به نام خدا

مرکز دانلود رایگان
مهندسی متالورژی و مواد

www.Iran-mavad.com

COMPREHENSIVE CORROSION

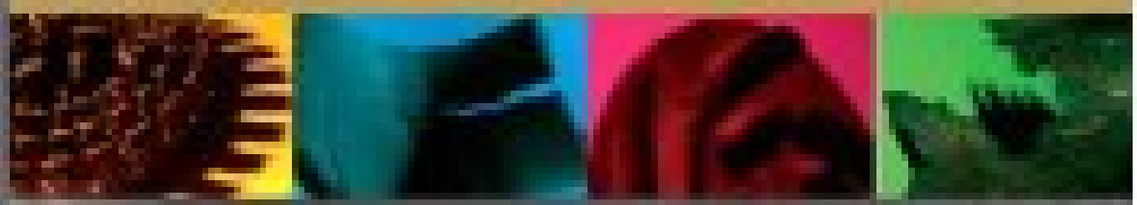

3.01 Corrosion of Carbon and Low Alloy Steels

S. B. Lyon
Corrosion and Protection Centre, School of Materials, University of Manchester, Oxford Road, Manchester M13 9PL, UK

Glossary

Akaganeite Hydrated iron oxide, β-FeO(OH,Cl), that is stable in the presence of chloride ions and thus generally forms in seawater.

Goethite Stable form of hydrated iron oxide, FeOOH and thus commonly found in nature.

LAMM phase The structure of the passive film on iron.

Lepidocrocite Metastable from of hydrated iron oxide, FeOOH and commonly found during atmospheric corrosion of iron-based alloys.

Abbreviations

ALWC Accelerated low water corrosion

BISRA British Iron and Steel Research Association

BS EN British Standard European Norm

FAC Flow-assisted corrosion
ISO International Standards Organisation
MIC Microbiologically assisted corrosion
NACE National Association of Corrosion Engineers
NBS National Bureau of Standards
RH Relative humidity
SIMS Secondary ion mass spectrometry

Symbols

ads Adsorbed
C Concentration of species
F The Faraday or Faraday's constant
i_{lim} Diffusion limited current density
k Mass transfer coefficient
n Number of electrons transferred in an electrochemical reaction
t Time
α Ferrite
γ Austenite
ω Angular velocity

3.01.1 Introduction

3.01.1.1 Historical Perspective

Prior to the sustained and deliberate production of iron, there is some evidence that ferrous materials (i.e., iron–nickel) derived from meteors were used intermittently in antiquity although they must have been relatively rare. The development of iron production dates back more than 3000 years (1500–1200 BC) when ferrous ores began to be smelted in the ancient Near East civilizations (i.e., Iran, India, Mesopotamia, and Anatolia), which apparently coincided with a shortage of tin for the production of bronze. In Europe, iron began to be produced somewhat later, in the period from the eight to the sixth century BC.[1]

A feature of early iron production was the relatively limited temperature that the furnaces of the time could achieve. In practice, this was not necessarily a disadvantage as the process involved the use of wood charcoal to reduce iron ore in the solid state leaving a porous mass of relatively pure solid iron (of variable composition) mixed with the ore residues (slag) resulting in a 'bloom.' Subsequently, the skill of the smith was required to repeatedly forge the hot bloom in order to remove the majority of the slag inclusions, resulting in a product known as 'wrought' (i.e., forged) iron. Subsequent adjustments in carbon content were made by cementation type processes, effectively by successively placing the semifinished object in hot charcoal or air.

This method of iron production remained, essentially unchanged in Europe, for 1500 years. However, in China development of iron smelting techniques that were able to reach temperatures of ~1150 °C and, consequently, were able to melt cast iron (when combined with ~4% carbon) was achieved in ~500 BC. Methods for reducing the carbon content of such cast irons were necessary in order to achieve a malleable material, and this was achieved by heating the molten material in air with stirring. During this process iron oxide, formed by oxidation of the molten metal, was stirred into the melt and reacted with dissolved carbon producing carbon monoxide, thus lowering the overall carbon content. In Europe, the development of water power was applied to the bloomery forging process in order to increase production of steels from 1000 AD onwards. However, cast irons were not generally produced as knowledge of how to reliably reduce their carbon content was not introduced until the Middle Ages (i.e., from 1100 to 1300 AD onwards) where a process similar to the Chinese one was used in so-called 'puddling' furnaces. Later developments included the manufacture of limited quantities of high quality steels via crucible and similar methods.

Large scale cast iron manufacture in blast furnaces developed only after the switch from wood charcoal (a limited resource) to coke derived from coal in the late seventeenth and early eighteenth centuries, while mass production of steel had to wait until Bessemer's invention of the converter in 1855, which utilized a hot air draught from below to remove carbon by reaction with oxygen. Until these developments, steel was an expensive commodity used only for niche applications where its combination of properties was essential. The widespread production of steel lowered its cost such that it could be used for an increasing number of applications, and eventually mild steel completely replaced wrought iron. Advances in the production of steel to further lower costs have continued as have alloy developments to further expand the use of ferrous materials. Nowadays, steel is a ubiquitous and essential component of modern life.

3.01.1.2 Iron–carbon Alloys

3.01.1.2.1 Phase diagram

Carbon is generally present in steel at room temperature as iron carbide (Fe_3C or cementite). This phase

is strictly metastable to decomposition to graphite and iron, however, the reaction is very sluggish at lower carbon contents although graphite evidently forms preferentially in, for example, grey cast irons. The iron–carbon phase diagram (drawn with cementite as the stable phase) is reproduced in **Figure 1**. The room temperature allotrope of unalloyed iron is known as ferrite (α-iron) and has a body-centered cubic structure; above 910 °C, this transforms to γ-iron or austenite (face-centered cubic) that, in turn, transforms to δ-iron (also body-centered cubic) above 1394 °C prior to melting at 1538 °C. Alloying with carbon lowers the melting point, eventually to the Fe–C eutectic temperature of 1140 °C forming effectively cast iron. Note that the solubility of carbon in ferrite is extremely low (around 0.03% at 723 °C and <0.01% at room temperature).

For practical purposes, iron may be defined as a material that contains carbon only up to its solubility limit in ferrite (i.e., <0.03% C by mass), while steel contains carbon within its solubility limits in austenite (i.e., from ~0.03% to 2.05% C by mass). In practice, most steels contain typically from 0.05% to 1.0% of carbon, with the majority of alloys lying at the lower end of this scale (i.e., 0.05–0.5% carbon), although some specialized alloys may have compositions that lie outside these values. Steel also contains elements such as silicon, phosphorus, and sulfur that arise inevitably from the steel-making process and which may affect properties detrimentally unless limited or controlled. For example, sulfur forms a low melting point eutectic with iron, and hence, limits the ability of the steel to be processed at higher temperatures. Thus, plain carbon steels traditionally contain sufficient added manganese (15–20 times that of sulfur) to 'mop-up' the sulfur via the formation of MnS precipitates. However, increased amounts of manganese are also beneficial in, for example, solid solution hardening of ferrite, and improving the ductility and toughness of the alloy.

'Plain carbon steel' may be defined as an alloy of iron with carbon where the total quantity of alloying elements is less than 2% by mass with compositional limits of 0.6% for copper, 1.65% for manganese, 0.04% for phosphorus, 0.6% for silicon, and 0.05% for sulfur and where no other elements are deliberately added in order to provide a specific property or attribute. This somewhat convoluted definition is necessary to exclude some low-alloyed steels (e.g., with small amounts of chromium, cobalt, niobium, molybdenum, nickel,

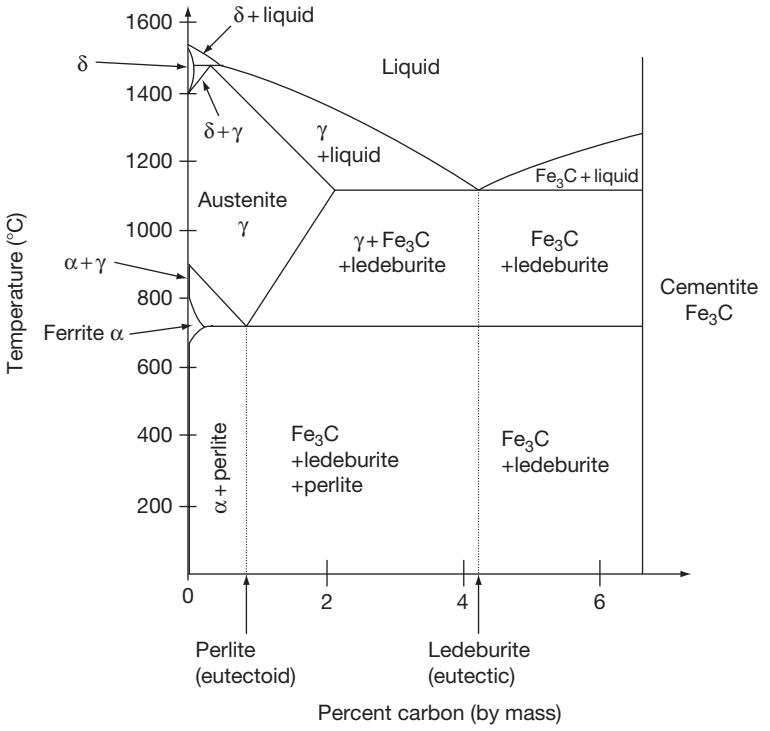

Figure 1 Iron–carbon phase diagram (note 'perlite' is an alternative spelling of 'pearlite'). Reproduced here under the Gnu Free Documentation License from its original source at www.wikipedia.org.

titanium, vanadium, etc.) that otherwise might be classed as 'plain carbon.' In contrast, 'low alloy steels' contain deliberate additions of alloying elements up to 10% by weight so as to develop enhanced mechanical properties. Finally, 'high alloy steels' contain more than 10% by weight of alloying additions and include materials such as stainless, tool, and maraging steels. Alloying additions may also be classed with respect to their effects on the stability of the ferrite and austenite phase regions. Thus, carbon, nitrogen, manganese, nickel, and cobalt all tend to expand the austenite phase region (i.e., are austenite stabilizers), while silicon, chromium, molybdenum, niobium, vanadium are ferrite stabilizers.

Carbon steels typically comprise more than 85% of steels produced and shipped worldwide and are, therefore, by far the most frequently used iron–carbon alloy. It is usual to categorize steels by their carbon content, but the specific boundaries are not well-defined. Generally, low-carbon steel ('dead mild' steel) contains up to ~0.15% carbon and 0.3–0.6% manganese by mass. It has relatively low strength but high formability, and is used typically in sheet and strip products. Mild steel contains from 0.15% to 0.3% carbon and is used in flat rolled products where higher strengths are required. For structural steelwork, plates and rolled sections, forgings and stampings of the manganese content can be increased to ~1.5% to improve toughness. Medium-carbon steels with 0.3–0.6% carbon and 0.60–1.65% manganese allow the use of quenched and tempered heat treatments with applications in axles, gears, forgings, rails, etc. Finally high-carbon steels containing 0.6–1.0% carbon and 0.3–0.6% manganese are used for high strength applications such as springs and wires. Materials with carbon content greater than 1% are typically insufficiently tough to be used for structural purposes, but find application where high hardness and abrasion resistance is required, for example, as machine tools, saw blades, etc.

3.01.1.2.2 Equilibrium microstructures

The iron–carbon phase diagram can be seen to be dominated by the pearlite eutectoid reaction (important for steel) and the ledeburite eutectic reaction (important for cast iron, and not considered further here). The pearlite reaction comprises the diffusion-controlled decomposition of austenite to ferrite and iron carbide at the eutectoid composition (~0.8% C by mass) and temperature (723 °C):

$$\gamma\text{-Fe} \rightarrow \alpha\text{-Fe} + \text{Fe}_3\text{C}$$

At carbon content below the eutectoid composition (hypoeutectoid <0.8% C), ferrite will form first, while at higher carbon content cementite will form first (hypereutectoid >0.8% C); both phases nucleating preferentially at the austenite grain boundaries. Pearlite (or perlite) is not a phase itself but it is rather a two-phase mixture of ferrite (~88%) and cementite (~12%) that forms in alternating laths (strips); it is so-called because of its characteristic pearl-like appearance. **Figure 2** shows representative steel microstructures of varying compositions. The individual laths of ferrite and cementite are often not easily resolved in commercial alloys using optical microscopy, however, they are visible in the higher carbon content material, **Figure 2(c)**.

Since the transformation is diffusion controlled, the spacing between the ferrite and cementite laths in pearlite varies as a function of cooling rate with slow (i.e., furnace) cooling giving the widest spacing and faster cooling giving closer spacing. Ferrite itself has a rather low yield stress, so the overall strength of the steel is dependent on the nature and spacing of second phase particles, including the individual pearlite colonies as well as the pearlite lamellae and any other phase that happens to be present.

3.01.1.2.3 Nonequilibrium microstructures

If steel is cooled faster than the rate at which carbon can be rejected by diffusion from the austenite lattice, the consequent formation of equilibrium iron carbide is partially or wholly suppressed. Under these circumstances, the austenite cannot retain the excess of carbon within its structure due to its thermodynamic instability and must transform via an alternative mechanism. At sufficiently low temperatures where essentially no significant diffusion of carbon can occur, the thermodynamic driving force is able to overcome the lattice strains inherent in a diffusionless (shear) transformation and martensite, which is a distorted body-centered tetragonal structure, will form directly. At intermediate temperatures where limited diffusion of carbon can still occur, the bainite structure forms by transformation of austenite to carbon-supersaturated ferrite with the subsequent diffusion of carbon and the precipitation of carbides either in untransformed austenite (upper bainite) or within the ferrite (lower bainite). The detailed mechanisms of these transformations and their microstructures are complex and beyond the scope of this work, however, the concept is important in understanding the properties of steel and particularly how they may be altered beneficially by heat treatment.

The advantage in rapid cooling (or quenching) of steel is that carbon is then held uniformly in the martensite phase in supersaturated solid solution. Martensite itself is very brittle and hard and, consequently, has limited uses. However, when martensite is reheated sufficiently, the retained carbon is able to diffuse and precipitate as fine carbides that are relatively evenly distributed in the material. In contrast, in pearlitic steel, the strengthening phase is both unevenly distributed (i.e., in pearlite colonies) and present in thin strips that are more likely to act as crack initiators. **Figure 3(a)** shows a quenched martensitic structure, while **Figure 3(b)** shows the same material but after aging (tempering) at an elevated temperature in order to precipitate the carbide particles. The even distribution of carbides is evident and compared with a pearlitic microstructure of similar carbon content, results in greatly increased fracture toughness at similar yield stress.

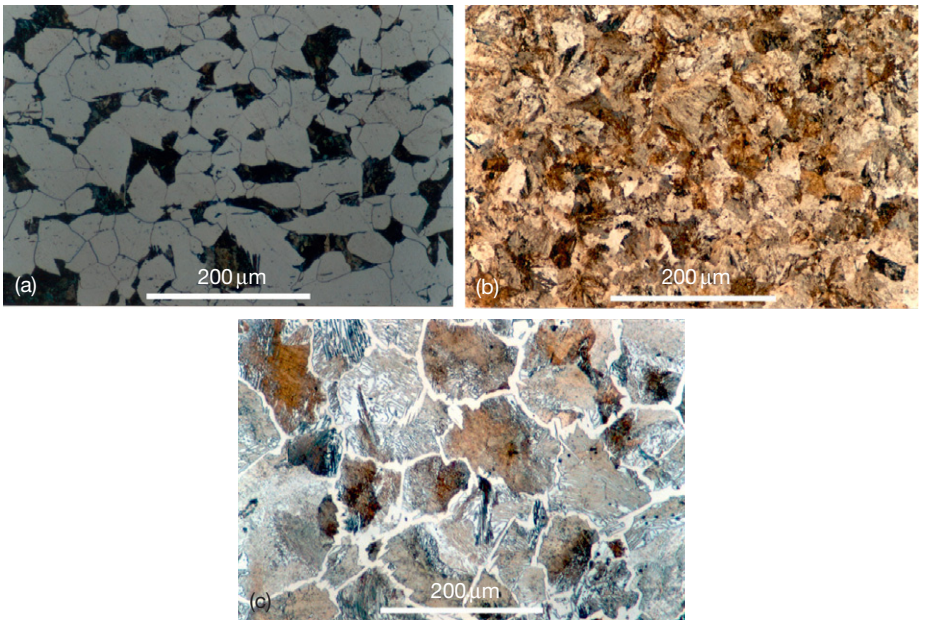

Figure 2 Pearlitic microstructures in steel (air cooled) (a) Hypoeutectoid (0.2% C; ferrite, light, with pearlite colonies, dark, elsewhere in the structure). (b) Eutectoid composition (0.8% C; fully pearlitic). (c) Hypereutectoid (1.3% C; cementite has nucleated on former austenite grain boundaries with pearlite elsewhere in the structure). Reproduced by kind permission of Cochrane, R. F. University of Leeds and the DoITPoMS Micrograph Library (www.doitpoms.ac.uk).

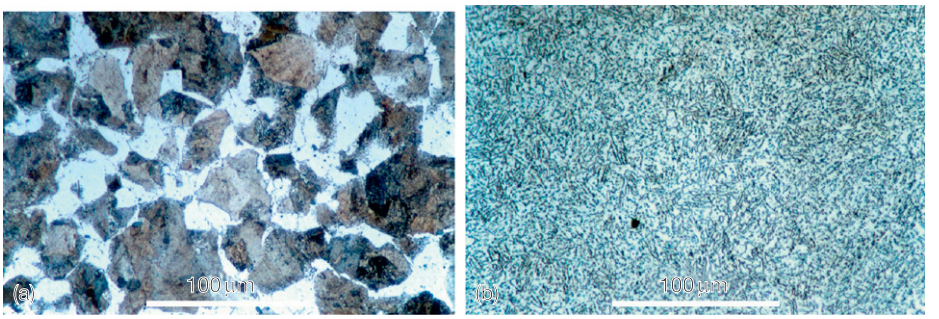

Figure 3 Annealed, compared with quenched and tempered, steel microstructures. (a) 0.31% C annealed showing pearlite colonies of ferrite and cementite between grains of ferrite. (b) as (a) but quenched to form martensite then tempered to precipitate a fine carbide distribution of cementite. Reproduced by kind permission of Cochrane, R. F. University of Leeds and the DoITPoMS Micrograph Library (www.doitpoms.ac.uk).

3.01.1.3 Mechanical and Physical Properties

Alloying greatly decreases the thermal and electrical conductivities of pure iron but has little effect on other physical properties such as the elastic modulus. Regarding mechanical properties, pure iron (ferrite) is soft and malleable but work-hardens rapidly, Table 1. Ferrite can be solid–solution strengthened by either interstitial (e.g., C, N, and P) or substitutional (e.g., Si and Mn) alloying additions. Silicon and manganese, which are always present in iron at levels of ~0.3–0.5%, provide some solid–solution strengthening of the ferrite; phosphorus gives much stronger solid-solution strengthening but is not commonly added deliberately as it can greatly reduce toughness. Carbon and nitrogen have the greatest potential effect but have very low solubilities in ferrite.

As noted above, carbon-containing alloys (i.e., steels) are mainly strengthened by the formation of second phase carbide precipitates. In plain carbon steels, these comprise iron carbides that may form as pearlite colonies or, after quenching and tempering, as a fine carbide distribution in the microstructure. In low alloy steels, the addition of elements such as molybdenum, titanium, vanadium, chromium, niobium, and nickel either promote the formation of alloy carbides or control the formation of martensite and/or the favorable precipitation of iron carbides.

Like other body-centered cubic metals, steels are subject to a ductile-to-brittle transition and this may occur close to ambient temperatures depending upon the type of steel, its alloying contents (including carbon, manganese, etc.), and how it has been processed. Clearly, it is usually advisable for the ductile-to-brittle transition temperature to fall well below operating temperatures in order to ensure adequate fracture toughness during service. Key factors that influence the transition temperature include microstructure, carbide distribution, internal stress, and the composition of the ferrite phase.

It is beyond the scope of this chapter to discuss the detailed effect of microstructure, composition, etc. on the overall mechanical properties of steels and, hence, interested readers are directed to Llewellyn *et al.*[3] and Bhadeshia *et al.*[4] for further information.

3.01.1.4 Processing

3.01.1.4.1 Heat treatment

The main purpose of heat treatment is to optimize the mechanical properties of a particular steel grade. This typically involves a single or a series of heating and cooling operations designed to produce an optimum microstructure for the particular end use. These processes can be divided conveniently into: softening (or annealing), normalizing, hardening, and tempering treatments.

General process annealing is carried out on cold-worked materials in order to relieve internal stresses and/or to soften them prior to further cold work. Full annealing is carried out by heating the steel into the austenite phase region (if a hypoeutectoid steel), or just above the eutectoid temperature (if hypereutectoid) followed by slow (e.g., furnace) cooling that results in a relatively coarse lamellar pearlite. Normalizing involves the same heat treatment, however, the cooling is more rapid and carried out in air, which results in a decrease in the size of microstructural features (grain size and pearlite lamellae spacing) and consequent increased final hardness.

Hardening of hypoeutectoid steels involves heating into the austenite phase region followed by rapid cooling (or quenching). As the cooling rate is increased, the formation of pearlite occurs at lower temperatures resulting in an increasingly finer lamellar structure, until at a critical cooling rate that depends on the alloy content of the steel, martensite is formed directly. Tempering of hardened steel is achieved by reheating to various temperatures below the austenite boundary with the intention to relieve internal stresses

Table 1 Generic properties for annealed ferrous alloys

Property	*Iron (>99.9% Fe)*	*Carbon steel (0.15%C)*	*Stainless steel (18%Cr, 10%Ni)*
Density ($Mg\,m^{-3}$)	7.86	7.86	8.00
Elastic modulus (GPa)	200	200	195
Thermal conductivity ($W\,m^{-1}\,K^{-1}$)	76.2	20–65	16.2
Electrical conductivity ($10^6\,\Omega^{-1}\,m^{-1}$)	11.2	6.23	1.45
Ultimate tensile strength (MPa)	>200	385	565
Proof Stress at 0.2% strain (MPa)	~70	285	210
Elongation (%)	>40	35	55

Source: Data taken from Smithells Metals Handbook.

induced by quenching and to permit the diffusion of carbon retained in the martensite matrix in order to precipitate a relatively even distribution of carbides. Tempering at 100–200 °C is sufficient to relieve quenching stresses only. However, at temperatures between 200 °C and 450 °C the martensite will decompose into ferrite by precipitation of fine particles of carbide throughout the structure decreasing yield strength but increasing toughness. At higher temperatures still (i.e., 450–650 °C) fewer but larger carbide particles are produced further increasing the toughness and reducing the strength. Microstructures formed in this way are known as tempered martensites and vary in microstructure from relatively large ferrite grains containing second phase carbides to small, fine-grained structures similar to bainite. Generically, these steels are known as quenched and tempered.

The details for steel heat treatments are complex and those given above merely summarize the main elements; further details can be found in *Steel Heat Treatment Handbook*.[5] In some cases, heat treatment alone cannot provide the desired structure, and some form of thermo–mechanical treatment is necessary. For example, some low alloy and microalloyed steels (high-strength low-alloy steels) develop exceptional combinations of strength, toughness, and low ductile-to-brittle transition temperature by virtue of a controlled process combining a gradually decreasing temperature with simultaneous rolling of the steel.

After processing (rolling, forging, forming, etc.) at elevated temperatures, a layer of oxide, called millscale, inevitably would have formed on the metal surface. The structure of millscale consists of three superimposed layers of iron oxides in progressively higher states of oxidation from the metal side outwards: ferrous oxide (FeO) on the inside, magnetite (Fe_3O_4) in the middle, and ferric oxide (Fe_2O_3) on the outside. The relative portions of the three oxides vary with the processing temperatures. A typical millscale on 9.5 mm mild steel plate would be ~50 μm thick, and contain ~70% FeO, 20% Fe_3O_4, and 10% Fe_2O_3. If millscale was perfectly adherent, continuous, and impermeable, it would form a good protective coating, but in practice millscale is liable to crack and flake off exposing the underlying metal. During atmospheric exposure, the presence of millscale on the steel may reduce the corrosion rate over comparatively short periods, but over longer periods, the rate tends to rise as the oxide flakes off the surface. In water, severe pitting of the steel may occur if large amounts of millscale are present on the surface. For example, pits up to 1.25 mm deep were found on as-rolled steel specimens after 6 months immersion in sea-water at Gosport.[6] It follows that for most practical purposes where steel is exposed without a protective coating, or indeed to achieve effective coatings adhesion to the substrate, it is essential to remove all millscale either before putting components into service or prior to application of a protective coating.

3.01.1.4.2 Mechanical deformation

The vast majority of steel products are produced by mechanical deformation either while 'hot' (i.e., above the recrystallization temperature of the alloy) or 'cold' (i.e., below the recrystallization temperature); in the latter case, if continued processing is required, periodic annealing is necessary in order to remove the effects of work-hardening. Such processes include: rolling (plate, strip, and bar products, etc.), forging, stamping, wire drawing, etc. Both hot and cold deformation will produce a varying degree of banding and texture in the resultant microstructure, which may result in properties that vary according to the deformation direction, **Figure 4**. Nonmetallic second-phase inclusions that originally derive typically from slag materials incorporated during the steel-making process will tend to form stringers in the metal during rolling operations. These can form planes of weakness in the steel, although modern clean steel making technology has greatly reduced the volume fraction and distribution of such unwanted second phases.

3.01.1.4.3 Metallurgical influences on corrosion

Generally, the process of manufacture has no appreciable effect on the corrosion characteristics of carbon steel. Slight variations in composition that inevitably occur from batch to batch in steels of the same quality have little effect with the exception of a limited number of elements in a small (but important) number of applications. For example, the addition of ~0.2% of copper results in a two- to threefold reduction in the atmospheric corrosion rate compared with a copper-free steel.[7,8] Variation in other alloying additions in carbon steel affects the corrosion rate to a marginal degree, the tendency being for the rate to decrease with increasing content of carbon, manganese, and silicon. Thus, steel containing 0.2% of silicon rusts in air ~10% slower than an otherwise similar steel containing 0.02% of silicon. Otherwise, all ordinary ferrous structural materials, that is, carbon and low-alloy steels, corrode at virtually the same rate when immersed in natural waters.

As shown in the historic data of Table 2, the process of manufacture and the composition of mild steel do not affect its corrosion rate appreciably.[9]

In carbon steels, the effect of microstructural anisotropy caused by processing is also generally not significant. Thus, in seawater immersion tests, carried out to determine the effects of rolling direction and tensile stress on the corrosion of a steel containing 0.14% C, 0.47% Mn and 0.04% Si,[10] specimens were cut from plates parallel to and perpendicular to the rolling direction. There was little difference in general corrosion performance, although pitting was somewhat worse on the plate cut parallel to rolling.

For low alloy steels generally under immersed conditions, alloying additions of at least 3% (e.g., of chromium, nickel, etc.) are necessary to obtain any marked improvement in the corrosion-resistance. The main elements that alter the rate of corrosion of low alloy steels when immersed in natural waters are aluminum, copper, chromium, molybdenum, and nickel, but other additions, for example, manganese, silicon, phosphorus, and sulfur, may have minor roles. The action of some alloying elements can be beneficial, neutral, or detrimental, depending upon whether localized or uniform corrosion is being considered and whether the steel is fully, partially, or intermittently immersed. A large program of work between a number of research laboratories in Europe was carried out over an extended period to study the influence of alloying elements on corrosion of low alloy steel[11] and the main findings, which are summarized in Table 3, are still relevant.

From a consideration of Table 3, steel containing copper and phosphorus might be chosen for its resistance to corrosion in the critical tidal and splash zone.

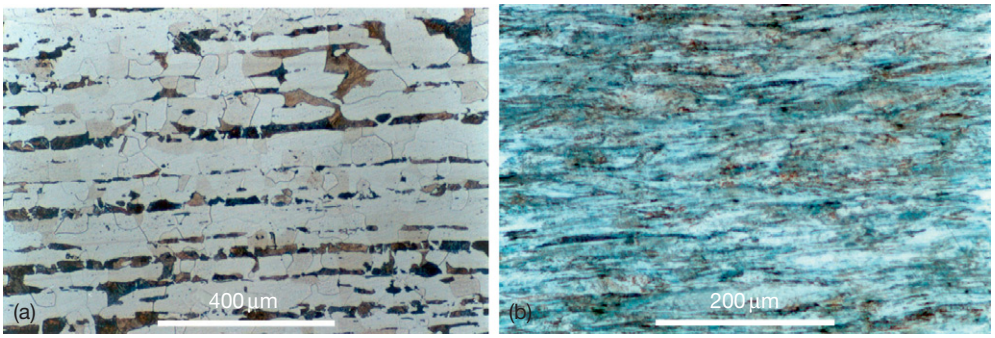

Figure 4 Directionality in microstructure after mechanical deformation. (a) 0.2% C steel after hot rolling showing banded carbide microstructure. (b) 0.6% C steel after cold wire drawing showing highly deformed grain structure Reproduced by kind permission of Cochrane, R. F. University of Leeds and the DoITPoMS Micrograph Library (www.doitpoms.ac.uk).

Table 2 Corrosion rates of mild steels in seawater, total immersion for 203 days at Plymouth

Type of steel[a]	*Analysis (%)*				*Average general penetration (mm year^{-1})*
	C	*Mn*	*P*	*S*	
Basic Bessemer, rimming ordinary	0.05	0.64	0.06	0.02	0.143
High phosphorus	0.03	0.31	0.14	0.04	0.143
High phosphorus and sulfur	0.03	0.30	0.10	0.07	0.148
Open-hearth, rimming ordinary	0.13	0.33	0.03	0.03	0.143
From haematite pig	0.06	0.32	0.01	0.03	0.140
Open-hearth, killed ordinary	0.10	0.35	0.03	0.02	0.140
From haematite pig	0.11	0.34	0.01	0.03	0.136
Open-hearth, killed ordinary	0.22	0.71	0.03	0.03	0.143
From haematite pig	0.21	0.58	0.02	0.03	0.158

[a]The copper contents of the steels, which were supplied through the courtesy of l'Office Technique pour l'Utilisation de l'Acier (France), varied from 0.03 to 0.11%. The killed steels contained 0.04% Al and 0.1% Si.
Source: After Hudson, J.C. *J. Iron Steel Inst*. **1950**, *166*, 123.

Table 3 Effect of alloying elements on marine corrosion resistance

Corrosion type	*Environment*	*Favorable*	*Neutral*	*Unfavorable*
Uniform corrosion	Marine immersion	Mn, Si, Al, Mo (> 4 years), Cr (< 4 years)	Ni	P, S, Cu, Mo (> 4 years), Cr (< 4 years)
Uniform corrosion	Tidal and splash zone	P	Cu, Cr, Ni	–
Uniform corrosion	Marine atmosphere	P, Si, Mn, Cu, Cr, Ni	–	–
Pitting corrosion	Marine immersion	–	Cu, Cr	Ni
Pitting corrosion	Tidal and splash zone	Cu	Ni	Cr

Source: After Songa, T. International Conference on Steel in Marine Structures, Paris, ECSC: Luxembourg, 1981.

However, in practice the sample-to-sample variation in corrosion rate is much greater than the difference between various alloy steels, so it is improbable that low-alloy steels will corrode more slowly than mild steel in most practical environments. This conclusion was supported by Forgeson *et al.* in the 1960s who concluded from extensive tests in fresh and salt waters of the Panama Canal Zone that: "proprietary low-alloy steels were not in general more resistant to underwater corrosion than the mild unalloyed carbon steel."[12] In any case, it is rare to expose unprotected steel in this way without a reliable corrosion control method such as cathodic protection also being applied.

The generally negligible effects of alloying additions on the corrosion of low alloy steels under immersed conditions were also reported in historic work from the 1930s to 1950s by the former British Iron and Steel Research Association (BISRA) in the UK[13] and the National Bureau of Standards (NBS) in the USA.[14] The latter work was rather extensive and involved ten varieties of steel (as well as cast irons), which were buried in 15 typical American soils from 1937 to 1950. The results showed that, with few exceptions, the corrosion of low-alloy steels containing copper, nickel, and molybdenum in various combinations did not differ by more than 20% from that of ordinary carbon steel. The main exception was chromium, where additions of 2% or 5% of chromium did increase the corrosion resistance somewhat, as is indicated in **Figure 5**.

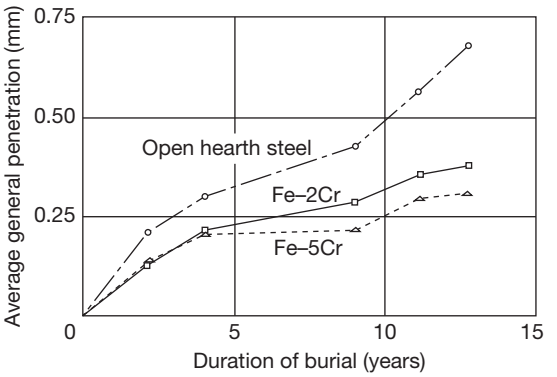

Figure 5 Effect of chromium content on the corrosion of buried steel. Reproduced from Romanoff, M. Underground Corrosion, National Bureau of Standards Circular 579, US Government Printing Office, Washington, 1957.

3.01.2 Electrochemistry

3.01.2.1 Thermodynamics

Iron is a relatively active element whose domain of stability resides completely below that of the domain of stability for water. Thus, in principle, iron can evolve hydrogen from aqueous solutions at all pH, **Figure 6**. In practice, hydrogen evolution occurs readily only at low pH (i.e., below ~pH 3); at higher pH, although it is thermodynamically possible, hydrogen evolution is very slow at ordinary temperatures due to the low driving force and sluggish kinetics. At intermediate pH, iron passivates and at higher pH iron may dissolve as the ferroate oxyanion, although this reaction is sluggish and passive iron is practically stable to pH 13 and above (e.g., in concrete). Iron corrodes readily, therefore, in near-neutral oxidizing environments, including: the atmosphere, natural waters in equilibrium with atmospheric carbon dioxide and seawater, however, the rate of corrosion in oxygen-free neutral waters is much less and controlled by the stability of the passive film. Iron is more active than elements such as nickel, copper, cobalt, etc. but is more noble than zinc, aluminum, magnesium, etc. Thus, the latter elements are, in practice, important for use as sacrificial anodes for the cathodic protection of steel. Apart from a few exceptions in specific circumstances, minor variations in the composition of steel generally have minimal effect on the overall electrochemistry and, hence, the corrosion rates.

Iron has two stable oxidation states: ferrous (+2) and ferric (+3). Typically, divalent ferrous species are

considerably more soluble in aqueous solution than the trivalent ferric species, which have significant solubility only at low and high pH. The oxides and hydroxides of iron are complex and interrelated crystallographically; furthermore, many of the ferric oxides undergo reductive dissolution to soluble ferrous species, such as the $Fe(OH)^{+}$ ion. Figures 6 and 7 show a Pourbaix diagram for the limits of stability of soluble iron species at a concentration of 10^{-5} M.

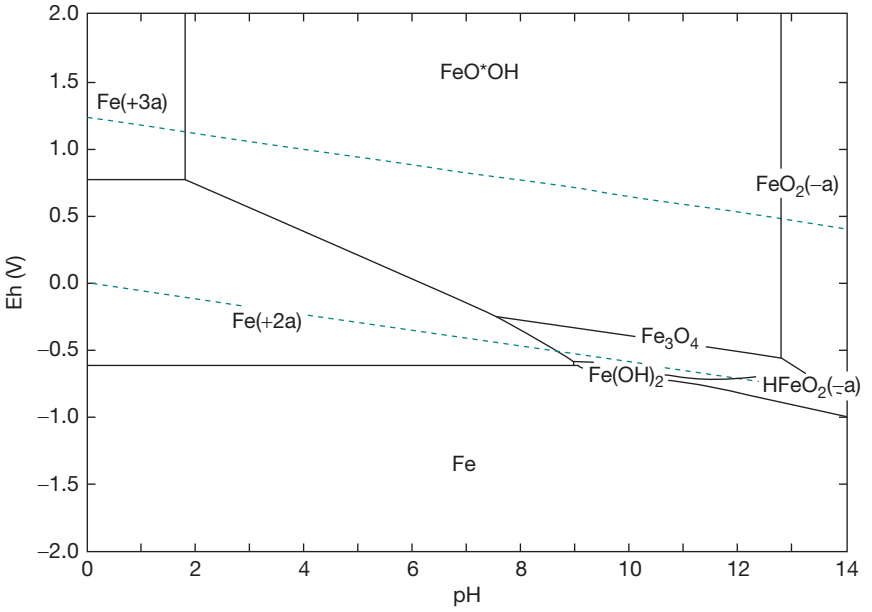

Figure 6 Pourbaix diagram for iron with soluble species at concentration of 10^{-5} M, and with the most frequent stable oxide species present. Calculated using HSC version 6.12 thermochemical modelling software, Outotec, Finland.

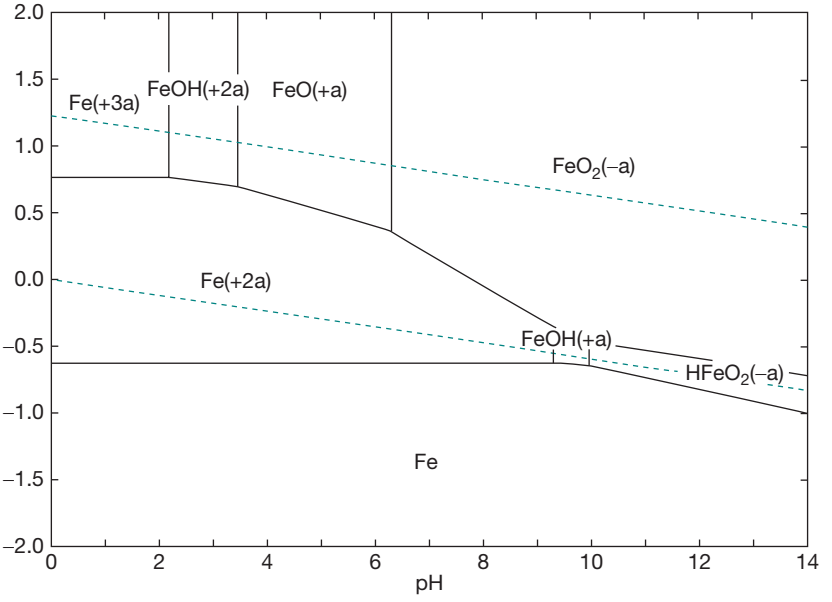

Figure 7 Pourbaix diagram for soluble species only (i.e., excluding solid species) at a concentration of 10^{-5} M. Calculated using HSC version 6.12 thermochemical modelling software, Outotec, Finland.

3.01.2.2 Anodic Dissolution

3.01.2.2.1 Oxygen-free (deaerated) conditions

The mechanism for the dissolution of iron, whether in aerated or deaerated conditions, varies as a function of pH and, despite extensive investigation by Bockris,[15–18] Drazic,[19,20] Lorenz,[21,22] Hackerman,[23] and others, is still not entirely resolved. One of the complications is that the mechanism is greatly influenced by a number of factors including the nature of the anions present in solution. The most commonly accepted generic reaction sequence in deaerated acid conditions is due to Bockris, Drazic, and Despic[17] where a reaction order of ~1 with respect to hydroxide ion concentration (i.e., the kinetics are a function of pH) was determined for the anodic dissolution of iron at pH <4. This broadly fits the following reaction sequence:

$$\mathrm{Fe} + \mathrm{H_2O} \rightleftarrows \mathrm{FeOH_{ads}} + \mathrm{H^+} + \mathrm{e^-} \quad [1]$$

$$\mathrm{FeOH_{ads}} \rightarrow (\mathrm{FeOH^+})_{\mathrm{ads}} + \mathrm{e^-}\,(\text{rate determining}) \quad [2]$$

$$(\mathrm{FeOH^+})_{\mathrm{ads}} + \mathrm{H^+} \rightleftarrows \mathrm{Fe^{2+}} + \mathrm{H_2O} \quad [3]$$

Thus, adsorption of water initially occurs onto the iron surface together with the first single electron transfer step giving rise to a transient intermediate ($\mathrm{FeOH_{ads}}$). The second electron transfer step, giving rise to the stable Fe(+2) oxidation state, occurs subsequently and is rate determining. In near neutral solution (4< pH <9) this sequence is modified slightly[24] and after reaction [2] above, the following sequence holds:

$$(\mathrm{FeOH^+})_{\mathrm{ads}} + \mathrm{H_2O} \rightleftarrows \left(\mathrm{Fe(OH)_2}\right)_{\mathrm{ads}} + \mathrm{H^+} \quad [4]$$

$$\left(\mathrm{Fe(OH)_2}\right)_{\mathrm{ads}} + 2\mathrm{H^+} \rightleftarrows \mathrm{Fe^{2+}} + 2\mathrm{H_2O} \quad [5]$$

In both cases, the overall reaction is the familiar:

$$\mathrm{Fe} \rightarrow \mathrm{Fe^{2+}} + 2\mathrm{e^-} \quad [6]$$

In alkaline solution (pH>9), and in the absence of oxygen, passivation of the iron surface occurs after reaction [4] with the initial formation of ferrous hydroxide, reactions [7] below and subsequent oxidization to magnetite:

$$(\mathrm{FeOH})_{\mathrm{ads}} + \mathrm{H_2O} \rightarrow \mathrm{Fe(OH)_2} + \mathrm{H^+} + \mathrm{e^-}\,(\text{rate determining}) \quad [7a]$$

$$(\mathrm{FeOH})_{\mathrm{ads}} + \mathrm{OH^-} \rightarrow \mathrm{Fe(OH)_2} + \mathrm{e^-}\,(\text{rate determining}) \quad [7b]$$

$$3\mathrm{Fe(OH)_2} \rightleftarrows \mathrm{Fe_3O_4} + 2\mathrm{H_2O} + 2\mathrm{H^+} + 2\mathrm{e^-} \quad [8]$$

Finally, strong alkali ferrous hydroxide can chemically dissolve as the dihypoferrite anion that is in equilibrium with the hypoferrite (ferroate) anion:

$$\mathrm{Fe(OH)_2} + \mathrm{OH^-} \rightleftarrows \mathrm{HFeO_2^-} + \mathrm{H_2O} + \mathrm{OH^-} \rightleftarrows \mathrm{FeO_2^{2-}} + 2\mathrm{H_2O} \quad [9]$$

3.01.2.2.2 Oxygen containing (aerated) conditions

When dissolved oxygen is present, ferrous species are unstable to further oxidation in solution to ferric species, which have considerably lower solubility products and are liable to precipitation giving rise to the familiar rust corrosion product. Thus, in aerated near-neutral to acid conditions, ferrous ions are oxidized by dissolved oxygen in solution, with FeO(OH) as the end product (other oxides/hydroxides are possible):

$$2\mathrm{Fe^{2+}} + 3\mathrm{H_2O} + \tfrac{1}{2}\mathrm{O_2} \rightarrow 2\mathrm{FeO(OH)} + 4\mathrm{H^+} \quad [10]$$

Any formed ferric oxide will immediately precipitate giving rise to the familiar brown staining that denotes rusting. If precipitation occurs close to the metal surface (as is likely in aerated solution), oxide will tend to build up on the iron, although this will not be in a coherent and impermeable manner. Hence, rust layers formed in this way can only provide a diffusion restriction for the corrosion of iron and steel and do not result in passivation.

In alkaline environments at pH >9, passive ferrous hydroxide and magnetite (in which 1/3 of the iron atoms are in the ferrous state and 2/3 ferric) are also susceptible to further oxidation to ferric hydroxide:

$$\mathrm{Fe(OH)_2} \rightleftarrows \mathrm{FeO(OH)} + \mathrm{H^+} + \mathrm{e^-} \quad [11]$$

$$\mathrm{Fe_3O_4} + 2\mathrm{H_2O} \rightleftarrows 3\mathrm{FeO(OH)} + \mathrm{H^+} + \mathrm{e^-} \quad [12]$$

However, in these cases, the reaction occurs in the solid state and the iron remains passive with the advantage that ferric hydroxide has a greater thermodynamic stability range. Note that the oxidation of ferrous hydroxide and magnetite to ferric hydroxide is reversible and, hence, the passive film is unstable to electrochemical reduction.

3.01.2.2.3 Anion adsorption effects on the mechanism of dissolution

As key steps in the anodic dissolution mechanism for iron involve the adsorption of water or hydroxyl ions,

it is evident that the presence of other anions that compete for adsorption will influence the concentration of the adsorbed hydroxyl intermediate and, in consequence, the corrosion rate. For example, the effect of halide ions on the corrosion rate of iron in acid media has been known for over 80 years.[25] Although, it is widely assumed that halides are uniformly aggressive (i.e., increase corrosion rates), this is not universally the case, and at low-to-intermediate concentrations in acid, they can act as effective inhibitors. For example, iodide ions inhibit corrosion of mild steel in 0.5 M H_2SO_4 at concentrations less than $\sim 10^{-2}$ M with an inhibition efficiency (i.e., percentage reduction in corrosion rate) of up to 90%.[26] The effectiveness of inhibition decreases in the order: I^-, Br^-, and Cl^-, which is consistent with the adsorption efficiency of the anions and confirmed by electrochemical impedance spectroscopy measurements of surface capacitance. Species that are only weakly absorbing (such as perchlorate) have no significant effect on the corrosion rate. Of course, a distinction here has to be made between species that interfere directly with the anodic dissolution process and species that interfere with a cathodic reaction such as hydrogen evolution. A large class of organic inhibitors for corrosion in acids (e.g., pickling inhibitors) act by adsorbing onto the surface of the steel and, hence, block either or both of the electrochemical reactions.[27]

3.01.2.3 Passivity

3.01.2.3.1 Passive oxide films

The phenomenon of passivity was probably first recorded by James Keir in 1790 on the exposure of iron to concentrated nitric acid.[28] He noticed that if the concentration of nitric acid was sufficiently high, gas evolution appeared to cease and the iron appeared to be in a quiescent state. This 'passive' state of iron was later explained by Michael Faraday in 1836 and, given the undeveloped state of knowledge at the time, his comments are immensely prescient[29]:

> . . . my impression is that the surface of the metal is oxidised or else that the superficial particles of the metal are in such relation to the oxygen of the electrolyte as to be equivalent to oxidation . . .

Passivity is now known to be caused by the formation of an oxidized species on a metal surface under the correct conditions of potential and pH. Thus, on formation of a more-or-less thermodynamically stable, compact, and continuous film on a metal surface, the kinetic processes involved in corrosion (e.g., electron and ion charge transfer, diffusion of reacting species, etc.) are slowed by many orders of magnitude. For ferrous alloys, and as indicated above, passivity occurs at intermediate pH and at sufficiently high oxidizing potentials and results in the formation of an oxide film. The literature on passivity in general, and on passivity of iron in particular, is extensive. Of interest are the mechanisms of passive oxide film formation, its structure and composition, the long-term stability of the film, and its local breakdown in the presence of species such as chloride ions and others (i.e., pitting).

Passive iron oxide is thermodynamically stable at sufficiently high potentials. Thus, the passive film on iron can itself participate in the corrosion process as a cathodic reactant, and is consequently destroyed in the process. In this way the passivity of iron is fundamentally more unstable than, for example, that of chromium or of aluminum. Also, unlike other passive films which are generally insulating, the passive oxide on iron (e.g., magnetite) is an electronically conducting n-type semiconductor[30] and forms an effective electrode for, for example, oxygen reduction.

Regarding the nature of the film, it was historically proposed to consist of a Fe_3O_4 inner layer with an outer layer of γ-Fe_2O_3,[31,32] results that appeared to be consistent with electrochemical data. However, later Mössbauer studies demonstrated that the passive film contained only ferric species with no evidence of significant Fe^{2+} present. Also, the films were likely to be microcrystalline or amorphous and did not appear to change structurally on drying in air.[33,34] For passive films formed on iron by anodic polarization in borate buffer solution at pH 8.4, the hydroxyl content of the film was shown by secondary ion mass spectrometry (SIMS) to be effectively zero,[35] thus confirming that the film was an oxide only and not a hydroxide.

A criticism of most research of this type is that it is necessarily carried out *ex situ* (i.e., the passive film was formed in solution the sample was removed and then analyzed elsewhere). Truly *in situ* measurements of the passive film structure were only achieved in the 1990s by use of X-ray absorption near edge fine structure[36] and scanning tunneling microscopy,[37] which showed that the film is either amorphous or a crystalline spinel (i.e., similar to Fe_3O_4 and γ-Fe_2O_3), thus confirming the previous results but leaving open the question of precisely which structure is correct.

The controversy on the structure of passive iron oxide appears now to have been solved by Toney *et al.* using careful *in situ* and *ex situ* synchrotron X-ray

diffraction measurements on high purity iron.[38] This confirmed that the diffraction peaks were similar to spinel, but that the structure factors did not conform to either Fe_3O_4 or γ-Fe_2O_3, or indeed any other known oxide or hydroxide of iron. Full X-ray structure refinement determined that the passive film consists of a nano-crystalline spinel unit cell (containing 32 oxide anions) with cation occupancy of ~80% for octahedral sites, 66% for tetrahedral sites, and with ~12% of cations occupying octahedral interstitial sites. Note that despite the superficial similarities to both the magnetite (Fe_3O_4) and maghemite (γ-Fe_2O_3) structures, it is a distinctly different material, termed the LAMM phase. Later work by the same authors, using a molecular modeling approach, has indicated that the LAMM phase is metastable.[39] However, this may not be so surprising considering that the film is formed under nonequilibrium conditions and, since it is thin, surface and interfacial free energies will dominate over the free energy of the macroscopic phase.

Similar experimental problems exist for determining the mechanism for passive oxide film growth. This is commonly assumed to occur via ion conduction caused by the electric field between the metal and the electrolyte. A clever experiment using isotopically labeled reagents studied the film formed after sequential anodizing of iron in ordinary and ^{18}O enriched water, using SIMS to monitor the $^{18}O/^{16}O$ ratio.[35] The results were consistent with the majority transport mechanism during film growth consisting of inward oxygen ion transport in the lattice; however, some ^{18}O was detected at the interface indicating that some short-circuit diffusion paths exist in the structure, presumably at crystalline boundaries.

3.01.2.3.2 Nonoxide passive films

In the strict sense, passivity relates to the process of oxidation leading to a solid corrosion product that forms in such a way (i.e., thermodynamically, or at least kinetically, stable, continuous, without substantive defects, relatively insoluble, and generally resistant to further oxidation or reduction) as to provide a significantly protective film. This definition does not have anything to say about the chemical nature of the passive film. Indeed, although passive oxide films are by far the most important type, passive films may also consist of sulfides, chlorides, etc.

In sulfide environments, for example, steel may passivate by the formation of an iron sulfide film, Figure 8. However, this film has distinctly different properties to passive oxides.[40] Firstly, the initially formed film is nonstoichiometric (FeS_{1-x}) and, like Fe_3O_4 (but unlike FeO(OH)) is electronically conducting and is an excellent cathode, especially for the hydrogen evolution reaction. Secondly, the film is unstable to further oxidation to FeO(OH) and FeS_2, which, due to volume expansion, disrupts the film and results in damage, including cracking. Cracks and

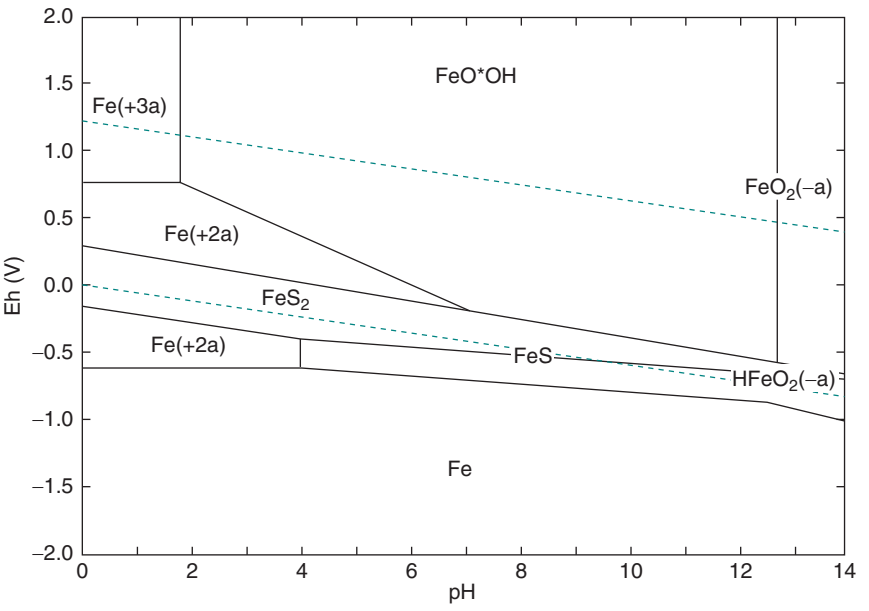

Figure 8 Pourbaix diagram for iron and sulfur at 10^{-5} M metal ion and 10^{-3} M sulfur species. Calculated using HSC version 6.12 thermochemical modelling software, Outotec, Finland.

other defects in the sulfide film effectively result in small local anodes that, when coupled to the large efficient external cathode (the remnant sulfide film), causes severe localized (pitting) corrosion.

Other forms of corrosion that result in the formation of surface films with significant protective properties are often the result not of direct oxidation to a solid species, but rather by precipitation of an insoluble salt that covers the metal surface, for example, iron phosphate. In the strict sense, this is not 'passivity,' although it is often described as such, particularly, if the end result (a greatly reduced corrosion rate and a tendency for corrosion to occur in a localized manner) is similar. In some cases, however, it is unclear whether the film forms by direct oxidation or by precipitation. For example, a protective ferrous sulfate film forms during corrosion of steel in concentrated sulfuric acid,[41] since iron sulfate is relatively insoluble in this environment. Also, corrosion of steel in environments containing dissolved carbon dioxide (so-called 'sweet' corrosion in the oil and gas industry) can result in a protective film of ferrous carbonate under some conditions.[42] Such films may either form by precipitation (salt films) or may form by direct oxidation to a solid product where the solubility of the species is extremely low. However, whether this is really passivity or not is ultimately a matter of semantics.

3.01.2.4 Cathodic Reactions

3.01.2.4.1 Hydrogen evolution reaction

The hydrogen evolution reaction is one of the most studied electrochemical processes partly due to its technological interest but also due to the relative ease of investigation (one only needs to place some zinc in sulfuric acid to observe hydrogen bubbles being produced). The mechanism for hydrogen evolution on iron involves initial discharge of hydrogen ions on the metal surface with corresponding adsorption of a hydrogen atom followed by the rate determining reaction[43]: most commonly, chemical desorption of adsorbed hydrogen [14a] or, at high overpotential, electrochemical desorption of adsorbed hydrogen [14b]:

$$H^+ + e^- \rightleftarrows (H_{ads}) \text{(rapid)} \quad [13]$$

$$(H_{ads}) + (H_{ads}) \rightleftarrows H_2 \text{ (rate determining, low overpotential)} \quad [14a]$$

$$(H_{ads}) + H^+ + e^- \rightleftarrows H_2 \text{ (rate determining, high overpotential)} \quad [14b]$$

Chemical desorption of adsorbed hydrogen [14a] is a potential independent reaction and consequentially, the surface coverage of hydrogen may build up to a high equivalent thermodynamic fugacity (i.e., equivalent pressure or chemical activity). This has the important consequence that the atomic hydrogen has sufficient residence time on the metal surface to enter the metal lattice (and cause embrittlement, hydrogen induced cracking, and other related phenomena) before combining to give molecular hydrogen that leaves the surface.

3.01.2.4.2 Oxygen reduction reaction

The oxygen reduction reaction on iron is important in all aerated conditions and particularly so in near-neutral to alkaline solutions where, in the majority of technologically important corrosion problems, oxygen is the dominant cathodic reactant. Unlike reduction of hydrogen ions, which is a 2-electron process that occurs via two successive single electron transfer reactions, the mechanism for the reduction of dissolved oxygen is intrinsically more complex due to the overall required transfer of four electrons. The initial step for the reduction of oxygen is generally believed to involve one or both of a superoxide or a peroxide intermediate species. However, hydrogen peroxide once formed is easily reduced in a 2-electron process that cleaves the central O–O bond.

The overall reaction for oxygen reduction differs according to whether the iron is passive (i.e., the reduction process occurs on an oxide or hydroxide surface) or whether the surface of iron is oxide-free (i.e., bare iron). An extensive investigation of the oxygen reduction reaction on iron in neutral solution was carried out by Jovancicevic.[44] For passive iron, the reaction scheme that best fits the observations involves rate determining adsorption of oxygen followed by stepwise reduction of the adsorbed intermediate initially to an adsorbed superoxide species (O_2H) then to peroxide ion (O_2H^-). This reacts immediately in water to form hydrogen peroxide, which may be detected in solution using a rotating ring disc electrode, and which is relatively easily reduced to hydroxide:

$$O_2 \rightleftarrows (O_{2ads}) \text{(rate determining)} \quad [15]$$

$$(O_{2ads}) + H_2O + e^- \rightleftarrows (O_2H)_{ads} + OH^- \quad [16]$$

$$(O_2H)_{ads} + e^- \rightleftarrows O_2H^- \quad [17]$$

$$O_2H^- + H_2O \rightleftarrows H_2O_2 + OH^- \quad [18]$$

$$H_2O_2 + 2e^- \rightleftarrows 2OH^- \quad [19]$$

The overall reaction being the familiar:

$$O_2 + 2H_2O + 4e^- \rightleftarrows 4OH^- \quad [20]$$

On bare iron, the situation differs in that no hydrogen peroxide species are detectable in solution; also, the kinetics of reduction are slower. In this case, therefore, the partly reduced intermediaries are expected to exist as adsorbed species on the metal surface. The rate-determining step is, in this case, consistent with adsorption and reduction of oxygen to an adsorbed superoxide species (O_2^-):

$$O_2 + e^- \rightleftarrows (O_{2\,ads}^-)\,(\text{rate determining}) \quad [21]$$

After this, the sequence is unclear but one that is consistent involves stepwise reduction, via an adsorbed peroxide intermediate, to hydroxide:

$$(O_{2\,ads}^-) + H_2O \rightleftarrows (O_2H)_{ads} + OH^- \quad [22]$$

$$(O_2H)_{ads} + H_2O + e^- \rightleftarrows 2OH_{ads} + OH^- \quad [23]$$

$$2OH_{ads} + 2e^- \rightleftarrows 2OH^- \quad [24]$$

3.01.2.5 Corrosion in Aqueous Environments

3.01.2.5.1 Anode and cathode separation

During corrosion, the local electrochemical potential at an anode is different from that at a cathode. Also, the local electrochemical reactions at anodes and cathodes result in significant chemical changes in their vicinity that encourage and maintain their spatial separation. Furthermore, the potential difference in solution gives rise to a voltage gradient, which attracts oppositely charged ions (or repels similarly charged ions), a process known as electro-migration. Additionally, there is the requirement for electro-neutrality in the electrolyte (by which is meant that an anion cannot exist in solution without a corresponding cation). The overall process for corrosion of iron with oxygen as the cathodic reaction is shown schematically in Figure 9, with migration and diffusion of ions carrying the flow of current.

3.01.2.5.2 Mass transport

For many, if not the majority, of the technical applications of carbon steel, the aqueous corrosion rate is controlled by the diffusion of reacting oxygen to the metal surface and/or the diffusion of dissolved species away from the surface. Under these conditions, mass transport in the solution becomes critical. In general, mass transport occurs by three fundamental processes:

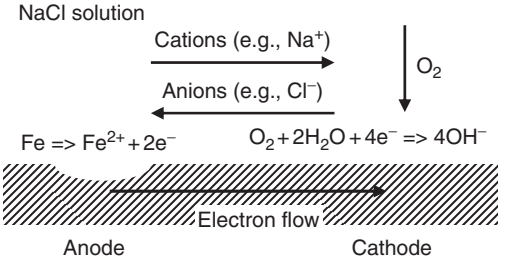

Figure 9 Schematic diagram showing spatial separation of anode from cathode with corresponding migration of ions in solution.

- Diffusion (i.e., movement under a concentration gradient)
- Migration (i.e., movement under an electric field gradient)
- Convection (i.e., natural or forced solution flow)

The total flux of reactant to a surface or interface (i.e., the total mass transport) is obtained simply by addition of the components of diffusion and migration to that of convection:

$$\text{Flux} = \text{Diffusional} + \text{Migrational} + \text{Convective}$$

In all flow conditions, a region of fluid exists adjacent to the surface of the electrode in which no convection occurs and only diffusion and migration occur; this is called the boundary layer, and may be equated with the diffusion distance in Fick's Law. Generally, as the convection rate increases, the boundary layer is compressed and reduced in extent and, hence, the overall rate of mass transport increases.

3.01.2.5.3 Effect of flow rate on corrosion

For corroding systems, under mass transport control, the flux of species to a surface where the rate-controlling reaction is occurring is described in the steady-state by Fick's first Law. This flux may be also measured electrochemically by the limiting current for that reaction (e.g., oxygen reduction). In this way, a mass transfer coefficient, k, may be defined by:

$$k = \frac{i_{lim}}{nFC_b} \quad [25]$$

where: i_{lim} is the limiting current density for a cathodic reaction, C_b is the bulk concentration of cathodic reactant, F is Faraday's constant and n is the number of electrons transferred in the reaction. For a corrosion process whose rate is controlled by mass transfer of cathodic reactant, for example carbon steel in neutral, oxygen-containing solutions,

knowledge of the mass transfer coefficient, k, enables prediction of corrosion rate.

Measurement of the diffusion flux may be carried out using standard electrochemical techniques as a function of fluid flow rate, either via rotating electrode systems, or via electrodes placed in flow channels. For laminar flow, the analytical solution predicts that the limiting current (i_{lim}) at a rotating electrode is proportional to the concentration of reacting species in solution and the square root of the rotation speed, the Levich equation[45]:

$$i_{lim} = A\ C\omega^{0.5}$$

where: ω is the angular rotation rate of the electrode (radians s^{-1}), C is the concentration of reacting species, and A is a constant that depends on the fluid properties and diffusion rate of the reacting species. Thus, if a plot of i_{lim} v. $\omega^{0.5}$ is a straight line, then the reaction is mass-transport controlled and the diffusion coefficient for the reacting species can be obtained from the slope of the straight line. This general kind of relationship holds for fluid flow in more complex geometries, including turbulent flow, where analytical solutions are not possible. Hence, experimental analogies for particular situations must be developed, commonly in terms of dimensionless parameters such as the Sherwood number (related to mass transport), the Reynold number (related to the fluid flow rate), and the Schmidt number (related to the fluid properties). For more detailed information on corrosion in flowing systems, the reader is referred to the relevant chapter of this book.

3.01.3 Corrosion Processes

Some of the technically more important corrosion processes for steel are summarized in this section. Note, however, that this is not intended as a comprehensive treatment and more detailed descriptions of these processes (both in general and in specific situations) will be found in the relevant chapters elsewhere in this book.

3.01.3.1 Corrosion Products

For general information, common compounds associated with the corrosion of steel are listed in Table 4.[46]

Table 4 Corrosion products formed on carbon steel in various environments

Compound	*Comments*
Oxides:	
FeO (wüstite)	Formed during high temperature oxidation, present in millscale with Fe_2O_3 and Fe_3O_4
α-Fe_2O_3 (hematite)	Iron ore mineral, also formed at elevated temperatures
Fe_3O_4 (magnetite)	Corrosion product formed in reducing aqueous conditions
γ-Fe_2O_3 (maghemite)	Oxidized form of magnetite and with the same crystal structure
Oxy-hydroxides:	
α-FeO(OH) (goethite)	Stable mineral, commonly found in nature
γ-FeO(OH) (lepidocrocite)	Metastable phase, formed during atmospheric corrosion
β-FeO(OH,Cl) (akaganéite)	Formed during corrosion in seawater – characteristic orange color
$Fe_5O_3(OH)_9$ (ferrihydrite)	Common iron mineral: metastable to hematite and goethite
Hydroxides:	
$Fe(OH)_2$ (ferrous hydroxide)	Intermediate corrosion product formed under reducing conditions
$Fe(OH)_3$ (ferric hydroxide)	Hydrated iron oxy-hydroxide, more properly written as: $FeO(OH).H_2O$
Sulfides:	
FeS_{1-x} (mackinawite)	Anion deficient FeS (troilite) formed during microbially influenced corrosion
$Fe_{1-x}S$ (pyrrhotite)	Iron sulfide mineral, cation deficient form of FeS (troilite)
FeS_2 (pyrite)	Iron sulfide mineral, known as 'fool's gold'
Carbonates:	
$FeCO_3$ (siderite)	Corrosion product that forms as a protective film in some forms of 'sweet' corrosion at high CO_2 partial pressures; occasionally also found as part of the corrosion product layer on archaeological iron objects after long-term burial
Phosphates:	
$3FeO{\cdot}P_2O_5{\cdot}8H_2O$ (vivianite)	Occasionally found within the corrosion product layer on archaeological iron objects after long-term burial in strongly anaerobic, typically water-logged, environments
Green rusts:	
$[Fe^{2+}_3\ Fe^{3+}\ (OH)_8]^+\ [Cl{\cdot}H_2O]^-$	Series of corrosion products that comprise mixed ferrous/ferric species together with incorporated anions, in particular: carbonates, sulfates and chlorides

3.01.3.2 Aqueous Corrosion

3.01.3.2.1 General corrosion

In the absence of inhibiting species, carbon and low alloy steel are not passive in most aqueous environments at pH less than ~9. Thus, for the majority of natural environments likely to be encountered in service, steel will undergo general corrosion. It is important to note that the term 'general corrosion' does not imply uniform thickness loss across a corroding surface rather it defines an active corrosion process that occurs in the absence of a passive film.

In practice, the general corrosion of uncoated steel in high conductivity media such as seawater will generally lead to an overall macroscopic roughening of the surface. This is exacerbated by the presence of surface-breaking second phase particles, the most important of which are sulfide inclusions that are always present in steels. For example, partial dissolution of sulfide inclusions results in aqueous sulfide species and the possible formation of adjacent iron sulfide films resulting in a surface electrochemical heterogeneity.[47–49] Hence, heterogeneity in the corrosion rate is developed across the material surface eventually resulting in variations in the thickness loss over the surface.

In low conductivity environments such as natural waters, the resistivity of the electrolyte is sufficiently large that the spatial separation of anodes and cathodes is greatly reduced. This tends to result in the localization of corrosion to specific regions of the surface with associated local precipitation of corrosion product giving the appearance of small protuberances. Such corrosion is often called tuberculation corrosion and can result in local attack underneath the precipitated corrosion product,[50] **Figure 10**. Although giving the appearance of pitting, the mechanism is in essence an extremely localized form of general corrosion combined with differential aeration corrosion. In the fullness of time, such regions will tend to merge together giving a macroscopically roughened surface.

Figure 10 Tuberculation corrosion of steel; corrosion is localized beneath rust protuberances (known as tubercules).

3.01.3.2.2 Concentration cell corrosion: Differential aeration

Where differences in concentration of an electrochemically active species are present in an environment then corrosion is likely to result. For example, for a buried structure, the local oxygen concentration will vary according to whether the soil is well-aerated or not, with the degree of aeration also varying as a function of soil depth. Thus, cathodes are likely to be localized at regions of relatively higher oxygen availability with anodes localized in regions of lower oxygen content. This is effectively a corrosion cell that is driven by a spatial variation in oxygen concentration in the environment (and is thus known as a concentration cell). Localization of the corrosion reactions can be readily demonstrated in a droplet of salt water on steel by the use of indicators that show the high pH generated at a cathode (e.g., by use of phenolphthalein, which turns pink) and the ferrous ions generated at an anode (e.g., by use of ferricyanide, which turns blue), **Figure 11**.

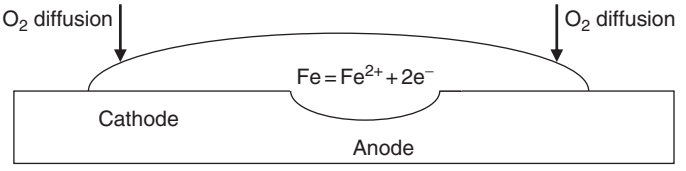

Figure 11 Corrosion in a salt water droplet showing the cathodic reaction localized at the droplet periphery (due to oxygen availability) and the anodic reaction localized in the droplet centre (due to oxygen depletion).

Differential aeration is an important factor in many corrosion processes where local oxygen depletion is present. For example, corrosion that is localized underneath deposits, and between mating surfaces, etc., is almost always caused by a differential aeration mechanism. In general, those localities that have a plentiful supply of oxygen will become cathodes with anodes occurring in regions of oxygen depletion.

3.01.3.2.3 Pitting and crevice corrosion

At alkaline pH and in the region where passivity of carbon steel is possible, then classical pitting and crevice corrosion mechanisms, that is, those involving local breakdown of a passive film, are possible. Localized corrosion may also result where the surface has been passivated by other means, such as oxidizing inhibitors (e.g., nitrite, etc.) or in sulfide environments.

For the pitting of pure iron in neutral electrolytes with a passive oxide film, pit initiation was found to be associated with a stage in the development of the film corresponding to a particular film thickness. This was found to be potential independent but dependent on the halide ion type (i.e., Cl^- or Br^-) and concentration as well as the anodic charge passed prior to pitting.[51,52] No incorporation of halide into the passive film was observed, which is in stark contrast to stainless steel, where halide ions do incorporate into the chromium passive film.[53] This is an evidence of the structural stability of the passive film on iron (which once formed is relatively stable) compared with the passive film on Fe–Cr alloys (which changes with time in accommodation to the environment). Note, of course, that passive iron oxide is unstable to reductive dissolution, which is not the case with stainless steel and is one of the reasons for the improved passivity of stainless alloys. Overall, iron (at a given pH in a given supporting electrolyte) appears to be susceptible to halide-induced pitting, if and only if, the passive oxide has reached a certain critical stage of growth.

Pitting can be generally prevented if there are sufficient alternative anion species present (e.g., nitrate, sulfate, and hydroxide). Thus, pitting generally is only feasible if the ratio of chloride to other anions exceeds certain critical values, which are environment, pH, and temperature dependent; for example, the chloride-to-hydroxide ratio for pitting corrosion of steel reinforcement in concrete.[54,55] Also, for a propagating pit, the chemistry must be consistent with the active regime of corrosion as indicated in the Pourbaix diagram. Given that the cathode area is large while that of the anode is small, the anodic current density (and hence the local rate of dissolution) in a pit must necessarily be high.

Pitting of steel also occurs in the presence of passive sulfide films such as mackinawite (FeS_{1-x}). Sulfide films are inherently unstable to oxidation with consequent disruption that results in the generation of defects and flaws in the film.[56] Since the film is an excellent cathode, anodes localize at the defects where the substrate is exposed thus resulting in severe local pitting.

Pitting and crevice corrosion are therefore associated with local development of chemical heterogeneity on the surface at the pit site. Furthermore, their occluded geometry, once formed, tends to maintain the solution at a significantly different local chemistry than the environment. This form of localized corrosion is much more likely to occur in stagnant conditions where the development of diffusion-driven solution heterogeneity over the metal surface is encouraged. Conversely, under flowing conditions, local diffusion-driven chemical changes cannot be maintained so effectively and pitting is less likely. Pumps and valves that operate intermittently with long periods of nonoperation are particularly prone to internal pitting and crevice corrosion.

3.01.3.2.4 Galvanic corrosion

Although the electrochemical series forms an outline guide for the tendency or not for galvanic corrosion, it is important to note that the position of alloys in the series is altered in specific environments and a galvanic series developed for the environment should therefore be consulted. Galvanic series for metals and alloys in seawater and potable waters are well-known and easily available.[57]

There are two necessary requirements for galvanic corrosion to occur: firstly, electrical connection to another electronically conducting material of a different electrochemical potential (commonly a metal, although conducting films such as magnetite and mackinawite as well as graphite can also act as electrodes) and secondly connection through the electrolyte solution (in order to permit ionic current to flow). Galvanic corrosion can also occur in a macroscopic sense between components differing materials, but may also occur microscopically at preexisting metallurgical features in the steel or, more commonly, where metal ions of a more noble element are present in solution and plate out locally on the steel surface. Thus, where copper ions plate out onto steel, for example from corrosion of a brass component elsewhere in the system, then local galvanic corrosion will initiate at such locations.

3.01.3.2.5 Flow-assisted corrosion (FAC)

The phenomenon of flow-assisted (or flow-accelerated) corrosion (FAC) is of fundamental importance and occurs particularly in high performance boilers and heat exchangers such as are used in power generating facilities (both conventional and nuclear), but also elsewhere.[58] The general mechanism of FAC is not limited to steel and involves the removal of a protective corrosion product, generally by dissolution, in a flowing environment. The process has long been known to occur in high flow rate systems, for example in copper alloy condenser tubing where the relatively soft and poorly adherent protective surface films are stripped from the surface by the shear stress across the boundary layer between the pipe wall and the moving turbulent fluid.

For carbon steel, the latter mechanism does not operate as the protective magnetite layer adheres strongly to the substrate. However, in common with all minerals, iron oxides are sparingly soluble in water and FAC involves the local or general thinning of the protective oxide film that forms on carbon steel in high temperature water. However, oxides where iron is entirely in the ferric (+3) oxidation state are considerably less soluble than magnetite as can be seen from Table 5.

In traditional boiler water treatment, the dissolved oxygen concentration is kept as low as possible (a few parts per billion, ppb) where magnetite is the stable oxide phase. It is thus susceptible to enhanced dissolution under high flow rate conditions. This leads both to unwanted deposition of oxide elsewhere in the system but, more importantly, enhanced corrosion of steel and often unexpected failures with typical scalloped surfaces.[59] However, if the oxygen concentration is controlled at a slightly higher level hematite becomes the stable phase. This is advantageous as it is considerably less soluble than magnetite and, hence, much more resistant to flow-accelerated corrosion (FAC).

Table 5 Solubility products for various iron oxides

Reaction	*Solubility product at 25 °C*	*Solubility product at 300 °C*
$Fe(OH)_2 \leftrightarrows Fe^{2+} + 2OH^-$	$10^{-15.04}$	$10^{-17.54}$
$Fe_3O_4 + H_2O \leftrightarrows Fe^{2+} + 2FeO(OH)$	$10^{-20.25}$	$10^{-21.40}$
$Fe_3O_4 + 4H_2O \leftrightarrows Fe^{2+} + 2Fe^{3+} + 8OH^-$	$10^{-33.68}$	$10^{-33.59}$
$Fe(OH)_3 \leftrightarrows Fe^{3+} + 3OH^-$	$10^{-37.94}$	$10^{-36.87}$
$FeO(OH) + H_2O \leftrightarrows Fe^{3+} + 3OH^-$	$10^{-41.58}$	$10^{-39.62}$
$Fe_2O_3 + 3H_2O \leftrightarrows 2Fe^{3+} + 6OH^-$	$10^{-40.40}$	$10^{-39.68}$

Source: Buecker, B. *Power Eng.* **2007**, *111(7)*, 20–24.

3.01.3.2.6 Erosion–corrosion

In the presence of two-phase flow in solution (i.e., solid particles, slurries, entrained gas, etc.) enhanced corrosion will generally occur due to a number of mechanisms including: increased mass transport of reacting species and impact of the 2nd phase onto the surface, see for example.[60] The latter process is the most important in causing erosion–corrosion as its effect on the protective surface film is critical. Thus, protective films may be thinned by abrasion or removed altogether causing rapid corrosion of the underlying material. This process is particularly prevalent where sharp changes in flow direction (e.g., pipe bends, etc.) or flow velocity (e.g., valves and chokes, etc.) occur. Careful design of plant components can minimize this form of attack.

3.01.3.3 Environmentally Assisted Cracking

3.01.3.3.1 Environments

Carbon steel is susceptible to stress corrosion cracking in a range of environments, often where it shows passivity or marginal passivity. These include anhydrous liquid ammonia, nitrate/nitrite, strong alkali and in carbonate/bicarbonate systems. Stresses in the steel can either arise from externally applied forces or be the result of processing, deformation, welding, etc. giving rise to a residual stress that is present at all times.

Historically the most important of these processes was caustic cracking prevalent in low-to-medium pressure riveted steel boilers. In such systems boiler waters that were traditionally dosed with carbonate or bicarbonate for pH control lost CO_2 to the steam resulting in a gradual increase in pH. Although in well-controlled systems, the bulk pH would be maintained within correct limits, local concentration in crevices or under deposits could give rise to a strongly alkaline region that initiated intergranular stress corrosion.[61] The phenomenon is not restricted to boilers but can occur in any system that handles strong alkali, for example during purification of bauxite via the Bayer process[62] or in Kraft process paper digesters.[63] The morphology of caustic cracking is intergranular with a lower limit for cracking of carbon steel in the range 1–5% NaOH (additions of nickel improve resistance). Cracking is observed to be potential dependent[64] occurring only in the passive region

and predominating in the region of the active-to-passive transition (i.e., from −800 to −600 mV vs. the Standard Hydrogen Electrode in 10% NaOH). Steels with lower carbon content appear to be more susceptible.[65] The failure mechanism is not thought to be associated with hydrogen embrittlement but is consistent with a slip dissolution model.[66]

Stress corrosion cracking of carbon and low alloy steels also occurs on buried structures under cathodic protection due to generation of alkalinity at coating defects by cathodic reduction. In aerated soil, carbon dioxide migrates to the cathodes in order to buffer the alkalinity thus producing the critical carbonate/bicarbonate environment. Failure surfaces are characterized by multiply branched intergranular cracks that tended to align along the principle stress axis of the pipe; fracture surfaces are often observed to be covered with magnetite.[67]

Transgranular stress corrosion cracking in anhydrous liquid ammonia is a separate phenomenon that unfortunately, because it was not understood, led to some catastrophic failures and loss of life.[68] The predominant risk factor for cracking in anhydrous ammonia is the presence of dissolved oxygen at >5 ppm (or >1 ppm in the presence of CO_2). Cracking can be inhibited effectively provided that the ammonia contains more than 0.1% of water to encourage passivity of the steel.[69]

3.01.3.3.2 *Hydrogen embrittlement*

Ferrite, like most body centered structures, has a high diffusivity and solubility for interstitial hydrogen in its lattice. Thus, carbon and low alloy steel are highly susceptible to hydrogen embrittlement and hydrogen-induced cracking. The former is caused by reduction in macroscopic ductility due to the presence of lattice hydrogen resulting in transgranular cleavage fracture, while the latter is due to the formation of hydrogen gas bubbles at extremely high pressure within the steel microstructure. There are numerous mechanistic models in the literature for the causes of hydrogen embrittlement and it is not clear whether a single mechanism prevails or whether several mechanisms coexist. A more detailed discussion of hydrogen embrittlement mechanisms and effects can be found elsewhere in the relevant chapter of this book.

3.01.3.4 Microbiologically Influenced Corrosion

In nonsterile systems (i.e., generally at temperatures below ~60–70 °C) the growth and multiplication of a wide range of microbial species is possible. For a microorganism to initially establish itself and then to grow and flourish, the environmental conditions must be favorable including a supply of a carbon food source and other trace essential nutrients (e.g., nitrogen, phosphorous, etc.) Many of the microbial species that have influence on the corrosion of carbon steel are anaerobic. Of these, sulfate reducing bacteria are the most frequently encountered. These metabolize oxidized sulfur species in their environment producing sulfide species in solution: that is, H_2S, HS^-, or S^{2-}, depending on pH. These will form sulfide corrosion product films on steel that are nonprotective and unstable, resulting in severe and often local corrosion.[70]

Other problematic families of anaerobic bacteria include: the nitrate-reducers (that metabolize nitrite corrosion inhibitors, reducing their concentration), the organic acid producers (acetic and other acids can be aggressive to carbon steel depending on the environment), and iron oxidizers that metabolize ferrous ions resulting in unwanted deposition of ferric oxides. Anaerobic bacteria can survive (but not metabolize) in aerobic environments and can often tolerate low levels of oxygen. Thus, they may colonize benign environments in locations of low oxygen concentration (i.e., under deposits of corrosion product, dirt, etc., and under bio-films of oxygen-tolerant species), even though the overall environment may be relatively well-oxygenated.

3.01.3.5 Aqueous Corrosion Protection

Although unprotected (bare) carbon and low alloys steel may be exposed without corrosion protection provided suitable allowances are made for corrosion losses during service, most steel is protected in some way. Methods available include: metallic coatings (e.g., galvanizing, electroplating, etc.), inorganic coatings (e.g., phosphate conversion coatings, etc.), organic coatings (i.e., paint coatings and linings) and cathodic protection. These topics are dealt with in detail elsewhere in this book and will not be considered further here.

3.01.3.6 High Temperature Oxidation

Plain carbon steels cannot be used at temperatures close to the lower critical temperature for austenite formation, as the microstructure becomes unstable, with spheroidization of pearlite and graphitization of iron carbide. Also, significant grain growth and creep occurs. In practice, plain carbon steel has an effective

temperature limit of ~400–420 °C. For higher temperature service, low-alloy steels hardened by stable alloy carbides should be used.

Iron readily oxidizes at elevated temperatures in air (and other oxidizing environments) resulting in a relatively adherent layered scale. Above 570 °C the ferrous oxide phase wüstite is stable and the oxide scale has three layers: a relatively thick inner layer of wüstite, a relatively thin intermediate layer of magnetite and a thin outer layer of hematite. The oxidation kinetics are controlled by diffusion of species through the scale thickness and are thus parabolic in nature. Wüstite has a large number of cation defects and is more properly written as $Fe_{1-x}O$. The oxide growth mechanism in wüstite is controlled by cation transport outwards,[71] resulting in relatively rapid oxidation rates. In view of this, the service temperature for carbon and low alloy steel should be below the formation temperature of wüstite.

Below ~570 °C, where wüstite is thermodynamically unstable, the oxide scale on iron contains an outer region of Fe_2O_3 (hematite) with an inner region of Fe_3O_4 (magnetite) adjacent to the metal. Since the transport processes (diffusion) through these phases is much less rapid, the oxidation rates are also less.[72] At these lower temperatures, the oxidation kinetics are not purely parabolic and are dependent on the surface preparation and degree of cold work present in the material; larger amounts of cold work resulting in more rapid oxidation. Plain carbon steel oxidizes somewhat (10–20%) more slowly than pure iron, which is almost certainly due to the presence of other alloying elements (e.g., silicon, manganese, and aluminum).[72] Below 570 °C, increased carbon content generally results in an increased oxidation rate because the scale formed over carbide particles and especially pearlite colonies is finer with a higher iron diffusion rate.

The high temperature oxidation and corrosion of iron and steel is discussed in greater depth elsewhere in this book, to which the interested reader is referred.

3.01.4 Atmospheric Corrosion

3.01.4.1 Environmental Influences

3.01.4.1.1 Humidity

Relative humidity (RH) is defined as the ratio of partial pressure of water vapor to the saturated water vapor pressure at the same temperature. Thus, the RH is a thermodynamic quantity that is equivalent to the fugacity of water vapor in the gas phase. Consequently, an RH of 100% defines a gas phase fugacity of 1, which is by definition in equilibrium with liquid phase water also at an activity of 1. In theory, therefore, atmospheric corrosion cannot occur at RH below 100% because no liquid water is present. However, in practice, water absorption readily occurs on bare metal surfaces at RH below 100% because, apart from gold, all metals are generally covered at standard conditions by hydrophilic thin oxide or hydroxide (passive) films.

Water adsorption on electropolished, uncontaminated surfaces as a function of RH from 0% to 80% was studied in the context of metrology in the precision weighing of stainless steel, silicon and platinum–iridium mass standards.[73,74] On these materials, water adsorption can be described well by a Brunauer–Emmett–Teller (BET) isotherm appropriate to multilayer adsorption on hydrophilic surfaces. On 20% Cr, 25%Ni stabilized stainless steel the water layer thickness was found to vary approximately linearly from 0% RH to 80% RH where it reached ~0.6 nm, corresponding to about three monolayers of water.

Generally, the corrosion of metals in the atmospheric environment is possible if and only if there is sufficient water present on the metal surface to solvate the ions produced during corrosion reactions. This was first demonstrated by Vernon[75] in a series of classical experiments, some of which are summarized graphically in **Figure 12**. He showed that rusting occurs at a low rate in pure air of less than 100% RH but that in the presence of minute concentrations of impurities, such as sulfur dioxide, serious rusting can occur without visible precipitation of moisture once the RH of the air rises above a critical and comparatively low value. This value depends to some extent upon the nature of the atmospheric pollution, but, when sulfur dioxide is present, it is in the region of 70–80%. Below the critical humidity, rusting is inappreciable, even in polluted air.

The results of Vernon have been confirmed many times. For example, more recent work has studied the integrity of carbon steel materials as a function of humidity in air at 65 °C.[76] On clean, uncontaminated steel, the corrosion at and below 75% RH was negligible and consistent with a dry oxidation mechanism. However, at 85% and above, the corrosion rate rapidly increased, consistent with a critical RH for the onset of aqueous atmospheric corrosion of ~80%.

The critical humidity for the onset of atmospheric corrosion varies considerably as a function of surface condition. Two factors are paramount in controlling this. Firstly, physical adsorption on porous surfaces

will occur below the expected bulk equilibrium value (i.e., the saturated vapor pressure) due to capillary condensation. This is of obvious relevance in the development of corrosion product (rust) layers, which will retain water in their pores well below the RH of condensation. Secondly, and importantly, liquid condensation will tend to occur at reduced RH where surface chemical contamination exists. This is because the activity of water at the saturated concentration of the solute, is lowered significantly, Table 6.

Thus, in the absence of other factors, a surface that is contaminated with sodium chloride will condense an aqueous phase at RH >75% while for seawater (containing magnesium and calcium cations) condensation of an aqueous phase might be expected at all RH >33%. In the presence of porous corrosion products, capillary condensation will lower these values further.

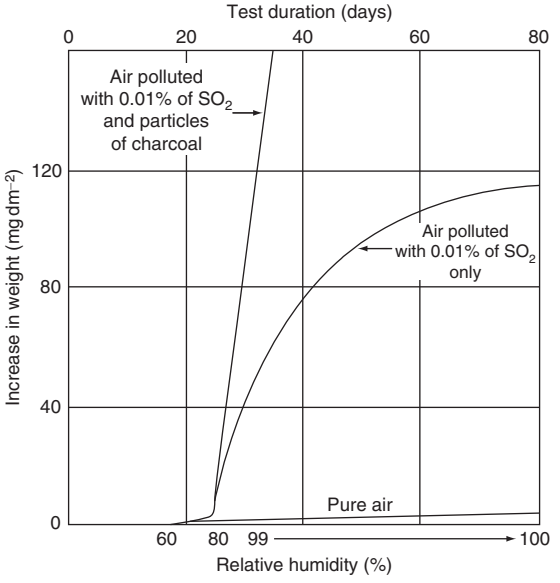

Figure 12 Effect of relative humidity and atmospheric pollution on the rusting of iron, after Vernon. Reproduced from Vernon, W. H. J. *Trans. Faraday Soc.* **1935**, *31*(1), 668.

Table 6 Equilibrium RH for saturated solutions of various solute species

Solute species	*Equilibrium RH in saturated solution*
$(NH_4)_2SO_4$	81.3% (20 °C); 79.0% (50 °C)
NaCl	75.5% (20 °C); 74.4% (50 °C)
$MgCl_2$	33.1% (20 °C); 30.5% (50 °C)
LiCl	11.3% (20 °C); 11.1% (50 °C)

Source: Greenspan, L. *J. Res. Natl. Bur. Stand.* **1977**, *81A*(1), 89–96.

3.01.4.1.2 Air-borne pollutants

Historically, the combustion-derived air-borne sulfur dioxide and nitrogen oxides have been the most important pollutant species in the atmosphere. Other air-borne pollutants including hydrochloric acid vapor, ammonia, dust, soot and salt aerosol particles are also of importance. However, given extensive pollution controls that are now placed on industry and transportation, combustion-derived species have been greatly reduced. For example, current European Union legislation[77] sets down limits for SO_2, NO_x and particulates of less than 10 μm for implementation no later than 2010, Table 7. Annual global sulfur dioxide emissions are estimated to have peaked at the end of the 1970s (75 MTonnes) and have since dropped ~20%.[78] In Europe, emissions have dropped much further and by 2010 are expected to be less than half their peak value. The impact on ground level pollutant concentrations is clearly considerable with a consequent reduction in atmospheric corrosion rates.

The significance of the amount of sulfur dioxide available for reaction at the metal surface (its presentation rate), rather than the concentration in the atmosphere, has been demonstrated by studying the effects of atmospheric flow rate. Thus, an increase in steel corrosion with increase in atmospheric flow rate at a constant volume concentration of sulfur dioxide has been observed by Vannerberg[79] and Walton *et al.*[80] Notwithstanding these findings, the effect of sulfur dioxide on the corrosion of steel is clearly seen in Figure 13, which plots historic data from the Sheffield area of the UK. This illustrates a clear relationship between sulfur dioxide in the atmosphere and the corrosion of steel exposed to it; the atmospheric SO_2 concentration accounting for ~50% of the observed variation in corrosion rate.[81]

The corrosion of steel in the presence of SO_2 has been studied as a function of RH by a number of

Table 7 EU air-borne pollution limits for 2010

Species	*Averaging period*	*Limit value*
SO_2	1 h	350 μg m^{-3}
	24 h	125 μg m^{-3}
	365 days	20 μg m^{-3}
NO_x	1 h	200 μg m^{-3}
	24 h	40 μg m^{-3}
	365 days	30 μg m^{-3}
Particulates	24 h	50 μg m^{-3}
< 10μm	365 days	20 μg m^{-3}

European Council Directive 1999/30/EC of 22 April 1999: Limit values for sulphur dioxide, nitrogen dioxide and oxides of nitrogen, particulate matter and lead in ambient air.

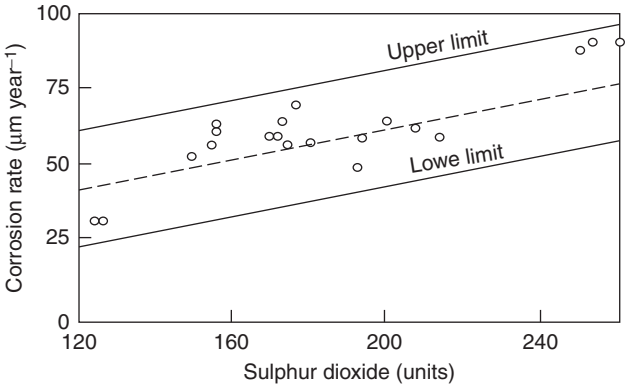

Figure 13 Relationship between sulfur dioxide (mg of SO_2 per m^3) and corrosion, after. Reproduced from Chandler, K. A.; Kilcullen, M. B. *Br. Corr. J.***1968**, *3*.

workers, the first being Vernon whose data are reproduced in **Figure 12**. Sydberger and Vannerberg later repeated this work extending it to include corroded surfaces.[82] Using isotopic labeling, they confirmed that on uncontaminated, polished iron, in 0.1 ppm SO_2 little or no SO_2 was absorbed at RH below 80% and no corrosion was observed. On precorroded iron at RH greater than 80% and in 0.10 ppm SO_2, sulfur was absorbed quantitatively.

This explains the historic observation that rust films formed in industrial atmospheres contain considerable amounts (5% or more) of ferrous sulphate.[83,84] However, the formation of iron sulfate only accounts for a small percentage of the overall metal loss and this does not explain fully the effect of SO_2 on iron corrosion.[85,86] For example, there is evidence that steel that has been allowed to corrode in an atmosphere containing sulfur dioxide, continues to corrode at a similar rate, at least for a time, after transferring it to a clean atmosphere.[87]

Historically, a cyclic variation in the amount of sulfate found in rust formed on steel exposed at different times of the year **Figure 14**, has been observed. The quantity present depends on the month of the year rather than on the period of exposure, at least for periods of up to 2 years.[88] Consequently, the month of initial exposure will have an important influence on the corrosion rate. For example, in one test, specimens exposed for 2 months from September corroded at 35 μm $year^{-1}$ compared with 136 μm $year^{-1}$ for specimens exposed from May. This effect was of importance in planning for atmospheric exposure tests for steel since different annual corrosion rates would be obtained depending on whether the initial exposure was carried out in the summer or the winter months. The observed variation was historically

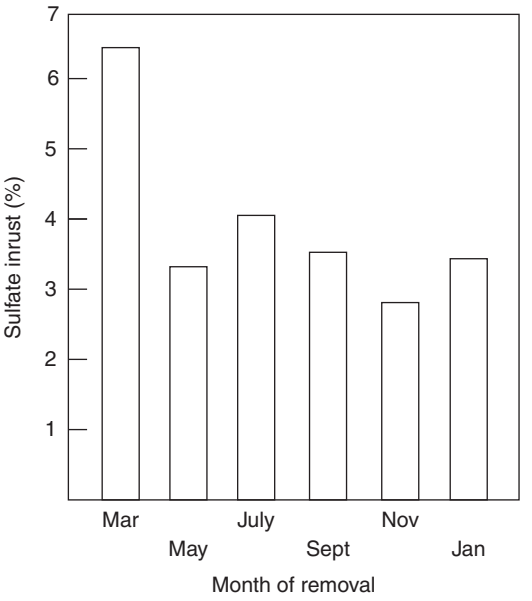

Figure 14 Sulfate in adherent rust on steel exposed at Battersea in January after. Reproduced from Chandler, K. A.; Stanners, J. F. *Proceedings of 2nd International Congress of Metallic Corrosion*; NACE: Houston, 1963; 325.

related to the quantity of ground-level atmospheric SO_2 present at different times of the year, which varied according to the burning of domestic coal for space and water heating. However, this source of SO_2 is no longer present and it might be assumed that the observed difference is now considerably less.

Historically, sulfur dioxide was the most important gaseous pollutant present in the atmosphere. However, given the considerable reduction in ground level SO_2 concentration over the last 30 years other species, particularly oxides of nitrogen (NO_x), have increased in importance.[89] Nitrogen oxides are

produced during combustion as a consequence of direct reaction between nitrogen and oxygen in the air at high temperature. Increased thermal efficiency of plant, where the combustion temperature is raised, inevitably increases the production of NO_x. Thus, at elevated temperatures the following reactions occur:

$$O_2 + N_2 \rightleftarrows 2NO \quad [25]$$

$$2NO + O_2 \rightleftarrows 2NO_2 \quad [26]$$

The ratio of NO to NO_2 is controlled by the reaction temperature and by the cooling time; faster cooling rates favoring NO_2 over NO.

Several attempts have been made to study the influence of nitrogen oxides alone and in combination with sulfur dioxide, on the corrosion of steel, however no clear answer exists. In multiregression studies under atmospheric exposure in Japan no significant correlation with measured NO_x levels was found.[90] Likewise Haynie, in laboratory tests, found no correlation with NO_x levels and the corrosion or weathering steel.[91] Later work by Johansson clarified this situation. He found that, on its own, the increase in the atmospheric corrosion rate of steel, which was not large, was independent of RH.[92] However, a strong synergism was found with small levels of NO_x in combination with SO_2, which were much more corrosive than either pollutant on its own. This behavior is believed to be caused by the considerably more rapid solution-phase oxidation of sulfite to sulfate species in the presence of NO_x as oxidizer.[93]

One of the confusing aspects to the effect of NO_x pollutant is that it is a mixture of NO and NO_2. In order to separate the effects of these species on steel, Oesch carried out a series of laboratory experiments[94] in controlled pollutant gas mixtures. He found that NO had almost no effect on corrosion irrespective of RH, which is no doubt due to its low solubility in water. Conversely, NO_2 caused a significant increase in corrosion rate although its effect was much lower than for SO_2 (the corrosion rate in 10 ppm NO_2 was about one-half that in 0.5 ppm SO_2).

Hydrochloric acid gas is produced during the combustion of coals containing chloride species. Given its high solubility in water it might be expected also to influence corrosion although in rainwater its presence will only be evident from a higher chloride concentration than expected from sea salt and a lower pH. Askey *et al.* studied the effect of hydrochloric acid gas on corrosion of steel at varying atmospheric presentation rates.[95] They found that the influence on corrosion of steel was high but reached a plateau where further increases in concentration did not increase the rate of corrosion. This was explained by the formation of iron chloride on the surface that oxidized to iron oxy-hydroxide liberating chloride. Thus, once sufficient chloride is present, further increases should have no additional effect.

Many other pollutant species are present in the atmosphere, including: H_2S, NH_3, etc. Most of these arise from biological processes and are present at low concentration or have limited effects. Ammonia, the only significant basic atmospheric constituent, is produced via biological activity (e.g., primarily farming) and industrially. It has an extremely high solubility in water and consequently has a low residence time in the air. It is, however, a significant component of atmospheric aerosols typically forming ammonium sulfate or chloride.

3.01.4.1.3 Particulates

Solid particles suspended in the atmosphere may also have influence on corrosion. They generally comprise three classes of material: dusts (e.g., from erosion of soil or sand), soots (i.e., derived from incomplete combustion) and aerosols (primarily sea salt and ammonium sulfate). Particles of all types play an important role in atmospheric corrosion as was found by Vernon and shown in **Figure 12**. They act as nuclei for the initial corrosion attack and as some particles are hygroscopic their presence tends to increase the periods of wetness of the steel surface. The most important particulate species in industrial atmospheres was historically ammonium sulfate, although chlorides[96] also have an effect. In marine environments (and as the ground-level SO_2 concentrations decrease, increasingly in most environments) sea-derived chlorides have the most pronounced effect. In the presence of chlorides, rusting can continue at humidities as low as 35%.[97,98] As a rule, the chloride concentration in the air falls off rapidly with distance inland, but steel rusts at almost incredible rates on surf beaches where it is exposed to a continuous spray of sea salts. This is shown by the results of some tests made in Nigeria that are given in **Table 8** and are confirmed in numerous other tests by other workers over many years. Cole and co-workers have developed a holistic model of atmospheric corrosion that considers the generation of salt in the ocean, its long-range transport and final deposition on materials as a function of distance form the sea.[99,100]

The number and composition of particulate matter in the atmosphere has changed markedly in view

of the change in overall pollution levels. Thirty years ago in the UK, the most aggressive species were: salt and salt/sand from marine or deiced locations, emitted ash from iron smelters, plume ash from incinerators and coal-fired boilers, and coal mine soot and dust.[101] However, the first of these sources now dominates the impact on corrosion. Detailed analysis of the nature and form of particulates is possible provided care is taken to separate and secure the water-soluble aerosol component. A recent analysis of air-borne solids in Hong Kong[102] has identified, for that location, three principle sources of ions derived from atmospheric particulates: fine aerosols derived from atmospheric transformations (e.g., the reaction of sulfate with ammonia to produce ammonium sulfate); coarse particles derived from soils and sea salt derived aerosol, **Table 9**.

Particles were found to have a bimodal size distribution with the larger particles in the size range 2–10 μm and the smaller particles in the range 0.1–1 μm. The effect on corrosion was found to depend on the size of the aerosols, which was also related to their composition. Thus, rusts formed from the finer aerosol particles have composition related to sulfates, while those from coarse particles are mainly related to chloride. Sea salt was found to contribute most to the corrosion of mild steel while calcium ions inhibited corrosion. Ammonium, potassium, and magnesium ions had much less of an effect on the corrosion of steel.

The effect on corrosion of combustion derived ashes (fly-ash) from coal and oil, as well as inert glass powder of similar size range as studied by Askey *et al.*[103] They found that the ashes from oil combustion were considerably more corrosive than those derived from coal combustion due to the much higher acidity of the former. In general, the effect of the fly-ash particulates was in approximate proportion to the quantity of ions that were released into solution indicating that a primary mechanism controlling corrosion was the resistance of the surface electrolyte. The presence of inert borosilicate glass particles on the steel surface was found to have a small, but statistically significant affect on the corrosion rate, increasing it by between 50% and 100% compared with the clean, uncontaminated surface. This effect was ascribed to a mechanism involving local differential aeration at the microcrevice formed between the particle and the surface.

Table 8 Effect of sea salts on the rate of corrosion of ingot iron[a]

Distance from surface	*Salt content of air*[b]	*Rate of rusting (mm year^{-1})*
50 yd	11.1	0.950
200 yd	3.1	0.380
400 yd	0.8	0.055
1300 yd	0.2	0.040
25 miles	–	0.048

Supply Tests in Nigeria carried out on behalf of BISRA.
Source: Sixth Report of the Corrosion Committee, Spec. Rep. No. 66, Iron and Steel Institute, London, 1959.
[a]The specimens were of ingot iron and were exposed for 1 year.
[b]The salt content of the air was determined by exposing wet cloths, and is expressed as mg NaCl per day (100 cm^2)$^{-1}$.

Table 9 Principle atmospheric particulate species collected in Hong Kong

Particle group	*Major ionic species*	*Variance of composition accounted*
Fine particles	SO_4^{2-}, NH_4^+, K^+	31%
Nonsea salt coarse particles	NO_3^-, Mg^{2+}, Ca^{2+}	30%
Sea salt	Cl^-, Na^+	22%

Source: Ngai T. Lau; Chak K. Chan; Lap I. Chan; Ming Fang *Corros. Sci.* **2008**, *50*(10), 2927–2933.

3.01.4.2 Mechanism of Atmospheric Corrosion of Iron

3.01.4.2.1 Acid regeneration cycle

Atmospheric corrosion of steel tends to initiate at local sites on the metal surface. The initial distribution of corroding sites is correlated with the presence of active surface-breaking manganese sulfide inclusions. These dissolve to form sulfide species that react locally with iron forming sulfide films that promote local corrosion.[104,105] As noted previously, sulfur dioxide from the air also absorbs onto the surface of clean steel, and into rust layers, and reacts to form a sulfate-containing electrolyte in the rust. During corrosion, ferrous sulfate is formed, which then reacts with atmospheric oxygen to form iron oxy-hydroxide:

$$FeSO_4 + 1.5H_2O + 0.5O_2 \rightarrow FeO(OH) + 2H^+ + SO_4^{2-} \quad [27]$$

In this way, the sulfate is regenerated and the local acidity is increased. Nests of sulfate species are frequently found in corrosion products after atmospheric exposure and the mechanism is consistent with these observations. Recent work using high-resolution analytical studies have found that the initial absorption of sulfur dioxide, and subsequent corrosion of steel, was local in nature. Importantly, it was found that SO_2 on its own is insufficient to

form sulfate nests and the presence of an additional oxidant (NO_2 or O_3) was essential for the detection of sulfate nests.[106]

3.01.4.2.2 The electrochemical mechanism

An electrochemical mechanism for atmospheric rusting was first proposed by Evans in 1963, but was not accepted at the time.[107] Its basic conception is that an electrochemical cell is formed between iron and iron oxy-hydroxide. At the anode, ferrous ions are produced in the normal way while at the cathode FeO(OH) is reduced. At some later point, the reduced iron oxide is reoxidized by atmospheric oxygen[108]; hence, a net increase in the amount of FeO(OH) ensues. Evans' original cycle is reproduced below:

$$Fe \rightarrow Fe^{2+} + 2e^- \quad [28]$$

$$Fe^{2+} + 8FeO(OH) + 2e^- \rightleftarrows 3Fe_3O_4 + 4H_2O \quad [29]$$

$$3Fe_3O_4 + 0.75O_2 + 4.5H_2O \rightleftarrows 9FeO(OH) \quad [30]$$

The above mechanism is now generally accepted although the indicated role of magnetite as the reduced species is probably only true under relatively reducing conditions. Thus, electrochemical reduction of lepidocrocite, γ-FeO(OH), results in a thin surface layer containing Fe^{2+} species which may either dissolve into the electrolyte or, at more negative potentials, may form magnetite.[109] The reduced surface layer, containing ferrous hydroxide, is easily reoxidized back to γ-FeO(OH). Hence, reactions [29] and [30] become:

$$Fe^{2+} + FeO(OH) + 2H_2O + e^- \rightleftarrows 2Fe(OH)_2 + H^+ \quad [31]$$

$$2Fe(OH)_2 \rightleftarrows 2FeO(OH) + 2H^+ + 2e^- \quad [32]$$

On the other hand, magnetite oxidizes preferentially to maghemite, γ-Fe_2O_3, which is relatively resistant to reduction, as is magnetite. Likewise, goethite, α-FeO(OH), is considerably more resistant to electrochemical reduction compared with lepidocrocite.[110] Hence, the electrochemical mechanism will only operate where there is sufficient lepidocrocite present while rusts largely containing goethite would be expected to be resistant to reduction and, hence, dimensionally more stable and more protective.

3.01.4.2.3 The wet–dry cycle

During atmospheric exposure of any material, a repeated, endless, and chaotic cycle of wetting and drying occurs, caused by precipitation, heat and wind drying of wetted surfaces, absorption and deposition of pollutants and wetting and drying of surfaces as a function of the RH. The cycles of wetting and drying strongly influence the corrosion of materials. For steel that this cycle is an essential part of the electrochemical mechanism described above was confirmed by an elegant series of experiments by Stratmann and co-workers.[111–114] In these studies, the mass loss of iron and the oxygen consumption rate were measured simultaneously as a function of the wetting and drying of the iron surface. The outstanding feature of the variation in corrosion rate with wetting and drying cycle, **Figure 15**, is the surprisingly large contribution that occurs during the drying part of the cycle. This was the first experimental evidence to demonstrate this unexpectedly large effect, which has since been confirmed for other materials during atmospheric corrosion.[115]

Notable from **Figure 15** is the profound effect on the corrosion rate during drying that is a result of the alloying copper with iron. This work thus provides insight into the well-known beneficial effect of copper on the atmospheric corrosion of low alloys steels. This is discussed in more detail below.

3.01.4.3 Corrosion Product Composition

Until quite recently, it was not thought useful to analyze rusts in detail partly because X-ray diffraction indicated that they were poorly crystalline. Notwithstanding this, it was known that corrosion products on steel during atmospheric exposure were similar to those formed in immersed conditions as might be expected by consideration of the electrochemical mechanism of corrosion. Thus, corrosion products on plain carbon steel after atmospheric rusting contain magnetite, Fe_3O_4, lepidocrocite, γ-FeO(OH) and goethite, α-FeO(OH) in varying amounts, the last being thermodynamically the most stable.

Recently, rather detailed studies have begun to be performed using a variety of techniques. A Mössbauer analysis of the corrosion products on mild steel after 35 years exposure in a semirural Japanese location found that the rusts were composed mostly of goethite with minor amounts of lepidocrocite and trace amounts of magnetite.[116] In addition, the crystallite size of the goethite component was found to be

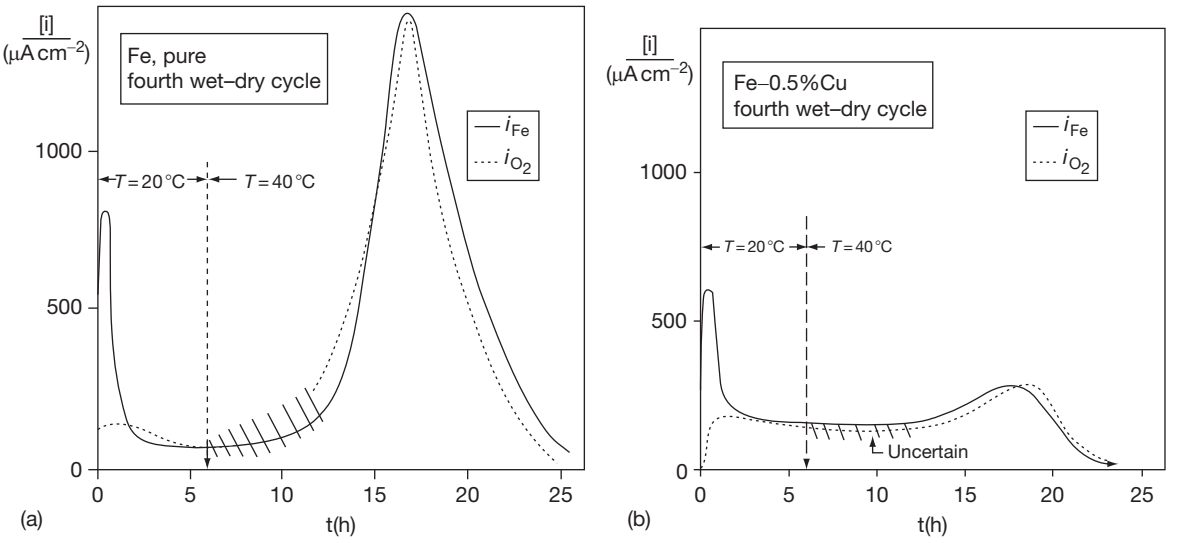

Figure 15 Atmospheric corrosion rate of Fe and Fe–0.5%Cu alloy over the 4th cycle of wetting (20 °C) and drying (40 °C), after. Reproduced from Stratmann, M.; Bohnenkamp, K.; Ramchandran, T. *Corros. Sci.***1987**, *27*(9), 905–926.

bimodal, with more than 80% larger than 12 nm but the remaining fraction smaller than 9 nm. In laboratory experiments, the composition of adherent and nonadherent rusts formed by artificially corroded steel at varying chloride concentrations were also studied by Mössbauer analysis. Nonadherent rust was found to consist of lepidocrocite, goethite, with traces of akaganeite and magnetite.[117] The composition of the corrosion products was essentially independent of the exposure times and chloride concentration. Studies of steels exposed over 16 years in various industrial locations in the United States found similar compounds with the difference that maghemite was identified rather than the isostructural magnetite.[118]

In summary, the corrosion product (rust) layer that is developed on steel after long-term exposure in the atmosphere contains species that may be expected from thermodynamic considerations. Thus, the majority component is the most stable phase (goethite), which appears as the outer, and thickest, layer. Depending on the environment and conditions of exposure, an intermediate layer of corrosion product contains lepidocrocite while magnetite and maghemite are concentrated in a region adjacent to the steel substrate, although they may also be present as isolated crystallites within the intermediate layer. In marine environments, minor amounts of akaganeite are also commonly present. The phases are all fined grained (and commonly nano-crystalline) with a decrease in grain size and an increase in the volume fraction of goethite associated with improved corrosion resistance.

3.01.4.4 Atmospheric Corrosion Kinetics

3.01.4.4.1 Climatic variation

Some representative figures to show how the rate of corrosion of carbon steel in the open air varies in different parts of the world are given in **Table 10**. They relate to 100 × 50 × 3.2 mm pieces of ingot iron freely exposed in a vertical position for 1 year and derive from historic data from the former BISRA.[8]

The results follow an expected pattern with by far the highest rate of corrosion being observed on a surf beach at Lagos, Nigeria. Indeed, this environment is so aggressive that the measured corrosion rate is several times that expected under immersed conditions. Conversely, the low rates of corrosion observed at Khartoum, Abisko, Delhi, Basrah, and Singapore are primarily associated with the absence of serious pollution. Moreover, at most of these locations the RH is low, for example, at Khartoum the RH lies below the critical value for rusting throughout the whole year.

Despite these results, it should not be assumed that corrosion rates of steel will necessarily be low in all comparatively nonpolluted desert environments. In regions such as the Arabian Gulf, considerable variations in corrosion rates may occur between inland and coastal sites. This arises not only from the salt content of the air but also from sand which is blown on to the steel. Although temperatures are high during the day, condensation occurs at night. The effects of different types of sand on the corrosion of mild steel have been studied.[119] It was concluded

Table 10 Atmospheric corrosion rates of mild steel exposed outdoors in different climates

Type of atmosphere	*Site*	*Corrosion rate (mm year^{-1})*
Great Britain		
Rural or suburban	Godalming	0.048
	Llanwrtyd Wells	0.069
	Teddington	0.070
Marine	Brixham	0.053
	Calshot	0.079
Industrial	Motherwell	0.095
	Woolwich	0.102
	Sheffiedl	0.135
	Frodingham	0.160
	Derby	0.170
Overseas		
Rural or suburban	Khartoum	0.003
	Abisko, North Sweden	0.005
	Delhi	0.008
	Basrah	0.015
	State College, PA, USA	0.043
	Berlin-Dahlem	0.053
Marine	Singapore	0.015
	Apapa, Nigeria	0.028
	Sandy Hook, NI, USA.	0.084
Marine/industrial	Congella, South Africa	0.114
Industrial	Pittsburgh, PA, USA	0.108
Marine, surf beach	Lagos	0.615

that fine sand has a higher salt content and is more corrosive than coarse sand within the size range <0.25–2.4 mm. Similarly in Canadian arctic and subarctic conditions corrosion rates as low as 2–5 μm year^{-1} were recorded at inland sites while within 1 km of the sea much higher rates (21–34 μm year^{-1}) were measured.[120] Thus, the rate of atmospheric corrosion is, as expected, dependent upon the local pollutant concentrations (e.g., affecting the surface chemistry and electrochemistry) as well as the local climatic conditions (e.g., controlling the total duration of corrosion, or time of wetness). It is important to remember that all quoted corrosion rates relate to average general penetration and take no account of pitting. Serious pitting of steel exposed to atmospheric corrosion is uncommon on simple test plates. However, it may be necessary to allow for this in some practical cases, where local attack may be occasioned by faulty design and other factors.

In reviewing this data, despite its historic nature, there is no reason to doubt the validity of the results in similar conditions. Thus, rates for the atmospheric corrosion of steel can be expected to vary from exceptionally high >600 μm year^{-1}, to very low <5 μm year^{-1}. What has changed, and this is an important consideration, is that the industrial pollutant concentrations have decreased dramatically over the last 20–40 years and that rate data for a particular location (especially if it is inland and was close to industry) may no longer be valid.

3.01.4.4.2 Conditions of exposure

It has long been known that sheltering and orientation of exposed steel during atmospheric corrosion testing influences significantly the measured corrosion rates. For example, the results of tests at Derby in the 1940s[121] show that specimens exposed at 45° to the horizontal corroded 10–20% more than specimens exposed vertically and that 54% of the total loss was on the underside. Likewise, for similar American tests[122] on specimens exposed at 30° to the horizontal, 62% of the total corrosion loss was on the underside. This influence is further demonstrated in experiments carried out 228 m from the sea at Kure Beach, North Carolina.[123] In these tests, the corrosion rates over a 4-year period varied by a factor of five depending on the orientation and degree of sheltering. Generally, east (sea) facing specimens exposed at 30° from the horizontal corroded at the highest rate while west (land) facing specimens exposed at the same angle corroded at the lowest rate. This can be ascribed to the prevailing wind direction driving sea salt aerosols onto the specimens.

The orientation of steel during atmospheric exposure tests is therefore found to have great influence on the final corrosion rates measured. This is because the amount of moisture and pollutants that can reach, and remain on, surfaces vary with compass direction, prevailing wind, sun, etc. In particular, the ground-facing side of a horizontal surface is protected from rain but it is also shielded from the drying action of the sun and often of the wind. Thus, condensation tends to remain in contact with the steel there for longer periods; moreover, harmful solid particles and soluble salts are not washed away by rain events. Consequently, and possibly counter intuitively, the ground-facing side is often found to corrode more rapidly than the sky-facing side. The same considerations apply to steel exposed obliquely. The relative corrosion of the opposite faces of a vertical steel plate will largely depend on the direction of the prevailing winds, pollution, rain and sun (i.e., whether the face is oriented towards the south (in the north of the equator) or the north (in the south of the equator).

3.01.4.4.3 Damage functions

Generally, in the majority of environments, except those that have exceptionally high levels of pollutant or salt aerosol, the corrosion rate of steel tends to decrease with time. This is a common observation, for example in recent work by Zhang *et al.*[124] for two different types of steel in a marine environment, **Figure 16**.

As may be seen in **Figure 16**, the tendency is for corrosion rates to decrease with time. Such behavior may be modeled simplistically by an exponential expression such as:

$$\text{Rate} = A\,t^{n} \qquad [33]$$

where A is a constant, t is time and n is the kinetic rate order (or exponent). For n equal to 1, linear kinetics ensue and the reaction rate is likely to be chemical reaction controlled however, for diffusion-controlled parabolic kinetics, n is equal to 0.5. Any other value for n implies a mixed control process. For atmospheric corrosion of steel, the value of n commonly lies between 0.5 (more typical of weathering steel) and 0.8 (more common for carbon steel).

Traditionally field exposures have been used to determine the corrosion rates of materials at particular environments. Initially, just corrosion rate data were collected but gradually such work was extended to include simultaneous collection of an increasing range of other atmospheric data, including: RH, air and metal temperature, precipitation, sunlight, as well as deposition of chloride, sulfate, nitrate, and analysis of rain water. The concept behind this considerable amount of effort is to develop damage functions (or dose–response relationships) for atmospheric corrosion so that predictive models may be developed. This approach culminated with an international program run under the auspices of the International Standards Organisation Technical Committee 156, Working Group 4 (ISO TC156/WG4) and the collaboration of 12 nations (Canada, Czechoslovakia, Finland, France, Germany, Japan, Norway, Spain, Sweden, UK, USA, and Russia) that commenced in 1986. The primary purpose of this was to verify the ISO 9223–9225 classification standards for the aggressiveness of atmospheres. A secondary, arguably more scientific, purpose was to collate the results across numerous and widely geographically separated locations in order to determine the best fit to the data by multivariate least squares regression analysis.

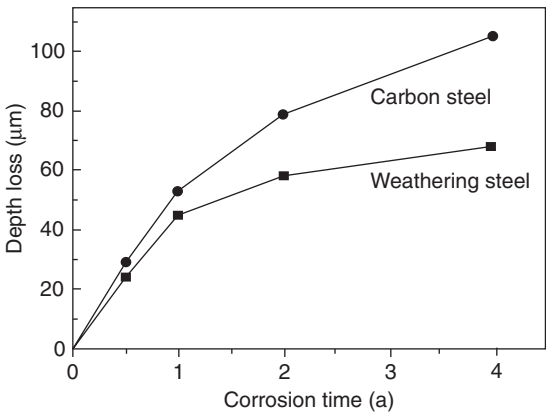

Figure 16 Thickness loss of weathering steel and mild steel versus exposure time. Reproduced from Zhang, Q. C.; Wua, J. S.; Wang, J. J.; Zheng, W. L.; Chen, J. G.; Li, A. B. *Mater. Chem. Phys.***2003**, *77*(2), 603–608.

Results from the ISO-CORRAG program were published gradually over a number of years for example by Dean *et al.*[125–127] Generally, the data show strong correlation between the corrosion rates for steel with the corrosion rates of the other tested materials (zinc, copper, aluminum) as might be expected. However, the scientific aim, which was to describe the corrosion rate of materials effectively as a regression equation over the main variables, was not completely successful. Thus, the use of the exponential rate expression alone was found to account for ~75% of the observed corrosion rate variation for steel. Regression of the time exponent against time of wetness and chloride deposition rate improved the regression fit only slightly. A more complete analysis of the data by Mikhailov, Tidblad, and Kucera[128] resulted in two rate expressions that reflect the observed increase in corrosion rate with temperature to 10 °C, thereafter decreasing:

Below 10 °C:

$$C = 1.77[\mathrm{SO_2}]^{0.52}\exp(0.020RH)\exp\{0.150(T-10)\} + 0.102[\mathrm{Cl^-}]^{0.62}\exp(0.033RH + 0.040T)$$

Above 10 °C:

$$C = 1.77[\mathrm{SO_2}]^{0.52}\exp(0.020RH)\exp\{-0.054(T-10)\} + 0.102[\mathrm{Cl^-}]^{0.62}\exp(0.033RH + 0.040T)$$

where: C is the corrosion rate of steel ($\mu m\ year^{-1}$), RH is relative humidity (%), T is temperature (°C), $[SO_2]$ is the concentration of sulfur dioxide ($\mu g\ m^{-3}$) and $[Cl^-]$ is the chloride deposition rate ($mg\ m^{-2}\ day^{-1}$). These expressions, regressed over 128 datasets, provide a correlation coefficient (R^2) of 0.85. Dean commented on the overall results of the ISO-CORRAG program:

Table 11 Kinetic parameters for the early stages of atmospheric corrosion of iron

Activation energy at 90% RH:	20 h	60 h	100 h
$\triangle E_{act}$ for 0.8 ppm SO_2	170 kJ mol^{-1}	140 kJ mol^{-1}	115 kJ mol^{-1}
$\triangle E_{act}$ for 20 μg cm^{-2} of NaCl;	70 kJ mol^{-1}	45 kJ mol^{-1}	35 kJ mol^{-1}
Chemical reaction orders at 90% RH:	*20 h*	*60 h*	*100 h*
f [SO_2]	1.56	1.46	1.40
f [NaCl]	0.70	0.60	0.61
Kinetic order (i.e., n in t^n) at 90% RH	*0.1 ppm*	*0.4 ppm*	*0.8 ppm*
n for the indicated pSO_2	0.78	0.76	0.68
n for the indicated [NaCl]	*10 μg cm^{-2}*	*20 μg cm^{-2}*	*40 μg cm^{-2}*
	0.89	0.84	0.64

Source: Cai, J.-P.; Lyon, S. B. *Corros. Sci.* **2005**, *47*(12), 2956–2973.

"Some other environmental variables will need to be found to improve this approach to predicting atmospheric corrosion." Nevertheless, the fact that comparatively simple rate expressions may be used to provide a guide to atmospheric corrosion prediction is helpful.

Kinetic rate parameters can be measured with more control in the laboratory. For example, activation energies and reaction rate orders as a function of chloride contamination and gas-phase SO_2 concentration have been determined in the laboratory for the early stages of the atmospheric corrosion of iron (i.e., between 0 and 120 h).[129] From the data in **Table 11** it can be noted that for exposure in gas-phase SO_2, activation energies, and kinetic and chemical rate orders, are consistent with the controlling mechanism for atmospheric corrosion of iron being slow solution-phase oxidation of sulfite to sulfate ion. Conversely, the corrosion process with surface chloride contamination is evidently much easier. These data provide input into corrosion models that may be extended out to longer exposure times in order to generate predictive corrosion models.

3.01.4.5 Weathering Steel

3.01.4.5.1 Alloying effects

Historically, from the 1940s, a large degree of effort was put into the development of low alloy steels that had improved overall corrosion resistance. By the early 1960s and into the 1970s, this program of testing had largely been completed with the development of a generation of optimized weathering steels based on steel compositions containing at least 0.2% Cu with small additional amounts of P and Cr. The beneficial effect of copper additions to steel has been referred to already in **Figure 15** and **Figure 16**. In turn, **Figure 17** refers to trials of 9 years duration at Rotherham in the United Kingdom[130] while similar curves based on American tests,[131] in **Figure 18**, show substantially the same features. The fact that the rates of corrosion are markedly slower in the American than in the British tests is mainly due to differences in the corrosiveness of the respective atmospheres.

The effects of the various alloying elements are not necessarily directly additive although same additions are synergistic (e.g., Cu+P is better than Cu on its own). Bearing this in mind, the practical effect of individual elements can be summarized as follows.

- Copper additions up to ~0.4% give a marked improvement, but further additions make little difference.
- Phosphorus, at least when combined with copper, is also highly beneficial. However, in practice, levels above ~0.10% adversely affect mechanical properties.
- Chromium, in fractional percentages, has a significant influence on corrosion rates.
- Nickel, while reducing corrosion rates a little, is not as important in its effect as the aforementioned elements.
- Manganese may have a particular value in chloride-contaminated environments, but its contribution is little understood.
- Silicon is in a similar position to manganese, with conflicting evidence as to its value.

3.01.4.5.2 Wetting and drying

The improvement in corrosion resistance for weathering steels compared with carbon steel is found to depend on the nature and amounts of the alloying elements and the corrosive environment. Thus, weathering steels show greatest advantage when they are freely exposed to the open air in industrial environments, that is, where they are subjected to atmospheric

wetting and drying. The effect of variations in surface wetting is illustrated in **Figure 19**, which compares the relative rates of corrosion of a weathering steel and a carbon steel at a UK industrial location after 9 years exposure.[132] The greatest rate of corrosion was on panels facing the north-westerly direction, which is wettest for the longest period of time.

Initially, weathering steel appears to corrode like mild steel. However, unlike mild steel whose oxide repeatedly spalls off, the surface rust layer on weathering steel stabilizes with time, provided that the exposure conditions allow the steel to dry out periodically. The rust then becomes darker, granular, and tightly adherent whilst any pores or cracks become filled. This protects the underlying steel by reducing the permeability of the oxide layer to water and air both of which must be present simultaneously at the metal surface for rusting to continue.

The distinguishing feature of the behavior of the slow-rusting low-alloy steels is the formation of this protective rust layer, which generally contains a finer grained (nano-crystalline) oxide particles and a higher proportion of the stable goethite phase compared with the rust layers formed on carbon steel. The first mechanistic evidence for this improvement in performance was made by Stratmann and is shown in **Figure 15**. In copper-free steel, a large fraction of the total corrosion process occurs during the drying phase of the wet–dry cycle. However, for copper-containing steel, the large increase in corrosion rate towards the end of the drying cycle is absent.[112] The precise reason for this suppression is not yet wholly clear however, it may be interpreted in terms either of a stabilization of iron oxy-hydroxide (rust) to reduction or in terms of the cathodic reduction of oxygen being inhibited.[133] Either way, the redox cycling (and associated volume changes) is suppressed resulting in a more compact and more protective rust layer.

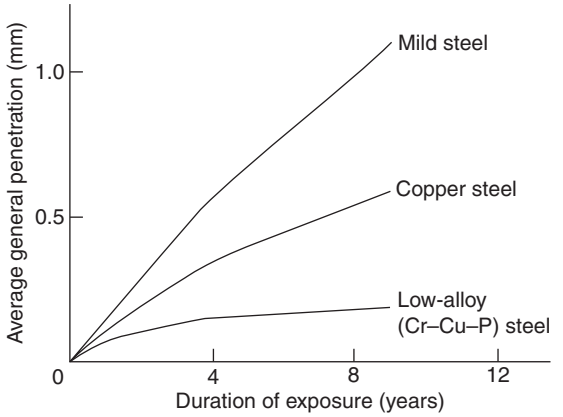

Figure 17 Effect of low-alloy additions on the corrosion of steel in Rotherham, UK. Reproduced from Edwards, A. M. Proc. Symp. on Developments in Methods of Prevention and Control of Corrosion in Buildings, British Iron and Steel Federation, London, 1966.

3.01.4.5.3 Applications

The most widespread use of weathering steels has been for structural steelwork in buildings, bridges, roadside furniture, etc. especially where maintenance painting is particularly difficult, dangerous, inconvenient, or expensive. Bridges over land, rivers, railways, roads and estuaries fall into this category, although in the last two cases care should be taken with respect to airborne salinity and ensuring adequate drainage to

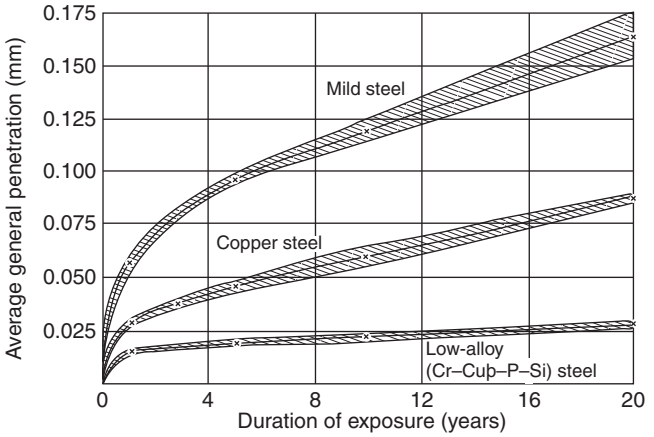

Figure 18 Effect of low-alloy additions on the corrosion of steel outdoors at Kearny, NJ, USA. Reproduced from Larrabee, C. P.; Coburn, S. K. *Proc. First International Congress on Metallic Corrosion*, 1962; Butterworths: London, pp 276.

avoid the possibility of continuous wetting. Road bridges can be affected by salt-laden atmospheres or water, produced as a consequence of winter ice and snow clearing with deicing salt and grit. Chloride can be in the form of an airborne spray thrown up by passing vehicles or as a result of leaks in the bridge deck. In the presence of salt-water many materials, including steel, paint, reinforced concrete, aluminum, etc. deteriorate at an accelerated rate. Weathering steels are no exception, and higher than normal corrosion rates should be expected if they are exposed to saline waters or frequent spraying with salt. Albrecht has described the applications and pitfalls of using weathering steel in US highway bridges in an informative paper that is well worth consultation.[134]

3.01.4.5.4 Next generation weathering steels

Recent research has been aimed at further optimization of the performance of weathering steels, partly by more detailed understanding of the nature of the rusts that are formed during exposures. Thus, X-ray diffraction, vibrational spectroscopy, and elemental analysis have all been applied to the analysis of various rusts on the micrometer scale. This has provided evidence of doping of the rust layers by Cr^{3+} and Ni^{2+}, which, in turn, limits cathodic oxygen reduction and promotes the stabilization of the goethite phase.[135,136] In the light of these results, more advanced weathering steels, based on modern high-strength, low-alloy compositions, have been developed,[137] Table 12.

The substitution of nickel for chromium, and the slightly increased level of copper, results in a considerably improved performance particularly in those atmospheres where the importance of chloride has increased due to the reduction in sulfur dioxide levels. The amount of corrosion on the novel material was less than 1/20 that of conventional weathering steel after 9 year exposure to a marine atmosphere in Japan.[136] It was suggested that this improved performance was due to nickel doping of the rust that resulted in an ion exchange process leaving a net negative charge at the inner rust layer, hence 'repelling' chloride ions.

3.01.4.6 Classification of Atmospheres

Classification of the atmosphere into various corrosivity (i.e., severity of corrosion) categories depending on local environment has been the work of a

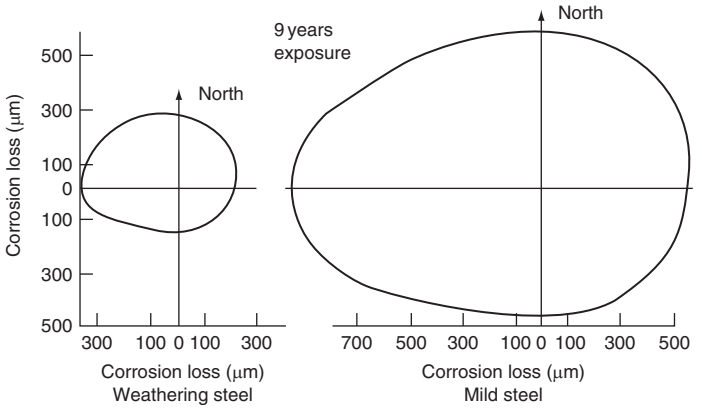

Figure 19 Corrosion losses of steels exposed vertically, facing different compass directions. Reproduced from Hooper, R. A. E.; Lee, B. V. Proc. 12th International COR-TEN Conference, Florida, 1985, United States Steel, Pittsburgh, 1985.

Table 12 Compositions of conventional and 'advanced' weathering steel

Material	*Chemical composition (mass %)*						
	C	*Si*	*Mn*	*P*	*Cr*	*Cu*	*Ni*
'Advanced' weathering steel	0.05	0.04	1.02	0.008	–	0.40	3.03
Conventional weathering steel	0.10	0.42	1.54	0.004	0.52	0.30	0.32

Source: Kimura, M.; Kihira, H.; Ohta, N.; Hashimoto, M.; Senuma, T. *Corros. Sci.* **2005**, *47*, 2499–2509.

number of national standards bodies. In the EU, this standardization is encompassed within BS EN 12500,[138] and consistent with ISO 9223–9226. The standard atmospheric corrosivity classifications are reproduced in **Table 13** with the corresponding expected corrosion rates for carbon steel in **Table 14**.

An example of this approach is given in **Table 15** where corrosion rates in various European (mainly Scandinavian) locations are matched to **Table 14** to derive an atmospheric corrosivity classification for that location.

3.01.5 Corrosion in Water

3.01.5.1 Water Composition

The composition of water is clearly of importance in determining the rate of corrosion of steel exposed to it. Some of the more important factors that contribute to corrosion are the dissolved gas content (primarily oxygen and carbon dioxide), the nature and amount of dissolved solids (which influences the electrical conductivity, pH and hardness of the water), the presence of organic matter (such as detergents, oils, wastes, etc.) and the presence or absence of microbial species such as bacteria, algae, or fungi.

3.01.5.1.1 Dissolved gases

Oxygen is the most important dissolved gas in water and, at pH > 3, is generally the main cathodic reactant for the corrosion of steel. Thus, in neutral or near-neutral water, dissolved oxygen is necessary for any appreciable corrosion of steel. Increasing the oxygen availability for reaction either by increasing the dissolved oxygen concentration or by increasing its mass transfer rate (i.e., in a flowing system) will, in almost every case, result in an increase in corrosion rate. In view of this, the control of oxygen concentration in solution is one of the primary methods for

Table 13 ISO standard classifications for atmospheric corrosivity

		Examples of typical environments	
Corrosivity category	*Corrosivity*	*Indoor*	*Outdoor*
C1	Very low	Heated spaces with low RH and insignificant pollution: schools, museums, etc.	Dry or cold zonesatmospheric environment with very low pollution and time of wetness for example, certain deserts, central Antarctica
C2	Low	Unheated spaces with varying temperature and RH. Low frequency of condensation and low pollution, for example, storage, rooms, sports halls	Temperate zones: environment with low pollution ($SO_2 < 12\ mg\ m^{-3}$), for example, rural areas, small towns. Dry or cold zones: environment with short time of wetness, for example, deserts, subarctic areas
C3	Medium	Spaces with moderate frequency of condensation and moderate pollution from production process, for example, food-processing plants, laundries, breweries, dairies	Temperate zone: environment with medium pollution (SO_2:12–40 $mg\ m^{-3}$) or some effect of chlorides, for example, urban areas, coastal areas with low deposition of chlorides Tropical zone: atmosphere with low pollution
C4	High	Spaces with high frequency of condensation and high pollution from production process, for example, industrial processing plants, swimming pools	Temperate zone: environment with high pollution, (SO_2: 40–80 $mg\ m^{-3}$) or substantial effect of chlorides, for example, polluted urban areas, industrial areas, coastal areas, without spray of salt water, strong effect of deicing salts. Tropical zone: environment with medium pollution
C5	Very high	Spaces with almost permanent condensation and/or with high pollution from production process, for example, mines, caverns for industrial purposes, unventilated sheds in humid tropical zones	Temperate zone: environment with very high pollution (SO_2: 80–250 $mg\ m^{-3}$) and/or strong effect of chlorides, for example, industrial areas, coastal and off shore areas, with salt spray. Tropical zone: environment with high pollution and/or strong effect of chlorides

Source: BS EN 12500: Protection of metallic materials against corrosion: Corrosion likelihood in atmospheric environment, classification, determination and estimation of corrosivity of atmospheric environments.

corrosion control of carbon steel (and indeed many other materials).

The presence of dissolved ambient carbon dioxide from the atmosphere (pCO_2 ~385 ppm in 2008) alters the pH of water by the reaction:

$$CO_2 + H_2O \rightleftarrows H_2CO_3 \rightleftarrows H^+ + HCO_3^- \quad K_a = 4.30 \times 10^{-7} \quad [33]$$

Indeed, the pH of most natural (nonsaline) water exposed to the atmosphere is acidic due to the above equilibrium. Thus, changes in the dissolved CO_2 level will tend to change the pH and, consequently, any process that depends upon pH. In near-neutral solutions, this will not affect the corrosion rate of steel directly. However, a change in pH may affect the stability of protective deposits and scales on the steel, particularly those containing calcium carbonate, which will tend to dissolve as the pH falls.

At higher CO_2 pressures the situation changes significantly. Thus, in 3% sodium chloride solution at 1 atm. of carbon dioxide the corrosion rate of steel is increased substantially above what might be expected at the equilibrium pH of ~3 with hydrogen evolution as the cathodic reaction. Although the concentration of hydrogen ions in solution is relatively low at pH 3 (i.e., 10^{-3}), carbonic acid dissociates as shown in eqn [34] to produce hydrogen ions immediately adjacent to the cathode. Thus, under these conditions, the hydrogen evolution reaction is controlled by mass transfer of carbonic acid to the cathode.[139] This mechanism largely explains the phenomenon of 'sweet' corrosion, due to CO_2 in oil and gas recovery and petrochemical production.

Table 14 Correspondence between mass loss of carbon steel after 1 year of exposure and ISO standard atmospheric corrosivity classifications

Corrosivity category	*Mass loss per unit area ($g\,m^{-2}$)*	*Thickness loss (μm)*
C1	≤10	≤1.3
C2	>10–200	>1.3–25
C3	>200–400	>25–50
C4	>400–650	>50–80
C5	>650–1500	>80–200

Source: BS EN 12500: Protection of metallic materials against corrosion: Corrosion likelihood in atmospheric environment, classification, determination and estimation of corrosivity of atmospheric environments.

3.01.5.1.2 Dissolved solids

The effect of dissolved solids is complex. The presence of inorganic salts, notably of chlorides and sulfates, should promote corrosion, because they increase the conductivity of the water, thereby facilitating the electrochemical reactions via improved ion transport in solution. Alkaline waters tend to be less aggressive than acid or near-neutral waters, and corrosion can be well-controlled in a closed system by appropriate water treatment; for example, addition of inhibitors and/or making the water alkaline and the metal passive. Unfortunately, at pH values just insufficient to give complete passivation, there is a high risk of severe pitting, even though the total corrosion rate is reduced, and this is a greater danger in many applications.

The most important property of dissolved solids in fresh waters is whether or not they lead to deposition of a protective film on the steel that will impede the corrosion process. This is determined mainly by the equilibrium between calcium carbonate, calcium bicarbonate, and carbon dioxide and is of fundamental significance and where an appropriate scaling index (e.g., the Langelier index) can provide guidance.[140] Since hard waters are more likely to deposit a protective calcareous scale than soft waters, the former tend to be considerably less aggressive than the latter; also, soft waters can often be rendered less

Table 15 Corrosion rates of carbon steel in various European locations

Environment	*Deposition rates ($mg\,m^{-2}\,day^{-1}$)*		*Corrosion rate ($\mu m\,year^{-1}$)*	*Atmospheric corrosivity classification*
	SO_2	*Cl^-*		
Rural	<20	<3	5–10	C2
Urban	20–100	<3–50	10–30	C2/C3
Industrial	110–200	–	30–60	C3/C4
Marine	<10	3>100	10–40	C3
Arctic	<10	<3	4	C2

Source: Bardal, E. *Corrosion and Protection*, Table 8.1; Springer: Berlin, 2004.

corrosive by treating them with lime (calcium hydroxide). Carbonate scales are not the only type that may form in water and, depending on water chemistry, scales of calcium sulfate, magnesium silicate, magnesium hydroxide and iron or manganese oxy-hydroxides may also form.

3.01.5.1.3 Microbial effects

Another important factor is that most natural waters are far from being sterile. They contain greater or lesser amounts of organic matter, both living and dead. Some of the dead organic matter, for example, peat residues, may render the water corrosive by making it acid, but in most cases, the living organisms probably exert the greater influence. In natural seawater, fouling occurs and in freshwaters, algae may grow. A more detailed discussion of microbial corrosion can be found elsewhere in this book.

3.01.5.2 Deposits and Scales

3.01.5.2.1 Fouling of surfaces

During service, the surface of steel in contact with the environment will inevitably tend to become covered with a deposit of some nature. Such deposits may arise from the water chemistry (i.e., carbonate scaling), from corrosion (i.e., the formation of a corrosion product), from bio-films (i.e., slimes from bacterial, algal and other origins), from sediments and silts (i.e., from suspended solids in the water), etc. In all cases, the fouling of surfaces will have an effect on corrosion rates of materials used and on the process or function of the system. These effects need to be understood and allowed for in the design of the system. However, if the anticipated effects are detrimental, the surface fouling must be controlled in some way depending on its origin.

In many systems or processes, fouling deposits tend to form preferentially in the hottest part of the system, often on heat transfer surfaces (e.g., boilers, heat exchangers, etc.), because the solubility of the depositing material is lowered; this is particularly prevalent for carbonate scaling. In other cases, deposits tend to form at the coolest part of the system (i.e., also in heat exchangers) for the same reason. The formation of bio-films is clearly not an issue where the system temperature is sufficient to ensure sterilization. Conversely, in chilled water and air conditioning systems, bio-film formation is a significant hazard.

In addition to a reduction in the efficiency of heat transfer due to the isolation of the metal surface from the water by a film of low thermal conductivity, fouling deposits can additionally cause significant problems due constriction of flow, blocking of valves, etc.

3.01.5.2.2 Under-deposit corrosion

Fouling deposits, depending on their nature, often result in enhanced corrosion underneath the deposit. On heat transfer surfaces at sufficiently high temperature, local boiling of water can occur beneath deposits giving rise to concentration of the species in solution at this point and consequent localized corrosion under the deposit. In the absence of heat transfer, under-deposit corrosion may still occur due to the differential aeration mechanism where the anode is localized to an area of lower oxygen concentration under the deposit.

Where water treatment is used to provide corrosion control, then the presence of deposits in the system will result in poor availability of the inhibitor at these locations and, again, increased corrosion will result. This is particularly significant where passivating inhibitors are used as the inhibitor concentration may locally (i.e., under the deposit) fall below the critical concentration required for passivity and, hence, give rise to a significant risk of pitting corrosion.

In many systems, a bio-film of an aerobic species may first colonize the steel surface, which will result local oxygen depletion under the bio-film. The effect of this is both to promote differential aeration cell corrosion but, more significantly, to create a beneficial environment for possible further colonization under the original film by an anaerobic species, including sulfate reducing bacteria. In this latter case, the metabolic products include reduced sulfur species, particularly sulfides and hydrogen sulfide, both of which are very likely to promote severe corrosion.

3.01.5.3 Natural Waters

3.01.5.3.1 Corrosion rates

As pointed out already, corrosion rates of carbon steel in water vary significantly depending, amongst other things, upon the specific water composition, oxygen concentration, and flow rate in the fluid (i.e., the mass transfer rate of oxygen to the corroding surface). In practice, some form of corrosion protection is generally used for carbon steel in aqueous environments. In a few situations however, unprotected bare steel may be used provided a corrosion allowance is provided for in the design. Such applications include: pipe internals on potable water systems and fire protection systems, where only minimal (or no) water treatment

Table 16 Rates of corrosion of mild steel in natural waters (total immersion)

Type of water	*Test authority*	*Test site*	*Test duration*	*Average corrosion rate ($\mu m\ year^{-1}$)*
Sea water	Institution of Civil Engineers[141]	Halifax, Nova Scotia	15	108
		Plymouth	15	65
	BISRA[142]	Emsworth	5	65
Fresh water	Institution of Civil Engineers[141]	Plymouth: reservoir water	15	43
River water	Office Technique pour l'Utilisation de l'Acier[143]	La Cadène: soft water	5	68
		Dôle: hard water	5	10

is possible, etc.; and steel piles for shoring work (e.g., on river banks, jetties, etc.).

For interest, some historic data for corrosion rates in a range of environments are given in **Table 16**; for low-carbon structural steel tested under the conditions stated. The figures are for the average general penetration over the whole test areas. As an indication of the maximum penetration depth, it may be noted that in the sea-water tests of the Institution of Civil Engineers[141] the maximum depth of pitting for descaled mild steel after 15 years immersion was ~2.3 mm; when the steel had been immersed in the as-rolled condition with its millscale, a Figure as high as 7.6 mm was observed. Under half tide immersion conditions, the corrosion rate of steel may be increased by a factor of 2–5 compared with the results for total immersion.

The rates of corrosion quoted in **Table 16** are sufficiently low that with a suitable corrosion allowance they can be used unprotected with an anticipated life for structures of 40–50 years. Traditionally, low-strength steel grades were used for pipes and structural elements (such as piling) and required a relatively thick section for strength. Increasingly, such steels are being replaced with higher strength materials of thinner section resulting, obviously, in a decreased lifetime. It is not clear that design engineers fully appreciate that the good lifetime previously achieved for steel in waters was often due to generous thickness allowances with respect to strength and corrosion.

3.01.5.3.2 Piped fresh water systems

It is not uncommon for unprotected ferrous materials (i.e., cast iron or carbon steel) to be used in potable (drinking) water systems (as pipes, pumps, valves, etc.), in fire protection systems, as foundation or shoring materials (i.e., steel piles) for support of riverside, or reservoir structures, etc. In fresh water distribution systems, cast iron (historically graphitic iron, recently nodular ductile iron) is more commonly used as a pipe material as opposed to steel; increasingly polymeric materials are now being used for water systems.

Corrosion problems of ferrous materials in domestic waters are a continuing problem.[144] In 1975, Larson comprehensively surveyed corrosion of steel in fresh water with data gathered from over 30 years of research in Illinois.[145] He developed a classification of waters for corrosion of steel in terms of dissolved oxygen, pH, and dissolved salts, **Table 17**.

The classification in **Table 17** assumes no significant effects from microbial corrosion. In practice, however, microbial effects are ubiquitous and it cannot be assumed that they will always be dealt with satisfactorily by disinfection (e.g., chlorination).[146] However, in potable water systems, where fluid flow is significant, microbial problems are more commonly considered in the industry to affect drinking water quality (e.g., odors and discolouration of the water) than corrosion. Fire protection systems (i.e., risers and sprinklers), on the other hand, in effect comprise a series of stagnant sections in which microbial growth can proliferate. Consequently, microbiologically influenced corrosion is a significant risk in these and similar systems. It is generally advisable to minimize the risk by thorough initial cleaning of new systems in order to remove internal debris as well as hydrocarbons that may comprise a food source. Following cleaning, appropriate (i.e., not too frequent) test schedules should be undertaken in order to reduce the ingress of fresh water. In severe cases, it may be necessary to dose the system with biocides in order to reduce the microbial load.[147]

3.01.5.3.3 Structural steel in waters

A major application for unprotected steel in water is in retaining walls (revetments) along river banks, in sea walls, docks and harbors, structural pilings, etc. Particularly in river systems with low salinity, unprotected revetments are traditionally used and have an adequate life. The higher conductivity of saline and sea water permits the option of applying cathodic

Table 17 Classifications for corrosivity of fresh water

Type of water	*Corrosivity*
Distilled water, no oxygen	Corrosion is negligible
Mineral salts present, oxygen and carbonate absent	Similar to previous case provided oxygen is kept out of the system
Distilled water and oxygen present	Corrosion rate decreases with increase in pH but danger of severe pitting corrosion if the steel has marginal passivity; danger of localized corrosion in crevices, under deposits and at the water line
Mineral salts and oxygen present, carbonate absent	Increased corrosion compared with distilled water due to higher conductivity; increased tendency for localized corrosion where passivity is marginal
Carbonate, mineral salts and oxygen present, calcium absent	In the absence of Ca^{2+}, carbonates act to inhibit corrosion with their maximum effect appeared at more than 5–10 times the concentration of other salts (Cl^- or SO_4^{2-}, etc.) at > pH 6.5–7
Dissolved calcium and carbonate present, oxygen present or absent	Significant reduction in corrosion rate if a carbonate scale is deposited, however this does not generally happen unless there is significant supersaturation of $CaCO_3$ at the pH of the water

Source: Larson, T. E. *Corrosion by Domestic Waters, Bulletin 59*; Illinois State Water Survey, 1975.

protection. However, designs often still rely on a corrosion allowance for unprotected steel. As noted above, although this strategy has worked well in the past, increasingly the use of thinner and higher strength steels is reducing the overall time to perforation. Additionally, increasing corrosion problems are being observed worldwide where severe corrosion of steel piles, retaining walls, etc. occurs at and just below the waterline. This phenomenon was observed from the 1970s onwards in sea water installations[148] and termed 'marine low-water corrosion'[149]; it also occurs in saline and estuarine locations as well as in fresh water at inland docks (e.g., on Lake Superior, USA).[150]

In marine locations, this corrosion is now called 'accelerated low-water corrosion' (ALWC). It manifests itself as severe attack leading to premature failure of steel structures with unusually high rates of corrosion (i.e., 0.3–1 mm $year^{-1}$ compared with expected rates of 50–100 μm $year^{-1}$). ALWC occurs at or close to the lowest astronomical tide and, hence, is only visible a few times per year and easily missed. The corrosion typically affects only a small percentage of the exposed surface area with a characteristic damage pattern that depends on the particular geometry and pile design.[70] The causal agent for ALWC appears to be a characteristic microbial colonization of the steel surface resulting in biofilms that contain synergetic populations of sulfur reducing and sulfur oxidizing bacteria. Laboratory *in vitro* studies found that an approximate ten-fold increase in corrosion rate for such colonization, similar to that observed in practice.[151] Control of ALWC in existing installations is probably best carried out by a combination of sterilization of the marine muds combined with cathodic protection. Future installations are recommended to employ cathodic protection in the design (possibly combined with coating) in order to avoid the problem in the future.

3.01.5.3.4 Variation of corrosion with height

The corrosion rate of steel will vary as a function of height above and below the water as the environment changes from predominantly atmospheric, through the splash zone, into water-saturated mud and eventually to an underground condition. In addition to the variation in environment, the available oxygen concentration will also vary with depth. Consequently, differential aeration corrosion is possible where an enhanced zone of corrosion occurs at the location of lowest oxygen concentrations (i.e., the anode becomes localized away from areas of higher oxygen concentration. **Figure 20** shows the variation in remnant thickness as a function of height.[149] The maxima in the corrosion rate are seen to occur in the splash zone immediately above mean high water and at just below mean low water. The former is due to rapid corrosion in intermittently wetted areas (similar to atmospheric corrosion on a surf beach) while the latter is due differential aeration corrosion. Note that the corrosion rate decreases as the pile depth increases into the mud/soil below the water line.

3.01.5.4 Process Waters

3.01.5.4.1 Heating and cooling systems

Corrosion in water systems that are used for process heating/cooling or space heating/air-conditioning is

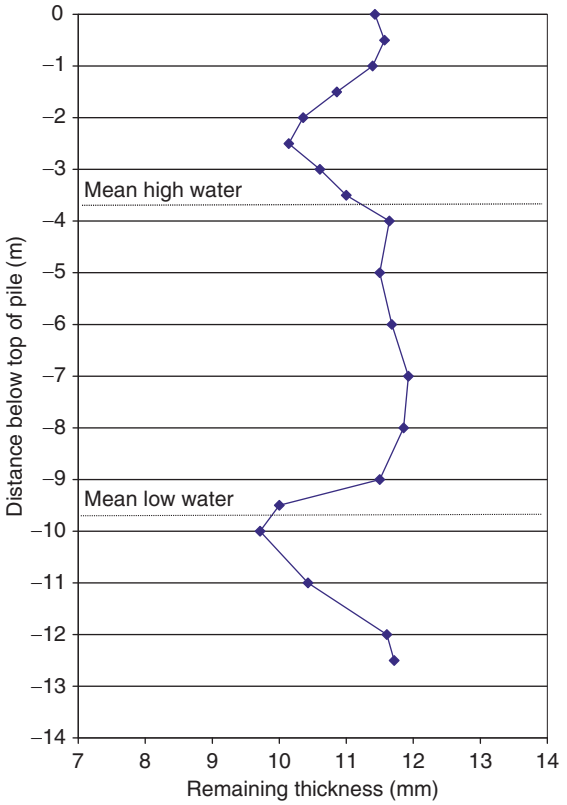

Figure 20 Thickness loss as function of height in a piled steel dockside. Reproduced from Morley, J. *Struct. Survey* **1989**, *7*(2), 138–151.

inevitable unless care is taken to condition the water environment. The principles for the control of corrosion, scaling and fouling in such systems are all well-known and summarized briefly in Table 18. They are discussed in more detail in the relevant chapter in this book.

In cooler waters, control of the microbiology is essential in order to achieve an effective system. Where the oxygen concentration is controlled at a relatively low level in order to limit corrosion, then anaerobic species are of concern. These include the sulfur reducing bacteria that produce sulfides in solution, which can be of concern due to the formation of unstable sulfide films on steel resulting in pitting corrosion. The presence of nitrate/nitrite reducing bacteria is of concern where nitrite corrosion inhibitors are present since these species will metabolize nitrite and reduce its concentration. Iron oxidizing bacteria can also be problematic due to their oxidation of dissolved ferrous species to ferric, resulting in enhanced deposition of rust deposits throughout the systems.

Table 18 Summary of main water treatments that are used to limit corrosion and related problems

Treatment	*Effect*
Water conditioning	Use of pH control, deaeration, softening and deionizing to pretreat the water supply and render it less likely to cause scaling and corrosion
Scale inhibition	Chemical addition made to prevent or modify the deposition of scales particularly on heat-transfer surfaces
Corrosion inhibition	Chemical addition made to reduce the rate of corrosion of metallic materials in the system
Microbial control	Chemical addition made to restrict microbial growth, essential where the water does not exceed sterilization temperatures (i.e., <60–70 °C)

3.01.5.4.2 Boiler waters

The principles of water treatment for the control of corrosion in boilers and related equipment are rather similar to those for heating and cooling systems (except for the absence of microbial corrosion since the water should be sterile) and are also well-established.[152] Clearly the main purpose of boiler water treatment is to maintain the lowest practical corrosion rate at reasonable cost. Traditional water treatment commonly attempts to maintain the steel in the passive region where magnetite is the stable phase and this is achieved by a combination of controlled pH, dissolved oxygen concentration, dissolved salts and addition of inhibitors for corrosion control not just in the boiler but also in the steam lines and condensers. The interested reader is directed to the chapter on boiler corrosion and its control in this book.

3.01.6 Underground Corrosion

3.01.6.1 Controlling Factors

In practice, bare carbon steel is rarely exposed underground without some form of functional corrosion protection system. Thus, cathodic protection is universally applied for the protection of buried metal underground almost always in combination with an effective protective coating system. Indeed, the performance of coating systems has been improved to such an extent that only a few milliamps of current per kilometer of buried pipeline might be required for adequate protection. Of course, the improvement in coatings (essentially a reduction in coating permeability to water and ions) leads to its own problems in

the shielding of protection currents where defects exist. The control of corrosion underground, including the influence of stray currents, is dealt with in more detail elsewhere and will not be considered further here.

Regarding the corrosion of buried steel, the seminal contributions from the 1950s and early 1960s of Romanoff in the USA[153] and Hudson in UK[154] for samples buried in some cases since the 1930s, still comprise the standard reference data for underground corrosion of bare, unprotected steel and other metals. Such data are of interest in situations where unprotected steel is used underground, which typically arise in construction applications where the use of steel for piles, revetments, shoring, etc. is not uncommon. More recent interest arises from the possible use of carbon steel as a cladding material for nuclear waste containers where knowledge of the long-term corrosion is essential for development of the relevant safety cases. In these cases, it is of merit to study the corrosion of buried archaeological artefacts as they are the only method for determining very long-term corrosion rates with any degree of certainty.

A detailed discussion of the effects of soil on corrosion of unprotected bare steel is beyond the scope of this article and the interested reader is directed to the relevant chapter on corrosion in soils in this book. In brief, soils vary greatly in corrosiveness according to their aeration, conductivity, composition, and microbial activity.[155] In general, dry, sandy, or calcareous soils, with a high electrical resistance, are the least corrosive. At the other end of the scale are the heavy clays and the highly saline soils, whose electrical conductivity is high. The depth of the water table is also important; much depends on whether the buried iron or steel is permanently above or below this, or even more perhaps on whether it is alternately 'wet' or 'dry.' The variation in corrosion rate with depth of burial is illustrated by the historic results quoted in **Table 19**, which also serve to indicate the rates of average general penetration in typical British soils.[156] It will be noted that the depth of burial had no consistent effect, which is not surprising since the average depth of the water table and the seasonal fluctuations in this varied from one site to another. Bacterial activity often plays a part in determining the corrosion of buried steel. This is particularly so in waterlogged clays and similar soils, where no atmospheric oxygen is present as such. If these soils contain sulfates, for example, gypsum and the necessary traces of nutrients, corrosion can occur under anaerobic conditions in the presence of sulfate-reducing bacteria. One of the final products is iron sulfide, and the presence of this is characteristic of attack by sulfate-reducing bacteria, which are frequently present.

Table 19 Corrosion of mild steel in various soils and depths over 5 years

Site	*Type of soil*	*Average general penetration (mm year^{-1})*	
		1.37 m	*0.6 m*
Benfleet	London clay	0.0185	0.0361
Gotham	Keuper marl	0.0132	0.0094
Pitsea	Alluvium	0.0353	0.0284
Rothamsted	Clay with flints	0.0201	0.0213

Source: Romanoff, M. Corrosion of steel piling in soils, National Bureau of Standards Monograph no. 58 (October 1962).

The maximum corrosion rate reported in tests carried out in the USA was ~70 μm year^{-1},[153,157] while the maximum rates obtained in tests carried out in the UK were between 35 and 50 μm year^{-1}.[156] However, the localized corrosion was much greater, with maximum rates of 250 μm year^{-1} reported from American, and 300 μm year^{-1} from British, tests.

3.01.6.2 Corrosion of Buried Steel

3.01.6.2.1 Piling

Unprotected steel is frequently used in construction as pilings for foundations and soil retention. This is because any protective coating is almost certainly going to be removed by abrasion during the piling operations. Generally, undisturbed soil and earth should have relatively low oxygen content and, hence, steel should have a relatively low corrosion rate. As noted above, **Table 19**, corrosion rates in a variety of different undisturbed soil types are indeed generally quite low, from ~10 to 35 μm year^{-1}.

Examinations of steel pilings recovered after considerable times of exposure have confirmed that the average corrosion rate is indeed acceptably low. Romanoff's study in the USA found that the load-bearing capacity of the pilings was not compromised.[158] Studies in the UK on pilings removed from the ground after up to 85 years service found that they were in excellent condition with an estimated average corrosion rate of the order of 10 μm year^{-1} with occasional rates up to 30 μm year^{-1}.[159] On the land (fill) side of piled harbor walls (i.e., in disturbed soil) the corrosion rates were about twice those found for undisturbed soil, but this is still

relatively low. A systematic study in Japan over 10 years showed that the corrosion of piles was not linear with time but was initially high and tended to decrease after time to a long-term rate that was ~10 μm year^{-1}.[160] In Australia, 52 year-old piles from Port Adelaide were removed and the average corrosion rate below the mud line was found to be ~30 μm year^{-1}.[161,162] What also seems clear from this historic data is that microbial corrosion did not seem to be of a significant risk provided the soil was undisturbed.[149]

3.01.6.2.2 Pipelines

Buried pipe, whether of steel or cast iron, are invariably coated and additionally protected by a cathodic protection system. It is not proposed to discuss this topic further here except, for completeness, to note the occurrence, during cathodic protection, of intergranular stress corrosion cracking in carbonate–bicarbonate environments and transgranular stress corrosion cracking of higher strength pipeline steels at neutral pH.

3.01.6.2.3 Long-term burial

Research on the nature of corrosion product layers on historic buried artefacts is an important component in understanding the progress of corrosion and in the modeling of proposed nuclear waste repositories. Most repository designs comprise a multibarrier system that consists of immobilized (e.g., vitrified) nuclear waste packed into a metallic container that is, in turn, emplaced into a suitable geological repository and backfilled with clay buffer layer. This design is expected to be initially relatively oxidizing (aerated) but will eventually become anaerobic. Since the function of the metal container is to prevent contact between the groundwater and the radioactive wastes for as long as possible, knowledge of the corrosion processes, including the expected corrosion products likely to form, are essential in order to provide a credible model of long-term corrosion over hundreds to thousands of years.

In the United Kingdom, historic iron commonly arises from the period of Roman occupation and later, with the most frequent artefact comprising iron nails. In Europe, buried iron can be found from much earlier. Commonly identified corrosion products include all those that might be expected to form, **Table 4**. In most buried environments the corrosion sequence commences with the development of 'green rusts,' which are mixed oxy-hydroxides of iron containing Fe (+2/+3) species and incorporating typically, carbonate, chloride or sulfate depending on the environment.[163] Generally, depending on local conditions of aeration and pH, this oxidizes further to form magnetite, maghemite, lepidocrocite or goethite; while in high chloride (e.g., marine) environments, akaganéite also forms. In anaerobic, waterlogged, conditions at higher pH (carbonated), siderite (iron carbonate) is a common corrosion product,[164] while at lower pH, vivianite (hydrated iron phosphate) has occasionally been observed.[165]

References

1. Tylecote, R. F. *A History of Metallurgy*; Institute of Materials, 1992.
2. Micrographs appear by kind permission of R.F. Cochrane, University of Leeds and the DoITPoMS Micrograph Library, University of Cambridge.
3. Llewellyn, D. T.; Hudd, R. C. *Steels: Metallurgy and Applications*; Butterworth-Heinemann, 1998.
4. Bhadeshia, H. K. D. H.; Honeycomb, R. W. K. *Steels: Microstructure and Properties*, 2nd ed.; Edward Arnold, 1995.
5. *Steel Heat Treatment Handbook*; Totten, G. E., Howes, M. A. H.; CRC Press, 1997.
6. Hudson, J. C.; *The Corrosion of Iron & Steel*; Chapman and Hall: London, 1940; p 61.
7. Larrabee, C. P.; Coburn, S. K. Proceedings of the 1st International Congress on Metal Corrosion, 1961; pp 276, Butterworths: London, 1962.
8. Sixth Report of the Corrosion Committee, Spec. Rep. No. 66, Iron and Steel Institute: London, 1959.
9. Hudson, J. C. *J. Iron Steel Inst.* **1950**, *166*, 123.
10. Mor, E. D.; Travesc, E.; Ventora, G. *Br. Corros. J* **1976**, *11*, 40.
11. Songa, T. International Conference on Steel in Marine Structures, Paris, ECSC: Luxembourg 1981.
12. Forgeson, B. W.; Southwell, C. R.; Alexander, A. L. *Corrosion* **1960**, *16*, 105t.
13. Hudson, J. C.; Banfield, T. A.; Holden, H. A. *J. Iron Steel Inst.* **1942**, *146*, 107.
14. Romanoff, M. *Underground Corrosion, National Bureau of Standards Circular 579*; US Government Printing Office: Washington, 1957.
15. Bockris, J. O'M.; Conway, B. E. *J. Phys. Colloid Chem.* **1949**, *53*(4), 527–539.
16. Bockris, J. O. 'M.; Drazic, D. M. *Electrochim. Acta* **1962**, *7*(3), 293–313.
17. Bockris, J. O. 'M.; Drazic, D. M.; Despic, A. R. *Electrochim. Acta* **1961**, *4*(2–4), 325–361.
18. Despic, A. R.; Raicheff, R. G.; Bockris, J. O. 'M. *J. Chem. Phys.* **1968**, *49*(2), 926–938.
19. Dražić, D. M.; Hao, C. S. *Electrochim. Acta* **1982**, *27*(10), 1409–1415.
20. Drazić, D. M.; Zećević, S. K. *Corros. Sci.* **1985**, *25*(3), 209–216.
21. El Miligy, A. A.; Geana, D.; Lorenz, W. J. *Electrochim. Acta* **1975**, *20*(4), 273–281.
22. Lorbeer, P.; Lorenz, W. J. *Electrochim. Acta* **1980**, *25*(4), 375–381.
23. Hackerman, N.; Stephens, S. J. *J. Phys. Chem.* **1954**, *58* (10), 904–908.
24. Drazic, D. M. In *Modern Aspects of Electrochemistry*; Conway, B. E., Bockris, J. O. M., White, R. E., Eds.; Plenum Press: New York, 1989; Vol. 19, p 69.

25. Walpert, G. *Z. Phys. Chem.* **1930**, *A.151*, 219.
26. Jeyaprabha, C.; Sathiyanarayanan, S.; Muralidharan, S.; Venkatachari, G. *J. Braz. Chem. Soc.* **2006**, *17*(1), 61–67.
27. Etzold, U.; Mohr, K. P.; Hulser, P. 38th Seminario de Laminacao Processos e Produtos Laminados e Revestidos; Florianopolis, SC; Brazil; 24–26 Oct. 2001, pp 210–223.
28. Keir, J. *Phil. Trans. R. Soc.* **1790**, *80*, 359–384.
29. Schonbein, C. F.; Faraday, M. *Phil. Mag.* **1836**, *9*, 53; 57; 122.
30. Kim, J. S.; Cho, E. A.; Kwon, H. S. *Corros. Sci.* **1989**, *29*, 183.
31. Nagayama, M.; Cohen, M. *J. Electrochem. Soc.* **1962**, *109*, 791.
32. Vetter, K. J.; Gorn, F. *Electrochim. Acta* **1973**, *18*, 321–326.
33. O'Grady, W. E. *Electrochim. Acta* **1980**, *127*, 555.
34. Eldridge, J.; Kordesch, M. E.; Hoffman, R. W. *J. Vac. Sci. Technol.* **1982**, *20*, 934.
35. Graham, M. J.; Bardwell, J. A.; Goetz, R.; Mitchell, D. F.; MacDougall, B. *Corros. Sci.* **1990**, *31*, 139–148.
36. Davenport, A. J.; Sansone, M. *J. Electrochem. Soc.* **1995**, *142*, 7254.
37. Ryan, M. P.; Newman, R. C.; Thompson, G. E. *J. Electrochem. Soc.* **1995**, *142*, L177.
38. Toney, M. F.; Davenport, A. J.; Oblonsky, L. J.; Ryan, M. P.; Vitus, C. M. *Phys. Rev. Lett.* **1997**, *79*, 4282–4285.
39. Hendy, S.; Walker, B.; Laycock, N.; Ryan, M. *Phys. Rev. B* 2003, 67, 085407.
40. Vera, J.; Kapusta, S.; Hackerman, N. *J. Electrochem. Soc.* **1986**, *133*(3), 461–467.
41. Froment, M.; Keddam, M.; Morel, P. *Compt. Rend.* **1961**, *253*, 2529.
42. Dugstad, A. Proceedings CORROSION'98; Paper No. 31; NACE: Houston, TX, 1998.
43. Bockris, J. O. 'M.; Reddy, A. K. N.; Gamboa-Aldeco, M. *Modern Electrochemistry* Springer: Berlin, 2001; Vol. 2b, p 1670.
44. Jovancicevic, V.; Bockris, J. O. 'M. *J. Electrochem. Soc.* **1986**, *133*, 1797–1807.
45. Levich, V. C. *Physicochemical Hydrodynamics*; Prentice-Hall: NJ, USA, 1962.
46. Udo Schwertmann; Cornell, Rochelle M. *The Iron Oxides: Structure, Properties, Reactions, Occurences and Uses*; Wiley-VCH: London, 2003.
47. Wranglen, G. *Corros. Sci.* **1969**, *9*(8), 585–592; 593–602.
48. Shifler, D. A.; Moran, P. J.; Kruger, J. *Electrochim. Acta* **1997**, *42*(4), 567–577.
49. Reformatskaya, I. I.; Rodionova, I. G.; Beilin, Yu. A.; Nisel'son, L. A.; Podobaev, A. N. *Prot. Met.* **2004**, *40*(5), 447–452.
50. Rothwell, G. P. *Corros. Prevention Control* **1979**, *26*(3), 9–13.
51. Bardwell, J. A.; MacDougall, B. *J. Electrochem. Soc.* **1988**, *135*, 2157.
52. Bardwell, J. A.; MacDougall, B.; Graham, M. J. *Corros. Sci.* **1991**, *32*, 139.
53. Mitrovic-Scepanovlc, V.; MacDougall, B.; Graham, M. J. *Corros. Sci.* **1984**, *24*, 479.
54. Li, L. *Corrosion* **2001**, *57*(1), 19–28.
55. Alonso, C.; Castellote, M.; Andrade, C. *Electrochim. Acta* **2002**, *47*(21), 3469–3481.
56. Vera, J.; Kapusta, S.; Hackerman, N. *J. Electrochem. Soc.* **1986**, *133*, 461–467.
57. Standard Guide for Development and Use of a Galvanic Series for Predicting Galvanic Corrosion Performance; ASTM G82–98, 2009.
58. Buecker, B. *Power Eng.* **2002**, *106*(9), 32–34.
59. Buecker, B. *Power Eng.* **2007**, *111*(7), 20–24.
60. Alan V. Levy *Solid Particle Erosion and Erosion–Corrosion of Materials*; ASM International, 1995.
61. Jones, D. D. *Corros. Technol. (Anti-Corros. Methods Mater.)* **1957**, *4*(2), 56–59.
62. Huy, Ha Le; Ghali, E. *Corros. Sci.* **1993**, *35*(1–4), 435–442.
63. Yeske, R. *Caustic Stress Corrosion Cracking Of Carbon Steels,* A Supplement To: Stress Corrosion Cracking Of Continuous Digesters, The Institute Of Paper Chemistry Appleton, Wisconsin, USA, Project 3589, October 17, 1986.
64. Parkins, R. N. *Fundamental Aspects of Stress Corrosion Cracking,* Proceedings of NACE Conference **1969**, p 361.
65. Zhagalya, N. N.; Marchak, I. I.; Melekhov, R. K. *Mater. Sci.* **1975**, *9*, 342–344.
66. Bandyopadhyay, N.; Briant, C. L. *Scr. Metall.* **1982**, *16*(8), 939–941.
67. Payer, J. H.; Berry, W. E.; Parkins, R. N. In *Stress Corrosion Cracking – The Slow Strain Rate Technique*; ASTM STP 665; Ugiansky, G. M., Payer, J. H., Eds.; American Society for Testing and Materials: Philadelphia, PA, 1979; pp 222–234.
68. Garverick, L. *Corrosion in the Petrochemical Industry*; ASM International, 1994; pp 212–213.
69. Farrow, K.; Hutchings, J.; Sanderson, G. *Br. Corros. J.* **1981**, *16*(1), 11–19.
70. Little, B. J.; Lee, J. S. *Microbiologically Influenced Corrosion*; Wiley: London, 2007.
71. Mrowec, S.; Podgorecka, A. *J. Mater. Sci* **1987**, *22*, 4181–4189.
72. Chen, R. Y.; Yuen, W. Y. D. *Oxid. Met.* **2003**, *59*(5–6), 433–468.
73. Picard, A.; Fang, H. *Metrologia* **2004**, *41*, 333–339.
74. Schwartz, R. *Metrologia* **1994**, *31*, 117–128.
75. Vernon, W. H. J. *Trans. Faraday Soc.* **1935**, *31*(1), 668.
76. Gdowski, G. E.; Estill, J. C. Proceedings Materials Research Society Fall Meeting, Nov. 27, Dec. 1, 1995.
77. European Council Directive 1999/30/EC of 22 April 1999: Limit values for sulphur dioxide, nitrogen dioxide and oxides of nitrogen, particulate matter and lead in ambient air.
78. Smith, S. J.; Conception, E.; Andres, R.; Lurz, J. Historical Sulfur Dioxide Emissions 1850–2000: Methods and Results, U.S. Department of Energy, Contract DE-AC06–76RL01830.
79. Vannerberg, N. G. *Electrochem. Soc.* **1978**, Pittsburg 78–82, (Extended abstract p. 314).
80. Walton, J. R.; Johnson, J. B.; Wood, G. C. *Br. Corros. J.* **1982**, *17*, 59.
81. Chandler, K. A.; Kilcullen, M. B. *Br. Corr. J.* **1968**, *3*, 80–84.
82. Sydberger, T.; Vannerberg, N.-G. *Corros. Sci.* **1972**, *12*, 775–784.
83. Chandler, K. A.; Stanners, J. F. *Proceedings of 2nd International Congress of Metallic Corrosion*; NACE: Houston, Tx, 1963; p 325.
84. Tanner, A. R. *Chem. Ind.* **1964**, *1*, 027.
85. Schikorr, G. *Werkstoffe Korros.* **1963**, *14*(2), 69.
86. Schwartz, H. *Werkstoffe Korros.* **1965**, *16*(3), 208.
87. Schikorr, G. *Korros. Metall.* **1941**, *17*, 305–313.
88. Chandler, K. A.; Stanners, J. F. *Proceedings of 2nd International Congress of Metallic Corrosion*; NACE: Houston, 1963; p 325.
89. Arroyave, C.; Morcillo, M. *Corros. Sci.* **1995**, *37*(2), 293–305.
90. Katoh, K.; Yasukawa, S.; Nishimura, H.; Yasuda, M. *Boshoku Gijursu* **1981**, *30*, 337.
91. Haynie, F. H., Spence, J. W., Upham, J. B. In *Atmospheric Factors Affecting the Corrosion of*

Engineering Metals; ASTM STP 646, 1978: Philadelphia, p. 30.
92. Eriksson, P.; Johansson, L.-G. Proceedings of 10th Scandinavian Corrosion Congress Stockholm 1986; p 43.
93. Johansson, L.-G. In *Proceedings of Symposium: Corrosion Effects of Acid Deposition and Corrosion of Electronic Materials*; Mansfeld, F., Kucera, V., Haagenrud, S. E., Haynie, F. H., Sinclair, J. D., Eds.; The Electrochemical Society: Pennington, 1986; p 267.
94. Oesch, S. *Corros. Sci.* **1996**, *38*, 1357–1368.
95. Askey, A.; Lyon, S. B.; Thompson, G. E.; Johnson, J. B.; Wood, G. C.; Cooke, M.; Sage, P. *Corros. Sci.* **1993**, *34* (2), 233–247.
96. Ross, T. K.; Callaghan, B. G. *Corros. Sci.* **1966**, *6*, 337.
97. Chandler, K. A. *Br. Corros. J.* **1966**, *1*, 264–266.
98. Evans, U. R.; Taylor, C. A. J. *Br. Corros. J.* **1974**, *9*(1), 26–28.
99. Cole, I. S.; Ganther, W. D.; Paterson, D. A.; King, G. A.; Furman, S. A.; Lau, D. *Corros. Eng. Sci. Technol.* **2003**, *38*(4), 259–266.
100. Cole, I. S.; Lau, D.; Paterson, D. A. *Corros. Eng. Sci. Technol.* **2004**, *39*(3), 209–218.
101. Walton, J. R.; Johnson, J. B.; Wood, G. C. *Br. Corros. J.* **1982**, *17*(2), 59–64; 65–70.
102. Ngai T. Lau; Chan K. Chak; Lap I. Chan; Ming Fang *Corros. Sci.* **2008**, *50*(10), 2927–2933.
103. Askey, A.; Lyon, S. B.; Thompson, G. E.; Johnson, J. B.; Wood, G. C.; Sage, P. W.; Cooke, M. J. *Corros. Sci.* **1993**, *34*(7), 1055–1081.
104. Schikorr, G. *Werkstoffe Korros.* **1963**, *14*, 69; **1964**, *15*, 457; **1967**, *18*, 514.
105. Barton, K.; Kuchynka, D.; Beranek, E. *Werkstoffe Korros.* **1978**, *29*, 199–201.
106. Weissenrieder, J.; Kleber, C.; Schreiner, M.; Leygraf, C. *J. Electrochem. Soc.* **2004**, *151*(9), B497–B504.
107. Evans, U. R. *Trans. Inst. Met. Finish* **1960**, *37*, 1.
108. Evans, U. R.; Taylor, C. A. J. *Corros. Sci.* **1972**, *12*(3), 227–246.
109. Stratmann, M.; Bohnenkamp, K.; Engell, H.-J. *Corros. Sci.* **1983**, *23*(9), 969–985.
110. Antony, H.; Perrin, S.; Dillmann, P.; Legrand, L.; Chaussé, A. *Electrochim. Acta* **2007**, *52*(27), 754–7759.
111. Stratmann, M.; Bohnenkamp, K.; Engell, H.-J. *Werkstoffe Korros.* **1983**, *34*(12), 604–612.
112. Stratmann, M.; Bohnenkamp, K.; Ramchandran, T. *Corros. Sci.* **1987**, *27*(9), 905–926.
113. Stratmann, M. *Phys. Chem. Chem. Phys.* **1990**, *94*(6), 626–639.
114. Stratmann, M.; Streckel, H. *Corros. Sci.* **1990**, *30*(6–7), 697–714.
115. Shirkhanzadeh, M.; Thompson, G. E.; Lyon, S. B.; Johnson, J. B. *Br. Corros. J.* **1987**, *22*(4), 243–249.
116. Okada, T.; Ishii, Y.; Mizoguchi, T.; Tamura, I.; Kobayashi, Y.; Takagi, Y.; Suzuki, S.; Kihira, H.; Itou, M.; Usami, A.; Tanabe, K.; Masuda, K. *Jpn. J. Appl. Phys.* **2000**, *39*, 3382.
117. García, K. E.; Morales, A. L.; Barrero, C. A.; Greneche, J. M. *Hyperfine Interact.* **2005**, *161*(1–4), 127–137.
118. Sei, J.; Oha, D. C.; Cook, H. E.; Townsend *Corros. Sci.* **1999**, *41*, 1687–1702.
119. Awad, G. H.; Abdel Halim, F. M.; El Arabi, R. M. *Br. Corros. J.* **1980**, *15*, 140.
120. Biefer, G. J. Exploratory corrosion tests in the Canadian Arctic, Canada Centre for Mineral and Energy Technology (CANMET), Ottawa Report, 1977, 77-45.
121. Dearden, J. *J. Iron Steel Inst.* **1948**, *159*, 241.
122. Larrabee, C. P. *Trans. Electrochem. Soc.* **1944**, *85*, 297.
123. Laque, F. L. *Mater. Perf.* **1982**, *21*, 17.
124. Zhang, Q. C.; Wua, J. S.; Wang, J. J.; Zheng, W. L.; Chen, J. G.; Li, A. B. *Mater. Chem. Phys.* **2003**, *77*(2), 603–608.
125. Dean, S. W. In *Degradation of Materials in the Atmosphere, ASTM STP 965*; Dean, S. W., Lee, T. S., Eds.; American Society for Testing and Materials: Philadelphia, PA, 1988; pp 385–431.
126. Dean, S. W. In *Atmospheric Corrosion, STM STP 1239*; Kirk, W. W., Lawson, H. H., Eds.; American Society for Testing and Materials, 2002; pp 3–18.
127. Dean, S. W.; Reiser, D. B. In *Outdoor Atmospheric Corrosion, ASTM STP 1421*; Townsend, H., Ed.; American Society for Testing and Materials, 2002; pp 3–18.
128. Mikhailov, A. A.; Tidblad, J.; Kucera, V. *Prot. Met.* **2004**, *40*(6), 541–550.
129. Cai, J.-P.; Lyon, S. B. *Corros. Sci.* **2005**, *47*(12), 2956–2973.
130. Edwards, A. M. Proceedings of Symposium on Developments in Methods of Prevention and Control of Corrosion in Buildings; British Iron and Steel Federation: London, 1966.
131. Larrabee, C. P.; Coburn, S. K. Proceedings of First International Congress on Metallic Corrosion; Butterworths: London, 1962; p 276.
132. Hooper, R. A. E.; Lee, B. V. Proceedings of 12th International COR-TEN Conference, Florida, 1985; United States Steel: Pittsburgh.
133. Kamimura, T.; Nasu, S.; Segi, T.; Tazaki, T.; Morimoto, S.; Miyuki, H. *Corros. Sci.* **2003**, *45*(8), 1863–1879.
134. Albrecht, P. In *Corrosion Forms and Control for Infrastructure ASTM STP 1137*; Chaker, V., Ed.; American Society for Testing and Materials: Philadelphia, PA, 1992; pp 108–125.
135. Kamimura, T.; Stratmann, M. *Corros. Sci.* **2001**, *43*, 429–447.
136. Kimura, M.; Kihira, H.; Ohta, N.; Hashimoto, M.; Senuma, T. *Corros. Sci.* **2005**, *47*, 2499–2509.
137. Kihira, H.; Ito, S.; Mizoguchi, T.; Murata, T.; Usami, A.; Tanabe, K. *Zairyo-to-Kankyo* **2000**, *49*, 30.
138. BS EN 12500: Protection of metallic materials against corrosion: Corrosion likelihood in atmospheric environment, classification, determination and estimation of corrosivity of atmospheric environments.
139. de Waard, C.; Milliams, D. E. *Corrosion* **1975**, *31*(5), 177.
140. Langelier, W. F. *J. Am. Water Works Assoc.* **1946**, *38*, 169–178.
141. Friend, J. N. *18th Report of the Committee of the Institution of Civil Engineers on the Deterioration of Structures of Timber*; Metal and Concrete Exposed to the Action of Sea Water: London, 1940.
142. Hudson, J. C.; Stanners, J. F. *J. Iron Steel Inst.* **1955**, *180*, 271.
143. Baudot, H.; Chaudron, G. *Rev. Met.* **1946**, *43*, 1.
144. *Internal Corrosion of Water Distribution Systems*, 2nd ed.; American Water Works Assocation, 1996.
145. Larson, T. E. *Corrosion by Domestic Waters, Bulletin 59*; Illinois State Water Survey, 1975.
146. Hu, J. Y.; Yu1, B.; Feng, Y. Y.; Tan, X. L.; Ong, S. L.; Ng, W. J.; Hoe, W. C. *Biofilms* **2005**, *2*, 19–25.
147. McReynolds, G. S. *Mater. Perf.* **1998**, *37*(7), 45–48.
148. Martini, A.; Mennenoh, S. *Stahl und Eisen*; **1981**, *10*(1).
149. Morley, J. *Struct. Survey* **1989**, *7*(2), 138–151.
150. Marsh, C. P.; Bushman, J.; Beitelman, A. D.; Buchheit, R. G.; Little, B. J. Freshwater Corrosion in the Duluth-Superior Harbor-Summary of the Initial Workshop Findings, Special publication ERDC/CERL SR-05–3, U.S; Army Corps of Engineers, 2005.

151. Beech, I. B.; Campbell, S. A. *Electrochim. Acta* **2008**, *54*, 14–21.
152. Buecker, B. *Power Plant Water Chemistry: A Practical Guide*; Pennwell Books: USA, 1997.
153. Romanoff, M. Underground Corrosion, National Bureau of Standards, Circular 579, Washington, 1957.
154. Hudson, J. C.; Acock, J. P. Symposium on the Corrosion of Buried Metals, The Iron & Steel Inst., Special Report No. 45, London, 1952.
155. Ismail, A. I. M.; El-Shamy, A. M. *Appl. Clay Sci.* **2009**, *42*, 356–362.
156. Hudson, J. C.; Watkins, K. O. BISRA Open Report No MG/B/3/68.
157. Romanoff, M. *J. Res. Natl. Bur. Stand* **1962**, *60*, 223–224.
158. Romanoff, M. Corrosion of steel piling in soils, National Bureau of Standards Monograph no. 58 (October 1962).
159. Morley, J. *Br. Corros. J.* **1986**, *21*, 177–183.
160. Ohsaki, Y. *Soils Found* **1982**, *22*(3).
161. Eadie, G. F. The Durability of Piles in Soils, Conference Paper 19, Australasian Corrosion Association, Perth, Western Australia (November 1979).
162. Eadie, G. R.; Kinson, K. Examination of Steel Piling Recovered from Port Adelaide after 52 Years' Service, Conference Paper 20, Australasian Corrosion Association, Adelaide, South Australia, (November 1980).
163. Neff, D.; Dillmann, P.; Bellot-Gurlet, L.; Beranger, G. *Corros. Sci.* **2005**, *47*, 515–535.
164. Matthiesen, H.; Hilbert, L. R.; Gregory, D. J. *Stud. Conservation* **2003**, *48*(3), 183–194.
165. Booth, G. H.; Tiller, A. K.; Wormwell, F. *Corros. Sci.* **1962**, *2*(3), 197–202.

3.02 Corrosion of Cast Irons

A. Reynaud
Centre Technique des Industries de la Fonderie, 44, av. de la Division Leclerc, F-92318 Sèvres Cedex, France

Glossary

Cast iron An alloy of iron with >1.7% carbon and including appreciable amounts of silicon and other elements. Compared with carbon steel, cast iron has a relatively low melting point and high fluidity permitting it to be cast into complex shapes.

Ductile or SG iron A form of cast iron in which the carbon is present as nodular spheroids of graphite and, consequently the iron is ductile.

Durichlor A high-silicon iron containing a minimum of 14.5% silicon with additions of chromium and molybdenum and optimised for service in hydrochloric acid.

Duriron A high-silicon iron containing a minimum of 14.5% silicon exhibiting extreme abrasion resistance and chemical resistance in acids.

Gray or LG iron A form of cast iron with a relatively high silicon content (> ~2%) in which the carbon is present as lamellar graphitic (LG) flakes; generally gray iron is brittle and fails with little or no ductility.

Hypersilid A high silicon iron containing from 14–18% silicon and similar to Duriron in performance and usage.

Malleable Iron A form of white cast iron that is traditionally produced by subjecting a casting to extended periods of heat treatment, this results in the nucleation of graphite in a nonlamellar form and, consequently, the iron is ductile (malleable).

Ni-Resist A form of cast iron containing sufficient nickel such that the iron is able to retain the austenite phase structure at room temperature, consequently, Ni-Resist is heat-resistant and relatively corrosion resistant compared with LG or SG irons.

White iron A form of cast iron of relatively lower silicon content in which the carbon is present as carbides and, consequently, white iron is extremely hard and abrasion resistant.

Abbreviations

ASTM American Society for Testing and Materials

BCIRA British Cast Iron Research Association (former body, no longer in operation)

BS British Standard

EN European Norm
ETIF Editions Technique des Industrie de le Fonderie
LG Lamellar graphitic
LSI Langelier saturation index
SG Spheroidal graphitic

3.02.1 General Introduction

Cast iron is the term applied to a wide range of ferrous alloys, whose principal distinguishing feature is carbon content in excess of ~1.7%. Cast iron can also be thought of as a composite material consisting of precipitated graphite or carbide particles in a metal matrix. The two major types of graphite morphology are flake, associated with gray iron and spherical (nodular), associated with ductile iron. While the properties of steel grades are determined (in addition to the composition) primarily by thermo–mechanical treatment, the properties of cast iron are controlled by inoculation, solidification, and cooling rate as well as alloy composition.

Four main types of iron are commonly encountered:

- white iron in which all the carbon is present in a metal carbide phase;
- gray iron in which most of the carbon is present as graphite flakes;
- nodular or ductile iron in which most of the carbon is present as graphite nodules, produced during solidification of the casting; and
- malleable iron in which most of the carbon is present as graphite nodules, produced subsequent to solidification by heat treatment of the casting.

Many properties of cast iron are first influenced by the form in which the carbon is present; that is, as graphite or as carbide and secondly by whether the matrix material is ferritic or pearlitic.

3.02.1.1 White Cast Iron

In white iron, carbon is in the form of iron carbide in a matrix of pearlite, the amount of which depends on the carbon content of the iron; such materials are hard and brittle. Alloying of white iron is possible and results in the formation of alloy carbides that are even harder and ideal for hard and abrasion-resistant applications such as extrusion dies and cement mixer liners.

3.02.1.2 Gray Cast Iron

Gray cast irons are by far the oldest and most common form of cast iron. Gray iron, named because of its characteristic fracture surface, has a gray appearance and consists of carbon in the form of flake graphite in a matrix consisting usually of pearlite or ferrite or a mixture of the two. The fluidity of liquid gray iron and its expansion during solidification due to the formation of graphite, has traditionally been ideal for the economical production of shrinkage-free, intricate castings such as motor blocks. These alloys are often known as lamellar graphitic (LG) cast irons; a sketch of the typical arrangement of lamellar graphite is shown in Figure 1.

Gray iron exhibits essentially no elastic behavior, and fails under tension without significant plastic deformation. The mechanical properties of gray cast iron result from the effects of chemical composition and the cooling history. In general, as the combined equivalent of carbon and silicon is reduced the strength of the cast iron is increased. For thicker sections requiring tensile strengths above 350 MPa, additions of chromium, nickel or molybdenum alloys are required.

The presence of graphite flakes gives gray iron an excellent machinability, damping, and self-lubricating characteristics. Consequently, gray cast iron has an outstanding resistance to sliding wear and has been used very successfully for sliding surfaces including cylinder bores, piston rings, and machine tools. Due to the effect of the graphite flakes, gray cast iron has an excellent resistance to galling and seizing, and has a low coefficient of friction. Finally, gray cast irons have an excellent capacity for absorbing

Figure 1 Sketch of lamellar (flake) graphite in cast iron.

vibration energy, and thus damping vibrations. This property is most evidenced with those materials with a high percentage of graphite flakes.

3.02.1.3 Malleable Cast Iron

Malleable irons are initially manufactured as white irons and subsequently heat treated in order to convert the carbide into graphite, which nucleates and grows from individual locations giving a more compact, nonlamellar form. Malleable irons are produced by two different processes, which result in either a ferrite or a pearlite matrix depending on the process adopted; however, even the pearlitic form is usually produced with a surface layer of ferrite. In malleable irons, the presence of graphite in a more compact or sphere-like form gives the material greatly increased ductility with tensile and yield strengths almost equal to cast, low-carbon steel.

3.02.1.4 Ductile Cast Iron

Ductile cast irons are similar to gray cast irons but have small amounts of alloying addition (e.g., magnesium) that promote the formation of carbon in a nodular form rather than as graphite flakes; they are often known as spheroidal graphitic (SG) irons or nodular graphitic irons; a schematic microstructure is shown in Figure 2. Ductile iron generally solidifies with a pearlite matrix, but in order to develop the full ductility of the iron, the castings are often subsequently annealed to give a ferrite matrix. They have properties similar to that of gray irons with a relatively low melting point (compared with steels), good fluidity, castability, excellent machinability, and wear resistance. However, compared to gray cast iron they have improved strength, toughness, and hot workability. Moreover, the nodular forms of graphite result in greatly increased facture toughness and offer the designer the option of choosing high ductility (with some grades guaranteeing more than 18% elongation), or high strength (with some tensile strengths exceeding 800 MPa).

Figure 2 Sketch of spheroidal graphite in cast iron.

3.02.1.5 Alloy Cast Irons

The properties of both white and gray cast irons can be altered and enhanced by the inclusion of alloying elements such as nickel, chromium, molybdenum, and silicon. For example, 4–5% nickel and 1.2% chromium additions are used to increase hardness and mechanical properties. Alloys containing over 14–25% nickel, are austenitic and have good heat and corrosion resistance. Alloys with 25–35% chromium result in a 'stainless' cast iron with good corrosion and high temperature properties, while irons containing up to 16% silicon offer enhanced hardness and excellent corrosion resistance at the expense of mechanical properties.

3.02.2 Production, Composition, and Microstructural Effects

A cast iron is an alloy of iron that contains 2–4% carbon, along with varying amounts of silicon and manganese and traces of impurities such as sulfur and phosphorus. The relatively low melting point of these alloys compared with that of steel and their tendency to expand slightly on solidification, which make them admirably suitable for the production of components by casting, result from this feature of their composition. The production of cast iron is relatively unsophisticated and mostly involves remelting charges consisting of pig iron (e.g., from a blast furnace), steel scrap, foundry scrap, and ferroalloys to give the appropriate composition. The composition figures quoted in Table 1 provides a general guide for the range of compositions for the various types of iron. Due to this variation in composition, cast irons are usually specified in terms of their mechanical properties rather than on an analytical basis. Cast iron is used extensively to make machine parts, engine cylinder blocks, stoves, pipes, steam radiators, and many other products.

Table 1 Composition ranges of cast iron alloys (nodular iron additionally: 0.04–0.1% Mg)

	Microstructure		*Carbon (%)*	*Carbide (%)*	*Si (%)*	*Mn (%)*	*S (%)*	*P (%)*
	Graphite	*Matrix*						
White iron	None	Pearlite	1.7–3.0	100%	0.8–1.3	0.4	<0.15	<0.5
Gray iron	Flake	Pearlite	2.7–4.0	<1	0.5–3.3	0.3–1.0	<0.15	<1.4
Nodular	Nodular	Pearlite/ferrite	3.3–3.9	<1	1.6–2.5	0.4	<0.01	<0.1
Malleable (blackheart)	Nodular	Ferrite	2.0–2.7	None	0.8–1.2	0.1–0.6	<0.15	<0.2
Malleable (whiteheart)	Nodular	Pearlite	3.3–3.9	0–1	0.3–0.8	0.1–0.5	<0.4	<0.1

3.02.2.1 Effect of Microstructure on Corrosion Resistance

The essential difference between the corrosion of cast iron and steel arises from the fact that cast iron contains in its microstructure several more or less corrosion-resistant phases that are largely or completely absent from steel. The most important of these corrosion-resistant phases are: graphite, phosphide eutectic, and, to a lesser extent, carbides, and carbide eutectic (i.e., pearlite). A close observation of the corrosion products of cast iron[1] can distinguish two distinct layers (see **Figure 3**).

The base layer, exactly occupying the place and volume of the original corroded metal and hence, sometimes called the 'topotaxial layer,' contains the inert, noncorroding elements of the cast iron, the graphite, in particular, possibly the phosphorous eutectic, and a few carbides for which the initial shape and distribution are preserved. The pores resulting from the selective attack of the ferrous matrix are generally filled by corrosion products of iron; additionally, the oxidation products of silicon (e.g., silicic acid) contribute to cohesion. This layer, which has no equivalent in steel, is often called the layer of 'graphitic corrosion residue.' This is because the species it contains, and which can most readily be identified (by X-rays), is graphite. This also explains terms such as graphitosis, graphitization, graphitic, or spongy corrosion, etc, that are often used to describe this form of corrosive attack.

The outer surface layer (epitaxial layer), which develops from the initial surface of the iron casting, results from the reaction of iron ions (Fe^{2+}), migrating through the graphitic layer from the underlying residual metal. This layer often takes the form of a voluminous gangue (up to 3.7 times the volume of iron lost to corrosion). It may also contain elements from the corrosive environment, either by incorporation, in the case of a solid aggressive medium (case of soils), or by precipitation, in the case of a liquid aggressive medium (e.g., calcareous rust). This layer (which has some protective capacity), thus, has variable density depending on the nature of the surrounding medium. Also, the layer may not even exist if the products of the reaction between the iron and the corrosive medium can be eliminated as they form, for example by an erosive action, or if they are immediately soluble.

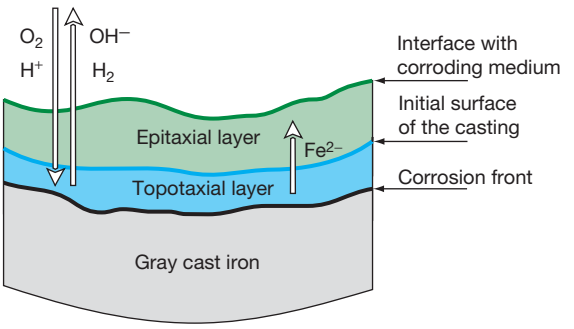

Figure 3 Schematic diagram showing layers of corrosion on gray cast iron. Based on a diagram by Tsuda M.; Murata Y., *IMONO*, **1982**, *54*, 605–611 and reproduced with permission from Reynaud, A. *Corrosion and Cast Iron*, ETIF, France, 2008.

These two layers are clearly distinct in both appearance and composition; one contains essential corrosion residues, while the other contains corrosion products. They can be separated more or less readily from one another (by scraping or as a result of an impact). Thus, after elimination of the outer layer of corrosion products, the casting most often appears in its initial form and may mask the actual extent of corrosion damage, which can be revealed only by sand blasting or by special measurements (ultrasound). The layer of corrosion products, consisting essentially of various hydrated iron oxides, is rather similar to the layer of

corrosion products that would form under the same conditions on steel.[2] However, it is anchored in a very different manner: in the case of steel, this layer develops from the evolving active corrosion front, while in the case of a cast iron, it develops on the unchanging inert surface of the layer of corrosion residues.

These layers, in particular the layer of corrosion residue, also act as a barrier that retard the progress of corrosion, as can be seen from the schematic representation (**Figure 4**) of the corrosion of a cast iron and of a steel in an acid medium: the graphite, highly cathodic with respect to the iron in an acid medium, at first speeds up the corrosion, then slows it by a barrier effect that limits the exchange between the acid medium and the corrosion front.

The amount of graphitic residue retained on a corroding surface depends partly on the morphology of the graphite and partly on the corrosivity of the medium. In general, coarse flake graphite tends to give a more permeable and less strong residue than finer graphite, while nodules produce an even weaker residue. However, these differences are only clear at very high corrosion rates. For example, while flake graphite iron retains virtually all the graphitic residue when corroded in 0.5% sulfuric acid, the residue from a nodular graphite iron is largely detached; in 0.05% sulfuric acid, however, there is little difference in the amounts retained by the two irons. Also, the effect of graphite on the corrosion of iron depends on the residue thickness – thus in 0.5% acid, graphite stimulates attack on the nodular graphite iron because of its ability to act as an efficient cathode for hydrogen evolution, however, in 0.05% acid, once the residue thickness reaches ~0.1 mm, the attack tends to become stifled.[3]

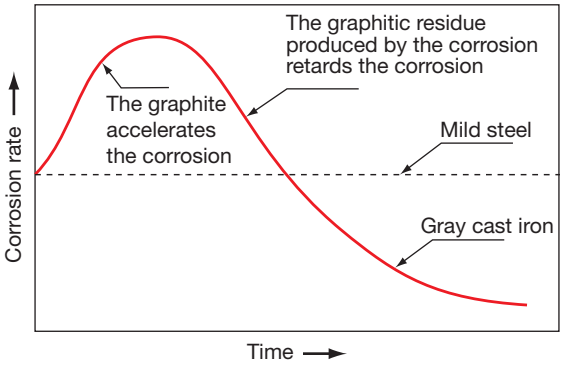

Figure 4 Schematic representation of the corrosion of a cast iron and of a steel in an acid medium. Based on a diagram by Hasson, D.; Karmon, M. *World Water*, **1983** (November), 44–45 and reproduced with permission from Reynaud, A. *Corrosion and Cast Iron*, ETIF, France, 2008.

Also note, that the original geometry of the material is often preserved after graphitic corrosion, unless the corrosion products disintegrate, and that the mechanical strength of this graphitic residue is generally good (especially if the graphite is lamellar). For example, water pipes made of graphitic cast iron, although severely corroded after ~30 years in service can still withstand high water pressures. However, ductile iron or steel pipes have burst under similar conditions. Similarly, some cast iron water pipes of the Château of Versailles are still functioning properly more than three centuries after they were installed (see **Figure 5**).

If the graphite form is spheroidal, the layer of graphitic residue is more friable and mechanically less strong because it receives less support from remaining graphite, which is distributed discretely, rather than continuously. On the other hand, the noncontinuity of graphite in SG cast irons also limits the penetration of the corrosion front, which occurs preferentially at the matrix–graphite interface. Otherwise, the often higher silicon content of spheroidal graphite cast iron implies, that the proportion of silica in the graphitic corrosion residue is slightly

Figure 5 Length of lamellar graphite cast iron water pipe in Versailles (more than three centuries old). Reproduced with permission from Reynaud, A. *Corrosion and Cast Iron*, ETIF, France, 2008.

larger in these materials. Despite these factors, it is important to remember that the slight benefits given by improved mechanical strength of the graphitic residue in lamellar graphite iron must not lead us to overlook the considerable superiority of the mechanical properties of spheroidal graphite cast iron.

3.02.2.2 Influence of Galvanic Couples in the Microstructure

In the case of cast iron, an eminent heterogeneous alloy, there is apparently an involvement of the galvanic couples that exist between the various metallographic phases. In addition to the couples formed with graphite (which is inevitably the cathode), they include, for example, the iron carbide–ferrite and iron phosphide–ferrite couples, which lead to the selective preferential dissolution of the ferrite (because cementite and iron phosphide are relatively noble).

Residues of islands of pearlite and coalesced carbides, after a ferritizing heat treatment of SG cast irons, can also lead to the formation of very fine microcells. This can result in the complete removal of the ferrite matrix, leaving the carbides, the phosphorous eutectic, and in particular the graphite in the corrosion products. Research has shown that SG cast iron has a higher susceptibility to corrosion than LG cast iron because of the magnesium sulfide inclusions (magnesium is used to inoculate the casting to promote formation of graphite nodules).[4,5] A Japanese electrochemical study[6] showed that, in the case of spheroidal graphite cast irons, the resistance to corrosion decreases as the size of the spheroids decreases. In the special case of SG cast irons obtained by stepped quenching, a bainitic microstructure results. The effect of graphite morphology on the corrosion resistance of this type of iron, austempered ductile iron (ADI) as defined for example by European standard BS EN 1564:1997, has shown, by corrosion potential measurements and anodic polarization tests, that in a 0.01 M HCl, the size of the graphite spheroids has little effect on corrosion resistance. Otherwise, corrosion resistance is diminished as the duration of the stepped quenching increases.

Researchers[6] have also studied the corrosion behavior of ADI cast irons as a function of nickel content and of the chill effect. The corrosion tests, in a 1 N NaCl solution, lasted from 12 to 72 h. Mass loss experiments showed that increasing the nickel content increased the corrosion resistance (especially at the longest test duration). The specimens taken in the vicinity of the chill had a greater corrosion resistance, which was attributed to a particular carbide content. Finally, this study reported that the corrosion resistance of ADI cast iron is superior to that of classical pearlitic cast iron.

3.02.3 General Corrosion Behavior

3.02.3.1 Low-Alloy Lamellar or Spheroidal Graphite Cast Irons

Apart from silicon, small variations in the composition of cast irons, or even the addition of minor amounts of alloying elements, generally have little effect on the corrosion resistance. This is illustrated by the work of Graham,[7] which related the corrosive wear of automobile cylinders and piston rings exposed to high sulfur fuels. Thus, iron exposed to 70% sulfuric acid at 130 °C is attacked at rates dependent on its silicon content, the rate being relatively low at below 1% Si but rising to a peak at ~2% Si (**Figure 6**).

Whittaker and Brandes[8] followed up this work, carrying out tests on iron containing small amounts of copper and nickel. The addition of 0.6% Cu to iron containing 2% Si improved the corrosion resistance significantly, but made little difference, or was detrimental, to iron containing less than 1.5% Si. Copper additions also appear to reduce the effect on corrosion of the sulfur content of an iron exposed to acid and the effect is thus lower in low sulfur irons. Since sulfur can stimulate corrosion in acidic

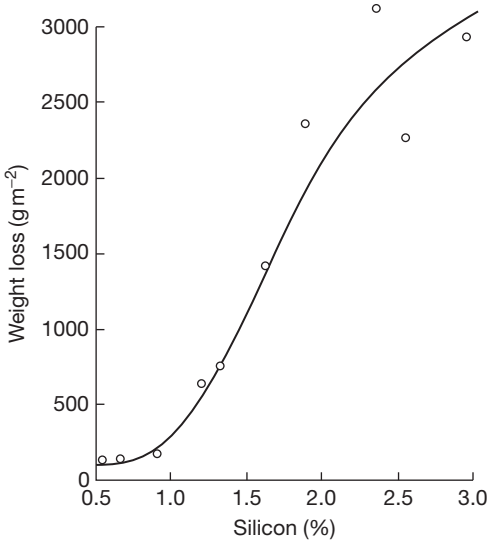

Figure 6 Weight loss for cast iron exposed in 70% H_2SO_4 at 130 °C for 16 h. Reproduced with permission from Graham, R.; Prado, O. S.; Collins, M. H.; Brandes, E. A.; Farmery, H. K. *Proc. Inst. Mech. Eng.* **1960**, *174*, 617.

environments, it is usually kept as low as possible in irons to be used under these conditions; a low sulfur content, is in any case, generally desirable.

3.02.3.2 High-Alloy Cast Irons

Significant additions of such alloy elements as nickel, chromium, and silicon have a great impact on the corrosion resistance of cast irons.[9] They modify the matrix, increasing its corrosion resistance and promote the formation of protective oxide (passive) films. The general outcomes of the most important additions are:

- nickel additions will tend to stabilize austenite;
- chromium cast irons, depending on the levels of chromium, carbon, and other added elements, including nickel, will be ferritic or austenitic;
- silicon cast irons will be ferritic.

3.02.3.2.1 Austenitic nickel cast iron

The addition of ~20% nickel to cast iron produces materials with a stable austenitic structure; these materials are sometimes known as austenitic cast irons but are more often referred to commercially as 'Ni-Resist' cast irons. The austenitic matrix of these irons gives rise to very different mechanical and physical properties compared with those obtained with the nickel-free gray cast irons. The austenitic matrix is more noble than the matrix of unalloyed gray irons, and it was shown in the early work of Vanick and Merica[10] that the corrosion resistance of cast iron increases with increasing nickel content up to ~20% (**Figure 7**).

Although the Ni-Resist irons, due to their austenitic matrix, are tougher and more shock resistant than the nickel-free gray irons, those with carbon in the lamellar graphite form (LG irons) still exhibit certain disadvantages due to the graphite structure. Much better strength and impact properties can be obtained by treating the iron with a small quantity of magnesium sufficient to give a residual content of 0.05–0.1%, which converts the graphite to a spheroidal form (SG irons). The Ni-containing austenitic irons are thus available in both LG and SG forms. The matrix also contains small amounts of second phase carbides, the quantity of which increases with increasing chromium content.

The first alloys in the Ni-Resist series, containing ~20% nickel, were introduced in the 1930s and soon became established in both corrosion and heat resistant applications. The range of alloys has been

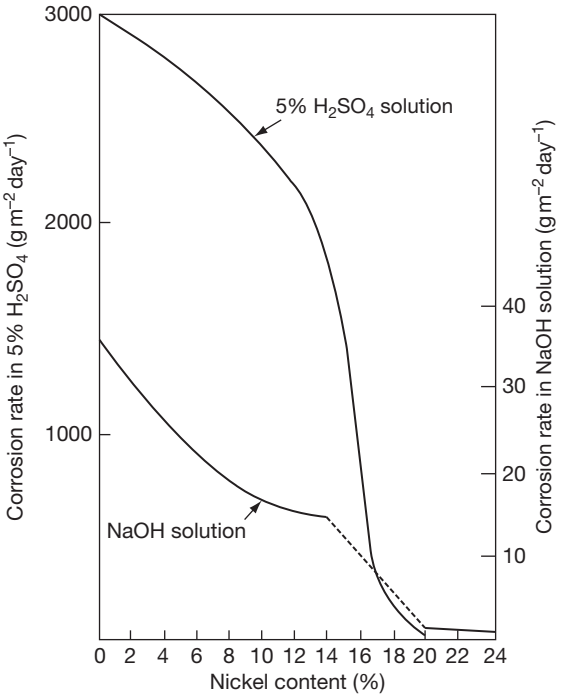

Figure 7 Effect of nickel content on corrosion resistance of cast iron.

extended over the years with nickel contents varying from 13% to 35%. Each material has a somewhat different characteristic such that the most appropriate grade must be selected to obtain the most advantageous properties for any particular application. The compositions and mechanical properties of the principal grades of austenitic cast irons are summarized in **Table 2**. There is no spheroidal austenitic iron corresponding to Type 1 Ni-Resist, since it is difficult to obtain a good spheroidal graphite structure in an austenitic iron containing more than 2% copper. A considerable number of modified grades, differing in both composition and properties from the basic grades, also exist. Specifications for eight commonly used grades of austenitic cast irons are given in BS EN 13835:2002.

The tensile strengths of the spheroidal graphite iron are generally about twice as those of their flake graphite equivalents and can be further improved, by ~80 MPa, by quenching the iron in oil or water from temperatures of 925–1000 °C. This treatment is even more effective when applied to chill castings but the resulting ductility is reduced because of the increased amount of carbide formed as a result of chilling. The impact resistance of the spheroidal graphite grades is much better than that of the equivalent flake graphite

Table 2 Composition and properties of principal grades of flake and spheroidal graphite austenitic case irons

BS 3468 designation	*Ni-resist type*	*Composition (wt%)*						*Minimum tensile strength* ($\times 10^7$ *N m*$^{-2}$)	*Brinell hardness*
		C	*Si*	*Mn*	*Ni*	*Cr*	*Cu*		
AUS101A	Type 1	3.0	1–2.8	1–1.5	13.5–17.5	1.75–2.5	5.5–2.5	170	130–170
AUS102A	Type 2	3.0	1–2.8	0.8–1.5	18–22	1.75–2.5	0.5 max.	170	125–170
AUS105	Type 3	2.6	1–2	0.4–0.8	28–32	2.5–3.5	0.5 max.	170	120–160
—	Type 4	2.6	5–6	0.4–0.8	29–32	4.5–5.5	0.5 max.	170	150–210
—	Type 5	2.4	1–2	0.4–0.8	34–36	0.1 max.	0.5 max.	140	100–125
AUS104	—	1.6–2.2	4.5–5.5	1–1.5	18–22	1.8–4.5	0.5 max.	190	248 max.
AUS202A	Type D-2	3.0	1.75–3	0.7–1	18–22	1.75–2.5	—	370	140–200
AUS205	Type D-3	2.6	1.5–2.8	0.5 max.	28–32	2.5–3.5	—	370	140–200
—	Type D-4	2.6	5–6	0.5 max.	29–32	4.5–5.5	—	420	170–240
—	Type D-5	2.4	1.5–2.8	0.5 max.	34–36	0.1 max.	—	370	130–180
AUS204	—	3.0	4.5–5.5	1–1.5	18–22	1–2.5	—	370	230 max.

irons and elongation values as high as 40% can be obtained with the SG irons. The mechanical properties of the austenitic irons are also good at low temperatures and can be useful in a number of chemical plants and cryogenic applications.

The austenitic irons show excellent casting properties and good machinability, which, in combination with the good mechanical properties and good corrosion resistance, ensures wide use of these materials in many applications.

3.02.3.2.2 High chromium cast iron

There is no clear demarcation between high-chromium steels and high-chromium cast irons other than the fact that components are fabricated from steels, and cast in the irons. In practice, however, irons are usually found to have carbon content varying between 0.6% and 3%, while most of the steels contain less than 0.3% carbon. Of the high-chromium irons, those used for components requiring a high degree of corrosion resistance, normally contain 25–35% chromium. It is established[11] that a useful formula to compute the minimum chromium content of a corrosion-resistant iron is: $\%Cr = (\%Cr \times 10) + 12$. That is, increased carbon content requires balancing with increased chromium content in the alloy. For example, a 1.5% carbon alloy should contain not less than 27% chromium.

The limitations imposed by this formula, together with the fact that the alloys in practice rarely contain more than 35% chromium, suggest that the maximum carbon content of the irons should be 2.3%, and that the irons normally contain between 1.0% and 2.0% carbon, unless some property other than corrosion resistance is of prime importance. Silicon may also be present in high-chromium irons in amounts varying between 0.5% and 2.5%; any value more than this has an embrittling effect. Silicon increases fluidity in the foundry and improve the surface quality of castings. Further effects are to refine the eutectic carbides in the iron, to produce a more uniform structure and to raise the temperature at which the matrix transforms from ferrite to austenite with consequent dimensional changes.

Irons with compositions discussed above have structures comprising a uniform dispersion of chromium–iron complex carbides in a matrix of chromium-containing ferrite. The chromium content of the ferrite is not known, although it is assumed to be ~10–13%. The carbides are probably mixtures of the types Cr_7C_3 and $Cr_{23}C_6$, in which some of the chromium has been replaced by iron.[12]

In general, the high-chromium irons are hard but not completely unmachinable. Typically, chromium cast irons, of the compositions described above, have tensile strengths ~450–480 MPa and hardness ~350 Brinell. The hardness of these alloys makes them particularly useful in environments where abrasion or wear resistance may be as important as corrosion resistance. However, the principal difficulties in the production of castings in this alloy are its high shrinkage, which entails some tendency to develop porosity, and the ready formation of an oxide skin, which may cause cold laps in the casting. Castings must, in consequence, be produced by methods similar to those employed for steel castings and care must be taken to avoid the introduction of oxide into the mould.

The high-chromium irons undoubtedly owe their corrosion-resistant properties to the development on the surface of the alloys of an impervious and highly tenacious film, probably consisting of a complex mixture of chromium and iron oxides. Since chromium oxide is derived from the chromium present in the matrix and not from that combined with the carbide, it follows that a stainless iron will be produced only when chromium in excess of the amount required to form carbides is present.

High chromium-containing cast irons are most useful in environments containing an abundant supply of oxygen or oxidizing agents; anaerobic or reducing conditions may lead to rapid corrosion since this may detrimentally affect passivity. Physical effects such as abrasion or sudden dimensional changes induced by temperature fluctuations may rupture the film and allow corrosion to take place. The iron will also be subject to corrosion by solutions containing anions, such as those of the halides, leading to pitting corrosion. With respect to mineral acids, the most important characteristic of chromium cast irons is its resistance to nitric acid, especially in dilute solution. On the other hand, these cast irons do not resist alkaline hydroxides and concentrated mineral acids. Ferritic chromium cast irons turn out to have excellent resistance to high temperature oxidation up to 950–1000 °C.

3.02.3.2.3 High silicon cast iron

Up to ~3%, increasing silicon content has little effect upon the corrosion resistance of the cast iron. In alloys containing much greater amounts of silicon, however, the silicon is responsible for the development of a marked increase in chemical resistance. These alloys can be divided into two types: those containing 4–10% silicon, which are used in

applications requiring an iron with good resistance to oxidation at high temperatures, and those containing 12–18% silicon, which are used in applications requiring an iron with very high resistance to acid attack. The latter are commonly referred to as the high-silicon irons. Compositions and mechanical properties of the high-silicon irons are given in **Tables 3** and **4**.

All these alloys are characterized by high values of hardness and low resistance to impact. Consequently, they are more similar to stoneware than to other metals but are superior to stoneware in thermal conductivity and in their resistance to thermal shock, which, however, is poor compared with that of other metals. Thus, high-silicon irons may be used at elevated temperatures if the process requires it. The principal limitation on their use is imposed by their relatively low thermal conductivities and susceptibility to cracking from thermal shock; this demands that the rate of application or removal of heat should not be rapid.

The microstructure of the high-silicon irons containing less than 15.2% silicon consists of a matrix of silico–ferrite[13] in which a majority of the carbon present in the alloy is distributed as fine graphite flakes. The addition of chromium or molybdenum in the alloy results in the formation of some alloy carbides. The hardness and brittleness of silicon-containing cast iron is predominantly due to the nature of the silico–ferrite, which is intrinsically brittle. Although attempts[14] have been made to produce high-silicon iron with a nodular graphite structure, because of the low strength of these alloys due to the matrix rather than to the graphite form, nodular graphite irons have little, if any, mechanical superiority.

Since the mechanical properties of high-silicon irons preclude any machining other than grinding, it is necessary to cast the materials essentially to net the final shape in such a way that subsequent treatment is kept to a minimum. Also, in view of their poor mechanical properties, the development of any stress in the castings during solidification is very dangerous, since they may cause the casting to crack in subsequent service. To overcome this risk, it is often desirable to strip the castings from the moulds while they are still red hot and to anneal them at 850 °C for several hours, followed by slow cooling.[15]

3.02.3.3 Typical Applications

3.02.3.3.1 Unalloyed cast irons

In spite of competition from other materials, cast iron has an extensive range of applications due to the improving number and variety of properties.[16,17] However, the adaptation of a type of cast iron to a given application calls for analysis and identification of the required properties, which are often very complex, among which the corrodibility and the cost price must in particular be considered. Austenitic cast irons and stainless steels cost roughly four and five times as much as unalloyed cast irons, respectively. These relative costs must be considered in the light of the respective service lives and replacement costs. Otherwise, the differences in properties between lamellar graphite unalloyed cast irons and austenitic cast irons are substantially of the same order as the differences between carbon steels and austenitic stainless steels.

When the service life of a unalloyed cast iron is mediocre, the addition of alloy elements (e.g., nickel, chromium, molybdenum, copper) can often extend it inexpensively. However, it must be borne in mind that possible casting defects (blowholes, porosities, inclusions of silica or slag, shrinkage cavities, irregularities of structure, segregation, undesirable constituents at grain boundaries, etc.) may be the locus of pitting or of local attack that may considerably shorten the life of the castings. Experience has shown that unalloyed iron castings of irreproachable quality and soundness, having a homogeneous structure, prepared using all the resources of the technique, can in some applications have longer service lives than parts made of special cast irons that are more delicate to work, more expensive, and not always free of defects.

Table 3 Analysis of typical silicon–iron alloys

Name	*Total carbon (%)*	*Si (%)*	*Mn (%)*	*S (%)*	*P (%)*	*Ni (%)*	*Cr (%)*	*Mo (%)*
Grey cast iron	3.5	2.0	0.5	0.1	0.1	—	—	—
Hypersilid 14/16	0.65	14.5	0.5	0.02	0.15	—	—	—
Duriron	0.85	14.5	0.6	<0.05	<0.1	—	—	—
Durichlor 51	1.00	14.5	0.6	<0.05	<0.1	—	5.0	1.0
Hypersilid 16/18	0.35	17.0	0.5	0.02	0.1	—	—	—

Table 4 Mechanical properties of silicon–iron alloys

Name	*Ultimate tensile strength (MN m^{-2})*	*Elongation 2 in (50 mm) gauge length*	*Brinell hardness no.*
Gray cast iron	23	2%	180
14.5% silicon iron	129	Nil	540
Durichlor	108	Nil	450

3.02.3.3.2 Alloyed ferritic cast irons

The addition of chromium allows the use of cast iron in the chemical industry (retorts, tanks, heat exchangers, etc.) where gray iron would have an unacceptably high corrosion rate. The degree of corrosion resistance of a cast iron (with chromium, for example) depends first on the nature of the film or layer that forms on the surface. If this film is dissolved or broken up or is destroyed because of the agitation of the aggressive medium, corrosion continues and can reach unacceptable levels comparable to unalloyed cast iron.

For example, with chromium contents from 12% to 20%, cast iron is satisfactory for the retorts used in the synthesis of carbon disulfide, which are generally exposed continuously to temperatures between 850 °C and 900 °C; their average life is of the order of 6 months.[16] In pyrite furnaces, it is the best material for the production of certain parts, notably because of its good resistance to sour gas (H_2S) at 1000 °C. The reaction between sodium chloride and concentrated sulfuric acid, producing gaseous hydrochloric acid at high temperature, requires ferritic chromium cast irons for the moving parts of the furnaces.[16] In aqueous corrosion conditions, chromium contents from 25% to 35% are often required to counter the removal of chromium from the matrix by the formation of carbides. If sufficient chromium is present, the cast iron has similar attributes to stainless steel and low corrosion rate when passive but is susceptible to pitting corrosion in chloride media and where oxidizing agents (e.g., cupric and ferric ion) are present in solution. The pitting corrosion of a high chromium cast iron in 4000 mg l^{-1} chloride ion is shown in Figure 8.

Since the corrosion resistance of the high-silicon ferritic cast iron depends on the permanence and impermeability of a thin silica film on the surface of the metal, it is obvious that any reagent which can damage the film will cause accelerated corrosion of the metal. For this reason all solutions containing hydrofluoric acid must be regarded as incompatible with the alloys.

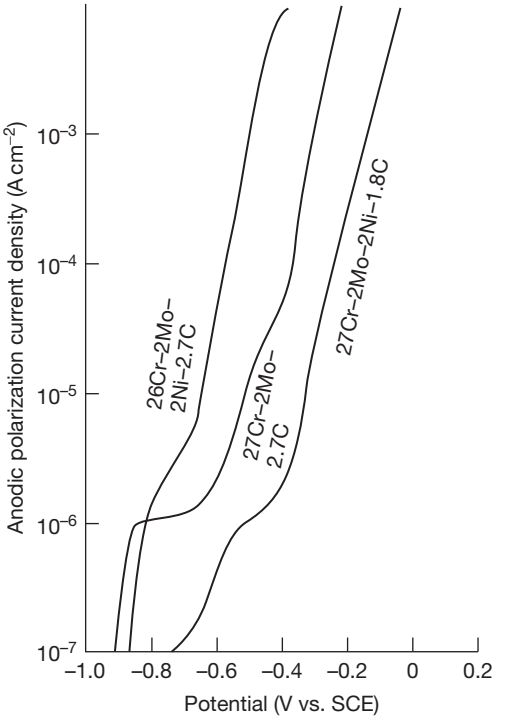

Figure 8 Potentiodynamic polarization curves for high-chromium white irons in nitrogen-saturated solution containing 4000 mg l^{-1} chloride at pH 7 and 25 °C. Reproduced with permission from Dodd, J. *J. Mater. Energy Sys.* **1980**, *2*, 65–76.

Apart from this, high silicon iron offers an excellent resistance to attack by all concentrations of nitric and sulfuric acids and their mixtures. It also provides good performance in hydrochloric acid and in phosphoric acid that is relatively free of fluoride.

Ferritic silicon cast irons (14–18%) are routinely used in parts for contact with acids of all concentrations and for acid effluents. For example, the mixers used to prepare sulfuric acids containing less than 25% water, for the production of explosives and of nitrated derivatives that are themselves used in the production of dyestuffs, are made of silicon cast iron.[16] The thesis by Y. Cetre[18] is a useful source of information about this subject.

3.02.3.3.3 Austenitic cast irons

In addition to the ferritic structures produced by additions of silicon or chromium, there is another

major family of cast irons, produced by addition of large quantities of nickel, cast irons having an austenitic structure; their resistance to electrochemical corrosion is much better than that of unalloyed cast irons. Austenitic cast irons show lower corrosion rates than ferritic irons primarily due to the nickel content of the austenitic matrix. Thus, in deaerated sulfuric acid, active dissolution of the austenitic irons occurs at more noble potentials resulting in an intrinsically lower active corrosion rate. Similarly, the critical current density (i_{crit}) for passivation of austenitic irons tends to decrease with increasing chromium and silicon content. Thus, austenitic irons, particularly those of higher chromium and silicon content, show superior corrosion resistance compared with ferritic irons.

In paper mills (installations processing pulp and paper), the standard practice is to use austenitic nickel cast irons for equipments operating in solutions of sulfites or sulfates or in caustic solutions. This type of cast iron is also used for parts of furnaces operating at high temperatures and for valves used in sulfuric, phosphoric, and concentrated brines. Spheroidal graphite austenitic cast irons, because of their good ductility and high impact energy, can be specified for vessels containing rather aggressive liquids at high pressures (see standard NF A 32-211 of January 1991)[19] and are also suitable for the production of pumps, valves, and turbo-expanders for low temperature duty in the petrochemical industry, and for the preparation, transport, and storage of liquefied gases.

The individual characteristics and uses of some of the basic grades of the austenitic irons are given in Table 5. The major uses of these materials occur in the handling of fluids in the chemical and petroleum industries and also in the power industry and in many marine applications. The austenitic irons are also used in the food, soap, and plastics industries where low corrosion rates are essential in order to avoid contamination of the product. Ni-Resist grades Type 2, 3, or 4 are generally used for such applications but the highly alloyed Type 4 Ni-Resist is preferred where low product contamination is of prime importance.

The modified grades of Ni-Resist are often different from the basic grades used in additional applications. Ni-Resist Types 1B, 2B, and D-2B have a higher chromium content than the corresponding basic grades which increases the erosion resistance of the materials; these grades are less expensive than the other grades with good erosion resistance, that is, Ni-Resist Types 3 and 4. A chromium-free grade of austenitic iron, Ni-Resist Type D-2C, has particularly good ductility and shows good mechanical properties below −100 °C. Even better low temperature properties are, however, obtained with Ni-Resist Type D-2M, a chromium-free 4% manganese grade, which was specially developed for cryogenic applications such as the separation of aromatic hydrocarbons and the production of ethylene. Ni-Resist Type D-4A is a recently developed grade of austenitic iron, which has particularly good resistance to high temperature oxidation and better ductility than the standard Type D-4 grade.

Table 5 Characteristics and uses of basic grades of austenitic cast irons

BS EN 13835 designation	*Ni-Resist Type*	*Characteristics*	*Uses*
AUS101A	Type 1	Least expensive austenitic iron: good corrosion resistance particularly in acidic media	Pumps, valves, furnace components
AUS102A AUS202A	Type 2 Type D-2	Good corrosion resistance; better than Type 1 in alkaline environments	As for Type 1 but preferable for alkaline solutions; used in soap and plastic industries
AUS105 AUS205	Type 3 Type D-3	Good thermal shock resistance; high resistance to erosion particularly in alkaline media	Pumps, valves, pressure vessels, filter parts, exhaust gas manifolds
— —	Type 4 Type D-4	Best corrosion resistance and erosion resistance of the austenitic irons	Castings for industrial furnaces; used in food industry for low contamination of product
— —	Type 5 Type D-5	Very low thermal expansion; good dimensional stability	Scientific instruments, glass moulds
AUS104 AUS204	— —	Good resistance to high temperature oxidation; good corrosion resistance in sulphuric acid	Pumps and valves

One of the outstanding properties of the austenitic irons is their resistance to graphitic corrosion or 'graphitization.' In some environments, ferritic cast irons corrode in such a manner that the surface becomes covered with a layer of graphite. This compact graphite layer, being more noble than the matrix, markedly increases the rate of attack. The austenitic irons rarely form this graphite layer and consequently, in environments where graphitic corrosion is a problem, perform much better than low-alloy cast irons. Practical experience indicates that the corrosion resistance of the flake and spheroidal graphite irons is similar in many environments; however, the spheroidal graphite irons have shown superior corrosion resistance compared to the equivalent flake graphite grades in a number of cases.[20]

3.02.4 Corrosion Environments

3.02.4.1 Atmospheric Corrosion

As cast iron components are normally very heavy in section, the relatively low rates of attack associated with atmospheric corrosion do not constitute a problem and little work has been carried out on the phenomenon. A summary of some data is given in **Table 6**. The most extensive work in this field was initiated by the American Society for Testing and Materials (ASTM) in 1958 and some of the results produced by these studies are quoted in **Table 7**.[21] It should be noted that there is a marked fall in corrosion rate with time for all the metals tested.

The atmospheric corrosion rate is generally determined by the atmospheric relative humidity (RH) and degree of air pollutants (i.e., gaseous, dust, and salt aerosols); at RH less than ~65%, atmospheric corrosion rates are usually relatively low. However, in areas of high humidity (above 70% for most of the year), unalloyed cast irons suffer generalized corrosion and results in the formation of rust similar to that in steel; that is, the corrosion product remains on the surface, **Figure 9**. In such cases, the initial corrosion rates vary from below 25 $\mu m\,year^{-1}$ in a pollution-free rural atmosphere to over 150 $\mu m\,year^{-1}$ in a polluted atmosphere (i.e., containing SO_2) or a marine atmosphere (i.e., containing sea-salt spray aerosol particles). However, this initial corrosion rate decreases as the duration of exposure increases due to the formation of an adherent and highly protective layer of corrosion product. The main characteristics of the two main types of atmospheric media (indoor and outdoor) are:

Indoors:

- partial pressure of water vapor generally less than the saturated vapor pressure at the same temperature (i.e., RH < 70%);
- no large variations of temperature;
- very thin films of water on the surfaces of metals;
- relatively low concentration of gaseous and solid pollutants.

Outdoors:

- presence of thick films of water on the surfaces of metals (e.g., rain, etc.);
- level of pollution by acid gases (SO_2, NO_x, Cl_2) generally higher than indoors;
- large variations of temperature (e.g., periodic diurnal temperature variations);
- variation (cyclic or not) of sunshine and of exposure to wind.

The atmospheric corrosion of cast irons is not a very acute problem: in many cases, a simple coat of paint will provide adequate protection. Otherwise, there seems to be rather little difference between lamellar graphite cast irons and spheroidal graphite cast irons; the latter are slightly better in an industrial environment, where the medium is more aggressive, because there is so little corrosion that the differences of behavior are hardly significant. The presence of small amounts of copper tends to improve the resistance of lamellar graphite cast irons to atmospheric corrosion in an industrial environment.[22]

Specific consideration must be given to local industrial environments in a plant that might give rise to more extensive corrosion. Generally, CO_2 in excess of the normal atmospheric level will not be a problem. However, acid gases or aerosols, such as SO_2, sulfuric acid and phosphoric acid (e.g., from industrial plant) and H_2S and NH_3 (e.g., from sewage works) generally require a highly alloyed material or effective surface protection by an organic coating. Thus, in principle, the atmospheric corrosion of unalloyed or low-alloy irons is similar to steel.

3.02.4.1.1 Nickel cast irons

Although the Ni-Resist irons will not remain rust-free when exposed to the atmosphere, their corrosion resistance is much better than that of plain cast iron or mild steel. The results of a 7.5 year exposure trial carried out in a marine environment at Kure Beach, North Carolina, USA are shown in **Figure 10**. The corrosion rates derived from the curves after 7.5 years of exposure are given in **Table 8**.

Table 6 Corrosion rate of steels and irons in the atmosphere (g $m^{-2}day^{-1}$)

Environment	*Rural*			*Urban*			*Industrial*			*Marine*	
Source	*ASTM*	*Roll*	*Friend*	*Nekrytyi*	*Roll*	*ASTM*	*Dearden*	*Friend*	*Roll*	*LaQue*	*ASTM*
Exposure period years	*12*	*2*	*6*	*1*	*2*	*12*	*1*	*6*	*2*	*–*	*12*
Material:											
Steel	0.23			1.2		0.27	3.4	2.4–3.2		3.6	1.38
Grey iron			1.4–2.1				3.2	1.1–1.2		0.6	2.0
White iron			0.1–0.3				1.3				
Malleable iron											
(a) <0.1% S	0.11			2.1		0.14			3.3		0.43
(b) >0.1% S	0.15	3.3			4.9–6.0	0.20			3.6		0.75
Nodular iron											
(a) Pearlitic	0.10					0.15				0.9	0.37
(b) Ferritic	0.11					0.17					0.72

Table 7 ASTM atmospheric corrosion data (g $m^{-2}day^{-1}$)

Location		*State College, PA (rural)*			*Kure Beach, NC (marine)*			*Newark, NJ (industrial)*		
Duration (years)		*1*	*3*	*12*	*1*	*3*	*12*	*1*	*3*	*12*
Metal	*Condition*									
Ferritic ductile iron	As cast	0.90	0.36	0.11	1.51	0.85	0.72	1.29	0.51	0.17
	Machined	0.56	0.31	0.09	0.90	0.63	0.60	0.88	0.36	0.12
Pearlitic ductile iron	As cast	0.62	0.30	0.10	0.96	0.53	0.37	0.15	0.43	0.15
	Machined	0.50	0.22	0.07	0.82	0.47	0.27	0.70	0.30	0.10
Malleable iron >0.1% S	As cast	0.75	0.40	0.15	1.41	1.11	0.75	1.53	0.70	0.20
Mild steel	Rolled	0.97	0.52	0.23	3.02	2.01	1.38	1.75	0.81	0.27

Source: Mannweiler, G. B. *Proc. Am. Soc. Test. Mater*. **1972**, *72*, 42.

Figure 9 Surface condition of a lamellar graphite iron casting exposed for several decades to atmospheric corrosion. Reproduced with permission from Reynaud, A. *Corrosion and Cast Iron*, ETIF, France, 2008.

3.02.4.2 Corrosion in Natural Water

3.02.4.2.1 Introduction

Water is a universal solvent for solids, liquids, and gases and, hence, water in its natural form is never chemically pure. It is likely to contain dissolved gases (O_2, CO_2, N_2, SO_2, Cl_2, etc.), organic or mineral matter (microorganisms, sand, etc.), and dissolved salts as ions (Ca^{2+}, Fe^{3+}, Cl^-, HCO_3^-, etc.). In order to specify the properties of water, it is necessary to determine the following parameters: pH, color (due to mineral salts, colloidal organic matter), turbidity (sands, etc.), temperature, total mineralization (or dry residue), total hardness, alkaline strength, total alkalinity, etc. and dissolved gases. For corrosion to occur an oxidizing agent must be present and, in most natural waters, this is usually dissolved oxygen. However, it is important to remember that other species (e.g., Cu^{2+}, sulfur, etc.) can also act as oxidizers.

3.02.4.2.2 Aggressiveness and corrosiveness of water

The aggressiveness of water is usually dependent on its acidity and this, in turn, depends on the presence of dissolved CO_2, which is in equilibrium with carbonate species and carbonic acid. Additional equilibria also exist with dissolved calcium and magnesium ions that result in these being undersaturated or supersaturated with respect to precipitation as the corresponding carbonate. For a given water chemistry, sufficient dissolved carbon dioxide must be present in order to prevent this precipitation. There is, therefore, a saturation equilibrium and pH for dissolved $CaCO_3$.[23–26] The governing equilibrium equations for this process are:

$$CO_2 + H_2O \leftrightarrows H_2CO_3 \leftrightarrows H^+ + HCO_3^-$$
$$CaCO_3 + H^+ \leftrightarrows Ca^{2+} + HCO_3^-$$

These equilibria control whether protective calcium carbonate films either deposit or not on the interior of the water pipe. In the absence of the carbonate film, the corrosion rate of the iron is increased and the water is therefore said to be aggressive (**Figure 11**).

Tillmans' formula gives the pH as a function of the free CO_2 and the alkalinity in $CaCO_3$ where the free CO_2 and ($CaCO_3$) have units of mg l^{-1} (i.e., ppm)[27]:

$$pH = 7 - \log \frac{3 \times \text{free}CO_2}{0.61 \times (CaCO_3)}$$

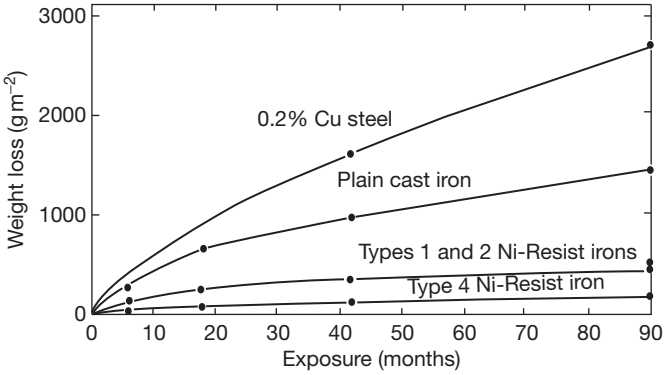

Figure 10 Results of a 7.5-year exposure test program on 150 × 100-mm panels at Kure Beach, N.C. Reproduced from Mannweiler, G. B. *Proc. Am. Soc. Test. Mater*. **1972**, *72*, 42.

Table 8 Corrosion rates after exposure for 7.5 years at Kure beach

Alloy	*Corrosion rate (mm year^{-1})*
0.2% Cu steel	0.020
Cast iron	0.010
Types 1 and 2 Ni-Resist	<0.003
Type 4 Ni-Resist	<0.003

Langelier's formula can be used to determine an index of aggressiveness, Langelier saturation index (LSI):

$$\mathrm{LSI} = \mathrm{pH} - \mathrm{pH_s}$$

where $\mathrm{pH_s}$ is the pH of saturation of $CaCO_3$

- If LSI is negative, the water is aggressive;
- if LSI is zero, the water is inert;
- if LSI is positive, the water is scale-forming, calcareous.

To limit attack, the corrosion rate of the iron must be less than the rate of formation of the protective carbonate containing the deposit. Various conditions must then be satisfied: the water must not contain excessive CO_2 and the pH must be above 7.4 for normally mineralized water, or 7.6 for soft water. To know whether water is calcareous or aggressive, it is also possible,[28] to refer to **Figure 12** and identify the water condition with respect to the carbonic acid equilibrium.

The corrosiveness of water in this context may be related to the presence of electrolytes in solution, mainly chlorides and sulfates, as measured by the conductivity. The point at which it starts to become significantly corrosive is also dependent on the dissolved oxygen concentration and other factors. However, **Table 9** provides general indications for the limits of Cl^- ions and SO_4^{2-} ions before water can be thought of being significantly aggressive.

Importantly, it must be realized that the action of water on a pipe is also a dynamic phenomenon in which the flow velocity of water, its content of dissolved gases (e.g., O_2), matter in suspension, and microbiological phenomena must be taken into account. Potable water can dissolve ~40 cm^3 of air per liter of water, of which 6 cm^3 is oxygen and 14 cm^3 is nitrogen. A dissolved oxygen content of less than this value is a sign of the presence of organic matter; the presence of hydrogen sulfide suggests active sulfate reducing bacteria.

3.02.4.2.3 *Influence of dissolved oxygen*

Dissolved oxygen plays a critical role on the corrosion of iron (as it does for most metals). It is usually the primary cathodic reactant (oxidant) and its rate of influx at the metal surface influences the corrosion rate. Thus, the corrosion rates of many systems are controlled by the mass transport of dissolved oxygen to the reacting surface and this, in turn, is controlled by the concentration of dissolved oxygen, the fluid flow rate and the presence or absence of films (such as calcium carbonate or rust) on the surface. In the case of ferrous alloys (including iron and cast irons), the corrosion products (iron oxides) on the surface are more or less hydrated and have different crystallographic structures. Rust, therefore, often has several constituents, in particular: goethite (α-FeOOH); lepidocrocite (γ-FeOOH) and magnetite (Fe_3O_4).

In the absence of dissolved oxygen, the corrosion rate of iron and of low-alloy cast iron is low. However, once the O_2 concentration increases, corrosion increases. In general, any process that modifies the

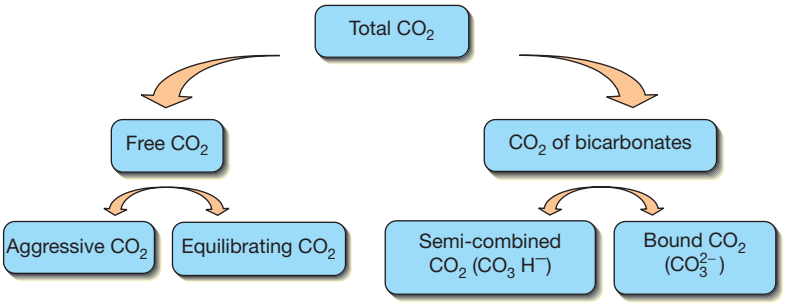

Figure 11 Distribution of carbon dioxide in water. Reproduced with permission from Reynaud, A. *Corrosion and Cast Iron*, ETIF, France, 2008.

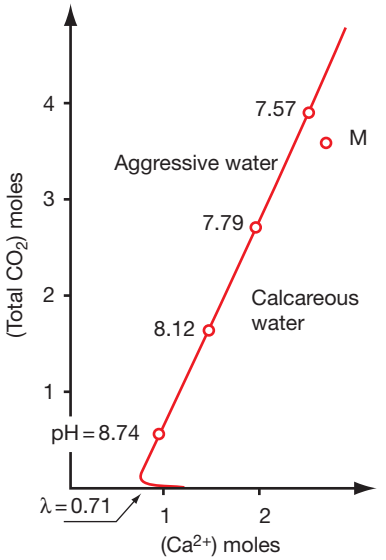

Figure 12 Definition of water condition as a function of CO_2 and Ca^{2+} contents. Based on a diagram by Lédion, J. *La corrosion par les eaux. La Revue des Laboratoires d'Essais*, no. 21, 1989, 9–13, and reproduced with permission from Reynaud, A. *Corrosion and Cast Iron*, ETIF, France, 2008.

Table 9 Approximate limits for chloride and sulfate before water becomes significantly aggressive

Chloride (Cl^-)	*Sulfate (SO_4^{2-})*	*Reference*
100 ppm	200 ppm	29
200 ppm	400 ppm	30
300 ppm	420 ppm	CEFRACOR

mass transport of oxygen to the metal surface for reaction (including the concentration of oxygen and the rate of agitation of the fluid) influences the corrosion rate. Note, however, that the presence of dissolved O_2 can assist in the passivation of some alloy cast irons. Moreover, the absence of oxygen, at least locally, can prevent the formation of a protective deposit or favor corrosion by differential aeration or crevice corrosion. This is the case, for example, of corrosion under deposits of scale, under joints, and on the plates of tube exchangers.

One interesting study has shown the influence of the concentration of dissolved oxygen on the mechanisms responsible for the corrosion of cast iron in water at 50 °C.[31] The results of this study can be summed up using **Figures 13** and **14**.

3.02.4.2.4 Corrosion of cast Iron in natural water

Generally, cast irons provide excellent service in water following the formation of a protective layer on the inside wall of the pipe (layer of carbonate, most often). However, water that contains carbon dioxide in solution, acid effluents, chlorides, etc., is significantly more corrosive.

The presence of alloying elements of moderate composition has no great influence on the corrosion rate of cast irons in water. For example, a German study[32] has shown that the addition of 0–3% nickel does not improve the corrosion resistance of cast iron in artificial seawater, cooling water, or soft water. However, according to the same authors, the corrosion rate can be reduced by 50% in water containing dissolved H_2S, but the corrosion is still so high that this is not considered a cost-effective solution. In practice, the conditions that the castings are exposed to influences the corrosion rates. Typical corrosion rates for graphitic and 18% nickel (austenitic) cast iron in various environments are given in **Table 10**.

The use of Ni-Resist cast iron is recommended in the following cases: borehole water, fresh water with a brackish tendency (pH = 7.6), water at 80 °C

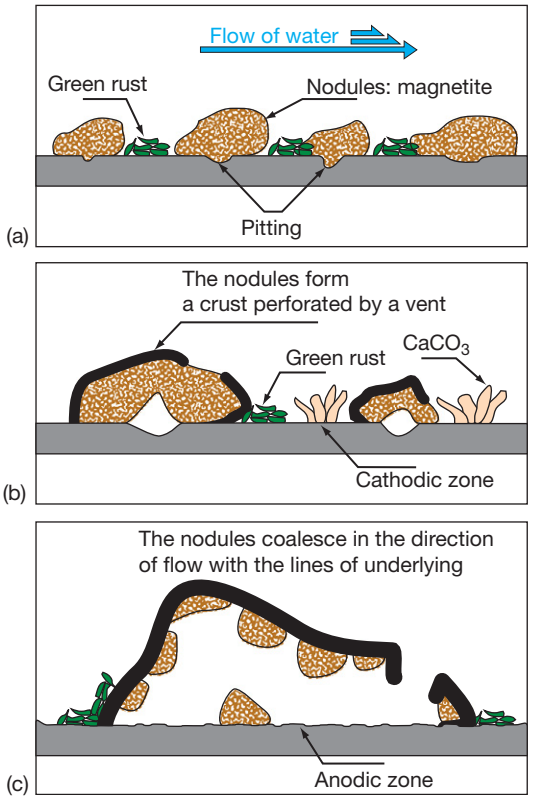

Figure 13 Steps in the development of the layer of oxides that forms on lamellar graphite unalloyed cast iron immersed in water at 50 °C containing 0.44 ppm oxygen: (a) from 3 to 7 h (b) after 10 h (c) from 16 to 40 h. Reproduced with permission from Smith, D. C.; MacEnaney, B. *Corros. Sci.* **1979**, *19*, 379–394.

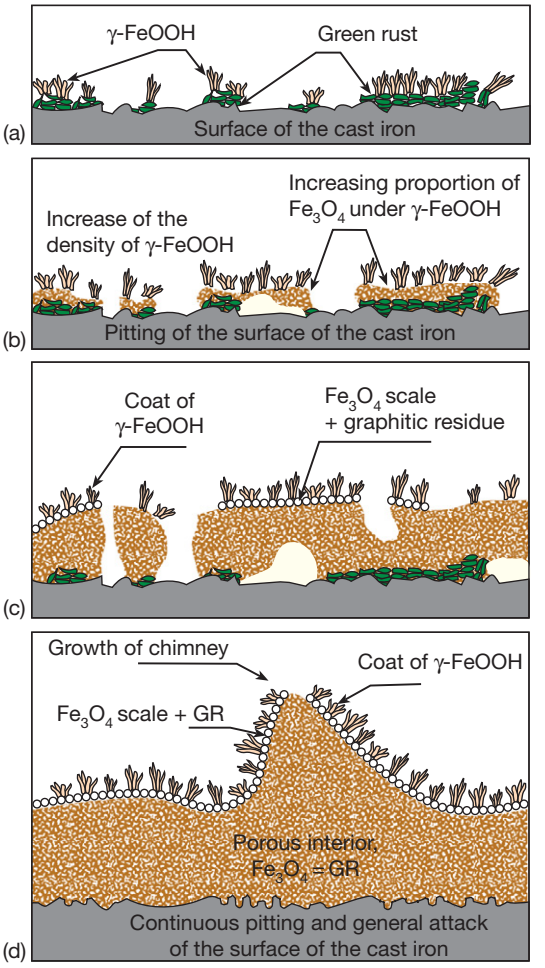

Figure 14 The same as Figure 13, but in water at 50 °C containing 3 ppm oxygen: (a) after 10 min (b) after 3 h (c) after 6 h (d) after 27 h. Reproduced with permission from Smith, D. C.; MacEnaney, B. *Corros. Sci.* **1979**, *19*, 379–394.

accompanied by ammonia vapors, and sulfite-rich water (pH = 3.5; e.g., from paper mills). On the other hand, low- or unalloyed cast irons can provide an adequate service life in the presence of more or less aerated water containing a large number of organic substances (low-alloy cast iron: 1.5% Ni + 0.5% Cr, for example). Small levels of copper and chromium also reduce the corrosion of lamellar graphite cast irons.

In certain cases, inhibitors may be used to protect cast irons against corrosion by water assuring that the materials are in a closed circulation system. The use of alkaline anodic inhibitors, such as 1% sodium silicate and 0.5% sodium nitrite, is effective. A mixture of phosphonocarboxylic acid and sodium nitrite also appears to be effective against the corrosion of cast irons by neutral solutions.[22] This results in the formation of a finer and more protective passive film than is formed in the presence of nitrite alone. A ranking of the inhibitors commonly used for closed cooling circuits has been proposed for cast irons although benzoates, known to be effective with steel, tend to aggravate the corrosion of cast irons:

- good protection: nitrites, phosphates;
- average protection: silicates, tannins;
- positive or negative effect according to conditions: borates.

Water containing sulfates generally has an electrochemical corrosive action on metals when the iron content exceeds 400–500 mg l^{-1}. Note also the possible appearance of pitting corrosion, by differential aeration, under scales containing sulfates.[33] To forestall corrosion of cooling circuits, we must ensure that the sum $(Cl^- + SO_4^{2-})$ is less than 250 mg l^{-1};

corrosion becomes likelier when this sum exceeds 500 mg l^{-1}.

In 2002, Indian researchers,[34] by means of electrochemical tests (measurements of Tafel slopes and of polarization resistance, for example), established a ranking for the aggressiveness of saline solutions at 28 °C on a cast iron. The concentrations tested were dilute (from a few ppm to a few hundred ppm), and likely to be encountered in drinking water. KCl and NaCl would seem to be more corrosive than $MnSO_4$, $Pb(NO_3)_2$, KI, and KBr. The variation of the corrosion rates over time (up to 360 h) were also tracked: the results are given in **Table 11**.

Table 10 Corrosion rates of unalloyed and austenitic cast irons in various waters

Types of water	*Corrosion rate (mm year)$^{-1}$*	
	Unalloyed Cast iron	*Austenitic Cast iron*
Distilled water	0.25	0.015
CO_2 purifier water	4.06	3.05
Water (pH = B) (+185 ppm $CaCO_3$)	0.76	0.5
Brackish water in oil well	0.5	0.025
Seawater	0.25	0.06
Seawater (8 m s^{-1})	4.47	0.20
Sour bath (pH = 4) +0.05% CO_2	1.78	0.5
Sour bath (pH = 4)+0.05% SO_2	1.01	0.25
Sewage	0.45	0.127

Table 11 Corrosion of gray cast iron in various saline electrolytes

Saline solution at 28 °C	*Corrosion rate after 360 h immersion (mm year^{-1})*
KCl	0.144
NaCl	0.141
Na_2SO_4	0.085
$CaCO_3$	0.027
$CaCl_2$	0.046
$MgSO_4$	0.034
$NaHCO_3$	0.038
$NaNO_3$	0.019
$MoSO_4$	0.004
$Fb(NO_3)_2$	0.002
KBr	0.010
KI	0.010
Water	0.759

Data taken from Mehra and Soni.[34]

In early 2000, Japanese researchers[35] studied the effect of pH on the corrosion behavior of underground SG cast iron pipes immersed in simulated underground water (using polarization curves and immersion tests). The intended application was corrosion resistance in clay-rich marine mud. The study highlighted the effects of an intensive selective dissolution of the ferrite of the pearlite where phosphorus and sulfur seem to have segregated; spheroidal graphite and cementite favor the evolution of hydrogen. The schematic diagrams in **Figure 15**, sum up the mechanisms.

3.02.4.2.5 Galvanic corrosion of cast iron in natural water

Scandinavian authors[36] have reported interesting data on the corrosion by galvanic coupling of unalloyed cast iron with various alloys in town water at 25 °C and 75 °C (temperatures encountered in household sanitary installations); **Table 12** groups these data.

These data show that the unalloyed cast iron is anodic, compared to the metals and alloys studied; only carbon steel and zinc are anodic with respect to

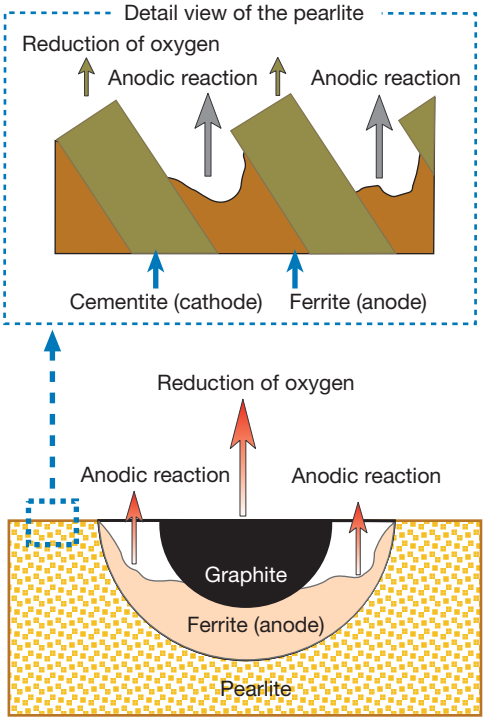

Figure 15 Selective dissolution of the ferrite of the pearlite where phosphorus and sulfur have segregated. Reproduced with permission from Reynaud, A. *Corrosion and Cast Iron*, ETIF, France, 2008.

Table 12 Corrosion potentials and galvanic currents for the listed materials coupled to LG iron

Alloys coupled to the cast iron	*Town water at 25°C*		*Town water at 75°C*	
	Current density ($\mu A\ cm^{-2}$)	*Corrosion potential (mV/SHE)*	*Current density ($\mu A\ cm^{-2}$)*	*Corrosion potential (mV/SHE)*
304 stainless steel	0.2	+250	1.0	+245
316 stainless steel	0.4	+250	0.9	+245
410 stainless steel	3.0	+250	1.0	+245
440 stainless steel	0.4	+250	1.0	+245
Carbon steel	−0.6	−470	−8.0	−390
Cu Zn39 TB3 brass	0.3	+190	0.7	+150
Cu Zn20 Al2 brass	0.4	+250	1.0	+245
Bronze	0.2	+250	3.0	+245
Cupro-nickel	0.2	+250	3.0	+245
Copper	0.09	+250	3.0	+245
Zinc	−0.6	−690	−4.0	−650
Cast iron alone	0.4	−90	–	−810

Data taken from Neumann *et al.*[36]

cast iron. On the subject of galvanic corrosion, reference to Bryant[37] will also be useful. Another type of 'galvanic' corrosion can occur on the same section of iron due to thermal-galvanic effects. Thus, the coexistence, in a single pipe, of hot zones and cold zones can create a chemical heterogeneity at the cast iron surface which leads to clearly separated anodic and cathodic regions. In this way a temperature difference of 20 °C can lead to a potential difference of 55 mV.[38]

Swedish work on the effects of galvanic coupling between SG cast iron and copper in water, published in 2005,[39] has shown that deaeration of water can diminish the galvanic corrosion of the cast iron, with the corrosion rate becoming equal to that observed in the absence of copper. The corrosion products formed on the surface of the cast iron under these conditions of deaeration have the appearance of a black film that consists of magnetite. However, if the temperature is raised from 30 °C to 50 °C, the galvanic corrosion current is multiplied by 10, even under conditions of deaeration.

3.02.4.2.6 Inhibition of corrosion in water

Traditionally, a standard range of species can be used to inhibit the corrosion of cast irons. Chromates were previously used as anodic passivating inhibitors, however, this is no longer permitted due to the toxicity of hexavalent chromium. Alternative anodic inhibitors include nitrites, molybdates and phosphates. Film-forming organic inhibitors such as octadecylamine can be used commonly in boilers and refrigeration installations, etc. Tannins are often used as an internal treatment for low-pressure steam boilers. Indian work in 2004, comparing the actions of different inhibitors of corrosion of cast irons in water,[40] showed that, among the products tested (molybdate, hydrogen phosphate, and nitrite), it is the molybdate ion that is the most effective. For potable water systems below 60 °C, sodium hexametaphosphate combines inhibition of scaling (at lower concentrations) and corrosion (at somewhat higher concentrations). It is one of the few chemicals that are permitted for use as a corrosion inhibitor for potable (drinking) water.

3.02.4.3 Corrosion in Steam

Ordinary cast irons are acceptable up to a few bar wet steam pressure (120–130 °C) while silicon cast irons (>15%) resist steam up to 300 °C. Under more severe conditions of service, austenitic cast irons are recommended. For example, in saturated steam at 170 °C (8 bar pressure) the loss of thickness for Ni20Cr3 (LG1 grade) is 0.02 mm $year^{-1}$. For steam at higher temperatures (up to 500 °C), castings must undergo a stabilization heat treatment (annealing at 760 °C for 4 h followed by cooling in the furnace down to ~500 °C). Generally, the high temperature corrosion of cast iron in steam is similar to steel. Thus, in the presence of superheated steam, from 450 °C to 600 °C, after 0.5–3 h of exposure, a film of magnetite (Fe_3O_4) forms on unalloyed cast irons, reinforced by wustite (FeO) if the temperature exceeds 575 °C. It is important to note that the relatively poor mechanical properties of cast iron compared with steel, constrain the application of cast irons to those at lower pressures.

3.02.4.4 Corrosion in Seawater

Evans,[41] in 1928, cites Hadfield, who describes various cases of cast iron foundations left in seawater for 25–50 years: they become extremely soft, to the point of consisting primarily of graphite and of the corrosion product. Evans points out that this 'graphitic softening' with no change of outward appearance is often found in cast iron objects that have remained immersed in the sea for a long time. He also recalls that cast iron objects from shipwrecks, found later, often seem at first glance not to have been affected, but are in fact constituted essentially of soft ferrous hydroxide held together by graphite lamellae; this ferrous hydroxide is subsequently oxidized when the objects are exposed to open air and akaganite (β-FeOOH).

Research has shown that the corrosion rate of cast iron in sodium chloride passes through a maximum at 3–3.5% NaCl,[42] a concentration that corresponds more or less to the composition of seawater (**Figure 16**). In short, seawater is an aggressive medium for cast irons, but their behavior is strongly influenced by the location and its specific conditions.

Tables 13 and **14** provide some examples. A corrosion rate of 50–100 μm year^{-1} is often given for unalloyed cast irons in seawater. All tests were conducted on small plates taken from pipes, machined and ground to eliminate the protective action of the casting skin. They clearly show that the corrosion of cast iron in seawater is not excessive (2–3 times that in distilled water) and that there is no significant difference between lamellar graphite cast iron and spheroidal graphite cast iron.

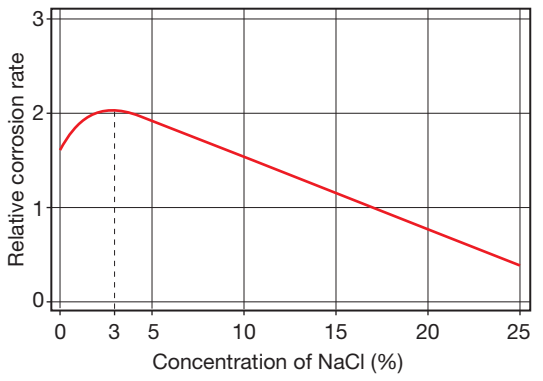

Figure 16 Effect of the concentration of NaCl on the corrosion rate of iron in aerated solutions at ambient temperature. Reproduced with permission from ASM. Corrosion of cast irons. Metals Handbook, Corrosion, 1987, Vol. 13; pp 566–572.

Alloying additions of nickel or chromium greatly reduce corrosion. As shown in **Figure 17**, austenitic cast irons stand up much better than other cast irons to seawater, water contaminated by certain industrial pollutants, and water rich in CO_2. For the desalination of seawater, austenitic nickel cast iron is specified for many pumps and valves operating in the feed seawater and in the brine. Similarly, many cooling water pumps made up of this type of cast iron have been installed in conventional power stations, refineries, and steel mills.

Even though seawater is an aggressive medium for cast irons, a unalloyed cast iron can provide satisfactory service if the seawater is still and not polluted. Japanese authors have shown that the resistance of cast irons to seawater corrosion improves as the carbon content decreases and the silicon content increases. In addition, the nature of the matrix seems to have a large influence: white cast irons having an extensive carbide structure are the most resistant, followed, in order of decreasing corrosion resistance, by ferritic, ferrito–pearlitic, and finally pearlitic gray cast irons. Low contents of chromium improve the resistance of lamellar graphite cast iron to corrosion by seawater. Small additions of molybdenum, vanadium, and titanium increase corrosion resistance by refining the graphite and the matrix.

In flowing seawater, the commonest type of exposure, the corrosion rate varies with the velocity of water and increases rapidly as the velocity increases because more oxygen is available. It is also stated that the corrosion rate can be up to 15–25 times as great as in stagnant seawater; but it would seem that at still higher velocities, the level of corrosion can be decreased by the formation of a protective oxide deposit. Some authors[43,44] recommend using austenitic nickel cast irons for cases of corrosion–erosion in seawater, since these cast irons have an excellent resistance to such attack. The resistance of high-silicon cast irons in seawater has also been studied. However, it turns out that these are sensitive to pitting corrosion in stagnant seawater (and at low flow rates). Such pitting is initiated at the matrix/graphite lamellae and matrix/interdendritic carbide interfaces. Otherwise, in flowing water, their resistance to corrosion–erosion is excellent (**Table 15**).

The water temperature also plays a more or less marked role according to the grade of cast iron, as shown in **Figure 18**. Additionally, some British studies[45] have shown that there are practically no differences in corrosion behavior among the various unalloyed gray cast irons (lamellar or nodular

Table 13 Corrosion rates of gray cast irons in various sea water environments

Type of Iron	*Duration of exposure (years)*	*Corrosion ($g\,m^{-2}\,day^{-1}$)*	*Maximum pitting depth (mm)*	*Location*
Continuous immersion				
Unalloyed gray cast iron, as-cast	4	2.0	6.4[a]	Bristol Channel (Great Britain)
Unalloyed gray cast iron, as-cast	15	2.95	1.5	Halifax, Nova Scotia (Canada)
Unalloyed gray cast iron, as-cast	15	1.3	5.0[a]	Plymouth (Great Britain)
Unalloyed gray cast iron, as-cast	15	4.25		Colombo (Sri Lanka)
Unalloyed gray cast iron, mean of S samples	3	2.4		Eastport, Maine (United States)
Austenitic gray cast iron, type L-NUC 15 6 2, as-cast	6	0.4	None	Kure Beach, North Carolina (United States)
Austenitic gray cast iron, type L-NO 20 2, as-cast	6	0.8	None	Kure Beach, North Carolina (United States)
Samples placed midway between high and low water				
Unalloyed gray cast iron, as-cast	15	0.75	1.3	Halifax, Nova Scotia (Canada)
Unalloyed gray cast iron, as-cast	15	1.0	4.6	Plymouth (Great Britain)
Unalloyed gray cast iron, mean of 9 machined samples	3	0.75		Eastport, Maine (United States)

[a]Extensive, graphic corrosion.
Data taken from Reynaud, A. *Corrosion and Cast Iron*, ETIF, France, 2008.

Table 14 Corrosion rates ($mg\,dm^{-2}\,day^{-1}$) of iron in various aqueous environments: $1\,mg\,dm^{-2}\,day^{-1} \sim 5\,\mu m\,year^{-1}$

Materials	*Natural seawater*	*Natural seawater*	*Natural seawater*	*Synthetic seawater*	*Distilled water*	*Distilled water*
	90 days, aerated	*180 days, aerated*	*360 days, aerated*	*360 days, aerated*	*360 days, aerated*	*360 days, stagnant*
Spheroidal (SG) iron	24	16.1	15.3	15.8	19.1	6.1
Lamellar (LG) iron	24.9	16.4	17	19.1	19.3	6.2

graphite, ferritic or pearlitic). According to the same authors, resistance of 'Ni-Resist' cast irons to seawater is better (2–3 times greater than that of unalloyed cast irons) even though it is the high-silicon and high-chromium grades that are generally thought to be the most resistant to corrosion in this medium.

This work also demonstrates the value of protection by coatings: examination of castings that had been metallized (by thermal spraying with aluminum) shows that the loss of mass is five times lower than for unprotected castings and significantly less than for austenitic cast irons. In the case of salt water mists at 100 °C, alloyed cast irons are generally recommended.

There is an interesting study[46] of the influence of ferrous sulfate (a corrosion inhibitor for copper alloy condenser tubes used in seawater) on the corrosion of an austenitic cast iron of the Ni20Cr2 LGI type in seawater. It showed that the presence of Fe^{2+} ions could make seawater more corrosive if the concentration of these ions was not too high (less than or equal to 100 ppm). On the other hand, contents 10–25 times as high would tend to diminish the corrosion rates.

Dutch work[47] has shown that the corrosion products formed on spheroidal graphite cast iron immersed in water differed substantially according to whether the iron is exposed under static or flowing conditions. For example, it was shown that these corrosion products consisted of α-FeOOH in a spongy form under static condition and of a hard mixture of γ- and α-FeOOH under dynamic condition.

The austenitic irons have also been shown to exhibit better corrosion resistance than the ferritic irons in seawater. Tests over long periods of time have shown

that Ni-Resist irons of Types 1, 2, and 3 corrode at rates of 0.020–0.058 mm year^{-1} in relatively quiet seawater. Under similar conditions low alloy cast irons have shown corrosion rates ranging from 0.066 to 0.53 mm year^{-1}.[22] The Ni-Resist irons maintain this superiority over a wide variety of conditions (**Figures 17** and **18**), both in stationary and flowing seawater. In a test lasting 740 days in seawater moving at 1.5 m s^{-1}, low-alloy cast iron showed a corrosion rate of 1.3 mm year^{-1} compared to 0.050 mm year^{-1} for Type 2 Ni-Resist. In tests carried out at controlled temperature at a higher velocity of 8 m s^{-1} (**Table 16**), the Ni-Resist irons again showed better properties than low-alloy cast irons or mild steel.

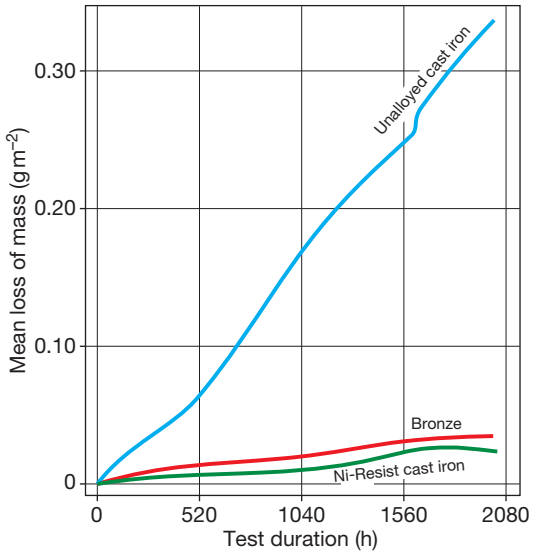

Figure 17 Comparison of the corrosion rates of a unalloyed cast iron, a 'Ni-Resist' cast iron, and a bronze in seawater. Reproduced with permission from Berenson, J.; Wranglen, G. *Corros. Sci.* **1980**, *20*, 937–941.

3.02.4.5 Soil Corrosion

Since buried pipes for water, sewage, and gas are a major use of cast iron, the corrosion of buried iron structures needs special consideration in any study of the corrosion properties of cast iron. With gray iron pipes, leakage usually arises because the pipe fractures as a result of soil stresses or top-loads that exceed the hoop strength of the pipe. With ductile iron pipes, leakage is usually through small corrosion pits. For this reason gray iron pipes are susceptible to both uniform and pitting corrosion while ductile iron pipes are only seriously affected by pitting. A characteristic of corrosion on buried ferrous metals is that the attack is mostly in the form of pitting, especially with the cast irons. This causes a problem in measuring the extent of corrosion in burial trials. Usually both the weight loss, measuring the average loss of section, and the deepest pit, measuring the maximum loss of section, are reported. For assessing the severity of the attack on buried pipes, the second parameter is clearly the most important.

The rate of attack on buried iron depends on the corrosivity of the soil in question. A good guide, which is still valid, is the work carried out by the National Bureau of Standards in the United States between 1922 and 1955.[48] In this very detailed and extensive study, the chemical characteristics of more than 100 soils drawn from all over the United States were examined and compared in relation to the

Table 15 Corrosion rates of cast irons in seawater

Source	*Hudson's study*	*Kress's study*	*Parts and de la Bruniere's study*	*Speidel and Witmoser's study*	*LaQue's study*
Location	*Emsworth, England*	*Cuxhaven, Germany*	*laboratory, France*	*artificial seawater*	*Harber Island USA*
Duration of test	*2 years*[a] *(g m^{-2} day^{-1})*	*6 months*[a] *(g m^{-2} day^{-1})*	*380 days*[a] *(g m^{-2} day^{-1})*	*220 days*[a] *(g m^{-2} day^{-1})*	*3 years*
Steel		4.4	2.4	1.6	
LGI	1.2	1.7	1.7	0.6	1.6[b]
White cast iron				0.65	
Malleable cast iron	1.6			0.9	
Pearlitic SGI		1.0		1.4	5.6[b]
Ferritic SGI		2.1	1.6	0.5	

[a]Results originally stated in mg cm^{-3} day^{-1} (based on loss of mass, with no indication of type of attack).
[b]Quantity measured: penetration depth of pitting.

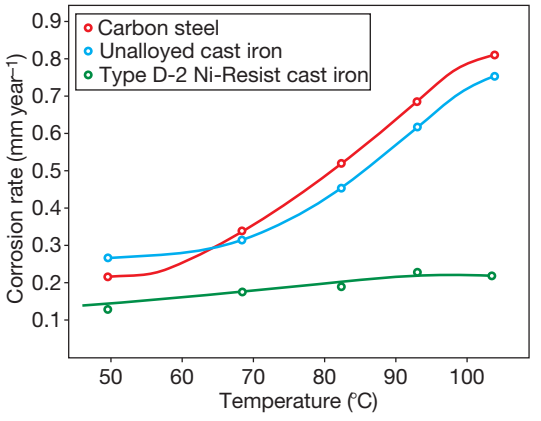

Figure 18 Corrosion rate in deaerated seawater of a carbon steel, of a unalloyed cast iron, and of a 'Ni-Resist' cast iron as a function of temperature (test lasting 156 days).

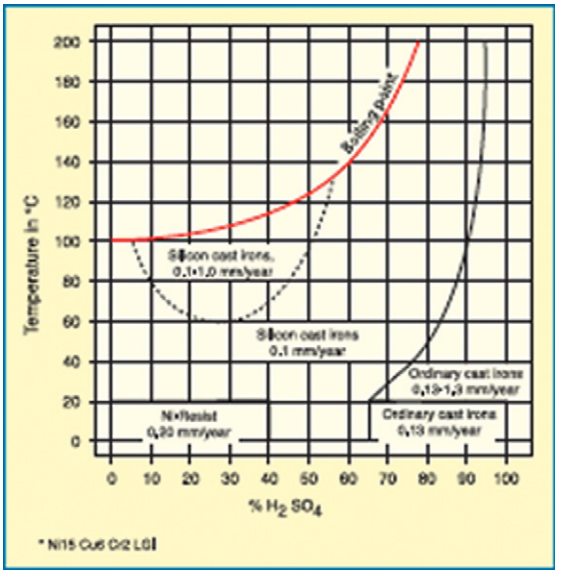

Figure 19 Resistance of cast irons to sulfuric acid. Reproduced with permission from Résistance des fontes à l'acide sulfurique concentré. Fonderie no. 393, Nov. 1979, 339.

corrosion behavior of small steel and iron specimens that had been buried in them for up to ~17 years. Detailed study of the published results suggests, however, that the only parameter to give any useful correlation with the severity of the corrosion is the electrical resistivity of the soil. Even this is only valid up to ~2000 ohm cm with a correlation coefficient of ~−0.5.[49] Currently, electrical resistivity is the factor used for dividing soils into corrosivity classes (Table 17).

Although resistivity surveys can decide which soils along a projected pipeline are probably aggressive to buried ferrous metals and which are not, it has been found that when unprotected pipes fail in service the local soil resistivity does not correlate to any significant extent with the corrosion rate at the pitted site. Indeed, Stokes[50] showed from a survey of statistics of ductile iron pipe failures in the United Kingdom, that the most likely pitting rate for an aggressive soil is ~1 mm $year^{-1}$ with a range of ~0.3–3 mm $year^{-1}$. Since the soil electrolyte is likely to be a dilute salt solution of low dissolved oxygen content and pH ~8.5, a consistent corrosion rate seems logical. Collins[51] has suggested that the tendency for low resistivity soils to be aggressive is due to the fact that for the most part they are poor in draining, and poorly aerated heavy clays are thus more liable to create differential concentration cells on the pipe surface than free-flowing soils such as sands. He argues that, as the soil resistivity falls, the probability of serious pitting increases but the pitting rate remains substantially constant. This would explain the poor correlation between the chemical parameters of the soil and its corrosivity. It also suggests that the physical characteristics of the soil should be better indicators of its corrosivity.

The results of tests on bare cast iron in soils that are relatively homogeneous on the scale of the size of the samples cannot be directly extrapolated to actual coated pipes; the latter, because of their length, will encounter a succession of soils (geological cells) that differ in their nature, their moisture content, their aeration – soils are sometimes made heterogeneous by borrowed materials or by differences of compaction. For example, in the case of a pipe passing in turn through a porous soil permeable to air, then a clay layer through which oxygen can pass only with great difficultly, a differential aeration cell may form, which results in the corrosion of the part of the pipe in the clay soil (which becomes the anode as it is in a region of oxygen restriction) while the part in the porous soil is only slightly corroded (since it is in a region with more easy oxygen access and is, hence, cathodic).[52] Additionally, corrosion of cast iron pipes in soils may also be affected by stray or induced currents: for example, from DC traction systems, induced AC current or from other cathodic protection systems.[53,54] Many of these conditions, which are difficult to circumvent, are likely to result in the formation of macrocells leading to a localized corrosion (pitting) that can be dangerous when the soil is highly corrosive.[55] Coupling with copper used for

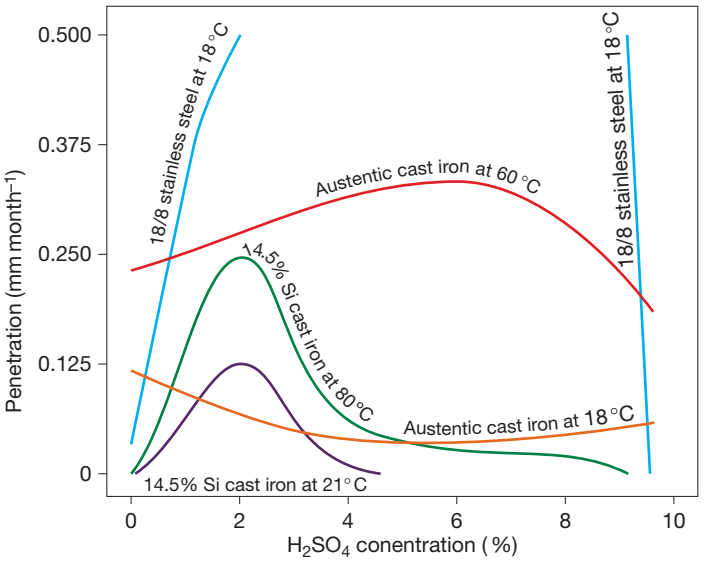

Figure 20 Iso-corrosion curves of LGI cast iron containing 15% Ni, 6% Cu, and 2% Cr in H_2SO_4.

Table 16 Seawater corrosion–erosion test carried out at 8 m s^{-1} at 28 °C for 60 days

Alloy	*Average corrosion rate (mm year^{-1})*
Cast iron	6.9
2% Ni cast iron	6.1
Type 1 Ni-Resist	0.74
Type 2 Ni-Resist	0.79
Type 3 Ni-Resist	0.53

Data taken from Berenson and Wranglen.[22]

Table 17 Soil corrosion classes as a function of soil resistivity

	Aggressive	*Nonaggressive*
Resistivity:	<2000 Ω cm	>2000 Ω cm
Redox potential at pH 7	<0.40 V SHE; (<0.43 V in clay)	>0.40 V SHE; (>0.43 V in clay)
Borderline cases resolved by water content	>20% by mass	<20% by mass

water distribution pipes can also result in the functioning of macrocells.[56]

In early 2000, Japanese researchers[57] studied more particularly the corrosion resistance of SG cast iron pipes in clay marine muds. In 2003, Kubota (Japan) patented a spheroidal graphite cast iron having improved corrosion resistance and high mechanical strength, for the production of pipes for underground applications.[58] Its composition is reported as: 3–4% C, 1–4% Si, <0.6% Mn, 0.02–0.08% Mg, 0.05–0.5% Co, <1.5% Ni, 0.2–0.8% Cr, and/or Cu.

It should be noted that it is extremely difficult to predict service lives of buried pipelines from the results of controlled trials with small specimens, whether in the laboratory or in the field. For example a study on the comparative corrosion resistances of ductile and gray iron pipes between 1964 and 1973[59,60] indicated a mean pitting rate of 0.35 mm year^{-1} for uncoated ductile iron pipe exposed in a typical heavy Essex clay of 500–900 Ω cm resistivity for 9 years. This contradicts the rate of 1 mm year^{-1} normally found on a corroded service pipe from such a soil. The discrepancy appears to be due to the use of specimens that were only a third of a pipe length each and were buried separately. It may reflect the contribution of the total surface area of the pipe as a cathode to the corrosion current at the anodic area of the pitting site.

3.02.4.6 Methods of Protection

Experience and knowledge of the corrosion caused by local geological differences (macrocells) in the soil have led to the development not only of methods of evaluation of the corrosiveness of soils on a pipe alignment (e.g., by soil resistance survey), but also of methods of protection capable of disrupting the

macrocells. These methods include: ensuring that electrical continuity along the pipe is broken by use of insulating joints (also limiting stray currents), using active coatings that are self-healing (e.g., zinc), use of an inert backfill[61] and, for difficult cases, placing a flexible polyethylene sleeve around the pipe when it is laid to prevent direct contact with the local heterogeneities of the soil.

Note that cathodic protection is also an excellent remedy for corrosion of cast iron by soils (although it is most often applied to steel pipes).[62,63] For steels, cathodic protection is often combined with a protective organic coating[64,65]; this is rarely done in the case of cast irons. However, cathodic protection of the town water supply network of Scarborough, United Kingdom has been undertaken.[62] This network, made up primarily of ductile cast iron and lamellar graphite cast iron pipes, is protected by magnesium sacrificial anodes to overcome the problems due to the corrosiveness of soils (resistivity from 1000 to 3000 Ω cm), which is due partly to the use of deicing salts, and also to galvanic coupling with the copper used in distribution pipes. It must be borne in mind that the cathodic protection of a structure may also generate stray currents in the soil. It may then create, in an adjacent metallic structure, zones of current input and zones of current output at which corrosion will occur. In practice, even though there are many networks of cast iron pipes that coexist in the soil with networks of steel pipes with cathodic protection, there are very few cases of corrosion ascribable to the influence of cathodic protection, because a few simple rules[66] can be applied to solve most of the problems.

3.02.5 Corrosion in Industrial Environments

In general, unalloyed gray or white cast irons possess no resistance to dilute mineral acids. In very dilute acids, the presence of air, or other oxidizing agents such as ferric salts, appreciably increases the corrosion rate. If corrosion rates are to be held below 0.25 mm year^{-1} in moderately aerated solutions, it is unwise to exceed a total acid concentration of 0.001 M (i.e., pH < 3), irrespective of the acid concerned.

3.02.5.1 Sulfuric Acid

The use of unalloyed cast irons is generally impossible in the presence of dilute sulfuric acid since the corrosion rates are very high (several millimeters a year).[67] By contrast, the same acid (sulfuric) in the concentrated state barely attacks unalloyed cast irons, even at high temperature. This is due to an iron sulfate salt film that forms at concentrations above ~70% such that corrosion rates do not exceed 0.13 mm year^{-1} at 20 °C.[67,68] In practice, thanks to this passivation effect, lamellar graphite cast irons, in the past, and spheroidal graphite cast irons, today, are used in coolers for concentrated sulfuric acid.

As for alloy cast irons, austenitic nickel grade can provide good corrosion resistance up to 20% sulfuric acid[67]; above this value, high-silicon cast irons must be used. For example, pumps used in the production of sulfuric acid are, in fact, often made of high-silicon cast irons. **Figure 19** shows the behavior of several cast irons under different conditions of service (temperature, concentration).[68] It can be seen that the resistance of these alloys to concentrated sulfuric acid is excellent up to its boiling temperature. Note that it is dangerous to use cast irons with oleum (concentrated sulfuric acid enriched with SO_3) because of the risk of oxidation of the silicon they contain.

The austenitic irons can be used in handling very dilute solutions of sulfuric acid at ambient or moderately elevated temperatures under conditions corrosive to ordinary cast iron and carbon steel. Austenitic irons have also given satisfactory service in handling concentrated sulfuric acids, but although they show low corrosion rates in such environments they are not markedly superior to the unalloyed cast irons. Type 1 Ni-Resist and the high silicon grades AUS104 and AUS204 are the types most generally used in sulfuric acid environments. The iso-corrosion curves of an austenitic lamellar graphite cast iron containing 15% Ni, 6% Cu, and 2% Cr in sulfuric acid are given in **Figure 20**.

High-chromium irons have no useful resistance to sulfuric acid of more than 10% concentration at any temperature. At temperatures above 20 °C corrosion rates in excess of 1.27 mm year^{-1} are probable even for acid of less than 10% concentration. The addition of 2% molybdenum increases the resistance to this acid at very low and very high concentrations (**Figure 21**).

Probably, the most useful characteristic of the high-silicon irons is their ability to withstand sulfuric acid at all temperatures and concentrations. The maximum rate of corrosion which can develop has been reported to be 0.482 mm year^{-1} in 30% sulfuric acid at boiling point,[3] and this falls to a minimum rate of 0.025 mm

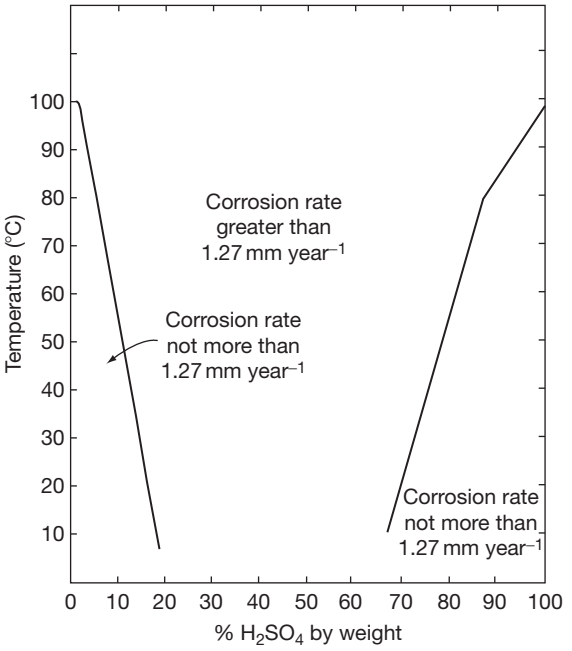

Figure 21 Resistance of high-chromium iron containing 2% molybdenum to sulfuric acid solutions.

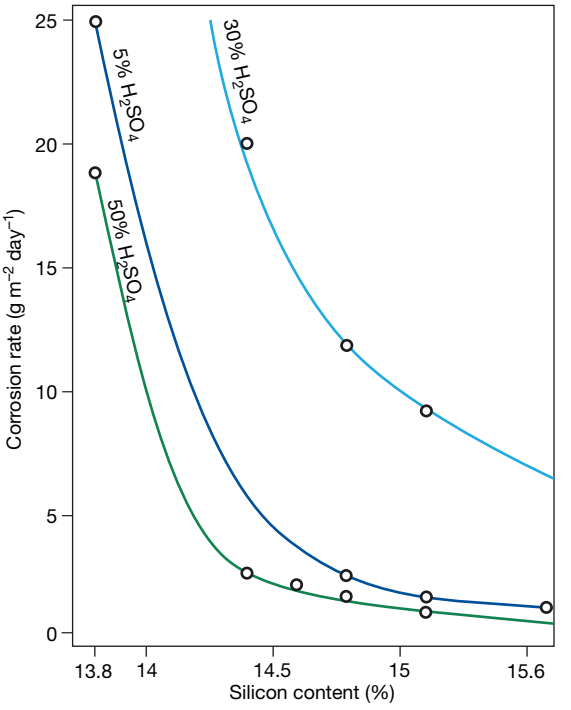

Figure 23 Influence of Si content on the corrodibility of cast irons in H_2SO_4 (5–30–50%).

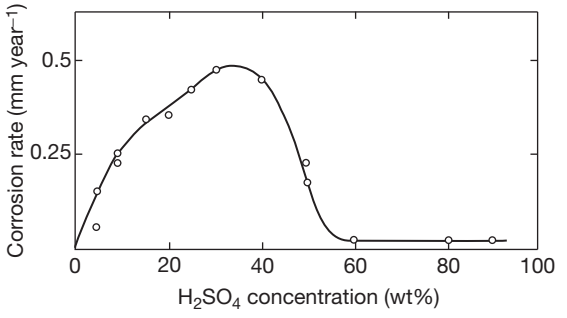

Figure 22 Variation of corrosion rate with concentration of boiling sulfuric acid (Duriron Co. data).

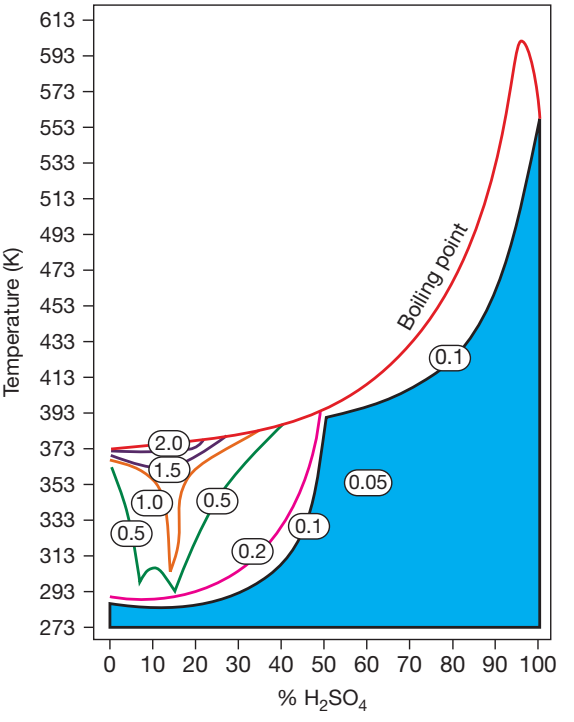

Figure 24 Iso-corrosion curves in H_2SO_4 of cast iron containing 15% Si.

year^{-1} when the acid concentration exceeds 60% and the temperature is at boiling point (Figure 22).

In order to achieve optimum performance over the widest possible acid concentration range, it is essential to ensure that the alloy content of silicon is optimal. The corrosion rates of silicon iron are illustrated in Figure 23, which shows the influence of the silicon contents from 13.8% to 15.6%, on the resistance to corrosion by boiling sulfuric acid at different concentrations. From this data, it is clear that silicon contents in excess of 15% provide the best performance. Figure 24 illustrates an iso-corrosion chart for 15% silicon iron in sulfuric acid.

3.02.5.2 Hydrochloric Acid

This commonly used acid attacks unalloyed cast irons very strongly, even in a dilute condition. High-chromium cast irons are only slightly better than unalloyed cast irons; the dissolution of these cast irons leaves a residue having a graphitic appearance and consisting of carbides.[69] Austenitic nickel cast irons are also attacked, especially by the cold concentrated acid and by boiling 20% acid. Attempts made to produce an alloy more resistant to hydrochloric acid have resulted in alloys containing 17–18% silicon or 14.5% silicon and chromium plus 3% molybdenum and both these alloys resist even concentrated hydrochloric acid relatively well. This is due to the protective layer of SiO_2 that forms on the surface of the material. If the acid is boiling, the attack of such cast irons will be much more intensive and this is illustrated in Figure 25. For example, with a cast iron containing 15% Si and 3% Mo in the presence of boiling 20% HCl, the loss of mass is $150\,g\,m^{-2}\,day^{-1}$.[69]

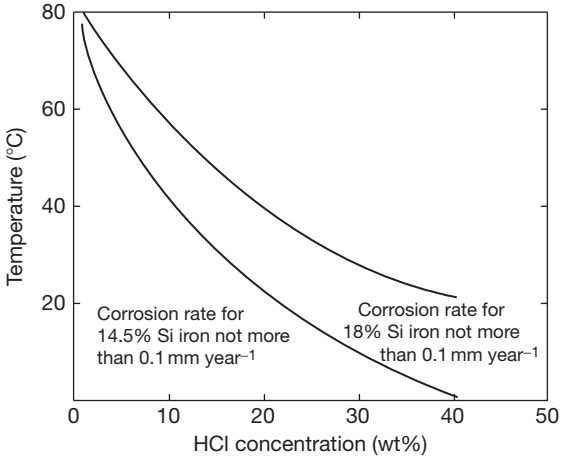

Figure 25 Limits of use of silicon irons in HCl for Fe–18Si and Fe–14.5Si alloys.

Table 18 Corrosion of Type 1 Ni-Resist, cast iron and carbon steel in deaerated HCl at room temperature

Acid concentration (%)	*Corrosion rate (mm year⁻¹)*		
	Ni-Resist	*Cast iron*	*Carbon steel*
1.8	0.13	23	15
3.6	0.38	30	36
5.0	0.46	38	46
10.0	0.41	30	48
20.0	1.1	32	69
27.0	3.0	30	60
36.0	9.4	28	30

The austenitic irons are superior to ordinary cast iron in their resistance to corrosion in deaerated hydrochloric acid at room temperature (Table 18). However, for practical uses where such factors as velocity, aeration and elevated temperatures have to be considered, the austenitic irons are mostly used in environments where the hydrochloric acid concentration is low, generally less than 1% and preferably below 0.5%. Such environments occur in process streams encountered in the production and handling of chlorinated hydrocarbons, organic chlorides and chlorinated rubbers.

3.02.5.3 Nitric Acid

Unalloyed cast irons are not suitable for castings resistant to nitric acid, at any concentration. Nitric acid also attacks high-nickel cast irons at all concentrations, but more specifically in dilute solutions. Only high-silicon and high-chromium cast irons display good resistance to this acid, due to the formation of passive oxide films. However, there may be some corrosion in boiling concentrated solutions. This will, for example, be the case of cast irons containing 29% chromium, the chemical composition of which will be adjusted according to the concentration and temperature of the nitric solutions.[69]

Figure 26 has been derived from data[2] for corrosion by nitric acid solutions of an alloy containing 29% chromium and 0.8% carbon. It is interesting to note that the resistance by this alloy in these solutions is roughly complementary to that of the high-silicon irons, the high-chromium iron being more suitable for dilute solutions and the high-silicon iron for concentrated solutions.

Nitric acid is also withstood by high-silicon iron. The concentrated acid is believed to reinforce the silica film by the formation of a passive iron oxide film, and this assumption is supported by the fact that the highest rates of attack are associated with hot dilute solutions. The iso-corrosion rate data for 14% silicon iron in nitric acid is shown in Figure 27.

3.02.5.4 Phosphoric Acid

Phosphoric acid attacks unalloyed cast irons at all concentrations. Austenitic cast irons are satisfactory when used at ambient temperature in solutions having concentrations less than or equal to 30%; above this threshold, the attack is rapid. High-chromium cast irons are suitable in most cases. The corrosion rates

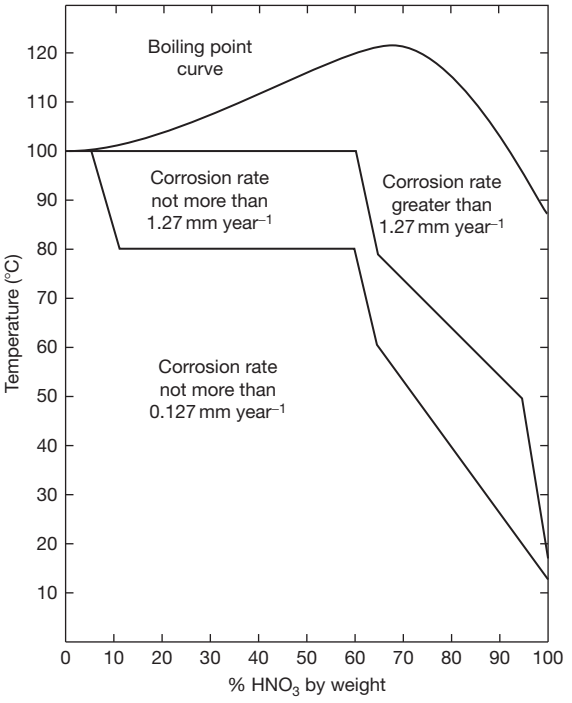

Figure 26 Resistance of high-chromium iron to nitric acid solution.

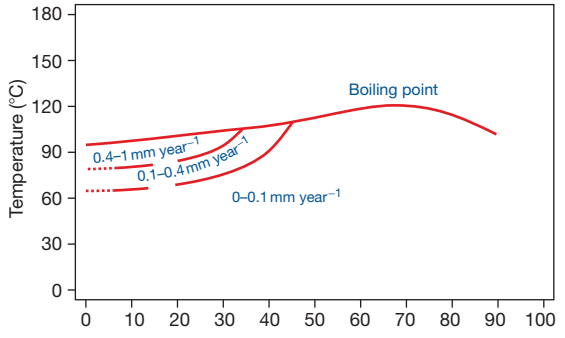

Figure 27 Corrosion resistance in HNO_3 of a cast iron containing 14% Si).

are ~0.12 mm year^{-1} up to a concentration of 60%, at all temperatures up to boiling.[69] High-silicon cast irons best resist this acid, at all concentrations and almost all temperatures (see **Figure 28**). Note that most crude phosphoric acid contains appreciable amounts of fluoride which can lead to excessive corrosion rates.

The results published in the literature suggest that solutions of phosphoric acid at all concentrations and temperatures are not corrosive to high-silicon irons. Kosting and Heins[70] quote long-term results given by the Duriron Co, together with figures obtained in their own tests of 24 h duration (**Table 19**).

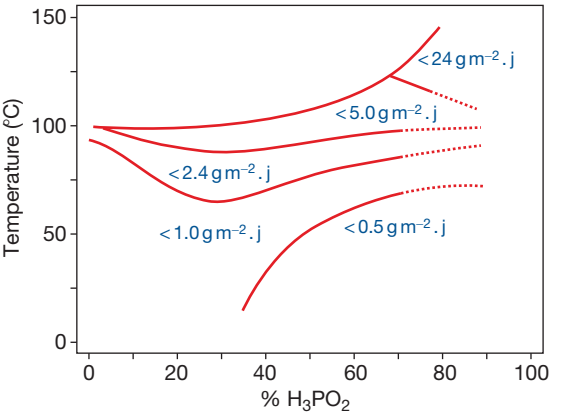

Figure 28 Resistance to corrosion by phosphoric acid of a cast iron containing 14.5% silicon as a function of concentration and temperature. Reproduced with permission from Reynaud, A. *Corrosion and Cast Iron*, ETIF, France, 2008.

3.02.5.5 Other Mineral Acids

Most cast irons are resistant to chromic acid at all concentrations due to passivation of the material. However, 15–17% silicon irons are recommended at higher temperatures up to 150 °C; the corrosion of these cast irons is less than 0.1 mm year^{-1}. In dry hydro–halide acids (i.e., HBr, etc.) unalloyeded irons suffice, however, in wet acids high silicon iron is essential, preferably containing molybdenum. Hydrogen cyanide is generally noncorrosive except at higher temperatures in the gas phase if the humidity is sufficiently high.[71]

3.02.5.6 Organic Acids

The short-chain organic carboxylic acids attack unalloyed cast irons, especially in dilute solutions. Thus, unalloyed cast irons should not be used in formic or acetic acids, however, chromium cast irons are acceptable for both, with nickel austenitic iron acceptable for acetic acid. As the chain length of the acid increases, the acidity diminishes and the unalloyed irons may have acceptable corrosion rates. Thus, in palmitic (hexadecanoic) acid unalloyed cast irons should not be used while nickel cast irons are recommended, and in stearic (octadecanoic) acid unalloyed irons may be acceptable at lower concentrations and temperatures.[71]

Therefore, for most organic acids, the corrosion resistance of cast iron is essentially dependent on the strength of the acid. Thus, unalloyed cast irons should not be used in citric, lactic, or oxalic acids (3 mm year^{-1} for unalloyed iron in citric acid) while for white chromium cast irons, the rate of attack is less than 0.01 mm year^{-1}.

Table 19 Corrosion of high-silicon irons by phosphoric acid

Acid concentration (%)	*Temperature (°C)*	*Corrosion rate (mm year^{-1})*	*Origin of data*
10	82–88	0.007	Duriron Co.
	98	0.147	Kosting & Heins
25	82–88	0.010	Duriron Co.
	98	0.038	Kosting & Heins
50	98	0.185	Kosting & Heins
87	82–88	0.010	Duriron Co.

Table 20 Corrosion of Type 1 Ni-Resist and ferritic cast iron in acetic acid at 15 °C

Acid concentration (%)	*Corrosion rate (mm year^{-1})*	
	Cast iron	*Ni-resist*
5	17	1.0
10	22	0.5
25	20	0.5
50	16	2.0

The austenitic irons are also useful in some circumstances for handling organic acids such as dilute acetic, formic and oxalic acids, fatty acids and tar acids. They are more resistant to organic acids than unalloyed cast irons, for example, in acetic acid the austenitic irons show corrosion rates 20–40 times lower than the ferritic iron (Table 20).

3.02.5.7 Corrosion by Alkalis

Dilute alkali solutions do not corrode cast iron at any temperature, but hot solutions exceeding ~30% concentration will attack it, with an accompanying evolution of hydrogen; this behavior is similar to that of steel. Broadly speaking, if the corrosion rates are to be held below 0.2 mm year^{-1} the temperature should not exceed 80 °C; corrosion rates may range as high as 1.25–2.5 mm year^{-1} in boiling solutions of more than 50% concentration. Molten caustic soda (650 °C) may attack cast iron initially at rates ~20 mm year^{-1}, but this decreases significantly after some exposure. In spite of these high corrosion rates, caustic concentration and fusion pots are made from cast iron, since the material is relatively cheap, and the thick wall necessary for mechanical strength also gives the pot a long life. It is of utmost importance to ensure that concentration and fusion pots are cast in sound metal, as any unsoundness, particularly at the bottom of the pan, will lead to pitting attack and

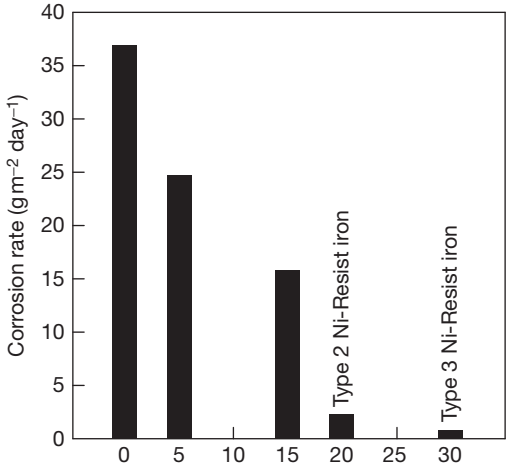

Figure 29 Effect of nickel additions to cast iron in reducing corrosion by caustic alkalis.

premature failure. On the other hand, high-silicon cast irons are less resistant to corrosion by alkalis than unalloyed cast irons and this is due to dissolution of the protective silicon oxide film by the alkali. Similarly, ferritic chromium cast irons should not be used in the presence of alkalis.

Austenitic cast irons show particularly good corrosion resistance in alkaline environments, even better than that shown by low alloy cast irons. The resistance to corrosion improves with increasing nickel content (Figure 29), and the irons containing ~30% nickel, such as Type 3 Ni-Resist, show the best resistance. An electrochemical study of the corrodibility of unalloyed SG cast irons in caustic soda has shown that some inhibition can be expected from the addition of thiourea[72]: 36% protection was found with the addition of 10^{-3} moles of thiourea per liter of a molar solution of sodium hydroxide at 30 °C.

The addition of 3–5% nickel improves the resistance of both lamellar graphite and spheroidal graphite cast irons to alkali attack and, with increasing nickel content, the corrosion resistance of austenitic

cast irons in these media is much lower than that of non or low-alloy cast irons and alloys containing 30% nickel are the least vulnerable to corrosion by alkalis. For a 50% solution of caustic soda at 50 °C, the use of a Ni-Resist cast iron containing 20–30% nickel and 2–3% chromium is recommended. **Figure 30** shows the corrosion rates of austenitic cast irons and of unalloyed cast irons in sodium hydroxide for various temperature–concentration domains.[73]

Test results cited by concerning the resistance of various cast irons in molten anhydrous caustic soda[75] at 510 °C (containing 0.5% NaCl, 0.5% Na_2CO_3, and 0.03% Na_2SO_4) are shown in **Table 21**. It can be seen here that the superiority of the austenitic grades

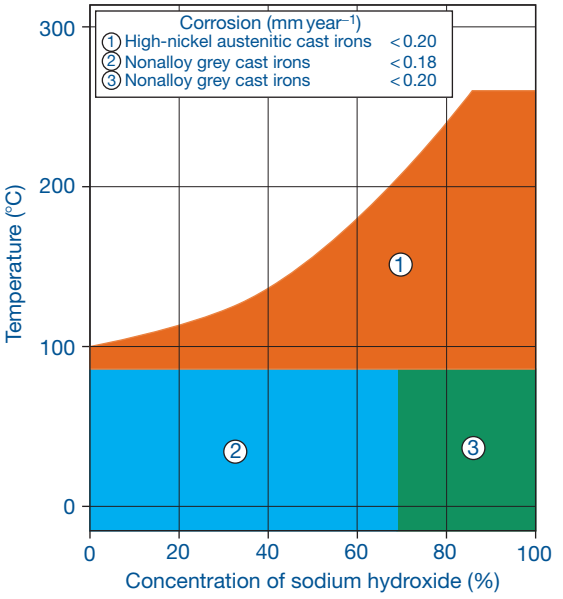

Figure 30 Corrodibility of austenitic cast irons and unalloyed cast irons in NaOH. Reproduced with permission from Higgins, R. I. *J. Res. Bcira* **1956** *6*, 165–177.

Table 21 Corrosion rate and pitting of cast iron in molten, anhydrous NaOH at 510 °C.

Cast iron	*Corrosion rate (mm year^{-1})*	*Pitting depth (mm)*
Unalloyed LGI	2.5–3.4	0.13
Unalloyed SGI	5.3	–
Unalloyed whise cast iron	3.8	0.5
3% NI cast iron	1.8	–
Ni15 Cr8 Cr2 LGI	15.9	1.5
N2O Cr2 LGI	24.9	1.8
N2O Cr2 SGI	11.8	1.5
N3O Cr3 LGI	2.2	0
Ni3O Si5 Cr6 LGI	13.6	1.0

disappears in the case of concentrated caustic soda. This superiority exists only up to concentrations of 70% and temperatures approaching the boiling point. Finally, **Table 22** confirms the favorable effect of nickel at lower concentrations[65] (81-day tests).

3.02.5.8 Salt Solutions

The corrosion rates of cast irons in salt solutions depend on the salt chemistry. Solutions which are alkaline or neutral in reaction are not generally so corrosive and even brines containing calcium and magnesium chloride can be safely handled by the austenitic irons (**Table 23**). Those salts which hydrolyze to give an acidic solution (e.g., divalent metal cations such as magnesium) are significantly more corrosive. The corrosion rates of Type 1 Ni-Resist and cast iron given in **Table 24** demonstrate that the austenitic iron shows better resistance than the nickel-free cast iron in a wide range of salt solutions.

3.02.5.9 Corrosion–Fatigue

Cast iron, exposed under conditions of cyclic stress, is liable to corrosion fatigue. Some data on this effect have been given by Collins and Smith,[75] but a more extensive study has been reported by Palmer[76] who generated stress-cycle (S–N) data using rotating bend at a cycle frequency of 50 Hz and a duration of up to

Table 22 Corrosion rate of cast iron as a function of nickel content in 30% NaOH solution

Nickel Content (%)	*Corrosion rate (mm year)$^{-1}$*
0	1.9–2.3
3.5	1.2
5	1.24
15	0.8
20	0.08
20 (+2% Cr)	0.15
30	0.01

Table 23 Corrosion of Type 1 Ni-Resist and cast iron in brine solutions

Environment	*Temperature (°C)*	*Corrosion rate (mm year^{-1})*	
		Ni-Resist	*Cast iron*
14% NaCl + 16.7% $CaCl_2$ + 3.4% $MgCl_2$. pH = 6	69	0.08	0.53
Saturated NaCl	93	0.12	1.85

Table 24 Corrosion of Type 1 Ni-Resist and cast iron in various inorganic salt solutions

Salt solution	*Concentration (%)*	*Temperature (°C)*	*Corrosion rate (mm year^{-1})*	
			Ni-Resist	*Cast iron*
Aluminum sulphate	5	16	0.41	1.0
Aluminum chloride	5	16	0.08	1.3
Aluminum chloride	5	93	0.15	4.8
Aluminum sulphate	5	16	0.15	0.76
Aluminum citrate	30	Room	1.5	550
Aluminum thiocyanate	50	27	0.38	3.3
Potassium aluminum sulphate	5	16	0.25	0.76
Zinc chloride	30	Boiling	2.0	16
Ammonium nitrate	5	Room	0.23	0.76
Manganese chloride	10	77	0.038	0.79
Ammonium chloride	20	93	0.25	5.8

10^7 cycles in demineralized water, 3% sodium chloride solution and demineralized water containing various inhibitors. The results for the uninhibited solutions are summarized in Table 25. Palmer found that corrosion fatigue due to water spray could be eliminated or mitigated by some of the inhibitor systems examined, but it was apparently easier to inhibit damage on gray irons than on ductile irons, which could only be inhibited by 0.25% potassium chromate solution. This was due to the inability of the other systems to maintain a continuous passive film on the iron; gray iron is less sensitive to a notch effect in fatigue so that the presence of local sites of attack would be less important to this metal provided that the overall corrosivity of the solution were depressed.

Various studies have also shown that it is possible to protect cast irons against corrosion fatigue by metallization with zinc or aluminum of thickness ~100–200 μm. The life of iron castings exposed to corrosion fatigue conditions in a saline medium is of the same order of magnitude as that of castings subjected to the same mechanical forces in air. Figure 31 clearly illustrates the effect of these coatings.

Another study emphasized, for different types of matrices, the low resistance of SG cast irons to corrosion fatigue in a 3% NaCl solution and the low aggressiveness of lubricating oils.[77,78] The results are shown in Table 26 and Figure 32. Fatigue resistance curves[79] in various media (air, water, salt water) are shown Figure 33. They concern a ferritic SG cast iron tested in rotary bending at 50 Hz. The influence of the aggressiveness of the medium is quite apparent.

An inhibitor consisting of 0.5% $NaNO_2$ plus 1% $NaSiO_4$ has been proposed[80] to prevent corrosion

Table 25 Corrosion fatigue limiting strengths (MPa)

Environment	*Air*[a]	*Water*[a]	*3% NaCl solution*[b]
Pearlitic gray iron	126	100	39
Ferritic gray iron	93	77	23
Pearlitic ductile iron	270	224	46
Ferritic ductile iron	208	178	46

Data taken from Higgins.
[a]Fatigue strength based on 50 × 10^6 cycles.
[b]Fatigue strength based on 100 × 10^6 cycles.

fatigue of pearlitic SG cast irons in water as a replacement for the toxic chromate. Further data, reproduced below (Figure 34), concerning the corrosion fatigue resistance of SG cast irons shows the harmful effect of the marine medium and the value of a metallic coating (zinc or aluminum), which can increase the resistance of the material to that observed in a nonmarine atmosphere.[81]

The fatigue limit under reversing stress and corrosion in hot water at 70 °C in pipes has been studied by Japanese researchers[82] on an as-cast SG cast iron alloyed with copper and molybdenum, and compared to a carbon steel. In the static corrosion test of water containing sulfates and chlorides, the latter was found to be less resistant, and its resistance, unlike that of the former, could not be improved by adding sodium nitrite as an inhibitor. With the cast iron, the corrosive attack practically stopped with inhibitor contents in excess of 6000 ppm. The resistance of this cast iron to corrosion fatigue was also improved; at 260 MPa with 6000 ppm nitrite, it was better than that of the carbon steel.

Japanese researchers considered the question of the corrosion fatigue of ferritic and bainitic spheroidal

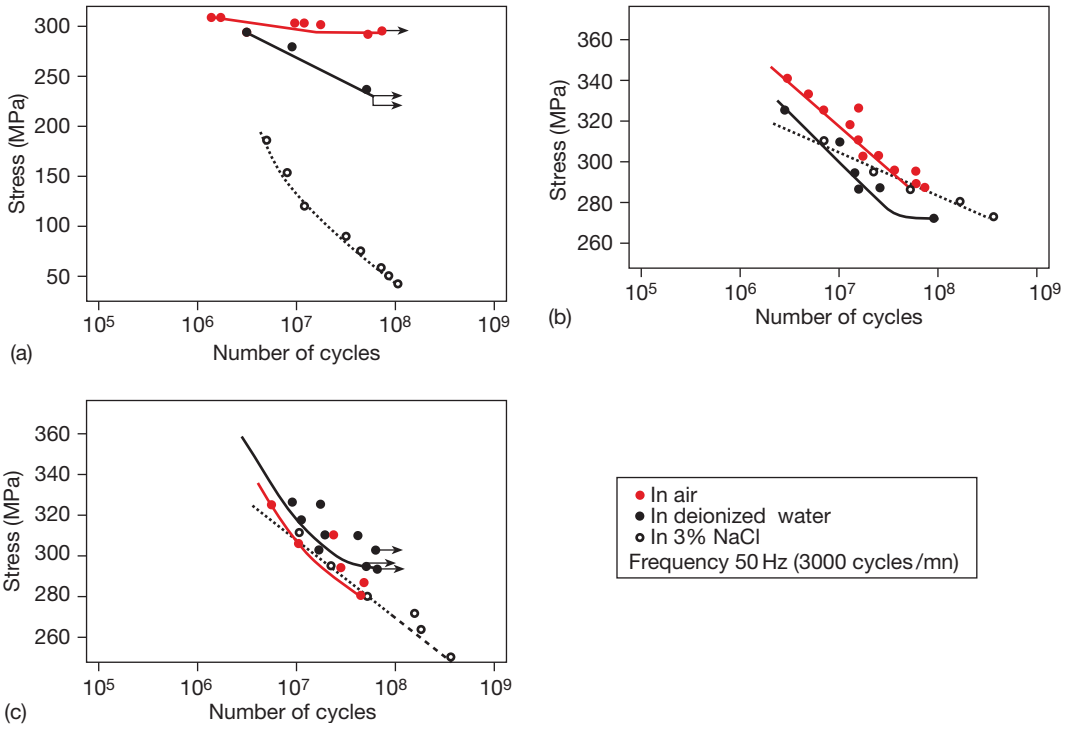

Figure 31 Corrosion fatigue curves of pearlitic SG cast irons: (a) shot-blasted, (b) metallized with Zn, and (c) with Al. Reproduced with permission from Reynaud, A. *Corrosion and Cast Iron*, ETIF, France, 2008.

Table 26 Fatigue resistance of some SG cast irons

Matrix	*Fatigues resistance in air (MPa)*	*Resistance to corrosion fatigue*	
		In 3% NaCl (MPa)	*In lubricating oil (MPa)*
Ferritic	240	100	225
Ferritic	350	75	330
Annealed martensite	350	145	540
Bainite	510	150	500

graphite cast irons (ADI) in water. They found that the fatigue limit of ADI cast irons declined in the course of time, apparently due to a selective dissolution of the acicular ferrite resulting from localized corrosion fatigue. It would seem that ferritic cast irons, in which the selective corrosion of ferrite does not occur, would perform better when exposed to water.

3.02.5.10 Stress Corrosion Cracking

In general, it can be said that cast irons are not liable to stress corrosion; however, in some particular media (concentrated sodium hydroxide solution for example), stress corrosion, cracking of spheroidal graphite cast iron, can be observed.[83] The mechanisms of this type of damage have been studied[84,85] and is similar to steel at the same pH. Lamellar graphite cast irons seem to be less liable to this type of attack; additions of nickel (3–5%) improve the stress corrosion resistance of lamellar and spheroidal graphite cast irons.[86] Tests of the stress corrosion resistance of a ferritic SG cast iron in a medium containing sulfur, (saturated solution of H_2S)[87] have shown that this type of material is barely liable to this mode of attack – at least not more than a work-hardened carbon steel.

Unalloyed and low-alloyed cast irons are susceptible to varying degrees of stress corrosion cracking in high pH (>13), in nitrite solutions, in H_2S, in acid (where a number of phenomena related to hydrogen occur), etc. These can be mitigated to a greater or lesser extent by alloying, as described elsewhere. Austenitic nickel cast irons are liable to stress corrosion in aerated sodium chloride solution[85] and this can be prevented by use of cathodic protection. Overall stress corrosion can be diminished or even eliminated by reducing the applied stress, by increasing the nickel content, and by reducing the dissolved oxygen content of the medium.

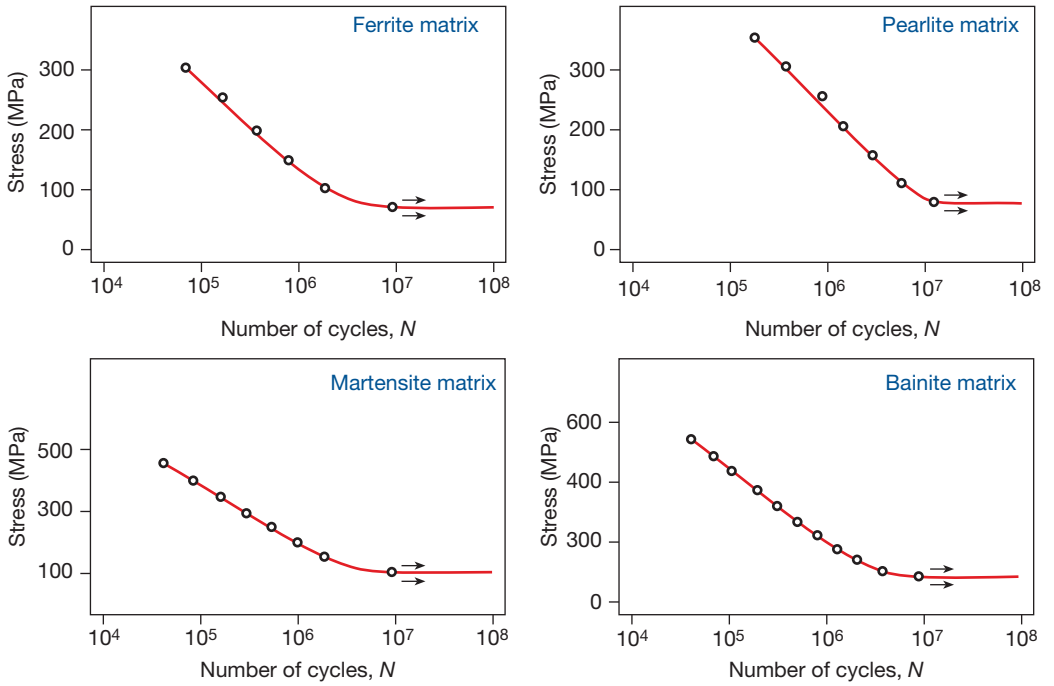

Figure 32 Corrosion fatigue resistance of SG cast irons having different types of matrices (in 3% NaCl). Reproduced with permission from Reynaud, A. *Corrosion and Cast Iron*, ETIF, France, 2008.

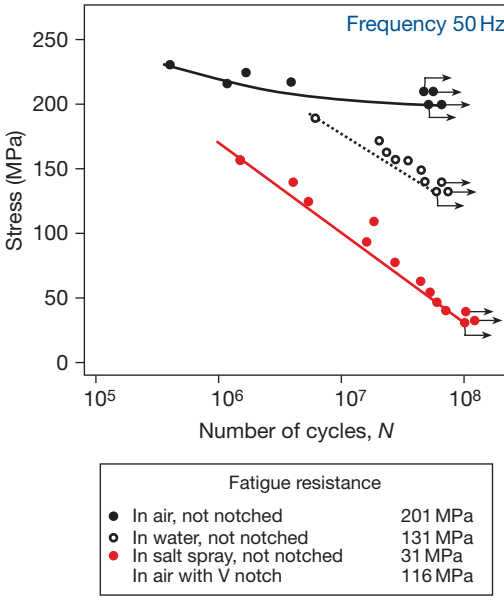

Figure 33 Corrosion fatigue curves of a ferritic SG cast iron in rotary bending (50 Hz).

Unlike most stainless steels, austenitic cast iron, for example the EN-GJSA-XNiCr20-2 type, is not affected by crevice corrosion or by corrosion cracking, even in stagnant solution. Moreover, it provides cathodic protection to any lower alloy cast steel or iron components. In many cases, however, cracks may occur by stress corrosion cracking in warm seawater, at temperatures above ~30 °C. The tensions that appear are not ascribable to the service loading; rather, they are due to internal stress. For this reason, a careful stress relieving annealing can reliably reduce the risk of stress corrosion cracking.[88,89]

The occurrence of stress corrosion cracking in EN-GJSA-XNiCr20-2 and EN-GJSA-XNiCr30-3 spheroidal graphite cast irons in magnesium chloride solutions containing 5–40% $MgCl_2$, at temperatures ranging from 20 °C to the boiling point, was studied by German authors[89,90] on tensile test pieces and a diagram of the stability as a function of stress in % of yield strength for the two cast iron types is shown in **Figures 35** and **36**.

There exists, for both cast irons and for each temperature, a clear limiting stress below which corrosion cracking no longer occurs. Concerning the influence of the concentration of the solution, it turns out that the life is shortest in a 10% solution of $MgCl_2$. The life is reduced by anodic polarization, while stress corrosion cracking can be blocked by a weak cathodic polarization of 50–100 mV from the resting potential. This implies that the stress

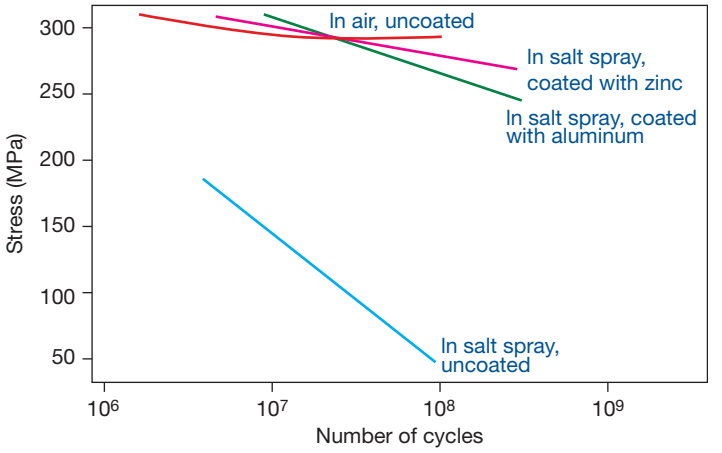

Figure 34 Effect of Zn and Al coatings on the corrosion fatigue resistance of an SG cast iron in a salt spray (3% NaCl). Reproduced with permission from Forecast Progress in Metal Casting, no. 46, October 1983.

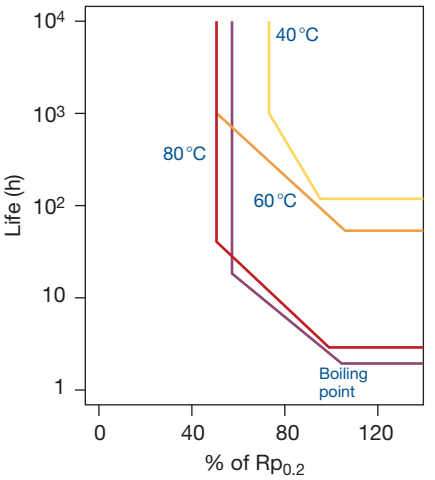

Figure 35 Diagram of resistance of an ENGJSA-XNiCr20-2 cast iron. Relation between the stress in % of yield strength (Rp0.2) and the temperature in 5–40% solutions of $MgCl_2$. Reproduced with permission from Baumel, A. *Werkstoffe Korros.* **1993**, *44*, 107–108.

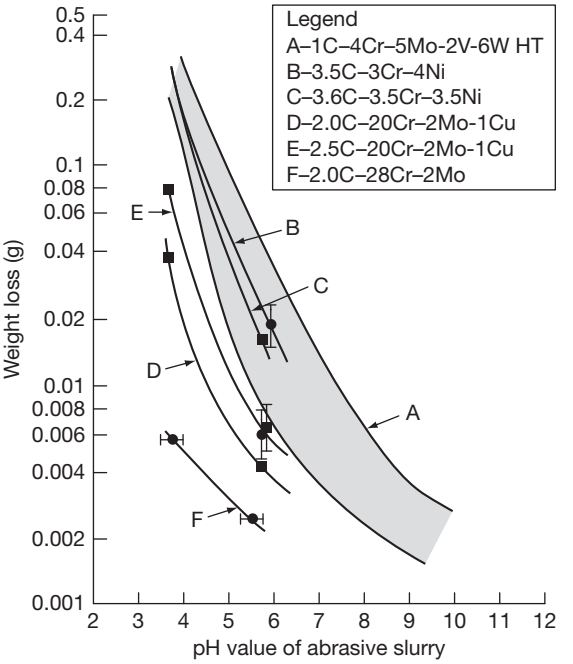

Figure 36 Diagram of resistance of an ENGJSA-XNiCr-30 cast iron: relation between the stress in % of yield strength (Rp0.2) and the temperature in 5–40% solutions of $MgCl_2$. Reproduced with permission from Baumel, A. *Werkstoffe Korros.* **1993**, *44*, 107–108.

corrosion cracking of austenitic cast iron is favored by contact with an austenitic stainless steel, even in highly dilute solutions, containing for example 0.1% $MgCl_2$, where there is still a sensitivity to stress corrosion cracking at high stresses and temperatures. Also, EN-GJSA-XNiCr-30 cast iron is considerably more resistant than EN-GJSA-XNiCr20-2 cast iron. As the most effective remedy against corrosion cracking under load, a reduction of internal stress by a stress-relieving annealing is recommended. Acceptable residual stress levels of 100 MPa for EN-GJSA-XNiCr20-2 cast iron and 150 MPa for EN-GJSA-XNiCr-30-3 cast iron are allowed.

3.02.5.11 Organic Compounds

3.02.5.11.1 Alcohol and glycol

Unalloyed cast irons and nickel cast irons can be used for ordinary applications in the presence of hydrocarbons, aldehydes, and amines although some slight attack occurs with the simultaneous presence of

water. Nickel cast irons have complete resistance at all concentrations of these species. On the other hand, alcohol–water mixtures will cause corrosion, the most common application occurring in the use of ethanediol and glycol compounds in automotive antifreeze and coolants. In order to combat this form of corrosion, one or more corrosion inhibitors, such as benzotriazoles and sodium benzoates, are often added, Table 27.[91]

3.02.5.11.2 Corrosion by food products

Unalloyed cast irons and nickel cast irons must not be used with wine, vinegar, beer, cider, fruit juices, milk, maltose, and mustard. By contrast, unalloyed cast irons can be used with concentrated beverage, alcohols, and liqueurs. Table 28 provides information about the corrosion resistance of two cast irons in the presence of a number of fruit juices and wine vinegar.

Table 27 Corrosion rate of unalloyed gray iron in ethanediol–water mixtures in the presence of various inhibitors

Medium	*Loss of mass after 50 days testing (mg cm^{-2})*
50% Aqueous solution of ethanediol at 70°C (Medium A)	19–21
Medium A + 1% sodium benzoate	25–28
Medium A + 5% sodium benzoate	0.63
Medium A + 0.5% benzotriazole	11–13
Medium A + 1% benzotriazole	6–8
Medium A + 1% benzoate 0.1% benzotriazole	0.3–5
Medium A + 1% benzoate 0.5% benzotriazole	0.3
Medium A + 1% benzoate 1% benzotriazole	0.2

Table 28 Corrosion rate of cast iron in various food products

Solution	*Temperature (°C)*	*Corrosion rate (mm/year)*	
		Unalloyed cast iron	*Ni-Resist cast iron (≤ 20% Ni)*
Pineapple juice	86	20	1.8
Pineapple juice	24	1.5	0.25
Grapefruit juice	Tb	59	0.5–1.5
Grapefruit juice	30	8.9	0.5–1.5
Tomato juice	50	2.8	0.5
Vinegar	15	3.3	–

3.02.5.12 Corrosion by Molten Materials

The resistance of cast iron furnace components, especially crucibles, to oxidation at elevated temperatures is important to ensuing dimensional stability and retaining a suitable wall thickness, especially in crucibles. The best material for crucibles from the standpoint of resistance to corrosion is a refractory alloy that can withstand a temperature of the order of 850 °C. According to Polish studies[88,92] a low-alloy chromium cast iron (1.5–3%) best meets this requirement: with such an alloy, the layers of oxides formed on the outside surfaces of the crucibles are relatively thin. The second problem for crucibles containing molten materials is their dissolution. First, a high, but nonuniform, dissolution of the crucible material can lead to the formation of deep local cavities, limiting the life of the crucible. Second, the crucible contents are polluted by iron, which can be a severe problem.

3.02.5.12.1 Corrosion by liquid aluminum or aluminum alloys

Unfortunately, not much is known about the transfer mechanisms of iron from a ferrous crucible into a molten aluminum. However, it is known that the general rate of dissolution of iron into a light alloy increases as the temperature and the silicon content increase.[64] Baths containing magnesium are also highly corrosive, but aluminum alloys containing copper are less so. Among ferrous alloys, cast irons generally resist better than cast steel. According to the Polish work mentioned earlier,[88,92] the best corrosion resistance is found for lamellar graphite cast irons and blackheart malleable cast irons. Some work indicates that high-phosphorus (1.29%) lamellar graphite cast iron displays the best corrosion resistance in liquid aluminum alloys. But that it would be difficult to apply these results in industry, because cast irons having an extensive phosphorus eutectic distribution are not, in other respects, sufficiently resistant to oxidation. As for the influence of chromium, it has been shown that the rate of iron dissolution has a minimum of 2.9% chromium.

Generally, in cast iron crucibles containing molten aluminum, the aluminum diffuses into the crucible surface forming an intermetallic compound ($FeAl_3$). This effect reduces the effective difference of aluminum content between the crucible and the liquid alloy, which is one of the drivers for the dissolution process. Some authors[93] have commented that since the $FeAl_3$ combination contains no carbon, there results an increase of the carbon content on

the perimeter of the ferrous sample, with a clear increase of the pearlite content. This local increase of the pearlite content favors the corrosion resistance of the metal. The same authors have also shown that ferritic white cast irons containing 32% chromium are among the materials that are least resistant to liquid aluminum.

Therefore, it appears that the optimum chemical composition for a cast iron that must resist corrosion by liquid aluminum and silicon alloys is: 3.4–3.5% C, 0.3% P, 2.5–3.0% Cr, 2.0–2.5% Si, 0.1% S, 4.0–5.0% Al, 0.4% Mn and a Polish patent (no. 55.549) was taken out for this grade of cast iron in 1968. In France, a similar cast iron, but containing no aluminum, is generally recommended. However, in practice, the problems of corrosion by liquid aluminum alloys are rarely solved at the metallurgical level; the recommendation most often made is to apply a good dye coating as the only way to ensure a satisfactory life.

3.02.5.12.2 Corrosion by liquid zinc and zinc alloys

A phenomenon of gradual dissolution also occurs in the cast iron crucibles used for melting zinc and its alloys. A detailed study at CTIF[94] of the corrosion of ferrous alloys by liquid zinc alloys found that ferrite is the most unfavorable constituent as regards resistance to this type of attack. Pearlite fairs better, even though there is a risk of progression of the corrosion between its lamellae, and a loosening of the latter. This last phenomenon is, however, rather rare: liquid surface tension generally prevents the molten zinc alloy from progressing between the lamellae when the pearlite is fine enough. Hence, it is preferable to avoid coarse structures. Since corrosion advances preferably along the graphite lamellae, it is also best to limit their size as much as is possible; spheroidal graphite once again seems preferable in this respect. As in the case of aluminum, corrosion by liquid zinc is chemical, not electrochemical. Thus, there is no reason to believe that the resistance of an austenitic cast iron of the 'Ni-Resist' type is better than that of a pearlitic cast iron.

3.02.5.12.3 Corrosion by other liquid metals

According to various sources, cast iron possesses good resistance ($<0.025\,mm\,year^{-1}$) to dissolution in liquid magnesium, at its melting temperature (651 °C), liquid calcium up to 700 °C, liquid lead up to 500 °C and liquid cadmium at 600 °C. It has limited resistance ($0.025–0.25\,mm\,year^{-1}$) in liquid tin at its melting point (322 °C), liquid magnesium from 700/800 °C and liquid sodium and potassium at 480 °C. However, cast iron has poor resistance ($>0.25\,mm\,year^{-1}$) in liquid sodium and potassium at 600 °C, liquid tin at 600 °C, and liquid antimony at its melting point (630 °C).

Note that the dissolution of cast iron crucibles used for the melting of metals can sometimes be ascribed to other processes that may accompany the iron dissolution, such as the erosion–corrosion resulting from the flow of the liquid metals, cracking by thermal fatigue or by creep, and high temperature oxidation processes.

3.02.5.12.4 Corrosion by liquid sulfur

Table 29[95] indicates the rate of attack in liquid sulfur of a unalloyed lamellar graphite cast iron and of a type EN-GJLA-XNiCuCr15-6-2 austenitic cast iron, as a function of temperature.

It can be seen here that nickel cast irons behave like unalloyed cast irons up to 250–300 °C, and then more poorly at higher temperatures.[96] The addition of silicon (15%), possibly reinforced by an addition of molybdenum (or of chromium or copper), significantly reduces the rates of attack (Table 30).[97]

3.02.5.13 Microbially Influenced Corrosion

The role played by microbes in nature is well known. Numerous in the soil and in water, they decompose organic and mineral matter and participate in the

Table 29 Dissolution rate of cast irons in liquid sulfur

Temperature (°C)	*Corrosion rate (mm year^{-1})*	
	Unalloyed LGI	*EN-GJLA-XNiCuCr15-6-2*
127	0.5	0.5
260	0.8	0.8
295	2.8	3.3
365	5.0	7.3
446	10.9	14.8

Table 30 Dissolution rate of 15% silicon iron in liquid sulfur

Temperature (°C)	*Corrosion rate (mm/year)*
120	<0.05
200–300	<0.1
430	0.5–1.25

grand cycles of carbon, nitrogen, and sulfur. Most of the microorganisms responsible for microbially influenced corrosion can adapt to temperatures between −10 and +99 °C, pH between 0 and 10.5 and concentration of oxygen between 0% and nearly 100%. Many bacterial species produce an extensive range of compounds and species capable of promoting corrosion, including organic acids, sulfuric acid, hydrogen sulfide, etc.

3.02.5.13.1 Iron oxidizing bacteria

Iron oxidizing bacteria utilize the transformation of ferrous salts into ferric salts as part of their life cycle. The bacteria secrete enzymes that favor the oxidation of iron. Thus, at local anodes where ferrous hydroxide is formed, this quickly turns into ferric and carbonated hydroxide by dissolved oxygen and carbon dioxide. Generally, the microbial process ends there; however, the rapid transformation of the ferrous ions into ferric salts, results in the formation of a voluminous clump of 'rust' containing the bacterial bodies, sometimes known as a tubercule, followed by a continuing attack of the metal.[98] The local environment under the rust is likely to be depleted in oxygen and this can provide a microclimate for the proliferation of anaerobic microbial species.

3.02.5.13.2 Sulfate-metabolizing bacteria

Sulfate-reducing bacteria, being anaerobic in nature, are found under the layers of rust, in contact with the metal, where oxygen does not reach them. They generally transform sulfate into reduced sulfur species ending in hydrogen sulfide, which combines with the ferrous salts to produce a black sulfide for example:

$$SO_4^{2-} + 4H_2O + 8e^- \leftrightarrows S^{2-} + 8OH^-$$

With the overall reaction:

$$4Fe + SO_4^{2-} \leftrightarrows FeS + 3Fe(OH)_2 + 2OH^-$$

Sulfur oxidizing bacteria, for their part, metabolize sulfur from sulfur or sulfide compounds, resulting in the production of sulfite or sulfate species and acidification of the medium, causing severe corrosive attack. For example:

$$S^{2-} + 4H_2O \leftrightarrows SO_4^{2-} + 8H^+ + 8e^-$$

Historically, microbial oxidation of ferrous sulfide (e.g., in tin, lead, and coal mines) resulting in the formation of strongly acidic mine waters, provided the first industrial examples of this type of corrosion. However, it is also found in many industrial water circuits (water sprinkler system, for example). In favorable circumstances, colonies of sulfate reducing and sulfate oxidizing bacteria may coexist giving rise to serious corrosion problem in water transport and in particular, the sewerage systems. The following conditions are generally favorable to biological corrosion by sulfur bacteria: an anaerobic medium, a pH of 5.5–8.5, the presence of sulfates, the presence of a food (carbon) source, the presence of essential nutrients such as phosphate, and an optimal development temperature (e.g., 30–40 °C).

3.02.5.13.3 Mechanisms of action

Together, microbiological knowledge of bacterial metabolisms and knowledge of corrosion on the chemistry of water in the presence of acid gases CO_2 and H_2S, lead to the conclusion that sulfate-reducing bacteria can regulate the pH of their environment to favor their growth. Secondary reactions with traces of oxygen or of ferrous iron can modify this pH value.[99]

It is important as well to remember that corrosion that occurs in an anaerobic medium is not necessarily bacterial; it may well be just a sign of the activity of a macrocell of the differential aeration type at its anodic zones, located precisely in the anaerobic zone. In the case of extended structures, these two types of activity are often found superimposed. Also, bacterial corrosion may be observed in soils that are not strictly anaerobic, but in which, as a result of corrosion previously initiated by classical processes, conditions favorable to the spread of bacterial activity have been established, for example under the corrosion product layers.

3.02.5.13.4 Microbial corrosion of cast iron

Often, the formation of a gelatinous vesicle is an initial visible sign of bacterial attack. This vesicle takes the form of a brown mass with smooth contours containing a blackish liquid with a strong hydrogen sulfide odor. At this stage sulfur compounds such as S, FeS, and FeS_2 are present in the gelatinous mass, which conceals corrosion, usually in the form of a crater that may perforate the metal. The craters contain pockets of bacteria, commonly with iron bacteria near the surface and sulfate-reducing bacteria in the interior, which is anaerobic. Generally, biological corrosion almost always follows as a result of electrochemical corrosion but can increase it substantially.

The process of development of corrosion vesicles on cast iron is shown schematically in **Figure 37**. From the outset, the ferrous ions that form at the

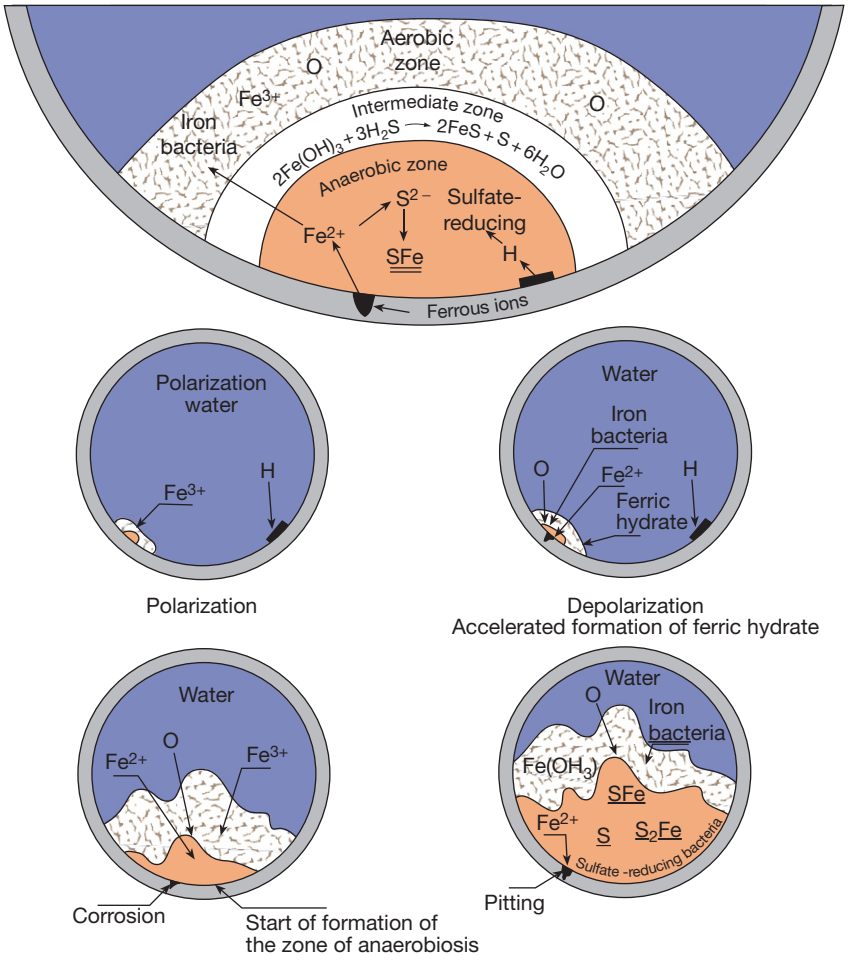

Figure 37 Formation of a gelatinous vesicle during microbial corrosion. Based on a figure in Badan, B.; Magrini, M.; Ramous, E. *J. Mater. Sci.* **1991**, *26*, 1951–1954, and reproduced with permission from Reynaud, A. *Corrosion and Cast Iron*, ETIF, France, 2008.

anode are transformed by oxidation into ferric hydroxide and hence, form a layer of rust, which gradually impregnates with ferrous salts that diffuse on the surface. These ferrous salts taken up by iron bacteria are quickly transformed into ferric hydroxide under aerobic conditions, and because of this the volume of the mass increases. It becomes more and more difficult for oxygen to diffuse to the interior. Aerobic development bacteria, therefore, can only thrive in the peripheral layers. This process creates, in the underlying layer, anaerobic conditions favorable to the development of sulfate-reducing bacteria, which reduce sulfates into hydrogen sulfide and iron sulfide. An Italian study[100] has confirmed the mechanisms stated above for microbial corrosion, in particular the formation of corrosion tubercules on the inside surface of cast iron pipes. In practice, in the case of water delivery pipes, cement mortar linings have been used for nearly 50 years as a mechanism for controlling corrosion in new pipes and for renovation of old pipes.

3.02.5.13.5 Combating microbial corrosion

Many chemicals (biocides) can, in principle, be used to combat bacterially influenced corrosion. Among these include oxidizing agents (e.g., chlorine, bromine, potassium permanganate, etc.), toxic heavy metals (e.g., Ag, Cu, Zn, Hg), and their salts, detergents and amine derivatives, and aromatic alcohols (e.g., phenol and derivatives). These compounds are extremely varied, but often have high toxicity not only to the microbial species, but also to other lives. The use of many of these is controlled by legislation over the discharge of materials is the

environment. Chantereau's book[98] contains a list of the main products used in the fight against bacteria, with all their characteristics and domains of use. Note that chlorine, even though it is normally a corrosive substance, is beneficial in this context; its bactericidal action generally reduces corrosion by two thirds.

3.02.5.14 Flow-Induced Corrosion

3.02.5.14.1 Cavitation corrosion of cast iron

When a liquid is subjected to a sudden fall of pressure, bubbles of vapor having a life of the order of a millisecond may form. This extremely brief existence ends when the local pressure increases in an implosion that, repeated thousands of times, can cause significant damage to some equipment. This is the phenomenon of cavitation. Some authors[101] have shown the impact of cavitation on corrosion damage: a ratio of 1–75 000 between 'simple' corrosion rates and cavitation corrosion rates. The interested reader may refer to Heuze[102] and for a theoretical examination of the phenomenon. In practice, two main types of cavitations are distinguished: 'flow' cavitation, which affects for example the vanes of turbines, and cavitation by vibrations. In cavitation by vibrations, the formation and implosion of bubbles result from the shock waves that a vibrating surface produces.

The apparently complex influence of temperature on the cavitation corrosion of cast irons has been the object of several studies.[103–105] It has, for example, been shown that the maximum attack occurs at a temperature approximately mid-way between the boiling and melting points of the corrosive medium (60 °C, in the case of water).[104] This critical temperature is assumed to be located differently according to the nature of the liquid and the ambient pressure.[106] It is found, in the case of water, that the deterioration of the material increases as the temperature rises from 0 to 50 °C. This seems to be explained by the concomitant lowering of the dissolved air content. Above 50 °C, the intensity of the cavitation decreases as the temperature increases; the lower air content of water is then offset by the higher vapor pressure. The nature of the fluid is also of some importance. Non-ionic liquids, such as toluene, are much less aggressive than water in the context of cavitation. The high vapor pressure of these liquids is invoked to explain this point. Otherwise, concerning the inhibition of this type of corrosion, in closed systems (cooling circuits), sodium nitrite or chromate and a few amines (triethanolamines, for example) have been proposed. The effectiveness of this protection by inhibitors proves the importance of the electrochemical factor in cavitation corrosion.

Cast irons as a whole are said to be more sensitive to cavitation than steels. Certain authors[107–110] have shown that pearlitic cast irons are less vulnerable to cavitation than ferritic grades, and that the shape and size of the graphite inclusions also play a role on the spheroidal graphite cast irons being more resistant. Often surface hardening can improve the resistance to cavitation corrosion and studies have shown the utility of a superficial nitriding treatment.[110,111] Otherwise, austenitic spheroidal graphite cast irons from 20% Ni, 2% Cr to 30% Ni, 5% Cr display excellent resistance to cavitation corrosion under the most severe conditions. Thus, fishing-boat propellers and pump rotors made of these materials provide better service than a bronze or a stainless steel containing 18% chromium, **Table 31**.[84]

Some laboratory studies have simulated cavitation phenomena using sonic or ultrasonic vibrations.[112] In one of these studies, the vibrations were of 40 µm in amplitude at 15 kHz. In such operating conditions, the losses of mass of the four types of cast iron were as follows: ferritic lamellar graphite cast iron: 298 mg h^{-1}; pearlitic lamellar graphite cast iron: 155 mg h^{-1}; ferritic spheroidal graphite cast iron: 124 mg h^{-1}; pearlitic spheroidal graphite cast iron: 67 mg h^{-1}. It was found that the intensity of the corrosion cavitation was proportional to the square of the amplitude of the vibrations. However, the general rates of cavitation corrosion in this type of laboratory test are much larger than those in the field.

Cavitation is not an uncommon problem in internal combustion engines using cast iron cylinder liners. It has been shown[113] that the radial vibrations of the walls of the lining due to the running of an engine can lead to severe cavitation damage of the cast iron. Other work has shown that the superimposition of an external mechanical effect (tension or compression) does not appear to affect the intensity

Table 31 Cavitation corrosion of various cast irons in seawater

Material	*Annual loss of thickness in seawater at 28°C at a velocity of 8.2 m s^{-1} (at mm)*
Unalloyed lamellar graphite cast iron	6.9
'Ni-Resist' cast iron (Ni20 Cr2 LGl)	0.75
88-10-2 Bronze	1.0

of the cavitation phenomenon (provided that it does not give rise to a significant stress phenomenon).

Some authors[114] have shown that the cavitation corrosion resistance of a lamellar graphite cast iron that has undergone superficial laser surface alloying by chromium (22%) in water (with or without 3% NaCl) at 50 °C is greatly increased. Similarly, other authors[109] have also shown the value of a surface hardening treatment. They found that a nitrided layer having the right hardness, thickness, and homogeneity is a good means of defence against cavitation corrosion.

An outline review of the literature on resistance of cast irons to cavitation[109] identified, or served to recall, a certain number of preliminary ideas. For example, it is known that the weakening effect of the graphite lamellae depends on their size, shape, and distribution in a given matrix. The spheroidal shape is optimal in this respect. Similarly, hard matrices (martensitic, bainitic, etc.) are preferable (the martensite must be tempered). Otherwise, note that saline solutions (3% NaCl) are much more aggressive than distilled water (up to seven times as corrosive). The use of inhibitors or of cathodic protection can be very effective. The presence of phosphorus (of phosphorus eutectic) has little effect other than a possible reduction of the incubation time of the phenomenon. Silicon, unlike chromium and molybdenum, increases cavitation resistance.

Kuwaiti researchers in 2001 studied the mechanisms of degradation of spheroidal graphite cast irons subjected to cavitation effects in seawater. They showed that the surfaces of iron castings, hollowed as wide craters, are prolonged in the cast iron by microcracks. The mechanism of initiation of the degradation seems to be related to the activity of a galvanic microcouple at the graphite–ferrite interface; the process is then prolonged by brittle fracture and ductile tearing of the material.[97]

3.02.5.14.2 Corrosion–erosion of cast iron

When the corrosive liquid also contains abrasive particles, there appears a phenomenon of erosion that strips away the corrosion products as they form, keeping the metal bare and therefore active. This mode of attack is commonly called 'corrosion–erosion' or 'erosion–corrosion' (the terms are often used interchangeably, but see below) or possibly 'cavitation–erosion' when the flow becomes highly turbulent.[115,116] The phenomenon of abrasion–corrosion (more correctly erosion–corrosion) is the result of mechanical damage by the action of solid particles and electrochemical damage due to the presence of a corrosive medium. This type of situation is often found in industry, for example in treatment and transport of fluids in the oil and mining industries. Many parameters are influential on the damage: for example, the shape, hardness, size, and velocity of the particles, angles of incidence, characteristics of the medium, etc. Gray cast irons can be used, given their low cost price, if the erosion conditions are not too severe. However, significant performance benefits accrue using more resistance materials such as a 'Ni-Hard' grade. Lower alloyed materials have carbides predominantly as M_3C type and, in order to obtain increased resistance to erosion effects, the chromium and nickel contents must be increased to irons largely free of pearlite and containing harder carbides of the M_3C_7 type.

Examination of the corrosion morphology of cast iron under erosion–corrosion conditions reveals that the erosion process generally begins with attack of the softer graphitic phase creating, in LG irons particularly, a network of voids that facilitates the penetration of the aggressive liquid. It follows that fine lamellar graphite is preferable to coarse lamellar graphite. After the preliminary stage, cracks form, essentially at the pearlite–phosphorus eutectic interfaces and at the boundaries between the various colonies of pearlite, leading to a gradual loss of cohesion of the cast iron. Ferrite seems to stand up better to this erosion process.

An ever-growing quantity of cast iron having high chromium and molybdenum contents is being used for the production of pumps that are harder and more resistant to abrasion. The results of tests on cast irons containing 15% Cr + 2% Mo or 25–27% Cr have, moreover, been published.[117] In this case, the advantages with respect to low-alloy white cast irons lie not only in their greater abrasion resistance and better fracture toughness, but also in their improved machinability. The housing and rotors of pumps transporting abrasive muds and of dredging pumps are manufactured by techniques that include annealing, machining, and quenching.[118] Elastic coatings to absorb impacts can also be considered.

High-chromium alloys with carbon contents in the range 0.5–2.0% afford a useful compromise between resistance to corrosion and resistance to abrasion. As the carbon content is increased, the resistance to abrasion improves, but corrosion resistance is reduced. The matrix structure of this range of high-chromium alloy irons can be largely austenitic or can be transformed to martensite by heat

treatment. There has been an increased interest in this series of alloy irons in recent years because they would seem to offer a cost-effective solution to problems encountered in handling abrasive slurries arising from gas scrubber installations in coal-fired power stations, **Figure 38**. They are also seen as candidate materials for the high-speed high-pressure pumps necessary in coal liquefaction projects, since they are able to resist abrasion at temperatures at which many abrasion-resistant steels would soften.

It is to be remembered that the hardness of the metal is not the only parameter to be considered in predicting resistance to corrosion–erosion. Allowance must also be made for factors related to the microstructure of the alloy, for example the size of the particles transported by the fluid relative to the size of the 'matrix' constituent. If the particle sizes are larger than the mean size of an 'island' of matrix in the microstructure, there will be less wear. There is a longstanding tendency to believe that, in these corrosion–erosion phenomena, the share of erosion prevails over the share of corrosion. In the light of certain tests, there seems to be less and less reason to believe this. Japanese authors[119] have shown that the erosion–corrosion of chromium cast irons is initiated at the matrix–carbide interface, and subsequently continues as corrosive and abrasive wear of the matrix

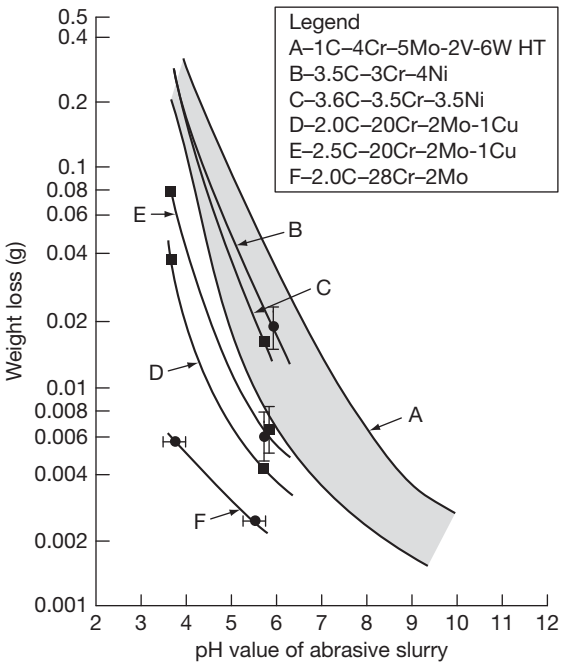

Figure 38 Influence of pH value on weight loss in the slurry abrasion test.

that can be reduced by increasing the chromium content. In general, additions of vanadium (5–8%), molybdenum (1–2%), and titanium (0.2%) seem to be effective ways to increase the resistance of grades containing 12–13% chromium.

Another Japanese study[120] has shown that the corrosion–erosion resistance of cast irons is often less than that of steels, because the preferential stripping of the graphite leads to the formation of craters, in which localized forms of corrosion are then initiated. These same authors have also shown that the deterioration of the material is inversely proportional to its hardness and that it can be prevented by cathodic protection. An electrochemical study of the corrosion–erosion resistance of white chromium cast irons has shown that the anodic corrosion current increases as the velocity of the abrasive substance increases and as the chromium content of the cast iron decreases.[121] Other work[122] has shown the value of austenitic–martensitic cast iron containing 5% manganese and 3% copper against corrosion–erosion, which would seem to have the same characteristics as a high-nickel alloyed grade. Finally, according to the same authors, a complementary addition of copper to chromium cast irons (5–6%) would seem to increase their resistance to this type of corrosion.

Many publications[123,124] report that laser surface hardening considerably increases erosion–corrosion resistance. Tests mentioned by American authors[125] have shown that, with gray cast irons (LG and SG), high power densities and long laser-cast iron interaction times result in very high hardness values (1200–1300 HV). The microstructures then observed correspond to fine carbide–ferrite aggregates. If the power density and interaction time are reduced, the hardness values are lower (600–800 HV) and the microstructure is found to be made up of dendrites of metastable austenite and films of interdendritic cementite. Depending on the values given to the various parameters of the laser treatment, the corrosion–erosion resistance can be improved by a factor of 2–5.

In the salt-rich and very polluted waters of the Persian Gulf, a comparative study of the corrosion–erosion resistance of a ferritic unalloyed SG cast iron, a silicon cast iron (14.5% Si), an austenitic lamellar graphite cast iron containing 20% Ni and 3% Si, and a duplex cast steel similar to a G-X 3 CrNiMo 26 6 3 cast steel with a reduced manganese content was carried out.[126] The objective was to test materials for ball valves. During these tests, the mechanism of corrosion and the formation of protective layers were also studied. The duplex cast steel suffered no measurable attack in the course of

25 days of tests. The corrosion losses of the three grades of cast iron are shown in Figure 39.

In stagnant water, only a small loss occurs, while in turbulent water the erosion increases significantly at first, except in the case of silicon cast iron where a coating made up of corrosion products forms. Gradually, the corrosion slows and the influence of the current velocity becomes weaker and weaker and forms, on the surface of the specimens, a thicker and thicker coating of corrosion products that slows the attack.

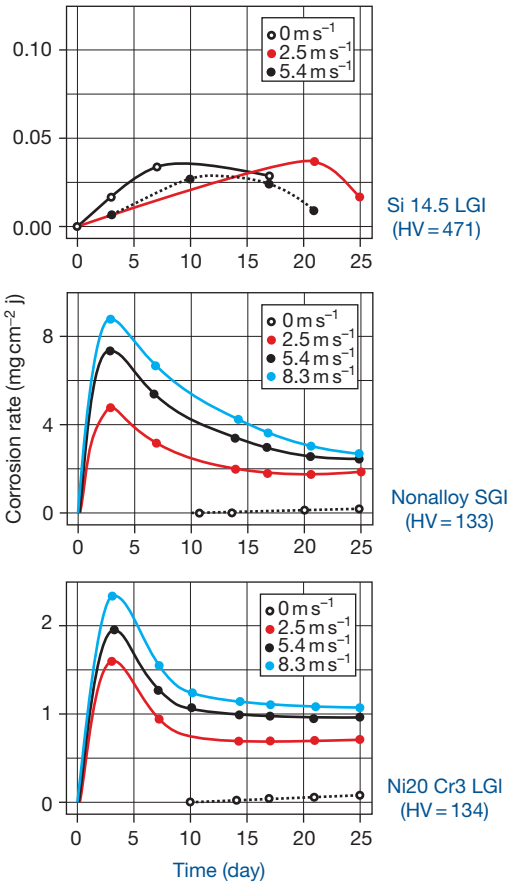

Figure 39 Corrosion rates of three grades of cast iron in turbulent Persian Gulf seawater at 28 °C.

Table 32 indicates the masses of the coating of corrosion products measured on the three grades of cast iron. On the silicon cast iron, the layer is very thin. At low current velocities and in still water, a phenomena similar to pitting or intergranular corrosion appeared on the cast irons; on the graphite lamellae and in the zones of segregation between the dendrites in particular. At higher current velocities, these phenomena disappear and the level of corrosion regresses to values too small to measure. The silicon cast iron suffered the least attack at all current velocities, thanks to its hardness, 470 HV, and to the thick coating of SiO_2.

Some authors[127] have proposed two grades of white cast iron containing manganese (4–5%) and chromium (5–6%), with and without copper (0 and 2–3%), that seem to have the same corrosion–erosion resistance as an austenitic–martensitic white nickel–chromium cast iron of the 'Ni-Hard' type; the addition of copper seems to increase the corrosion resistance. Ageing these grades for 6 h at 800 °C is recommended, in order to precipitate very fine carbides in the austenitic matrix to increase the erosion resistance.

3.02.6 Corrosion by Gases

3.02.6.1 High Temperature Oxidation and Corrosion

At temperatures above ~500 °C, unalloyed cast iron in an oxidizing atmosphere becomes covered with a

Table 32 Mass of corrosion product on cast iron after exposure to seawater at different flow velocities

Duration of test (days)	*Mass of corrosion product on surface (g)*							
	Slicon cast iron ($m\ s^{-1}$)		*Unalloyed SGI iron ($m\ s^{-1}$)*			*Ni20 Cr3 LGI*		
	2.5	*5.4*	*2.5*	*5.4*	*8.3*	*2.5*	*5.4*	*8.3*
3	0.00	0.00	N.A	19.71	18.89	N.A	3.35	3.84
7	0.00	0.00	10.89	28.90	33.70	4.05	5.64	3.79
10	0.00	0.00	20.91	35.09	37.80	5.11	2.53	2.22
14	0.27	0.00	23.95	39.10	31.25	6.81	3.64	4.36
17	0.29	0.13	25.07	42.39	30.77	9.33	4.67	1.08
21	0.22	0.03	31.82	50.08	37.55	11.33	3.85	1.87
25	0.20	0.15	49.13	54.78	37.00	16.31	4.19	5.72

scale made up of several layers of oxides plus a layer consisting of ferrous oxide and oxides of the alloy element X: $FeO + Fe_yX_zO$. Thus, its behavior is very similar to steel under the same conditions. The effect of chromium, aluminum and silicon additions to cast iron alloys on oxidation at high temperature has long been known. Thus, alloyed irons preferentially form more protective oxide scales consisting of, respectively, Cr_2O_3, Al_2O_3, and SiO_2. Reaction with FeO at the oxide–metal interface may additionally result in the formation of a spinel: $FeCr_2O_4$ or $FeAl_2O_4$, or a silicate such as Fe_2SiO_4. At greater distances from the basic metal, the oxygen pressure increases and, at a certain level, FeO is transformed into Fe_3O_4, then Fe_2O_3. The diffusion velocity of the iron ions in the lower layer of compound oxides, highly adherent and more compact than the superficial layers of pure iron oxides, is very low and hence, protects alloys containing chromium, aluminum, and silicon. The presence of molybdenum also favors this oxidation resistance.

In this particular case of lamellar graphite cast irons,[128] oxidation at high temperature is not limited to the superficial layer, but progresses along the graphite–matrix interfaces in the interior of the casting. The oxygen first combines with carbon, which at the temperatures in question gives carbon dioxide, CO_2, which in turn oxidizes the metal as it turns into CO. This gas tends to crack the protective oxide film, thereby facilitating the entry of oxygen. The formation of the oxidized compounds combines with the graphitization to cause a swelling of the cast iron. The progression of the oxidation, therefore, follows the path traced by the graphite; the layers of oxides are interposed between the matrix and the graphite lamellae.

Figure 40 below gives an idea of the intensity of the superficial oxidation that occurs when gray cast iron is held at 900 °C in air. Generally, the relative importance of the layer of oxides formed is measured using the change of mass of the sample. The absorption of oxygen is reflected by an increase of the mass due to the formation of the layer of oxides, while the removal of this layer causes a reduction of this mass. For specific graphite contents, the lamellar shape is therefore the most unfavorable; resistance to the penetration of the oxidation increases as the shape becomes more compact, with the spheroidal shape being the most favorable. Figure 41, which compares the swelling of five lamellar graphite cast irons having different silicon contents with the swelling of five spheroidal graphite cast irons having the same composition, shows the superiority of the latter very clearly.

A Japanese study of the effect of chromium, aluminum, nickel, and silicon on the oxidation rate of SG cast irons between 700 and 850 °C was

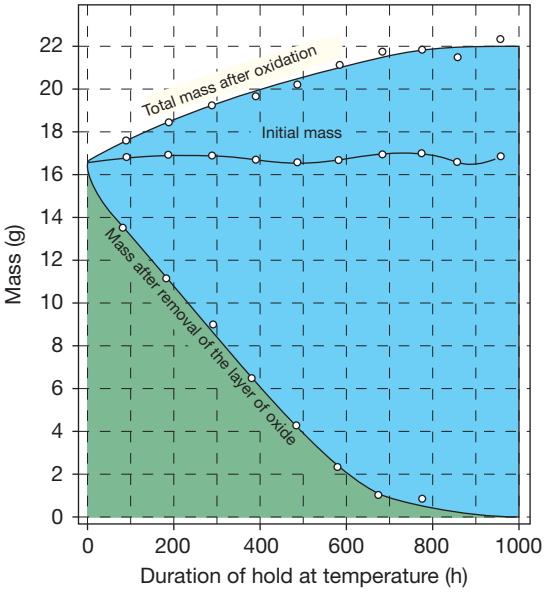

Figure 40 Superficial oxidation of a unalloyed cast iron held in air at a temperature of 900 °C (the initial specimen was 10 mm in diameter and 30 mm long). Reproduced with permission from Sawamoto, A.; Usami, T.; Ogi, K.; Matsuda, K. *Imono* **1984**, *10*, 597–601.

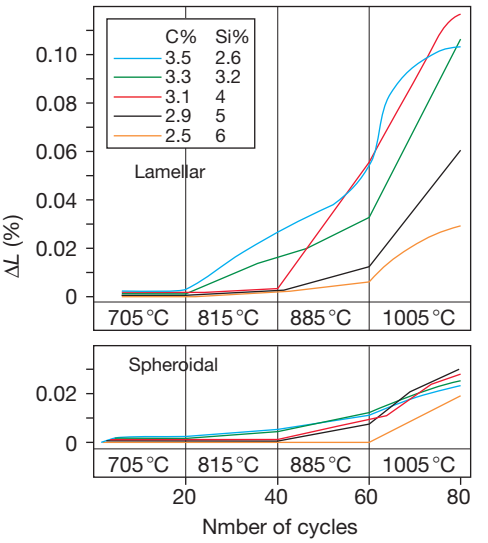

Figure 41 Samples 10 cm long were subjected to cycles of heating (30 min at the temperature indicated) and cooling in air. Reproduced with permission from Bechet, S. *Hommes Fonderie* **1981**, *112*, 15–28.

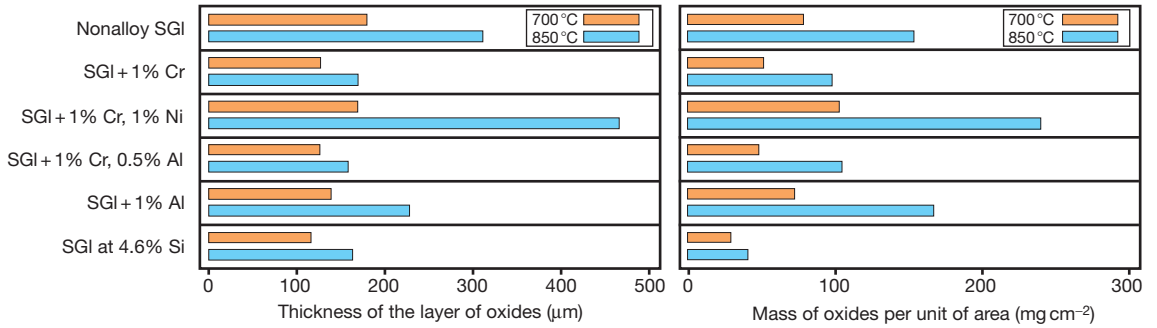

Figure 42 Oxidation behavior at high temperature of various SG cast irons held for 100 h at 700 and 850 °C.

investigated[129] with the elements classified in order of decreasing effectiveness, as follows: Si–Cr–Al–Ni. Information on the influence of moderate additions of chromium, aluminum, nickel, and/or silicon on oxidation resistance at high temperature is shown in Figure 42.[130]

The beneficial effect of chromium on the oxidation resistance of cast irons is shown in Figure 43. This effect is very substantial from the first additions of chromium; this is a significant advantage, given that the chromium content of gray cast irons is always limited because of its strong tendency to produce carbides, which can for example result in machining difficulties.

In general, the types of cast iron used as a function of temperature are as follows:

- cast iron at 1–2% chromium for combustion gas with temperatures of not more than 850 °C or for preheating, up to a maximum of 350 °C, of gas having a high carbon monoxide content;
- cast iron at 30% chromium in the case of combustion gas of which the temperature is less than or equal to 1050 °C, or for the preheating of air to 650 °C.

The resistance of 30% chromium cast iron to destruction by gases having high carbon monoxide content is excellent in the temperature range from 400 to 600 °C.

The influence of the silicon content in conjunction with the carbon content shows that the oxidation resistance of hypoeutectic cast irons is better than that of hypereutectic cast irons. The harmful effect of carbon is also recognized. The influence of silicon content (between 2.4% and 6.4%) on the oxidation of five SG cast irons as a function of temperature is evident in Figure 44. This figure clearly shows that

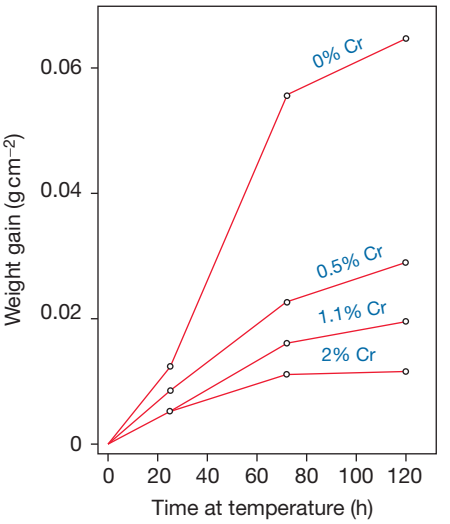

Figure 43 Influence of chromium on the oxidation of cast irons at 800 °C. Reproduced with permission from Murakami, N.; Kobayashi, T. Owadano *Imono* **1986**, *58*(7), 275–280.

the higher the temperature, the more important the role of silicon.

Certain American tests measured oxidation depths of 0.18 mm in a eutectic cast iron containing 4.7% silicon and 0.025 mm in a eutectic cast iron containing 5.9% Si, after exposure in air at 870 °C for 1000 h. It follows that increasing the silicon content very quickly reduces oxidation at high temperature.

Oxidation resistance is also greatly improved by the addition of aluminum. Figure 45 illustrates the oxidation resistance of a cast iron containing 3% C and 0.8% Si as a function of its aluminum content (2.4, 4.3, and 6%), after 200 h exposure to temperatures up to 980 °C. Figure 46 shows the influence of

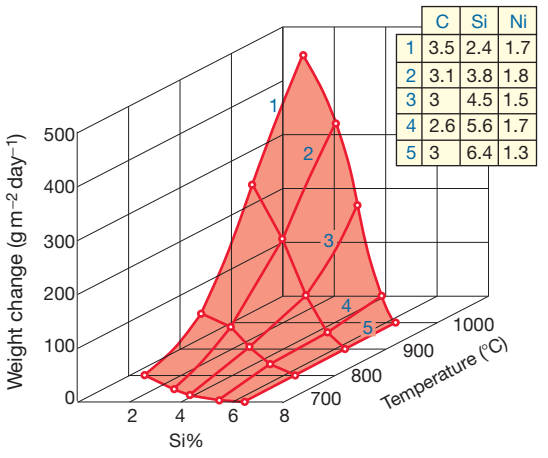

Figure 44 Influence of silicon content on the oxidation resistance of SG cast irons as a function of temperature. Reproduced with permission from Murakami, N.; Kobayashi, T. Owadano *Imono* **1986**, *58*(7), 275–280.

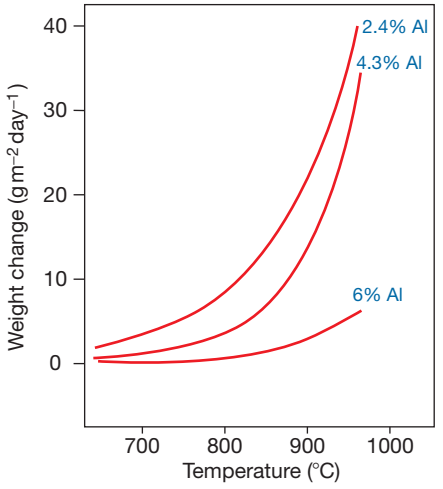

Figure 45 Influence of aluminum content on oxidation resistance of cast irons containing 3% C, exposed for 200 h at the temperature indicated. Reproduced with permission from Murakami, N.; Kobayashi, T. Owadano *Imono* **1986**, *58*(7), 275–280.

aluminum content on the oxidation resistance of gray cast irons as a function of temperature. Otherwise, with aluminum contents of the order of 20–25%, there is practically no oxidation: ~20 mg m^{-2} day^{-1} at 1050 °C.

Combining silicon with aluminum provides significant improvement in oxidation resistance. The best resistance to oxidation at 950 °C compatible with acceptable mechanical properties seems to be obtained with fine graphite cast irons containing 6.5–7% Al and 5–6% Si; better performance occurs with a carbon content close to the eutectic, that is, close to 1.8% C. The addition of aluminum also increases the resistance of cast iron in a sulfurous atmosphere. There is literature evidence[128] that the lowest oxidation rate occurs in alloys having compositions close to 5% Al, 2% Mo, and 2–3% Si: the penetration of oxidation in a cast iron of this type, after 1000 h at 925 °C, is 8 µm. The resistance of some spheroidal graphite high-nickel high-alloy cast irons (e.g., 30% Ni, 5% Cr, 5% Si) to heat and to corrosion by hot gases, chlorine, and chlorides is excellent.[131,132] Their drawback is that they are very expensive. Otherwise, the resistance of 'Ni-Resist' cast irons to oxidation at high temperature is generally high. They are often used for certain applications, such as exhaust manifolds for extreme conditions and some turbocharger parts.[133]

3.02.6.2 Corrosion by other Gas Atmospheres

A precise, exhaustive treatment of this subject would greatly exceed the scope of this article. Thus, a few general remarks for a few of the most commonly encountered corrosive gases will be made.

Cast irons stand up rather well to hydrogen sulfide gas from −60 to +20 °C provided it is dry; otherwise, there is risk of a form of hydrogen cracking.[134] The losses of thickness, in the case of a mixture of 98% H_2S and 2% air at 32 °C, are 0.075 mm year^{-1} (1.75 mm year^{-1} for damp H_2S) for unalloyed cast irons and 0.050 mm year^{-1} for austenitic cast irons. At higher temperatures, cast irons perform satisfactorily (especially unalloyed cast irons); the losses of thickness are shown in **Table 33**. Silicon cast irons are also relatively resistant to hydrogen sulfide up to 100 °C. The presence of chromium, even at moderate contents (2%), improves resistance to this gas; such cast irons in fact have acceptable performance up to 300 °C.

In hot sulfur dioxide, the gas temperature significantly affects the corrodibility of cast iron. Thus, in roasting furnaces (8% SO_2), an SG cast iron containing 0.5% Cr is acceptable provided the temperature remains below 300 °C. At 550 °C, it is still possible to use an ordinary cast iron provided that it is metallized by spraying with aluminum; at higher temperatures, at 1000 °C, it becomes necessary to use a cast iron containing 30% chromium or 16% silicon and 3% molybdenum.

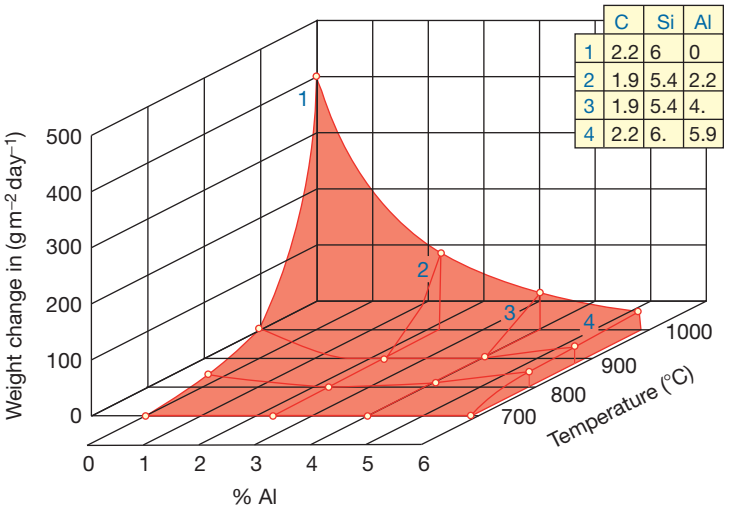

Figure 46 Influence of aluminum content on the oxidation resistance of gray cast irons containing 6% Si and 2% C. Reproduced with permission from Murakami, N.; Kobayashi, T. Owadano *Imono* **1986**, *58*(7), 275–280.

Table 33 Corrosion of cast iron in hydrogen sulphide

Medium	*Loss of thickness (mm year^{-1})*	
	Unalloyed cast irons	*Austenitic cast irons*
H_2S at 80–85°C	0.64	0.21
H_2S at 92°C	1,75	0,25

Table 34 Corrosion of cast iron in chlorine gas as a function of temperature

Alloy	*Temperature (°C)*	*Corrosion rate (mm year^{-1})*
Unalloyed LGI	93	0.76
	120	1.52
	177	3.05
	232	30.00
18–8	280	0.76
Stainless steel	315	1.52
	400	15.20

At ordinary temperatures (and at low temperatures), dry gaseous (or liquid) chlorine does not attack cast irons. Also, provided that the temperature is sufficient to avoid water condensation, chlorine containing some water vapor is not significantly aggressive. However, at higher temperatures, above ~350 °C, chlorine reacts with water vapor to form hydrochloric acid and hypochlorite, which is highly aggressive and requires the use of high-alloy cast irons (e.g., containing 15% silicon and 3% molybdenum or Ni14Cu6Cr3 'Ni-Resist' LGI cast irons or again cast irons containing 30% chromium). **Table 34** indicates the corrosion rates of a unalloyed cast iron and of carbon steel in chlorine as a function of temperature.[135]

Specific studies of corrosion risk are often performed for recuperators and heat exchangers for the cooling or heating of air that may contain chlorine traces. This is because, among the many causes of corrosion of heating installations, there is one that is especially insidious, namely corrosion by the action of halogens in air.[136] Note that any halogen present in a combustion atmosphere potentially react to produce aggressive products such as HCl. Halogen sources include chlorinated substances that have household, industrial, and recreational uses and, hence, incineration of wastes can produce a highly aggressive atmosphere.

Given the very large number of gases and mixtures of gases, an exhaustive study is impossible, so **Tables 35** and **36** indicate the cast irons recommended for given gas conditions.

3.02.6.3 Corrosion in Gas Transport and Distribution Pipes

The gas flowing in these pipes may, in the course of its travel, either remain at all times at a temperature above its dew point or occasionally cool to a temperature below this dew point. In the former case,

Table 35 Recommended cast irons for use in the specified gas atmosphere

Gaseous mixture	*Recommended cast iron*
Mixture	
Gas mixture with CO_2 or $CO_2 + CO$	
+ CO_2 (95 %) + H_2O (2,5 %) + NH_3 (1,5 %)	'Ni-Resist' cast iron
+ CO_2 (87 %) + H_2O (2 %) + inert gases (11 %) NH_3 (traces)	'Ni-Resist' cast iron
+ CO_2 (70 %) + air (16 %) + H_2O (10 %) + NH_3 (4 %)	'Ni-Resist' cast iron
+ CO_2 (17 %) + CO (25 %) + H_2O (2 %) + H_2 (50 %) + N_2 (4 %) + CH_4 (52 %)	'Ni-Resist' cast iron or 15% Si cast iron
+ CO_2 (13 %) + CO (11 %) + H_2 (7 %) + O_2 (2 %)	15% Si cast iron or ferritic white Cr+Mo cast iron
+ CO_2 (11.6 %) + N_2 (77 %) + H_2O (8 %)	'Ni-Resist' cast iron or 15% Si cast iron
+ CO_2 (5 %) + N_2 (74 %) + H (20 %) + O_2 + CH_4 + CO (1 %)	Unalloyed cast iron
+ CO_2 (4 %) + CO (70 %) + N_2 (18 %) + H_2 (6 %) + water and hydrocarbon vapours	1.5% Ni Pearlitic LGI
+ CO_2 (0.5 %) + H_2O (6.6 %) + air (93 %)	Unalloyed cast iron
Gas mixture with CO_2 and SO_2	
+ CO_2 (10 %) + SO_2 (17 %) + O_2 (10 %) + N_2 (63 %)	Unalloyed cast iron
+ CO_2 (12 %) + SO_2 (0.1 %) + O_2 (3.4 %) + N_2 (74.5 %) + water vapour (10 %)	'Ni-Resist' cast iron
+ CO_2 + SO_2 (0.3 %) saturated with moisture	'Ni-Resist' cast iron
Gas mixture with SO_2, SO_3, SO_2 + SO_3, or SO_2 + NO_2	
+ SO_2 (18 %) + N_2 (79 %) + O_2 (3 %)	Unalloyed cast iron
+ SO_2 (8 %) + N_2 (79 %) + O_2 (13 %) nearly dry (50 mg/m3 H_2O)	300 LGI, 1.8% Ni and 0.6% Cr
+ SO_3 (9 %) + N_2 (85 %) + O_2 (6 %) dry	Unalloyed cast iron
+ SO_2 + SO_3 (traces) dry (30°C)	2% Ni SGI
+ SO_2 (9.5 %) + NO_2 (84.7 %) + air (5.8 %) dry	Unalloyed cast iron
Other gas mixtures	
+ H_2 saturated with water + O_2 (3 %) + Cl_2 (2 ppm) (35°C)	'Ni-Resist' cast iron, Ni15 Cu5 Cr2 LGI
+ HCl (50 %) + N_2 (50 %) (dry)	Unalloyed cast iron
+ HCl (50 %) + N_2 (50 %) (dry) (damp)	15% Si cast iron
+ Vinyl chloride saturated with water vapour (36–100°C)	Unalloyed cast iron
+ O_2 Damp + CO_2	'Ni-Resist' cast iron
+ Perchloric vapours	15% Si cast iron
+ CH_4 (62.5 %) + CO (12 %) + H_2 (5 %) + N_2 (10.4 %) + CNH_2N (8.7 %) + O_2 (1.5 %)	Unalloyed cast iron
+ Dimethylether (38 %)/Methanol (27 %) + N_2 (28 %) + O_2 (3 %) + H_2O (3 %) + CO_2 (1 %) + CO	Unalloyed cast iron
+ H_2S (60–68 %) + CO_2 (22–28 %) + HCN (6–8 %) + water vapour (4 %)	None
+ H_2S (13.4 %) + CO_2 (34 %) + HCN (1.5 %) + H_2 (24 %) + CO (22 %) + sodium aluminate (4.5 %) dry	Unalloyed cast iron
+ Air + heavy water (vapour)	'Ni-Resist' cast iron
+ Monochlorobenzene vapour saturated with water	15% Si cast iron

Data taken from Reynaud, A. *Corrosion and Cast Iron*, ETIF, France, 2008.

there is no condensation, while in the latter water is deposited. Such condensates are likely to form a thin film of moisture, continuous or not, which can lead to corrosion generally at the base of the pipes. For this reason, gas networks have traps, to be able to eliminate condensates. When this is done, centrifugal cast iron pipes only rarely suffer this type of internal corrosion due to the gas transported, even if it contains water vapor. Industrial experience has in fact shown that the cast iron tubes used for natural gas distribution can survive for many decades without undergoing significant internal corrosion. In the case of oxygen-free natural gas, the principal aggressive constituents are sulfides. However, distributors will purify and condition gases so as to avoid these phenomena.

Table 36 Recommended cast iron for use in specified gas atmosphere

Gaseous mixture	*Recommended cast iron*
Pure gases	
H_2 100 % – 49°C	'N-Resist' cast iron (Ni23 Mn4 SGl)
HCl 100 %	32–34% Chromium cast iron
NH_3 100 %	Unalloyed cast iron
Freon 113 – 50°C	Unalloyed cast iron
CCl4, dry, 40°C	Unalloyed cast iron
CCl4, damp, 40°C	'Ni-Resist' cast iron
Phenols (vapours)	Unalloyed cast iron
Acetone	Unalloyed cast iron
Tolueno	Unalloyed cast iron
Ethanol	Unalloyed cast iron
Haptane	Unalloyed cast iron
NO, dry	Unalloyed cast iron
NO_2 dry	Unalloyed cast iron
Propane	Unalloyed cast iron
Bulane	Unalloyed cast iron
Ethane	Unalloyed cast iron
Mathane	Unalloyed cast iron
Ethylene	Unalloyed cast iron
Ethylene oxide	Unalloyed cast iron
Monochloroethylene, dry	Unalloyed cast iron
Dichloroethylene, dry	Unalloyed cast iron
Dichloroethylene, damp	15% Si cast iron
Oxygen	'Ni-Resist' cast iron

Data taken with permission from Reynaud, A. *Corrosion and Cast Iron*, ETIF, France, 2008.

References

1. Tsuda, M.; Murata, Y. *IMONO.* **1982**, *54*, 605–611.
2. Fontana, M. G.; Greene, N. D. *Corrosion Engineering*, 2nd ed.; McGraw-Hill.
3. Collins, H. H. *BCIRA J.* **1962**, *10*, 543.
4. Landolt, D. *Corrosion et chimie de surfaces des métaux.* Traité des matériaux; Presses polytechniques et universitaires romandes, 1993; Vol. 2.
5. Ikenaga, A.; Nitta, Y.; Kavamoto, M. *J. Jpn. Foundry Eng. Soc.* **1996**, *68*(7), 585–591.
6. Hemanth, J. *J. Mater. Process. Technol.* **2000**, *101*(1/3), 159–166.
7. Graham, R.; Prado, O. S.; Collins, M. H.; Brandes, E. A.; Farmery, H. K. *Proc. Inst. Mech. Engs.* **1960**, *74*, 617.
8. Whittaker, J. A.; Brandes, E. A. *Foundry* **1962**, *90*, 70.
9. Wons, W. *Wasser Boden.* **1982**, *4*, 138–144.
10. Vanick, J. S.; Merica, P. D. *Trans. Am. Soc. Steel Treat.* **1930**, *18*, 923.
11. Kinzel, A. B.; Franks, R. Alloys of Iron and Chromium. In *High Chromium Alloys*; McGraw-Hill: New York, 1940; Vol. 2, pp 228–260.
12. Jackson, R. S. *J. I. S. I.* **1970**, *208*, 163–167.
13. Hurst, J. E.; Riley, R. V. *J. Iron Steel Inst.* **1947**, *155*, 172.
14. Dumitrescu, T.; Medeleanu, V.; Nicolaid, M.; Dinu, I. *Rev. Metall. (Roumania)* **1958**, *3*(2), 19.
15. Hurst, J. E. *Proc. Inst. Brit. Foundrym.* **1944**, *37*, B46.
16. Kulikov, V. I. *Chem. Pet. Eng.* **1981**, *16*(7/8), 441–443.
17. CIFOM. Emploi des fontes dans l'industrie chimique. Supplement à l'Usine Nouvelle, June 1967, pp 1–8.
18. Cetre, Y. Etude du comportement à la corrosion de divers matériaux métalliques dans l'acide sulfurique concentré à chaud. Doctoral dissertation in engineering, INSA, Lyon, September, 1985.
19. Norme, N. F. A32–211, January 1991. Produits de fonderie – Fontes à graphite sphéroïdal pour robinetterie et appareils à pression.
20. Swales, G. L. *Ind. Chem. Chem. Manufacturer* **1963**, *39*, 16–21, 79–83, 142–144.
21. Mannweiler, G. B. *Proc. Am. Soc. Test. Mater* **1972**, *72*(1), 42.
22. Berenson, J.; Wranglen, G. *Corros. Sci.* **1980**, *20*(7), 937–941.
23. Labbe, J. P. *L'agressivité des eaux dans les chauffe-eau électriques. Materiaux et techniques* 1983, pp. 126–130.
24. Jakobs, J. A.; Hewes, F. W. *Mater. Perf.* **1987**, *26*(5), 42–49.
25. Smith, D. C. *Br. Corros. J.* **1980**, *15*(4), 192–194.
26. Sontheimer, H.; Koelle, W.; Snoeyink, V. *J. AWWA.* **1981**, *73*(11), 572–579.
27. Degremont *Mémento Technique de l'Eau*, 8th ed., 1978.
28. Lédion, J. *La Corrosion par les Eaux. La Revue des Laboratoires d'Essais,* no. 21, 1989, pp 9–13.
29. AFNOR standard, Protection électrochimique contre la corrosion, Recommandations concernant les traitements des influences du courant continu sur les structures métalliques enterrées. Standard NF A 05-615, July 1993.
30. Waanders, F. B.; Vorster, S. W. A Mössbauer Spectroscopy Study of the Corrosion of Nodular Cast Iron in Mine Waters. In *Hyperfine Interactions*; Springer: Netherlands; pp 1027–1033, Vol. 92, no. 1.
31. Smith, D. C.; Mac Enaney, B. *Corros. Sci.* **1979**, *19*, 379–394.
32. Suery, P.; Hiltbrunner, K. *Archiv Für Das Eisenhuettenwesen* **1979**, *50*(11), 493–498.
33. Degremont *Mémento Technique de l'Eau*, 8th éd. 1978.
34. Mehra, R.; Soni, A. *Bull. Mater. Sci.* **2002**, *25*(1), 53–58.
35. Katz, W. *Giessen für die Chemie*; VDI-Verlag GmbH: Düsseldorf.
36. Neumann, E.; Behrendt, B.; Hecht, A. Nachweis von Korrosion (Spongiose) an den Innen Wänden von Orangußrohren mit Hilfe einer rechnergeführten Ultraschall prüfeinrichtung (Abakus) Materialprufung. no.3, March 1987, pp 60–66.
37. Bryant, M. D. *BCIRA J.* **1972**, *20*, 345–350.
38. Degremont *Mémento Technique de l'Eau*, 8th éd. 1978.
39. Smart, N. R.; Rance, A. P.; Fennell, P. A. H. Galvanic corrosion of copper–cast iron couples. Technical report TR-05-06, Svensk Kärnbränslehantering, January 2005.
40. Mehra, R.; Soni, A. Inhibition of corrosion of cast iron by nitrite, hydrogen phosphate, and molybdate ions in corrosive water. In *Chemical Engineering Communications*; Taylor & Francis: London, 2004; Vol. 191, no. 11, pp 1502–1524.
41. Evans, U. R. *La corrosion des Métaux;* Dunod: Paris, 1928.
42. ASM *Metals Handbook, Corrosion*; ASM International: Ohio, 1987; Vol. 13; pp 566–572.
43. Marshall, A. *Corros. Prevention Control* 1983, pp 177–181.
44. Une nouvelle nuance de fonte Ni-Resist à graphite sphéroïdal. INCO NICKEL, no. 33, 1971, pp 4.
45. Forecast Progress in Metal Casting; no. 46, 1983.

46. Daub, M. B.; Venkateswaran, G.; Venkateswarlu, K. S. *Br. Corros. J.* **1990**, *25*(4), 303–307.
47. Waanders, F. B.; Vorster, S. W. *Hyperf. Interact.* **1994**, *92*(1), 1027–1033.
48. Romanoff, M. Underground Corrosion US Nat. Bur. Stnd.: Washington DC, Circular No. 579, 1957.
49. Schwerdtfeger, W. J. *J. Res. Bur. Std.* **1985**, *69C*, 71.
50. Stokes, R. F. *Chem. Ind.* **1983**, (17), 659–663.
51. Collins, H. H. Conference on Corrosion and the Water Industry, UMIST: Manchester, 1986.
52. Akimov, G. V. *Théorie et Méthodes d'Essai de la Corrosion des Métaux,* DUNOD: Paris, 1957.
53. Stadler, F. *AQUA* **1983**, *4*, 183–187.
54. Heims, W. D. In *Gras Influence des Sources de Courant Électrique Extérieures sur la Corrosion et la Sécurité des Canalisations en Fonte Ductile Enterrées dans leur Voisinage;* FGR, Vol. 18, 1983; pp 17–31.
55. A.G.H.T.M. *Les canalisations d'eau et de gaz*, Editions Lavoisier: Paris, 1987.
56. Domerty, B. J. *Mater. Perf.* **1990**, *29*(1), 22–28.
57. Katz, W. *Giessen für die Chemie*; VDI-Verlag GmbH: Düsseldorf.
58. Ductile cast iron having high strength and high corrosion resistance. Japanese patent, 09/04/2003, no. JP 2003105484.
59. Collins, H. H.; Fuller, A. G.; Harrison, J. T. In 12th World Gas Conference, Nice, Report 19 U/D 1973.
60. De Rosa, P. J.; Parkinson, R. W. Water Research Engineering Technical Report 241, 22, 1986.
61. Pont-à-Mousson. Les canalisations en fonte ductile. L'eau, l'industrie, les nuisances, no. 90, March 1985, pp 65–66.
62. Domerty, B. J. *Mater. Perf.* **1990**, *29*(1), 22–28.
63. Garrity, K. C.; Jenkins, C. F.; Corbett, R. A. *Mater. Perf.* **1989**, *28*(8), 25–29.
64. Jakobs, J. A.; Hewes, F. W. *Mater. Perf.* **1987**, *26*(5), 42–49.
65. Schiff, M. J.; McCollom, B. *Mater. Perf.* **1993**, *32*(8), 23–27.
66. AFNOR standard, Protection électrochimique contre la corrosion, recommandations concernant les traitements des influences du courant continu sur les structures métalliques enterrées. Standard NF A 05-615, July 1993.
67. Résistance des fontes à la corrosion de l'acide sulfurique. Fonderie-fondeur d'aujourd'hui, no. 61, January 1987, 19.
68. Résistance des fontes à l'acide sulfurique concentré. Fonderie no. 393, November 1979, 339.
69. Reynaud, A. Les fontes alliées au chrome et au silicium pour l'industrie chimique. Fonderie-fondeur d'aujourd'hui, no. 124, April 1993, pp 32–34.
70. Kosting, P. R.; Heins, C. *Ind. Eng. Chem.* **1931**, *23*, 140–150.
71. Leconte, J. Protection contre la corrosion. Techniques de l'ingénieur métallurgie/génie industriel, pp A830.1–A835.4.
72. Lammia Al-Shama; Jalal Mohammed Saleh; Naema A. Hikmat, *Corros. Sci.* **1987**, *27*(3), 221–228.
73. Higgins, R. I. *J. Res. Bcira* **1956**, *6*, 165–177.
74. ASM. Corrosion of cast irons In *Metals Handbook, Corrosion,* 1987; Vol. 13, pp 566–572.
75. Collins, B. L.; Smith, J. O. *Proc. ASTM* **1942**, *42*, 639.
76. Palmer, K. B. Proceedings of Conference on Engineering Properties and Performance of Modern Iron Castings, BCIRA, 1972, p 110.
77. Muthukumarasamy, S.; Seshan, S. *Bull. Electrochem.* **1991**, *7*(1), 1–3.
78. Muthukumarasamy, S.; Seshan, S. *Transact. AFS* **1992**, *92*(16), 873–879.
79. Dawson, J. V. *BCIRA J.* **1978**, *26*, 135–144.
80. Palmer, K. B. *BCIRA J.* **1975**, *23*, 40–43.
81. Forecast Progress in Metal Casting, no. 46, October 1983.
82. Yamamoto, S.; Ono, S.; Fukada, M. *Imono* **1993**, *65*(9), 712; 717.
83. Smith, S. H. *BCIRA J. Res. Deterior.* 1957.
84. Morrison, J. C. *Anticorrosion* **1983**, *30*(8), 8.
85. Miysaka, M.; Ogure, N. *Corrosion* **1987**, *43*(10), 582–588.
86. Borel, P. Propriétés des fontes à graphite nodulaire. Techniques de l'ingénieur, metallurgie, p M392–19
87. Diegle, R. B.; Treseder, R. S. *Mater. Perf.* **1978**, *17*, 31–32.
88. Kosowski, A. *Przeglad Odlewnictiva* **1966**, *16*, 362–367.
89. Baumel, A. *Werkstoffe Korros.* **1993**, *44*, 107–108.
90. Atkinson, R.F. *Nickel*, *9*(2), 10–11
91. Mercer, A. D. *Br. Corros. J.* **1979**, *4*(3), 179–182.
92. Podrzucki, C. *Revue Métallurgie* **1968**, *65*, 137–144.
93. Bastien, P.; Daeschner, S. Recherche sur la corrosion des fontes par l'aluminium et les alliages légers au silicium liquides. 21st ATF congress, October, 1947.
94. Charbonnier, J.; Parisien, J. Résistance des organes de machines à couler sous pression à la corrosion par les alliages de zinc liquides. Booklet CTIF, November, 1964.
95. Laque, F. L.; Uhlig, M. H. *Corrosion Handbook*; Wiley: London, 1978; p 197.
96. Eisensiliziumguss. Werkschrift der Rheinhütte: Wiesbaden, 1968.
97. Al-Hashem, A.; Abdullah, A.; Riad, W. *Mater. Charact.* **2001**, *47*(5), 383–388.
98. Chantereau, J. *Tech. Documentation* 1980.
99. Crolet, J. L.; Daumas, S.; Magot, M. *Materiaux Tech.* **1992**, *9/10*, 71–77.
100. Badan, B.; Magrini, M.; Ramous, E. *J. Mater. Sci.* **1991**, *26*, 1951–1954.
101. Gouda, V. K.; Al-Hashem, A. H.; Abdullah, A. M.; Riad, W. T. *Br. Corros. J.* **1991**, *26*(2), 109–116.
102. Heuze, J. L. Endommagement par érosion de cavitation de métaux et alliages de structure cubique à faces centrées. Thesis University of Paris 6, 27/10/1988
103. Okada, T.; Iwai, Y.; Yamamoto, A. Division of Research Development and Administration University of Michigan, USA, Report UMICH 014571-43–I, March 1982.
104. Iwai, Y.; Okada, T.; Hammit, F. G. *Wear* **1983**, *88*(3), 181–191.
105. Eisensiliziumguss. Werkschrift der Rheinhütte, Wiesbaden, 1968.
106. La cavitation par vibrations dans les fontes grises. Fonderie Fondeur d'Aujourd'hui no. 1, 1981, pp 35–37.
107. Okada, T.; Iwai, Y.; Yamamoto, A. *Wear* **1983**, *88*(2), 167–179.
108. Tomlinson, W. J.; Talks, M. G. *Tribol. Int.* **1991**, *24*(2), 67–75.
109. Berger, J.; Phol, M.; Sitnik, L. *Prakt. Metallograp.* **1986**, *23*, 513–527.
110. La cavitation par vibrations dans les fontes grises. Fonderie Fondeur d'Aujourd'hui no. 1, 1981, pp 35–37.
111. Lopez Vazquez, L. B. *Colada* **1979**, 231–241.
112. Lopez Vasquez, L. B. Cavitation vibratoire dans les pièces en fonte. Fonderie Fondeur d'Aujourd'hui no. 1, January, 1981, pp 35–37.
113. Zhou, Y. K. L.; He, J. G.; Hammit, F. G. *Wear.* **1982**, *76*(3), 329–336.
114. Tomlinson, W. J.; Brandsen, A. S. *Surf. Eng.* **1988**, *4*(4), 303–308.

115. Zhou, Y. K. L.; He, J. G.; Hammit, F. G. *Wear.* **1982**, *76*(3), 329–336.
116. Tomlinson, W. J.; Brandsen, A. S. *Surf. Eng.* **1988**, *4*(4), 303–308.
117. Koutny, A.; Nakladal, V.; Vogel, M. *Strojir.* **1982**, *32*(11), 599–604.
118. Fairhust, W.; Rohrig, K. *Foundry Trade J.* **1984**, 685–698.
119. Sawamoto, A.; Usami, T.; Ogi, K.; Matsuda, K. *Imono.* **1984**, *56*, 597–601.
120. Murakami, N.; Kobayashi, T. Owadano *Imono*. **1986**, *58*(7), 275–280.
121. Rajagopal, V.; Iwasaki, I. *Corrosion* **1992**, *48*(2), 132–139.
122. Chakraborty, I.; Basak, A.; Chatterjee, U. K. *Wear* **1991**, *143*, 203–220.
123. Vasil'ev, V. Y.; Edneral, N. V. *Zashichita Metallov.* **1982**, *18*(3), 450–453.
124. Chen, C. H.; Alstetter, C. J.; Rigsbee, J. M. *Metallurg. Trans.* **1984**, *15A*, 719–728.
125. Internal document Cavitation-érosion des fontes, 1985.
126. Shalaby, H. M.; Attari, S.; Riad, W. T.; Gouda, V. K. *Corrosion* **1992**, *48*(3), 206–217.
127. Chakrabarty, I.; Basak, A. *Transact. AFS* **1990**, *98*, 707–716.
128. Bevan, J. E. Climax Molybdenum Co, Report L-194-38, March 1974.
129. Komatsu, Y.; Sugimoto, S. *Imono.* **1978**, *50*(12), 727–732.
130. Tomlinson, W. J.; Brandsen, A. S. *Surf. Eng.* **1988**, *4*(4), 303–308.
131. Kurof, O. V.; Abramyan, E. S. *Fizko-Khimickeskaya Mekhanika Materialov.* **1973**, *9*(2), 104.
132. CENTRE d'information du NICKEL. Fontes austénitiques au nickel, Ni-Resist, 1965.
133. Thouvenin, D. *Revue Française de Mécanique* **1990**, *1*, 33–38.
134. Rabald, E. *Corrosion Guide*; Elsevier: Amsterdam, 1968.
135. Giessen für die Chemie. VDI-Düsseldorf.
136. Dugniolle, E.; Guillaume, M. La corrosion des chaudières et des cheminée métalliques par les halogènes PROCLIM, Tome 24, no. 7, December, 1993, pp 403–409.

3.03 Corrosion of Iron Nickel Alloys and Maraging Steel

G. N. Flint
Nickel Development Institute
J. W. Oldfield
Cortest Laboratories Ltd, Sheffield, UK
D. P. Dautovich
International Nickel Company

This article is a revision of the Third Edition articles 3.4 and 3.5 by D. P. Dautovich, G. N. Flint and J. W. Oldfield, volume 1, pp 3:78–3:100, © 2010 Elsevier B.V.

Glossary

Aging A heat treatment process whereby an alloy, that has been previously quenched in order to retain alloying additions in solid solution, is reheated into a temperature range in which the rate of solid state diffusion is sufficient to permit the precipitation of strengthening second phase particles.

Maraging steel An ultrahigh strength low-carbon iron–nickel alloy that is strengthened by the precipitation of second phase intermetallic compounds rather than carbides.

U-bend A form of corrosion test specimen that is prepared in the shape of a 'U' and commonly used to determine the resistance of a material to SCC.

Abbreviations

AISI American Iron and Steel Industry

Symbols

a_{cr} Critical crack length for propagation of stress corrosion crack

K_{ISCC} Critical stress intensity threshold for the onset of stress corrosion cracking

3.03.1 Introduction

Alloys of iron with nickel have a number of important applications. The first class are of interest due to their unique magnetic characteristics and their abnormally low thermal expansion coefficients in the compositional region of Fe–36%Ni. Although not specifically used as corrosion-resistant materials, their high resistance to attack from many common environments is of benefit in their specialized applications. The second important class, 'maraging steels,' are ultra-high strength low-carbon iron–nickel alloys that derive their outstanding mechanical properties from the precipitation of second phase intermetallic compounds rather than carbides.

3.03.2 Iron–Nickel Alloys

3.03.2.1 Electrochemistry

The potentiodynamic polarization curves of Beauchamp,[1] Figure 1, demonstrate the effect of increasing nickel content on the anodic behavior of iron–nickel alloys in 0.5 M H_2SO_4. The maximum current in the active region is reduced and the potentials moved to more noble values; the current in the passive region is increased and some evidence of secondary passivity appears. The greater nobility with increasing nickel content in the active region is of importance in acid environments where hydrogen evolution is the major cathodic reaction, and results in significantly lower rates of corrosion. In neutral environments, the protection provided by a layer of insoluble corrosion products is of greater significance.

3.03.2.2 Atmospheric Corrosion

The addition of small amounts of nickel to iron improves its resistance to corrosion in industrial atmospheres due to the formation of a protective layer of corrosion products. Larger additions of nickel, for example, 36% or 42%, are not all that beneficial with respect to overall corrosion, since the rust formed is powdery, loose, and nonprotective, leading to a linear rate of attack as measured by weight loss. Figure 2 of Pettibone[2] illustrates the results obtained.

With respect to resistance to pitting corrosion, there is an increasing advantage to be obtained by increasing the nickel content up to 50%. There is little distinction between the Fe–50Ni alloy and pure nickel. Data on the corrosion of Fe–36Ni alloy at an industrial site in the United States are reported by La Que and Copson[3] and at a European site by Evans.[4] In marine atmospheres, the overall rates of corrosion are reduced progressively with increase in nickel content up to 35%, but with small improvement thereafter. The rates of corrosion at various sites, reported by Friend,[5] show the superiority of Fe–36Ni over mild steel with respect to both average and localized corrosion (Table 1).

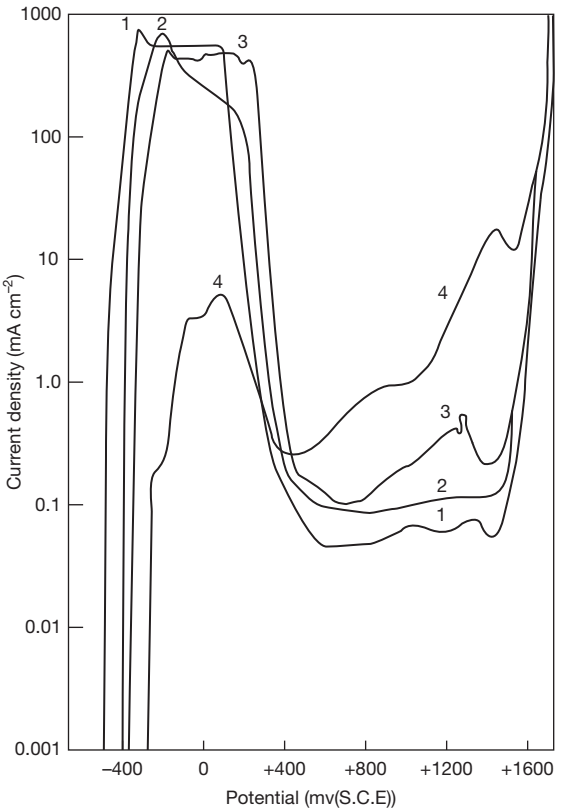

Figure 1 Effect of nickel on the anodic behavior of iron alloys in 1 M H_2SO_4 at 25 °C. Curve 1 – Fe; Curve 2 – Fe–10Ni; Curve 3 – Fe–36Ni; Curve 4 – Ni. Reproduced from Beauchamp, R. L. Dissertation, Ohio State University, 1966; Figure 27.

3.03.2.3 Corrosion in Natural Environments

3.03.2.3.1 Seawater

The average rates of corrosion of Fe–36Ni alloy exposed to alternate immersion in seawater are appreciably greater than those that occur when the alloy is exposed to marine atmospheres. Although the rates of corrosion are significantly below those observed for mild steel (Table 2), the superiority over mild steel is not all that great with respect to pitting attack.

Nickel–iron alloys fully immersed in seawater may suffer localized corrosion, which can be severe under conditions where oxygen is constantly renewed at the surface and the formation of protective corrosion products is hindered, for example, in fully-aerated flowing seawater. In quieter, less oxygenated conditions, average corrosion rates of Fe–36Ni are low and well below those for mild steel, as exemplified in the data given in Table 3. However, the resistance to localized attack is not improved to the same extent.

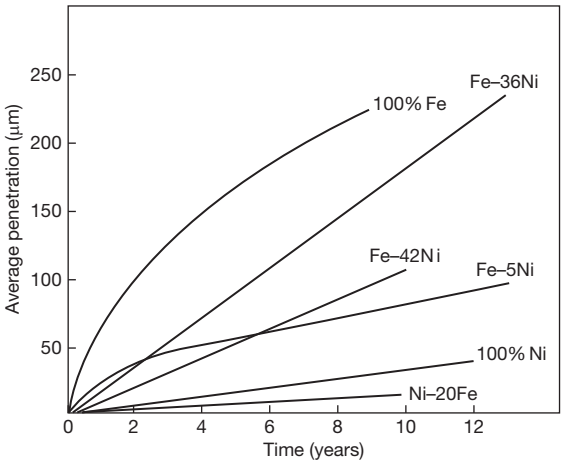

Figure 2 Resistance of nickel–iron alloys to corrosion by an industrial atmosphere in Bayonne NJ, USA. Reproduced from La Que, F. L.; Copson, H. R., Ed. *Corrosion Resistance of Metals and Alloys*, 2nd ed.; Reinhold Publishing Corporation/Van Nostrand Reinhold Ltd: New York/London, 1963; p 458.

3.03.2.3.2 Freshwater

Nickel–iron alloys suffer significantly less corrosion than mild steel when exposed to a soft, freshwater, but Friend[5] found that the resistance to pitting is only slightly greater. For example, the average corrosion rate for mild steel after 15 years' exposure was 0.94 g m^{-2} day^{-1} as against 0.07 g m^{-2} day^{-1} for Fe–36Ni. On the other hand, the maximum pit depths were similar, 2.2 and 2.0 mm for mild steel and Fe–36Ni respectively.

Table 1 Resistance of Fe–36Ni and mild steel to corrosion in marine atmospheres[5]

Location	*Corrosion after exposure for 15 years*			
	Average (g m^{-2} day^{-1})		*Localized (max. pit depth, mm)*	
	Fe–36Ni	*Mild steel*	*Fe–36Ni*	*Mild steel*
Colombo, Ceylon	0.08	5.5	0	–
Auckland, New Zealand	0.02	1.5	0	2.43
Halifax, Nova Scotia	0.03	0.65	0.1	1.64
Plymouth, England	0.08	3.5	0.19	1.09

Table 2 Resistance of Fe–36Ni and mild steel to corrosion during alternate immersion in sea-water[5]

Location	*Corrosion after exposure for 15 years*			
	Average (g m^{-2} day^{-1})		*Localized (max. pit depth, mm)*	
	Fe–36Ni	*Mild steel*	*Fe–36Ni*	*Mild steel*
Colombo, Ceylon	0.64	3.4	1.0	2.55
Auckland, New Zealand	0.09	0.32	0.24	0.36
Halifax, Nova Scotia	0.24	1.5	2.59	2.15
Plymouth, England	0.36	1.4	0.25	1.58

3.03.2.4 Corrosion in Industrial Environments

3.03.2.4.1 Acids

Much of the information available on the resistance of nickel–iron alloys to corrosion by mineral acids is summarized by Marsh.[6] In general, corrosion rates decrease sharply as the nickel content is increased from 0 to 30–40%, with little further improvement above this level. The value of the nickel addition is most pronounced in conditions where hydrogen evolution is the major cathodic reaction, that is, under conditions of low aeration and agitation. Results reported by Hatfield[7,8] show that the rates of attack of Fe–25Ni alloy in sulfuric and hydrochloric acid solutions, although much lower than those of mild steel, are still appreciable (**Table 4**). In solutions of nitric acid, nickel–iron alloys show very high rates of corrosion.

Bourelier *et al.*[9] and Raicheff *et al.*[10] investigated the inhibitive effect of chloride ions on corrosion in sulfuric acid. The inhibition efficiency was found to depend on the alloy composition, alloy surface, and chloride concentration. The more aggressive the environment, the greater the inhibition efficiency. Yagupol'skaya *et al.*[11] studied the effect of iodine additions to sulfuric acid on the corrosion resistance of Ni and Ni–Fe alloys. Again there was an inhibitive effect caused by the halide ion. Uto *et al.*[12] studied Ni–Fe–Si alloys, adding Si to improve the castability of the simple Ni–Fe materials. They found that alloys containing 0–70% Fe and 5–10% Si, with the balance being Ni, are usable in 0–85% sulfuric acid at temperatures of up to 80 °C and in 0–10% hydrochloric acid at temperatures of up to 40 °C.

Cid *et al.*[23] studied the corrosion resistance of Ni, 5% Fe–Ni and 10% Fe–Ni alloys in the transpassive region in sulfuric acid. For a given acid concentration, the addition of iron reduced the corrosion rate. It was concluded that the addition of small percentages of Fe was doubly beneficial, decreasing both general and intergranular corrosion.

3.03.2.4.2 Salt solutions

Nickel–iron alloys are more resistant than iron to attack by solutions of various salts. In alternate immersion tests in 5% sodium chloride solution, Fink and De Croly[13] determined values of 2.8, 0.25, and 0.5 $g\,m^{-2}\,day^{-1}$ for alloys containing 37%, 80%, and 100% nickel as against 46 $g\,m^{-2}\,day^{-1}$ for iron. Corrosion rates of about 0.4 $g\,m^{-2}\,day^{-1}$ are reported by Hatfield[7] for Fe–30Ni alloy exposed to solutions containing 5% magnesium

Table 3 Resistance of Fe–36Ni alloy and mild steel to corrosion when fully immersed in seawater[5]

Location	*Corrosion after exposure for 15 years*			
	Average (g m^{-2} day^{-1})		*Localized (max. pit depth, mm)*	
	Fe–36Ni	*Mild steel*	*Fe–36Ni*	*Mild steel*
Colombo, Ceylon	0.8	2.0	2.5	6.5
Auckland, New Zealand	0.5	2.0	1.08	2.59
Halifax, Nova Scotia	1.3	2.2	3.49	1.23
Plymouth, England	0.8	1.5	1.82	2.75

Table 4 Resistance of Fe–25Ni and carbon steel to corrosion by sulfuric and hydrochloric acids

Alloy	*Corrosion rate (mm $year^{-1}$)*					
	5% H_2SO_4		*25% H_2SO_4*		*50% H_2SO_4*	
	15 °C	*40 °C*	*15 °C*	*40 °C*	*15 °C*	*40 °C*
Carbon steel	62	183	93	378	0.95	2.8
Fe–25Ni	0.45	1.4	0.45	1.8	0.9	1.8
	5% HCl			*25% HCl*		
	15 °C	*40 °C*	*60 °C*	*15 °C*	*40 °C*	*60 °C*
Carbon steel	23	40	41	63	188	185
Fe–25Ni	0.45	2.3	5.4	0.9	0.9	19

sulfate, 10% magnesium chloride, and 10% sodium sulfate; the same alloy corroded at a rate of about 1.2 g m^{-2} day^{-1} in 5% ammonium chloride.

In a study of the corrosion of 10 binary nickel–iron alloys in 3% sodium chloride solution, Schwerdtfeger[14] found the average corrosion rate to decrease from 1.4–1.6 g m^{-2} day^{-1} for alloys containing 0–16% nickel alloy to 0.1 g m^{-2} day^{-1} for a 57% nickel–iron alloy. There was little further reduction in the rate of weight loss for the higher-nickel alloys. However, the alloys showed an increasing tendency to suffer pitting and crevice corrosion with increasing nickel content.

3.03.2.4.3 Stress corrosion

In tests lasting for 14 days, Copson[15] found that the susceptibility of steel to stress corrosion cracking (SCC) in hot caustic soda solutions increased with increase in the nickel content up to at least 8.5%. Alloys containing 28% and more of nickel did not fail in this period. In boiling 42% magnesium chloride, the 9% nickel–iron alloy was the most susceptible of those tested to cracking (**Table 5**) with alloys containing 28 and 42% nickel not failing within 7 days. Couper[16] reports cracking of an Fe–36Ni alloy in 10–55 days in this medium. Radd *et al.*[17] have noted cracking of Fe–36 Ni alloys at ambient temperatures in an unspecified environment, but this possibly may have been residual traces of acid copper chloride etching solution.

Marquez *et al.*[18] studied the effect of cold rolling on the resistance of Ni–Fe alloys to hydrogen cracking. It was found that low-carbon, 10–19% Ni–Fe alloys become considerably more resistant to hydrogen cracking after severe cold rolling. The observed resistance decreased with increasing carbon content and the improvement was directional, the optimum effect applying to specimens stressed in the longitudinal direction.

3.03.2.4.4 Galvanic corrosion

Galvanic corrosion of nickel–iron alloys may be of significance in welding operations. Ni–45Fe alloys are used as filler materials in the welding of cast irons but the favorable area relationship of weld metal to base plate mitigates the effect of the more noble characteristics of the nickel–iron alloy. Thus, their application in corrosive environments is rarely of concern.

Of more serious practical significance is iron contamination of nickel-clad steel welds. **Tables 6** and **7** show the increase in corrosion of various nickel–iron alloys that may occur when coupled to nickel in calcium chloride or sodium hydroxide solutions. It is evident that in the calcium chloride solution, 5% iron contamination of weld metal can be tolerated, while in the sodium hydroxide solution bimetallic corrosion will not become significant until contamination exceeds 20%.

3.03.3 Maraging Steels

3.03.3.1 Composition

Notwithstanding their name, maraging steels are a class of high-strength iron alloys of very low carbon content. Strengthening is achieved by the use of substitutional alloying additions that result in the precipitation of secondary phases during age hardening of a quenched martensitic iron–nickel matrix. The term maraging was thus coined from the words 'martensite' and 'age hardening.'

The development of maraging steels began in the late 1950s, on steels containing 20 and 25% Ni using a combination of aluminum, titanium, and niobium as age-hardening elements.[19] Later work[20] revealed the important synergistic age-hardening effect of cobalt plus molybdenum and led to the development of the 18% Ni maraging steels. Using titanium as a

Table 5 Resistance of iron–nickel alloys to SCC in boiling 42% magnesium chloride

Composition of alloy					*Hardness*	*Time to cracking (days)*	*Comments*
Ni	*C*	*Mn*	*Si*	*Fe*			
Nil	0.19	1.65	0.20	Bal.	89 Rb	No cracking after 11 days	
2.02	0.19	0.46	0.18	Bal.	77 Rb	7	Few shallow cracks
4.96	0.15	0.51	Nil	Bal.	96 Rb	<3	Profuse deep cracks
8.67	0.10	0.76	0.23	Bal.	24 Rc	<3	Cracked in two
27.88	0.03	0.18	0.06	Bal.	81 Rb	No cracking after 7 days	
41.79	0.02	0.18	0.08	Bal.	77 Rb	No cracking after 7 days	
99.41	0.10	0.24	0.02	0.13	20 Rc	No cracking after 7 days	

Source: Rhodin, T. H. Ed. *Physical Metallurgy of Stress Corrosion Fracture*; Interscience: New York, 1959; pp 259–262.

supplementary hardening element, and with appropriate balancing of cobalt and molybdenum, nominal yield strengths in the range of 1370–2400 MPa can readily be achieved. Table 8 lists the nominal composition of the 18% Ni maraging steels. Other types of maraging steel include an alloy (17% Ni) developed for use as a casting,[21] and a 12Ni–5Cr–3Mo alloy. Stainless-type alloys have also been developed[22] but are outside the scope of this section.

During the 1970s, the price of cobalt increased enormously and then declined. These price fluctuations plus the concern about the future supply of cobalt caused serious declines in the use of the cobalt-containing grades of maraging steel. In response to this market change, a new cobalt-free grade of maraging steel was developed.[23] The composition of this steel is given as 18.5Ni, 3.0Mo, 1.4Ti, and 0.1A1. Its strength is 1720 MPa and its mechanical properties approximate those of the 18% Ni 240 maraging steel. Discussion in this chapter is restricted to the 18% Ni maraging steels.

Table 6 Bimetallic corrosion between nickel and nickel–iron alloys in 16% calcium chloride solution[2]

Alloy	*Corrosion rate[a] (mm year^{-1})*	
	Coupled	*Uncoupled*
100 Ni	–	0.02
Ni–5Fe	0.045	0.045
Ni–10Fe	0.7	0.055
Ni–20Fe	1.0	0.044

[a]Room temperature test of duration 120 days, solution agitated. Cathode:anode area = 100:1.

3.03.3.2 Structural Features

On cooling to room temperature after annealing, maraging steels transform completely to martensite. The as-annealed structure consists of packets of parallel lath-like martensite platelets arranged within a network of prior austenite grain boundaries. The platelets have a high dislocation density but are not twinned.

On heat treating at 485 °C, a very rapid age-hardening reaction takes place and greatly strengthens the material. Although the nature of the precipitates formed is still uncertain, the consensus of opinion is that ageing for several hours at 485 °C results in a Ni_3Mo phase, while longer times produce the Fe_2Mo phase. There may also be a titanium precipitate, η-Ni_3Ti or $Ni_3(Mo,Ti)_3$. Ageing at higher temperatures or longer times results in some reversion to austenite, which may be stable at room temperature (depending on time and temperature of ageing), and to a lower strength.

3.03.3.3 Physical and Mechanical Properties

Summaries of the physical and mechanical properties of the 18% Ni maraging steels are given in Tables 9 and 10. The mechanical properties are highlighted by good ductility, toughness, and a lack of notch sensitivity. The plane strain fracture toughness of maraging steels is superior to other alloys at comparable strength levels (Table 11).

3.03.3.4 Fabrication

Maraging steels have been produced by both air and vacuum melting. Small amounts of impurities can

Table 7 Bimetallic corrosion between nickel–iron alloys in sodium hydroxide[2]

Galvanic couple	*Corrosion rate[a] (mm year^{-1})*				
	23% NaOH		*50% NaOH*	*75% NaOH*	
	Coupled	*Uncoupled*	*Coupled*	*Coupled*	*Uncoupled*
Ni–5Fe	0.04	0.035	0.06	0.0250	0.02
Nickel	0.015	0.01	0.02	0.04	0.04
Ni–10Fe	0.07	0.03	0.48	0.38	0.035
Nickel	0.01	0.01	0.015	0.02	0.04
Ni–20Fe	0.095		0.04	0.05	0.015
Nickel	0.015		0.01	0.03	0.04
Ni–30Fe	0.04	–	0.2	0.31	–
Nickel	0.02	0.01	0.01	0.02	0.04
Ni–40Fe	0.04	–	0.21	0.34	–
Nickel	0.02	0.01	0.01	0.02	0.04

[a]Area ratio Ni:Ni–Fe = 10:1.

Table 8 Nominal composition of 18% Ni maraging steels[24]

Maraging steel type	*Nominal composition (%)*					*Nominal yield strength (MN m^{-2})*
	Ni	*Co*	*Mo*	*Ti*	*Fe*	
18% Ni 200	18	8.5	3	0.2	Balance	1380
18% Ni 250	18	8	5	0.4	Balance	1720
18% Ni 300	18	9	5	0.6	Balance	2050
18% Ni 350	17.5	12.5	3.75	1.7	Balance	2390
Cast alloy	17	10	4.6	0.3	Balance	1580

Table 9 Summary of physical properties for the 18% Ni 200 to 18% Ni 350 alloys

Density 8.0–8.1 g cm^{-3}
Crystal structure Martensite (body-centered cubic); austenite (face-centered cubic)
Lattice parameter Martensite 2.856–2.862 Å at room temperature; austenite (retained) 3.58 Å
Thermal conductivity 19.68–20.93 kW m^{-2} °C (20–100 °C)
Electrical resistivity 60–70 μΩ cm when solution annealed at 815 °C; 35–50 μΩ cm when maraged at 485 °C for 3 h
Melting temperature 1430–1445 °C
Transformation temperature *M* 145–200 °C; *M* 77–145 °C; *A* 445 °C
Nominal length change −0.06% to −0.10% during maraging

decrease toughness significantly. Sulfur in particular is detrimental and should be kept as low as possible. Silicon and manganese also have a detrimental effect on toughness and should be maintained below a combined level of 0.20%. Such elements as C, P, Bi, O, N, and H should be kept to the lowest levels practicable.

The maraging steels are readily hot worked by conventional rolling and forging operations. A preliminary homogenization at 1210–1260 °C is normally used prior to hot working at that temperature. During subsequent hot working, extended times at, or slow cooling through, temperatures from 760 to 1100 °C should be avoided, since they produce embrittlement.[25] Maraging steels can be cold worked up to 85% before requiring intermediate annealing (because of low work-hardening characteristics) but are usually annealed after smaller reductions.

Heat treatments are relatively simple and normally consist of annealing for 1 h at 815 °C followed by ageing for 3 h at 485 °C. Recently, double annealing treatments have grown in favor. Machining or fabrication is easily performed in the as-annealed condition. Subsequent age hardening generally introduces small and predictable dimensional changes.

3.03.3.5 Corrosion of Maraging Steels

3.03.3.5.1 Natural environments

In atmospheric exposure, 18% Ni maraging steel corrodes in a uniform manner[22] and becomes completely rust covered. Pit depths tend to be less deep than for low-alloy high-strength steels.[26] Atmospheric corrosion rates[27] in industrial (Bayonne, NJ) and marine (Kure Beach, NC) atmospheres are compared with those for low-alloy steel in **Figures 3** and **4** respectively. The corrosion rates drop substantially after the first year or two, and in all cases, the rates for maraging steel are about half the corrosion rate for HY80 and AISI 4340 steels.

The corrosion rates for both maraging steel and the low-alloy steels in seawater are similar initially, but from about 1 year onwards, the maraging steels tend to corrode more slowly as indicated in **Figure 5**. The corrosion rates for both low alloy and maraging steel increase with water velocity.[5] During seawater exposure, the initial attack was confined to local anodic areas, whereas other areas (cathodic) remained almost free from attack; the latter were covered with a calcareous deposit typical of cathodic areas in seawater exposure. In time, the anodic rust areas covered the entire surface.[6]

Polarization tests[27] indicate that maraging steel does not exhibit passive behavior in 3% NaCl, and that the polarization curves are unaffected by changes in heat treatment.

3.03.3.5.2 Industrial environments

The corrosion rates of maraging steels in acid solutions such as sulfuric, hydrochloric, formic, and stearic acids are substantial, although lower than those of the low-alloy high-strength steels.[28] Polarization studies[29] indicate that maraging steels exhibit active–passive behavior in 1 and 0.1 M sulfuric acid. The corrosion potential, critical current density, primary passivation potential, and passive current density are all affected by variations in ageing treatment.

Table 10 Summary of nominal mechanical properties for the 18% Ni maraging alloys

Property	*18% Ni 200*	*18% Ni 250*	*18% Ni 300*	*18% Ni 350*
Yield strength −0.2% offset ($MN\,m^{-2}$)	1310–1550	1650–1820	1780–2060	2270–2480
Ultimate tensile strength ($MN\,m^{-2}$)	1340–1580	1680–1860	1820–2100	2300–2510
Elongation in 25.4 mm (1 in.), (%)	11–15	10–12	7–11	6–10
Reduction in area (%)	35–67	35–60	30–50	25–45
Modulus of elasticity E ($kN\,m^{-2}$)	18.0×10^7	18.5×10^7	18.9×10^7	19.3×10^7
Hardness (Rockwell *C*)	44–48	48–50	51–55	56–59
Impact Charpy V-notch (J)	35–68	24–45	16–26	7–14
Notch tensile				
0.0128 m bar $K_1 = 10(MN\,m^{-2})$	2390	2350–2510	2900–3100	–
0.00762 m bar $K_1 = 10\ (MN\,m^{-2})$	–	2560–2660	–	1360–1490
Fracture toughness (K_{tc}) ($MN\,m^{-2}\,m$)	101–176	98–165	88–143	44–82
Endurance limit ($MN\,m^{-2}$)				
Smooth bar 10^8 cycles	620–795	620–760	760–900	690
Notched bar 10^8 cycles ($K_t = 2.2$)	275–345	275–380	275–415	–
($K_t = 2.8$)	–	–	–	352

In all cases treatment was for 1 h at 815 °C plus 3 h at 485 °C.

Table 11 Comparison of toughness of maraging steels and other high strength alloys

Alloy	*Yield strength ($MN\,m^{-2}$)*	$K_{tc}(MN\,m^{-2}\sqrt{m})$
18% Ni 200	1380	110–176
18% Ni 250	1720	98–165
18% Ni 300	1930	88–143
D6 AC	1380	88–99
H–11	1790	66–71
AISI 4340	1790	61–66
AMS 6430	1510	61–71
Ti–16V–2.5A1	1170	49–55
Aluminum 7075.T6	415–485	39–66

Source: K_{tc} is the place strain fracture roughness (see Section 8.9). Bourelier, F., Vu Quang, K. In Proceedings of the Conference, 10th International Congress Metallic Corrosion, Madras, India, November 1987, 1988; p 2813.
Data Bulletin on 18% Ni Maraging Steels, The International Nickel Company, Inc. 1964.

The critical and passive current densities increase as the structure is varied from fully annealed to fully aged. The normal heat treatment produces critical and passive current densities of 0.4 and 0.2 $mA\,cm^{-2}$ respectively ($0.1\ mA\,cm^{-2} \sim 1.2\ mm\,year^{-1}$).[30]

3.03.3.6 Stress Corrosion Cracking

3.03.3.6.1 Mechanisms

The 18% Ni maraging steels do not display passivity and normally undergo uniform surface attack. Of more serious consequence, however, for all high strength steels, is the degree of susceptibility to SCC. For high-strength steels in general, the stress corrosion process in aqueous media is characterized by delayed failure, which consists of an incubation period followed by slow, and at times, intermittent crack growth. Failure can occur on loading to some fraction of the yield stress or through the action of residual stresses, often in environments as mild as humid air.[31] The degree of susceptibility depends on the mode of loading and is highest in cases of plane strain loading (triaxial stresses), with tensile loading and plane stress bending, in that order, representing less severe loading conditions[32] (tensile stresses of course are present in all these modes of loading). In general, susceptibility to SCC increases with increasing yield strength. Different alloy types, however, vary in their degree of resistance, and at comparable strength levels, maraging steels compare favorably in cracking resistance with other high-strength steels.

For a variety of steels, including maraging steels, it was found that under freely corroding conditions, the pH of the solution near the crack tip was about 3.8 for the materials studied.[33] Furthermore, potential measurements indicated that thermodynamic conditions were satisfied for hydrogen ion reduction. Further potential–pH measurements were made on AISI 4340 steel exposed to 0.6 N NaCl solutions of different pH and polarized to potentials both negative and positive with respect to the corrosion potential.[34] It was found that the pH of the solution in the crack was determined

solely by electrochemical reactions at the crack tip irrespective of starting pH. It was also apparent that, regardless of the impressed potential, the electrochemical conditions in the crack satisfied the thermodynamic requirements for the production of hydrogen. These results indicate that it is not necessary to invoke an active path mechanism and that hydrogen is available even during anodic polarization of AISI 4340 steel.

Activation energy measurements for SCC of H-11 steel and AISI 4340 in water and moist air are similar[34,35] and suggest that the cracking rate in these alloys is controlled by the diffusion of hydrogen, since these are in close agreement with the value for the diffusion of hydrogen through AISI 4340 membranes.[36] There is little question that at strongly negative potentials, cracking occurs by hydrogen embrittlement. For all other cases, there does not appear to be a strong basis for favoring one mechanism over the other or to discard the possibility that each mechanism shares in the control of the cracking process. The latter possibility for maraging steel has been supported by a study of cracking response to polarization, fractographic studies, and pH determinations of the corrodent at the tip of the crack.[37] Craig and Parkins[38] have shown good evidence that cracking can proceed by hydrogen embrittlement at more negative potentials, by anodic dissolution at more positive potentials, and possibly by combinations of both mechanisms at intermediate potentials. The effects of precracking or pitting of smooth specimens was also examined. In many instances, the local changes in chemistry of the test solution in the cracks or pits was more important than the stress concentrations at these locations.

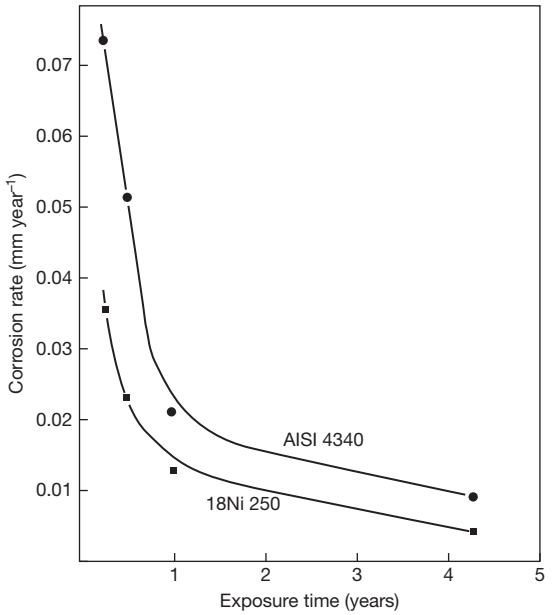

Figure 3 Corrosion rates of maraging and low alloy steels in an industrial atmosphere at Bayonne NJ, USA. Reproduced from Kenyon, N.; Kirk, W. W.; van Rooyen, D. *Corrosion* **1971**, *27*, 390.

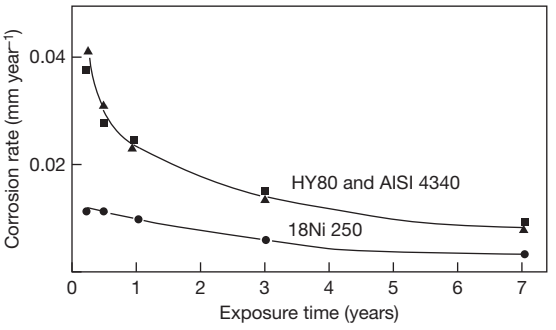

Figure 4 Corrosion rates of maraging and low alloy steels 244 m from the sea at Kure Beach NC, USA. Reproduced from Kenyon, N.; Kirk, W. W.; van Rooyen, D. *Corrosion* **1971**, *27*, 390.

3.03.3.6.2 Testing for SCC

The stress corrosion resistance of maraging steel has been evaluated both by the use of smooth specimens loaded to some fraction of the yield strength and taking the time to failure as an indication of resistance, and by the fracture mechanics approach,[39] which involves the use of specimens with a preexisting crack. Using the latter approach, it is possible to obtain crack propagation rates at known stress intensity factors (K) and to

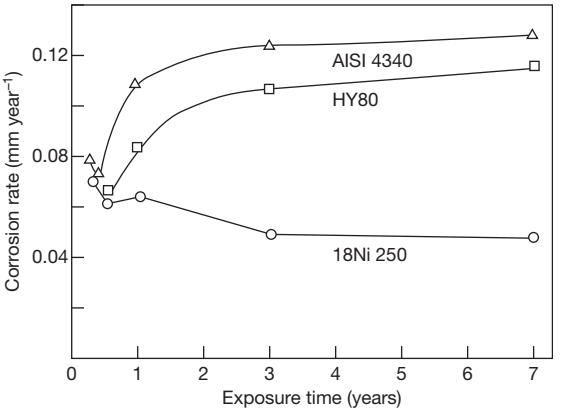

Figure 5 Corrosion rates of maraging and low alloy steels in seawater flowing at 0.6 m s^{-1}. Reproduced from Kenyon, N.; Kirk, W. W.; van Rooyen, D. *Corrosion* **1971**, *27*, 390.

determine critical stress intensity factors (K_{ISCC}) below which a crack will not propagate.

Any test in which time to failure of smooth specimens is determined is an overall measure of the incubation period to initiate a crack, the ability to resist the propagation of a stress corrosion crack, and the ability to resist final mechanical fracture. Since this test does not indicate the relative merits of an alloy in each individual aspect of the cracking process, it is probably of less benefit to a design engineer. The use of precracked specimens in the fracture mechanics approach follows from the philosophy that structures are likely to contain crack-like defects. The use of precracked specimens promotes a rapid change in the chemistry of the solution at the crack tip and shortens or eliminates the initiation time for crack propagation.

3.03.3.6.3 Cracking resistance in smooth materials

Maraging steel in the strength range 1240–1720 MPa tested as U-bends in seawater displayed good resistance, as it did not fracture in periods of up to 2–3 years although there was considerable general corrosion and fouling. However, microcracks were observed after 6 months. Similar behavior[22,26] of U-bend and bent beam specimens can be expected in industrial or marine atmospheres, although general corrosion is less severe. By comparison, AISI 4340 at strength levels of 1660 MPa failed in about 1 week in both seawater and atmospheric tests. Maraging steel of yield strength at or above 2060 MPa was not resistant and failed rapidly. Welds in maraging steel are somewhat less resistant than base plate. U-bend exposure of 1240 MPa strength welds survived for up to 2 years in seawater, while at 1380 MPa, failures occurred in 2–18 months.[28]

It is possible to provide cathodic protection to materials of up to 1720 MPa yield strength, by coupling to mild steel or possibly to zinc.[22,26] However, zinc and metals more active than zinc tend to induce hydrogen embrittlement. Welds up to 1380 MPa may be cathodically protected by zinc, but at impressed potentials of −1.25 V (vs. the standard calomel electrode), both 1240 and 1380 MPa welds fail rapidly due to hydrogen embrittlement.[28] Hence, although tests on smooth specimens indicate that cathodic protection of maraging steel is possible, tests on specimens with preexisting cracks indicate a greater sensitivity to hydrogen embrittlement during cathodic polarization.[28] The use of cathodic protection on actual structures must therefore be applied with caution, and the application of less negative potentials than are indicated to be feasible in smooth specimen tests is to be recommended if it is assumed that structures contain crack-like defects. Further evidence of the relative resistance of maraging steel is reproduced in **Figure 6**. Also shown is the beneficial effect in smooth surface tests of cold rolling; shot peening has a similar beneficial effect.[28]

3.03.3.6.4 Critical stress intensity factor

It has become common to use K_{ISCC}, the critical stress intensity factor, as a measure of the resistance of an alloy to SCC. Tests are performed on specimens that are precracked by a fatigue machine and must be of sufficient dimensions to ensure plane strain conditions. **Figure 7** presents a summary comparing the K_{ISCC} values of maraging steel, with values for H-11, AISI 4340, AM 355, AISI410, 17–4 PH, 13–8 Mo PH, D6AC, and 9Ni–4Co–C steels. The data have been taken from a number of sources[28,40–43] and are for exposures in aqueous environments, with and without NaCl. No attempt has been made to distinguish between different environments, since they do not affect the results appreciably.

Plotted points marked W in **Figure 7** refer to data for welds; also included are lines of critical crack depth a_{cr}. The region below a line of specified critical crack depth corresponds to combinations of strength and K_{ISCC} for which a long crack of the specified depth will propagate when stressed to the yield point, whereas the region above the line corresponds

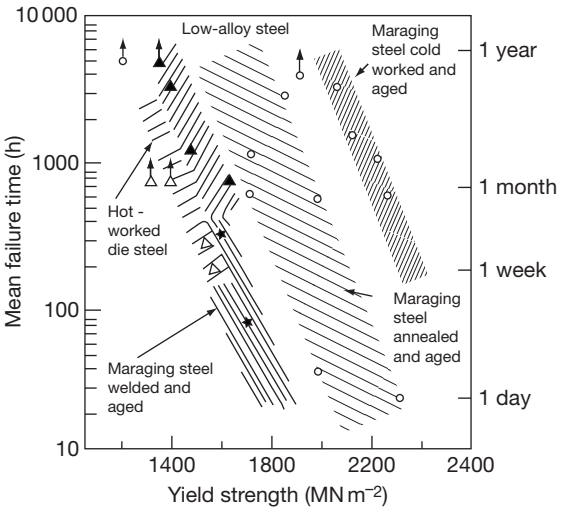

Figure 6 Bent-beam test results in aerated distilled water. These specimens were exposed to the environment at a stress of 70% of yield. Reproduced from Setterlund, R. B. *Mater. Protect.* **1965**, *4*(12), 27.

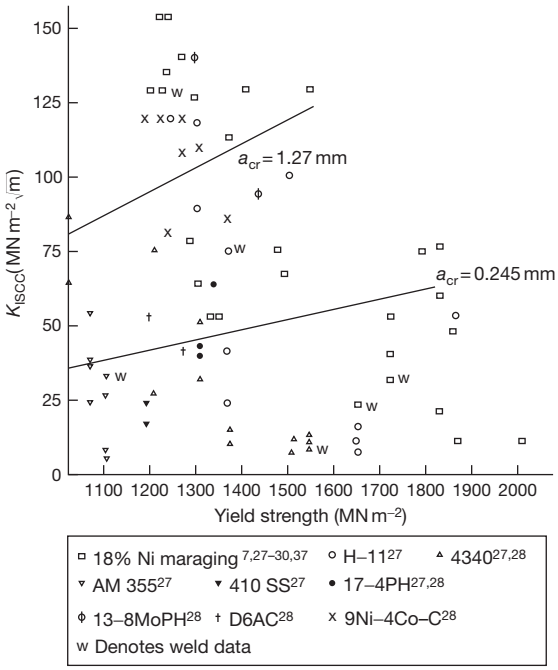

Figure 7 Comparison of K_{ISCC} as a function of yield strength of 18% Ni maraging and other high strength steels.

to the strength and K_{ISCC} combinations for which the crack will not propagate. The critical crack depth (assuming yield point stresses) for cracks the length of which greatly exceeds their depth is given by:

$$a_{cr} = 0.2\left(\frac{K_{ISCC}}{\sigma_y}\right)^2$$

where σ_y is the yield stress.[44]

In general, it is clear that maraging steels compare favorably with other high-strength steels and offer comparatively high K_{ISCC} values over a wide range of strength. It is also clear that maraging steels can withstand a greater crack depth without crack propagation.

A further estimation of the corrosion resistance of maraging steel can be obtained from data on the rate of crack propagation. Although the rate of crack propagation has been found to be a function of stress intensity in some alloys, for many alloys and heat treatments, there is a range of stress intensity above K_{ISCC} and approaching K_{IC} at which the rate of crack propagation is independent of stress intensity (Table 12).[45] The cracking rate for maraging steel is seen to be slower than for 4340 and D6AC and equivalent to H-11 and HP 9Ni–Co–C steels, at a strain rate of 10^{-5} mm s^{-1}. The fact that cracks propagate very slowly in maraging steels has an important consequence related to their stress corrosion testing.

Table 12 Crack propagation rates for a number of high strength steels

Alloy	*Yield strength (MN m^{-2})*	*Crack velocity (mm s^{-1})*
Maraging 250	1570	1.31×10^{-5}
Maraging 250	1690	1.40×10^{-5}
Maraging 300	1950	2.75×10^{-4}
Modified maraging 300[a]	2180	1.18×10^{-4}
Modified maraging 300[a] (underaged)	1810	0.72×10^{-3}
Modified maraging 300[a] (overaged)	1760	2.88×10^{-5}
4340	1430	1.65×10^{-3}
D6AC	1540	1.74×10^{-4}
H–11	1420	1.19×10^{-5}
HP 9–4–25	1330	2.54×10^{-5}
HP 9–4–45 (bainitic)	1460	1.06×10^{-5}

Source: Carter, C. S. *Met. Trans.* **1970**, *1*, 1551.
[a]No details on the modification were available.

In determining K_{ISCC} by dead-weight loaded cantilever beam tests, it has been recommended[46] that maraging steel should withstand 1000 h without failure to ensure that the applied stress intensity is at, or lower than, K_{ISCC}.

3.03.3.6.5 Effect of metallurgical variables on SCC

It is notable that while it is possible to produce maraging steels with consistently uniform mechanical properties, the stress corrosion properties are subject to scatter, as indicated in Figure 7. To a large extent, this scatter is an indication of the greater sensitivity of SCC to metallurgical variables. Although the variation in cracking resistance is not well understood, and the reaction to certain treatments not always consistent, certain observations may be used to indicate guidelines for improved properties. Cracking in maraging steels has generally been observed to be intergranular with isolated cases of transgranular cracking.[26,47,48] Both Ti_2S and Ti(C,N) on prior austenite boundaries have been suggested to be related to greater susceptibility. Thus, since prolonged time in the temperature range 760–1100 °C favors the precipitation of Ti_2S and Ti(C,N) on prior austenite boundaries, such exposures should be avoided both in processing and in annealing.

Studies of the effect of ageing temperature on cracking behavior have shown rather marked effects. Under-ageing at temperatures of 455 °C or lower was found to increase greatly the rate of crack propagation without affecting the mode of crack propagation

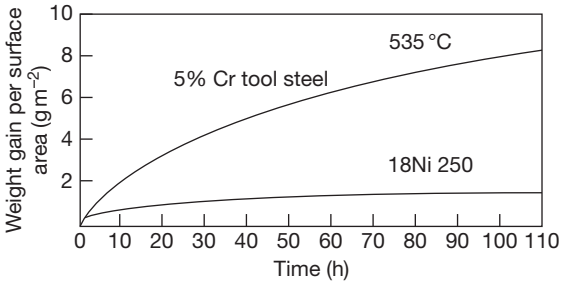

Figure 8 Oxidation rate at 535 °C of 18Ni250 maraging steel compared with a generally-available tool steel. These tests were performed on 6.35 mm cubes exposed to still air for 5, 25, and 100 h. The weight gain includes the scale formed during heating and cooling. Reproduced from Data Bulletin on 18% Ni Maraging Steels, The International Nickel Company, Inc. 1964.

(intergranular) or K_{ISCC}.[45,47,49] However, over-ageing appears to offer slightly slower crack growth rates (Table 12), but it did not significantly improve K_{ISCC}.[29] The best combination of properties is obtained with the normal ageing treatment at 485 °C.

Studies on welds showed that cracking resistance as indicated in U-bend tests[28] was substantially increased by a postweld anneal (1 h at 815 °C) prior to the normal ageing treatment. Material aged in the as-welded condition was less resistant. The most significant structural difference resulting from the two heat treatments was a finer dispersion of austenite ribbons in material annealed before ageing.

3.03.3.7 High Temperature Corrosion

Little data are available on hot corrosion behavior. Figure 8 indicates maraging steel to have better resistance to air exposure at 535 °C than a 5% Cr tool steel.[24] Metallographic examination indicates that exposure to air at elevated temperatures results in reaction with both oxygen and nitrogen, forming both oxides and titanium carbonitrides. Under some conditions of reduced oxygen partial pressure, selective subsurface oxidation of iron can occur.

3.03.3.8 Applications

Maraging steels have found varied uses in the aerospace and aircraft industries. These uses have included rocket motor cases, landing gear components, aircraft forgings and fasteners. Other areas of usage include machine tool and die applications, and extrusion hardware. Marine uses include hydrofoil foil systems and aircraft arrester hooks.

References

1. Beauchamp, R. L. Dissertation Ohio State University, 1966; Figure 27.
2. La Que, F. L.; Copson, H. R. Eds. *Corrosion Resistance of Metals and Alloys*, 2nd ed.; Reinhold Publishing Corporation/Van Nostrand Reinhold Ltd: New York/London, 1963; p 458.
3. Symposium on Atmospheric Corrosion of Non-Ferrous Metals, American Society for Testing and Materials, 58th Annual Meeting. June 29, 1955, Special Techical Publication No. 175, pp 141–158.
4. Evans, T. E. In 4th International Congress on Corrosion Amsterdam, 1969.
5. Friend, J. N. In 18th Report of the Committee of the Institution of Civil Engineers 1940.
6. Marsh, J. S. *The Alloys of Iron and Nickel: Vol. I Special-Purpose Alloys*; McGraw-Hill: New York, London, 1938; p 495 et seq.
7. Hatfield, W. H. *Engineer* **1922**, *134*, 639.
8. Hatfield, W. H. *J. Iron Steel Inst.* **1923**, *108*, 103.
9. Bourelier, F.; Vu Quang, K. In Proceedings of the Conference, 10th International Congress Metallic Corrosion, Madras, India, November 1987, 1988; p 2813.
10. Raicheff, R.; Aroyo, M.; Aropadjan, S. *Werkst. Korr.* **1982**, *33*, 25.
11. Yagupol'skaya, L. N.; Lavrenko, V. A.; Kozachenko, E. V. *Zasch. Metal.* **1974**, *109*, 291.
12. Uto, Y.; Kitajima, H.; Kai, T. *Nippon KInzoku Gakkaishi* **1963**, *27*, 18.
13. Fink, C. G.; De Croly, C. M. *Trans. Am. Electrochem. Soc.* **1929**, *56*, 239.
14. Schwerdtfeger, W. J. *J. Res.* **1966**, *70C*, 187.
15. Rhodin, T. H. Ed. *Physical Metallurgy of Stress Corrosion Fracture*; Interscience: New York, 1959; pp 259–262.
16. Couper, A. S. *Mater. Product.* **1969**, *8*(10), 17.
17. Radd, F. J.; Wolfe, L. H.; Crowder, L. H.; Crowder, L. H. In The World Petroleum Conference 1967.
18. Marquez, J. A.; Matshusima, I.; Unlig, H. H. *Corrosion* **1970**, *26*, 216.
19. Bieber, C. G. *Met. Prog.* **1960**, *78*, 99.
20. Decker, R. F.; Eash, J. T.; Goldman, A. J. *Trans. Quart. ASM* **1962**, *55*, 58.
21. Sadowski, E. P.; Koppi, W. A. *Trans. Am. Foundrymen's Soc.* **1967**, *75*, 294.
22. Kirk, W. W.; Covert, R. A.; May, T. P. *Met. Eng. Quart.* **1968**, *8*, 31.
23. Floreen, S. *U.S. Patent 4* **1984**, *443*, 254.
24. Data Bulletin on 18% Ni Maraging Steels, The International Nickel Company, Inc. 1964.
25. Novak, C. J. D.M.I.C. Memo 1964; p 196.
26. Dean, S. W.; Copson, H. R. *Corrosion* **1965**, *21*, 95.
27. Stavros, A. J.; Paxton, H. W. Paper presented at NACE Meeting, Chicago, Illinois 1971.
28. Kenyon, N.; Kirk, W. W.; van Rooyen, D. *Corrosion* **1971**, *27*, 390.
29. Bui, N.; Pieraggi, B.; Dabosi, F. *Mem. Sci. Rev. Met.* **1971**, *68*, 223.
30. France, W. D., Jr.; Mazzatenta, E. D. *Mater. Eng.* **1970**, *62*.
31. Johnson, H. H. In Proceedings of Conference of Fundamental Aspects of Stress Corrosion Cracking, National Association of Corrosion Engineers 1969; p 439.
32. Hayden, H. W.; Floreen, S. *Corrosion* **1971**, *27*, 429.
33. Brown, B. F. In Extended Abstract of paper presented at Fourth International Congress on Metallic Corrosion, Amsterdam, Netherlands, 1969.
34. Smith, J. A.; Peterson, M. H.; Brown, B. F. *Corrosion* **1970**, *26*, 539.

35. Johnson, H. H.; Willner, A. M. *Appl. Mater. Res.* **1965**, *4*, 34.
36. Beck, W.; Bockris, J. O'M.; McBreen, J.; Nanis, L. *Proc. Roy. Soc. London A* **1966**, *290*, 221.
37. Syrett, B. C. *Corrosion* **1971**, *27*, 270.
38. Craig, I. H.; Parkins, R. N. *Br. Corros. J.* **1984**, *19*, 3–16.
39. Setterlund, R. B. *Mater. Protect.* **1965**, *4*(12), 27.
40. Freedman, A. H. *J. Mater.* **1970**, *5*(12), 431.
41. Brown, B. F. Naval Research Laboratory Report 7168, 1970.
42. Steigerwald, E. A. Presented at ASM Conference on Stress Corrosion Cracking, Philadelphia, PA, August 1970. Original work by Carter, C. S., Boeing Co. Report D6–19770 November 1967.
43. Dautovich, D. P.; Floreen, S. Paper presented at the International Conference on Stress Corrosion Cracking and Hydrogen Embrittlement of Iron Base Alloys, Unieux-Firminy, France, June, 1973.
44. Brown, B. F. *Met. Rev.* **1968**, *13*, 171.
45. Carter, C. S. *Corrosion* **1971**, *27*, 471.
46. Brown, B. F. Paper presented at ASM Conference on Fracture Control, Philadelphia, PA, January 1970.
47. Carter, C. S. *Met. Trans.* **1970**, *1*, 1551.
48. Parkins, R. N.; Haney, E. G. *Trans. Met. Soc.* **1968**, *242*, 1943.
49. Stavros, A. J.; Paxton, H. W. *Met. Trans.* **1970**, *1*, 3049.

3.04 Aqueous Corrosion of Stainless Steels

A. Iversen
Outokumpu Stainless AB, PO Box 74, SE 774 22 Avesta, Sweden
B. Leffler
Outokumpu Stainless, Hot Rolled Plate, SE 693 81 Degerfors, Sweden

Glossary

Active Describes a metal which corrodes in the negative direction of electrode potential.

Activation polarization Corrosion reaction determined kinetically by the participating electrode reactions.

Anaerobic Free of air or oxygen.

Anode The electrode of an electrolyte cell at which oxidation occurs.

Anodic polarization The change in the electrode potential in the noble positive direction.

Austenite A face-centered cubic crystalline phase of iron-base alloy.

Cathode The electrode of an electrolytic cell at which reduction is the principal reaction.

Cathodic polarization The change of the electrode potential in the active negative direction.

Cathodic protection Reduction of corrosion rate by shifting the corrosion potential of the electrode towards a less oxidizing potential by applying an external electromotive force.

Cold work The operation of shaping metals at temperatures below their recrystallization temperatures so as to produce strain-hardening.

Corrosion – fatigue Fatigue type cracking of metal caused by repeated or fluctuating stresses in a corrosive environment.

Corrosion potential, E_{corr} The potential of a corroding surface in an electrolyte, relative to a reference electrode, also called open circuit potential.

Double layer The interface between an electrode or a suspended particle and an electrolyte created by charge-charge interaction leading to an alignment of oppositely charged ions at the surface of the electrode or particle.

Ductility Ability of materials to be deformed by working process and to retain strength and freedom from cracks when their shape is altered.

Electrolyte A chemical substance or mixture, usually liquid, containing ions that migrate in an electric field.

Elongation The percentage plastic extension produced in a tensile test.

Embrittlement Loss of ductility of a material resulting from a chemical or physical change.

Equilibrium potential The potential of an electrode in an electrolytic solution when the forward

rate of a given reaction is exactly equal to the reverse rate.

Erosion Destruction of materials by abrasive action of moving fluids, usually accelerated by the presence of solid particles.

Fatigue The phenomenon leading to fracture under repeated or fluctuating stresses having a maximum value less than the tensile strength of the material.

Ferrite A body-centered cubic crystalline phase of iron-base alloys.

Galvanic corrosion Corrosion associated with the current resulting from the electrical coupling of dissimilar electrodes in an electrolyte.

General corrosion A form of deterioration that is distribute more or less uniformly over a surface.

Hardening The process of making steel hard by cooling from above the critical range at a rate that prevents the formation of ferrite and pearlite and results in the formation of martensite.

Heat affected zone (HAZ) That portion of the base metal that was not melted by welding but whose microstructure and properties were altered by the heat of the welding process.

Inclusion A nonmetallic phase such as an oxide, sulfide or silicate particle in a metal.

Martensite Metastable body-centered phase of iron super-saturated with carbon, produced from austentite by shear transformation during quenching or deformation.

Mixed potential A potential resulting from two or more electrochemical reactions occurring simultaneously on one metal surface.

Noble The positive direction of electrode potential.

Open circuit potential The potential of an electrode measured with respect to a reference electrode when no current flows to or from it (see also corrosion potential).

Passivation A reduction of the anodic reaction rate of a metal.

Passive A metal corroding under the control of a surface reaction product.

Passivity The state of being passive.

Pits, pitting Localized corrosion of a metal surface that is confined to a small area and takes to form of cavities.

Polarization The deviation from the open circuit potential of an electrode.

Polarization curve or polarization diagram A plot of current density versus electrode potential for a specific electrode-electrolyte combination.

Potentiodynamic The technique for varying the potential of an electrode in a continuous manner at a present rate.

Potentiostate An instrument for automatically maintaining an electrode at a constant potential or controlled potential with respect to a reference electrode.

Potentiostatic The technique for maintaining a constant electrode potential.

Precipitation hardening Improving the strength of solid solutions alloys by controlling the formation of precipitates on a crystal lattice scale.

Reference electrode A reversible electrode used for measuring the potentials of other electrodes.

Relative humidity, RH The ratio, expressed as a percentage, of the amount of water vapor present in a given volume of air at a given temperature to the amount required to saturate the air at that temperature.

Scanning electron microscope (SEM) An electron optical device that images topographical details with maximum contrast and depth of field by the detection, amplification and display of secondary electrons.

Sensitizing heat treatment A heat treatment, which causes precipitation of constituents at grain boundaries.

Solution heat treatment Heating a metal to a suitable temperature and holding at that temperature long enough for one or more constituents to enter into solid solution, then cooling rapidly enough to retain the constituents in solution.

Tempering The reheating of hardened steel at any temperature below the critical range, in order to decrease the hardness. Sometimes drawing.

Toughness Condition intermediate between brittleness and softness, as indicated in tensile tests by high ultimate tensile stress and low to moderate elongation and reduction in area, or by high values of energy absorbed by impact tests. More precisely it

is the value of the critical strain energy release rate.

Transpassive The noble region of potential where an electrode exhibits a current density higher than passive current density.

Abbreviations

BCC Body centered cubic structure
CCT Critical crevice corrosion temperature (°C)
CPT Critical pitting temperature (°C)
FCC Face centered cubic structure
GS Grain size
HISC Hydrogen-induced stress cracking
LT-MED Low temperature multi effect, desalination plant
Me Metal
MIC Microbially influenced corrosion
MIG Gas metal arc welding
MSF Multistage flash
OCP Open circuit potential (V)
PRE Pitting resistance equivalent
REM Rare earth metals
RH Relative humidity (%)
RO Reverse osmosis
RT Room temperature
SCC Stress corrosion cracking
SCE Saturated calomel electrode
SEM Scanning electron microscope
SHE Standard hydrogen electrode
SSC Sulfide stress cracking
SWRO Seawater reverse osmosis
TIG Gas tungsten welding
TTS Time temperature sensitization
WPA Wet process phosphoric acid

Symbols

α Body centered cubic ferrite rich in iron
α' Body centered cubic ferrite rich in chromium
A_5 Elongation or permanent extension of the gauge length after fracture, as expressed as a percentage of the original gauge length.
b_a Anodic Tafel slope
C_s Concentration of metal ion
δ Diffusion length (m)
D Diffusion coefficient of component i ($m^2\ s^{-1}$)
E Potential (V)
E_τ Transition potential (V)
E_{corr} Corrosion potential (V)
E_p Pitting Potential (V)
E_{pp} Passivation Potential (V)
E_{rp} Repassivation Potential (V)
E_{tr} Transpassive Potential (V)
F Faraday's constant (A s mol^{-1})
I Current (A)
I_{crit} Critical current density for passivation ($A\ cm^{-2}$)
i_L Anodic limiting current density ($A\ cm^{-2}$)
K Equilibrium constant
K_{ISCC} Threshold stress intensity factor ($MPa\ m^{1/2}$)
M_{d30} The temperature at which martensite will form at a strain of 30%
M_d The temperature below where martensite will form
M_s Martensite temperature, the starting temperature for martensite transformation
n Charge number
N Number of cycles
φ_s Ohmic potential drop in a pit cavity
R Stress ratio
R_m Tensile strength (MPa)
$R_{p0.2}$ Proof strength at which the material undergoes a 0.2% nonproportional (permanent) extension during a tensile test (MPa)
$R_{p1.0}$ Proof Strength at which the material undergoes a 1.0% nonproportional (permanent) extension during a tensile test (MPa)
S Stress amplitue (MPa)

3.04.1 Introduction

The corrosion resistance of stainless steels, in combination with their good mechanical properties and manufacturing characteristics, makes them an extremely valuable and flexible material for designers. Although the usage of stainless steel may have traditionally been relatively low compared with that of carbon steels, growth has been steady, in contrast to the growth of structural steels. The most dominant product form for stainless steels is cold rolled sheet and the major application areas include consumer products and plant and equipment for the oil and gas, chemical process, and food and beverage industries. The most widely used stainless steels are the austenitic grade S30400 and ferritic grades such as S41000, followed by the molybdenum-alloyed austenitic grades, notably S31600.

In terms of their durability and corrosion resistance, iron and most iron-alloyed steels are relatively poor materials, since they easily corrode in air and acid environments unless protected by some external coating and scale in furnace atmospheres. Stainless steels, however, although also belonging to the category of iron-base alloys, offer superior corrosion resistance properties and durability in such diverse environments as seawater, diluted and concentrated acids, and high temperature environments up to 1100°C.

It was the discovery, made about 100 years ago, of the effect of chromium on the resistance of iron in many environments that triggered the development of what is currently the most common group of corrosion-resistant alloys. The first patent for stainless steel was registered in the United Kingdom in 1912 and the development of stainless steels was then sparked off simultaneously in the United Kingdom, the United States, and Germany. Even if most of the stainless steel types currently in use had been available in the 1930s, it was not until the 1960s that developments in process metallurgy gave rise to the growth and widespread use of modern stainless steels.

Early research found that increasing the chromium content of iron to about 10–14% produced a massive drop in corrosion rate in many diverse environments. In time it was also realized that increasing the chromium content above 18–20% improved the corrosion resistance by decreasing the corrosion rate even further. This is the reason that even today many common stainless steel grades contain about 18% chromium. It is the resistance to many common corrosive environments, in combination with good mechanical and fabrication properties, that makes stainless steels universally useful whenever corrosion resistance and long-lasting endurance are required.

3.04.2 The use of Stainless Steels

Steel is the predominant metal used in industry. The global production of steel is around 1 billion metric tons a year, of which stainless steel accounts for about 2.5%.

The use and production of stainless steels have for many years been dominated by the industrialized Western nations and Japan, but in recent years, Asian countries, such as India and China, as well as some South American countries, have emerged as important producers and consumers of stainless steels.

The most common product form for stainless steels is cold rolled sheet. Other products, such as hot rolled plate and sheet, bar, tube and pipe, individually account for only a third or less of the total volumes of cold rolled sheet produced.

The use of stainless steels can be divided into a few major areas, with consumer products, industrial equipment, transport, and construction being the biggest. Table 1 gives a breakdown of the use of stainless steel by end-user segment.

The most widely used stainless grades are austenitic steels, which typically contain 18% chromium and 8% nickel, that is, S30400/304L. These steels account for more than 50% of the global production of stainless steel. The next most widely used grades are ferritic steels, for example, S41000 (EN 1.4000), followed by molybdenum-alloyed austenitic steels, for example, S31600/316L (EN 1.4401/1.4404). Together, these grades account for over 70% of the total tonnage of stainless steels. However, the use of duplex stainless steels, such as UNS S32205 (EN 1.4462), has been growing considerably recently and this group of stainless steels now accounts for a considerable proportion of the stainless market. The use of duplex grades will certainly increase in future. Figure 1 shows an

Table 1 Use of stainless steel divided into application categories

End-user segment	%
Catering & household	32
Industrial equipment	26
Transport	16
Construction	15
Tubular products	5
Other	6

Figure 1 White liquor tank from the pulp and paper industry built in a recently developed stainless steel grade, S32101 (1.4162).

example of the use of a recently developed duplex stainless steel grade, S32101 (1.4162), in a white liquor tank for the pulp- and paper industry.

3.04.3 Definition of Stainless Steels, Alloying Elements, and Microstructure

3.04.3.1 Classification of Stainless Steels

Stainless steels are generally defined as iron-based alloys containing at least 10.5% chromium (by weight) and a maximum of 1.2% carbon (by weight). This is the definition given in the European standards. Other definitions may vary slightly, for example, requiring minimum chromium content of 12%, but all definitions agree that stainless steels are iron-based alloys with a substantial amount of chromium, usually in the range of 10.5–12%.

Stainless steels are normally subdivided into five major families or categories based on their crystalline structure and microstructure or hardening mechanism. Each category or family shares a distinct set of general properties, including chemical composition, mechanical properties, fabrication properties, and resistance to certain types of corrosion. Within each of the stainless families there is a considerable range of chemical compositions, and therefore each family consists of several steel grades with variations within the general property profile of the specific category/family.

Stainless steels are divided into different categories according to the three basic microstructures: ferrite, austenite, and martensite. The first two are phases with distinct crystalline structures; ferrite has a body-centered cubic structure and austenite has a face-centered cubic structure. Martensite, on the other hand, is a microstructure that is formed by a complex transformation of an austenitic microstructure under certain conditions. The different categories of stainless steel are refined further from these basic criteria, either as a single-phase microstructure or as combinations of these structures, to result in five categories of stainless steel, as follows:

- ferritic stainless steels
- austenitic stainless steels
- ferritic–austenitic (duplex) stainless steels
- martensitic stainless steels
- precipitation-hardening (PH) steels

The most common alloying elements used in stainless steels are chromium, nickel, molybdenum, carbon, nitrogen, silicon, and manganese. Silicon and manganese are present in almost all stainless steels in concentrations of 0.2–0.7% and 1–2%, respectively. Other elements are also used for various purposes, but the first five named earlier are the most common alloying elements used to influence the composition of the steel in such a way that the grade falls into a specific category. Different typical combinations of these basic alloying elements are thus characteristic of the different categories of stainless steel, and in Table 2, the typical ranges of the main alloying elements for the different categories of stainless steel are shown.

As can be seen from Table 2, relatively low alloy content characterizes martensitic steels, whereas ferritic steels have high chromium content and no – or virtually no – nickel. This is in contrast to austenitic steels, which always contain nickel and have comparatively high chromium content. Duplex steels fall somewhere in between ferritic and austenitic steels as they typically have high chromium content but less nickel than standard austenitic grades. The use of nitrogen as an alloying element is restricted almost exclusively to austenitic and duplex steels. In some austenitic steel grades, nickel may, to some extent, be replaced by manganese.

Table 2 Typical ranges for alloying elements in different stainless steel categories

Category	*Composition (wt%)*					*Others*
	C	*N*	*Cr*	*Ni*	*Mo*	
Martensitic	>0.10	–	11–14	0–1	–	
	>0.15	–	16–18	0–2	0–2	
	<0.10	0.05	12–18	4–6	0–2	
Precipitation hardening	0.03–0.20	–	12–17	4–8	0–2	Al, Cu, Ti, Nb, V
	0.05–0.15	–	15–18	4–8	1–3	
Ferritic	<0.08	–	12–27	0–5	0–5	Ti
	<0.25	–	24–28	–	–	
Austenitic	<0.08	0.03–0.7	16–30	8–35	0–7	Cu, Ti, Nb, Mn
Duplex	<0.05	0.05–0.4	18–33	0–7	1–5	Mn

Figures 2 and 3 show examples of a normal microstructure for austenitic and duplex stainless steel.

For commercial stainless steel grades, several international and national standards describe and specify the composition and required properties of stainless steel products. One of the most comprehensive catalogs of steel grades is the Unified Numbering System (UNS). This system does not contain specifications but provides a unified list of alloys that have compositions specified in standards or elsewhere. All stainless steels have the letter 'S' as a prefix in the UNS number. European stainless steel grades are listed along with their compositions in EN 10088-1.[1] American steel grades and their compositions are normally listed in the material and product standards published by ASTM or ASME, for example, ASTM A 240 or ASME SA 240. Table 3 shows the typical chemical composition for a number of commercial stainless steels of various types based mainly on American and European standards.

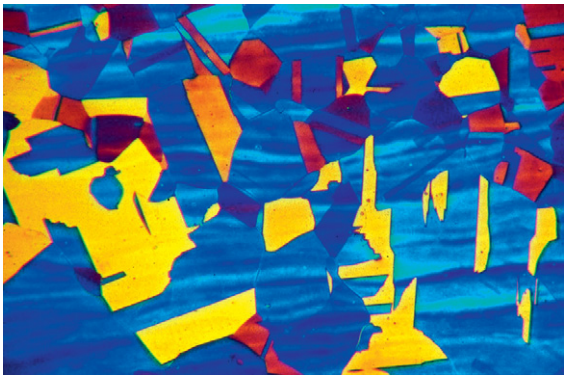

Figure 2 Typical microstructure of an austenitic stainless steel.

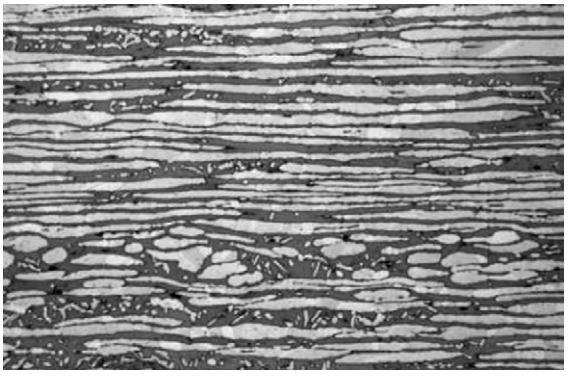

Figure 3 Typical microstructure of a duplex stainless steel.

3.04.3.2 Alloying Elements and Microstructure

Stainless steels contain a number of different alloying elements, each of which has a specific effect on the properties of the steel. The properties of a specific steel grade will thus be determined by the combined effect of the alloying and trace elements in that specific grade. A brief overview of the alloying elements and their effects on the structure and properties of the steel are given in the following sections together with an explanation of why various elements are added to certain grades.[2] It should also be noted that the effect of the alloying elements differs in some aspects between the hardenable and the nonhardenable stainless steels.

3.04.3.2.1 Chromium (Cr)

This is the most important alloying element as it provides stainless steels with their basic corrosion resistance. Generally speaking, the higher the chromium content, the better the corrosion resistance. Chromium also enhances the steel's resistance to oxidation at high temperatures and promotes a ferritic structure.

3.04.3.2.2 Nickel (Ni)

The main reason for adding nickel is to promote an austenitic structure. Nickel generally increases ductility and toughness. It also lowers the corrosion rate and can thus be used to good effect in acid environments. In precipitation-hardening steels, nickel is also used to form the intermetallic compounds to increase the strength of the steel.

3.04.3.2.3 Molybdenum (Mo)

Molybdenum substantially enhances the resistance to both general and localized corrosion and increases the mechanical strength of steels. In addition to promoting a ferritic structure, molybdenum promotes the formation of secondary phases in ferritic, duplex, and austenitic steels. In martensitic steels, it will increase the hardness at higher tempering temperatures because of its effect on carbide precipitation.

3.04.3.2.4 Copper (Cu)

Copper enhances the corrosion resistance of steels in certain acid environments and promotes an austenitic structure. In precipitation-hardening steels, copper is used to form the intermetallic compounds to increase the strength of the steel.

Table 3 Typical chemical compositions for some commercial stainless steel grades

Steel grade			*Microstructure*	*Typical chemical composition (wt%)*				
UNS	*ASTM*	*EN*		*Cr*	*Ni*	*Mo*	*N*	*Other*
S41000	410	1.4006	Martensitic	12			0.04	
S41600	416	1.4005	Martensitic	13			0.04	S
S42000	420	1.4021	Martensitic	13				
S43000	430	1.4016	Ferritic	16				
S43400	434	1.4113	Ferritic	17		1		
S44400	444	1.4521	Ferritic	17		2		
S20100	201	1.4372	Austenitic	17	5		0.15	Mn(7.08)
S20400	204		Austenitic	16	2.2		0.17	Mn(9.07)
S30100	301	1.4310	Austenitic	17	7			
S30100	301LN	1.4318	Austenitic	17.7	6.5		0.14	
S30300	303	1.4305	Austenitic	17.3	8.2			
S30400	304	1.4301	Austenitic	18.1	8.3			
S30403	304L	1.4307	Austenitic	17.5	8			
S30500	305	1.4303	Austenitic	17.7	12.5			
S34700	347	1.4550	Austenitic	18	9.5		0.04	Nb,Mn(2.0)
S31600	316	1.4401	Austenitic	17.2	10.2	2.1		
S31603	316L	1.4404	Austenitic	17.2	10.2	2.1		
S31635	316Ti	1.4571	Austenitic	16.8	10.9	2.1		Ti
S31653	316LN	1.4406	Austenitic	17.2	10.3	2.1	0.14	
S31600	316	1.4436	Austenitic	16.9	10.7	2.6		
S31703	S31703	1.4438	Austenitic	18.2	13.7	3.1		
N08904	N08904	1.4539	Austenitic	20	25	4.5		Cu(1.5)
S31254	S31254	1.4547	Austenitic	20	18	6.1	0.20	Cu
S34565	S34565	1.4565	Austenitic	24	17	4.5	0.45	5Mn(5.5)
S32101	S32101	1.4162	Duplex	21.5	1.5	0.3	0.22	
S32304	S32304	1.4362	Duplex	22	3.5	0.1	0.10	
S32205	S32205	1.4462	Duplex	22	5.5	3	0.17	
S32750	S32750	1.4410	Duplex	24	6	3	0.27	

3.04.3.2.5 Manganese (Mn)

Manganese is generally used in stainless steels to improve hot ductility. Its effect on the ferrite/austenite balance varies with temperature; at low temperatures, manganese is an austenite stabilizer, whereas at high temperatures, it will stabilize ferrite. Manganese increases the solubility of nitrogen and is used to obtain high nitrogen contents in austenitic steels.

3.04.3.2.6 Silicon (Si)

Silicon increases the resistance to oxidation, both at high temperatures and in strongly oxidizing solutions at lower temperatures. It promotes a ferritic structure.

3.04.3.2.7 Carbon (C)

Carbon is a strong austenite former and strongly promotes an austenitic structure. It also substantially increases the mechanical strength. Increasing carbon content reduces the resistance to intergranular corrosion. In ferritic stainless steels carbon will strongly reduce both toughness and corrosion resistance. In the martensitic and martensitic–austenitic steels, carbon increases hardness and strength. In the martensitic steels, an increase in hardness and strength is generally accompanied by a decrease in toughness and in this way carbon reduces the toughness of these steels.

3.04.3.2.8 Nitrogen (N)

Nitrogen is a very strong austenite former and promotes an austenitic structure. It also substantially increases the mechanical strength of steel and enhances its resistance to localized corrosion, especially when used in combination with molybdenum. In ferritic stainless steels, nitrogen will lead to a significant reduction in toughness and corrosion resistance. In martensitic and martensitic–austenitic steels, the addition of nitrogen will increase hardness and strength but reduce the toughness of the steel.

3.04.3.2.9 Titanium (Ti)

Titanium is a strong ferrite former and a strong carbide former, and, as such, helps lower the effective

carbon content and promote a ferritic structure in two ways. In austenitic steels, it is added to improve the resistance to intergranular corrosion, but it also enhances the mechanical properties of the steel at high temperatures. In ferritic stainless steels, titanium is added to improve toughness and corrosion resistance by lowering the amount of interstitials in solid solution. In martensitic steels, titanium reduces the martensite hardness and increases the tempering resistance. In precipitation-hardening steels titanium is used to form the intermetallic compounds used to increase the strength of the steel.

3.04.3.2.10 Niobium (Nb)

Niobium is both a strong ferrite and carbide former. Like titanium, it promotes a ferritic structure. In austenitic steels, it is added to improve the resistance to intergranular corrosion, but it also enhances mechanical properties at high temperatures. In martensitic steels, niobium reduces the hardness and increases the tempering resistance. It is also referred to as columbium (Cb).

3.04.3.2.11 Aluminum (Al)

Aluminum improves the oxidation resistance, if added in substantial amounts. It is used in certain heat resistant alloys for this purpose. In precipitation-hardening steels, aluminum is used to form the intermetallic compounds that increase the strength in the aged condition.

3.04.3.2.12 Cobalt (Co)

Cobalt is only used as an alloying element in martensitic steels in which it increases the hardness and tempering resistance, especially at higher temperatures.

3.04.3.2.13 Vanadium (V)

Vanadium increases the hardness of martensitic steels due to its effect on the type of carbide present. It also increases tempering resistance. Vanadium stabilizes ferrite and will, at high contents, promote ferrite in the structure. It is only used in hardenable stainless steels.

3.04.3.2.14 Sulfur (S)

Sulfur is added to certain stainless steels in order to increase the machinability. At the levels present in these grades, sulfur will substantially reduce corrosion resistance, ductility, and fabrication properties, such as weldability and formability.

3.04.3.2.15 Cerium (Ce)

Cerium is one of the rare earth metals (REMs) and is added in small amounts to certain heat-resistant, high temperature steels and alloys in order to increase the resistance to oxidation and high temperature corrosion.

Since it is the combined effect of the alloying elements that decide both the microstructure and the properties of a certain grade, the effect of the alloying elements can be summarized in various ways. One such summary of the effect of alloying elements on the microstructure is the Schaeffler–Delong diagram presented in **Figure 4**. A guide to the composition of the stainless steels presented in **Figure 4** is given in **Table 4**.

The diagram is based on the fact that the alloying elements can be divided into ferrite-stabilizers and austenite-stabilizers. This means that they favor the formation of either ferrite or austenite in the microstructure of the steel. Assuming that the ability of austenite-stabilizers to promote the formation of austenite is related to the nickel content, and that the ability of ferrite-stabilizers is related to the chromium content, it becomes possible to calculate the total ferrite and austenite stabilizing effect of the alloying elements in the steel, and thereby obtain the

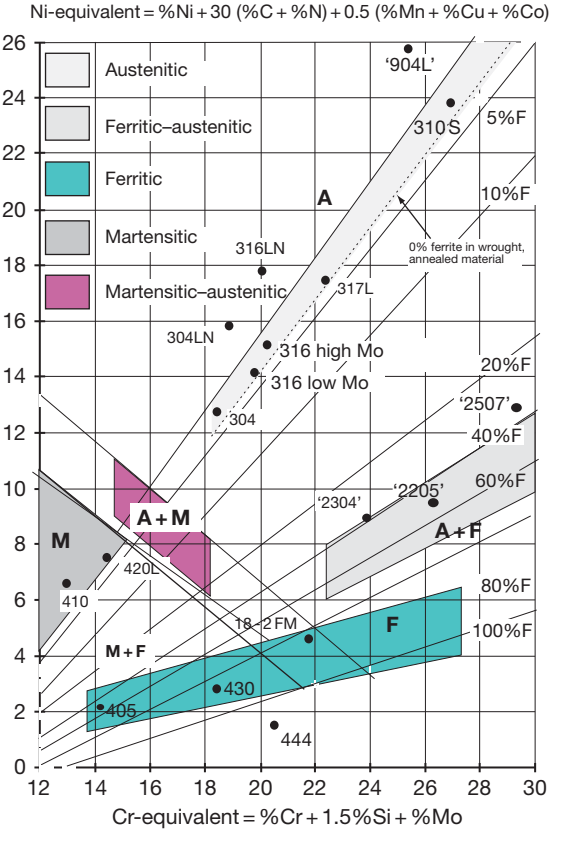

Figure 4 The Schaeffler–Delong diagram. A guideline to the steel grades is presented in **Table 4**.

Table 4 Guide to the compositions of the stainless steels presented in Figure 4

Note in Figure 4	*Steel grade*			*Typical chemical composition (wt%)*				
	UNS	*ASTM*	*EN*	*Cr*	*Ni*	*Mo*	*N*	*Other*
410	S41000	410	1.4006	12			0.04	
420L	S42000	420	1.4021	13				
430	S43000	430	1.4016	16				
444	S44400	444	1.4521	17		2		
304	S30400	304	1.4301	18.1	8.3			
304LN	S30451	304LN	1.4311	18.5	10.5		0.14	
316LowMo	S31600	316	1.4401	17.2	10.2	2.1		
316LN	S31653	316LN	1.4406	17.2	10.3	2.1	0.14	
316HiMo	S31600	316	1.4436	16.9	10.7	2.6		
317L	S31703	317L	1.4438	18.2	13.7	3.1		
904L	N08904	N08904	1.4539	20	25	4.5		Cu(1.5)
2304	S32304	S32304	1.4362	22	3.5	0.1	0.10	
2205	S32205	S32205	1.4462	22	5.5	3	0.17	
2507	S32750	S32750	1.4410	24	6	3	0.27	
310S	S31008	310S	1.4845	25	20			

chromium and nickel equivalents in the Schaeffler–Delong diagram. It is thus possible to take into account the combined effect of alloying elements on the microstructure of a steel grade.

The Schaeffler–Delong diagram was originally developed for weld metal, that is, it describes the structure after melting and rapid cooling, but the diagram has also been found to give a useful picture of the effect of the alloying elements for wrought and heat-treated material. However, in practice, wrought or heat-treated steels with ferrite contents in the range 0–5% according to the diagram in fact contain smaller amounts of ferrite than that predicted by the diagram. It should be noted that the Schaeffler–Delong diagram is not the only diagram for assessing the ferrite content and microstructure of stainless steels. Several other diagrams have been published, all with slightly different equivalents, phase limits, or general layout.

Precipitation-hardening stainless steels can be divided into three subcategories: martensitic, semiaustenitic, and austenitic grades. The common denominator here is not the microstructure but the hardening mechanism, precipitation hardening. This involves the formation of second-phase particles from a supersaturated solution which induces an internal strain in the microstructure and thus increases the strength of the material. The elements most commonly used to induce precipitation hardening, either individually or in combination, are aluminum, titanium, and copper.

3.04.4 Mechanical Properties

The difference in the mechanical properties of different stainless steels is perhaps seen most clearly in the stress–strain curves in Figure 5. The high yield and tensile strengths but low ductility of the martensitic steels are apparent, as are the low yield strength and excellent ductility of the austenitic grades. Duplex and ferritic steels both lie somewhere between these two extremes. Ferritic steels generally have a slightly higher yield strength than austenitic steels, whereas duplex steels have an appreciably higher yield strength than both austenitic and ferritic steels. The ductility of ferritic and duplex steels is of the same order of magnitude, even if the latter are somewhat superior in this respect.

3.04.4.1 Mechanical Properties at Room Temperature

In terms of their mechanical properties, stainless steels can be roughly divided into four groups: martensitic, ferritic, duplex, and austenitic, and the properties within each group are relatively similar. Table 5 shows the typical mechanical properties at room temperature for a number of stainless steels.

Stress values are given as the nearest 10 MPa. Standard deviations are normally about 20 MPa for proof strengths, $R_{p0.2}$, $R_{p1.0}$ and tensile strength, R_m; and 3 wt% for the elongation, A_5. More detailed information can be found in Nordberg *et al.*[4]

Martensitic steels are characterized by their high strength and the fact that this strength is strongly affected by heat treatment. Martensitic steels are usually used in the hardened and tempered condition.

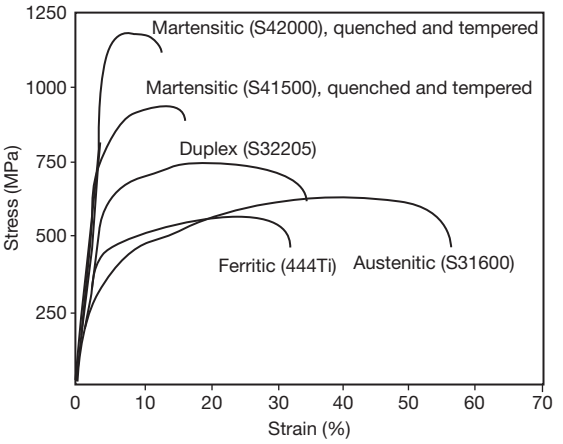

Figure 5 Stress–strain curves for some stainless steels. Reproduced from Leffler, B. *Stainless – Stainless Steels and Their Properties*; Avesta Sheffield AB Research Foundation, Stockholm, Sweden, 1996.

In this condition, the strength of the steel improves in relation to the carbon content. Steels with more than 13 wt% chromium and a carbon content above 0.15 wt% are completely martensitic after hardening. A reduction in the carbon content causes an increase in the ferrite content and thus has an adverse effect on the strength of the steel. The ductility of martensitic steels is relatively low. Low carbon martensitic grades, often alloyed with nickel, have high strength in the hardened and tempered condition and good ductility. The mechanical properties of martensitic stainless steels are heavily influenced by the heat treatments to which the steels are subjected. A brief description of the general heat treatment of martensitic stainless steels and the effect on the mechanical properties is given as follows.[5,6]

To obtain useful properties, martensitic stainless steels are normally used in the hardened and tempered condition. The hardening treatment consists of heating to a high temperature in order to produce an austenitic structure with carbon in solid solution followed by quenching. The austenitizing temperature is generally in the range 925–1070°C. The effect of

Table 5 Typical mechanical properties for stainless steels at room temperature for hot rolled plate

Micro structure	*Steel grade*		$R_{p0.2}$ *(MPa)*	$R_{p1.0}$ *(MPa)*	R_m *(MPa)*	A_5 *(%)*
	EN	*UNS(ASTM)*				
Martensitic	1.4006	S41008	540		690	20
	1.4021	S42003	780		980	16
		S43100	690		900	16
		ASTM 248 SV	790	840	930	18
Ferritic		ASTM446	340		540	25
	1.4521	S44400	390		560	30
Duplex (ferritic–austenitic)	1.4162	S32101	450		650	30
	1.4362	S32304	470	540	730	36
	1.4462	S31803	500	590	770	36
	1.4410	S32750	600	670	850	35
Austenitic	1.4301	S30400	310	350	620	57
	1.4307	S30403	290	340	590	56
	1.4311	S30453	340	380	650	52
		S30451	350	400	670	54
	1.4541	S32100	280	320	590	54
	1.4404	S31603	310	350	600	54
	1.4571	S31635	290	330	580	54
	1.4401	S31600	320	360	620	54
	1.4432	S31603	300	340	590	54
	1.4438	S31703	300	350	610	53
	1.4439	S31726	320	360	650	52
	1.4529	N08904	260	310	600	49
	1.4547	S31254	340	380	690	50
Austenitic (heat-resistant steels)	1.4845	S31008	290	330	620	50
	1.4818	S30415	380	410	700	50
	1.4835	S30815	410	440	720	52
	1.4854	S35315	360	400	720	50

austenitizing temperature and time on hardness and strength varies with the composition of the steel, especially the carbon content. In general, the hardness will increase in relation to the austenitizing temperature up to a maximum and then decrease. The effect of increased time at the austenitizing temperature is normally a slow reduction in hardness with increased time. Quenching, after austenitizing, is done in air, oil, or water depending on the steel grade. On cooling below the M_s temperature, the starting temperature for the martensite transformation, the austenite transforms to martensite. The M_s temperature lies in the range 70–300 °C and the transformation is usually completed at about 150–(200–248) °C below the M_s temperature. Almost all alloying elements will lower the M_s temperature, with carbon having the greatest effect. This means that in higher alloyed martensitic grades, the microstructure will contain retained austenite due to the low temperature (below ambient) needed to finish the transformation of the austenite into martensite.

In the hardened condition, the strength and hardness are high but the ductility and toughness is low. To obtain useful engineering properties, martensitic stainless steels are normally tempered. The tempering temperature used has a large influence on the final properties of the steel. The effect of tempering temperature on the mechanical properties of a martensitic stainless steel (Type 431) is shown in **Figure 6**. Normally, increasing tempering temperatures above 400 °C will lead to a small decrease in tensile strength and an increase in reduction of area while hardness, elongation, and yield strength are more or less unaffected. Above this temperature, there will be a more or less pronounced increase in yield strength, tensile strength, and hardness because of the secondary hardening peak, around 450–500 °C. In the temperature range around the secondary hardening peak, there is generally a dip in the impact toughness curve. Above about 500 °C, there is a rapid reduction in strength and hardness, and a corresponding increase in ductility and toughness. Tempering at temperatures above the AC1 temperature (780 °C for the steel in **Figure 6**) will result in partial austenitizising and the possible presence of nontempered martensite after cooling to room temperature.[7]

Ferritic steels have relatively low yield strength and the work hardening is limited. The strength increases as the carbon content is increased, but the effect of increased chromium content is negligible. However, ductility decreases at high chromium levels and good ductility requires very low levels of carbon and nitrogen.

Duplex (ferritic–austenitic) steels have a high yield strength, which increases with higher carbon and nitrogen levels. Increased ferrite content will, within limits, also increase the strength of duplex steels. Their ductility is good and they exhibit strong work hardening properties.

Austenitic steels generally have a relatively low yield strength and are characterized by strong work hardening properties. The strength of austenitic steels increases with higher levels of carbon, nitrogen, and, to a certain extent, also molybdenum. The detrimental effect of carbon on corrosion resistance

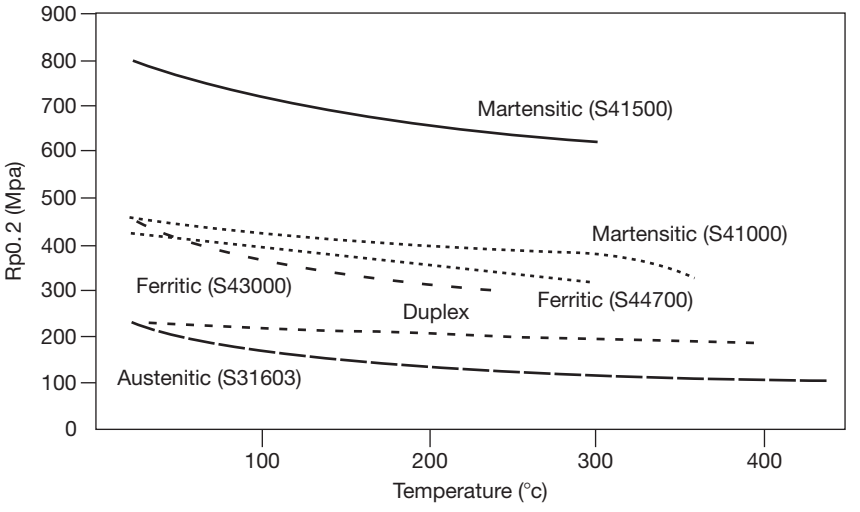

Figure 6 Effect of tempering temperature on the mechanical properties ($R_{p0.2}$ – 0.2% proof strength).

means that this element cannot be used for increasing strength. Austenitic steels exhibit very high ductility; they have a high elongation and are very tough.

Some austenitic stainless steels with a low overall content of alloying elements, for example, type 301 and 304 steels, can be metastable and may form martensite, either due to cooling below ambient temperatures or through cold deformation, or a combination of both. The formation of martensite will cause a considerable increase in strength, as illustrated in Figure 7. The M_d temperature is defined as the temperature below which martensite will form. The stability of the austenite depends on the composition of the steel; the higher the content of alloying elements, the more stable the austenite. A common equation for relating austenite stability to alloy composition is the M_{d30}, which is defined as the temperature at which martensite will form at a strain of 30%:

$$M_{d30} = 551 - 462(C + N) - 9.2Si - 8.1Mn - 13.7Cr - 29(Ni + Cu) - 18.5Mo - 68Nb - 1.42\ (GS - 8.0)(^{\circ}C)$$

where GS is the grain size, ASTM grain size number.

This type of equation gives a good idea of the behavior of lean austenitic stainless steels, but it must be noted that it is only approximate as interactions between the alloying elements are not taken into account.

The effects of alloying elements and structure on the strength of austenitic and duplex steels have been discussed over the years and several regression equations have been proposed for identifying the effects of the various alloying elements in stainless steels. Most of the regression equations proposed apply to austenitic stainless steels but some have also included duplex stainless steels in the equations.[8,9,10] These equations may be used to estimate the strength of austenitic and duplex steel.

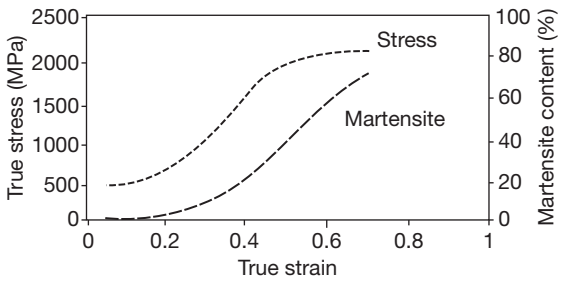

Figure 7 The effect of strain on martensite and yield strength of AISI 301. Reproduced from Peckner, B. *Handbook of Stainless Steel*; McGraw-Hill, 1977.

In contrast to the constructional steels, austenitic steels do not exhibit a clear yield stress but begin to deform plastically at a stress around 40% of the tensile strength, $R_{p0.2}$.

It should be noted that although the different elements are included in the equation through rather simple expressions, the actual strengthening mechanism might be more complex. At chromium contents over 20%, austenitic steel with 10% Ni will contain d-ferrite, which in turn causes a smaller grain size, and this will enhance both yield strength and tensile strength. Nitrogen has a strong strengthening effect but is also a powerful austenite stabilizer. In duplex stainless steels, the strengthening effect of nitrogen is, to a certain extent, countered by the increased austenite content caused by the addition of nitrogen.

3.04.4.2 The Effect of Cold Work

Stainless steels will harden during deformation and the mechanical properties of stainless steels are strongly influenced by cold deformation. The amount of hardening depends on both the composition and the type of steel. The work hardening of austenitic and duplex steels in particular causes considerable changes in properties after cold forming operations. The general effect of cold work is to increase the yield and tensile strengths and at the same time decrease the elongation. Figure 8 shows cold hardening curves for some stainless steels.

The work hardening is greater for austenitic steels than for ferritic steels. The addition of nitrogen in austenitic steels makes these grades particularly hard and strong: compare S31603 and S31653. The strong work hardening of the austenitic steels means that large forces are required for forming operations even though the yield strength is low. Work hardening can, however, also be deliberately used to increase the strength of a component.

3.04.4.3 Toughness

The toughness of the different types of stainless steel shows considerable variation, ranging from excellent toughness at all temperatures for austenitic steels to the relative brittleness of martensitic steels.

Toughness is dependent on temperature and generally increases with increasing temperature. One measure of toughness is impact toughness, that

is, the toughness measured on rapid loading. **Figure 9** shows the impact toughness for different categories of stainless steel at temperatures ranging from −200 to +100°C. It is apparent from the diagram that there is a fundamental difference at low temperatures between austenitic steels on the one hand and martensitic, ferritic, and duplex steels on the other.

The martensitic, ferritic, and duplex steels are characterized by a transition in toughness, from tough to brittle behavior, at a certain temperature, the transition temperature. For the ferritic steel, the transition temperature increases with increasing carbon and nitrogen content, that is, the steel becomes brittle at successively higher temperatures. For the duplex steels, increased ferrite content gives a higher transition temperature, that is, more brittle behavior. Martensitic stainless steels have transition temperatures around or slightly below room temperature, while those for the ferritic and duplex steels are in the range 0–60°C, with the ferritic steels in the upper part of this range.

The austenitic steels do not exhibit a toughness transition as the other steel types but have excellent toughness at all temperatures. Austenitic steels are thus preferable for low-temperature applications.

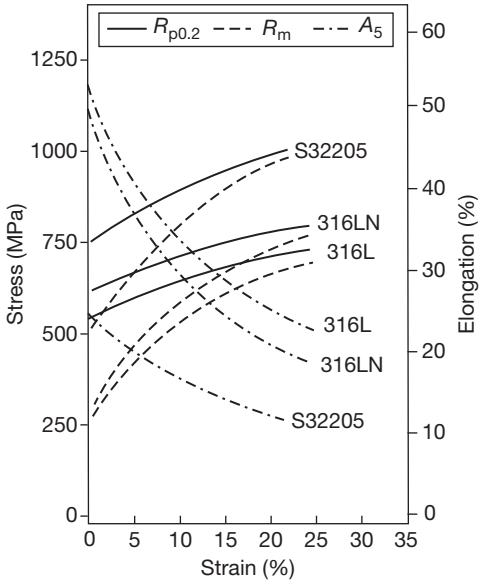

Figure 8 Effect of cold work on some stainless steels. Reproduced from Leffler, B. *Stainless Steels and Their Properties*, 2nd revised ed.; Outokumpu Stainless Research Foundation, Stockholm, 1998.

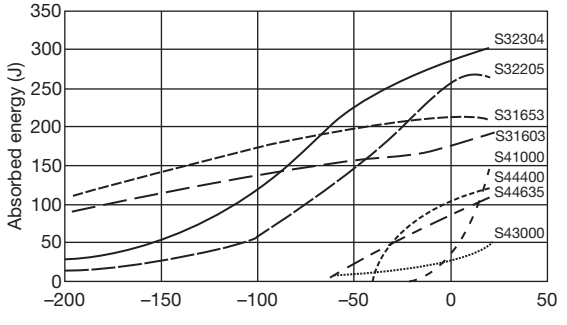

Figure 9 Impact toughness for different types of stainless steels.

3.04.4.4 Fatigue Properties

During cyclic loading, stainless steels, like other materials, will fail at stress levels considerably lower than the tensile strength measured during tensile testing. The number of load cycles the material can withstand is dependent on the stress amplitude. **Figure 10** shows how the lifetime, that is, the number of cycles to failure, increases with decreasing load amplitude until a certain amplitude is reached, below which no failure occurs. This stress level is called the fatigue limit. In many cases, there is no fatigue limit, but the stress amplitude shows a slow decrease with an increasing number of cycles. In these cases, the fatigue strength, that is, the maximum stress amplitude for a certain time to failure (number of cycles) is called the fatigue strength and it is always given in relation to a certain number of cycles.

The fatigue properties of ferritic–austenitic and austenitic stainless steels with a fatigue limit at a lifetime of 10^6–10^7 load cycles can be described by the Wohler curve or *S*–*N* curve and related to their tensile strength, as shown in **Table 6**. The relation between the fatigue limit and tensile strength is also

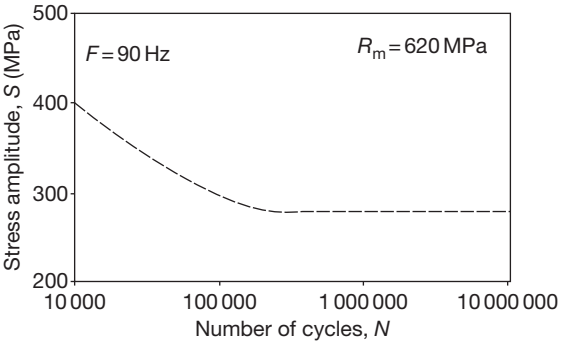

Figure 10 *S*–*N* curve (Wohler curve) for an austenitic stainless steel of Type S31600 (hMo) in air. *S* – stress amplitude, *N* – number of cycles. Reproduced from Leffler, B. *Stainless Steels and Their Properties*, 2nd revised ed.; Outokumpu Stainless Research Foundation, Stockholm, 1998.

Table 6 Fatigue properties of stainless steels, relation between tensile strength and fatigue strength

Microstructure	S_o/R_m, *Stress ratio*		*Maximum stress*
	R=−1	*R=0*	
Ferritic	0.7	0.47	Yield strength
Austenitic	0.45	0.3	Yield strength
Duplex	0.55	0.35	Yield strength

dependent on the type of load, which is the stress ratio (R). The stress ratio is the ratio of the minimum stress to the maximum stress during the loading cycle. The compressive stresses are defined as negative.

3.04.5 Precipitation and Embrittlement

Under various circumstances, the different stainless steel types can suffer undesirable precipitation reactions, which can cause a decrease in both corrosion resistance and toughness.

3.04.5.1 Embrittlement at 475°C

If martensitic, ferritic, or duplex steels are exposed to temperatures in the range 350–550°C, a serious decrease in toughness will occur after some time. The phenomenon is encountered in grades containing more than 15–18% chromium and the origin of this embrittlement is the decomposition of the ferrite into two phases of body-centered cubic, bcc, structure, α and α'. The former is very rich in iron and the latter very rich in chromium. This type of embrittlement is usually called 475°C embrittlement after the midpoint of the temperature range.

3.04.5.2 Carbide and Nitride Precipitation

If ferritic steels are heated to temperatures above approximately 950°C, they suffer precipitation of chromium carbides and chromium nitrides during the subsequent cooling, which cause a decrease in both toughness and corrosion resistance. This type of precipitation can be reduced or eliminated by decreasing the levels of carbon and nitrogen to very low levels and/or stabilizing the steel by additions of titanium as in 18Cr–2Mo–Ti.

Carbide and nitride precipitation in austenitic and duplex steels occurs in the temperature range 550–800°C. Chromium-rich precipitates form in the grain boundaries and can cause intergranular corrosion and, in extreme cases, even a decrease in toughness. However, during the short times in the critical temperature range experienced in the heat-affected zone adjacent to welds, the risk of deleterious precipitation is very small for the low-carbon steels.

3.04.5.3 Intermetallic Phases

In the temperature range 700–900°C, iron alloys with a chromium content above about 17% form intermetallic phases such as σ phase, χ phase, and Laves phase. These phases all have high chromium content and are brittle and consequently large amounts of these phases in the microstructure will lead to a drop in toughness and a decrease in resistance to certain types of corrosion.

Chromium, molybdenum, and silicon promote the formation of intermetallic phases, so the majority of ferritic, duplex, and austenitic steels show some propensity to form these phases. Intermetallic phases form most readily from highly alloyed ferrite. In ferritic and duplex steels, intermetallic phases therefore form readily but are, on the other hand, relatively easy to dissolve on annealing. In the austenitic steels, it is the highly alloyed grades that are particularly susceptible to intermetallic phase formation. The low chromium content and low molybdenum grades are considerably less sensitive to the precipitation of these phases.

Heat treatment may remove all types of precipitates by redissolving them. Renewed heat treatment of martensitic steels and solution annealing and quenching ferritic, duplex, or austenitic steels restore the microstructure. Relatively long times or high temperatures may be required for the dissolution of intermetallic phases in highly alloyed grades.

Stainless steels can pick up nitrogen if exposed to nitrogen-containing atmospheres such as nitrogen, nitrogen mixtures, and cracked ammonia. During nitrogen pick-up, nitrides and other brittle compounds of chromium, molybdenum, titanium, vanadium, and aluminum can form. Atmospheric oxygen, even at relatively low levels, reduces the risk for nitridation. At temperatures between 400 and 600°C, a layer of nitrides is formed at the steel surface; at higher temperatures, nitrogen uptake and nitride formation occur throughout the material. Nitridation, that is, nitride formation, causes chromium depletion and reduced oxidation resistance in the same way as carburization. This can lead to catastrophically high oxidation rates on the outer surface of equipment, which is subjected to a nitriding atmosphere on the inside – for example, the muffles in annealing

furnaces. Nitrogen pick-up can also cause embrittlement because of to surface or internal nitride formation. Nickel is the alloying element, which provides the greatest protection against nitridation, as nickel does not form stable nitrides.

3.04.5.4 Carburization

If a material is exposed to gases containing carbon, for example, in the form of CO, CO_2, or CH_4, it can pick up carbon. The degree of carburization is governed by the levels of carbon and oxygen in the gas, also the temperature and steel composition. The carbon, which is picked up by the steel will largely form carbides, primarily chromium carbides.

The formation of a large amount of chromium carbides causes chromium depletion and thus a reduced resistance to oxidization, because carbides, or even a network of carbides, form in the grain boundaries as well as within the grains. The resistance to thermal cycling is reduced and, since carburization leads to an increase in volume, there is a danger of cracks developing in the material. Carbon pick-up can occur even at relatively low temperatures (400–800°C) in purely reducing–carburizing atmospheres and gives rise to catastrophic carburization or metal dusting. Attack is severe and characterized by 'powdering' of the steel surface because of the breakdown of the protective oxide layer and inward diffusion of carbon, which forms grain boundary carbides. The increase in volume on carbide formation means that grains are rapidly broken away from the steel surface, giving rapid and serious attack.

Chromium, nickel, and silicon are the alloying elements, which most improve resistance to carburization.

3.04.5.5 Heat Treatment

The aim of heat treatment of stainless steels is to restore the microstructure after forming or other fabrication and production operations thereby removing or at least minimizing any possible negative effects. However, in the case of the hardenable stainless steels, that is, martensitic and precipitation-hardening grades, heat treatment is used to set the mechanical properties at the required level. In other cases, that is, stress relief heat treatment, the aim is to reduce the level of residual stresses caused by fabrication operations such as cold forming and welding.

3.04.5.5.1 Solution annealing

Solution annealing is the most common heat treatment for ferritic, austenitic, and duplex stainless steels, that is, the types of stainless steel in which the mechanical properties cannot be set by heat treatment. Instead the aim of the heat treatment is to restore the microstructure by allowing recrystallization to occur and deleterious phases, such as carbides and intermetallic phases, to be dissolved.

During solution annealing the material is heated to a temperature where detrimental phases will be dissolved, held at temperature for a time long enough to allow the unwanted phases to dissolve, and then rapidly cooled or quenched. Solution annealing is normally performed on austenitic and duplex stainless steels at temperatures above 1020°C. A higher alloying content will normally require a higher solution annealing temperature in order to produce a precipitate-free microstructure. For the stabilized austenitic grades, the temperature used should allow chromium carbides and other unwanted phases to dissolve but should be low enough to retain the titanium or niobium carbides used to stabilize the steel. Ferritic stainless steels are normally only annealed using temperatures below 1000°C. Table 7 presents typical heat treatment as solution annealing or annealing temperatures for stainless steels.

Rapid cooling after heat treatment is normally required to ensure that unwanted reactions in the microstructure do not occur. Whether air- or water-cooling is required depends on parameters such as section thickness and the type of steel. It is not the cooling rate *per se* that is important, but the time spent in the temperature range in which precipitation or other unwanted reactions may occur. Higher alloyed grades and thicker sections will thus generally require water quenching rather than air-cooling.

3.04.5.5.2 Quenching, tempering, and ageing

Martensitic grades

Heat treatment of the martensitic stainless steels is essentially the same as the heat treatment of other hardenable steels. The difference is that the high

Table 7 Heat treatment temperatures for ferritic, austenitic and duplex stainless steels

Category	*Temperature (°C)*	*Quenching*
Ferritic	700–850	Water/forced air
Ferritic (high alloyed)	750–950	Water/forced air
Austenitic	1020–1100	Water/forced air
Austenitic (high alloyed)	1080–1200	Water
Duplex	1020–1150	Water

alloy content slows the transformation reactions and increases hardenability.

The normal heat treatment cycle of martensitic stainless steels is

1. hardening by austenitizing at temperatures of 950–1050 °C followed by quenching in oil or water, and
2. tempering at temperatures of 300–700 °C to set final properties.

Quenched hardness will increase with increasing austenitizing temperature in the lower end of the temperature range, but austenitizing in the high end of the temperature range will lower the as-hardened hardness.

Tempering is designed to allow the material to reach an optimum between strength and ductility. The tempering temperature is thus dependent on the strength level specified and these may normally be found in the appropriate product standards.

Precipitation hardening Grades

These steels can be divided into three subcategories: martensitic, semiaustenitic, and austenitic grades. All of the precipitations hardening grades depend on a precipitation reaction to induce the strengthening during aging. The precipitates may differ from grade to grade, but the principle is that a solution anneal is used to put some alloying elements into solution at high temperature followed by quenching to low temperature at which a supersaturated solution is obtained. Ageing at an elevated temperature will then cause the precipitation and hardening resulting in an increased strength. The heat treatment cycles of the different types of precipitation-hardening steels can be summarized as follows:

1. Martensitic grades
   a. solution anneal in the austenite region (1020–1050 °C)
   b. quench to room temperature
   c. age at 470–630 °C to produce precipitation and hardening
2. Semiaustenitic grades
   a. solution anneal in the austenite region (1020–1050 °C)
   b. quench to room temperature followed by sub-zero cooling or tempering at about 750 °C
   c. age at 470–570 °C to produce precipitation and hardening
3. Austenitic grades
   a. solution anneal (1000–1100 °C)
   b. quench to room temperature
   c. age at 700–800 °C to produce precipitation and hardening

3.04.5.5.3 Stabilization annealing

A stabilization heat treatment is applied to titanium- or niobium-stabilized grades in order to enhance the resistance to intergranular corrosion, that is, to make sensitization more difficult. The aim of this treatment is to ensure that the carbon dissolved in the matrix is forced to combine with the stabilizing element, for example, titanium or niobium, thus becoming securely locked up in as titanium or niobium carbides and therefore not unavailable for chromium carbide formation.

Titanium and niobium both form more stable carbides than do chromium and these carbides precipitate at higher temperatures than do chromium carbides. The stabilizing treatment therefore consists of heat treatment at a temperature slightly above the temperature range for chromium carbide precipitation. The temperature selected is normally in the range as low as possible in order to obtain maximum driving force for the precipitation. Stabilization heat treatment is usually performed at temperatures in the range 850–980 °C on material that has previously been solution annealed. The lower part of the temperature range should be used with some caution, as this type of treatment is not equally effective in all environments.

3.04.6 Physical Properties

The physical properties of the different stainless steels are dependent on both the microstructure (crystal structure) and the amount of alloying elements added. In many cases the physical properties cannot be manipulated by heat treatment or fabrication practices and are more or less 'locked' in the atomic arrangement of the steel. Again, the grouping of the property values follows the division of steel grades into the main stainless categories.

Ferromagnetism is a characteristic property of ferrite and martensite while austenite is not ferromagnetic. This means the ferritic and martensitic stainless steels are strongly magnetic while the fully austenitic stainless steels are nonmagnetic. However, since many of the more common and lower alloyed austenitic grades contain small amounts of ferrite the might show a weak magnetic behavior. The duplex steels containing about 40–60% ferrite will naturally be magnetic even if their magnetism is weaker that that of the ferritic or martensitic stainless steels.

Regarding the other physical properties it may be noted that the thermal expansion is strongly related to

the microstructure and this gives the austenitic steels a thermal expansion that is about 50% higher than that of the ferritic and martensitic stainless steels. The thermal conductivity is lower for austenitic steels compared with that of the ferritic or martensitic steels and within each category the thermal conductivity decreases with increasing alloying content. Other properties such as thermal capacity and the modulus of elasticity show relatively little variation across the different stainless steel categories. The most highly alloyed austenitic grades have a somewhat lower modulus compared with other stainless steels.

Typical values of the physical properties for the some stainless steels from the different categories are shown in Table 8.[11,12]

3.04.7 Property Relationships for Stainless Steels

Martensitic and martensitic–austenitic stainless steels are characterized by their high strength but limited corrosion resistance. An increased carbon content increases strength, but at the expense of lower toughness and considerable degradation of weldability. The martensitic 13% chromium steels, with higher carbon contents, are not designed to be welded, even though it is possible under special circumstances. In order to increase high temperature strength, alloying with strong carbide formers such as vanadium and tungsten are used. An increase in the nickel content also increases toughness. In contrast to the martensitic steels, the martensitic–austenitic steels do not have to be welded at elevated temperatures except in thick sections; even then only limited preheating is required.

The areas of use of martensitic and martensitic–austenitic steels are naturally those in which the high strength is an advantage and the corrosion requirements are relatively low. The martensitic steels with low carbon contents and the martensitic–austenitic steels are often used as stainless constructional materials. The martensitic steels with high carbon content are used for springs, surgical instruments, and for sharp-edged tools such as knives and scissors.

The ferritic steels are characterized by good corrosion properties, very good resistance to chloride-induced stress corrosion cracking (SCC), and moderate toughness. The toughness of ferritic stainless steels is generally not particularly high. Lower carbon and nitrogen levels give a considerable improvement in both toughness and weldability, although toughness is limited for thicker dimensions. Consequently ferritic steels are usually only produced and used in thinner dimensions. Ferritic stainless steels are used in household products and in applications with fairly low demands of the corrosion resistance of the material in combination with aesthetic reasons. Examples of such application areas are cookware lids, washing machine drums, refrigerator doors etc. They have stress–strain data similar to carbon steel; generally have higher yield strength than the austenitic stainless steels. Their

Table 8 Typical physical properties of some stainless steels[1]

Stainless steel grade	*Density (kg dm^{-3})*	*Modulus (GPa)*	*Thermal expansion (10^{-6} °C^{-1})*	*Thermal conductivity (W m^{-1} °C^{-1})*	*Thermal capacity (J kg^{-1} °C^{-1})*	*Electrical resistivity (m)*
	RT	*RT*	*RT–400 °C*	*RT*	*RT*	*RT*
Ferritc						
S43000	7.7	220	10.5	25	460	0.60
Martensitic						
S42000	7.7	215	12.0	30	460	0.65
Duplex						
S32205	7.8	200	14.5	15	500	0.80
Austenitic						
S30100	7.9	200	18.0	15	500	0.73
S20100	7.8	200	17.5	15	500	0.70
S30403	7.9	200	18.0	15	500	0.73
S31603	8.0	200	17.5	15	500	0.75
N08904	8.0	195	16.9	12	450	1.00
S31254	8.0	195	18.0	14	500	0.85
S34565	8.0	190	16.8	12	450	0.92

RT, room temperature.

thermal conductivity is high and they transmit heat efficiently, which is one of the reasons to frequent use in electric irons and heat exchangers. They have further a low thermal expansion coefficient, lower than for the austenitic stainless steels, which give them less distortion when heated. Ferritic stainless steels are widely used in large tonnage all over the world.

The modern duplex steels span the same wide range of corrosion resistance as the austenitic steels depending on the alloy composition. Duplex equivalents can be found to both the ordinary austenitic grades, such as S31600 (1.4401), and to the high-alloyed austenitic grades, such as S31254 (1.4547). The corrosion resistance of S32304 (1.4362) type duplex is similar to that of S31600 (1.4401) while S32205 (1.4462) is similar to N08904L (1.4539) and S32750 (1.4410) is similar to the high-alloyed austenitic grades with 6% molybdenum, such as S31254 (1.4547). High strength, good toughness, and very good corrosion resistance characterize the duplex steels in general and excellent resistance to chloride-induced SCC and corrosion fatigue in particular. An increased level of chromium, molybdenum, and nitrogen increases corrosion resistance, while the higher nitrogen level also contributes to a further increase in strength above that associated with the duplex structure. Applications of duplex steels are typically those requiring high strength, good corrosion resistance and low susceptibility to SCC or combinations of these properties. The lower alloyed S32304 (1.4362) is used for applications requiring corrosion resistance similar to S31600 (1.4401) or lower and where strength is an advantage. Some examples of such applications are: hot water tanks in the breweries, pulp storage towers in the pulp and paper industry, tanks for storage of chemicals in the chemical process industry, and tank farms in tank terminals in the transportation industry. The higher alloyed S32205 (1.4462) is, for example, used in pulp digesters and storage towers in the pulp and paper industry where it is rapidly becoming a standard grade. It is also used in piping systems, heat exchangers, tanks and vessels for chloride-containing media in the chemical industry, in piping and process equipment for the oil and gas industry, in cargo tanks in ships for transport of chemicals, and in shafts, fans, and other equipment which require resistance to corrosion fatigue. High alloyed grades, for example, S32750 (1.4410), are used in piping and process equipment for the offshore industry, that is, oil and gas and in equipment for environments containing high chloride concentrations, such as seawater.

Very good corrosion resistance, very good toughness, and very good weldability characterize the austenitic steels. They are also the most utilized stainless steels. Resistance to general corrosion, pitting, and crevice corrosion generally increases with increasing levels of chromium and molybdenum. The low-carbon grades exhibit good resistance to intergranular corrosion and consequently the higher alloyed steels are only available with low carbon contents. Austenitic steels are generally susceptible to chloride-induced SCC; only the highly alloyed steels such as N08904 (1.4529), and S31254 (1.4547) exhibit good resistance to this type of corrosion.

The austenitic stainless steels are used in almost all types of applications and industries. Typical areas of use include piping systems, heat exchangers, tanks and process vessels for the food, chemical, pharmaceutical, pulp and paper, and other process industries. Nonmolybdenum alloyed grades, for example, S30400, are normally not used in chloride-containing media but are often used where demands are placed on cleanliness or in applications in which equipment must not contaminate the product. The molybdenum-alloyed steels are used in chloride-containing environment with the higher alloyed steels, N08904, S31254, being chosen for higher chloride contents and temperatures. S31254 is used to handle seawater at moderate or elevated temperatures. Applications include heat exchangers, piping, tanks, process vessels, etc. within the offshore, power, chemical and pulp- and paper industries. The low-alloyed grades, especially S30400 and 31600, are used in equipment for cryogenic applications. Examples are tanks, heaters, evaporator, and other equipment for the handling of condensed gases such as liquid nitrogen. Finally it is worth mentioning that austenitic stainless steels are often used in applications requiring nonmagnetic materials since they are the only nonmagnetic steels.

3.04.8 Corrosion Properties of Stainless Steels

Stainless steels are widely used throughout the world in a variety of applications in both industrial and domestic environments, for example, as a construction material, in the manufacture of everyday utensils. The use of stainless steels has been growing steadily and new areas of application, often in demanding service environments, are constantly being developed. The serviceability of stainless steels

in many of these applications is determined by the material properties of the steels and how they perform when exposed to different service environments. Historically, the success stories of stainless steel usage have been widely accounted for in corrosion engineering. Extensive research has been carried out with the aim of reducing further the risk of various types of corrosion by choosing appropriate stainless steel grades for specific service environments. The following chapter is intended as a guide for explaining the different types of corrosion mechanisms that can affect stainless steel and their causes. This section also aims to increase the knowledge of stainless steels and their corrosion resistance in different service environments. Depending on the service environment involved, several types of corrosion may affect stainless steels.

Figure 11 shows part of a stainless steel pipe after service in a very severe corrosive environment consisting of high amounts of chlorides, water, and oxygen in combination with high temperatures under evaporative conditions. The pipe suffered from several corrosion forms that affect stainless steels, notably pitting corrosion, crevice corrosion and SCC.

3.04.8.1 Passivity

The reason for the good corrosion resistance of stainless steels is that they form a very thin, invisible surface film, so called passive film or passive layer in oxygen containing environments. The passive film is mainly a chromium oxide, which protects the steel from corrosion attack in an aggressive environment. For a passive film to form on a stainless steel surface, a certain amount of chromium is required in the steel as an alloying element. As chromium is added to steel, a rapid reduction in corrosion rate is observed around 10 wt% because of the formation of this protective layer or passive film, as illustrated in Figure 12.

The commercial alloys of austenitic stainless steels typically contain between 16 and 28 wt% of chromium, while the chromium content of ferritic stainless steels ranges from 10.5 to 30 wt%. The chromium content varies in martensitic stainless steels, from 11.5 to 18 wt% and in duplex stainless steels; it is usually between 21 and 29 wt%. A passive film on a stainless steel surface consists of an inner layer of mixed iron/chromium oxides and an outer layer of chromium hydroxide. This film has self-healing properties when damaged in the presence of oxygen and a repair of the passive film can easily form after a scratch or other surface damage.

The thickness of a passive film is commonly considered to be in the range of 1–3 nm, depending on the service environment and the steel grade, but it also depends on pH values and the electrochemical properties in contact with a surrounding solution.

Figure 11 SCC, crevice corrosion, and pitting corrosion on a stainless steel pipe, after service in a very aggressive environment consisting of high amounts of chlorides, water, and oxygen in combination with high temperatures under evaporative conditions. Photo: Outokumpu Stainless.

3.04.8.2 Contribution of Main Alloy Elements to Passivation

As already indicated, chromium is the most important alloying element for corrosion resistance in stainless steels as it helps to form a passive film on

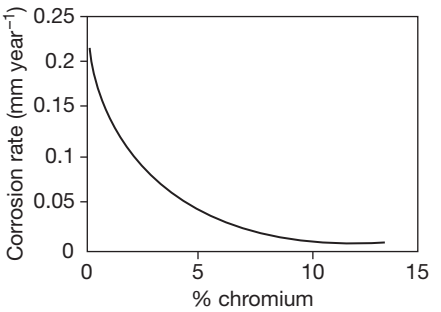

Figure 12 The effect of chromium content on passivity. Reproduced from Design Guidelines for the selection and use of stainless steel, specialty steel Industry of the United States, Washington, DC, USA.

the surface. The spontaneous formation of intact chromium oxide on the surface acts as a barrier layer and the surface electrochemistry is changed as a result of equilibrium reactions between the passive film and any surrounding solution.

It is also well-accepted and proved that the addition of molybdenum, as an alloying element, offers an efficient method for preventing corrosion in stainless steel by improving the passive film properties. The molybdenum content in stainless steels can be as much as 8%. However, the exact mechanism of detailed chemistry of molybdenum in a passive film with respect to passivity, interaction, and formation of compounds is the subject of extensive discussion, since molybdenum as an alloying element shows a complex oxide chemistry in the passive film with many oxidation stages.

The addition of nitrogen contributes to enhancing the resistance to pitting and crevice corrosion on austenitic stainless steels.[14] As the nitrogen stays soluble in the stainless steel, without any precipitation, the localized corrosion resistance is improved for rather high amounts. However, if nitrides are formed in the stainless steel the corrosion resistance is drastically decreased. More about nitride precipitation can be read in **Section 3.04.5**.

Nickel contributes to improved corrosion properties by assisting the repassivation process and helping reduce the rate of corrosion, for example, in strong acid solutions.

3.04.8.3 General Electrochemical Considerations in Corrosion of Stainless Steels

The basic electrochemical reactions for corrosion are that the metal, Me, is defined as the anode and balances the oxygen reduction attributed to the cathode.

$$Me \rightarrow Me^{n+} + ne^{-}$$

In the classical electrochemical oxygen cathodic reaction there are two pathways accepted for the reduction according to.

$$O_2 + 2H_2O + 4e^{-} \rightarrow 4OH^{-}$$

(neutral or alkaline environment)

$$O_2 + 4H^{+} + 4e^{-} \rightarrow 2H_2O \quad \text{(acid environment)}$$

The oxygen reduction is, however, a known complex process with many proposed pathway, for example:

Four electron pathway:

$$O_2 + 4H^{+} + 4e^{-} \rightarrow 2H_2O \quad E_{01} = 1.229\,\text{V/SHE}$$

Two electron pathway:

$$O_2 + 2H^{+} + 2e^{-} \rightarrow H_2O_2 \quad E_{02} = 0.695\,\text{V/SHE}$$
$$H_2O_2 + 2H^{+} + 2e^{-} \rightarrow 2H_2O$$

The reduction pathway is influenced by many factors, for example, the surface composition of the electrodes.

In strongly reducing environments, reduction of hydrogen ions is often the cathodic reaction to balance the metal dissolution:

$$2H^{+} + 2e^{-} \rightarrow H_2 \quad E = 0\,\text{V/SHE}$$

The oxidation of a metal, that is, corrosion, requires always a counter balance by a reduction.

A common test procedure for the investigation of stainless steel's resistance to corrosion in wet environments is to perform dynamic anodic polarization measurements in a conductive solution to obtain a polarization curve. **Figure 13** shows a schematic polarization curve undertaken for a stainless steel presenting the different potential area and the current density response.

The high current densities shown in **Figure 13** represent a corrosion process and the very low current response represents the passivity of a stainless steel. At low cathodic potentials, a line of high current densities represents the cathodic reaction. At the potential, when the cathodic reaction and the anodic reaction meet in the active area on occurring corrosion is denoted the corrosion potential, E_{corr}.

At the higher anodic potential, the passivity is represented by a decrease in current densities corresponding to the passivation current to stabilize in the passive potential area to a very low current density, the passive current density. Pitting corrosion or crevice corrosion is typically represented by a steep increase in the current response at an even higher potential, the pitting potential, E_p. Transpassive corrosion is represented by an increase in current density response in a rather extended potential area at even higher anodic potentials, associated with the transpassive potential, E_{tr}. In order to investigate the ability of a stainless steel to repassivate in, for example, chloride environment, a reverse scan is commonly performed while performing polarization measurements. The current response on the repassivation process is a clear decrease in the passive current and the potential for the steep decrease is noted repassivation potential, E_{rp}.

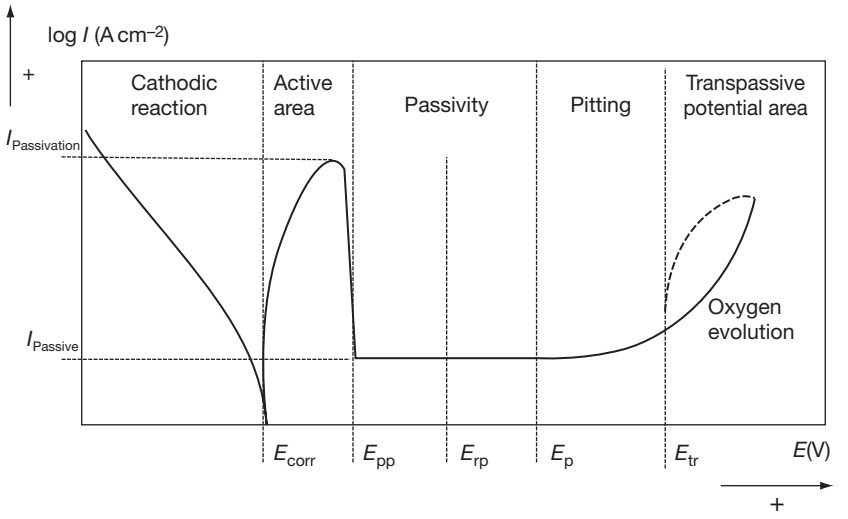

Figure 13 Schematic polarization curve for a stainless steel.

3.04.8.4 Breakdown of Passivity

All corrosion forms on stainless steels are related to any permanent damage of the passive film, either as a complete breakdown of the film causing uniform corrosion or locally as in pitting and crevice corrosion. Intergranular corrosion occurs along grain boundaries due to local breakdown of the passive film where chromium has been depleted. Once the passivity of stainless steel is broken down, completely or locally, and repassivation is not promoted by the aggressiveness of the surrounding solution, active corrosion occurs.

Local breakdown such as pitting and crevice corrosion is commonly initiated in neutral solutions, but can also occur in solutions with a low pH. The general aspect to consider in pitting and crevice corrosion is the very fast corrosion rate that can cause penetration through the steel in a short time and may lead to catastrophic failure.

Complete breakdown of the passive film causing uniform corrosion may occur in solutions of either low or high pH. Uniform corrosion or general corrosion occurs when the passive layer on a stainless steel surface breaks down partly or completely. The corrosion then propagates at a rate determined by a corrosive environment and the alloy composition in combination. Uniform corrosion causes a corrosion rate that can be expressed as a mean value of the attacked surface, making it possible to calculate a material loss, from weight loss determinations.

An even worse type of corrosion from the construction service point of view is SCC, which is characterized by the cracking of materials that are subjected to both a tensile stress and a corrosive environment. Most reported failures due to SCC occur in the standard stainless steel grades S30400 and S31600 with tensile stress in aqueous solutions containing chlorides at elevated temperatures, $>60\,^{\circ}C$. However, solutions containing chlorides are not the only environments that cause SCC in stainless steels. Similar cracking can also occur in hot caustic solutions and in environments containing impurities such as hydrogen sulfide.

3.04.8.5 Localized Corrosion – Pitting and Crevice Corrosion

Smialowska recently reviewed the tremendous work performed on pitting and crevice corrosion and the use of electrochemistry to characterize stainless steel regarding pitting and crevice corrosion.[15] Detailed information about pitting and crevice corrosion and the historical research can be read in this review.

Defects in the passive film enhance the risk of pitting and crevice corrosion. Manganese sulfides are identified to be initiation points to pitting and crevice corrosion. However, in modern commercial stainless steels, the sulfur content is normally so low that there are only few recent reports about sulfur causing pitting corrosion.

Environments, which represent the greatest risk of pitting and crevice corrosion of stainless steels,

include seawater and process solutions in which there is a high concentration of chlorides sometimes also in combination with an increased temperature. High halide concentration, commonly chlorides, low pH, and high temperature increase the probability of pitting and crevice corrosion on stainless steels. Pitting corrosion may also be caused by the presence of thiosulphate in combination with chloride ions. The risk of pitting corrosion increases when the relative levels of thiosulfate, sulfate, and chloride reach a certain amount, but can be avoided by controlling the amount of thiosulfate.

Different types of formulas have been proposed to rank the resistance of stainless steels to pitting corrosion and to compare a steel grade among other grades by the influence of main alloying elements. The pitting resistance equivalent (PRE) of a specific steel grade can be estimated by formulas in which the relative influence of a few elements, that is, chromium, molybdenum, and nitrogen, are considered. The higher the PRE value of a stainless steel, the better the resistance to pitting corrosion in neutral chloride containing solutions. Table 9 shows the compositions of some commercial stainless steels and calculated PRE, indicating their relative pitting corrosion resistance.

One frequently used expression is:

$$\mathrm{PRE} = \%\mathrm{Cr} + 3.3\%\mathrm{Mo} + 16\%\mathrm{N}$$

There are also other formulas with different alloying elements included, such as manganese, wolfram, sulfur, and carbon.

Alfonsson and Qvarfort investigated some formulas for PRE, based on the chromium, molybdenum, and nitrogen content and compared the PRE values with critical pitting temperatures (CPT) measured potentiodynamically, using the Avesta cell.[16] They found an acceptable linearity between the CPT and PRE values for any of the PRE formulas studied.

3.04.8.5.1 Influence of alloy composition on localized corrosion

The increase in the chromium content and molybdenum content enhances the passive potential area to more anodic potentials and consequently increases the stainless steel's ability to passivate in more aggressive solutions. The higher alloyed stainless steel grades, for example, those containing 6% of molybdenum, do not often show any pitting potential due to pitting corrosion in polarization measurements at room temperature, and elevated temperatures are often required to break down the passivity in high amounts of chlorides.

Horvath and Uhlig investigated the influence of chromium, nickel, and molybdenum on the pitting potential in sodium chloride, NaCl, and sodium bromide, NaBr. They showed that the alloying elements, which had the greatest influence on the pitting

Table 9 Typical chemical compositions and PRE numbers for some commercial stainless steel grades

Steel grade			*Typical chemical composition (wt%)*					*PRE*
UNS	EN	Microstructure	Cr	Ni	Mo	N	Other	
S41000	1.4006	Martensitic	11.5			0.04		11.5
S42000	1.4021	Martensitic	12					12
S43000	1.4016	Ferritic	16					16
S44400	1.4521	Ferritic	17		1			20
S20100	1.4372	Austenitic	17	5		0.15	Mn (7.08)	19
S20400		Austenitic	16	2.2		0.17	Mn (9.07)	19
S30100	1.4310	Austenitic	17	7				17
S30100	1.4318	Austenitic	17.7	6.5		0.13		20
S34700	1.4550	Austenitic	18	9.5		0.04	Nb, Mn(2.0)	18
S30400	1.4307	Austenitic	17.5	8				17.5
S31600	1.4404	Austenitic	17.2	10.2	2.1			25
S31600	1.4571	Austenitic	16.5	10.5	2		Ti	23
N08904	1.4539	Austenitic	20	25	4.5		Cu (1.5)	36
S31254	1.4547	Austenitic	20	18	6.1	0.20	Cu	43
S32101	1.4162	Duplex	21.5	1.5	0.3	0.22		26
S32304	1.4362	Duplex	22	3.5	0.1	0.10		23
S32205	1.4462	Duplex	22	5.5	3	0.17		35
S32750	1.4410	Duplex	24	6	3	0.27		38

potential, were chromium and molybdenum. The addition of nickel resulted in a minor increase of the pitting potential compared with the results obtained by the addition of chromium and molybdenum.[17] Figure 14 shows the influence of alloying elements on pitting potentials in NaCl extracted from Horvarth and Uhlig.[17] Comparing the data with an increasing addition of chromium in a Cr–Fe alloy, the pitting potential was around 0.2 V/SHE for 20 wt% chromium, which rose to around 0.9 V/SHE at 38 wt% of chromium. For nickel in a 15% Cr–Fe alloy, the pitting potential was at 20% Ni, 0.28 V/SHE, which at 40 wt% Ni increased to only 0.35 V/SHE. In contrast to the low increase in the pitting potential produced by the addition of nickel, the addition of molybdenum produced a significant influence, even at very low amounts. The pitting potential increased from 0.3 V/SHE for 0.48 wt% up to 0.76 for 2.4 wt% in a 15%Cr–13%Ni stainless steel.

As previously mentioned the presence of nitrogen increases the resistance of pitting and crevice corrosion on stainless steels. Jargelius-Pettersson showed that the effect of nitrogen was depressing both the active dissolution and passive current. The author also showed that the positive effect was pronounced in combination with molybdenum.[18] There are further methods to increase the surface content of nitrogen to enhance the pitting and crevice corrosion resistance of a stainless steel.

3.04.8.5.2 Pitting corrosion

Pitting is a type of localized corrosion that is characterized by attacks at small discrete spots on the stainless steel surface. The pits often appear to be rather small on the surface, but may have larger cross section areas deeper inside the metal as indicated in Figure 15. When the metal corrodes inside the pit, dissolved metal ions generate an environment with a low pH and chloride ions migrate into the pit to balance the positive charge of the metal ions. The environment inside a growing pit gradually becomes more aggressive by the generation of hydrogen ions contributing to the ingress of chloride ions through a lacy cover to maintain the electroneutrality in the pit solution. The repassivation becomes less likely due to the increased aggressiveness in the pit solution and also by the restriction to mix the pit solution to the surroundings by the diffusion barrier of the lacy cover on top of the pit. Figure 16 shows schematically the

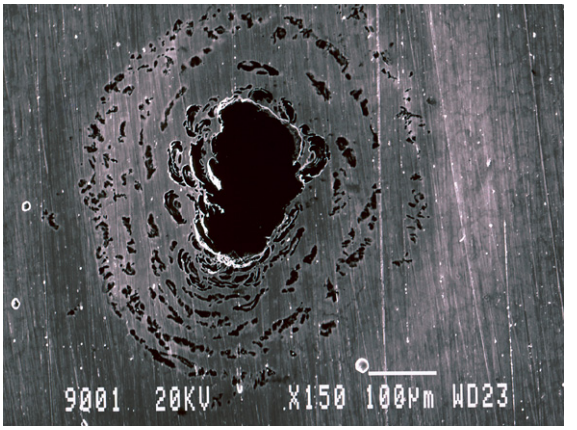

Figure 15 Pitting corrosion on stainless steel, image from scanning electron microscope, SEM, Outokumpu Stainless, R. Qvarfort.

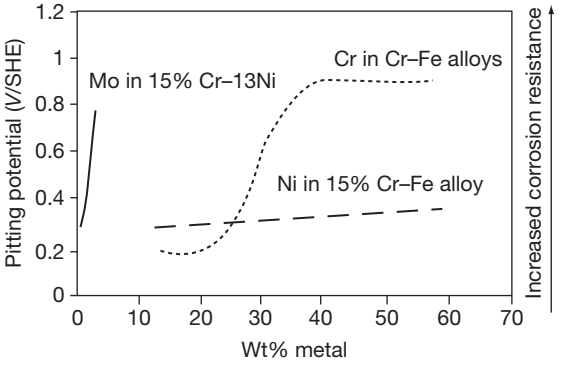

Figure 14 Dependence of chromium, nickel and molybdenum in 0.1 M NaCl at 25 °C. Reproduced from Horvath, J.; Uhlig, H. H. *J. Electrochem. Soc.* **1968**, *115*(8), 791.

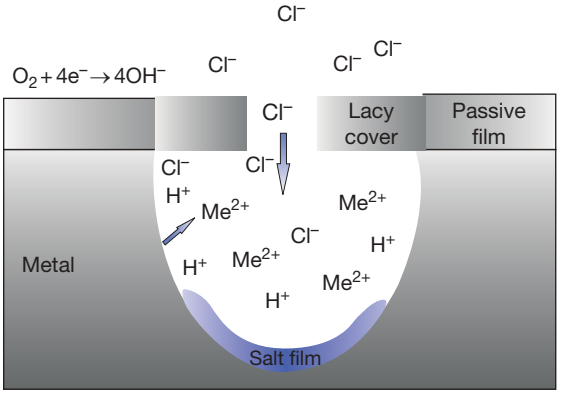

Figure 16 Schematic presentation of the pit chemistry and the diffusion restriction due to corrosion product formation and the lacy cover of a stainless steel suffering from pitting corrosion.

pit chemistry and the diffusion restriction due to corrosion product formation and the lacy cover of a stainless steel suffering from pitting corrosion. Since pitting may not be immediately visible from a surface inspection and may indeed be concealed altogether if the propagation occurs inside the pit rather than close to the surface, a pitting attack often remains undiscovered until it causes perforation and leakage.

In order for pitting corrosion to propagate and thrive in stainless steels, a concentrated pit solution is needed, else passivation processes would interrupt active corrosion. This solution is produced inside the pit as a result of the increase in the concentration of the dissolved metal. However, the exact chemistry of the solution inside an active pit is not yet determined. Newman has reviewed the research undertaken in recent years to explain the concept of pitting corrosion in stainless steels.[19] The author simplifies the complexity in the chemical reactions inside the pit by indicating that the low pH level results from a large ionic activity coefficient superimposed on hydrolysis reaction such as

$$Cr^{3+} + H_2O = CrOH^{2+} + H^+ \quad (K = 10^{-3.8})$$

Newman also describes the dependence of active dissolution rate on the concentration of dissolved products inside the pit.[19] Tester and Isaacs associated this anodic dissolution process in the pit by anodic diffusion control across an iron-rich salt film formed in the bottom of the pit.[20] The salt film stabilizes the dissolution process by providing a reservoir of acid but at the same time, it consumes acidity in the interface, leading to passivation when the aggressive solution inside the pit is not maintained. Landolt and Grimm showed further that this diffusion-controlled anodic dissolution process reaction was hindered when the amount of chromium in the steel increased to about 25%.[21]

Donker and Dengg showed already in 1927 that, by applying an external potential to an iron anode, a pitting potential corresponds to a large increase in the current passing through an electrochemical cell using a cathode of silver and solutions of various salts.[22] The technique was then used by Brennert to study the passivity of stainless steels.[23] Streicher showed in 1956 that by applying a constant current instead of a potential the number of pits per unit of area found for a specific combination of steel and corrosive solution depends directly on the density of the current passing through the surface of a specimen. He also demonstrated the differences in the extent of pitting at increasing current densities and that the pitting data obtained for a certain stainless steel at one temperature cannot be used to predict the behavior of other stainless steels or for the same steel at other temperatures.[24]

The pitting potential is characterized by the susceptibility of alloys to a defined environment and has been used extensively to rank different steel grades regarding pitting corrosion resistance in various environments containing halides such as chlorides. Laycock *et al.* recently stated that there was an obvious similarity between the pitting potentials of pits and crevices and related the pitting potential to the transitions potential between the two regimes to activation control at lower potentials for metastable pitting, where crevice corrosion commonly occurs and diffusion control at higher potentials, where pitting corrosion occurs.[25]

In Smialowska's review of pitting corrosion, the induction time for pit initiation is referred to as the time required to form the first pit on a passive metal exposed to a solution containing aggressive anions (e.g., Cl^-).[26] Schwenk showed that this induction time at constant chloride content varies as a function of applied potential.[27] The induction time is shorter at a higher applied potential than at a lower potential.

Critical pitting temperature (CPT)

Brigham and Tozer introduced the postulation of temperature dependence in pitting corrosion in 1973 to use for comparison of a large range of stainless steels with varying pitting corrosion resistance.[28] The authors introduced a method to test pitting corrosion properties in a potential area where temperature showed the main influence on pitting corrosion regardless of the potential. However, later the method was further developed by the introduction of a crevice-free cell by Qvarfort and he showed by polarization measurements that there is a temperature, above which the corrosion is pitting corrosion, but below this temperature pitting corrosion is impossible. This critical pitting temperature was illustrated in dynamic anodic polarization measurements showing a pitting potential above the CPT and transpassive corrosion at higher anodic potentials at a temperature below the CPT. He also showed that the transition between the transpassive corrosion and pitting corrosion was very abrupt at a temperature range $\pm 1^\circ C$.[29] The concept of critical pitting temperature was thereafter developed to measure potentiostatically at 700 mV/SCE in 1 M sodium chloride and it is, at present, widely used as standard (ASTM G 150). The method is used for ranking purposes of higher alloyed stainless steel grades

containing high levels of molybdenum and chromium. **Figure 17** illustrates the potential dependence and independency of the CPT.

Newman has summarized the concept of CPT for stainless steel to understand the corrosion of stainless steel by the emphasis on the temperature as the main parameter for pitting corrosion.[19] The CPT is suggested to be the temperature at which passivation occurs simultaneously as the precipitation of an anodic salt film in the pit. The CPT for a specific stainless steel currently refers to the temperature at which passivation reactions intervene in active corrosion. Newman suggests further that two regimes of pit growth can be identified one under mixed activation/ohmic control, which is usually found at lower potentials, and the second under diffusion control, generally at higher potentials with a salt film in the pit bottom.[19] As a lacy cover at the pit mouth develops, it stabilizes the dissolution of the pit, but the dissolution is still metastable at this stage and as pitting corrosion is established, the cover will finally collapse. Repassivation occurs either because of the absence of the salt film or as the lacy cover ruptures. As long as the pit is growing and the salt film is present, the pitting corrosion is under diffusion control. The transition between those two domains is characterized by a transition potential, E_T. In general, the pitting potential E_p is the lowest transition potential E_T, the potential at which stable pitting can be distinguished for a specific stainless alloy and aggressive environment.

Nyman suggests that in order to compare two different stainless steels, for example, S30400 and S31600 the following relation has to be considered[19]:

$$E_T = E_{corr} + b_a \log(i_L/i_{corr}) + \varphi_s$$

where E_{corr} and i_{corr} are the corrosion potential and corrosion current density, respectively, in the saturated pit solution; b_a is the anodic Tafel slope; i_L is the anodic limiting current density; and φ_s is the ohmic potential drop in the pit cavity, which is constant.

When the concentration of the metal cations is at, or slightly above the saturation concentration of metal cat ions, precipitation of the salt film occurs. In order to precipitate, an anodic current density greater than or equal to the limiting current density, has to flow in the cavity where pitting initiates. The anodic current density required to maintain the local chemistry is then compared with the critical current density for passivation i_{crit} from Salinas-Bravo and Newman[30]. For relatively concentrated solutions very clean linear plots of E_T vs log i_L can be generated using artificial pits.

$$I_{crit}(T, C_s) = nFDC_s/\delta$$

where i_{crit} is the critical current density for passivation, D is the diffusivity of metal ions, δ the diffusion length (pit depth), C_s is the metal ion concentration at the pit surface, n the charge number, and F the Faraday's constant.

Salinas-Bravo and Newman also considered that this critical current density exists in the most aggressive pit environment and also considered it to be a steeper function of the temperature than the anodic limiting current density. The concept of CPT was

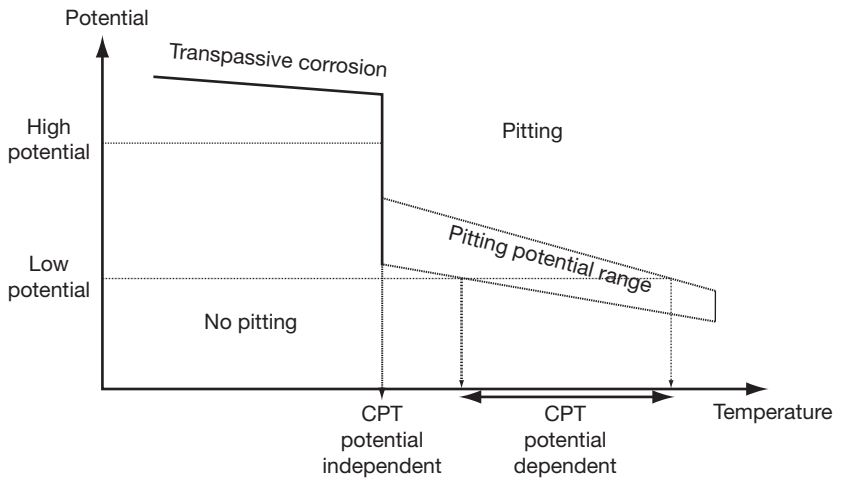

Figure 17 Potential dependence in transpassive and pitting corrosion.

then concluded to be when the critical current density equals the anodic limiting current density and the temperature at which the salt precipitation is possible.[30] Newman concludes recently, however, that the steeper function of the temperature is trivially true for experiments carried out in strong HCl solution mimicking the pit environment but that there are no precise data available for real pit environments at present.[19]

Moreover, the diffusion length is included in the concept of temperature dependence, which can explain why crevice corrosion appears at lower temperatures than pitting corrosion. Notable is, that the diffusion length in a crevice is generally longer and consequently any CCT, critical crevice corrosion temperature, is lower than CPT for a defined stainless alloy.

Figure 18 shows a photograph of a stainless steel surface with pitting corrosion after CPT measurement using a crevice-free flush port cell.

Even if the CPT has proved to be a useful value for ranking a wide range of stainless steels with regard to their pitting resistance, it does not necessarily accurately reflect their performance and properties in actual environments. Figure 19 shows examples of CPT for increasing chromium and molybdenum contents in various stainless steel grades represented by their PRE values. The figure indicates the very strong dependence of corrosion properties on the alloy composition of stainless steels. The difficulties associated with obtaining CPT values for lower alloyed stainless steels are obvious. Lower alloyed stainless steels such as ferritic stainless steels containing 12% of chromium seem to have CPT values well below room temperature and these steel grades commonly corrode at temperatures of only a few or even below 0°C under these very aggressive conditions.

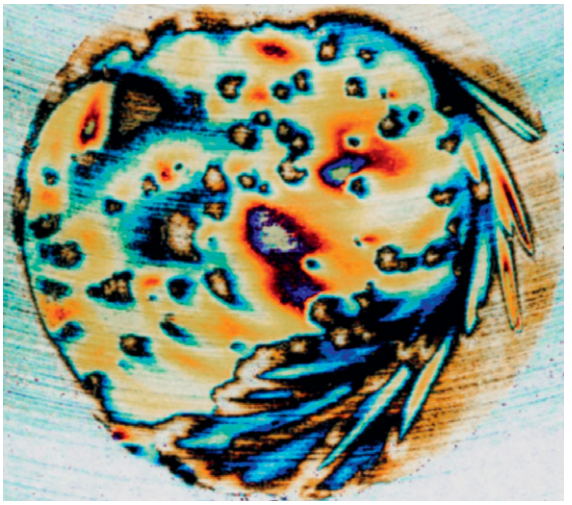

Figure 18 Stainless steel surface with pitting corrosion after CPT measurement in a crevice-free flush port cell.

3.04.8.5.3 Crevice corrosion

Crevice corrosion attacks start in a narrow crevice or under a deposit on the stainless steel surface. Crevices, such as those found at flange joints or at threaded connections, are thus often the most critical sites for corrosion of stainless steels.

In narrow crevices, it is possible for a liquid to penetrate into the crevice and cause stagnant conditions by capillary forces. Oxygen and other oxidants are then consumed for the maintenance of the passive layer inside the crevice. In the stagnant solution inside the crevice, the supply of oxygen is after some time restricted, causing a weakened passive layer. Small amounts of dissolved metal ions inside the crevice cause a further decrease of the solution's pH levels and finally, the presence of chlorides facilitates the breakdown of the passive layer. Thus the environment inside the crevice gradually becomes more aggressive and repassivation becomes less likely. As a result, crevice corrosion attacks often propagate at a high rate, thereby causing corrosion failure in a relatively short time.

The mechanisms for under deposit corrosion or crevice corrosion bear several similarities to pitting. However, one of the differences between pitting and crevice corrosion is that pitting initiates at points which are susceptible to corrosion and to which the

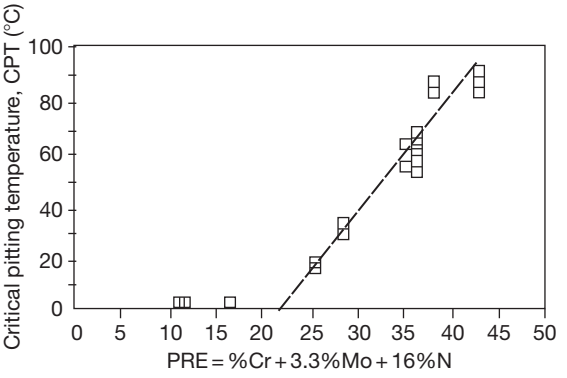

Figure 19 Critical pitting temperatures (CPT) measured according to ASTM G 150 for stainless steels with different PRE. All data from surfaces of 320 mesh (Outokumpu Stainless data).

environment has free access. Crevice corrosion, on the other hand, is initiated on the metallic surface where the surrounding solution has restricted access.[15] The rate determining factors in this stage are proposed by Valen to be that the large current density consumes high mounts of oxygen and the narrow crevice, contains less amounts oxygen.[31] Both factors lead to more rapid oxygen depletion inside the crevice. Since oxygen depletion occurs in the crevice or under the deposit the oxygen reduction occurs as cathodic on the outside of the crevice. This causes a potential difference between the inside and the outside of a crevice, which causes the corrosion process to thrive.

Crevice corrosion can be unpredictable and one reason for this is that the critical potential, for crevice corrosion to occur, is dependent on the type of crevice. It is further experimentally more difficult to find universal crevice formers to predict all types of crevice corrosion since the type of crevice found in actual structures may come in many different shapes and forms. Examples of crevice formers are gaskets, flanges joining stainless steel structures, or almost any partial blocking of the stainless surface. It is almost impossible to avoid crevices completely in practical operations, but the principles of good design emphasize that crevices should be kept to a minimum.[32] **Figure 20**, shows crevice corrosion in a flange after exposure in high temperature and high amounts of chlorides exceeding the corrosion resistance of the steel grade.

One important parameter, which influences the risk of crevice corrosion, is the geometry of the crevice. A narrow crevice of a few micrometers in width is typically more prone to crevice corrosion than a wider crevice, due to the influence of capillary forces in a narrow gap. The practice of draining the crevice area from the stagnant chloride containing solution may further decrease the risk of crevice corrosion.

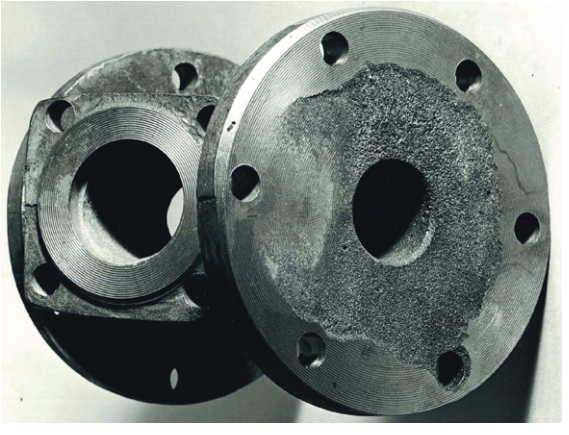

Figure 20 Example of crevice corrosion in a flange.

In the case of deposits, it can be difficult to measure the crevice area, the degree of porosity and consequently the exact influence of this parameter. Dense deposits will cause more severe corrosion attacks compared with a porous deposit, which allows the solution to diffuse from the narrow area between the stainless surface and the deposit.

There are several ways to prevent crevice corrosion and several courses of action may be taken to minimize the risk, for example, selecting gasket materials that are nonporous and do not contain chlorides, since the chlorides can be released to the surrounding solution. However, in areas where crevices cannot be avoided weld-overlaying the sealing surface can be performed using a filler material that is higher alloyed and thus more corrosion resistant than the flange itself. Sharp corners or angles can be sites for collecting dirt or other solids that act like deposits and consequently increase the risk of corrosion under deposits. As regards other types of corrosion, the risk of crevice corrosion attacks decreases as the alloy content increases in the stainless steel, particularly with regard to chromium, molybdenum, and nitrogen. One stainless steel grade can be resistant to localized corrosion on open surfaces but another higher alloyed stainless steel might be used for creviced conditions.

In some cases when crevices cannot be avoided, there are ways of positioning beams, channels, and stiffeners to encourage smooth flow and to avoid the trapping of solids or deposits. If crevice corrosion occurs on a certain steel grade, the material selection process should take this into account and specify a better and more corrosion-resistant stainless steel grade.

3.04.8.6 Stress Corrosion Cracking

A material failure may be accelerated by the combined effect of a corrosion process and mechanical tensile stress. Two examples of such processes are SCC and corrosion fatigue. SCC does not occur if only one of the two conditions is present. For example, tensile stress present in a stainless steel in a noncorrosive environment is unable to cause SCC.

Different manufacturing processes can introduce stresses in the material. Examples of such processes are coarse grinding, forming, and welding. Any machining on the stainless steel surface that

introduces residual stresses, hardening or martensitic transformation can influence the resistance to SCC. Examples of machining operations of this kind are abrasion or machining techniques that involve deep grooves or notches.[33] However, the degree of the impact from machining on SCC properties is not easily evaluated and ranking methods are most commonly used to test any deterioration or improvement in SCC resistance.

The electrochemical potential of the stainless steel in solution has some effect on the risk for SCC. The susceptible potential zones at which SCC can occur for a given alloy/solution with a typical active–passive behavior are shown in **Figure 21**.

Two zones of susceptibility appear at the potential boundaries where the passive film is less stable. In the active–passive potential zone, SCC occurs where the passive film is relatively weak at active potentials almost inadequate forming the film A, and B in **Figure 28**. In the other potential zone C, in the passive potential area, SCC and pitting corrosion are associated in adjacent or overlapping potential ranges. The common example of SCC in the active–passive potential zone (B) is austenitic stainless steel in hot $MgCl_2$ solutions. However, a material, which is not susceptible to SCC, will not crack in despite being in the susceptible zones. SCC in the active–potential area is commonly associated with a low pH contributing to the corrosion mechanism and the cracking in the passive-potential area is associated with high amounts of chlorides contributing to localized breakdown of the passive film.

3.04.8.6.1 SCC mechanisms

There are many attempts to explain the SCC by mechanism taking into consideration both the corrosion process and the role of stresses in the material. Sedriks summarizes some of the numerous mechanisms and concludes that the lack of agreement as to which mechanisms are operative have lead to a simplistic nomenclature to describe SCC in terms of the environments that cause it. For example, chloride SCC and caustic SCC describe SCC in chloride environment and in caustics respectively. Hydrogen embrittlement describes cracking in environments in which the cracking process is facilitated by the entrance of hydrogen into the metal.[34]

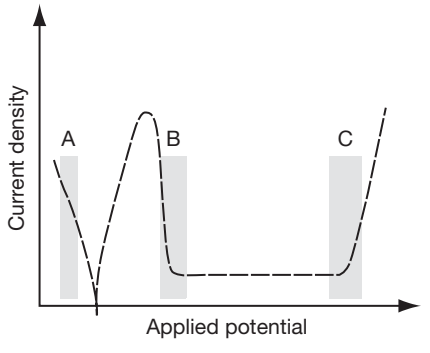

Figure 21 Susceptible zones in the potential area for stainless steels and SCC.

Some general processes were, however, concluded by Sedriks to provide a basis for a classification of SCC mechanisms based on either removal of material by dissolution or by film formation for separation of the material.[34] In the following section are some mechanisms summarized briefly that were chosen by Newman as three testable cracking models that may account for most known cases of SCC in metals: Slip-dissolution, film-induced cleavage, and hydrogen embrittlement.[35]

Slip dissolution

This mechanism is mainly used to explain intergranular cracking in ferritic stainless steels in environments where the stainless steel is passive and in sensitized stainless steels. The crack growth in the slip dissolution model is the result of an extremely localized anodic dissolution. Propagation of the cracks occurs as a result of film rupture, dissolution, and repair. The sides of the crack are considered to be protected by a film, an oxide, which is fractured as a result of plastic strain in the metal at the crack tip.

Film-induced cleavage

Film-induced cleavage occurs when the crack is going through a face cubic centre metal, fcc, as an austenitic stainless steel, with a very high velocity in a very short time. The stress corrosion crack introduces a brittle crack in the propagation direction, which is then widened by plastic arrests in the metal. The crack propagates in steps by a brittle crack, which is then widened in steps. As the crack goes further into the material the outer cracks get wider and wider.

Hydrogen embrittlement model

Hydrogen embrittlement is assisted by the absorption of hydrogen into the material from an aqueous environment. If the acidification from the hydrogen contributes to passive film breakdown in a crack, the absorbed hydrogen can promote cleavage, intergranular separation or a highly localized plastic fracture.[35] Microstructure plays an important role in

hydrogen embrittlement as in the other mechanistic approaches for SCC. In susceptible steel hydrogen enters under both anodic and cathodic conditions.

Hydrogen embrittlement is accounted for in the presence of hydrogen sulfide H_2S as in oil wells and releasing hydrogen is also commonly assisted with an acid environment in the presence of sulfur adsorption.

3.04.8.6.2 Impact of mechanical stress on corrosion: stress intensity factor and crack rate

Generally, it is considered that decreasing the applied stress on the material increases the time to failure. Threshold stress intensities (K_{ISCC}) are often referred to as stress intensity factors below which the rate of cracking in a given environment is very low. The threshold stress intensity factor indicates a level below which stress corrosion cracks will not propagate. Increasing the stress factor above K_{ISCC} failure will occur.[34] Stress intensity factors are usually derived from laboratory measurements in environments such as boiling magnesium chloride and care has to be taken since these environments do not coincide with real service in different applications. Precracked specimens are used for measurements of the rate of growth as a function of the stress intensity factor at the tip of the crack. The presence of different microstructure phases, for example, in duplex stainless steels, can result in different stress intensity factor, depending on the microstructure. It is also generally considered that the duplex stainless steels have better SCC resistance than the corresponding austenitic stainless steels. Newman attributes these properties to the differences in the stress intensity factor in the different phases as ferritic and austenite in the microstructure. The effect seems to be that one phase is considered to assist to arresting the crack propagation.[35]

Figure 22 shows a schematic representation of the stress intensity factor and crack rate for S31600 cold worked at 25 and 50% in a hot chloride solution.

The plateau in the schematic representation of the stress intensity factor is proposed by Newman to occur due to chemical reactions controlling the crack rate, rather than mechanical properties. These chemical reactions might be dissolution, diffusion or adsorption.

3.04.8.6.3 Chloride-induced SCC

Circumstances where there is a pronounced risk of SCC include evaporative conditions in chloride solutions on stainless steel grades with low resistance to SCC, such as the austenitic grade S30400 subjected to stresses by manufacturing processes. The chloride content on the surface increases to very high values as a result of the evaporative conditions, causing corrosion to occur. Failure from SCC is very rapid; there are no warning signs before the failure and the corrosion propagates very rapidly, causing the construction to fail in a short time.

The most common type of SCC on austenitic stainless steel is transgranular SCC, which may develop in concentrated chloride-containing environments at elevated temperatures at around or above 50–60 °C. The crack propagation is in many cases perpendicular to the introduced tensile stresses and in transgranular stress corrosion, the cracks run across the grains – to be compared with intergranular SCC, where the cracks run in the grain boundaries. Figure 23 shows typical transgranular SCC in austenitic stainless steel.

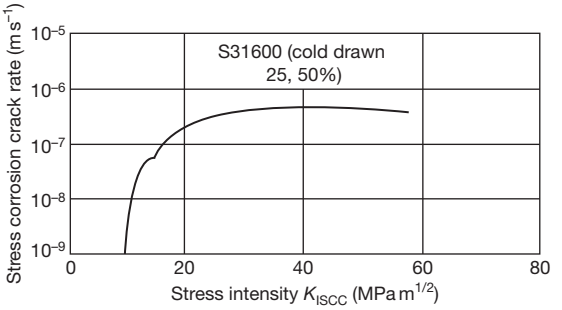

Figure 22 Schematic representation of the Stress Intensity factor and crack propagation rate for S31600 cold worked 25 and 50% in a hot chloride solution. Reproduced from Extracted from Dickson, J. I.; Russel, A. J.; Tromans, D. *Can. Met. Q* **1980**, *19*, 161.

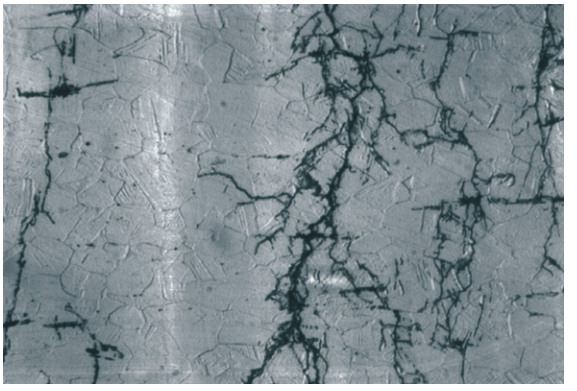

Figure 23 Transgranular SCC in an austenitic microstructure.

Another frequently mentioned cause to SCC of stainless steels is the sensitization of the material. Sensitization occurs when stainless steel is submitted to a high temperature treatment for too long a time, which can cause carbide precipitation to occur if the steel's carbon content is too high. By avoiding sensitization and carbide precipitation; the risk of SCC can in many cases be eliminated. Most commercially available modern stainless steels have low carbon content and amounts below 0.05 wt% are seldom sensitized, even in welding operations. For use in hot concentrated nitric acid, the maximum carbon content is proposed not to exceed more than 0.03 wt%. These improved properties not only contribute to higher resistance to cracking but also enhance the steel's intergranular corrosion properties.

Solutions containing chlorides are not the only environments that can cause SCC of stainless steels. Solutions of other halides may also cause cracking. Sensitized 1.4301 (30400) stainless steels are also susceptible to intergranular SCC in steam and water environments, for example, in boiling water reactors if the stress level is sufficiently high.

3.04.8.6.4 Caustic SCC

Another risk scenario that may give rise to SCC, particularly in low alloy steels, is very alkaline solutions at high temperatures, where the pH values are above 14 at concentrations between 20 and 70 wt% and temperatures above 120°C. Caustic SCC has been of particular interest to some industries, such as chemicals, petrochemicals, and pulp and paper. Sedriks concludes that any heat treatment or sensitization to produce 475°C embrittlement in duplex stainless steels will promote caustic cracking but also that duplex stainless steels generally offer better resistance to cracking in hot caustic solutions.[33]

The alloy compositions of stainless steels influence the cracking of the material and it would appear that alloys including molybdenum have a different ranking in hot alkaline solutions compared with that obtained for other wet chloride-induced corrosion in stainless steels.

3.04.8.6.5 Sulfide stress cracking (SSC) by hydrogen sulfide

Contaminants, such as hydrogen sulfide, H_2S, may increase the risk of SCC in stainless steels in chloride containing environments. Hydrogen sulfide exists in oil and gas wells and stainless steels intended for applications in the oil and gas industry are typically tested for use under these circumstances. The most important environmental aspects of SCC in the sour service environments common in oil and gas production are hydrogen sulfide, H_2S partial pressure, pH, and the chloride concentrations.

The cathodic reaction in chloride containing hydrogen sulfide solutions is mainly the reduction of hydrogen ions to hydrogen, which may form either as hydrogen gas or dissolve in the metal as hydrogen atoms:

$$2H^+ + 2e^- \rightarrow H_2 \ (\text{or} 2H)$$

The adsorption of hydrogen sulfide on the surface promotes the hydrogen absorption in iron alloys. The cathodic rate depends on several parameters such as temperature, pH, concentration of weak acids, and the electrochemical potential of the material. The role of the weak acid is to donate hydrogen ions.

Duplex stainless steels are frequently used in the oil and gas industry because of their mechanical properties and corrosion resistance in chloride environments, for example, in subsea components working at high pressures and high temperatures. Some examples are pipelines, flow lines, and pipe work.

3.04.8.6.6 Hydrogen-induced stress cracking (HISC) using cathodic protection

Martensitic and ferritic microstructures are susceptible to hydrogen embrittlement whereas austenitic stainless steels are much less likely to suffer from this type of cracking. The resistance to SCC can be influenced by cathodic currents applied to stainless steel in wet environments. For example, the super ferritic grade, UNSS44735, is prone to hydrogen embrittlement when polarized to potentials in the range of 0.9–1.4 V/SCE, caused by overprotection at potentials more negative than −0.8 V/SCE, so potential in this range should be avoided.

High strength steels, including many martensitic grades, are susceptible to hydrogen embrittlement. Yield strength seems to be an important factor and cause of hydrogen embrittlement along with the tempering and precipitation hardening of the material.[33]

Subsea duplex stainless steels are usually subjected to cathodic protection since these steels are typically connected to other carbon and low alloy steel structures that are already protected. Overall, duplex stainless steels have an excellent track record in subsea conditions but hydrogen-induced stress cracking is a risk if cathodic protection is applied in sour environments, containing H_2S. The reported failures under

cathodic protection have been associated with unusually high mechanical loads, an unfavorable microstructure in the base metal, characterized by large grains, intermetallic phases, etc. or a high ferrite content in welds. Lowering the hydrogen sulfide concentration to below 0.1 g l^{-1} can reduce the susceptibility to SCC or by reducing the applied stress level to below 60% of the yield stress.

Many tests on hydrogen embrittlement are carried out using cathodic charging in sulfuric acid solutions that contain arsenic, Hydrogen embrittlement occurs if the applied stress is higher than the yield stress and the presence of hydrogen ions recombines in the presence of the poison arsenic compound in sulfuric acid. The presence of molybdenum in ferritic stainless steel can reduce the steel's resistance to hydrogen embrittlement.

3.04.8.6.7 SCC in atmospheric environments

A number of accidents have occurred where ceilings in swimming pool houses have collapsed due to corrosion, mainly involving 304 type steel grades. For example, in Steenswijk in the Netherlands in 2001, suspended air channels were collapsed due to corrosion. Analysis revealed that the reason for the collapses was SCC and also that it occurred at lower temperatures than expected based on previous experience. Most other reports of SCC related to atmospheric environments have been at temperatures above 50 °C in combination with chlorides under evaporative conditions and not typically at room temperature.

In recent decades, the atmospheric environment in swimming pool houses has changed as modern pool houses use higher water and atmospheric temperatures for convenience. Furthermore, in many cases, dehumidifiers are installed and the pools have higher water agitation and heavier bather loadings. The swimming pool house atmosphere may also be subjected to changes in humidity and temperature during both day and night.

Experience has shown that items of stainless steel furniture and equipment immersed in or washed by pool water do not suffer from corrosion problems.

Chlorine-based disinfectants are used in most swimming pool water in a form of hypochlorous acid, HClO, hypochlorite, ClO^-, and chlorine, Cl_2, independent of the particular disinfection procedure. Assuming the most typical pH level for swimming pools, that is, between 7.2 and 7.4, the concentration of hypochlorite and hypochlorous acid in the pool water is approximately equal and the concentration of chlorine gas is negligible. The amount of free chlorine in the pool water, that is, the total concentration of hypochlorite, hypochlorous acid, and chlorine, is usually kept at 0.5–2 mg l^{-1}.

Free chlorine reacts with ammonia and amine compounds introduced to the pool water by bathers forming relatively stable intermediate products, chloramines. Chloramines are volatile substances responsible for 'swimming pool smell' and causing most of the eye and nose irritations to pool users. Chlorine seems to be transported to the metal surface from the pool water in the form of volatile chlorine-based chemicals, probably mainly as trichloramines. Chloramines are sufficiently stable to be carried to relatively distant locations and dissolve in condensed water on a metal surface. However, the deposition of chlorine-based chemicals in the form of water aerosol has also to be considered. Regular maintenance, such as routine cleaning with clean water, reduces the risk of corrosion in these environments significantly.[37]

Iversen and Prosek simulated the worst possible conditions in a swimming pool atmospheric environment by exaggerating the concentration of chloride in the surface electrolyte, the level of tensile stress, the temperature, and the relative humidity of the atmosphere in comparison with values reported from real swimming pool environments to simulate extremely severe conditions.[37] The test method they used consisted in applying droplets of saturated magnesium and calcium chloride spots on the top of U-bent samples of eight grades of stainless steel. A part of each of the samples was exposed at 50 °C over saturated water solutions of respective chloride salts to keep the relative humidity at the deliquescence point. The stainless steel grades S30400 (1.4301) and S31600 (1.4404) were susceptible to SCC in the presence of magnesium and calcium chloride deposits at 50 °C and at the deliquescence point. Transgranular cracks were initiated rapidly, probably within the first week of exposure.

No SCC was found on samples of the higher alloyed austenitic stainless steel grades N08904 (1.4539) and S31254 (1.4547). These were completely free of corrosion or suffered from pitting corrosion. **Figure 24** shows SCC on S31600 from laboratory tests exposed with $MgCl_2$ spots at 50 °C and at 31% RH for 22 weeks.

Common austenitic stainless steel grades without molybdenum or with a maximum of 3% molybdenum have been recognized to suffer from SCC under the specific conditions that can occur in swimming pool atmospheres. Therefore, these stainless steels should be excluded from being used as safety-relevant fastening components in swimming pool buildings.

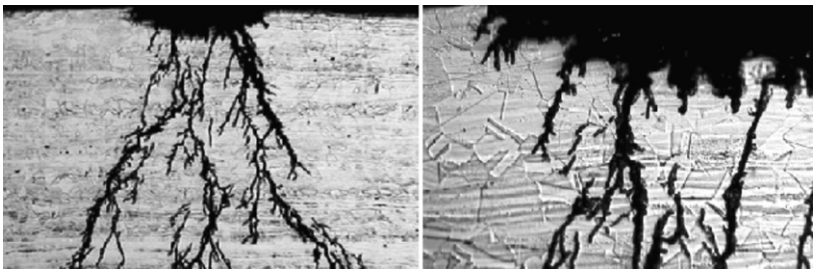

Figure 24 SCC on S31600 (1.4404) from laboratory tests exposed with $MgCl_2$ spots at 50 °C and at 31% RH for 22 weeks. Reproduced from Iversen, A.; Prosek, T. Eurocorr 2007, Freiburg im Breisgau, Germany, 9–13 September, 2007.

It seems that highly corrosion-resistant stainless steels are necessary for the successful and safe application of stainless steels in swimming pool atmospheres in combination with maintenance such as regular cleaning of the stainless steel surfaces.

3.04.8.6.8 SCC of martensitic stainless steels

Martensitic stainless steels such as S41000 are very susceptible to both SCC and hydrogen embrittlement. Martensitic grades are especially susceptible to hydrogen embrittlement in tempered conditions. This susceptibility to hydrogen embrittlement can have an adverse effect on any cathodic protection of martensitic stainless steels in applications such as in seawater. The cathodic protection sets the potential in a risk area, at low negative potentials, for hydrogen embrittlement to occur. Another risk scenario for martensitic stainless steels is grain boundary precipitation caused by tempering, which leads to an increased risk of intergranular SCC. The hardness of the material is often an important factor in the selection of martensitic stainless steels, but comes at a cost, since the mechanical toughness decreases with increasing hardness. This will also influence the stress levels in the material, particularly in welded components.

3.04.8.6.9 SCC of ferritic stainless steels

Ferritic stainless steels are highly resistant to chloride-induced SCC, but even if ferritic grades do not crack under such conditions, their resistance to other types of corrosion, such as localized corrosion and uniform corrosion, is determined by a combination of the alloy composition and the service environment.

High chromium ferritic alloys can suffer from embrittlement under incorrect and prolonged heat treatment often referred to as 475°C embrittlement. Even though ferritic stainless steels exhibit excellent resistance to stress corrosion in chloride solutions, sensitization or high temperature embrittlement at 475°C leads to cracking of these grades in a chloride or caustic solution. Another operation that increases the susceptibility to cracking in ferritic grades is cold work. Alloying elements in ferritic grades identified as causes of SCC include nitrogen, copper, nickel, and carbon. Microstructure effects on increasing cracking properties, are probably related to the reduction of ductility, which occurs where precipitation of carbides and nitrides occur in high temperature embrittlement at 475°C.[33]

The most common reported cause of sensitization in ferritic stainless steels is high carbon content. Low carbon and nitrogen levels in ferritic stainless steels are beneficial as they improve the toughness of the material and also help prevent the precipitation or carbides and nitrides. Alloying elements that improve the resistance to cracking of ferritic stainless steels are titanium (Ti) and niobium (Nb).

3.04.8.6.10 SCC of austenitic stainless steels

The alloying element nickel has been widely discussed in terms of its contribution to resistance to chloride-induced SCC of austenitic stainless steels in sodium chloride solutions. Copson showed that for low and high levels of nickel in austenitic stainless steels no SCC occurred in boiling magnesium chloride at 154°C.[38] However, it should be pointed out that these measurements were carried out under conditions that cannot be transferred to any real environment. Nevertheless, Nickel has a beneficial effect and is known to prevent SCC when the nickel content exceeds 30–40 wt%. Very high amounts of nickel as an alloying element are accounted for in nickel-based materials. Any beneficial effect attributable to nickel only is excluded in the ferritic stainless steels as they normally do not contain nickel and are anyway highly resistant to chloride-induced SCC. An increase in the molybdenum content in austenitic stainless steels has produced a significant improvement in the resistance to SCC in sodium chloride solutions. The resistance to SCC generally increases

in line with the PRE number, as the chromium, molybdenum, and nitrogen content is increased in austenitic stainless steels. The super austenitic stainless steels are highly resistant to chloride-induced SCC. One of the reasons for this is that the assisting corrosion reaction to SCC does not initiate as easily in super stainless steels with a high PRE number as in the standard grades S30400 (1.4301) and S31600 (1.4401).

3.04.8.6.11 SCC of duplex stainless steels

Generally, duplex stainless steels are more resistant to SCC compared with austenitic stainless steels with corresponding PRE values and alloy composition. This is because duplex stainless steels have a two-phase microstructure. An austenite stabilizing alloying element such as nitrogen and nickel does not dissolve easily in the ferritic phase. The effect of the duplex microstructure on the overall material is a two-phase system and a possible reason mentioned in the literature is different stress intensity factors for the two phases.[35] There are also some theoretical considerations suggesting that the SCC process can be arrested by the differences between the two phases and that propagation is, to some extent, hindered between the two phases. However, occurrences of SCC in duplex stainless steels have been reported in strong alkaline solutions at very high temperatures.

3.04.8.7 Corrosion Fatigue

It is well-documented that material subjected to a cyclic load far below the ultimate tensile stress can fail, due to fatigue. If the metal is simultaneously exposed to a corrosive environment, the failure can take place at low loads and after a short period of time. Contrary to pure mechanical fatigue, there is no fatigue limit in corrosion-assisted fatigue. The fatigue fracture is brittle and the cracks are typically transgranular, as in SCC, but not branched. Fatigue properties of stainless steels can be read in **Section 3.04.4.4**.

The fatigue strength is sensitive to the service environment and under both cyclic loading and corrosive conditions; the fatigue strength will generally decrease. In many cases there is no pronounced fatigue limit, as observed in air, but a gradual lowering of the fatigue strength with increasing number of load cycles. The more aggressive the corrosive conditions and the lower the loading frequency, the higher the effect of the environment. During very high frequency loads there is little time for the corrosion to act and the fatigue properties of the material will mostly determine the service life. At lower frequencies the corrosive action is more pronounced and an aggressive environment may also cause corrosion attacks that will act as stress concentrations and thus contribute to a shorter life. There is a clear tendency that duplex stainless steels resist fatigue and corrosion fatigue better than austenitic stainless steels. The reason is a high strength combined with good corrosion resistance.

3.04.8.8 Corrosion on Stainless Steels Related to Welding Procedures

The procedure of welding changes mechanical properties, the surface geometry, surface appearance, and microstructure in the weld compared with the base material. These changes have an impact on the corrosion properties of the steel grades and have to be accounted for in a construction, welding procedure, the choice of filler material but also by the postweld treatment.

Welding defects, which occur in connection with the welding procedure, can in some cases have an adverse effect on corrosion resistance. The effects of weld defects will depend on the service environment in which the construction or application is placed. Weld defects in mild environments, for example, clean and moist air, do not normally cause any severe corrosion damage, whereas in more aggressive environments, such as those, which might occur in process industry, could lead to more severe damage. One good rule is to aim to eliminate defects and if they occur, to remove them to ensure optimum corrosion resistance of the welded construction.

In most cases where weld defects cause corrosion attacks, the types of corrosion typically seen are localized corrosion, such as pitting and crevice corrosion. Other types of corrosion attacks might be caused by nonproper welding procedures, as previously mentioned. The combination of unsuitable welding procedures and an aggressive environment can give rise to general corrosion, SCC and/or intergranular corrosion.

Defects possibly causing pitting corrosion are local areas of holes, microcrevices, surface pores, crater pores, spatter, slag or any other surface defect, which naturally can be a location for the initiation of pitting corrosion attacks. Crevice corrosion resistance is decreased by any defect that forms a crevice. Examples of such defects are all types of cracks, incomplete penetration or lack of fusion. Service environments causing deposits under service are also a trigger to the initiation of crevice corrosion.

Uniform corrosion may occur in strong acid environments in connection to oxides or defects caused by ignition spark. If a weld is underalloyed compared with the parent metal, the weld could corrode uniformly leaving the parent metal as if the service environment is too aggressive for the filler material used.

SCC is caused by a combination of factors. These include an aggressive environment as well as an elevated temperature in combination with tensile stresses in the surface. Welding can introduce tensile stresses in the material that can initiate SCC if the other two requirements are present. All types of defects known to cause SCC must be avoided, for example, cracks, or heavy undercuts. The presence of oxygen on the root side during gas tungsten welding, TIG or gas metal arc welding, MIG can, if present in the same concentrations as in the service atmosphere, lead to excessive oxidation of the melted metal during welding. The result is a weld with a totally unacceptable geometry combined with an excessive heat tint – thereby leaving the root side with an unacceptably low corrosion resistance. To avoid excessive oxidation, an inert root gas must always be used during welding.

All types of stainless steels ferritic, duplex, and austenitic must be thoroughly cleaned after welding to accomplish sufficient and acceptable corrosion resistance of the weld.

3.04.8.8.1 Ferritic stainless steels

The weldability of ferritic stainless steels depends on the chemical composition and more specifically on the ratio of alloying elements such as carbon and nitrogen in relation to the chromium content. Precipitation of chromium carbides along grain boundaries should be avoided since this increases the risk of intergranular corrosion. After welding, heat treatment may be necessary to restore the corrosion resistance of these steels. However, a low ratio of (C+N/Cr) reduces the risk of chromium carbide/nitride precipitation and any intergranular corrosion in connection with welding.[32]

If insufficient gas protection is used during welding, chromium nitrides may form, caused by an uptake of nitrogen from the atmosphere. These precipitates can cause embrittlement and lower the corrosion resistance.

3.04.8.8.2 Duplex stainless steels

The modern duplex stainless steels have much better welding characteristics than the ferritic stainless steels and require in general no preheating or postweld heat treatment. However, duplex stainless steels show ferritic microstructure at very high temperatures and too rapid a cooling can conserve this structure. This could lead to the precipitation of nitride or carbide and consequently increase the risk of intergranular corrosion. However, modern duplex stainless steels contain high nitrogen content and low carbon contents, favoring a two-phase structure free from precipitates. The use of fillers with higher Ni-content ensures a weld metal with sufficient austenite level.

3.04.8.8.3 Austenitic stainless steels

Austenitic stainless steels are generally easy to weld and do normally not require any preheating or postweld heat treatment. Highly alloyed austenitic stainless steels – also known as super austenitic grades – generally have good weldability, but the micro segregation of molybdenum reduces the pitting resistance in the weld deposit. To counter the reduction in pitting resistance, these grades are welded with a nickel-based filler that has been overalloyed with molybdenum. Super austenitic steels should be welded with a minimum of heating. The presence of ferrite might influence the corrosion resistance in the ferrite phase in some specific environments as nitric acid. To rectify this, the use of fully austenitic electrodes and filler are used in some applications, such as the production of urea and acetic acid.

Intergranular corrosion was previously a problem for stainless steels with high carbon content. Nowadays, modern stainless steel manufacturers have no difficulties in maintaining a low carbon content so intergranular corrosion caused by chromium carbide precipitation after the welding of austenitic and duplex stainless steels is no longer a problem.

3.04.8.8.4 Postweld treatment

The presence of weld oxides can also cause decreased resistance to pitting corrosion.

Heat tint seen on stainless steels after welding is caused by an oxidation of even fairly minor amounts of oxygen at the high welding temperature during welding. The heat tint influences the passive film and the corrosion properties of the passive film negatively adjacent to the weld. Any oxides, tarnish or scale, should be removed by grinding and/or pickling to maintain the localized corrosion resistance of stainless steels. However, in some cases where the environment will lead to general corrosion such as in strong acids, the service environment will remove the oxide scale.

Grinding of the surface produces a more or less rough surface depending on the grit used. Generally,

the finer the surface finish, the better the corrosion resistance, and grinding coarser than grit 80 very often produces a surface with an unacceptably low pitting resistance compared with the pitting resistance actually inherent in the alloy composition. Coarse grinding can introduce tensile stresses in the surface, which increases the risk of SCC if the environment is too corrosive.

3.04.8.9 General Corrosion

General corrosion occurs uniformly over the stainless steel surface when the passive layer is completely broken down. Anodic and cathodic reactions occur on the same surface and the corrosion rate is similar over the entire surface.

General corrosion is easier to predict from corrosion rates and thinning of the material over time compared with localized corrosion such as pitting, crevice, and SCC. The corrosion rate can be used for lifetime predictions and in material selection, a stainless steel grade is generally chosen for its low corrosion rate. Material with a corrosion rate of less than 0.1 mm $year^{-1}$ is generally regarded as being corrosion-proof, whereas a corrosion rate that exceeds 1.0 mm $year^{-1}$ means that the material is regarded as unusable in terms of its corrosion resistance. Extensive data are available on the uniform corrosion properties of commercial stainless steels.[32] However, laboratory tests are not strictly comparable with actual service conditions, where the corroding medium often contains impurities. These may in some cases increase corrosion, in others, decrease it. In unfavorable cases, the increase can be very high. The best material advice is based on results obtained from the actual process or service environment concerned.

The uniform corrosion rate is also affected if the acid contains chemicals that are oxidizing or reducing. Reducing impurities, for example, hydrogen sulfide may increase the corrosion rate. An oxidizing acid that has a positive effect at a lower concentration is nitric acid, since this promotes passivation of the stainless steel surface at some concentrations rather than initiating uniform corrosion. Nevertheless, there is a limit to how oxidizing the environment may be from a corrosion point of view. Some exceptions occur in strongly oxidizing solutions such as in hot concentrated nitric acid or in chromic acid. In these environments, molybdenum is an undesirable alloy addition. A hot concentrated nitric acid can dissolve the passive layer and transpassive corrosion may occur. The mechanism of transpassive corrosion is not similar to uniform corrosion as the passive layer will be oxidized to more soluble species but the consequence is the same, the passive layer breaks down partly or completely and uniform corrosion occurs. As for many other environments, in common mineral acids and organic acids the higher alloyed stainless steel grades containing higher amounts of chromium, nitrogen, and molybdenum are more resistant to uniform corrosion than the lower alloyed stainless steel grades. Severe environments from a general corrosion point of view are high concentrations of hydrochloric or hydrofluoric acid in which the corrosion may propagate at a rate that can be detrimental to a construction.

Severe environments from a general corrosion point of view are those with high concentrations of hydrochloric or hydrofluoric acid in which the corrosion may propagate at a rate that can be detrimental to a construction.

Engineering with stainless steels relies, in many cases, on test results obtained in laboratory measurements. As with other types of corrosion, a number of different methods are used to describe the susceptibility to uniform corrosion. Isocorrosion diagrams are available for a number of stainless steel grades tested in pure chemicals.[32] The test methods introduce activation of the stainless steel to corrosion in between test periods to forward either propagating uniform corrosion or repassivation.

3.04.8.9.1 Sulfuric acid

When stainless steels are exposed to acids, the aggressivity of the solution is generally related to the level of concentration and general corrosion increases with temperature, but as far as sulfuric acid is concerned, there are some exceptions to this rule, even with regard to the increase in the concentration. At low concentrations and in concentrated sulfuric acid, the aggressiveness towards stainless steels is low and at intermediate concentrations, sulfuric acid causes high uniform corrosion rates.

The isocorrosion line in the diagram shows the limit for use of the specific stainless steel grade. The line, one for each alloy, represents a corrosion rate of 0.1 mm $year^{-1}$. At concentrations or temperatures above this line the corrosion rate is unacceptably high. In other words, above the isocorrosion line, the corrosion rate is too high and below the line, the material is regarded as corrosion-proof. A safety limit is typically adopted to provide materials selection advice well below the line and not on the line.

As can be seen from the isocorrosion diagrams in Figures 25 and 26 the steel grade N08904 (1.4539) performs better in sulfuric acid at intermediate concentrations than some other stainless steel grades. Increased nickel, molybdenum, and copper content in the steel sustain the uniform corrosion rate in sulfuric acid.

Comparing the corrosion resistance of N08904 in aerated and deaerated sulfuric acid, Figures 25–27, show that in the aerated sulfuric acid some increase in the corrosion rates were observed at intermediate concentrations.

Figure 25 shows, at very high concentrations of sulfuric acid, above 90 wt% and, at temperatures below 30 °C, that there is a possibility of using the standard grade of S31600, since the aggressiveness of the highly concentrated sulfuric acid is less for stainless steel compared to intermediate concentrations of sulfuric acid.

To understand the change in the corrosiveness of sulfuric acid solutions, which is higher at intermediate concentrations than at high concentrations, we must look to the hydrogen ion concentration in the sulfuric acid. At intermediate concentrations, the

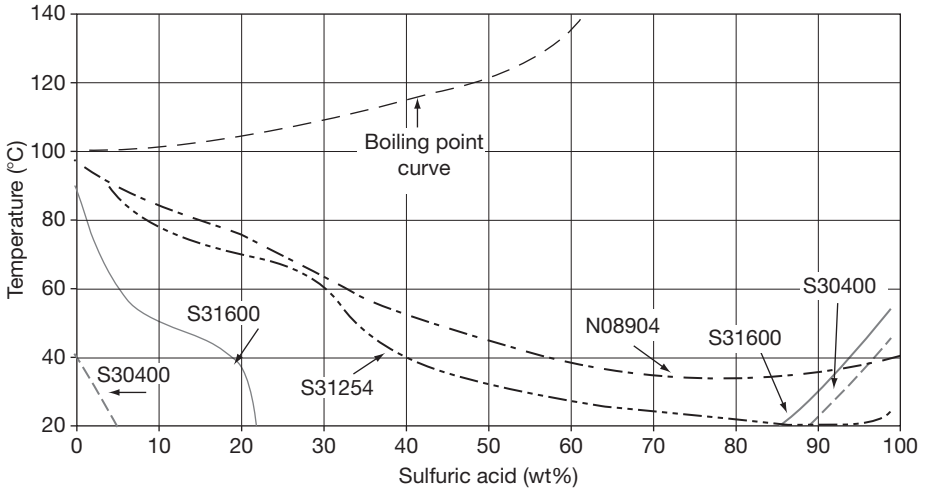

Figure 25 Isocorrosion diagram at 0.1 mm year^{-1} for some austenitic stainless steels in aerated sulfuric acid. Reproduced from Alfonsson, E.; Arnvig, P.E.; Bergquist, A.; Ivarsson, B.; Iversen, A.; Leffler, B.; Nordström, J.; Olsson, J.; Stenvall, P.; Wallén, B.; Vangeli, P.; Outokumpu Stainless Corrosion Handbook, 9th ed.; Outokumpu Stainless Oy, Sandviken 2004, pp I:8–I:103.

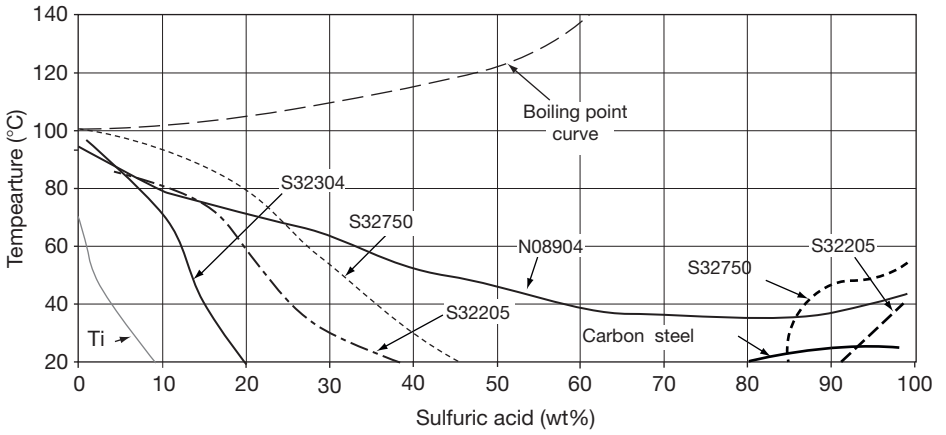

Figure 26 Iso corrosion diagram at 0.1 mm year^{-1} for some duplex stainless steels in aerated sulfuric acid. Reproduced from Alfonsson, E.; Arnvig, P.E.; Bergquist, A.; Ivarsson, B.; Iversen, A.; Leffler, B.; Nordström, J.; Olsson, J.; Stenvall, P.; Wallén, B.; Vangeli, P.; Outokumpu Stainless Corrosion Handbook, 9th ed.; Outokumpu Stainless Oy, Sandviken 2004, pp I:8–I:103.

hydrogen ions are able to dissolve into the water more easily than in the higher concentrations since there are minor amounts of water present in the higher concentrations. The ability of sulfuric acid to be either reductive or oxidizing is also affected by the concentration.

3.04.8.9.2 Hydrochloric acid

Hydrochloric acid is one of the most severe mineral acids for stainless steels. Generally, the corrosion resistance in this type of environment increases with increasing alloy content of chromium, molybdenum, and nitrogen. However, stainless steels are only used at low concentrations of this acid and at low temperatures. The isocorrosion diagram, **Figure 28**, shows that the corrosion rate increases rapidly when the steel is exposed to hydrochloric acid. Care must also be taken in chemicals where the risk of hydrochloric acid production is possible.

The beneficial effect from molybdenum as an alloying element in stainless steel can be seen from the results in the isocorrosion diagram, where S32654, containing approximately 7 wt% of molybdenum, performs better than the other stainless steels containing lower amounts of molybdenum. It should also be pointed out that even if a low general corrosion rate is obtained for a stainless steel in hydrochloric acid, there would still be an increased risk of pitting at moderate temperatures, as well as a risk of SCC at higher temperatures. Hydrochloric acid is the most

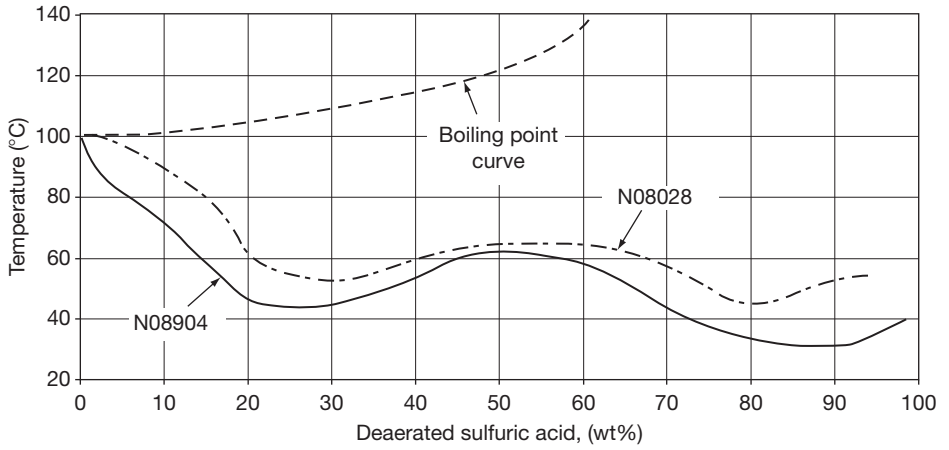

Figure 27 Isocorrosion diagram at 0.1 mm year^{-1} for deaerated sulfuric acid. Reproduced from Alfonsson, E.; Arnvig, P.E.; Bergquist, A.; Ivarsson, B.; Iversen, A.; Leffler, B.; Nordström, J.; Olsson, J.; Stenvall, P.; Wallén, B.; Vangeli, P.; Outokumpu Stainless Corrosion Handbook, 9th ed.; Outokumpu Stainless Oy, Sandviken 2004, pp I:8–I:103.

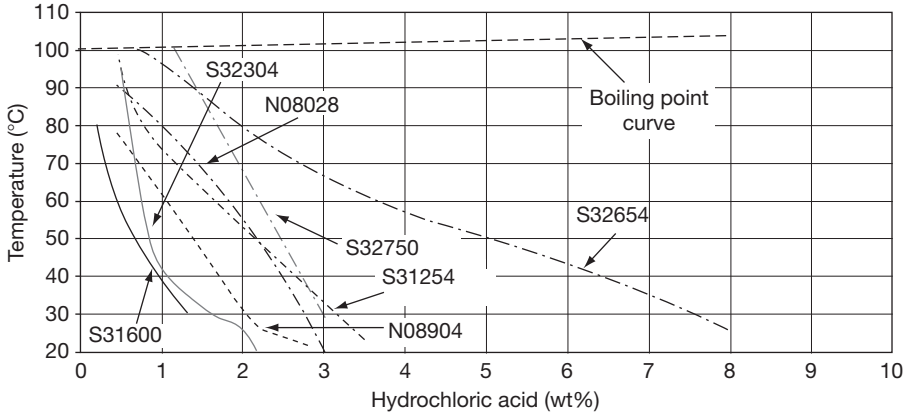

Figure 28 Isocorrosion diagram at 0.1 mm year^{-1} for hydrochloric acid. Reproduced from Alfonsson, E.; Arnvig, P.E.; Bergquist, A.; Ivarsson, B.; Iversen, A.; Leffler, B.; Nordström, J.; Olsson, J.; Stenvall, P.; Wallén, B.; Vangeli, P.; Outokumpu Stainless Corrosion Handbook, 9th ed.; Outokumpu Stainless Oy, Sandviken 2004, pp I:8–I:103.

corrosive mineral acid and when a stainless steel is activated there is little or no chance of repassivation of the material.

3.04.8.9.3 Phosphoric acid

Phosphoric acid is used in many industrial processes and the quality of the acid varies in many cases depending on impurities. If oxidizing chemicals are present, passivity can be obtained, and in pure phosphoric acid, many stainless steel grades are capable of existing without any severe corrosion, as shown in the isocorrosion diagram for pure phosphoric acid (see Figure 29).

Many types of phosphoric acids are used in industrial applications. The common classification of these is wet-process phosphoric acids (WPA) and usually means that the acid contains impurities in combination with phosphoric acid. Some triggers to increased corrosiveness in technical phosphoric acids are fluorides, chlorides, and bromides. Care has to be taken while using phosphoric acids containing chlorides and at increased temperatures. A temperature change of 50–100 °C would cause the corrosion rate to increase more than 10-fold on a typical stainless steel grade such as S31600, even where only low amounts of chlorides are present in the acid. If the chloride content were to increase to values exceeding 500 mg l^{-1} (ppm), even the S31600 grade would be unsuitable due to the high corrosion rate at this temperature range (see Figure 30).

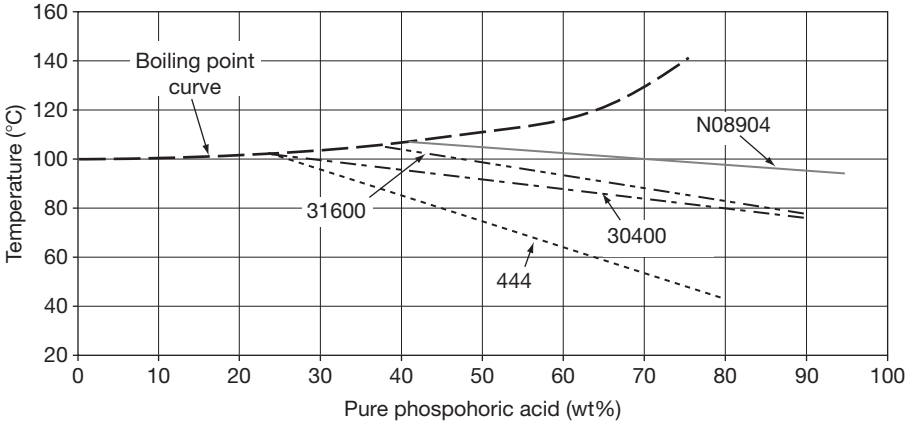

Figure 29 Isocorrosion diagram at 0.1 mm $year^{-1}$ for pure phosphoric acid. Reproduced from Alfonsson, E.; Arnvig, P.E.; Bergquist, A.; Ivarsson, B.; Iversen, A.; Leffler, B.; Nordström, J.; Olsson, J.; Stenvall, P.; Wallén, B.; Vangeli, P.; Outokumpu Stainless Corrosion Handbook, 9th ed.; Outokumpu Stainless Oy, Sandviken 2004, pp I:8–I:103.

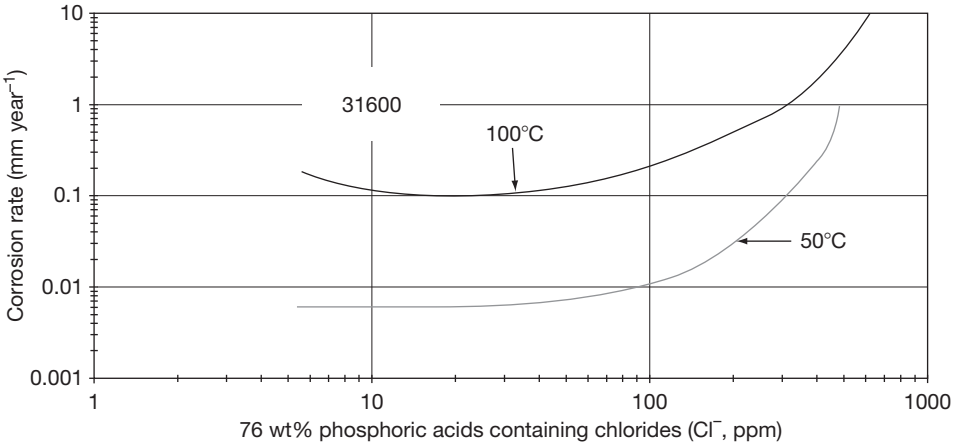

Figure 30 Corrosion rate for the stainless steel grade S31600 in phosphoric acid containing chlorides. Reproduced from Alfonsson, E.; Arnvig, P.E.; Bergquist, A.; Ivarsson, B.; Iversen, A.; Leffler, B.; Nordström, J.; Olsson, J.; Stenvall, P.; Wallén, B.; Vangeli, P.; Outokumpu Stainless Corrosion Handbook, 9th ed.; Outokumpu Stainless Oy, Sandviken 2004, pp I:8–I:103.

Fluorides in phosphoric acids may also have an adverse effect on corrosion resistance if the amounts are too high in combination with temperature increase, see **Figure 31**. The worse conditions, however, are those where there are synergetic effects between chlorides and fluorides in combination with other impurities. In complex WPA that contains different impurities, it is usually advisable to seek additional information and advice from corrosion experts. Examples of WPA can be found in the literature, however, only as examples and in real applications, the amounts of impurities are typically not the same as published.[32]

3.04.8.9.4 Nitric acid

Nitric acid is generally a passivation acid for common austenitic and duplex stainless steels containing 18 wt% chromium at concentrations of 20 wt% and below 100 °C. It is used for cleaning and passivation after any alterations in the stainless steel surfaces in different applications. Nitric acid is also one of the chemicals in pickling acids used in the manufacturing of stainless steels. The use of the stainless steel grade S30400 in nitric acid of different concentrations up to 60 wt% and below 100 °C is widely adopted. Even ferritic grades containing 13 wt% chromium are resistant to corrosion in nitric acid at concentrations of 20–60 wt% below 40 °C.[32] However, in hot nitric acid there is a risk of intergranular corrosion in most stainless steel grades due to the oxidizing power of the solution. Sedrik reviewed that high silicon alloys have been used for service in concentrated nitric acid solutions and the stainless steel grade 310L has been used for very hot concentrated nitric acid.[34]

3.04.8.9.5 Organic acids

Most organic acids are less aggressive than the mineral acids. However, formic acid is one exception, as this is aggressive to S30400 at intermediate temperatures and concentrations. The temperature plays a significant role in determining the corrosiveness of formic acid and at intermediate concentrations ranging from 25–85 wt% in combination with a high temperature, that is, 100 °C, most stainless steels corrode. However, at lower temperatures, most of the stainless steels containing higher amounts of chromium, nitrogen, and molybdenum are resistant to corrosion in formic acid, see **Figure 32**. Other organic acids such as acetic and lactic acid are less corrosive and the stainless steel grades S30400 and S31600 are resistant to corrosion at most temperatures and concentrations. However, the stainless steel grades S30400 and S31600 corrode at higher temperatures and concentrations close to boiling point in lactic acid solutions, so higher-alloyed stainless steel must be used in such service environments. In acetic acid, S30400 is prone to corrosion at temperatures above 90 °C at concentrations above 10 wt% and even to localized corrosion above 70 °C at concentrations above 80 wt%. There are many organic chemicals in pure conditions, many of which are not at all corrosive to stainless steels such as S30400 and S31600. Some examples are fatty acids, such as oleic acid, stearic acid

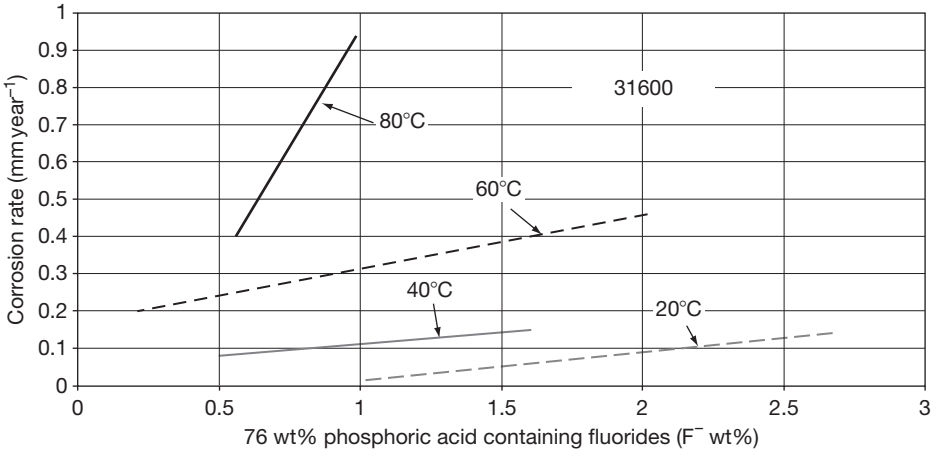

Figure 31 Corrosion rate for the stainless steel grade S31600 in phosphoric acid containing fluorides. Reproduced from Alfonsson, E.; Arnvig, P.E.; Bergquist, A.; Ivarsson, B.; Iversen, A.; Leffler, B.; Nordström, J.; Olsson, J.; Stenvall, P.; Wallén, B.; Vangeli, P.; Outokumpu Stainless Corrosion Handbook, 9th ed.; Outokumpu Stainless Oy, Sandviken 2004, pp I:8–I:103.

or ethanol. The S31600 grade can also cope with most concentrations and temperatures of citric acid.

Oxalic acid has two organic acid functional groups and can release two protons per molecule. This acid is more corrosive for standard stainless steel grades such as S30400 and S31600 and is further highly corrosive to titanium, see **Figure 33**.

3.04.8.9.6 Alkaline solutions

Stainless steels such as S30400 and S31600 are highly resistant in alkaline environments such as sodium hydroxide and potassium hydroxide at lower and intermediate temperatures at all concentrations, see **Figure 34**. The tolerance to chloride contamination in sodium and potassium hydroxide is also much higher compared with neutral water solutions. Uniform corrosion tests have shown that resistance was obtained in solutions containing 1–20 wt% sodium chloride in 40 wt% sodium hydroxide solution using activation and at a temperature as high as 80 °C.[32] However, at high temperatures above 115 °C and at intermediate concentrations above 20 and 70 wt%, stainless steels are prone to SCC in sodium and potassium hydroxide.

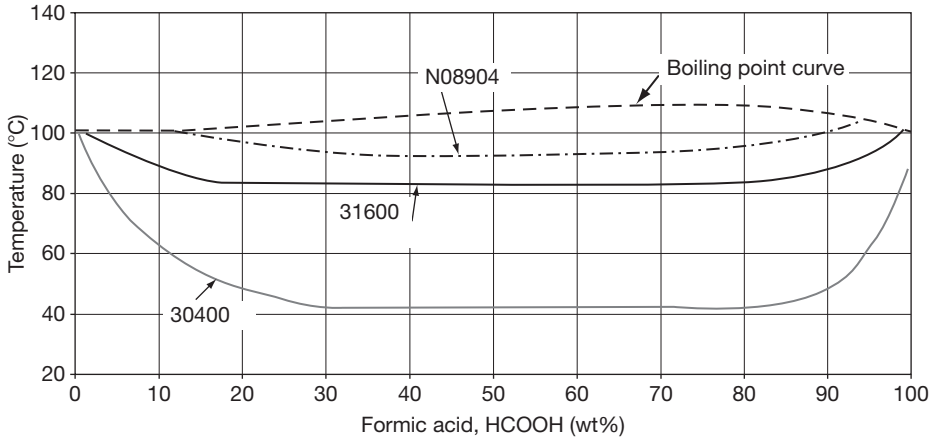

Figure 32 Isocorrosion diagram at 0.1 mm year^{-1} for formic acid. Reproduced from Alfonsson, E.; Arnvig, P.E.; Bergquist, A.; Ivarsson, B.; Iversen, A.; Leffler, B.; Nordström, J.; Olsson, J.; Stenvall, P.; Wallén, B.; Vangeli, P.; Outokumpu Stainless Corrosion Handbook, 9th ed.; Outokumpu Stainless Oy, Sandviken 2004, pp I:8–I:103.

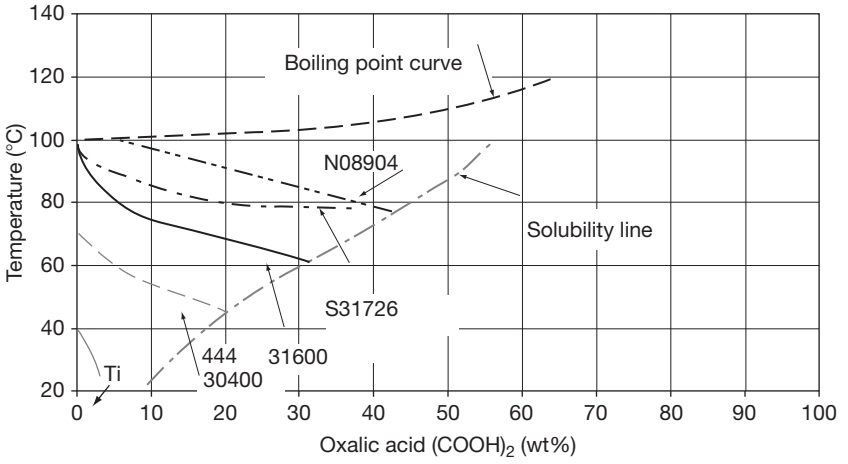

Figure 33 Isocorrosion diagram at 0.1 mm year^{-1} for pure oxalic acid. Reproduced from Alfonsson, E.; Arnvig, P.E.; Bergquist, A.; Ivarsson, B.; Iversen, A.; Leffler, B.; Nordström, J.; Olsson, J.; Stenvall, P.; Wallén, B.; Vangeli, P.; Outokumpu Stainless Corrosion Handbook, 9th ed.; Outokumpu Stainless Oy, Sandviken 2004, pp I:8–I:103.

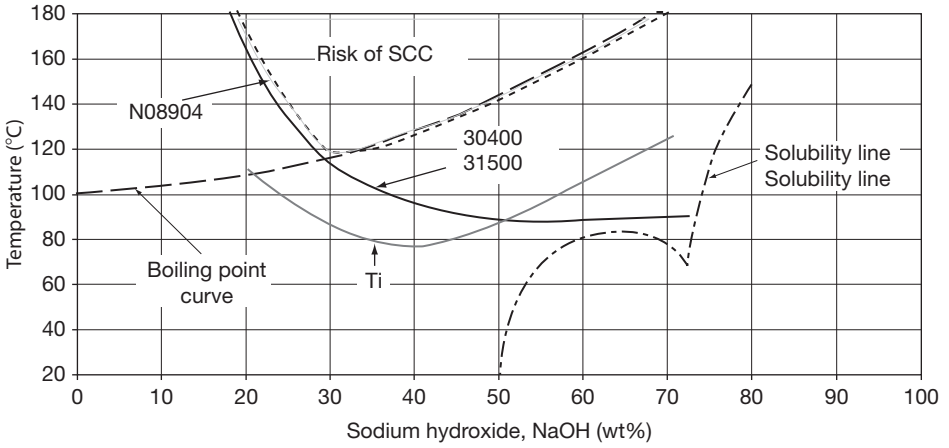

Figure 34 Isocorrosion diagram at 0.1 mm year^{-1} for sodium hydroxide. Reproduced from Alfonsson, E.; Arnvig, P.E.; Bergquist, A.; Ivarsson, B.; Iversen, A.; Leffler, B.; Nordström, J.; Olsson, J.; Stenvall, P.; Wallén, B.; Vangeli, P.; Outokumpu Stainless Corrosion Handbook, 9th ed.; Outokumpu Stainless Oy, Sandviken 2004, pp I:8–I:103.

3.04.8.10 Galvanic Corrosion

Galvanic corrosion may occur when two dissimilar metals are in electrical contact in a conductive solution, an electrolyte. The corrosion rate is dependent on the conductivity of the electrolyte, on the difference in the galvanic series between the metals and also on the surface ratio between the metals. The position of a metal in the galvanic series, at a specific temperature, in a specific electrolyte can be represented as the corrosion potential of the metal, E_{corr} or open circuit potential, OCP. For example, in seawater at 10 °C, passive stainless steel is a more noble metal and has a higher corrosion potential in the galvanic series than the less noble mild steel. If a stainless steel construction is in conductive electrical contact with a less noble metal, the less noble metal will corrode at a higher corrosion rate. Furthermore, if the less noble metal has a small surface ratio compared with the more noble metal, the corrosion rate will increase even more.

Two different stainless steel grades in the passive state, coupled in an electrolyte, are quite close in the galvanic series and the risk of galvanic corrosion is less as long as the stainless steels remain in the passive state. If the passivity of one of the steel grades breaks down and corrosion occurs, the corrosion potential thus changes to the stainless steel active corrosion potential and the corrosion rate is influenced by this change between the two materials. Knowledge about the series in the specific environment is necessary to predict galvanic corrosion. The corrosion potential for a stainless steel can vary as the pH level of the solution changes and if oxidizing or reductive chemicals are present in the solution.

In summary, the following circumstances influence the extent of galvanic corrosion:

- The relative area between the dissimilar metals. A smaller area of the less noble metal suffers from more aggressive corrosion attack. This relation is often referred to as a small anode to a large cathode.
- The magnitude in variation of nobility of the metals. The higher the potential difference between the dissimilar metals in the galvanic series, the higher the galvanic corrosion rates under wet conductive conditions. The solution's electrical conductivity. The worse leading ability of a solution contribute to limited corrosion attack close to the contact area between the two dissimilar metals.
- The corrosion rate of galvanic corrosion is further decreased by the decrease in temperature of the electrolyte.
- The solution's electrical conductivity. A high conductivity, that is, a high leading ability of a solution contributes to increased electron flow from the corrosion reactions and thereby a higher corrosion rate at the contact area between the two dissimilar metals.
- The rate of galvanic corrosion may be decreased by a reduction in the temperature of the electrolyte.

All passive stainless steels are relatively high up in electrochemical potential, compared with other material, whereas, for example, zinc is relatively low down in potential in the galvanic series, see **Figure 35**.

There are several ways of preventing galvanic corrosion. Painting operations prevent the electrolyte from reaching the contact area. The use of wax or adhesives in narrow crevices prevents the electrolyte from reaching any contact area and thus prevents corrosion. The use of electrochemical knowledge between metals in construction can also prevent the occurrence of galvanic corrosion as well as being used in corrosion protection.

The risk of galvanic corrosion is severe in seawater applications. To predict the risk of galvanic corrosion the comparison of the different corrosion potentials can be utilized. The larger the difference the greater the risk of attack of the less noble component.

3.04.8.11 Intergranular Corrosion

Intergranular corrosion occurs as the name indicates along grain boundaries on. This corrosion form is sensitive to high carbon contents in the stainless steel and occurs if chromium carbides are precipitated in between the grains. Precipitation reactions in stainless steels can be read about in Section 3.04.5. A stainless steel, which was heat-treated to conditions for grain boundary precipitations to occur, is referred to as sensitized. Other circumstances for intergranular corrosion to occur are when carbon is diffusing into the surface layer of the solid stainless steel as in carburization. If the stainless steel components are heat treated with oil, plastic tape or other organic substances on the surface or in atmosphere containing carbon monoxide or hydrocarbons there is a risk of carburization and intergranular corrosion as a result.[32] More about carburization can be read in Section 3.04.5.4.

Intergranular corrosion occurs in solutions where the grain boundaries of chromium carbide are activated and the rest of the material is in a passive condition, which means under strong oxidizing conditions. But it should also be pointed out that a sensitized stainless steel is vulnerable to other forms of corrosion as pitting, crevice corrosion, and SCC.

Measures to increase the resistance of stainless steels to intergranular corrosion caused by chromium carbide precipitations are to perform solution annealing or lowering the carbon content by stabilizing with titanium and niobium.

The addition of titanium or niobium to the steel, so-called stabilization, means that the carbon is bound as titanium or niobium carbides. Since titanium and niobium have a greater tendency to combine with carbon than chromium, this means that carbon is not available to form chromium carbides. The risk of intergranular corrosion is therefore appreciably reduced. There is, however, a disadvantage associated with stabilization. In the area closest to a weld, the temperature during welding can be so high that titanium or niobium carbides are dissolved. There is then a danger that they do not have time to re-precipitate before the material has cooled sufficiently to allow the formation of chromium carbides in the grain boundaries. This leads to so-called knife line attack in which a narrow zone of material very close to the weld suffers intergranular corrosion. Since the carbon level in stabilized steels is often quite high (0.05–0.08 wt%) this can give serious attack.

Nevertheless, a low carbon content in the stainless steel extends the time required for sensitization to occur and modern steel manufacturing methods enable lower carbon contents to provide a considerable decrease of the risk of intergranular corrosion to occur.

The effect of a decrease in the carbon content is most easily illustrated by a time–temperature-sensitization, TTS-diagram, an example of which is shown in Figure 36. The curves in the diagram show the longest time an austenitic steel of type 18Cr–8Ni can be maintained at a given temperature before there is a danger of corrosion. This means that for

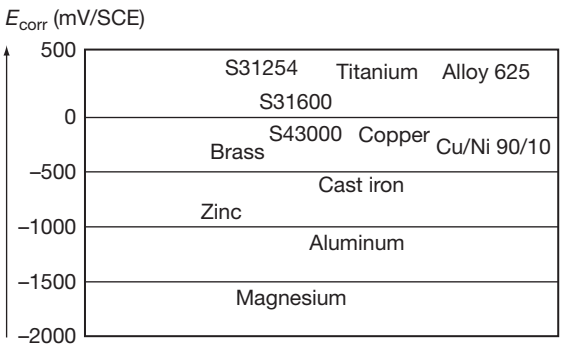

Figure 35 The corrosion potential, E_{corr} of stainless steels in flowing seawater at 10°C.[32,39]

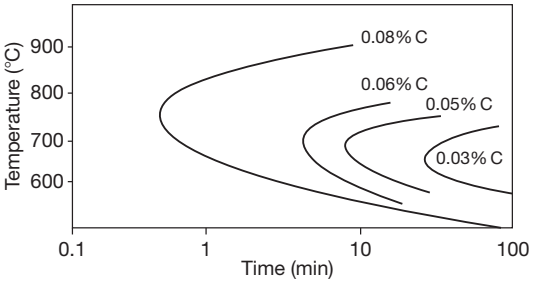

Figure 36 TTS diagram for S30400 steels with different carbon contents. The curves are based on the Strauss test.[40]

standard low-carbon austenitic steels (L-grades) the risk of intergranular corrosion cracking is, from a practical point of view, eliminated. All high-alloyed austenitic and all duplex grades intended for aqueous corrosion service have carbon contents below 0.03 wt % and are consequently 'L-grades.' Due to the low solubility of carbon in ferrite, the carbon content will have to be extremely low in ferritic stainless steels if the risk of intergranular corrosion is to be eliminated. In ferritic stainless steels, stabilizing element and extra low carbon contents are often used to eliminate the risk of intergranular attack after welding or other potentially sensitizing treatments.

The stainless steels are usually delivered in the solution-annealed conditions which is a heating process causing the chromium carbides to dissolve, followed by rapid cooling. Such an operation leaves the carbon in solid solution in the steel. Even if a sensitized structure occurs, solution annealing recovers the stainless steel microstructure.

3.04.8.12 Erosion Corrosion

In construction systems where a flow of the solution is a part of the process, a sufficiently high rate to avoid deposits or marine growth is of preference. The mechanical impact from a flowing solution in combination of corrosion reaction might raise the risk of erosion corrosion in tubular systems. However, stainless steels commonly provide high tolerance against erosion corrosion in neutral chloride solutions and an optimum of flow rate avoiding erosion corrosion but mitigate deposits beneficial for both corrosion performance and economics of operation.

Erosion corrosion is a form of corrosion, which occurs at high relative metal–liquid velocities. This form of corrosion includes a mechanical wear of corrosion products. In a solution containing solid particles, for example, sand, the corrosion rate is higher. Stainless steels can be attacked if the composition of the steel grade provides unstable passivity in an aggressive solution. Attacks can occur on, for example, pump impellers. The resistance of stainless steels to erosion corrosion is generally increased by the same alloying elements as those, which increase resistance to general corrosion in the solution in question.[40]

3.04.8.13 Common Test Procedures and Standards for Stainless Steels

The most reliable test method for stainless steel's performance in an environment is the field-testing procedure. A number of stainless steel grades are then tested in the service environment for a long period of time, a year or longer. However, there are a number of good test methods for ranking purposes of different stainless steel grades and also in some cases used for control purposes of the steel grades. Below are some of the most common test methods presented, used in the laboratory for research purposes and also for the screening of different stainless steel grades. The test methods are commonly based on the type of corrosion expected to occur.

Laboratory methods offer the most efficient way of ranking different stainless steel grades and their resistance to pitting and crevice corrosion. However, care has to be taken while using laboratory results in real environments, and field tests should, in some cases, be carried out to provide information about the optimum stainless steel grade to use. Laboratory tests can, nevertheless, still be very informative since some of the parameters that have the greatest influence on the corrosion properties of stainless steels may be used to simulate the most aggressive conditions, such as the amount of chlorides, temperature, pH levels, type of acid, any oxidizing chemicals, etc. Advice on material selection can then be formulated on the basis of these results.

3.04.8.14 Localized Corrosion Testing of Stainless Steels using Electrochemical Methods

The most common electrochemical method currently used to demonstrate the passivity and corrosion of standard alloy stainless steels in different solutions is to perform polarization measurements. **Figure 37** shows a schematic polarization curve for a stainless steel suffering from pitting corrosion at anodic potentials where the electrochemical response of active corrosion is a high current density.

The characteristic of pitting and crevice corrosion is the breakdown of the passive film, represented in polarization measurements by the pitting potential, E_p. The pitting potential can be defined as the potential at which the current density exceeds 100 $\mu A\ cm^{-2}$ for more than a minute. The most common polarization measurements show typically spikes in the current density before the breakdown to corrosion, which are referred to as metastable pitting corrosion.

Both the pitting potential E_{pr} and the repassivation potential, E_r are dependent on the scan rate. A higher scan rate will influence the chemical equilibrium reactions at the metal surface. If the scan rate is too high the pitting potential increases and the

repassivation potential, E_r, will typically decrease.[15] The effect of too high a scan rate is independent of the steel grade.[41]

The distinction between localized corrosion, such as pitting and crevice corrosion, and transpassive corrosion in the polarization measurements, is shown by the slope in the polarization measurements in the higher potential area, shown in Figure 38. In the case of pitting the increase in current density is much steeper than in the case of transpassive corrosion. Even more pronounced is the difference in the repassivation potential, where in transpassive corrosion this is closer to the transpassive potential, E_{tr} than for pitting corrosion.

Figure 38 shows the polarization measurements illustrating transpassive corrosion at higher anodic potentials.

Comparing the pitting potentials, in solutions containing sufficient amounts of sodium chloride can successfully provide a ranking of the standard stainless steel grades S30400, S31600 and low alloy stainless steel grades. However, the test temperature in combination with the aggressiveness of the solution must exceed the critical pitting temperature (CPT) of the tested steel grade for pitting corrosion to occur.

3.04.8.15 Different Stainless Steel Grades and their Resistance to Pitting and Crevice Corrosion

Two common methods for determining the critical pitting temperature, CPT, are prescribed in ASTM G 150 and ASTM G 48. The former is an electrochemical method that uses a set potential at 700 mV/

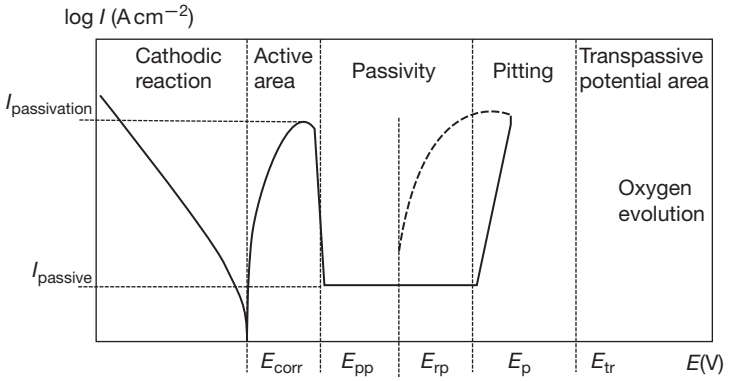

Figure 37 Schematic polarization diagram of pitting potential, E_p and repassivation potential, E_r in a solution containing chlorides.

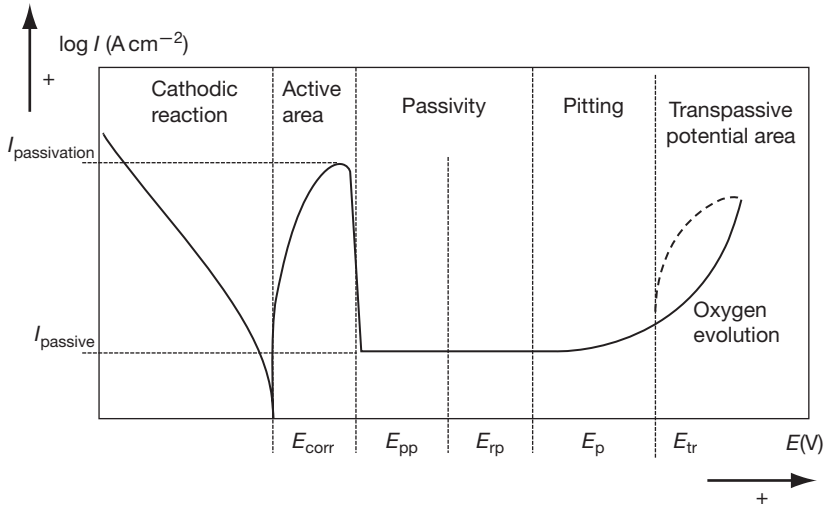

Figure 38 Polarization measurements illustrating transpassive corrosion.

SCE in 1 M NaCl as the electrolyte and then screens the temperature from 0°C to the CPT where pitting corrosion of the steel grade propagates in a crevice-free electrochemical cell. This method provides a different CPT than ASTM G 48, which is an immersion test for 24 h in a 6% $FeCl_3$ solution that produces an oxidizing effect from the chemical solution instead of from a potentiostate. The temperature is then increased in intervals of 2.5°C until pitting corrosion occurs. Both methods show similar ranking properties with regard to the resistance to pitting corrosion among stainless steel grades, but ASTM G 150 offers better reproducibility than ASTM G 48. **Figure 39** shows critical pitting temperatures for higher-alloyed stainless steel grades according to ASTM G150 and **Figure 40** shows CPT according to ASTM G 48. It should be pointed out that these values do not represent exact values for each steel grade but may deviate due to effects from corrosion kinetics for various surfaces, welding or other mechanical treatments, etc.

The drawback of these methods is that it is extremely difficult to measure lower-alloyed stainless steels, such as 12% chromium ferritic stainless steels or austenitic S30400 (1.4301) grades, due to the aggressiveness of the methods. Both environments cause these types of stainless steel grades to corrode almost immediately when exposed. Today, pitting potentials are typically used for ranking lower-alloyed stainless steels in solutions with different chloride contents. For comparison, pitting potentials are presented for some standard stainless grades, S30400 (1.4301) and S31600 (1.4401), in **Figure 41**.

There are several standardized methods for measuring stainless steels' susceptibility to crevice corrosion. One concept is to measure the critical crevice temperature CCT, using standard crevice formers of the MTI-2 type in a ferric chloride solution, according to a modified ASTM G 48 method, which is very aggressive to crevice corrosion in stainless steels due to the combination of acidity and oxidizing power. The higher-alloyed, more resistant stainless steel grades provide a higher CCT than the lower-alloyed stainless steels, but this method also has the disadvantage of being too aggressive for the lowest-alloyed stainless steel grades, such as the 12% ferritic stainless steels and S30400. This measure is similar to the CPT measurements only if used for ranking purposes and do not really provide data about the actual service environment. **Figure 42** presents some CCT values for higher-alloyed stainless steels. In testing crevice corrosion resistance of stainless steels a crevice former is used. Depending on the type of crevice former different results can be obtained. It can, in many real environments, be very difficult to translate the type of crevice to the laboratory since crevice corrosion is dependent on the pressure from the crevice former, the ability to drainage the solution out from the crevice and also the crevice area. Generally

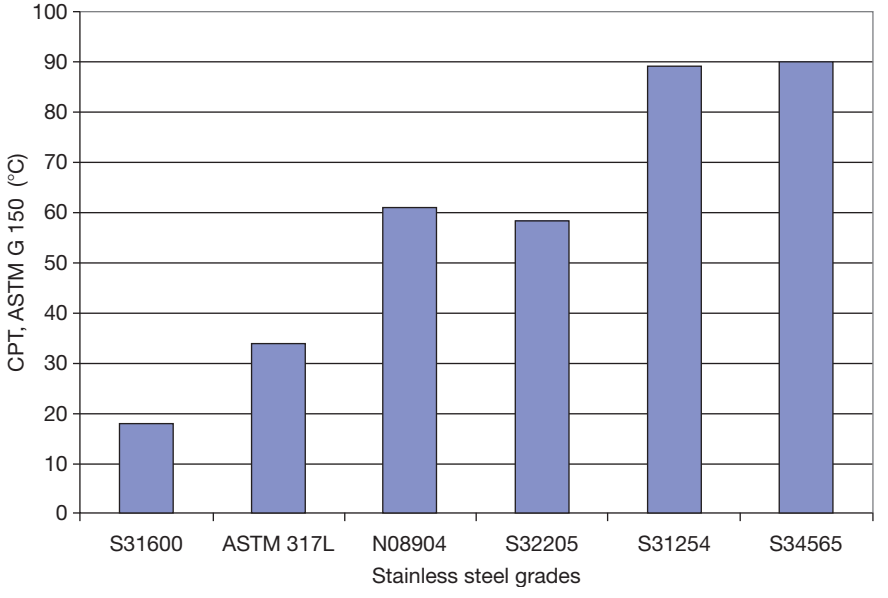

Figure 39 CPT according to ASTM G 150; some examples of single measurements for surface 320 grit, for higher alloyed stainless steels.

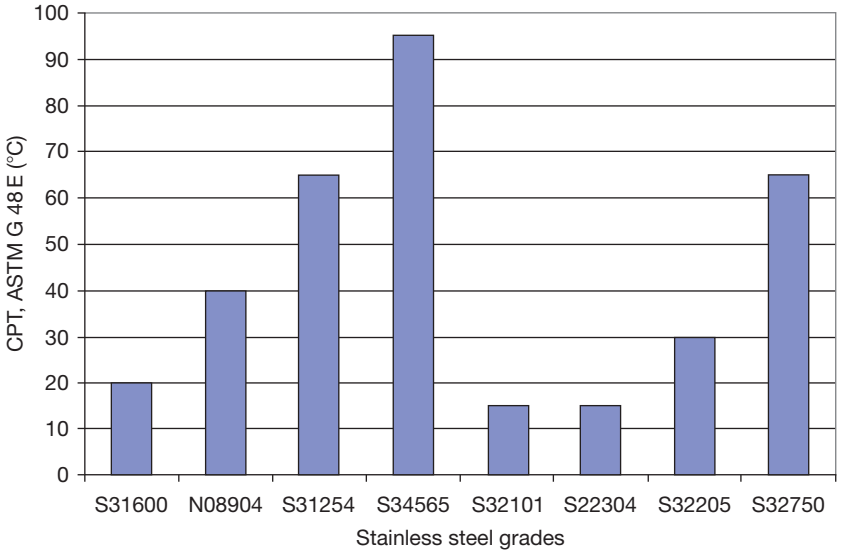

Figure 40 CPT according to ASTM G 48E for some stainless steels.

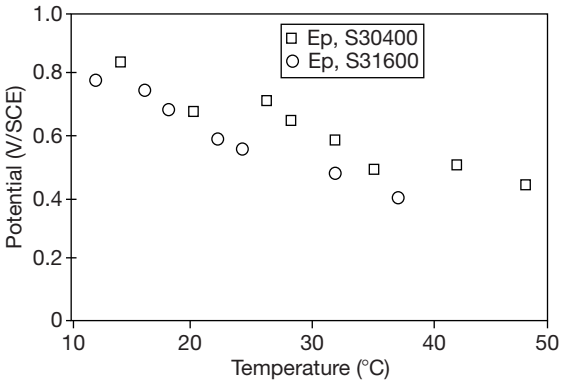

Figure 41 Pitting potentials, E_p, for some standard stainless steels, S30400 and S31600, at different temperatures in 0.1 M NaCl. Scan rate 20 mV min^{-1} and defined at 100 μA cm^{-2}.

standardized types of crevices are used for comparison of laboratory purposes. Figure 43 shows an example of a crevice former of MTI type with heals.

3.04.8.16 Screening of General Corrosion Properties of Stainless Steel Grades

One frequently used method to screen a stainless steel grade for many acids and to use for ranking purposes is ASTM G 157-98. The original test method was developed by MTI that has issued a number of strictly specified laboratory tests, which facilitate direct comparison between stainless steel grades. Control alloys supplied by MTI are included in the tests. The stainless steel is considered to be passive and unaffected by corrosion when the corrosion rate is lower than 0.127 mm $year^{-1}$ (5 mpy) and in ASTM G157-98 the lowest temperature at this measure is referred to as the critical temperature T_c.

A screening of the different stainless steel grades shows a clear influence of the alloy composition on the uniform corrosion properties. The super austenitic stainless steel grades S32654, S31254, and N08904 and the super duplex stainless steel grades S32750 and S32205 provide much better resistance to general corrosion compared with the standard grades of type S30400 and S31600, as can be seen in Figure 44.

3.04.8.17 Testing Stress Corrosion Cracking of Stainless Steels in Environments Containing Hydrogen Sulfide Under Acidic Conditions

Tests are adopted for material selection in environments containing hydrogen sulfide under acid conditions. The most internationally prevalent standardized method used for testing in these environments is NACE TM 0177, which employs a 5% NaCl + 0.5% CH_3COOH solution, saturated with H_2S by continuous bubbling after nitrogen de-aeration and a pH of 2.7–2.8. The test specimens are immersed in acidified solutions by the addition of acetic acid

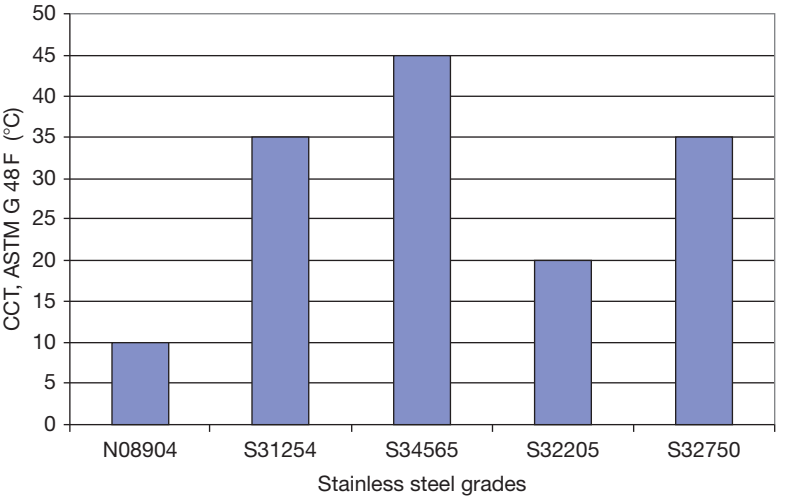

Figure 42 CCT for higher alloyed stainless steel grades.

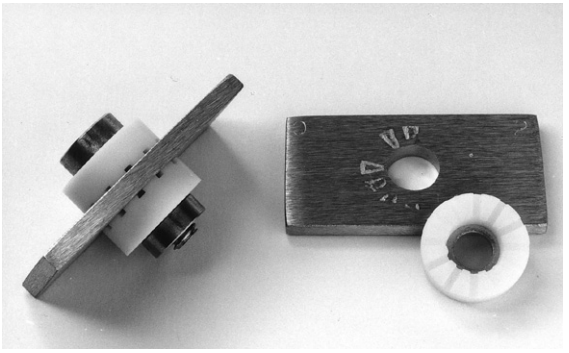

Figure 43 Example of a MTI crevice former with heales.

containing sodium chloride, which is saturated with hydrogen sulfide at room temperature prior to the test. The solution is also deaerated with nitrogen gas. Some test results obtained for duplex stainless steels tested according to NACE TM 0177 for 720 h are presented in Table 10. Material selections based on this standardized method are included in NACE MR-0175.

3.04.8.18 Laboratory Tests of SCC

Several methods can be used to test resistance to SCC. However, it can be very difficult to translate

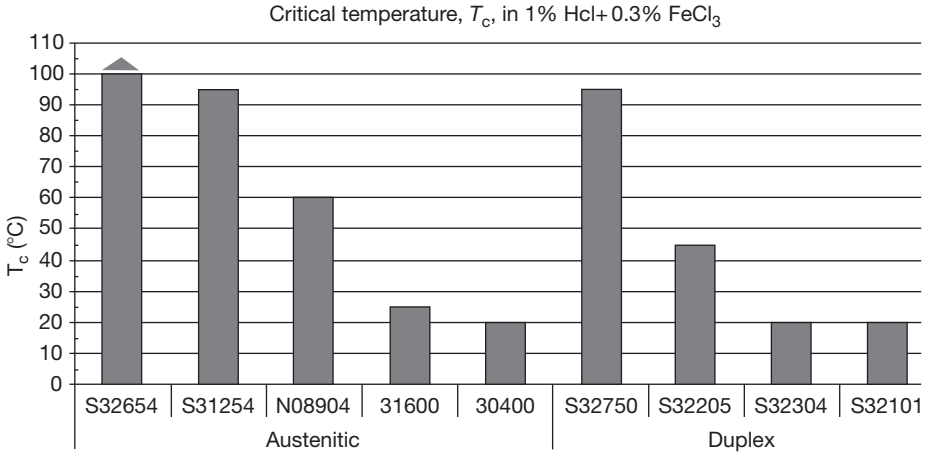

Figure 44 Critical temperatures, T_c, at 0.127 mm $year^{-1}$ for different stainless steel grades in 1% hydrochloric acid containing 0.3% $FeCl_3$ additions.

the results of many of these more or less accelerated tests to reflect performance in an actual service environment, particularly in terms of the tensile stresses that can occur in the material. U-bent samples are used for many tests but can lose the introduced stress level in the test sample by test time. Nevertheless, the practice of ranking the results for different stainless steels can, in combination with experience, provide valuable data for the material selection process. One test method used for testing evaporative conditions is the 'Wick-test,' ASTM G-692-71, which was developed to simulate evaporative conditions at ~100 °C in an insulation material wetted with dilute chloride solution. The results obtained from this test for different stainless steel grades after 600 h of exposure are presented in Table 11.

Austenitic stainless steels seems much more prone to SCC in this test compared with the duplex corresponding duplex stainless steel grades.

3.04.9 Stainless Steels in Natural Wet Environments

Experience has shown that natural water is considerably more corrosive for stainless steel than artificial water. Nevertheless, to understand the interactions between metal surfaces and microbial life in water, in terms of degradation and corrosion, a multidisciplinary view has to be adopted and there are several definitions used in the field of investigation of the interactions between microbial life and materials resulting in corrosion and/or deterioration of materials.

Microbially influenced corrosion (MIC) can be referred to as the influence of microorganisms on the kinetics of corrosion processes of metals, caused by microorganisms adhering to the interfaces. A prerequisite for MIC is the presence of microorganisms.

3.04.9.1 Microbially Influenced Corrosion

MIC on stainless steels in natural water is commonly related to an attached biofilm growth on a stainless steel surface. If the conditions favor microbial activity in the water, one of the effects of the adhesion of a biofilm to the stainless steel surface is ennoblement of the open circuit potential OCP or corrosion potential E_{corr}. The increase in the potential may cause localized corrosion on stainless steel if it reaches a value exceeding the pitting potential of the steel grade. Cases of MIC on stainless steels have been reported for alloys with relatively low molybdenum content as localized corrosion and deposits were often found at or close to the corrosion sites.[41]

Figure 45 shows typical ennoblement on stainless steels S30400 (1.4301) and S31600 (1.4401) in a natural water containing microorganisms.

Parameters that influence microbial activity on metal surfaces are considered to be:

- temperature
- availability of nutrients

Table 10 Some test results obtained for duplex stainless steels tested according to NACE TM 0177 for 720 h

Material	*H_2S (bar)*	*Load (% $R_{p0.2}$)*		
		70	*95*	*100*
S32205	0.01	No cracking	Not tested	No cracking
S32205	0.1	SCC	Not tested	SCC
S32750, welded tube	0.1	Not tested	No cracking	Not tested
S31254	1	No cracking	Not tested	No cracking

Table 11 Results from the Wick-test, ASTM G-692-71 for some duplex and austenitic stainless steels after 600 h

Microstructure	*Material*	*Number of tested specimens*	*Failed due to SCC*	*PRE*
Duplex	S32101	6	0	26
	S32304	6	0	23
	S32205	2	0	35
	S31803	4	1	35
Austenitic	S30400	5	5	17.5
	S31603	4	4	24
	N08904	4	1	36
	S31254	3	0	43

- flow velocity
- pH
- oxygen level
- cleanliness
- toxic effects from chemicals

Biofilms may grow under favorable conditions to such proportions that they can be regarded as deposits and the risk of under deposit corrosion or crevice corrosion increases with the density of the deposits.

From early investigations by Mollica and Trevis of stainless steels immersed in seawater, an increase of the open circuit potential or corrosion potential, to high values ranging from 350 to 450 mV/SCE was observed and attributed to the formation of a biofilm on stainless steel surfaces.[42] These values were also reported by many other investigations and the results appeared to be similar and independent of geographical location or hydrological properties, but sensitive to temperature changes. Mollica and Trevis attributed the ennoblement to an increased rate of the cathodic reaction, which has an effect on the corrosion rate in the propagation stage. Feron investigated the temperature effect and the ennobled potential fell above 40 °C.[43]

Another explanation for the mechanism of ennoblement is the action of manganese oxidizing bacteria. Tverberg, Pinnow, and Redmerski reported manganese-rich deposits in combination with corrosion in standard stainless steel grades.[44]

While evaluating and predicting MIC in stainless steels, several parameters that influence local corrosion have to be considered. The ennoblement from active microorganisms increases the risk of exceeding the pitting potential of the passive layer. However, the pitting potential is dependent on factors such as the alloying elements used in the steel grade, welding procedures, chloride content, nitrate content, and deposits. In addition, while considering the risk of MIC in water passing through different industrial water systems, one must also take into account the fact that the water quality varies with respect to factors such as oxygen content and chloride content.

3.04.9.1.1 Chlorination

The conventional way to prevent biofouling or to reduce its effects is to chlorinate the water. This is normally done by continuously or intermittently, adding a strong hypochlorite solution. High chlorine concentrations may increase the corrosivity of water due to the oxidizing effect imposed on the stainless steel. For this reason, the chlorine addition should be restricted to a minimum. The addition of free chlorine in quantities as low as 0.1 mg l^{-1} is just sufficient to prevent the formation of an active biofilm but not enough to increase the potential.

Figure 46 shows an example of the time dependence of the open circuit potential on addition of sodium hypochlorite for stainless steel grade S32205 (1.4462). The efficiency of the hypochlorite addition releasing chlorine in this case is approximately ~14%.

By intermittent chlorination, high potentials are reached during a short chlorination period. After chlorination, the potentials decrease to low values

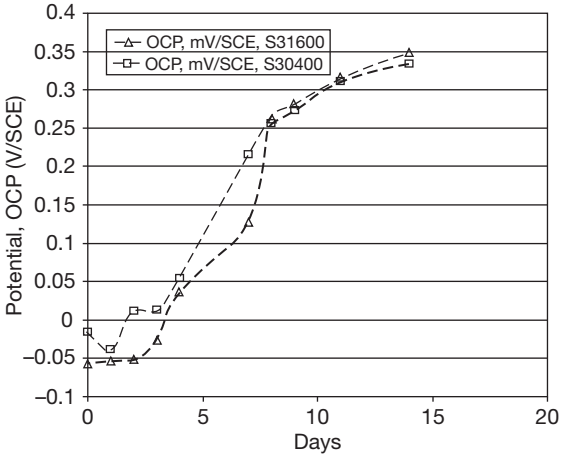

Figure 45 Ennoblement of the open circuit potential (OCP) on stainless steel in natural water containing microorganisms.

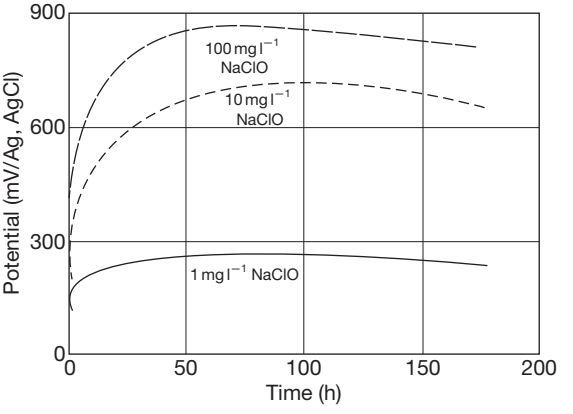

Figure 46 Time dependence of the open circuit potential for S32205 at different additions of sodium hypochlorite (NaClO) in 1000 mg l^{-1} chloride solution. Reproduced from Tverberg, J.; Pinnow, K.; Redmerski, L. NACE Corrosion, Paper 151, April 23–27, Nevada, 1990.

similar to sterile chloride solutions, before the next chlorination period. If the interval between two chlorination periods is very long, an active biofilm will be formed and the potentials will increase once again after a couple of weeks.

The risk of crevice corrosion initiation is increased by the chlorination but the propagation rate of the crevice attack is reduced if intermittent chlorination is used. Crevice corrosion on type S31600 (1.4401) specimens exposed to, for example, nonchlorinated and chlorinated seawater showed the strongest attack in the nonchlorinated water while intermittent chlorination causes only a minor shallow attack.[32]

3.04.9.2 River Waters and Freshwater

3.04.9.2.1 Drinking water[32]

Drinking water may seem a relatively harmless environment from a corrosion point of view, and the common austenitic stainless steels, that is, S30400 (1.4301), S31600 (1.4401), and similar grades are suitable for most equipment used in the production and distribution of potable water, but may in rare circumstances suffer corrosion. Standard grade stainless steels such as S30400 and S31600 are widely used in the manufacture of vessels, piping, and heat exchanger tubing for handling all kinds of freshwater. Four primary environmental parameters must be defined for the serviceability of S30400 and S31600 in freshwater. These are the chloride content of the water, the presence of oxygen or any other strong oxidant, the temperature, and the presence of crevices. If one or more of these environmental parameters exceeds these empirical limits, the possibility of localized corrosion is introduced. In most countries, the chloride concentration is limited in potable water, often to a maximum of 0.250–0.300 g l^{-1}. However, chemicals added at various stages in the water plant may contain chlorides, with the result that higher chloride concentrations than those specified for drinking water may occur close to the dosage points of such chemicals.

The corrosiveness of the water increases as its temperature rises. Most countries require the temperature of drinking water to be less than 25 °C. In consumer applications, stainless steels may also be used in water heaters and hot water tubing, where the water temperature usually exceeds 60 °C. In hot water systems, heat transfer may occur through the wall of a tube or a vessel. In such situations, the corrosion risk will also be influenced by the direction of the heat flux. In systems handling hot water, the risk of SCC must sometimes be considered. In the case of a hot water tube, where the heat flux direction is from the water to the tube wall, the maximum temperature of the stainless steel wall will be that of the water. For the outside of the tube, there should be no risk of corrosion as long as the surface is dry or just wetted by water without chlorides. However, if the outside is welled by water containing an appreciable amount of chloride ions, evaporation of the water may result in a concentrated solution that promotes pitting and crevice corrosion that, in turn, may act as starting points for SCC. Examples of this situation are water leaking through a chloride containing thermal isolation, or water leaking to the surface of a tube embedded in wall plaster containing a chloride-rich antifreeze agent. The 1.4301 grade (S30400) is sensitive to this type of SCC even after a short wet period whereas type 1.4401 (31600) can tolerate such conditions for a longer period than 1.4301 (30400). However, if the wall temperature is less than 50 °C, SCC is not likely to occur in ordinary drinking water systems. Duplex stainless steels such as 1.4361 (S32304) and 2205 (S32205) offer better resistance to SCC than the 1.4301 and 1.4401 grades and should be considered for hot water tubing that might be subject to welling from the outside.

Several oxidizing chemicals may be added at a water treatment plant and in the distribution system, for example, potassium permanganate for the precipitation of metal ions, iron (III) ions for coagulation, and various chlorine compounds and ozone for disinfection purposes. In the presence of strong oxidants, the corrosion potential of the steel will be polarized in the positive anodic direction and the pitting or crevice corrosion potential may be exceeded. Accordingly, there may be a greater risk of localized corrosion attack close to the points where oxidants are added to the water.

3.04.9.2.2 Freshwater

Freshwaters such as lakes and rivers contain much less amounts of chlorides compared with seawater. The material choice of stainless steels relies, in many cases, on the chemical analysis of the water and the temperature. For example, the stainless steel grade chosen should rely on the chloride content of the water but in some cases there are beneficial effects of, for example, sulfates and nitrates solved in the water. However, no systematic studies are available on how beneficial those effects are but in some cases tentative engineering diagrams are used for the determination of a useful stainless steel. There are, however, circumstances when unexpected pitting

or crevice corrosion occurs in freshwater systems and experiences from real systems can be a guide to material advice. One example of tentative engineering diagrams is presented in Figure 47. A significant decrease in the tolerance to chlorides and temperatures is seen from the tentative engineering diagram when crevice corrosion is a risk compared with a base material without any crevices.

Data from tentative engineering diagrams should be a guidance and also taken with care, since there are a number of factors not included such as the impact of different crevices, other impurities, etc.

3.04.9.3 Seawater

As seawater contains high amounts of chlorides (~21 000 ppm), standard stainless steels such as 30400 and 31600 are susceptible to localized corrosion such as pitting and crevice corrosion. In addition, natural seawater contains microorganisms, which under beneficial conditions are able to cause ennoblement of the open circuit potential and thereby impose an oxidizing effect. Typical values found in seawater are 300–350 mV/SCE, reached within 10–20 days of exposure. The ennoblement caused by active microorganisms is independent of stainless steel grade. Where ennoblement occurs in combination with biofouling by microorganisms or barnacles on a stainless steel surface, super austenitic or super duplex stainless steels are often required to ensure corrosion resistance in seawater, even at low temperatures.

Also in seawater as in other natural waters, the ennoblement is sensitive to temperature and imposes a catalytic effect of the cathode reaction, which causes a high current density in corrosion reactions. Practical experience and numerous corrosion tests have shown that conventional stainless steels are prone to localized corrosion in seawater. Over the last decades a number of highly alloyed steels with excellent corrosion resistance have been introduced into the market. Some of the new steels are being used extensively in seawater applications, especially in the seawater systems on offshore platforms.

A common factor of the super austenitic and super duplex stainless steels is a high content of the alloying elements chromium, molybdenum and, in most cases, nitrogen. Typical compositions of seawater-resistant stainless steels, S31254 (1.4547) and S32750 (1.4410) with different structures are shown in Table 12. The two stainless steels, S31254 (1.4547) and S32750 (1.4410) have approximately the same resistance to crevice and pitting corrosion.

3.04.9.3.1 Material selection

Figure 48 shows up to which approximate temperatures stainless steel can be used in oxygen-saturated, slightly chlorinated water of varying chloride content. The diagram is based on studies of literature,

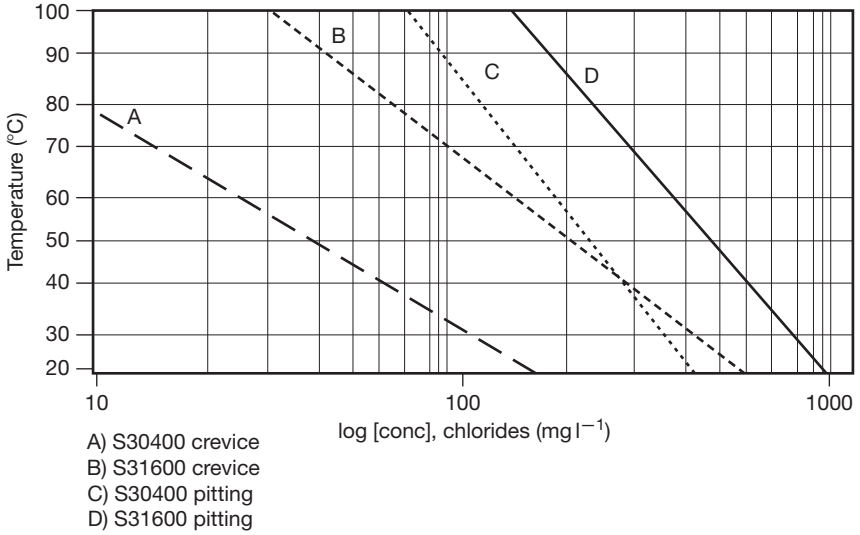

Figure 47 Tentative engineering diagram for S30400 and S31600 for different chloride contents and temperatures extracted from Outokumpu Corrosion handbook. Reproduced from Alfonsson, E.; Arnvig, P.E.; Bergquist, A.; Ivarsson, B.; Iversen, A.; Leffler, B.; Nordström, J.; Olsson, J.; Stenvall, P.; Wallén, B.; Vangeli, P.; Outokumpu Stainless Corrosion Handbook, 9th ed.; Outokumpu Stainless Oy, Sandviken 2004, pp I:8–I:103.

Table 12 Chemical composition and mechanical strength (min, values) of some seawater-resistant and conventional stainless steels

		Typical composition (%)						*Mechanical properties N mm^{-2} (20 °C)*		*Microstructure*
EN	*ASTM*	C_{max}	*Cr*	*Ni*	*Mo*	*Cu*	*N*	$R_{p0.2}$	R_m	
1.4547	S31254	0.020	20	18	6.1	0.7	0.2	300	650	Austenite
1.4410	S32750	0.030	25	7	4	–	0.3	550	800	Duplex
1.4436	S31600	0.050	17.5	11	2.6	–	–	220	510	Austenite
1.4539	N08904	0.020	20	25	4.5	1.5	–	220	500	Austenite
1.4462	S31803	0.030	22	5.7	3.1	–	0.17	480	680	Duplex

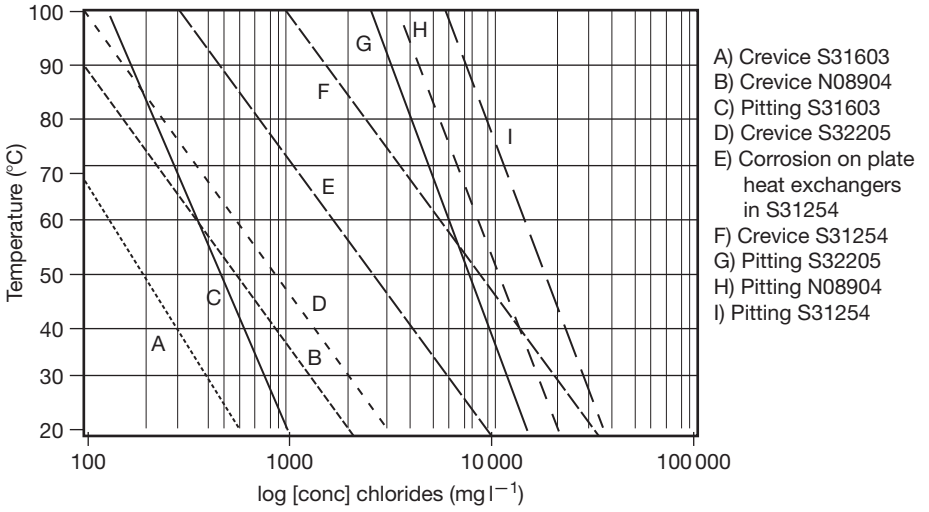

Figure 48 Risk of pitting and crevice corrosion on high alloyed stainless steel in water of different chloride contents or temperatures. Reproduced from Alfonsson, E.; Arnvig, P.E.; Bergquist, A.; Ivarsson, B.; Iversen, A.; Leffler, B.; Nordström, J.; Olsson, J.; Stenvall, P.; Wallén, B.; Vangeli, P.; Outokumpu Stainless Corrosion Handbook, 9th ed.; Outokumpu Stainless Oy, Sandviken 2004, pp I:8–I:103.

combined with practical experience, but it must be underlined that the resistance of a material is also influenced by factors other than temperature and chloride content. Examples of such factors are weld defects, presence of oxide from welding or other heat treatment, contamination of the steel surface by particles of nonalloyed or low-alloyed steel, pH, microbial activity, and the degree of chlorination. The crevice geometry is normally more difficult in a plate heat exchanger than for flange joints, a deeper and more effective crevice due to the curved contact surface, thereof two boundary lines for crevice corrosion on S31254 (1.4547). It should, however, be noted that the crevice geometry of a flange joint is dependent on the pressure that is obtained while tightening screws and bolts. Therefore, the boundary line for crevice corrosion under 'normal' conditions can, in practice, be similar to that which applies to crevice corrosion for plate heat exchangers.[32]

Data from tentative engineering diagrams should be used as a guidance and also taken with care since there are a number of factors not included such as the impact of different crevices, other impurities etc.

3.04.9.3.2 Polluted seawater

In practice, the organisms most dangerous to stainless steels are the sulfate reducing bacteria, which receive their energy, by reducing sulfate ions to hydrogen sulfide while simultaneously oxidizing organic substances. The growth of these bacteria is promoted by anaerobic conditions, which, for instance, exist in bottom sediments containing decomposing organic matter.

Several investigations show that hydrogen sulfide stimulates the anodic reaction in the corrosion process

of stainless steels and consequently increases the corrosion rate. Accordingly, very high levels of hydrogen sulfide lower the pitting potential of a stainless steel and increase the rate of the active corrosion existing in the pit. However, hydrogen sulfide acts reducing on the potential, which lowers the corrosion potential. These low potentials mean that the risk of initiation of crevice and pitting corrosion will decrease.

3.04.9.3.3 Cathodic protection and hydrogen embrittlement

Naturally, cathodic protection of seawater-resistant stainless steels is not necessary. However, such steels might be included in a protection system if they are parts of a construction in which other components have to be protected, one example being subsea templates in the offshore industry. Another example can be found in power plant condensers when stainless steel tubes have been roller-expanded into tube sheets made of bronze and brass.

However, examples of intentional protection of stainless steel can be found in offshore flow lines, which are placed on the bottom of the sea to transport corrosive oil and gas from satellite platforms to the main platform. In this case, the environment inside the flow line determines the choice of material and this seldom justifies seawater-resistant steel. Therefore, cathodic protection of the outside of the flow line is often necessary in spite of extensive passive corrosion protection.

In cathodic protection with sacrificial anodes, there are always parts of the object where the potential is more negative than the reversible potential of hydrogen evolution, so significant hydrogen evolution always takes place. Under such circumstances certain alloys may pick up hydrogen and thus suffer embrittlement and cracking. The risk is particularly high if the material is cold worked and subjected to high mechanical stresses and fatigue loading. The austenitic steel is not influenced by seawater and cathodic protection despite being cold worked to 30%. However, embrittle effect on the duplex steel is under debate. The phenomenon needs further investigation, but caution is recommended if severely cold-worked duplex stainless steels are used in seawater constructions equipped with cathodic protection.

3.04.9.3.4 Seawater exposures

One of the largest exposure programme run in Europe, the MAST II programme, studied the effects of biofilm growth and the impact of chloride concentrations from different locations in Europe.[46] In this programme, several commercial stainless steels for marine application were chosen and the electrochemical effects induced by biofilm growth were measured and collected on samples exposed in all European seas, from the Mediterranean to the North Sea. Table 13 presents a list of the stainless steel grades tested. Potential ennoblement of the stainless steels in the passive state occurred at all marine stations and in all four seasons. The initial corrosion potential and the rate of ennoblement showed significant differences between the sites but the reasons for the varying rates were not explained. The ennoblement was related to the seasons of the year and was strongly dependent on the temperature being less rapid in winter than in the summer for all stations.

The samples were immersed in coastal seawaters adjacent to Trondheim (Norway), Kristineberg (Sweden), Cherbourg (France), Brest (France) and Genoa (Italy).

The main risk of corrosion attack for stainless steels in seawater where there is heavy biofouling is crevice corrosion. Table 14 illustrates the risk of

Table 13 Stainless steel grades exposed in the MAST II Programme[46]

EN	*Trade name*	*Chemical composition (wt%)*				
		Cr	*Ni*	*Mo*	*Cu*	*N*
1.4435	316L	17.2	12.6	2.6		
1.4462	2205	22	5.5	3.2		0.17
1.4460	UR47N	24.7	6.6	2.9		0.18
1.4507	UR52N+	25	6.3	3.6	1.5	0.25
1.4410	SAF 2507	24.9	6.9	3.8		0.28
1.4547	254SMO	19.9	17.8	6	0.69	0.2
1.4652	654SMO	24.5	21.8	7.3	0.43	0.48
1.4563	SAN28	26.7	30.3	3.4	0.9	0.07
1.4537	URSB8	24.9	25	4.72	1.4	0.21
1.4529	URB26	20	24.7	6.3	0.8	0.19

Table 14 Results from crevice corrosion tests carried out at five marine stations[46]

EN	Trade Name	Genoa, Italy	Cherbourg, France	Brest France	Kristineberg Sweden	Trondheim Norway
1.4435	316L	5/5	0/4	0/4	0/4	4/4
1.4462	2205	++	+	+	0/5	+
1.4460	UR47N	++	+	0/4	0/4	0/4
1.4507	UR52N+	+	+	0/5	0/5	+
1.4410	SAF 2507	0/4	+	0/5	+	+
1.4547	254SMO	+	+	0/5	0/5	0/5
1.4652	654SMO	+	0/5	0/5	+	0/4
1.4563	SAN28	+	+	+	0/5	+
1.4537	URSB8	+	+	0/5	0/5	0/5
1.4529	URB26	0/5	0/5	0/5	+	0/5

+/++, one/several depassivated areas, no weight loss; 5/5 crevice corrosion on 5 coupons out of 5.

crevice corrosion for different stainless steels exposed to seawater.

The more-alloyed stainless steel grades either austenitic or duplex grades, appeared to be resistant to crevice corrosion in all marine stations after at least a 6000 h of immersion at ambient temperature. The winter and summer tests lasted 3000 h respectively. Some depassivation as discoloration was observed under the crevice washers on many of the samples but no weight losses were observed.

3.04.9.3.5 Anaerobic seawater environments

The presence or absence of a cathodic reaction can determine the extent of corrosion. Oxygen reduction is not the most natural cathodic reaction in natural waters and by the absence of such a reaction may have a beneficial effect in terms of low or virtually zero oxygen content. Mollica, Montini, Scotto, and Marcenaro investigated three stainless steel grades, EN 1.4016(S43000), 1.4301(S30400), and 1.4401 (S31600) that were exposed in an anaerobic clay environment in seawater at the harbor in Genoa, Italy. The exposure time was six months and the coupons were exposed at six various levels of depth to the waterline, where the first level was just under the waterline. During exposure, the open circuit potentials were measured and weight loss measurements were performed after the test. Analysis of free sulfur and pH was carried out at the different levels of exposure. The pH was 7.6 and the sulfur content varied from 2.65 to 3.15 mol l^{-1} in the clay. The OCP for EN 1.4301(304) and 1.4401(S31603) was after 40 days at the potential of -500 ± 10 mV/SCE without any initiation of local corrosion. The stainless steel grades EN 1.4301 and 1.4401 remained corrosion resistant under anaerobic conditions and their corrosion potential coincided with the redox potential of the medium, indicating that the level of oxygen determined the open circuit potential, or corrosion potential. However, the less noble grade EN 1.4016 suffered local corrosion at potential levels ranging from -500 and -600 mV/SCE.[47]

These results indicate that in a completely oxygen-free environment, even where there are high amounts of chlorides, there is an electrochemical effect of the oxygen removal that coincides with the cathodic protection of the stainless steel. However, in an anaerobic clay or similar environment, any oxidizing coupling effect of the steel, that is, an oxidizing chemical is added or oxygen is present from another source, causes an increase in the potential which can have an adverse effect on the corrosion resistance of stainless steels.

Mollica and Ventura tested crevice samples of the following stainless steel grades: EN 1.4652 (S31654), EN S31254 (1.4547), EN N08904 (1.4539), ENS31600 (1.4404), and EN S32205 (1.4462) in an anaerobic marine environment and simulated a coupling effect between anaerobic and aerobic environments potentiostatically to simulate the rate of ennoblement found in aerobic conditions.[48] They found that the stainless steels were in the passive state at an open circuit potential close to -450 to -500 mV/SCE, almost independent of the alloy composition. However, the passivity was destroyed by a cathodic polarization at a potential below -700 mV/SCE. An activity peak was observed at the potential range -600 to -700 mV/SCE, independently of alloy composition and tested temperatures. Nevertheless, spontaneous repassivation of activated stainless steels was also observed. The spontaneous initiation of crevice

corrosion attacks in stainless steels in totally anaerobic seawater seemed impossible. However, under oxidizing conditions, localized corrosion such as crevice corrosion was initiated.[48]

3.04.10 Stainless Steels Performance in Atmospheric Environments[32]

In architectural applications, that is, wall claddings and decorations, stainless steel is often chosen for its aesthetic qualities, since it can be supplied with a variety of surface finishes, and because of its cost benefits – it is virtually maintenance-free.

In structural applications, stainless steel is used for components within the building and construction industry where the emphasis is more on the strength and ductility of the material. In such cases, superficial staining and minor shallow corrosion are not necessarily a cause for concern as there is seldom any risk of structural or mechanical failure of the component. However, for stainless steel roofing, some superficial staining need not be critical, but any penetrating pitting attack will mean that the material chosen will have failed to serve its purpose.

Whatever the reason for choosing stainless steel for architectural applications, material selection must be based on experience and knowledge of the performance of specific grades in specific circumstances. Figure 49 shows the Sickla bridge constructed in duplex stainless steel. The bridge is located close to Stockholm in Sweden.

Figure 49 The Sickla bridge, constructed in duplex stainless steel.

3.04.10.1 Types of Atmosphere, Corrosivity, and Material Selection

Outdoor atmospheres were previously divided into four categories:

- rural
- urban
- industrial
- marine

Revisions of standards from the international standardization organization, for example, ISO define corrosivity classes rather than atmospheres. The corrosivity of the different atmospheres are calculated and evaluated by pure metals such as carbon, steel, and zinc. The results and corrosivity of environment have been compared with the performance of stainless steels and Table 15 shows stainless steels performing with corrosion resistance in the different corrosivity classes.

Table 15 A comparison between corrosivity classes according to ISO 9223 and ISO 12944–2, including appropriate stainless steel grades

ISO	*Typical environments*	*Grades*
C 1	Indoor, heated. Outdoor, deserts and arctic areas (rural)	S43000, S30400
C 2	Indoor, nonheated. Outdoor, arid and low pollution (rural)	S43000, S30400
C 3	Indoor, humid, low pollution. Coastal areas with low deposits of salt. Urban and industrialized areas with moderate pollution	S30400, S31600
C 4	Indoor with volatile aggressive chemical compounds, swimming pool buildings.[a] Polluted urban and industrialized atmosphere. Coastal areas with moderate salt deposits	S31600, S32205, N08904, S32750, S31254
C 5	Severely polluted industrial atmospheres with high humidity and marine atmosphere with high degree of salt deposits, splashes	N08904, S31254

[a]Attention must be paid to cold stainless steel surfaces well above the water level where volatile compounds, especially chloramines, can condense and cause a special type of SCC. It has been found that only the most resistant grades, that is, N08904 (1.4539) and S31254 (1.4547), are capable of withstanding such conditions. See the previous section on SCC.

3.04.10.1.1 Indoor, heated, nonheated. Outdoor, arid, low pollution, deserts and arctic areas (Rural), C1–C2

A rural atmosphere is characterized by clean air, that is, a low level of pollutants, including airborne chlorides from the sea. Acid rain resulting from emissions of sulfur oxides due to the combustion of fossil fuels at remote power stations does not normally cause any problems for stainless steel as long as there are no chlorides present.

Ferritic grades with 17% chromium, for example, 1.4016 (S43000), can normally be used in this type of atmosphere.

Austenitic steels such as S30400 (1.4301) and similar grades are still very common, but these are often selected for their availability and fabrication aspects rather than for their corrosion resistance. Certain forming operations can be facilitated by the use of austenitic grades.

Ferritic grades have a transition temperature, that is, a temperature below which the material becomes brittle. This does not normally create any problems for thin gauges since the transition occurs at temperatures well below zero (°C). However, this phenomenon cannot be totally neglected in countries with cold winters. Austenitic grades are safer in that respect.

3.04.10.1.2 Indoor, humid, low pollution. Coastal areas with low deposits of salt. Urban and industrialized areas with moderate pollution, C3

The use of 1.4301 (304) should be limited to indoor nonpolluted atmospheres as described in Table 1.

Urban and industrial atmospheres normally contain oily exhaust fumes from engines and soot and dust, including metal dust. A fall in temperature during the night may expose the stainless steel surface to a slightly acidic condensate, which in turn may cause staining. However, serious corrosion will never occur provided that the atmosphere is free from chlorides. Metal dust, especially if the source is a steel plant or a mechanical workshop fabricating steel items, can attach itself to stainless steel surfaces and affect both the aesthetic and corrosion resistance properties of the stainless steel surface unless it is cleaned regularly.

Stainless steel is commonly used for architectural applications in major cities, and in such an environment, regular cleaning is recommended if the material has been selected for its aesthetic qualities, particularly if the surface is close to street level.

Grades containing 2–2.5% molybdenum, that is, type S31600 (1.4401) and similar, normally offer adequate corrosion resistance even when used for applications in cities situated close to the sea.

The principles of material selection for industrial areas are virtually the same as those, which apply for major cities. However, in an industrial environment, the staining from nearby metal industries can sometimes be so severe that it is almost impossible to maintain a shiny surface appearance. In such cases, if the aesthetic aspects are a prime consideration in material selection, other materials are to be preferred. If the integrity of a structural component is more important, stainless steel is still an excellent material.

3.04.10.1.3 Indoor with volatile aggressive chemical compounds, roof parts with mechanical load in swimming pool buildings. Polluted urban and industrialized atmosphere. Coastal areas with moderate salt deposits, C4–C5

A marine atmosphere is characterized by its location to the sea resulting in airborne and depositing chlorides, either as salt crystals or close to water spray. The distance from the sea is important, as is the geographical location. Temperature and humidity are almost as important as the presence of chloride ions.

Molybdenum alloyed grades of type S31600 (1.4401) or comparable grades are normally specified for a marine atmosphere, regardless of whether the application is a prestigious building in a coastal city or an offshore platform. However, this material has inadequate resistance if used close to the sea in tropical countries with high levels of humidity and high daytime temperatures. Examples include cases of SCC reported from industrial installations along the Arabian Gulf coast and in South East Asia. A duplex grade such as 1.4462 (S32205) is a good alternative in those conditions. This grade has also been used for hand railings along beach promenades in the Canary Islands. For high prestigious buildings situated very close to the sea in such countries, it may be necessary to select a very highly alloyed grade such as 1.4547, S31254 or S32750 (1.4410).

Indoor atmospheres are often, to a certain extent justifiably, neglected. They do not normally contain chlorides and the low relative humidity and high temperature make the risk of condensation almost negligible. The criteria for material selection will, in such circumstances, be the same as for rural atmospheres, that is, either a ferritic grade or S30400

(1.4301) or similar as described earlier. This is also what we face while entering a modern office building, an elevator, or a hamburger bar.

However, there are indoor atmospheres for which serious consideration is warranted prior to the installation of stainless steel, whether stainless steel is chosen for its aesthetic properties or for load carrying structural components.

One such case is swimming pool buildings. In such an environment, the combination of high humidity, relatively high temperatures, and the evaporation of volatile chloramines can create very harsh conditions for stainless steel. Chloramines are formed from nitrogenous compounds such as sweat and urine from bathers, and from chlorine, which is used as a disinfectant. Grade S31600 (1.4401) can normally be used for components intended for use or installation below or just above the water surface, for example, handrails, ladders, stairs, etc., whether they are actually immersed in the water or merely exposed to it in the form of splashes. For weight-bearing structural components installed well above the surface of the water, sometimes towards the ceiling, more highly alloyed grades such as 1.4439 (N08904) and S31254 (1.4547) should be selected, for example, ceiling wires and wire ropes, strapping and hose clips, and various types of fasteners.

Another harsh indoor atmosphere can be found on industrial sites which handle acids or chlorinated hydrocarbons. These chemicals can evaporate and later condense on cold metal surfaces. Material selection must be based on actual conditions but grades lower alloyed than S31600 (1.4401) should not be considered. It might sometimes be necessary to use grades as highly alloyed as S32205 (1.4462) or, on rare occasions, even S31254 (1.4547).

3.04.10.2 Factors Influencing Atmospheric Corrosion on Stainless Steels

The importance of keeping the surface clean cannot be stressed enough. 'Cleanliness' in this context can either be achieved by regular washing to avoid staining by soot and dust, or by a carefully prepared postweld cleaning procedure to restore the surface after welding.

The surface finish of the steel is another very important parameter, as it not only has a direct influence on the corrosion resistance, but can also determine the efficiency of cleaning operations.

Narrow crevices always involve a potential risk of crevice corrosion but pockets that collect dirt and moisture should also be avoided.

In some cases, when a design prevents postweld cleaning operations or contains crevices that cannot be avoided, it may be advisable to use a more highly alloyed grade than would otherwise have been chosen in normal service conditions.

3.04.11 Application Areas of Commercial Significance

3.04.11.1 Domestic – Kitchenware

The corrosion resistance of stainless steel is an appealing property of items used in domestic cutlery and kitchenware. The stainless steel grade S30400 (1.4301) or similar grades are frequently used and widespread in these applications. It is used in a wide variety of applications, ranging from brewing vessels to kitchen sinks and milk tankers. The deep drawing properties required to produce beer kegs are good for this steel grade. Stainless steels are tolerant to the wide range of temperatures common in cooking and resist thermal shock very well. A stainless steel surface is also easy to clean. The surface finish is important in applications such as domestic cutlery and kitchenware. A rough surface attracts food deposits, promoting an environment in which microorganisms can proliferate, whereas a smooth and easily cleaned surface will prevent this. The European Hygienic Engineering & Design Group provides guidelines on surface finish, recommending R_a 0.8 mm or better, which can easily be achieved with cold-rolled stainless steels. The R_a value alone, however, is not a reliable indicator of whether the surface will attract solids or deposits. The cleaning procedure becomes even more important on rough surfaces than on smooth surfaces and it is important to establish how easy it is to clean the surface in actual service conditions.

The environments to which domestic cutlery and kitchenware are exposed often vary from very mild, indoor, dry, and less corrosive environments in the living room to warm, wet environments such as those found in kitchens, in which chloride may be present, or even to outdoor environments such as a patio close to the sea or coastal areas. The dry/wet environment in households varies depending on the chloride content in the water, the temperature and, to a large extent, the humidity and the stainless steel chosen must be capable of withstanding such environments. Typical variations are

- chloride contents: 0.020–0.250 g l^{-1}
- temperatures: 20–100 °C
- relative humidity: 20–100% RH
- cyclic drying and wet variations, as in flush shower, bath etc.

Some examples of corrosive parameters for using table salts and cooking in kitchenware are:

- food deposits in boiling chloride solution (table salt).
- long-term exposure to chloride water, for example, leaving the pasta in the saucepan.
- partly heated water with table salt for a long time
- acids in the food, for example, in jam, juice, rhubarb.

Examples of stainless steel grades used in cutlery blades and kitchens utensils are presented in Table 16. The use of lower-alloyed and standard grade of S30400 (1.4301) are the most common in these applications. It is important to remember that, for certain application areas in a kitchen environment, corrosion might occur if stainless steel grades at the lower end of the scale are selected. An example is the use of the martensitic grade 1.4006 (410), which provides a sharp edge but is not really a suitably corrosion-resistant steel grade for use in hot chloride water environments.

The main source of corrosion resistance in the stainless steel grades presented in Table 12 is chromium. The lower the chromium content, the lower the corrosion resistance. To test the corrosion resistance of stainless steels used for cutlery, there is an easy and useful test described in EN-ISO8442 – Material and articles in contact with foodstuff. A mild test for the lower end martensitic stainless steels is an immersion test in 0.050 g l^{-1} sodium chloride for 6 hours at room temperature, between 18 and 26°C. Another more aggressive test is EN-ISO8442 – Annex A, part 1 and Annex C part 2, where 1.0 wt% NaCl at 60°C of cyclic immersion 2–3 times per minutes for 6 h.

3.04.11.2 Process Industry

3.04.11.2.1 Hydrometallurgy[32]

Many metals are extracted from mined ores and subsequently refined by hydrometallurgical processes, which usually involve dissolving of the metals in an acid. Some examples of common hydrometallurgical processes are recovery of zinc, copper, and nickel. These processes vary not only in the sense of corrosive environments but also in process routes. Nevertheless, there are some general operations in the hydrometallurgy processes to recover the desired metals. These stages can include pressure or atmospheric leaching, separation by, for example, solvent extraction or ion exchange. Depending on the desired product the downstream process stages can include purification of solution, product recovery by electrorefining, electrowinning and/or thereafter casting to slabs as, for example, in the zinc production.

Because of its relatively low cost, sulfuric acid is the most important acid used in these processes and it is often produced on-site. Stainless steels are usually the basic materials of construction used for withstanding the acid environment and. have several advantages from design and process flexibility point of view. Under the most severe conditions, there are possibilities to identify applications for the super duplex or super austenitic stainless steel grades as well as other steel grades for less severe environments.

The leaching stages have the most demanding environments for stainless steels, since these stages contain not only acid, but also chlorides and metal ions from the ores, concentrate or matte. The presence of metallic ions in combination with chlorides and sulfuric acid complicates the prediction of corrosion of stainless steels in hydrometallurgical process environments. The metal ions, that is, Fe^{2+}/Fe^{3+} and Cu^{2+}, have, due to the oxidizing influence, an inhibitive effect on uniform corrosion of stainless steels, when added to sulfuric acid. Conversely, in combination with chlorides this oxidizing effect increases the risk for localized corrosion and too high amounts of chlorides can also lead to increased uniform corrosion. In summary, the combination of sulfuric acid, chloride ions, oxidizing metal ions, and the elevated temperature creates harsh conditions for stainless steels.

Table 16 Stainless steel grades used in cutlery blades and kitchen utensils

Material		*Microstructure*	*Typical composition (wt%)*			*PRE*
EN	*UNS*		*Cr*	*Ni*	*N*	
1.4006	S41000	Martensitic	11.5–13.			11.5–13.5
1.4028	S42000	Martensitic	12.0–14.			12–14
1.4016	S43000	Ferritic	16.0–18.0			18–18
1.4301	S30400	Austenitic	17.0–19.5	8.00–10.5	<0.11	17–19.5

Zinc production

One of the hydrometallurgical processes used for zinc production is the Jarosite process. This process can be divided into several stages. Neutral leaching is performed in sulfuric acid at a concentration of ~50–60 g l^{-1}, that is, at a low pH and a temperature of 60 °C. Oxygen is blown into the process stage from below for further oxidation of the product stream. One stream of the outlets from the neutral leaching stage continues to purification and a separation stage where cadmium, copper, and cobalt are reduced from the product. The other product stream from the neutral leaching stage proceeds to the Jarosite process. The pH in the Jarosite stage is 1.5, containing ~7–10 g l^{-1} sulfuric acid. From the Jarosite stage a part of the process solution is recycled to the neutral leaching stage.

A large part of the product stream continues to the hot leaching stage, or concentrate leaching, where Jarosite $NaFe_3(SO_4)_2(OH)_6$, is precipitated. The hot leaching is carried out in tanks made of super-austenitic or super-duplex stainless steels at elevated temperatures of ~95 °C, at chloride contents of 300–400 mg l^{-1} and sulfuric acid concentrations of 60–80 g l^{-1}. In the hot leaching stage manganese oxide is partly circulated as an oxidizing agent and it can cause deposits on the tanks. Corrosion can occur on grade 1.4539 (N080904) in this very hostile environment while S32750 (1.4410) or S31254 (1.4547) are examples of more corrosion-resistant grades. **Figure 50** shows a tank on the road in S32750 (1.4410) manufactured for a hydrometallurgy process solution.

When cadmium, copper, and cobalt have been removed from the neutral leaching process solution, it continues to the product recovery, the electrowinning stage, where pure zinc is precipitated electrochemically on large cathodes. In this stage manganese dioxide can precipitate on the anode surfaces (lead) causing efficiency loss in due time. For this reason, the manganese dioxide has to be removed. Chlorine can be used, solving the manganese dioxide by oxidation. However, there is an increased risk of localized corrosion on stainless steels, due to the oxidizing effect of chlorine.

Figure 50 A tank on the road in stainless steel grade S2750 (1.4410).

The leaching processes in zinc production are under continuous development to increase production efficiency and new processes operate commonly with direct leaching. Zinc concentrate is in the direct leaching process leached in acid slurry at atmospheric conditions by the use of oxygen.

In addition to the hydrometallurgical production of zinc, sulfuric acid is also commonly produced on the site. Before entering the sulfuric acid production, the product stream is filtered electrostatically to remove mercury in a corrosive environment. An example of a steel grade used in the electrostatic precipitator is the super austenitic EN S31254 (1.4547).

Copper production

Copper refining is an electrolytic production process using direct current for transporting copper in an electrolyte to large cathodes. The electrolyte has a low pH and contains, for example, copper ions, sulfuric acid, and chlorides.

Copper is precipitated on large cathodes of stainless steels in the electrolytic process. The steel grade used is EN S31600 (1.4404). The high purity copper on the cathodes is then stripped mechanically from the cathodes. The electrolyte might be corrosive for EN 1.4404 when the cathodes are exposed in the solution for longer periods of time when the current is shut off, for example, at maintenance stops, but during operation the cathodes are cathodically protected at low potentials.

Nickel production

A very harsh environment for stainless steels can be found in solutions in nickel production using autoclaves at elevated temperatures in combination with chlorides and sulfuric acid. An example of the hostile conditions is the processes operating at a temperature as high as 250 °C and under high pressure. In some of the more demanding environments, metals such as titanium and titanium alloys, zirconium, or even tantalum must be used in the leaching tanks to withstand

the severe conditions. Nonmetallic materials may also be suitable for certain applications in these environments.

Corrosion resistance of stainless steels in simulated hydrometallurgical solutions

Hydrometallurgical solutions are indeed very complex and in order to document the corrosion properties of stainless steels systematically, the most corrosive parameters have to be considered such as the sulfuric acid, oxidizing chemicals Fe^{2+}/Fe^{3+}, Cu^{2+}, and chlorides and any synergistic effects in between. Laboratory tests have been performed in environments simulating some conditions in hydrometallurgy plants, that is, including chloride ions, ferric ions, cupric ions, and sulfuric acid. Selected temperature was 98°C and immersion time 30 days. Cold-rolled sheets were used for the preparation of samples, which also were equipped with crevice washers.

Table 17 shows typical compositions of tested stainless grades and Table 18 show the test compounds. Table 19 presents the indications of corrosion resistance in stainless steel grades in these compounds.

Both localized and uniform corrosion occurred simultaneously on the test coupons. In some cases the uniform corrosion was dominating, at very high corrosion rates.

At intermediate chloride contents, between 0.1 and 0.5 g l^{-1}, only the super duplex S32750 (1.4410), and super austenitic S31254 (1.4547) were resistant. Severe corrosion occurred while increasing the chloride content above the 0.5 g l^{-1} and the temperature was close to the boiling point. Table 20 shows the test results in compounds C and D. Increasing the sulfuric acid content to 100 g l^{-1}, but maintaining the low chloride amounts (0.1 g l^{-1}) did not seem to initiate any corrosion on any of the steel grades, Table 21. These results emphasize the importance on maintaining the chloride levels very low in these very harsh environments.

The corrosion tests were carried out without any activation of the samples during the tests which can have an impact on direct comparison with real service conditions as also other impurities most commonly included in hydrometallurgical service environments.

3.04.11.2.2 Desalination[32]

Water management will be one of the most important infrastructural tasks for the future to solve all over the world. Desalination, that is, the production of potable water or industrial boiler feed water by removing salt from brackish water, seawater or salty aquifers, involves several stages, each of which places different demands on the construction materials. Figure 51 shows an example of a desalination plant, Melitha.

Multistage flash

The oldest distillation process, and also the most common for the larger desalination plants, is multistage flash (MSF). In this process, hot deaerated seawater or a seawater/brine mixture at a temperature of around 110–115°C, occasionally with some residual chlorine, enters the first stage flash chamber, where some of it evaporates and also condenses. During each stage, the seawater/brine mixture loses some of its energy and the temperature drops far below 100°C towards the end of the process. However, creating a vacuum, which enables boiling to take place at these low temperatures, counterbalances this. The distillate is achieved by cooling the steam down via numerous condenser tubes running above the flashing seawater.

The most common stainless steel found in MSF plants is S31600 (1.4404), which in the past has been used for the lining of evaporator vessels and for a number of internal components, for example, orifice plates, distillate trays, demisters, and condenser tube support plates. More modern design calls for clad plates in the evaporator vessels, sometimes using S31700 (1.4438). The condenser tubes are mostly

Table 17 Typical chemical compositions of tested stainless steel grades in weight %

Steel grade, EN	*UNS*	*Cr*	*Ni*	*Mo*	*N*	*Others*
1.4435	31600	17.1	12.7	2.64	0.060	
1.4539	N08904	19.8	24.0	4.30	0.060	1.5 Cu
1.4462	S32205	21.9	5.67	2.99	0.190	
1.4410	S32750	24.7	7.11	3.82	0.280	
1.4547	S31254	20.1	18.1	6.28	0.210	Cu
Hastelloy, C-276		15.3	REM	15.6		
ATi-24						

made of copper alloys, but titanium has also been used. Highly alloyed stainless steel grades, such as S31254 (1.4547) and 1.4565 (S34565) could be an option for the tubes, but neither grade has yet been used for this particular application in MSF plants. However, stainless steel tubes in the S31254 (1.4547) grade have successfully been used for condensers in ventilation systems.

The latest concept for evaporator vessels is solid stainless steel, which has been successfully used for recycling and also once-through plants. Hidd, a 135 000 m^3 day^{-1} MSF recycling plant in Bahrain, was commissioned in February 2000 and Melittah, a 15 800 m^3 day^{-1} recycling plant in Libya, will start water production during 2004. The evaporator vessels were made of S31600 (1.4404) and S32205 (1.4462) respectively, and in the latter case the higher strength of 1.4462 (S32205) was used for redesigning the shells, making them around 30% thinner and less costly than if made of S31600 (1.4404).

Solid stainless steel has also been used for once-through plants, that is, MSF with no recycling of brine. The material used for the evaporator vessels must thus resist a very hostile internal environment and also a potentially aggressive external environment, which may include exposure to boiling seawater on a hot wall. Once through implies no deaeration, that is, the water entering the first stage is air saturated with an oxygen level of a few milligrams per liter, and it may contain some residual chlorine.

There are three MSF once-through plants in service in Chile, the oldest was commissioned in 1996, and solid 254 SMO has been used for the first six stages while ASTM 317LMN (1.4439) was used for the remaining six. However, plant tests have shown that 2205 would be a more cost effective alternative than ASTM 317LMN (1.4439) for stages downstream the first six stages. The total capacity of these plants is 10 400 m^3 day^{-1}.

Table 18 Test compounds for immersion tests at 98 °C

Test compound	*Me^{n+}*		*H_2SO_4 (g l^{-1})*	*Cl^- (g l^{-1})*
	Fe^{3+}	*Cu^{2+}*		
A	5	4	10	0.1
B	5	4	10	0.5
C	5	4	100	0.1
D	25	4	100	0.1

Table 19 Summary of test results at 98 °C in test compounds A and B, containing 5 g l^{-1} Fe^{3+}, 4 g l^{-1} Cu^{2+}, 10 g l^{-1} H_2SO_4 and two levels of chloride amounts according to the table

Chloride content, Cl^- (g l^{-1})	*S31600 (1.4435)*	*N80904 (1.4539)*	*S32205 (1.4462)*	*S32750 (1.4410)*	*S31254 (1.4547)*	*C-276*
0.1	No corrosion	No corrosion	No corrosion	No corrosion	No corrosion	No corrosion
0.5	Corrosion	Corrosion	Corrosion	No corrosion	No corrosion	No corrosion

Table 20 Summary of test results in test compound C containing 4 g l^{-1} Cu^{2+}, 100 g l^{-1} H_2SO_4 0.1 g l^{-1} chlorides, and 5 g l^{-1} Fe^{3+} and D with the same composition but with an increase in the amount of Fe^{3+} to 25 g l^{-1}

Fe(III) content Fe^{3+} (g l^{-1})	*S31600 (1.4435)*	*S32205 (1.4462)*	*S2750 (1.4410)*	*S31254 (1.4547)*	*C-276*
5	No Corrosion	No Corrosion	No Corrosion	No Corrosion	Corrosion
25	No Corrosion	No Corrosion	No Corrosion	No Corrosion	Corrosion

Table 21 Steel grades used in field and laboratory tests

UNS	*EN*	*ASTM*	*CPT (°C)*	*PRE*	*Cr*	*Ni*	*Mo*	*N*
S30400	1.4301	304	–	19	18	8.7	–	0.06
S31600	1.4436	316	27	27	17	11	2.7	0.06
S32205	1.4462	2205	52	35	22	5.5	3	0.17

Figure 51 An example of a desalination plant, Melitha.

Low-temperature multieffect, desalination plants (LT-MED)

One major operational drawback of MSF plants is the formation of scale, calcareous deposits, created by the high temperatures. This has led to the development of LT-MED, where the main deviation is a maximum brine temperature of 55–60 °C, as opposed to 110–120 °C, resulting in reduced corrosivity towards metallic materials. The physics behind this process are the same as in MSF plants, that is, an applied vacuum causes boiling and evaporation of the incoming seawater at a temperature far below 100 °C, but the design of the evaporators and condenser tubes is totally different. There is no flashing but evaporation due to a falling film on tubes where the internal side acts as a condenser while the external side causes boiling.

Different types of material have been used for the evaporator shells; epoxy coated mild steel, clad steel, solid S31600 (1.4404), and even S31254 (1.4547). A duplex grade, such as 1.4462 (S32205), would be an appropriate alternative. A pronounced advantage for a high strength grade such as 1.4462 (S32205) is the cylindrical shape of the LT-MED evaporators making an even more cost-effective design possible than in the case for MSF shells.

There is one LT-MED plant in service with highly alloyed stainless steel condenser tubes, AVR's Demi Water Plant, a 24 000 m^3 day^{-1} plant in the Netherlands, where 1.4 million meters of 1.4565 (S34565) tubes were installed.

Reverse osmosis and seawater reverse osmosis

The reverse osmosis (RO) process is performed at ambient temperature but at a high pressure, for an seawater reverse osmosis (SWRO) plant it is often in the range 70–80 bar. The feed, seawater or brackish water, is first pretreated, which implies mechanical filtering, chlorination to avoid biofouling, and the addition of chemicals to adjust pH values, etc.

However, the membranes used in RO plants do not tolerate chlorine, so also if the feed has been chlorinated as part of the water treatment, any residual chlorine must be removed prior to the membrane passage, often by an addition of sodium bisulfite or similar. The feed is still air saturated and as the design contains a number of crevices, there is an obvious risk of pitting and, above all, crevice corrosion in these plants.

Highly alloyed austenitic stainless steels, such as S31254 (1.4547), have frequently been used, very successfully, in a number of SWRO plants in the Middle East, on Mediterranean islands, on the Canary Islands, in the West Indies and in the USA. Most of the 'biggest in the world' plants are equipped with high-pressure piping made of S31254 (1.4547) or similar. Materials of type N08904 (1.4539), S32205 (1.4462), 1.4438 (S31700), and 1.4404 (31600) have previously been used, but the failures have been numerous, not least for 1.4404 (31600) and 1.4438 (S31700).

Highly alloyed grades have also been used for high-pressure pumps and the super duplex S32750 (1.4410) can be an extremely attractive option for energy recovery systems. The first plant to utilize the properties, that is, strength and corrosion resistance, for the energy recovery system of this grade will be Ashkelon, a 275 000 m^3 day^{-1} plant in Israel.

Highly alloyed stainless steels, for example, S31254 (1.4547), can also be used for different filters upstream the high pressure pumps although other materials are often preferred for cost reasons.

3.04.11.2.3 Stainless steel within the pulp and paper industry

The stainless steel manufacturers have been developing specific stainless steel grades optimized in pulp- and paper process environments. Cost efficiency and sustainability of stainless steels in the pulp- and paper solve corrosion problems. One of the first fields of application for duplex grades was the pulp and paper industry, where the first digesters were mounted in New Zealand in 1988.

Apart from economic factors, a growing concern for the environment has led to a number of new processes being introduced and existing processes being modified. Effluent recycling has also become more common in modern plants. The positive environmental benefits of 'closing-up' the mills have been accompanied by a rise in the concentrations of

chemicals used in process streams, and in operating temperatures. These factors have drastically increased the demands made on the corrosion resistance of the structural materials used in such plants.

Process environments and their impact on corrosion varies in a great extent in different pulp- and paper processes, which also leads to that advice concerning material selection require modification while considering a particular environment at a particular mill.

The duplex alternative, for example, 1.4462 (S32205), is constantly gaining ground at the expense of the other alternatives and many duplex vessels have been started up. The selection of an appropriate duplex grade will, among other things, depend on the process environment in service.

3.04.11.2.4 Architecture – Art [32]

The most visible and perhaps also the most common outdoor applications of stainless steel are for facades, wall claddings, and roofs. The surface finish is selected according to the aesthetic impression required by the architect, whilst the surrounding atmosphere determines the steel grade.

One of the oldest examples of this is the Chrysler Tower in New York, which was crowned with an Art Deco cap of stainless steel as early as 1929. It is still in perfect condition and the extra sheets shipped from Germany during the building's construction and intended for use in future maintenance were still held in storage as recently as 1995. This means that the stainless steel has stood the test of time for more than 70 years without any mass loss or localized corrosion. The steel grade selected was of type 1.4301 (S30200), which would today be regarded as a borderline steel grade in terms of its alloy composition, considering the previous discussion on corrosion hazards. Another equally old landmark is the canopy at London's Savoy Hotel. Both are clearly excellent examples of the understated elegance of stainless steel.

More recent installations that are equally well known are the Court of Human Rights in Strasbourg in France, Canary Wharf in London, and Petronas' 450 m high Twin Towers in Kuala Lumpur, that are all clad with stainless steel of type S31600 (1.4401). The same material was also used for the roof of the new departure terminal at Stockholm's central railway station, built in the late 1980s.

Another recent installation is the Tsing Ma Bridge along the highway to Chep Lap Kok, the new airport of Hong Kong. Whilst this construction is, in some respects, similar to those named earlier, there is an important difference. In this case, the stainless wind deflectors were not only installed for aesthetic reasons; they are also intended to protect the traffic from strong side winds during the hurricane season.

The elegance of stainless steel can be seen in a number of monuments all over the world. **Figure 52** shows a bridge constructed in stainless steel located at the island Menorca.

The famous Finnish composer Jean Sibelius has been honored with a monument in Helsinki, a stainless steel 'organ,' created by Eila Hiltunen. The same sculptress also created 'The Sun Flower Field,' which was raised in a man-made seawater lagoon outside Jeddah. The selection of steel grade was in both cases based on the respective atmospheres, with type S31600 (1.4436) being selected for the urban atmosphere of the Finnish capital and S31254 (1.4547) for the harsh marine conditions of the Red Sea.

The steel grade S31254 (1.4547) was also used for Carl Milles' sculpture "God and the Rainbow", seen in **Figure 53**, which was inaugurated in 1995 by HRH King Carl XVI Gustaf of Sweden. Its location means that the rainbow is sprayed with water from the Baltic Sea and such conditions would be too harsh for a conventional grade such as S31600 (1.4401).

Maintenance-free structural components can be found in a number of industries, but in selecting a grade for a specific application, it is always important to consider the intended operating environment.

The cable ladders on the Norwegian platform Statfjord A were originally made of painted mild steel, which lasted four years. The replacement ladders made of zinc coated (galvanized) steel lasted another 7 years but were then replaced by stainless steel ladders made of S31600 (1.4401) in 1990.

Figure 52 Bridge constructed in stainless steel, located at Menorca.

Figure 53 S31254 (1.4547), used for Carl Milles' sculpture 'God and the Rainbow', seen in Figure 53, which was inaugurated in 1995.

Another example is the internal wall lining of a building for the pickling of steel at a Swedish carbon steel producer. The original lining was made of stainless steel, 1.4436hMo (S31600), which, from an aesthetic point of view, offered inadequate corrosion resistance to the acid condensate precipitated on the walls. The result was heavy rusting and a thorough evaluation of several highly alloyed grades was performed prior to the selection of the wall lining for an expansion in 1998. However, despite the heavy rusting, it was eventually concluded that type 1.4436 was good enough from a functional point of view and this grade was also selected for the expansion.

If similar problems occur at other plants, it is recommended that an exposure test be performed prior to the selection of steel grade.

3.04.11.2.5 Stainless steel in oil and gas production[32]

Although oil is not corrosive in itself, production of oil can involve highly corrosive environments because of the simultaneous presence of water and dissolved aggressive species such as oxygen, chlorides, carbon dioxide, and hydrogen sulfide. To a certain degree oil can in fact act as an inhibitor, though it is somewhat unreliable with regard to stainless steels when only a thin oil film is 'isolating' the metal from the corrosive water. Thick films of oil may totally inhibit corrosion.

Initially, mainly carbon steels were used in oil and gas production. However, because of the often increasing amounts of corrosive agents after years of production in old wells and the exploitation of more and more corrosive wells, stainless steels are used increasingly in this industry. Furthermore, environmental considerations have also led to the increased use of stainless steels, since carbon steel demands the addition of vast amounts of various artificial corrosion inhibitors, even under fairly mild corrosive conditions, and most of these inhibitors are more or less hazardous to the environment.

Looking at long term economics, by means of life cycle cost calculations, the use of a stainless steel can often repay the initial extra investment cost, mainly through low maintenance costs and weight savings since stainless steel components do not need to be over dimensioned to compensate for general corrosion, as do carbon steel components. Finally, much longer lifetimes can be achieved with stainless steels than with carbon steels.

Environmental factors

'Sweet' or 'sour' environments Production fluids and gases in the oil and gas industry are traditionally classified as 'sweet' or 'sour' environments, depending on whether hydrogen sulfide is absent or present in significant amounts respectively.

Sweet environments are those containing no or negligible amounts of hydrogen sulfide. High amounts of carbon dioxide may be present in sweet environments, causing accelerated corrosion on carbon steel. Sour environments are those containing significant amounts of hydrogen sulfide. The main concern regarding H_2S is its ability to embrittle metals thereby causing cracking, 'sulfide stress cracking (SSC),' under certain conditions.

Hydrogen sulfide Hydrogen sulfide is one of the main factors to consider, while choosing a material for oil and gas production equipment, because of the risk of SSC.

Sulfides, S_2, HS or H_2S adsorbed to the metal surface, catalyze the absorption of hydrogen atoms by the metal, which may subsequently crack due to hydrogen, induced stress cracking (HISC) depending among other factors on the amount of hydrogen absorbed. It is this cracking that is usually termed 'SSC.' The full mechanism of hydrogen embrittlement by H_2S is still under debate.

The hydrogen absorption caused by H_2S may work synergistically with the factors involved in

chloride SCC, thereby increasing the risk of environmentally induced cracking.

Hydrogen embrittlement seems to be the most active cracking mode at low temperatures, whereas chloride SCC predominates at high temperatures. Consequently, the combined risk of cracking due to H_2S and chlorides tends to be most severe for the nonferritic stainless grades at intermediate temperatures, approximately in the range 80–100°C.

When H_2S is present, it is generally the risk of cracking that is of concern. However, very small amounts of H_2S should not necessarily be seen as a negative factor since the presence of H_2S guarantees a low redox potential in the environment and thereby lowers the risk of chloride-induced localized corrosion, for example, SCC, pitting and crevice corrosion.

Actual limiting critical values of H_2S partial pressures are difficult to give, due to several other factors temperature, pH, and chloride concentration probably being the dominating ones.

Carbon dioxide Stainless steels are not susceptible to the general CO_2 corrosion as are carbon steels. For example, pipelines in carbon steel suffering CO_2 corrosion have been replaced with stainless steel and have given very long service lives. However, CO_2 can indirectly affect the performance of stainless steels by dissociation of carbonic acid, which leads to a lowering of pH.

$$CO_2 + HOH\ {}_2CO_3\ H - + HCO_3$$

It is not surprising that a higher hydrogen ion activity will increase the driving force for hydrogen being absorbed into the metal, so that the metal becomes more prone to cracking (SSC). A significant hydrogen uptake is, however, still only possible when H_2S above a certain concentration is present.

It should be borne in mind that most actual systems have natural pH buffering systems such as from bicarbonate present initially. Therefore the full pH lowering effect caused by CO_2 may not be felt because of buffering action. So, in many practical situations, the system may not be as aggressive as expected from the knowledge only of the partial pressures of CO_2 and H_2S.

Chlorides Chlorides are very often present in high concentrations in water associated with oil and gas formations. Localized corrosion on stainless steels induced by chlorides is well-known. However, the oxygen content of these fluids is mostly extremely low and significantly higher chloride levels are therefore acceptable than under oxygen-saturated conditions. The main cathodic reaction in these systems is the reduction of hydrogen ions.

Temperature As is well-known, normally the higher the temperature the more aggressive the environment with regard to localized corrosion induced by chlorides. However, as mentioned earlier, nonferritic stainless steels seem to show their greatest sensitivity to SSC at around 80–100°C in terms of critical partial pressure of H_2S. This effect is most pronounced in the duplex stainless steels and lower-alloyed austenitic stainless steels. This phenomenon is thought to be explained by the reverse temperature dependency of sulfide-induced SSC and chloride-induced SCC.

Sulfur The presence of elemental sulfur has shown to be highly deleterious for stainless steels and may reduce the critical partial pressure of H_2S appreciably. One possible explanation for the deleterious effect of elemental sulfur is that it can be reduced by hydrogen ions to form H_2S. However, elemental sulfur does not seem to be present in most wells.

Galvanic effects

Creating a galvanic contact between stainless steels and carbon steels will often result in full cathodic protection of the stainless steel with regard to chloride-induced localized corrosion. However, ferritic and duplex stainless steels may, during long periods of exposure, develop hydrogen embrittlement from the increase in the cathodic reaction (hydrogen ion reduction) on the stainless steel surface. Obviously this effect is most pronounced at a low pH.

Artificial environments

In many cases the limiting environment with regard to corrosion may not be the gas or formation water present in the well. A number of chemicals are frequently added to the well in order to optimize the productivity or as part of the initial drilling and set-up procedures.

Stimulation acids are widely used to increase formation permeability. These acids are most often inhibited, however many of these inhibitors have been developed for carbon steel, and there is no guarantee that the inhibition is effective on stainless steels without prior testing.

In general, the use of organic acids is recommended. Excessively large injections should be avoided. This will minimize the risk of creating an unnecessarily aggressive local environment with a low pH. It should be recognized that even though the pH is lowered during acidifying, the concentration of dissolved sulfides is also lowered by general dilution in the near vicinity of the metal.

Completion fluids are sometimes used to counter balance the formation pressure. These fluids may contain high concentrations of chlorides or bromides that inherently introduce an enhanced risk of chloride (halide)-induced localized corrosion.

Injected waters to help secondary recovery may be seawater in the case of offshore production, or produced water in either onshore or offshore production. These waters can be treated in various ways, which influence their corrosivity like dc aeration (less aggressive) or chlorination (more aggressive).

Offshore production – seawater

Topside equipment may be exposed to seawater internally in the case of seawater being used as a cooling liquid or used for the production of freshwater. The unavoidable splashing from the marine environment causes external exposure of topside equipment to seawater.

In these cases, the selection of a stainless steel grade should be based on the maximum temperature and the condition (aerated and untreated, chlorinated, deaerated, etc.) of the seawater. In the case of splashing from the marine environment, possible evaporative conditions should be considered. The super austenitic 6Mo stainless steel grade S31254 (1.4547) has shown excellent performance in many seawater environments.

Submerged pipelines are another example where the outside environment is sometimes potentially more aggressive than that on the inside.

Metallurgical factors

It is generally accepted that the sensitivity to hydrogen embrittlement increases with increasing strength. This has led to the practice of specifying a maximum hardness of the material when used in sour service, as in NACE standard MR0175, which is discussed as follows.

It should be recognized that the traditional correlation between strength, hardness, and SSC sensitivity was based on industry experience with carbon steels. The application of this rule is not so straightforward for stainless steels, where the strength in the annealed condition can vary greatly depending on a number of different metallurgical factors. For example, a high nitrogen content in the fully austenitic stainless steel S31254 (1.4547) or in the super duplex stainless steel S32750 (1.4410) introduces a high strength in the annealed condition, but these steel grades are in general less sensitive to SSC compared with the similar stainless steels containing lower amounts of nitrogen and having lower annealed strength.

Certain stainless steels do, however, become more susceptible to SSC, when they have been cold worked.

Ferritic and martensitic stainless steels Ferritic stainless steels are fairly susceptible to SSC, especially in the cold-worked condition. For common ferritic grades the resistance to chloride-induced pitting and crevice corrosion is also limited. Ferritic stainless steels have therefore found limited use in sour production environments.

Martensitic stainless steels are used mainly when high strength is needed in sweet environments, where they have shown to be cost effective in replacing carbon steel suffering from CO_2 corrosion.

Martensitic stainless steels have a fairly limited chloride-induced localized corrosion resistance, and they show a high susceptibility to SSC.

Austenitic stainless steels Low-alloyed austenitic stainless steels, types S30400 (1.4301) and S31600 (1.4401), are being used for a large number of components. These alloys are far less prone to SSC than ferritic and martensitic alloys as long as they are in the annealed condition. However, heavy cold work of these alloys does increase their susceptibility to SSC even at ambient temperature. Stainless steel S30400 (1.4301) cold worked 30% exhibits susceptibility to SSC even at very low chloride concentrations.[37]

The super austenitic 6Mo stainless steel grade, S31254 (1.4547) has shown excellent resistance to SSC and SCC. Even after cold work up to 80% and coupled to carbon steel, S31254 (1.4547) is highly resistant to SSC. The carbon steel coupling increases the driving force for hydrogen-induced cracking as discussed earlier.

At high temperatures the high chloride-induced SCC resistance is a further argument for the wide spread use of S31254 (1.4547) in oil and gas production.

Duplex stainless steels The high strength of duplex stainless steels together with their high resistance to chloride-induced localized corrosion is

important reasons for their popularity in oil and gas production.

However, it is necessary to observe some restrictions on their use in severe sour environments, since laboratory investigations have indicated moderate SSC susceptibility. It should be borne in mind that pH and stresses in practical applications try tests. This is clearly illustrated by a number of successful applications of duplex steels at far higher partial pressures of H_2S than a number of laboratory investigations have indicated should be possible.

SSC test method NACE MR0175 NACE standard MR0175 presents material requirements for resistance to SSC in oil and gas production equipment and related equipment. The document is a broadly written document. Certainly not all materials listed in MR0175 are satisfactory for all practical sour service applications. However, MR0175 is frequently used as a minimum requirement for the selection of materials for sour service.

In this standard a sour gas environment is defined as containing water as a liquid and hydrogen sulfide in the gas at a partial pressure exceeding 3 mbar (0.05 psi), and with total pressures greater than 4.5 bar (65 psi).

In the case of multiphase systems (gas/'oil'/water) MR0175 defines sour environments as systems with H_2S partial pressure exceeding 3 mbar (0.05 psi) at a total pressure above 18.3 bar (265 psi). At total pressures below 18.3 bar, the partial pressure of H_2S above 0.7 bar (10 psi) or more than 15% H_2S also defines a sour environment. Sour multiphase systems that have operated satisfactorily with standard equipment are outside the scope of MR0175.

MR0175 lists a wide range of metallic materials and product forms that under certain conditions are found to be acceptable for use in sour service. In general the main restriction put on the materials is a maximum hardness level. Requirements for welds are generally the same as for the annealed wrought material with regard to the maximum hardness level.

It should be remembered that MR0175 only addresses SSC in the context of the H2S partial pressure, whereas effects of pH and chloride-induced localized corrosion are not taken into account.

3.04.11.2.6 Stainless steel in wastewater treatment [32,49]

The first methods used to treat wastewater involved reducing the amount of suspended matter in rivers. Biological treatment for further reduction of suspended matter and phosphorus reduction was added as a cleaning process in the 1970s followed by methods for nitrogen removal. During the 1990s, the use of an activated sludge process in the biological treatment of wastewater has increased. New biological purification treatments have been introduced in wastewater treatment plants worldwide, which efficiently reduce nitrates from the water.

Methods of purification

The design of a wastewater treatment plant will usually depend on what methods are required for purification of the wastewater. Both chemical and biological cleaning processes are used to clean the incoming wastewater.

Wastewater treatment plants may contain several stages involving different processes of purification. Main purification processes are mechanical treatment, chemical treatment with removal of phosphorous, biological treatment (including nitrogen reduction), and removal of organic matter. Figure 54 shows a schematic representation of the main stages in a wastewater treatment plant.

Mechanical treatment The sewage enters a wastewater treatment plant through screens that remove

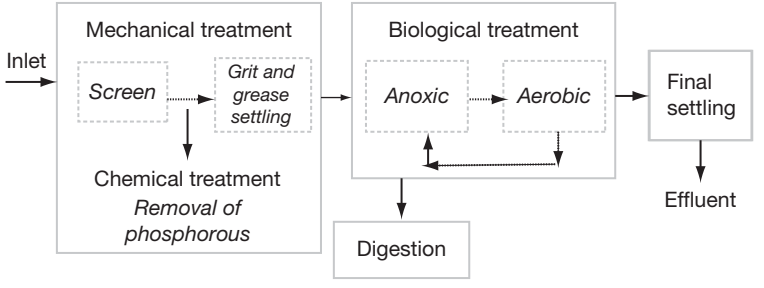

Figure 54 Schematic view of the main processes in a wastewater treatment plant.

large particles. It then continues to a grit chamber, where grit, gravel, oil, and fat are removed from the wastewater, and thereafter to the primary settling stage.

Chemical treatment Phosphorus in wastewater consists of several compounds such as phosphorus in organic compounds and phosphates. However, the organic phosphorus compounds undergo hydrolysis in water and orthophosphate, which is the main compound, is usually removed from the sewage water by precipitation. A variety of precipitation chemicals can be used for this purpose and different plants may have different preferences.

Some examples of precipitation chemicals are ferrous sulfate, aluminum sulfate or iron (III) chloride. In Sweden, the use of poly aluminum chlorides and poly aluminum sulfates in wastewater treatment is a relatively recent development. The dosage point may be prior to the primary settling stage and/or, in some plants, before the final settling tank to ensure low phosphorus content in the effluent.

Biological treatment The biological treatment involves both the removal of nitrogen and the removal of biological carbons. In some plants, it may also involve the reduction of phosphorus. This purification process can be divided into several stages. The biological treatment can alternate between anaerobic (anoxic) conditions and aerobic conditions where air is blown into the water. Biological nitrogen is removed in the processes of nitrification and denitrification. An anaerobic environment assists the denitrification process and an aerobic environment assists the nitrification process. During nitrification, ammonia is converted to nitrate, whilst during denitrification; nitrate is converted to free nitrogen. The end product, nitrogen gas, is then released into the atmosphere.

The internal position of the aerobic nitrification and the anaerobic denitrification stages in the biological treatment may vary from plant to plant. In some plants, the aerobic stage may come first, whereas in others, it may occur at the end, followed by recycling to the anaerobic process. Biological carbons are removed during the aerobic stage where nitrification also occurs. During this process, the biological carbons are converted to carbon dioxide and water.

Final settling After the biological treatment the wastewater passes on to the final settling tanks where the remaining active sludge settles. The sludge may thereafter be passed back and recycled into the biological treatment or transferred into the process of digestion. The temperature of the flowing water in the final settling tanks varies commonly between 10 and 15 °C. After the final settling stage, the effluent can be released into the sea, lakes, or rivers.

Digestion Sludge is removed during the biological treatment and later transferred to large digesters where it undergoes a process of digestion. The active digestion of the sludge is oxygen consuming and the process is considered to be anaerobic. The temperature during the digestion process remains relatively constant at 38 °C while the pH level of the sludge can vary between 6 and 8. During biological digestion, biogas containing hydrogen sulfide gas is produced.

The sludge may be dewatered after digestion by centrifugation. If it contains no heavy metals, the dried sludge may be used as fertilizer.

Corrosion conditions in waste water treatment plants

Chloride Content The chloride ions present in the water promote local corrosion such as crevice corrosion and pitting, and the higher the chloride content, the more corrosive the water. The chloride concentration of the water that passes through sewage treatment plants is usually lower than the chloride concentration of seawater. In Sweden, where the use of de icing salt on the roads is common during the winter period, the chloride content passing through a plant may vary according to season. High values of chloride may be recorded during a few days in the winter season.

MIC and requirements for localized Corrosion on Stainless Steels Ennoblement from microbial activity such as, for example, after the biological cleaning stages, that is, in the final settling of a wastewater treatment plant might provide a high potential closer to, or in the vicinity of, the pitting potential for standard stainless steel grades of type S30400 (1.4301) and S31600 (1.4401) under certain conditions such as in the presence of chlorides, crevices, and deposits. In these environments, localized corrosion can be initiated and propagated with an increased corrosion rate due to the enhanced cathodic reaction caused by the microbial activity.

Addition of Chemicals The most common chemicals used in Scandinavian wastewater treatment plants to precipitate phosphates are aluminum

sulfate, iron (III) chloride, and iron sulfate. At the point where the dosage is in the plant, there is an increased risk of local corrosion using iron (III) chloride. However, the risk of corrosion on stainless steels declines very fast with the distance to this dosage point since the chemicals are diluted in the flowing water. Less corrosive chemicals with no chloride content are iron sulfate and aluminum sulfate.

If, at any stage of the purification process, any other chemicals are added, for example, strong oxidizing agents such as chlorine as a disinfectant, or potassium permanganate for precipitation reactions, care must be taken with the dosage. The dosage must be low enough to ensure that the effect on stainless steels does not promote any increase in the free corrosion potential. This is essential in both the aerobic and anaerobic stages. The effects of strong oxidizing agents such as chlorine and potassium permanganate are well-documented in **Section 3.04.9**.

Corrosion results from field tests in wastewater treatment plants

Field exposures were carried out at different wastewater treatment plants at various locations in Sweden and Denmark to evaluate the risk of corrosion in wastewater treatment plants. The most corrosive part of the plants based on the processes was considered to be the final stages, the settling tanks where chlorides in combination with grown biofilm on the surfaces have to be taken into account. The test materials were welded standard austenitic stainless steel grades S30400, S31600 (1.4301, 1.4436), and a welded duplex stainless steel grade S32205 (1.4462). The chemical compositions of these steels are shown in **Table 21**. The pitting resistance equivalent (PRE) numbers and the critical pitting temperatures CPT according to ASTM G 150 for the steel grades are also presented in **Table 22**.

Field tests were carried out over a 12-month period several wastewater treatment plants in Sweden and Denmark, where the samples were exposed in the final settling tanks. The chemical compositions of the water from three of the exposure sites in the plants are shown in **Table 22**.

The open circuit potentials were measured in for the test coupons exposed in the plants. From these results it was shown that in aerobic conditions the potential increased to a maximum of 340 mV/SCE, schematically shown in **Figure 55**, whereas, in more anaerobic conditions the OCP increase was low and even decreased as schematically shown in **Figures 56**.

At plant 1, corrosion was found on stainless steel grades S30400 (1.4301), and S31600 (1.4436) in combination with heavy deposits, a high chloride content and ennoblement. **Figure 57** shows the extent of corrosion on the base material and on the welds of steel grade S31600 after the removal of the deposits containing both sulfur and manganese.

Base material welds

Table 23 shows the potential values obtained in the field tests in combination with the chloride content and visual observations after the field tests. Biofilms or biological deposits were observed on all samples after the exposure at the plants, but ennoblement was only observed at some plants.

The combination of a high OCP value generated by microbial activity in a biofilm and high chloride content will lead to a higher susceptibility of localized corrosion for steel grade S30400 (1.4301), and S31600 (1.4436). The Localized corrosion was observed in plant 1 for S30400 (1.4301), and S31600

Table 22 Chemical compositions of treated wastewater from the field-test locations

Compound	*Plant 1*	*Plant 3*	*Plant 5 (anaerobic)*
Nitrate-N (mg l^{-1})	10.2	1.5	4.1
Sulphate (mg l^{-1})	129	150	69
Chloride (mg l^{-1})	515	585	78
Iron (mg l^{-1})	0.16	0.083	0.98
Manganese (mg l^{-1})	0.18	0.045	0.069
Aluminium (mg l^{-1})	<0.01	<0.01	0.06
pH	6.8	7.1	7.6
Conductivity (mS m^{-1})	208	263	60.2
COD[a] (mg l^{-1})	4.3	6.6	16[b]

[a]Oxygen consumption measured as chemical oxygen demand (COD).
[b]Higher value than expected from the anaerobic process.

(1.4436) because of a high OCP and high chloride content in combination with heavy deposits. On the other hand, for plants with a low chloride content in the water, no corrosion was observed.

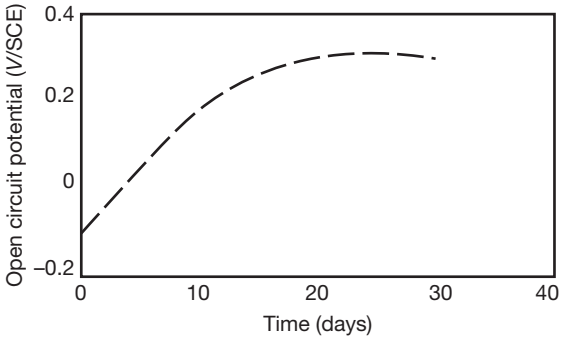

Figure 55 Time dependence of OCP during exposure of stainless steels in the final stage of a wastewater treatment plant in Sweden (aerobic biodegradation of wastes in plant 1).

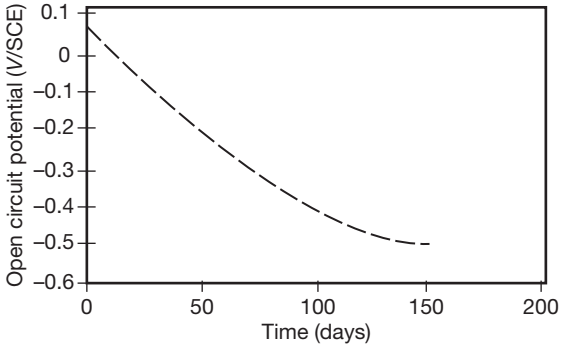

Figure 56 Time dependence of OCP during exposure of stainless steels in the final stage of a wastewater treatment plant in Sweden (anaerobic biodegradation of wastes in plant 3).

3.04.12 High Temperature Corrosion[32]

When stainless steels are exposed to hot gases, chemical reactions take place between the steels, or rather between their alloying elements, and elements or compounds in the gases. As a rule, these reactions will lead to the formation of gas–metal interface layers of reaction products. The chemical compositions and morphologies of these products are determined by, among other factors, the steel and gas compositions and temperatures. These surface layers are more or less protective against further attacks from the gas.

The chemical composition and various standards' designations for some high temperature steels are given in Table 24.

In practice, all stainless steels rely on the formation of an oxide layer. All other reaction products either form a porous, less adherent, and hence nonprotective scale, or are liquid or even volatile and will flux off any existing scale or evaporate. Thus, one condition that must be fulfilled for good high temperature corrosion resistance is that the gas must be oxidizing, that is, it must contain enough oxygen for the formation of a protective layer, consisting of oxides of one or several of the alloying elements. Even so, all oxide scales will eventually experience a breakdown due to growth stresses in the scale. Any measure taken to reduce the scale growth rate will therefore increase the time to breakdown. A low growth rate will also reduce the subscale depletion of the oxide forming element(s), thus improving the ability of the alloy to heal any cracks or other damage to the scale.

The terms oxidizing and reducing are common in the context of high temperature environments, but are not very well-defined and should be used with care. A gas may, for example, be reducing to some of

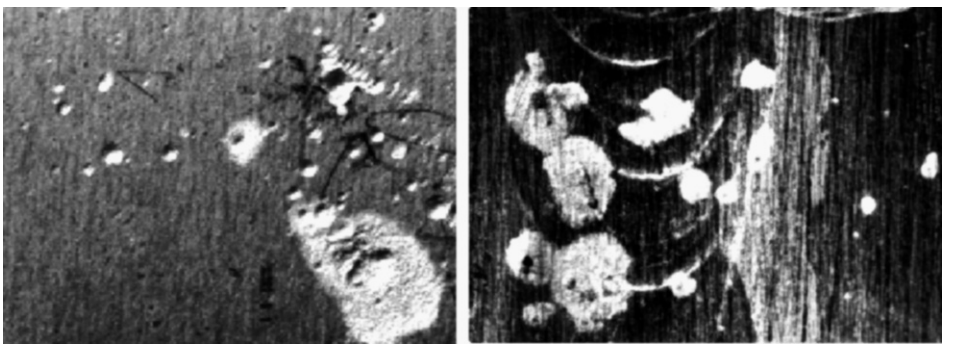

Figure 57 Localized corrosion found on S31600 (1.4436) under heavy deposits after a field test at plant 1. (Magnification×3).

Table 23 Results from visual inspections made after the field tests in the final stages of six treated wastewater treatment plants

Plant	*S30400 weld*	*S31600 base*	*S31600 weld*	*S32205 weld*	*Max OCP (mV/SCE)*	*Chloride content (mg l^{-1})*
1	Corrosion	Corrosion	Corrosion	No corrosion	337	515
2	Corrosion	No corrosion	No corrosion	No corrosion	219	585
3	No corrosion	No corrosion	No corrosion	No corrosion	50	78

Table 24 Typical chemical composition for some examples of high temperature stainless steels

Steel grade		*Typical chemical composition (wt%)*					
EN	*ASTM, UNS*	*C*	*N*	*Cr*	*Ni*	*Si*	*Others*
1.4948	304H	0.05	–	18.3	8.7	0.5	–
1.4878	321H	0.05	–	17.5	9.5	0.5	Ti
1.4818	S30415	0.05	0.15	18.5	9.5	1.3	Ce
1.4828		0.04	–	20	12	2.0	–
1.4833	309S	0.06	–	22.5	12.5	0.5	–
1.4835	S30815	0.09	0.17	21	11	1.7	Ce
1,4841	314	0.10	–	24	19	1.5	–
1.4845	310S	0.05	–	25	20	1.0	–
1.4854	S35315	0.05	0.15	25	35	1.5	Ce

the alloying elements but oxidizing to others. Another gas may contain enough oxygen for the formation of a protective layer; yet at the same time contain other elements that form other, faster growing but less protective compounds.

Gases and/or construction materials are generally chosen to ensure that such a protective layer is in fact formed on the material. For example, the type of gas chosen for heat treatment applications, where oxidation of the treated material is undesired, will generally be reducing, or at least nonoxidizing, to the treated material, but oxidizing to the higher-alloyed furnace construction materials.

In certain processes, however, truly reducing gases are used or produced, and in such circumstances, no oxide layer will form and any existing layer will, as a rule, dissolve. Preoxidation is often used to increase the corrosion resistance in such atmospheres. However, the resulting oxide layer has a limited lifetime and the process of preoxidation has to be repeated at certain intervals.

Heat resistant stainless steels are mainly developed for strength and corrosion resistance at elevated temperatures. As the technical requirements are different, the resistance of these alloys to room temperature 'wet' corrosion may be less satisfactory. The risk of condensation or deposition of aggressive compounds during temporary disturbances or shutdowns must therefore be considered while selecting the construction material. Alternatively, removal of the aggressive gas may be specified in the service instructions for such events.

Several common corrosion types are described as follows. Since some of these corrosion types are generally active, simultaneously or in sequence, in practical cases, one often has to choose between fulfilling contradictory demands for the material's corrosion resistance. Whilst the mechanical or physical properties of the material may sometimes be paramount, this can to some extent be overcome by design.

The very complex nature of high temperature corrosion and the lack of standardized testing practices make it virtually impossible to present corrosion data in tables.

While choosing material for high temperature applications, one must have an extensive knowledge of existing or expected service conditions, such as gas temperature, gas composition and the temperature of the material. Knowledge of previously used materials, their service performance, and of the cause(s) of previous failures are usually of great support in the process of material selection to identify an optimum high temperature grade.

The demands on the corrosion resistance vary depending on the processes and constructions involved. In some plants, components can be maintained,

repaired, or replaced with minor if any interference to normal service, but in other applications, maintenance and repair must be carefully planned and can only be performed during annual or semiannual shutdowns. Obviously, a more careful choice of materials must be made in those cases.

3.04.12.1 Oxidation

When steel is heated in air or another oxygen containing gas, an oxide layer is formed on the surface, acting as a barrier between the steel and the gas. A dense and adherent layer will retard further oxidation, whilst a porous and crack-prone layer will be less protective. Chromium alloyed steels have a better resistance to oxidation than carbon steels since the presence of chromium and mixed chromium–iron oxides in an oxide layer makes it more protective than a pure iron oxides layer. When the chromium content is increased from 0 to 27 wt%, the scaling temperature increases from around 500 to 1125 °C. At temperatures above 1000 °C, aluminum oxides are more protective than chromium oxides. The amount of aluminum required for the formation of a protective layer will, however, make the alloy rather brittle and hence the fabrication difficult and costly.

The scaling temperature is a common measure of the oxidation resistance and is defined as the temperature above which the oxidation rate exceeds a certain value, and is usually determined in different short time cyclic tests, which differ between testing laboratories. The scaling temperature is primarily used for ranking different alloys. The maximum service temperature in air is usually set some 50 °C lower.

Additions of silicon and rare earth metals (REM) improve the oxidation resistance of steels by reducing the oxide layer growth rate further. The protectiveness of the oxide layer also depends on the oxygen activity of the oxidizing gas, as this affects the morphology and composition of the scale.

Rapid temperature changes are detrimental, since thermal stresses will be induced in the oxide layer due to lower thermal expansion of the oxide relative to that of the base metal. This will eventually lead to cracking and spalling of the layer. Ferritic stainless steels have lower thermal expansion coefficients than austenitic high temperature stainless alloys and are therefore more resistant to oxidation under varying temperature conditions. Unfortunately, this advantage cannot generally be fully exploited at higher temperatures due to the poor mechanical strength and the greater tendency for embrittlement of the ferritic stainless steels. The negative effect of temperature variations on the performance of austenitic alloys can be reduced by several means, for example, by increasing the nickel content. Thereby, satisfactory oxidation resistance up to 1150 °C can be reached. REM additions will lead to the formation of a thinner, more ductile, and hence more adherent oxide layer.

In Figure 58, the oxidation behavior of some common austenitic high temperature stainless steels is compared.

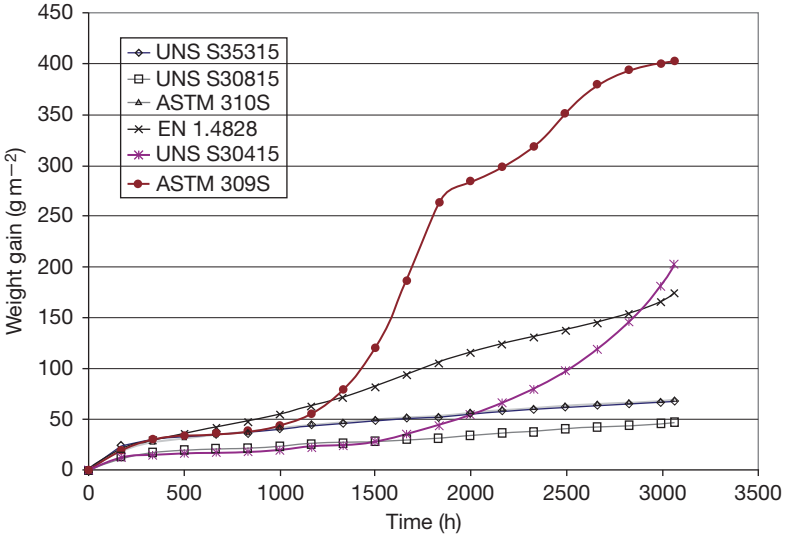

Figure 58 Comparison between common high temperature steels in oxidation behavior at 1000 °C, 165 h cycles.

Although oxides as a rule are beneficial, there are a few elements which tend to form liquid or even gaseous oxides – especially in stagnant atmospheres – which may lead to "catastrophic oxidation," that is, fluxing of the scale by the liquid oxide. Molybdenum (Mo), known to be one of these elements, however, is often used to increase wet corrosion resistance, but should be avoided in materials for service at temperatures above 750°C. A similar behavior is reported for tungsten (W). For niobium (Nb), even worse behavior than for Mo and W has been reported, although some sources claim that it can have a positive effect on the oxidation resistance, at least at lower temperatures.

Two other elements, which form liquid oxides, are vanadium and lead. Their concentration in alloys as either alloying or trace elements is too low to be harmful, but they are sometimes present as contaminants in the environment.

3.04.12.2 Sulfur Attack

Different sulfur compounds are often present as contaminants in flue gases and some process gases. Chemically, sulfidation is similar to oxidation. However, as a rule, sulfides have lower melting points than the corresponding oxide, so the risk for a fluxing of the scale is greater. Especially nickel is a nonfavorable alloying element in that respect. Moreover, the diffusion rates in sulfide scales are generally much higher than in the corresponding oxides, making the scale growth rate higher and the time to scale breakdown shorter.

In oxidizing gases, that is, when a protective oxide layer can be formed, the corrosion resistance is determined by the properties of that layer. Sulfur attacks generally start at cracks in the layer. A ranking of the corrosion resistance of different materials in oxidizing sulfur-containing environments is often equivalent to the oxidation resistance ranking. On the other hand, under conditions where it is difficult to form a protective oxide layer, the corrosion resistance is considerably lower and directly dependent on the bulk chemical composition of the tested alloys. Under these conditions, steels with high chromium content and little or no nickel are superior.

3.04.12.3 Halogen Gas Corrosion

Gases containing halogens, that is, F, Cl, Br, and I or hydrohalides are very aggressive against all metallic materials. Under reducing conditions, nickel and chromium additions generally improve the corrosion resistance. In oxidizing environments, chromium and especially molybdenum and tungsten are very detrimental due to their tendency to form highly volatile oxychlorides and fluorides.

The halogens of practical interest are fluorine and chlorine. Fluorine is considered to be more corrosive than chlorine, which, on the other hand, is more common and more concentrated in most applications. Although theoretical considerations and laboratory tests yield very low maximum service temperatures (<300°C), in practice, stainless steels can often be used up to 600°C.

Other halogen compounds may be equally corrosive, but only after deposition or condensation, see molten salt corrosion in the following section.

3.04.12.4 Molten Salt corrosion

There are several industrial applications in which molten salts are intentionally used, the most important areas being heat treatment, metal extraction, and energy conversion. However, there are also many cases in which the presence of molten salts is far from intentional.

Mixtures of chloride salts are frequently used in salt pots for heat treatment. These 'neutral salts' will neither oxidize nor decarburize heat-treated or construction materials when they are pure, but their corrosivity can increase dramatically if they become oxidized or otherwise contaminated. The salt pots often experience localized attacks at the salt–air interface. Salt pot life can be extended by using special inserts at this transition zone, by using an inert gas instead of air, and/or by rectification (deoxidation) of the salt bath. As for chlorine gas corrosion, low-chromium, high- or medium-nickel alloys are the best material choices. Some recent tests have also shown a good performance for low-nickel, high-silicon alloys. In general, however, salt pot failures are due to poor manufacturing, operational, or maintenance procedures, rather than to poor alloy selection.

Fluoride salts have been suggested for use in nuclear power systems. Those mentioned earlier also apply to them.

In the case of hardening salt pots, cyanides are added to the common chloride mixture. The pot material should then be able to withstand carburization and nitridation, that is, high nickel content is beneficial. Since the cyanide keeps the oxygen content at a low level, these salt pots often show longer service lives than 'neutral salt' pots.

3.04.12.5 Molten Metal Corrosion

Construction materials are deliberately exposed to liquid metals in several applications, for example, heat treatment, energy conversion, and the actual production of those metals. The main corrosion mechanisms in those cases are massive or selective material dissolution, or possibly mass transfer.

Some general observations can be made. With respect to austenitic Ni–Cr–Fe alloys, the higher the nickel content, the more rapidly the alloy dissolves in liquid metal. Ferritic Fe–Cr stainless steels tend to be more resistant, and are not as likely to suffer intergranular attack, as are austenitic alloys.

Specific metals and alloys will not be treated separately in this article. The reader is referred to specialist literature on this subject.

A more unpredictable and hence more dangerous threat is liquid metal embrittlement – a phenomenon caused by local contamination by metals such as Ag, Cu, and Zn. When molten, these metals, or alloys of them, will penetrate austenitic alloys' intergranular and may cause rupture within seconds. Examples where this has been reported to occur are:

- Welding stainless steels to galvanized carbon steels or other zinc contaminated steels, for example, from melting off galvanized steel (e.g., during fire) or from zinc containing paint;
- Weld cracking due to copper contamination, for example, from cold forming tools or back-up bars;
- Cracking caused by copper containing antiseize compounds;
- Cracking from manual, and hence less well-controlled, silver brazing.

References

1. European Committee for Standardization, Brussels, Belgium, EN 10088-1.
2. Leffler, B. *Stainless – Stainless Steels and Their Properties*; Avesta Sheffield AB Research Foundation, Stockholm, Sweden, 1996.
3. MNC Handbok nr 4, Rostfria stål, Metallnormcentralen, Stockholm, Sweden, 1983.
4. Nordberg, H.; Fernheden, K. Nordic Symposium on Mechanical Properties of Stainless Steels. Avesta Research Foundation, 1990.
5. Peckner, B. *Handbook of Stainless Steel*; McGraw-Hill, 1977.
6. *Metals Handbook*, 9th ed.; American Society for Metals, 1981; Vol 4.
7. Leffler, B. *Stainless Steels and Their Properties*, 2nd revised ed.; Outokumpu Stainless Research Foundation, Stockholm, 1998.
8. Nordberg, H. *La Metallurgica Italiana* **1994**, *85*(3), 147–154.
9. Skuin, K. *Neue Hütte,* **1970**, *15*(8), 477–479.
10. Sieurin, H.; Zander, J.; Sandström, R. *Mater. Sci. Eng.* **2006**, *415*(1–2), 66.
11. Richter, F. *StahlEisen-Sonderberichte*; Verlag StahlEisen, 1973; Heft 8.
12. Richter, F. *StahlEisen-Sonderberichte*; Verlag StahlEisen, 1983; Heft 10.
13. Design Guidelines for the selection and use of stainless steel, specialty steel Industry of the United States, Washington, DC, USA.
14. Truman, J. E.; Coleman, M. J.; Pirt, K. R. *Br. Corros. J.* **1977**, *12*(4), 236.
15. Szklarska-Smialowska, Z. *Pitting and Crevice Corrosion,* NACE International, Houston, TX, 2005.
16. Alfonsson, E.; Qvarfort, R. Investigation of the applicability of some PRE expressions for austenitic stainless steels, ACOM 1-1992, Avesta, 1992.
17. Horvath, J.; Uhlig, H. H. *J. Electrochem. Soc.* **1968**, *115*(8), 791.
18. Jargelius-Pettersson, R. F. A. *Corros. Sci.* **1999**, *41*, 1639.
19. Newman, R. C. *Corrosion* **2001**, *57*(12), 1030–1041.
20. Tester, J. W.; Isaacs, H. S. *J. Electrochem. Soc.,* **1975**, *122*(11), 1438.
21. Grimm, R. D.; Landolt, D. *Corros. Sci.* **1994**, *36*, 1847.
22. Donker, H. J.; Dengg, R. A. *Korrosion Metallschutz* **1927**, *3*, 217.
23. Brennert, S. J. *Korrosion Metallschutz* **1937**, *13*, 379.
24. Streicher, M. A. *J. Electrochem. Soc.* **1956**, *103*(7), 375.
25. Laycock, N. J.; Stewart, J.; Newman, R. C. *Corros. Sci.,* **1997**, *29*(10–11), 1791–1809.
26. Szlarka-Smialowska, Z. *Pitting Corrosion of Metals*, NACE, Houston, 1986; p 103.
27. Schwenk, W. *Corrosion* **1964**, *20*(4), 129t.
28. Brigham, R. J.; Tozer, E. W. *Corrosion* **1973**, *29*(1), 33.
29. Qvarfort, R. *Corros. Sci.* **1988**, *28*, 135 (ACOM, No 2–3).
30. Salinas-Bravo, V. M.; Newman, R. C. *Corros. Sci.* **1964**, *36*, 67.
31. Valen, S. I. PhD thesis, University of Trondheim, 1991.
32. Alfonsson, E.; Arnvig, P. E.; Bergquist, A.; Ivarsson, B.; Iversen, A.; Leffler, B.; Nordström, J.; Olsson, J.; Stenvall, P.; Wallén, B.; Vangeli, P. *Outokumpu Stainless Corrosion Handbook*, 9th ed.; Outokumpu Stainless Oy, Sandviken, 2004, pp I:8–I:103.
33. Sedriks, A. J. *SCC of Stainless Steels*; ASM International: Materials Park, OH, 1992; pp 91-130.
34. Sedriks, A. J. *Corrosion of Stainless Steels*, 2nd ed.; John Wiley, 1996.
35. Newman, R. C. In *Corrosion Mechanisms in Theory and Practice*; Marcus, P., Oudar, J., Eds.; Marcel Dekker, 1995; pp 311, 372.
36. Extracted from Dickson, J. I.; Russel, A. J.; Tromans, D. *Can. Met. Q* **1980**, *19*, 161.
37. Iversen, A.; Prosek, T. Eurocorr 2007, Freiburg im Breisgau, Germany, 9–13 September, 2007.
38. Copson, H. R. *Physical Metallurgy of Stress Corrosion Fracture*; Interscience, New York, 1959; p 247.
39. Extracted from Valen, S. I. Proceedings 11th Scandinavian Corrosion Congress, Stavanger, Norway, June 19–21, 1989 and from reference 32.
40. Wallén, B.; Olsson, J. In *Handbook of Stainless Steel*; Peckner, D., Bernstein, I. M., Eds.; McGraw-Hill, 1977; pp 16.1–16.89.
41. Leckie, P. J. *Electrochem. Soc.* **1970**, *117*, 1152.
42. Thierry, D.; Sand, W. *Microbially Influenced Corrosion, Corrosion Mechanisms in Theory and Practice*; Marcel Dekker, 199; pp. 457–499.

43. Mollica, A.; Trevis, E. Proceedings 4th International Congress on Marine Corrosion and Fouling, Juan les Pins, France, 1976, p 351.
44. Feron, D.; Dupont, I.; Novel, G. Eurocorr 96 (1996), European Federation of Corrosion, Publications No 22. Aspects of microbially induced corrosion, 1997.
45. Tverberg, J.; Pinnow, K.; Redmerski, L. NACE Corrosion, Paper 151, April 23–27, Nevada, 1990.
46. Mameng, S. Amase master thesis, EEIGM Nancy, École Européenne d'ingénieurs en Génie des Matériaux, Institut Nation Polytechnique de Lorraine, France, 2007.
47. MAST II Program. Biofilm Project Contract No MAS2 CT92 001.1, CNR-ICMM: Scotto, V. (coordinator), Mollica, A., Ventura, G., Traverso, E., Trentin, I., Marcenaro, G., Piccarolo, C., Martinoli, O., Andrei, E., Lai, E., Dellepiane, R., Decarolis, G., CEA: Féron, D., Dupont, I., Delepine, J., Blanchard, D., Letouze, J. M., Bourneuf, F., Laniece, V., Massilian, R., Lefevre, Y. ENRICERCHE: Carrera, P., Camilli, M., Pietrangeli, B., Gianna, R., IFREMER: Compère, C., Festy, D., Mazeas, F., Leroux, J. P., Riou, L., IRSID: Audouard, J. P., Dowling, N. J., Bonnet, C., SCI: Thierry, D., Taxen, C., Kivisäkk, U., Aronsson, C., Linder, M., SINTEF: Rogne, T., Steinsmo, U., Drugli, J. M., Solem, T., Bjordal, M., Final report Marine Biofilms on Stainless Steels: Effects, Monitoring and Prevention, European Commission, 1996.
48. Mollica, A.; Montini, U.; Scotto, V.; Marcenaro, G. Comportement face a la corrosion d'alliages ferreux en sediments anaerobies portuaires, Communication par affice à ''Biocorrosion prevention et maintenance'' Strasbourg (France), Octobre 1989.
49. Mollica, A.; Ventura, G. Crevice corrosion resistance of Stainless Steels in anaerobic seawater enriched by sulfides produced by SRB's activity, Technical Report, CNR-ICMM-BC-1/97.
50. Iversen, A. *Br. Corros. J.* **2001**, *36*(4), 277–291.

3.05 Aqueous Corrosion of Nickel and its Alloys

H. Alves
ThyssenKrupp VDM GmbH, Plettenberger Str. 2, D-58791 Werdohl, Germany
U. Heubner
Consultant, Borgheller Str. 28, D-58791 Werdohl, Germany

Abbreviations

ABS Acrylonitrile butadiene styrene (copolymer)
AOD Argon-oxygen-decarburization
ASTM American Society for Testing and Materials
BAM Bundesanstalt Fuer Materialforschung und-pruefung (Germany)
CCT Critical crevice corrosion temperature
CPI Chemical process industry
CPT Critical pitting temperature
EDC Ethylene dichloride
EN European standardization
FGD Flue gas desulfurization
FM Filler metal
HAZ Heat affected zone
IC Intercrystalline corrosion
LC Low carbon
MDI Methylene di-paraphenylene
NACE National Association of Corrosion Engineers
PRE Pitting resistance equivalent
PVC Polyvinyl chloride
SAN Styrene acrylonitrile (plastic resin)
SBR Styrene butadiene rubber
SEP Stahl-Eisen-Pruefblaetter (Germany)
TDI Toluene di-isocyanate
TIG Tungsten inert gas welding process
UNS Unified numbering system (North America)
VCM Vinyl chloride monomer
VOD Vacuum-oxygen-decarburization

Symbols

A_V Notch impact energy (J)
mV_{NHE} Potential versus a normal hydrogen electrode (mV)
M_6C Metal carbide
p.a. Analytical grade purity
pH Negative logarithm of the concentration of dissolved hydrogen ions (H^+)
V_{SCE} Potential versus a saturated calomel electrode (V)

3.05.1 Introduction

Within the chemical process industry (CPI), as well as other industries, the austenitic corrosion-resistant stainless steels have been, and will continue to be, the most widely used tonnage material after carbon steel. Materials of construction for the modern chemical process and petrochemical industries must not only resist uniform corrosion caused by various aqueous media, but must also have sufficient resistance to localized corrosion as pitting, crevice corrosion and stress-corrosion cracking. Chemical process and petrochemical industries have to cope with the technical and commercial challenges of rigid environmental regulations, the need to increase the production efficiency by utilizing higher temperatures and pressures and more corrosive catalysts and, at the same time, possess the necessary versatility to handle varied feedstock and upset conditions. Over the past 50 years, improvements in alloy metallurgy, melting technology, and thermomechanical processing, along with a better fundamental understanding of the role of various alloying elements, have led to new nickel alloys that not only extend the range of usefulness of the existing alloys by overcoming their limitations, but are also reliable and cost-effective, and have opened new areas of applications.

Nickel and nickel alloys have useful resistance to a wide variety of aqueous corrosive environments typically encountered in various industrial processes. In many instances, the corrosive conditions are too severe to be handled by other commercially available materials, including stainless and super stainless steels. Nickel by itself is a very versatile corrosion-resistant metal finding many useful applications in industry. More importantly, its metallurgical compatibility over a considerable composition range with a number of other metals as alloying elements has become the basis for many binary, ternary, and other complex nickel alloy systems having unique and specific corrosion-resistant behavior for handling the modern-day corrosive environments of chemical processing, petrochemical, marine, pulp and paper, agrichemicals, oil and gas, energy conversion, and many other industries. These alloys are more expensive than are the standard austenitic corrosion-resistant stainless steels because of their higher alloy content and more involved thermomechanical processing, and hence, are used only when stainless steels are not suitable or when product purity and/or safety considerations are of critical importance. Corrosion resistance depends on the chemical composition of the alloy, the alloy's microstructural features developed during thermomechanical processing, the chemical nature of the environment, and the various reactions occurring at the alloy–environment interface.

In this chapter, the major nickel alloy systems are discussed, including their major characteristics, the effects of alloying elements, and most

importantly, the strengths, weaknesses, and applications of these systems. A few words on fabrication are also included, because an improper fabrication may destroy the corrosion resistance of an otherwise fully satisfactory nickel alloy.

3.05.2 Brief Survey of Nickel and Nickel Alloy Groups for Aqueous Corrosive Applications

Nickel and nickel alloy systems for aqueous corrosive applications can be divided into various groups according to their composition as shown in Table 1.

Table 1 gives, in its first column, the internationally used, but not standardized, alloy designation, followed in the second column by the materials' number in use for European standardization (EN). In the third column, the designation according to the unified numbering system (UNS) of the Unified States is indicated. The following columns describe nickel and the various nickel alloys by means of their main alloying elements, indicating typical values only.

With reference to Table 1 from top to bottom, the first alloy group is unalloyed nickel in its high-carbon (maximum 0.05 mass%) and special low-carbon (maximum 0.02 mass%) forms, designated as alloys 200 and 201, respectively. Second are the nickel–copper alloy 400 and its age-hardenable version alloy K-500, which are widely used. Third is the nickel–molybdenum group, where only one of its members, the quasibinary nickel–molybdenum alloy B-2 is mentioned, due to the very limited use of this type of alloy in special applications. The nickel–chromium alloy group can be considered to be an extension of the austenitic nickel–chromium stainless steels up to very high nickel and to rather low iron content.

The group of nickel–chromium–molybdenum alloys has restricted iron content only and may contain tungsten besides some other elements like niobium, copper, and tantalum. Since the corrosion behavior of these alloys is largely dependent on the amounts of

Table 1 Principal nickel alloy groups for aqueous corrosive applications

Designation			*Main alloying elements, typical values (mass%)*					
Alloy	EN	UNS	Ni	Cr	Mo	Cu	Fe	Other elements/remarks
Nickel								
200	2.4066	N02200	99.5					Ni >99.2
201	2.4068	N02201	99.5					Ni >99, C ≤0.02
Nickel–copper								
400	2.4360	N04400	64			32	1.8	1.0 Mn
K-500	2.4375	N05500	65			30	1.0	0.6 Mn, 2.8 Al, 0.45 Ti
Nickel–molybdenum								
B-2	2.4617	N10665	69	0.7	28		1.7	
Nickel–chromium								
600 L	2.4817	N06600	73	16			9	0.25 Ti, C ≤0.025
690	2.4642	N06690	61	29			9	0.25 Ti
Nickel–chromium–molybdenum with (Cr + Mo) in ascending order								
625	2.4856	N06625	62	22	9		3	3.4 Nb
C-4	2.4610	N06455	66	16	16		1	
C-276	2.4819	N10276	57	16	16		6	3.5 W
22	2.4602	N06022	56	22	13		4	3 W
686	2.4606	N06686	58	21	16		1.5	3.8 W
MAT 21		N06210	58	19	19		<1	1.8 Ta
2000	2.4675	N06200	57	23	16	1.6	1.5	
59	2.4605	N06059	59	23	16		1	
Nickel–chromium–iron–molybdenum–copper with (Cr + Mo) in ascending order								
20	2.4660	N08020	38	20	2.4	3.4	34	0.2 Nb
825	2.4858	N08825	40	23	3.2	2.2	31	0.8 Ti
G-3	2.4619	N06985	48	23	7	2.0	19	0.3 Nb
31	1.4562	N08031	31	27	6.5	0.9	45	0.20 N
33	1.4591	R20033	31	33	1.6	0.6	32	0.40 N
G-30	2.4603	N06030	43	30	5	1.7	15	2.5 W, 0.7 Nb
Age-hardenable nickel–chromium–iron–molybdenum(–Copper)								
718	2.4668	N07718	53	19	3		18	5.2 Nb, 0.9 Ti, 0.6 Al
925	2.4852	N09925	44	21	3	2	27	2.1 Ti, 0.3 Al

chromium and molybdenum being added as alloying elements, the alloys are arranged in Table 1 according to the sum of these elements in ascending order.

For the same reason, the members of the following nickel–chromium–iron–molybdenum–copper alloy group are arranged according to the sum of their alloying elements chromium and molybdenum in ascending order. However, other alloying elements like copper and nitrogen, and last but not least, nickel, exert an influence on the corrosion behavior too. This will be pointed out more in detail in the following subsection devoted to this alloy group. The alloys of this group are higher in iron than are the alloys of the nickel–chromium–molybdenum alloy group, and are, in this way, closely related to or – depending on the formalities of classification – at the same time part of the corrosion-resistant high-alloy special stainless steels.

At the bottom of the table is the age-hardenable nickel–chromium–iron–molybdenum (–copper) alloy group that is of great importance in the special application of oil and gas extraction.

Although the list of the principal nickel alloy groups for aqueous corrosive applications presented in Table 1 seems to be quite large, it shows a selection of the most important alloys only. The great number of nickel alloys for aqueous corrosive applications that are available today is the result of a phenomenal recent growth in the development of new nickel alloys, with special emphasis on the high-performance nickel–chromium–molybdenum alloy group. This development of new alloys has become possible by the introduction of new metallurgical techniques like argon–oxygen-decarburization (AOD) and vacuum–oxygen-decarburization (VOD) in the 1960s. These new metallurgical techniques allow easy decarburization of large volumes of molten alloys down to very low carbon contents as, for instance, 0.005 mass%. Table 2 gives a brief listing of developments of some nickel alloys during the pre-1950s and since the 1950s.[1] As is evident from this listing, today's corrosion and material engineers have a much wider selection of alloys to meet their specific needs than had been the case prior to the 1950s when the alloy choices available for combating aqueous corrosion were very limited. This historical development has to be kept in mind when reading older literature on corrosion-resistant materials. New alloys and refinements of old ones are constantly under way.

3.05.3 Nickel and Nickel Alloy Groups for Aqueous Corrosive Applications

3.05.3.1 Nickel

As Friend[2] points out, the standard reduction potential of nickel that is shown in the electrochemical series of metals is nobler than that of iron and less noble than that of copper. Owing to nickel's marked hydrogen overpotential, hydrogen is not so easily liberated from the usual nonoxidizing acids, and the presence of oxygen, for example, from dissolved air is generally necessary here in order to allow corrosion to proceed. The general rule is that oxidizing conditions promote the corrosion of nickel in chemical solutions, whereas reducing conditions retard it. However, nickel has the ability to protect itself against certain forms of corrosive attack by forming a passive layer of oxide or hydrated oxide, and in practice often exhibits a more noble behavior than does copper. Therefore, corrosion is not always accelerated by oxidizing conditions. A certain amount of pitting may occur if the passive layer is locally destroyed, for example, in hot chloride solutions. The results of the studies of the mechanism of passivation of nickel have been reviewed extensively by Friend.[2]

If the temperature is not excessively high, nickel has a useful measure of resistance to corrosive attack by dilute nonaerated solutions of most of the nonoxidizing mineral acids, for example, sulfuric, hydrochloric, and phosphoric acid. This also applies to the nonoxidizing salts of such acids, which can hydrolyze with the formation of dilute solutions of these

Table 2 Historical development and introduction to the market of selected nickel alloys

	Period					
Alloy	*Pre-1950s*	*1950s*	*1960s*	*1970s*	*1980s*	*1990s*
Ni, Ni–Cu, Ni–Cr	200, 400, 600					
Ni–Mo	B			B-2		B-2 'controlled composition'
Ni–Fe–Cr–Mo–Cu		825	20, G	G-3	G-30	31, 33
Ni–Cr–Mo	C		C-276, 625	C-4	22	59, 686, 2000, MAT 21

acids. Nickel may corrode rapidly in oxidizing acids, for example, nitric acid, or in other mineral acids containing significant amounts of oxidants.

Nickel has a useful measure of corrosion resistance to most nonaerated organic acids and other organic compounds. This enables it to be used in the plastics industry. When being used in the food industry, nickel itself might exhibit a sufficient level of corrosion resistance in the medium under consideration, nevertheless attention has to be paid to the amount of nickel ions that might migrate into the food, and for this reason, nickel-plated food contact materials should not be used.[3]

Nickel is very resistant to corrosion by most kinds of natural and highly purified water. However, if water intended for human consumption is considered, the size of the surface of the nickel-plated parts being exposed to the water should be limited and a sufficient amount of flow maintained as well, in order to avoid an excessive uptake of nickel by the drinking water, and in this way, meet the requirements of the European Council Directive 98/83/EC on the quality of drinking water.[4]

Nickel is also resistant to fast-flowing seawater. Under stationary conditions, however, it is susceptible to substantial growth of organisms, with the result that severe local attack may occur under this and other deposits.

Nickel is outstandingly resistant to alkalis such as sodium and potassium hydroxide, even at high concentrations and temperatures, with the exception of more highly concentrated ammonium hydroxide solutions, and to nonoxidizing alkaline and neutral salts. This property is the reason for nickel's use in chemical process equipment manufacturing for the production and processing of caustic soda and caustic potash. **Figure 1** shows an isocorrosion diagram of nickel in caustic soda solution originally established more than 30 years ago[5] and redrawn more recently,[6] due to its unique importance for the industrial application of metallic nickel. Obviously, in practice, this diagram can only be used as an initial guide, because admixtures and impurities that may be present in the caustic soda influence the metal's corrosion behavior.

More detailed information on nickel's corrosion behavior is provided by Friend.[2] In traditional parlance, unalloyed nickel in wet-corrosion applications is referred to as 'pure nickel.' The most popular grades for wet-corrosion service are the standard grade alloy 200 (EN 2.4066/UNS N02200) and the low-carbon grade alloy 201 (EN 2.4068/UNS N02201) shown in **Table 1**. The low-carbon grade must be used at temperatures in excess of 315 °C (600 °F) in order to avoid loss of ductility because of the precipitation of graphite at the grain boundaries within the metal's microstructure.[2] In addition, unalloyed nickel when used in electroplated form, mainly on steel and brass, may be exposed to wet-corrosive attack too.

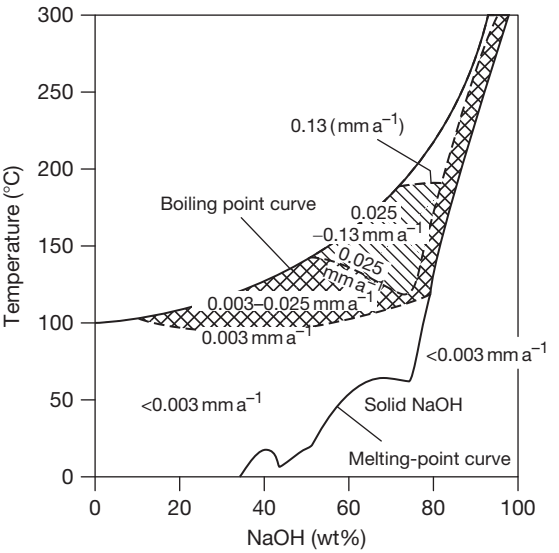

Figure 1 Corrosion resistance of unalloyed nickel in sodium hydroxide, related to concentration and temperature. Reproduced from Heubner, U. In *Nickel Alloys and Special Stainless Steels*; 3rd ed.; Heubner/Klöwer, *et al*., Ed.; Expert Verlag: Renningen, 2003; Chapter 2, pp 47–93.

3.05.3.2 Nickel–Copper Alloys

Copper is reasonably corrosion-resistant in dilute, nonoxidizing, nonaerated solutions of mineral acids such as sulfuric, hydrochloric, phosphoric, or hydrofluoric acid, and also of most organic acids, for example, acetic and formic acid, even at quite high temperatures. It is attacked by hot concentrated solutions of these acids. When nickel and nickel alloys are alloyed with copper, their resistance to these nonoxidizing acid solutions is generally improved. In particular, copper is often added to increase the corrosion resistance of nickel alloys and high-alloy special stainless steels in sulfuric acid.

Nickel–copper alloys containing, for instance, 27–34 mass% copper may have a useful measure of corrosion resistance in nonaerated sulfuric acid at concentrations of up to 80% at room temperature, 60% at 70 °C, and 20% at boiling temperature (Craig and Anderson[7] indicate data that are at variance with this).

Nickel–copper alloys are reasonably resistant to dilute hydrochloric acid solutions, provided that, like

the aforementioned sulfuric acid solutions, they are kept free of air. These alloys can then be used at hydrochloric acid concentrations of up to ~15% at room temperature and ~5% at ~70 °C. Therefore, they can be used for handling nonoxidizing chlorides, which form hydrochloric acid in low concentrations by hydrolysis in the presence of water.

Nickel–copper alloys are one of the few types of metallic materials that exhibit good corrosion resistance in nonaerated hydrofluoric acid of all concentrations. In aerated solutions, on the other hand, severe metal dissolution and stress-corrosion cracking may occur. The corrosion rates are shown in detail in the isocorrosion diagram for nonaerated and aerated solutions.

Nickel–copper alloys are resistant to most kinds of water; their resistance to seawater with a high flow-velocity is particularly relevant for their use in actual service. They can therefore be used for, among other things, heat exchanger tubes and for shielding in seawater spray and tidal zones. The age-hardenable variant is used in places where not only resistance to seawater but also high strength are important, for example, for ship propeller shafts, valve seats, studs, bolts, and pump components. Under stationary conditions, incrustation by marine organisms can occur, causing concentration cells to form, which result in pitting. This, however, tends to slow down with time and even, in tropical waters, seldom exceeds penetration depths of ~0.75 mm (30 mils) after a few years.

Thanks to their high nickel content, nickel–copper alloys are resistant to most alkalis (except ammonium hydroxide) and most nonoxidizing alkaline and neutral salts. They have good resistance in caustic soda and caustic potash, similar to that of unalloyed nickel. Rates of corrosion of less than 0.05 mm $year^{-1}$ were found up to a concentration of 75% NaOH and a temperature of 130 °C. When 75% NaOH is evaporated to anhydrous NaOH, the corrosion rates are higher than with unalloyed nickel, and in molten NaOH, stress-corrosion cracking was observed in equipment items subjected to high mechanical stress. Under such conditions, therefore, the components must undergo stress-relief annealing.

Neutral and alkaline salt solutions such as chlorides, carbonates, sulfates, nitrates, and acetates have only a minimal corrosive effect on nickel–copper alloys, even at high concentrations and temperatures up to the boiling point; consequently, corrosion rates are generally less than 0.025 mm $year^{-1}$. Nickel–copper alloys are, therefore, used in plants in which salts are crystallized from saturated brines.

Nickel–copper alloys are not resistant to highly oxidizing solutions such as nitric and chromic acid, moist chlorine, and hypochlorites.

The most important nickel–copper alloys for engineering purposes are alloy 400 (EN 2.4360/UNS N04400) and the age-hardenable variant alloy K-500 (EN 2.4375/UNS N05500) as mentioned in **Table 1**.

Related, in the broader sense, to the nickel–copper alloys are the copper–nickel alloys, which are dealt with in **Chapter 3.07, Corrosion of Copper and its Alloys**.

3.05.3.3 Nickel–Molybdenum Alloys

Molybdenum exhibits a very good corrosion resistance to nonoxidizing solutions of hydrochloric, phosphoric, and hydrofluoric acid at most concentrations and temperatures and to boiling sulfuric acid up to a concentration of ~60%. The alloying of nickel and nickel alloys with molybdenum improves their corrosion resistance in these media approximately in proportion to the percentage of added molybdenum. Nickel–molybdenum alloys, which typically contain 26–30 mass% molybdenum, are among the few metallic materials that are resistant to nonaerated hydrochloric acid at all concentrations and temperatures.[6] The prerequisite is the absence of oxidizing additions such as dissolved oxygen and heavy metal ions. Otherwise, the corrosion rates can increase significantly, as the isocorrosion diagrams shown by Craig and Anderson[7] for the alloy type B-2 make clear by way of example.

In nickel–molybdenum alloys, the practicable molybdenum content is subject to an upper limit owing to the constitutional situation.[8–10] As shown in **Table 1**, the commercial alloy B-2 typically contains 28 mass% molybdenum. As **Figure 2** makes clear,[6,11] at this molybdenum content, a minimal rate of corrosion, which depends only to a slight extent on variations in the molybdenum content, can be anticipated in tests in boiling 10% hydrochloric acid as a test method, which is widely used in such circumstances.

Up to the mid-1990s, problems were frequently encountered when working and using the technologically established alloy B-2 (EN 2.4617/UNS N10665) because of fractures during working and stress-corrosion cracking while in service. The cause of both the fall in ductility and the stress-corrosion cracking is considered to be the formation of the ordered Ni_4Mo phase,[9,10] a phenomenon that is accelerated by cold deformation.[12] A thorough

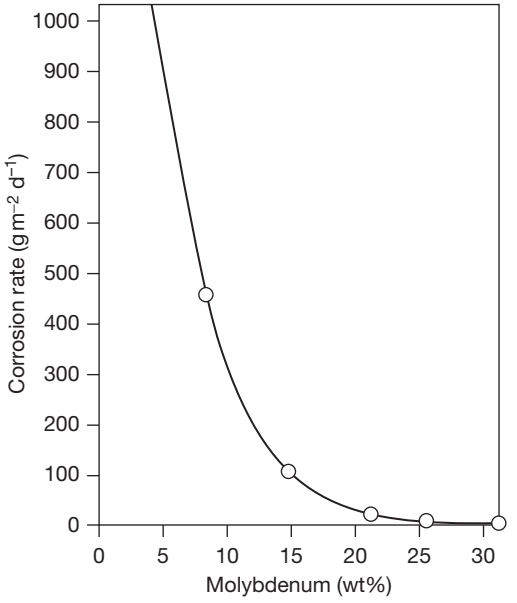

Figure 2 Influence of the molybdenum content on the corrosion resistance of nickel–molybdenum alloys in boiling 10% hydrochloric acid.[6,11]

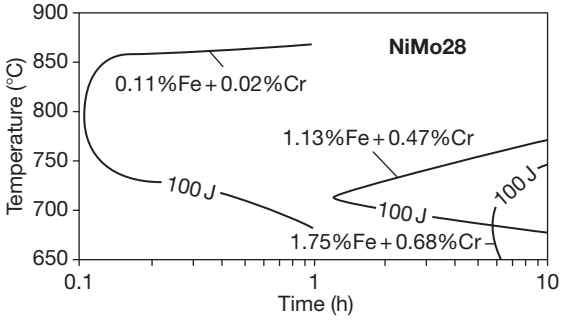

Figure 3 Time–temperature–notch impact energy diagrams for the alloy NiMo28 – alloy B-2 (EN 2.4617/UNS N10665), established using three melts with different iron and chromium contents.[6,8]

analysis showed that the risk of such damage can be greatly reduced if the iron and chromium contents of this type of alloy are set close to the upper limit of what is acceptable according to the specification.[10] Figure 3 reveals by way of example how with this material the decrease in ductility during a working-related input of heat in the medium temperature range is delayed with increasing iron and chromium contents. It is due to these findings that a new alloy B-2 'controlled composition' with Fe at 1.7 and Cr at 0.7 mass% as typical values, as shown in Table 1, had been introduced to the market in the 1990s (cf. Table 2). Nevertheless, solution annealing of cold-formed parts, for example, heads, may be necessary when deformation is greater than 7% outer fiber elongation of cold work in order to avoid susceptibility to cracking at welds and heat affected zones during subsequent fabrication or later service.

The isocorrosion diagram plotted for alloy B-2 (EN 2.4617/UNS N10665) in nonaerated sulfuric acid shows interesting areas of resistance, for example, at concentrations between 60% and 80% and at temperatures above 120 °C. This too is subject to the prerequisite that clearly reducing conditions must be present; oxygen inputs due to aeration, heavy metal ions, and other oxidants accelerate corrosion.[6,7]

The corrosion resistance of alloy B-2 (EN 2.4617/UNS 10665) in organic acids, especially acetic acid, is tied to similar conditions.[2]

Thanks to its extremely low carbon and silicon contents, the NiMo28 alloy B-2 (EN 2.4617/UNS 10665) has good resistance to knife-line corrosion and selective corrosion in the heat-affected zone (HAZ) and can therefore usually be used in the welded state without further heat treatment.

3.05.3.4 Nickel–Chromium Alloys

Nickel and nickel alloys are alloyed with chromium to improve their resistance to strongly oxidizing media. Substances of this kind include nitric acid, chromic acid, and some acidic solutions containing oxidizing salts, with the exception of chlorides. In this case, corrosion resistance increases approximately in proportion to the chromium content, provided that it is more than 10 wt%. In the case of aerated acidic solutions, especially at elevated temperatures, chromium contents of more than 18% are preferable.[2] Figure 4 serves as a typical example of the effect of chromium on the reduction of the corrosion rate in strongly oxidizing solutions, referring as much to iron–chromium–nickel alloys as to nickel–chromium–iron alloys as shown by the example of alloy 690 (cf. Table 1). The difference between the older data and the newer data reflects the introduction of the melting technologies AOD and VOD, which occurred in the 1960s and resulted in cleaner alloys. Internal cleanness of the metallic grain structure is an often overlooked prerequisite for an enduring resistance to corrosive attack in the passive/transpassive and in the transpassive area, as may happen in strongly oxidizing solutions such as boiling azeotropic nitric acid as in Figure 4.

Since nickel–chromium alloys require the presence of further alloying elements in order for them

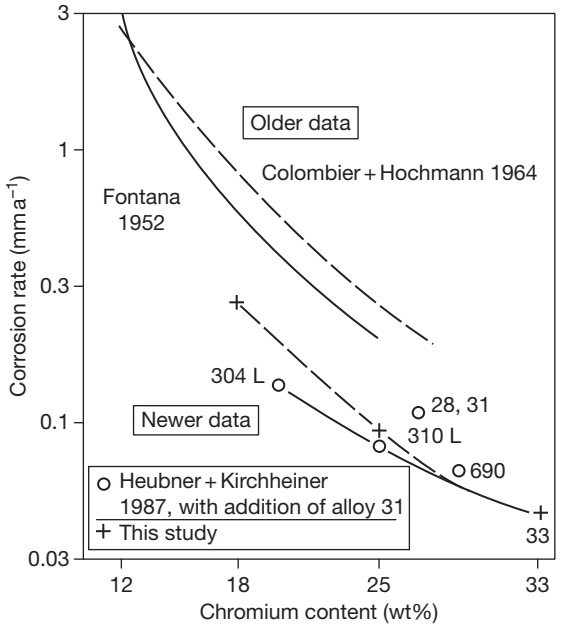

Figure 4 Corrosion of iron–chromium–nickel and nickel–chromium–iron alloys in boiling azeotropic nitric acid.[13,14]

to be universally suitable for wet-corrosion service, they are few in number and their use tends to be limited to special cases. In current engineering practice, there are only two that are commonly used: alloy 600 L (EN 2.4817/UNS N 06600) and alloy 690 (EN 2.4642/UNS N 06690). As shown in **Table 1**, these alloys also have a nominal iron content of 9 mass%. This means that, strictly speaking, they are nickel–chromium–iron alloys. Owing to their high nickel content, both can be considered for corrosive attack by hot alkaline solutions if they contain oxidants; examples are chlorates from diaphragm cells or sulfur compounds. These types of alloy are also used for steam generators in nuclear power stations. Owing to its high chromium content, alloy 690 has also been considered for corrosive attack by strongly oxidizing media. Nowadays, however, as is evident from **Figure 4**, the more recently developed alloy 33 (EN 1.4591/UNS R20033) is probably a better alternative.[13,14]

3.05.3.5 Nickel–Chromium–Molybdenum Alloys

3.05.3.5.1 General

As is to be expected, nickel–chromium–molybdenum alloys combine the good resistance to corrosion of nickel–molybdenum alloys under reducing conditions with the good resistance to corrosion exhibited by nickel–chromium alloys under oxidizing conditions. The most important for engineering purposes are the so-called C-type alloys, the first of which was introduced as long ago as the 1930s. This was a nickel alloy with typically (figures in mass%) 16% chromium and 16% molybdenum, which also contained 4% tungsten and 6% iron together with 0.7% silicon and 0.05% carbon; this alloy is no longer in common use.[15] With the discovery that to reduce precipitation-readiness, it is important to reduce both the carbon and the silicon content of such materials to very low levels, it was developed into the alloy C-276 (EN 2.4819/UNS N10276), which is in use today, as shown in **Table 1**. Since the 1960s, this has also been possible on a large scale without major problems, thanks to the new AOD and VOD production processes, which were introduced from that date onwards (cf. **Section 3.05.3.4**). Low silicon contents of typically 0.04 mass% and very low carbon contents of typically 0.005 mass% are nowadays characteristic of all the commonly used C-type nickel–chromium–molybdenum alloys,[15] which also include the alloys C-4 (EN 2.4610/UNS N06455), 22 (EN 2.4602/UNS N06022), and 59 (EN 2.4605/UNS N06059) in **Table 1**.

3.05.3.5.2 Alloy C-276

Alloy C-276 (EN 2.4819/UNS N10276) has its main areas of use for prevailing corrosive attack by reducing acids such as sulfuric acid, phosphoric acid, hydrochloric acid, and organic acids. Its isocorrosion diagram in technical grade sulfuric acid is reproduced in **Figure 5**.

Owing to its good corrosion resistance in predominantly reducing media, even in the presence of halogens, it has succeeded in conquering a wide range of applications in the chemical industry; today, however, these are increasingly being taken over by the subsequently developed alloy 59 (see later text), which can be used on a more universal scale. This applies, for example, to plate-type heat exchangers in sulfuric acid production, which operate at reduced temperatures. Alloy C-276 is also used in applications where its resistance to hydrochloric acid solutions comes to the fore, for example, in the production of vinyl chloride monomer (VCM), methylene di-*para*-phenylene isocyanate (MDI), and toluene di-isocyanate (TDI). Moreover, this type of alloy has good resistance to acetic acid at all concentrations and temperatures,[7] and is used for handling oxidizing acetic acid solutions and in places where acetic acid occurs in combination with inorganic acids and salts,

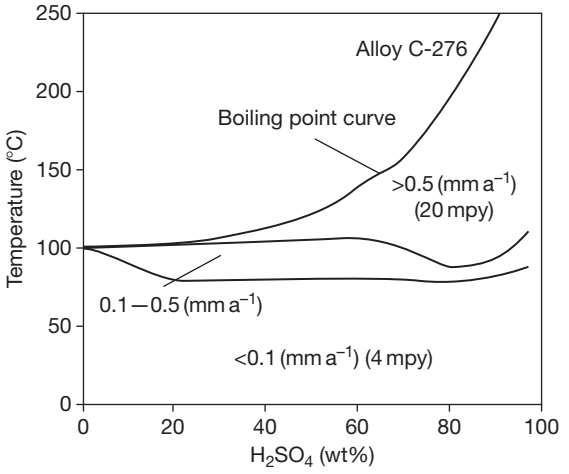

Figure 5 Isocorrosion diagram of alloy C-276 (EN 2.4819/UNS N10267) in slightly aerated technical grade sulfuric acid, determined by immersion tests over at least 120 h. Reproduced from Kirchheiner, R.; Wahl, V. In *Nickel Alloys and Special Stainless Steels*; 3rd ed.; Heubner/Klöwer, *et al.*, Ed.; Expert Verlag: Renningen, 2003; Chapter 8, pp 255–294.

which restrict the use of stainless steels.[7] Alloy C-276 has proved to be resistant to chloride-induced stress-corrosion cracking under very aggressive sour-gas conditions, even in the presence of elemental sulfur, but is susceptible to hydrogen-induced stress-corrosion cracking in such media below a temperature of 100 °C.[16] The material's capabilities are also well proven in environmental technology where it has a broad area of use in flue gas desulfurization (FGD).[17] Other important industries in which this type of alloy has become established together with its C-4 variant, which is described in the following section, are listed by Agarwal *et al.*[15] Some details of this material and its corrosion behavior are discussed in the following section in comparison with the other C-alloys.

3.05.3.5.3 Alloy C-4

Alloy C-4 (EN 2.4610/UNS N06455) is a variant of alloy C-276, which is in common use in the European chemical industry in particular. As shown in **Table 1**, it differs from the latter material in the absence of tungsten as an alloying element and greatly reduced iron content. Consequently, the alloy is less resistant in predominantly reducing media, but is much less prone to precipitation and very much easier to work, with the result that, on its commercial launch in the 1970s, it rapidly gained acceptance in the chemical industry. The important chemical industry applications include fertilizer and pesticide production processes and the production of pharmaceutical intermediates, acetic acid, and inorganic chemicals. In the version without the addition of titanium that is supplied by ThyssenKrupp VDM GmbH, it is free from titanium nitrides. This enables a uniformly smooth surface, which remains smooth, to be obtained in electropolishing and comparable conditions, for example, current feeding rollers in electrolytic plating.

3.05.3.5.4 Alloy 22

With alloy 22 (EN 2.4602/UNS 06022), a nickel–chromium–molybdenum alloy typically containing 22 mass% chromium and 13 mass% molybdenum together with 3 mass% tungsten and 3 mass% iron, which was brought into the market in the mid 1980s,[15] a material became available which, owing to the increased chromium content, has better corrosion resistance than do alloy C-276 and alloy C-4 in oxidizing media. However, owing to the reduced molybdenum content, the effect of which can only be partly compensated for by the tungsten addition, it is inferior to alloy C-276 in strongly reducing media and in conditions of extreme crevice corrosion attack.[15] The subsequently developed alloy 59 also exhibits, according to Heubner[6] and the following remarks, a more favorable behavior than does alloy 22 in many respects.

3.05.3.5.5 Alloy 59

Alloy 59 (EN 2.4605/UNS N06059), with its composition of 23 mass% chromium and 16 mass% molybdenum, is a considerable advance on alloy 22. This material,[15] which was introduced into engineering practice in the early 1990s, is not only far superior to the other nickel–chromium–molybdenum alloys listed in **Table 1** in handling reducing acids, even if contaminated, their main area of application, but has also been successfully qualified for further duties such as the handling of highly corrosive salt solutions resulting from waste water treatment in FGD[18] and control of critical crevice corrosion problems in seawater,[15] including those occurring in plate-type heat exchangers cooled with chlorinated seawater.[19]

Its isocorrosion diagram in aerated technical grade sulfuric acid, plotted using results from immersion tests, is depicted in **Figure 6**. It shows a broad range of resistance, which, in these test series, falls only slightly below 100 °C up to a concentration of ~60% H_2SO_4. The corrosion behavior of alloy 59 in sulfuric acid is not influenced greatly by the amounts of oxidants present in the acid and is also less impaired by the presence of chlorides than is the

corrosion behavior of alloys that are more difficult to passivate.[20]

Figure 7 depicts the isocorrosion diagram for alloy 59 in hydrochloric acid, also plotted using results from immersion tests. It shows that this material is resistant at all HCl concentrations up to at least 40 °C. This, however, means among other things, that it is corrosion resistant in many organic process media in which hydrochloric acid is formed, which with other materials would lead to corrosion damage.

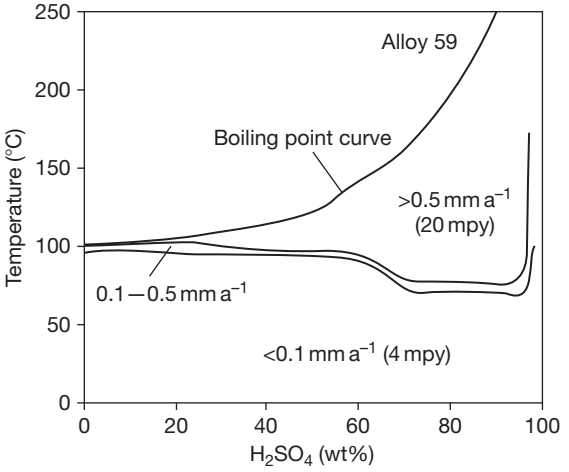

Figure 6 Isocorrosion diagram of alloy 59 (EN 2.4605/UNS N06059) in slightly aerated technical grade sulfuric acid, determined by immersion tests over at least 120 h. Reproduced from Kirchheiner, R.; Wahl, V. In *Nickel Alloys and Special Stainless Steels*; 3rd ed.; Heubner/Klöwer, *et al*., Ed.; Expert Verlag: Renningen, 2003; Chapter 8, pp 255–294.

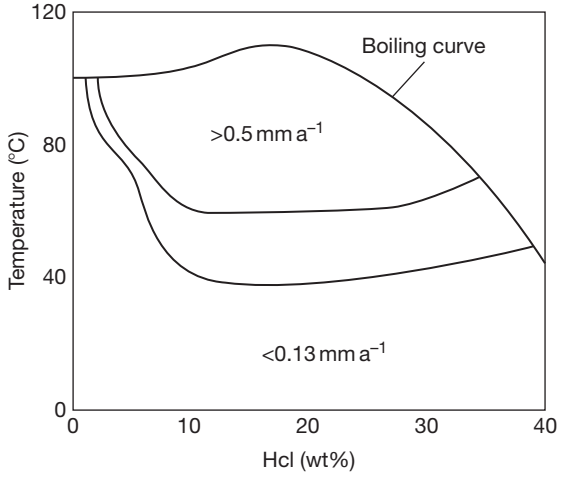

Figure 7 Isocorrosion diagram for alloy 59 (EN 2.4605/UNS N06059) in hydrochloric acid, determined by static immersion tests.[14,21]

Alloy 59 should also be considered as a very attractive material for handling aerated hydrofluoric acid.[15] Finally, as shown in **Figure 8**, the results of testing in an oxidizing sulfuric acid solution in accordance with ASTM G-28 method A are also of interest. Even though they are not directly relevant to practical use, they illustrate, by way of example, the influence of the chromium to molybdenum plus tungsten ratio on the corrosion behavior of nickel–chromium–molybdenum alloys under oxidizing conditions.[6,21]

The 'Green Death' solution (11.5% H_2SO_4 + 1.2% HCl + 1% $FeCl_3$ + 1% $CuCl_2$), which is widely used for testing the pitting resistance of nickel–chromium–molybdenum alloys and which simulates acidic condensates of the kind that can occur in the flue gas ducts of coal-fired power stations, shows a critical pitting temperature (CPT) of >120 °C for alloy 59, compared with 120 °C for alloy 22, 115–120 °C for alloy C-276, and 100 °C for alloy C-4.[22] The Green Death solution decomposes at temperatures above 120 °C, which means that there is no point in measuring temperatures in excess of 120 °C. However, a further differentiation of the pitting behavior of very high-alloyed materials is enabled by the $CaCl_2$ test,[23] a potentiostatic holding test at

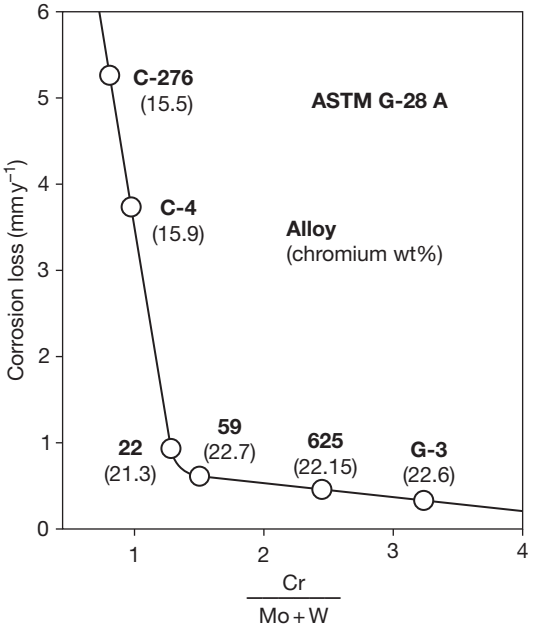

Figure 8 Corrosion loss of nickel–chromium–molybdenum alloys in boiling 50% H_2SO_4 with 42 g l^{-1} $Fe_2(SO_4)_3 \cdot 9H_2O$ in accordance with ASTM G-28 A as a function of their ratio of chromium to molybdenum plus tungsten.[6,21]

0.2 V_{SCE} in a 4.5 mol l^{-1} (500 g l^{-1}) $CaCl_2$ solution boiling at 115 °C, which for alloy 59 gives a CPT of 100 °C, compared with 83 °C for alloy C-276. A realistic pitting test for FGD is the testing of unwelded and welded specimens at the chloride–pH–temperature matrix intersection Cl^- 7%/pH 1/T 105 °C, which is described with results in Figure 9 and which likewise shows that the performance of alloy 59 is superior to that of other nickel–chromium–molybdenum alloys.[17]

The time–temperature–sensitization diagram, which is discussed in the following section, shows that alloy 59 is supremely resistant to thermal influences. The harmonious relationship of outstanding corrosion behavior accompanied by good workability is the special distinguishing feature of alloy 59. This alloy is therefore used in many areas of chemical process technology and other process industries,[24] in marine technology,[25] as well as in environmental engineering on a very large scale.[17,26]

3.05.3.5.6 Additional C-alloys and thermal stability as a criterion for alloy selection

The additional alloy C variants, which have been brought onto the market since the introduction of alloy 59 are alloy 2000 (EN 2.4675/UNS N06200), which typically contains 23 mass% chromium and 16 mass% molybdenum plus 1.6 mass% copper and 1.5 mass% iron, alloy MAT 21 (UNS N06210) which, as shown in Table 1, typically contains both 19 mass% chromium and molybdenum and 1.8 mass% tantalum in addition, and alloy 686 (EN 2.4606/UNS N06686), which, as shown in Table 1, typically contains 21 mass% chromium, 16 mass% molybdenum and also 3.8 mass% tungsten and 1.5 mass% iron. With respect to alloy MAT 21, insufficient data are available to discuss its localized corrosion behavior and thermal stability. Alloy 2000 clearly attempts to take advantage of the well known influence of copper on the corrosion resistance of

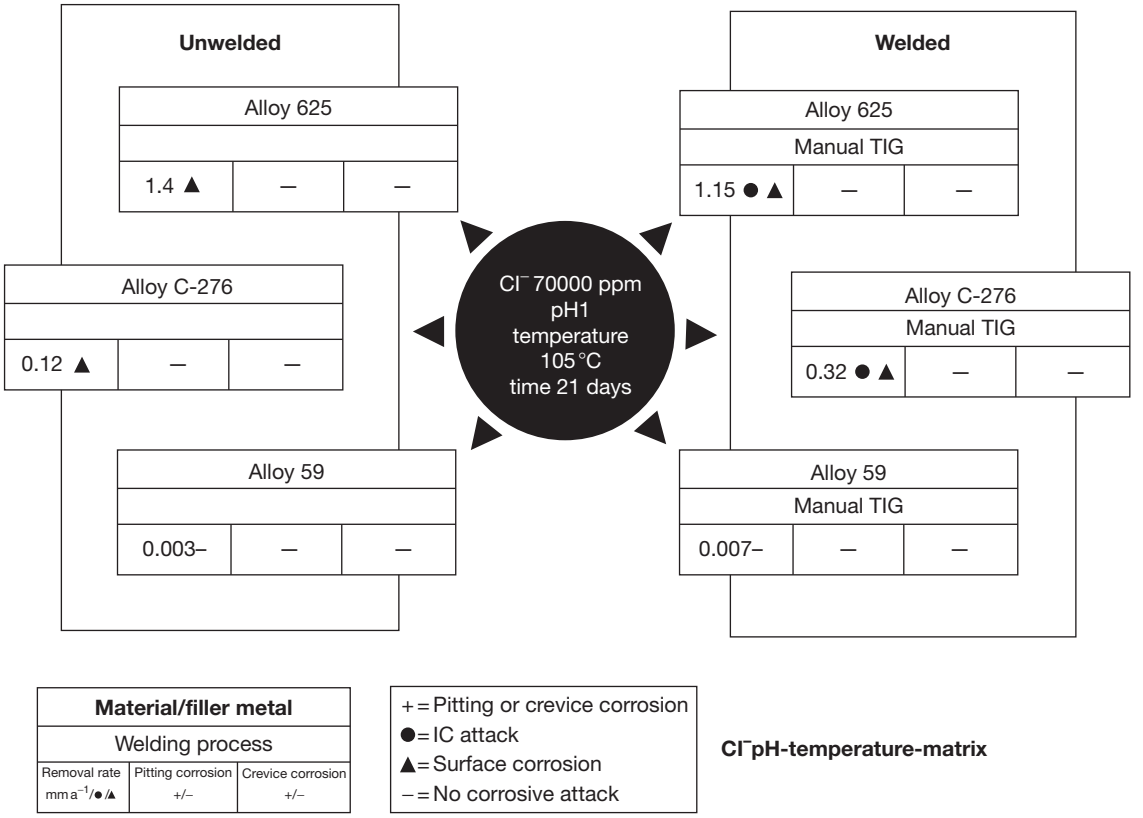

Figure 9 Comparison of the corrosion behavior of NiCrMo materials in a diluted sulfuric acid-containing solution with 7% chloride addition; base materials unwelded and base materials welded with matching filler metal using the tungsten inert gas (TIG) process; corrosion rate given in mm $year^{-1}$, see legend for local corrosion assessment. Reproduced from Kirchheiner, R.; Wahl, V. In *Nickel Alloys and Special Stainless Steels*; 3rd ed.; Heubner/Klöwer, *et al*., Ed.; Expert Verlag: Renningen, 2003; Chapter 8, pp 255–294.

nickel alloys and high-alloyed special stainless steels in sulfuric acid.[27] In case of alloy 686, it is evident from the composition that the intention was to shift the best available corrosion resistance more toward reducing conditions. Both alloys achieve their special corrosion behavior at the expense of a thermal stability that is markedly inferior to that of alloy 59, as shown in Table 3 by reference to the corrosive attack after sensitizing annealing treatment.[15]

The thermal stability of nickel–chromium–molybdenum alloys is an important criterion for their use, for example, in welding of thick-walled vessels where multipass welding is necessary, or in hot deformation of thick cross-sections. A fuller idea of the outstanding thermal stability of alloy 59 compared with alloy 686 and alloy 2000 with reference to the corrosive attack after sensitizing annealing treatment for periods ranging from 0.3 to 10 h at temperatures between 650 and 1000 °C is given[6] in Figure 10.

A further comparison is given by the time–temperature–sensitization diagrams[26] as shown in Figure 11. It is evident that alloy C-276 is very susceptible to intercrystalline corrosion (IC) under such criteria. In fact, this alloy is neither intended nor suitable for use under the kind of oxidizing conditions that are specified by the test in accordance with ASTM G-28 A. By contrast, alloy 59 performs significantly better under these oxidizing conditions, also in comparison with the other two nickel–chromium–molybdenum alloys C-4 and 22. Sensitization in the sense of an intercrystalline 50 µm depth of penetration IC criterion only begins after 2 h at the earliest. This is an adequate time in practice for avoiding IC after hot-forming, heat treatment, and welding even of thick dimensions.

3.05.3.5.7 Alloy 625

Alloy 625 (EN 2.4856/UNS N06625) is listed in Table 1 as the leanest of the nickel–chromium–molybdenum alloy group. As is evident, it differs from the previously described C-type nickel–chromium–molybdenum alloys in that it is stabilized with niobium. Also, it has the lowest molybdenum content of 9 mass%, and hence the lowest pitting resistance of this group of alloys, but owing to its niobium content, the effect of which is similar to that of molybdenum, it gives the appearance, in terms of its corrosion behavior, of having a somewhat higher alloying content of molybdenum. This alloy was originally developed for high temperature applications, but is now widely used in wet-corrosion service. The isocorrosion diagram for this type of material in sulfuric acid is shown in Craig and Anderson.[7] Its high mechanical strength and good resistance to acids[7] enable the fabrication of thin-walled components with good heat transmission. As can be inferred from the chromium-to-molybdenum ratio and is confirmed by Figure 8, its preferred area of use is more on the oxidizing side. It is used in the processing of phosphate ores with fairly high impurity content because of its corrosion and erosion resistance to the phosphate slurries in the digestion reactor and in the evaporation equipment of the final stage.[7] However, in the processing of phosphate ores, alloy 625 is increasingly replaced by alloy 31 (EN 1.4562/UNS N08031), which, due to its higher chromium content, performs much better, and is more cost-effective in addition (cf. Section 3.05.5.4). Alloy 31 has increasingly taken the place of alloy 625 in flue gas cleaning too, where alloy 625 was typically used under less aggressive conditions not requiring the use of alloy 59. Also, worthy of mention is the use of alloy 625 for borehole equipment and flow lines under sour-gas conditions.

Table 3 Thermal stability, stated as corrosion loss in millimeter per year after a sensitizing heat treatment for 1, 3, and 5 h at 87 °C (1600 °F) in tests in accordance with ASTM G-28 A and with ASTM G-28 B, according to data from Agarwal and Herda[15]

Test	*Sensitization (h)*	*Alloy*				
		C-276	*22*	*686*	*C-2000*	*59*
ASTM G-28 A	1	>12.5[a]	>12.5[a]	22.2[a]	3.0[a]	1.0[b]
	3	>12.5[a]	>12.5[a]	>25.4[a]	4.5[a]	1.3[b]
	5	>12.5[a]	>12.5[a]	>25.4[a]	5.3[a]	–
ASTM G-28 B	1	>12.5[a]	8.6[a]	0.4[a]	>12.5[a]	0.1[b]
	3	>12.5[a]	8.0[a]	2.2[a]	>12.5[a]	0.1[b]
	5	>12.5[a]	>12.5[a]	>12.5[a]	>12.5[a]	0.4[b]

[a]The alloys C-276, 22, C-2000, and 686 exhibit severe pitting and intercrystalline corrosion with grains dropping out.
[b]Alloy 59 exhibits no pitting.

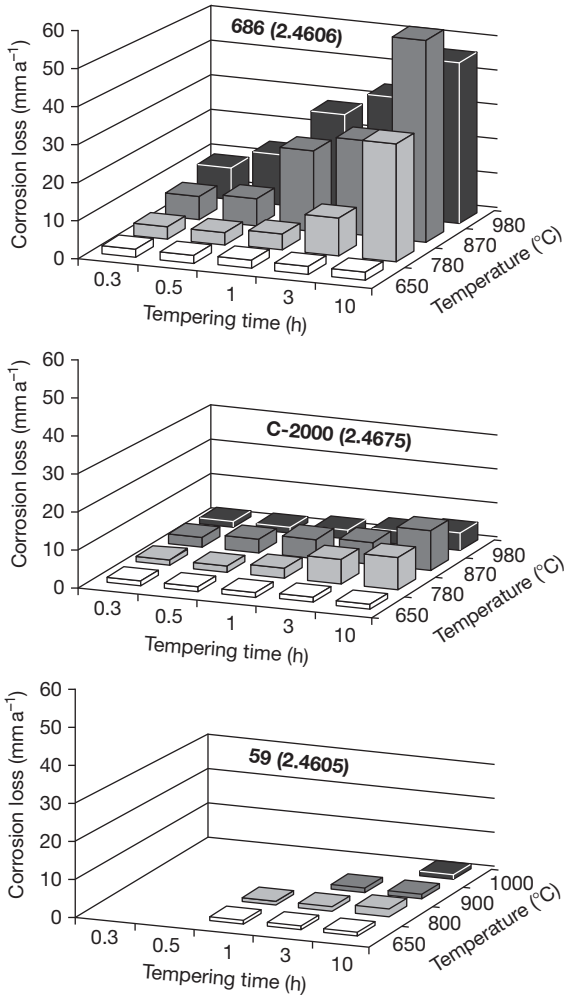

Figure 10 Thermal stability of alloy 59 (EN 2.4605/UNS N06059) compared with alloys 686 (EN 2.4606/UNS N06686) and 2000 (EN 2.4675/UNS N06200), measured as corrosive attack in tests in accordance with ASTM G-28 A after sensitizing heat treatments for 0.3–10 h at between 650 and 1000 °C. Reproduced from Heubner, U. In *Nickel Alloys and Special Stainless Steels*; 3rd ed.; Heubner/Klöwer, *et al*., Ed.; Expert Verlag: Renningen, 2003; Chapter 2, pp 47–93.

3.05.3.6 Nickel–Chromium–Iron–Molybdenum–Copper Alloys

3.05.3.6.1 General

Nickel–chromium–iron–molybdenum–copper alloys occupy a position between the nickel–chromium–molybdenum alloys and the high-alloy steels. Consequently, they are more limited in their application than the nickel–chromium–molybdenum alloys, but are significantly more corrosion resistant than the popular stainless steels in a large number of industrial

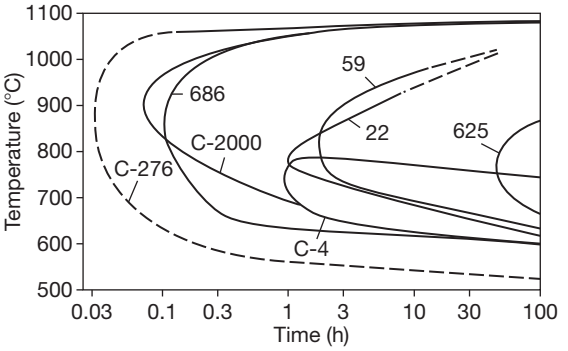

Figure 11 Time–temperature–sensitization diagrams of various nickel–chromium–molybdenum alloys,[26] established in tests in accordance with ASTM G-28 A.

media. One of their characteristics is that, due to their still relatively high nickel content, they have excellent resistance to stress-corrosion cracking in aqueous and acidic media containing chloride ions. With the exception of alloy 33, these alloys are particularly intended for use in the reducing acids sulfuric acid and phosphoric acid. The alloys in question with their chromium, molybdenum, and tungsten contents in ascending order (cf. **Table 1**) are alloy 20 (EN 2.4660/UNS N08020), alloy 825 (EN 2.4858/UNS N08825), alloy G-3 (EN 2.4619/UNS N06985), alloy 31 (EN 1.4562/UNS N08031), alloy 33 (EN 1.4591/UNS R20033), and alloy G-30 (EN 2.4603/UNS N06030). Their resistance in sulfuric acid is significantly improved by the alloying addition of copper.[27]

3.05.3.6.2 Traditional materials: Alloys 20, 825, G-3, and G-30

The alloys 20, 825, G-3, and G-30 can be considered traditional materials in that they are making use of titanium or niobium as stabilizing additions in combination with rather high nickel contents. Alloy 825's high stabilization with titanium marks it out as a veteran of material technology, which was developed before the 1960s (cf. **Table 2**). According to the isocorrosion diagram reproduced in Craig and Anderson,[7] it can be considered resistant to sulfuric acid of all concentrations up to a temperature of at least 50 °C with a corrosion rate of <0.13 mm year^{-1}. Its corrosion resistance is further improved by the presence of nitric acid and oxidizing salts.[7] If the requirements are not too stringent, this very traditional yet versatile material can also be used for handling nitric acid and caustic soda solutions.[7] Alloy 20 can be regarded as a variant of alloy 825 with reduced nickel, chromium, and molybdenum

contents but an enhanced copper content. According to the comparative isocorrosion diagram,[7] its corrosion resistance in sulfuric acid is predominantly somewhat lower than that of alloy 825. Alloy 20 is a material of construction for sulfuric and phosphoric acid heat exchangers and pipes, which is in common and widespread use in the United States in particular. Alloy 825, on the other hand, is also used in the offshore sector as a preferred material for heat exchangers, product piping, and conveying pipes. Both the alloys are resistant to hydrofluoric acid of all concentrations at room temperature and at concentrations up to 10% HF at 70 °C.[7]

In view of the pitting resistance equivalent (PRE) relationship, which plays a dominant role here, both alloy 825 and alloy 20 can be expected to exhibit comparatively low resistance to pitting and crevice corrosion in chloride-containing media, including seawater. However, alloy 825 has a remarkably high resistance to chloride-induced stress-corrosion cracking with preceding pitting corrosion in aggressive sour-gas media.[28] Therefore, for this kind of attack, a parameter $\sum = Ni + 2Mo + 0.5Cr$ (for $Mo \geq 2.5$) calculated as mass% has been tentatively proposed by Rhodes[16] as a measure of alloy resistance in place of the commonly used PRE written for instance[16] as $PRE = Cr + 3.3Mo + 30N$. However, as the PRE shows very clearly, in the case of alloy 825, the fixing of all the available nitrogen by the titanium is not an advantage, and in the case of alloy 20, the high copper content is more likely to have a detrimental effect on its crevice corrosion resistance.[6] This weakness is counteracted by the higher molybdenum content of the variant alloy G-3, which is increased to 7 mass % nominal as shown in **Table 1**. Besides the handling of sulfuric and phosphoric acid, this type of alloy can also be used in acetic acid production[7] and for tubular products in oil and gas extraction. However, there are applications where more advanced materials such as alloy 31 (EN 1.4562/UNS N08031) have been substituted successfully for the traditional alloy G-3, and this change is expected to continue.

Alloy G-30 is a modification of alloy G-3, with increased chromium content and lower molybdenum content. Alloy G-30 has excellent corrosion resistance in commercial phosphoric acids as well as in many complex and mixed acid environments of nitric/hydrochloric and nitric/hydrofluoric acids. The alloy also shows good corrosion resistance to sulfuric acid. Typical applications of alloy G-30 are in phosphoric acid service, mixed acid service, nuclear fuel reprocessing, components in pickling operations, agrichemicals manufacture, and mining industries.[1]

3.05.3.6.3 Advanced materials: Alloys 31 and 33

As shown in **Table 1** the alloys 31 and 33 are a new type of nickel–chromium–iron–molybdenum–copper materials characterized by lower content of nickel in order to save on the cost of raw materials, and instead of stabilizing alloying additions they contain appreciable amounts of nitrogen, which provides increased resistance to pitting corrosion and increased strength. It is for these reasons that they deserve a more detailed presentation.

According to **Table 1**, alloy 31 (EN 1.4562/UNS N08031) with the sum of its alloying elements chromium, molybdenum, and copper is higher than alloy G-3, whereas it is remarkably lower in nickel. In view that the amount of the alloying elements chromium, molybdenum, and copper, to a large extent, determines the corrosion behavior, alloy 31 can be taken as an excellent example for what can be done more with respect to corrosion resistance with less cost of raw materials. The isocorrosion diagram established by means of immersion tests in aerated technical grade sulfuric acid is reproduced in **Figure 12**. However, the presence of oxidants is important for the corrosion resistance of alloy 31 in sulfuric acid at concentrations above ~10%. Therefore, when testing in analytical grade sulfuric acid instead of aerated technical grade sulfuric acid, the 0.1 mm $year^{-1}$ isocorrosion line will be shifted to lower temperatures as shown in **Figure 13**, which results from detailed studies.[20] The presence of chlorides will shift the 0.1 mm $year^{-1}$ isocorrosion line of alloy 31 to lower temperatures too.[20]

In the production of phosphoric acid, the presence of chlorides, fluorides, oxidizing metal ions, and possibly further corrosion-accelerating impurities such as an influence of erosion or deposit formation should be anticipated depending on the composition of the phosphate ores. This means that for the concentration stage (>50% H_3PO_4), only special stainless steels or nickel alloys with very high alloying contents of chromium and molybdenum are suitable. Alloy 31 has been tested for such applications, both in the laboratory and directly in the plant, *inter alia* with specimens that were fixed to the agitating arms of acid digestion tanks as well as with tube specimens that were installed in the concentration units. As is evident from the results reproduced in **Table 4**, alloy

31 exhibits an attractive behavior in comparison with other materials that are commonly used for the production and processing of phosphoric acid. In fact, alloy 31 has proved its capabilities superbly under the particularly aggressive conditions of phosphoric acid production,[29] being probably the most cost-effective alloy to meet these harsh requirements[30] and having thus successfully replaced the higher-alloyed material alloy G-30 (cf. **Table 1**) in this application too.[31]

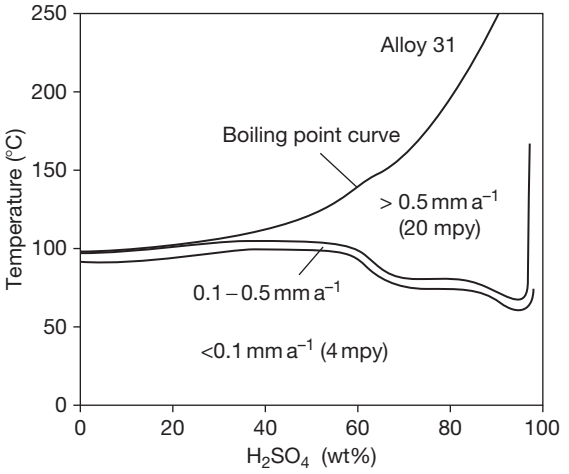

Figure 12 Isocorrosion diagram of alloy 31 (EN 1.4562/UNS N08031) in slightly aerated technical grade sulfuric acid, determined by immersion tests over at least 120 h. Reproduced from Kirchheiner, R.; Wahl, V. In *Nickel Alloys and Special Stainless Steels*; 3rd ed.; Heubner/Klöwer, *et al*., Ed.; Expert Verlag: Renningen, 2003; Chapter 8, pp 255–294.

According to the isocorrosion diagram in hydrochloric acid shown in **Figure 14**, which was established on the basis of immersion tests,[32] alloy 31 is resistant at room temperature up to a concentration of 8% and at 80 °C up to a concentration of ~3% HCl. It may be inferred from this that alloy 31 should have good resistance in chemical processes in which traces of HCl can form.[6]

Alloy 31 (EN 1.4562/UNS N08031) has been tested in 67% boiling HNO_3 solution (Huey test). Even after 10 boiling periods of 48 h each, alloy 31 base material exhibits exceptionally low corrosion rates of 0.11 mm year^{-1}, as shown by its position in **Figure 4**. Notwithstanding its high Mo content, alloy 31 is therefore also outstandingly resistant in strongly oxidizing media.

Alloy 31 (EN 1.4562/UNS N08031) has also been tested under sour-gas conditions (10 bar H_2S at 232 °C). In this test, the rate of uniform corrosion after 35 days was 0.01 mm year^{-1} with no signs of pitting and stress-corrosion cracking at a load of 95% $Rp_{0.2}$. Alloy 31 complies with NACE specification MR-0175 (Level VI) and the requirements of the Exxon Slow Strain Rate Test (177 °C, 7 bar H_2S, 980 MPa).[33]

The critical pitting corrosion temperature of alloy 31 is close to the upper 85 °C limit of the of the widely used $FeCl_3$ test.[17] Therefore, a direct comparison of the pitting corrosion resistance of alloy 31 with the pitting corrosion resistance of higher-alloyed nickel-base materials is better done by testing in a $CaCl_2$ test solution.[34] The results are demonstrated in **Figure 15**. In this test, the critical pitting corrosion temperature

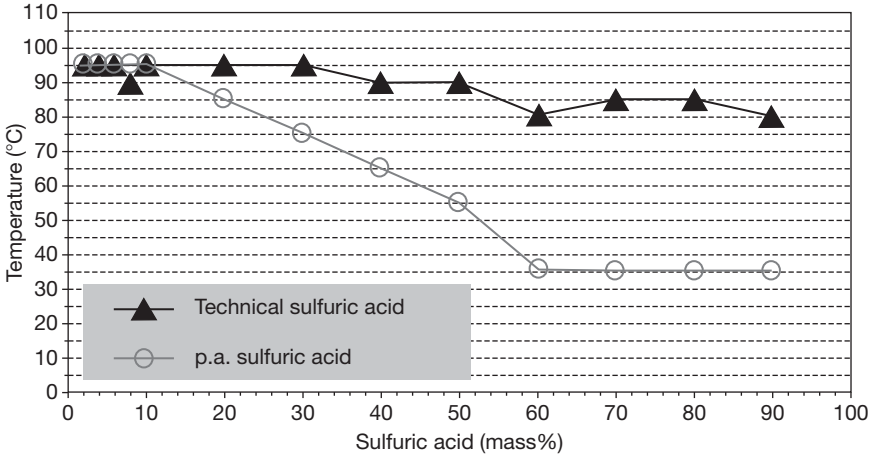

Figure 13 Corrosion resistance of alloy 31 (EN 1.4562/UNS N08031) in sulfuric acid and its dependence on the presence of oxidants in the acid as shown by the position of the 0.1 mm year^{-1} isocorrosion lines in aerated technical grade sulfuric acid and in analytical-grade (p.a.) sulfuric acid, as published by Alves *et al*. Reproduced from Alves, H.; Werner, H.; Agarwal, D. C. CORROSION 2006; NACE International: Houston, TX, 2006, Paper No. 06222.

Table 4 Corrosion loss in millimeters per year of alloy 31 (EN 1.4562/UNS N08031) and other alloys in technologically relevant phosphoric acid solutions,[6] according to data from White *et al.*[29]

Test – Medium	*Temperature (°C)*	*Alloy*			
		Alloy 31 (EN 1.4562)	*Alloy 926 (EN 1.4529)*	*Alloy 28 (EN 1.4563)*	*Alloy G-3 (EN 2.4619)*
72% H_3PO_4 + 4.5% H_2SO_4 + 0.9% H_2SiF_6 + 1.5% Fe_2O_3 + 400 ppm Cl^-	80	0.02	0.06	0.075	
	120	0.78			
52% P_2O_5	116	0.08[a]		1.2	0.28
42% H_3PO_4 + 2.4% H_2SO_4 + 2.3% H_2SiF_6 + 1% Fe_2O_3 + 1000 ppm Cl^-	80	0.015	0.03		
54% P_2O_5	116	0.05[a]		1.4	0.40
54% P_2O_5 + 2000 ppm Cl^-	116	2.35[a]		2.3	0.40
	100	1.30			

[a] Temperature: 120 °C.

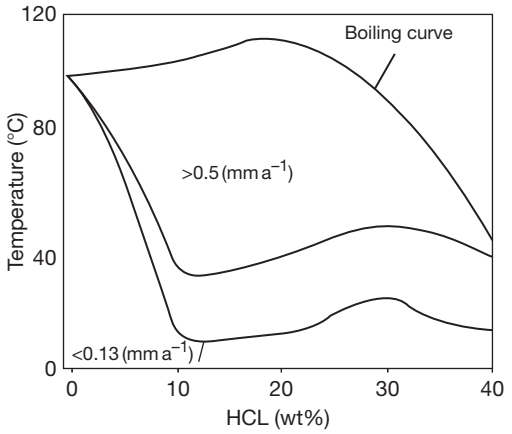

Figure 14 Isocorrosion diagram for alloy 31 (EN 2.4605/UNS N08031) in hydrochloric acid, determined by static immersion tests.[14,32]

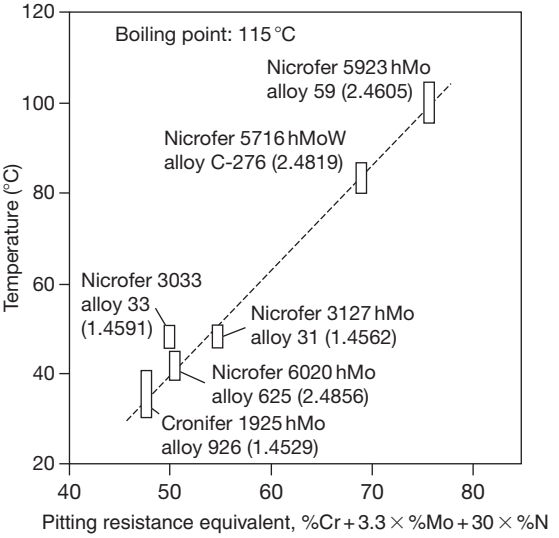

Figure 15 Critical pitting temperatures (CPTs) in the $CaCl_2$ test as a function of the pitting resistance equivalent (PRE), according to Voigt *et al.*[34]

of alloy 31 (EN 1.4562/UNS N08031) is at ~48 °C, well above the critical pitting corrosion temperature of alloy 625 (EN 2.4856/UNS N06625).

To obtain an initial indication of the relationship between temperature and pitting resistance in chloride-contaminated aqueous media, the pitting potential of alloy 31 (1.4562) was measured in ASTM artificial seawater.[6] The pitting potential is plotted against the temperature in **Figure 16** in comparison with the other two high-alloy materials, alloy 28 (EN 1.4563) and alloy 926 (EN 1.4529). Obviously, the potentials for the two reference materials fall sharply as the temperature rises, whereas for alloy 31 the pitting potential remains almost constantly high, even at temperatures up to 90 °C. This indicates outstanding resistance to pitting in actual media such as seawater, brackish water, and chloride-contaminated cooling water.

Besides its pitting resistance, the crevice corrosion resistance of alloy 31 in actual seawater service is also superior to that of the conventional 6% molybdenum steels such as EN 1.4529. As **Figure 17** shows,[14] when used as a flange material, the resistance limits are correspondingly broadened in the direction of higher temperatures and chlorine contents.

With regard to resistance to IC, the time–temperature–sensitization diagram plotted in the test according to ASTM G-28 Method A shows that sensitization in the sense of an intercrystalline 50 µm depth of penetration IC criterion only occurs after 2 h in the temperature range between ~650 and 700 °C.[6] To complement this, individual tests were also carried out on welded specimens (plate thickness

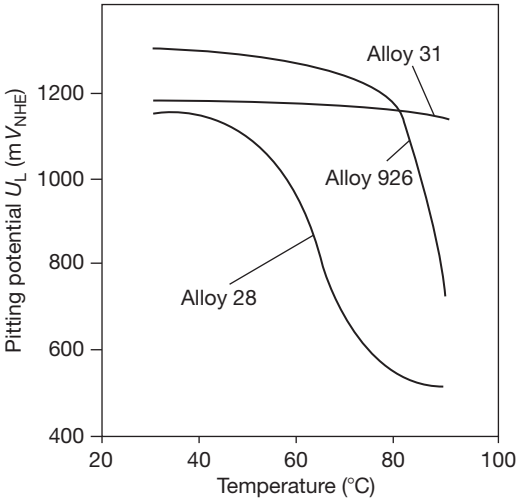

Figure 16 Pitting potential of three high-alloy corrosion-resistant steels in ASTM seawater, agitated and air-saturated. Reproduced from Heubner, U. In *Nickel Alloys and Special Stainless Steels*; 3rd ed.; Heubner/Klöwer, *et al*., Ed.; Expert Verlag: Renningen, 2003; Chapter 2, pp 47–93.

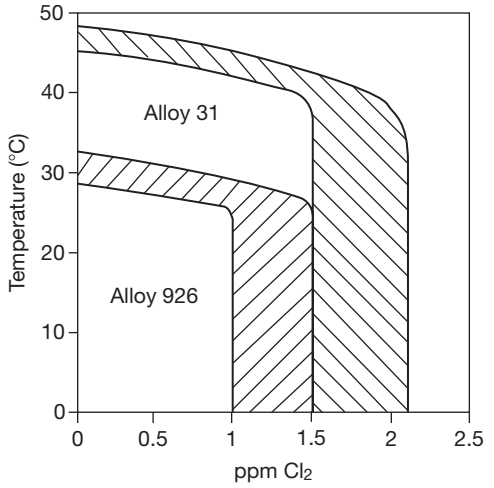

Figure 17 Stability limits of alloy 926 (EN 1.4529/UNS N08926) when used as a flange material in chlorinated seawater up to the onset of crevice corrosion and their extension when using alloy 31 (EN 1.4562/UNS N08031), determined in tests in realistic conditions (North Sea, Norway), from Heubner. Reproduced from Heubner, U. In *Nickel Alloys and Special Stainless Steels*; 3rd ed.; Heubner/Klöwer, *et al*., Eds.; Expert Verlag: Renningen, 2003; Chapter 1, pp 1–46.

6 mm) according to both ASTM G-28 Method A (120 h) and SEP 1877 Method II (24 h). The results are compared with those obtained for the two high-alloy special steels EN 1.4529 and EN 1.4563 in

Table 5 Results of testing of TIG-welded alloy 31 (EN 1.4562/UNS N08031) specimens and reference materials in accordance with (a) ASTM G-28, Method A, 120 h, (b) testing in accordance with SEP 1877, Method II, 24 h. Surface ratio weld metal/base material of the corrosion specimens as 1:6, corrosion loss in millimeters per year, according to data taken from Heubner[6]

(a) ASTM G 28 A	*Base material*	*Welded specimen*
Alloy 926 (EN 1.4529)	0.43; 0.37	0.45; 0.58
Alloy 28 (EN 1.4563)	0.18; 0.14	0.20; 0.23
Alloy 31(EN 1.4562/ UNS N08031)	0.18; 0.13	0.17; 0.20
(b) SEP 1877 II	*Base material*	*Welded specimen*
Alloy 926 (EN 1.4529)	0.13	0.24
Alloy 28 (EN 1.4563)	0.03	0.08
Alloy 31(EN 1.4562/ UNS N08031)	0.04	0.05

Table 5. In both the tests, alloy 31 (1.4562) exhibits the lowest corrosion rates. The weld metal, HAZ and base metal are all free from IC. Hence, the IC resistance after welding that is required in actual service is guaranteed. It should be noted, however, that in the case of alloy 31 only the carbides that are precipitated at low temperatures manifest themselves in the form of sensitization; this is not the case with the sigma phase, which can form at high temperatures. Particularly after hot-forming work, which is critical for this, such as pressing of heads, a test for pitting resistance and notch impact toughness can indicate more readily than can an IC test whether the material is in perfect condition. This applies to welding as well.

The results of the corrosion tests and service experience to date indicate the following typical areas of application for alloy 31 (EN 1.4562/UNS N08031): equipment for production and the handling of phosphoric acid, pipes, and heat exchangers in contact with sulfuric acid and seawater, components for oil and natural gas extraction under sour-gas conditions, components for the pulp and paper industry, salt manufacturing industry, and, last but not least, flue gas desulphurization, where the use of alloy 31 is preferred especially for regulating and shut-off systems operating under extremely demanding conditions in modern coal-fired power stations. It is also qualified for the evaporation of effluents from flue gas cleaning (first evaporation stage).[18]

While alloy 31 (EN 1.4562/UNS N08031) has a wide-ranging scope for application, alloy 33

(EN 1.4591/UNS R20033) is suitable for specific applications. Although it was originally intended chiefly for use in oxidizing media in view of its high chromium content, it has also proven to be an attractive material for the handling of nonoxidizing acids and alkaline media and for use in chloride-containing aqueous solutions, for instance, seawater.

Alloy 33 exhibits lower corrosion rates in the passive state and a greater ease of passivation in 15–80% sulfuric acid at temperatures between 50 and 90 °C than do the traditional materials alloy 825 (EN 2.4858/UNS N08825) and alloy 20 (EN 2.4660/UNS N08020) that are well established for such applications. As a result, its range of use in the passive condition is broadened in comparison with these materials. Low oxidant contents enable the range of application to be extended to higher acid concentrations and temperatures. For example, as can be seen from the corrosion resistance diagram in **Figure 18**, ~6 mg l^{-1} Fe^{3+} is sufficient to allow it to be used in conditions of up to 45% H_2SO_4 and 80 °C, and ~28 mg l^{-1} Fe^{3+} is sufficient in order to extend the range of application to 45% H_2SO_4 and 90 °C.

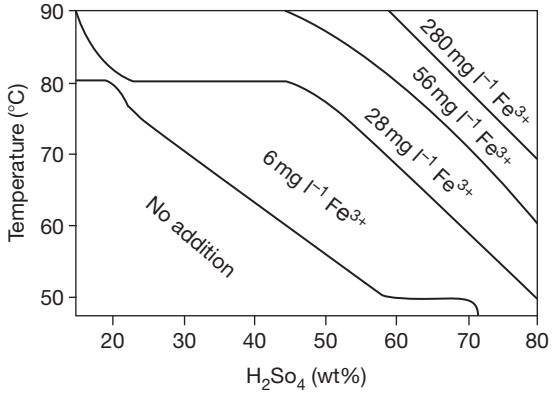

Figure 18 Corrosion resistance of alloy 33 (EN 1.4591/UNS R20033) in stationary analysis-grade sulfuric acid of medium concentration for corrosion rates <0.13 mm $year^{-1}$ and various additions of Fe^{3+} as oxidant, added in the form of $Fe_2(SO_4)_3$, established using three parallel specimens in each case over a test period of 7 days. Reproduced from Heubner, U. In *Nickel Alloys and Special Stainless Steels*; 3rd ed.; Heubner/Klöwer, *et al*., Ed.; Expert Verlag: Renningen, 2003; Chapter 2, pp 47–93.

In boiling 67% nitric acid (Huey test), alloy 33 exhibits a corrosion loss of only 0.04 g m^{-2} h^{-1} in tests over 15 × 48 h, and hence has the lowest level of corrosive attack of all known iron–nickel–chromium alloys under these corrosive conditions, as shown in **Figure 4**. On the basis of the results of extensive corrosion testing for up to 100 days, the alloy can be regarded as corrosion resistant, even in the welded state, at a HNO_3 concentration of up to 95% at 25 °C, up to 90% HNO_3 at 50 °C, up to slightly below 85% HNO_3 at 75 °C, and in 67% HNO_3 up to boiling point.[13] Alloy 33 is also of interest for handling nitric–hydrofluoric acid mixtures, as shown by the test results in **Tables 6** and **7**. It is therefore an attractive material not only for nuclear fuel reprocessing, but in particular for lining of pickling tanks for stainless steels.

The corrosion behavior of alloy 33 in highly concentrated sulfuric acid has been comprehensively tested.[35–37] **Figure 19** reproduces the isocorrosion diagram of alloy 33 for corrosion losses of 0.1 and 0.5 mm $year^{-1}$ in stationary highly concentrated industrial-grade sulfuric acid according to the data given in Renner and Michalski-Vollmer.[36] It is evident that toward lower sulfuric acid concentrations, there are obviously two different corrosion mechanisms at work, depending on the temperature, which have their maximum reaction rates at ~110 and ~190 °C, respectively. However, under different test conditions and especially with a different test period, the situation may differ[37] from that shown in **Figure 19**, making the small window of corrosion resistance even narrower. Therefore, for practical applications, prior corrosion tests under the specific operating conditions are strongly advised.

It is not only in oxidizing acids and in reducing acids, whose composition has been sufficiently adjusted

Table 6 Results of corrosion testing of alloy 33 (EN 1.4591/UNS R20033) and other materials for comparison in nitric/hydrofluoric acid solutions, immersion tests over 21 days at 90 °C, corrosion loss in grams per square meter per hour, according to data taken from Heubner[6]

Alloy	*12% HNO_3*			*0.4% HF*			
	+0% HF	*+0.9% HF*	*+3.5% HF*	*+32% HNO_3*	*+44.5% HNO_3*	*+56% HNO_3*	*+67.5% HNO_3*
28 (EN 1.4563)	<0.01	5.74	20.74	0.96	1.78	3.38	5.46
690 (EN 2.4642)	<0.01	0.61	6.34	1.46	1.97	4.69	7.42
G-30 (EN 2.4603)	<0.01	0.28	1.21	0.49	1.45	2.39	4.49
33 (EN 1.4591)	<0.01	0.24	1.19	0.27	0.67	1.66	3.08

Table 7 Results of corrosion testing of alloy 33 (EN 1.4591/UNS R20033) and other materials for comparison in 20% nitric acid solutions with additions of 3, 5, and 7% hydrofluoric acid, immersion tests over 21 days at 25 and 50 °C, corrosion loss in grams per square meter per hour, according to data taken from Heubner[6]

Alloy	*25 °C*			*50 °C*		
	+3% HF	*+5% HF*	*+7% HF*	*+3% HF*	*+5% HF*	*+7% HF*
316 Ti (EN 1.4571)	3.33	6.20	5.68	17.3[a]	24.4[a]	33.45[a]
28 (EN 1.4563)	0.03	0.04	0.06	0.18	0.29	0.41
33 (EN 1.4591)	0.01	0.01	0.02	0.08	0.11	0.17

[a]Duration of test: 7 days.

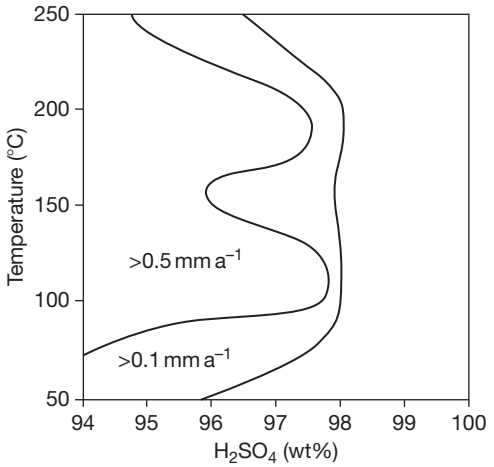

Figure 19 Isocorrosion diagram for alloy 33 (EN 1.4591/UNS R20033) in stationary highly concentrated industrial grade sulfuric acid,[6] based on the data established by Renner *et al.*[36] over a test period of 21 days.

to oxidizing, that alloy 33 exhibits a corrosion behavior that is attractive for practical applications of many kinds; this also applies to alkaline media. For example, a corrosion loss of <0.01 mm year^{-1} was measured in 25% and 50% caustic soda solution up to the boiling point.[35] Even for 70% caustic soda at 170 °C, a corrosion loss of only 0.03 mm year^{-1} is stated.[38] To complement this, field tests were carried out in NaOH tanks with added chlorine, the specimens therefore being exposed to both the liquid and the vapor phase. The material performed faultlessly, with only slight signs of crevice corrosion.[6] In a further field test with chloride- and chlorate-contaminated caustic soda from the diaphragm cell process, an outstanding resistance was measured,[39] as reported in **Section 3.05.5.2**.

The resistance of alloy 33 to pitting, which has been comprehensively tested[34] with regard to the handling of chloride-containing cooling water and use in seawater, is comparable with that of alloy 31 (EN 1.4562/UNS N08031), alloy 31 tending to perform somewhat better. This is made clear by the results of the $FeCl_3$ test shown in **Table 8**. In the $CaCl_2$ test, on the other hand, both alloys have practically the same CPT, as is evident from **Figure 15**.

Table 8 Critical pitting temperatures (CPT) and crevice corrosion temperatures (CCT), established in $FeCl_3$ tests,[34] indicating the pitting resistance equivalent (PRE) as % Cr + 3.3 × % Mo + 30 × % N

Alloy	*EN*	*UNS*	*PRE*	*CPT (°C)*	*CCT (°C)*
20	2.4660	N08020	28.3	15	<5
825	2.4858	N08825	33	30	<5
904L	1.4539	N08904	37	45	25
926	1.4529	N08926	47	70	40
33	1.4591	R20033	50	85	40
31	1.4562	N08031	54	>85	65

In terms of crevice corrosion resistance, on the other hand, alloy 33 (EN 1.4591/UNS R20033) is comparable with alloy 926 (1.4529/UNS N08926), as is again evident from **Table 8**. This confirms that higher nitrogen contents have a lesser effect on the crevice corrosion resistance than on the pitting resistance, in accordance with the data in Kirchheiner and Wahl[17] for the material EN 1.4565. Alloy 33 and alloy 926 can also be rated equally with regard to their repassivation potential in the case of crevice corrosion in seawater according to Voigt *et al.*[34] Combined with its high strength, excellent ductility, and high resistance to stress-corrosion cracking, even under sour-gas conditions,[40] possibilities for application in seawater and offshore service are therefore open to alloy 33.

In conclusion, it should be noted that alloy 33 (EN 1.4591/UNS R20033) exhibits a high degree of thermal stability. During ageing between 700 and 900 °C, its notch impact toughness decreases slightly because of precipitation of sigma phase, but nevertheless still exceeds 100 J even after a tempering time of 8 h. When tested for sensitization in boiling azeotropic nitric acid (Huey test), there are no signs of

either grain boundary attack or an increase in the rate of uniform corrosion even after tempering for up to 1000 h.[35]

3.05.3.7 Age-Hardenable Nickel–Chromium–Iron–Molybdenum (–Copper) Alloys

Positioned at the bottom of Table 1 is an alloy group consisting of two important age-hardenable nickel–chromium–iron–molybdenum (–copper) alloys. They are used for bars, tools, pump shafts, valves, and forgings in oil and gas production where low weight and hence high strength is a requirement. Their high mechanical strength is achieved by so-called age-hardening in an intermediate range of temperatures where intermetallic phases are precipitating within the metallic matrix, causing an increase of strength. Alloy 925 (EN 2.4852/UNS N09925) is the age-hardenable version of alloy 825 (EN 2.4858/UNS N08825), with an almost identical corrosion behavior (cf. Section 3.05.3.6.2). Alloy 718 (EN 2.4668/UNS N07718), however, has its origin in high temperature/high-strength applications and has been adapted very successfully for the wet corrosive requirements of oil and gas extraction.

3.05.4 Corrosion Behavior of Nickel Alloys in the Welded State

3.05.4.1 The Specific Surface and Structural Condition of the Weld Metal and the HAZ

In chemical, environmental, power, and marine engineering, welding is the most popular joining method. In these fields, there are very few material applications where welding is not required. The corrosion resistance that is determined for a material in its various mill product forms should therefore generally apply to this material in the welded state as well, that is, to the weld metal and the whole area of the weld. The weld area of a construction may well be the location of preferential corrosive attack, because here – in contrast to the homogeneous solution-annealed or stabilized and subsequently (if necessary) shot-blasted and pickled state – a clean, bright metal surface may not be obtained easily. Instead, the weld may have slag residues or may be oxidized depending on the welding process used. The adjacent HAZ is also likely to be coated with surface oxides to varying extents, which are generally recognizable as temper colors. A lookout should also be kept for spatter and contamination away from the weld, which are usually detrimental to corrosion resistance. Moreover, in the weld area the microstructure is heterogeneous not only in the weld metal with its cast structure, but often also in the HAZ directly adjoining the weld. The extent of the structural changes caused by the welding operation in the HAZ depends on the material and its susceptibility to precipitation of carbides and intermetallic phases at medium temperatures, as well as on the heat input and the rate of cooling during welding. Problem-free welding of a material by means of the particular welding process is only possible if welding techniques and welding parameters can be used to keep the heat input so low that the agreed testing methods fail to discover any intolerable structure-related impairment of the corrosion behavior and the mechanical properties in the HAZ. Moreover, care should be taken where necessary to ensure, by appropriate posttreatment of the surface, that any scale and any surface oxides manifesting themselves as temper colors do not adversely affect the material's corrosion behavior.

Some possible defects in the weld area are depicted schematically in Figure 20. Slag residues

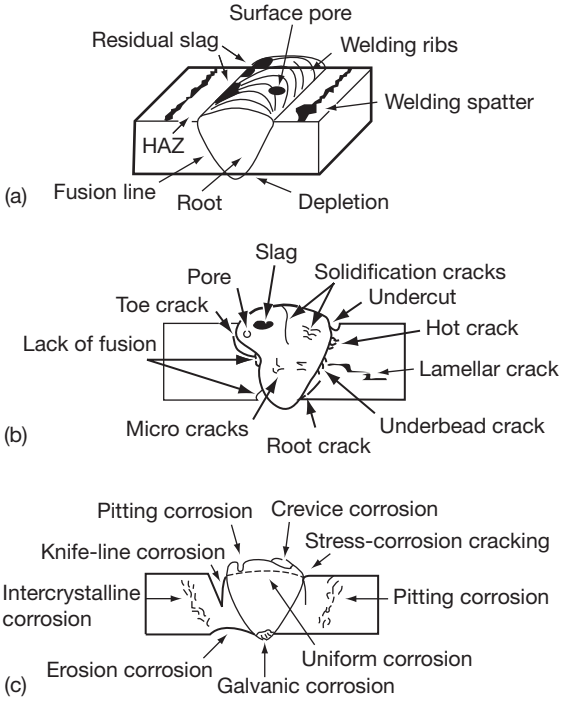

Figure 20 Possible defects in the weld area and their effects on corrosion behavior, from Heubner. Reproduced from Heubner, U. In *Nickel Alloys and Special Stainless Steels*; 3rd ed.; Heubner/Klöwer, *et al*., Ed.; Expert Verlag: Renningen, 2003; Chapter 2, pp 47–93.

on the surface of the weld are sites of preferential attack, because they offer ideal conditions for crevice corrosion and pitting. The same applies to pores, which, in the form of solidification porosity, cannot be ruled out for nickel alloys, but can be controlled by alloying techniques with respect to the filler metal or by other welding engineering measures. An excessively rough material surface (ribbed texture), edge misalignment, or severe cases of drop-through chiefly allow room for the formation of sediments, deposits, and incrustations, which, acting like a sponge, result in local concentrations of corrosive media constituents such as chloride ions that can lead to localized corrosion. Solidification cracks, hot cracks, weld undercuts, weld interface, and root cracks and incomplete root fusion are ideal locations for crevice corrosion attack. With materials that require a higher-alloyed filler metal, unmixed fusion zones in the root area, but also on the capping pass side, can be sites of preferential corrosive attack. High mechanical stresses in the weld area, including thermally caused stresses, may result in an increased likelihood of stress-corrosion cracking, depending on the material and the surrounding medium. A rough-ribbed structure of the weld metal can also contribute to this on account of the stress peaks, which then arise.

3.05.4.2 Surface Condition and Necessary Surface Treatment after Welding

Oxide layers on the weld metal and oxides over the HAZ, which manifest themselves as temper colors, weaken the resistance of nickel alloys to pitting. As known from stainless steels,[6] the differences in corrosion resistance may be greatest between pickled surfaces and those with 'light,' that is, straw-yellow temper colors. As temper colors become darker, corrosion resistance further decreases. The surface oxide layers either consist almost exclusively of chromium oxide, Cr_3O_4 (spinel type)[41] or are, at any rate, generally significantly enriched with chromium.[42] The chromium required for oxide formation is extracted from the matrix of the material, which consequently becomes depleted in chromium. As the resistance of nickel–chromium–molybdenum alloys to pitting is almost exclusively determined by their chromium and molybdenum contents, a decrease in the chromium content is synonymous with reduced resistance to this type of corrosion.[41] There is even a strong possibility that immediately beneath the oxide coating, there is a thin metallic surface layer, which no longer corresponds to the intended material grade at all. Therefore, it is understandable that in such a case, simply removing the temper colors may not be sufficient to restore the resistance of the unwelded base material; it may in fact be necessary to remove the chromium-depleted metallic surface layer lying immediately beneath them at the same time. In practice, the situation may become really problematic, for the technical corrosion resistance of a material depends less on the pitting potential than on the lower repassivation potential, because it is only below this repassivation potential that pitting, once begun, can be stopped again.

In industrial engineering practice, therefore, full-immersion pickling of welded components is recommended for critical situations. This, however, is feasible only in certain cases and to a limited extent. Moreover, its success depends on the material and on the pickling method employed. As a rule, it is necessary to use a different means for removing the surface oxides. In modern fabrication practice, the methods of *in situ* pickling of the component, abrasive blasting, and grinding are mainly used. The effectiveness of each of these measures was investigated by, among other things, measuring the critical pitting potential in artificial seawater.[43,44] It turned out that, among the methods of grinding with disc wheels, blasting with glass beads and pickling with HNO_3/HF pickling pastes, grinding was the least effective – at least with a very rough finish – and the best results were obtained with the pickling pastes. For the some types of stainless steels, the results of the investigation show that when using the pickling pastes, it is at best possible to obtain a corrosion resistance that is virtually equivalent to that of the metal in the bright, unwelded state. On the other hand, in the case of higher-alloyed materials such as alloy 625 (EN 2.4856/UNS N06625), there was only a slight dependence of the corrosion resistance on the method of surface treatment. With this material, the pickling action achieved was insufficient to remove not only the oxide coating but also an adequate amount of the chromium-depleted metallic surface layer beneath it, because even in a chromium-depleted surface condition, this material is too corrosion-resistant in relation to the pickling agent for this to be achieved within the treatment time. This is true not only of treatment with pickling paste, but has also been observed with nickel–chromium–molybdenum alloys in the case of post-treatment by immersion or spray pickling.

Consequently, brushing of welds with a stainless steel wire brush immediately after welding while

the metal is still hot, at the least, is vital in order to remove surface contamination, slag residues, and temper colors to the greatest possible extent. Subsequent pickling is then likely to produce a further marked improvement in corrosion resistance, but mechanical removal of the chromium and molybdenum-depleted metallic surface might be an additional requirement in case of very corrosion-resistant materials when used near to the limit of their corrosion resistance. The highest resistance to pitting is obtained with electrochemical polishing. If there are doubts regarding the nature and extent of postweld treatment, the testing of expertly executed and experimentally posttreated welded joints in a manner which corresponds or at least approximates to the level of corrosive attack in practice is essential.

3.05.4.3 IC in the HAZ

In chromium-alloyed nickel-base materials, with a sufficiently high carbon content of the HAZ adjacent to a welded joint, preferential precipitation of chromium carbides at the grain boundaries may occur, with the consequence of chromium depletion in the region near the grain boundaries. This may go so far that under corrosive attack, adequate corrosion resistance no longer exists in this region, and IC occurs. This can also take the form of pitting along the grain boundaries; it is then referred to as sensitization. In the case of the chromium-alloyed nickel-base materials for wet-corrosion service that are the focus of interest here, only LC grades or stabilized materials are in use today; as a result, IC, owing to simple precipitation of chromium carbide, only rarely comes up for discussion in the case of these materials – for instance, if it is necessary to consider a high temperature material with a high carbon content, such as the nickel–chromium alloy 600 (EN 2.4816/UNS N06600) with regard to temporary service under wet-corrosion conditions (e.g., shutdown dew point corrosion and during cleaning) among other factors.

However, in the case of the chromium-alloyed nickel-base materials, IC in the HAZ of welded joints may well be a matter, which requires consideration owing to the precipitation of intermetallic phases, including the M_6C type of carbide. On the other hand, the sigma phase, which is precipitated in, for example, the nickel–chromium–iron–molybdenum–copper alloy 31 (EN 1.4562/UNS N08031) in the medium temperature range[45] leads, when tested in the conventional tests according to ASTM G 28 A or SEP 1877 II, not to IC but to an increased susceptibility to pitting;[46] however, this does not usually cause problems in fabrication by welding.

Figure 11 shows a summary of the time–temperature–sensitization diagrams that have been plotted for nickel–chromium–molybdenum alloys.

Leaving aside the more stringent Strauss test, which is little used, the test methods employed for IC testing of high-alloyed materials range from the Huey test, which specifies very strongly oxidizing conditions, *via* the Streicher test in accordance with ASTM G 28 A, which likewise specifies oxidizing conditions, to – with decreasing aggressiveness – the testing of nickel–molybdenum alloys in hydrochloric acid. However, there is no standardized method of IC testing for slightly oxidizing conditions, which would be typical of the corrosive conditions to which nickel–chromium–molybdenum alloys are frequently exposed, for example, in the aqueous media encountered in FGD plants of fossil-fired power stations. To fill this gap, the anodic polarization behavior of welded nickel–chromium–molybdenum alloys in solutions containing sulfuric acid with the addition of anions with a structure-specific effect, such as SCN^- and Cl^-, was investigated.[47] The results showed that in the transitional active/passive range of the materials, it is actually possible to distinguish between the behavior of different heat treatment states with regard to IC of the HAZ and pitting-like selective corrosion of the weld metal, which also occurs under these test conditions. In such a test, after welding with a heat input in excess of 8 kJ cm^{-1}, the tendency for increased IC within the HAZ and for selective corrosion of the weld metal is most marked in the case of alloy C-276, followed by alloy C-4. With the alloy 59 (2.4605), any influence of the heat input during welding only becomes noticeable if the values for the energy inputs per unit length of weld are as extreme as 6.2 kJ cm^{-1} on the one hand, or 15.1 kJ cm^{-1} on the other. In this respect too, therefore, alloy 59 (EN 2.4605/UNS N06059) proves to be the least susceptible nickel–chromium–molybdenum alloy.

3.05.4.4 Resistance of Weld Metal and Heat Affected Zone to Pitting

The cast structure of the weld metal and the associated segregations have widely differing effects on corrosion resistance, depending on the material and the surrounding medium. Because of this, unalloyed nickel and the nickel–copper, nickel–molybdenum, and nickel–chromium alloys are welded with fillers of identical or at least similar composition to the base

metal; here, peculiarities in the chemical composition of the filler metals have more to do with the technical requirements of the welding operation than with the demands of corrosion resistance.

If nickel–chromium–molybdenum alloys are welded with filler of identical composition to the base metal, practical experience clearly shows that the identical-composition weld metal generally has the same high corrosion resistance, in spite of its heterogeneous nature,[22] as the homogeneous austenitic base metals, at least below certain threshold conditions of attack. Electrochemical tests in oxidizing ASTM G-28 A solution have revealed only minor differences, the weld metal, in fact, having a more noble corrosion and passivation potential.[48] Potential profiles relating to joint welding of nickel–chromium–molybdenum alloys with filler of the same composition as the base metal show no or only slight differences between the wrought alloy and the weld metal.[49] However, marked differences arise in the testing of the pitting resistance. For instance, in the 'Green Death' test[23] the CPT established for the weld metal of FM 625 (EN 2.4831/UNS N06625) was on average ~12 K lower than that established for the corresponding homogeneous austenitic material alloy 625 (EN 2.4856/UNS N06625), and for the weld metal of FM C-276 (EN 2.4886/UNS N10276) the CPT was on average ~18 K lower than that of the corresponding homogeneous austenitic material alloy C-276 (EN 2.4819/UNS N10267).[23] In the $CaCl_2$ test,[23] which is more sensitive and can be used over a wider range of alloys, this difference is on average c. 25 K for alloy C-276 (EN 2.4819/UNS N10267).[23,50] If the actual conditions of service make it necessary to do so, for example, as a result of realistic tests in the chloride/pH/temperature matrix (cf. **Figure 9**), it is probable, based on the test results available so far,[22,23] that the reduced corrosion resistance of the weld metal of FM 625 and FM C-276, as shown by the 'Green Death' test,[23] can be avoided by instead using FM 59 (EN 2.4607/UNS N06059) as filler metal.

A good guide to the anticipated behavior of materials on welding is also given by cooling tests at different rates from the solution-annealing temperature.[46] **Table 9** shows the results obtained from tests with alloy 31 (EN 1.4562/UNS N08031). This alloy should preferably be solution-annealed at 1150–1180 °C. If the CPT in the HAZ, to be measured in the $FeCl_3$ test, must not fall below 75 °C, the cooling rate in the range between the solution-annealing temperature and 600 °C should, according to these test results, be at least 150 °C min^{-1}. The associated notch impact energy values, which are often of interest to the design engineer, are also shown in **Table 9** for comparison. It is interesting to note that in this case the notch impact energy does not fall in parallel with the pitting resistance, but initially rises; this has been observed, to a far greater extent, with alloy 926 (EN 1.4529/UNS N08926) as well in the case of isothermal ageing.[51]

Table 9 Influence of the cooling rate from the solution-annealing temperature down to 600 °C on the CPT to be measured in the $FeCl_3$ test and the notch impact energy (A_v) of alloy 31 (EN 1.4562/UNS N08031)[6,46]

Condition	*CPT (°C)*	*A_v (J)*
Solution-annealed	85	266
At 150 °C min^{-1} to 600 °C	75	270
At 50 ° C min^{-1} to 600 °C	70	280
At 25 ° C min^{-1} to 600 °C	55	240

3.05.5 Application of Nickel and Nickel Alloys as Materials Resistant to Aqueous Corrosion in the CPI and in Environmental Technology

3.05.5.1 General

The CPI and environmental technology have to cope with a large variety of adverse operating conditions, including a wide range of temperatures, all kinds of static and dynamic loads, as well as numerous solid, liquid, and gaseous products and product mixtures. Safety, cost-efficiency, and even the feasibility of a process depend on whether the materials envisaged for the plant and its components can handle the required range of different operating conditions.

Nickel and nickel alloys are needed in all areas of halogen chemistry/chlorine chemistry to withstand both general and localized forms of corrosion. Further applications can be found in chemical processes involving alkalis (e.g., caustic soda) or acids (e.g., sulfuric acid and acetic acid) at different concentrations and temperatures. These high corrosion-resistant materials are well established in wide areas of chemical processing, and in the following section, some selected examples of their application are presented.

Beyond the scope of the CPI and environmental technology, nickel alloys are finding wet corrosive applications in many other industrial sectors, for example, marine technology[14] and oil and gas extraction.[28,33]

3.05.5.2 Production of Caustic Soda

Caustic soda (NaOH) is one of the most important chemical feedstocks, with a total annual production of 10^6 tons. NaOH is used in organic chemistry, in the production of aluminum, in the paper industry, in the food processing industry, in the manufacture of detergents, etc. Caustic soda is a coproduct in the production of chlorine, 97% of which takes place by the electrolysis of sodium chloride.

Caustic soda has an aggressive impact on most metallic materials, especially at high temperatures and concentrations. It has been known for a long time, however, that nickel exhibits excellent corrosion resistance to caustic soda at all concentrations and temperatures, as shown by **Figure 1**. In addition, except at very high concentrations and temperatures, nickel is immune to caustic-induced stress-corrosion cracking. The nickel standard grades alloy 200 (EN 2.4066/UNS N02200) and alloy 201 (EN 2.4068/UNS N02201) are therefore used at these stages of caustic soda production, which require the highest corrosion resistance. The cathodes in the electrolysis cell used in the membrane process are made of nickel sheets as well. The downstream units for concentrating the liquor are also made of nickel. They operate according to the multistage evaporation principle mostly with falling-film evaporators. In these units, nickel is used in the form of tubes or tube sheets for the preevaporation heat exchangers, as sheets or clad plates for the preevaporation units, and in the pipes for transporting the caustic soda solution. Depending on the flow rate, the caustic soda crystals (supersaturated solution) can cause erosion on the heat exchanger tubes, which makes it necessary to replace them after an operating period of 2–5 years. The falling-film evaporator process is used to produce highly concentrated, anhydrous caustic soda. In the falling-film process developed by Bertrams, molten salt at a temperature of ~400 °C is used as the heating medium. Here, tubes made of low-carbon nickel alloy 201 (EN 2.4068/UNS N02201) should be used, because at temperatures higher than ~315 °C (600 °F), the higher carbon content of the standard nickel grade alloy 200 (EN 2.4066/UNS N02200) can lead to graphite precipitation at the grain boundaries. Nickel is the preferred material of construction for caustic soda evaporators where the austenitic steels cannot be used. In the presence of impurities such as chlorates or sulfur compounds – or when higher strengths are required – chromium-containing materials such as alloy 600 L (EN 2.4817/UNS N06600) are used in some cases. Also of great interest for caustic environments is the high-chromium-containing alloy 33 (EN 1.4591/UNS R20033). If these materials are to be used, it must be ensured that the operating conditions are not likely to cause stress-corrosion cracking. Alloy 33 (EN 1.4591/UNS R20033) exhibits excellent corrosion resistance in 25% and 50% NaOH up to boiling point and in 70% NaOH at 170 °C. This alloy also showed excellent performance in field tests in a plant exposed to caustic soda from the diaphragm process.[39] **Figure 21**

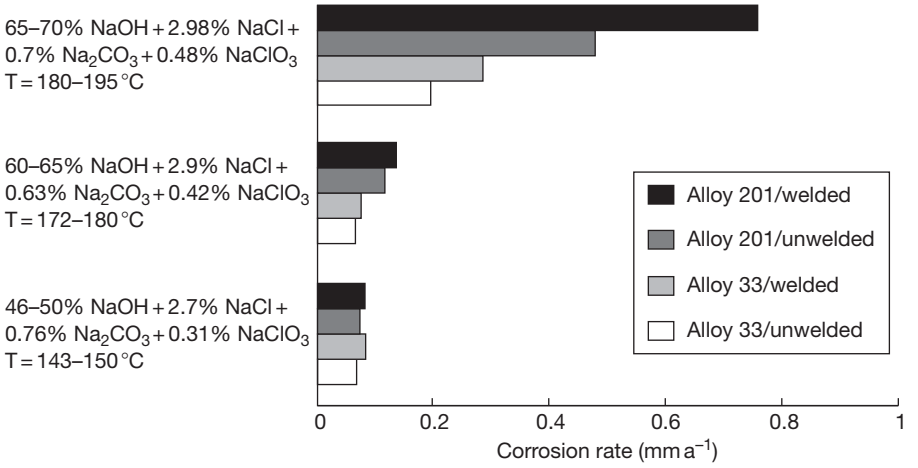

Figure 21 Corrosion rates of alloy 33 (EN 1.4591/UNS R20033) and low carbon nickel alloy 201 (EN 2.4068/UNS N02201) after almost 3 months of exposure to diaphragm caustic soda contaminated with NaCl, Na_2CO_3, and $NaClO_3$ in various ranges of concentrations and temperatures. Reproduced from Alves, H.; Horn, E. M.; Klöwer, J. In Nickel *Alloys and Special Stainless Steels*; 3rd ed.; Heubner/Klöwer, *et al.*, Ed.; Expert Verlag: Renningen, 2003; Chapter 7, pp 226–254.

shows some results regarding the concentration of this diaphragm caustic liquor, which was contaminated with chlorides and chlorates. Up to a concentration of 45% NaOH, the materials alloy 33 (EN 1.4591/UNS R20033) and nickel alloy 201 (EN 2.4068/UNS N02201) show a comparable outstanding resistance. With increasing temperature and concentration, alloy 33 becomes even more resistant than nickel. Thus, as a result of its high chromium content, alloy 33 seems to be advantageous to handle caustic solutions with chlorides and hypochlorite from the diaphragm or mercury cell process.

3.05.5.3 Production and Handling of Sulfuric Acid

Sulfuric acid (H_2SO_4) is one of the basic raw materials for the chemical industry. It is used in numerous processes as a reagent, as a catalyst, and as a drying agent. Examples of the wide-ranging applications of this acid include the treatment of raw phosphates in the fertilizer industry, the treatment of titanium ores for the production of titanium dioxide, the manufacture of phosphoric and hydrofluoric acid, and the wide field of organic chemical synthesis, for example, in sulfonation and nitration.

Today, primarily elemental sulfur but also pyrite is used as raw material for the production of sulfuric acid. Combustion produces sulfur dioxide (SO_2) which is subsequently converted catalytically to form sulfur trioxide (SO_3) and thereafter is absorbed in concentrated sulfuric acid, usually in several stages. The absorption of SO_3 in concentrated sulfuric acid takes place in packed towers. Absorption occurs in a counter-current system, the SO_3 gas flowing upwards and the concentrated sulfuric acid flowing downwards. This process is highly exothermic.

So far, only a few materials were available which offer adequate corrosion resistance to highly concentrated sulfuric acid at high temperatures. As a result, the operating temperatures for the downstream equipment such as heat exchangers, pumps, and piping had to be reduced. For components operating at these lower sulfuric acid temperatures, various special materials are used. The nickel alloy C-276 (EN 2.4819/UNS N10276) is used for plate-type heat exchangers serving as acid coolers. Alloy 59 may also be used for this purpose. The isocorrosion diagram of alloy C-276 in technical grade sulfuric acid (**Figure 5**) at its extreme high concentration side on the right shows a large horizontal distance between the 0.1 and the 0.5 mm $year^{-1}$ isocorrosion line, indeed. This represents an excellent safety margin in case of temporary excursions of the sulfuric acid to lower concentrations.

Alloy 33 (EN 1.4591/UNS R20033) had been developed with the aim to use it, for example, for large acid distribution systems and plate heat exchangers.[36] **Figure 19** shows the isocorrosion diagram for this material in highly concentrated sulfuric acid. However, it must be emphasized that sulfuric acid can exhibit very complex behavior toward materials. For example, the temperature dependence of the corrosion rate of alloy 33 in highly concentrated sulfuric acid is not monotonous.[36,37] For certain acid concentrations, it is possible to cause the corrosion rate to rise by decreasing the temperature, an effect which can be observed in the isocorrosion diagram of **Figure 19**. Furthermore, traces of impurities, changes in the rate of flow, slight changes in concentration and/or slight increases in temperature can cause markedly higher rates of corrosion. In view of this, the isocorrosion diagram presented in **Figure 19** can only serve to provide an initial orientation and extensive testing in the actual plant acid and environment is necessary when selecting alloy 33 (EN 1.4591/UNS R20033).

Depending on the actual operating conditions, deviations can be expected to occur to a lesser or greater extent. This is true not only for the highly concentrated sulfuric acid discussed here in detail but for the whole range of sulfuric acid concentrations as shown in **Figures 5, 6,** and **12**, in particular for those temperatures under which materials are near their limits of resistance. If the operating parameters cannot be closely controlled, it may, in some cases, be necessary to select a material not as a function of its resistance to the theoretical operating conditions, but rather because of its ability to absorb variations in these conditions. As is so often the case, only plant testing under true service conditions is likely to give a reliable indication on the suitability of materials in most circumstances.

With these considerations in mind, the handling of sulfuric acid and sulfuric acid-based aqueous solutions constitutes a very broad field of application for nickel alloys. Standard stainless steel grades can be used only to handle much diluted acid at low temperatures. At higher concentrations and temperatures, the use of materials like high-alloy stainless steels and nickel alloys becomes necessary. Alloy 20 (EN 2.4660/UNS N08020), alloy 825 (EN 2.4858/UNS N08825), alloy 31 (EN 1.4562/UNS N08031), alloy 59 (EN 2.4605/UNS N06059), and alloy B-2 (EN 2.4617/UNS N10665) are some examples.

As pointed out in **Section 3.05.3.3**, the use of alloy B-2 may become necessary at sulfuric acid concentrations between 60% and 80% and temperatures even above 120 °C, but clearly reducing conditions must be present.

The use of the alloys 825 and 20, on the other hand, is restricted to the lower temperature range, but is facilitated by the presence of oxidants, as mentioned in **Section 3.05.3.6.2**. The newer alloys 31 (EN 1.4562/UNS N08031) and 59 show a more extended suitability. This is obvious from their isocorrosion diagrams in technical grade aerated sulfuric acid shown in **Figure 6** for alloy 59 (EN 2.4605/UNS N06059) and in **Figure 12** for alloy 31 (EN 1.4562/UNS N08031). However, it has to be kept in mind that the 0.1 mm year^{-1} isocorrosion line of alloy 31 in sulfuric acid is shifted to lower temperatures if no oxidants are present as demonstrated in **Figure 13** with the comparison of the corrosion behavior in technical grade sulfuric acid and in a p.a. sulfuric acid, established by Alves *et al.*[20] Although oxidants can extend the region of passivity of alloy 31, the corrosion behavior of alloy 59 is not influenced greatly by the amounts of oxidants present in the acid.[20]

Besides the influence of oxidants, the influence of the temperature deserves a closer look, too. Near the isocorrosion line, temperature is an extremely important variable influencing the corrosion rate, since above that line corrosion rate rises above 0.1 mm year^{-1} and materials may become unsuitable for service. Alloy 31 (EN 1.4562/UNS N08031) and alloy 59 (EN 2.4605/UNS N06059) behave differently in this respect. While for alloy 31, a small temperature increase above the isocorrosion line can cause a jump in corrosion rate, for alloy 59 the corrosion rate also increases but more moderately, as shown in **Figure 22**. This is because the corrosion rate in active state, which depends directly on the test temperature and on the alloy composition, is significantly higher for alloy 31 than for alloy 59. Particularly, high Ni and Mo contents are known to reduce the rate of active current density giving rise to the lower active corrosion rates of alloy 59.[20] Anodic polarization curves, which had been established in this context by Alves *et al.*,[20] indicate that alloy 31 is not so easy to passivate as alloy 59, but once passive, it exhibits lower passive current density than does alloy 59. This is probably related to the copper content of alloy 31 (EN 1.4562/UNS N08031), since copper is known to influence the passive current density in sulfuric acid.[20]

In many sulfuric acid applications, chlorides are also present, for example, in wall condensate in FGD units. Chlorides impair the corrosion resistance in sulfuric acid in shifting the anodic curve to higher current densities, making passivation more difficult, increasing the corrosion rates and may produce pitting corrosion. Indeed, as shown by Alves *et al.*,[20] the 0.1 mm year^{-1} isocorrosion line of alloy 31 (EN 1.4562/UNS N08031) is shifted to significantly lower temperatures when 1 g l^{-1} chloride is added to the sulfuric acid. However, in sulfuric acid contaminated with chlorides, alloy 59 (EN 2.4605/UNS N06059) has advantages over alloy 31, as exemplified in **Figure 23**, and its resistance to pitting is higher.

Many chemical processes use 98–99% sulfuric acid. After reaction is completed, the acid is not totally consumed, but is discharged in a diluted and

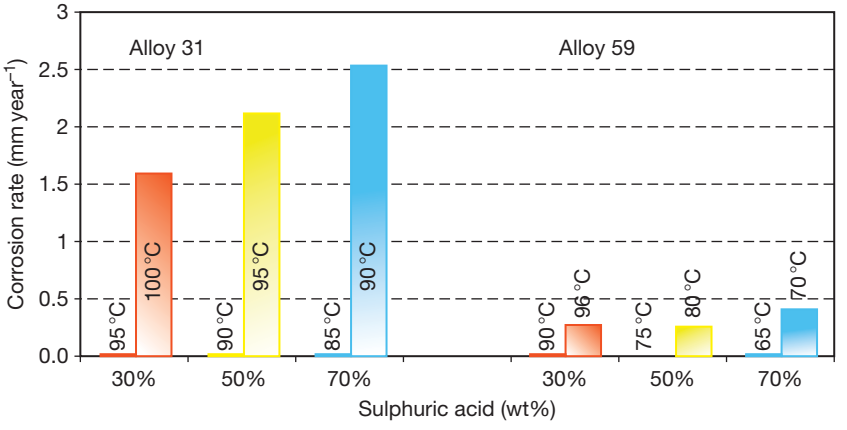

Figure 22 Corrosion rates of alloy 31 (EN 1.4562/UNS N08031) and of alloy 59 (EN 2.4605/UNS N06059) in aerated technical grade sulfuric acid closely below and above the 0.1 mm year^{-1} isocorrosion line, 24 h immersion test, according to Alves *et al.*[20]

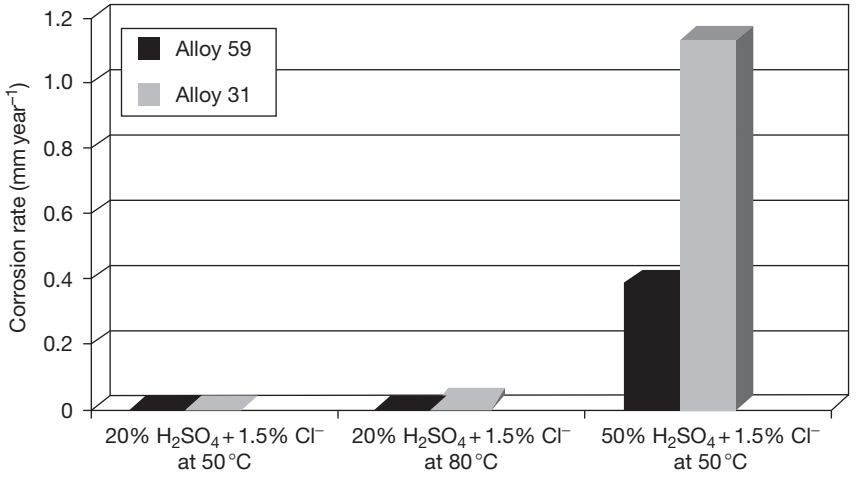

Figure 23 Corrosion rates of alloy 31 (EN 1.4562/UNS N08031) and of alloy 59 (EN 2.4605/UNS N06059) in aerated technical grade sulfuric acid with addition of 1.5% chloride, graph published by Alves *et al*.[20]

contaminated form. This waste acid is totally useless unless it can be concentrated (e.g., up to 75–80%) and purified for further use in chemical process reactions. Both alloy 31 (EN 1.4562/UNS N08031) and alloy 59 (EN 2.4605/UNS N06059) are in use in the regeneration of waste sulfuric acid.

For example, in viscose Rayon plants, alloy 31 (EN 1.4562/UNS N08031) is used in the regeneration of sulfuric acid. In the spinning step, the viscose is forced through a spinneret to produce the fine filaments and then comes into contact with a solution of sulfuric acid, sodium sulfate, and usually Zn^{2+} ions. The waste sulfuric acid from this step is regenerated by condensation under vacuum at temperatures between 30 and 40 °C and further adjusted with highly concentrated sulfuric acid, the dissociation heat of which can raise the temperature to up to 60 °C. The resulting 80–85% acid can be used for further processes.

In the production of titanium dioxide by the sulfate process, finely ground ilmenite ($FeTiO_3$) or ilmenite slag is digested with sulfuric acid in a concentration of ~90% and the cleaned titanium oxide sulfate is hydrolyzed to form titanium oxide hydrate, which is then calcined to form TiO_2. Modern plants incorporate a downstream dilute sulfuric acid processing facility. Alloy 31 (EN 1.4562/UNS N08031) is used in this application.

Further examples of waste acid recovery systems can be found in the metal-producing industry. In the copper production, alloy 31 (EN 1.4562/UNS N08031) is used in autoclaves to concentrate spent waste-contaminated sulfuric acid from 25% to ~75–80% in evaporators under vacuum. The presence of oxidizing metal ions in the contaminated acid helps maintain the passivity of alloy 31 (EN 1.4562/UNS N08031).

3.05.5.4 Production of Phosphoric Acid

A large amount of the world's fertilizer production is based on phosphoric acid (H_3PO_4). Two principal production methods are used. Thermal phosphoric acid is produced by the combustion of phosphorus with atmospheric oxygen, followed by the hydration of the oxide obtained. Owing to its high purity, this acid is primarily used as a food additive. Because of the high energy requirement, this method is of secondary importance. In the wet process, phosphoric acid is produced by digesting phosphate rock (apatite), usually with sulfuric acid. The by-products of this process are calcium sulfate, in the form of dihydrate (gypsum), and fluosilicic acid. About 95% of the global demand for phosphoric acid is met by the wet process. After filtration, the phosphoric acid, usually at a concentration of ~28% P_2O_5, is concentrated either to the standard commercial grade of 54% P_2O_5 or to super phosphoric acid with 70% P_2O_5.

The action of phosphoric acid on most metals is not particularly aggressive. However, the sulfuric acid and the presence of fluorine, chloride, and silica in the phosphate ores, which leads to the formation of hydrofluoric acid, fluosilicic acid, and also hydrochloric acid, give rise to very complex corrosion conditions. Silica and aluminum are used to complex with fluorine and reduce its corrosive effect. The chloride concentration strongly depends on the origin of the apatite and increases if the ores are washed using

seawater. Corrosiveness is further increased by the presence of sulfides. In addition, the degree of corrosive attack is aggravated by erosion resulting from the presence of abrasive solids such as phosphate rock particles and gypsum crystals, by turbulence and high velocity fluid flow, by deposit formation and by increases in temperature. From literature and plant experience, it is known that high chromium levels in the alloys used are required for sufficient corrosion resistance to phosphoric acid under those conditions.

In the wet process, the first stage for which corrosion-resistant materials are required is the reactor for digesting the ore. The reactor vessel is made of carbon steel throughout with a nonmetallic lining, sometimes augmented with acid-resisting bricks, particularly in locations of impingement and abrasion. The agitators are often made of special stainless steels. The application of these alloys, however, is limited by the increasing impurities in the phosphate ores and higher temperatures for digesting the ore. Experience gained under real service conditions proved that the materials alloy 31 (EN 1.4562/UNS N08031) and alloy 625 (EN 2.4856/UNS N06625) are particularly resistant to erosion and corrosion in phosphoric acid slurries.[29]

The filtration equipment requires special materials, in particular, with good resistance to pitting and crevice corrosion. The materials used for this equipment item are high-alloy stainless steels, but higher resistance to pitting and crevice corrosion can be achieved with alloy 31 (EN 1.4562/UNS N08031).

After filtration, the raw phosphoric acid, which may be contaminated with sulfuric acid, chlorides, fluorides, and fluosilicic acid, is concentrated to 54% P_2O_5. This takes place in an evaporator that is either equipped with metal tubes or is made of graphite. It has been shown that metallic heat exchangers operate satisfactorily when hot water is used as the heating medium. The solids settling on the tube walls, mainly gypsum, are easily removed by routine cleaning, which prevents corrosion under the deposits. Alloy 28 (EN 1.4563/UNS N08028) and alloy 31 (EN 1.4562/UNS N08031) are used for the heat exchangers.

In the further processing to produce super phosphoric acid (70–72% P_2O_5), usually no particular corrosion problems arise, because most of the fluorine contaminants have been removed in the upstream stages. The nickel–chromium–molybdenum alloy 625 (EN 2.4856/UNS N06625) is the standard material here. Nickel alloys are also used for further equipment in the phosphoric acid production, such as plate heat exchangers, equipment for the removal of gaseous fluorine compounds, pumps, and fans.

According to **Table 4**, alloy 31 (EN 1.4562/UNS N08031) exhibits high resistance to uniform and localized corrosion in industrial phosphoric acid under diverse conditions.[29] In phosphoric acid contaminated with sulfuric acid, fluosilicic acid, oxidizing metallic ions, and high amount of chlorides at 80 °C, this alloy shows outstanding corrosion resistance. At 120 °C, the corrosion rate becomes considerably higher. At these high temperatures, contamination is extremely important and must be well defined and controlled. In the example of **Table 4**, the contaminated 52% phosphoric acid at 120 °C is ~10 times more corrosive than is the technical pure one.

It should be emphasized that the performance of alloy 31 (EN 1.4562/UNS N08031), which combines a high chromium content with a sufficient molybdenum level is comparable or even many times superior to higher-alloyed materials of significantly higher price. As an example, **Figure 24** shows the corrosion rate of various alloys in attack acid with different

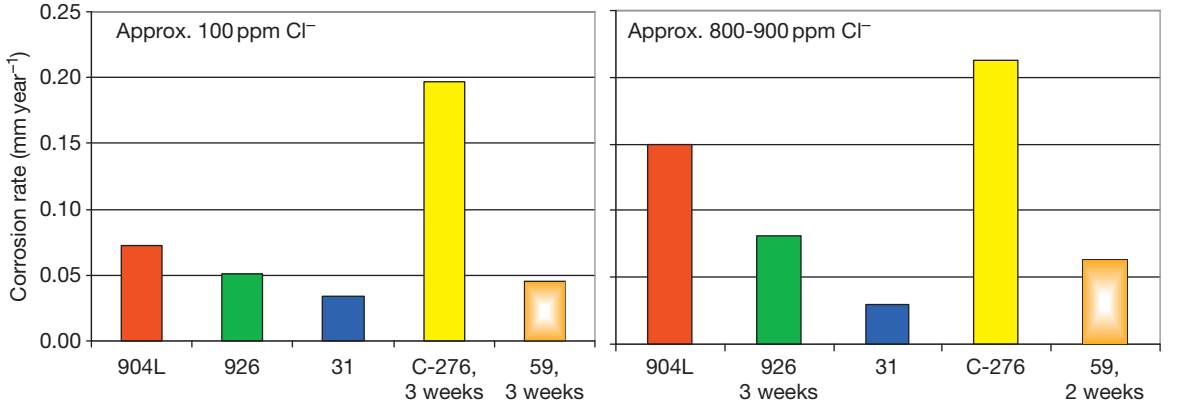

Figure 24 Corrosion rate of various alloys upon immersion in attack acid with (mass%) 33 P_2O_5, 1.6 SO_3, 1.8 F, and different chloride content at 90 °C.

chloride content at 90 °C, demonstrating that alloy 31 excels with the lowest corrosion rate.[30,52] This alloy also resists well to erosion–corrosion conditions,[29] which is in accordance with studies suggesting that under the mixed erosion–corrosion conditions found in the phosphoric acid industry, it is primarily corrosion resistance rather than hardness that determines the performance of the material. Typical applications for alloy 31 (EN 1.4562/UNS N08031) in phosphoric acid production include mixers, filter components, piping systems, heat exchanger tubes in concentration units, sulfuric acid coolers, vapor systems in concentration plant, flash coolers, and others. In particular, the use of alloy 31 (EN 1.4562/UNS N08031) in phosphoric acid production increases feedstock flexibility by contributing in a cost-effective manner to the solution of corrosion problems in the processing of, for example, phosphate ores containing high levels of chlorides.[30,31] Additional information on suitable alloys for application in phosphoric acid and on tackling chloride corrosion in phosphoric acid production is provided by Alves *et al.*[52] and by Hoxha *et al.*[53]

3.05.5.5 Production of Hydrofluoric Acid and Aluminum Fluoride

Hydrofluoric acid (HF) is produced by the reaction of concentrated sulfuric acid with fluorspar (calcium fluoride): $CaF_2 + H_2SO_4 \rightarrow 2\ HF + CaSO_4$. The reaction can take place in two stages. In the first stage, preheated fluorspar and preheated sulfuric acid are mixed together. The reaction is exothermic and the temperatures can reach 150 °C. The materials used here must therefore be able to resist hot concentrated sulfuric acid as well as hydrofluoric acid and possess adequate erosion resistance to fluorspar and calcium sulfate crystals. Depending on concentration and temperature, the materials alloy 20 (EN 2.4660/UNS N08020), alloy C-276 (EN 2.4819/UNS N10276), and alloy 59 (EN 2.4605/UNS N06059) are successfully used for these equipment items.

The second stage is a rotary kiln, in which the reaction is taken to completion. Some kilns, or their linings, are made of alloy 20 (EN 2.4660/UNS N08020), while in others, special stainless steels are used. Recently, good experience has been achieved with alloy 59 (EN 2.4605/UNS N06059) as a material for the rotary kiln. The gaseous hydrogen fluoride leaving the kiln is contaminated with entrained sulfuric acid and silicon tetrafluoride; these contaminants are removed in a sulfuric acid scrubber. The material for the scrubber will be determined by the concentration of sulfuric acid in the scrubber liquid. In some plants, the high-alloyed stainless steel alloy 926 (EN 1.4529/UNS N08926) is successfully used; depending on the sulfuric acid concentration, alloy 31 (EN 1.4562/UNS N08031) or alloy 59 (EN 2.4605/UNS N 06059) may also be considered.

The HF gas is liquefied at ambient temperature in condensers made of carbon steel and then distilled in two stages to remove impurities. The volatile constituents are first removed in a carbon steel column. In the second stage, the less volatile impurities are removed. The residue is an aqueous mixture of hydrofluoric acid and sulfuric acid. In the upper part of the distillation column, carbon steel can be used, while alloy 400 (EN 2.4360/UNS N04400) is generally used for the lower part and the reboiler.[39]

Only a few special stainless steels and nickel alloys can be used for handling aqueous hydrofluoric acid solutions; alloy G-3 (EN 2.4619/UNS N06985), alloy 31 (EN 1.4562/UNS N08031), and alloy 59 (EN 2.4605/UNS N06059) are suitable within very narrow temperature and concentration limits.[39] If alloy 400 (EN 2.4360/UNS N04400) is used, it must be kept in mind that stress corrosion cracking can occur in air containing hydrofluoric acid vapors, and to a lesser extent also in the liquid phase.

Aluminum fluoride is produced in fluidized beds of aluminum oxide and hydrogen fluoride at a temperature of 650 °C. Owing to the excellent corrosion resistance of alloy 600 L (EN 2.4617/UNS N06600) at high temperatures in the presence of gaseous HF, this alloy is used to make the reactors and the tubes for the product coolers.[39]

3.05.5.6 Production of Acetic Acid

Acetic acid (CH_3COOH) is the most important of the organic acids. It is used as a raw material in a large number of chemical processes. For example, acetic acid is used for the production of cellulose acetate, vinyl acetate monomer, acetic ester, pharmaceuticals, plastics, dyes, and insecticides. Acetic acid can be produced by fermentative oxidation of methanol. More common is the catalytic oxidation of hydrocarbons (e.g., butane) or the catalytic reaction of methanol and carbon monoxide: $CH_3OH + CO \rightarrow CH_3COOH$.

The most well known process using this route was developed by Monsanto, the license now being held by BP Chemicals. Rhodium activated with iodide acts as the catalyst. From carbon monoxide and the methyl groups, a complex compound is produced,

which is converted into acetic acid by hydrolysis, carbon dioxide and water arising as by-products. The exothermic reaction takes place at temperatures of 180–200 °C and a pressure of 15 bars in a special reactor. The acetic acid formed is then collected in an overhead condenser from where the iodine compounds are recycled to the reactor. The raw acetic acid is then distilled in two stages, with the unconverted methanol also being returned to the reactor.

The combination of hydroiodic acid, acetic acid, and water in the reactor, scrubber, and distillation columns produces extremely corrosive, reducing conditions. The materials in use for these items are alloy B-2 (EN 2.4617/UNS N10665), which is particularly corrosion resistant under reducing conditions, or alternatively zirconium.

After separation of the halogen ions, the acetic acid is less corrosive, so that the materials alloy C-276 (EN 2.4819/UNS N10276), alloy 59 (EN 2.4605/UNS N06059), alloy G-3 (EN 2.4619/UNS N06985), or alloy 31 (EN 1.4562/UNS N08031) can then be used in the downstream process equipment.

In other acetic acid processes like the Eastman process, in which no iodine is used, nickel–chromium–molybdenum alloys such as alloy C-276 (EN 2.4819/UNS N10276) and alloy 59 (EN 2.4605/UNS N06059) are likewise used.

3.05.5.7 Production of VCM

VCM is a feedstock for the manufacture of PVC and is nowadays produced from ethylene and chlorine. Ethylene is either converted directly with chlorine to form ethylene dichloride (EDC), which is then thermally cracked to produce VCM or ethylene is subjected to oxychlorination followed by pyrolysis.

As would be expected in pyrolysis processes, many equipment items are exposed to high temperatures and severe corrosive attack. The highly corrosive nature of dissolved chlorine and hydrogen chloride comes to the fore at elevated temperatures and, to a particularly strong extent, in the presence of moisture. Priority therefore attaches to the operation of a dry process. Any introduction of moisture or water would lead to the formation of hydrochloric acid and other corrosive media. As the demand for absolute dryness cannot be fulfilled in actual practice (start-up and shutdown, downtimes, leaks, decoking with steam), suitable measures must be found to prevent premature material failure as a result of corrosion. Where the process temperature permits, such measures include coatings (in most cases organic-based) and the use of corrosion-resistant materials. According to Alves *et al.*,[39] here it is mainly nickel alloys that have proved successful in the relevant operating conditions. Thus, alloy 825 (EN 2.4858/UNS N08825) is used for gas inlet tubes and alloy 59 (EN 2.4605/UNS N06059) or alloy C-276 (EN 2.4819/UNS N10276) for tube sheets and as cladding material in the catalysis section of fluidized bed reactors. The fixed-bed reactors are equipped with vertical tubes that are usually made of the nickel standard grade alloy 200 (EN 2.4066/UNS N02200), alloy 600 (EN 2.4816/UNS N06600), or alloy 625 (EN 2.4856/UNS N06625).

Thermal cracking of the EDC to form VCM and hydrochloric acid takes place in a pyrolysis kiln at 425–550 °C. Alloy 800 H (EN 1.4958/UNS N08810) is the standard material for this application. A few facilities are also constructed in alloy 600 (EN 2.4816/UNS N06600). In the EDC purification section, the main corrosion problem is created by hydrochloric acid. Here, various nickel materials such as alloy 400 (EN 2.4360/UNS N04400), alloy B-2 (EN 2.4617/UNS N10665), and 6Mo stainless steels such as alloy 926 (EN 1.4529/UNS N08926) are used for columns, heat exchangers, pumps, and valves. The use of standard chromium–nickel steel grades cannot be recommended owing to their high susceptibility to pitting corrosion and stress-corrosion cracking in the special conditions of VCM production.

A characteristic feature of some older VCM plants is the flare stack used to burn off waste gases. Alloy 59 (EN 2.4605/UNS N06059) is suitable for the stack head, which is subject to heavy corrosive attack. For environmental reasons, in new facilities, this gas is no longer burnt off but recycled to the process. The same materials can be used for the recycling process as for the VCM process itself, because their corrosion behavior has to meet similar requirements.

3.05.5.8 Production of Styrene

Styrene ($C_6H_5CH{:}CH_2$) is an important chemical for the production of a range of plastics, including polystyrene, SBR, ABS, and SAN resins, synthetic latexes, and polyesters. The main process used to produce styrene is the production of ethylbenzene in a first step by catalytic reaction of benzene and ethylene followed by the dehydrogenation of ethylbenzene.

In the first reaction stage, in which the ethylbenzene is produced, it is the corrosiveness of the catalyst that determines the type of material required. The Union Carbide/Badger process employs aluminum chloride as catalyst. Aluminum chloride is extremely

corrosive, meaning that only acid-resistant glass or ceramic linings come into consideration here. For metal linings, heating coils, and other internals, alloy B-2 (EN 2.4617/UNS N10665) and alloy C-276 (EN 2.4819/UNS N10276) can be used. The same alloys are also used in the downstream heat exchangers and piping systems. Columns and heat exchangers that come into contact with traces of chlorides are often made of the nickel–copper alloy 400 (EN 2.4360/UNS N04400). Special stainless steels such as the 6Mo grade alloy 926 (EN 1.4529/UNS N08926) can also be considered.

Other ethylbenzene processes use noncorrosive catalysts, and therefore, only low-alloy materials are required in the first stage.

The second process stage, in which hydrogen is split off, runs at high temperatures (950–1000 °C) in the presence of superheated steam. The steam is produced in furnaces in which the tubes and the manifolds are generally made of alloy 800 H (EN 1.4958/UNS N08810). The connection line from the superheater to the reactor may also be made of the same material. High temperature materials are also used for the reactor in which dehydrogenation takes place. These are mainly heat-resistant steels such as alloy 800 H (EN 1.4958/UNS N08810) or nickel alloys such as alloy 617 (EN 2.4663/UNS N06617). The exact choice of material depends on the design and the degree of attack.

3.05.5.9 Production of Acrylic Acid and Acrylate Esters

Acrylic acid (C_2H_3COOH) is a feedstock for the production of polyacrylic acid and acrylic esters. Acrylate esters (such as methyl acrylate, ethyl acrylate, butyl acrylate, etc.) are used in polymerized form for the production of dyes and paints, adhesives, textiles, and plastics. Polyacrylic acid is used in the production of hygiene products, cleaning products, and water treatment agents.

The most important process for the production of acrylic acid is the partial oxidation of propylene. In general, this process is regarded as 'noncorrosive,' enabling low-alloy steels to be used. Recently, however, a number of cases of corrosion damage have occurred in the extraction column. These problems have been attributed to traces of formic acid in the plant. Field tests have led to the selection of different materials according to the corrosiveness of the medium. Thus, in one plant, the 6Mo stainless steel grade alloy 926 (EN 1.4529/UNS N08926) was selected, in another plant the nickel alloy C-276 (EN 2.4819/UNS N10276), and in a third plant alloy 31 (EN 1.4562/UNS N08031).

Acrylate esters are produced by reacting acrylic acid with the corresponding alcohol in the presence of a catalyst. The catalyst can, for example, be sulfuric acid or sulfonic acid; the reaction temperature is in the order of 130 °C. An oxidizing or reducing stabilizer is added to prevent polymerization. The corrosiveness of the process is determined by the type of catalyst. Therefore, the choice of material for the reactor, heating tubes, and mixer will be determined by its corrosion resistance to sulfuric or sulfonic acids under either oxidizing or reducing conditions.

When reducing conditions are encountered, the copper–nickel alloy 400 (EN 2.4360/UNS N04400) can be successfully employed. It should be kept in mind, however, that alloy 400 loses its resistance to corrosion under oxidizing conditions. In one plant, severe corrosive attack was observed when the stabilizer was converted from reducing to oxidizing. Extensive exposure tests as much with high-alloy stainless steel grades as with the nickel alloy grades alloy G-3 (EN 2.4619/UNS N06985), alloy 625 (EN 2.4856/UNS N06625), alloy 31 (EN 1.4562/UNS N08031), alloy C-276 (EN 2.4819/UNS N10276), alloy 59 (EN 2.4605/UNS N06059), etc. showed that alloy 59 was the only material exhibiting an overall corrosion rate below 0.01 mm $year^{-1}$ and no pitting or crevice corrosion. For this reason, alloy 59 (EN 2.4605/UNS N06059) was selected for the particularly critical part of the plant, the heating tubes. As Alves *et al.*[39] report, after 3 years in use without any problems, the entire reactor was constructed in alloy 59.

3.05.5.10 Production of MDI and TDI as Feedstocks for Polyurethanes

Polyurethanes are produced by the polyaddition of isocyanates and alcohol. The most common processes use MDI and TDI as feedstocks. MDI and TDI are synthesized by conversion of diamines in the presence of carbonyl chloride (phosgene).

In the synthesis of both MDI and TDI, hydrogen chloride is generated as a by-product. Owing to the corrosiveness of HCl it is generally necessary to use corrosion-resistant materials. The heat exchangers downstream of the reactor are exposed to corrosive attack from a mixture of TDI, HCI, and phosgene (in traces) at temperatures of ~200 °C. The nickel–chromium alloy 600 L (EN 2.4817/UNS N06600) is generally used for these heat exchangers. Under normal conditions, this material lasts ~10 years. Under

particularly critical conditions, alloy 59 (EN 2.4605/UNS N06059) has been successfully selected.

In other areas of the plant, materials are required that are resistant to hydrochloric acid in aqueous solution. Depending on the overall process, the process stage and the precise composition of the medium, the nickel alloy grades alloy B-2 (EN 2.4617/UNS N10665), alloy 400 (EN 2.4360/UNS N04400), alloy C-276 (EN 2.4819/UNS N10276), or alloy 59 (EN 2.4605/UNS N06059) are used.[39]

Recently, a new gas phase technology has emerged whereby alloy C-4 and alloy 59 have proved to withstand corrosion in key equipment parts. In the reactor sump vessel, the mixture of TDI, hydrogen chloride, and phosgene at high temperature leads to strong pitting on standard stainless steel. In field tests and long-term pilot plant operation, alloy C-4 (EN 2.4610/UNS N06455) and alloy 59 (EN 2.4605/UNS N06059) have proved to be the material of choice.

3.05.5.11 Production of Fine and Specialty Chemicals

The fine and specialty chemicals industry produces a wide variety of chemical ingredients and active intermediates to be used, for example, in the pharmaceutical, food, agrochemical, and home and care industries. The selection of materials for the production of fine chemicals is made more difficult by the fact that the chemical plants involved are increasingly used to produce different types of substances to satisfy fast-changing market demands, so that reactors, vessels, piping systems, and heat exchangers are frequently exposed to changing corrosive media requiring the use of equally versatile multipurpose materials.

In addition, metallic contamination of the final product is not tolerable in many cases. Dissolved metallic ions may either lead to a discoloration of the products or trigger undesired catalytic reactions within the products or their amount may be limited by legal requirements. For this reason, specifications have to be met in many cases where tolerable mass loss is far below the corrosion rate of $\leq$ 0.1 mm year^{-1}, which is usually considered the limit for the technical corrosion resistance in case of metallic alloys.[54] The requirement for resistance to a broad spectrum of different media, which is given in most cases leads to the selection of either nonmetallic materials, like glass-linings and polymers, or special metallic materials. Such special metallic materials are alloys belonging to the family of C-type nickel–chromium–molybdenum alloys, titanium, zirconium, and tantalum. Lower-alloyed materials like alloy 31 (EN 1.4562/UNS N08031) are useful to a certain extent.

C-type nickel–chromium–molybdenum alloys, particularly alloy 59 (EN 2.4605/UNS N06059) can be considered for critical equipment as synthesis reactors and distillation columns. In the case of centrifuges, fittings, agitators, and valves, the material selection is mainly restricted to metals due to mechanical and design requirements.

Furthermore, cleanability is an important issue in multipurpose plants. In the case of nickel alloys, a high degree of cleanability can be achieved by electropolishing. Electropolishing of nickel alloys allows obtaining extremely smooth surface structures to which it is difficult for the products to adhere. In addition, the true surface area of an extremely smooth surface is considerably reduced compared with a surface of greater roughness, which results in a lower corrosion rate of the alloy and less migration of alloying constituents to the product. However, obtaining smooth surfaces by electropolishing requires a high degree of homogeneity of the alloy that has to be part of the material specification for this reason.

The wide variety of service media encountered in this industry is outside the scope of this work. As an example, reactions involving organic acid or solvents and catalyzed by small amounts mineral acids like sulfuric acid or hydrochloric acid can be found in the production of fine chemicals. Although more corrosive than the sulfuric acid, the hydrochloric acid is sometimes preferred owing to its higher catalytic activity. Oxidizing contaminants like oxygen, ferric, or cupric ions should also be considered, because they tend to shift the redox potential.

Figures 25 and **26** present data from laboratory tests intended to simulate in a simplified manner such type of environments.[55] Distinct levels of dissolved oxygen were achieved by bubbling nitrogen or oxygen into the solution and different concentrations of ferric ions were added in the form of sulfate. As indicated by the results, alloy 31 (EN 1.4562/UNS N08031) may sometimes require a shift of the free corrosion potential to more oxidizing conditions in order to make it corrosion resistant in these media. Alloy 59 (EN 2.4605/UNS N06059), however, exhibits very low corrosion rates under all conditions tested. Nickel–molybdenum alloys of the B-type are not considered for changing conditions in multipurpose plants, as they are resistant to few specific media only. In addition, their corrosion rate is increasing strongly with increasing amounts of accompanying oxidizing substances.

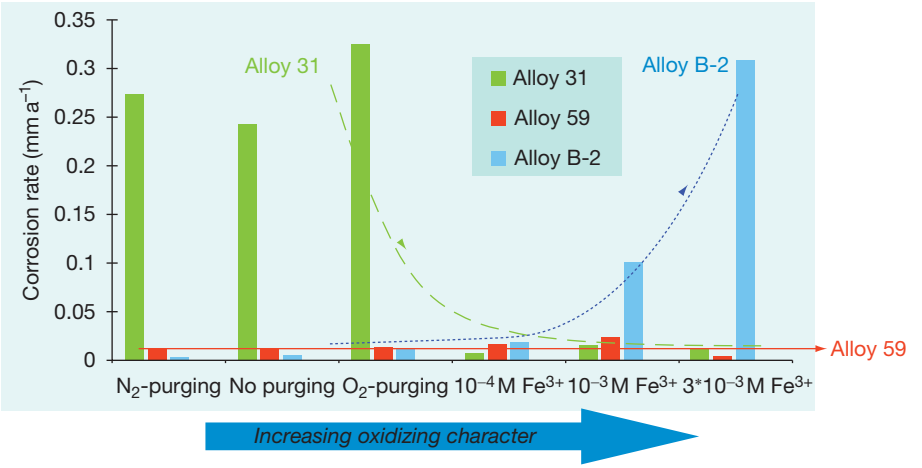

Figure 25 Corrosion behavior of alloy 31 (EN 1.4562/UNS N08031), alloy 59 (EN 2.4605/UNS N06059), and alloy B-2 (EN 2.4617/UNS N10665) in 50% CH_3COOH + 40% HCOOH + 5% H_2SO_4 + 5% H_2O under different oxidizing conditions at 95 °C, graph made from data (**Table 3** in Alves and Werner[55]) determined by Alves *et al*. in a 24 h immersion tests.

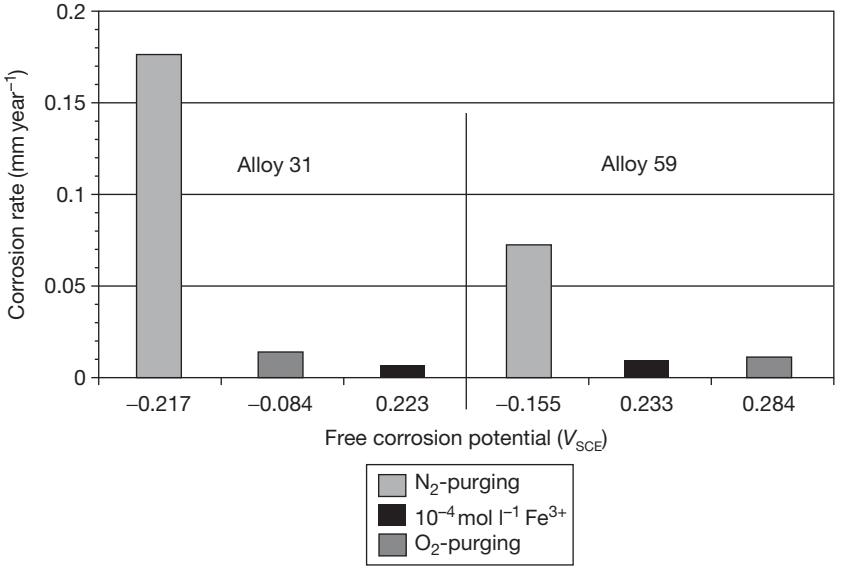

Figure 26 Dependence of corrosion rate on the free corrosion potential of alloy 31 (EN 1.4562/UNS N08031) and alloy 59 (EN 2.4605/UNS N06059) in 94% C_2H_5OH + 2% HCl + 4% H_2O at 60 °C, determined by Alves *et al* in a 24 h immersion tests. Reproduced from Alves, H.; Werner, H. *CORROSION 2004*; NACE International: Houston, TX, 2004, Paper No. 04235.

An additional study by Alves *et al.*[56] on the corrosion resistance in organic solvents with small amounts of sulfuric acid or hydrochloric acid showed again that alloy 31 (EN 1.4562/UNS N08031) requires a threshold oxidizing capacity to passivate, being preferred for the more oxidizing conditions. Alloy 59 (EN 2.4605/UNS N06059), however, revealed to be the more versatile alloy, having good resistance in the most environments studied. Alloy 59 (EN 2.4605/UNS N06059) shows higher ability to passivate and little susceptibility to variations on the content of oxidants or chlorides. Another interesting conclusion of the same study is that the corrosive impact of the small additions of HCl (2%) depends on the solvent and decreases in the sequence: methanolic solution > ethanolic solution > aqueous solution as a result of the different protonic activity. If methanol is used as a solvent, a certain threshold of water is required to maintain the passivity of nickel alloys. The water contents required to maintain

passivity and the corrosion rate <0.1 mm year^{-1} were found to be 8% at 40 and 50 °C for the unwelded alloy 31 (EN 1.4562/UNS N08031), and 12% at 40 °C and 18% at 50 °C for the welded alloy 31. Alloy 59 (EN 2.4605/UNS N06059) requires significantly lower amounts of water to maintain passivity (2% at 40 °C and 4% at 50 °C) and is not influenced by the welding conditions.

The C-type family of nickel–chromium–molybdenum alloys, in particular, alloy 59 (EN 2.4605/UNS N06059), offers a high level of reliability when equipment items are exposed to a variety of corrosive media. Indeed, this versatile alloy is suitable for a wide variety of corrosive environments, including mineral and organic acids, acid mixtures, halides, etc., and resists high levels of chlorides, oxidizing and reducing contaminants, and stress-corrosion cracking. Thus, alloy 59 (EN 2.4605/UNS N06059) can often be considered to replace more expensive materials like zirconium and tantalum or the mechanically fragile enamel.

3.05.5.12 Transport of Corrosive Dangerous Goods in Tanks

In Germany, the "BAM – List Requirements for Tanks for the Transport of Dangerous Goods" with compatibility evaluations of selected metallic material groups as well as of polymeric gasket and lining materials under the influence of dangerous goods and water-polluting substances is the basis for substance-related prototype approvals for tank containers designed for the carriage of dangerous goods.[57] Such information is applicable also to tanks, trucks, and rail cars. There are a large number of dangerous goods with high corrosivity to metals where the standard steels are not corrosion resistant. One possibility to solve corrosion problems is to line the tank with a polymeric material. An alternative possibility is the application of high-alloyed stainless steels and nickel alloys as there are alloy 31 (EN 1.4562/UNS N08031) and alloy 59 (EN 2.4605/UNS N06059). For lack of corrosion test results with welded test samples of these high-alloyed materials under the influence of corrosive dangerous goods, a comprehensive test program was performed in 14 relevant groups of media at 55 °C.[58,59]

The results obtained indicate that alloy 59 (EN 2.4605/UNS N06059) showed the most universal corrosion resistance of the materials tested. This alloy is suitable as material for tanks transporting almost all corrosive substances having been included in the test series. One exception is the limitation of temperature during the transport of hydrochloric acid.

Alloy 31 (EN 1.4562/UNS N08031) is very corrosion resistant, but more restricted in its use than alloy 59. Exceptions for the use of this material are hydrochloric acid, perchloric acid, and molten monochloroacetic acid at 110 °C. Limitations for the use exist in the concentration range of aqueous solutions of aluminum chloride, copper (II) chloride, ferric chloride, and 2-chloropropionic acid. Alloy 31 can be considered corrosion-resistant tank material for the transport of mixtures of concentrated nitric acid and 96% sulfuric acid if the content of the nitric acid does not exceed 50% or the temperature does not exceed 30 °C. Alloy 31 has excellent prospects for application in transportation tanks because of the multipurpose corrosion resistance characteristics in combination with the beneficial cost ratio in comparison with the standard stainless steel grade AISI 316L.

All details of those and future test results will be included in the most recent edition of the BAM-List – Requirements for Tanks for the Transport of Dangerous Goods.

3.05.5.13 Environmental Technology

Air pollution control occupies a leading position in the market for environmental technology. Therefore, the subject of this section[16] is the removal of oxidation products of the sulfur and of the accompanying HCI/HF gases from the combustion processes of organic materials (coal, lignite, oil) by chemical gas scrubbing. This process is generally known as 'FGD' and the associated plants as 'FGD plants.'

The wide range of scrubbing processes developed can be divided into scrubbing processes with regeneration of the scrubbing solution, spray absorption processes, and scrubbing processes without regeneration of the scrubbing solution. The scrubbing processes without regeneration, the so-called limestone processes are used throughout the world in ~90% of all FGD plants.

In a typical single-circuit process limestone FGD plant, the flue gas passes through an electrostatic precipitator; subsequently, the dust-free raw gas is sprayed with a scrubbing suspension in a quencher, whereby it is cooled and saturated with water vapor. In plants with a heat recovery system, the raw gas is cooled from ~200 to 300 °C (with/without NO_x reduction) to 150 °C by means of a so-called clean gas preheater before entering the scrubber. The gas flow and the circulation of the scrubbing suspension are adjusted so that the temperature of the scrubbing suspension is ~60 °C. The pH is adjusted to between

4.5 and 6. In the scrubber sulfur dioxide/sulfur trioxide (SO_2/SO_3) are transformed by the addition of limestone into calcium sulfite ($CaSO_3$) and subsequently transformed by the injection of air or oxygen into essentially insoluble $CaSO_4 \times 2\ H_2O$, that is, gypsum. This essentially insoluble gypsum precipitates out, and thus promotes the very high SO_2/SO_3 conversion rate of over 90%. A suspension of quicklime (CaO), hydrated lime ($Ca(OH)_2$), or limestone ($CaCO_3$) is used as the scrubbing solution. Chemical buffer reactions provide a constant pH in the absorber after the start-up phase of a FGD plant. Secondary reactions that take place after entry into the quencher or the bottom section of the integrated absorber are the almost 100% removal of hydrogen chloride (HCl) and hydrogen fluoride (HF), which are produced in the combustion process by chemical reactions and carried over with the flue gas. In counter-current systems, the flue gas is again sprayed with the scrubbing suspension in the upper region of the scrubber, the limestone excess in the added suspension resulting in a further increase in the degree of desulphurization. A pH shift toward a pH of ~6 is obtained by the buffer reaction of hydrogen carbonate. The main reaction in the FGD therefore consists in the transformation of sulfur oxides into inert insoluble end products (gypsum) in a weakly acidic medium. The resultant attack of the material arising from this process is in principle not critical. Practice shows, however, that particular zones within the plant are more sensitive with regard to materials than others, apparently because of secondary reactions or nonequilibrium conditions. Effects such as local temperature variations, catalytically acting surface conditions, and the tendency toward formations of incrustations and concentrations of individual harmful ions contribute to this. This results in zones ranking in their aggressiveness from slight to very severe requiring a whole spectrum of corrosion-resistant materials, from high-alloy stainless steels to nickel alloys.

The lower-alloyed stainless steels can – as a simplification – only be used in the area of the FGD absorber in very mild conditions, at low temperatures and if the development of concentrations under incrustations or deposits can definitely be ruled out, that is to say, in the neutral to weakly acidic region, if the chloride ion concentration is adjusted to = 0.5%. The operating range of the alloys mentioned in **Table 1**, for example, alloy 31 (EN 1.4562/UNS N08031) commences in weakly acidic solutions and extends to strongly acidic solutions with moderate chloride ion attack. Higher-alloyed nickel alloys are usually used at chloride concentrations >0.5% and in acidic to very strongly acidic conditions as well as where temperature increases to well over 70 °C are expected. At temperatures over 100 °C, with large fractions of chloride in the flue gas and much incrustation with dust or gypsum deposits, only the highest-alloyed materials such as alloy C-276 (EN 2.4819/UNS N10276) and alloy 59 (EN 2.4605/UNS N06059) turned out to have long-term resistance, but even these two broadly similar materials in practice exhibited marked differences in resistance to the most aggressive FGD conditions. In the past, countless reference plants have shown that alloy 59 (EN 2.4605/UNS N06059) is the only material that is still in use in an undamaged condition, even after many years of operation, in areas that are at greatest risk of corrosion such as the raw gas inlet of an FGD plant in a lignite-fired power station, and can also guarantee safe operation of the plant for its entire service life.

With this simplified representation of the areas of application of the special steels and nickel alloys, it is, however, vital to bear in mind that the actual material specification is only possible with reference to the specific project and by the material manufacturer, the equipment fabricator, the engineering consultant, and the plant operator working together. In doing so, a large number of other parameters such as processing, fuels, mode of plant operation, operating temperatures, magnitude, and frequency of deviations from the state of equilibrium, proportion of particulates, incrustations, design, and geometry of the components have to be taken into account.

It is economically sensible to produce in metal all the components of the heat recovery system, the quencher with the raw gas inlet, the absorber, the ducting, the second heat exchanger, and the stack. Nickel alloys are to be used for the components that will be subjected to the most aggressive media. Heat recovery systems, raw gas inlet areas, as well as fixing and sealing elements of dampers, are as a rule the components that are usually subjected to high condensate attack, and must therefore be made from the most-resistant materials. In recent years, alloy 59 (EN 2.4605/UNS N06059) has been used to a large extent for this application. Alloy C-276 (EN 2.4819/UNS N10276) may also be selected for these components; however, with this, the reserve capacity of alloy 59 is not quite attained. Since failure of fastening components could be disastrous and because of the extreme crevice conditions encountered there, alloy 59 (EN 2.4605/UNS N06059) is recommended for any fastening components too.

Alloy 59 is also recommended as a universal filler metal in welding, taking advantage of its high corrosion resistance combined with its high thermal stability.

If a stable chemical system with pH values in the range 4.5–6.5 is formed in the absorber sump and thus the aggressiveness can be calculated, and also as long as the chloride content is not too high, even alloy 31 (EN 1.4562/UNS N08031) can be used, given an exact knowledge of the operating conditions. The condition for the use of the latter material, however, is the avoidance of gypsum deposits by designing the agitating units accordingly. If there are any doubts, it is better to manufacture the absorber sump region in alloy 59 (EN 2.4065/UNS 06059), for example, in clad form (10 + 4 mm). In the transition zone from the raw gas inlet to the wet–dry interface of the sump, certain areas have to be constructed with a greater amount of alloy 59 or alloy C-276.

This also applies to the quencher nozzle system up to the process-specific transition into the absorber region (bowl in the dual-circuit scrubber). The first absorption planes, that is, the first spray pipe layers above the quencher nozzle system, can be made from alloy 31 (EN 1.4562/UNS N08031). The head of a dual-circuit absorber may be made from a high-alloy stainless steel, depending on the effectiveness of the mist eliminator. The heat recovery system, which is coupled with the raw gas inlet must, even in the parts where the gas is clean, be fabricated from nickel alloys of the type alloy 59 (EN 2.4605/UNS N06059).

It is necessary to make a distinction between coal-fired and lignite-fired power stations where the clean-gas connections to the stack are concerned. While, as a rule, in lignite-fired power stations with heat recovery systems, very clean treated gas duct conditions usually occur and thus limited deposits form, the situation in coal-fired power stations is the opposite. In particular, if there is no heat recovery system and the mist eliminator system is not working effectively or is not rinsed out frequently, thick deposits form in coal-fired power stations, which can give rise to an extremely high risk of corrosion with simultaneous condensate formation, particularly in the 6 o'clock position and in the flow deviation areas, and at design-related flow interruption points. Clean-operating treated gas ducts can, in some cases, even be fabricated from alloy 31 (EN 1.4562/UNS N08031) or even from a 6Mo stainless steel such as alloy 926 (EN 1.4529/UNS N08926). With all other methods of operation, higher-alloyed nickel alloys must be used, particularly in the 6 o'clock position and at the other flow interruption points, to achieve a corresponding increase in corrosion resistance. Stack inlet pipes or stacks built of solid metal usually require the materials alloy C-276 (EN 2.4819/UNS N10276) and alloy 59 (EN 2.4605/UNS N06059), since it is not possible to calculate accurately over the stack height and cross-section where the condensation zone occurs as a function of the external climate. Massive damages to coating systems (resin coatings with flake filling) as well as serious rotting of unprotected concrete stacks have recently increased the use of metallic nickel–chromium–molybdenum materials in stack construction.

Despite some fluid mechanics-related requirements, materials for shut-off fittings, for example, dampers and gates, must naturally be assessed according to their location in the gas stream. The material selection is obviously based on the aforementioned remarks.

On the basis of past experience, the selection of suitable materials specific to the component can guarantee a better long-term reliability and thus higher plant availability. If costs dictate thin-walled application of highly corrosion-resistant materials, this can be produced by the cladding of existing or new carbon steel structures with thin large sheets of nickel–chromium–molybdenum materials (wallpapering), or by the use of explosively or roll-bond clad composites with highly corrosion-resistant cladding materials.

References

1. Agarwal, D. C. Nickel and Nickel Alloys In *Uhlig's Corrosion Handbook*; 2nd ed.; Winston Revie, R., Ed.; John Wiley & Sons, 2000; Chapter 45, pp 831–851.
2. Friend, W. Z. *Corrosion of Nickel and Nickel-Base Alloys*; John Wiley & Sons: New York, 1980.
3. Council of Europe's Policy Statements Concerning Materials and Articles Intended to Come into Contact with Foodstuffs – Policy Statement Concerning Metals and Alloys – Technical Document – Guidelines on Metals and Alloys Used as Food Contact Materials – 13.02.2002, – www.coe.fr/soc-sp, Partial Agreement Department in the Social and Public Health Field, Council of Europe, Avenue de l'Europe, F-67000, Strasbourg.
4. Council Directive 98/83/EC of November 1998 on the quality of water intended for human consumption, Official Journal of the European Communities, 5.12.98, L 330/32–54.
5. International Nickel Co., Inc., Corrosion Resistance of Nickel and Nickel Containing Alloys in Caustic Soda and Alkalis, Corrosion Engineering Bull. CEB-2, 1973.
6. Heubner, U. In *Nickel Alloys and Special Stainless Steels*; 3rd ed.; Heubner/Klöwer, *et al.,* Ed.; Expert Verlag: Renningen, 2003; Chapter 2, pp 47–93.
7. Craig, B. D.; Anderson, D. S. Eds.; *Handbook of Corrosion Data*, 2nd ed.; ASM International: Materials Park, OH, 1995.

8. Büth, H. J.; Köhler, M. *Werkstoffe Korrosion* **1992**, *43*, 421–425.
9. Köhler, M.; Heubner, U. CORROSION 94; NACE International: Houston, TX, 1994, Paper No. 230.
10. Agarwal, D. C.; Heubner, U.; Köhler, M.; Herda, W., *Mater. Perform.* **1994**, *33*(10), 64–68.
11. LaQue, F. L.; Flint, G. N. *Nickel und Nickellegierungen*; Springer: New York, 1970; Chapter H, pp 356–398.
12. Alves, H.; Godinho, V.; Köster, U.; Ferreira, M. G. Proceedings EUROCORR. 2005, Lisbon, Sept. 2005.
13. Köhler, M.; Heubner, U.; Eichenhofer, K.-W.; Renner, M. CORROSION 97; NACE International: Houston, TX, 1997, Paper No. 115.
14. Heubner, U. In *Nickel Alloys and Special Stainless Steels*; 3rd ed.; Heubner/Klöwer, *et al.,* Eds.; Expert Verlag: Renningen, 2003; Chapter 1, pp 1–46.
15. Agarwal, D. C.; Herda, W. *Mater. Corros.* **1997**, *48*, 542–548.
16. Rhodes, P. R. *Corrosion* **2001**, *57*(11), 923–966.
17. Kirchheiner, R.; Wahl, V. In *Nickel Alloys and Special Stainless Steels*; 3rd ed.; Heubner/Klöwer, *et al.,* Eds.; Expert Verlag: Renningen, 2003; Chapter 8, pp 255–294.
18. Riedel, G.; Voigt, C.; Werner, H.; Heubner, U. *Mater. Corros.* **1999**, *50*, 452–462.
19. Alves, H.; Aberle, D.; Stenner, F. CORROSION 2007; NACE International: Houston, TX, 2007, Paper No. 07215.
20. Alves, H.; Werner, H.; Agarwal, D. C. CORROSION 2006; NACE International: Houston, TX, 2006, Paper No. 06222.
21. Heubner, U.; Köhler, M. *Werkstoffe Korrosion* **1992**, *43*, 181–190.
22. Kirchheiner, R.; Köhler, M.; Heubner, U. *Werkstoffe Korrosion* **1992**, *43*, 388–395.
23. Riedel, G.; Voigt, C.; Werner, H. *Mater. Corros.* **1997**, *48*, 518–527.
24. Agarwal, D. C.; Herda, W. R.; Klöwer, J. CORROSION 2000; NACE International: Houston, TX, 2000, Paper No. 501.
25. Agarwal, D. C.; Brill, U.; Behrens, R. CORROSION 2004; NACE International: Houston, TX, 2004, Paper No. 04281.
26. Butts, M. D.; Cripps, P. R.; Gilbertson, O.; Agarwal, D. C. In AIRPOL Symposium 2004, August 29, 2004, Washington, DC; NACE International: Houston, TX, 2004.
27. Heubner, U.; Rockel, M. B.; Wallis, E. *ATB Metall.* **1985**, *XXV*(3), 235–241.
28. Hibner, E. L.; Pucket, B. C.; Patchell, J. K. *CORROSION 2004*; NACE International: Houston, TX, 2004, Paper No. 04110.
29. White, F. E.; Jallouli, E. M.; Moustaqssa, A.; Agarwal, D. C. In AIChE Central Florida Section, 23rd Annual Memorial Weekend Conference on Phosphate Technology, Clearwater, Florida, May 28–30, 1999.
30. Alves, H.; Stenner, F.; Agarwal, D. C.; Hoxha, A. *CORROSION 2006*; NACE International: Houston, TX, 2006, Paper No. 06221.
31. Thomas, B.; Agarwal, D. C. *CORROSION 2007*; NACE International: Houston, TX, 2007, Paper No. 07216.
32. Heubner, U.; Kirchheiner, R.; Rockel, M. *CORROSION 91*; NACE International: Houston, TX, 1991, Paper No. 321.
33. Klöwer, J.; Schlerkmann, H.; Pöpperling, R. *CORROSION 2001*; NACE International: Houston, TX, 2001, Paper No. 01004.
34. Voigt, C.; Riedel, G.; Werner, H.; Köhler, M. *Mater. Corros.* **1998**, *49*, 489–495.
35. Köhler, M.; Heubner, U.; Eichenhofer, K. W.; Renner, M. *Stainless Steel World* **1999**, *11*(4), 38–49.
36. Renner, M. H.; Michalski-Vollmer, D. In Proceedings of Stainless Steel World 99 Conference, KCI Publishing BV, Zutphen, 1999; Book 2, pp. 443–452.
37. Werner, H.; Riedel, G.; Brill, U. *Mater. Corros.* **2002**, *53*, 893–897.
38. Gramberg, U. *Stainless Steel World* **1996**, *8*, 24–29.
39. Alves, H.; Horn, E. M.; Klöwer, J. In *Nickel Alloys and Special Stainless Steels*; 3rd ed.; Heubner/Klöwer, *et al.,* Eds.; Expert Verlag: Renningen, 2003; Chapter 7, pp 226–254.
40. Klöwer, J.; Rommerskirchen, I.; Kolb-Telieps, A.; Köhler, M. *CORROSION 2000*; NACE International: Houston, TX, 2000, Paper No. 636.
41. Herbsleb, G. *BBR* **1989**, *40*, 554–559.
42. Koppe, J.; Lausch, H.; Heubner, U.; Brill, U. *Chem. Ingenieur Technik* **1999**, *71*, 609–612.
43. Vollmer, T.; Gümpel, P.; Blaise, M.; Racky, W. *Mater. Corros.* **1995**, *46*, 92–97.
44. Gümpel, P.; Vollmer, T.; Blaise, M.; Racky, W. *Stainless Steel Eur.* **1995**, 47–51.
45. Heubner, U.; Hoffmann, T.; Köhler, M. *Mater. Corros.* **1997**, *48*, 785–790.
46. Köhler, M. *Mater. Corros.* **1997**, *48*, 528–534.
47. Riedel, G.; Kirchheiner, R.; Heubner, U. *Mater. Corros.* **1997**, *48*, 113–124.
48. Heubner, U. L.; Altpeter, E.; Rockel, M. B.; Wallis, E. *Corrosion* **1989**, *45*, 249–259.
49. Altpeter, E.; Heubner, U.; Rockel, M. *Werkstoffe und Korrosion* **1992**, *43*, 96–105.
50. Riedel, G.; Werner, H.; Voigt, C. *Werkstoffwoche;* Wiley VCH, 1999; Vol. 3, pp 275–280.
51. Heubner, U.; Rockel, M.; Wallis, E. *Werkstoffe Korrosion* **1989**, *40*, 459–466.
52. Alves, H.; Hoxha, A.; Stenner, F.; Coppe, P. Proceedings COVAPHOS II Conference, Marrakech, 9–11 November 2006.
53. Hoxha, A.; Stenner, F.; Alves, H.; Novello, F. Proceedings IFA 2006, Vilnius, 25–28 April 2006.
54. Korkhaus, J. Materials for Future Chemical Plant Concepts, Achema Conference, Workshop Nickel Alloys Selection in the Chemical Process Industry, Frankfurt/Main, 15–19 May 2006.
55. Alves, H.; Werner, H. *CORROSION 2004*; NACE International: Houston, TX, 2004, Paper No. 04235.
56. Alves, H.; Werner, H. Proceedings of the 16th International Corrosion Congress, Beijing, 19–24 September 2005.
57. BAM – List – Requirements for Tanks for the Carriage of Dangerous Goods – 8th edition, Federal Institute for Materials Research and Testing (BAM), Berlin 2005.
58. Weltchev, M.; Baessler, R.; Werner, H.; Alves, H.; Behrens, R. *CORROSION 2006*; NACE International: Houston, TX, 2006, Paper No. 06688.
59. Weltchev, M.; Baessler, R.; Werner, H.; Alves, H. *CORROSION 2008*; NACE International: Houston, TX, 2008, Paper No. 08180.

3.06 Aqueous Corrosion of Cobalt and its Alloys

A. Neville
Institute of Engineering Thermofluids, Surfaces and Interfaces, School of Mechanical Engineering, University of Leeds, Leeds LS2 9JT, UK
U. Malayoglu
Faculty of Engineering, Dokuz Eylul University, Bornovo, Izmir, Turkey

Glossary

Stellite A family of cobalt–chromium based alloys typically containing additions of carbon, tungsten, and molybdenum and notable for their extreme hardness and good corrosion resistance.

Abbreviations

Bcc Body centred cubic
Fcc Face centred cubic
GTAW Gas tungsten arc welding
Hcp Hexagonal close packed
HIP Hot isostatic pressing
MoM Metal-on-metal
SFE Stacking fault energy
TCP Topologically close packed
THR Total hip replacement
TJR Total joint replacement
TWL Total weight loss

Symbols

E_{corr} Corrosion potential
i_{corr} Corrosion current density

3.06.1 Metallurgy

3.06.1.1 Introduction

Cobalt is one of the transition metals appearing between iron and nickel; it was discovered by Brandt in 1735. Depending on temperature, there are two allotropic modifications of cobalt: face centered cubic (fcc), which is stable above 690 K and hexagonal close packed (hcp), stable below 690 K. Pure cobalt is soft and it has poorer oxidation resistance than nickel and iron. However, the alloying of cobalt with chromium and various quantities of carbon and tungsten results in the family of Stellite alloys, which have excellent corrosion and wear resistance. Cobalt is generally obtained as a secondary product from the mining of other elements, particularly copper and

nickel; relatively minor quantities (15%) derive from primary cobalt mining.[1] Current production is around ~50 000 tonnes per annum at a producer cost generally from three to five times that of nickel.

The cobalt-base alloys are extremely resistant to many forms of wear and moderately resistant to many forms of corrosion. For example, alloys optimized for wear resistance generally include significant carbon addition, which results in the formation of carbides in the microstructure during alloy solidification. These carbides increase the hardness of the alloys and their resistance to low-stress abrasion. Key applications are in wear and erosion-resistant alloys (e.g., the Stellite family and cemented carbides) and in high temperature oxidation-resistant alloys: these comprise ~40% of cobalt use. The balance of production is used in batteries (25%), magnetic alloys (6%), colors and pigments (10%), catalysts (9%), etc.

Alloys designed for service in severely corrosive environments typically contain low carbon levels. Not only does this markedly improve resistance to corrosion, but also it increases ductility. The chief benefits of high carbon content are increased hardness and enhanced resistance to low-stress abrasion, both of which increase with increasing carbon content. Aspects of the corrosion resistance are discussed in detail later in the chapter.

In forming carbides, the carbon ties up a portion of vital alloying elements, such as chromium. The effective chromium content from a corrosion standpoint (the chromium remaining in the solid solution) is therefore considerably lower than indicated by the nominal composition. Carbide forming elements such as tungsten (which forms W_6C type carbides) may reduce the amount of carbon required to reach the eutectic composition.

3.06.1.2 Alloying

Historically, many of the commercial cobalt-base alloys are derived from the cobalt–chromium–tungsten and cobalt–chromium–molybdenum ternaries first investigated by Elwood Haynes in the beginning of the twentieth century.[2] He discovered the high strength and stainless nature of the binary cobalt–chromium alloy, and he later identified tungsten and molybdenum as powerful strengthening agents within the cobalt–chromium system. When he discovered these alloys, Haynes named them the Stellite alloys after the Latin 'stella' (star), because of their star-like microstructure. Having discovered their high strength at elevated temperatures, Haynes also promoted the use of Stellite alloys as cutting tool materials. In **Figure 1** a typical microstructure of the Stellite 6 alloy is shown and the

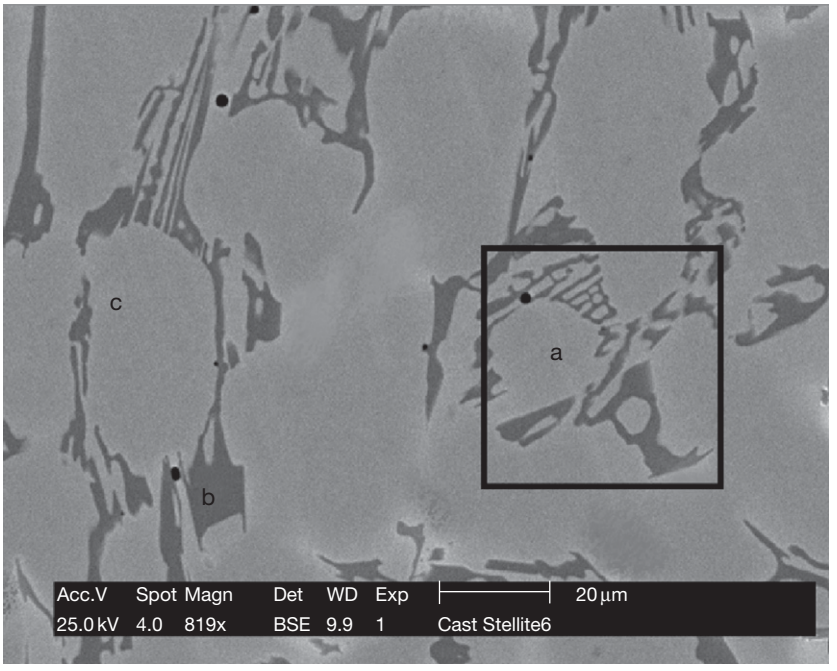

Figure 1 Typical microstructure of Stellite 6 alloy: (a) analysis area composition in wt% is 60.8% Co, 29.8% Cr, 6.2% W, 1.7% C, 1.4% Fe (b) is eutectic Cr-rich carbide, and (c) is the Co rich matrix. Reproduced from Malayoglu, U. PhD Thesis, Heriot-Watt University, 2005.[3]

complex structure of eutectic carbides and the Co-rich matrix is clear.

The chemical constitution of cobalt alloys is analogous to the general family of stainless steels and the role of major and minor alloying elements is virtually identical throughout these austenitic alloy systems. The addition of alloying elements alters the thermodynamic stability of the fcc compared with the hcp phases by either enlarging or constricting their fields. These alloys also effect the martensitic transformation by influencing the Ms (martensitic start) and As (austenite start) temperatures.

In cobalt-base alloys, the key element, chromium, is added in the range of 20–30 wt% to improve corrosion and wear resistance and for some measure of solid–solution strengthening. Where carbide precipitation strengthening is a desirable feature, chromium also plays a strong role through the formation of a series of varying chromium–carbon ratio carbides such as M_7C_3 and $M_{23}C_6$. M_7C_3 carbides, which have a hexagonal crystal structure and contain ~70 wt% Cr, ~12 wt% Co, and small amounts of other metallic elements in the alloy.

The refractory elements, tungsten and molybdenum, are utilized as the major solid–solution strengtheners for both wrought and cast cobalt alloys, while those of lower solubility such as tantalum, columbium, zirconium, and hafnium are generally more effective in their carbide forming role. Molybdenum and tungsten produce strengthening by formation of intermetallic compounds of Co_3M and MC carbides and the formation of M_6C carbides

For cast alloys, Morrow *et al.*[4] demonstrated that replacing tungsten with an atomic equivalent addition of molybdenum improves elevated tensile and rupture ductility without decreasing strength in alloys such as FSX 414 and MM 509. Additionally, alloy cost and density decreases with little change in expansion coefficient or microstructural characteristics. However, molybdenum addition slightly decreases the solidus and liquidus temperatures and increases the total solidification range, which somewhat alters the carbide morphology and produces additional eutectic carbides.

The refractory element rhenium has been successfully utilized in nickel alloys for solid solution strengthening; however, its potential in cobalt alloys has not fully been explored. Like tungsten, it exhibits extensive solubility in the matrix and increases the solidus and liquidus temperatures. Of the alloying elements, tungsten produces a favorable increase in melting temperature. Tantalum has been successfully utilized as a replacement for tungsten in high temperature sheet alloys MM-918 and S-57, where some improvement in oxidation resistance was also demonstrated. The effect of different alloying elements is summarized in Table 1.

Table 1 The effect of several elements in cobalt-base superalloys

Element	*Effect*
Chromium	Improves oxidation and hot-corrosion resistance; produces strengthening by formation of M_7C_3 and $M_{23}C_6$ carbides
Molybdenum	Solid–solution strengtheners; produce strengthening by formation of intermetallic compound Co_3M; formation of M_6C carbide
Tungsten	
Tantalum	Solid–solution strengtheners; produce strengthening by formation of intermetallic compound Co_3M and MC carbide; formation of M_6C carbide
Columbium	
Aluminum	Improves oxidation resistance; formation of intermetallic compound CoAl
Titanium	Produces strengthening by formation of MC carbide and intermetallic compound Co_3Ti; with sufficient nickel produces strengthening by formation of intermetallic compound Ni_3Ti
Nickel	Stabilizes fcc form of matrix; produces strengthening by formation of intermetallic compound Ni_3Ti; improves forgeability
Boron	Produce strengthening by effect on grain boundaries and by precipitate formation; zirconium produces strengthening by formation of MC carbide
Zirconium	
Carbon	Produces strengthening by formation of carbides MC, M_7C_3, $M_{23}C_6$, and possibly M_6C
Yttrium	Increases oxidation resistance
Lanthanum	

Source: Anon, Cobalt Monograph, Centre d'Information du Cobalt/Battelle, 1958.

3.06.1.3 Microstructure and Microstructural Influences

The microstructure of Stellite alloys varies considerably with composition. They may either be in the form of hypoeutectic structure consisting of primary dendrites of a cobalt-rich solid solution surrounded by eutectic carbides, or of hypereutectic type containing large idiomorphic primary chromium rich carbides and eutectic.

Among the alloying elements, carbon is found to have a large influence on the microstructure, causing a change from a hypoeutectic to hypereutectic alloy. Figure 2 shows the phase diagram for the

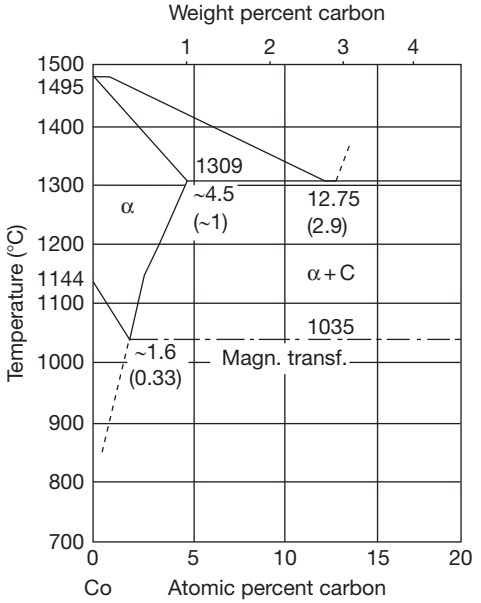

Figure 2 Cobalt–carbon binary system. Reproduced from Atamert, S. Stability, wear resistance and microstructure of iron, cobalt and nickel-based hardfacing alloys, PhD thesis, University of Cambridge UK, 1989.[5]

carbon–cobalt alloy system. As can be seen in the hypoeutectic side of the system (<1.6at% of C) the liquidus temperature of the alloy decreases by ~14 °C for each 1% increase in carbon content. Carbon is clearly critical to those casting alloys formulated for the highest creep rupture strength levels, since carbide strengthening is the primary precipitation hardening mechanism utilized in the cobalt alloy system. The control of carbon is critical for tensile and rupture strength and ductility since it has been shown that a nonlinear increase in strength occurs over a range of ~0.3–0.6% carbon.

The strength of most cobalt base superalloys is derived from the carbide phases present in the matrix and distributed around the grain boundaries. The carbides that form depend on the composition and thermal history of the material. The carbide former elements are from group IV (Ti, Zr, Hf), group V (Cb, Ta), and group VI (Cr, Mo, W). The types of carbides that are formed are as follows (M and C represents metal and carbon atoms respectively):

M_3C_2: rhombic, a high chromium content carbide which forms at low Cr/C ratio;
M_7C_3: trigonal, a high chromium content carbide which forms at a slightly higher Cr/C ratio;
$M_{23}C_6$: cubic, a high chromium content carbide which forms at an higher Cr/C ratio, when the Cr is greater than 5 wt% of the alloy;
M_6C: complex cubic, a carbide phase whose volume fraction increases as refractory metals are introduced;
MC: fcc NaCl structure, a carbide comprising metal groups IV and VI.

These carbides are listed above in the order of increasing stability, or free energy of formation. The stronger the carbide formers used, the greater is the tendency to form M_6C and MC carbides. The type of carbides that form is dependent upon both thermal history and composition. Lane and Grant[6] suggested a transformation of M_7C_3–$M_{23}C_6$ during aging in an X-40 casting, which is described by the reaction

$$23M_7C_3 = 7M_{23}C_6 + 27C \quad [1]$$

This demonstrates that a nonequilibrium structure exists in Co castings at high temperatures.

The microstructure of cobalt base superalloys is thus a combination of MC, M_7C_3, $M_{23}C_6$, and M_6C carbides. In the cast structures, both composition and shape help to distinguish one carbide from another. The MC carbides have two characteristic shapes, a Chinese script and a block-like angular particles. The differences are believed to be the result of formation at various times during solidification. Block-like angular MC carbides may form initially before the bulk of the melt has started to solidify, whereas in the Chinese script, MC carbide is formed within the eutectic composition.[7]

$M_{23}C_6$ carbides are found mostly as fine plates interlayered with the cobalt matrix. This eutectic structure has a block-like shape. Subsequent heating of the cast structure can dissolve the $M_{23}C_6$ carbides. Upon aging, the carbides are precipitated as fine particles, usually near the eutectic $M_{23}C_6$ islands. In contrast to other carbides, the M_6C carbides do not have a characteristic morphology. Other important microstructural features of cobalt base superalloys are stacking faults, which have been reported to be present on all {111} planes.[8] Stacking faults appear to be related to the tendency to form hcp. Since stacking faults in fcc materials have an hcp structure, this is not surprising.

Many of the chemical attributes of the cobalt-based alloys derive from their crystallographic characteristics, which are summarized in **Figure 3**. The influence of alloying elements such as iron and nickel is explained through their effect on the stacking fault energy (SFE). Ni, Mn, and Fe have a strong effect on the SFE stabilizing the fcc allotrope, but Mo, W and Cr tend to stabilize the hcp allotrope and decrease the SFE. The excellent erosion resistance of cobalt-based

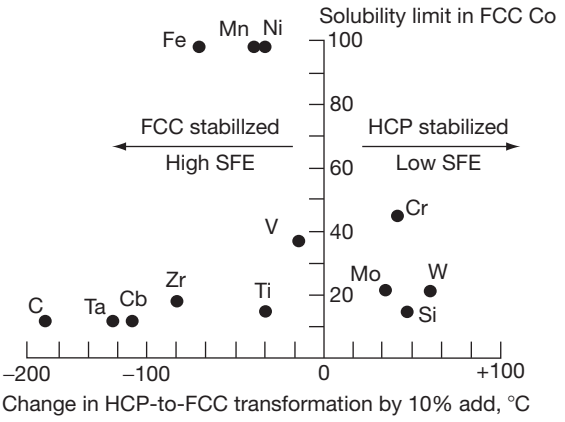

Figure 3 Effect of alloying elements on the fcc–hcp transformation in cobalt as a function of solubility. Reproduced from Sims Chester, T.; Stoloff, N. S.; Hagel, W. C. *Super Alloys II*; John Wiley & Sons: London, 1987.[9]

Stellite alloy is greatly attributed to the low SFE, which in turn means higher stacking fault probability and a greater chance for the formation of ε hcp platelets. The lower the SFE (the greater the width of stacking fault), the more difficult cross-slip is and the higher the work hardening and the strain to fracture. The materials with low SFE tend to strain harden rapidly, and show the highest galling resistance.

The effect of stacking faults may be detrimental to overall mechanical properties of cobalt base superalloys. Stacking faults have been shown to contribute to the strength of materials by inhibiting dislocation flow.[5] They also serve as sites for precipitation of second phases in cobalt base superalloys, which can likewise increase strength.[10] In contrast, it has been suggested that excessive stacking faults decrease the ductility of cobalt base superalloys to a value unacceptable for commercial use.

Stellite 6B is more likely to transform to hcp phase than most cobalt-base alloys since the fcc stabilizing elements iron and manganese are present in small amounts. Although carbon has a strong stabilizing effect in solution, most of it is tied as carbides. In fact, by suitable heat treatment, partial transformation may be achieved by thermal exposure alone.

Addition of iron and nickel are known to increase the stability of the fcc phase (and therefore, the SFE) of cobalt-base alloy. Furthermore, an increase in the SFE results in a change in the mode of deformation. The α→ε transformation occurs to a lesser extent and there is a greater tendency towards slip of undissociated dislocations {111} phase. The α→ε phase transformation and the formation of mechanical twins have been found to cause rapid increase in the work hardening rate while also producing a maximum in the strain to fracture. These two phases are considered necessary for erosion resistance and therefore, any factor suppressing these structural changes must lead to a decrease in resistance.

3.06.1.4 Alloy Systems

The cobalt–chromium–carbon system is characterized by the affinity of chromium for the formation of carbides of various types in which cobalt can replace some of the chromium. Wever and Haschimoto[11] carried out extensive studies on the solidification behavior of cobalt–chromium–carbon alloys of various compositions by thermal analysis. According to their findings the 30% Cr, 1% C alloy has a solidification range (the temperature difference between the solidus and liquidus temperatures) of ~150 °C. In the carbon content range of 1.0% to 1.7%, the solidification range decreases by ~5.5 °C with each 0.1% increase in carbon content. Also, they showed that at 1% carbon, an increase in chromium from 20% to 30% results in reduction of the solidification range by ~50 °C.

Koster and Spencer[12] studied the constitution of the cobalt–chromium–tungsten alloy system and their work showed for up to ~30% chromium and 15% tungsten the microstructure at room temperature consists of only the cobalt base solid solution. At higher chromium and tungsten contents various intermetallic phase would form in addition to the solid solution.

The carbon–tungsten–carbon system has been the subject of many investigations concerning cemented tungsten carbides (WC and W_2C), dealing mainly with alloys containing less than 25% cobalt. However, Rautala and Norton[13] covered most of the alloy system and produced diagrams showing phase equilibria at 1400 °C. These studies show that if the carbon content is maintained close to that required for stoichiometric formation of WC there will be a stable two-phase region of Co + WC below 1400 °C. Carbon deficiencies lead to formation of Co_3W_3C while carbon excess leads to the formation of graphite. However, it has to be mentioned that up to ~7.5% WC is soluble in cobalt.[13] Thus in alloys containing small quantities of carbon and tungsten, the formation of WC phase would not be expected.

3.06.1.5 Processing

There are numerous processing techniques depending on the application and the environment available to provide good wear and corrosion resistance parts from

cobalt base alloys. The effect of different processing techniques on the microstructure and the mechanical properties has been studied by different researchers and a short review is presented later in the chapter.

Wrought cobalt–tungsten base alloys were studied by Adkins *et al.*[14] In the binary alloys, the room temperature hardness increased with increasing tungsten content up to 15%. There was a slight drop in hardness for alloys containing over 15% tungsten. Solution-treated and quenched alloys showed a martensitic Co_3W phase.

Stellite alloys are often used as a coating for hard-facing applications or as castings. The casting and hard-facing of Stellite is, however, difficult and leads to an inhomogeneous coarse grain structure and also to excess dilution and improper adherence when there is overlaying.

Mohamed *et al.* studied the localized corrosion behavior of alloy Stellite 6 produced by hot isostatic pressing (HIP) and by wet powder pouring using electrochemical techniques.[15] In another work Wong-Kian *et al.* compared the erosion corrosion behavior of HIPed and welded Stellite coatings[16] and showed that HIPed alloys have lower mass loss due to finer microstructure. Malayoglu also confirmed the superior resistance of HIPed Stellite 6 and attributed this to the different microstructure with spherical carbides and the enriched Cr in solid solution in the matrix.[3] **Figure 4** shows the HIPed microstructure of Stellite 6.

Frenk and Kurz[17] investigated the solidification conditions and microstructure of a cobalt base alloy.

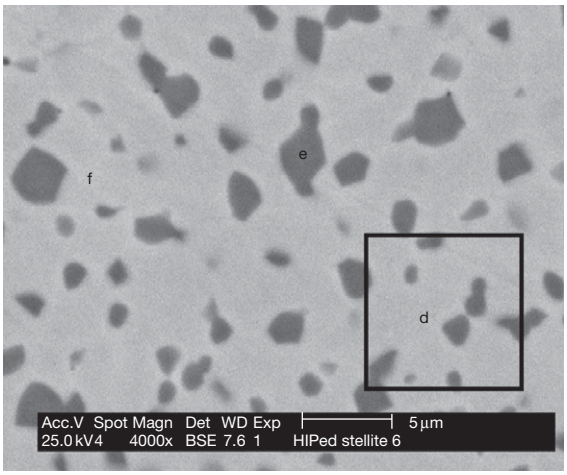

Figure 4 Microstructure of HIPed Stellite 6 (e) Cr-rich carbides, (f) Co-rich matrix. Reproduced from Malayoglu, U. PhD Thesis, Heriot-Watt University, 2005.

They concluded that different processing conditions can be achieved using laser surface cladding. For example, a variation in the laser scanning rate over two orders of magnitude from 1.67 up to 167 mm s^{-1} led to a considerable refinement of the microstructure. Antony[18] compared the wear performance of various forms of Stellite alloy 6B. He showed that gas tungsten arc welded (GTAW) alloy had better cavitation resistance compared to investment cast, wrought and oxyacetylene Stellite 6B deposit. Berns and Wendl analyzed the microstructure of the alloy Stellite 6 in the cast, forged and powder metallurgy state and compared them to the mechanical and wear properties.[19]

Weld overlays are used for economic and technical reasons. From an economic standpoint, it is sensible to use relatively expensive wear and corrosion resistant alloys only where their properties are necessary. From a technical standpoint, many wear-resistant alloys are brittle by nature and thus unsuitable for use in bulk form. The largest problem associated with the use of weld overlay material is dilution that is, the intermixing which occurs with the substrate material, generally stainless steel. It has been reported that dilution of iron into the cobalt-base alloy is detrimental to the corrosion and cavitation resistance of cobalt-base alloys.[20]

Cobalt and cobalt–molybdenum binary alloys have been the subject of work by Bibring and coauthors.[21] In alloys containing 8% or 10% molybdenum, quenching results in a structure that consists primarily of the hcp low temperature phase, and a significant proportion of the fcc nonequilibrium high temperature phase. When aged at a temperature below the solubility limit, the supersaturated hcp phase increases rapidly in hardness, while the fcc phase remains unchanged. This selective hardening of the hcp phase is due to the appearance of a phase with a composition corresponding to Co_3Mo. Darby and Beck[22] investigated the cobalt–chromium–molybdenum alloys and they reported an existence of $Co_{13}Cr_{17}$, which had a beneficial effect on the mechanical properties of the alloy. Silverman *et al.*[23] increased the proportion of chromium and molybdenum in commercial alloy Stellite 21. They found that room temperature hardness increased with increasing proportion of chromium and molybdenum.

Precipitation of an intermetallic compound in cobalt–chromium–molybdenum alloys was found to increase the room-temperature hardness in alloys containing 20% chromium and up to 16% molybdenum. A study of precipitation hardening in alloys containing 12.0% to 17.5% chromium and from 15% to 20% molybdenum was made by Lux and

Bollmann.[24] The alloys as-cast all contained a coarse precipitate of Co_7Mo_6. Some of the alloys in the cast condition showed Widmanstatten structure. It was suggested that this structure was associated with the formation of a Co_3Mo super lattice. Generally speaking, the precipitate observed in cast specimens that had been aged for 100 h at 1000 °C gave an X-ray pattern that corresponded to Co_7Mo_6, but chemical analysis of precipitates indicated a partial replacement of the molybdenum by chromium. The amount of chromium in the precipitate increased with aging temperature. At room temperature, the data offered three possible relationships between the precipitate and the matrix: a Co_3Mo super lattice, a coherent Co_3Mo precipitate, or a coherent Co_7Mo_6 precipitate.

3.06.1.6 Strengthening Mechanisms

Intermetallic compounds play an important role in the microstructure of Co-base alloys and the next few paragraphs discusses the nature of these and their role in affecting the properties of Co-base alloys.

Geometrically close-packed (GCP) phases are usually designated by the chemical formula A_3B, where A is the larger atom. For example, in nickel base superalloys a fine precipitate $Ni_3(Al,Ti)$ contributes greatly to high temperature strength. Because of its strengthening characteristics and high solution temperature, this phase has improved tremendously the high temperature properties of nickel superalloys, and even surpassed the properties of the cobalt systems. The generation of GCP phases within cobalt alloys is substantially more difficult since the chemical and crystallographic stability is affected by a lattice mismatch that is rarely less than 1%. In contrast, topologically close-packed phases (TCP) are usually detrimental to high temperature mechanical properties of cobalt superalloys. These phases are made up of close-packed layers of atoms separated from one another by relatively large interatomic distances forming a characteristic topology. By contrast, GCP phases are characterized as close-packed in all directions. The most common TCP phases are σ, μ, and R which are electron compounds. The general formula for a TCP phase is: $(Co,Ni)_x(Cr,Mo,W)_y$; where x and $y = 1–7$. The structure of the TCP-type phases (σ, μ and R) are as follows:

σ = complex body centre tetragonal	30 atoms/unit cell
μ = rhombohedral	13 atoms/unit cell
R = rhombohedral	53 atoms/unit cell

Laves phases are the most common intermetallic compounds of the TCP type. The chemical formula for Laves phase is A_2B, where A and B are two different metallic elements and occur in high temperature superalloys when excessive amounts of refractory metals are added. These phases precipitate as both plate and block structures and are generally detrimental to mechanical properties.

The primary strengthening mechanism in cobalt base alloys is precipitation hardening; principally by the presence of carbides in the matrix and grain boundaries. The carbides, especially $M_{23}C_6$, precipitate at the grain boundaries, pin the grain boundaries preventing grain boundary sliding, or in the case of higher carbon content, the carbide network may support some of the load. The large carbide particles can act as dislocation generators under the influence of a stress and the subsequent dislocation interaction can give rise to an increase in the flow stress of the metal. Regarding carbides, another important mode of strengthening arises from precipitation of fine $M_{23}C_6$ particles on stacking faults. This provides a rather uniform dispersion of interlocking structural effects caused by the hard carbide particles at stacking faults and stacking fault intersections.

Beside carbides, another form of second phase particles in cobalt-based alloys are intermetallic compounds as mentioned earlier. These phases have to be considered as they can cause a significant loss of both strength and ductility. Their deleterious effect is due primarily to the chemical partitioning effect caused by the mass presence of the phase itself, thus depleting the matrix of solute-strengthening atoms. As mentioned earlier, solid solution strengtheners include mainly the refractory elements such as chromium, molybdenum and tungsten. These atoms contribute to strengthening in a number of ways: they inhibit recovery by binding vacancies; and also they impede dislocation glide through the existence of interstitial complex around the refractory atoms. The fcc–hcp transformation in cobalt alloys has not been fully utilized in the development of desired mechanical properties. This is primarily due to the fact that the details of the allotropic transformation have not been well understood. The first detailed examination using transmission electron microscopy of the fcc–hcp transformation in the Co–Cr–Mo–C system was carried out by Vander Sande *et al.*[25] Their work was initiated by earlier findings of property modifications in response to heat treatment and processing variables and associated microstructural changes.

3.06.2 Corrosion

3.06.2.1 Electrochemistry

Compared with iron, cobalt is significantly more noble and part of its domain of stability lies above the hydrogen stability line for water. Compared with nickel, it is slightly less noble; the main difference in chemistry being a considerably larger stability for the Co(III) oxidation state compared to the corresponding nickel species. Cobalt is passive in neutral to alkaline pH but dissolves in aerated and dearated acids below pH 7. The Pourbaix diagram for cobalt is shown in Figure 5.

3.06.2.2 Passive Films on Co-Base Alloys

It is generally acknowledged that the susceptibility of passive metals to localized corrosion (including pitting) and the rate at which this corrosion process occurs are closely related to the ability of the passive film to resist breakdown and to repassivate once corrosion has initiated.[26] The chemical composition of the passive film, its structure, physical properties, coherence and thickness are of paramount importance in the nucleation and propagation of localized corrosion.

Investigations into the composition and structure of passive oxide films on stainless steels and other related passive alloys, of which the Co-base superalloys are one class, are much more difficult than in the case of analysis of oxide films on iron because the films are thinner, their chemical composition is complicated, and they cannot be reduced cathodically. A major part of the information available on composition and structure of passive films on stainless steels has been obtained with spectroscopic techniques, particularly X-ray photoelectron spectroscopy (XPS) and Auger electron spectroscopy (AES). Other methods such as ion scattering spectroscopy (ISS) and secondary ion mass spectrometry (SIMS) also provide valuable data.

The XPS method was used to study the composition and structure of oxide films on iron-chromium alloys. Li *et al.*[27] used this method to compare the film formed on Fe–30Cr and Fe–30Cr–2Mo alloys during passivation in 1 M KCl. They did not find any substantial differences in the film composition, which was primarily hydrated chromium oxyhydroxide. XPS and AES methods were also used by Olefjord and Elfstrom to study oxide films on austenitic stainless steels passivated in 0.1 M HCl + 0.4 M NaCl solution.[28] The passive film consisted primarily of chromium oxide. Iron was preferentially dissolved even during passivation. Mo enrichment was observed in high Mo alloyed (6%) steel. Ni was present only to a small extent in the film.

Compared to the extensive literature on Fe-based alloys (especially stainless steels) there is very little information available on other alloys which exhibit

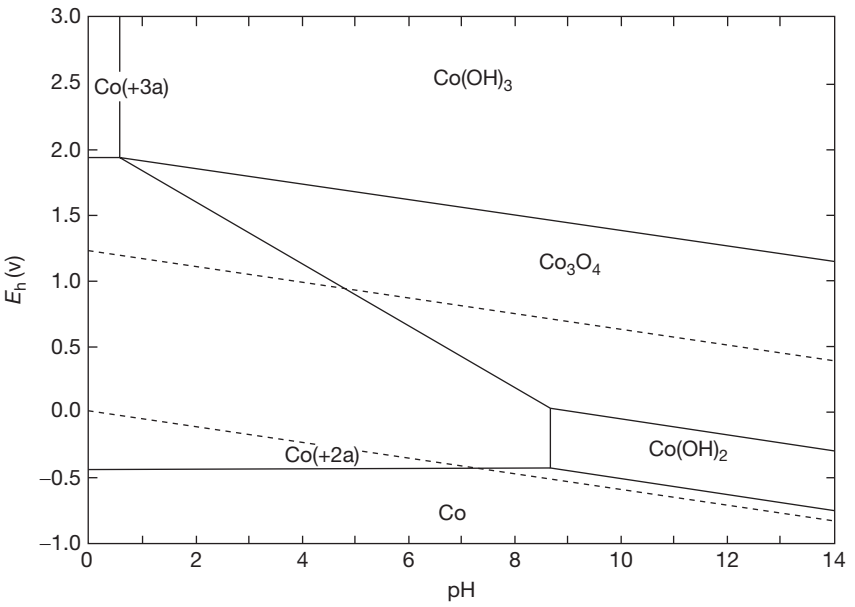

Figure 5 Pourbaix diagram for cobalt at a metal ion concentration of 10^{-5} M.

passivity (e.g., Ni and Co-based alloys). Hocking *et al.*[29] studied the corrosion of Stellite 6 in lithiated high temperature water used in pressurized water reactors (PWR) coolant circuits. By using XPS, they determined the chemical composition at the outer surface of the corrosion layer and concluded that oxidation of Stellite 6 alloy is believed to occur by preferential dissolution of Co at the solution interface, leaving a Cr-rich oxide. An increase in oxygen activity leads to a change in the mechanism from diffusion controlled to solution transport, dissolution-precipitation process and the corrosion rate increases.

McIntyre *et al.* also studied on the formation of the corrosion film on Stellite 6 alloy[30] According to their work there are two major mechanisms controlling the corrosion behavior of the alloy during aqueous oxidation. One is migration via solid-state processes, while a second results from dissolution of the cation and its subsequent reprecipitation on the oxide surface. As a result of their work, they concluded that during aqueous exposure in either reducing or mildly oxidizing conditions, a depletion of the cobalt surface composition was observed. This implies that there is a preferential dissolution of cobalt, which had already migrated preferentially to the interface.

It is also known for passive alloys that there is generally an inverse relationship between the thickness of the film and its protective property. This was seen in work by Malayoglu *et al.*[3] where the breakdown potential in anodic polarization tests was shown to be reduced aligned with a thinning of the passive film detected by XPS on HIPed Stellite 6 in 3.5% NaCl.

For the as-polished sample of Stellite 6, the C 1s spectrum revealed the presence of an overlay of carbonaceous contamination, and the O 1s spectrum the presence of oxide/hydroxide species at the surface. The carbon contamination and oxygen-containing species are readily removed by argon etching. The C 1s spectrum also reveals the presence of metal carbide species below the contamination over layer. The Cr 2p spectrum comprises the presence of Cr metal, carbide and oxide/hydroxide species and the W 4f spectrum is consistent with the metal but not W oxides. The Co 2p spectrum is consistent with the presence of Co metal and oxide/hydroxide species. The XPS signals of the metal oxide/hydroxide species decrease with argon ion etching, hence the model for the as-polished surface is of a matrix of metal and metal carbide species with an over layer of Cr and Co oxide/hydroxide and carbonaceous contamination.

The analysis of the spectra after anodic polarization on HIPed Stellite 6 indicates a multilayer duplex structure, where the composition changes continually with depth. At the outer surface, the film contains no metallic Co, Cr or W and consists of $Cr(OH)_3/Cr_2O_3$ and WO_2. Immediately beneath this layer, depending on the test temperature, the film is composed of $Cr(OH)_3/Cr_2O_3$ and metallic Cr, from the bulk material can be observed. Similarly, W was detected in the form of WO_3 and metallic W. A schematic representation of the key components of the air-formed film and corroded surface was presented as shown in **Figure 6**.

Maffiotte *et al.*[31] confirmed the qualitative similarity in oxide film composition on a 30%Cr, 4.5%W, 2.5% Ni alloy when exposed to different environments representative of operating conditions in PWR. The film in both solutions was Cr-enriched and Co-depleted but the depth profile of the oxide film composition was dependent on the solution composition. Longer exposure to the solution further enriched the oxide with Cr as shown in **Figure 7**.

3.06.2.3 Corrosion of Cobalt-Based Alloys

Co-base alloys have seen extensive use in wear environments mainly due to their high strength, corrosion resistance and hardness. Application of cobalt-based superalloys was traditionally most prevalent in the nuclear industry in the 1960s and 1970s and, for this reason, much research into corrosion of Stellite was focused in conditions relevant to nuclear power applications such as simulated pressurized water reactor and primary heat transfer conditions, for example.[32]

Currently, use of Stellite alloys has extended into various industrial sectors (e.g., pulp and paper processing, oil and gas processing, pharmaceuticals, chemical processing) and the need for improved

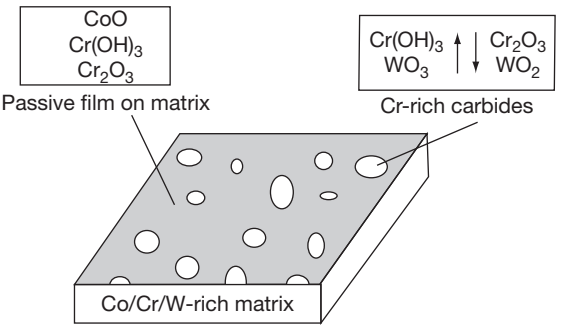

Figure 6 Key components of the air-formed passive film. Reproduced from Malayoglu, U. PhD Thesis, Heriot-Watt University, 2005.

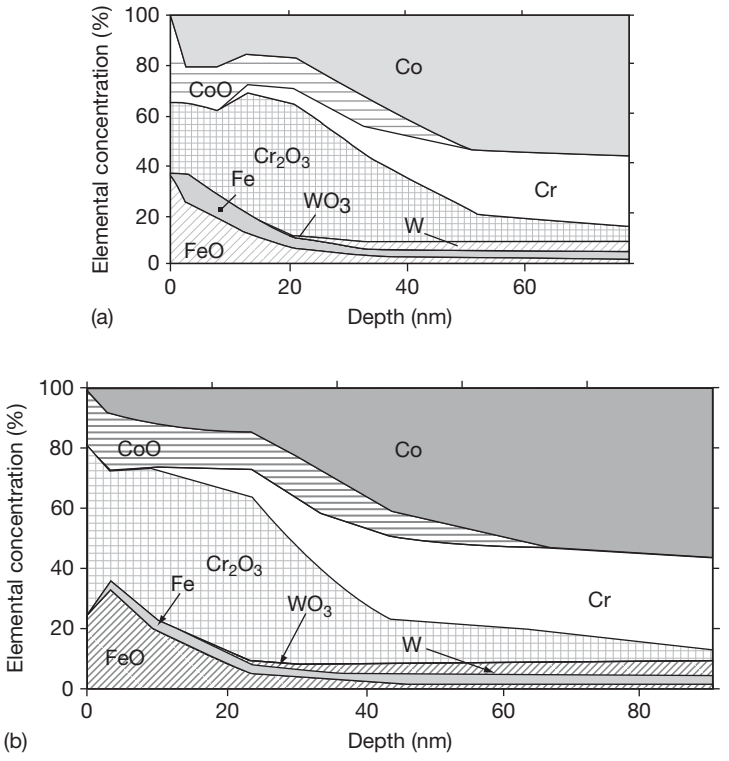

Figure 7 XPS composition depth profiles from Stellite 6 immersed in 300 ppm H_2BO_3, 2.65 ppm LiOH, 2 ppm H_2 for 250 h (a) and 2000 h (b). Reproduced from Maffiotte, C.; Navas, M.; Castaño, M. L.; Lancha, A. M. *Surf. Interface Anal.* **2000**, *30*(1), 161–166.

information regarding corrosion (and often tribo-corrosion) of Stellite alloys has increased. It has been recognized that processing changes, which affect the microstructure of Stellite alloys, affect the corrosion behavior. Stellite alloys have been used as surface engineering systems as weld overlays, laser-clad overlays and HVOF coatings, and because of the very different microstructures as a result of the thermal cycling, the corrosion properties can vary. In a study by Kim and Kim[33] the corrosion resistance of Stellite 6 resulting from the plasma transferred arc (PTA) welded surfaces was compared to spray-fused and open arc-welded surfaces. Their corrosion results showed that the corrosion resistance of PTA weld surfaced Stellite 6 is better than that of the open arc weld surfaced Stellite 6 because dilution (~15%) with the iron substrate for the open arc weld surfaced Stellite 6 is higher than that (~5%) of the PTA weld surface Stellite 6. **Figure 8** shows the increase in corrosion current density (i_{corr}) for the alloys experiencing higher dilution.

Mohamed *et al.*[15] studied the localized corrosion behavior of powder metallurgy processed cobalt-base alloy Stellite 6 in a chloride environment. They showed that the Stellite 6 alloys produced by the HIP technique had the highest pitting and crevice corrosion resistance compared with identical alloys manufactured by the rolling or wet powder process. They discussed how the Oldfield–Sutton model of acidification was more appropriate for crevice corrosion in HIPed alloys than the models used to describe Cl^- accumulation. The finer microstructure for the HIPed alloy was thought to be the main reason for the improved resistance.

Human *et al.*[34] studied the electrochemical polarization and corrosion behavior of a cobalt–tungsten–carbon alloy in 0.5 M sulfuric acid. They showed that tungsten and carbon additions influence the corrosion behavior of the alloy. With increasing tungsten and carbon additions, the corrosion current density and the critical current density were reduced. The corrosion potential shifted to more positive values with increasing additions. As the corrosion studies have not necessarily been made with high purity elements, the effect of small amounts of impurity or alloying elements and the synergistic

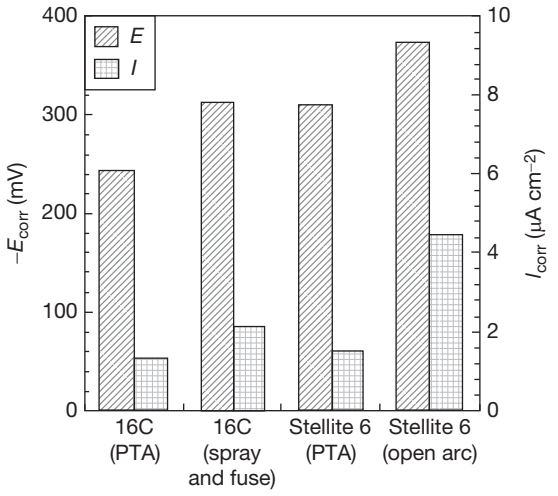

Figure 8 Comparisons of free corrosion potential and corrosion current density for surface engineered Stellite alloys in 3%NaCl. Reproduced from Kim, H. J.; Kim, Y. J. *Surf. Eng.* **1999**, *15*, 495–501.

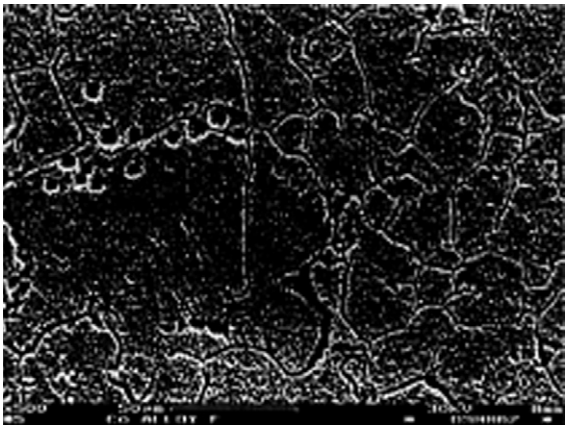

Figure 9 Cracks and pores in the surface layer of Co—WC alloy in sulfuric acid. Reproduced from Human, A. M.; Roebuck, B.; Exner H. E. *Mater. Sci. Eng.* **1981**, *A241*, 202–210.

effects of them on the corrosion performance of the metals and alloys is difficult to determine and understand.

In this work empirical relationships were developed for the alloys of the form

$$E_{corr} = -372 + 70V_v^{fcc}(C, W)[mV]$$

where V_v^{fcc} is the volume fraction of fcc phase. In this nonpassivating system, the cracks and pores in the surface layer are clearly visible (**Figure 9**).

Malayoglu assessed the corrosion resistance of three Stellite alloys in the cast and HIPed form. The Stellite 12 has a similar composition to Stellite 6 but with a much higher content of W of 9%. In Stellite 706, the W in Stellite 6 is replaced with Mo. As shown in **Figures 10a** and **10b** the resistance to passivity breakdown (E_b) is affected by temperature and the alloys are affected to a different extent. At low temperature for the cast alloy Stellite 12 and Stellite 706 are comparable and more resistant than Stellite 6. Between 30 and 40 °C, there is a significant loss of resistance for Stellite 6. In potentiostatic tests on HIPed alloys, it was shown that the critical temperature was higher for Stellite 12 and Stellite 706. However, severe tunneling pitting was seen on Stellite 12 – not seen on Stellite 6.

3.06.2.4 Oxidation

The effect of alloying elements on the high temperature corrosion performance of the metals and alloys, and the corrosion resistance of films and scales have been summarized by Frantsevich[35] who stated that;

- Small amounts of alloying elements will affect the parent metal oxide by changing its conductance. Factors influencing this will be the alloying element's valence, ion radius, and the heat of formation of the oxide.
- Large amounts of alloying elements will affect, more significantly, the properties, such as: electrical conductivity, mechanical and thermodynamic stability, and mutual solubility of the oxide phase. Changes in the dissolution pressure, concentration defects in the lattice, appearance of physical defects in the scale owing to stresses originating in the oxide film can be expected.

The effects of the alloying elements on improving the oxidation resistance of an alloy may be due to one or more of the following main factors:

- Reduction of the diffusion rate of reaction components in the oxide layer and metal through the decreased concentration of lattice defects and the formation of new phases of combined oxides.
- An increase of the ion mobility in the oxide may improve the mechanical properties of the scale phase and permit some plastic deformation.
- The decrease of the metal/oxide volume ratio, due to the change of parameters of the oxide and metal lattices, occurs when the cations are replaced with ions of smaller radii.

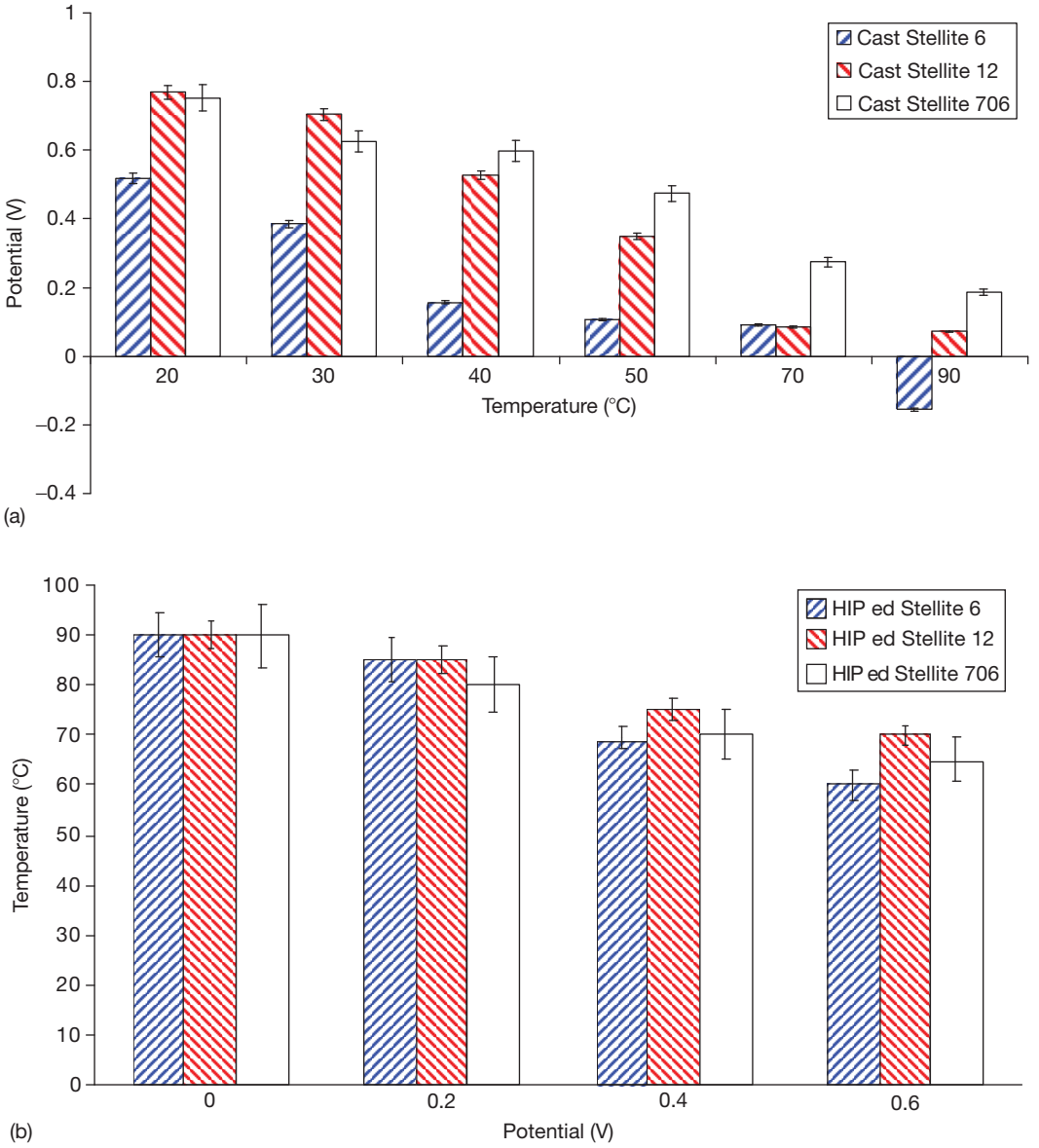

Figure 10 (a) Breakdown potential of cast 6, 12 and 706 Stellite alloys as a function of temperature in 3.5% NaCl. Reproduced from Malayoglu, U. PhD Thesis, Heriot-Watt University, 2005. (b) Breakdown temperature from potentostatic tests on HIPed 6, 12 AND 706 Stellite alloys in 3.5% NaCl. Reproduced from Malayoglu, U. PhD Thesis, Heriot-Watt University, 2005.

3.06.2.5 Corrosion in Biomedical Applications

3.06.2.5.1 Joints

CoCrMo alloys have been widely and successfully used in hip joints due to their high corrosion resistance and good mechanical properties. Many authors have studied effects of the microstructure and elemental content on the joint-bearing performance. It has been shown that many factors influence their performance.[36–39] However, one major concern about the use of CoCrMo alloys is the toxicity of the released Co and Cr ions. From clinical examinations, released metal ions lead to various phenomena: transportation, metabolism, accumulation in organs, allergic reactions, and carcinoma. If a large amount of metal ions are released, it is generally thought to be harmful to human health.[40–42] Some researchers have found Co, Cr, and Ni ions can be eliminated through urine.[43] Nevertheless, how they affect different organs, and the safe level of metal ions, are still

under investigation. Their effects are thought to be also dependent on the individual. Since the release of metal ions depends on the electrochemical reactions or on tribocorrosion processes, a full understanding of how corrosion and wear processes lead to the loss of ions from the surface is necessary.

Many authors have been studying metal on metal wear behavior *in vivo* and *in vitro*. A running-in (or bedding-in, wearing-in) stage is found for most cases, followed by a lower wear rate steady-state.[44] The length of running-in varies depending on the different simulators and geometry of contacts (pin-on-plate, ball-on-plate, etc.) from thousands of cycles to one million cycles.[44–46] Small wear debris particles are created in the running-in phase and cause abrasive wear. From clinical examinations, for the first few days after implantation of metal-on-metal joints, metal ions were found to increase dramatically. The metal ion level then stabilized,[47–49] which is possibly related to differences between the running-in and the steady-state phases phenomena and the saturation of metal ions in the body.

Corrosion has been considered as one of the major problems for metallic biomaterials. When devices are implanted into the human body, they are immediately surrounded by biological fluids. Even though corrosion can occur on plastics, ceramics, and glasses, the term is often associated with metals. In this section, corrosion of metallic bio-implant materials is the focus. From a corrosion engineering point of view, these liquids are not as aggressive as some industrial process fluids, but the body is still a harsh environment due to the oxygenated saline solution and the involvement of organic species. Ever since metallic biomaterials were adapted for surgical use, studies have been done to assess corrosion resistance of those materials. Three major metallic materials; stainless steel, cobalt chromium alloys, and titanium/titanium alloys are normally used and the understanding of their performance and improvement has been under investigation for several years.

Corrosion can severely limit the fatigue life and ultimate strength of materials, leading to the mechanical failure of implants. Corrosion has been implicated in causing local pain and swelling in the region of the implant and affect the performance of those implants resulting in failure and revision. The release of ions from implanted metallic biomaterials to the local host environment is also a great concern. Ions are released by chemical and electrochemical processes (corrosion).

One point which should not be ignored is the corrosion of wear debris. Even though nano-size metal debris is very difficult to be collected and analyzed, it is still a potentially important source of the metal ion release which has not largely been studied until now.

The corrosion mechanisms of these metallic materials for surgical use have been extensively investigated, from both *in vitro* experiments and *in vivo* observations.

Pitting corrosion: Pitting corrosion is the most common type of localized corrosion. It was found on stainless steel implant materials resulting in extensive damage and causing release of significant amounts of metal ions.[50]

Crevice corrosion: Compared to the other types of metallic implant materials, Type 316L stainless steel is highly susceptible to this corrosion attack. In the area of contact between stainless steel screw heads and the bone plate, the occurrence of corrosion was found. It also induced crack propagation of bone plate.[51]

Fretting corrosion: Fretting corrosion phenomena are associated with micromotions between components.[52] When an oscillating rubbing action is continuously applied on two opposing surfaces such as bone plates and the screw heads of the prosthetic devices, fretting corrosion can occur.[53] It is the major factor to cause the initiation of cracks and fracture failures for surgical screws.

3.06.2.5.2 Galvanic corrosion

When metals of different types from different devices are in physical contact in body fluid, galvanic corrosion can occur. For example, a bone screw and a bone plate made of dissimilar metals and alloys can form a galvanic couple.

Wear-corrosion: When implant materials are under cyclic loading, wear-corrosion is always present.[54] Wear-corrosion resistance is an important factor of consideration for load-bearing surgical implants such as hip and knee replacement implants.

Metallic materials used for bearing surfaces in hip arthroplasties normally rely on a stable passive film, which forms spontaneously in air, for their biocompatibility. The passive film can form a barrier, which can efficiently separate the metal from the corrosive environment and protect it from further corrosion processes. The passive film inhibits corrosion and keeps current flow and the release of corrosion products at a very low level. Nonetheless, the release of metal into the body is a well-documented fact. Uniform passive dissolution resulting from the slow diffusion of metal ions through the passive film, transpassive dissolution under high oxidizing conditions,

or the local breakdown of passivity as a consequence of localized forms of corrosion such as pitting or crevice corrosion, or as a consequence of mechanical events, such as fretting and wear corrosion, are all possible mechanisms.

XPS and other surface analysis techniques have been used to determine the nature of passive films on Co-base alloys. Primarily Cr_2O_3, CoO, and MoO_3 are found in the top layer (1.6 nm) of the spontaneously formed passive film in air for CoCrMo alloys. The inner layer of the passive film contains Cr_2O_3 and Co and Mo metal species.[55] The total thickness of the passive film on CoCrMo alloys in the atmosphere is ~4–5 nm.

Hanawa *et al.*[56] examined the surfaces of metallic stainless steel, CoCrMo alloys, and titanium. A preferential release of Co ion for CoCrMo alloys and Fe ion for stainless steel 316L were obtained. The release of Mo in CoCrMo was reported to be insignificant. A ratio of approximately 2.9:1 of Co/Cr for pin-on-disk tests on CoCrMo was reported.[57] However, the amount of Co released from cast CoCrMo alloys was found to be very small in the biological solution.[58] In addition it was found that the amount of Ni released from 316L gradually decreased with increasing pH; similarly, the amount of Cr and Mo ions released from CoCrMo decreased at pH 4 and higher. One thing which should be noticed is that, in the natural body serum condition, the pH is ~7.4. Calcium phosphate was found as precipitates on implant metals and alloys surfaces. They also suggested that the formation of oxide or hydroxides of metal ions was less toxic than the complex of protein-bond-metal.[59]

The CoCrMo alloys are highly corrosion resistant with only a minimal susceptibility whilst stainless steel quite readily suffers crevice and pitting corrosion. CoCrMo alloys are considered biocompatible. However, very high levels (20–30 times as reference normal serum cobalt value ($0.15\,\mu g\,l^{-1}$) and serum chromium value ($0.26\,\mu g\,l^{-1}$)) of metal ions are reported cytotoxic with increasing concern over the biocompatibility of implant materials and especially in terms of the significance of corrosion, wear, hypersensitivity and carcinogenicity.[60] The quantity of organometallic production over longer periods after total joint replacement (TJR), correlation with patient health medication and activity levels remain the objective of many studies.[61] There can be no doubt, therefore, that patients with metal-on-metal (MoM) implants will be exposed to elevated levels of metal ions locally. The outstanding question is the clinical impact of these elevated ion levels. Brondner *et al.*[62] examined patients with CoCrMo MoM total hip replacement (THR) and found that the Co and Cr concentration in blood serum and urine are high. They seem to fall after the initial one-year running-in phase. Average preparative blood serum cobalt levels of $0.15\,\mu g\,l^{-1}$ were cited as reference values for patients who had MoM hip implants from Muniz's studies on elements trace[63] and it is generally in line with the others. Black *et al.*[64] showed a disagreement concerning 'normal' levels for these elements in serum. Because it is still unclear what constitutes a normal level for an individual patient and what the consequences are of transient or chronic deviations from that level, a question mark still exists over MoM implantation.

Visuri and Koskenvuo[65] showed that there was no increase in the risk of cancer in patients with McKee-Farrar type CoCrMo MoM THR and Willert[66] found no proof that the release of metal is teratogenic but did show the possibility of hypersensitivity to metals. Koegel and Black[67] and others disagreed. An increased incidence in cardiomyopathy (a disease or disorder of the heart muscle) and tumors was found from animal tests. Because the number of patients with a MoM TJR for 10, 20, or more, years increases, it suggested that long-term studies are still required to fully address the issue of metal-ion associated diseases. Investigations to clarify the importance of toxicology are currently being undertaken by many researchers and clinicians.

Electrochemical methods have been employed to understand corrosion behavior for implant materials and then to assess their biocompatibility. Many authors have been trying to monitor the performance of TJR by measuring metal levels.[68–69]

At this stage, it is important that a more detailed understanding of the effects of implanted metals must be gained.[69] A wide variety of serum proteins exists *in vivo* and it is reasonable to assume that many of these become rapidly adsorbed onto the metal surfaces upon implantation. It is suggested that the adsorbed proteins influence the material corrosion rate.

3.06.2.6 Erosion-Corrosion

In certain environments, either where two moving surfaces come into contact or where there is impingement of a slurry onto a surface, wear is unavoidable. There is usually progressive deterioration of the surface resulting from the removal of material by at least one of the following mechanisms, abrasion, erosion, and erosion-corrosion. Additionally, forms of corrosion may occur locally to exacerbate the damage.

Neville *et al.*[70] discussed the effect of temperature on the erosion rate of Stellite X40 and BS 3468 cast

iron in the slurry erosion conditions. The focus of this work was to validate the use of Stellite X40 as an optimum material for subsea drill bit castings (**Figure 11**). Drill bits for subsea use have to be able to tolerate the impingement of the drilling fluid injected through the nozzle onto the faces of the bit which contain the diamond cutters. Material loss in this region is serious as the support for the cutters is lost, as seen in **Figure 11(b)**. In their work, it was shown that the damage on the face is a complex mix of erosion and corrosion processes and that Stellite X40, is in fact the optimum material when compared with a variety of Fe and Ni base materials.

The synergistic effect between erosion and corrosion has received more and more attention in recent years because of the widespread occurrence of such problems in material processing industries. In such conditions, material selection can be a problem and, in many cases, is only carried out on the basis of empirical evidence. Erosion-corrosion can cause high material degradation rates because the action of the erodent particles can remove a stable passive film on the surface of the material. Hence, the wastage rates of the material can be significantly higher than the combined effects of erosion and corrosion acting separately.

The literature has not been consistent in the use and meaning of the synergistic effect in aqueous erosion-corrosion. Some authors describe it as the sum of the enhancement of erosion due to corrosion and vice versa (dE_C and dC_E).[71] Some authors used the term 'additive effect' to refer to an enhancement, but there is a difference between these two terms. Often an 'additive effect'[72] is when the sum of pure erosion in the absence of corrosion (E), the pure corrosion in the absence of erosion (C) and the change of corrosion rate due to erosion (dC_E) is equal to the total weight loss (TWL). If this is not the case the 'synergistic effect' is observed. In other words, the term synergism is restricted to the erosion enhancement due to corrosion (S or dE_C). The following equations [2] and [3] show the differences between the additive effect and the synergy (S) effect from on which this work is based.

$$\mathrm{TWL} = E + C + dC_E + dE_C \quad [2]$$

$$\mathrm{TWL} = E + C + S \quad [3]$$

In order to define the synergistic effect, both erosion and corrosion must be studied independently of each other under controlled conditions. To obtain the corrosion rate, a potentiostat or galvanostat is used to control the electrical potential or current of the erosion sample.

Neville *et al.*[70,73,74] used a range of engineering alloys ranging from low grade C–Mn steel to super alloys, Stellite X40, to calculate the percentage damage caused by synergy.

They measured the TWL at the free corrosion potential; anodic polarization with presence of liquid–solid impingement and by using Tafel extrapolation *in situ* pure corrosion component of TWL (C)

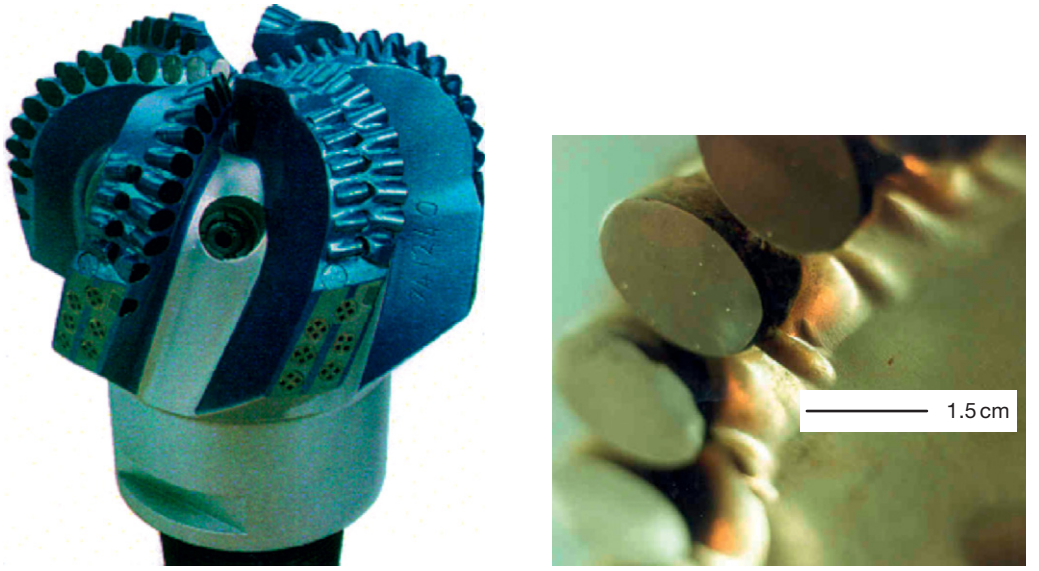

(a) (b)

Figure 11 New subsea drill bit (a) and erosion-corrosion of the Stellite X40 around the polycrystalline diamond cutters (b).

is calculated. By applying a cathodic potential to the sample the pure erosion component (E) of the TWL was obtained.

The TWL of the material was identified as pure erosion, corrosion and synergistic effects. In the literature, the effect of temperature, salinity, and solid particles content in the impingement jet was analyzed and their effect on the different mechanisms were quantified. Das *et al.*[75] showed that the corrosive wear rate increases with increasing angle of inclination and a higher wear rate was obtained for the impingement angle 90° and, the lowest weight loss was obtained at 30°. Similar findings were reported by Fan *et al.*[76,77] where they related these findings to the properties of the passive film. They showed that in the areas where the tangential component of impact velocity is large, the main mechanism is a cutting mode. On the contrary, in the areas where the normal component of impact velocity is larger, the failure mode consists of the formation of microcracks and the removal of second phases.

The performance of the different alloys under erosion-corrosion conditions has been studied with various techniques. Important variables relating to erosion such as load, fluid velocity, impact angle and solid loading have been studied to determine the erosion-corrosion behavior of materials. However, there is virtually no information available on cobalt-based superalloys under erosion-corrosion conditions and in particular, the effect of alloying elements on the mechanical and electrochemical damage, which is one of the main objectives of the current project.

3.06.2.7 Wear and Wear-Corrosion of Cobalt-Base Alloys

Cobalt-base alloys have enjoyed extensive use in wear-related engineering applications for well over 50 years because of their inherent high-strength corrosion resistance and ability to retain hardness at elevated temperatures. In recent years, a concentrated effort has been made to understand the deformation characteristics of cobalt-base alloys exposed to erosive environments in order to optimize those factors contributing to their erosion resistance.

In Stellite alloys the cobalt-rich solid solution incorporating elements such as chromium, tungsten and molybdenum, is highly resistant to erosion. This is due to rapid increase in the work hardening rate and the strain to fracture, which are caused by deformation twinning and presence of a small amount of strain-induced ε phase.

The wear properties of the cobalt-based alloys are believed to be influenced by:

- the limited mobility of the stacking faults generated by mechanical stress, which limits plastic deformation;
- interaction between stacking faults (this results rapid hardening);
- mechanical twinning which occurs extensively in certain alloys and absorbs energy;
- the formation of hcp platelets, which are believed to absorb energy; and
- the characteristics of this hcp phase once formed.

Most cobalt-based alloys possess good cavitation resistance and moderate abrasion and slurry erosion resistance. The last two features are independent of the carbon content, and have been attributed by Crook[78] to crystallographic transformation, under stress, from the fcc to hcp structure by twinning. During deformation, energy is absorbed and the effect of the stress is decreased.

Cobalt-based superalloys have been recognized as an alloy type one of the most resistant to both cavitation and liquid impact erosion.[79] The underlying reason for their superior erosion resistance behavior however, is not yet clear. Investigations have attempted to obtain universal correlation between the erosion resistance of the materials and the mechanical properties such as hardness and strain energy to fracture but all such attempts have been unfortunately unsuccessful. For example, austenitic stainless steel had higher erosion resistance than martensitic stainless steel of the same hardness and cobalt-base alloys had much higher resistance in relation to hardness.[80]

Lee *et al.*[80] compared the liquid impact erosion resistance of 12 Cr steel with a Vickers hardness of 380 kg mm^{-2} and Stellite 6B with a hardness value of 420 kg mm^{-2}. The liquid impact erosion resistance of Stellite 6B was at least six times greater than that of 12 Cr steel, implying that hardness is not the governing factor for liquid erosion. Stellite 6B also showed very different behavior in liquid impact erosion in comparison with 12 Cr steel (**Figure 12**). They concluded that the superior erosion resistance of Stellite 6B results from the cobalt matrix whose deformation appeared as mechanical twins. Other studies showed a trend of increasing erosion resistance with decreasing grain size. The twins are produced by the passage of partial dislocations, which had a Burgers vector equal to a fraction of the lattice vector, giving twinned

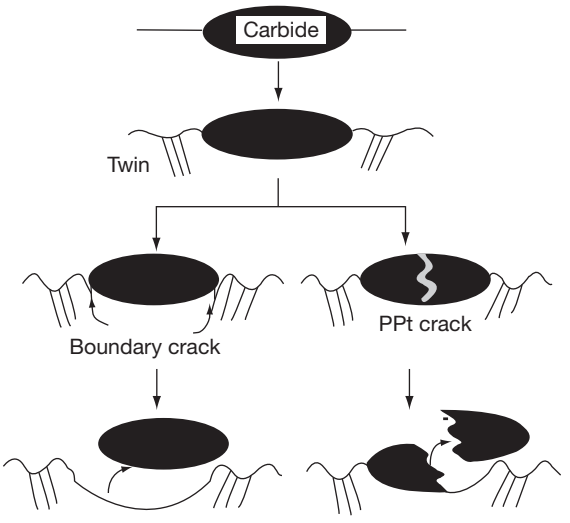

Figure 12 Liquid impact erosion mechanisms of Stellite No. 6B.

regions and untwinned regions of different orientations. Therefore, the increase in density of twins with a number of impacts would play the role of fragmentation of the grains in the cobalt matrix into a submicrometer level. This would decrease the mean free path of dislocations to a limit surface distortion severely and given a much higher erosion resistance.

In the case of cavitation erosion, it is observed that the dynamic and localized nature of the stresses generated by the imploding cavities produce a material response which is quite different from that obtained under bulk quasi-static loading. A striking example of this is that cobalt and its alloys exhibit far greater erosion resistance than other metals and alloys comparable strength.[81] In fact pure cobalt is the most erosion resistant of comparable pure metals known.

Wong-Kian *et al.*[16] showed that under erosion-corrosion conditions HIPed Stellite alloys 1, 6, and 21 had lower mass loss than the welded specimens of the same Stellites. They related their finding to the finer and homogeneous microstructure, which was obtained after HIPing. They also showed that wear resistance of the cobalt-based alloys is promoted by the harder complex carbides of chromium and tungsten, while corrosion resistance is enhanced by the presence of cobalt in the matrix.

From almost all of the work done on the wear properties of Stellite alloys it has been concluded that the exceptional erosion resistance of the Stellite alloys can be ascribed to the drastic change in mechanical properties brought about by the formation of mechanical twins and by the presence of platelets of the ε hcp phase. It has been shown that the formation of twins and ε phase is controlled by the SFE.

Strain hardening occurs as a result of interactions of dislocations with each other, and with barriers, which impede dislocation motion. One of the earliest explanations for strain hardening is that dislocations pile up on slip planes at barriers in the crystal, and produce a back stress, which opposes the applied stress on the slip plane.[82] Possible dislocation interactions and intersection of the active slip planes were suggested as another dominating mechanism for strain hardening. Mechanical twinning, and the presence of hcp platelets may also contribute to the work-hardening in cobalt base alloys. The effectiveness of each mechanism in terms of work-hardening depends upon the strain increment characteristics of each process. This concept was studied by Roebuck *et al.*,[83] who found the best strengths and ductilities in extruded Co–C–W alloys correspond with the highest fcc content. They suggested that when the fcc phase is stabilized deformation occurs by twinning or slip rather than by fcc–hcp martensitic transformation.

The strength of the matrix is considered in detail here. Kosel *et al.*[84] showed the effect of the matrix strength can affect the wear rate. They used the normalized alloy content (NAC) as a measure of the matrix strength. They defined the NAC as the sum of the weight percentages of Ni, V, W, Mo and in **Table 2** they are normalized with respect to Stellite 6 alloy. The alloys that are used as solid–solution strengtheners give an approximate measure of the degree of solid–solution strengthening.

By using the same approach the NAC of the alloys Stellite 6, Stellite 12, and Stellite 706 were calculated and normalized against cast Stellite 6 as shown in **Table 2**.

Figures 13 and **14** show the change in the weight loss as a function of NAC. In **Figure 12**, only Stellite 6 and Stellite 12 are compared to assess the effect of increased tungsten on the NAC and the resistance to wear. **Figure 13** is a comparison of Stellite 6 and Stellite 706 and the factor being considered here is replacing tungsten and molybdenum. From **Figure 12** it can be clearly seen that an increase in the tungsten amount increases the NAC and the weight loss at both test temperatures and both solid loadings is not affected by the increase in NAC. However, as shown in **Figure 13**, there is a linear relationship between the NAC and the erosion-corrosion resistance of the alloys. The alloys with high NAC gave a lower weight loss in all test conditions. These two results show that molybdenum as a solid–solution strengthener is much more

effective in providing erosion-corrosion resistance than tungsten.

It is apparent that SFE has a significant influence in changing the deformation mode. The excellent erosion resistance of cobalt-based Stellite alloys is generally attributed to the low SFE,[85] which, in turn, means higher stacking fault probability and a greater chance for the formation of ε hcp platelets. The lower the SFE (the greater the width of the stacking fault) the more difficult is cross-slip, and the higher is the rate of work-hardening and the strain to fracture. Bhansali and Miller[86] examined the role of SFE on the galling and wear behavior of Stellite 6 modified by the addition of Ni, which in turn increases SFE and stabilizes the fcc matrix. Their results showed that materials with low SFE tend to strain harden rapidly, and to show the highest galling resistance.

Remy and Pineaue[87] found that in Co–Cr–Ni–Mo alloys an SFE of ~20 mJ m^{-2} resulted in an Md temperature (i.e., the maximum temperature at which the fcc–hcp reaction can be stress induced of ~25 °C). This low value of the SFE also gives rise to the optimum mechanical properties, that is, the highest work-hardening rate and the maximum strain to fracture.

Heathcock and Ball,[79] compared the cavitation erosion resistance of a number of Stellite alloys, (3, 4, 6, 8, 20, and 2006), cemented carbides and surface-treated alloy steels. They showed that among the Stellite alloys, Stellite 3 has the highest resistance to cavitation erosion. Stellite 4, 6, 8, and 20 have similar resistance and Stellite 2006 is a little less resistant than all the Stellite alloys. They considered this difference to be a consequence of the microstructure. Stellite 3 has carbides Cr_7C_3 and W_6C which form a fine interdentritic network in a cobalt-rich matrix whereas in Stellite 20 acicular Cr_7C_3 carbide formation and islands of cobalt-rich solid solution were observed. They also showed that acicular carbides in Stellite 20 are much harder than those in Stellite 3 (1860 HDP compared with 1100 HDP), which also showed the inverse relation between the hardness and the cavitation erosion resistance of the alloys. They concluded that in Stellite alloys the cobalt-rich solid solution, incorporating elements such as chromium, tungsten, and molybdenum is highly resistant to erosion, due to a rapid increase in the work-hardening rate and the strain to fracture which is caused by deformation twinning and the presence of a small amount of strain-induced ε phase.

Although some attempts have been made to correlate hardness with erosion resistance, a good

Table 2 Normalized alloy content of Stellite 6, Stellite 12, and Stellite 706 (both cast and HIPed)

Alloy	*Normalized alloy content (NAC)*
Stellite 6 Cast	1
Stellite 6 HIPed	1.2
Stellite 12 Cast	2.5
Stellite 12 HIPed	2.4
Stellite 706 Cast	1.36
Stellite 706 HIPed	1.39

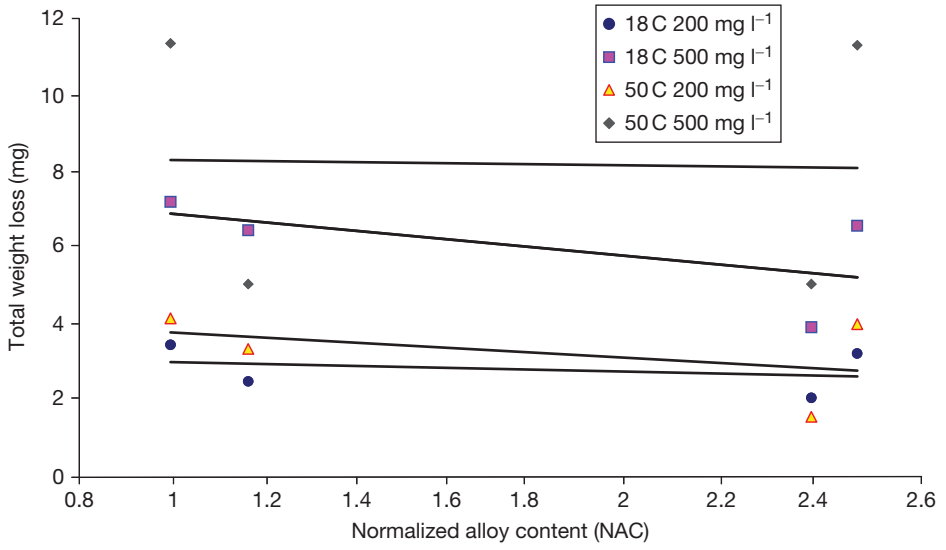

Figure 13 Total Weight Loss (TWL) test results plotted versus normalized alloy content for Stellite 6 and Stellite 12. Reproduced from Malayoglu, U. PhD Thesis, Heriot-Watt University, 2005.

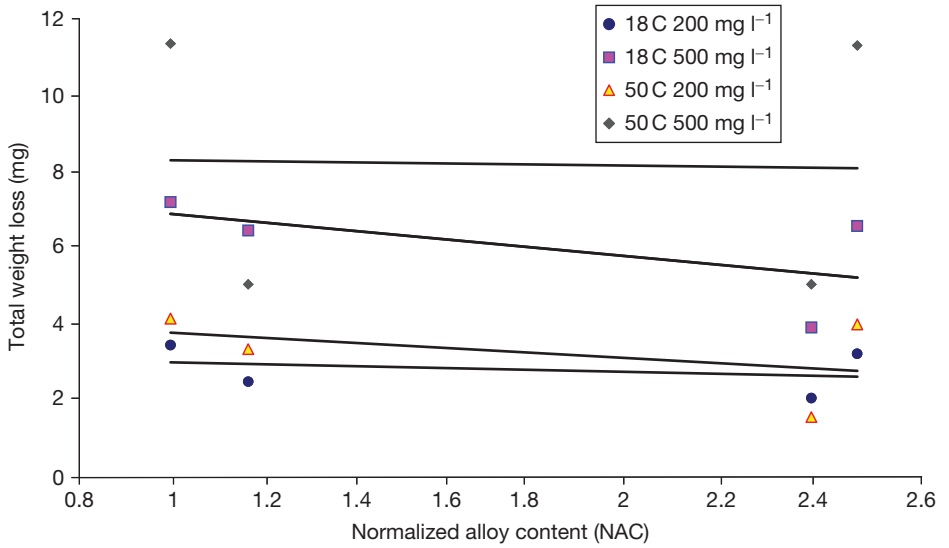

Figure 14 Total Weight Loss (TWL) test results plotted versus normalized alloy content for Stellite 6 and Stellite 706. Reproduced from Malayoglu, U. PhD Thesis, Heriot-Watt University, 2005.

correlation generally has been recognized only for pure metals or alloys with the same compositional system. For example, Finnie *et al.*[88] showed that a good relationship between material hardness and erosion resistance existed for pure metals but not for heat-treated carbon steel (the erosion resistance was nearly constant, independent of the heat treatment). In another study, the cobalt alloy Stellite 6 B was shown to have a steady-state rate of volume loss, an order of magnitude less than many titanium- and iron-base alloys of comparable hardness.[89] These results may suggest that it is not possible to use material hardness as the sole parameter in evaluation of erosion resistance for all materials.

Frenk and Kurz[81] investigated the influence of the microstructure on the dry sliding wear resistance of a hypoeutectic Stellite 6 alloys. They showed that the hardness is dependent on the microstructure and in particular, on the size of the dendrites and the chemical composition of the matrix, in particular elements modifying the SFE. They reported a severe delamination wear of the Stellite under the sliding conditions investigated. During the stationary wear regime, no dependence of the wear rate on the as-solidified microstructure was determined. They suggested addition of alloying elements which decreases the SFE, which could improve the dry sliding wear resistance.

Desai *et al.*[90] studied the effect of carbide size on the abrasion resistance of two cobalt-based powder metallurgy alloys 6 and 19. As a result of their SEM investigation they divided the wear scar into three parts, entrance, central, and exit regions. In the entrance region, many of the abrasive particles move at angles to the length of the wear scar, while in the central and exit regions the particles create long straight grooves. Stellite 6 gave a greater mass loss than alloy 19 at any given carbide size. They attributed this to the combined effect of the higher matrix microhardness of alloy 19. They also concluded that the wear rate decreased monotonically with increasing carbide size. The effect of carbide size is attributed primarily to the fact that the smaller carbides are often found to be contained wholly within micromachining chips, indicating that these carbides contribute little to wear resistance.

References

1. Cobalt Development Institute, Facts About Cobalt (www.theecdi.com)
2. Anon, Cobalt Monograph, Centre d'Information du Cobalt/ Battelle, 1958
3. Malayoglu, U. PhD Thesis, Heriot-Watt University, 2005
4. Morrow, H.; Danes, W. P.; Sponseller, D. L. *Cobalt* **1973**, *4*, 93–102.
5. Atamert, S. Stability, wear resistance and microstructure of iron, cobalt and nickel-based hardfacing alloys, PhD thesis, University of Cambridge: UK, 1989.
6. Lane, J. R.; Grant, N. J. *Tran. Am. Soc. Met.* **1952**, *44*, 113–121.
7. Wagner, H. J.; Hall, A. M. The physical metallurgy of cobalt-base superalloys, Defence Metals Information Centre, 1962.
8. Woodfor, D. A. *Metall. Transac* **1972**, *3*, 1137–1145.

9. Sims Chester, T.; Stoloff, N. S.; Hagel, W. C. *Super Alloys II*; John Wiley & Sons: London, 1987.
10. Kuzucu, V.; Ceylan, M.; Celik, H.; Aksoy, I. *J. Process. Technol.* **1997**, *69*, 257–263.
11. Wever, F.; Haschimoto, U. *Mitt. Kaiser Wilhelm Inst. Einsenforch* **1929**, *11*, 293–301.
12. Koster, W.; Spencer, F. *Arch. Eisehuttenwesen* **1955**, *29*, 555–565.
13. Rautala, P.; Norton, J. T. *J. Met.* **1952**, *4*, 1045–1050.
14. Adkins, E. F.; Williams, D. N.; Jaffe, R. I. *Cobalt* **1960**, *8*, 16–25.
15. Mohamed, K. E.; Gad, M. M. A; Nassef, A. E.; El-Sayed, A. W. A. *Z. Metallkd.* **1990**, *90*, 195–201.
16. Wong-Kian, M.; Cornish, L. A.; Van Bennekom, A. *J. South African Inst. Mining Metall.* **1995**, 319–335.
17. Frenk, A.; Kurz, W. *Wear* **1994**, *174*, 81–91.
18. Antony, K. C. *J. Met.* **1983**, *35*, 52–60.
19. Berns, H.; Wendl, F. Microstructure and properties of CoCr29W (Stellite 6) in the as-cast, forged and powder metallurgical conditions, 2nd International Conference on Cobalt, Venice **1985**; pp 292–305.
20. Crook, P. *Corros. Sci.* **1993**, *35*, 647–653.
21. Bibring, H.; Seibel, G. *Comptes Rendus Hebdomadaires Des Seances De L Academie Des Sciences Serie C* **1969**, *268*(2), 144.
22. Darby, J. B., Jr.; Beck, P. A. *J. Met.* **1955**, *7*(203), 765–766.
23. Silverman, R.; Arbiter, R.; Hodi, F. *Trans. Amer. Soc. Met.* **1957**, *49*, 805–815.
24. Lux, B.; Bollmann, W. *Cobalt* **1961**, *11*, 4–12.
25. Vander Sande, J. B.; Coke, J. R.; Wulff, J. *Metall. Trans. A* **1976**, *7A*, 389–397.
26. Morral, F. R. *Corros. NACE* **1969**, *25*, 307–322.
27. Li, X. Y.; Akiyama, E.; Habazaki, H.; Kawashima, A.; Asami, K.; Hashimoto, K. *Corros. Sci.* **1997**, *39*, 1365–1375.
28. Oleford, I.; Elfstron, B. O. *Corrosion* **1982**, *38*(1), 46–52.
29. Hocking, W. H.; Stanchell, F. W.; McAlpine, E.; Lister, D. H. *Corros. Sci.* **1985**, *25*(7), 531–557.
30. McIntyre, N. S.; Zetaruk, D.; Murphy, E. V. *Surf. Interface Anal.* **1979**, *1*(4), 105–110.
31. Maffiotte, C.; Navas, M.; Castaño, M. L.; Lancha, A. M. *Surf. Interface Anal.* **2000**, *30*(1), 161–166.
32. Mirza, N. M.; Rafique, M.; Hyder, M. J.; Mirza, S. M. *Ann. Nucl. Energy* **2003**, *30*(7), 831–851.
33. Kim, H. J.; Kim, Y. J. *Surf. Eng.* **1999**, *15*, 495–501.
34. Human, A. M.; Roebuck, B.; Exner, H. E. *Mater. Sci. Eng.* **1981**, *A241*, 202–210.
35. Frantsevich, I. N. *Poroshkovaya Metall.* **2002**, *9–10*, 11–29.
36. Zhu, J.; Xu, N.; Zhang, C. *Adv. Contracept* **1999**, *15*, 179.
37. Khan, M. A.; Williams, R. L.; Williams, D. F. *Biomaterials* **1999**, *20*, 631.
38. Goldberg, R. J.; Gilbert, L. J. *Biomaterials* **2004**, *25*, 85.
39. Lewis, A. C.; Kilburn, M. R.; Papageorgiou, I.; Allen, G. C.; Case, C. P. *J. Biomed. Mater. Res. A* **2005**, *73*, 456.
40. Hanawa, T.; Ota, M. *Biomaterials* **1991**, *12*, 767.
41. Hallab, N. J.; Bundy, K.; O'Connor, K.; Moses, R.; Jacobs, J. *Tissue Eng.* **2001**, *7*, 55.
42. Yan, Y.; Neville, A.; Dowson, D. *J. Phys. D: Appl. Phys.* **2006**, *39*, 3200.
43. Beamson, G.; Briggs, D.; Davies, S. F.; Fletcher, I. W.; Clark, D. T.; Howard, J.; Gelius, U.; Wannberg, B.; Balzer, P. *Surf. Interface Anal.* **1990**, *15*, 541.
44. Walker, P. S. *Acta Orthop. Belg.* **1973**, *39*, 43.
45. Lebugle, A.; Subirade, M.; Gueguen, J. *Biochem. Biophys. Acta* **1995**, *1248*, 107.
46. Franks, F. *Biophys. Chem.* **2002**, *96*, 117.
47. Contu, F.; Elsener, B.; Bohni, H. *Biomed. Mater.* **2002**, *62*, 412.
48. Hanawa, T.; Hiromoto, S. *Corros. Eng.* **1998**, *47*, 895.
49. Adelina, B. Synopses of International Tribology Conference (Kobe) **2005**; p 21 Vol C-04.
50. Contu, F.; Elsener, B.; Bohni, H. *Corros. Sci.* **2004**, *47*, 1863–1875.
51. Roberge, P. R. *Handbook of Corrosion Engineering;* McGraw Hill: New York, 2000.
52. Kuhn, A. T. *Biomaterials* **1981**, *2*, 68–77.
53. Yang, J.; Meritt, K. *J. Biomed. Mater. Res.* **1994**, *28*, 1249–1258.
54. Khan, M. A.; Williams, R. L.; Williams, D. F. *Biomaterials* **1999**, *20*, 762–772.
55. Jacobs, J. J.; Skipor, A. K.; Campbell, P. A.; Hallab, N. J.; Urban, R. M.; Amstutz, H. C. *J. Arthroplasty* **2004**, *19*, 59–65.
56. Hanawa, T. *Corros. Eng* **2000**, *49*, 687–699.
57. Stemp, M.; Mischler, S.; Landolt, D. *Wear* **2003**, *255*, 466–475.
58. Jacobs, J. J.; Skipor, A. K.; Patterson, L. M.; Hallab, N. J.; Paprosky, W. G.; Black, J.; Galante, J. O. *J. Bone Joint Surg.* **1998**, *80*, 1447–1458.
59. Lindsley, B. A.; Marder, A. R. *Wear* **1999**, *225–229*, 510–516.
60. Hensten-Pettersen, A.; Jacobsen, N. *Systemic Toxicity and Hypersensitivity, Biomaterials Science;* Elsevier Academic Press: London, 2004.
61. Barril, S.; Mischler, S.; Landolt, D. *Wear* **2004**, *256*, 963–972.
62. Brodner, W.; Bizan, P.; Meisinger, V.; , Kaider, A.; *et al. J. Bone Joint. Surg.* **1997**, *79*, 316–321.
63. Muniz, C. S.; Fernandez-Martin, J. L. *Biol. Trace Elem. Res.* **2001**, *82*, 259–269.
64. Black, J.; Maitin, E. C.; Gelman, H.; Morris, D. M. *Biomaterials* **1983**, *4*, 160–164.
65. Visuri, T.; Koskenvuo, M. *Orthopedics* **1991**, *14*, 137–142.
66. Willert, H. G.; Buchhorn, G. H.; Gobel, D. *Clin. Orthop. Relat. Res.* **1996**, *329*, 160–186.
67. Koegel, A.; Black, J. *Soc. Biomater.* **1983.**
68. Rossi, S.; Fedrizzi, L.; Deflorian, F.; Zen, M. *Mater. Corros.* **2000**, *51*, 552–556.
69. Micheli, S. M. d. D.; Riesgo, O. *Biomaterials* **1982**, *3*, 209–212.
70. Neville, A.; Reyes, M.; Xu, H. *Tribol. Int.* **2002**, *35*, 643–650.
71. Stack, M. M.; Corlett, N.; Zhoi, S. *Wear* **1997**, *215*, 67–76.
72. Stack, M. M.; Stott, F. H. *Corros. Sci.* **1993**, *35*, 1027–1034.
73. Neville, A.; Hodgkiess, T. *Br. Corros. J.* **1997**, *32*, 197–205.
74. Neville, A.; Hodgkiess, T.; Dallas, J. T. *Wear* **1995**, *186–187*, 497–507.
75. Das, S.; Mondal, D. P.; Dasgupta, R.; Prasad, B. K. *Wear* **1999**, *236*, 295–302.
76. Fan, A.; Long, J.; Tao, Z. *Wear* **1995**, *181–183*, 876–882.
77. Fan, A.; Long, J.; Tao, Z. *Wear* **1996**, *193*, 73–77.
78. Crook, P. *Cobalt and Cobalt Alloys*, 10th ed.; ASM International: Materials Park, OH; 447–454, Vol. 2
79. Heathcock, C. J.; Ball, A. *Wear* **1982**, *74*, 11–26.
80. Lee, M. K.; Kim, W. W.; Rhee, K. C.; Lee, J. W. *J. Nucl. Mater.* **1998**, *257*, 134–144.
81. Vaidya, S.; Mahajan, S.; Preece, C. M. *Metall. Transac. A* **1980**, *11A*, 1139–1150.
82. Honeycombe, R. W. K. Steel, *Microstructure and Properties, E* Arnold: London, 1981.
83. Roebuck, B.; Almond, E. A. *Mater. Sci. Eng.* **1984**, *66*, 179–194.
84. Kosel, T. H.; Fiore, N. F. *J. Mater. Energy Sys.* **1981**, *3*, 7–27.
85. Remy, T. L.; Pineau, A. *Mater. Sci. Eng.* **1976**, *26*, 123–132.

86. Bhansal, K. J.; Miller, A. E. *Wear* **1982**, *75*, 241–251.
87. Remy, L. *Metall. Transac. A* **1981**, *12A*, 387–407.
88. Finnie, I.; Stevick, Gr; Ridgely, Jr. *Wear* **1992**, *152*, 91–98.
89. Hansen, J. S. *Am. Soc. Test. Mater*; 1979, 148–162.
90. Desai, V. M.; Rao, C. M.; Kosel, T. H.; Fioren, F. *Wear* **1984**, *94*, 89–101.

Further Reading

Cobalt Development Institute, 167 High Street, Guildford, Surrey, GU1 3AJ: http://www.thecdi.com/
Cobalt News – published, and available for free download, by the Cobalt Development Institute.

3.07 Corrosion of Copper and its Alloys

C. D. S. Tuck
Lloyd's Register EMEA, London, UK
C. A. Powell
Copper Development Association, Hemel Hemstead, UK
J. Nuttall
European Copper Institute, Belgium

Glossary

Antimicrobial Capable of destroying or inhibiting the growth of microorganisms.

Dealloying A corrosion process whereby one constituent of a metal alloy is preferentially removed from the alloy, leaving an altered residual microstructure.

Dezincification A corrosion process specific to brasses (copper–zinc alloys) whereby zinc is preferentially removed from the alloy, resulting in a porous residual microstructure.

Shape memory alloy An alloy which, after it is deformed, will automatically regain its original geometry when it is heated.

Abbreviations

BTAH Benzotriazole
FPSO Floating production, storage and offloading vessel
MIC Microbiologically influenced corrosion
MRSA Meticillin-resistant *Staphylococcus aureus*
SCC Stress corrosion cracking
SEM Scanning electron microscopy
STEM Scanning transmission electron microscopy
WHO World Health Organization

Symbols

A_i Activity of species *i*
K Equilibrium constant and rate constant
Q Activation energy
R Copper run-off rate
R Gas constant
T Temperature (K)

3.07.1 Introduction

Copper and copper alloys are among the earliest metals known to man, as they have been used from prehistoric times, and their present-day importance is greater than ever before. Their widespread use depends on a combination of good corrosion resistance in a variety of environments, excellent workability, high thermal and electrical conductivity, and attractive mechanical properties at low, normal, and moderately elevated temperatures.

A wide range of cast and wrought alloys is available. For detailed expositions of properties and uses, the reader is referred to publications of many specialized aspects obtainable from the Copper Development Association offices in various countries. Relevant publications of the British Standards Institution include BSEN1982, *Copper Alloy Ingots and Castings*,[1] and those covering wrought products.[2,3] All ASTM standards relating to copper and copper alloys are included in a volume published annually.[4]

3.07.1.1 Alloy Compositions and Properties

The mechanical properties of wrought alloys[5,6] depend on composition and metallurgical condition. At the extremes, annealed pure copper has a tensile strength of 220 MN m^{-2} and a hardness of 40 HV, and heat-treated beryllium copper can have a tensile strength of 1450 MN m^{-2} and a hardness of 400 HV. Summaries of typical properties of some of the more important wrought and cast copper alloys are given in Tables 1–4.

3.07.1.1.1 Coppers

The purest grade of copper commercially available, and that with the highest electrical conductivity, is oxygen-free high-conductivity copper. The minimum copper content required by some specifications is 99.99% and the method of manufacture is such that no residual deoxidant is present. Oxygen itself has very little effect on conductivity, and the 'tough pitch' coppers (either electrolytic or fire-refined), containing ~0.04% oxygen are high-conductivity materials.

One disadvantage of tough pitch coppers is embrittlement, which is liable to occur when they are heated in atmospheres containing hydrogen. Therefore, for many purposes (and particularly where fabrication is involved) deoxidized coppers are preferred. The usual

Table 1 Compositions of wrought copper alloys.[2]

Alloy												
Description	*EN No.*	*Cu*	*Al*	*Fe*	*Mn*	*Ni*	*P*	*Pb*	*Si*	*Sn*	*Zn*	*Other*
HC copper Cu–ETP	CW004A	99.90Min						0.005				0.0005Bi 0.040 O
Deoxidized nonarsenical copper Cu–DHP	CW024A	99.90Min					0.015–0.040					
Oxygen-free copper, Cu–OF	CW008A	99.95Min						0.005				0.0005Bi
Silver-alloyed copper, Cu–EPT	CW012A	Rem										0.06–0.08Ag 0.0005Bi 0.040 O
Tellurium copper	CW118C	Rem					0.003–0.012					0.4–0.7Te
Beryllium copper	CW100C	Rem		0.2		0.3						1.6–1.8Be 0.3Co
85/15 brass	CW502L	84.0–86.0	0.02	0.05		0.3		0.05		0.1	Rem	
70–30 brass	CW505L	69.0–71.0	0.02	0.05		0.3		0.05		0.1	Rem	
60/40 brass	CW509L	59.5–61.5	0.05	0.02		0.3		0.3		0.2	Rem	
Dezincification resistant brass	CW602N	61.0–63.0	0.05	0.1	0.1	0.3		1.7–2.8		0.1	Rem	0.02–0.15 As
Free machining brass	CW614N	57.0–59.0	0.05	0.3		0.3		2.5–3.5		0.3	Rem	
Aluminum brass	CW702R	76.0–79.0	1.8–2.3	0.07	0.1	0.1	0.01	0.05			Rem	0.02–0.06As
Naval brass	CW712R	61.0–63.0		0.1		0.2		0.2–0.6		1.0–1.5	Rem	
High tensile brass	CW705R	65.0–68.0	4.0–5.0	0.5–3.0	0.5–3.0	1.0		0.2–0.8		0.2	Rem	
18% Nickel silver	CW409J	60.0–63.0		0.3	0.5	17.0–19.0		0.03		0.03	Rem	
5% Tin bronze	CW451K	Rem		0.1		0.2	0.01–0.4	0.02		4.5–5.5	0.2	
Silicon bronze	CW116C	Rem	0.05	0.2	0.7–1.3		0.05	0.05	2.7–3.2		0.4	
High strength bronze	CW111C	Rem		0.2	0.1	1.6–2.5	0.02		0.4–0.8			Additions of Co, Mg, Cr
10% Aluminum bronze	CW307G	Rem	8.5–11.0	3.0–5.0	1.0	4.0–6.0		0.05	0.2	0.1	0.4	
90–10 Cupronickel	CW352H	Rem		1.0–2.0	0.5–1.0	9–11	0.02	0.02		0.03	0.5	
70–30 Cupronickel	CW354H	Rem		0.4–1.0	0.5–1.5	30–32	0.02	0.02		0.05	0.5	

Values are given in % mass fraction and are maximum values unless indicated otherwise.

Table 2 Typical properties of wrought alloys

Alloy		*Melting point (°C)*	*Density (g cm^{-3})*	*Coeff of expansion ($\times 10^{-6}$ °C^{-1})*	*Electrical Cond (% IACS)*	*Thermal conductivity (W mK^{-1})*	*Tensile Strength (MN m^{-2})*	*Elongation (%)*	*Hardness (HV)*
Description	*EN No.*								
HC copper Cu–ETP	CW004A	1083	8.94	18	103	390	220–385	4–55	40–110
Deoxidized nonarsenical copper Cu–DHP	CW024A	1082	8.93	18	80	340	220–385	4–60	40–120
Oxygen-free copper, Cu–OF	CW008A	1083	8.94	18	100	395	220–385	4–60	40–110
Silver-alloyed copper, Cu–EPT	CW012A	1083	8.94	18	102	390	220–385	4–55	40–110
Tellurium copper	CW118C	1075	8.93	18	96	360	250–360	2–7	90–110
Beryllium copper	CW100C	955	8.2	18	23	85	680–1450	3–35	100–400
85/15 Brass	CW502L	1025	8.74	19	35	155	260–420	4–50	55–135
70–30 Brass	CW505L	955	8.53	20	27	125	270–490	9–50	55–150
60/40 Brass	CW509L	905	8.38	21	29	125	340–480	6–43	85–140
Dezincification resistant brass	CW602N		8.43	21	26	117	280–520	15–45	70–140
Free machining brass	CW614N		8.47	21	27	120	350–450	20–30	100–150
Aluminum brass	CW702R	980	8.33	19	23	100	300–390	25–35	70–110
Naval brass	CW712R	890	8.41	21	25	110	340–460	10–30	85–140
High tensile brass	CW705R	890	8.35	21	23	105	550–650	8–12	150–200
18% Nickel silver	CW409J		8.69	16	7	35	380–900	2–40	85–230
5% Tin bronze	CW451K	1050	8.89	18	17	80	340–740	1–60	70–220
Silicon bronze	CW116C	1030	8.52	18	8	40	380–900	3–50	90–220
High strength bronze	CW111C	1060	8.86	17	50	220	600–800	5–15	100–250
10% Aluminum bronze	CW 307G	1075	7.5	18	8	40	430–770	15–25	200–240
90–10 cupronickel	CW352H	1150	8.91	16	10	50	290–520	8–35	80–160
70–30 cupronickel	CW354H	1240	8.94	16	5	30	350–520	12–35	90–130

Table 3 Compositions of cast copper alloys[1]

Alloy														
Description	*EN No.*	*Cu*	*Al*	*Fe*	*Mn*	*Ni*	*P*	*Pb*	*S*	*Sb*	*Si*	*Sn*	*Zn*	*Other*
High conductivity copper	CC040	Not specified												
Dezinification resistant brass	CC752S	61.5–64.5	0.3–0.70	0.35	0.15	0.25		1.5–2.5		0.15	0.02	0.4	Rem	0.15As
High tensile brass	CC765S	57.0–65.0	0.5–2.5	0.5–2.0	0.5–3.0	6.0	0.03	0.5		0.08	0.1	0.1	Rem	
Tin bronze	CC481K	87.0–89.5	0.1	0.1	0.05	0.1	0.5–1.0	0.25	0.05	0.05	0.01	10.0–11.5	0.05	
Leaded gunmetal	CC491K	83.0–87.0	0.1	0.3		2.0	0.10	4.0–6.0	0.1	0.25	0.01	4.0–6.0	4.0–6.0	
Aluminum bronze	CC331G	83.0–89.5	8.5–10.5	1.5–3.5	1.0	1.5		0.1			0.2	0.2	0.5	0.05Mg
Copper nickel chrome	CC382H	Rem	0.01	0.5–1.0	0.5–1.0	29.0–31.0	0.01	0.005	0.01		0.15–0.50		0.2	1.5–2.0Cr, 0.15Zr 0.25Ti
Copper chromium	CC140C	Rem												0.4–1.2Cr

Values are given in % mass fraction and are maximum values unless indicated otherwise.

Table 4 Properties of cast copper alloys[1]

Alloy		*Tensile strength, minimum (MN m^{-2})*	*Elongation, minimum (%)*	*Brinell hardness HB, minimum*
Description	*EN No.*			
High conductivity copper	CC040A	150	25	40
Dezincification resistant brass	CC752S	280	10	70
High tensile brass	CC765S	500	18	120
Tin bronze	CC481K	350	4	85
Leaded gunmetal	CC491K	230	10	65
Aluminum bronze	CC331G	550	18	130
Copper nickel chrome	CC382H	440	18	115
Copper–chromium	CC140C	300	10	95

deoxidizing agent is phosphorus, and specifications require residual phosphorus contents of between 0.004% and 0.06%. Phosphorus-deoxidized coppers with lower phosphorus content have electrical conductivities ~98% of that of pure copper.

3.07.1.1.2 High conductivity coppers

Pure copper has the highest electrical conductivity of any metal apart from silver. However, it has poor strength and suffers from creep at temperatures above ~150 °C. A small addition of silver (0.03–0.12%) gives an increase in creep strength and resistance to softening up to 250 °C (up to 350 °C for short times). Copper–silver alloys are widely used in electrical motors and for contact and catenary wires for electric railways and tramways. They have a nominal conductivity of 100% IACS. In the past, copper–cadmium alloys (0.5–1.2% Cd), which have an excellent combination of strength and electrical conductivity, were widely used for such applications. However, due to health concerns regarding cadmium when the alloy is molten, the use of copper–cadmium alloys is declining. Other high conductivity alloys such as copper–magnesium and copper–tin (0.1–0.5%) have been developed. For all of these high conductivity alloys, a compromise has to be made between high strength and electrical conductivity.

3.07.1.1.3 Heat treatable copper alloys

Copper alloyed with 0.5–1.2% chromium with or without 0.03–0.3% zirconium gives precipitation hardening alloys with strengths up to 450 MN m^{-2}. Such alloys have electrical conductivities of 80% IACS together with good thermal conductivity properties.

Precipitation hardening Cu–Ni–Si alloys are also available. One type is based on copper, nickel, and silicon (described as 'High strength bronze' in Table 3), which, with further alloy additions, can reach tensile strengths of around 800 MN m^{-2} while retaining its high conductivity. For this material, which is widely used for plastic moulding equipment, the main precipitating phase is Ni_2Si. Stress relaxation and the ability to withstand high temperatures under stress without losing spring properties or ease of bending are importance for this material.

The highest strength of any copper alloy (up to 1450 MN m^{-2}) is obtained by precipitation hardening and cold working copper–beryllium (1.8–2.0% Be). However, due to the toxic nature of beryllium, care must be exercised in melting and machining this alloy.

3.07.1.1.4 Brasses

Brasses are basically alloys of copper and zinc, containing between ~10% and 45% Zn, but many other additions can be made.[7] The single-phase (α) brasses, containing up to ~37% Zn in the binary alloys, may have additions of 1% Sn (Admiralty brass), 2% Al (aluminum brass), or 1–3.5% Pb for ease of machining. Duplex (α–β) brasses containing more than 37% Zn, may have additions of 1% Sn (Naval brass), or 1–3% Pb to assist machining. Both α and α–β brasses, with and without lead, are used in the cast as well as the wrought form. High-tensile brasses are α–β alloys containing up to 5% Al and 1–2% of one or more of the following: Sn, Pb, Fe, or Mn. These alloys also are used in both wrought and cast form.

3.07.1.1.5 Cupronickel alloys

Cupronickel alloys contain between 5% and 30% Ni and are mainly used in the wrought condition.[8] The more popular grades have 10% and 30% Ni and are recognized for their very good corrosion and biofouling resistance in marine applications.[9,10] Small controlled alloying additions of iron and manganese are essential to optimize their resistance to localized corrosion and seawater flow. The addition of chromium has also been shown to improve resistance to flow

velocity and a cast (30Ni–1.6Cr)[11] as well as a wrought version (16Ni–0.5Cr)[12] have been developed. The cast version has been predominantly used by the British Navy and is covered by DEF STAN 02-824.[11]

Other higher strength cupronickels have additions of aluminum or tin, producing two ranges of products. The Cu–Ni–Al alloys[13] are thermally age-hardened to form Ni_3Al precipitates in the matrix whereas Cu–Ni–Sn alloys display spinodal strengthening through the development of submicroscopic chemical composition fluctuations.[14]

3.07.1.1.6 Tin bronze

Copper alloys with 1.5–9% Sn and 0.01–0.4% P are wrought alloys known as phosphor bronzes. They have good elastic properties combined with good resistance to corrosion and corrosion fatigue.

Cast copper alloys with between 2% and 11% Sn and 1–10% Zn are termed gunmetals. Modified forms may contain lead (up to 7%) giving leaded gunmetal or nickel (up to 6%) giving a nickel gunmetal. Gunmetals are the most widely used copper casting alloys combining good corrosion resistance with modest strength and good castability.

3.07.1.1.7 Aluminum–bronzes

Wrought aluminum bronzes contain between 4% and 12.5% Al. If less than 8% Al is present, the alloys are α-phase and may be cold worked. The two phase (α–β) alloys, which may be wrought or cast, contain 8–12.5% Al with possible additions of iron (0.5–7%), manganese (1.5–3.5%), nickel (2–7%), and silicon (2%). In terms of its influence on corrosion resistance, the addition of nickel is the most important, as it acts to reduce dealuminification (see **Section 3.07.3.3.3**).

Aluminum bronzes can be hardened by heat treatment and have an enhanced corrosion resistance due to the existence of a complex naturally-formed protective film which includes both aluminum oxide[15] and copper oxide. If damaged, the film is self healing and this gives aluminum bronzes good wear, cavitation, and antigalling characteristics.

3.07.1.1.8 Silicon–bronzes

Silicon–bronzes usually contain 2.8–4.5% Si and 0.8–1.5% Mn. The wrought alloys combine high tensile strength (see **Table 2**) with good corrosion resistance and an attractive color. They are used in chemical equipment and marine hardware. The cast alloy has found application in statuary, art castings, and plaques.

3.07.1.1.9 Nickel silvers

Nickel silvers do not contain silver but are essentially copper–zinc brasses with nickel in the range of 9–18%. The 18% nickel alloy polishes to a white color (like silver) and has good corrosion resistance. All have excellent ductility and are available as tube, wire, plate, sheet, and strip.

3.07.1.1.10 Copper–nickel--chromium

Copper–nickel–chromium alloys have been developed chiefly as cast alloys, the most prominent of which is CC382H. A version of this is DEF STAN 02-824, which is commonly used by the British Navy.

3.07.2 Theoretical Aspects of Copper Corrosion

Copper is the first member of Group IB of the periodic table, having atomic number 29 and electronic configuration $[Ar]3d^{10}4s^1$. Loss of the outermost s electron gives the cuprous ion Cu^+ and a second electron may be lost from the filled d shell to form the cupric ion Cu^{2+}. The availability of the d electrons for coordination allows copper to readily form complexes with such species as NH_3 and CN.

Copper occurs in the uncombined state in nature and is relatively easily obtained by the reduction of its compounds. It is not very active chemically and oxidizes very slowly in air at ordinary temperatures. In the electrochemical series of elements, copper is near the noble end and will not normally displace hydrogen, even from acid solutions. Indeed, if hydrogen is bubbled through a solution of copper salts, copper is slowly deposited, a process which occurs more rapidly if it is carried out under pressure.

As copper is not an inherently reactive element, it is not surprising that the rate of corrosion, even if unhindered by films of insoluble corrosion products, is usually low. Nevertheless, although the breakdown of a protective oxide film on copper is not likely to lead to such rapid attack as with a more reactive metal (e.g., aluminum), in practice the good behavior of copper, and, more particularly, of some of its alloys often depends to a considerable extent upon the maintenance of a protective film of oxide or other insoluble corrosion product.

In many environments, alloys of copper can be more resistant to corrosion than is copper itself, owing to the incorporation either of relatively corrosion-resistant metals, such as nickel or tin, or of metals such as aluminum or beryllium which would

be expected to assist in the formation of protective oxide films. Several types of copper alloys are liable to undergo a selective type of corrosion in certain circumstances, the most notable example being the dezincification of brasses (see **Section 3.07.3.3.2**). Some alloys are liable to suffer stress corrosion by the combined effects of internal or applied stresses and the corrosive effects of certain specific environments. The most widely known example of this is the season cracking of brasses (see **Section 3.07.3.6**). In general, brasses are the least corrosion-resistant of the commonly used copper-based alloys.

The various grades of commercial copper available do not differ to any marked extent in their corrosion resistance, and a choice between them is usually based on other grounds. Subsequent references to the corrosion behavior of copper may therefore be taken to apply broadly to all types of copper. The choice of alloy for any particular application is determined by the desired physical, mechanical, and metallurgical properties. Within these limits, however, a range of materials is usually available. It is essential that, at the very earliest stage, the choice of materials and the detail of design of the installation should be considered from the point of view of corrosion if the best performance is to be obtained in service. This is particularly true for copper alloys, where protective measures are not normally applied.

3.07.2.1 Electrode Potential Relationships

The electrode potentials for the equilibria:

$$Cu^{2+} + 2e \leftrightarrows Cu \quad [1]$$

$$Cu^{+} + e \leftrightarrows Cu \quad [2]$$

$$Cu^{2+} + e \leftrightarrows Cu^{+} \quad [3]$$

are +0.34, +0.52, and + 0.17 V respectively, as measured against a standard hydrogen electrode. For the equilibrium

$$2Cu^{+} \leftrightarrows Cu^{2+} + Cu \quad [4]$$

$$K_c = a_{Cu^{2+}} / \left(a^2_{Cu^{+}}\right)^2$$

K_c has the value of $\sim 1 \times 10^6$ at 298 K, and in solutions of copper ions in equilibrium with metallic copper, cupric ions therefore greatly predominate over cuprous ions, except in very dilute solutions. Cupric ions are therefore normally stable and become unstable only when the cuprous ion concentration is very low. A very low concentration of cuprous ions may be produced in the presence of a suitable anion, by the formation of either an insoluble cuprous salt or a very stable complex cuprous ion. Cuprous salts can therefore exist in contact with water only if they are very sparingly soluble (e.g., cuprous chloride) or are combined in a complex, for example, $[Cu(CN)_2]^-$ and $[Cu(NH_3)_2]^+$. Cuprous sulfate can be prepared in nonaqueous conditions, but because it is not sparingly soluble in water, it is immediately decomposed by water to copper and cupric sulfate. The equilibrium between copper and cuprous and cupric ion is disturbed by the presence of oxygen in solution, since the reaction shown in eqn [3] is facilitated, the oxygen acting as an electron acceptor.

3.07.2.2 Behavior of Copper Electrodes

The electrode potential behavior of copper in various solutions has been investigated in detail by Gatty and Spooner.[16] According to these workers a large part of the surface of copper electrodes in aerated aqueous solutions is normally covered with a film of cuprous oxide and the electrode potential is usually close to the potential of these film-covered areas. The filmed metal simulates a reversible oxygen electrode at the oxygen concentration and pH, less an overvoltage determined by the existing current density. The principal factors which affect the electrode potential are thus the nature of the solution, the way in which this influences the area of oxide film, and the supply of oxygen to the metal surface. In solutions containing chloride, there is a tendency for the establishment of the $Cu/CuCl/Cl^-$ electrode potential, so that the activity of chloride ions is an important factor in determining the electrode behavior. From a knowledge of the solubility products of cuprous chloride and cuprous oxide, it is possible to predict under what conditions chloride or hydroxyl ions are the potential-determining ions. According to Gatty and Spooner, chloride determines the potential if $a_{OH^-} < 10^{-8.1} \times a_{Cl^-}$ and hydroxyl determines the potential if $a_{OH^-} > 10^{-8.1} \times a_{Cl^-}$. However, this will not hold in concentrated solutions as complex $[CuCl_2]^-$ ions as well as simple ions will be present. A further factor to be considered is the ready formation of insoluble basic compounds. In solutions which do not contain chloride (e.g., sulfate or nitrate solutions), corrosion rates are usually lower and the electrode potential is more steady over a wide range of conditions.

Gatty and Spooner consider that the rate of corrosion is probably determined by the rate at which metal ions can escape through pores in the protective oxide film, and this is supported by the results of

experiments on the anodic and cathodic polarization of copper.

One of the potential–pH equilibrium diagrams devised by Pourbaix[17] relating to the Cu–H_2O system is shown in **Figure 1**. Such diagrams are of considerable assistance in discussing many problems associated with the chemistry, electrochemistry, electrodeposition, and corrosion of copper. It must be pointed out that the thermodynamic approach on which these are based has limitations, the most important being that, although predictions can be made about the possibility of a given reaction proceeding in certain circumstances, no information can be gained about the rate at which it will proceed.

A similar method of representing the behavior of copper in dilute aqueous solutions by means of corrosion-current/pH diagrams has been given by Rubinic and Markovic.[18] A study of the behavior of copper when anodically polarized has been made by Hickling and Taylor[19] and, more recently, by Kuksina *et al.*[20] using electrochemical methods which record the variation of potential with the Faradaic charge passed. In alkaline solutions, the main stages of polarization have been found to be (1) the charging of the double layer, and (2) the formation of a film of cuprous oxide which was almost at once oxidized to cupric oxide. Mayer and Muller[21] report evidence that this converts to Cu_2O_3 at potentials above −25 mV versus Hg/HgO in 1 M KOH. However, in 0.1 M NaOH,[20] the Cu_2O film was found to be around four molecules thick when oxygen evolution first commenced. In buffer solutions of decreasing pH, the formation of sparingly soluble salts preceded or accompanied the formation of the oxide film. In acid solutions yielding soluble copper salts, no passivity developed, the anodic process being merely dissolution of copper. In nitrate solutions, the cathodic process has a significant effect on the

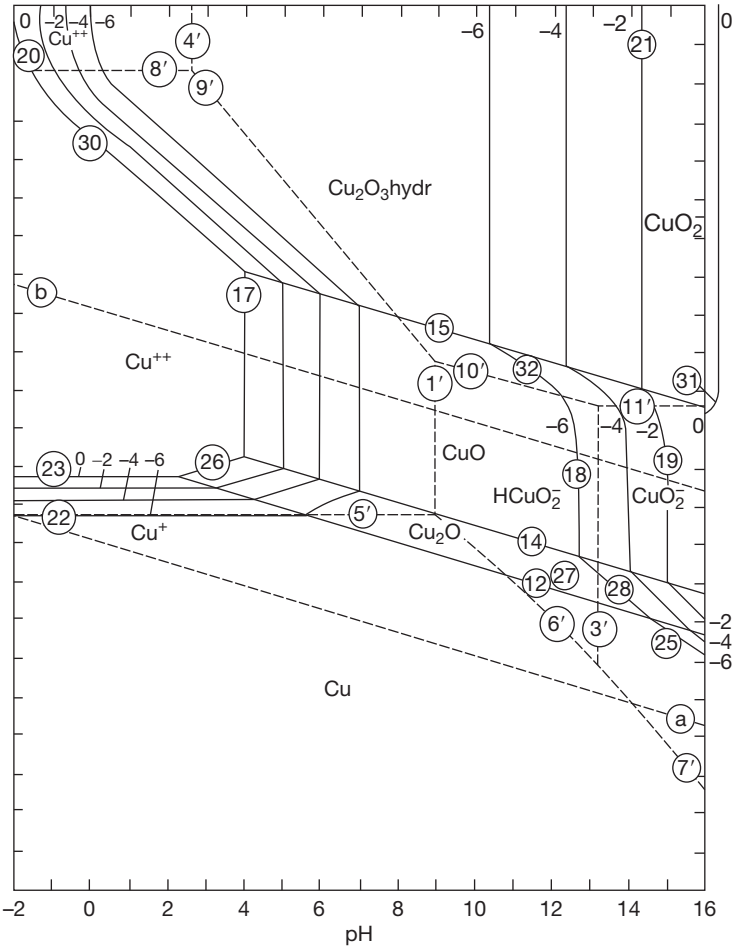

Figure 1 Potential–pH equilibrium for the system copper–water at 25 °C.

anodic dissolution of copper. Low-frequency AC polarization techniques have shown[22] that OH^- ions adsorbed during the cathodic half-cycle facilitate copper dissolution in the anodic half-cycle through the production of an insoluble hydroxide layer. Other workers have also studied the anodic behavior of copper or copper alloys in alkaline[23] and in acid[24,25] solutions, using both static conditions and turbulent conditions, such as those generated by rotating cylinder electrodes[26] and the presence of light has been found to have an influence on the electrochemistry.[21] For instance, in Cu–Al–Sn anodically polarized in sodium sulfate solution,[27] an enrichment of the passive film with aluminum oxide can be detected as the photocurrent spectrum changes from a 'copper-type' to an 'aluminum-type' with time.

The excellent corrosion resistance of cupronickel alloys is related to the formation of a particularly effective protective film of corrosion products in the early stages of exposure. A number of studies have been carried out involving a wide range of analytical techniques.[28] The film formed is dark brown in color and there is general agreement that it contains an inner layer of Cu_2O which is enriched with nickel and iron. Recent electrochemical studies[29] have identified that over this layer, a thin outer layer of CuO develops and an increasing nickel content in the alloy produces a decrease in the overall corrosion rate. The corrosion rate also falls as the chloride ion concentration rises above 0.3 M due to an enhanced formation of the passive Cu_2O film.[30] On this subject, in a seawater context, see **Section 3.07.3.5**.

3.07.3 Corrosive Environments Experienced

Copper and its alloys have a very diverse range of properties and their application exposes them to many types of environment. Artifacts dating back thousands of years are testimony to the resilience of copper alloys to atmospheric corrosion, waters, and soils. Also, they have been recognized for marine use for several decades and are still selected even though other noncopper alloy systems have been developed in the interim. The release of copper ions and the cuprous oxide film have antifouling properties and, in addition, recent work has proved their antimicrobial properties; investigations into the mechanisms for these beneficial effects are ongoing, as are their development into new applications. More traditional applications requiring corrosion resistance of copper alloys involve roofing, plumbing, naval and commercial shipping, and desalination plant. The level of corrosion and corrosion mechanisms occurring in different environments depend on the alloy group chosen and can vary from mildly resistant to highly resistant. Various corrosion mechanisms exist and these have been found to be related to the type of alloy and to the environment to which it is exposed. The following sections give details of the effects seen in a range of different corrosive environments experienced.

3.07.3.1 Atmospheric Corrosion

Copper has a high degree of resistance to atmospheric corrosion and is widely used for roofing sheets, flashings, gutters, and conductor wires as well as for statues and plaques. The corrosion resistance of copper and its alloys is due to the development of protective layers of corrosion products, which act to reduce the subsequent rate of attack. The formation, in course of time, of the typical green 'patina' gives copper roofs a pleasing appearance; indeed, methods are used to produce it artificially or to accelerate its formation.[31] The nature of the corrosion products formed on copper exposed to the atmosphere has been exhaustively studied by Vernon and Whitby.[31–33] A comprehensive review of the literature on atmospheric corrosion including copper and copper alloys up to 1995 has been produced by Dechema[34] It has been found that in the early periods of exposure, the corrosion deposit contains sulfide, oxide, and soot. By the action of sulfuric acid and by the oxidation of sulfide, copper sulfate is formed and this hydrolyzes and forms a coherent and adherent basic form of this compound. Initially, this approximates to $CuSO_4$–$Cu(OH)_2$ but it gradually increases in basicity until after 70 years or so it becomes $CuSO_4$–$3Cu(OH)_2$ and is identical with the mineral brochantite. In some cases, small quantities of basic carbonate, $CuCO_3$–$Cu(OH)_2$ (malachite), are also present, and, near the sea coast, basic chloride $CuCl_2$–$3Cu(OH)_2$ (atacamite) is produced. However, even very near the sea coast, sulfate usually predominates over chloride.

In laboratory tests, Vernon[33] showed that the relative humidity and the presence of sulfur dioxide have a profound effect on the rate of corrosion of copper, as they do with many other metals. He found that when the relative humidity was less than 63%, there was little attack even in the presence of much sulfur dioxide, but when the relative humidity was raised to

75%, corrosion became severe and increased with the concentration of sulfur dioxide present. By exposing specimens to the atmosphere at different times of the year, Vernon found that the rate of attack on copper was determined by the conditions prevailing at the time of first exposure. For specimens first exposed in winter, there was a linear relationship between increase in weight and time of exposure, indicating that the layer of corrosion product formed under these conditions was nonprotective. For specimens first exposed in summer, the square of the increase in weight was proportional to the time of exposure. This indicated that the coating formed in summer (when the atmospheric pollution was relatively low) was protective. It was found that the parabolic law holds when the corrosion product layer obstructs the access of the corrosive agent to the metal, the rate of attack then being inversely proportional to the thickness of the layer. It was apparent that the protective character of the layer persisted through subsequent periods when the pollution was relatively high.

Copper tarnishes rapidly when exposed to atmospheres containing hydrogen sulfide. Atmospheric corrosion tests on copper and several copper alloys were carried out by Hudson[35] at a number of sites in the United Kingdom. Corrosion damage was assessed by one or more of the following methods: gain in weight, loss of weight after cleaning, loss of electrical conductivity, and loss of tensile strength. Hudson found that the resistance to atmospheric corrosion was high and that the rate of attack tended to decrease with time of exposure. Little difference was found between the behavior of arsenical copper and high-conductivity copper, and most of the alloys tested behaved very similarly except for the brasses, which deteriorated more rapidly owing to dezincification (see **Section 3.07.3.3.2**). Several series of atmospheric exposure tests have been carried out since Hudson's work, and the loss in weight data obtained in six of the most important investigations are summarized in **Table 5**. In all cases, losses in tensile strength were also determined, and the results from the two methods were, in general, in good agreement. However, for alloys suffering selective attack (such as with the dezincification of brasses) change in mechanical properties usually provided a more reliable indication of deterioration than weight loss. Some other findings common to all the tests were that (1) corrosion rates decreased with time, (2) least attack occurred at rural sites and most in urban and industrial atmospheres, (3) corrosion was uniform, and (4) with a few exceptions, there was no significant pitting.

Tracy *et al.*[36] exposed specimens of 11 different grades of copper in the form of sheet and wire to rural, marine, and industrial atmospheres in the United States for periods up to 20 years. The differences in the behavior of the materials were small and of little, if any, practical significance. Very similar results for various types of copper were found by Mattsson and Holm[37] in Sweden and Scholes and Jacob[38] in the United Kingdom (see **Table 5**).

Table 5 gives the results of tests on copper alloys by Tracy,[36] Thompson,[40] and Mattson and Holm,[37] Scholes and Jacob[38] and, more recently, Morcillo[39] together with their co-workers. The tests of Tracy and Scholes were for periods up to 20 years; in the work of Thompson and Mattson, specimens were

Table 5 Atmospheric corrosion tests on copper and copper alloys

	No. of types of copper	*No. of different alloys*	*No. of sites*	*Period of exposure (years)*	*Average rates of attack from weight losses (mm year^{-1} × 10^{4})*		
					Rural sites	*Marine sites*	*Urban/ Industrial sites*
Tracy, Thompson, and Freeman[36]	11	–	4	20	5.6–4.3	6.9–9.4	8.6–12
Tracy[43]	2	9	7	20	0.5–7.6	1.3–23[a]	13–30[a]
Thompson[40]	1	17	4	7	3.3–10	4.3–25	13–27
Mattson and Holm[41]	4	–	3	7	5–6	7–8	10–12
	–	18	3	7	2–5	6–11	9–22
Scholes and Jacob[38]	4	–	2	20	–	6–10	11–20
	–	17	2	20	–	8–26	14–38
Morcillo *et al.*[39]	1	–	66	4	0.1–0.2		

[a]Rates of attack for high tensile brass were (45–115) × 10^{-4} mm year^{-1}.

removed after 2 and 7 years and further specimens were removed after 16 years.[41] The average penetration during the 16-year period was found to be about the same as during the first 7 years, but considerably lower than during the initial 2 years. The materials tested included brass, nickel–silvers, cupronickels, copper–beryllium alloys, and various bronzes. Recent studies have involved the investigation of seasonal effects of industrial pollutants (NO_x) and comparison of rural and marine locations in South America.[42]

In the tests described by Tracy,[43] a high-tensile brass suffered severe dezincification (see **Table 5**). The loss in tensile strength for this material was 100% and, for a non-arsenical 70–30 brass, 54%; no other material lost more than 23% during 20 years' exposure. In Mattsson and Holm's tests, the highest corrosion rates were also shown by some of the brasses. Dezincification caused losses of tensile strength of up to 32% for a β brass and up to 12% for some of the α–β brasses; no other materials lost more than 5% in 7 years. Dezincification also occurred, though to a lesser degree, in the α brasses tested, even in a material with as high a copper content as 92%. Incorporation of arsenic in the α brasses consistently prevented dezincification only in marine atmospheres.

In Thompson's reported work, the alloy showing the lowest rate of attack at all sites was a bronze containing 7Al–2Si. Relatively high corrosion rates were shown by Cu–5Sn–0.2P at a marine site and Cu–2.5Co–0.5Be in an industrial environment. The beryllium–copper alloys were the only materials to show measurable pitting, the deepest attack being 0.6 mm after 7 years. In Scholes and Jacob's tests pitting, intergranular (or transgranular) penetration, or selective attack occurred on some alloys. The maximum depth of attack exceeded 0.2 mm in 20 years on 6 of the 21 materials (three brasses, two nickel silvers, and Cu–20Ni–20Mn), but exceeded 0.5 mm in 20 years only on Cu–20Ni–20Mn and 60/40 brass. These two latter alloys lost up to 73% and 13% respectively of their tensile strength; no other alloys lost more than 10% in 20 years.

The work of Ramos *et al.*[42] has demonstrated a clear correlation between seasonal increases in SO_2 and NO_x concentrations in urban atmospheres with higher corrosion rates and the presence of sulfates in the corrosion products. This broadly agreed with a previous study of comparative weight gains of copper over a 2-year period at 39 sites spread across Europe,[44] where a clear correlation was found between weight gain and SO_2 content of the environment, although attempts to find mathematical correlations of weight increase with other atmospheric species was not found to be possible. However, other works report that the corrosion of copper by sulfur dioxide is measurably accelerated by the presence of NO_2[45] or ozone.[46] The recent study conducted in South America, which involved the comparison of 21 unpolluted sites with 45 marine locations, showed that there is a threshold chloride concentration of 20 mg m^{-2} day^{-1} in the environment above which the corrosion rate intensifies. Other recent studies have involved comparing the effects of different types of climates throughout four continents.[47]

From the work described and other investigations,[48] it is evident that copper and most copper alloys are highly resistant to atmospheric corrosion. The reported results indicate that copper itself is as good as, or better than, any of the alloys with regard to atmospheric corrosion. Some of the brasses are liable to suffer rather severe dezincification and it is unwise to expose these to the more corrosive atmospheres without applying some protection.

When unusually rapid corrosion of copper and its alloys occurs during atmospheric exposure, it is likely to be for one of the following reasons:

1. Extreme local pollution by products of combustion.
2. Bad design or construction, for example, the presence of crevices where moisture may lodge for long periods, including, for instance, coiled wire.[49]
3. Constant dripping of rain water contaminated by atmospheric pollution (e.g., from near-by chimney stacks) or by organic acids from lichens, etc.
4. Corrosion fatigue due to inadequate allowance for expansion and contraction with consequent buckling as the temperature fluctuates.

Most of these disorders can be avoided by attention to design.[50]

The discussions in recent years of the possibility of pollution occurring as a result of released copper due to atmospheric corrosion have resulted in studies of runoff from roofs and facades by several workers.[51–54] A number of research results have been published by the Royal Institute of Technology, Stockholm, Sweden[55–61] and the EMPA laboratories, Switzerland. It has been found that, after a short initiation period, the runoff rate of copper per year is constant over a long time.[55,56,58,62] This makes it possible to model the copper runoff rate, R,[57] based on SO_2 concentration, the pH of the rainwater, and its quantity. The roof surface angle of inclination Θ has

also been taken into account,[61] according to the following equation:

$$R = (0.37[SO_2]^{0.5} + 0.95[\text{Rain}]10^{-0.62\text{pH}})\frac{(\cos\Theta)}{(\cos 45^\circ)} \quad [5]$$

The seasonal variation of copper corrosion rate and the runoff rate have also been studied.[60]

Some workers note that the released metal from the corrosion reaction is in ionic form directly on the roof and the environmental impact of these released ions has been determined. Other workers state that the run-off is mainly in particulate form. However, the interaction with solid surfaces in the near vicinity of buildings has been looked at together with the changes of transport which occur from the source to the end product. Investigations of reactivity have been made toward various natural and manmade surfaces, such as different soil systems, limestone, and concrete. The results illustrate that, for scenarios where copper ions come in extensive contact with solid surfaces, a large fraction of released copper is retained in the immediate vicinity of the building.[56] The potential ecotoxic effects from released copper have also been investigated. Copper biosensor testing with a bacteria and growth inhibition testing with green algae have been used. The runoff water directly after release was found to cause significant reduction of the green algae growth rate, indicating that the copper is bioavailable. However, it was found that contact with solid surfaces effectively reduces this bioavailable copper.

The fate of released copper in runoff has also been studied in the United States.[62–64] The results obtained also show that the bioavailable copper fraction is low after contact with solid surfaces.

Sundberg[62] followed the runoff from a new copper roof for 3.5 years. A relatively stable runoff rate per year was found after 0.5 years. The result was compared with the runoff from a roof prepatinated 40 years ago, which was found to have a copper runoff rate which was 10% lower.

3.07.3.2 Soil Corrosion

Several extensive series of soil-corrosion tests have been carried out by the National Bureau of Standards in the United States, and the results summarized by Romanoff.[65] In one series, 2 types of copper and 10 copper alloys were exposed in 14 different soils for periods up to 14 years. The results for the copper specimens are summarized in **Table 6**.

The behavior of the phosphorus-deoxidized and tough-pitch coppers was, in general, very similar. At the less corrosive sites, with a few exceptions, copper was the best material. Most of the alloys lost weight ranging up to twice that of copper, with maximum depths of attack up to three times greater. At the other sites, although the coppers were usually rather better than the alloys, some of the alloys were occasionally superior.

The three most corrosive sites were rifle peat (pH 2.6), cinders (pH 7.6), and tidal marsh (pH 6–9). Corrosion of some of the alloys was particularly severe in the cinders. The behavior of the brasses tested, particularly those high in zinc, was rather different from that of the other materials. In most cases dezincification occurred and the brasses were the worst behaved materials; in the cinders, for instance, several brass specimens were completely destroyed by dezincification. However, in some of the soils rich in sulfides, the brasses were the best materials.

The British NonFerrous Metals Research Association carried out two series of tests, the results of which have been given by Gilbert[66] and Gilbert and Porter[67]; these are summarized in **Table 6**. In the first series,[66] tough pitch copper tubes were exposed at

Table 6 Soil-corrosion tests on copper by National Bureau of Standards and British Nonferrous Metals Research Association (BNFMRA)

	Period of exposure (years)	*Average rate of attack from loss in weight (mm year^{-1} × 10^{-4})*	*Maximum rate of pitting (mm year^{-1})*
BNFMRA first series five least corrosive soils	10	0.5–2.5	Nil
BNFMRA second series four least corrosive soils	5	5.0–25	0.140
Nat. Bur. Standards nine least corrosive soils	14	4.0–25	0.043
Nat. Bur. Standards two next most corrosive soils	14	23–130	0.033
BNFMRA first series acid clay and acid peat	10	53–66	0.046
BNFMRA second series cinders	5	66	0.32
Nat. Bur. Standards three most corrosive soils: rifle peat, cinders, tidal marsh	14	160–355	0.115

seven sites for periods of up to 10 years. The two most corrosive soils were a wet acid peat (pH 4.2) and a moist acid clay (pH 4.6). In these two soils, there was no evidence that the rate of corrosion was decreasing with duration of exposure. In the second series,[67] phosphorus deoxidized copper tube and sheet were exposed at five sites for 5 years. Severe corrosion occurred only in cinders (pH 7.1). In these tests, sulfides were found in the corrosion products on some specimens and the presence of sulfate-reducing bacteria at some sites was proved. However, it was not clear to what extent the activity of these bacteria was a factor accelerating the corrosion of copper.

Cinders and acid peaty soils are obviously among the soils most corrosive toward copper. There is, however, no direct relationship between the rate of corrosion and any single feature of the soil composition or constitution.[68] For instance, in the American tests, corrosion in several soils with either low pH or high conductivity was not particularly severe, while the British tests show that chloride or sulfate contents are not necessarily harmful. The latter tests showed that bare copper can safely be buried in a wide range of soils without fear of excessive corrosion. Experience of the behavior of copper water service pipes, which are used widely, confirms this. Difficulties are generally confined to 'made-up' ground containing cinders, etc. and a few other aggressive soils, and in these circumstances it is necessary to apply protection such as bitumen-impregnated wrappings or plastic coatings. Tin coatings cannot be recommended as experience shows that accelerated attack is liable to occur at pores and scratches in the coating, leading to premature failure. Copper water pipes have been known to fail by the action of stray electric currents, but this is not a common occurrence.

There is agreement between the soil-corrosion tests carried out by National Bureau of Standards and practical experience of the behavior of hot-pressed brass fittings used for joining copper water service pipes. These duplex-structure brass fittings are liable to suffer attack by dezincification in many soils in which copper behaves satisfactorily, and, for burial underground, fittings of copper, gunmetal, or dezincification-resistant brass are to be preferred. In general, it may be said that, unless there is some special reason for using a copper alloy, it is preferable to choose copper for applications involving subterranean service. A comparison of the corrosion produced through the influence of possible ionic species present around buried copper has shown[69] that the major damage is caused by chloride ions. Ammonium and sulfide species appear to be relatively benign. The corrosion products which result are cuprite and malachite, the latter being favored for soils with higher water content.[70]

3.07.3.3 Corrosion in Natural Waters

Copper and copper alloy pipes and tubes are used in large quantities both for conveying fresh and salt water and in condensers and heat exchangers where fresh or salt water is used for cooling. Pumps, screens, valves, and other ancillary equipment may also be largely constructed of copper alloys. Large tonnages of these materials are therefore used on offshore structures, multistage flash desalination plants, power stations, on board ships, in sugar factories, and in oil refineries, as well as in hot and cold water circuits and heating and cooling systems in hospitals, factories, hotels, and homes.

Corrosion problems that arise frequently are discussed under separate headings, depending on whether the environment is seawater or freshwater. In fact, there is no sharp dividing line between these environments, since some harbor, estuarine, and brackish well waters are mixtures of seawater and freshwater and are often variable in composition. Corrosion has been found to occur in all these media, particularly in seawater, but this is more frequently seen as a result of poor design or operation than as a result of lack of materials suitable for the application. This section will deal with the types of corrosion which can be seen in all types of natural water; seawater, brackish water, or freshwater. Separate sections will follow which deal with corrosion types seen almost entirely solely in freshwater and with the behavior of copper alloys specifically in seawater.

3.07.3.3.1 Impingement attack

Copper alloys have good corrosion resistance under moderate fluid flow rates. However, above a certain flow velocity, called the breakaway velocity, the shear stress of the liquid on the alloy protective surface film is sufficient to damage it and much higher corrosion rates occur. This phenomenon is called impingement attack or erosion–corrosion. Therefore, tube and piping systems are designed to operate satisfactorily up to a maximum velocity and it is important that this is not exceeded in service. Breakaway velocity can be influenced by many factors, including the alloy being used, the resilience of the surface film, the geometry of the product and system, the corrosive nature of the

fluid being handled, pollution, solids (e.g., sand in seawater), and turbulence.[71]

Copper tubes have been found to suffer from impingement attack in systems where the speed of water flow is unusually high. The phenomenon has been discovered to be dependent in some degree on the quality of the water, for instance where no protective scale is able to form, for example, in a soft water containing appreciable quantities of free carbon dioxide.[72] Impingement attack is most often seen downstream of poorly installed fittings or sharp bends in pipework systems. Such obstructions to flow and sharp changes in direction where the speed of the water is high can lead to eddy currents concentrating the flow on specific parts of the tube, the creation of bubbles at areas of low pressure (which subsequently collapse), and the streaming of particulate matter. The latter can act alone or in concert to remove any protective scale that has formed on the copper surface, thus exposing the metal to further corrosion and subsequent removal of corrosion product. In such a way, severe metal loss can occur, leading eventually to failure of the tube. Impingement attack is characterized by areas of bright metal and horseshoe-shaped undercut areas, their direction being as though the horse was walking upstream. In the middle of such undercut areas, there may be islands of bright metal or metal still retaining some protective corrosion product. An example of this phenomenon is shown in **Figure 2**. Ball valve seatings may also suffer an erosive type of attack. The corrosion of ball valves, including the effect when the water is chlorinated, has been studied by several workers.[73] Avoidance of impingement attack is usually achieved by reducing the flow velocities by one or a combination of the following: reducing the pump output, increasing the pipe size, modification of the change of direction to one which is less abrupt, opening partially closed valves, etc. The maximum flow velocity quoted in European Standard EN806 part 3 is 2.0 m s^{-1} for header, riser, and floor service pipes and 4.0 m s^{-1} for (replaceable) connection pipes to one fitting. The Swedish Building Standard 2522 recommends a reduction in velocity as the design operating water temperature increases viz, 2 m s^{-1} at 10 °C, 1.5 m s^{-1} at 50 °C, 1.3 m s^{-1} at 70 °C, and 1.0 m s^{-1} at 90 °C.

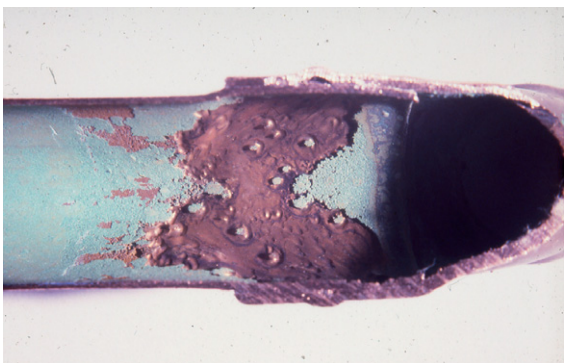

Figure 2 Photograph showing typical impingement attack caused by eddy currents which were present as a result of burrs on the internal wall. The tube type is 15 mm diameter copper tube to EN 1057, R250 (half-hard condition).

The actual velocity at which impingement commences depends on the fluid and varies from alloy to alloy.[74] In general, the nickel aluminum bronzes and copper–nickel alloys have the highest velocity tolerances in seawater and are somewhat better than gunmetals, brasses and tin bronzes[75] (see **Table 7** and **Section 3.07.3.5**). The cupronickel 90–10 and 70–30 alloys are commonly used for seawater condensers, heat exchangers, and pipework in naval vessels as well as merchant shipping. For tube sizes used in heat exchangers and condensers, the velocity is limited to ~2–2.5 m s^{-1}. For seawater pipework of internal diameter 100 mm and with bends of long radius, the recommended maximum seawater flow velocities are 3.5 m s^{-1} for the 90–10 alloy and 4 m s^{-1} for the 70–30 alloy[76]. This has worked well in practice although it is now believed to be a little on the conservative side.[77,78] Areas causing high turbulence such as bends with tight radiuses, partially throttled valves, and partial obstructions need to be avoided.

Other cupronickel alloys have been developed and have been found to offer even better resistance to impingement attack. In particular, a 16.5% Ni–0.5% Cr alloy first developed by INCO in the 1970s has a much higher, critical shear stress than the 70–30 alloy.[12] Also a 2% Mn–2% Fe–30% Ni alloy, developed for extra impingement resistance in situations where entrained sand is present in seawater, is now successfully used in the more demanding areas of desalination plants.[9]

Gunmetals and aluminum bronzes have good resistance to impingement attack but these alloys are not normally used for heat exchange tubing, the former because they are casting alloys and the latter because it may pit in quiescent conditions. However, both groups are used for components such as pumps and valve bodies. The nickel aluminum bronze alloy is used for propellers and pump components as it has excellent resistance to cavitation compared to many other copper based alloys.

Table 7 Comparative results showing corrosion and erosion/corrosion performance of a number of copper alloys[a]

Alloy	*General corrosion rate (mm year^{-1})*[b]	*Crevice corrosion rate (mm year^{-1})*[b]	*Minimum flow rate to produce erosion/corrosion (m s^{-1})*[c]
Wrought Alloys:			
Phosphorus deoxidized copper, CW024A	0.04	<0.025	1.8
Admiralty brass, CW706R	0.05	<0.05	3
Aluminum brass, CW702R	0.05	0.05	4
Naval brass, CW712R	0.05	0.15	3
HT brass, CW705R	0.18	0.75	3
90–10 cupronickel	0.04	<0.04	3.6
70–30 cupronickel	0.025	<0.025	4.5
5% Al–bronze	0.06	<0.06	4.3
8% Al–bronze	0.05	<0.05	4.3
9% Al–bronze	0.06	0.075	4.5
Nickel aluminum bronze	0.075	<0.30	4.3
Aluminum silicon bronze	0.06	<0.075	2.5
High strength cupronickel (Cu–Ni–Al–Mn–Fe)	0.02	<0.02	4.8
Cast alloys:			
Gunmetal, CC491K	0.04	<0.04	3.6
Gunmetal, CuSn10Zn2	0.025	<0.025	6
High tensile brass, CC765S	0.18	0.25	2.5
Aluminum bronze, CC331G	0.06	<0.06	4.5
Nickel aluminum bronze, CC333G	0.06	<0.5	4.3
Manganese aluminum bronze, CC212E	0.04	3.8	4.3

[a]Due to difficulties of achieving consistent results for tests in seawater, data should be used for comparing relative performance rather than being taken as absolute.[75]
[b]The figures for general corrosion rate and crevice corrosion rate were determined using samples fully immersed beneath rafts in Langstone Harbour, Portsmouth, UK, for 1 year.[75]
[c]The corrosion/erosion resistance tests were carried out using the following method (known as the Brownsdon and Bannister method): the specimens were fully immersed in natural sea water and supported at 60 °C to a submerged jet, 0.4 mm diameter placed 1–2 mm away, through which air was forced at high velocity. From the minimum air jet velocity required to produce corrosion/erosion in a fourteen-day test, the minimum sea water velocity required to produce corrosion/erosion under service conditions was estimated on the basis of known service behavior of some of the materials.

A number of studies have evaluated the impingement resistance for marine condensers and piping involving several types of test apparatus, including rotating discs, rotating spindles, model condensers, multivelocity jet tests, and jet impingement tests.[79] This work has proved reliable in ranking materials as a function of impingement resistance and has been an important factor in the development of alloys resistant to impingement attack.

Experience has shown that for intermittent flow (as might be the case of firewater systems used on offshore platforms which are tested periodically), short-term high velocities in the order of 7–15 m s^{-1} for cupronickels are not detrimental. Also open geometries need not have the velocity restrictions of pipe and tubing; for example, 90–10 cupronickel has been successfully used on ship hulls operating at 24 knots (12 m s^{-1}) with little thinning experienced.[9]

3.07.3.3.2 Dezincification of brasses

Historically, the most common dealloying phenomenon seen in copper alloys has been the dezincification of brasses. In recent years, the development of dezincification-resistant brasses and a greater understanding of the required conditions under which dezincification manifests itself have lessened its occurrence, but it retains a high degree of scientific interest. Dezincification is characterized by regions of the brass becoming replaced by a porous mass of copper which, though retaining the shape of the original article, has virtually no strength. There has long been discussion as to whether there is selective corrosion of the zinc in the brass, which leaves the copper behind, or whether complete dissolution of the brass occurs, followed by redeposition of copper. Possibly both processes occur under different circumstances.

The mechanism of dezincification of brass has been investigated and discussed by Evans,[80] Fink,[80] Lucey,[81] Feller,[82] and Heidersbach,[83] and is referred to in many other papers.[84–92] Recent extensive studies[93,94] which have investigated the distribution of copper isotopes and the effects of specimen rotation during testing, show that redeposition of copper is a major mechanism.

With a single-phase brass, the whole of the metal in the corroded areas is affected. Dezincification may proceed fairly uniformly over the surface, and this 'layer type' takes much longer to cause perforation than the more localized 'plug type' which more often occurs.[95] With a two-phase brass, the zinc-rich β phase is preferentially attacked and eventually the α phase may be attacked as well. The zinc corrosion products which accompany dezincification may be swept away, or, in some conditions, may form voluminous deposits on the surface. These may in turn lead to blockages, for example, in fittings. In general, the rate of dezincification increases as the zinc content rises, and great care needs to be exercised in making brazed joints with copper/zinc brazing alloys, particularly if they are to be exposed to seawater. Under these conditions, a properly designed capillary joint may last for some time, but it is preferable to use corrosion-resistant jointing alloys such as silver solders[96], as specified in BS EN 1044:1999.

Factors which cause increased rates of dezincification are high temperature, high chloride content of water, and low water speed.[97–100] Dezincification is also likely to occur preferentially beneath deposits of sand or silt on the metal surface, or in crevices where there is a low degree of aeration.

Addition of ~0.04% arsenic will inhibit dezincification of α brasses in most circumstances and arsenical α brasses can be considered to be immune to dezincification for most practical purposes.[101] There are conditions of exposure in which dezincification of these materials has been observed, for example, when exposed outdoors well away from the sea[37] or when immersed in pure water at high temperature and pressure, but instances are rare. In other conditions, for example, in polluted seawater, corrosion can occur with copper redeposition away from the site of initial attack, but this is not truly dezincification, which, by definition, requires the metallic copper to be produced *in situ*. The work of Lucey[81] goes far in explaining the mechanism by which arsenic prevents dezincification in α brasses but not in α–β brasses. An interesting observation is that the presence of a small impurity content of magnesium will prevent arsenic in α brass from having its usual inhibiting effect.[102]

The addition of antimony or phosphorus, in amounts similar to arsenic, are claimed to be also capable of preventing dezincification of α brasses. However, most manufacturers use arsenic. It appears desirable to avoid using phosphorus, as Bem[103] has shown that this element can, in some circumstances, lead to an undesirable susceptibility to intergranular corrosion. The same can be true for arsenic additions over ~0.05%.

A dezincification resistant alloy, CW602N, was first introduced in 1980. This alloy is a leaded brass with a zinc content sufficiently high to permit hot forging and extrusion in the β range without cracking. After hot working, a heat treatment of up to 6 h at 500 °C followed by slow cooling transforms any residual β phase to α so that the finished component is essentially α brass. Dezincification is inhibited by adding arsenic (0.02–0.15%) which protects the α phase, and good machinability is assured by adding lead (1.7–2.8%). The impurities iron and manganese, which combine with arsenic, must be carefully controlled for the arsenic to be effective. A rule of thumb is that the percentage of arsenic must be greater than the combined percentage of iron and manganese to provide resistance to dezincification. There is practical evidence that the maximum limits for iron and manganese allowed in the specification (0.1% each) are too high as, at these levels, the arsenic may be rendered ineffective.

Newer studies of intergranular corrosion attack (IGA) of arsenic-containing dezincification resistant brass[93,104] show that there is a close relationship with the degree of precipitation of iron–arsenic compounds in the grain boundaries. The precipitates are formed during low temperature heat treatment or slow cooling after hot forging or a prior heat treatment. Sulfide corrosion and dezincification in the grain boundary appear to be the result as the arsenic is bound to impurities like iron. IGA has also been reported for aluminum brass (CW 702R) and Mazza and Torchio[105] have presented a laboratory test method to reveal IGA in this material. The method has also been used successfully for dezincification resistant brass[104] and correlation with field tests in seawater is good.

The addition of 1% tin can markedly reduce the rate of dezincification in two phase brasses, and naval

brass (61Cu–38Zn–1Sn) is attacked considerably more slowly than 60/40 brass in seawater, although there may be virtually no difference between them in most freshwaters. Some of the cast complex high-strength two-phase brasses containing tin, aluminum, iron, and manganese appear to have relatively good resistance to dezincification, but they are by no means immune to it.

Dezincification of brasses in drinking water may occur, particularly in stagnant or slowly-moving warm or hot waters relatively high in chloride and containing little carbonate hardness.[106] Dezincification of α brasses is inhibited by the usual arsenic addition, but two-phase brasses are liable to severe attack in some waters. In such cases, dezincification-resistant brass or gunmetal fittings should be used. If copper/zinc brazing alloys are used, these may dezincify in water known to support this type of corrosion and may consequently give rise to leaks.[106]

3.07.3.3.3 Selective attack in other alloys

Selective attack analogous to dezincification can occur in other copper alloys, particularly in aluminum bronzes and, less frequently, in tin bronzes,[107] cupronickels,[108] and other alloys. Dealuminification of aluminum bronzes has been studied extensively[109] and the results indicate that, while α-phase alloys suffer such attack comparatively rarely, alloys of higher aluminum content can be more susceptible. The electrochemical relationships are such that preferential corrosion of the second phase is liable to occur in α–γ_2 alloys, but α–β alloys are relatively resistant to attack. Retention of β phase is favored by rapid cooling after casting or after high temperature heat treatment, and also by incorporating manganese in the alloy. A tempering heat treatment in the temperature range of 650–740 °C has been found to hinder the occurrence of dealuminification due to the transformation of the more corrosion-prone β phase to a combination of α phase and comparatively benign κ phases.[110]

The addition of nickel to aluminum bronze has been found useful in controlling the occurrence of the γ_2 phase, which has a corrosion potential ~100 mV less noble than the α phase, thereby undergoing selective attack in seawater. Weill-Couly and Arnauld[111] have determined an empirical relationship, eqn [6] shown below, which denotes the aluminum content of nickel–aluminum bronze castings below which a resistance to dealuminification is found.

$$\mathrm{Al} \leq 8.2 + \frac{\mathrm{Ni}}{2} \qquad [6]$$

3.07.3.3.4 Deposit attack and pitting

When water speeds are low and deposits settle on the surface, pitting in copper and copper alloys is liable to occur by differential aeration effects. This is particularly so at water speeds below ~1 m s^{-1}. In seawater systems, such attack may occur under dead barnacles or shellfish, the decomposing organic matter assisting the corrosion process. Pitting is most likely to occur in polluted in-shore waters, particularly when hydrogen sulfide is present. In such contaminated waters, non-protective sulfide scales are formed and these tend to stimulate attack. It has been found possible to develop a mathematical model which can be successfully used to calculate the electrode potential below which copper is immune to pitting in tap water or seawater in the temperature range 25–75 °C.[112] Of the 26 ionic species which have been included in the calculation, CO_3^{2-} and SO_4^{2-} were found to be the most aggressive.

3.07.3.4 Corrosion in Freshwater

Freshwaters are, in general, less corrosive toward copper than is seawater and copper is widely and satisfactorily used for distributing cold and hot waters in domestic and industrial installations.[113–116] Copper and copper alloys are used for pipes, hot-water cylinders, ball valves, taps, fittings and heater sheaths. In condensers and heat exchangers using freshwater for cooling, tubes of 70/30 brass or Admiralty brass are usually used, and corrosion is rarely a problem. Nevertheless, the widespread use of copper and copper alloys since the early part of last century especially in domestic water systems has meant that all adverse situations have been experienced and the following are rare but notable corrosion issues. Two British Standards give guidance on the likelihood of corrosion in water distribution and storage systems and in water recirculating systems. These are BSEN 12502:2004 and BSEN14868:2005.

3.07.3.4.1 Pitting

Occasionally copper water pipes fail prematurely by pitting. This a general term and is used for any failure of the pipework system leading to a leak. Pitting corrosion of copper in drinking water systems is often categorized as Type I, II, or III but other types of localized corrosion are also known. However, there may be no strict limits between Type I and Type II pits; in relatively saline tap waters, corrosion pits showing traits of both types have been found. Only through proper investigation can the cause of pitting be identified, such as in the following sections.

3.07.3.4.1.1 Carbon film pitting

Carbon film pitting, also known as 'Type I' pitting, has been a frequent problem. An example of this in a copper tube from a domestic water supply is shown in **Figure 3** with the corrosion products removed from the main pit. The characteristics of the pits are hemispherical cavities with large crusts of corrosion products outside. The composition of the crusts is mainly basic cupric carbonates for example, malachite. Cuprous chloride and reddish cuprous oxide crystals may be found inside the cavity. The presence of $CaCO_3$ in the crust outside the cavity led Lucey[117] to propose a particular mechanism for this type of pitting. Contrary to conventional descriptions of the pitting processes, Lucey postulated that the cathodic reaction that is, the oxygen reduction, takes place at the crust of corrosion products which cover the cavity. The phenomenon was found to occur in organically pure, cold waters originating from deep wells and boreholes and was shown by Campbell[118] to be associated with residual films of carbon on the bore of the tubes. This carbon was caused by decomposition of residual drawing lubricant during bright (reducing atmosphere) annealing. It is therefore necessary for manufacturers to take steps to avoid these harmful residues. This type of pitting attack has been identified in many different countries[119] and may be assisted by iron-rich precipitates which can be present at the grain boundaries.[120,121] There is evidence that it could be inhibited by the presence of organic species in the water.[122]

This evidence has been corroborated in the United Kingdom by Campbell, who found failures due to this effect were confined to certain districts that is, supply waters. He showed that for many supply waters this pitting cannot proceed even in tubes containing carbonaceous cathodic films. He proposed that this is most probably due to the presence of small amounts of a naturally-occurring inhibitor in the water, probably an organic colloidal material, which stifles pitting of copper. Pipe failures therefore only occur in waters which contain little or none of this inhibitor.

Figure 3 Photograph showing carbon film pitting on a copper tube.

Pitting problems also occasionally occur in copper water cylinders[123] and, as a result of a study of this problem, Lucey[117] has made suggestions about the mechanism of pitting of copper in potable water supplies. Several suggested methods of avoiding pitting failures in copper cold-water tubes have been evaluated.[124–126]

3.07.3.4.1.2 Hot soft water pitting and Type II pitting

In hot water pipes, failures sometimes occur in certain areas supplied with soft waters from moorland gathering grounds. The waters concerned contain a few hundredths of a part per million of manganese, and in the course of several years' exposure, a deposit rich in manganese dioxide is laid down in the hottest parts of the system. This may cause pitting which could eventually lead to failure.

Hot-water pitting of another type, often referred to as 'Type II' pitting, is sometimes experienced in soft waters having high sulfate content in relation to the carbonate hardness and a relatively low pH value and it has been described by Mattson and Fredriksson.[127] The crusts covering these pits are less voluminous than Type I pits, the cavities are branching and they may be almost completely filled with black cuprous oxide. The occurrence of Type II pitting is associated with waters with pH ≤ 7 and low carbonate contents. A successful remedy has been to increase pH, introduce carbonate dosing to give a minimum of 70 mg HCO_3^- per liter, or reduce the water temperature to less than 60 °C.

3.07.3.4.1.3 Type III pitting

This type of pitting occurs in cold soft waters with a pH above 8.0 and it is geographically localized, being mainly confined to Sweden. It is generalized form of pitting where the pits are sparse[128,129]. Mattson[128] describes the phenomenon, noting its morphology and means of avoidance through a method involving bicarbonate dosing of the drinking water.

3.07.3.4.1.4 Electrochemistry of pitting

Drogowska *et al.*[130] have used solutions designed to mimic natural waters containing bicarbonate and chloride ions to study the anodic oxidation of copper and onset of pitting corrosion. They have found that,

as the anodic polarization of copper increases in this environment, a porous layer of Cu_2O initially forms on the metal surface. This is found to convert to basic $CuCO_3$ at more positive anodic potentials or in higher concentrations of HCO_3^- ions. A passivity breakdown potential is recorded at which pitting initiates, and this becomes more positive when HCO_3^- ions are present. The presence of Cl^- ions shifts the pitting potential to lower values, but the HCO_3^- ions are found to act to prevent this effect. Sulfate ions are found to have a very similar effect to chloride ions in lowering the breakdown potential[131] and pitting is found to be avoided if the pH $\geq$ 7.4 and the $[HCO_3^-]/[SO_4^{2-}]$ ratio is $\geq$1. The effect of increasing the solution temperature to 60 °C is found to give improvement to the passivity of the oxide film.[132] Two new international standards have been produced which give guidance on corrosion prevention in water distribution and storage systems.[133]

3.07.3.4.2 Chemical attack

Joining copper should be accomplished according to recommended practice to avoid corrosion issues. Copper pipework installations are joined using capillary attraction of solder or braze material or by mechanical means.

In the case of capillary joints, fittings, or in some cases specifically formed tube ends, are used to form an annular capillary gap into which molten solder or braze is run. Fluxes containing chlorides have to be used when soldering. The chlorides act to remove surface oxide and reduce the surface tension, allowing the solder to be drawn into the capillary gap. Excessive use of flux can lead to its retention in the pipework and attack by the chloride ions present. This will normally take place in the first few months after installation. An example of this is shown in **Figure 4**. Over longer periods when the active elements of the flux are exhausted, the presence of residue can lead to deposit attack. In both of these cases, pitting corrosion and failure of the tube can result. Good installation practice which ensures complete removal of any flux residue by washing (as given by BS 6700:1997) will prevent this type of corrosion. Capillary joints formed using copper/phosphorus, copper/silver/phosphorus, or silver brazing alloys do not need flux and therefore cannot suffer this type of attack.

3.07.3.4.3 Microbiologically influenced corrosion

Microbiologically influenced corrosion (MIC), describes a form of pitting considered to be due to the action of microbes. This form of corrosion of metals has been known for many years, for instance in the oil industry, and an early description of its occurrence with copper alloys was given by Rogers in 1948.[134] In some instances, MIC has been associated with soft water which is high in organic content which has been allowed to maintain temperatures in the region of 20–30 °C under low velocity conditions. In such circumstances, the resulting warm high concentration of organic material at the bottom of horizontal tubes provides ideal conditions for MIC to take place.[135] Other circumstances with a different water quality have been described by Wagner *et al.*[136] However, the exact MIC mechanism has not been elaborated. The general view is that a region of low pH is created under a biofilm containing polysaccharides and that the organic materials present provide transport for the metal ions to the liquid phase.[137]

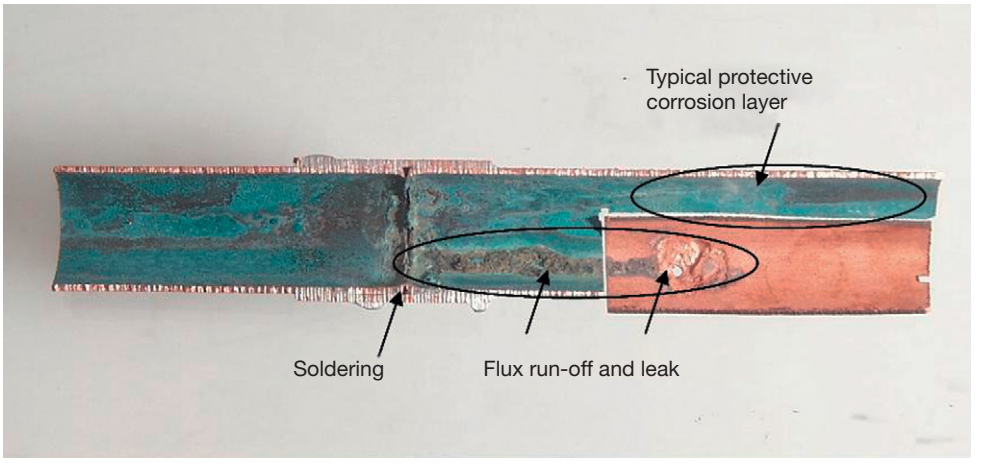

Figure 4 Photograph showing flux attack on a soldered copper tube.

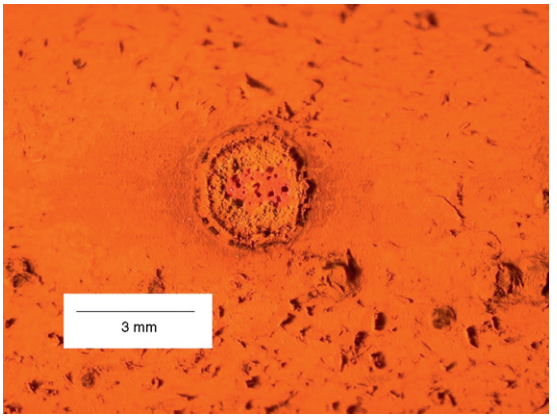

Figure 5 Optical micrograph showing an example of the typical pit morphology found in MIC.

Figure 6 Photograph showing longitudinal stress corrosion cracking of a 15 mm diameter copper tube (EN 1057, R250, half-hard condition).

MIC of copper water pipes in institutional buildings has been reported in several countries. The results of research, leading to remedial measures, have been summarized by Geesey.[138]

An example of this type of corrosion associated with soft high organic content water is shown in Figure 5. Avoidance entails operating the system at correct temperatures and flow rates as well as providing water with a low organic burden and with the implementation of appropriate disinfection measures.

3.07.3.4.4 Stress corrosion cracking

Stress corrosion cracking (SCC) may occur with brass fittings (see Section 3.07.3.6.1) due to traces of ammonia in the environment or arising from nitrates in the water. In certain rare instances, copper tubes are known to suffer SCC, an example of which is shown in Figure 6. In the great majority of cases of stress corrosion encountered, traces of ammonia have been found in the cracks.

3.07.3.4.5 Dissolution

The corrosion of copper in contact with drinking water soon reduces to a very low rate due to the formation of stable scale. However, some waters continuously dissolve appreciable amounts of copper.[139–141] Factors which favor this action are waters with low pH and low total dissolved solids. Therefore, most dissolution is found in hot, soft, acid waters. Desalination plants will produce such an aggressive water and unless treated to increase its mineral content this water should not be used with copper. This type of corrosion is general and the resulting pipe wall thinning is so slight that the useful life of the pipe or component is virtually unaffected unless impingement attack occurs. A few very hard waters can also give rise to copper dissolution. Research has indicated that the difference between a scale forming water (with a resulting low copper dissolution rate) and a 'dissolving' hard water appears to be organic content.[142]

High levels of copper complexed with organic material gives the water a distinctive blue color, and is hence given the term 'blue water corrosion.' It tends to be confined to soft, unstable water types and, to date, appears to be confined to Australia and New Zealand. This form of dissolution has been found to be due to microorganisms[143] and restoring the disinfection agent (e.g., free chlorine) to its desired level will stop the effect and prevent the occurrence of further episodes.

A review of the current state of knowledge on dissolution in drinking water has been prepared by Merkel and Pehkonen.[144] In considering copper dissolution, this paper subdivides general copper corrosion into the subprocesses (oxidation, scale formation, and scale dissolution) enabling a better understanding of the influence of water quality parameters and operating conditions on copper release. This work also considers that research needs to be carried out to distinguish between organic components which promote or reduce the dissolution process.

Once copper has been dissolved, it may then lead to problems downstream. For instance, the dissolved copper can (1) plate out and cause galvanic corrosion on other products such as zinc-coated steel,[145] light alloys,[146] or bare steel and (2) cause blue–green staining in baths, sinks, and sometimes clothes or hair due

to the combination of copper with stearates in soaps and shampoos.

The World Health Organization (WHO) Guidelines for Drinking Water Quality 1993[147] notes that copper is an essential element necessary for human health and that in most parts of the world deficiency was a problem. However, it was decided that setting an upper limit for the allowable concentration was necessary. Following this guideline, many countries have regulated the maximum weekly average of drinking water to 2 mg Cu per liter. Araya *et al.*[148] showed that the likely taste level for copper in drinking water was 4 mg l^{-1} or above for 95% of the population.

In deaerated conditions, for instance, in most central heating systems, little attack on copper occurs.[149–151] Further reference to the subject of copper in water can be found in an extensive review by Grunau.[152]

3.07.3.5 Corrosion in Seawater

Copper alloys have had an extensive history of use in a wide range of marine applications[9,153] due to their advantageous properties with respect to corrosion and biofouling resistance, conductivity, and ease of fabrication.

Exposure tests of various copper alloys have been carried out in natural seawater by the UK Ministry of Defence laboratories.[154] Weight loss measurements were used to measure general corrosion rates, crevice corrosion rates, and erosion/corrosion flow velocity limits. The results are shown in **Table 7**, although some anomalies have been reported for the dta as presented[75]. It was found that the brasses exhibited the highest corrosion rates and the alloys most resistant to corrosion and erosion/corrosion were the cupronickels.

Regarding practical applications of copper alloys in seawater, a major example is their use for condensers and heat exchangers, which has been long established. Recent reviews have considered potential corrosion in this application, the likely causes and remediation procedures.[76,155–157] Specific aspects covered include the effects of surface films, the commissioning process, stagnant conditions, flow velocity, ferrous sulfate treatment, and cleaning techniques. The latter may lead to greater corrosion, though ferrous sulfate treatment can offset the effect. Chlorination can cause increased attack in some circumstances, aluminum brass being more susceptible to attack than cupronickels. The presence of sulfide contamination causes serious corrosion if polluted and aerated conditions alternate, or if oxygen and sulfide are simultaneously present.

Corrosion of condenser tubes was a problem of great magnitude during the first quarter of the twentieth century. In those times, 70–30 brass condenser tubes failed by dezincification and Admiralty brass (70Cu–29Zn–1Sn) was brought into use. This proved little better, but some time later the addition of arsenic was found to inhibit dezincification. Failures of Admiralty brass by impingement attack became a serious problem, particularly as cooling water speeds increased with the development of the steam turbine. The introduction of alloys resistant to impingement attack was a great step forward and immediately reduced the incidences of failure. A history of condenser tubes up to 1950 has been published by Gilbert.[158]

The alloys most commonly employed today are cupronickels,[159] containing appropriate iron and manganese levels and aluminum brass (76Cu–22Zn–2Al–0.04As). Three cupronickel alloys are in widespread use and these are: (1) 30Ni–0.7Fe–0.7Mn, (2) 30Ni–2Fe–2Mn, and (3) 10Ni–1.5Fe–1 Mn. These materials are extensively and successfully applied in ships, power stations, oil refineries, desalination plants, etc., in condensers and heat exchangers, with limitations on water flow velocities, sometimes with much entrained air present. At the highest water flow velocities, there is a rather greater factor of safety with 70–30 cupronickel. The 30Ni–0.7Fe–0.7Mn variant is usually to be preferred under most polluted water conditions.

A number of studies have been carried out on the reasons for the high seawater corrosion resistance of cupronickels. In 70–30, a nickel-rich zone is formed in the oxide layer at the metal surface.[160] This acts to anodically protect the matrix from further corrosion. If the film develops defects, which may be caused by prior deformation of the metal,[161] then corrosion initially accelerates in those areas, but quickly diminishes, resulting in a smooth overall surface.

The occasional failures which still occur in condenser tubes are usually due to one (or sometimes several) of the following factors:

1. Localized attack or pitting in badly contaminated waters.
2. Pitting under decaying barnacles, shell fish, or other deposits.
3. Impingement attack due to high local water velocities, e.g., at partial obstructions in a tube such as barnacles or *Hydra*.

4. Erosion due to sand or other abrasive particles suspended in the water.
5. Use of tubes of the wrong alloy, or of incorrect composition or which contain manufacturing defects.
6. Poor welding techniques causing welds to protrude into the flow.

The material most commonly used when suspended abrasive matter is a problem is the 30% Ni alloy containing 2% each of Fe and Mn.[156,157]

A difficult condenser-tube corrosion problem arises from the use of polluted cooling waters from harbors and estuaries, which may be severely contaminated, particularly when warmer climates are involved.[162] Many condenser-tube materials are liable to suffer corrosion in these circumstances, and the choice of materials is made difficult by the fact that different orders of merit apply at different locations and even at the same location at different times. The state of the water when the tubes are commissioned and first enter service, which influences the type of surface film formed, may well determine whether or not a satisfactory service life will be obtained.[159,163] Full salinity seawater, free from sulfides, is reported to be the most effective passivating medium[162] although the 14–60 days which this takes to complete may put it at a lower ranking than other methods, particularly those involving dosing with ferrous sulfate[76].

In power plants, the condenser tubes must be able to withstand corrosive cooling waters and complex boiler water treatments. Also, the use of recirculating water can cause dissolved salts to concentrate between twice and eight times the initial concentration, making the water significantly more aggressive.[164] Corrosion of power-station condenser tubes by polluted waters was at one time particularly troublesome in Japan. Improved results have been reported using tin brasses or special tin bronzes.[165] Elsewhere, pretreatments have been investigated with mixed success[76,166] and sodium dimethyldithiocarbamate is reported to give protective films which will withstand the action of polluted waters[167] and has had some naval use.[76]

Methods of maintaining tube cleanliness include chlorination and mechanical methods such as water lancing and the use of the Taprogge system of circulating sponge-rubber balls.[157] Hot acid is now not environmentally acceptable and the use of commercial descaling agents invariably results in the near complete loss of the passive surface layers on the material.[168] Thus, it is recommended that, after their use, a period of 3 weeks or more should be imposed during which natural seawater is allowed to flow through the system to restore passivity.

Condenser tube-plates of naval brass usually undergo some dezincification in seawater service, but this is normally not serious in view of the thickness of the metal involved. Use has been made of tube-plates of more resistant materials such as aluminum bronze, or cupronickel. Plates that are too large to be rolled in one piece can be fabricated by welding together two or more items. In some special applications, the tubes are fusion welded or explosively welded to the tube plates. Fusion welding operations are rather more difficult with brasses than with other copper alloys due to the evolution of zinc fume during the process.

Condenser water-boxes were at one time made of unprotected (or poorly protected) cast iron and these afforded a measure of cathodic protection to the tube plates and tube ends. This beneficial effect has been lost with the general adoption of water-boxes which are completely coated with rubber or some other impervious layer, or which are made from resistant materials such as gunmetal, aluminum–bronze, or cupronickel. Steel water-boxes which are clad with cupronickel are also used. To prevent attack on tube-plates and tube-ends in these circumstances, either a suitable applied-current cathodic protection system can be applied or sacrificial soft-iron or mild-steel anodes can be installed, the required protection voltage being fairly low (50 mV minimum).[169] Ferrous wastage plates have the additional advantage that the iron corrosion products introduced into the cooling water assist in the development of good protective films throughout the length of the tubes. This is particularly important in the case of aluminum–brass tubes; indeed, with such tubes it may be desirable, as an additional preventative measure, to add a suitable soluble iron salt (such as ferrous sulfate) regularly to the cooling water.

As it has become increasingly necessary to supplement natural sources of freshwater in various parts of the world, processes for producing freshwater from seawater have been intensively studied. Distillation is one method widely used and, during recent years, large numbers of multistage flash-distillation plants have been installed in various countries particularly in the Middle East. Many of the larger flash-distillation units are capable of producing several millions of gallons of freshwater per day. In these plants, seawater passes through horizontally disposed tubes and steam, which is 'flashed' from the brine, condenses

on the outside. In some parts of the plant, the conditions are similar to those in steam condensers, but in other parts the seawater has been treated to remove dissolved gases and is at much higher temperatures. Copper alloy tubes are used in large numbers for the heat exchange units in this type of desalination plant,[170,171] these being mainly aluminum–brass and the various cupronickel alloys.

For cooling-water trunking and saltwater services in the engine room and elsewhere, including fire mains, plumbing, and air-conditioning systems in ships, more resistant alloys are taking the place of copper or galvanized steel. The latter were formerly extensively employed, but they do not have adequate resistance to attack by seawater. Cu–10Ni–1.5Fe alloy has been widely utilized and normally gives excellent service. In some special naval applications, pipelines of 70–30 cupronickel are used and it has been found that adequate attention must be given to correct fabrication and installation techniques. Carbonaceous residues from fillers used in bending operations must be avoided or pitting corrosion may occur in service. Jointing materials of low corrosion resistance should not be used, silver brazing or appropriate welding methods being the correct techniques. Residual stresses, if present, can cause stress-corrosion failures of aluminum–brass pipelines in service.

Copper alloys in wrought or cast form are employed for other purposes in ships and marine installations, such as for propellers, bearings, valves, and pumps. For instance, aluminum–brass is used for heating coils in tankers carrying crude oil or petroleum products. However, some corrosion problems encountered in this and other applications on board ship have been described by Gilbert and Jenner.[172]

Cupronickels have been shown to possess extremely low long-term corrosion rates in quiet or slowly-moving seawater. The 90–10 alloy is of particular interest[28,163]: this alloy is now well established for use for pipelines on ships and it has become widely used for piping systems on floating production, storage and offloading vessels (FPSO's), and offshore platforms. In addition to its good corrosion resistance, 90–10 cupronickel has a high resistance to marine macrofouling providing that it is not cathodically protected. This has led to applications such as the construction or sheathing of ships' hulls, fish cages for aquaculture and cladding of steel offshore structures in the tidal/splash zones.[9]

Investigations into the effects of arsenic and phosphorus in single phase brasses on their susceptibility to intergranular attack and SCC in seawater have shown that the normal additions of arsenic to inhibit dezincification (~0.04%) have no significant adverse effect. Other possible consequences of exposing copper alloys to seawater which have been investigated included dealloying of aluminum bronzes[109] and the effects at bimetallic contacts.

Major efforts have been made to understand the nature of films formed on copper alloys in natural seawater. These films have quite different characteristics to those formed in sodium chloride solution, the differences being associated with the presence of organic material in the natural environment. However, the structure of the films is affected by variables such as water velocity, temperature, and oxygen content. Protective films often have a multilayered structure,[157] with an outer layer rich in iron providing impingement resistance and an inner layer giving chemical/electrochemical protection. With aluminum brass, a colloidal mixed hydroxide inner layer provides a buffering action, with tin-containing brass there is a tin-rich layer near the copper surface[173] and, with cupronickel, there is a chloride-rich layer which strongly inhibits the cathodic reaction. A study on Cu–Si alloys in seawater has found that the formation of copper silicide at the alloy surface acts to prevent corrosion.[174]

3.07.3.6 Effect of Exposure to Contaminated Environments

As with many metallic materials, failure of copper alloys may occur by cracking due to the combined influence of tensile stress and exposure to a debilitating environment due to the presence of a contaminant. Failures of brass components due to this form of stress corrosion cracking have been known for many years[175] and has been termed *season cracking*. In this case, the stresses in the material are produced in components during their manufacture and the contaminant is ammonia vapor produced by the natural decay of organic matter.

Only certain specific environments appear to produce stress corrosion of copper alloys, most notably ammonia,[176–178] ammonium compounds, or amines. Interestingly, pure copper does not suffer from ammonia-induced stress corrosion but will display the phenomenon in the presence of nitrites.[179] Stress corrosion can also occur with moist sulfur dioxide, sulfites, and some organic acids.[180] Mercury or solutions of mercury salts (which cause deposition of mercury), or other molten metals will also cause cracking, but the mechanism is undoubtedly

different.[181] Cracks produced by mercury are always intergranular, but ammonia, according to the exact conditions, may produce cracks which are fully transgranular, fully intergranular, or a mixture of both. As an illustration of this, Edmunds[182] found that mercury would not produce cracking in a stressed single crystal of brass, whereas ammonia could do so.

In certain circumstances, corrosion of copper alloys can occur through seemingly random interconnected microtunnels which spread out into the metal from what appears to be only a discoloration of the surface film. As a result of this phenomenon, through-thickness perforation of tube can result in weeks or months. This type of corrosion has been termed formicary corrosion due to its morphological similarity to an ants nest. Elliott[183] has produced a summary of knowledge of formicary corrosion up to 1999. The cause has been ascribed to contamination of the outside of the tube by carboxylic acids.

3.07.3.6.1 Stress corrosion of brasses

Brasses containing only a few percent of zinc may crack under load if the stresses are high and the environment is sufficiently corrosive and most types of brass appear to be susceptible to the occurrence of this phenomenon of stress corrosion. An investigation of the effect of additions to 70–30 brass has been carried out by Wilson *et al.*,[184] who found that an addition of ~1% Si was markedly beneficial. Other additions were beneficial under some circumstances but none of the 36 additions tested accelerated stress-corrosion cracking. Further results have been given in later papers.[185,186]

In general, the susceptibility to stress corrosion in brasses appears to rise with an increase of zinc content, but in some circumstances alloys containing 64–65% Cu were found to be rather more affected than those containing 60% Cu.[187]

Many workers[188–193] have investigated the residual stresses introduced by different working processes in brasses of various compositions and the annealing treatments necessary to remove these stresses or reduce them to a safe level. A 'stress-relief anneal' at ~300 °C will usually lower internal stresses to comparatively small values without much effect on hardness of the material.

Specifications for brass products customarily include the provision for carrying out a mercurous nitrate test[194,195] (EN ISO 196:1995) to ensure that unduly high residual tensile stresses are not present, but a satisfactory result in this test does not guarantee freedom from cracking in environments containing ammonia. More searching tests involving exposure to ammonia have therefore been devised, such as ISO 6957:1988. The standardization of stress-corrosion cracking tests and their correlation with service experience have been the subject of several papers.[196–200] A European standard for the assessment of susceptibility to SCC was published in 2006: EN 14977, Copper and copper alloys – detection of tensile stress – 5% ammonia test. Many authors[201–205] have described practical cases of stress-corrosion cracking usually involving tensile stresses applied in service. Two possible preventive measures are the use of coatings[206–208] or inhibitors.[209]

The behavior of a wide range of α, α–β, and β brasses in various corrosive environments was studied by Voce and Bailey and their results have been summarized by Whitaker.[210] Penetration by mercury and by molten solder was found to be intergranular in all three types of brass. In moist ammoniacal atmospheres, the penetration of unstressed brasses of all types was intergranular. Internal applied stresses accelerated the intergranular penetration of α brasses and initiated some transgranular cracking. It also caused severe transgranular cracking of β alloys and transgranular cracking across the β regions in the two-phase brasses. Immersion in ammonia solution, however, caused intergranular cracking of stressed β brasses. β brasses containing 3% or more aluminum failed with an intergranular fracture when stressed at ~0.1% proof stress in air. The behavior of alloys of this type was subsequently studied by Perryman[211] and Bailey[212] who showed that cracking in air occurs only when moisture is present. It has been confirmed that β brasses are prone to crack in service.[213]

High-strength α–β brasses containing up to ~5% Al (with small amounts of Fe, Mn, Sn, etc.) used for propellers, parts of pumps, nuts and bolts, and similar applications usually give good service but occasionally suffer intergranular failure, for instance in contact with seawater. Examination of such failures usually reveals thin dezincified layers along the cracks, but it is often difficult to decide whether the crack or the dezincification occurred first.

The theoretical aspects of stress-corrosion cracking have attracted much attention in recent years. Among the copper alloys, the behavior of brasses in ammoniacal environments has been most studied. While cracking has been shown to be possible in contact with some other corrosive agents, ammonia has the most powerful effect. Evans[214] suggests that

this is because ammonia is a feeble corrodent which produces little attack except at regions such as grain boundaries or other lattice imperfections. Also, it prevents accumulation of copper ions in the crevices formed owing to the formation of stable complexes such as $Cu[(NH_3)_4]^{2+}$. The mode of cracking (intergranular or transgranular) can be affected by changes in composition of the brass or by changes in the nature of the environment.[215] Mattsson[216] found that, on immersion in ammoniacal solutions of different pH values, stressed brasses cracked most rapidly at pH 7.1–7.3 and that in this range black surface films formed on the metal. The role of tarnish films has been further studied subsequently.[217–219] Many authors have studied electrochemical[220–235] or metallurgical[236–241] aspects of the stress corrosion of copper alloys and discussed theories of the mechanism. Papers on the subject have been included in several symposia or conferences on stress corrosion of metals.[242–244] The stress cracking of brasses has been reviewed by Bailey[245] and other workers[246–254] and reviews of stress corrosion as a general subject have also been published.[255–257]

3.07.3.6.2 Stress corrosion of other copper alloys

Evidence indicates that pure copper is not likely to be susceptible to stress corrosion[258–260] but instances of the failure of copper are known, when it contains 0.4% As[261] or 0.02% P.[258] SCC has also been found to occur in copper–beryllium,[262] copper–manganese,[263–265] aluminum–bronzes,[266,267] tin–bronzes, silicon–bronzes, nickel silvers,[268] and cupronickels.[268,269] Most of these alloys are much less susceptible to cracking than brasses,[270] although under some conditions aluminum–bronzes can be particularly prone to cracking.[271] In ammoniacal environments, the cracking tends to be transgranular, and in steam atmospheres, intergranular cracking is favored.[272] Additions of 0.35% Sn or Ag are claimed to be effective in preventing intergranular cracking.[273,274] Aluminum–bronzes containing 2% Ni and 0.5–0.75% Si are claimed to have good resistance to stress corrosion,[273,275] although there is evidence that silicon bronzes can show accelerated intergranular fracture in the presence of moist air.

Thompson and Tracy[258] carried out tests in a moist ammoniacal atmosphere on stressed binary copper alloys containing zinc, phosphorus, arsenic, silicon, nickel, or aluminum. All these elements gave alloys susceptibility to stress corrosion. In the case of zinc, the failure time decreased steadily with increase of zinc content, but with most other elements there was a minimum in the curve of concentration of alloying elements against time to failure. In tests carried out under a static load of 70 MN m^{-2}, these minima were found to occur at concentration levels of ~0.2% P, 0.2% As, 1% Si, 5% Ni, and 1% Al. In most cases, the cracking was observed to be intergranular.

A series of slow strain rate tests have been carried out on high strength Cu–Ni–Al alloys in environments which could be encountered by the offshore oil and gas industry[276] and these have found that the application of a cathodic potential (as applied in cathodic protection) gives protection against stress corrosion. However, molybdenum disulfide greases mixed with seawater and greases containing bentone were found to promote stress corrosion as did the more well known debilitating species such as amines. Work on relating the microstructural aspects of these alloys to their possible susceptibility to stress corrosion has identified[277] that the production process should be undertaken in such a way that the presence of iron-rich phases on the grain boundaries is restricted, the material has a fine grain size and that it is supplied in an under-aged condition.

Cupronickels (90–10 and 70–30) have generally been considered immune to sulfide stress corrosion in most seawater environments.[9] However, there have been recent trials[278] in seawater containing severe sulfide levels of 100–1000 ppm which indicate a cracking possibility for the 90–10 alloy.

A related debilitating effect to stress corrosion cracking is hydrogen embrittlement, and it is interesting to note that copper alloys have not been reported to suffer from this phenomenon. In particular, testing has demonstrated that high strength Cu–Ni–Al and Cu–Ni–Sn alloys do not embrittle under hydrogen charging conditions[277] whereas nickel alloys containing copper and aluminum (Ni–Cu–Al) lose ductility under the same conditions. Detailed electrochemical work carried out by Pound[279] allowed him to suggest that this is because the internal hydrogen becomes associated with both reversible and irreversible trap sites. He postulates that the trap sites in a Cu–Ni–Al alloy are measurably more reversible than those in Ni–Cu–Al, preventing the former from being susceptible to hydrogen embrittlement.

3.07.3.7 Corrosion in Industrial Chemicals

A number of publications are available which give detailed information on the action of a wide range of chemicals on copper and copper alloys.[280–285]

When contemplating the use of copper-based materials for industrial purposes it is necessary to bear in mind that, even though a satisfactory life of the component may be obtained, possible difficulties may arise from the following other causes:

1. Copper compounds can be tolerated only in small amounts in potable waters or food substances. The WHO current safe concentration limit for copper in drinking water of 2.0 mg l^{-1}.
2. Copper compounds are highly colored, and a very small amount of corrosion may lead to staining and discoloration of products.
3. Stimulation of the corrosion of vital parts made of more anodic metals may occur if they are connected to copper.
4. Very small amounts of copper taken into solution may cause considerable corrosion of more anodic metals elsewhere in the system, particularly zinc,[145] aluminum,[146] and sometimes steel.[286] Small particles of copper deposited from solution set up local cells which can cause rapid pitting.

Despite these qualifications, copper and its alloys are used extensively and successfully in many types of chemical production equipment. Uses include condensers and evaporators, pipelines, pumps, fans, vacuum pans, and fractionating columns. Tin–bronzes, aluminum–bronzes, silicon–bronzes, and cupronickels are used in some circumstances because they present better corrosion resistance than copper or brasses.

3.07.3.7.1 Acid solutions

Copper does not normally displace hydrogen, even from acid solutions, and it is therefore virtually unattacked in nonoxidizing conditions. For strongly reducing conditions in the temperature range 300–400 °C, corrosion resistance is comparable, if not better, than stainless steel. However, when copper alloys come into contact with most solutions, which invariably contain dissolved air, cathodic depolarization can occur which increases the chances that corrosion will take place.[287] Therefore, it is difficult to lay down any general recommendations for the use of copper in acid solutions, since the rate of attack significantly depends on the particular circumstances. Under fairly mild conditions copper or copper alloys are successfully used for handling solutions of hydrofluoric,[280,288,289] hydrochloric,[280,290] sulfuric,[291] phosphoric,[280,292] acetic, and other fatty acids.[280,293] Rates of corrosion, in general, increase with concentration of acid, temperature, amount of aeration,[294,295] and speed of flow.[296] Tin–bronzes, aluminum–bronzes,[297–299] silicon–bronzes, and cupronickels are among the copper alloys most resistant to acids. For instance, aluminum bronze will withstand 50% sulfuric acid at 120 °C and 60% sulfuric acid at 30 °C. Silicon bronze is resistant to hydrochloric acid over the range 10% HCl at 70 °C/20% HCl at 50 °C/35% HCl at 15 °C. Brasses should not normally be used in acids. All copper-based materials are attacked rapidly by oxidizing acids such as nitric acid, strong sulfuric acid, or chromic acid (including dichromates) and also by hydrocyanic acid. The maximum temperature of operation of copper in dry HCl is 93 °C and in dry chlorine it is 200 °C.

The dissolution of copper and brasses in acid solutions has been studied by several authors.[300–305] In sulfuric acid, pitting attack has been found to occur in 95% sulfuric acid at 50 °C, in 80% sulfuric acid at 70 °C, and in 60% sulfuric acid at 100 °C. Various substances have been found to have an inhibiting effect on the rate of attack of copper or brasses in nitric acid[306–310] and in hydrochloric acid.[311]

3.07.3.7.2 Neutral and alkaline solutions

Copper-based materials are resistant to alkaline solutions over a wide range of conditions,[312] but may be appreciably attacked by strong solutions, particularly if hot. Cupronickel alloys usually give the best results in alkaline solutions. Copper and its alloys should be avoided if ammonia, ammonium compounds, or organic amines are present[313–317] owing to the danger of both general corrosion and stress corrosion.

Copper is satisfactory for handling solutions of most neutral salts[280,318] unless aeration and turbulence are excessive. All exception is provided by those salts that form complexes with copper, such as cyanides, and solutions containing oxidizing agents, such as ferric or stannic compounds.

3.07.3.7.3 Hydrogen sulfide pollution

Polluted and stagnant waters can be a source of corrosion to copper alloys because of the metal reaction with hydrogen sulfide to form sulfide surface films. Higher corrosion rates and pitting corrosion can result because the films do not provide the same protection as those normally formed. Sources of hydrogen sulfide include industrial waste, decomposition of organic matter, and sulfate reducing bacteria.

When there is little or no oxygen present in the system, then the corrosion rate of copper alloys with a sulfide film is only slightly higher than in aerated seawater.[319] However, when aerated seawater mixes with sulfide-containing seawater, higher rates of

corrosion can occur. Such corrosion is also velocity sensitive and is found to be more pronounced in regions of highest flow velocity.

A sulfide film can gradually be replaced by an oxide film in seawater during subsequent exposure to aerated conditions,[9,162] although this may take several days and high corrosion rates can be expected in the interim. However, if an established cuprous oxide film is already present, then periodic exposure to polluted water can be tolerated without damage to the film. Therefore, exposure to sulfides should be restricted wherever possible and this should be particularly so during commissioning and during the first few months of exposure to seawater, during which time the oxide film is maturing. Typical guidelines for commissioning or shut down/standby of copper alloy piping systems are given in **Table 8**.

The addition of ferrous ions to seawater systems, usually as a result of dosing with ferrous sulfate or by the use of a stimulated iron anode, has been found to improve the corrosion resistance of aluminum brass and cupronickels when exposure to polluted conditions are anticipated.[76] Other pretreatments have been investigated with variable success.[76,166]

The common cast alloys used for seawater systems are gunmetals, high tin bronzes, and nickel aluminum bronze. In clean water, nickel aluminum bronze is the favored alloy for pumps and valves[319] but 10% tin bronzes can be better in mildly polluted conditions, particularly for erosion resistance.

Francis has reported[319] that the presence of sulfides can reduce the temperature above which hot spot corrosion can be found in heat exchangers from ~130 °C down to 80 °C. This type of attack is caused by thermogalvanic effects under slow flow or stagnant conditions. Cupronickel (70–30) is the most susceptible alloy for hot spot corrosion and aluminum brass is the most resistant. Again, ferrous sulfate dosing, or higher flow rates, can provide improved resistance.

A microstructural study of the behavior of high strength Cu–Ni–Al alloy toward aqueous H_2S has been carried out using STEM and SEM surface analysis.[320] The morphology of the surface is shown in **Figure 7** together with a schematic diagram derived from microanalysis explaining the chemical composition of the various corrosion product layers formed. It was concluded that the large copper sulfide crystals were deposited on the surface following preferential corrosion of copper from the alloy surface. The general corrosion rate was about three times lower than that of 70–30 cupronickel as a result of the formation of an aluminum-rich oxide layer directly at the solid/solution interface.

3.07.3.7.4 Other chemicals

Copper and copper alloys are unsuitable in hydrogen peroxide[279,321] or molten sulfur.[279,322] Halogens have little action on copper at room temperature when dry, but are corrosive when wet. Hypochlorite solutions are corrosive.[323] Most organic compounds are without appreciable action,[279] although contact with moist acetylene should be avoided, as explosive compounds are formed. Moisture also accelerates

Table 8 Guidelines for shutdown and standby conditions of a copper alloy piping system in order to avoid possible problems caused by the presence of sulfides

Conditions in the system		
Duration	***Clean seawater or freshwater without deposits***	***Polluted seawater or freshwater where deposits are present***
4–6 days	Keep the system filled	Commissioned system: • Avoid high flow rates • If possible, drain the system and fill with clean seawater or freshwater New system: • Clean the system and fill with clean seawater or freshwater.
>4–6 days	Keep the system filled and replace the water by oxygenated water every 2–3 days	Possibility I: • Clean the system and fill with clean seawater or freshwater • Replace the water by oxygenated clean water every 2–3 days. Possibility II: • Clean the system and keep it dry.

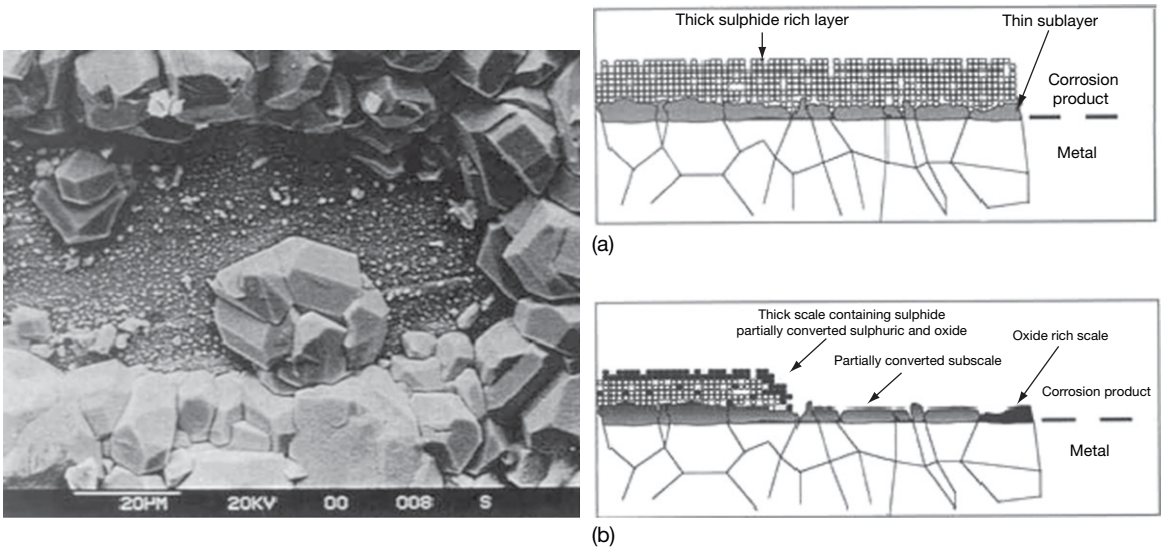

Figure 7 Scanning electron image and schematic diagram of Cu–Ni–Al surface after exposure to saturated aqueous H_2S at 25 °C.

attack by halogenated organic compounds, particularly carbon tetrachloride and trichloroethylene, which hydrolyze to give traces of hydrochloric acid. Cupronickels show most resistance to these chemicals.

Copper alloys are widely used for handling hydrocarbon oils, although, if sulfur compounds are present, attack can be serious. The effects of synthetic detergents on copper have been investigated[324,325] and several authors[279,326–328] have discussed various aspects of the behavior of copper and its alloys in the food-processing industry, where direct contact with copper alloys can result in the alteration of taste or color.

3.07.3.8 High Temperature Oxidation and Scaling

Several authors have reviewed the literature on the oxidation and scaling of metals, including copper.[329–332]

3.07.3.8.1 High temperature oxidation of copper

The volume ratio for cuprous oxide on copper is 1.7, so that an initially protective film is to be expected. Such a film must grow by a diffusion process and should obey a parabolic law. This has been found to apply for copper in many conditions, but other relationships have been noted. For instance, in the very early stages of oxidation, a linear growth law is found (e.g., at 1000 °C).[333]

At 180–290 °C, it has been determined[334] that the parabolic law first applies but, subsequently, this changes to a logarithmic relationship of the type shown in eqn [7]:

$$Y = K \log B(t + 1/B) \qquad [7]$$

B being a constant. However, other workers have reported a cubic relationship under some conditions. Evans[335,336] has shown how the effect of internal stresses in growing films may have various effects which can lead to any one of the three growth laws referred to above.

At medium and high temperatures[337–345] copper ultimately follows the parabolic law.[346] It has been shown using radioactive tracers[347,348] that the diffusion of copper ions in cuprous oxide is the rate-determining step at 800–1000 °C, and there is considerable evidence in favor of the view that metal ions move outwards through the film by means of vacant sites in the oxide lattice.[133]

When oxidation is a diffusion-controlled process, the oxidation rate should be related to the temperature by the Arrhenius relationship, eqn [8]:

$$K = A \exp(-Q/RT) \qquad [8]$$

where K is the rate constant, A a constant, R the gas constant, T the absolute temperature, and Q the activation energy. Values which have been obtained for A and Q are summarized by Tylecote,[349] Pilling and Bedworth,[350] Feitknecht,[351] and others

and give values of Q of ~0.17 MJ for temperatures of 700–1000 °C, while at lower temperatures (up to 500 °C) Vernon[352] and others have obtained values of about 85 kJ. These values are in agreement with calculations by Valensi,[353] based on the assumption that, at high temperatures, the oxidation proceeds by the reaction of oxygen with metallic copper to produce cuprous oxide while at lower temperatures the rate is determined by the reaction between oxygen and cuprous oxide to form cupric oxide.

At low temperatures (e.g., 300 °C) the film consists almost entirely of CuO. As the temperature increases, the film consists of a layer of Cu_2O beneath a layer of CuO, the proportion of Cu_2O increasing until, at high temperature, the film is almost entirely Cu_2O. The precise composition of the film depends, however, on a number of factors, including temperature, time, and oxygen concentration in the atmosphere. Tylecote[346] has investigated the composition, properties, and adherence of scales formed on various types of copper at temperatures between 400 and 900 °C. At the higher temperatures, the scales formed on copper containing phosphorus were more brittle and less adherent than those formed on copper containing no phosphorus.

Studies have been carried out on the effects at high temperature of sulfur[349] and of atmospheres containing hydrogen sulfide,[354–356] steam,[357,358] sulfur dioxide,[358] and hydrogen chloride.[358]

3.07.3.8.2 High temperature oxidation of copper alloys

In the case of copper alloys which contain elements which are more noble than copper, the resulting surface oxide will be substantially pure copper oxide as the oxides of the noble metals have higher dissociation pressures than the copper oxides. Conversely, for alloys containing baser metals, the alloying element will appear as an oxide in the scale often in greater concentration than in the alloy itself, and sometimes to the exclusion of copper oxides. The dissociation pressures of many oxides have been calculated by Lustman.[359]

Whether the rate of oxidation of an alloy of copper with a base metal is less or more than that of copper will depend on the concentration of the alloying element and the relative diffusion velocities of metal atoms or ions in the oxide layers. There is extensive literature on the oxidation behavior of copper alloys.[346,347,360–367] According to Wagner's theory[368–371] the rate of oxidation will be largely influenced by the electrical conductivity of the film and this theory is supported by the fact that the alloying elements giving maximum oxidation resistance to copper, that is, beryllium, aluminum, and magnesium, form oxides having very low conductivities, as shown by Price and Thomas.[372] Wagner calculated that when sufficient aluminum was present in copper to cause the formation of an alumina film, the oxidation rate should be decreased by a factor of more than 80 000. Experiment showed the factor to be only 36, but when Price and Thomas carried out initial oxidation under only slightly oxidizing conditions, producing only a film of alumina, the oxidation rate on subsequent exposure to full oxidizing conditions was decreased by a factor of ~240 000. Hallowes and Voce[358] found that selective oxidation of a 95Cu–5Al alloy by this method gave protection from atmospheric oxidation up to 800 °C unless the film was scratched or otherwise damaged, or the atmosphere contained sulfur dioxide or hydrogen chloride.

The effects on oxidation resistance of copper as a result of adding varying amounts of one or more of aluminum, beryllium, chromium, manganese, silicon, and zirconium are described in a number of papers.[360–367] Other authors have investigated the oxidation of copper–zinc[373,374] and cupronickel alloys,[374,375] the oxidation of copper and copper–gold alloys in carbon dioxide at 1000 °C[376] and the internal oxidation of various alloys.[377–379]

Copper alloys have been used extensively in high-pressure feed-water heaters in power generating plant.[380] Experience has shown that when such heaters are operated intermittently, 70Cu–30Ni or 80Cu–20Ni alloy tubes suffer fairly rapid and severe steam-side (external) oxidation with the formation of exfoliating scales. This corrosion, which may be associated with ingress of air during shutdowns, has been the subject of several published papers.[381–385] The behavior of other alloys for feed-water heater service has also been discussed.[380,386–388]

3.07.4 Protective Measures

The good corrosion behavior of copper and copper alloys is dependent upon correct choice of material, good design of equipment, and proper methods of operation. Brasses and bronzes may often be effectively protected by polishing followed by periodic waxing. If proper attention is given to these factors, there will usually be no need for protective measures. In special cases, however, for example, to prevent the dissolution of small amounts of copper or to maintain

a high-grade finish, metallic coatings of one or more of the following metals may be applied: tin, lead, nickel, silver, chromium, rhodium, or gold. In other cases painting, varnishing, or lacquering may be desirable, or if the conditions are very severe (as in some corrosive soils) heavier protection such as bituminous or plastic coatings may be necessary. Brasses that are liable to suffer dezincification or stress corrosion may need protection where other copper alloys would be satisfactory in an unprotected condition. Sometimes use is made of the principles of cathodic protection, for example, steel 'protector blocks' in condenser water-boxes.

In some circumstances, use of inhibitors may be a desirable remedial measure. For instance, benzotriazole (BTAH) has been found of considerable value for preventing staining and tarnishing of copper products.[389] The characteristics of the behavior seen indicate that an inhibiting film is formed by adsorption of neutral BTAH molecules on the copper surface followed by adsorption of a thin layer of copper BTAH in polymeric form. Also, a synergistic effect has been found when BTAH and iodide ions are used together to prevent copper corrosion in sulfuric acid.[390] Sodium diethyldithiocarbamate also has useful inhibiting properties.[391] Other types of inhibitors can be of value in condensate systems[392,393] and in acid solutions.[305–310] Reviews have been given of corrosion inhibitors for copper[394] and brasses.[395,396] The effects and efficiencies of various inhibitors continues to be the subject of much research.[397–400] Low concentrations (0.1 mM) of amino acids (glycine and cysteine) have been demonstrated to provide over 95% inhibition efficiency for 95–5 cupronickel corrosion.[401]

The danger of accelerated attack on copper-base materials due to coupling with other metals is small in many environments since copper is usually the cathodic member of the couple, but precautions are often necessary to prevent excessive corrosion of the anodic member. Surveys of the behavior of couples involving copper and copper alloys have been given.[319] Titanium, high nickel alloys, and super stainless steels can be sufficiently more noble than copper alloys in seawater environments to cause galvanic attack of the copper alloy and electrical isolation or insulated spool pieces may be required. This is less of a problem in chlorinated systems as prevention of the biofilm can reduce the efficiency of the cathode.[319,402] Another material that has been found capable of accelerating attack on copper in practice is graphite; hence graphitic paints or graphite in gasketing, etc., are undesirable. Occasionally the action between different copper-based materials may be appreciable particularly if the relative surface areas are unfavorable, for example, gunmetal may stimulate the corrosion of copper or brass in seawater and due care should be taken.

3.07.5 Areas of Future Development

3.07.5.1 Antimicrobial Benefits of Copper Corrosion

The formation of cuprous Cu^{+} and cupric ions Cu^{2+} has been described earlier. The ability of copper to gain and lose outer electrons is the source of many of copper's important physical properties such as high electrical and thermal conductivity, chemical stability, and its reddish color. Copper ions also play a crucial role in copper's antimicrobial action and the main hypotheses for the mode of actions in damaging the functionality of a cell of a microorganism are:

1. Their competing with and hindering uptake of major minerals such as sodium and potassium. This causes serious imbalances in the mineral composition of the cell of the microorganism.[403]
2. Their binding to proteins inside the cell which do not require copper, creating a dysfunction of that protein.[404,405]
3. Their causing oxidative damage, thereby damaging the cell wall and other cellular structures and finally causing bacterial cell death.[406]

Recent work[407–409] has shown the effectiveness of copper in inactivating pathogens such as *Escherichia coli*, Meticillin-resistant *Staphylococcus aureus* (MRSA), and *Influenza A* and in reducing environmental contamination in a clinical setting.[410,411]

3.07.5.2 Alloy Developments

Cupronickel alloys in particular are being developed for applications in seawater and oil and gas well environments. Copper nickel chrome (DEF STAN 02-824) cast components are beginning to replace those made from nickel aluminum bronze when long-term seawater corrosion resistance is required. This is due to the fact that, after 10 years of seawater service, only such components have been found to have lost only ~0.15 mm from their original thickness through corrosion, performing significantly better than cast nickel aluminum bronze under the same conditions.[412] Cu–Ni–Al and Cu–Ni–Sn alloys are

being developed as high strength corrosion resistant alloys for seawater applications requiring hydrogen-embrittlement-free, antigalling properties, and as alternative corrosion resistant, nonmagnetic bearing alloy to Be–Cu in directional oilfield drilling equipment.

Shape memory effect alloys have recently been under development for use in electronics and dentistry. Those based on Cu–Al and Cu–Ag–Al have been found to exhibit curious electrochemical effects during dissolution in alkali media if oxygen is present.[413] This has been explained in terms of fast preferential dissolution of aluminum followed by the slow transport of aluminate ions from the surface. This influences the formation of Cu_2O, which is the main corrosion reaction, such that an unusual oscillatory electro-potential effect is produced.

Acknowledgements

This section is comprised of a revised version of the chapter by P.T. Gilbert, which appeared in the previous edition. This, in turn, was based on 'Chemical Properties and Corrosion Resistance of Copper and Copper Alloys,' which formed Chapter XVIII of the American Chemical Society Monograph No. 122, '*The Science and Technology of the Metal its Alloys and Compounds*,' edited by Professor Allison Butts, and published by the Reinhold Publishing Corporation, New York, in 1954. Acknowledgement is hereby made to the Reinhold Publishing Corporation for permission to make derivations from this work. The revisions of the current chapter have also been contributed to by Peter Webster, Technical Consultant, and Angela Vessey, Director, Copper Development Association UK, Claes Taxén of KIMAB, Sweden and Rolf Sundberg of Västerås, Sweden, to whom further acknowledgements are given.

References

1. BSEN. *Copper and Copper Alloys – Ingots and Castings*, BSI: London, 1982.
2. CEN TC 133. CR 13388. *Copper and Copper Alloys – Compendium of composition and products*, BSI: London.
3. EN1652. *Specifications for Copper and Copper Alloys: Plate, sheet, strip and circles for general purposes*, EN 12163 *Rod*, EN12166 *Wire*, EN 12449 *Tubes*, EN12420 *Forgings*, BSI, London.
4. *Copper and Copper Alloys*; ASTM: Pittsburg, 2006.
5. A1322. *Standards Handbook for Wrought and Cast Copper and Copper Alloy Products*; Copper Development Association Inc., New York, 2003.
6. *Copper and Copper Alloys Compositions, Application and Properties*; Publication 120, Copper Development Association: UK, 2004.
7. *The Brasses-Properties and Applications*; Publication 117, Copper Development Association: UK, 2005.
8. DKI German Copper Institute Booklet: Copper nickel alloys; Properties, Processing, Application, DKI: Germany, 2000.
9. Powell, C. A.; Michels, H. T. *Cupronickel Alloys for seawater corrosion resistance and antifouling – a state of the art review*; Corrosion, NACE: Houston, 2000.
10. Powell, C. *Corr. Management.* **2005**, *63*, 8.
11. DEF-STAN 02-824. *Copper Nickel Chromium Sand Castings and Ingots*; UK Ministry of Defence, Abbey Wood: UK, 2002.
12. Gaffoglio, C. J. *Power Eng.* **1982**, 60.
13. Tuck, C. D. S.; Bendall, K. C.; Radford, G. W. J.; Campbell, S. A.; Grylls, R. J. Paper No. 78, Corrosion/96, NACE: Houston, 1996.
14. Ratka, J. O.; Maligas, M. N. Paper No. 04298, *Corrosion 2004*, NACE: Houston, 2004.
15. Ateya, B. G.; Elsayed, A. A.; Sayed, M. S. *J. Electrochem. Soc.* **1993**, *141*(1), 71–78.
16. Gatty, O.; Spooner, E. C. R. *Electrode Potential Behaviour of Corroding Metals in Aqueous Solutions*; Clarendon Press: Oxford, 1938.
17. Pourbaix, M. J. N. *Atlas of Electrochemical Equilibria in Aqueous Solutions*; Pergamon: Oxford, 1966.
18. Rubinic, L.; Markovic, T. *Werkst. Korrosion* **1959**, *16*, 666.
19. Hickling, A.; Taylor, D. *Trans. Faraday Soc.* **1948**.
20. Kuksina, O. Y.; Kondrashin, V. Y.; Mashakov, I. K. *Protec. Met. (Russia)* **2006**, *42*(2), 144.
21. Mayer, S. T.; Muller, R. H. *J. Electrochem. Soc.* **1992**, *139*(2), 426–434.
22. Kusina, O. Y.; Kondrashin, V. Y.; Marshakov, I. K. *Protect. Met. (Russia)* **2004**, *40*(6), 581.
23. Wilde, B. E.; Teterin, G. A. *Br. Corros. J.* **1967**, *2*, 125.
24. Mansfield, F.; Uhlig, H. H. *J. Electrochem. Soc.* **1970**, *117*, 427.
25. Varenko, E. S.; Galushko, V. P.; Kovtan, V. N.; Fedash, P. M.; Loshkarev, Y. M. *Zashchita Metallov* **1970**, *6*, 103.
26. Gavgahi, M.; Kaymaz, I.; Totik, Y.; Sadeler, R. *Corr. Rev.* **2002**, *20*(4–5), 403.
27. Virtanen, S.; Wojtas, H.; Schmuki, P.; Böhni, H. *J. Electrochem. Soc.* **1993**, *140*(10), 2786–2790.
28. Parvizi, M. S.; Aladjem, A.; Castle, J. E. *Int. Mater. Rev.* **1988**, *33*(4), 169.
29. Mathiyarasu, J.; Palaniswamy, N.; Muraldharan, V. S. *Corr. Rev.* **2000**, *18*(1), 65.
30. Badawy, W. A.; Ismail, K. M.; Fathi, A. M. *Electrochimica Acta* **2005**, *50*(18), 3603.
31. Vernon, W. H. J. *J. Inst. Met.* **1932**, *49*, 153.
32. Vernon, W. H. J.; Whitby, L. *J. Inst. Met.* **1929**, *42*, 181; **1932,** *44*, 389.
33. Vernon, W. H. J. *Trans. Faraday Soc.* **1931**, *27*, 255, 582.
34. Baumann, K.; Ruhrberg, U.; Kreysa, G. DECHEMA-Werkstoffe-Tabelle, 37th Supplement (Atmosphere), DECHEMA: Frankfurt, 1995.
35. Hudson, J. C. *Trans. Faraday Soc.* **1929**, *25*, 177; *J. Inst. Met.* **1930**, *44*, 409; *J. Birmingham Met. Soc.* **1934**, *14*, 331; *Met. Ind.* **1934**, *44*, 415; *J. Inst. Met.* **1935**, *56*, 91.
36. Tracy, A. W.; Thompson, D. H.; Freeman, J. R. *Special Technical Publication No. 175*; ASTM: Pittsburgh, 1955; pp 77–87.
37. Mattsson, E.; Holm, R. *Metal Corrosion in the Atmosphere*; STP 435; ASTM: Pittsburgh, 1968; p 187.
38. Scholes, I. R.; Jacob, W. R. *J. Inst. Met.* **1970**, *99*, 272.
39. Morcillo, M.; Almeida, E.; Marmcos, M.; Rosales, B. *Corrosion* **2001**, *57*(11), 967.

40. Thompson, D. H. *Metal Corrosion in the Atmosphere*; STP 435; ASTM: Pittsburgh, 1968; p 129, 199.
41. Holm, R.; Mattsson, E. *Atmospheric Corrosion of Metals*; STP 767; ASTM: Pittsburgh, 1982; p 85.
42. Ramos, A. C.; Camoes, M. F.; Mendonca, M. H.; Foneca, I. I. E. *Corr. Prot. Mater.* **2001**, *20*(4), 16.
43. Tracy, A. W. STP No. 175; ASTM: Pittsburgh, 1955; pp 67–76.
44. Tidblad, J.; Leygraf, C.; Kucera, V. *J. Electrochem. Soc.* **1991**, *138*(12), 3592–3598.
45. Eriksson, P.; Johansson, L.-G.; Strandberg, H. *J. Electrochem. Soc.* **1993**, *140*(1), 53–59.
46. Strandberg, H.; Johansson, L.-G. *J. Electrochem. Soc.* **1998**, *145*(4), 1093.
47. Knotkova, D. Proceedings of 12th International Corrosion Congress, Houston; NACE: Houston; Sept 1993; Vol. 2, p 51.
48. Laub, H. *Metallurgy* **1968**, *22*, 1116.
49. Veleve, L.; Luja, M. *Br. Corr. J.* **1999**, *34*(1), 34.
50. Hullman, H. Proceedings of UN ECE Workshop, Munich, May 2003; Swedish Corrosion Institute, Stockholm, 2003.
51. Priggemeyer, S. Report AZ 10730, *Deutsche Bundesstiftung Umwelt*; 1998.
52. Priggemeyer, S.; Priggemeyer, S. *Metallurgy* **1999**, *53*, 204.
53. Leuenberger-Minger, A. U.; Faller, M.; Richner, P. *Mat. Corr.* **2002**, *54*(3), 157.
54. UN ECE-Report. *Investigation of the Metal Run-off from Copper Surfaces exposed to Atmosphere*; Bulletin – Korrosions Institutet, 2003, ISSU 109E.
55. Odnevall Wallinder, I.; Leygraf, C. *J. Corr. Sci.* **1997**, *39*, 2039.
56. Bertling, S.; Odnevall Wallinder, I.; Berggren Kleja, D.; Leygraf, C. *Environ. Toxicol. Chem.* **2006**, *25*, 891.
57. Odnevall Wallinder, I.; Bahar, B.; Leygraf, C.; Tidblad, J. *J. Environ. Monit.* **2007**, *9*, 66.
58. Sandberg, I.; Odnevall Wallinder, I.; Leygraf, C.; Le Bozec, N. *J. Corr. Sci.* **2006**, *39*, 4316.
59. Karlén, C.; Odnevall Wallinder, I.; Heijerick; Leygraf, C. *Environ. Pollut.* **2002**, *120*, 691.
60. Odnevall Wallinder, I.; Leygraf, C. *J. Corr. Sci.* **2001**, *43*, 2379.
61. Odnevall Wallinder, I.; Verbiest, P.; He, W.; Leygraf, C. *J. Corr. Sci.* **2000**, *42*, 1471.
62. Sundberg, R. *Metallurgy* **2005**, *59*, 10.
63. Arnold, R. *Integrat. Environ. Assess. Mgmt.* **2005**, *1*, 333.
64. Boulanger, B.; Nikolaidis, N. P. *J. Am. Water Resources Assn.* **2003**, *39*, 325.
65. Romanoff, M. *Underground Corrosion*; Nat. Bur. Stand. Circ. 579; Supt.of Documents: Washington, D.C, 1957.
66. Gilbert, P. T. *J. Inst. Met.* **1947**, *7*, 139.
67. Gilbert, P. T.; Porter, F. C. *Iron and Steel Institute Special Report No. 45,* 1952, pp 55–74, pp 127–134.
68. Markovic, T.; Sevic, M.; Rubinic, L. *Werkst. Korrosion* **1960**, *11*, 87.
69. Maeda, M.; Tenyama, K.; Shibayanagi, T.; Naka, M. *Mater. Charac.* **2005**, *55*(2), 127.
70. Angelini, E.; Mongiatti, A.; Grassini, S.; Rosalbino, F.; Ingo, G. M.; De Caro, T. EUROCORR 2004, Nice, Sept 2004. Published CEFRACOR: Paris, 2004.
71. Efird, K. D. *Corrosion* **1977**, *33*(1), 347.
72. Obrecht, M. F. *Corrosion* **1962**, *18*, 189t.
73. Solelev, A. *J. Inst. Wat. Engrs.* **1955**, *9*, 208.
74. Gilbert, P. T. *Br. Corr. J.* **1979**, *14*, 20.
75. *Aluminium Bronze Alloys Corrosion Resistance Guide*; Publication 80, Copper Development Association, UK, 1981.
76. Defence Standard 01-782. *Protection of Seawater System Pipework and Heat Exchanger Tubes in HM Surface Ships and Submarines*; UK Ministry of Defence, Abbey Wood, 2009.
77. Kirk, W. Evaluation of Critical Seawater Hydrodynamic Effects of Erosion Corrosion of CuNi, INCRA Report 396 1987.
78. Beckmann, W.; Hecht, M.; Jasner, M.; Steinkemp, K. Kuala Lumpur Fabrication Technology Corrosion 2001, Kuala Lumpur; Institute of Materials: London, 2000.
79. LaQue, F. L. *Proc. Am. Soc. Test. Mater.* **1952**, *52*, 1.
80. Evans, U. R. *J. Electrochem. Soc.* **1939**, *75*, 446; Fink, F.W. *J. Electrochem. Soc.* **1939**, *75*, 446, 441.
81. Lucey, V. F. *Br. Corr. J.* **1965**, *1*(9), 53.
82. Feller, H.-G. *Z. Metallkunde* **1967**, *58*, 875.
83. Heidersbach, R. *Corrosion* **1968**, *24*, 38.
84. Kenworthy, L.; O'Driscoll, W. G. *Corr. Technol.* **1955**, *2*, 247.
85. Piatti, L.; Grauer, R. *Werkst. Korrosion* **1963**, *14*, 551.
86. Hashimoto, K.; Ogawa, S.; Shimodaira, S. *Trans. Jpn. Inst. Met.* **1963**, *4*, 42.
87. Sugawara, H.; Ebiko, H. *Corr. Sci.* **1967**, *7*, 513.
88. Joseph, G.; Arce, M. T. *Corr. Sci.* **1967**, *7*, 597.
89. Langenegger, E. E.; Robinson, F. P. A. *Corrosion* **1968**, *24*, 411; **1969,** *25*, 59.
90. Horton, R. M. *Corrosion* **1970**, *26*, 160.
91. Rothenbacher, P. *Corr. Sci.* **1970**, *10*, 391.
92. Pötzl, A.; Lieser, K. H. *Z. Metallkunde* **1970**, *61*, 527.
93. Sundberg, R.; Holm, R.; Hertzman, S.; Hutchinson, B.; Lindh-Ulmgren, E. *Metallurgy* **2003**, *57*, 721.
94. Hutchinson, B.; Oliver, J.; Lindh-Ulmgren, E.; Symniotis, E. In *Investigation into the Dezincification of α-Brass*; Proceedings of the International Conference Copper 2006; Welter, J.-M. Ed.; Wiley-VHC, 2006.
95. Bengough, G. D.; Jones, R. M.; Pirret, R. *J. Inst. Met.* **1920**, *23*, 65.
96. Upton, B. *Br. Corros. J.* **1966**, *1*, 134.
97. Baldwin, A. B.; Campbell, H. S. *Brit. Waterworks Assoc. J.* **1961**, *43*, 13.
98. Schafer, G. J.; Dall, R. A. *Aust. Corr. Eng.* **1966**, *10*, 39.
99. Ladeburg, H. *Metallurgy* **1966**, *20*, 33.
100. Simmonds, M. A.; Huxley, W. G. S. *Aust. Corr. Eng.* **1967**, *11*, 9.
101. Bengough, G. D.; May, R. *J. Inst. Met.* **1924**, *32*, 81; Discussion of Bradbury, E. J.; Johnson, L. W. *Trans. Inst. Mar. Engrs.* **1951**, *63*, 59.
102. Breckon, C.; Gilbert, P. T. *Chem. Ind.* **1964**, *4*, 35.
103. Bem, R. S. *The Engineer* **1958**, *206*, 756.
104. Sundberg, R.; Hertzman, S.; Linder, M. In *Intergranular Corrosion (IGA) of Brass*; Proceedings of the International Conference Copper 2006 Welter, J.-M. Ed.; Wiley-VHC, 2006.
105. Mazza, F.; Torchio, S. *J. Corr. Sci.* **1983**, *23*, 1053.
106. Tumer, M. E. D. *Proc. Soc. Water Treatm. Exam.* **1961**, *10*, 162; **1965,** *14*, 81.
107. Clark, W. D. *J. Inst. Met.* **1947**, *73*, 263.
108. Breckon, C.; Gilbert, P. T. Proceedings of the first International Congress on Metal Corrosion, London; Butterworths: London, 1962; p 624.
109. Meigh, H. *Cast and Wrought Aluminum Bronzes – Properties, Processes and Structure;* IOM Communications, 2000.
110. Brezina, P. *Int. Met. Rev.* **1982**, *27*(2), 1.
111. Weill-Couly, P.; Arnoud, D. *Fonderie* **1973**, 322.
112. Taxen, C. *Korrosioninstitutet Rapport* **1996**, *8*, 1.
113. Campbell, H. S. *Chem. Ind.* **1955**, 692.
114. Hatch, G. B. *J. Am. Waterworks Assn.* **1961**, *53*, 1417.
115. Hatch, G. B. NACE Tech. Rep. 60–11; *Corrosion* **1960**, *16*, 453t.
116. Schafer, G. J. *New Zealand J. Sci.* **1962**, *5*, 475.

117. Lucey, V. F. *Br. Corr. J.* **1967**, *2*, 175.
118. Campbell, H. S. Proceedings of the second International Congress on Metal Corrosion, New York (1963); NACE: Houston, 1966; p 237.
119. Gilbert, P. T. *Aust. Corr. Eng.* **1969**, *13*, 513.
120. Zhu, X.; Lei, T. *J. Mat. Sci. Technol. (China)* **1998**, *14*(1), 57.
121. Lin, L.; Lui, S.; Lui, Z.; Xu, J. *Corr. Sci. Protect. Technol.* **1999**, *11*(1), 37.
122. Sundberg, R. *Metallurgy* **2002**, *56*(11), 714.
123. Schafer, G. J.; Dall, R. A. *Aust. Corr. Eng.* **1963**, *7*(10), 33.
124. Proceedings of the International Corrosion of Copper & Copper Alloys in Building; Tokyo, Japanese Copper Development Association, 1982.
125. Cornwall, F. J.; Wildsmith, G.; Gilbert, P. T. *Br. Corr. J.* **1973**, *8*, 202.
126. Oliphant, R. J. *Causes of Copper Corrosion in Plumbing Systems;* Foundation for Water Research, 2003.
127. Mattson, E.; Fredriksson, A.-M. *Br. Corr. J.* **1968**, *3*, 246.
128. Mattson. *E., Werkst. U Korros.* **1988**, *39*, 499.
129. Linder, M. *Proceedings of the 9th Scandinavian Corrosion Congress, Copenhagen,* 1983, pp 569–581.
130. Drogowska, M.; Brossard, L.; Menard, H. *J. Electrochem. Soc.* **1992**, *139*(1), 39–47.
131. Milosev, I.; Metikos-Hukovic, M.; Drogowska, M.; Menard, H.; Brossard, L. *J. Electrochem. Soc.* **1992**, *139*(9), 2409–2418.
132. Drogowska, M.; Brossard, L.; Menard, H. *J. Electrochem. Soc.* **1993**, *140*(5), 1247–1251.
133. BSEN 12502:2004. Protection of metallic materials against corrosion. *Guidance on the assessment of corrosion likelihood in water distribution and storage systems. Influencing factors for cast iron, unalloyed and low alloyed steels* and BSEN 14868:2005*, Protection of Metallic Materials against Corrosion. Guidelines on the assessment of corrosion likelihood in closed water circulation systems*, BSI, UK, 2005.
134. Rogers, T. H. *J. Inst. Met.* **1948**, *75*, 19–38.
135. Keevil, C. W.; Walker, J. T.; McAvoy, J.; Colbourne, J. S. In *Biocorrosion*; Gaylarde, C. C., Moreton, L. H. G., Eds.; Biodeterioration Society: Kew, 1988.
136. Wagner, D.; Fischer, W.; Tuschewitzki, G. J. Microbiologically influenced corrosion of copper pipes Final report, ICA project number 453, 1992.
137. Geesey, G. G; Mittleman, M. W.; Iwaoka, T.; Griffiths, P. R. *Materials Performance* **1986**, 37–40.
138. Geesey, G. C.; Lewandowski, Z.; Fleming, H.-C. *Biofouling/Biocorrosion in Industrial Water Systems*; Lewis Publishers: Chelsea, MI, 1993.
139. Tronstad, R.; Veimo, R. *J. Inst. Met.* **1940**, *66*, 17.
140. Kenworthy, L. *J. Inst. Heat. Vent. Engst.* **1940**, *8*, 15.
141. Gilbert, P.T. *Proc. Soc. Water Treatm. Exam*. **1966**, *15*, 165.
142. Priggemeyer, St.; Priggemeyer, S.; Meyer, E.; Sauter, W.; Breu, M.; Schüz, G.; Arens, P.; Baukloh, A. In *Copper Release of Copper Tubes in Contact with Hard Drinking Waters*, Conference Proceedings of CEOCOR Plenary Meeting 2001; Biarritz.
143. Critchley, M.; Taylor, R.; O'Halloran, R. *Mater. Perform.* **2005**, *44*(6), 56.
144. Merkel, T. H.; Pehkonen, S. O. *Corr. Eng. Sci. Technol.* **2006**, *41*(1), 21–37.
145. Kenworthy, L. *J. Inst. Met.* **1943**, *69*, 67.
146. Porter, F. C.; Hadden, S. E. *J. Appl. Chem.* **1953**, *3*, 385.
147. Guidelines for Drinking Water Quality, 3rd ed.; WHO: Geneva, 2008.
148. Araya, M.; McGoldrick, M. C.; Klevay, L. M.; Strain, J. J.; Robson, P.; Nielsen, F.; Olivares, M.; Pizarro, F.; Johnson, L.; Poirier, K. A. *Regulat. Toxicol. Pharmacol.* **2001**, *34*, 137–145.
149. Davenport, W. H.; Nole, V. F.; Robertson, W. D. *J. Electrochem. Soc.* **1959**, *106*, 1005.
150. Ives, D. J. G.; Rawson, A. E. *J. Electrochem. Soc.* **1962**, *109*, 447.
151. Obrecht, M. F.; Pourbaix, M. *J. Am. Waterworks Assoc.* **1967**, *59*, 977.
152. Grunau, E. B. *Städtehygiene* **1967**, *7*, 153.
153. Tuthill, A. H. *Mater. Perfor.* **1987**, *26*(9), 12.
154. Defence Standard 01/2 and Angell, B.; Tuck, C. D. S., private communications, UK Ministry of Defence, Bristol, UK.
155. Shone, E.; Grim, G. *Trans I. Mar. Eng.* **1976**, 98, Paper 11.
156. Kirk, W.; Tuthill, A. The Application of Copper Nickel Alloys in Marine Systems. Copper Nickel Condenser and Heat Exchanger System, CDA Inc Seminar Technical Report 7044–1919, CDA, Inc: New York, 1992.
157. Jasner, M.; Hecht, M.; Beckman, W. *Heat Exchangers and Piping Systems from Copper Alloys – Commissioning, Operating and Shutdown*; KME: Osnabruck, 1998.
158. Gilbert, P. T. Conference of Historical Metallurgy Society, Birmingham, Paper Copper 4, 1984.
159. Powell, C. A.; Michels, H. T. *Cupronickel Alloys for seawater corrosion resistance and antifouling – A State of the Art review;* Corrosion 2000; NACE: Houston, 2000.
160. Zhu, X.; Lin, L.; Lei, T. *Acta Metall. Sinica (China)* **1997**, *33*(12), 1256.
161. Zhu, X.; Lin, L.; Xu, J.; Lei, T. *Chin. J. Non-ferrous Met.* **1997**, *7*(2), 79.
162. Nicklin, G. J. E. *Living with the threat of microbiologically influenced corrosion in submarine seawater systems-the Royal Navy's perspective.* Proceedings of 9th International Naval Engineering Conference (INEC 2008), Hamburg, IMarEST, London, 2008.
163. Schleich, W. Corrosion 2005; NACE: Houston, 2005, Paper No. 5222.
164. Theile, E. W. Proceedings of CDA Heat Exchanger Seminar; New York, April; Copper Development Association: New York, 1981.
165. Sato, S. Proceedings of the fourth International Congress of Metal Corrosion Amsterdam, 1969; NACE: Houston, 795, 1972.
166. i,s Lee, T. S. *Pre-treatment of Condenser Tubing for Enhanced Corrosion Resistance*; INCRA Project 284 Final Report, NiDI, 1985.
167. Rowlands, J. C. *J. Appl. Chem.* **1965**, *15*, 57.
168. Lemieux, E.; Wolejsza, T. M.; Grolleau, A. M. *Corrosion 2002*; Denver; NACE: Houston, 2002, Paper No. 02210.
169. Berthagen, L. *The use of Cathodic Protection for Copper Alloys in Seawater Cooling Systems*, EFC Working Party Report, EuroCorr 2001, Maney Publishing: London, 2001.
170. Tuthill, A. H.; Todd, B.; Oldfield, J. *IDA World Congress on Desalination and Water Reuse; Madrid* **1997**; Vol. IIIp 251p 25, paper No. 73.
171. Oldfield, J. W.; Todd, B. *A Review of Materials and Corrosion in Desalination-Key Factors for Plant Reliability*; IDA World Congress on Desalination and Water Science: Abu Dhabi, 1995.
172. Gilbert, P. T.; Jenner, B. J. *International Marine and Shipping Conference*; Institute of Marine Engineers: London, 1969.
173. Li, W.; Lui, D.; Wei, K. *Corr. Sci. Protect. Technol.* **1995**, *7*(3), 232.
174. Sigh, I.; Basu, D. K.; Singh, M. N.; Battamishra, A. K. *Anti-Corrosion Meth. Mat.* **1993**, *44*(3), 195.
175. Nelson, G. A. *Bull. Am. Soc. Test. Mat.* **1959**, *240*, 39.
176. Agarwal, D. C. *Br. Corr. J.* **2002**, *37*(2), 105.
177. Agarwal, D. C. *Corr. Eng. Sci. Technol.* **2003**, *38*(4), 275.

178. Agarwal, D. C.; Sarin, S.; Wadhura, R.; Vishwakarma, R.; Deshmukh, M. B.; Kurian, S. *J. Failure Anal. Prev.* **2005**, *5*, 70.
179. Slusser, J. W.; Dean, S. W.; Drummer, D. M. Corrosion '86 NACE: Houston, 1986, Paper 330.
180. Parkins, R. N.; Holroyd, N. J. H. *Corrosion* **1982**, *38*, 245.
181. Robertson, W. D. *Trans. Amer. Inst. Min. (Metall.) Engrs.* **1951**, *191*, 1190.
182. Edmunds, G. *Symposium on Stress-corrosion Cracking in Metals*; ASTM: Philadelphia, 1944; pp 67–89.
183. Elliot, P.; Corbett, R. A. In Corrosion/1999 NACE: Houston, 1999, Paper No. 342.
184. Wilson, T. C.; Edmunds, G.; Anderson, E. A.; Peirce, W. M. *Symposium on Stress-corrosion Cracking in Metals*; ASTM: Philadelphia, 1944; pp 173–193.
185. Sato, S.; Nosetani, T. *Sumitomo Light Metal Tech. Rep.* **1969**, *10*(2), 83.
186. Syrett, B. C.; Parkins, R. N. *Corr. Sci.* **1970**, *10*, 197.
187. Uhlig, H. H. Ed. *Corrosion Handbook*; Wiley: New York, 1948; pp 78–79.
188. Sato, S. *Sumitomo Light Met. Tech. Rep.* **1960**, *1*(3), 45.
189. Kamath, K. V.; Erdmann-Jesnitzer, F. *Metallurgy* **1960**, *14*, 1061.
190. Thompson, D. H. *Chem. Eng.* **1961**, *68*(3), 130.
191. Laub, H. *Metallurgy.* **1966**, *20*, 1174.
192. Adamson, K. *Corr. Sci.* **1967**, *7*, 537.
193. Erdmann-Jesnitzer, F.; Kacslingk, N. *Werkst. Korrosion* **1969**, *20*, 493.
194. Copper Alloys-ammonia test for stress corrosion resistance, ISO 6957; BSI: London, 1988.
195. Wrought copper and copper alloys. Detection of residual stress. Mercurous nitrate test, ISO 196; BSI: London, 1995.
196. Helling, S.; Lissner, O.; Rask, S.; Ström, B. *Werkst. Korrosion* **1957**, *8*, 569.
197. Aebi, F. *Z. Metallk.* **1958**, *49*, 63.
198. Thompson, D. H. *Mater. Res. Standards* **1961**, *1*, 108.
199. Szabo, E. *Werkst. Korrosion* **1963**, *14*, 162.
200. Mattsson, E.; Lindgren; Rask, S.; Wennström, G. *Current Corrosion Research in Scandinavia*; Kemian Keskususliitto: Helsinki, 1965; p 171.
201. Baumann, G. *Werkst. Korrosion* **1962**, *13*, 737.
202. Sato, S. *Sumitomo Light Metal Tech. Rep.* **1963**, *4*(1), 48.
203. Uhlig, H. H.; Sansone, J. *Mater. Protection* **1964**, *3*(2), 21.
204. Peters, B. F.; Carson, J. A. H.; Barer, R. D. *Mater. Protect.* **1965**, *4*(5), 24.
205. Logan, H. L.; Ugiansky, G. M. *Mater. Protect.* **1965**, *4*(5), 79.
206. Laub, H. *Metallurgy* **1966**, *20*, 597.
207. Laub, H. *Metallurgy* **1967**, *21*, 173.
208. Laub, H. *Metalloberfläche* **1966**, *20*, 413, 453, 493.
209. Sato, S.; Nosetani, T. *Sumitomo Light Metal Tech. Rep.* **1969**, *10*(3), 175.
210. Whitaker, M. E. *Metal. Manchr.* **1948**, *39*, 21, 66.
211. Perryman, E. C. W.; Goodwin, R. J. *J. Inst. Met.* **1954**, *13*, 378.
212. Bailey, A. R. *J. Inst. Met.* **1959**, *87*, 380.
213. Sheehan, T. L.; Dickerman, H. E. *J. Am. Soc. Nav. Engrs.* **1946**, *58*, 586.
214. Evans, U. R. *Symposium on Internal Stresses in Metals and Alloys*; Institute of Metals: London, 1947; pp 291–310.
215. Pugh, E. N.; Craig, J. V.; Montague, W. G. *ASM. Trans. Quart.* **1968**, *61*, 468.
216. Mattsson, E. *Electrochim. Acta* **1961**, *3*, 279.
217. Forty, A. J.; Humble, P. *Philos. Mag.* **1963**, *8*(86), 247.
218. Proceedings of the Second International Conference of Metal Corrosion, New York (1963); NACE: Houston, 1966; p 80.
219. McEvily, A. J., Jr.; Bond, A. P. *J. Electrochem. Soc.* **1965**, *112*, 131.
220. Forty, A. J. *Met. Progr.* **1959**, *75*, 154.
221. Graf, L.; Lacour, H. R. *Z. Metallk.* **1960**, *51*, 152; **1962,** *53*, 764.
222. Graf, L.; Richter, W. *Z. Metallk.* **1961**, *52*, 834.
223. Aebi, F. *Z. Metallk.* **1955**, *46*, 547; **1956,** *47*, 421.
224. Bakish, R.; Robertson, W. D. *J. Electrochem. Soc.* **1956**, *103*, 320.
225. Edeleanu, C.; Forty, A. J. *Philos. Mag.* **1960**, *5*(58), 1029.
226. Graf, L. *Metallurgy* **1964**, *18*, 1163, 17.
227. Lynes, W. *Corrosion* **1965**, *21*, 125.
228. Pugh, E. N.; Westwood, A. R. C. *Philos. Mag.* **1966**, *13*, 167.
229. Pugh, E. N.; Montague, W. G.; Westwood, A. R. C. *ASM. Trans. Quart.* **1965**, *58*, 665.
230. Hoar, T. P.; Booker, C. J. L. *Corr. Sci.* **1965**, *5*, 821.
231. Fairman, M. *Corr. Sci.* **1966**, *6*, 37.
232. Takano, M.; Shimodaira, S. *Corr. Sci.* **1968**, *8*, 55.
233. Lahiri, A. K. *Br. Corr. J.* **1968**, *3*, 289.
234. Lahiri, A. K.; Banerjee, T. *J. Corr. Sci.* **1968**, *8*, 895.
235. Hoar, T. P.; Rothwell, G. P. *Electrochim. Acta* **1970**, *15*, 1037.
236. Swann, P. R.; Nutting, J. *J. Inst. Met.* **1960**, *88*, 478.
237. Swann, P. R. *Corrosion* **1963**, *19*, 102t.
238. Swann, P. R.; Pickering, H. W. *Corrosion* **1963**, *19*, 369t, 373t.
239. Tromans, D.; Nutting, J. *Corrosion* **1965**, *21*, 143.
240. Brown, B. F. *Met. Mater.* **1968**, *2*(12), 171.
241. Graf, L. *Werkst. Korrosion* **1969**, *20*, 408.
242. Robertson, W. D. Ed. *Stress Corrosion Cracking and Embrittlement (Electrochem. Soc. Symposium)*; Wiley: New York, 1956.
243. Rhodin, T. N. Ed. *Physical Metallurgy of Stress-Corrosion Fracture (AIME Symposium)*; Interscience: New York, 1959.
244. Conference on Fundamental Aspects of Stress Corrosion Cracking, Ohio State University, 1967; NACE: Houston, 1969.
245. Bailey, A. R. *Metall. Rev.* **1961**, *6*(21), 101.
246. Sparks, J. M.; Scully, J. C. *J. Corr. Sci.* **1974**, *16*, 619.
247. Kermani, M.; Scully, J. C. *J. Corr. Sci.* **1978**, *18*, 833; **1979,** 89, 489.
248. Scully, J. C. *Met. Sci.* **1978**, *12*, 290; *J. Corr. Sci.* **1980**, *20*, 297.
249. Takano, M.; Staehle, R. W. *Trans. Jpn. Inst. Met.* **1978**, *19*, 1.
250. Takano, M. *Trans. Jpn. Inst. Met.* **1977**, *18*, 787.
251. Takano, M. *Corrosion* **1974**, *30*, 441.
252. Kawashima, A.; Agrawal, A. K.; Staehle, R. W. *Spec. Tech. Pub.* **1979**, *665*, 266.
253. Uhlig, H.; Gupta, K.; Liang, W. *J. Electrochem. Soc.* **1975**, *122*, 343.
254. Holroyd, N. J. H.; Hardie, D.; Pollock, W. J. *Br. Corr. J.* **1982**, *17*, 103.
255. Logan, H. L. *Meta. Eng. Quart.* **1965**, *5*, 32.
256. Parkins, R. N. *Metall. Rev.* **1964**, *9*(35), 201.
257. Engel, H.-J.; Speidel, M. O. *Werkst. Korrosion* **1969**, *20*, 281.
258. Thompson, D. H.; Tracy, A. W. *J. Met. N.Y.* **1949**, *1*, 100.
259. Pugh, E. N.; Montague, W. G.; Westwood, A. R. C. *Corr. Sci.* **1966**, *6*, 345.
260. Uhlig, H. H.; Duquette, D. J. *J. Corr. Sci.* **1969**, *9*, 557.
261. White, L. F.; Blazey, C. *Met. Ind.* **1949**, *75*, 92.
262. Sylwestrowicz, W. D. *Corrosion* **1969**, *25*, 168, 405; **1970,** *26*, 160.
263. Lahiri, A. K.; Banerjee, T. *Corr. Sci.* **1965**, *5*, 731.

264. Chatterjee, U. K.; Sircar, S. C.; Banerjee, T. *Corrosion* **1970**, *26*, 141.
265. Chatterjee, U. K.; Sircar, S. C. *Br. Corros. J.* **1970**, *5*, 128.
266. Blackwood, A. W.; Stoloff, N. S. *ASM. Trans. Quart.* **1969**, *62*, 677.
267. Harry Meigh. *Cast and Wrought Aluminum Bronzes-Properties, Processes and Structure*; IOM Communications, 2000.
268. Helliwell, B. J.; Williams, K. J. *Metallurgia* **1970**, *81*, 131.
269. Nishimara, R.; Yoshida, T. *Corr. Sci.* **2008**, *50*(4), 1205.
270. Thompson, D. H. *Corrosion* **1959**, *15*, 433t.
271. Marshall, T.; Hugil, A. J. *Corrosion* **1957**, *13*, 329t.
272. Klement, J. F.; Maersch, R. E.; Tully, P. A. *Corrosion* **1959**; 15p 295t.
273. Norden, R. B. *Chem. Eng.* **1958**, *65*, 194, 196.
274. Klement, J. F.; Maersch, R. E.; Tully, P. A. *Met. Prog.* **1959**, *75*, 82; *Corrosion*, **1960,** *16*, 519t; U.S. Pat. 2 829 972.
275. Robertson, W. D.; Grenier, E. G.; Davenport, W. H.; Nole, V. F. *Met. Prog.* **1959**, *75*, 152; U.K. Pat. 802 044.
276. Andersen, M. W.; Joosten, M.; Murali, J.; Milliams, D. E. Corrosion/96; NACE: Houston, 1996, Paper No. 78.
277. Tuck, C. D. S. Corrosion 2005; NACE: Houston, 2005, Paper No. 5462.
278. El Domiaty, A.; Alhajji, J. N. *J. Mat. Eng. Perform.* **1997**, *6*(4), 534.
279. Pound, B. G. *Corrosion* **1994**, *50*(4), 301.
280. Lee, J. A. *Materials of Construction for Chemical Process Industries*; McGraw-Hill: New York, 1950.
281. Rabald, E. *Corrosion Guide*; Elsevier: New York, 1951.
282. LaQue, F. L. *Corrosion* **1954**; 10p 391.
283. Heim, A. T. *Ind. Eng. Chem.* **1957**, *49*, 63A, 64A, 66A.
284. Baker, S. *Corr. Technol.* **1961**, *8*, 8.
285. Tracy, A. W. *Chem. Eng.* **1962**, *69*, 130, 152.
286. Gould, A. J.; Evans, U. R. *J. Iron Steel Inst.* **1947**, *155*, 195.
287. Lacan, M.; Markovic, T.; Rubinic, L. *Werkst. Korrosion* **1959**, *10*, 767.
288. Holmberg, M. E.; Prange, F. A. *Ind. Eng. Chem.* **1945**, *37*, 1030.
289. Lingnau, E. *Werkst. Korrosion* **1957**, *8*, 216.
290. Fontana, M. G. *Ind. Eng. Chem.* **1950**, *42*, 69A.
291. Groth, V. J.; Hafsten, R. J. *Corrosion* **1954**, *10*, 368.
292. Bulow, C. L. *Chem. Eng.* **1946**, *53*, 210.
293. Friend, W. Z.; Mason, J. F. *Corrosion* **1949**, *5*, 355; NACE, Report; *Corrosion* **1957**, *13*, 757t.
294. Russell, R. P.; White, A. *Ind. Eng. Chem.* **1927**, *19*, 116.
295. Damon, G. H.; Cross, R. C. *Ind. Eng. Chem.* **1936**, *29*, 231.
296. Cornet, I.; Barrington, E. A.; Behrsing, G. U. *J. Electrochem. Soc.* **1961**, *108*, 947.
297. Caney, R. J. T. *Aust. Eng.* **1954**, *64*, 54; U.K. Pat 718,987.
298. Zitter, H.; Kraxner, G. *Werkst. Korrosion* **1963**, *14*, 80.
299. Piatti, L.; Fot, E. *Werkst. Korrosion* **1964**, *15*, 27.
300. Gregory, D. P.; Riddiford, A. C. *J. Electrochem. Soc.* **1960**, *107*, 950.
301. Talati, J. D.; Desai, M. N.; Trivedi, A. M. *Werkst. Korrosion* **1961**, *12*, 422.
302. Graydon, W. F. *J. Electrochem. Soc.* **1962**, *109*, 1130.
303. Kagetsu, T. J.; Gradon, W. F. *J. Electrochem. Soc.* **1963**, *110*, 856.
304. Feller, H.-G. *Corr. Sci.* **1968**, *8*, 259.
305. Otsuka, R.; Uda, M. *Corr. Sci.* **1969**, *9*, 703.
306. Rana, S. S.; Desai, M. N. *Indian J. Technol. S* **1967**, 393.
307. Desai, M. N.; Shah, Y. C. *Anti-Corr. Meth. Mater.* **1968**, *15*(12), 9.
308. Desai, U.; Gandhi, M. H. *Corr. Sci.* **1969**, *9*, 65.
309. Padma, D. K. *Anti-Corr. Meth. Mater.* **1969**, *16*, 4.
310. Desai, M. N.; Shah, Y. C.; Punjani, B. K. *Br. Corr. J.* **1969**, *4*, 309.
311. Ammar, I. A.; Riad, S. *Corr. Sci.* **1969**, *9*, 423.
312. Desai, M. N.; Rana, S. S. *Werkst. Korrosion* **1966**, *17*, 870.
313. Radley, J. A.; Stanley, J. S.; Moss, G. E. *Corr. Technol.* **1959**, *6*, 229.
314. Schaefer, B. A. *Corr. Sci.* **1968**, *8*, 623.
315. Bartoníček, R.; Holinka, M.; Lukašovská, M. *Werkst. Korrosion* **1968**, *19*, 1032.
316. Green, J. A. S.; Mengelberg, H. D.; Yolken, H. T. *J. Electrochem. Soc.* **1970**, *117*, 433.
317. Jenkins, L. H.; Durham, R. B. *J. Electrochem. Soc.* **1970**, *117*, 768.
318. Dubrisay, R.; Chesse, G. *Comp. Rend. Acad. Sci. Paris* **1945**, *220*, 707.
319. Francis, R. *The Selection of Materials for Seawater Cooling Systems – A Practical Guide for Engineers*; NACE Publication, 2006.
320. Campbell, S. A.; Radford, G. J. W.; Tuck, C. D. S.; Barker, B. D. *Corrosion* **2002**, *58*(1), 57.
321. Reichert, J. S.; Pete, R. H. *Chem. Eng.* **1947**, *54*, 218.
322. West, J. R. *Chem. Eng.* **1951**, *58*, 281.
323. Botham, G. H.; Dummett, G. A. *J. Dairy Res.* **1949**, *16*, 23.
324. Holness, H.; Ross, T. K. *J. Appl. Chem.* **1951**, *1*, 158.
325. Bukowiecki, A. *Schweizer Archiv. Angew. Wiss.* **1958**, *24*, 355.
326. Mason, J. F. *Corrosion* **1948**, *4*, 305.
327. Inglesent, H.; Storrow, J. A. *J. Soc. Chem. Ind.* **1945**, *64*, 233.
328. Clendenning, K. A. *Canad. J. Res. F (Technol.)* **1948**, *26*, 277.
329. Mimura, K.; Lim, J.-W.; Isshika, M.; Zhu, Y.; Jiang, Q. *Met. Mat. Trans. A* **2006**, *37*(4), 1231.
330. Vernon, W. H. J. *Chem. Ind. (Rev.)* **1940**, *59*, 87.
331. Kubaschewski, O.; Hopkins, B. E. *Oxidation of Metals and Alloys*; Butterworths: London, 1953.
332. Hauffe, K. *Oxydation von Metallen und Legierungen*; Springer-Verlag: Berlin, 1956.
333. Wagner, C.; Grunewald, K. *Z. Phys. Chem.* **1938**, *40*, 455.
334. Dighton, A. L.; Miley, H. A. *Trans. Electrochem. Soc.* **1942**, *81*, 321.
335. Evans, U. R. *Trans. Electrochem. Soc.* **1947**, *91*, 547.
336. Evans, U. R. *Res. Lond.* **1953**, *6*, 130.
337. Mott, N. F. *Trans. Faraday Soc.* **1939**, *35*, 1175; **1940,** *36*, 472; **1947,** *43*, 429.
338. McKewan, W.; Fassell, W. M. *J. Met. M. Y.* **1953**, *51*, 1127.
339. Paidassi, J. *Acta Metall.* **1958**, *6*, 216.
340. Lohberg, K.; Wolstein, P. *Z. Metallk.* **1955**, *46*, 734.
341. Baur, J. P.; Bridges, D. W.; Fassell, W. M. *J. Electrochem. Soc.* **1956**, *103*, 273.
342. Gulbrausen, E. A.; Copan, T. P.; Andrew, K. F. *J. Electrochem. Soc.* **1961**, *108*, 119.
343. Ro¨nnquist, A. *J. Inst. Met.* **1962**, *91*, 89.
344. Yoda, E.; Siegel, B. M. *J. Appl. Phys.* **1963**, *34*, 1512.
345. Wallwork, G. R.; Smeltzer, W. W. *Corr. Sci.* **1969**, *9*, 561.
346. Tylecote, R. F. *J. Inst. Met.* **1950**, *78*, 327; **1952**, *81*, 681.
347. Bardeen, J.; Brattain, W. H.; Shockley, W. *J. Chem. Phys.* **1946**, *14*, 714.
348. Castellan, G. W.; Moore, W. J. *J. Chem. Phys.* **1949**, *17*, 41.
349. Tylecote, R. F. *J. Inst. Met.* **1950**, *78*, 301.
350. Pilling, N. B.; Bedworth, R. E. *J. Inst. Met.* **1923**, *19*, 529.
351. Feitknecht, W. *Z. Elektrochem.* **1929**, *35*, 142, 500.
352. Vernon, W. H. J. *J. Chem. Soc.* **1926**, 2273.
353. Valensi, G. *Pittsburgh International Conference on Surface Reactions*; Corrosion Publishing: Pittsburgh, 1948; pp 156–165.

354. Oudar, J. *Metaux* **1960**, *35*, 397, 445.
355. Dyess, J. B.; Miley, H. A. *Trans. Am. Inst. Min. (Metall.) Eng.* **1939**, *133*, 239.
356. Vernon, W. H. J. *Trans. Faraday Soc.* **1924**, *19*, 839.
357. Preston, G. D.; Bircumshaw, L. L. *Philos. Mag.* **1935**, *20*, 706.
358. Hallowes, A. P. C.; Voce, E. *Metal. Manchr.* **1946**, *34*, 95.
359. Lustman, B. *Met. Prog.* **1946**, *50*, 850.
360. Dennison, J. P.; Preece, A. *J. Inst. Met.* **1952**, *81*, 229.
361. Blade, J. C.; Preece, A. *J. Inst. Met.* **1959**, *88*, 427.
362. Maak, F.; Wagner, C. *Werkst. Korrosion* **1961**, *12*, 273.
363. Wallbaum, H. J. *Werkst. Korrosion* **1961**, *12*, 417.
364. Maak, F. *Z. Metallkunde* **1961**, *52*, 538.
365. Zwicker, U. *Metallurgy* **1962**, *16*, 1110.
366. Kapteijn, J.; Couperus, S. A.; Meijering, J. L. *Acta Metall.* **1969**, *17*, 1311.
367. Sanderson, M. D.; Scully, J. C. *Corr. Sci.* **1970**, *10*, 165.
368. Dunwald, H.; Wagner, C. *Z. Phys. Chem.* **1933**, *22*, 212.
369. Wagner, C. *Z. Phys. Chem.* **1933**, *21*, 25.
370. Wagner, C. P*ittsburgh International Conference on Surface Reactions*; Corrosion Publishing: Pittsburgh, 1948; pp 77–82.
371. Hoar, T. P.; Price, L. E. *Trans. Faraday Soc.* **1938**, *34*, 867.
372. Price, L. E.; Thomas, G. J. *J. Inst. Med.* **1938**, *63*, 21.
373. Schu¨ckher, F.; Lampe, V. *Prog. Met.* **1965**, *105*, 192.
374. Wood, G. C.; Chattopadhyay, B. *J. Inst. Met.* **1970**, *98*, 117.
375. Whittle, D. P.; Wood, G. C. *J. Inst. Met.* **1968**, *96*, 115, *J. Corr. Sci.* **1968**, *8*, 295.
376. Swaroop, B.; Wagner, J. B., Jr. *J. Electrochem. Soc.* **1967**, *114*, 685.
377. Ashby, M. F.; Smith, G. C. *J. Inst. Met.* **1963**, *91*, 182.
378. Bolsaitis, P.; Kahlweit, M. *Acta Metall.* **1967**, *15*, 765.
379. Pötschke, J.; Mathew, P. M.; Frohberg, M. G. *Z. Metallkunde* **1970**, *61*, 152.
380. *Alloy 400 for use in High Pressure Feedwater Heaters*; Nickel Institute Publication 14021, Nickel Institute: Alvechurch, UK, 1993.
381. Moore, C.; Bindley, D. Proceedings of the Second International Congress on Metal Corrosion, New York, 1963; NACE: Houston, 1966; p 391.
382. Castle, J. E.; Harrison, J. T.; Masterson, H. C. Proceedings of the Second International Congress on Metal Corrosion, New York (1963) NACE: Houston, 1966; p 822.
383. Hopkinson, B. E. ASME 1962, Paper No. 62-WA.
384. Wiedersum, G. C.; Tice, E. A. ASME WA/CT-3, ASME, 1964, Paper No.64.
385. Castle, J. E.; Harrison, J. T.; Masterson, H. G. *Br. Corros. J.* **1966**, *1*, 143.
386. Otsu, T.; Sato, S. *Trans. Jpn. Inst. Met.* **1961**, *2*, 153.
387. Sato, S. *Sumitomo Light Metal Tech. Rep.* **1964**, *5*(1), 2; **1964,** *5*(2), 27; **1964,** *5*(3), 231; **1964,** *5*(4), 290.
388. Brush, E. G.; Pearl, W. L. *Corrosion* **1969**, *25*, 99.
389. Tromans, D.; Sun, R. *J. Electrochem. Soc.* **1991**, *138*(11), 3235–3244.
390. Wu, Y. C.; Zhang, P.; Pickering, H. W.; Allara, D. L. *J. Electrochem. Soc.* **1993**, *140*(10), 2791–2800.
391. Bhatt, I. M.; Soni, K. P.; Triveda, A. M. *Werkst. Korrosion* **1967**, *18*, 968.
392. Tinley, W. H. *Chem. Ind.* **1964**, *12*, 2036.
393. Obrecht, M. F. Proceedings of the Second International Congress on Metal Corrosion, New York (1963); NACE: Houston, 1966; p 624.
394. Desai, M. N.; Rana, S. S.; Gandhi, M. H. *Anti-Corr. Methods Mater.* **1970**, *17*(6), 17.
395. Desai, M. N.; Shah, Y. C.; Gandhi, M. H. *Aust. Corros. Eng.* **1968**, *12*(3), 3.
396. Desai, M. N.; Shah, Y. C. *Werkst. Korrosion* **1970**, *21*, 712.
397. Gupta, P.; Chaudhary, R. S.; Prakash, B. *Br. Corr. J.* **1983**, *18*, 98.
398. Walker, R. *Corrosion* **1973**, *20*, 290.
399. Lewis, G. *Br. Corr. J.* **1981**, *16*, 169.
400. Subramanyan, N. C.; Sheshadri, B. S.; Mayanna, S. M. *Br. Corr. J.* **1984**, *19*(4), 177.
401. Badawy, W. A.; Ismail, K. M.; Fathi, A. M. *Electrochim. Acta* **2006**, *51*(20), 4182.
402. Francis, R. *The Selection of Materials for Seawater Cooling Systems: A Practical Guide for Engineers;* NACE: Houston, 2003.
403. Avery, S. V.; Howlett, N. G.; Radice, S. *Appl. Environ. Microbiol.* **1996**, *62*(11), 3960.
404. Kim, J. H.; Cho, H.; Ryu, S. E.; Choi, M. U. *Arch. Biochem. Biophys.* **2000**, *382*(1), 72.
405. Karlstrom, A. R.; Levine, R. L. *Proc. Natl. Acad. Sci. USA* **1991**, *88*(13), 5552.
406. Pena, M. M.; Lee, J.; Thiele, D. J. *J. Nutr.* **1999**, *129*(7), 1251.
407. Noyce, J. O.; Michels, H.; Keevil, C. W. *J. Hosp. Infect.* **2006**, *63*, 289.
408. Noyce, J. O.; Michels, H.; Keevil, C. W. *Appl. Environ. Microbiol.* **2006**, *72*, 4239.
409. Noyce, J. O.; Michels, H.; Keevil, C. W. *Appl. Environ. Microbiol.* **2007**, *73*, 2748.
410. Casey, A. L.; Lambert, P. A.; Miruszenko, L.; Elliot, T. S. J. *Copper for preventing microbial environmental contamination;* Interscience Conference on Antimicrobial Agents and Chemotherapy (ICAAC) ASM, Washington, 2008.
411. Casey, A. L.; Adams, D.; Karpanen, T. J.; Lambert, P. A.; Cookson, B. D.; Nightingale, P.; Miruszenko, L.; Shillam, R.; Christian, P.; Elliott, T. S. J. *The role of copper in the reduction of contamination of the hospital environment,* submitted to J. Hospital Infection, March 2009.
412. Mawella, J. UK Ministry of Defence, Abbey Wood, Bristol, Communication on Corrosion performance of NES 824 copper-nickel chrome www.marinecorrosionforum.org, 2005.
413. Hurtado, M. R. F.; Sumodjo, P. T. A.; Benedetti, A. V. *J. Electrochem. Soc.* **1993**, *140*(6), 1567–1571.

3.08 Corrosion of Aluminum and its Alloys

G. M. Scamans
Innoval Technology Limited, Beaumont Close, Banbury, Oxon OX16 1TQ, UK; Brunel Centre for Advanced Solidification Technology, Brunel University, Uxbridge, Middlesex UB8 3PH, UK
N. Birbilis
Department of Materials Engineering, Monash University, Clayton VIC 3800, Australia
R. G. Buchheit
Department of Materials Science and Engineering, The Ohio State University, Columbus, OH 43210, USA

3.08.1 Introduction

Having been discovered some 180 years ago, aluminum has a relatively short history and only recently completed its first century of commercial manufacture. The key to its extensive use today is its corrosion resistance and its extreme versatility that make it suitable for a wide range of products from household foil to armor plate and the essential construction material for generations of aircraft and space vehicles. Aerospace applications, which demand strength, toughness, corrosion resistance and light weight, have provided the greatest stimulus for alloy development and corrosion research, which continues even today.[1] Durable aluminum has provided a vast web of power transmission cables, cladding for all types of buildings and the versatile extruded section for glass house construction. It is increasingly the metal chosen for reducing the weight, thereby reducing emissions from the world's vast and rapidly expanding population of cars and trucks.

Aluminum and its alloys offer a diverse range of desirable properties that can be matched precisely to the demands of each application by the appropriate choice of composition, temper and fabrication mode. Aluminum can be rolled, forged, slit and sheared and shaped by extrusion through dies of a multiplicity of shape or can be cast directly into shaped products. In addition to its low density and high corrosion resistance, its other major attributes are its high thermal and electrical conductivity, heat and light reflectivity, cryogenic compatibility, nonferromagnetic property as well as its hygienic and nontoxic qualities for food contact applications.[2]

Aluminum as an engineering material ranks in tonnage use only behind iron and steel, and its growth in production has been continually increasing year by year. The global tonnage shipped in 2007 was 60 Mt, of which 37 Mt was provided by primary production and 23 Mt by recycled scrap.[3] Aluminum is unique in its high level of recyclability, which can compensate for the high energy cost of its primary production.

Aluminum is an essential material for modern economies and often substitutes as the preferred material for steel and plastics in automotive and building applications; copper in electricity production and transmission; magnesium, titanium, composites and plastics in aerospace and defense applications; steel, plastics and glass in packaging applications; and wood and vinyl for building and construction applications.

This chapter provides a general, yet concise, account of the corrosion behavior of aluminum and its alloys with reference to their classification, processing and surface treatment.

3.08.2 Historical Perspective

Aluminum was first produced in impure form in 1825 by Hans Christian Ørsted and in pure form in 1827 by Friedrich Wöhler. The first commercial preparation of aluminum was in 1855 in France when Henry Etienne Sainte-Claire Deville reduced aluminum chloride with sodium. He also, most likely, conceived the idea of the electrolysis of aluminum oxide dissolved in cryolite, which in 1886 was used independently by Charles Martin Hall in the United States and Paul Héroult in France for the development of electrolytic extraction of high-purity aluminum in an economical manner and remains the basis for production even today.[4,5] Before the Hall–Héroult process was developed, aluminum was more valuable than gold and was used for dinner plates by Napoleon

III and the apex of the Washington Monument in 1884. Commercial production started in 1888 at the Pittsburgh Reduction Company, today known as Alcoa, and in 1889 in Switzerland at Aluminium Industrie, now part of Alcan.

Aluminum is the most abundant metal and comprises about 8% of the earth's crust. It occurs naturally as bauxite, the name given to its ore containing 30–50% hydrated alumina (along with impurities including iron oxide, titania and silica). The processing of bauxite is carried out by the chemical process invented by Karl Joseph Bayer in 1888,[6] which converts bauxite to alumina by digestion in caustic soda followed by precipitation and calcination. Impurities from bauxite and from the steel vessels and pipework of the alumina plants have a significant influence on the corrosion behavior of aluminum and its alloys.

The Hall–Héroult process is carried out in aluminum primary production plants, known as smelters, where the alumina from the Bayer plant is dissolved in molten cryolite, and electrolysis is carried out in an electrolytic reduction cell (or 'pot') consisting of baked carbon anode rods (which are consumed), a carbon-lined vessel to hold the electrolyte and a molten pool of liquid aluminum (the cathode).[4,5] The reduction cell is operated at about 950 °C. The anodes are consumed during the process as they react with the oxygen coming from the alumina. A typical smelter has hundreds of cells arranged in potlines operating at currents up to 500 kA. All potlines built since the early 1970s use prebake anode technology, where the anodes, manufactured from a mixture of petroleum coke with coal tar pitch binder, are prebaked in separate anode plants. In the earlier Soederberg technology, the carbonaceous mixture is fed directly into the top part of the pot, where self-baking anodes are produced using the heat released by the electrolytic process. Potlines of this type are being progressively phased out.

At regular intervals, molten aluminum is tapped from the pots and is transported to the cast house where it is alloyed in holding furnaces by the addition of other metals, cleaned of oxides and gases and then cast into ingots. These can take the form of extrusion billets for extruded products, or rolling ingots for plate, sheet and strip products, depending on the way they are to be further processed. Aluminum castings are produced by foundries using a number of molding techniques to manufacture shaped components.

Generally, the purity of aluminum from electrolysis cells is adequate (i.e., 99.7–99.9%) for alloying, the main impurities being iron and silicon together with lower levels of zinc, magnesium, manganese and titanium; however, if high- or super-purity aluminum is required, a second stage of refining is carried out in a three-layer Hoopes cell producing purities between 99.99% and 99.999%. Higher purities can be achieved by zone-refining super-purity aluminum. World aluminum production grew rapidly from 180 kt in 1918 to 2 Mt in 1952 to 20 Mt in 1989. Since that time, the rate of increase has been more modest, rising steadily to 24 Mt in 2000 and recently, more rapidly to 37 Mt in 2007. Aluminum has been traded on the London Metal Exchange (LME) since 1978, and from 1985, the LME price was adopted as the market price. Over the past 30 years, the average LME quoted price of aluminum has been $1.5 per kilogram but has ranged between $1.00 and $3.00 per kilogram depending on the variation in supply and demand.[7,8]

From a corrosion perspective, aluminum has been a remarkably successful metal, and many of the earliest artifacts remain like the mill-finished roof of the church of St. James in Rome built in 1897 and the statue of Eros by Albert Gilbert unveiled in London in 1893. The aluminum industry maintained strong corrosion technology support groups for many years as aluminum production and its range of applications expanded. The major corrosion issues addressed during this time were the tropicalization of aluminum alloys containing magnesium, the stress corrosion cracking of alloys used in aerospace applications, the galvanic corrosion of aluminum in architectural and automotive applications and, most recently, the filiform corrosion of painted aluminum sheet in both architectural and automotive applications. The most significant aluminum corrosion challenges at present are the ramifications from the elimination of chromates and the tolerance of increased impurity levels due to the increased use of recycled metal.

3.08.3 Production and Types of Aluminum Alloys

3.08.3.1 Aluminum Production

Bauxite production has increased from 144 Mt worldwide in 2002 to 178 Mt in 2006. Most of this is mined from open cast mines in Australia (62 Mt), Brazil and China (both 20 Mt) followed by Guinea (15 Mt), Jamaica (15 Mt), and India (13 Mt). In 2006, Alcoa, Chinalco, Alcan, Rusal and BHP Biliton accounted for or controlled almost 60% of the

69 Mt of worldwide alumina production from the 178 Mt of bauxite.[9] The largest alumina producers in 2006 were Australia (18 Mt) and China (14 Mt). Like many commodities, alumina is sold both on spot prices and contract terms, for which it is typically priced between 11.5% and 13.5% of the aluminum price quoted on the LME. The recent rapid growth in Chinese demand for aluminum has led to a predicted increase in annual demand from 69 Mt per year in 2006 to 88 Mt per year by 2011. The largest producers of primary aluminum in 2003 were China (5.5 Mt), Russia (3.5 Mt), Canada (2.8 Mt), United States (2.7 Mt), Australia (1.8 Mt) and Norway (1.1 Mt). By 2007, Chinese production had increased to 12.6 Mt out of the total world primary production of 34 Mt.[9] The amount of electrical energy to produce aluminum has been reduced from more than 50 kW h kg^{-1} in 1890 to 16.1 kW h kg^{-1} in 1990 and to 15.2 kW h kg^{-1} in 2006.

Four tons of bauxite is used to produce 2 tons of alumina, which then produces 1 ton of aluminum. The industry average emissions associated with primary aluminum production is 9.73 kg CO_2e per kilogram, 55% of this from electricity generation, so this varies considerably depending on how the electricity is generated.[3] Historically, over 50% of the electricity used to produce aluminum has been hydroelectrically generated, and although it is expected that this trend will continue, recently significant smelter capacity has been installed, particularly in the Middle East, using gas. Aluminum production consumes 3% of the world's electricity and about 10% of its hydropower.

The aluminum industry maintains a close watch on the composition of primary aluminum by regular chemical analysis of samples from each individual electrolysis cell. Purity is calculated by subtracting all the trace element concentrations from 100%. Trends are noted with respect to age of the cell, anode technology and alumina source, as well as the use of recycled alumina from the environmental control systems (scrubbers) used in smelters that are used to trap elements that volatilize from reduction cells. Use of this scrubber alumina results in higher levels of nickel, lead, gallium and vanadium. From the corrosion perspective, the most significant impurities are iron (typically 0.03–0.2 wt %) and silicon (0.03–0.1 wt%) and the lower levels of elements such as copper, manganese, nickel, titanium, zinc, vanadium and gallium. Volatile elements such as sodium, calcium and phosphorous are removed by flux treatments prior to ingot casting.

Aluminum and its alloys are readily recyclable, with recycled scrap providing an increasingly important and growing contribution of 23 Mt per year to the more than 60 Mt total annual metal supply.[3,10] The ever-growing environmental concerns over raw material processing and primary aluminum production as well as the favorable economics of recycling have led to a strong secondary aluminum production industry based on reclaimed scrap accounting for about 30–35% of total aluminum production since the early 1990s. The recycling of aluminum requires 95% less energy than that is required for primary aluminum production, and recycling of used aluminum products generates only 0.5 kg of CO_2e per kilogram of aluminum produced.

However, in order to meet the mechanical and corrosion performance requirements of many alloy and product specifications, much of the recycled metal must be 'sweetened' with primary metal to reduce impurity levels. The result is that in many cases (except beverage cans) recycled metal tends to be used primarily for lower grade casting alloys and products. While a certain amount of this is acceptable, the recycle-friendly world will be truly optimized only when the recycle loop is closer to a closed loop within a number of product lines. Elements that increase in the recycled metal are mainly iron and silicon, and other elements such as magnesium, nickel and vanadium.[11] It is generally advisable to separate wrought alloys from cast alloys.

The total weight of aluminum products in use in 2006 was estimated to be 584 Mt, of which 32% is in building products, 28% in transport applications, 28% in engineering and cable, 1% in packaging and 11% in other products. Since the 1880s, close to 800 Mt of aluminum have been produced, and about three-quarters of this metal, more than 580 Mt, is still in productive use. This is a testament to the excellent corrosion resistance and recyclability of aluminum in almost all its applications. Recycling the metal currently in use would equal 17 years' primary aluminum output.[3]

3.08.3.2 Physical Metallurgy

The properties of aluminum alloys (mechanical, physical and chemical) depend on both alloy composition and alloy microstructure as determined by casting conditions and the thermomechanical processing history. While certain metals alloy with aluminum rather readily,[12] comparatively few have sufficient solubility to serve as major alloying elements. Of the commonly

used alloying elements, magnesium, zinc, copper and silicon have significant solubility, while a number of additional elements (with <1% total solubility) are also used because of the important improvements to alloy properties they confer. Such elements include manganese, chromium, zirconium and titanium.[1,13]

The low yield strength of pure aluminum (~10 MPa) mandates strength increase by alloying for subsequent engineering applications. The simplest strengthening technique is 'solution hardening,' whereby alloying additions as solute must have appreciable solid solubility over a wide range of temperatures and must remain in solution after any heating/cooling cycles, ultimately not being removed from solution by reacting with elements to form insoluble phases. Solid solution strengthening can lead to strength increases of about a factor of 2–4.

However, the most significant increase in strength for aluminum alloys is derived from age-hardening, and in the extreme, this can result in strengths up to 800 MPa. Age-hardening requires a decrease in solid solubility of one (or more) alloying elements with decreasing temperature. The age-hardening process can be summarized by the following stages

- solution treatment at a temperature within a single-phase region to dissolve the alloying element(s);
- quenching or rapid cooling of the alloy to obtain what is termed a supersaturated solid solution;
- decomposition of the supersaturated solid solution at ambient or moderately elevated temperature to form finely dispersed (nanoscale) precipitates.

The fundamental aspects of decomposition of a supersaturated solid solution are complex and still under debate.[14–16] Typically, however, Guinier–Preston (GP) zones and intermediate phase (as shown in **Figure 1**) are formed as precursors to the equilibrium precipitate phase.[13]

In addition, increases in yield strength may also be achieved by grain refinement by exploiting the Hall–Petch relationship.[1] Grain refinement in aluminum alloys is achieved at the casting stage (by additions of small amounts of low-solubility additions such as Ti and B to provide grain nuclei) or by recrystallization control using dispersoids (formed by making trace alloying additions of Cr, Zr or Mn to promote submicron-sized insoluble particles which subsequently restrict or pin grain growth).

Strength development can be further enhanced or modified by careful thermomechanical processing which may include heat treatments such as duplex aging and retrogression and reaging. Maximum hardening in commercial alloys is often achieved when the alloy is cold-worked by stretching after quenching and before aging, increasing dislocation density and providing more heterogeneous nucleation sites for precipitation.[14]

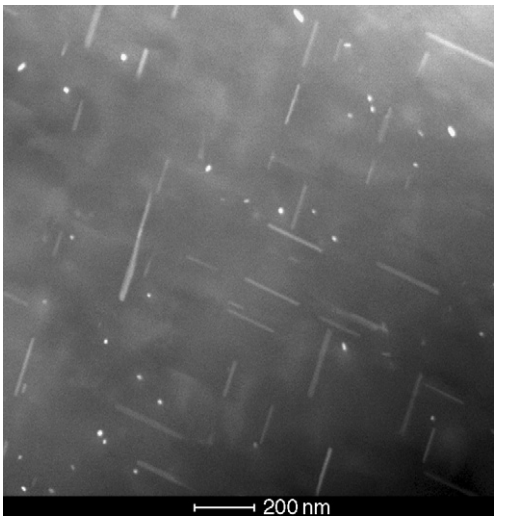

Figure 1 Dark field scanning transmission electron micrograph of fine precipitate Al_2CuMg particles in an Al–Mg–Cu–Si alloy – imaged down the <100> zone axis. Courtesy of Nick Birbilis.

In reality, the microstructures developed in aluminum alloys are complex and incorporate a combination of equilibrium and nonequilibrium phases. Typically, commercial alloys have a chemical composition incorporating up to 10 deliberately made alloying additions. It is prudent, from a corrosion point of view, to understand the role that impurity elements have on the microstructure. While not of paramount significance to alloy designers, impurity elements such as Fe and Si with additional elements form insoluble/high-melting-point compounds that form constituent particles at the alloy casting stage. These constituent particles are comparatively large and irregularly shaped, with characteristic dimensions ranging from 1 to 10 μm. These particles are formed during alloy solidification and are not appreciably dissolved during subsequent thermomechanical processing. Rolling and extrusion tend to break up and align constituent particles into bands within the alloy as shown in **Figure 2**. Often, constituents are found in colonies made up of several different intermetallic compound types. Because these particles are rich in alloying elements, their electrochemical behavior is often significantly different from that

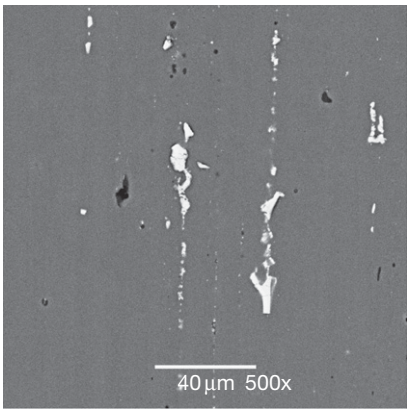

Figure 2 Scanning electron micrograph of constituent particles in AA7075-T651 imaged in the backscattered electron mode. Courtesy of Katja Meyer.

of the surrounding matrix phase. In most alloys, pitting is associated with specific constituent particles present in the alloy.[17,18] A range of alloying elements are found in constituent particles: examples include Al_3Fe, Al_6Mn and Al_7Cu_2Fe.

3.08.3.3 Description of Alloys and Tempers

Traditionally, the global prescription of aluminum alloys for use in engineering was difficult owing to the alloy designations differing from country to country.[1] For this reason, the introduction of an International Alloy Designation System (IADS) introduced in the 1970s was a welcome rationalization and advance. The IADS, and its European Standard equivalent (EN 573), give each wrought alloy a four-digit number of which the first digit is assigned on the basis of the major alloying element(s), as is summarized in **Table 1**, along with the associated temper description.

In the case of cast aluminum alloys, the alloy designations used in a global sense principally adopt the notation of the Aluminium Association system summarized in **Table 2**. The casting compositions are described by a four-digit system which incorporates three digits followed by a decimal. The .0 decimal indicates the chemistry limits applied to an alloy casting; the .1 decimal indicates the chemistry limits for ingot used to make the alloy casting; and the .2 decimal indicates ingot composition but with somewhat different chemical limits (typically tighter, but still within the limits for ingot).[19] Generally, the XXX.1 ingot version can be supplied as a secondary product (remelted from scrap, etc.), whereas the XXX.2 ingot version is made from primary aluminum. Some alloy designations include a letter. Such letters, which precede an alloy number, distinguish between alloys that differ only slightly in percentages of impurities or minor alloying elements (e.g., 356.0, A356.0, B356.0 and F356.0).

The temper designation system adopted by the Aluminium Association is similar for both wrought and cast aluminum alloys. Comprehensive details of alloy properties and characteristics are provided in the publications of the major aluminum companies and independent organizations.[19] Aluminum alloys tend to fall into several distinct groups, sometimes with apparently small differences within the group. Characteristics that could influence the selection of the most appropriate wrought products for a specific application are tabulated (in **Table 4**), but further details are provided as successful utilization of aluminum begin with the selection of alloy.

3.08.3.3.1 *Pure aluminum*

Corrosion resistance of unalloyed aluminum increases with increasing metal purity. The use of the 99.8% and 99.9% grades is usually confined to those applications in which very high corrosion resistance or ductility is required. The chemical industry can advantageously use these purities for handling some products, but because of their low mechanical strength, they are sometimes used as a cladding material for a stronger substrate. Decreasing the purity results in modestly increased strength for the 99% and 99.5% grades, which still retain a high resistance to corrosion. The 99% pure metal may be considered the more useful general-purpose metal for lightly stressed applications such as cooking utensils. These alloys are known as the 1xxx series alloys, and the last two of the four digits indicate the minimum aluminum percentage. For example, 1050 is aluminum with a minimum purity of 99.5%. Alloys for electrical use are of special composition (i.e., AA1350 conductor alloys).

3.08.3.3.2 *Manganese-containing alloys*

Manganese has a relatively low solubility in aluminum but improves its corrosion resistance in solid solution and can moderate the harmful influence of iron-bearing primary intermetallic phases. Additions of manganese of up to 1% form the basis for an important series of non-heat-treatable (3xxx series) wrought alloys, which have good corrosion resistance, moderate strength and high formability. For example, AA3003 displays a tensile strength of ~110 MPa. In sheet form, its attractive combination of properties has resulted in large tonnages being used in buildings cooking utensils, and many general engineering

Table 1 Wrought aluminum alloy and temper designations

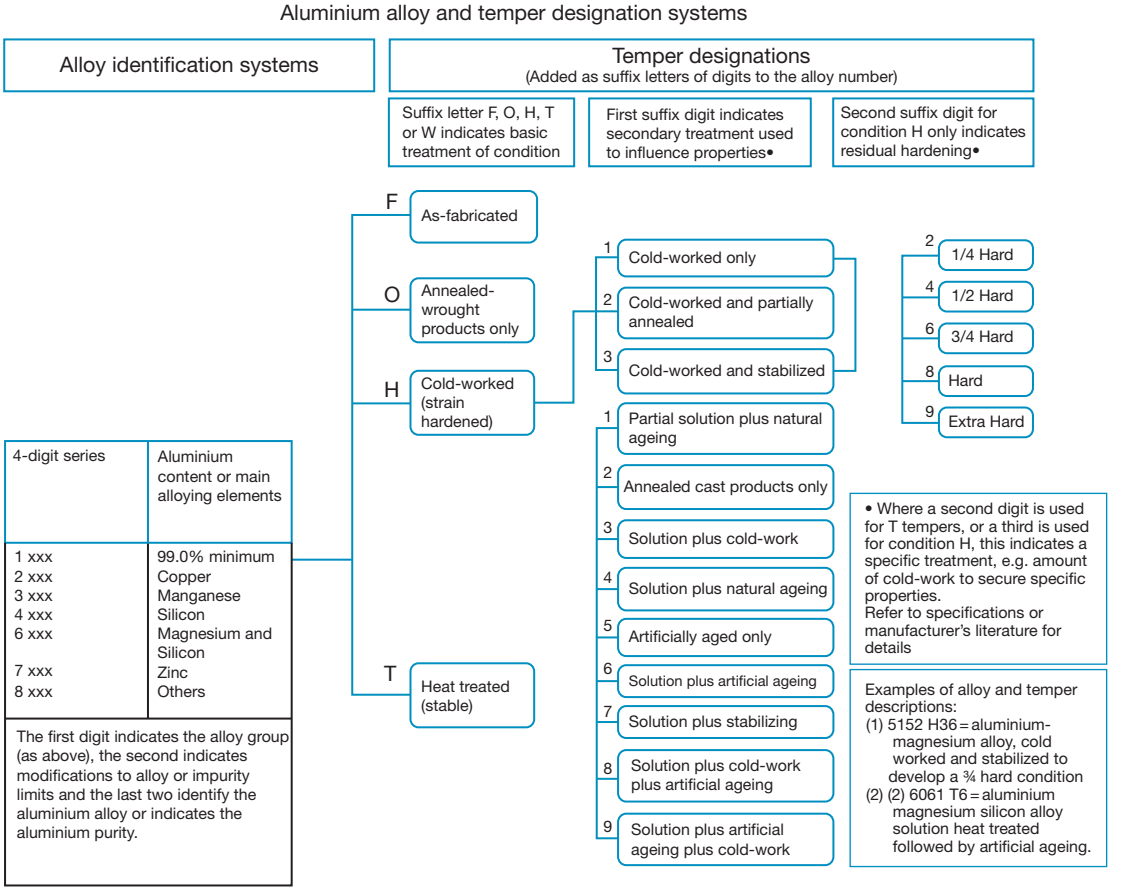

Source: Polmear, I. J. *Light Alloys: Metallurgy of the Light Metals*, 3rd ed.; Arnold: London, 1995.
Schlesinger, M. *Aluminium Recycling*; CRC Press: Boca Raton, FL, 2006.

Table 2 Four digit system for cast aluminum alloy designations

Alloy class	*Designation*
Aluminum of ≥99.0%	1xxx.x
Al + Copper	2xxx.x
+ Silicon (with copper and/or magnesium)	3xxx.x
+ Silicon	4xxx.x
+ Magnesium	5xxx.x
(Series is unused)	6xxx.x
+ Zinc	7xxx.x
+ Tin	8xxx.x
+ Other elements	9xxx.x

Source: Polmear, I. J. *Light Alloys: Metallurgy of the Light Metals*, 3rd ed.; Arnold: London, 1995.
Schlesinger, M. *Aluminium Recycling*; CRC Press: Boca Raton, FL, 2006.

applications. The predominant architectural sheet alloys are AA3005 and AA3105, and alloys such as AA3104 are used for beverage cans because of their deep-drawing capability.

3.08.3.3.3 Magnesium-containing alloys

Magnesium that has a relatively high solubility in aluminum can impart substantial solid solution strengthening and improvement of work-hardening characteristics. The 5xxx series alloys (containing <7% Mg) do not age-harden. Nominally, the corrosion resistance of these weldable alloys is good, and their mechanical properties make them ideally suited for structural use in aggressive conditions. These alloys are used both for boat and shipbuilding, for which a long history of satisfactory corrosion

performance is on record, and for automotive structural applications. However, elevated temperatures should be avoided, since for alloys containing more than 3 wt% Mg, the precipitation of β-type phase (Mg_2Al_3, Mg_5Al_8) over a period of time can lead to serious corrosion in the form of intergranular attack or stress corrosion cracking. Fully work-hardened AA5456 (Al–4.7Mg–0.7Mn–0.12Cr) has a tensile strength of 385 MPa.

3.08.3.3.4 Silicon- and magnesium–silicon-containing alloys

Silicon additions alone can lower the melting point of aluminum while simultaneously increasing fluidity, which is very important and is largely the basis of aluminum casting alloys and the associated shape-casting industry. These alloys are making an increasingly important contribution in automotive applications for engine and drive train components. Generally, corrosion issues with aluminum casting alloys are rare or at least underreported unless they are in contact with other metals, fasteners or fixtures that promote galvanic corrosion. Wrought 4xxx series aluminum–silicon alloys are used extensively as cladding materials for brazing alloys. Where free machining characteristics are required, this may be achieved by additions of cadmium, antimony, tin or lead.

The heat-treatable Al–Mg–Si alloys are predominantly structural materials, all of which have a high resistance to corrosion, immunity to stress corrosion cracking (SCC) and a satisfactory degree of weldability. These 6xxx series alloys are mainly used in extruded form, although increasing tonnages of automotive closure sheet are being produced. Magnesium and silicon additions are made in balanced amounts to form quasibinary Al–Mg_2Si alloys, or excess silicon additions are made beyond the level required to form Mg_2Si. Alloys containing magnesium and silicon in excess of 1.4% develop higher strength upon aging. AA6061 (Al–1Mg–0.6Si–0.25Cu–0.2Cr) in the United States and AA6063 (Al–0.6Mg–0.4Si–0.10Cu) in the EU are used as general-purpose building materials. Automotive closure sheet is made from AA6016 in the EU and AA6111 in North America.

3.08.3.3.5 Copper- and copper–magnesium-containing alloys

Copper is one of the most common alloying additions to aluminum since it has both good solubility and a significant strengthening effect by its promotion of age-hardening response. Copper is added as a major alloying element in the 2xxx series of alloys. The copper–magnesium alloys led to the accidental discovery of age-hardening by Wilm in 1906.[20] These alloys were the foundation of the modern aerospace construction industry, and, for example, AA2024 (Al–4.4Cu–1.5Mg–0.8Mn) can achieve strengths of up to 520 MPa depending on temper. Such Al–Cu–Mg alloys develop their strength by precipitation of the S-phase (Al_2CuMg).

3.08.3.3.6 Zinc- and zinc–magnesium-containing alloys

Zinc is added to certain types of casting alloys, and wrought binary aluminum–zinc alloys are used as clad layers to sacrificially protect aerospace and armor alloys. However, binary alloys show a limited age-hardening response, which is significantly increased by the addition of magnesium and copper. The Al–Zn–Mg alloy system provides a range of commercial compositions, primarily where strength is a major consideration along with weldability, although this requirement limits the maximum amount of copper that can be added to less than 0.3 wt%. Al–Zn–Mg–Cu alloys have traditionally offered the greatest potential for age-hardening, and as early as in 1917, a tensile strength of 580 MPa was achieved; however, such alloys were not suitable for commercial use until their high susceptibility to stress-corrosion cracking could be moderated. Military and commercial aerospace needs following World War II led to the introduction of a range of high-strength aerospace alloys of which AA7075 (Al–5.6Zn–2.5Mg–1.6Cu–0.4Si–0.5Fe–0.3Mn–0.2Cr–0.2Ti) is perhaps the most well known.

The high-strength 7xxx series alloys derive much of their strength from the precipitation of the η-phase ($MgZn_2$) and its precursor forms. The heat treatment of the 7xxx series alloys is complex, involving a range of heat treatments that have been developed to balance strength and stress corrosion cracking performance.[21]

3.08.3.3.7 Lithium-containing alloys

Lithium is soluble in aluminum to a maximum level of about 4 wt%; however, as this is 16 at.%, it means that significant density improvements result from lithium additions. The strong response of these alloys to heat treatment has led to intense research and development on these alloys of high specific strength and stiffness for aerospace applications. Although research into Al–Li alloys dates back to the 1950s, there are continuing

concerns relating to low ductility and poor toughness and low corrosion resistance.

Recent studies have focused on Al–Cu–Li, Al–Li–Mg and Al–Li–Cu–Mg alloys (including the use of minor Ag additions). These alloys derive their strength from age-hardening, involving intermetallics such as Al_2CuLi and S′ phase resulting in strengths in excess of 700 MPa.[22] Such alloys are very attractive for aerospace applications such as, for example, the launching of payloads into space orbit. The new Airbus A350XWB aircraft (expected 2013) is proposed to be predominantly comprised of Al–Li-based alloys. The corrosion challenge that remains to be resolved is the susceptibility to intergranular corrosion (IGC).

3.08.3.3.8 Other alloys classified as 8xxx alloys

Certain alloys high in lithium are classified as 8xxx alloys. This designation also includes alloys containing high levels of iron and manganese near the ternary eutectic content, such as 8006, that have useful combinations of strength and ductility at room temperature and retain their strength at elevated temperatures. These properties are due to the fine grain size stabilized by the finely dispersed iron-rich second phase. Alloys such as 8011 are based on Al–Fe–Si but with more than 1 wt% total alloying element present to give correspondingly higher strengths. Such alloys find application as foil and closures as well as heat exchanger finstock.

An Al–Ni–Fe alloy 8001 is used in nuclear power generation for applications demanding resistance to aqueous corrosion at elevated temperatures and pressures. Other alloys included in the 8xxx series are bearing alloys commonly used in cars and trucks which are based on the Al–Sn system (e.g., 8280 and 8081).

3.08.3.4 Properties of Aluminum Alloys

The basic physical properties of aluminum are given in Table 3.

The diverse and exacting technical demands made on aluminum alloys in different applications are met by the considerable range of alloys available for general and specific engineering purposes, each of which have been designed and tested to provide various combinations of useful properties. These include strength/weight ratio, corrosion resistance, workability, castability or high temperature properties, to mention a few. Some basic properties of these standard alloys are given in Table 4.

Table 3 Properties of aluminum

Physical	
Atomic number	13
Atomic weight	10.0
Atomic volume	26.97
Valency	3
Crystal structure	Face-centered cubic
Interatomic distance	2.863 Å
Electrochemical equivalent	0.3354 g A^{-1} h^{-1}
Density at 293 K	2700 kg m^{-3}
Thermal	
Melting point	931 K
Sp. heat at 293 K	896 J kg^{-1} K^{-1}
Mean sp. heat (293–931 K)	1047 J kg^{-1} K^{-1}
Latent heat of fusion	387 kJ kg^{-1}
Coeff. of linear exp. (293–393 K)	0.61 × 10^{-6} m K^{-1}
Thermal conductivity at 273 K	214 W m^{-1} K^{-1}
Electrical	
Elec. vol. resistivity at 293 K	2.7–3.0 μΩ. cm
Elec. vol. conductivity at 293 K	63–57% IACS
Temp. coeff. of elec. resistance per K for 293 K	0.0041
Thermoelectric power vs. platinum	+0.41 mV/100 K

Wrought aluminum alloys are fabricated into the familiar semifabricated forms such as plates, sheets, extruded sections and drawn tubes from direct chill (DC) cast blocks or billets as appropriate. The largest DC cast rolling blocks are of the order of 20 tons, and most of these are made from primary metal alloyed and cast at smelters. These large rolling blocks are processed through a series of breakdown mills as well as hot and cold tandem mills to produce the wide range of plate and sheet products that represent the largest tonnage of aluminum alloy usage. Continuous casting (CC) of aluminum for sheet products has grown from its commercial inception in the early 1960s to more than 6 Mt per year capacity today. These CC alloys have both modified composition and microstructure when compared to their DC cast equivalents, and this results in modified corrosion behavior. Joining may be carried out by mechanical methods (such as riveting and bolting), brazing, soldering, adhesive bonding or welding. The argon-shielded arc welding methods (MIG and TIG), and more recently, friction stir welding are particularly appropriate where corrosion resistance of the welded joints is of importance.[23]

3.08.3.4.1 Wrought aluminum alloys

The wrought aluminum alloys are often classified according to two major groups, which are the

Table 4 Properties of selected aluminum alloys

Alloy	*Temper*	*Wrought/cast*	*Density ($g\ cm^{-3}$)*	*Electrical conductivity (% IACS)*	*Thermal conductivity at 25 °C ($W\ m^{-1}\ K^{-1}$)*	*Yield strength (MPa)*	*Tensile strength (MPa)*	*Elongation (%)*
1199	O	W	2.71	60	237	10	45	50
1100	O	W	2.71	59	222	34	90	35
3003	H14	W	2.73	50	193	145	152	8
5005	H38	W	2.70	52	200	200	186	5
5052	H38	W	2.68	35	138	290	255	7
2024	T4	W	2.77	30	121	324	469	20
	T861					490	517	6
6061	T6	W	2.7	43	167	276	310	12
7075	T6	W	2.80	22	130	503	572	11
	T73					434	503	13
201.0	T4	C (sand cast)	2.80	30	121	215	365	20
356.0	T51	C (sand cast)	2.69	41	150	140	175	2
413.0	F	C (die cast)	2.66	39	154	140	300	2.5

Source: Polmear, I. J. *Light Alloys: Metallurgy of the Light Metals*, 3rd ed.; Arnold: London, 1995.
Grjotheim, K.; Welch, B. J. *Aluminium Smelting Technology*, 2nd ed.; Aluminium-Verlag: Dusseldorf, 1988.
Hatch, J. E. *Aluminium: Properties and Physical Metallurgy*; ASM International: Materials Park, OH, 1984; pp 424.

non-heat-treatable, and heat-treatable wrought alloys. Non-heat-treatable alloys derive their strength from a combination of solid solution or dispersion hardening. Such alloys can be further strengthened by strain-hardening and cold work.

In contrast, the heat-treatable alloys are strengthened by solutionizing and subsequent age-hardening. The designations, properties and applications of wrought alloys are covered elsewhere in this chapter.

3.08.3.4.2 Cast aluminum alloys

Naturally, casting alloys may not be worked or strain-hardened; however, they may be heat-treated. It was estimated that in 1997 ingots for casting represented a total of ~26% of the total aluminum market in the United States. Of this amount, about 60% was die cast, with the remainder either sand cast, permanent mold cast, etc. The strength of the cast component is typically lower than that of wrought alloys; however, a tensile strength of up to 485 MPa may be realized with heat-treated 2xx.x series casting alloys, with a number of commercial casting displaying a good medium strength in the vicinity of 300 MPa.

3.08.4 Processing of Aluminum Alloys

3.08.4.1 Shape Casting

Cast products are usually produced in foundries from prealloyed metal supplied from secondary smelters, although certain high-performance castings are made from primary metal. The three most commonly used processes are sand casting, permanent mold casting and die casting. Sand molds are gravity fed, whereas the metal molds used in permanent mold casting are either gravity fed or by using air or gas pressure to force the metal into the mold. In high pressure, diecastings, parts up to 5 kg are made by injecting molten aluminum alloy into a metal mold under substantial pressure using a hydraulic ram. Sand castings and permanent mold castings are made from alloys that respond to heat treatment; however, because of their entrapped gas content, die castings are not easily welded or heat treated. Approximately, 85% of aluminum alloy die castings are produced in aluminum–silicon–copper alloys. Permanent mold castings are used for higher production runs than diecastings and, as the metal mold produces rapid solidification, such castings have excellent mechanical properties, low porosity and good dimensional tolerances. Sand casting is a versatile and low-cost process used for a wide range of alloy types although such castings do not have dimensional accuracy and have a relatively poor surface finish. Plaster molds have better surface finish than sand castings, allowing castings to be made with fine detail and close tolerances. Investment casting uses refractory molds formed over expendable wax or thermoplastic patterns. The molten aluminum is then cast into the fired mold to produce precision parts with thin walls, good

dimensional tolerance and a fine surface finish that require little further machining.

Aluminum castings are found in most of the vehicles in use today from cars, buses and trains, to ships, aircraft and spacecraft. The wide variety of aluminum casting alloys available allows the selection of materials with good strength, good corrosion resistance and other special properties. Approximately, 60% of aluminum castings are used in transport applications, 15% in domestic and office equipment, 6% in general engineering applications and 5% in the building and construction industry. Aluminum castings form parts used in cooking pots, washing machines, refrigerators, chairs and tables, and in offices castings are used in furniture, computers and other small, lightweight, high-technology equipment.

However, despite their wide use comparatively, little work has been carried out to date to understand the corrosion behavior of aluminum casting alloys. Because of their high content of alloying elements such as silicon, iron and magnesium, casting alloys have a higher density of intermetallic particles when compared to wrought aluminum alloys. Processing parameters such as cooling rate and pouring temperature and even minor alloying element content variation lead to significant changes in the microstructure of these alloys.

3.08.4.2 Direct Chill Casting

This is a semicontinuous process used for the production of rectangular ingots or slabs for rolling into plate, sheet and foil and cylindrical ingots or billets for extruded rods, bars, shapes, hollow sections, tube, wires and rods. Most of the production is from primary aluminum and process scrap or selected post-consumer scrap. The shallow mold for a DC casting is made from an aluminum- or copper-based alloy with good thermal conductivity, and the walls of the mold are water cooled. The base of the mold is lowered hydraulically or mechanically at a speed that depends on the size and composition of the alloy being cast.

Casting starts by pouring molten metal into the mold which solidifies on contact with the water-cooled base of the mold. Before the mold is filled, it is lowered and the pouring rate is controlled to maintain a constant level of metal in the mold. The solidified shell holding the molten metal is directly chilled by water sprays directed onto the emerging ingot, and pouring is continued until the required ingot length is cast. For small diameter ingots, multiple ingots in lengths of 3 to 4 m may be cast in one drop. This requires a high degree of automation and control for both quality and safety.

Before DC casting, the melt is degassed, filtered and grain-refined. The cast surface is often uneven, and the outermost 20 cm of the cast surface is often of a coarser grain structure than the interior and can contain higher levels of segregates. The outer cast surface is commonly scalped off.

An ideal structure for a DC cast ingot is a fine and uniform grain size, and this is achieved by using a grain refining master alloy in rod form that is fed into the molten alloy during casting at a rate of 0.2 –1 kg t^{-1} of alloy. Grain refiner is usually an alloy that contains 5% titanium and 1% boron as intermetallic phases of titanium aluminide and titanium diboride. These provide the nuclei for solidification in the cooled melt. Cast ingots have a 5–20-mm-thick coarse-grained shell zone with fine grain and a coarse-grained center. DC cast ingots also suffer from macrosegregation and the middle of the ingot can have a significantly different composition.

The stress in the cast ingot depends on the alloy composition, the size and shape of the ingot, the casting speed and the cooling rate, but can be large enough to result in ingot splitting. Certain high-strength 7xxx alloys require stress relieving by heating to 450 °C and slow cooling to prevent splitting.

Thermodynamic considerations often fail to predict correctly the phase content and solid solution content of the as-cast microstructure because of the nonequilibrium nature of solidification during DC casting. This is important, as alloy corrosion properties are controlled by solid solution levels and intermetallic phase crystallography and morphology, which depend on complex kinetic competitions for nucleation and growth. An understanding of the factors that govern phase selection in aluminum alloys under conditions of nonequilibrium solidification is important since varying solidification conditions can lead to variations in secondary Al–Fe and ternary Al–Fe–Si phase contents at different positions in the casting, which in turn can lead to a degradation in the corrosion resistance of the fabricated products.[24]

Following DC casting, ingots are homogenized at high temperature between 450 and 630 °C prior to rolling or extrusion. Homogenization reduces segregation, encourages the transformation of metastable secondary and ternary phases into equilibrium phases and acts to equilibrate solid solution levels of soluble elements, resulting in certain cases in the precipitation of dispersoids. Homogenization can

therefore exert a significant influence on corrosion performance. The transformation of Al–Fe phases to Al–Fe–Si phases, known as beta to alpha transition, is particularly important in the processing of 6xxx extrusion alloys and 3104 can stock.[25] These transitions can exert a controlling influence on subsequent corrosion behavior.

3.08.4.3 Hot and Cold Rolling

Rolling blocks or slabs that are up to 30 tons in weight are scalped by milling away the cast surface and usually have their tops and bottoms sawn off. Slabs are heated to a temperature in the range 400–500 °C and passed through a reversing breakdown mill using heavy reductions per pass to reduce the slab gauge down to 15–35 mm. The surface of the slab undergoes intense shear deformation during this process, and a thin deformed layer is developed that can have a major influence on the subsequent corrosion performance of the rolled sheet if the layer is not removed by chemical or electrochemical cleaning.[26] The slab from the breakdown mill is then hot-rolled on a multistand tandem mill down to a gauge of 2.5–8 mm. Strip is coiled from the hot mill in tandem. Hot rolling deforms the original cast structure and the as-cast grains are elongated in the rolling direction. Depending on the alloy composition, temperature and rolling reduction, recovery processes and partial recrystallization can take place during hot rolling and the slow cooling of the hot-rolled coil. The elongated microstructure developed during hot rolling can have a profound effect on corrosion properties such as stress-corrosion cracking and exfoliation corrosion. For example, the exfoliation corrosion of 7xxx alloys was shown to be due to manganese segregation during DC casting, which developed into a banded microstructure during hot rolling, and exfoliation corrosion occurred as a result of preferential matrix attack adjacent to bands of manganese-containing intermetallic phases.[27]

Cold rolling is usually carried out continuously on multiple-stand tandem mills in which each stand has four rolls and the small diameter work rolls are prevented from bending by large diameter backup rolls. Surface roughness is controlled by the surface finish of the steel rolls. In cold rolling, there is still asperity contact between the roll and the aluminum surface and this can also produce a deformed surface layer with lower corrosion resistance than the underlying alloy. Removal of this surface has been shown to be important for the control of filiform corrosion of coil-coated aluminum architectural sheet.

3.08.4.4 Extrusion

In aluminum extrusion, a hydraulic ram forces a preheated billet held in a fixed container against a die and squeezes the metal through the die opening. The billet surface sticks to the container wall and a new surface is generated on the extrudate. However, this is not the case in backward or indirect extrusion, where the billet surface becomes the surface of the extrusion. Control of temperature and speed is important to avoid problems associated with overheating. However, most of these problems relate to surface defects seen during finishing operations such as anodizing rather than to direct corrosion issues. As with rolling corrosion of extruded sections is controlled largely by the distribution of primary intermetallic phases from DC casting and how these phases are broken up and elongated in the extrusion direction. Grain size and shape are important particularly if recrystallization does not occur and the as-cast grain structure is elongated in the extrusion direction. Partial recrystallization of an outer band of the extrusion can lead to a duplex structure with a predominately fibrous core and a thin, recrystallized outer zone.

3.08.4.5 Continuous Casting

Aluminum flat products can also be produced by twin roll casting or twin belt casting. This effectively removes the requirement for DC casting, formal homogenization and hot rolling. Molten aluminum is directly cast onto a water-cooled hollow steel roll or onto a cooled belt or block. Growth in continuous casting capacity has increased to more than 6 Mt per year from almost zero in 1960. Continuous casting has proven to be remarkably effective for the production of coiled strip suitable for coil coating for use as painted architectural sheet and for foilstock.

From a corrosion perspective, as solidification is more rapid in continuous casting, higher levels of supersaturation are achieved and the size of iron-bearing intermetallic phases is refined. This can be beneficial from a corrosion perspective. However, the surface quality is generally inferior to more conventionally cast and rolled strip, as the cast surface is not removed by scalping and variations in casting conditions can lead to surface streaks that persist at the final gauge after cold rolling. The range of alloys that can be made by continuous casting is more limited, and to date, only limited success has been achieved with automotive sheet alloys although belt

casting capacity for this purpose has been installed in Japan.

Continuous casting is particularly suitable for making strip from secondary metal sources such as recycled post-consumer scrap. This, together with the lower surface quality, has raised concerns about corrosion resistance, but service experience of painted architectural sheet has been positive provided that the sheet is properly cleaned prior to pretreatment and coating.

3.08.5 Corrosion of Aluminum Alloys

Aluminum is a very reactive metal with high affinity for oxygen. This is indicated from its position on the electromotive force series. The metal is nevertheless highly resistant to most atmospheres and to a great variety of chemical agents. This resistance is due to the inert and protective character of the aluminum oxide film which forms on the metal surface and reforms rapidly if damaged. In most environments, therefore, the rate of corrosion of aluminum decreases rapidly with time.

The protective oxide film on aluminum attains a thickness of about 1 nm on freshly exposed metal in seconds. Oxide growth is modified by impurities and alloying additions and is accelerated by increasing temperature and humidity and immersion in water. The protective oxide film inhibits corrosion because it is both resistant to dissolution and a good insulator that prevents electrons produced by oxidation of the metal from reaching the oxide/solution interface, where either the cathodic reduction of oxygen or water can take place. Restricting these cathodic reactions reduces the amount of aluminum oxidation that can occur.

The oxidation of aluminum at room temperature is reported to conform to an inverse logarithmic equation for growth periods up to 5 years.[28] At elevated temperatures, oxidation studies over shorter periods illustrate conformity to parabolic, linear and logarithmic relationships according to time and temperature. These kinetic variations are attributed to different mechanisms of film formation.[29,30]

Corrosion of aluminum is an electrochemical process that involves the dissolution of metal atoms; so it can take place only once the protective oxide film has been dissolved or damaged. Aluminum is amphoteric in nature, meaning its oxide film is stable in neutral conditions but soluble in acidic and alkaline environments. The thermodynamic stability of aluminum's oxide film is expressed by the potential versus pH (Pourbaix) diagram shown in **Figure 3**.[31]

This diagram indicates the theoretical circumstances in which aluminum should show corrosion (forming Al^{3+} at low pH values and AlO_2^- at high pH values), passivity due to hydrargillite, that is, $Al_2O_3{\cdot}3H_2O$ (at near-neutral pH values) and immunity (at high negative potentials). The nature of the oxide actually varies according to temperature, and above about 75 °C boehmite ($Al_2O_3{\cdot}H_2O$) is the stable form. It should be noted that the potential versus pH diagram does not indicate one of the most important properties of aluminum, that is, its ability to become passive in strongly acidic solutions of high redox potential such as concentrated nitric acid.

3.08.5.1 Forms and Causes of Corrosion

Corrosion is an electrochemical process, and hence the corrosion potential of different aluminum alloys is of considerable importance. In addition, the difference between the potential of aluminum alloys and other metals is important, as is the relationship between the potential of microstructural constituents of a single alloy. As we discuss in the following, the compositions of solid solutions and additional phases, in addition to the spatial distribution and number density of additional phases, impact both the extent and the morphology of resultant corrosion. The major forms and causes of corrosion are covered individually below.

3.08.5.1.1 General dissolution

As a general rule, general dissolution occurs spontaneously in strongly acidic or strongly alkaline solutions (as predicted by the Pourbaix diagram), but there are specific exceptions. Thus, in concentrated nitric acid, the metal is passive and the kinetics of the process is controlled by ionic transport through the oxide film, while inhibitors such as silicates permit the use of some alkaline solutions (up to pH 11.5) to be used with aluminum. Even where corrosion may occur to a 'limited' extent, aluminum is often preferred to other metals because its corrosion products are colorless.

3.08.5.1.2 Pitting and localized corrosion

This is the most commonly encountered form of aluminum corrosion. In certain near-neutral aqueous solutions, a pit once initiated will continue to propagate as the solution within the pit becomes acidified and the alumina is no longer able to form a protective film to prevent pit growth.[32]

Pitting arises from the creation of a very localized and 'aggressive' environment that breaks down the

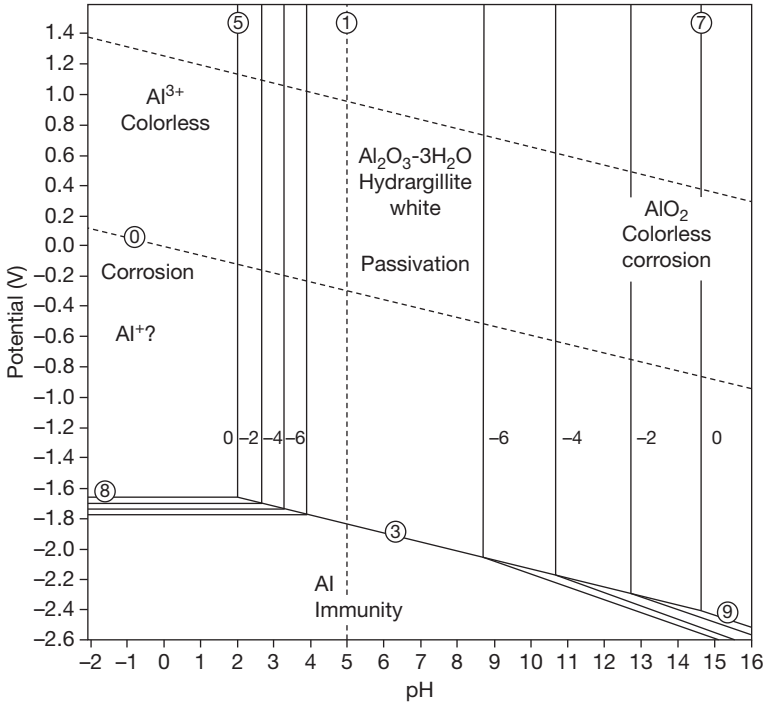

Figure 3 Pourbaix diagram for aluminum.

nominally passive and corrosion-resistant film on the metal. Such an environment usually contains halide ions, of which chlorides are the most common. Solutions containing chlorides are very harmful, while the presence of chlorides can create local corrosion potential 'drops' between the metal surface and the occluded region at which the chloride is concentrated or accumulated. Pits may form at scratches, mechanical defects or stochastic local discontinuities in the oxide film. Pitting occurs only in the near-neutral pH range since the oxide is unstable in a bulk sense under acidic or alkaline conditions. Chlorides facilitate the breakdown of the film by forming $AlCl_3$, which is also usually present in the solution in the pits. When aluminum ions migrate away from the pits, alumina precipitates as a membrane, further isolating and intensifying local acidity, and sustained pitting of the metal results.

With increasing purity of aluminum, greater resistance to pitting corrosion is developed. On high-purity materials, however, any pits that develop are likely to be deeper though fewer in number than those formed in more impure metal. In some special applications, notably in contact with ammonia solutions or pure water at elevated temperatures and pressures, the iron and silicon present in commercial-purity metal are beneficial and retard corrosion. Up to about 5% magnesium improves the corrosion resistance to seawater.

While the shape of the pits can vary rather significantly depending on the alloy type and environment, pit cavities are nominally hemispherical. This distinguishes pits from other forms of corrosion such as intergranular or exfoliation corrosion. Pitting is strongly influenced by the alloy type and microstructure, and **Section 3.08.5.2** covers the effect of microstructure on the corrosion mode in more detail.

The pitting potential defines the conditions under which metals in the passive state are subject to corrosion by pitting, and also serves as a means of discriminating the pitting propensity of alloys. However, the pitting potential yields no information regarding the number and size of pits which may form upon a given alloy, but it does give a measure of the driving force required for pitting to proliferate for a given alloy. There is a definite pitting potential for aluminum and its alloys in near-neutral pH environments, which has been readily and reproducibly measured by many investigators.[33–35]

A review of certain aspects of pitting corrosion of aluminum was given by Smialowska.[18,36] This review highlighted that from a detailed mechanistic point of view, the processes (at the atomic level) that lead

to breakdown of the film due to halide interaction are presently not understood in sufficient detail. However, different analytical techniques including selected ion monitoring (SIM), X-ray photoelectron spectroscopy (XPS) and autoradiography have revealed a clear adsorption of Cl^- on passive films of aluminum.[36]

In addition, since the 1980s, the work of Macdonald and coworkers has endeavored to explain the role of the film structure on pitting using the point defect model.[37–41] This model hypothesizes that chloride ions may be incorporated into the passive film by occupying anion vacancies resulting in a decrease of anion vacancies and an increase in cation vacancies. Cation vacancies are then posited to pile up at the metal interface leading a film breakdown.

More recently, certain researchers have observed current oscillations at a constant anodic potential below the pitting potential for different aluminum alloys.[42–45] The occurrence of these oscillations was explained by the formation and repassivation of nano/micropits termed 'metastable' pits. These investigations have been largely carried out to understand the processes that lead to the formation of stable pits. A typical current versus time record is shown below in **Figure 4**.

Recent studies have shown that the surface of rolled, ground or machined aluminum alloys have deformed surface layers that range in thickness from 100 to 200 nm up to several microns[46,47] and that the presence of these layers has a strong effect on the initiation of pitting corrosion. These deformed layers are characterized by ultrafine grains formed as a result of the high levels of shear strain locally experienced by the aluminum alloy surface. The surface layer grains are 50–100 nm in diameter, are stabilized by oxide particles on their boundaries and are more susceptible to corrosion than the underlying bulk alloy. Deformed layers on AA3005 and similar architectural alloys are activated by the preferential precipitation of manganese-containing dispersoids, whereas the similar layers on AA6016 and AA6111 automotive AA7075 aerospace alloys are more susceptible to pitting due to the preferential precipitation of the aging precipitate. High-shear processing of the surface of aged alloys results in the dissolution of the aging precipitate and this can lead to double breakdown potentials in polarization tests, as the surface is effectively in an underaged state and the pits are at a lower potential than the underlying bulk alloy.[48]

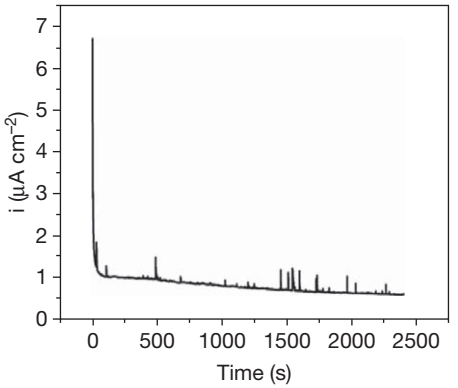

Figure 4 Current vs. time record for AA7075-T651 in deaerated 0.1 M NaCl held potentiostatically at −0.755 V_{SCE}. Courtesy of Mary K. Cavanaugh.

3.08.5.1.3 Bimetallic or galvanic corrosion

Aluminum is anodic to many other metals, and when it is joined to them in a suitable electrolyte which may even be a damp, porous solid, the resultant potential difference (see **Table 5**) causes a current to flow and result in considerable corrosion. Corrosion is most severe when the resistance of the electrolyte is low, for example, seawater. In some cases, surface moisture on structures exposed to an aggressive atmosphere can give rise to galvanic corrosion.

Table 5 Comparison of measured corrosion potentials according to ASTM G-69

Alloy/material	*Corrosion potential (V_{SCE})*
Al (99.999)	−0.75
Cr (99.9)	+0.23
Cu (99.999)	+0.00
Fe	−0.55
Mg	−1.64
Zn	−0.99
1100	−0.74
2014-T6	−0.69
2024-T3	−0.60
3003	−0.74
5052	−0.76
5154	−0.77
6061-T4	−0.71
6061-T6	−0.74
6063	−0.74
7039-T6	−0.84
7055-T77	−0.75
7075-T6	−0.74
7075-T7	−0.75
7079-T6	−0.78
8090-T7	−0.75

The corrosion potentials for a range of non-heat-treatable (wrought), heat-treatable (wrought), and cast aluminum alloys with some other standard corrosion potentials based on measurements made according to ASTM G 69 are shown in Table 5.

In practice, copper, brasses and bronzes in marine conditions cause the most trouble. The danger from copper and its alloys is enhanced by the slight solubility of copper in many solutions and its subsequent redeposition on the aluminum to set up active local cells. This can occur even when the copper and aluminum are not originally in contact: for example, when water running over cuprous surfaces subsequently comes into contact with aluminum. Similarly, water washings from lead can cause pitting of aluminum. The controlling factor with lead and cuprous washings is the solvency of the water, so soft water is the most damaging in this respect. The successful utilization of these metals in close proximity to aluminum, for example, in plumbing and roofing, therefore requires careful design to avoid the transfer of a harmful solute to the aluminum.

Contact with steel, though less harmful, may accelerate attack on aluminum, but in some natural water and other special cases, aluminum can be protected at the expense of ferrous materials. Stainless steels may increase attack on aluminum, notably in seawater or marine atmosphere, but the high electrical resistance of the two surface oxide films minimizes bimetallic effects in less aggressive environments. Titanium appears to behave in a similar manner to steel. Aluminum–zinc alloys are used as sacrificial anodes for steel structures, usually with trace additions of tin, indium or mercury to enhance dissolution characteristics and to render the operating potential more electronegative. Aluminum–55% zinc alloys applied as hot dip coatings are also used extensively as a protective coating for steel for roofing and automotive applications.

Additions of elements such as zinc, tin, indium and mercury activate aluminum electrochemically and are 4 of the 10 elements that can enhance aluminum dissolution in aqueous electrolytes when contained as solute in the aluminum solid solution. The full list of these activators is antimony, zinc, lead, cadmium, thallium, bismuth, tin, indium, gallium and mercury in the order of increasingly negative potential. When these activators are mixed, the potential is controlled by the dominant activator which is the one with the highest melting point.[49] Aluminum alloys are similarly activated by additions of the activator elements to the electrolyte. These additions may be used to turn aluminum into an anode plate for dry cells or metal–air batteries. The best addition for this purpose has been found to be tin together with an addition of magnesium. The magnesium addition is required to prevent a higher level of activation, and hydrogen production associated with the use of activators that can form hydrides.[50]

Aluminum in contact with galvanized steel may accelerate attack on the zinc coating and this is particularly noticeable when there is an unfavorable area ratio, as with galvanized fittings on aluminum sheets. In alkaline solutions, however, aluminum may be preferentially attacked. The copper-bearing aluminum alloys are nobler than most other aluminum alloys and this can accelerate galvanic attack on these, notably in seawater. Mercury and all the precious metals are harmful to aluminum.

Bimetallic corrosion of aluminum is a frequent cause of service-related corrosion failures, as the rate of attack can be rapid and corrosion can be severe and unexpected. In automotive applications, galvanic corrosion of aluminum is found in accelerated vehicle and component tests, particularly where aluminum is in direct electrical and electrolytic contact with a nobler metal. The solution is generally simple and involves providing sufficient protection using combinations of paints and barrier tapes to ensure that either electrical or electrolytic continuity is broken.

3.08.5.1.4 Crevice corrosion

If a crevice is formed between two aluminum surfaces, or between the surfaces of aluminum and a nonmetallic material (i.e., a polymer) localized corrosion may occur within the crevice in the presence of electrolyte.

Crevice corrosion is due to the formation of a local cell, since at the mouth of the crevice (whether it is submerged or not) the concentration of oxygen is higher than that within the crevice. The difference in oxygen concentration leads to a difference in local corrosion potentials leading to corrosion in the 'less noble' area, which is the oxygen depleted zone. Concomitantly, the oxygen rich zone (i.e., the mouth) assumes the role of the cathode. This mode of attack is often termed 'differential aeration cell corrosion' or 'concentration cell corrosion,' which are terms that may be applied more generally to describe corrosion phenomena other than crevice corrosion.

Crevice corrosion can be a very problematic form of corrosion in an engineering sense, as the sites for crevice corrosion are often difficult to avoid in 'real' constructions which include welded lap joints,

rivetings, valve seats, or even deposits that arise in service.[51] Crevice geometry is the governing factor that determines the susceptibility, or conversely the resistance, to crevice corrosion. As a result, crevices are defined by their degree of tightness and their depth (distance from the mouth).

The general rules for the severity of crevice corrosion are presently under active research for several metal alloy systems, including aluminum.[51–53] Typically, in aluminum, tighter crevices lead to more rapid initiation of attack (owing to less electrolyte and a steeper oxygen concentration profile being achieved more rapidly). In addition, increasing crevice depth may also increase the likelihood of crevice initiation. Elimination of crevices should be done at the design stage where possible, and when unavoidable, they should be kept as open and shallow as possible or possibly even sealed with some type of appropriate non-crevice-forming sealant.

3.08.5.1.5 Filiform corrosion

Filiform corrosion may be considered as a specific type of differential aeration cell corrosion that occurs from defects where the bare metal is exposed on painted or coated aluminum surfaces.[2] Filiform corrosion attack has a unique appearance that resembles fine filaments (worm-like threads) emanating from one or more defects in semirandom directions. Much like crevice corrosion, filiform attack is driven by a differential aeration cell with an anodic head growing under the coating and a cathodic tail where oxygen is reduced. The filiform filaments are filled with corrosion products that can include alumina gel and partially hydrated corrosion products. Typical filiform filament growth rates average about 100 μm per day.[2] Filiform corrosion has been an issue for aluminum alloys in the aging aircraft sector. This is because aircraft are routinely painted for corrosion protection with polyurethanes and more complex coating systems.[53–56] Filiform corrosion, however, is not observed in cases where aluminum has been anodized or conversion-coated. More recently, filiform corrosion has also been observed in automobiles with aluminum closure sheet, in architectural sheet in Northern Europe and in packaging products.[46,47]

Recent work has shown that susceptibility to filiform corrosion in architectural and automotive applications in most if not all cases is due to the presence of a deformed layer on the surface of the sheet. For architectural applications, this is the residual surface layer from the high levels of surface shear induced by hot and cold rolling that becomes corrosion susceptible as a result of the preferential precipitation of manganese-containing dispersoid particles. This type of deformed layer-induced filiform corrosion can be prevented by acid or alkaline etching to remove the deformed surface layer, by reducing the manganese level in the alloy or by heat treatment to precipitate the manganese from solid solution before rolling. In automotive applications, the susceptibility to filiform corrosion is induced by the grinding treatment that is used to rectify surface blemishes prior to painting. This type of corrosion is prevented by limiting the rectification grinding treatments in vehicle areas susceptible to stone chip damage in service or by providing additional protection to the painted surface to prevent stone chip damage.[57]

3.08.5.2 Effects of Microstructure on Corrosion

The microstructure of aluminum alloys develop as a result of alloy composition, including impurities, casting practice and thermomechanical treatment. From the corrosion perspective, the dominant features of alloy microstructures are grain structure and the distribution of second phase (intermetallic) particles as constituent particles, dispersoids or precipitates. Such particles have electrochemical characteristics that differ from those of the surrounding alloy matrix, making the alloys susceptible to localized forms of galvanic attack, that has been termed microgalvanic corrosion.

Over the years, a number of studies have been carried out in order to assess the effect of specific intermetallic particles on the corrosion susceptibility of specific aluminum alloys.[34,58–62] In the mid-1990s, Buchheit collected the corrosion potential values for intermetallic phases common to aluminum alloy families mainly in chloride-containing solutions.[18] More recently, various groups have focused on the electrochemical properties of Fe-containing intermetallics[63,64] and Cu-containing intermetallics[65–67] and this has been expanded into a more comprehensive treatise covering a variety of common intermetallics present in commercial aluminum alloys (both wrought and cast).[32] A summary of the results of these studies is shown in **Table 6**.

The identification and structural characterization of intermetallic particles present in aluminum alloys have been quantified by particle extraction techniques combined with X-ray diffraction, by automated electron probe microanalysis and by scanning and transmission electron microscopy combined with X-ray microanalysis. For example, Buchheit *et al.*[67]

quantitatively determined the chemical composition of constituent particles in AA2024-T3 and were able to determine both their stoichiometry and relative surface area.

Intermetallic particles in aluminum alloys may be either anodic or cathodic relative to the matrix. As a result, two main types of pit morphologies are typically observed.[68,69] The so-called circumferential pits appear as a ring of attack around a more or less intact particle or particle colony and the corrosion attack is mainly in the matrix phase. This type of morphology arises from localized galvanic attack of the more active matrix promoted by the more noble (cathodic) particle, as shown in **Figure 5**.

The second pit type of morphology is due to the selective dissolution of the constituent particle. Pits of this type are often deep and may have the remnants of the particle in them. This morphology has been interpreted as particle fallout, selective particle dissolution in the case of electrochemically active particles, or in the case of some Cu-bearing particles, particle dealloying and non-faradaic liberation of the Cu component.

Localized corrosion activity is, however, a complex phenomenon that is still under active research. Localized corrosion leads to local pH gradients, as recently studied by Scully *et al.*[61] Cathodic sites of enhanced oxygen reduction will naturally generate hydroxyl ions and promote local pH increases, which can then modify the subsequent rate and morphology of corrosion propagation. The precise morphology of particle-induced pitting is important for the emerging damage accumulation models. For these models to be predictive, it is necessary to develop a comprehensive,

Table 6 Summary of corrosion potentials in NaCl at the given concentration for intermetallic particles common to Al alloys

Stoichiometry	*Phase*	*Corrosion potential (mV_{SCE})*		
		0.01 M	*0.1 M*	*0.6 M*
Al_3Fe	B	−493	−539	−566
Al_2Cu	θ	−592	−665	−695
Al_3Zr	β	−752	−776	−801
Al_6Mn	–	−839	−779	−913
Al_3Ti	β	−620	−603	−799
$Al_{32}Zn_{49}$	T′	−1009	−1004	−1063
Mg_2Al_3	β	−1124	−1013	−1162
$MgZn_2$	M, η	−1001	−1029	−1095
Mg_2Si	β	−1355	−1538	−1536
Al_7Cu_2Fe	–	−549	−551	−654
Mg(AlCu)	–	−898	−943	−936
Al_2CuMg	S	−956	−883	−1061
$Al_{20}Cu_2Mn_3$	–	−550	−565	−617
$Al_{12}Mn_3Si$	–	−890	−810	−858
Al–2%Cu	–	−813	−672	−744
Al–4%Cu	–	−750	−602	−642

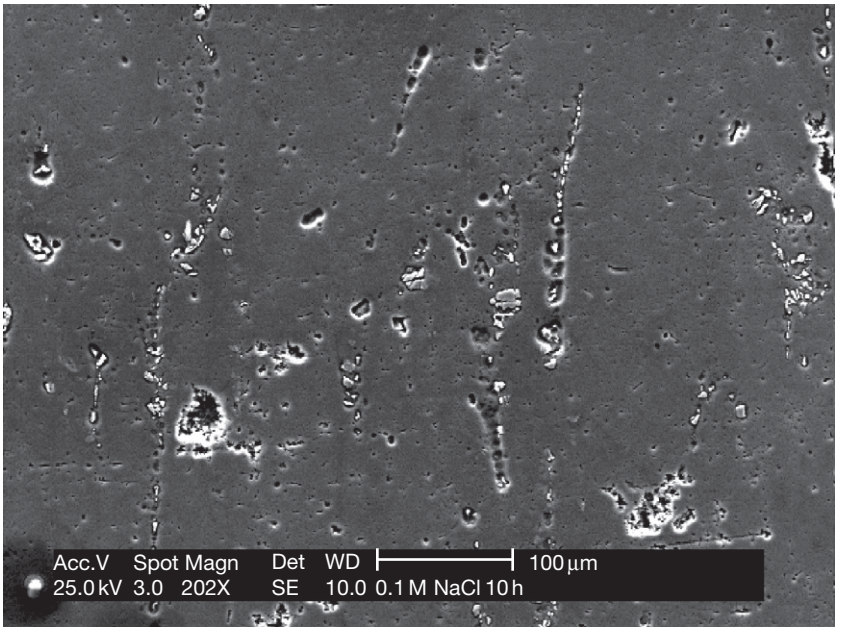

Figure 5 Scanning electron micrograph of early stage corrosion development upon AA7075-T651 immersed in quiescent 0.1 M NaCl for 10 h. Courtesy of Mary K. Cavanaugh.

self-consistent account for this type of pitting. In cases where the electrochemical characteristics of constituent particles have been rigorously characterized, they have been found to have much more complicated behavior than that could becategorized by simple characterizations such as 'noble' or 'active.'

Generally, the constituent intermetallics of interest for a particular aluminum are those that appear in the greatest proportion either by size or by frequency. Variations in thermal treatments will have marked effects on the local chemistry (hence local electrochemistry) and hence the local corrosion resistance of the alloy. Similarly, the impact of mechanical working will influence the number of grain boundaries (hence grain boundary precipitates) and the distribution and size of constituent type particles (which tend to break up and align in the direction of working). Furthermore, directional solidification and segregation from casting will influence the resultant microstructure, all of which will impact the type and number of particles that form and their location within the material.

3.08.5.3 Intergranular Forms of Corrosion

IGC is a phenomenon of which the precise mechanisms have been under debate for almost half a century.[70–76] While in a global sense we can consider IGC as a special form of microstructurally influenced corrosion, in a generic sense, IGC can be summarized as a process whereby the grain boundary region of the alloy is anodic to the bulk or adjacent alloy microstructure.

Corrosion is often microgalvanic (or even nanogalvanic), with activity developing as a result of some heterogeneity in the grain boundary structure. In aluminum–copper alloys, precipitation of Al_2Cu particles at the grain boundaries leaves the adjacent solid solution anodic and more prone to corrosion.[76] With aluminum–magnesium alloys, the opposite situation occurs, since the precipitated Mg_2Al_3 phase is less noble than the solid solution. However, serious intergranular attack in these two alloys may be avoided, provided correct manufacturing and heat treatment conditions are observed.

In the case of the aluminum–magnesium system, almost all commercial alloys are supersaturated as the magnesium solubility at ambient temperatures is less than 1 wt%. This effectively means that for alloys with more than 3 wt% magnesium elevated service temperatures can lead to grain boundary precipitation and sensitization of grain boundaries to corrosion as intercrystalline attack. The extent of this sensitization may be approximately deduced from the continuity of Mg_2Al_3 precipitation at the boundaries as determined by optical metallography of polished and etched cross sections. Apparently, continuous or nearly continuous etched boundaries correspond to high levels of sensitization to IGC.

Although the precipitation of Mg_2Al_3 may appear continuous from examination of polished and etched sections in an optical microscope, examination of microstructures at higher resolution in a scanning or transmission electron microscope invariably reveals the precipitation to be discontinuous. Susceptibility of AA5xxx alloys is controlled in practice either by limiting the level of magnesium in the alloy to below 3 wt%, as such alloys can be sensitized to IGC only under extreme conditions or by the use of a deliberate stabilization treatment for a more magnesium-rich alloy. Stabilization of AA5xxx alloys with more than 3% magnesium is achieved by a deliberate heat treatment to promote intragranular precipitation of Mg_2Al_3. The temperature and time of this treatment depend on the precise magnesium level in the alloy. In production sometimes, this process is carried out by a specific formal heat treatment, and sometimes the rolling practice is modified so that the required level of intragranular precipitation is achieved during warm rolling. The level of sensitization to IGC of a fabricated sheet, plate or extrusion can be easily determined by measurement of the NAMLT value. This is a 24 h exposure to nitric acid and a measurement of weight loss due to IGC and loss of grains. A NAMLT value of more than 30 g cm^{-2} of surface is necessary before an alloy has become sensitized to IGC or cracking.

In the case of Al–Zn–Mg alloys, where the precipitated phase is the highly anodic $MgZn_2$ phase, IGC can occur rather readily. However, susceptibility to IGC is strongly dependent on the heat-treated condition and its effect on grain boundary solute segregation and the morphology and composition of the grain boundary precipitate and the surrounding alloy matrix.[77] The most resistant heat treatments are based on the use of overaging to the T7 condition. More complex heat treatments that involve retrogression and reaging are also used to provide a high level of IGC resistance with a lower loss of strength.[1,2]

The images in **Figure 6** help rationalize the origins of IGC.

IGC differs from pitting corrosion. While IGC may initiate from a pit, propagation of IGC proceeds more rapidly than pitting corrosion, and while both may have a deleterious effect on corrosion fatigue,

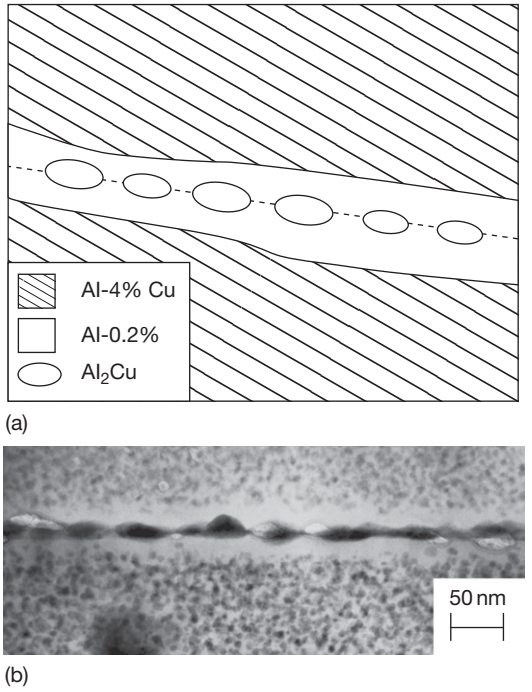

Figure 6 (a) Schematic of hypothetical grain boundary in an Al–Cu alloy. This schematic indicates the different chemistry that exists in the grain interior, solute depleted zone (precipitate-free zone) and grain boundary precipitates – giving rise to electrochemical heterogeneity localized at the grain boundary region. (b) Conventional bright field TEM image of high-angle grain boundary in AA7022-T651, revealing grain boundary precipitates ($MgZn_2$) and a distinguishable precipitate-free zone. Courtesy of Steven P. Knight.

IGC is more detrimental as the sharper corrosion front compared to a more rounded pit front is a higher stress concentrator that reduces the number of cycles to failure.

The test method used to evaluate susceptibility to IGC depends on the alloy type. For 5xxx series alloys, the NAMLT method (ASTM G 67) is adopted, whereas for 2xxx and 7xxx series alloys, ASTM G 110 is most common, employing testing in sodium chloride solutions containing hydrogen peroxide.

Exfoliation corrosion[78] of aluminum alloys is also frequently due to IGC. It generally occurs in cases where the alloy microstructure has been heavily deformed by rolling, extrusion or forging where the grain structure has been flattened and significantly extended in the direction of working. IGC attack from transverse edges and pits then runs along grain boundaries parallel to the alloy surface, and the resulting layers of corrosion attack are sometimes referred to as 'layer corrosion.' Exfoliation corrosion is characterized by leafing off of layers of relatively uncorroded intragranular metal caused by the swelling of the corrosion product in the layers of IGC. Exfoliation corrosion is observed on aircraft components, for example, around riveted or bolted components or wing brackets. Testing for exfoliation corrosion is carried out by a number of ASTM tests, including the acidified salt spray test (ASTM G 85), the ASSET immersion test (ASTM G 66) and the EXCO immersion test (ASTM G 34).

3.08.5.4 Environmentally Assisted Cracking

Environmentally assisted cracking is a generic term that includes stress corrosion cracking (SCC), liquid metal embrittlement (LME), corrosion fatigue (CF) and hydrogen embrittlement (HE).

3.08.5.4.1 Stress-corrosion cracking

Stress-corrosion cracking is a time-dependent, predominantly intergranular fracture mode in aluminum alloys that requires the simultaneous presence of a susceptible alloy, a sustained tensile stress and a corrosive environment.

The minimum tensile stress required to cause SCC in susceptible alloys is usually small and significantly less than the macroscopic yield stress.[79,80] Susceptibility to SCC has restricted the use of aluminum alloys, particularly the weldable 7xxx series alloys, to well-controlled and well-protected applications. There are several theories postulated for the mechanism of SCC. The main theories are either corrosion dominated where cracking is due to preferential corrosion along the grain boundaries by anodic dissolution (i.e., analogous to IGC) or hydrogen dominated where cracking along grain boundaries is enhanced by absorbed atomic hydrogen. The origin of this hydrogen is from IGC itself, and it is considered that the presence of absorbed hydrogen weakens grain boundaries.

While SCC is a very important corrosion-related phenomenon for aluminum alloys, in order to do justice to the topic, the reader is referred to specific monographs on the topic for a more detailed treatise of the SCC theories.[81,82] As previously mentioned, SCC in aluminum alloys is predominately intergranular, and this is seen in **Figure 7**.

Whether or not SCC develops will depend on both the duration and magnitude of the applied tensile stress. Fracture mechanics tools for the determination of crack growth rates are commonly used in the evaluation of SCC resistance for aluminum

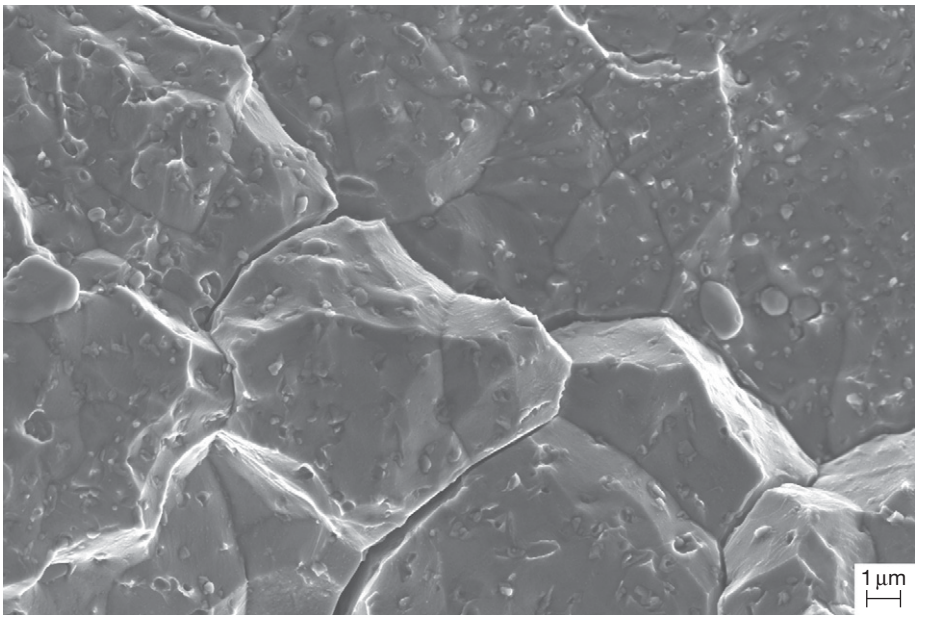

Figure 7 High-resolution SEM micrograph of an SCC fracture surface taken from an AA7079-T651 DCB specimen exposed to 75% relative humidity (specimen was from the T/6 position from a 3-in.-thick rolled plate). Courtesy of Steven P. Knight.

alloys. Such tests suggest a minimum (threshold) stress intensity is required for cracks to develop. This empirical test is largely the basis on which susceptibility to SCC is compared between different alloys under the specific conditions of a particular test or environment.[2]

Residual stresses in aluminum products that may arise as a result of quenching following solution heat treatment and cold working may play an important role in SCC should the level of residual stress be significant. After solution heat treating and quenching of aluminum aerospace and defense plates, it is a common practice to 'stress relieve' the cold-rolled plate by controlled plastic deformation typically to 1.5% by tensile stretching using a plate stretcher. The stress-relieved temper is designated by the Tx5x designation following the temper designation: examples include AA7075-T651 or AA2124-T351.[1]

SCC of 7xxx alloys occurs in water and water vapor in addition to chloride-containing electrolytes. Most other susceptible alloys fail only because of exposure to environments containing chloride ions.

Grain structure has a major influence on SCC of thick section aluminum wrought products. Generally, these products, of which plate is the main example, are not recrystallized and have directional, highly anisotropic grain structures. This means that cracks can grow only in directions parallel to the rolling direction along the flattened grain boundaries. This means that testing the plate in the short transverse direction determines the lowest SCC resistance, followed by the long transverse, and then the longitudinal direction where the intergranular crack path is the most tortuous. This is a very important consideration for the use of plates in the aerospace and defense sector, where thin sections need to be designed such that there is little or no stress in the short transverse direction, or that the most SCC-resistant tempers are used. For welded aluminum alloys in defense applications, exposed short transverse edges are protected by buttering with weld metal or by the use of flame-sprayed protective coatings of sacrificial alloys based on aluminum zinc alloys.

Generally speaking, the low-strength and relatively pure aluminum alloys are not susceptible to SCC. The alloys most prone to SCC are the 7xxx, 2xxx and the higher strength 5xxx series alloys. Most service failures involving SCC have occurred as a result of residual stresses acting in the short transverse direction.[83] The relative resistance of certain aluminum alloys to SCC is tabulated in **Table 7** (adapted from Davies).[2] As noted, progressively overaging beyond the peak (T6) condition generally improves SCC resistance (while lowering strength).

3.08.5.4.2 Liquid metal embrittlement

While LME is not commonly observed in the routine use of aluminum alloys, it can be defined as a mode of attack that results in a complete loss of alloy ductility of a solid metal, below the normal yield stress, as a result of the surface being wetted by a liquid metal. LME-induced fractures may be both intergranular and transgranular but are generally intergranular in aluminum alloys. A micrograph of intergranular fracture due to LME in mercury is shown in Figure 8.

It is well known that gallium in contact with aluminum can result in the disintegration of aluminum (or aluminum alloy) into individual grains. In addition, mercury can also embrittle aluminum and its alloys, though to a lesser extent. Aluminum has also been noted as being embrittled appreciably by tin–zinc and lead–tin alloys, indium and sodium.

Table 7 Qualitative SCC resistance of aluminum alloys (in the rolled plate form)

Alloy and temper	*SCC resistance*
2014-T3	Poor
2024-T3, T4	Poor
2024-T8	Good
2124-T851	Good
2219-T3, T4	Poor
2219-T6, T8	Excellent
6061-T6	Excellent
7049-T73	Good
7x75-T6	Poor
7x75-T73	Excellent
7x75-T76	Intermediate

Source: Davies, J. R., Ed. *Corrosion of Aluminium and Aluminium Alloys*; ASM International: Materials Park, OH, 1999.
US Air Force Research Laboratory, Wright Patterson Air Force Base, OH.

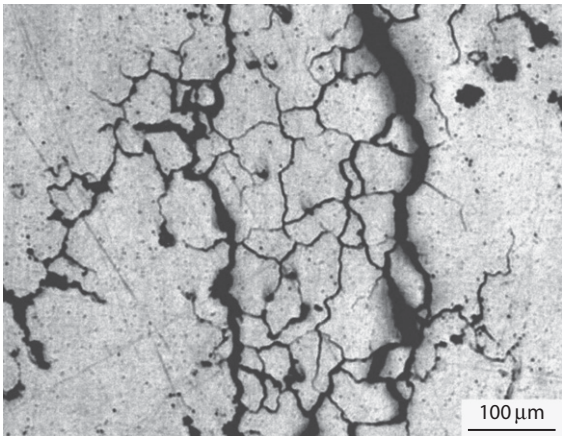

Figure 8 Intergranular failure of an Al alloy pressure vessel in a natural-gas plant due to LME by Hg. Courtesy of Stan P. Lynch.

3.08.5.4.3 Corrosion fatigue

Corrosion fatigue is the interaction of irreversible cyclic plastic deformation with localized corrosion (electrochemical) activity. The combination of each of the mechanisms, as well as the transition from initiation to propagation, is an issue under research currently and of considerable technological importance. However, corrosion pits have been observed to nucleate crack growth in structures subject to fatigue loading.[84]

Recent work has emphasized that in a fatigue study of aluminum alloy 7075-T6 all specimens in that study fractured from cracks associated with pitting.[85] Indeed, the numerous studies referenced with Ref. 2 support the notion that pitting has a critical and detrimental effect on fatigue life.

Corrosion fatigue is an area that is of relevance to the aerospace sector and, indeed, a significant amount of work exists in the area, including several technical publications, dedicated monographs and handbooks.[86,87]

A fatigue crack can initiate from a corrosion pit or surface flaw when the flaw reaches a critical size at which the stress intensity factor reaches a threshold for fatigue cracking, or conversely when the rate of fatigue crack growth exceeds that of pit growth.[88,89]

A simple expression revealing the relationship between the critical pit size and the stress concentration can be given by:[90]

$$a_{p-c} = \pi\left(\frac{\Delta K_{th}}{2.2K_t\,\Delta\sigma}\right)^2$$

where a_{p-c} is the pit–crack transition size and K_t is the stress concentration factor.

As noted in recent works,[91] aerostructures nominally experience corrosion between flights and fatigue loading during flight, suggesting the notion of 'prior corrosion.' This eludes to corrosion pits as precursors to fatigue cracking, a notion that can be seen elegantly in Figure 9 as adapted from Harlow.[92]

Corrosion fatigue phenomena are diverse and specific to the environment and particular application at hand; however, certain variables that can influence corrosion fatigue crack growth propagation naturally include stress intensity, frequency of loading, stress ratio, alloy composition and microstructure (hence electrochemical potential) and the environment composition (and temperature).

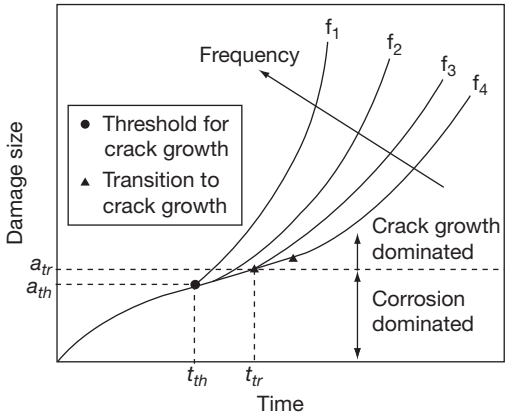

Figure 9 Schematic diagram of the development of corrosion and corrosion fatigue crack growth, indicating the transition from one mode to another via some threshold pit depth.

3.08.5.4.4 Hydrogen embrittlement

Hydrogen is capable of dissolving in aluminum and its alloys both in the molten state and during thermal treatments at temperatures close to the alloy melting temperature where the atmosphere may include water vapor or excessive hydrocarbons. Hydrogen from molten aluminum results in porosity in cast products but does not have an influence on corrosion performance or hydrogen embrittlement.

However, there is experimental evidence that hydrogen generated during corrosion can penetrate into the grain boundaries and lead to embrittlement, a factor in the initiation and propagation of cracking (in particular SCC).[93–96] The mechanism by which hydrogen causes the embrittlement is difficult to study and is posited to act by either facilitating enhanced dislocation emission ahead of an advancing crack or by bond weakening and enhanced plasticity ahead of an advancing crack. The strongest evidence for the involvement of hydrogen in the SCC of 5xxx and 7xxx aluminum alloys comes from the observations of recovery and hydrogen evolution, from the measurement of sufficiently rapid grain boundary hydrogen diffusion and the precise matching of intergranular fracture surfaces that are striated with crack arrest markings.

Understanding hydrogen embrittlement is important in unraveling the mechanism and modes of failure processes including SCC; however, this far it has not been a key factor that has restricted the usage of high-strength aluminum alloys. There are no specific and generally accepted tests for assessing hydrogen embrittlement susceptibility of aluminum alloys, as embrittlement in hydrogen gas has not been observed irrespective of the test pressure.

3.08.5.5 Influence of Environment and Processing

3.08.5.5.1 Influence of alloy processing

The bulk microstructure of aluminum alloys is determined by the complex interaction between the cast microstructure and any subsequent thermomechanical processing operation. The situation is then complicated by any forming, finishing or joining operations that may locally modify alloy microstructures. Any deformation or heat-treatment processes that modify the local or bulk microstructure of the alloy will have an attendant influence on alloy corrosion. This is mainly due to the modification of the size and distribution of intermetallic phases at the micron, submicron and nanoscale and the change in grain size and grain shape from the cast state.

Soldered or brazed joints will usually have lower corrosion resistance than the parent metal, but sound-welded joints with resistance to attack equal to that of the parent metal can be obtained in most alloys.[97] Many assemblies contain angles, pockets or crevices that attract moisture originating either from external sources or from condensation. The corrosion so caused could often be avoided by redesign of the assembly, the provision of drain holes if possible (of at least 5 mm diameter) and the avoidance of horizontal surfaces being among the more important features.

3.08.5.5.2 Atmospheric corrosion

The aluminum alloys as a group present with a pleasant gray color outdoors, which may deepen to black in industrial atmospheres. Superficial pitting occurs initially but gradually ceases, being least marked on high-purity aluminum. With some alloys, including the copper-bearing alloys and the medium-strength Al–Zn–Mg alloys, additional protection, for example, painting, is desirable in the more aggressive atmospheres to avoid any risk of IGC.

Gases such as hydrogen sulfide and carbon dioxide do not typically increase the corrosivity of the atmosphere towards aluminum.[98] Service experience extends over 100 years and includes such well known examples as Eros, which is in an excellent condition although cast in a low purity (98%) aluminum, and the cupola of San Gioacchino (St. James), a church in Rome that was covered in 1897 with a sheet 1.25 mm thick and now shows attack to a depth of less than 0.13 mm. Twenty-year tests at selected marine,

industrial and rural sites in the United States[99] have shown that the greater part of the attack takes place in the first or second year and that thereafter the rate of attack maintains a low value.

The relatively high percentage strength losses are due to the extremely thin test specimens. After 20 years, the average measured depth of attack for an aluminum–copper alloy at a sea coast test site did not exceed 0.15 mm. The falling-off in the rate of pitting with time is in sharp contrast to the behavior of the older established structural metals that have a fairly uniform corrosion rate throughout their life, and indicates that the relative merit of aluminum increases with scheduled life.

Aggressive environments include marine conditions and particularly industrial atmospheres containing high concentrations of acid gases such as sulfur dioxide; rain washing is beneficial in both environments, while dampness and condensation alone can accentuate the rate of attack in the presence of chlorides and acidic sulfates. The relative severity of industrial, marine and rural conditions has been demonstrated by the results of 7-year tests in the United States and the United Kingdom,[100] and in this work the benefit from rain washing was especially manifest for the industrial sites in the United Kingdom. While the continual removal of atmospheric pollution by rain washing is beneficial, the removal of the protective corrosion product is obviously undesirable. The retention of the weathered surface is therefore usually preferred unless aesthetic considerations are of major importance, in which case abrasive or specialist chemical cleaning are effective.

Over many years Alcan used the CLIMAT test originally developed by Bell Laboratories[101] to "classify industrial and marine atmospheres." The test that has been standardized[102] involves the exposure of wire-on-bolt samples to the atmosphere of interest for a period of 90 days. Following the exposure, the wire-on-bolt samples are disassembled, cleaned and weighed, and the CLIMAT indices are determined from the percentage weight losses. Generally, three wire-on-bolt samples are exposed with aluminum wires wound on to plastic, copper and mild steel bolts. The relative values of the weight loss indexes enable the corrosivity of different sites to be compared and ranked. By 1988, it was estimated that Alcan had carried out over 13 000 individual CLIMAT tests in locations all over the world, and summarized versions of the test results have been published.[103–105] More recently, the CLIMAT test has been used to monitor and compare the severity of outdoor exposure sites in Europe and to assess the corrosivity of the automotive environment. The test has also begun to be used to compare the severity of different types of cabinet tests compared to outdoor exposure sites.

In urban areas, atmospheric fallout of carbon from partially burned fuel can cause severe localized pitting by galvanic action, although this is not commonly encountered. Indoors, aluminum retains its appearance well, and even after prolonged use may show no more than slight dulling, or on aluminum–magnesium alloys a slight bloom. This superficial deterioration can be accelerated by the presence of moist conditions and condensation which in extreme cases may lead to staining.

In order to enhance the durability of structural aluminum, anodizing provides a good level of protection. Anodized aluminum extrusions can survive even prolonged exposure in accelerated salt spray testing, indicating that the anodizing process where applicable is an industrially acceptable means of protection.

3.08.5.5.3 Natural waters

Immersed aluminum and its alloys have excellent resistance to attack by distilled or pure condensate water, and are used in industry in condensing equipment and in containers for both distilled and deionized water, as well as in steam-heating systems.[106]

Of the commercial alloys, only those that contain copper as a major alloying element are likely to corrode in unpolluted seawater, but pollution of the seawater may cause localized pitting attack to occur on other aluminum alloys. The Al–Mg alloys containing up to about 4.5% magnesium offer particularly good combinations of corrosion resistance and strength. Fouling collects readily on aluminum alloys, as on other materials, and where it may be necessary to use paints containing cuprous oxide for antifouling purposes, the risk of bimetallic corrosion must be substantially inhibited by a chemical pretreatment. Nowadays, the use of chromate priming paint in addition to mercury-containing antifouling compositions is not considered as a best practice. The behavior of aluminum in natural fresh water and tap water may vary, as these types of water differ widely in their dissolved solid content. No corrosion occurs immediately on immersion of aluminum and its alloys in these kinds of near-neutral water, and aluminum gives satisfactory service with all types of tap water provided regular cleaning and drying takes place, as occurs with aluminum hollowware. In some types of water, black or brown stains, which are largely due to

optical effects associated with the oxide film on the metal surface, occur. Although somewhat unsightly, the film is quite harmless and can be removed by simple methods such as boiling of fruits (e.g., rhubarb). Alternatively, preliminary boiling with pure water provides some protection against the staining, but can hardly be considered justifiable in most of the cases.

The combination of carbonate, chloride and copper is more damaging than if they are present singly or if one of them is absent,[107,108] so that some kinds of supply water are naturally more aggressive than others. The role of copper is of particular relevance, since as little as 0.02 ppm can initiate pitting in hard waters,[109] although more is required in soft waters which are otherwise less aggressive. In this context, however, it must be remembered that soft waters are inherently more cupro-solvent than hard waters; consequently, the conjoint use of aluminum and copper fittings is rarely advisable irrespective of the necessity for avoiding galvanic interaction when the two metals are in direct contact. This latter point has traditionally stifled the usage of aluminum in more routine plumbing applications, although use of aluminum in such applications is likely to be considered again as the price of brass- and copper-based fittings and pipework increases relative to the price of aluminum.

Once pitting has started, it may continue in solutions which would themselves be incapable of initiating corrosion. In water of all types, the rate of increase in the depth of pitting falls off rapidly with time. Water movement (of the order of 0.3 m s^{-1} or more) will reduce pitting or prevent its initiation. A rise in temperature tends to lead to higher corrosion rates at existing pits, but even with the most aggressive hard waters, above about 50 °C the oxide-forming mechanisms act to prevent the initiation of pitting as shown by the long and satisfactory service given by aluminum hollowware, which is assisted in some waters by scale formation.

Where aluminum is to be used in direct contact with cold, natural water with no possibility of regular cleaning, clad aluminum alloys are the preferred materials. Aluminum–zinc alloys are used for cladding that is anodic to the core alloy and corrosion is therefore restricted to the surface cladding, thereby obviating the risk of perforation. Cladding with super-purity aluminum is preferable where it is important to have the minimal degree of total corrosion, but in this case, the potential relationship with the core is more critical and in some circumstances the cladding can actually become cathodic. Sacrificial protection may also be obtained from sprayed coatings of appropriate composition which can be applied to extrusions and castings as well as to sheets, rods, plates and tubes. In practice, unclad aluminum–manganese alloys have been used for piping soft water in the United Kingdom and, more widely, in the United States.

3.08.5.5.4 Underground corrosion by soils

This is largely related to the presence of moisture which can leach out soluble constituents from the soil. As it is the case with natural water, the nature of the corrosive environment is a more important factor than the alloy used, provided that copper-bearing alloys are avoided. At present, it is difficult to produce a satisfactory classification of soils with respect to their aggressive action on aluminum alloys. Made-up ground, particularly when it includes carbonaceous cinders, is usually extremely corrosive, while neutral clays are often the least corrosive. It is desirable that protection should be given to all aluminum materials buried in soils[110] except where there is previous experience of satisfactory service from aluminum in a given soil. Pipe wrappings based on bitumen (or the now legislated-against chromates) are effective, while for cable sheathing, a continuous plastic coating provides both electrical and corrosion protection. Cathodic protection has been utilized for pipelines[111] but is not widely practiced; close control is necessary since overprotection can result in alkali attack (from excessive accumulation of hydroxyl ions generated from the CP). Potentials in the region of −1.0 V versus saturated $Cu/CuSO_4$ are favored although some divergence of opinion exists in this respect.

3.08.5.5.5 Corrosion in chemical environments

Detailed information about the behavior of specific chemicals is given in several works of reference.[112–115]

Acids

Most acids are corrosive to aluminum-based materials. The oxidizing action of nitric acid at concentrations above about 80%, however, causes passivation of aluminum. Very dilute and concentrated sulfuric acid dissolves aluminum only slowly. This is seen graphically in **Figure 10**.

Boric acid also exerts little attack on aluminum, while a mixture of chromic and phosphoric acids can be used for the quantitative removal of corrosion products from aluminum without attacking the metal.

Organic acids usually have low rates of attack on aluminum, notable exceptions to this generalization

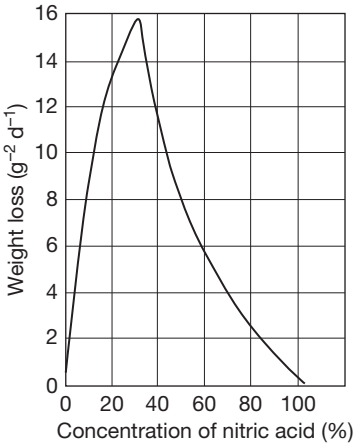

Figure 10 Action of nitric acid of various concentrations on commercial-purity aluminum at 20 °C. Adapted from *Aluminium in the Chemical and Food Industries*; British Aluminium: London, 1959.

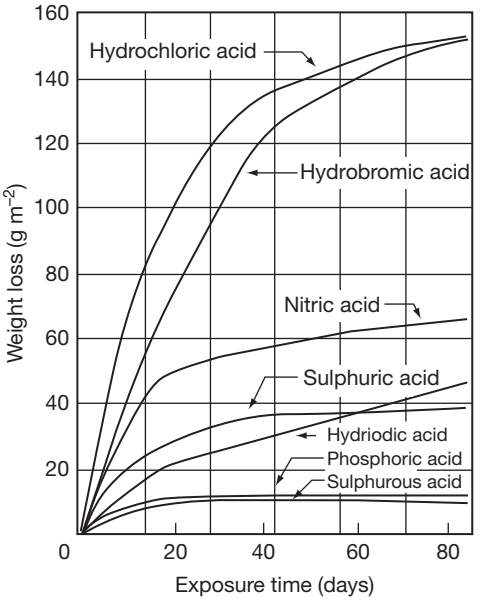

Figure 11 Action of dilute (0.1 N) solutions of inorganic acids on commercial-purity aluminum at 25 °C. Adapted from *Aluminium in the Chemical and Food Industries*; British Aluminium: London, 1959.

being formic acid, oxalic acid and some chloride-containing acids such as trichloroacetic acid. Glacial acetic acid (pH 3) has no significant corrosive effect on aluminum but the rate of attack increases rapidly with decreasing concentration or in the absence of the traces of water normally present. The rate of corrosion in an acid solution rises rapidly with temperature, often doubling or more with a 10 °C rise.

A summary of the effect of dilute inorganic acids on the corrosion of aluminum is seen in **Figure 11**.

Alkalis

Alkalis are generally corrosive to aluminum; caustic soda is in fact used for chemical milling of aluminum. Ninety-nine percent pure aluminum is, however, resistant to ammonium hydroxide, even at pH 13, while the action of more dilute caustic alkalis can be inhibited by the use of silicates. Mild alkalis such as sodium carbonate are moderately corrosive and are not recommended for washing aluminum hollow-ware. Synthetic detergents, in general, give satisfactory service in cleaning aluminum, but those containing uninhibited sodium carbonate may give some surface roughening. Inhibitors such as silicates can prevent attack by the more dilute solutions.

Alloys of aluminum with magnesium or magnesium and silicon are generally more resistant than other alloys to alkaline media. The corrosion rate in potassium and sodium hydroxide solutions decreases with increasing purity of the metal, but with ammonium hydroxide the reverse occurs.

Inorganic salts

Most simple inorganic salt solutions cause virtually no attack on aluminum-based alloys unless they possess the qualities required for pitting corrosion, which have been considered previously, or hydrolyze in solution to give acid or alkaline reactions, as do, for example, aluminum, ferric and zinc chlorides. With salts of heavy metals, notably copper, silver and gold, the heavy metal deposits on the aluminum, where it subsequently causes serious bimetallic corrosion.

Some salts, notably chromates, dichromates, silicates, borates and cinnamates, have marked inhibitive power and are very effective in closed-circuit water systems. Care must be taken to ensure that a sufficient quantity of such anodic inhibitors as chromates is added, as otherwise attack, though occurring at fewer points, may be more severe at these points. Chromates and dichromates have little inhibitive power in strongly acidic solutions. It is emphasized that while chromates are mentioned herein for historical purpose, the toxicity of chromates has resulted in a dramatic decrease in their use in the past decade, and may result in a zero-usage policy on the global scene within the coming few years.

Aluminum is used in hydrogen peroxide processing and storage equipment partly because of its high corrosion resistance and also because it does not cause degradation of the peroxide.

Organic compounds

With many organic compounds, aluminum shows high corrosion resistance either in the presence or absence of water. The lower alcohols and phenols are corrosive when they are completely anhydrous, although this is rarely encountered in practice since repair of breaks in the natural protective oxide film on aluminum cannot take place in the absence of water. Amines generally cause little attack unless very alkaline.

Processing and storage equipment for many chemicals, including acetaldehyde, formaldehyde, nylon salt, methyl methacrylate, carbon tetrachloride, glycerol, triacetin, proprionic acid, acetic acid and acetic anhydride, is manufactured from aluminum alloys, primarily because of their excellent corrosion resistance.

Aluminum has good resistance to petroleum products, and an Al–2Mg alloy is used for tank heating coils in crude-oil carriers. Caked-on deposits must be removed from the coils by hot seawater cleaning in order to maintain effective heat transfer and prevent corrosion. Aluminum is also used in the petroleum industry for sheathing for towers, heat exchangers, transport and storage tanks and scrubbers. Many industries use aluminum alloys for heat exchangers, clad alloys being used where pitting corrosion is liable to be initiated by one of the contacting materials. Heat exchangers in the gas industry have utilized duplex tubes, with aluminum on the water side and steel on the gas side in cases where aluminum is unsuitable owing to the presence of catechol which can attack it.

Aluminum does not become brittle at low temperatures and for this reason (and because of its corrosion resistance), it has been adopted for the carriage and storage of liquefied methane.

3.08.5.5.6 High temperature corrosion

Dry atmospheres

When exposed to high temperatures in dry atmospheres, aluminum is highly resistant to corrosion by most of the common gases, other than the halogens or their compounds.

High temperature aqueous systems

When aluminum corrodes at temperatures below 90 °C in aqueous systems, attack is usually by pitting. At temperatures between 90 and 250 °C (for the attainment of which considerable pressures are needed), uniform attack is the commonest form of aqueous corrosion. Above about 250 °C, uniform attack is merely the prelude to highly destructive intergranular attack. The corrosion products from the uniform attack form a film which includes a barrier layer and a bulk film analogous to those formed during anodizing; it is the bulk film that controls the corrosion rate, which is not significantly affected by most common dissolved ions. The onset of intergranular attack occurs at about the same time as the crystallization of the amorphous barrier layer oxide. Kinetic studies indicate that over the temperature range from 100 to 363 °C the oxidation rate law is successively inverse logarithmic, parabolic and linear.[116]

The requirements of nuclear energy application fostered an interest in special alloys for service in high temperature aqueous environments, but their utilization has not been widespread. Encouraging results have been reported for alloys of 2Ni–0.5Fe and 1.2Ni–1.8Fe.[117]

Steam forms a protective white film at temperatures up to about 250 °C, but above this temperature steam can, under some conditions, react with aluminum progressively to form aluminum oxide and hydrogen. Sintered aluminum powder (SAP) has relatively good resistance to steam at 200 °C, but at about 300 °C an addition of 1% nickel to the SAP is needed to prevent rapid disintegration.

Molten salts and metals

Aluminum alloys resist the action of many molten salts which are nearly neutral in reaction. Molten sodium nitrate or mixtures of sodium nitrate and potassium nitrate are, even nowadays, most commonly used for salt-bath heat treatment of most aluminum alloys.

Molten metals generally attack aluminum alloys. Both zinc and tin form alloys by dissolution of aluminum, although the aluminum does not melt. Molten lead is inert to aluminum, and molten lead baths can be used for heating aluminum alloys.

3.08.5.5.7 Aluminum in contact with other materials

The aluminum alloys recommended for structural and architectural purposes (not including the high-strength alloys containing copper) have relatively good resistance to concretes, mortars, plasters and cement products. When freshly mixed, some of the materials release traces of alkaline products that are sufficient to stain aluminum (that is, to etch it). As soon as the mixture is set, the attack, however, is noted to cease, and even after many years' service attack on embedded aluminum is found – empirically – to be negligible.[118]

With cement and concrete under continuous wet conditions, there may, however, be surface attack. This decreases with time, and the strength of components is not significantly affected. Under embedment conditions, bituminous protection is advisable to avoid risk of cracking of the concrete due to stresses set up by the bulk of the voluminous aluminum corrosion product. Plasters are generally less aggressive than Portland cement. In damp environments, some corrosion of aluminum may arise in contact with the more open-grained building stones and brickwork, but the hard stones, such as granite, are inert. With building stone and brickwork, as with soils, it is the nature of the products that can be leached out which will determine whether aluminum corrodes. Unprotected aluminum, in the form of nails for example, can be satisfactorily used in contact with precast concrete blocks, which are usually noncorrosive to aluminum. Magnesium oxychloride compositions (used for flooring), on the other hand, stimulate corrosion of aluminum under moist conditions, as well many insulation materials based on magnesium and calcium silicates.

Plastics generally do not react with aluminum and are widely used to provide insulation between other metals and aluminum. Rubber has no effect upon aluminum unless it is filled with carbon.

A few acid woods, such as oak, chestnut and Western red cedar, accelerate surface weathering of aluminum, but do not usually give rise to serious attack.[119] Timber preservatives containing soluble copper compounds should be avoided; creosote and zinc napthenate are satisfactory preservatives for wood in contact with aluminum.

Common packaging materials are a potential source of aggressive substances,[120,121] and careful selection is recommended to avoid surface deterioration. Where paper is in contact with aluminum, the chloride content should be below 0.05%, sulfate content below 0.25% and copper content below 0.01%, and the pH of aqueous extracts in the range pH 5.5–7.5, in order to avoid corrosion in damp conditions. Papers and felts used in building applications should also conform to this specification as a minimum requirement and be of the highest quality, since metallic copper found in materials of inferior origin can result in severe local galvanic attack of aluminum. Tarpaulins are sometimes treated with copper-containing preservatives, and water leached from these has been found to cause corrosion of underlying aluminum sheets.

Fiberglass insulation produced from soda glass can cause pitting in conditions where leaching of alkali occurs, for example, by condensation: the use of fiberglass produced from Pyrex glass is therefore preferred. Common putties of whiting/linseed oil composition do not attack aluminum; adhesion is obtained by allowing the metal surface to weather, or by applying an etch primer treatment to the metal. Both thermosetting adhesives (e.g., the phenolic types) and thermoplastic adhesives (such as paraffin and microcrystalline waxes or bitumen) are noncorrosive to aluminum. In general, adhesives applied to aluminum should not contain chlorides in excess of 0.05% (as NaCl) of the solid content, and should be free from copper- or mercury-containing fungicides. The presence in the adhesive of borax or sodium silicate is beneficial when one of the adhesive components is of an acidic character.

3.08.5.5.8 Applied stress

Stress below the proof stress does not normally affect corrosion rates. Cyclic stresses in combination with a corrosive environment (corrosion fatigue) can produce failure at below the ordinary fatigue limit. Alloys susceptible to intergranular attack may corrode faster when stressed (see **Section 3.08.5.4**).

3.08.6 Corrosion Prevention Strategies

3.08.6.1 Inhibitors

Corrosion of aluminum and aluminum alloys can be controlled by use of inhibitors added to aggressive aqueous environments. For the purpose of this discussion, an inhibitor is a chemical substance, soluble in water, that slows the corrosion cell process on aluminum. The range of inhibitors that slow corrosion of aluminum is large, and there are a number of useful ways to deliver chemical inhibitors when corrosion is a risk.

Soluble corrosion inhibitors act by slowing either the anodic reaction or the cathodic reaction or both. This gives rise to a useful scheme for classifying chemical inhibitors. Those that slow the anodic reaction are referred to as ‘anodic’ inhibitors, those that slow the cathodic reaction are ‘cathodic’ inhibitors, and those that slow both reactions are ‘mixed’ inhibitors.

For aluminum alloys, anodic inhibitors typically act to increase the pitting potential in electrochemical testing, or slow or suppress the onset of pitting in exposure testing. Even with good anodic inhibitors, pitting may occasionally occur if pre-existing defects

on the alloy surface are weak enough. Additionally, anodic inhibitors may have no effect on slowing the growth of existing pits.

Cathodic inhibitors are usually substances that slow the rate of the oxygen reduction reaction on aluminum alloy surfaces. By slowing down oxygen reduction, the companion aluminum oxidation reaction must also slow down. This results in an overall decrease in the corrosion cell kinetics, as well as a decrease in the free corrosion potential. For the best inhibitors, the decrease in the corrosion potential is usually to a value well below the alloy's pitting or repassivation potential. Cathodic inhibitors have the advantage of being able to improve corrosion resistance at very low concentrations. For example, chromate added at micromolar concentrations to an aerated dilute chloride solution is enough to significantly reduce the rate of oxygen reduction leading to significant corrosion protection.

Soluble corrosion inhibitors are usually ions in solution. Important inorganic anions that inhibit aluminum corrosion include chromate, phosphate, permanganate, nitrate, vanadate, molybdate, tungstate and silicate. Cations of strontium, cerium and the lanthanides as well as zinc are inorganic cationic inhibitors. Organic substances that are inhibitors of aluminum corrosion include phosphonates, sulfonates, benzoates, thiols, azoles, amines, fatty acids and natural compounds such as tannins. Among these, special attention must be given to chromates. Chromate is an exceptionally powerful inhibitor of oxygen reduction and an excellent inhibitor of aluminum corrosion. Chromates are used across all industries as aluminum corrosion inhibitors. However, their use is becoming increasingly restricted over concerns for work-place safety and environmental pollution because chromates are human carcinogens.

Inhibitors can be incorporated into coating systems in a variety of ways. Sparingly soluble inorganic compounds and ion exchange materials are used as corrosion inhibiting pigments in coating formulations. Inhibitor ions can be attached to reactive sites on coating resin polymers or directly applied to aluminum surfaces using an evaporable solvent.

3.08.6.2 Conversion Coatings

Conversion coatings, which are frequently referred to as pretreatments or pretreatment coatings, are applied to aluminum and aluminum alloys to improve corrosion resistance or to improve adhesion of subsequently applied organic coatings and adhesives. From a technological and processing perspective, conversion or pretreatment coating of aluminum is analogous in some ways to phosphating of steel and passivation of stainless steels. The conversion coating process involves contacting the surface to be coated with an aqueous solution containing surface activators and coating-forming ingredients. Contact times in commercial processes range from seconds on a continuous coil processing line to minutes for certain aerospace applications, and solution contact with the surface can be applied by immersion, spraying or rolling. Coating solutions are operated at or slightly above room temperature, and bath stability is maintained under careful control using guidelines from the pretreatment system supplier. Commercial conversion coating processes are well supported by suppliers, and methods for maintaining coating baths and ensuring coating quality are almost always provided.

Conversion coatings are not as protective as anodized coatings, and in most cases, conversion-coated surfaces are subsequently primed or painted. Conversion coatings are used for stand-alone corrosion protection when mild to moderate, occasionally condensing, atmospheric exposure conditions are expected, or for temporary corrosion protection.

Pretreatment of aluminum has relied extensively on chromate-based systems. There are two general classes of chromate conversion processes: the activated acidic formulations such as the chromium chromate processes that use a sodium fluoride–chromic acid chemistry, and alkaline oxide processes based on a sodium chromate–sodium hydroxide or carbonate chemistry. Activated acid processes have been the dominant process across many industry sectors for over 50 years. In finished form, conversion coatings produced are a light to deep yellow, continuous, and conformal across the surface with thicknesses ranging from 0.1 to 1.5 μm depending on coating bath contact time. Freshly formed coatings are gelatinous and require at least a day to harden before handling. Such coatings can prevent pitting for several thousand hours of continuous salt spray exposure. Alkaline oxide coatings fell out of common use with the emergence of activated acidic formulations. Alkaline oxide coatings are thicker, less uniform and occasionally dusty. Coating baths produce much sludge and are difficult to maintain.

Chromate conversion coatings are noted for their ability to self-heal. Self-healing refers to the ability of the coating to resist corrosion from scribes or defects in the coating. This phenomenon is attributed to the release of labile hexavalent chromium in the coating

into an aggressive solution contacting the surface. Chromate ions are released by the coating, and can be transported to the site of damage to participate in repair of the film by reduction of the chromate to a chromic species that bond with the aluminum substrate and the existing conversion coating.

Chromate is a human carcinogen, and chromate-based coatings are banned in many countries. In response to this ban, trivalent chromium conversion coatings have been developed. These coatings provide useful levels of corrosion protection, but are not as protective as chromate conversion coatings. They are also observed to perform better on certain alloys than others.

There has been a major worldwide initiative to develop chrome-free pretreatment systems for aluminum alloys. Successful chrome-free pretreatment of aluminum alloys depends on a number of critical factors ranging from alloy and process route selection through to appropriate surface cleaning and how corrosion or durability testing is carried out to compare chrome-free and chrome-based systems.

Recent results have shown that the severity of corrosion of coil-coated aluminum architectural sheet is directly related to the manganese content of the alloy. This means that alloys such as AA3003, AA3103, AA3004, AA3104 and AA3005 are all potentially more susceptible to corrosion than alloys with a lower manganese level, such as AA3105, or AA5050, AA5251, AA5754, etc. It is quite difficult to make the low-manganese AA3xxx or AA5xxx alloys susceptible to corrosion under paint films.

Generally, the corrosion susceptibility of painted aluminum is due to an active surface layer.[122–128] This arise from the high level of surface shear induced during rolling, which transforms the near-surface microstructure. Deformed surfaces are characterized by an ultrafine grain size that can be stabilized by magnesium oxide pinning in magnesium-containing alloys.[129] A typical deformed surface layer on an AA3104 alloy after hot rolling is shown in Figure 12.

However, it is not the fine grain size that is responsible for the corrosion susceptibility of the surface layer. This susceptibility is promoted by the preferential precipitation of manganese-rich dispersoids during annealing treatments. Susceptibility is directly related to density of precipitated dispersoids, which, in turn, depends on the manganese solid solution level and the temperature and time of annealing. This is why manganese has such a strong influence on corrosion susceptibility.[130–132]

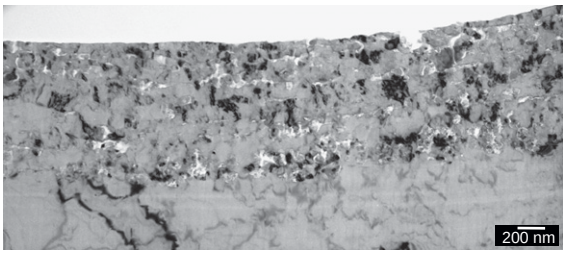

Figure 12 TEM image of an ultramicrofomed section of a hot-rolled AA3104 alloy after breakdown rolling showing the ultrafine grains pinned by magnesium oxide particles. Courtesy of Yanwen Liu.

Deformed surface layers on aluminum alloys are produced most readily by hot rolling, and generally the layer thickness of sheets and plates after hot rolling is of the order of a micrometer. The deformed layer thickness is progressively reduced by cold rolling, so alloys that have been extensively cold rolled have thinner deformed layers that can more readily be removed by conventional etch-cleaning operations. This means that resistance to corrosion can be improved by increasing the transfer gauge thickness so that after cold rolling the amount of surface to be removed at final gauge is 0.2 μm or less.

Another route to reduce susceptibility is to homogenize rolling blocks before hot rolling to precipitate out the manganese from solid solution. This is equivalent to using a lower manganese-containing alloy. A further possibility is to eliminate hot rolling by using either roll-cast or thin belt-cast production routes. This is particularly effective when used in combination with appropriate alloy selection.

Cleaning is the most critical process step to provide alloy surfaces that can be successfully pretreated with a chrome-free pretreatment. Basically, the corrosion active surface layer must be removed using either an acidic or alkaline treatment. The amount of metal to be removed depends directly on the layer thickness, and this means that cleaning is facilitated where there has been significant cold rolling to reduce layer thickness. In low-magnesium alloys, the ultrafine grains are usually annealed out, but there is still a preferential precipitation of dispersoids compared to the bulk microstructure. The entire corrosion sensitive layer must be removed. For most AA5xxx alloys, the only requirement is to remove magnesium oxide from the surface, as this can reduce adhesion particularly for bonding applications. This means that cleaning of AA5xxx alloys is much more straightforward than cleaning AA3xxx alloys, particularly those with high manganese content.

Aluminum alloys generally become immune to underfilm corrosion following effective cleaning to remove any corrosion-susceptible layers. However, it is very important to avoid accumulation of copper on the alloy surface during the cleaning operation and/or to ensure that any copper enrichment is removed by a suitable desmutting treatment. Copper is readily enriched on the surface of aluminum alloys in both acid and alkaline etching solutions. Generally, it is important that surfaces are not overcleaned and that the cleaning operation is calibrated such that the end of cleaning coincides with active layer removal. Copper enrichment during cleaning can be measured on alloys where the nominal copper level in the alloy is less than 0.1%.

The principal function of pretreatment or conversion treatment after cleaning of architectural and automotive sheet alloys is to provide good adhesion. This can be achieved by using a treatment to enhance the natural oxide layer, such as anodizing or hydrothermal treatment in water or steam. Anodizing pretreatments have been used very effectively for many years, although they are not in widespread use as coil-line treatments. Coil-line treatments are based on fast anodizing in either sulfuric acid or phosphoric acid. These types of preteatment have the advantages of speed, control and uniformity compared to most chemical conversion treatments. They are much underutilized as chrome-free pretreatments for aluminum alloys.

Fluorotitanic- and fluorozirconic-acid-based pretreatments are in widespread use as chrome-free alternatives. Such pretreatments are effective but are more difficult to monitor in production compared to traditional chrome-based systems. This is particularly an issue where polymeric additions are made to the formulation to improve performance. For such systems, good adhesion is achieved through good surface coverage of a uniform film of either zirconium and/or titanium oxide. However, adhesion is severely compromised if the film is too thick, and this can lead to coating failure in service that is unrelated to corrosion sensitivity.

Pretreatment systems based on the use of adhesion promoters such as silanes, phosphonates and polyacrylic acids have been extensively researched. These pretreatments can be very effective especially when applied as monolayers rather than thick films. They are probably most useful when used in combination with a thin anodizing treatment or similar treatment to increase barrier film thickness and to develop a microsurface roughness to enhance adhesion.

There is very little systematic information on the field performance of painted aluminum products. Most useful information has come from the carefully monitored exposure of sets of test panels on exposure sites. The results of these studies correlate extremely well with filiform corrosion tests and with certain cyclic corrosion tests that are not overaccelerated by acidification or the use of additions of copper salts. There is generally poor correlation with the results of acidified salt spray tests either in terms of performance ranking or in the observed mode of corrosion. It is inappropriate to use corrosion tests designed for steel substrates for aluminum, as the conditions that promote corrosion are quite different. Corrosion of painted aluminum requires the presence of chloride and a high humidity. Corrosion of aluminum under conditions of total immersion or at humidity levels of more than 95% does not show the filamental corrosion mode that is seen on exposure sites or in service.[133]

Corrosion on painted panels occurs most readily on marine sites when panels are exposed vertically, facing north, and the panel is protected by an overhang so that accumulated chloride is not removed by rain. Such conditions are not reproduced in most cabinet-based corrosion tests.

Although the surface of wrought aluminum products can be made corrosion resistant by cleaning to remove active surface layers, it is important that such surfaces are not damaged by subsequent high shear processes such as grinding or machining operations. This is particularly important for aluminum automotive alloys, such as AA6111 and AA6016, which are used in external closure panel applications. Mechanical grinding during processes such as rectification can readily produce an ultrafine-grain-sized surface layer as shown in **Figure 13**. This layer is not removed during cleaning and phosphating as part of the body-in-white finishing operation. The layer can become more corrosion-active than the underlying bulk metal following paint baking. This is due to preferential precipitation of the aging precipitate in the surface layers compared to the bulk microstructure.

The situation of aluminum external closure panels is similar to using galvanized steel, in that rectification must be minimized in the areas that are susceptible to stone chip damage. For galvanized steel, surface grinding removes the protective zinc layer, whereas for aluminum, a corrosion active layer is created by the grinding and finishing operation. However, corrosion in service can occur only if the paint film is damaged to expose the bare metal.

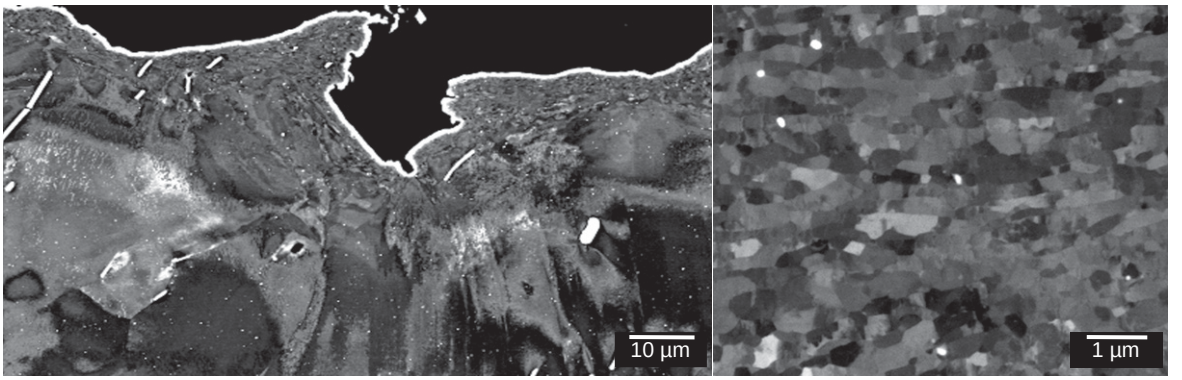

Figure 13 Scanning electron micrographs of the surface of an AA6016 alloy after rectification by grinding. The higher magnification image shows the ultrafine grain size of the deformed layer. Courtesy of George Thompson.

Although as-cast surfaces have not been found to be susceptible to filiform corrosion, it is possible to develop active layers on castings by grinding or machining and subsequent thermal treatment. This is probably the main influence on the corrosion of cast aluminum wheels. The surface of extruded aluminum has been studied extensively, although ultrafine grain microstructures have not been reported. However, transformed surface microstructures, particularly those with coarse grain structures, have been well documented. Resistance to filiform corrosion is also significantly improved by deep surface etching. Cutting, grinding and machining operations, following cleaning and pretreatment either before or especially after painting, are probably highly significant in promoting corrosion in service.

Secondary metal generally contains higher levels of impurities compared to primary metal. This can lead to higher levels of elements such as iron, silicon and copper and also contamination by elements such as lead, bismuth, zinc and tin. Aluminum alloys made from secondary metal can be highly resistant to corrosion using chrome-free pretreatments, provided that alloy compositions are optimized. In addition, continuous casting production routes should be chosen to minimize active layer development by eliminating hot rolling. Effective cleaning is critical, and surface enrichment of elements such as copper, lead, bismuth, zinc and tin must be avoided or such enriched layers must be removed. After such cleaning, continuously cast alloys made from secondary metal can be shown to be highly resistant to corrosion using simple chrome-free pretreatments that promote good adhesion.

3.08.6.3 Anodizing

Aluminum and aluminum alloys can be anodized to enhance corrosion protection and improve adhesion of subsequently applied organic coatings, and improve a range of other surface properties. For this reason, it is a very widely used process. Anodized coatings are formed electrochemically in an aqueous solution that results in an aluminum oxide surface film (see **Figure 14**). Anodized coatings on aluminum alloys are on the order of 2–50 µm in thickness. Aluminum anodization is usually carried out in an acidic bath that contains ingredients which promote formation of an adherent oxide film. Anodization is most commonly carried out in chromic acid solutions and sulfuric acid solutions. To improve corrosion protection, anodized coatings can be sealed in a second step in the process.

Chromic acid anodization is carried out in solutions that are at or slightly above room temperature. Coating times range from 30 to 60 min, and result in a 2–5-µm-thick gray-colored coating. This process does not consume much of the base metal, making it suitable for applications where precise part dimensions must be maintained. Among various anodization processes, the chromic acid process causes the smallest fatigue strength debit. The chromic acid process is the process of choice for porous surfaces and complex shapes where rinsing of the anolyte may be difficult. The residual anolyte is rich in chromate, which is passivating and protective for aluminum alloys.

Sulfuric acid anodization is carried out at ambient temperatures in H_2SO_4 solutions. Coating times range from 30 to 60 min. The process yields coatings that are 5–10 µm in thickness. These coatings possess

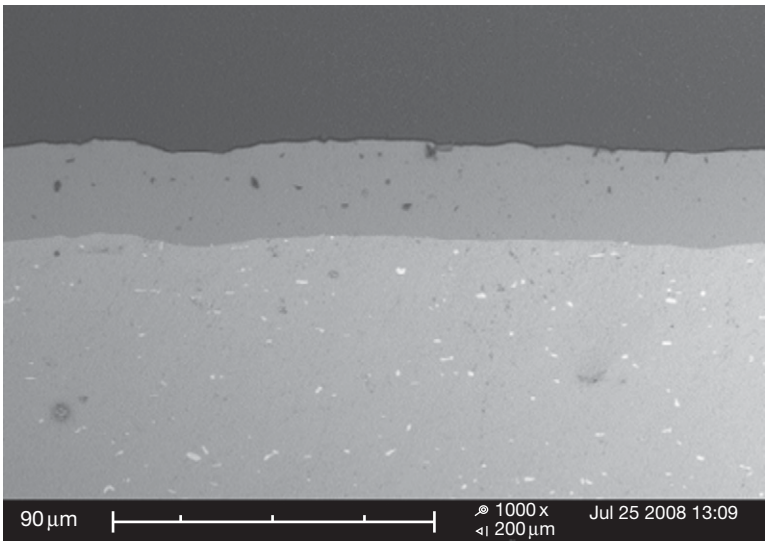

Figure 14 Backscattered SEM image revealing the anodized coating upon a sectioned piece of extruded AA6060. Courtesy of Brendan Stafford.

good corrosion resistance, which can be improved by sealing the coating through subsequent immersion in the sodium chromate solution. Coatings produced by this process can be dyed to take on a range of colors.

Changes to the sulfuric acid anodization process can be made to produce anodized layers with high hardness. The so-called hard coat anodization processes are carried out in solutions chilled to near freezing (about 1 °C). Coating times range from 20 to 120 min. These coatings can be as much as 50 µm in thickness. Coatings are very hard and suitable for applications where wear resistance is needed. The intrinsic porosity of the coatings makes them well suited for adhesive bonding applications. Corrosion resistance of these coatings is excellent and can be further improved by sealing in boiling water or nickel-based sealing solutions.

The protectiveness of anodized coatings is commonly tested using accelerated exposure testing. When anodized coatings fail, the substrate is subjected to localized corrosion, which occurs mainly in the form of pitting. Electrochemical methods are appropriate for characterizing the corrosion resistance of anodized coatings. In particular, electrochemical impedance methods are useful for determining the effectiveness of sealing treatments as well as the overall protectiveness of the anodized layer.

3.08.6.4 Organic Coatings

The natural passivity of aluminum is often insufficient to protect against corrosion in many common service environments. Alloying aluminum further degrades protection conferred by passivity, and alloys are almost always coated when the application requires prolonged exposure to outdoor environments.[134] A broad range of organic coatings can be applied to aluminum alloys. For many engineering applications, and certainly the most demanding ones, a coating system consisting of multiple coating layers is used. Each layer contributes to the functionality of the overall coating system. Functions imparted may include adhesion to the underlying alloy, flexibility, impermeability, chemical resistance, abrasion resistance, electromagnetic signature control and, of course, corrosion protection.

There are two general strategies for imparting corrosion protection by organic coatings: barrier protection and active corrosion protection. The barrier protection strategy is based on the simple concept of preventing contact of the underlying aluminum substrate with the environment. The vast majority of protective coatings systems used today are based on this concept. While simple and straightforward, this concept is remarkably difficult to implement and sustain in practice in engineered systems. There are two reasons for this. First, coatings contain defects that are formed during the application process. These defects can serve as corrosion initiation sites when a coated component is placed in service. In modern coating operations, great effort is made to apply coatings on scrupulously clean surfaces under very well controlled conditions. This minimizes defect

formation and leads to higher quality, longer lasting coating systems. Second, coatings will sustain damage in service. Damage can arise from mechanical action at the surface that scrapes or scratches. Damage can also arise by exposure to aggressive chemical agents. This can degrade the organic component of the coating destroying the barrier properties. Exposure to thermal energy and ultraviolet radiation can also degrade the integrity of the organic component of the coating.

In the active corrosion protection strategy, barrier properties of the coating are not necessarily important. Coatings that protect by this mechanism contain a releasable corrosion inhibitor. As moisture from the environment penetrates the coating, the corrosion inhibitor is released. In well-designed coatings, any moisture that reaches the coating–metal interface will have enough inhibitor in it so that the natural passivity of the underlying alloy is preserved. This protection strategy is not as widely employed as barrier protection, but strontium chromate-pigmented organic primer coatings used widely in aerospace applications depend critically on this protection mechanism.

Corrosion of aluminum under organic coatings generally occurs as filiform corrosion, although blistering is observed on samples exposed to accelerated corrosion tests or where coating adhesion is entirely inadequate. In thick and opaque coating systems, corrosion under the coating may be difficult to detect until corrosion has progressed to a significant extent.

Corrosion of organically coated metals is typically characterized using outdoor exposure tests or simulated service testing. Overaccelerated corrosion tests should be avoided, as their relative ranking of corrosion susceptibility is usually erroneous and the observed mode of corrosion is not that found in service. The extent of corrosion damage accumulation is normally characterized visually. Early stages of coating degradation and undercoating substrate corrosion can be characterized by electrochemical methods including electrochemical noise and electrochemical impedance spectroscopy. The application of impedance spectroscopy for characterizing degradation of organically coated metal surfaces has been thoroughly reported in the scientific literature.

3.08.7 Applications of Aluminum Alloys

In recent years, the aluminum industry has become a global industry, just as the business interests of its customers have become global. The world economy has integrated, and major industry consolidation has occurred. Today, Alcoa is the only independent major producer in North America, as Alcan has become part of Rio Tinto. Alcoa, Alcan (as Rio Tinto Alcan) and Rusal are the three largest aluminum companies.

Total global aluminum consumption (as measured as aluminum semis, castings and forgings) grows each year by about 5% on average. Rolled products are the largest product form at 35% (16.4 mt) followed by castings at 26% (12 mt), extrusions at 24% (11.3 mt), wire and cable at 10% (4.8 mt), and forgings and other forms at 5% (2.5 mt). In 2005, the geographical market was split among North America (24%), Western Europe (22%), China (22%), Asia (21%), Latin America (5%), Africa and Oceania (2%), Eastern Europe (2%) and CIS (2%).[3]

Presently, there are three main markets for the aluminum industry: packaging (cans and foil), transportation (automotive and light trucks) and building and construction. About 25 years ago, building and construction was the largest aluminum market, packaging was second and transportation was third. Then, 10 years ago, transportation became the largest market, followed by packaging and then construction. However, more recently in the emerging economies, building and construction has been the greatest source of growth and this is now the second largest market for aluminum after transportation. In terms of global consumption of the 43 Mt of aluminum produced in 2005, transportation was 27%, building and construction 20% and containers and packaging 16%. These main uses were followed by electrical (10%), machinery and equipment (8%), consumer durables (7%) and other uses (12%). In 2007 ~14.5 Mt of aluminum was used in transportation, 13 Mt in building and construction, and 4.5 Mt in beverage cans.[3]

In packaging, aluminum cans are in competition with plastic containers and, to a much lesser degree, glass, although this varies considerably from country to country. In North America, steel is not much of a factor, whereas in Europe it still is, and in certain markets like the United Kingdom, there is direct and sustained competition between aluminum and steel cans. Presently, the recycling rate of aluminum used beverage cans (UBCs) varies significantly from country to country and from state to state in the United States. Critical factors are legislation and the use of financial incentives (e.g., returnable deposits on cans) to promote collection and return. Corrosion concerns in packaging applications are not a major factor.

There is a direct relationship between the weight of a car and its fuel consumption, and although there are global legislative initiatives to reduce fuel consumption and carbon emissions, the weight of cars has in fact progressively increased since the 1970s. This is shown by the increase in weight of the VW Golf from the Mark 1 (750 kg) to the Mark 2 (770 kg), the Mark 3 (960 kg), the Mark 4 (1060 kg) and the Mark5 (1200 kg). The main factors that have led to this weight increase are safety, both for crash and pedestrians, comfort and build quality. The weight of a car is mainly from its structure or 'body-in-white' (BIW) (34%), its drive train (25%) and its engine (17%), and the increase in BIW weight has been the most significant contributor to vehicle's weight increase. There is strong competition between high-strength steel, aluminum, magnesium high pressure die castings and plastics for BIW construction. The average aluminum content of European cars increased from 32 kg in 1978 to 120 kg in 2002 and is predicted to be 160 kg by 2010. This total use of 160 kg is split between BIW hang-on panels (50 kg), suspension and wheels (50 kg), engine and drive train (43 kg) and interior components (17 kg). Audi has led the way in making aluminum-intensive cars exemplified by the A2 1.2TDi introduced in 1999, which was the first mass-producible car with a fuel consumption of 3 l of fuel per 100 km traveled. The emissions from this car were only 80 g of CO_2 per kilometer. In North America, it is estimated that an average car or a light truck has about 160 kg of aluminum and the major applications are in hang-on panels (bonnets and deck lids) and engines, with aluminum engines representing about 90% of current production. The potential for increased use of aluminum in cars is enormous, particularly as number of vehicles on the road is predicted to increase from 800 million to more than 1450 million in 2030 with nearly all of this increase in developing economies like India and China.

Forming and joining issues associated with the use of aluminum in cars have been solved, and the only reported corrosion issues have been galvanic corrosion where protection systems were not in place and filiform corrosion associated with rectification by grinding prior to painting. The main barrier remains the relatively high cost of aluminum automotive sheet as compared to its steel equivalent. Just as aluminum beverage cans compete favorably with steel cans through their high level of recyclability, it is the same for aluminum in transportation applications. Aluminum automotives become both cost and energy competitive with steel if the aluminum sheet is recycled back to the same sheet and this is maintained over repeated construction and end-of-vehicle life cycles. Aluminum-intensive vehicles also offer increased vehicle life. Durability and corrosion issues associated with the use of recycled sheet will need to be addressed.

Although aluminum has enjoyed a dominant position as the material of choice for airframe construction, it has become increasingly threatened by composite materials. However, the overall tonnage of aluminum aircraft plate required by major manufacturers such as Airbus and Boeing is predicted to increase. For example, Airbus have estimated that their plate demand, which was 20.2 kt in 2002 and was 88 kt in 2007, will be more than 100 kt from 2010 onwards. Airbus consider the latest generation of aluminum lithium alloys such as 2050 with less than 2 wt% lithium to be competitive with composites for fuselage applications, and that their corrosion resistance is such that they can be used without cladding for fuselage skin applications. They are also considering an increased use of weldable alloys (AlMgSc) and using joining procedures like laser welding and friction stir welding to decrease the buy-to-fly ratio. The competition between aluminum plate and sheet and composites for airframe construction has stimulated the development of 2xxx, 7xxx (7449 and 7140) and 6xxx (6056) alloys with improved mechanical performance in terms of both strength and toughness. The development of improved alloys and the use of new joining techniques have stimulated significant corrosion-testing activity.[135,136]

Acknowledgements

The authors gratefully acknowledge Ms. Julie Fraser (Monash University) for the careful production of diagrams, figures and tables.

References

1. Polmear, I. J. *Light Alloys: Metallurgy of the Light Metals*, 3rd ed.; Arnold: London, 1995.
2. Davies, J. R. Ed. *Corrosion of Aluminium and Aluminium Alloys*; ASM International: Materials Park, OH, 1999.
3. http://www.world-aluminium.org (accessed December 2008).
4. Grjotheim, K.; Kvande, H. Eds. *Introduction to Aluminium Electrolysis*, 2nd ed.; Aluminium-Verlag: Dusseldorf, 1993.
5. Grjotheim, K.; Welch, B. J. *Aluminium Smelting Technology*, 2nd ed.; Aluminium-Verlag: Dusseldorf, 1988.

6. Hetherington, L. E.; Brown, T. J.; Benham, A. J.; Lusty, P. A. J.; Idoine, N. E. *World Mineral Production 2001–05*; British Geological Survey: Keyworth, Nottingham, 2007.
7. http://www.infomine.com/commodities/aluminium.asp (accessed September 2008).
8. http://www.lme.co.uk/aluminium.asp (accessed October 2008).
9. http://www.indexmundi.com/en/commodities/minerals/bauxite_and_alumina (accessed December 2008).
10. Schlesinger, M. *Aluminium Recycling*; CRC Press: Boca Raton, FL, 2006.
11. Das, S. K. *Light Metal Age*, June 2006, 26.
12. Van Horn, K. R. Ed. *Aluminium*, ASM International: Materials Park, OH, 1967; Vol. 1.
13. Hatch, J. E. *Aluminium: Properties and Physical Metallurgy*; ASM International: Materials Park, OH, 1984; pp 424.
14. Raviprasad, K.; Hutchinson, C. R.; Sakurai, T.; Ringer, S. P. *Acta Materialia* **2003**, *51*(17), 5037–5050.
15. Kovarik, L.; Miller, M. K.; Court, S. A.; Mills, M. J. *Acta Materialia* **2006**, *54*(7), 1731–1740.
16. Winkelman, G. B.; Raviprasad, K.; Muddle, B. C. *Acta Materialia* **2007**, *55*(9), 3213–3228.
17. Szklarska-Smialowska, Z. *Pitting and Crevice Corrosion*; NACE International: Houston, 2005; pp 650.
18. Buchheit, R. G. *J. Electrochem. Soc.* **1995**, *142*, 3994.
19. www.aluminium.org (The Aluminium Association) (accessed October 2008).
20. Polmear, I. J. 100 years of Aluminium Alloys, ICAA 2004 Queensland Australia.
21. Sprowls, D. O. *Aluminum* **1978**, *54*(3), 214–217.
22. Rao, K. T. V.; Ritchie, R. O. *Int. Mater. Rev.* **1992**, *37*(4), 153–185.
23. *The Properties of Aluminium and its Alloys*, 6th ed.; The Aluminium Federation: Birmingham, 1968.
24. Allen, C. M.; O'Reilly, K. A. Q.; Cantor, B.; Evans, P. V. *Prog. Mater. Sci.* **1998**, *43*, 89–170.
25. Alexander, D. T. L.; Greer, A. L. *Acta Mater.* **2002**, *50*, 2571.
26. Fishkis, M.; Lin, J. C. *Wear* **1997**, *206*, 156.
27. Evans, D. G.; Jeffrey, P. W. In *NACE 3, Localised Corrosion,* 1971, pp 614, 622.
28. Godard, H. P. *J. Electrochem. Soc.* **1967**, *114*, 354.
29. Aylmore, D. W.; Gregg, S. J.; Jepson, W. B. *J. Inst. Met.* **1959–1960**, *88*, 205.
30. Bartlett, R. W. *J. Electrochem. Soc.* **1964**, *111*, 903.
31. Pourbaix, Atlas of Electrochemical Equilibria
32. Frankel, G. S. *J. Electrochem. Soc.* **1998**, *145*(6), 2186–2198.
33. Kaesche, H. *Werkstoffe Korros.* **1963**, *14*, 557.
34. Birbilis, N.; Buchheit, R. G. *J. Electrochem. Soc.* **2005**, *152*, B140–B151.
35. Wall, F. D. *J. Electrochem. Soc.* **2003**, *150*(4), B146–B157.
36. Szklarska-Smialowska, Z. *Corros. Sci.* **1999**, *41*, 1743.
37. Chao, C. Y.; Lin, L. F.; Macdonald, D. D. *J. Electrochem. Soc.* **1981**, *128*(6), 1187–1194.
38. Lin, L. F.; Chao, C. Y. *J. Electrochem. Soc.* **1981**, *128*(6), 1194–1198.
39. Chao, C. Y.; Lin, L. F.; Macdonald, D. D. *J. Electrochem. Soc.* **1982**, *129*(9), 1874–1879.
40. Macdonald, D. D. *J. Electrochem. Soc.* **1992**, *139*(12), 3434–3449.
41. Macdonald, D. D. *J. Electrochem. Soc.* **2006**, *153*(7), B213–B224.
42. Pride, S. T.; Scully, J. R.; Hudson, J. L. *J. Electrochem. Soc.* **1994**, *141*(11), 3028–3040.
43. Kim, Y.; Buchheit, R. G. *Electrochimica Acta* **2007**, *52*, 2437–2446.
44. Cavanaugh, M. K. ECS Transactions, 2008.
45. Trueman, A. R. *Corros. Sci.* **2005**, *47*(9), 2240–2256.
46. Zhou, X.; Thompson, G. E.; Scamans, G. M. *Corros. Sci.* **2003**, *45*(8), 1767–1777.
47. Scamans, G. M.; Afseth, A.; Thompson, G. E.; Zhou, X. Ultra-fine Grain Sized Mechanically Alloyed Surface Layers on Aluminium Alloys, 8th International Conference on Aluminium Alloys, Aluminium Alloys their Physical and Mechanical Properties 2002, pp 1461–1466.
48. Zhao, Z.; Frankel, G. S. *Corros.Sci.* **2007**, *49*(7), 3089–3111.
49. Hunter, J. A.; Scamans, G. M.; Sykes, J. M. *J. Power Sources* **1990**, *13*, 193–211.
50. Scamans, G. M.; Hunter, J. A.; Holroyd, N. J. H. *A Surface Engineering Approach to the Corrosion of Aluminum, Aluminium Alloys Contemporary Research and Applications*; Academic Press, 1989.
51. Burleigh, T. D. *Corrosion* **1991**, *47*(2), 89–98.
52. Roberge, P. R. *Handbook of Corrosion Engineering*; McGraw-Hill Professional, 2000.
53. Chen, Z. Y.; Cui, F.; Kelly, R. G. *J. Electrochem. Soc.* **2008**, *155*(7), C360–C368.
54. Schneider, O.; Ilevbare, G. O.; Kelly, R. G.; Scully, J. R. *J. Electrochem. Soc.* **2007**, *154*(8), C397–C410.
55. McMurray, H. N.; Coleman, A. J.; Williams, G.; Afseth, A.; Scamans, G. M. *J. Electrochem. Soc.* **2007**, *154*(7), C339–C348.
56. Coleman, A. J. *Electrochem. Solid State Lett.* **2007**, *10*(5), C35–C38.
57. Scamans, G. M. International Conference on Environmental-friendly Pretreatment of Aluminium and Other Metals, ICEPAM 2004, Oslo, June 2004.
58. Zamin, M. *Corrosion* **1981**, *37*, 627.
59. Mazurkiewicz, B.; Piotrowski, A. *Corros. Sci.* **1983**, *23*, 697.
60. Seri, O. *Corros. Sci.* **1994**, *36*, 1789.
61. Scully, J. R.; Knight, T. O.; Buchheit, R. G.; Peebles, D. E. *Corros. Sci.* **1993**, *35*, 185.
62. Nişancioğlu, K. *J. Electrochem. Soc.* **1990**, *137*, 69.
63. Pryor, M. J.; Fister, J. C. *J. Electrochem. Soc.* **1984**, *131*, 1230.
64. Afseth, A.; Nordlien, J. H.; Scamans, G. M.; Nişancioğlu, K. *Corros. Sci.* **2002**, *44*, 2543.
65. Searles, J. L.; Gouma, P. I.; Buchheit, R. G. *Met. Mat. Trans. A* **2001**, *32A*, 2859.
66. Birbilis, N.; Buchheit, R. G. *J. Electrochem. Soc.* **2008**, *155*(3), C117.
67. Birbilis, N.; Cavanaugh, M. K.; Buchheit, R. G. *Corros. Sci.* **2006.**
68. Park, J. O. *J. Electrochem. Soc.* **1999**, 146(2), 517.
69. Ramgopal, T.; Gouma, P. I.; Frankel, G. S. *Corrosion* **2002**, *58*, 687.
70. Illevbare, G. O. *J. Electrochem. Soc.* **2002**, *148*(5), 687.
71. Liao, C. M.; Olive, J. M.; Gao, M.; Wei, R. P. *Corrosion* **1998**, *54*, 451.
72. Buchheit, R. G.; Montes, L. P.; Martinez, M. A.; Michael, J.; Hlava, P. F. *J. Electrochem. Soc.* **1999**, *146*, 4424.
73. Büchler, M.; Watari, T.; Smyrl, W. H. *Corros. Sci.* **2000**, *42*, 1661.
74. Schneider, O.; Ilevbare, G. O.; Kelly, R. G.; Scully, J. R. *J. Electrochem. Soc.* **2004**, *151*, 465.
75. Ilevbare, G. O.; Schneider, O.; Kelly, R. G.; Scully, J. R. *J. Electrochem. Soc.* **2004**, *151*, 453.
76. Hunter, M. S.; Frank, G. R.; Robinson, D. L. 2nd International Congress on Metallic Corrosion 1963, 66.
77. Knight, S. P. A review of Heat Treatments, Australasian Corrosion Association 2003.
78. Zhao, X. Y.; Frankel, G. S. *Corros. Sci.* **2007**, *49*(2), 920–938.

79. Scamans, G. M.; Holroyd, N. J. H.; Tuck, C. D. S. *Corros. Sci.* **1987**, *27*(4), 329–347.
80. Scamans, G. M.; Holroyd, N. J. H. *J. Electrochem. Soc.* **1986**, *133*(8), C308–C308.
81. Sedriks, A. J. *Stress Corrosion Cracking: Test Methods*; National Association of Corrosion Engineers: Houston, Texas, 1990.
82. Jones, R. H. Ed. *Stress-Corrosion Cracking*; ASM International: Materials Park, Ohio, 1992.
83. Summerson, T. J.; Sprowls, D. O. In *Corrosion Behavior of Aluminium Alloys*, International Conference of the Hall-Heroult Process, Conference Proceedings of Engineering Materials Advisory Services Ltd. (University of Virginia), 1986; Vol. 3, pp. 1576–1662.
84. van der Walde, K.; Brockenbrough, J. R.; Craig, B. A.; Hillberrya, B. M. *Int. J. Fatigue*; **2005**, *27*.
85. Jones, K.; Hoeppner, D. W. *Corros. Sci.*; **2005**, 47.
86. Suresh, S. *Fatigue of Materials*; Cambridge University Press: Cambridge; New York, 1998.
87. Hertzberg, R. W. *Deformation and Fracture Mechanics of Engineering Materials 1989–01*; John Wiley & Sons Inc.
88. Hoeppner, D. W. Model for Prediction of Fatigue Lives based upon a Pitting Corrosion Fatigue Process. In *Fatigue Mechanisms*; Fong, J. T., Ed.; Proceedings of ASMT-NBS-NSF Symposium, Kansas City, Mo. ASTM STP675, ASTM, 1979, pp 841.
89. Kondo, Y. *Corrosion* **1989**, *45*, 7.
90. Wang, Y. Q.; Wang, X. S.; Liang, F.; Zeng, Y. P. *Acta Mech. Sin.*; **2003**, *19*(3).
91. Sankaran, K. K.; Perez, R.; Jata, K. V. *Mater. Sci. Eng.* **2001**, *A297*, 223.
92. Harlow, D. G.; Wei, R. P. *Key Eng. Mater.* **2001**, *200*, 119.
93. Thakur, A.; Raman, R.; Malhotra, S. N. *Mater. Chem. Phy.* **2007**, *101*(2–3), 441–447.
94. Osaki, S.; Kondo, H.; Kinoshita, K. *Mater. Trans.* **2006**, *47*(4), 1127–1134.
95. Kannan, M. B.; Raja, V. S. *J. Mater. Sci.* **2006**, *41*(17), 5495–5499.
96. Lynch, S. P. Paper from Hydrogen Conference, Wyoming 2008.
97. Blewett, R. V.; Skerry, E. W. *Metallurgia* **1965**, *71*, 73.
98. Aziz, P. M.; Godard, H. P. *Corrosion* **1959**, *15*, 529t.
99. Symposium on Atmospheric Corrosion of Non-Ferrous Metals. American Society for Testing Materials Special Technical Publication No. 175, 1956.
100. Metal Corrosion in the Atmosphere, American Society for Testing Materials, Special Technical Publication No. 435 (1968). Papers by McGeary, *et al.*, p. 141 and Ailor, J. R., p. 285
101. Compton, K. G.; Mendizza, A.; Bradley, W. W. *Corrosion* **1955**, *11*, 383t.
102. Standard Practice for Conducting Wire-on-Bolt Test for Galvanic Corrosion. ASTM G116, 1993.
103. Doyle, D. P.; Godard, H. P. *Nature* **1963**, *200*, 1167–1168.
104. Doyle, D. P.; Wright, T. E. In *Atmospheric Corrosion*; Ailor, W. H., Ed.; 1982, pp. 227–243.
105. King, G. A. *Assessment of the Corrosivity of the Atmospheres in an Intensive Piggery using CLIMAT Testers*; Corrosion Australasia, 1987; p 14.
106. Symposium on Corrosion by High Purity Water. *Corrosion* **1957**, *13*, 151t.
107. Davies, D. E. *J. Appl. Chem.* **1959**, *9*, 651.
108. Rowe, L. C.; Walker, M. S. *Corrosion* **1961**, *17*, 353t.
109. Porter, F. C.; Hadden, S. E. *J. Appl. Chem.* **1953**, *3*, 385.
110. Raine, P. A. *Chem. Ind. (Rev.)* **1956**, *1102*, 1196.
111. Sprowls, D. O.; Carlisle, M. E. *Corrosion* **1961**, *17*, 125t.
112. *Aluminium in the Chemical and Food Industries*; British Aluminium: London, 1959.
113. *Aluminium with Food and Chemicals*; Alcan Booth Industries, 1966.
114. Ritter, F. *Korrosionstabelien Metallischer Werkstoffe*; Springer-Verlag: Vienna, 1944.
115. *Aluminium with Food and Chemicals*; The Aluminium Association: New York, 1967.
116. Troutner, V. H. *Corrosion* **1959**, *15*, 9t.
117. Dillon, R. L. *Corrosion* **1959**, *15*, 13t.
118. Dillon, R. L.; Bowen, H. C. *Corrosion* **1962**, *18*, 406t.
119. Porter, F. C. *Metallurgia* **1962**, *65*, 65.
120. Farmer, R. H.; Porter, F. C. *Metallurgia* **1963**, *68*, 161.
121. Scott, D. J.; Skerrey, E. W. *Br. Corros. J.* **1970**, *5*, 239.
122. Leth-Olsen, H. Ph.D. thesis, NTNU, 1996.
123. Afseth, A. Ph.D. thesis, NTNU, 1999.
124. Scamans, G. M.; Amor, M. P.; Ellard, B. R.; Hunter, J. A. *Aluminium Surf. Sci. Technol.* **1997**, p 229, Antwerp.
125. Nisancioglu, K.; Nordlien, J. H.; Afseth, A.; Scamans, G. M. *Significance of Thermomechanical Processing in Determining Corrosion Behavior and Surface Quality of Aluminum Alloys* 7th International Conference on Aluminium Alloys their Physical and Mechanical Properties 2000, pp 111–125.
126. Scamans, G. M.; Afseth, A.; Thompson, G. E.; Zhou, X. Thermomechanical Processing Induced Corrosion of Aluminium Alloy Sheet, Aluminium Surface Science and Technology 2, Manchester, p9, May 2000.
127. Scamans, G. M.; Afseth, A.; Thompson, G. E.; Zhou, X. In *Control of the Filiform Corrosion Susceptibility of Aluminium Alloy Sheet* DFO/DGO Conference on Light Alloys, Munster, 2001.
128. Scamans, G. M.; Afseth, A.; Thompson, G. E.; Zhou, X. In *Ultra-fine Grain Sized Mechanically Alloyed Surface Layers on Aluminium Alloys,* 8th International Conference on Aluminium Alloys, Aluminium Alloys their Physical and Mechanical Properties 2002, pp 1461–1466.
129. Scamans, G. M.; Afseth, A.; Thompson, G. E.; Zhou, X. *Surface Microstructure and Corrosion Resistance of Aluminium-Manganese Alloy*, Aluminium Surface Science and Technology 3, Bonn, May 2003.
130. Zhou, X.; Thompson, G. E.; Scamans, G. M. *Corros. Sci.* **2003**, *45*(8), 1767–1777.
131. Ambat, R.; Davenport, A. J.; Afseth, A.; Scamans, G. M. *J. Electrochem. Soc.* **2004**, *151*(2), B53–B58.
132. Scamans, G. M.; Afseth, A.; Thompson, G. E.; Zhou, X. In *Control of the Cosmetic Corrosion of Aluminium Automotive Alloys,* DFO/DGO Conference on Light Alloy Applications, Dusseldorf, March 2004.
133. Scamans, G. M.; Afseth, A.; Remmers, U.; van der Meer, W.; Hallenstvet, M.; schauzier, F. E.; Katgerman, L.; Nisancioglu, K. In *Analysis of the Exposure Site and Accelerated Test Results of the FICARP (Filiform Corrosion of Aluminium Rolled Products) Project,* ECCA Conference, Budapest, May 2001.
134. Vilche, J. R.; Bucharsky, E. C.; Giudice, C. A. *Corros. Sci.* **2002**, *44*, 1287.
135. Leque, P.; Lassince, P.; Warner, T.; Raynard, G. M. *Int. J. Aircraft Eng.* **2001**, *73*(2), 147–159.
136. Dif, R.; Bes, B.; Warner, T.; Leque, P.; Ribes, H.; Lassince, P. Recent developments in AA6056 aluminum alloy used for aerospace. Presented at the ASM International Conference, 2001.

3.09 Corrosion of Magnesium and its Alloys

K. U. Kainer, P. Bala Srinivasan, C. Blawert, and W. Dietzel
Institute of Materials Research, GKSS-Forschungszentrum Geesthacht GmbH, D 21502 Geesthacht, Germany

Abbreviations

CVD Chemical vapor deposition
EB Electron beam
EMF Electromotive force
IG Intergranular
LB Laser beam
MAO Micro arc oxidation
PEO Plasma electrolytic oxidation
PVD Physical vapor deposition
RA (%) Percentage reduction in area
RE Rare earth
SCC Stress corrosion cracking
SCE Saturated calomel electrode
SSRT test Slow strain rate tensile test
TG Transgranular
UTS Ultimate tensile strength
YS Yield strength

3.09.1 Introduction

There is great concern about the weight of vehicles in automobile, aircraft, and aerospace sectors. With the existing rules of the European Commission on CO_2 emissions, the drive for a reduction in the consumption of petrol in automobiles has already be felt. A reduction in the weight of vehicles would not only help in minimizing the fuel consumption and emission levels, but would to a great extent enable the automobile and aviation industries to improve passenger and

transportation capacities, with considerable control of overall operating costs. However, it becomes essential to ensure passenger comfort and safety when such a design is being looked into.

So far, high-strength low alloy steels have a major share in the automobile industry, whereas age-hardenable aluminum alloys and titanium alloys mainly cater to the needs of the aircraft and aerospace sectors. With recent developments, the requirement for lightweight constructions can be fulfilled to a great extent by magnesium and its alloys. Magnesium alloys with lower density levels are destined to be the construction material in the aforementioned industries in the days to come. Weight savings of up to 30% could be achieved with magnesium in place of aluminum. This could be further improved by appropriate processing and additional treatments on magnesium alloys, and thus these alloys have a great potential for many applications. However, there are issues concerning magnesium alloys which limit their usage for critical applications. The low ductility of some of the alloys is one problem, and the galvanic corrosion of magnesium in contact with other materials is another big concern.

In this chapter, a comprehensive discussion of the magnesium alloys with reference to their classification, processing, and treatments is provided. The different forms of corrosion and their associated mechanisms, including environmentally assisted cracking, are dealt with in detail. The methods of combating the problems of corrosion, including some of the recent advancements and modern practices, are addressed in the last segment.

3.09.2 Historical Perspective

Magnesium was discovered in 1808 by Sir Humphrey Davy. He achieved this by the electrolytic splitting of magnesium oxide with the help of cinnabar. Subsequently, different production techniques were developed by Bussy (1828), Liebig (1830), Bunsen (1852), and Sainte-Claire Deville (1857) for the extraction of magnesium, and magnesium found its first application as an explosive. Magnesium was first produced industrially by a procedure developed by Grätzel in an aluminum and magnesium factory at Hemelingen in 1886.

In 1896, magnesium was produced by molten bath electrolysis in a chemical factory in Bitterfeld. Until 1900, the global production of magnesium amounted to only 10 tons. With further developments, the production of magnesium rose steadily from 2200 tons in 1932 to about 14 000 tons in 1935. By 1939, this amount was doubled to 30 000 tons and then reached a level of 235 000 tons in 1943 owing to the high demand for materials during the Second World War. At the end of the war, the production dropped down again to 17 000 tons, with a more or less continuous increase in usage up to the present day. As of 2002, the global production of magnesium was around 400 000 tons per annum (**Figure 1**) and by the end of 2006 the

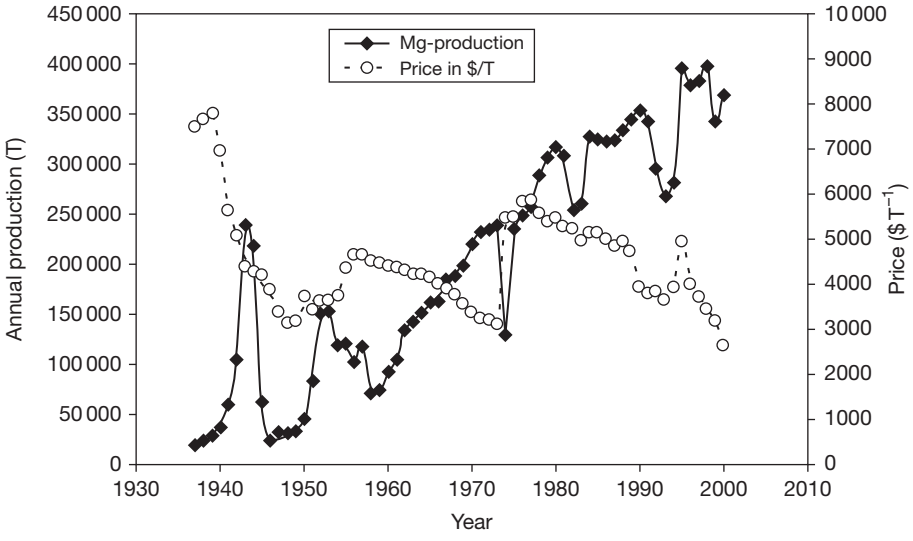

Figure 1 Trend of global production and price of primary magnesium since 1937.
Source: http://minerals.usgs.gov/minerals/pubs/commodity/magnesium/

production of primary magnesium has been reported to be approximately 726 000 tons per annum.

In the early days, magnesium alloys were accepted by the automotive and aviation industry[1] owing to their light weight and good strength-to-weight ratio. In the 1970s, magnesium alloys were virtually forced out of applications owing to their poor corrosion properties and the low prices of aluminum alloys. Nevertheless, with increase in crude oil prices and stringent requirements from the environmental viewpoint (CO_2 emissions), magnesium alloys are experiencing a renaissance; they are popular today with wide acceptance and a large number of applications since the early 1990s.

3.09.3 Production and Types of Magnesium Alloys

3.09.3.1 Extraction of Magnesium

Magnesium is the eighth most abundantly available element in the earth's crust, but it is not available in the metallic form in nature. Table 1 shows the essential source materials for magnesium. Magnesite appears to be the most important ore of magnesium and is reported to be available with 95% purity level.

More than 50% of the global production of primary magnesium today is in China, and production installations are also found in Russia, Canada, Israel, Brazil, and the United States. In Australia and Congo, some projects are underway. Owing to the very high operating costs in the EU, no primary magnesium is produced there nowadays. Compared to the early stages in the 1980s when primary magnesium was sold at $3.6 per kg, the prices touched $2 per kg in 2002. However, with the increase in demand for raw materials, the prices have gone up again. Today, the primary production of magnesium is dominated by two routes *viz.*, (a) molten salt bath electrolysis and (b) thermal reduction. In the first case, $MgCl_2$ obtained from the source products is reduced by the electrolytic process, and in the thermal reduction process either dolomite or magnesite is processed with the addition of ferrosilicon. The composition and characteristics of some of the typical electrolytes used in the electrolytic reduction of $MgCl_2$ are provided in Table 2.

Table 1 Raw materials and their magnesium con tent[2,6,7]

		Percentage
Carnallite	$MgCl_2 \cdot KCl \cdot 6H_2O$	8.7
Magnesite	$MgCO_3$	28.8
Dolomite	$MgCO_3 \cdot CaCO_3$	13.2
Brucite	$Mg(OH)_2$	41.7
Kieserite	$MgSO_4 \cdot H_2O$	17.6
Kainite	$MgSO_4 \cdot KCl \cdot 3H_2O$	9.8
Forsterite	Mg_2SiO_4	17.3
Periclaso	MgO	60.3
Sea water	$MgCl_2$	0.5
Natural brines	$MgCl_2$	3–10

3.09.3.2 Physical Metallurgy

While magnesium was primarily used as an alloying element for aluminum alloys in the early days, it took until 2003 to reach the same level of use as a construction material (Figure 2). Other applications such as desulphurization of iron are also shown in the figure. The effect of alloying elements and important alloys of magnesium are introduced in the following sections. Most alloying elements form intermetallic phases with magnesium, resulting in either eutectic or peritectic systems. Table 3 lists a group of binary alloys based on magnesium, indicating the solubility of alloying elements, the possible intermetallic phases, and also the melting point of each system.

The first industrially useable magnesium alloys were developed at the beginning of the twentieth century. The basic works at that time showed very clearly the influence of essential alloying elements on the property profile and the workability of magnesium alloys. The effect of alloying elements on the properties of a variety of magnesium alloys has been addressed in the literature.[1–5] An overview concerning the effect of the alloying elements on the properties is given in Table 4. Table 5 shows the essential physical properties of pure magnesium and a very popular alloy containing aluminum and zinc, called AZ91. Furthermore, the chemical compositions of some of the commonly used alloys are provided in Table 6.

3.09.3.3 Alloying Elements

Aluminum is considered as one of the primary alloying elements for magnesium alloys. The addition of aluminum to magnesium improves the strength and corrosion resistance, reduces the melting point and increases the melting range. Aluminum is also known to cause microporosity. In alloys containing more than 6% (by weight) aluminum, the intermetallic phase $Mg_{17}Al_{12}$ (Figure 3) is formed. These alloys are heat

Table 2 Typical electrolyte composition for electrolytic reduction of magnesium[3]

Electrolyte	*Composition (wt%)*	*Melting point (°C)*	*Density (kg m^{-3})*	*Conductivity (S m mm^{-2})*	*Viscosity (mPa s)*	*Surface tension (mN m^{-1})*
Potassium Electrolyte	5–12 $MgCl_2$ 70–78 KCl 12–16 NaCl	650	1600	183	1.35	104
Sodium–Potassium Electrolyte	10 $MgCl_2$ 50 NaCl 12–16 NaCl	625	1625	200	1.58	108
Sodium–Calcium Electrolyte	8–16 $MgCl_2$ 30–40 $CaCl_2$ 35–45 NaCl 0–10 KCl	575	1780	200	2.22	110
Lithium–Pottasium–Electrolyte	10 $MgCl_2$ 70 LiCl 20 KCl	550	1500	420	1.20	Data not available
Lithium–Sodium Electrolyte	10 $MgCl_2$ 70 LiCl 20 NaCl	560	1521	488	Data not available	Data not available
Sodium–Barium Electrolyte	10 $MgCl_2$ 20 $BaCl_2$ 50 NaCl 20 KCl	686	1800	217	1.70	110
Mg		650	1580	22.4	1.25	563

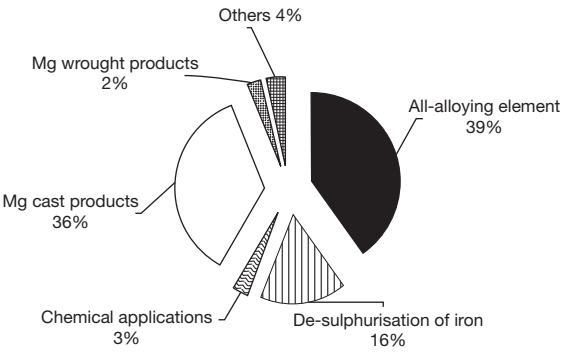

Figure 2 Applications of magnesium (statistics as of 2002).
Source: http://minerals.usgs.gov/minerals/pubs/commodity/magnesium/
http://www.intlmag.org

treatable and thus an improvement in mechanical properties is feasible. Aluminum has no adverse influence on the weldability of magnesium. Nevertheless, aluminum in excess of 1.5% has been reported to increase the stress corrosion cracking (SCC) susceptibility of magnesium alloys. An aluminum content of about 10% favors fine grained solidification and also weldability. With regard to high temperature mechanical properties and creep strength, aluminum shows no positive effect.

Zinc is used, very often in combination with aluminum, in magnesium alloys. Because of its low melting point, the addition of zinc lowers the melting range of Mg–Al alloys, which on the other hand causes problems in solidification. A zinc content of more than 1% in magnesium alloys can lead to hot cracking problems during solidification, and a content higher than 2% can cause cracking during welding. Nevertheless, in combination with zirconium and/or thorium, zinc positively influences the mechanical properties. In addition, zinc improves the corrosion behavior of magnesium alloys.

Zirconium is used as a grain refiner in magnesium alloys which do not contain Al, Mn, Sn, Sb, Ni, Fe, Co, or Si or contaminants such as C, N, O or H. Zirconium helps in the development of a fine grain structure in the welding of magnesium alloys and in addition Zr minimizes the loss of ductility in welded joints. Furthermore, the presence of zirconium prevents excessive grain growth during heat treatment.

Alloying elements of the group of rare earth (RE) elements as well as thorium results in eutectic systems with limited solubility. The level of porosity is reduced in the presence of RE elements. In general, these elements form stable precipitates/intermetallic phases which improve the elevated temperature strength and creep resistance. In addition, an improvement in the

Table 3 List of selected binary magnesium alloy systems[9]

System	Max solubility		Phase	Melting point (°C)
	wt%	at.%		
Mg–Ag[a]	15.5	4.0	Mg_3Ag	492
Mg–Al[a]	12.7	11.6	$Mg_{17}Al_{12}$	402
Mg–Bi[a]	8.85	1.12	Mg_3Bi_2	821
Mg–Ca[a]	0.95	0.58	Mg_2Ca	714
Mg–Ce[a]	0.74	0.13	$Mg_{12}Ce$	611
Mg–Dy[a]	25.8	4.83	$Mg_{24}Dy_5$	610
Mg–Ga[a]	8.5	3.1	Mg_5Ga_2	456
Mg–In[b]	53.2	19.4	Mg_3In	484
Mg–Li[a]	17.0	5.5	–	–
Mg–Mn[b]	2.2	1.0	Mn	1245
Mg–Nd[a]	3.6	0.63	$Mg_{41}Nd_5$	560
Mg–Pb[a]	41.7	7.75	Mg_2Pb	538
Mg–Sc[b]	25.9	15.9	MgSc	–
Mg–Sm[a]	5.8	0.99	$Mg_{6.2}Sm$	–
Mg–Sn[a]	14.85	3.45	Mg_2Sn	770
Mg–Tb[a]	24.0	4.57	$Mg_{24}Tb_5$	–
Mg–Th[a]	5.0	0.49	$Mg_{23}Th_6$	772
Mg–Tl[a]	60.5	15.4	Mg_5Tl_2	413
Mg–Tm[a]	31.8	6.26	$Mg_{24}Tm_5$	645
Mg–Y[a]	12.0	3.6	$Mg_{24}Y_5$	620
Mg–Yb[a]	3.3	0.48	Mg_2Yb	718
Mg–Zn[a]	8.4	3.3	MgZn	347
Mg–Zr[b]	3.6	0.99	Zr	1855

[a]Eutectic.
[b]Peritectic.

corrosion behavior is also observed with the addition of these elements. Yttrium is used as an alloying element along with RE elements. The other RE elements, *viz.*, Nd, Ce, La, and Pr, are often used in combinations. For example, the magnesium alloy designated as 'QH21A,' contains 2.5% Ag, 1.0% Th, 0.7% Zr, and 1.0% Di. Didymium (Di) consists basically of about 85% Nd and 15% Pr.

Beryllium has a very low solubility in magnesium; nevertheless, it has great potential to control the melt oxidation while melting or welding. However, the addition of beryllium needs to be done very carefully as it may cause grain coarsening. As a rule, the addition of beryllium should be restricted to a maximum of 30 ppm in magnesium alloys.

Additions of calcium in quantities >0.03% will increase the susceptibility to hot cracking. During solidification, the calcium-rich low melting eutectic mixture wets the grain boundaries, consequently leading to cracking assisted by the solidification stresses. In aluminum containing magnesium alloys, calcium additions lead to the formation of a stable intermetallic phase Al_2Ca in preference to $Mg_{17}Al_{12}$, which helps in improving the high temperature properties.

The addition of strontium in small quantities is reported to reduce the porosity during welding of high pressure die cast alloys, as it improves the solubility of hydrogen. Further, in conjunction with RE additions, strontium is found to improve the high temperature properties of magnesium alloys.

Silicon improves the castability if added in small quantities. With addition of up to 1% it forms the high-melting intermetallic phase magnesium silicide (Mg_2Si) and thus improves the high temperature properties. However, in the presence of iron it deteriorates the corrosion resistance of magnesium to a great extent. Higher silicon content (>1%) in magnesium alloys decreases the castability drastically because of primary precipitation of Mg_2Si in the melt.

Lithium can be used in large quantities in order to reduce the density of magnesium even further. Besides, an increase in Li content beyond 11%, leads to a change in the crystal structure from hexagonal close packed to body centered cubic structure. With the availability of more slip systems, the formability of the alloys is greatly improved, but the strength of Mg–Li alloys is generally reduced. Further, the problems of burning and vaporization arise while melting in presence of higher levels of lithium. In addition, the corrosion resistance of magnesium alloys in presence of lithium has been reported to be poor.

Manganese is found in most of the magnesium alloys. Primarily, manganese in magnesium alloys improves the ductility, and as it forms stable compounds with iron and other alloying elements, the corrosion resistance is improved on account of control of 'free' iron. Manganese also has a positive effect on the weldability and shows some grain refinement effect, too.

Copper has been reported to improve the high temperature properties of magnesium alloys. At the same time, Cu levels greater than 0.05% have been found to be highly detrimental for the corrosion resistance of the magnesium alloys. Other elements with similar adverse effect on the corrosion resistance of magnesium alloys are, Fe, Ni, Cr and Co. However, they are generally regarded as impurities in magnesium alloys.

3.09.3.4 Alloy Designations

As for ferrous systems, there are quite a number of alloy designation systems for magnesium alloys, too. An overview of the universally accepted alloy designation for magnesium systems, as recommended by the German Institute for Standardization (DIN) and

Table 4 Selection of alloying elements and their effect on properties of magnesium alloys[13]

Alloying element	*Tensile strength*	*Ultimate strain*	*Compressive strength*	*Hardness*	*Ductility*	*Liability of cracks/notches*	*Creep resistance*	*Hot strength*	*Corrosion resistance*	*Grain refinement*	*Castability*
Aluminum	+	+		+					+	+	+
Copper	☹	+	☹						☹☹	☹	
Chromium								+		+	
Yttrium	+					☹			+	+	+
Cobalt		+							☹☹		
Strontium	+	+	+							+	
Zirconium	+	☹			+			+		++	
Lithium	☹		☹		+				☹		
Manganese	+				+	+	+		+	+	
Nickel									☹☹☹		
Silicon		☹	+	+							☹
Zinc	+										
Calcium						☹	+			+	+

+ Beneficial; ☹ Deleterions.

Table 5 Characteristic physical properties of pure magnesium and AZ91 alloy[14]

	Mg	*AZ91*
Density (g cm^{-3}, RT)	1.74	1.81
Liquidus temperature (°C)	650	598
Thermal expansion coefficient (10^{-6} K^{-1}, 20–100 °C)	24.8	26.0
Specific enthalpy (kJ kg^{-1})	382	370
Specific heat (kJ kg^{-1} K^{-1}, RT)	1.03	1.02
Thermal conductivity (W K^{-1} m^{-1}, RT)	156	51
Electrical conductivity (10^6 Ω^{-1} m^{-1}, RT)	22.6	6.6

RT – room temperature.

the American Society for Testing of Materials (ASTM) is provided below.[3,4,6] As per the German Institute for Standardization (DIN) EN 1754 the materials receive a prefix EN M followed by the marking of the product form as below:

- A: Anodes (Ingots)
- B: Block metals
- C: Castings

After this marking, the chemical composition is provided. Therefore, the marking EN M C MgAl9Zn1 is the designation for a magnesium alloy casting with 9% Al and 1% Zn.

The identification of magnesium alloys is also standardized worldwide by the ASTM standards; each alloy is marked with letters indicating the main alloying elements, followed by the rounded figures of each element in weight percentage. **Table 7** shows the key letters for each of the available alloying elements. The last letter in each identification number indicates the stage of development of the alloy (A, B, C, etc.). The alloy AZ91D, for example, is an alloy with a rated content of 9% aluminum (A) and 1% zinc (Z). Its development stage is 4 (D). The corresponding DIN specification would be MgAl9Zn1.

ASTM specifies the following composition for the above designation D (all values wt%): Al 8.3–9.7; Zn 0.35–1.0; Si (max.) 0.10; Mn (max.) 0.15; Cu (max.) 0.30; Fe (max.) 0.005; Ni (max.) 0.002; others (max.) 0.02.

Some of the alloy designations may also contain the history of heat treatment. The designation of heat treatment follows the rules of aluminum alloys.[3] The purpose of the heat treatments in the case of magnesium alloys would be to achieve the desired microstructural state and properties. The different temper designations concerning the heat treatment of magnesium alloys are presented in **Table 8**.

3.09.3.5 Cast Magnesium Alloys

The first commercial magnesium alloys, among them many AZ systems, were developed in the mid 1930s, and in recent times significant developments have taken place on alloy development. Even though new alloys have been developed with specific properties viz., high strength, creep and corrosion resistance etc., the AZ system of alloys still remains as the prime group. These alloys are of importance because of good casting properties, especially in high pressure die casting, and in general these alloys possess a good combination of properties. The main alloying elements are aluminum and zinc, with both the elements improving the castability. Alloys belonging to the category of AM designations, with Al and Mn as the major alloying elements, have relatively inferior castability. However, these alloys have better toughness and reasonable strength. Both these categories of alloys are suitable for both cold and hot chamber pressure die casting. Nevertheless, the properties of the AZ and AM series alloys are highly insufficient for applications at temperatures higher than 130 °C.[7]

For elevated temperature applications (>130 °C), AE and AS categories of alloys are preferred, in which the RE elements or silicon, respectively, are the essential alloying elements in addition to aluminum. These alloys have poor castability, and owing to the high melting points and formation of precipitates in the melt, the alloys are not suitable for hot chamber high pressure die casting. These alloys can successfully be employed at temperatures up to 180 °C.

Other alloys for high temperature applications are available in the WE, ZE, or QE systems. The WE group of alloys contains yttrium and RE elements as main constituents are currently used in the aviation industry, e.g. for gear cases in helicopters. They can be used up to temperatures of 300 °C.[8–10] While the alloys of the ZE system are based on zinc and RE elements, the QE alloys are based on silver and RE elements. These alloys are processed predominantly by sand casting and are not suitable for high pressure die casting. The processing capabilities of these alloys in the semisolid state have not yet been fully understood. Further, both the above systems are not used any more for major industrial applications. The newly developed alloys MRI, AJ, and ACM appear to be superior compared to the old ZE and QE type of alloys for the high temperature applications, as can be seen from **Tables 9** and **10**.

All aforementioned alloys are used nowadays in the form of high purity alloys. The level of impurities in

Table 6 Nominal chemical compositions of standard magnesium alloys[9,10,15,16]

	Al	*Zn*	*Mn*	*Zr*	*RE*	*Ag*	*Th*	*Si*	*Y*	*Others*
High pressure die casting alloys										
AE42	4.0		0.10		2.5					
AJ52x	5.0									1.95 Sr
AJ62x	6.0									2.4 Sr
AJ62Lx	6.15									1.9
AM50A	4.9		0.26							
AM60A	6.0		0.13							
AS21	2.2		0.10					1.0		
AS41A	4.2		0.20					1.0		
AZ91D	8.7	0.7	0.13							
Sand and gravity die casting alloys										
AM100A	10.0		0.1							
AZ63A	6.0	3.0	0.15							
AZ81A	7.6	0.7	0.13							
AZ91E	8.7	0.7	0.13							
AZ92A	9.0	2.0	0.1							
EQ21A				0.7	2.1 Di					
EZ33A		2.7		0.6	3.3					
HK31A				0.7			3.3			
HZ32A		2.1		0.7			3.3			
K1A				0.7						
QE22A				0.7	2.1 Di	2.5				
QH21A				0.7	1.0 Di	2.5	1.0			
WE43A				0.7	3.4				4.0	
WE54A				0.7	3.0				5.2	
ZC63A		6.0	0.25							2.7 Cu
ZE41A		4.2		0.7	1.2					
ZE63A		5.8		0.7	2.6					
ZH62A		5.7		0.7			1.8			
ZK51A		4.6		0.7						
ZK61A		6.0		0.7						
Wrought alloys										
AZ10A	1.2	0.4	0.2							
AZ31B	3.0	1.0	0.2							
AZ61A	6.5	1.0	0.15							
AZ80A	8.5	0.5	0.12							
M1A			1.2							
ZC71		6.5	0.5							1.25 Cu
ZK21A		2.3		0.45						
ZK31		3.0		0.6						
ZK40A		4.0		0.45						
ZK60A		5.5		0.45						
ZK61A		6.0		0.7						
ZM21		2.0	0.5							

RE – Rare earth elements.
Di – Nd + Pr.

the magnesium alloys is of great importance from the viewpoint of corrosion resistance. Even small levels of nickel, iron or copper as impurities may adversely influence the corrosion behavior of magnesium alloys. These elements are controlled in the primary processing stages, for example, by the addition of elements like manganese to form an intermetallic compound with iron. The high purity magnesium alloys offer a much superior corrosion resistance compared to those with intolerable levels of impurities.[8]

A new trend in alloy development is to check the current alloys on their ability to be processed in the semisolid state and to modify them for better semisolid processing. The modification is done by additions of calcium, strontium and also RE elements. These elements have been reported to improve the

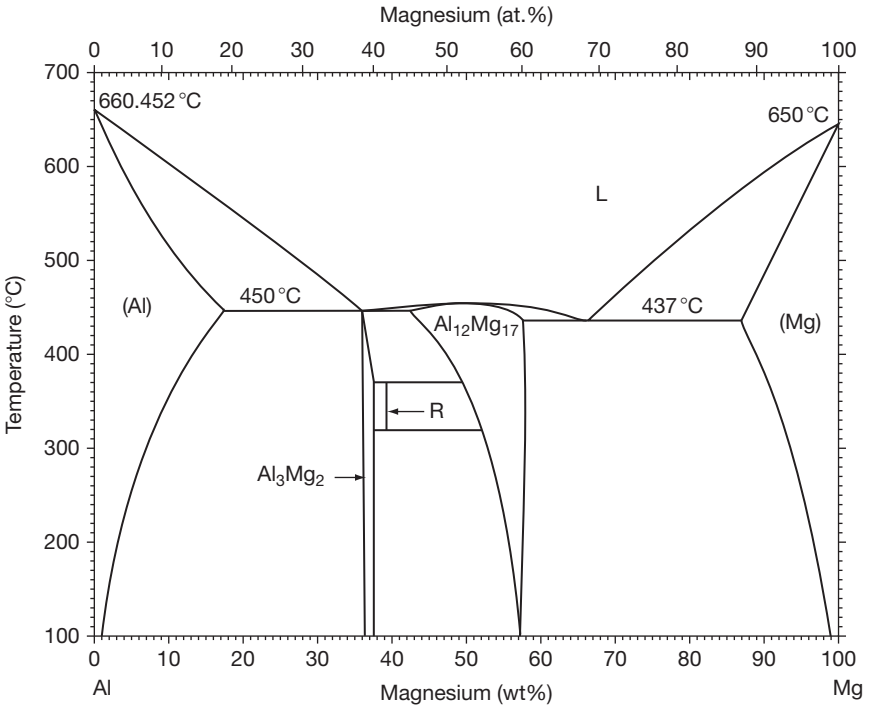

Figure 3 Binary phase diagram of Mg–Al system.[3]

Table 7 Codes for alloying elements in magnesium alloys[9,10]

Element	*Letter*	*Element*	*Letter*
Aluminum	A	Manganese	M
Bismut	B	Nickel	N
Copper	C	Phosphorous	P
Cadmium	D	Silver	Q
Rare earth	E	Chromium	R
Iron	F	Silicon	S
Thorium	H	Tin	T
Zirconium	K	Yttrium	W
Lithium	L	Antimony	Y
		Zinc	Z

mechanical properties and corrosion behavior as well.[10,11] The RE elements especially improve the mechanical properties at high temperatures due to formation of stable precipitates. Thus, the creep behavior is strongly improved.[12–14]

Unlike aluminum alloys, grain refiners for use with magnesium alloys are not well known. Only a few elements such as Zr, Sr, Si and C are known as effective grain refiners.[1,3,15,17] Zirconium works only in magnesium alloys which are free from Al, Si, Sn, Mn, Sb, Ni, Fe and Co. In such alloys Zr addition has been reported to provide finer grain size and this contributes to better formability. Particles such as SiC can work as grain refining agents as well.[17] However, none of the mechanisms for the grain refinement of magnesium alloys is completely understood. Most of the grain refiners work only in certain alloys and combinations of them may influence the effectiveness or may even have an opposite effect.[2,3,17]

Magnesium castings are also produced by squeeze and thixocasting techniques. In the first case, the material is handled in a completely molten state and in the latter it is processed in a semisolid state. The squeeze cast magnesium alloys exhibit a good strength and ductility, owing to the fact that the squeeze casting develops fine grained structures.[18] Even though the squeeze cast alloys are expected to exhibit good fatigue behavior, their creep properties are poor, essentially because of the fine grains. Properties of semisolid processed alloys are still under investigation. As the main applications are housing for electronic components, the property requirements are not that stringent for these alloys.

3.09.3.6 Wrought Magnesium Alloys

Wrought magnesium alloys have a great potential for light weight construction, especially in the automobile

industry, owing to the excellent strength to weight ratio. For rolling into sheet alloys, low levels of alloying elements are generally used (e.g., AZ31), while for extrusion and forging, basically, all alloys can be used. The AZ family of alloys with low zinc content and different levels of aluminum is the dominant alloy system, as they exhibit an attractive combination of strength and ductility. The increase in aluminum content in the alloy leads to an increase in the secondary phase content ($Mg_{17}Al_{12}$), which in turn results in increased strength levels with acceptable drop in ductility. In the wrought systems, the most commonly used alloys are AZ31, AZ61, and AZ80. Furthermore, Mg–Mn alloys (M1 and M2) are used for extrusions. The advantage is the high press rate; however, the ductility is rather low, hence this alloy system is of less importance.[19] Other alloys used are based on the Zn system (ZK30, ZK60) in which Zr is working as grain refiner and providing an improved formability to the material. Furthermore, typical cast alloys of the AZ (AZ91) and AM (AM50, AM60) systems are used mainly for extrusions,[20–22] and also for forgings. The WE system (WE43, WE54) has also gained commercial importance in extrusions and forgings in recent times. The mechanical properties of typical wrought alloys are given in **Tables 11** and **12**.

Table 8 Temper designations in magnesium alloys[9]

F		As-manufactured
O		Heat treated and recrystallized
H		Cold deformed
	H1	Only cold deformed
	H2	Cold deformed and partially annealed
	H3	Cold deformed and stabilized
T		Heat treated to obtain conditions other than mentioned under F, O or H
	T1	Cooled down and naturally aged
	T2	Annealed (only cast alloys)
	T3	Solution treated and cold deformed
	T4	Solution treated
	T5	Cooled down and artificially aged
	T6	Solution treated and artificially aged
	T7	Solution treated and stabilized
	T8	Solution treated, cold deformed, and artificially aged
	T9	Solution treated, artificially aged, and cold deformed
	T10	Cooled down, artificially aged, and cold deformed t
W		Solution treated (unstable condition)

3.09.3.7 Magnesium Matrix Composites

In addition to conventional magnesium alloys, metal matrix composites (MMCs) based on magnesium are studied to extend the field of applications. MMCs, as they are defined, contain at least 5% of strengthening phases/constituents in the alloy matrix. The secondary strengthening constituents may be present in the form of long fibers, short fibers, whiskers or particles and in addition, a mixture of particles and fibers is also feasible. Generally, all magnesium alloys can be used as matrix material, but in view of the intended applications, the heat-resistant alloys are mostly used as matrix.

The MMCs have been reported to possess higher specific strength than the monolithic magnesium alloys. MMCs have shown better properties in terms of Young's modulus, thermal expansion coefficient, electrical and thermal conductivity and creep resistance.[23,24] The creep rates of the magnesium MMCs are reported to be about 10–100 times lower than those of the monolithic alloys, and in fact these MMCs are believed to compete with some class of steels in terms of creep properties. However, corrosion resistance is most of the time adversely affected because of galvanic effects between the reinforcement

Table 9 Comparison of typical properties of newly developed magnesium alloys and standard alloys[15,39]

	MRI 153 M	*MRI 230D*	*AJ62Lx*	*AJ62x*	*AJ52x*	*AZ91D*	*AE42*	*AS41*	*AS21*
R_p (RT)	170	180	147	142	134	160	135	130	125
R_p (150 °C)	135	150	116	108	110	105	100	–	87
R_m (RT)	250	235	270	239	212	260	240	240	230
R_m (150 °C)	190	205	166	163	163	160	160	–	120
A (%, RT)	6	5	11	8	6	6	12	10	16
A (%, 150 °C)	17	16	27	19	12	18	22	–	27
Corrosion rate (mg cm^{-2} day^{-1})	0.09	0.10	0.04	0.08	0.09	0.10	0.21	–	0.34

Corrosion data: Based on salt spray tests, ASTM B117.

Table 10 Mechanical properties of sand gravity and die cast magnesium alloys[9,10]

		UTS (MPa)	*YS (MPa)*	*% RA*
AM100A	T61	275	150	1
AZ63A	T6	275	130	5
AZ81A	T4	275	83	15
AZ91E	T6	275	145	6
AZ92A	T6	275	150	3
EQ21A	T6	235	195	2
EZ33A	T5	160	110	2
HK31A	T6	220	105	8
HZ32A	T5	185	90	4
K1A	F	180	55	1
QE22A	T6	260	195	3
QH21A	T6	275	205	4
WE43A	T6	250	165	2
WE54A	T6	250	172	2
ZC63A	T6	210	125	4
ZE41A	T5	205	140	3.5
ZE63A	T6	300	190	10
ZH62A	T5	240	170	4
ZK51A	T5	205	165	3.5
ZK61A	T5	310	185	–
ZK61A	T6	310	195	10

Table 11 Mechanical properties of forged magnesium alloys[9,10]

		UTS (MPa)	*YS (MPa)*	*% RA*
AZ31B	F	260	170	15
AZ61A	F	295	180	12
AZ80A	T5	345	250	6
AZ80A	T6	345	250	11
M1A	F	250	160	7
ZK31	T5	290	210	7
ZK60A	T5	305	215	16
ZK61	T5	275	160	7
ZM21	F	200	125	9

and the matrix. Nonconducting reinforcements are generally a better choice to minimize the galvanic corrosion attack.

3.09.4 Processing of Magnesium Alloys

3.09.4.1 Casting Technologies

About 95% of the magnesium components are produced by liquid metallurgy route, and the processing temperatures are normally in the range of 600–800 °C. Magnesium and its alloys are extremely reactive in the molten state and extreme care is required for protecting the melt. In the early days, salt-fluxes were used to protect the melt, and in addition these are useful to clean the impurities in the melt, to some extent.[1] However, today, these fluxes are seldom used and the modern foundries, which process magnesium alloys mostly employ controlled atmospheres. In the beginning, a mixture of inert gases, e.g. N_2, with SF6, was used for protection,[25,26] with SF6 offering an efficient protection against oxidation to the molten baths up to temperatures of around 700 °C by forming a thick protective film. However, since 2007, the use of SF6 has been restricted on account of environmental regulations. SO_2 has been recommended by the European Commission as an alternative to SF6. However, SO_2 is a toxic gas, and handling it is more difficult than SF6; thus, the magnesium producers are exploring the possibilities of employing SO_2 on the production scale.

Sand casting belongs to the traditional casting techniques and was already employed for magnesium in the early days, but the problems that were encountered are partly unsolved up to now. The exothermic reaction between the components of sand (silicon dioxide, iron oxide, and water) and molten magnesium can damage the mould and the surface of the component. In order to minimize this problem, sulfur, boric acid, calcium fluoborate, ammonium fluorine silicate and urea (referred to as inhibitors) are used individually or in combination.[1,4]

For gravity die casting, moulds from steel are normally used. Even though the problem of reaction between the mould and the molten metal does not arise in this case, the steel moulds are expensive, and the surface finish is rather inferior. However, generally good quality casting can be produced by gravity die casting procedure, if the wall thickness is high enough. Thin walled parts are better produced by pressure assistance.

Magnesium components are produced predominantly by pressure die casting techniques and both the cold and hot chamber die casting procedures are adopted in the industry. Both techniques yield components with fine grain structure, excellent quality surface finish and a greater dimensional accuracy. The major disadvantage of these techniques, however, is the inevitable gas inclusions in the castings, preventing the use of heat treatments to fully utilise the potential of the alloys. Employment of either cold or hot chamber technique for the production of castings depends also on the type of alloys. AZ91, AM50 and AM60 alloys are most suitable for the production of castings by hot chamber pressure die casting technique. The AS and AE systems of magnesium alloys, which have relatively higher melting points than the

Table 12 Mechanical properties of wrought magnesium alloys[40]

Alloy	*Tensile strength (MPa)*	*Yield strength $R_{p0,2}$ (MPa)*	*Compressive strength (MPa)*	*Elongation (%)*
AZ31	250	180	110	14
AZ61	300	220	130	12
AZ80	340	240	145	10
M1A	260	170	–	10
M2A	250	180	110	4
ZK31	290	240	190	14
ZK60	320	290	230	12
WE34	260	170	165	12
WE54	280	190	180	10

AZ or AM alloys, are more suitable for casting in cold chamber pressure die casting machines. The latter can also be used for processing AZ and AM based alloys.

Squeeze-casting is a special process with a vertical arrangement of a slewable casting unit and molding direction. When the unit is filled, it closes and docks to the mould. Then, the piston rises up and the actual filling begins. In contrast to die-casting, the molding is done slowly (minimum turbulence and hence low porosity), though the final compression is the same. In squeeze-casting, however, the pressure is maintained until freezing is complete and even allows for further feeding in the semi-solid condition. Injection pressures are usually between 70 and 100 MPa, so as to obtain a compact and fine-grained microstructure. Squeeze-casting is an excellent method for producing pressure-sealed, low-porosity, weldable, heat-treatable parts with reproducible high quality. It is increasingly being used in place of classical gravity casting. Magnesium alloy casting can be made by employing both direct and indirect squeeze casting techniques and the same is applied for the production of MMCs, too.

Thixocasting is a fairly new method based on the thixotropic properties of semi liquid alloys. The material while processing would reach the liquidus temperature and would consist of a mixture of solid and liquid phases (also known as semi-solid metal forming). For example, intense stirring can be used to prevent the usual formation of dendritic grains, instead, globular grains form. This condition is characterized by thixotropic flow behavior; with increasing viscosity the shearing strain falls off. The actual procedure requires suitably manufactured raw material. Technically, it is carried out by electromagnetic stirring (rheocasting) within a slab-casting machine.

Recently, much effort has been directed towards shortening the time required for the electromagnetic stirring so as to lower the processing costs. A first step towards this goal is the so-called NRC process (new rheo-casting process). This process tries to avoid dendritic growth by a customized melting–cooling process and simultaneous turning of the melting crucible. The advantages of this procedure compared to conventional casting are as follows: (a) complete automation of the production process, (b) high productivity, (c) cost savings due to low energy consumption, (d) higher tool lifecycles, (e) parts free from gas inclusions and hence weldable, (f) low cooling shrinkage and no blow holes, (g) parts with excellent mechanical properties, and (h) final parts with near-net-shape quality.[27–30] Even though all the three procedures, NRC, thixocasting, and thixomoulding can process the material in the partially liquid state, the source, state, pretreatment and realization of the process differ in each case.[31] Thixocasting, in general, promises improved mechanical properties and comparable wall strengths for magnesium alloy components compared to high pressure die castings.[32,33] Microstructures of some of the commercial alloys in the various cast conditions are presented in **Figure 4**.

3.09.4.2 Forming Technologies

The three major metal forming processes that are widely employed for the processing of magnesium alloys are (a) rolling, (b) extrusion, and (c) forging. The deformation behavior of magnesium alloys is greatly influenced by a number of variables, *viz.*, crystal structure, initial microstructure, thermodynamic conditions, state of stress, method of deformation etc. At ambient temperatures, the formability of magnesium alloys is limited, owing to the hexagonal close packed structure. However, with increase in temperatures to about 225 °C a higher number of slip systems becomes active and an improved metal forming behavior is observed.

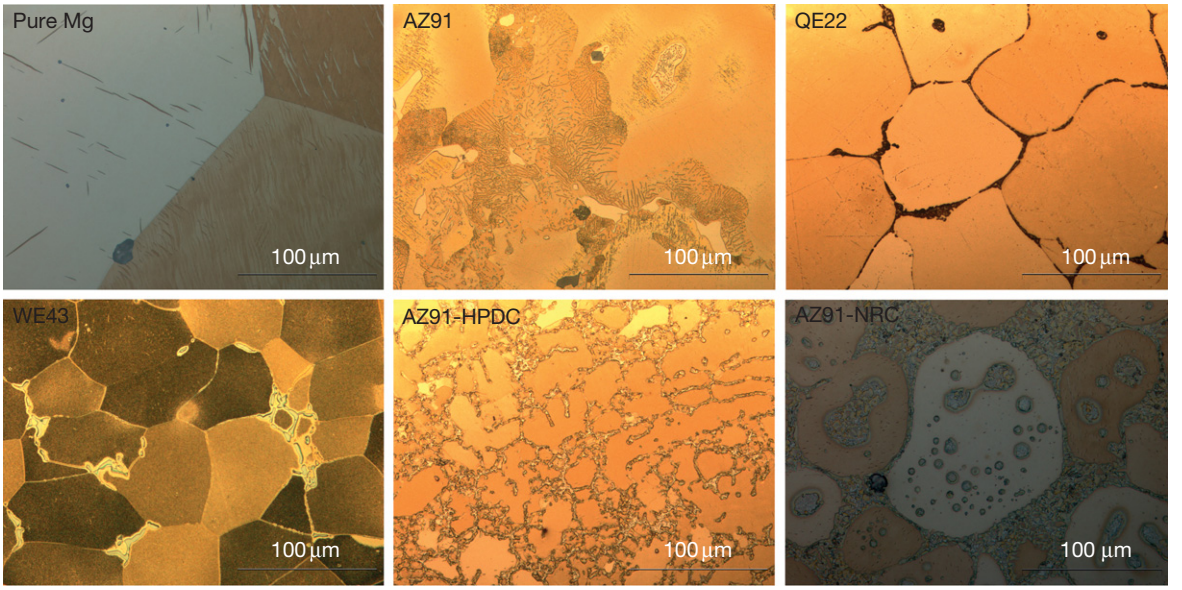

Figure 4 Optical micrographs of some cast magnesium alloys.

Magnesium alloy sheets have to compete with aluminum and steel sheets for automotive applications, offering at least the same economical and technical benefits. For economic reasons, rolling is preferred to be done at temperatures as close as possible to ambient temperature. However, considerable optimization is required for obtaining sheets with acceptable mechanical, thermal and corrosion properties and surface finish.[34] The surface quality is controlled by the use of appropriate lubricants, either oil based or solid lubricants like molybdenum disulphide.[35] The anisotropy that is observed in the magnesium alloy sheets can be minimized by appropriate use of thermo-mechanical treatments and the choice of alloys.

The coarse grained structure of magnesium cast alloys can be readily converted into fine grained ones by hot working processes, such as extrusion. The mechanical properties of the extruded alloys depend on the chemical composition and the thermo mechanical pretreatment that is given to the alloys.[36] The extrusion processes have three variants, *viz.*, direct extrusion, indirect extrusion and hydrostatic extrusion, but most commonly used industrial processes are direct and indirect extrusion. Cylindrical ingots are heated to 300–400 °C depending on the alloy and pressed through matrices with manifold cross-sections. The maximum extrusion length is 50 m. Because of the required complexity, only AZ31 or M2 alloys with restrictions, and AZ61 alloys as well, can be extruded with economical speed, the minimum wall thickness that could be achieved is determined by the alloy and the type of profile. For small to medium-sized AZ31 profiles, the minimum wall thickness that is achievable is 1.2 mm.[37,38] Hydrostatic extrusion is still under examination, but it seems to allow higher extrusion rates and lower extrusion temperatures. Representative micrographs of typical wrought alloys are shown in **Figure 5**.

Magnesium alloy components can also be produced by forging. However, there are limitations in terms of availability of suitable alloy systems, formability and corrosion behavior of these alloys. Nevertheless, wheel rims have been successfully forged and used in commercial vehicles and racing cars.

3.09.4.3 Joining Technologies

The joining technologies for magnesium alloys can generally be classified into two broad categories, *viz.*, mechanical fastening and metallurgical bonding. Screwed connections, riveted joints and use of adhesives form the first group, and the second group is constituted by fusion or solid state joining processes, viz., power beam welding, friction stir welding, diffusion bonding, etc.

An overview of the different aspects of preparing screwed connections for magnesium alloys was given by Weissert.[39] It is important to bear in mind the different thermal expansion coefficient values of

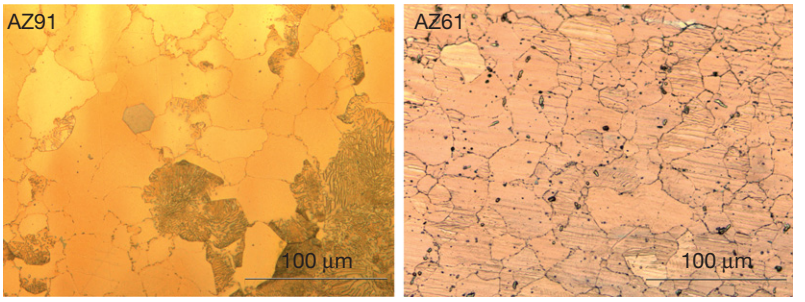

Figure 5 Optical micrographs of wrought magnesium alloys (extruded).

magnesium and steel/aluminum when designing components for elevated temperature operation (especially above 100 °C) in a multi-material mix design. From the design and the material selection perspective, it is necessary to ensure that the screwed/bolted assemblies do not lose their pre-stress during application, and the materials chosen as screw do not foster galvanic corrosion. The latter can be minimized by the right choice of material combinations, appropriate coatings, and constructive measures.

Welding is one of the most widely used joining technologies for magnesium alloys. The weldability of magnesium alloys is influenced by (a) chemical and physical properties, (b) chemical composition, and (c) production process, and the quality of base material. The physical properties that are considered relevant for welding are the melting point, the boiling point, the thermal conductivity, and the coefficient of thermal expansion. A wide solidification range in the alloys, increases the possibility of hot cracking as well as the localized melting of some of the eutectic phases in the alloy.

Joining of magnesium alloys can be accomplished by different fusion welding processes *viz*., gas tungsten arc welding, gas metal arc welding, plasma arc welding, laser beam welding and electron beam welding. Solid state joining processes *viz*., friction welding, friction stir welding, and diffusion bonding are also employed for this purpose.[40–42]

Even though the gas tungsten arc (GTA) and gas metal arc (GMA) welding are still popular,[43–45] with the advent of power beam processes and friction stir welding, the trend moves towards the modern techniques for the joining of magnesium alloys.[46,47] The GTA and GMA welds suffer from the inherent drawbacks of large weld pool/heat affected zone, low welding speeds and higher degree of distortion and residual stress. In some cases, hybrid welding with laser and GTA/GMA combination has proved to be successful for achieving deeper penetration welds in magnesium alloys,[48] also overcoming some of the issues mentioned above. Recently, the activated-GTA (popularly called as A-TIG) with flux addition was employed for the welding of AZ31B, and full penetration joints in 5 mm thick plates were claimed to have been realized with acceptable quality.[49]

The absorption of laser beam on the surface of materials being joined plays a crucial role in the case of magnesium alloys, and this has been treated extensively in literature.[50,51] Even though both CO_2 and Nd:YAG lasers are employed for welding of magnesium alloys, the weldability with Nd:YAG has been reported to be much superior due to shorter wave length and stable molten pool.[52,53] Quite a large number of researchers have investigated the evolution of microstructures and the mechanical properties of magnesium alloy laser beam welds.[54,55] The mechanical properties of the resultant weldments were observed to be dependent on the alloy composition, and a wide range of property variations have been reported for these weldments. However, in almost all the cases, a distinct reduction in the fracture strain values of the weldments was reported. Also, the electron beam welding of magnesium alloys is attempted by researchers, especially, for welding of higher section thickness magnesium alloys.[47]

The application of the friction stir welding process for joining of magnesium alloys is described in the literature.[4,56] The development of this modern solid state joining technique has given a new dimension to the joining of the so-called difficult to weld aluminum and magnesium alloys. However, in contrast to the aluminum alloys, the published literature on the characterization of friction stir welded joints of magnesium alloys is quite limited.[57–59] The investigations made and documented so far, suggest, that there exists a great potential for employing FSW for making not only similar, but dissimilar welds containing

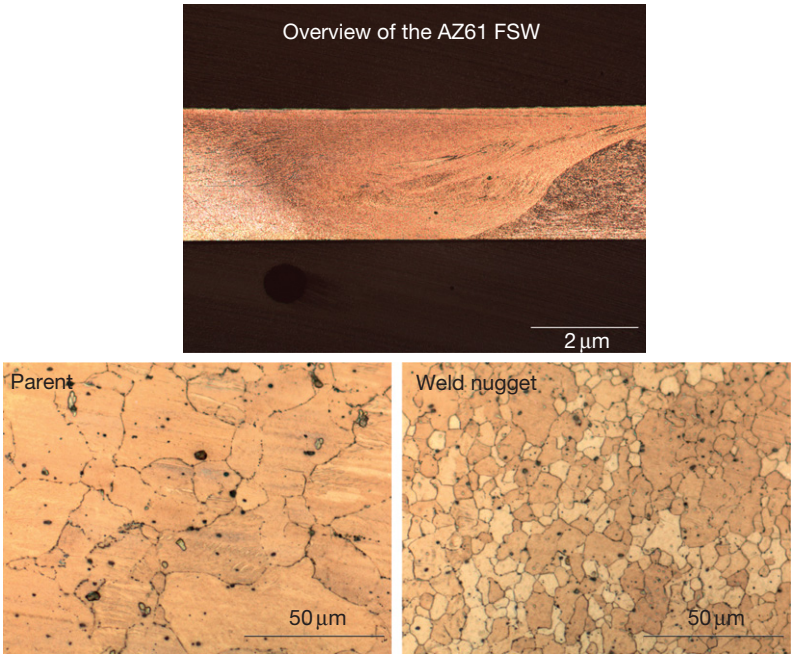

Figure 6 Microstructural features of a friction stir weldment.

magnesium alloys, as well. The macrostructure and the microstructural features of the parent and weld nugget regions of the friction stir weldment of AZ61 alloy are depicted in Figure 6.

3.09.5 Corrosion of Magnesium Alloys

Until recently, it was believed that magnesium has a poor corrosion resistance amidst the metals and alloys known to the engineering industry. This widespread view was essentially owing to a variety of reasons which include, but are not limited to: (a) poor alloy design (with higher levels of impurities like Fe, Ni, and Cu, and or inclusions of melting salts), (b) improper design of the components, or (c) none or a wrong or inadequate surface protection for the chosen application. But, today's magnesium alloys show corrosion properties similar to or better than some of the structural grade carbon steels and copper-containing high strength aluminum alloys (Figure 7). With the right choice of alloy and the developments in the field of surface engineering, the so-called 'susceptible magnesium' alloys are nowadays used for a variety of applications in the electronic, automobile and aircraft industry with appropriate surface protection.[60–63]

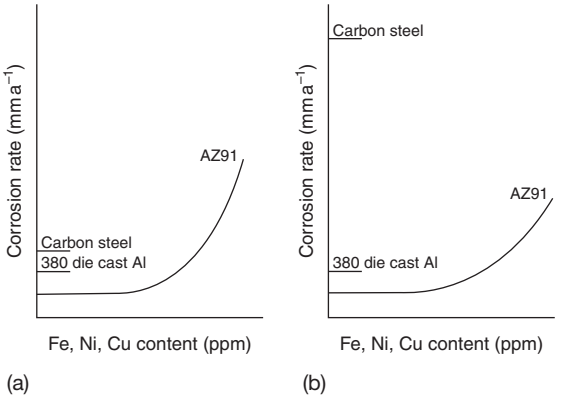

Figure 7 Corrosion rates of AZ91 die cast alloy with different impurity levels. (a) In salt spray test and (b) atmospheric exposure at the Brazos River on the Texas Gulf Coast for 2 years.

On the one hand, the uniform or general corrosion of magnesium alloys in various environments is relatively well controllable, whereas on the other hand, the galvanic corrosion and the environmentally assisted cracking (SCC and corrosion fatigue) are the causes of failures of components made from these alloys. Other forms of corrosion such as pitting corrosion, filiform corrosion, and crevice corrosion apparently play an assisting role in the damage.

Intergranular corrosion of magnesium alloys does not seem to happen because of the fact that the grain boundaries outlined with secondary phases are nobler than the matrix/interior grains.

3.09.5.1 Forms and Mechanisms

Like all the metals which do not exist in the metal state in nature, magnesium has to be extracted from its ores, requiring considerable quantum of energy. Hence, magnesium also tends to return to its stable natural state by reactions with elements of the environment, that are mainly oxygen and water. Magnesium has a standard electrode potential of −2.37 V for bare magnesium in contact with a solution containing Mg divalent ions, and is the most active construction material in the EMF series (**Figure 8**). Its free corrosion potential in neutral chloride solution is around −1.7 V *versus* SCE, and is in the active end of the galvanic series (**Figure 9**). The shift of the potential is caused by the polarization due to passive film formation.

The fact that magnesium reacts instantaneously with air and water leads to the formation of corrosion products on the surface. The nature of the layer is determined by the surrounding environment, and in many instances, this leads to a reduction of the corrosion rate due to the effect of passivation, which by itself is an effective corrosion protection means. Thus, in normal atmospheres, the level of corrosion damage on magnesium alloys is insignificant. However, with increase in relative humidity of air the extent of corrosion damage in general increases. At low ambient humidity magnesium reacts with the oxygen of the air to form magnesium oxide (MgO), which forms as a thin passive layer on the surface of the material. In more humid conditions (>93% relative humidity) first, a surface layer of magnesium hydroxide ($Mg(OH)_2$) develops, which subsequently converts into magnesium carbonate ($MgCO_3$) as a result of the reaction with the CO_2 in the air. In marine and industrial atmospheres, chlorides, sulfates, and nitrates can destroy this protective layer and may induce corrosion damages.

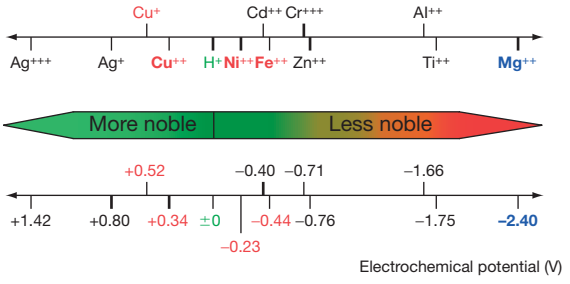

Figure 8 Electromotive force series (EMF series).

In aqueous solutions, the process of corrosion of magnesium, which is dependent on the pH and temperature, is described below:

$$Mg(s) + 2H_2O(1) \rightarrow Mg(OH)_2(s) + H_2(g) \quad [1]$$

The dissolution of magnesium is the partial anodic reaction

$$Mg(s) \rightarrow Mg^{2+} + 2e^- \quad [2]$$

and/or

$$Mg(s) + 2(OH)^- \rightarrow Mg(OH)_2(s) + 2e^- \quad [3]$$

and the hydrogen evolution is the partial cathodic reaction

$$2H^+ + 2e^- \rightarrow H_2(g) \quad [4]$$

The following cathodic reaction can lead to the evolution of hydroxyl ions

$$2H_2O + 2e^- \rightarrow H_2(g) + 2OH^- \quad [5]$$

The potential–pH diagram, known as the Pourbaix diagram, for the system magnesium–water is shown in **Figure 10**. It is obvious from this diagram that magnesium undergoes active dissolution in the pH range from 0 to 11, and magnesium hydroxide is stable only above pH 11. In contrast to aluminum, magnesium forms stable and self healing passive oxide/hydroxide layers in aqueous solutions without additional ions, only if the pH values are higher than 11. Immunity, the state in which corrosion cannot take place due to thermodynamic reasons, exists only below −2.5 V, because of the very low negative standard potential of magnesium. Nevertheless, the corrosion rate is normally very low in small sealed off water volumes because of the low solubility of $Mg(OH)_2$ (the saturation equilibrium is reached fast), and owing to the dissolution of magnesium, a pH value above 10 is quickly reached. However, if the exchange of water becomes constant, this equilibrium will not be reached and the corrosion progresses continuously. An increase in temperature also accelerates the corrosion rate.

In aqueous chloride solutions with heavy metal ions such as Ni, Fe, and Cu, the corrosion rate of magnesium alloys is generally very high. These metal ions will be deposited on the anodic magnesium surface and act as very active cathodes, thus driving

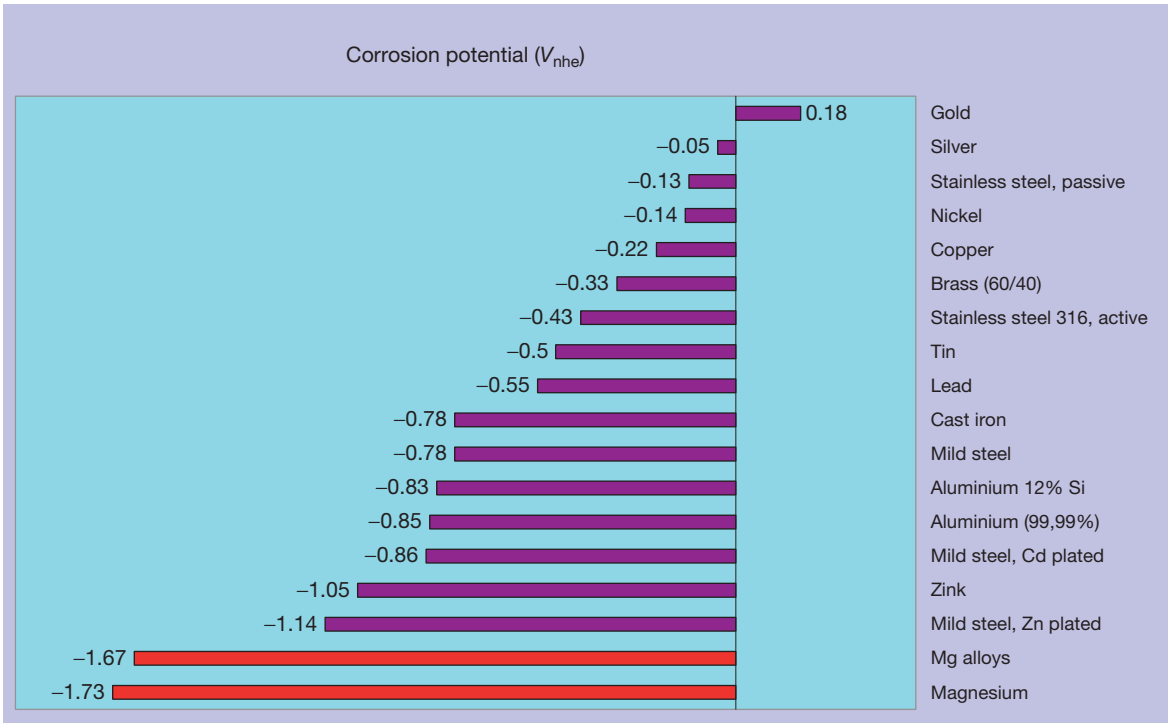

Figure 9 Free corrosion potentials of metallic materials in neutral sodium chloride solution.

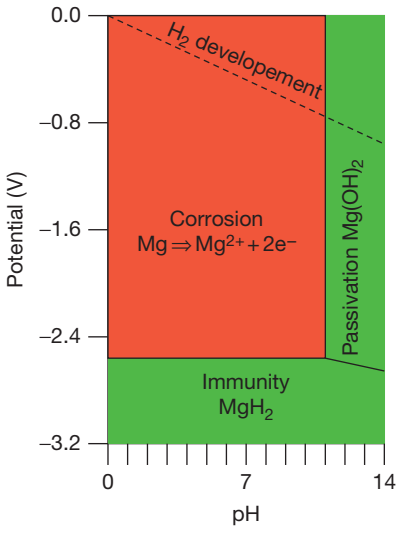

Figure 10 Potential–pH diagram (Pourbaix diagram) of Mg–H_2O system.

magnesium to dissolve at a rapid rate by galvanic action. Various anions, too, have an effect on the localized dissolution of magnesium hydroxide, and chlorides play a much more prominent role than sulfates and nitrates. However, there is a group of anions that help in the formation of a protective layer on the surface, upon forming hardly soluble and adherent compounds with marginal dissolution of magnesium. Such salts are used in the electrochemical surface treatment of magnesium alloys (fluorides, chromates, vanadates, phosphates, etc.). Dissolved oxygen in water or salt solutions has no additional corrosive effect.

As magnesium is stable in solutions with pH > 11, due to a stable $Mg(OH)_2$ layer, it does not corrode in alkaline solutions. All acids, except HF and H_2CrO_4, tend to attack and dissolve magnesium strongly. In the aforementioned exemptions, the formation of a stable film upon initial dissolution helps in preventing further dissolution. An aqueous chromic acid (180 g l^{-1}) solution is often used to clean magnesium alloys from corrosion products.

Most of the organic compounds (aliphatic and aromatic hydrocarbons, ketones, ether, glycol, etc.) have very little effect on the corrosion of magnesium alloys. The corrosion effect on magnesium alloys by ethanol is rather light, and anhydrous methanol inflicts a strong attack. Sour liquids like fruit juices, carbonated drinks, milk, etc., also cause measurable corrosion attack.

The resistance of magnesium alloys to almost all gases, including the aggressive chlorine, is very good

as long as the gases are dry. Even very small quantities of humidity lead to the formation of acids and hence, may result in a strong damage to the magnesium alloys, for example, in the presence of chlorine and sulfur dioxide. In contrast, the performance of magnesium alloys in ammonia containing atmosphere is good, regardless of whether the conditions are dry or humid. The oxidation of magnesium in the presence of oxygen increases with temperature; however, the applications at elevated temperatures are limited mostly by the creep resistance and not by the oxidation rates. As mentioned earlier, the corrosion performance is dependent on the pH value, and apparently the corrosion performance of magnesium alloys in soils depends on the pH value of the soil. Thus, the corrosion rate is higher in saline acidic soils than in neutral or alkaline soils.

Because of the basic nature of magnesium alloys with very active corrosion potentials, the corrosion is accelerated when in contact with other metals due to the galvanic effect. This is taken as an advantage for applications, wherein, magnesium alloys are used as sacrificial anodes for the cathodic protection of metals. However, for structural applications in aggressive media some additional coating and/or constructional measures are required on components to be protected.

The compatibility of magnesium (so-called anodes) and a second metal (cathodes) to be used as a couple in a given environment, is determined by the potential difference of the couple and the polarization resistance. In principle, these potential differences should be as low as possible and the resistance polarization (of the cathode material) should be as high as possible. Aluminum alloys belonging to the 5XXX and 6XXX series are the most compatible materials due to a relatively low potential difference with magnesium, compared to most other acceptable materials. Interestingly, despite a very large potential difference 80Sn/20Zn alloy coatings are also acceptable because of their high polarization resistance characteristics. The following materials are absolutely not acceptable to be used as a direct couple with magnesium alloys: practically all steels, nickel and aluminum alloys containing copper. However, in the case of steels, a coating of zinc plus a cataphoretic painting to the tune of 15 μm would be helpful for making a couple with magnesium alloys.

Magnesium alloys are not only susceptible to galvanic corrosion when in contact with other metals, but also for a special kind of galvanic corrosion in the form of so-called 'microgalvanic cells'. The potential differences between the anodic and cathodic regions within the alloy is the reason for this type of corrosion that can occur in chloride-containing neutral as well as in alkaline media. Impurities such as iron, copper, and nickel, although mostly present as intermetallic compounds in the matrix, have very noble potentials compared to the matrix and thus, accelerate the corrosion damage of the matrix. The corrosion damage can at times be highly localized and lead to pits. The effect is similar in alloys containing the secondary phase $Mg_{17}Al_{12}$, wherein the regions with this intermetallic compound exhibit more noble potentials than the matrix in chloride solutions. The same effect can be observed for almost all intermetallics, formed between magnesium and alloying elements.

Even though the galvanic drive is expected to accelerate the dissolution of the surrounding matrix, it is feasible to tailor the properties of magnesium alloys with proper distribution of the secondary phase in the matrix. For example, in pressure die cast alloys with fine grained structure, the distribution of $Mg_{17}Al_{12}$ secondary phase can be made more favorable, and this phase can form a coherent corrosion barrier network along the grain boundaries (**Figure 11**),[65] and thus, may lead to lowering of the corrosion rate.

3.09.5.2 Environmentally Assisted Damages

The term environmentally assisted cracking, in general, refers to failures under conditions of either static or dynamic loading with considerable assistance from

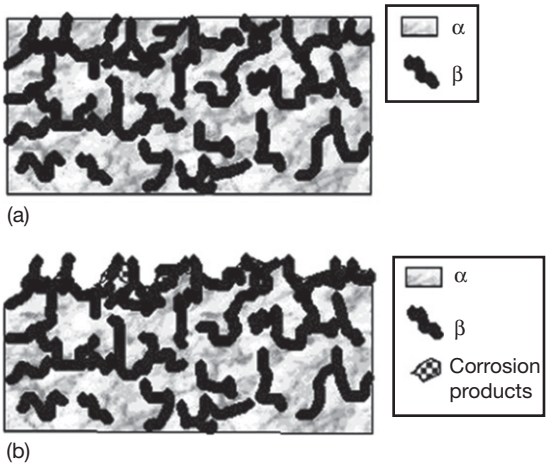

Figure 11 Schematic representation of the change of surface conditions during corrosion of a magnesium alloy with nearly continuous $Mg_{17}Al_{12}$ phase near to the surface.[65] (a) Initial surface and (b) final surface.

the environment. In the case of statically loaded components, this failure is influenced by the dissolution of the alloy, known as SCC, or induced by the entrapped/picked up/generated hydrogen at the tip of the crack, referred to as hydrogen induced cracking (HIC), or hydrogen embrittlement (HE). Under conditions of cyclic loading, the failures that happen with the influence of the environment are termed as corrosion fatigue (CF).

SCC is generally considered to be a dangerous form of damage, as it often leads to catastrophic failures. The mechanisms of SCC vary from one system to the other, and mechanistically SCC is quite subtle. The failure under these circumstances can be without any signs of visible deterioration of surfaces, but can happen due to highly localized damage. In fabricated components, apart from the external stresses, the residual stress in the components itself can lead to failures. The SCC susceptibility of wrought magnesium alloys has been widely looked at by researchers. Nevertheless, cast Mg alloys too, have been reported to be susceptible to SCC, especially when the stress levels are higher.

The SCC behavior of magnesium alloys is very similar to that experienced in the metals/alloys with a passive layer. There has always been a debate, as to whether pure magnesium is susceptible to SCC or not[66–70]; however, the alloys of magnesium are susceptible to this form of damage to a great extent. Stampella *et al.*[70] reported the susceptibility of 99.95% (high pure) magnesium to SCC in sulphate solutions based on slow strain rate tensile (SSRT) tests. The susceptibility of magnesium alloys to SCC was reported based on the laboratory tests performed by numerous researchers and compiled by Winzer *et al.*[71] SCC of a variety of magnesium alloys was observed in environments containing very low concentrations of (as low as 0.001 N) sulfates or chlorides or even in distilled water. Further, SCC has been observed in chromate containing solutions.

A fairly large amount of work has attempted to understand the effect of alloying elements on the SCC behavior of magnesium alloys. Aluminum, one of the major elements for strengthening, has been reported to adversely influence this behavior, with the threshold concentration level of around 2.5%.[69,70] Higher aluminum containing alloys have been found to fail by SCC, even in distilled water. Miller[72] reported that zinc increases the SCC susceptibility, which was contradicted by Fairman and Bray.[73] Surprisingly, the manganese containing magnesium alloys are generally considered to be immune in the atmosphere, chloride solutions, and chloride–chromate solutions,[72] but have been reported to be susceptible in distilled water.[74] Addition of cadmium and neodymium to Mg–Zn–Zr alloy has been reported to improve the SCC resistance[75] and, conversely, the deleterious effect of Cd was also reported.[69] The presence of Fe as impurity plays a crucial role in SCC, especially in the impure alloys. The presence of intermetallic compounds such as FeAl is reported to influence the SCC,[76] the micro galvanic effect in these alloys leads to stronger hydrogen evolution, and the cracking is expected to be with the assistance of hydrogen.[77,78]

In a recent work, the SCC susceptibility of an extruded magnesium alloy (AZ31) in ASTM D 1384 test solution (**Figure 12**) was addressed.[79] The fracture was observed at a stress level of around 100 MPa with a strain of 2% compared to the strain level of about 45% in the tests in air. The fracture surfaces of SSRT tested AZ31 magnesium alloy (in air and in ASTM D 1384 solution) presented in **Figure 13** show characteristic fine dimples in the specimen tested in air, and a distinct transgranular cleavage fracture in the specimen tested in ASTM D 1384 solution.

The documented literature on the SCC of magnesium alloys suggests that in a majority of the cases the failure was transgranular (TG) in nature. SCC of magnesium alloys in intergranular (IG) or mixed modes are also reported in literature.[80,81] The differences in fracture modes have been attributed to the heterogeneities at the grain boundaries, leading to the formation of micro galvanic cells and subsequent dissolution along the grain boundaries, thus resulting in IGC.

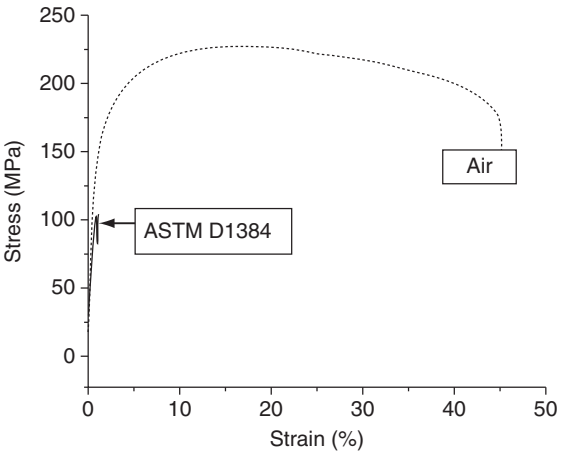

Figure 12 Stress–strain plots of SSRT tested AZ31 magnesium alloy.[79]

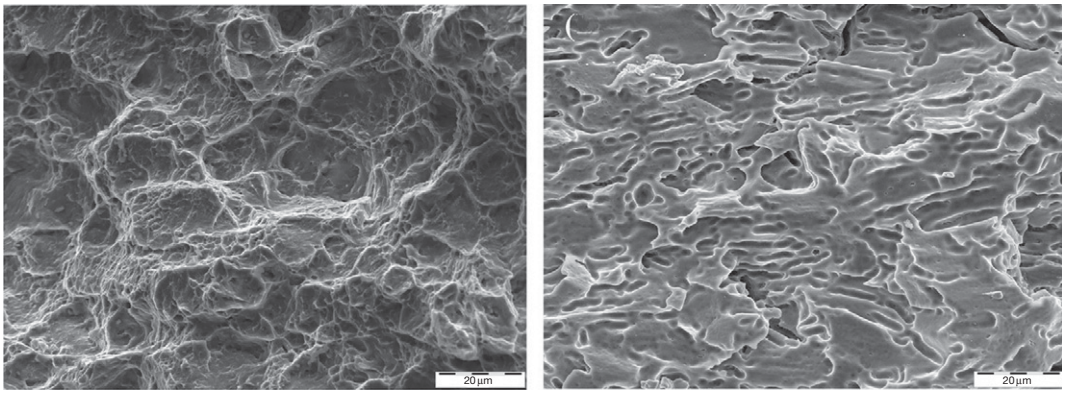

Figure 13 Fracture surface appearance of SSRT tested AZ31 alloy (10^{-6} s^{-1})[79]: (a) in air and (b) in ASTM D 1384 solution.

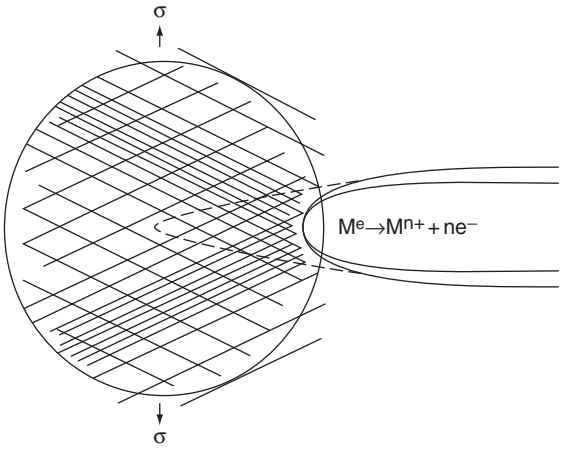

Figure 14 Continuous crack propagation by dissolution following film rupture.[82]

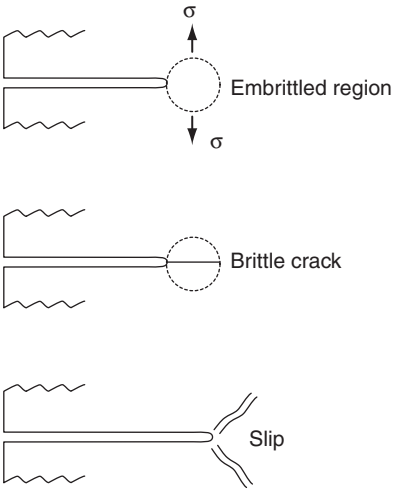

Figure 15 Model for transgranular cracking in Mg–Al alloys.[83]

The SCC propagation mechanisms for magnesium alloys fall in one of the following two groups: (a) continuous crack propagation by anodic dissolution at the crack tip (**Figure 14**)[82] or (b) discontinuous crack propagation by a series of mechanical fractures at the crack tip (**Figure 15**).[83] The dissolution mechanisms could be (a) preferential attack, (b) galvanic attack by film rupture, or (c) tunneling. The mechanical fracture mechanisms are broadly either (a) cleavage fracture or (b) hydrogen embrittlement. A comprehensive description of the SCC mechanisms in magnesium alloys can be found in the review by Winzer *et al.*[71]

There is not much published information on the effect of processing conditions on the cracking susceptibility of magnesium alloys. The data presented in **Figure 16**[84] suggests that the processing conditions have a definite influence on the mechanical properties of AZ31 alloy. However, it is interesting to note that the strain to failure of the specimens in chloride environment is nearly the same although the difference in air is quite large.

The information on the SCC behavior of welded magnesium alloys is also quite scarce. Welds produced by the modern joining technologies *viz.*, friction stir welding and laser beam welding, seem to have good mechanical properties. The SCC of laser and friction stir weldments addressed recently,[79] suggest that the fusion boundary region is susceptible to SCC. A mixed mode of fracture (transgranular + intergranular) has been reported in both these weldments subjected to SSRT tests in ASTM D1384 solution, and further, the

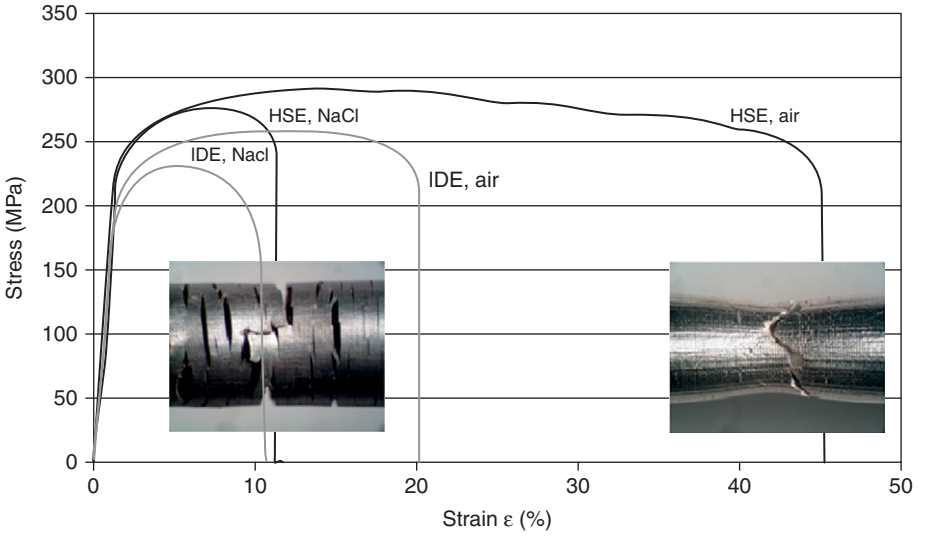

Figure 16 Effect of processing conditions on the SCC of AZ31.[84] IDE – indirect extrusion; HSE – hydrostatic extrusion.

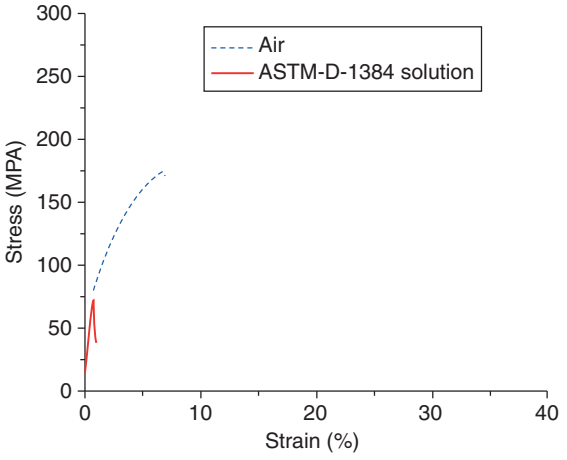

Figure 17 Stress–strain plot of SSRT tested friction stir weldment of AZ31.[79]

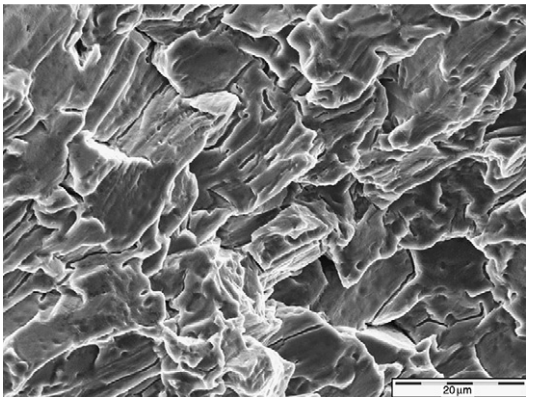

Figure 18 Fracture surface appearance of FSW weldment of AZ31.[79]

weldments showed a higher susceptibility to SCC than the parent alloy (**Figures 17** and **18**).

Cathodic polarization of magnesium alloys is reported to reduce or even prevent SCC of magnesium alloys in aqueous solutions.[66,70,72] However, yet in another recent work,[85] it has been found that AZ80 alloys undergo SCC–HE under conditions of continuous charging under cathodically polarized conditions in distilled water. **Figure 19** shown below explains the effect of cathodic charging on the cracking behavior. The exact role of hydrogen and the precise underlying mechanisms of SCC under such conditions are still being debated.

3.09.5.3 Influence of Alloying and Processes

The corrosion behavior of magnesium alloys is influenced substantially by the impurities. The heavy metals contained as impurities (*viz.*, Fe, Cu, and Ni) form galvanic cells and enhance the corrosion rate, and the effect of these impurities on the corrosion rate is depicted in **Figure 20**.[86]

The tolerance limit depends on the alloy composition. For pure magnesium, the tolerable limits for Cu, Fe, and Ni are 0.1%, 0.005%, and 0.0005%, respectively. These impurities in magnesium alloys arise from various sources; the iron pick up is primarily from the melting crucibles and tools, copper comes from impure aluminum, while nickel gets in

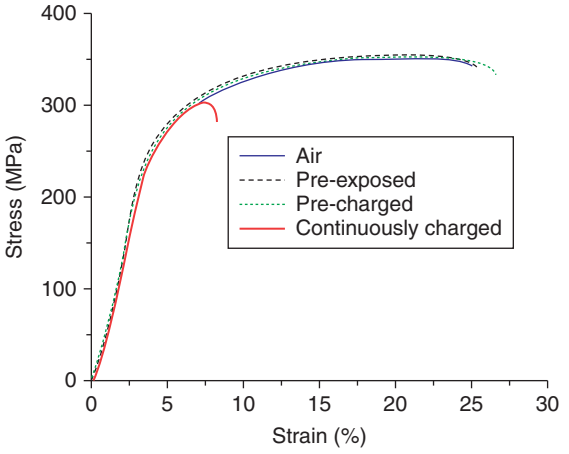

Figure 19 Stress–strain curve of AZ80 alloy at a strain rate of 10^{-6} s^{-1}: in air; preexposed in distilled water for 24 h and then immediately strained in air; precharged at ~300 mV cathodic to the open circuit potential (OCP) for 24 h in distilled water and then immediately strained in air; continuously charged at ~300 mV cathodic to OCP in distilled water during the test.[85]

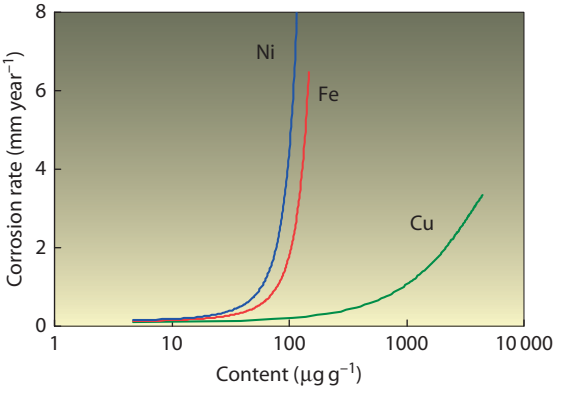

Figure 20 Effect of impurities on the corrosion rate of magnesium alloy AZ91.[86]

from nickel containing stainless steel crucibles or at times very low levels of Ni may be contained in the raw magnesium itself.[87] If these impurities are restricted within tolerable limits, a substantial improvement in the corrosion resistance of magnesium alloys could be accomplished.

Magnesium alloys in which the total content of these impurities is restricted to 'ppm' levels are referred to as high purity (HP) alloys, and these alloys can virtually compete with aluminum alloys in terms of corrosion resistance.[86] In the salt spray tests performed as per ASTM B 117, the high purity magnesium alloys (with the exception of AM20) showed very low corrosion rates, (**Figure 21**)

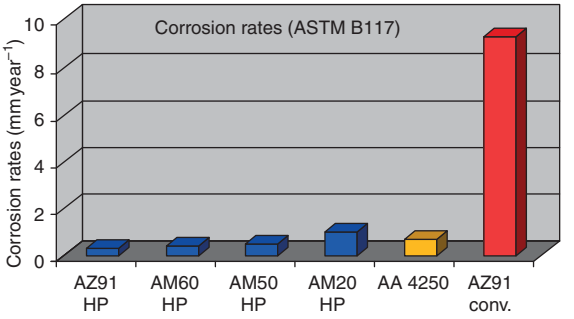

Figure 21 Comparison of corrosion rates of HP magnesium alloys and $AlSi_9Cu_3$. (Note the corrosion rate of AZ91 with impurities beyond the tolerable limits.)

compared to a silicon and copper containing aluminum alloy (AA4250), which is used as a secondary alloy in the automobile industry.

The micro galvanic effects, as well as the formation of passive layers to minimize the corrosion can be influenced by addition of specific alloying elements. Besides the production of HP alloys, the susceptibility to corrosion of magnesium alloys can be controlled by the addition of RE elements. It is believed that these elements stabilize the passive film formed on the surface of magnesium alloys. In addition, the intermetallic phases formed in the magnesium alloys containing SE, show corrosion potentials similar to the aluminum containing matrix and thus, eliminate the galvanic effect. Additions of manganese to magnesium alloys help in reducing the galvanic corrosion, as manganese preferentially forms an intermetallic compound with aluminum, incorporating Fe and Ni, thus bringing down the effect of potential differences between free iron or nickel and the magnesium matrix in the alloys. The tolerance limits for impurities (especially Fe) in such alloys can be higher, without many of its problems. Aluminum improves the corrosion resistance in magnesium alloys when the alloying addition is increased from 2% to 9%. The benefit is two fold, first, $Mg_{17}Al_{12}$ forms a favorable corrosion resistant network along the grain boundaries, and second, the incorporation of aluminum oxide in the $Mg(OH)_2$ layer improves the stability of the passive layer and thus enhances the corrosion resistance. Owing to the superior passive layer on the surface in aluminum containing magnesium alloys, a special form of corrosion, so-called filiform corrosion, is observed which is otherwise observed only underneath thin coatings. Zinc increases the corrosion potentials and thus reduces the corrosion rate. Also, the elements such as zirconium added as grain refiners to magnesium alloys can influence the corrosion behavior positively.

The microstructure with a given grain size and precipitate has a great influence on the corrosion resistance. Small grain size is often reported to be more corrosion resistant than larger grains. Thus, corrosion resistance can be optimized by the choice of the production process. So, the same alloy processed with HPDC has generally a better performance than sand or gravity die casting, and this can be explained by higher cooling rates resulting in a finer microstructure. Using special melt or powder metallurgical production processes or thermo mechanical treatments, even smaller grain size can be obtained. The new production processes, such as semi-solid processing, result in specific microstructures and thus have an influence on the corrosion performance. The globular microstructure with surrounding intermetallic phases is often reported to have good corrosion resistance. The best corrosion resistance, however, is often found with the products of rapid solidification processes. Precipitates and impurities are often finer and more uniformly distributed or the alloying elements remain in solid solution without forming precipitates. Passive films on supersaturated alloys are more easily formed and are more uniform and stable. In Mg–Al alloys, the β-phase ($Mg_{17}Al_{12}$) formation can be suppressed by rapid solidification, and there is sufficient Al available to stabilize the passive layer by the formation of $MgAl_2O_4$ spinels.[88]

Heat treatment of magnesium alloys influences the corrosion behavior, as the involved diffusion process has an effect on the distribution of alloying elements in the matrix and also influences the secondary phase formation. In general, magnesium alloys subjected to heat treatment (solution treatment, ageing, etc.) exhibit a higher corrosion rate when compared to the as-cast condition. The latter is especially the case if the precipitates have a barrier function in the as-cast condition, owing to the formation of a dense network along the grain boundaries.

3.09.6 Corrosion Prevention Strategies

3.09.6.1 Coatings

Magnesium and magnesium alloys can hardly be protected by alloy development against general corrosion in acidic environments and against galvanic corrosion. Instead, for this purpose, a wide variety of coatings are available. The coatings are also used for improving the aesthetic appeal and for increasing the decorative finish. The following techniques are available for the surface modification of magnesium and its alloys:

- Chemical conversion coatings
  - Chromating, phosphating
- Electro-chemical coatings
  - Anodizing
  - Electroplating (Zn, Cu, Ni, Cr)
  - Plasma electrolytic oxidation
- Physical techniques
  - Physical vapor deposition
  - Plasma/laser assisted vapor deposition
  - Thermal spraying
- Nonmetallic coatings
  - Varnish, wax, polymeric coatings, paints.

The physical techniques are still in the research stage, and only the other surface modification technologies are adopted in the industry to some extent as of today. A detailed overview, description of the processes, and information about the advantages and disadvantages of many surfaces treatments for magnesium alloys is given by Gray and Luan.[89] Before selecting a coating system for a given application, it is necessary to understand the corrosion behavior of the magnesium alloy in question in the service environment and the suitability of the material for processing, to deposit the coating. The surface preparation plays a crucial role in making the coating system perform well in the field of operation.

A number of problems are specific for coatings on magnesium alloys. No coating system polarizes magnesium in the cathodic direction, since all the coatings are more noble than the magnesium alloy matrix. Coating of magnesium, especially with a metallic coating, may lead to an accelerated galvanic attack in aqueous environments, if the deposited layers are not sufficiently thick enough or if there are any defects/damages in the coatings. However, magnesium surfaces can be modified and effectively protected by multilayered systems. For reasons of cost, the coating system is mostly decided, based on the aggressiveness of the environment and the application demand. Pickling, conversion coating, anodizing, plating, and organic coatings are available and multiple combinations of these are possible.

3.09.6.1.1 Chemical conversion coatings

Chromating is a known surface treatment for aluminum, zinc, and magnesium for years and this treatment develops a very thin layer (to about 1 μm maximum). The treatment can be used for the prevention of damage by corrosion of magnesium alloy

components during storage and transport. In addition to corrosion protection, these films offer an inhibitive effect inherent to the chromate film. The adhesion to organic coatings is also greatly improved by this treatment.[90] Nevertheless, the use of chromates is limited by the new environmental regulations in Europe since 2003, owing to growing health concerns associated with hexavalent chromium.[91,92]

New alternatives to the chromating process based on phosphate permanganate or fluoride zirconate have been proposed.[90] Alternate chrome-free conversion coatings based on alkali potassium permanganate solutions (MAGPASS-COAT®) and from solutions containing vanadates, molybdates and tungstates have also been attempted.[93,94] As these conversion coatings impart good adhesion properties, a few attempts have been made to produce chrome-free coatings in electrolytes based on stannates [95] and RE salts.[96] Effort was also made to produce conversion coatings based on zinc manganese phosphating electrolytes on magnesium alloys.[97] In general, all these conversion coatings need to be used in combination with an overlay coating for efficient corrosion protection, especially in aggressive environments.

3.09.6.1.2 Electrochemical conversion coatings

The anodic oxidation of magnesium alloys result in a relatively thick and electrically insulating layer with good wear resistance. Like the chemical conversion coatings, the anodic oxide films also provide a good base for organic coatings, and in addition these can be impregnated as well. In particular, the newer processes are capable of developing very hard ceramic layers (ANOMAG®, KERONITE®, TAGNITE®, and MAGOXID®). These treatments are carried out in electrolytes at higher operating voltages with low current density levels leading to a plasma discharge.[98] The temperature of the bulk electrolyte tends to rise, typically to around 50 °C (depending on the degree of cooling provided to the system). The local temperature in the plasma zone would probably be in excess of 1000 °C, this results in the formation of 'glassy' or 'ceramic' anodic coatings. The process is called by various names, *viz.* plasma anodizing, micro arc oxidation (MAO), and plasma electrolytic oxidation (PEO).

The composition and the thickness of the conversion layers developed, depend on the processing conditions, *viz.* the chemical composition of the alloy, electrolyte composition, operating voltage, current density, temperature of electrolyte, duration, etc. The thickness of the layers ranges from a few microns to as high as 150 μm. Electrolytes containing combinations of hydroxides, carbonates, silicates, phosphates, aluminates, and borates have been explored. The processing voltages are in general a function of the composition of electrolytes, and voltage levels as high as 600 V are achieved during this PEO processing. The current density for the PEO operation ranges generally from 5 to 50 mA cm^{-2}, which is decided depending on the electrolyte/material combination. A few of the conventional and plasma anodizing processing electrolytes, processing conditions and resultant films are presented in **Table 13**.[99]

Figure 22 represents schematically a typical PEO coating obtained in an electrolyte based on silicate and hydroxide. The various zones that are observed in the PEO coatings are: Zone 1 (interface): The interface is very rough. It appears as if there were thin layers of less than 1 μm thickness with a finer and more dense structure in the interface region; Zone 2 (micro porosity): This has an extension from 20 to 80 μm. Here, the ceramic oxide film is denser, and only a small number of larger pores or cavities are visible; Zone 3 (pore band): This is observed in all specimens and can be identified by a pronounced band of cavities at a depth of 20–40 μm from the surface. Most of the visible surface pores (craters with discharge channels) seem to end in this band of cavities; Zone 4 (near surface): This is the outermost surface with the crater structure on the top. The ceramic layer is enforced by a large number of discharge channels reaching from the crater surface toward Zone 3. The porosity is the most striking feature of the anodized layers (**Figure 23**), and the size and distribution of pores strongly influence the properties of the layers. It should be noted that the other coatings can vary from this layered structure.

As almost all PEO layers are more or less porous, a secondary seal coat would be preferred for an enhanced corrosion protection, depending on the environment in which the components are to be used. However, their use in the commercial market as of date, is somewhat restricted owing to the high operating costs associated with the processing.

3.09.6.1.3 Electro and electroless deposition

The deposition of metals and/or alloys from aqueous solutions containing the respective metal salts is practiced for many of the components made of both ferrous and nonferrous metallic substrates for imparting better surface finish, aesthetic appeal, corrosion resistance, electrical conductivity, solderability etc.

Table 13 Some commonly used anodic oxidation processes for magnesium alloys[99]

Process	*Electrolyte Components*	*Current density (A cm^{-2})*	*Type of current*	*Electrolyte temperature (°C)*	*Layer color*
HAE	Potassium fluoride Sodium phosphate Potassium hydroxide Aluminum hydroxide Potassium permanganate	1.5–2.5	AC or DC	27	Brown
DOW 17	Ammonium difluoride Sodium dichromate o-Phosphoric acid	0.5–5.0	DC	70–80	Green
AHC Magoxid-Coat®	Mineral acid (fluoric, phosphoric. boracic acids) Organic matters	1–5	Special types of signals with plasma-chemical reaction	15–20	White

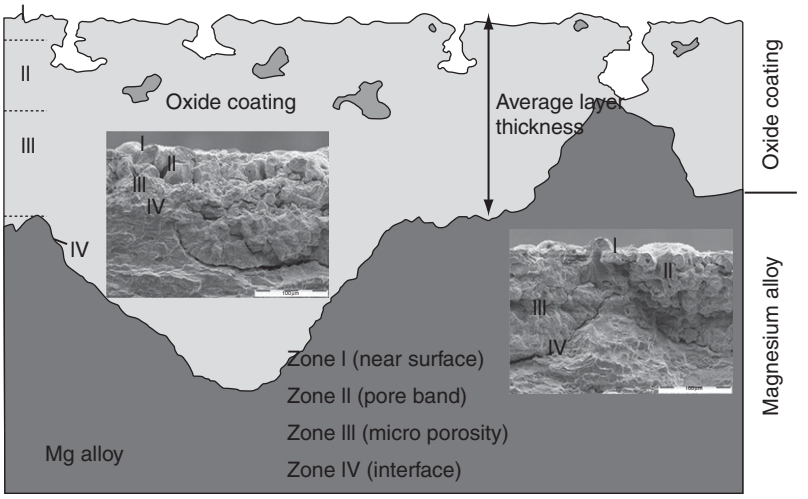

Figure 22 Schematic representation of a typical cross section of PEO-coated magnesium alloy.[100] (Typical features of the scanning electron micrographs inserted.)

There is not much older literature on the established practices for the deposition of metals/alloys on magnesium, but recently the interest manifested in the number of publications is increasing, especially in China.

There are lots of issues in the deposition of metals/alloys on magnesium alloys. First, magnesium is quite active and can react with oxygen to form a layer on the surface which very strongly inhibits effective deposition. Hence, it calls for a specific and careful preplating treatment procedure. Second, magnesium undergoes active dissolution in acidic or near neutral solutions upon immersion, and hence needs to be handled carefully while plating. Nevertheless, there have been a number of research attempts for the prevention of corrosion of magnesium by plating techniques. Plating of nickel/gold has proved to be good for some space applications, while plating with silver was rated good from electrical conductivity. Plating of gold is reported to be done in stages with the first stage being zinc immersion plating, followed by nickel electro flash and finally the gold coating.[101] Recently, in an interesting work, plating of zinc from ionic solutions was demonstrated by Bakkar and Neubert and it is claimed that deposits were free from defects and showed corrosion behavior (**Figure 24**) similar to that of pure zinc in chloride solutions.[102]

Electroless nickel plating is also contemplated for magnesium alloys with a careful pretreatment of the substrates. In order to promote better coating

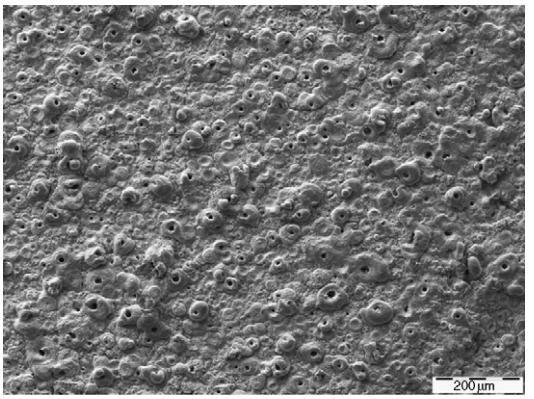

Figure 23 SEM image showing the topography of the PEO-coated magnesium alloy.[100]

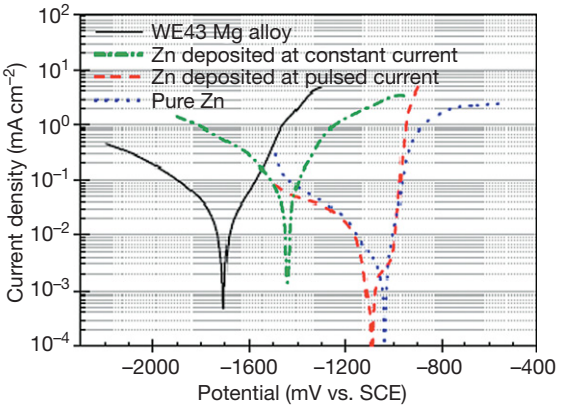

Figure 24 Potentiodynamic polarization behavior of WE43 magnesium alloy with and without Zn electrodeposit in 0.1 M NaCl solution.[102]

characteristics, magnesium surfaces may be given a zinc or copper flash coating over which nickel can be deposited by the electroless technique,[98] and the deposition of flash coating is similar to that performed for the deposition of gold. The electroless nickel deposits are harder than most of the magnesium alloys ($\leq$80 $HV_{0.1}$), in general to about 500 $HV_{0.1}$. Such coated magnesium alloys find applications in electronics and telecommunications, guaranteeing a stable electrical contact with good resistance to adhesive wear and corrosion. It is mandatory to ensure that the deposits are free from pores and cracks as these defects can very adversely influence the corrosion behavior of the coated magnesium alloy (galvanic effect), despite the presence of a layer intended for protection. Further, recycling of such coated alloys is not feasible, especially if one looks at the production of high purity magnesium alloys. This is true despite the fact that there are quite a number of stripping solutions available for the removal of coatings from magnesium substrates.

3.09.6.1.4 Physical techniques

Advanced techniques like laser beam (LB) and electron beam (EB) processing offer large scope for the modification of the surface of engineering alloys. Thus, magnesium alloys can be tailored by just heating to critical temperatures, or remelting with or without the addition of alloying elements, or by depositing coatings (cladding).

The thermal spray coatings often have a good amount of porosity, and this could be a major disadvantage from the corrosion point of view. The modern thermal spray techniques like high velocity oxy fuel or detonation gun spray process could produce effective coatings as the porosity levels are substantially low. Thermal spray coatings on magnesium alloys have been reported for space applications.[103]

With the LB, EB and thermal spray processing, surfaces resistant to wear and corrosion can be produced by means of alloying and diffusion and it is even feasible to develop functionally graded layers. The physical and chemical vapor deposition technologies can also be used for coating a number of metallic and ceramic layers on magnesium alloys. The advantage and disadvantage at the same time is that they can be used economically only for reinforcement of smaller local areas whereas large area coatings are normally too time consuming. The coatings that can be achieved by thermal sputtering in highly controlled atmospheres are free from oxidation, and it is possible to produce thin and thick corrosion resistant protective coatings depending on the requirement.

Laboratory scale experiments on chemical vapor deposition (CVD) of molybdenum are reported to improve the corrosion resistance significantly, by the formation of a stable thin film (<0.5 µm) of molybdenum on magnesium alloy substrates.[104] Deposition of titanium nitride and zirconium nitride by plasma assisted CVD have also been attempted.[105] PVD coatings based on Mg alloys can be used for cathodic protection of conventional magnesium substrates.[106–108] However, the applicability of PVD and CVD coatings on large scale industrial components has not yet been fully explored.

3.09.6.1.5 Organic coatings

The effect of organic coatings is generally to prevent or reduce the contact of water, oxygen, or other electrolytes with the metal surface. They are generally used in combination with conversion or anodized

coatings and offer in this combination an excellent corrosion protection (paint). If they are used alone, then normally only a temporary protection is intended, for example, the use of wax or oil for storage or shipping. The most important aspect for the selection is a resistance against alkaline corrosion products of magnesium alloys.

3.09.6.2 Choice of Coating Systems and Design Aspects

The damage caused by galvanic corrosion of the magnesium components in contact with other metallic materials can also be reduced or fully suppressed by employing appropriate constructive measures. The most effective method is to avoid the accumulation of electrolyte in the area of contact of materials, as this virtually eliminates the formation of a galvanic cell.

The other way of controlling the galvanic corrosion of magnesium alloys is to control the cathodic reaction so that the net anodic reaction (galvanic attack) on magnesium can be reduced correspondingly.[109] The galvanic current (I) is expressed as

$$I = (E_C - E_A)/(R_C + R_E + R_M)$$

where E_C and E_A are the open circuit potentials of the cathode and anode, respectively, R_M and R_E are the resistances of the metal circuit and the electrolyte, respectively, and R_C is the cathodic polarization resistance.

Based on the above equation, the net galvanic current flow can be controlled by selecting an appropriate and compatible material as a couple, thus keeping the potential difference as low as possible. By using suitable coatings and insulation materials, the resistances R_C and R_M can be increased, resulting in lower galvanic current. As mentioned earlier, keeping the electrolyte away will result in an increased R_E, hence, in that case, too, a better galvanic corrosion resistance can be expected.

The choice of protective systems for magnesium alloys depends on the size, shape and geometry of the components and the joining technologies employed. Screwed and riveted joints offer the most varied possibilities to control, as one can alter the anode, cathode and the electric contact between these as well as the contact with the electrolyte. In some cases, by providing insulation between the magnesium and the other contacting material, the magnesium component can be left as such without any coating. There have been instances in which failure of a coating on magnesium alloys led to accelerated form of damage by the galvanically driven corrosion.

Conventionally galvanized steel screws can be employed with a silicate sealing for fastening of magnesium alloys, and it has been proven to be successful for applications in commercial vehicles.[110] The steel screws can also be electroplated with an alloy deposit of 80%Sn–20%Zn for a better performance.[111] The steel fasteners can also be used with nylon or plastic caps as cover for the screw heads.[109] In addition, washers made of an aluminum alloy (6XXX series, anodized) or polymer can be used with steel screws to minimize the galvanic corrosion. The use of Al screws instead of steel, if the loading conditions are not that severe, is a good idea. Fiber reinforced plastic screws on PEEK base with carbon or polyamide fibers can also be used considering the fact that the polymers are free from galvanic corrosion.[112]

The surface treatment procedures described above can also be applied for the treatment of magnesium alloy weldments. In principle, these weldments can be treated as an individual component; however, it is well known that the heat affected zones could be the vulnerable region in the weldments.[113] Nevertheless, by appropriate selection of processing parameters, a good protection from corrosion damage can be offered to these weldments.

3.09.7 Applications of Magnesium Alloys

Magnesium alloys have had applications since the early 1930s, when they were first used in the cast form in automobiles. Since the start of its production in 1939, more and more parts, such as the crank case, camshaft sprocket, gearbox housing, several covers, and the arm of an electric generator, were added, until the total magnesium weight reached 17 kg in 1962, which meant a reduction of 50 kg in total mass compared to steel. The production of the VW Beetle used almost 21 000 tons of magnesium alloys in 1960,[114] and the Volkswagen Group reached a total consumption of 42 000 tons of magnesium alloys in 1972,[115] until the change from air-cooled to water-cooled engines reduced the use of magnesium alloys. Other manufacturers used magnesium in their technical applications as well as in complex parts such as tractor hoods made of die-castings (dimensions: 1250 mm × 725 mm × 480 mm; weight 7.6 kg), main gear boxes for helicopters (casting weight 400 kg, machined 200 kg), crank cases for zeppelin engines, air intake cases for propjet engines (weight 42 kg), frames,

rims, instrument panels, fan blades for cooling towers (weight 169 kg), etc.

The development of high purity (HP) alloys, with their much improved corrosion resistance, contributed to the rapidly expanding production. In the past, the corrosion behavior of the available alloys had often been the overriding factor preventing their application. The factor favoring the use of magnesium is that it counts as a substitute for polymers for which no satisfactory recycling solution has yet been found. Furthermore, it allows light-weight construction for reduced energy consumption or simply easier handling.

With regard to the processing of magnesium alloys, pressure die-casting is preferred in view of its advantages compared to the processing of aluminum and zinc, which are both amenable to this type of casting. Besides the specific properties of magnesium mentioned above, the other favorable factors are its low casting temperature (650–680 °C, depending on the alloy) and the relatively low energy needed for melting. The energy needed for AZ91 (2 kJ cm^{-3}) is about 77% of that required to melt the aluminum alloy AlSi12CuFe.[116] The high price of magnesium usually refers to its mass not its volume, and the lower density coupled with other factors can actually make it cheaper in real terms. Thus, the low thermal heat content allows the casting process to be 50% faster than with aluminum; a high clock cycle of parts is possible, maintaining high precision and good surface quality.

Thus, magnesium can be found in a variety of applications today. The density, its shielding against electromagnetic radiation, and the possibility of producing thin-walled parts has led to furthering the use of magnesium die-cast parts in the computer industry, in mobile phones (**Figures 25(a)** and **25(b)**), and in hand tools (e.g., chainsaws).

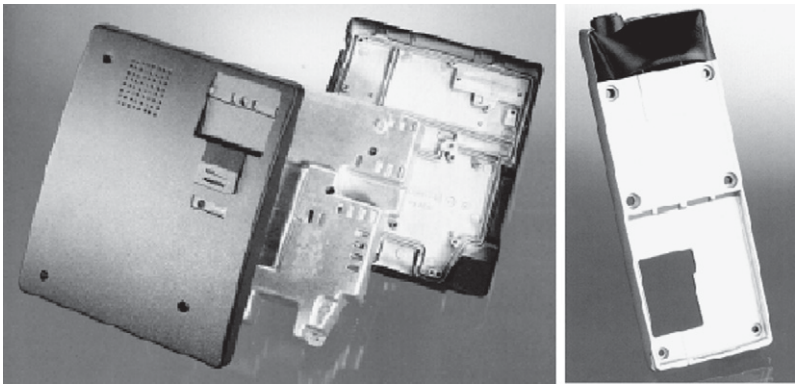

(a) (b)

Figure 25 Applications of magnesium alloys in the communications sector.[122] (a) Parts for a telephone switch board and (b) a mobile case.

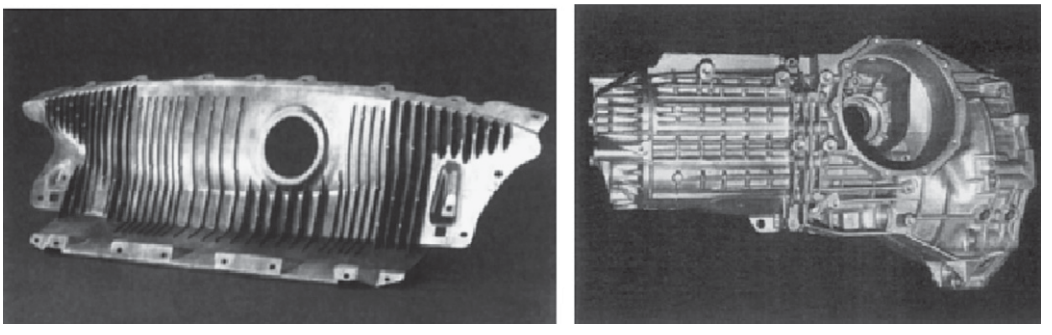

(a) (b)

Figure 26 Applications of magnesium alloys in automobiles.[122] (a) Fuel tank cover in Mercedes Benz and (b) gearbox housing in VW-Passat (Volkswagen AG).

Other examples of magnesium parts in vehicles include:

- gearbox housing, e.g., in the VW Passat, Audi A4
- the inner tailgate in the Lupo ('3-liter car'), which was made of AM50 (3.2 kg)
- tank cover in the Mercedes-Benz SLK
- cylinder head caps, for example, made of AZ91HP by cold-chamber high pressure die casting, and having a weight of 1.4 kg[117]
- dashboard, for example, in the Audi A8 and in the Buick Park Avenue/Le Sabre[118]
- seat-frames[119]
- steering wheels, for example, in the Toyota Lexus, Celica, Carina, and Corolla[118]
- rims, for example, in the Porsche Carrera RS (9.8 kg AM70 HP; low-pressure ingot casting).[117]

The list of magnesium parts in cars could be further continued[120,121] and new examples are constantly being added. Two recent applications of magnesium are illustrated in **Figures 26(a) and 26(b)**. The Mercedes-Benz SLK fuel tank cover is used as an example to show the advantages resulting from converting the construction from conventional materials to magnesium alloys. The part supports the car body and serves as a separation between the trunk and the back seats. Previous solutions consisted of a welded conduit frame. The first alternatives were steel and aluminum welding (7–8 kg each) and a magnesium cast part. The magnesium casting could be established as a serial part with a total weight of 3.2 kg, a decreased spatial requirement, and fewer components. Moreover, no post processing was necessary and the part could be used uncoated. The use of magnesium in the gearbox housing in the VW Passat is also primarily based on the weight savings achieved by replacing aluminum alloys. The use of the AZ91 alloy instead of aluminum led to a total weight reduction of almost 25%, and the geometry and production equipment remained identical.

References

1. Beck, A. *Magnesium und seine Legierungen;* Julius Springer Verlag: Berlin, 1939.
2. Emley, E. F. *Principles of Magnesium Technology;* Pergamon Press: New York, USA, 1966.
3. Avedesian, M. M.; Baker, H. *ASM Specialty Handbook Magnesium;* ASM International: Materials Park, OH, USA, 1999.
4. Kammer, C. *Magnesium-Taschenbuch;* Alumiumverlag: Düsseldorf, 2000.
5. Neite, G.; Kubota, K.; Higashi, K.; Hehmann, F. In *Materials Science and Technology, Volume 8, Structure and Properties of Non-Ferrous Alloys*; Cahn, R. W., Haasen, P., Kramer, E. J., Eds.; VCH Weinheim, 1996.
6. Annual book of ASTM Standards. Nonferrous metal Products. Volume 02.02. Aluminium and Magnesium alloys. ASTM West Conshohocken, 1996.
7. Fink, R. In *Magnesium – Eigenschaften, Anwendungen, Potenziale*; Kainer, K. U. Ed.; Wiley-VCH, 2000; pp 26–49.
8. Zeumer, N.; Fuchs, H.; Betz, G. *Proc. Int. Conf. Magnesium Technology;* London 1987; pp 18–24.
9. Unsworth, W.; King, J. F. *Proc. Int. Conf. Magnesium Technology;* London 1987; pp 25–36.
10. King, J. F. In *Magnesium Alloys and their Applications*; Kainer, K. U., Ed.; Wiley-VCH, 2000; pp 14–22.
11. Alves, H.; Köster, U. In *Magnesium Alloys and their Applications*; Kainer, K. U., Ed.; Wiley-VCH, 2000; pp 439–444.
12. Mordike, B. L.; Buch, F. V. In *Magnesium Alloys and their Applications*; Kainer, K. U., Ed.; Wiley-VCH, 2000; pp 35–40.
13. Pettersen, K.; Westengen, H.; Skar, Y. I.; Videm, M.; Wei, L.-Y. In *Magnesium Alloys and their Applications*; Kainer, K. U., Ed.; Wiley-VCH, 2000; pp 29–34.
14. Pekguleryuz, M. O. *Mater. Sci. Forum* **2000**, *350–351*, 131–140.
15. Du, W.; Sun, Y.; Min, X.; Xue, F.; Zhu, M.; Wu, D. *Mater. Sci. Eng. A* **2003**, *356*, 1–7.
16. Yuan, G. Y.; Liu, L.; Wang, Q. D.; Ding, W. J. *Mater. Lett.* **2002**, *56*, 53–58.
17. Lee, Y. *Grain Refinement of Magnesium*; PhD Thesis, University of Queensland: Australia, 2002.
18. Sillekens, W. H.; Bohlen, J. In *Magnesium, Proc. 6th Int. Conf. and Exhibition on Magnesium Alloys and their Applications*; Kainer, K. U., Ed.; Wiley VCH, 2003; pp 1046–1052.
19. Becker, J.; Fischer, G. In *Magnesium-Eigenschaften, Anwendungen, Potenziale*; Kainer, K. U., Ed.; Wiley-VCH Verlag, 2000; pp 95–110.
20. Mabuchi, M.; Yamada, Y.; Higashi, K. In *Magnesium Alloys and their Applications*; Wiley-VCH Verlag, 2000; pp 280–284.
21. Lin, H. K.; Huang, J. C. *Key Eng. Mater.* **2003**, *233–236*, 875–880.
22. Kainer, K. U.; Doege, E.; Janssen, S.; Ebert, T. *Magnesium Alloys and their Applications*; Wiley-VCH Verlag, 2000; pp 596–601. (ISBN: 3-527-30282-2).
23. Everett, R. K.; Arsenault, R. J. *Metal Matrix Composites: Mechanisms and Properties;* Academic Press, 1991.
24. Clyne, T. W.; Withers, P. J. *An Introduction to Metal Matrix Composites;* Cambridge University Press, 1993.
25. Freuling, J. W.; Hanawalt, J. D. *Trans. AFS* **1969**, *77*, 159–164.
26. King, J. F. Proc. 60th Annual World Magnesium Conference, Stuttgart, 2003; pp 10–15.
27. Kainer, K. U.; Benzler, T. U. In *Magnesium – Eigenschaften, Anwendungen, Potenziale*; Kainer, K. U., Ed.; Wiley-VCH, 2000; pp 59–75.
28. Wabusseg, H.; Kaufmann, H.; Uggowitzer, P. J. *Giesserei* **2000**, *87*(3), 39–43.
29. Mundl, A.; Kaufmann, H. *Giesserei* **2001**, *88*(8), 55–58.
30. Noll, T. R.; Freiedrich, B.; Mueser, H.; Budak, I. *Giesserei* **2001**, *88*(8), 60–66.
31. Gräf, T.; Hauer, H. *Giesserei* **2001**, *88*(10), 38–41.
32. Czerwinski, F.; Zielinska-Lipiec, A.; Pinet, P. J.; Overbeeke, J. *Acta Mater.* **1991**, *49*, 1225–1235.
33. Sasaki, H.; Adachi, M.; Sakamoto, T.; Takimoto, A. *Giesserei-Praxis* **1997**, *15/16*, 341–246.
34. Kainer, K. U.; Dietzel, W.; Blawert, C. *Reaktionsfreudig – Korrosionsschutz von Magnesium-werkstoffen Maschinenmarkt – Das Industrie Magazin* **2003**, *Vol. 14*, 66.

35. Haferkamp, H.; Zilberg, J.; Rodman, M.; Nicmeyer, M.; Weber, J.; Holzhamp, U. *Theorie Praxis Metall.* **2000**, *19*(5), 23–24.
36. Swiostek, J.; Bohlen, J.; Letzig, D.; Kainer, K. U. In *Proc. 6th Int. Conf. and Exhibition on Magnesium Alloys and their Applications*; Kainer, K. U., Ed.; Wiley VCH, 2003; pp 278–284. (ISBN: 3-527-30975-6).
37. Becker, J.; Fischer, G. In *Magnesium – Alloys and Technology*; Kainer, K. U., Ed.; Wiley-VCH Verlag GmbH: Weinheim, 2003. ISBN: 3-527-30570-X.
38. Müller, K. B. In *Magnesium Technology*; Kaplan, H. I., Ed.; 2002; pp 187–192.
39. Weissert, W. *Mat.-wiss. U. Werkstofftechn.* **2001**, *32*, 81–83.
40. AWS, *Welding Handbook*, 8th ed.; American Welding Society: Miami, 1991; Vol. 2, pp 739–762.
41. *Welding of Magnesium Alloys; In ASM Handbook*; ASM international, 1990; pp 772–782.
42. Ryavov, V.; Ryazantsev, V. *Arc Welding of Aluminium and Magnesium Alloys;* Backbone Publishing: USA, 1998.
43. Rethmeier, M.; Wohlfahrt, H.; Wiesner, S. Joining of Lightweight Mg-Alloys by MIG Welding, IIW-Doc. IX-2042-02, 2002.
44. Liu, L.; Dong, C. *Mater. Let.* **2006**, *60*, 2194–2197.
45. Munitz, A.; Cotler, C.; Stern, A.; Kohn, G. *Mater. Sci. Eng. A* **2001**, *302*, 68–73.
46. Xunhong, W.; Kuaishe, W. *Mater. Sci. Eng. A* **2006**, *431*, 114–117.
47. Chao-Ting, C.; Chuen-Guang, C. *J. Mater. Process. Technol.* **2007**, *182*, 369–373.
48. Liming, L.; Jifeng, W.; Gang, S. *Mater. Sci. Eng. A* **2004**, *381*, 129–133.
49. Liu, L. M.; Cai, D. H.; Zhang, Z. D. *Scripta Mat.* **2007**, *57*, 695–698.
50. Haferkamp, H. H.; Niemeyr, M.; Schmid, C.; Kaese, V.; Cordini, P. Magnesium 2000: Proceedings of the Second Israeli International Conference on Magnesium Science & Technology, Dead Sea, Israel, MRI, 2000; pp 449–455.
51. Weisheit, A.; Galun, R.; Mordike, B. L. *Magnesium Alloys and Their Properties;* DGM: Wolfsburg, 1998.
52. Sanders, P. G.; Keske, J. S.; Leong, K. H.; Kornecki, G. *J. Laser Appl.* **1999**, *11*(2), 96–103.
53. Leong, K.H.; Kornecki, G.; Sanders, P.G.; Keske, J.S. ICALEO 98: Laser Materials Processing Conference, Orlando, FL, 16–19 November 1998; pp 28–36.
54. Weisheit; Galun, R.; Mordike, B.L. Proceedings of the Conference: Magnesium Alloys and Their Applications, Wolfsburg, Germany, 28–30 April 1998; pp 619–624.
55. Coelho, R. S.; Kostka, A.; Pinto, H.; Riekehr, S.; Koçak, M.; Pyzalla, A. R. *Mater. Sci. Eng.* **2008**, *485*, 20–30.
56. Schram, S.; Kettler, C.; Mazac, K.; Goldstein, C. *Schweissen Schneiden* **2000**, *52*(6), 349–353.
57. Lackyer, S., Friction stir welds in magnesium alloys – Just how good are the mechanical properties, TWI: Bulletin March/April 2001.
58. Kato, K.; Tokisue, H. *Weld. Int.* **1994**, *8*, 452–457.
59. Nagasawa, T.; Otsuka, M.; Yokota, T.; Ueki, T. Magnesium Technology 2000, TMS, Nashville, 12–17 March 2000, pp 383–387.
60. Hawke, D. L. In *ASM Speciality Handbook Magnesium and Magnesium Alloys*; ASM International, 1987; pp 194–210.
61. Song, G.; Atrens, A. *Adv. Eng. Mater.* **1999**, *1*, 11–33.
62. Boese, E.; Göllner, J.; Hevn, A.; Strunz, A.; Baierl, C.; Schreckenberger, H. *Mater. Corros.* **2001**, *52*, 247–256.
63. Makar, G. L.; Kruger, J. *Int. Mater. Rev.* **1993**, *38*(3), 138–153.
64. Hillis, J. E.; Reichek, K. N. High purity magnesium AM60 alloy: The critical contaminant limits and the salt water corrosion performance, SAE Technical Paper Series #860 288, Detroit, 1986.
65. Song, G.; Atrens, A.; Dargusch, M. *Corros. Sci.* **1998**, *41*, 249–273.
66. Ghali, E. In *Uhlig's Corrosion Handbook*; Revie, R. W., Ed.; John Wiley: New York, 2000; ch. 44, pp 793–830.
67. Lynch, S. P.; Trevena, P. *Corrosion* **1988**, *44*, 113.
68. Meletis, E. I.; Hochman, R. F. *Corrosion* **1984**, *40*, 39.
69. *ASM Speciality Handbook: Magnesium and Magnesium Alloys*; ASM International: USA, 1999; p 211.
70. Stampella, R. S.; Procter, R. P. M.; Ashworth, V. *Corros. Sci.* **1984**, *24*, 325–341.
71. Winzer, N.; Atrens, A.; Song, G.; Ghali, E.; Dietzel, W.; Kainer, K. U.; Hort, N.; Blawert, C. *Adv. Eng. Mater.* **2005**, *7*, 659–693.
72. Miller, W. K. In *Stress Corrosion Cracking: Materials Performance and Evaluation*; ASM International: USA, 1992; p 251.
73. Fairman, L.; Bray, H. J. *Corros. Sci.* **1971**, *11*, 533–541.
74. Tomashov, N. D.; Modestova, V. N. Proceedings of the Inter-crystalline Corrosion and Corrosion of Metals Under Stress; Levin, I. A. Ed.; Consultants Bureau: New York, 1962; pp 251.
75. Rokhlin, L. L. *Magnesium Alloys Containing Rare Earth Metals*; Taylor and Francis: UK, 2003; p 221.
76. Perryman, E. C. W. *J. Inst. Metals* **1951**, *78*, 621.
77. Pelensky, M. A.; Gallaccio, A. Stress Corrosion Testing, STP 425, ASTM 1967; p 107.
78. Pardue, W. M.; Beck, F. H.; Fontana, M. G. *Trans. Am. Soc. Metals* **1961**, *54*, 539.
79. Bobby Kannan, M.; Dietzel, W.; Zeng, R.; Zettler, R.; dos Santos, J. F. *Mater. Sci. Eng. A* **2007**, *460–461*, 243–250.
80. Fairman, L.; Bray, H. J. *Br. Corros. J.* **1971**, *6*, 170.
81. Priest, D. K.; Beck, F. H.; Fontana, M. G. *Trans. Am. Soc. Metals* **1955**, *47*, 473.
82. Jones, R. H.; Ricker, R. E. *Stress Corrosion Cracking: Materials Performance and Evaluation*; ASM International: USA, 1992; p 1.
83. Bursle, A. J.; Pugh, E. N. *Mechanisms of Environment Sensitive Cracking of Materials*; Materials Society: London, 1977; p 471.
84. Blawert, C.; Swiostek, J.; Dietzel, W.; Leitzig, D.; Atrens, A. Proceedings of the Inzeynieria Powierzchni 2A, 2005, Corrosion 2005, Warsaw, Poland, 8–10 June 2005; pp 183–189.
85. Bobby Kannan, M.; Dietzel, W.; Singh Raman, R. K.; Lyon, P. *Scripta Mater.* **2007**, *57*, 579–581.
86. Hillis, J. E. The effects of heavy metal contamination on magnesium corrosion performance, SAE Technical Paper No. 830523, Detroit, 1983.
87. Bühler, K. *Metall* **1990**, *8*, 748–753.
88. Bray, D. J. Cast and rapidly solidified magnesium alloys – New light alloys. Advisory Group for Aerospace Research and Development, 92 – Neuilly sur Seine; NATO, Brussels; AGARD Conference on New Light Alloys 1990, Monterey, CA, USA 1990; pp 7.1–7.29.
89. Gray, J. D.; Luan, B. *J. Alloys Compounds* **2002**, *336*, 88–113.
90. Schreckenberger, H. Proceedings of Fortschritte mit Magnesium im Automobilbau; Bad Nauheim 2000; pp 41–50.
91. Murray, R. W.; Hillis, J. E. Magnesium finishing – Chemical treatment and coating practices, SAE Technical Paper No. 900791, Detroit, 1990.
92. Kurze, P. Proceedings of Berichtsband 23, Ulmer Gespräch 2001, pp 82–88.

93. Zeng, A. P.; Xue, Y.; Qian, Y. R.; Want, Z. J. *Acta Metall. Sin.* **1999**, *12*, 946–951.
94. Gonzalez-Nunez, M. A.; Nunez-Lopez, C. A.; Skeldon, P.; Thompson, G. E.; Karimzadeh, H.; Lyon, P.; Wilks, T. E. *Corros. Sci.* **1995**, *37*, 1763–1772.
95. Rudd, A. L.; Breslin, C. B.; Mansfeld, F. *Corros. Sci.* **2000**, *42*, 275–288.
96. Reinhold, B. *OWT & WTK, Chemnitz* **2001**, 151–158.
97. Leyendecker, F. *DFO Leichtmetall-Anwendungen–Neue Entwicklungen in der Ober-flächentechnik* **2001**, *46*, 131–142.
98. Hillis, J. E. *Proc. of 40th Annual Conf. of Metallurgists of CIM* 2001; pp 3–26.
99. Kurze, P. In *Magnesium – Alloys and Technology*; Kainer, K. U. Ed.; Wiley-VCH Verlag GmbH: Weinheim, 2003. ISBN: 3-527-30570-X.
100. Blawert, C.; Heitmann, V.; Dietzel, W.; Nykyforchyn, H. M.; Klapkiv, M. D. *Surf. Coat. Technol.* **2005**, *200*, 68–72.
101. Sharma, A. K. *Metal Finishing* **1991**, *89*(7), 16.
102. Bakkar, A.; Neubert, V. *Electrochem. Commun.* **2007**, *9*, 2428–2435.
103. Yoshinori, Y. Method for plating magnesium alloy, JP60024383, 1985.
104. Feurer, R.; Bui-Nam; Morancho, R.; Larharfi, M.; Calsou, R. *Br. Corros. J.* **1989**, *24*, 126–130.
105. Rie, K. T.; Whole, J. *Surf. Coat. Technol.* **1999**, *112*, 226–233.
106. Seeger, D. M.; Blawert, C.; Dietzel, W.; Bohne, Y.; Maendl, S.; Rauschenbach, B. In *Magnesium Technology 2005, TMS 2005, 134th Annual Metting and Exhibition;* San Fransisco, CA (USA), 13–17, February; Neelameggham, N. R., Kaplan, H. I., Powel, B. R., Eds.; 2005; pp 323–328. ISBN:0-87339-582-4.
107. Bohne, Y.; Seeger, D. M.; Blawert, C.; Dietzel, W.; Maendl, S.; Rauschenbach, B. *Surf. Coat. Technol.* **2006**, *200*(22–23), 6527–6532.
108. Blawert, C.; Heitman, V.; Dietzel, W.; Stoermer, M.; Bohne, Y.; Gerlach, J. W.; Manowa, D.; Maendl, S. Proceedings of the Light Metals Technology Conference, Saint-Sauveur (CDN), 24–26 September 2007; pp 135–139.
109. Hydro Magnesium, Corrosion and Finishing of Magnesium Alloys, Technical Brochure.
110. Reinhold, B.; Kose, S. G.; Strobl, C. *Mater. Corros.* **1999**, *50*, 517–522.
111. Lehmkuhl, H.; Mehler, K.; Reinhold, B.; Bangard, H.; Tesche, B. *Adv. Eng. Mater.* **2001**, *3*, 412–417.
112. Skar, J. I.; Albright, D. *Magnesium Technology 2002*; TMS, 2002; pp 255, 261.
113. Lübbert, K.; Kopp, J.; Wendler-Kalsh, E. *Mater. Corros.* **1999**, *50*, 65–72.
114. Serwe, G. Magnesiumgußteile im Volkswagen, VDI-Berichte Nr. 58, VDI-Verlag, Düsseldorf, 1962.
115. Höllrigl-Rosta, F.; Just, E.; Köhler, J.; Melzer, H.-J. *Metall* **1980**, *34*, 12.
116. Cahn, R. W.; Hassen, P. In *Materials Science and Technology – A Comprehensive Treatment*; Kramer, E. J., Ed.; *Structure and Properties of Nonferrous Alloys* Matucha, K. H.; Ser Ed.; VCH Weinheim, 1996; Vol. 8.
117. Olsen, A. L. *Metall* **1992**, *46*, 570–574.
118. Magers, D. Einsatzmöglichkeiten von Magnesium im Automobilbau, Leichtmetalle im Automobilbau (Sonderausgabe der ATZ und MTZ 1995), Franckh-Kosmos Verlags-GmbH, Stuttgart, 1995.
119. Hector, B.; Heiss, W. Magnesium die-castings as structural members of the new Mercedes-Benz Roadster, SAE-Technical Paper Series No. 900798, 1990.
120. Müller, C. M. *Giesserei*; **1991**, *78*(19).
121. Polmear, I. J. *Mater. Sci. Technol.* **1994**, *10*, 1–16.
122. Kainer, K. U.; Von Buch, F. In Magnesium – Eigenschaften, Anwendungen, Potenziale; Kainer, K. U., Ed.; Wiley–VCH, 2000; pp 1–26.

3.10 Corrosion of Titanium and its Alloys

D. W. Shoesmith and J. J. Noël
Department of Chemistry, The University of Western Ontario, London, ON, Canada N6A 5B7

Glossary

Adsorption The surface retention of atoms, molecules, or ions by a solid or a liquid.

Alloy A metal product containing two or more elements as a solid solution, intermetallic compound, or mixture of metallic phases.

Anatase A tetragonal polymorph of titanium dioxide, also called octahedrite.

Cathodic modification Enhancement of cathodic kinetics by alloying additions leading to depolarization of the cathodic reaction and a shift of the corrosion potential to the passive region.

Complexation Formation of a coordination compound between a metal ion and a molecular or ionic entity known as a ligand.

Corrosion allowance An excess amount of metal included in a component, beyond that required for mechanical considerations, to compensate for expected corrosion losses.

Creep Slow, time-dependent strain of a solid caused by stress.

Diffusion coefficient The mass of a species, in grams, diffusing across an area of 1 cm^2 in one second in a unit concentration gradient. Also known as diffusivity.

Environmentally-assisted cracking A cracking process driven by tensile stress in the presence of particular favorable environmental conditions (e.g., stress corrosion cracking, hydrogen-induced cracking).

Film fracture events Spontaneous and sudden rupture of the passive film on a metal, resulting in exposure of the underlying metal to the environment.

Fretting Wear and corrosion damage at the asperities of contact surfaces induced by repeated relative surface motion under load.

Galvanic coupling The joining of two dissimilar metals in an electrolyte, potentially leading to galvanic corrosion.

Halide The anion of an element belonging to the halogen group (F, Cl, Br, I, At).

Hydriding The formation of a covalent compound between hydrogen and a metal

Hydrolysis The reactions of metal cations with water to produce oxides or hydroxides and increase acidity.

Initiation The start of a localized corrosion process.
Intermetallic compound A covalent compound of two or more metals, or the alloy of two metals in which a progressive change in composition is accompanied by a progression of phases, differing in crystal structure.
Lamination A layered arrangement.
Load The mechanical force that is applied to a body.
Metallosis Infiltration of metal ions and/or particles into, and inflammation of, soft and/or bony tissues proximate to metallic biomedical implants as a result of wear, corrosion, and/or hypersensitivity reaction.
n-Type A semiconductor whose electrical conduction is associated with electrons (as opposed to holes) as the majority charge carrier.
Nitinol A TiNi shape-memory alloy.
Propagation The active stage of ongoing reaction and damage formation during a localized corrosion process.
Repassivation The cessation of corrosion and return to passivity of a surface after loss of passivity caused by localized corrosion or mechanical damage.
Rolling Reducing or changing the cross-sectional area of a workpiece by the compressive forces exerted by rotating rollers.
Rutile A tetragonal polymorph of titanium dioxide.
Semiconductor A solid material whose electrical conductivity is intermediate between that of a conductor and insulator, and is usually strongly temperature-dependent.
Stress intensity factor A measure of the stress at a point in a structure due to pressure resulting from combined tensile and compressive stresses.
Texture The anisotropic ordering of size, shape, and crystallographic orientation of grains in a polycrystalline solid.
Toughness A property of a material capable of absorbing energy by plastic information (see fracture toughness).
Young's modulus The ratio of a simple tensile stress applied to material to the resultant strain parallel to the tension.

Abbreviations

ASTM American Society for Testing and Materials
BCC Body-centered cubic
HCP Hexagonal close-packed
HIC Hydrogen-induced cracking
MIC Microbiologically-influenced corrosion
ppm Parts per million (by weight)
SCC Stress corrosion cracking
SCE Saturated calomel electrode
UNS No. Unified Numbering System number

Symbols

H_c Critical hydrogen concentration for hydrogen-induced cracking [ppm]
pH $-\log$ (hydrogen ion activity)
pK_a $-\log$ (acid dissociation constant)
Ti_xFe Intermetallic compound of titanium and iron with uncertain stoichiometry represented by x
TiH_x Titanium hydride with uncertain stoichiometry represented by x
α The hexagonal phase of titanium
β The cubic phase of titanium

3.10.1 Introduction

The key attributes of titanium and its alloys are high strength-to-density ratios and corrosion resistance, making these materials attractive choices for aerospace applications and the chemical process industry, respectively.[1–6] More recently, improvements in the corrosion resistance of the higher strength alloys by minor alloying additions have led to their expanded usage as medical and dental implants.[7]

3.10.2 General Physical Properties

Titanium has two elemental crystalline structures, the hexagonal close-packed (HCP) α structure and the body-centered cubic (BCC) β structure.[8–11] While commercially pure Ti has the α structure, the impurity Fe and added alloying elements can produce a range of alloy microstructures. Depending on the predominant phase, Ti and its alloys are classified as α, near-α, α–β, or β.[9] The commercially

pure materials have the α structure and vary in oxygen content depending on strength requirements. The already good corrosion resistance of these materials can be further improved by the addition of small amounts of Pd and Ru.[7] The near-α alloys retain the HCP structure, but the addition of metals such as Al, Sn, V, Mo, and Ni may stabilize small amounts of the β-phase. This leads to increases in strength and toughness. The addition of very small amounts (<1 wt%) of Mo and Ni, and especially Pd or Ru, improves their corrosion resistance. Further increases in alloy content, particularly V and Al, lead to a range of higher strength α–β alloys, whose corrosion resistance can again be enhanced by Pd or Ru additions. The β alloys, predominantly used in aerospace applications, contain additional alloying elements, such as Cr, Zr, and Nb.

When corrosion resistance is paramount, α or near-α alloys are the appropriate choice, while α–β and β alloys are more appropriately selected for high-strength applications. **Table 1** shows a representative selection of materials and properties. More extensive listings and a general description of mechanical properties are available elsewhere.[2,5–7]

Small variations in impurity Fe content (generally <0.2 wt%) and distribution influence the microstructure by inhibiting grain growth during fabrication. This leads to decreased α-grain size and Fe-stabilized β-phase along grain boundaries. Fe contents (≥0.03 wt%) can lead to the precipitation of Ti_xFe particles on grain boundaries and at triple points.[12–14] The time spent in the temperature range 700–860 °C (during fabrication, welding, or heat treatments) enhances β-phase and Ti_xFe formation.

Small microstructural changes also occur on addition of the slightly soluble Pt group metals.[7] Pd can form intermetallic compounds in the α-matrix without affecting grain growth, while Ru additions stabilize β-phase and inhibit α grain growth. For near-α Ti containing 0.15 wt% of Ru, β-phase Ru content can exceed 10 wt%.[15] In α–β alloys, both Pd and Ru are accommodated in the β-phase and the microstructure is unaffected.[7] Since both noble metals and Fe stabilize β-phase and intermetallics, their cosegregation can occur. For example, β-phase containing 12 wt% Ru and 5 wt% Fe is observed in Ti containing 0.15 wt% Ru,[16] and grain boundary phases containing 2.6–6.9 wt% Fe and 0.3–0.8 wt% Pd are observed in Grade-7 (0.15 wt% Pd).[16]

3.10.3 General Corrosion Properties

Titanium is highly reactive with oxygen, and its corrosion resistance is attributable to the presence of a chemically inert, adherent, oxide film. This film forms spontaneously in air and aqueous environments and can be amorphous or crystalline, depending on the mode and rate of formation, slow growth favoring crystallinity.[17–19] The crystalline oxide can be anatase or the more stable rutile.[20–22] The presence of oxygen vacancies and Ti^{III} interstitial ions makes the oxide an n-type semiconductor.[23–25] Its composition is close to $Ti^{IV}O_2$ with Ti^{III}/Ti^{II} states at the metal–oxide interface.[26,27] The oxide–solution interface is commonly hydrated.[20]

For α and near-α alloys, alloying elements (Pd, Ru, Ni) do not incorporate into the oxide, but, for α–β

Table 1 Composition and properties of selected ASTM grades of titanium

ASTM grade (UNS No.)	*Alloy type*	*Nominal composition (wt%)*	*Minimum yield strength (MPa)*	*Minimum tensile strength (MPa)*
1	α	0.06 O	170	240
2	α	0.12 O	275	345
4	α	0.3 O	483	550
7	α	0.12 O, 0.15 Pd	275	345
16	α	0.12 O, 0.05 Pd	275	345
26	α	0.12 O, 0.1 Ru	275	345
9	Near-α	3 Al, 2.5 V	483	620
18	Near-α	3 Al, 2.5 V, 0.05 Pd	483	620
12	Near-α	0.3 Mo, 0.8 Ni	345	483
28	Near-α	3 Al, 2.5 V, 0.1 Ru	483	620
5	α–β	6 Al, 4 V	828	895
24	α–β	6 Al, 4 V, 0.05 Pd	828	895
25	α–β	6 Al, 4 V, 0.5 Ni, 0.05 Pd	828	895
19	β	3 Al, 8 V, 6 Cr, 4 Zr, 4 Mo	759	793
20	β	3 Al, 8 V, 6 Cr, 4 Mo, 4 Zr, 0.05 Pd	759	793

alloys the oxide on the β-phase is slightly enriched in Al and V.[28,29] The oxide thickness and crystallinity may vary spatially.[30] The film at grain boundaries may be less protective than that on the grains when secondary phases are present.[16,31] The durability of this film is essential for corrosion protection, and the parameters most likely to influence its properties are (i) environmental redox conditions (i.e., corrosion potential), (ii) pH, and (iii) temperature.

3.10.3.1 Influence of pH

For pH < 4, the oxide can dissolve[31] and the Ti become active. An active to passive transition is observed over the potential range –0.7 to –0.3 V (vs. SCE).[32] Active corrosion can be rapid, leading to surface hydride (TiH_x) formation,[2] but the rate is significantly suppressed on Pd- and Ru-containing alloys,[7] which become surface-enriched in Pd/Ru.[33–38] Even for hot, strongly reducing acidic conditions, enrichment can catalyze proton reduction and shift the corrosion potential into the passive region; this process is known as cathodic modification,[39,40] and is also observed with the Grade-12 alloy.[41]

In a sufficiently oxidizing environment, the corrosion potential will be >–0.3 V (vs. SCE) and the alloy passive. Corrosion rates are negligible and insensitive to environment and to temperature well above 100 °C.[2,5] An increase in potential thickens the oxide and makes it less defective.[42] For an applied potential >1 V (vs. SCE), a current for water oxidation to O_2 is observed,[43,44] and often mistaken for the onset of pitting in α and near-α alloys. Pitting only occurs in Br^- solutions, an effect which has been attributed to Br^- adsorption at sites associated with impurity inclusions containing either Al and Si or Fe.[50–52] In Cl^- solutions, polarization to >5 V (vs. SCE) is required to induce pitting,[53,54] and temperatures >100 °C are required before pitting potentials decrease to ~2 V (vs. SCE). Pitting requires high film stresses leading to film breakdown/recrystallization and the introduction of enhanced transport pathways for Cl^- ions.[44,55–57]

Since potentials >1 V (vs. SCE) are unattainable under natural corrosion conditions, pitting does not occur in Ti and its alloys, and protection against active corrosion is ensured at corrosion potentials >–0.3 V (vs. SCE). Protection can be ensured by anodic protection[58–60] or by the addition of small concentrations of oxidants (e.g., O_2, Fe^{3+}).[2,5] Anodic or thermal oxidations are also options,[61,62] but anodic oxidation produces only short term protection. In dry environments (e.g., Cl_2 gas) and organic process streams, only small amounts of moisture or O_2 are needed to maintain passivity.[2,63]

Corrosion rates increase in alkaline solutions as the protective oxide is more soluble, but, except at high temperatures, they remain low.[2,5,64] In peroxide solutions at pH >12, commonly encountered in the pulp and paper industry, corrosion rates can be extremely high.[65,66] These high rates are attributed to the aggressive HO_2^- anion, the dominant form of peroxide above pH 10.6 (the pK_a for H_2O_2).[67–69] By contrast, peroxide, while modifying the passive oxide, does not cause rapid corrosion at lower pH values.[70,71]

3.10.3.2 Influence of Temperature

For active conditions (reducing acids and alkaline peroxide), increasing the temperature increases corrosion rates, but its influence under passive conditions is marginal. As the temperature is increased up to ~70 °C, the passive film becomes more crystalline and absorbs water,[17,72,73] and flaws begin to appear.[57,74] Although observable through the fluctuations in corrosion potential that they cause, these flaws rapidly self-repair and no significant loss of passivity is observed up to 150 °C in Cl^- solutions.[75,76] In fact, extensive corrosion testing in extremely saline environments to temperatures well above 200 °C shows that corrosion rates are not significantly enhanced.[39,77–84]

3.10.3.3 Influence of Fluoride

Fluoride appears to be the only ion in aqueous solution that is able to destroy passivity. Its influence has been studied widely for dental applications,[85–101] since dental gels and rinses can contain 1000–10 000 $\mu g\,g^{-1}$ (ppm) of F^- in the pH range 3.5 to neutral, and in flue gas scrubber environments,[102,103] in which the liquors formed can contain up to ~1000 $mg\,l^{-1}$ of F^-. This aggressiveness is attributed to the solubilization of Ti as TiF_6^{2-} and TiF_6^{3-} aqueous complexes. It is generally recognized that a substantial F^- concentration and a low pH must coexist[104,105] for passivity to be lost. The pH threshold varies with F^- concentration and the Pd/Ru content of the alloy; for example, for a Pd content >0.1 wt%, passivity in 900 $mg\,l^{-1}$ of F^- is maintained at pH 4, while at 9000 $mg\,l^{-1}$ no general corrosion was observed at pH 6.5 but shallow (up to ~ 2 μm in cross section) pitting was observed.[98] The most likely location of these pits is at Fe impurity sites in grain boundaries. Their extensive propagation is unlikely because it will be limited by the cathodic modification process.[98–101]

Despite the much more aggressive environments, the influence of F^- in flue gas scrubbers is muted. These environments contain Cl^- up to 15 700 $\mu g\,g^{-1}$, SO_4^{2-} in the range 9000–26 000 $\mu g\,g^{-1}$, F^- up to 12 000 $\mu g\,g^{-1}$, and the pH can be as low as 1 (at $T \sim$ 170–180 °C).[102,103] For Ti Grades-2 and-12, F^- led to a loss of passivity for pH $\leq$ 3 and <1.5, respectively. The relatively minor influence of F^- was attributed to its removal by complexation with cations (e.g., NaF, Na_2F^+, CaF^+) and its reaction with the silica in fly ash. The resilience of Pd/Ru-containing alloys in extreme environments has been demonstrated by testing of the Ti–6Al–4V–Ru alloy (Grade-29) in deep gas well environments.[106]

3.10.3.4 Hydrogen Absorption into Ti

Under active conditions (reducing acid and alkaline peroxide solutions) corrosion is driven by H^+ reduction leading to H absorption.[24] Since the solubility of H in α-Ti is low (20–100 $\mu g\,g^{-1}$ at room temperature, depending on alloy composition[107]), brittle hydrides then precipitate in α- and near-α alloys, and embrittlement may be possible. Also, even relatively small H contents (>70 $\mu g\,g^{-1}$) can cause a loss of impact toughness.[108] However, at room temperature, the diffusion coefficient of H in the α-phase is low,[109,110] and H is retained in a surface hydride layer[2,5,111–113] and material integrity is not challenged.

The rate and extent of absorption depend on alloy composition, microstructure, and temperature. On Pd/Ru alloys, catalysis of H^+ reduction leads to enhanced absorption,[40,114] but this can be limited by solution aeration.[115] In the Grade-12 alloy, Ti_2Ni particles act as galvanically-coupled cathodes in the α-matrix and form hydride readily.[116] Furthermore, the Ni-stabilized β-phase in the grain boundaries facilitates H transport into the bulk of the alloy, as the β-phase diffusion coefficient is $\sim 10^5$ times that in the α-phase.[110,117]

The passive oxide is generally impermeable to H, and the absorption efficiency approaches zero for pH > 3,[118] unless the alloy is cathodically polarized to <–0.6 V (vs. SCE) when redox transformations in the oxide are accompanied by H absorption ($TiO_2 + H^+ + e^- \rightarrow TiOOH$).[119–124] Although the oxide is then rendered permeable, significant H transport through it requires a potential <–1.0 V (vs. SCE).[119,125]

Polarization to these potentials requires either galvanic coupling to active metals (e.g., Zn or carbon steel) or the application of cathodic protection. To avoid significant hydrogen absorption, an operating threshold of >–0.7 V (vs. SCE) is recommended.[2] Although the potentials during galvanic coupling to carbon steel can be below this value (at temperatures in the range 18–60 °C[126]), the H absorption rate (generally measured at –1.0 V (vs. SCE)) decreases parabolically with time as H accumulates in a surface hydride layer[127,128] and absorption becomes controlled by diffusion into the alloy. For α-alloys, the transport is slow and little damage is done. For Grade-12 Ti, however, β-phase transport accelerates diffusion and the overall absorption rate is higher.[129] Since diffusion coefficients are temperature-dependent, embrittlement below 80 °C is not expected.[2] Generally, this is observed to be the case,[130] although high stress levels promote absorption and hydriding.[131]

Cathodic protection is common in marine applications, with relative absorption tendencies in the order Ti-12 > Ti-2 > Ti-5/Ti-9.[132] Noble metal additions to near-α and α–β alloys increase absorption only slightly (up to ~40%).[128] Thermal oxidation prior to exposure suppresses absorption (in 6% NaCl, up to 120 °C),[135] and H absorption in deaerated HCl (2 $\leq$ pH $\leq$ 4) up to 250 °C can be prevented by aeration.[115]

3.10.4 Localized Corrosion Processes

A major asset of Ti alloys is their apparent immunity to many localized corrosion processes, especially pitting and vapor phase corrosion[2,5,134,135] and microbially-influenced corrosion (MIC).[134–143] The two predominant localized corrosion failure modes are crevice corrosion and hydrogen-induced cracking (HIC).

3.10.4.1 Crevice Corrosion

Crevice corrosion is generally observed in hot oxidizing halide (or, less commonly, sulfate) environments, under tight gaskets, in metal–metal joints, and under adherent deposits produced in industrial process streams. Reviews summarizing industrial observations and laboratory studies have been published.[2,5,144] For the most commonly used Ti material, Grade-2, it is accepted that crevice corrosion will not occur for T < 70 °C, regardless of pH and Cl^- concentration, and for pH > 10, regardless of temperature.

The initiation of crevice corrosion requires a loss of passivity and the establishment of active corrosion

conditions within the creviced region. The importance of temperature shows that initiation is primarily dependent on the film breakdown events, which commence around 70 °C.[57,74–76] The rapid repair observed on open surfaces does not occur within a tight crevice, and the acidity developed by dissolved metal cation (Ti^{3+}/Ti^{4+}) hydrolysis leads to the establishment of active conditions.[145] Once initiated, propagation is rapid and extensive, being supported both within the crevice by H^+ reduction (70–80%) and outside the crevice by O_2 reduction (30–20%).[12,146]

For Grade-2 Ti, the depth of crevice penetration is dependent on the amount and distribution of the impurity Fe. When Fe is present in grain boundaries, but not separated into Ti_xFe precipitates, penetration (at 95 °C) is rapid (up to 2 mm) and limited only by the ohmic potential drop caused by corrosion product accumulated within the crevice.[147] When Ti_xFe precipitates are present, the crevice is polarized to repassivation (by the cathodic modification mechanism), and penetration is limited to $\leq$0.8 mm.[12,119] For Grade-12, which contains a large number of Ti_2Ni precipitates, repassivation occurs more rapidly, and penetration is limited to <0.4 mm.[148] The inherent instability of this alloy is clear from the observation that >95% of the damage is due to proton reduction within the creviced site.[148]

The threat of crevice corrosion can be effectively eliminated by alloying Ti with Pd or Ru.[7] Despite the presence of film fracture events for $T > 70$ °C,[12] no significant damage occurs up to 200 °C on near-α and α–β alloys, even in extremely aggressive environments such as 10% $FeCl_3$ (pH 2) and Cl_2-saturated 20% NaCl.[81] Other methods of preventing, mitigating, or at least detecting, crevice corrosion have been discussed.[5,149,150]

3.10.4.2 Environmentally-Assisted Cracking

The primary factors influencing these processes, which include stress corrosion cracking (SCC), corrosion fatigue cracking, and HIC have recently been reviewed.[5] These processes can often occur simultaneously, and a case can be made that H absorption is a key feature of crack propagation in all three processes.

3.10.4.2.1 Stress corrosion cracking

Since passivity is difficult to breach, the majority of Ti alloys do not suffer SCC except in aqueous halide systems and in a few nonaqueous environments, such as dry methanol, where the addition of even small amounts of water is enough to ensure passivity and avoid cracking.[5] In aqueous halides, SCC is more likely at high concentrations, low pH, and high temperature, and appears to progress via oxide rupture and local acidification leading to H absorption and crack tip embrittlement.[151,152]

The ductility and passivity of Ti alloys means industrial failures are unusual and generally observed only for higher strength near-α alloys containing Al and Sn. When SCC is feared, susceptibility can be reduced by using alloys with low interstitial ion (O, C, N) contents. Generally, initiation requires the presence of stressed surface cracks or flaws. Recently, extensive testing of Grades-12 and-7 over a 4 year period in a range of saline environments (pH 2.7 to >12; 60–90 °C) confirmed the resistance of these materials to SCC,[153] although cracking could be forced to occur when low-frequency cyclic loading was applied.[154]

3.10.4.2.2 Hydrogen-induced cracking

For HIC to occur, a considerable amount of H must be absorbed by the alloy, which is most likely to occur when cathodic protection is applied. The tolerance of an alloy for H will be a function of H solubility, and the material's microstructure and texture. The solubility of H is very different in the α and β phases (20–100 and >9000 $\mu g\,g^{-1}$, respectively), making β-alloys generally insensitive to HIC. However, this difference, and the more rapid transport of H through the β-phase than through the α-phase, mean that the microstructure of near-α and α–β alloys has a strong influence on HIC.

Even H contents as low as 70 $\mu g\,g^{-1}$ can lead to a decrease in impact toughness,[5,155] although the resistance can be improved by increasing the Al content of the alloy.[5] However, under slow straining or sustained load conditions, tolerance for H is much higher. Slow strain rate tests on Ti Grades-2 and -12 indicate no influence on fracture toughness below a critical level (H_c),[156–158] which is taken to be the concentration below which fast crack growth will not occur. The combinations of stress intensity factor and H concentration leading to either fast crack growth (brittle failure) or slow crack growth by either sustained load cracking or ductile rupture, or to no failure have been determined.[156–158]

The values of H_c were found to be very sensitive to material microstructure and texture with respect to the orientation of the crack and the applied stress.[159]

For Grade-2 Ti, depending on crack orientation with respect to the laminations introduced by rolling, H_c varied between ~400 and 1000 $\mu g\,g^{-1}$.[157] For Ti Grade-12, H_c for cracks aligned with the rolling direction was 500 $\mu g\,g^{-1}$ compared with 2000 $\mu g\,g^{-1}$ for cracks perpendicular to this direction. Values of H_c rose markedly with temperature, which was attributed to the prevention of stress concentration by enhanced creep deformation.[157] Similar measurements for the Grade-5 α–β alloy yielded $H_c = 200\,\mu g\,g^{-1}$.[159] On the basis of these measurements, models to predict HIC failures of Ti nuclear waste containers have been developed.[160–163]

3.10.5 Specific Applications

Because titanium is an expensive material, its practical use is limited to applications that require one or both of the material's particular performance advantages: superior corrosion resistance and high strength-to-density ratio. Alloying to improve these properties adds further expense. As a commercial material, Ti and its alloys have an established history of reliable long term performance in aggressive environments, including hot oxidizing acids, hot saline solutions, chlorine- and sulfur-bearing gases, and organic solvents. Its industrial and commercial usage continues to grow, and Ti is now the material of choice for many chemical, marine, biomedical, and energy systems applications. Two recent extensive reviews are available.[164,165]

3.10.5.1 Aerospace

The emergence of Ti as an industrial material in the late 1940s and 1950s was driven primarily by the demands of military, and subsequently commercial, aircraft production. While corrosion resistance is important, the primary reasons to use Ti in aircraft and spacecraft are its high strength-to-density ratio and high temperature performance.[165,166] While maintaining the strength of steel, Ti is 45% lighter, and is twice as strong as Al, but only 60% heavier.[164] Ti is an effective replacement for Al alloys for temperatures above 130 °C, the normal limit for conventional Al. The right choice of alloy permits Ti engine components to function at temperatures up to 600 °C.[166]

The main, general-purpose aerospace alloy is Grade-5, although many others are adopted for specific situations. Ti comprises ~10 wt% of the airframe of a modern commercial aircraft[167] and up to 95 wt% in military planes. Gas turbine engines have ~30 wt% Ti.[165] Ti bands are even wrapped around Al fuselages to prevent propagation of fatigue cracks.[165]

Except for hot hydraulic fluids, few media encountered in the aerospace environment can corrode Ti, allowing the use of unpainted/uncoated Ti throughout the aircraft. Paint is only necessary at Ti interfaces with Al or low-alloy steels to prevent galvanic corrosion.[166] The use of Ti alloys is mandated for lavatory and galley floors because of the corrosiveness of those environments to Al and steels.[165,166] Even the hydraulic fluid problem, in which organophosphoric acids produced by high temperature breakdown can cause severe etching of Ti alloys and H absorption to embrittlement, has been managed using the β-alloy Timetal 215. This alloy is immune to attack by hydraulic fluid, purportedly through the synergistic effects of its Nb and Mo contents.[166]

3.10.5.2 Seawater and Brine

Ti alloys have supplanted cupronickel alloys, such as Monel, as the preferred materials for heat exchangers and condensers in brackish water, seawater, and polluted waters. Unlike the cupronickel alloys, Ti is immune to general corrosion up to 260 °C, and resistant to localized corrosion processes, sulfide attack, and flow-accelerated forms of corrosion. Flow rates over 36 m s^{-1} do not cause erosion corrosion, cavitation corrosion, or impingement attack in the presence of abrasive particles such as sand.[164,165,168] This allows the use of thin-walled tubing (with good heat transfer properties), as a zero corrosion allowance can be specified. This reliability is demonstrated by the industrial use of millions of meters of tubing over many decades without corrosion failures.[164,165,168]

Other seawater and brine applications include submarine hulls, surface ships, oil and gas platforms, desalination and salt production evaporators, and water jet propulsion systems.[165,166,168] Wet–dry cycling, water line exposure, and salt spray have no effect on corrosion.[167] Since Ti does not suffer MIC, it can withstand biofouling. It is not biotoxic, nor does it suffer corrosion in the presence of biocides.[136,164,165,168] Although it may require the specification of Pd/Ru-containing alloys, crevice corrosion can be avoided. As discussed earlier, galvanic corrosion can be an issue for Ti in seawater environments. Since Ti is normally the cathode in the galvanic couple, it can accelerate attack of the active anodic material while absorbing H itself. While

embrittlement and HIC are not issues at low temperatures, they can be at higher temperatures (**Sections 3.10.3.4** and **3.10.4.2.2**).

3.10.5.3 Biomedical and Dental Implants

The oxygenated, warm (37 °C), neutral (pH ~ 7.4) saline conditions encountered in the human body are not aggressive towards Ti. Its corrosion resistance, including resistance towards processes involving stress and fatigue, and biocompatibility make Ti an ideal implant material.[169] Its major uses include cranial plates, orthopedic fracture plates, joint replacements, stents, catheters, pacemaker cases, dental implants and wires, and maxillofacial and orbit reconstruction plates.[170] The extremely low corrosion rates mean Ti dental implants have no taste.[164]

Nitinol shape-memory materials, often used in orthodontics and stents, have been known to undergo pitting and crevice corrosion *in vivo* if heat treatments leave a crystalline oxide on the surface. However, this can be avoided by applying surface treatments to produce an amorphous oxide.[171] Corrosion fatigue, though rare, has been observed on Ti–6Al–4V implants.[172] Some cases of metallosis involving this alloy have also been encountered, but these are primarily due to fretting and wear producing fine metal particulates, rather than to corrosion.[173,174] Care must also be taken to avoid galvanic corrosion, even between materials as similar as commercially pure Ti and Ti–6Al–4V implants.[170]

Although Ti alloys are corrosion resistant *in vivo*, and there have been no clinically substantiated reports of problems stemming from the presence of Al and V in the implants,[174] some concern over the long term impact of these alloying elements remains.[174] Studies on alternative materials to Ti–6Al–4V to avoid potentially toxic alloying compounds are underway.[174–178] In these new materials, V and Al are being replaced by various amounts of other less toxic elements, including Fe, Zr, Mo, Ta, and Sn. These materials possess similar corrosion properties to Ti–6Al–4V but have improved mechanical properties, such as a decreased Young's modulus.

3.10.5.4 Chemical Processing and Power Generation

The use of Ti and its alloys in the chemical process industry has been extensively reviewed[2,5] and will not be dealt with here, except to note that their usage is still expanding. The key corrosion issues, as discussed earlier, are crevice corrosion and hydrogen absorption leading to embrittlement and cracking.

Titanium alloys have recently been extensively studied as candidate materials for the fabrication of high-level nuclear waste containers and container dripshields.[134,135,153,160,179,180] The critical requirement in these applications is the need to maintain corrosion resistance over tens of thousands of years. The ability of Ti alloys to maintain extremely low corrosion rates over extensive time periods and their lack of susceptibility to localized corrosion processes[135,160] make them ideal candidates for this application. A particularly attractive feature is their insensitivity to γ-radiation even at extremely high dose rates.[181]

References

1. Schutz, R. W.; Grauman, J. S. Titanium for marine applications; Presented at the Second Corrosion Control Workshop, sponsored by The Colorado School of Mines, New Orleans, LA, February 1997.
2. Schutz, R. W.; Thomas, D. E. In *Metals Handbook*, 9th edn.; ASM: Metals Park, OH, 1987; Vol. 13, pp 669–706.
3. Schutz, R. W.; Grauman, J. S. In *Industrial Applications of Titanium and Zirconium;* ASTM: Philadelphia, PA, 1986; Vol. 4, STP 917, pp 130–143.
4. Schutz, R. W. *Beta Titanium Alloys in the 1990's*; The Minerals, Metals and Materials Society: Warrendale, PA, 1993; pp 75–91.
5. Been, J.; Grauman, J. S. In *Uhlig's Corrosion Handbook*, 2nd edn.; Revie, R. W., Ed.; John Wiley: New York, NY, 2000; pp 863–885.
6. Boyer, R. Welsch, G.; Collins, E. W. Eds. *Titanium Alloys, Materials Properties Handbook*; ASM: Materials Park, OH, 1994.
7. Schutz, R. W. *Corrosion* **2003**, *59*, 1043–1057.
8. Lide, D. R. Ed. *CRC Handbook of Chemistry and Physics*, 82nd edn.; CRC Press: Boca Raton, FL, 2002.
9. Donachie, M. J., Jr. Ed. *Titanium: A Technical Guide*, 2nd edn.; ASM International: Materials Park, OH, 2000.
10. Blackburn, M. *The Science, Technology and Application of Titanium*; Pergamon Press: New York, NY, 1970; pp 633.
11. Margolin, H.; Farrar, P. *Ocean Eng.* **1969**, *1*, 329.
12. He, X.; Noel, J. J.; Shoesmith, D. W. *Corrosion* **2004**, *60*, 378–386.
13. Watanabe, T.; Kondo, M.; Naito, H.; Sakai, K. In *Sixth World Conference on Titanium, Cannes, June 6–9, 1988*; Lacombe, P., Tricot, R., Beranger, G., Eds.; 1988; Vol. IV, pp 1735–1740.
14. Tsujikawa, S.; Kojima, Y. *Mat. Res. Soc. Symp. Proc.* **1990**, *212*, 261.
15. van der Lingen, E.; Sandenbergh, R. F. *Corros. Sci.* **2001**, *43*, 577–590.
16. Zhu, R.; Qin, Z.; Noel, J. J.; Shoesmith, D. W.; Ding, Z. *Anal. Chem* **2008**, *80*, 1437–1447.
17. Shibata, T.; Zhu, Y. C. *Corros. Sci.* **1995**, *37*, 253–270.
18. Tyler, P. S.; Kozlowski, M. R.; Smyrl, W. H.; Atanasoski, R. T. *J. Electroanal. Chem.* **1987**, *237*, 295–302.
19. McAleer, J. F.; Peter, L. M. *Faraday Discuss.* **1980**, *70*, 67–80.

20. Noel, J. J. Ph.D. Thesis, University of Manitoba, Winnipeg, Manitoba, Canada, 1999.
21. Kim, Y. J.; Oriani, R. A. *Corrosion* **1987**, *43*, 92–97.
22. Kim, Y. J.; Oriani, R. A. *Corrosion* **1987**, *43*, 85–91.
23. Torresi, R. M.; Camara, O. R.; dePauli, C. P.; Giordano, M. C. *Electrochim. Acta* **1987**, *32*, 1291–1301.
24. Casillas, N. Ph.D. Thesis, University of Minnesota, St. Paul, MN, 1993.
25. da Fonseca, C.; Boudin, S.; da Cunha Belo, M. *J. Electroanal. Chem.* **1994**, *379*, 173–180.
26. Tomashov, N. D.; Al'touski, P. M. Corrosion and Protection of Titanium, Government Scientific–Technical Publication of Machine – Building Literature (Russian Translation), Moscow, Russia 1963.
27. Huang, Y. Z.; Blackwood, D. J. *Electrochim. Acta* **2005**, *51*, 1099–1107.
28. Ask, M.; Lausmaa, J.; Kasemo, B. *Appl. Surf. Sci.* **1988–1989**, *35*, 283–301.
29. Ask, M.; Rolander, U.; Lausmaa, J.; Kasemo, B. *J. Mater. Res.* **1990**, *5*, 1662–1667.
30. Kudelka, S.; Michaelis, A.; Schultze, J. W. *Ber. Bunsenges, Phys. Chem* **1995**, *99*, 1020–1027.
31. Blackwood, D. J.; Peter, L. H.; Williams, D. E. *Electrochim. Acta* **1988**, *33*, 1143–1149.
32. Kelly, E. J. *J. Electrochem. Soc* **1979**, *126*, 2064–2075.
33. Sedriks, A. J. *Corrosion* **1975**, *31*, 60–65.
34. Kitayama, S.; Shida, Y.; Ueda, M.; Kudo, T. In *CORROSION92*; NACE: Houston, TX, 1992; Paper No. 52.
35. Cotton, J. B. *Platinum Met. Rev.* **1967**, *11*, 50–52.
36. Higginson, A. *Br. Corros. J.* **1989**, *24*, 297–302.
37. Brossia, C. S.; Cragnolino, G. A. In *Corrosion/2001*; NACE: Houston, TX, 2001; Paper No. 127.
38. Kornienko, L. P.; Tomashov, N. D.; Chernova, G. P. *Zasch. Met* **1993**, *29*, 359–367.
39. Satoh, K.; Shimogori, K.; Kamikubo, F. *Platinum Met. Rev.* **1987**, *31*, 115–121.
40. Schutz, R. W.; Xiao, M. In *Corrosion Control for Low-Cost Reliability, 12th International Corrosion Congress;* Houston, TX, Sept. 19–24 1993; Vol. 3A, pp 1213–1225.
41. Hall, J. A.; Banerjee, D.; Wardlaw, J. L. In *Titanium Science and Technology*; Proceedings of the Fifth International Conference on Titanium, Munich, Germany, Sept. 10–14, 1984; Lutjering, G., Zwicker, U., Bunk, W., Eds.; 1985; Vol. 4, pp 2603–2610.
42. Ohtsuka, T.; Masuda, M.; Sato, N. *J. Electrochem. Soc.* **1985**, *132*, 787–792.
43. Casillas, N.; Charlebois, S.; Smyrl, W. H.; White, H. S. *J. Electrochem. Soc.* **1994**, *141*, 636–642.
44. Kolman, D. G.; Scully, J. R. *J. Electrochem. Soc.* **1994**, *141*, 2633–2641.
45. Raetzer-Scheibe, H. J. *Corrosion* **1978**, *34*, 437–442.
46. Beck, T. R. *J. Electrochem. Soc.* **1973**, *120*, 1310–1316.
47. Beck, T. R. *J. Electrochem. Soc.* **1973**, *120*, 1317–1324.
48. Petit, J. A.; Kondro, B.; Dabosi, F. *Corrosion* **1980**, *36*, 145–151.
49. Basame, S. B.; White, H. S. *J. Electrochem. Soc.* **2000**, *147*, 1376–1381.
50. Garfias-Mesias, L. F.; Alodan, M.; James, P. I.; Smyrl, W. H. *J. Electrochem. Soc.* **1998**, *145*, 2005–2010.
51. Kamikubo, F.; Satoh, H.; Shimogori, K.; Fukuzuka, T. In Proceedings of the Eighth International Congress on Metallic Corrosion, DECHEMA, Frankfurt/Main, Germany 1981; pp 1378–1383.
52. Curty, C.; Virtanen, S. *Electrochem. Soc. Proc.* **1999**, *99–27*, 445–452.
53. Koizumi, T.; Furuya, S. In Proceedings of the Second International Conference: Titanium, Science and Technology; Jaffe, R. I., Burte, H. M., Eds.; Plenum Press: New York, NY, 1973; pp 2382–2393.
54. Posey, F. A.; Bohlman, E. G. *Desalination* **1967**, *3*, 269–279.
55. Leach, J. S. L.; Pearson, B. R. *Corros. Sci.* **1988**, *28*, 43–56.
56. Shibata, T.; Zhu, Y. C. *Corros. Sci.* **1995**, *37*, 253–270.
57. Dyer, C. K.; Leach, J. S. L. *J. Electrochem. Soc* **1978**, *125*, 1032–1038.
58. Cotton, J. B. *Chem. Eng. Prog.* **1970**, *66*, 10, 57.
59. Cotton, J. B. *Br. Corr. J* **1975**, *10*, 2, 66.
60. Tomashov, N. D.; Chernova, G. P.; Ruscol, Y. S.; Ayuyan, G. A. *Electrochim. Acta* **1974**, *19*, 159.
61. Schutz, R. W.; Covington, L. C. *Corrosion* **1981**, *37*, 585.
62. Fukuzuka, T.; Shimogori, K.; Satoh, H.; Kamikubo, F. In *Titanium 80, Science and Technology*; Kimura, H., Izumi, O., Eds.; 1980; Vol. 4, pp 2783–2787.
63. Millaway, E. E.; Kleinmann, M. H. *Corrosion* **1972**, *23*, 88.
64. Popa, M. V.; Vasilescu, E.; Mirza-Rosca, I.; Gonzalez, S.; Llorente, M. L.; Drob, P.; Anghel, M. In Eurocorr'97, Trondheim, Norway 1997; Vol. II, pp 687–692.
65. Been, J. Ph.D. Thesis, University of British Columbia, Vancouver, Canada, 1998.
66. Been, J.; Tromans, D. *Pulp Paper Can.* **1999**, *100*, 50.
67. Varjonen, O. I.; Hakkarainen, J. J. *Tappi J.* **1995**, *78*, 161–166.
68. Hyokyvirta, O. A. *Mater. Corros.* **1997**, *48*, 376–387.
69. Wyllie, W. E., II; Brown, B. E.; Duquette, D. J. In *CORROSION94*; NACE International: Houston, TX, 1994, Paper No. 421.
70. Pan, J.; Thierry, D.; Leygraf, C. *J. Biomed. Mater. Res.* **1994**, *28*, 113.
71. Pan, J.; Thierry, D.; Leygraf, C. *Electrochim. Acta* **1996**, *41*, 1143.
72. Shibata, T.; Zhu, Y. C. *Corros. Sci.* **1994**, *36*, 1735–1749.
73. Noel, J. J.; Ikeda, B. M.; Miller, N. H.; Shoesmith, D. W.; Sunder, S.; Tun, Z. In *Proceedings Symposium on Surface Oxide Films*; Bardwell, J. A., Ed.; Electrochemical Society: Pennington, NJ, 1996; pp 246–257, 996–918.
74. Yahalom, J.; Zahavi, J. *Electrochim. Acta* **1970**, *15*, 1429–1435.
75. He, X.; Noel, J. J.; Shoesmith, D. W. *Corrosion* **2007**, *63*, 781–792.
76. Noel, J. J.; Yan, L.; Ofori, D.; Jakupi, P.; Shoesmith, D. W. In *Passivation of Metals and Semiconductors*; Marcus, P., Maurice, V., Eds.; Elsevier BV: Amsterdam, 2006; pp 199–204.
77. Smailos, E.; Koster, R. In *Materials Reliability in the Back End of the Nuclear Fuel Cycle;* Proceedings of a Technical Committee Meeting of the International Atomic Energy Agency (IAEA), Vienna, Austria, Sept. 2–5, 1986, IAEA-TECDOC-421, 1986.
78. Molecke, M. A.; Ruppen, J. A.; Diegle, R. B. Materials for high level waste canisters/overpacks in salt formations; Sandia National Laboratory Report, SAND82-0429, 1982.
79. Schutz, R. W. *Mater. Perform.* **1985**, *24*(1), 39–47.
80. Schutz, R. W.; Grauman, J. A. In *Corrosion 88*; NACE International: Houston, TX, 1988; Paper 162.
81. Schutz, R. W. *Platinum Met. Rev.* **1996**, *40*, 54–61.
82. Schutz, R. W. In *CORROSION97*; NACE International: Houston, TX, 1997; Paper No. 32.
83. Schutz, R. W.; Porter, R. L.; Horrigan, J. M. *Corrosion* **2000**, *56*, 1170–1179.
84. Schutz, R. W. In *CORROSION03*; NACE International: Houston, TX, 2003; Paper No. 03455.
85. Lausmaa, J.; Kasemo, B.; Hansson, S. *Biomaterials* **1985**, *6*, 23–27.
86. Boere, G. *J. Appl. Biomater.* **1995**, *6*, 283–288.

87. Oda, Y.; Kawada, E.; Yoshinari, M.; Hasegawa, K.; Okabe, T. *J. Dent. Mater. Dev.* **1996**, *15*, 317–322.
88. Mimura, H.; Miyagawa, Y. *Jpn. J. Dent. Mater. Dev.* **1996**, *15*, 283–295.
89. Toumelia-Chemla, F.; Rouelle, F.; Burdairon, G. *J. Dent.* **1996**, *24*, 109–115.
90. Probster, L.; Lin, W.; Hutteman, N. *Int. J. Oral Maxillofac. Implants* **1992**, *7*, 390–394.
91. Nakagawa, M.; Matsuya, S.; Shiraishi, T.; Ohta, M. *J. Dent. Res.* **1999**, *78*, 1568–1571.
92. Johansson, B. I.; Beregman, B. *Dent. Mater.* **1995**, *11*, 41–46.
93. Siirila, H. S.; Kokonen, M. *Int. J. Oral Maxillofac. Implants* **1991**, *5*, 50–54.
94. Nakagawa, M.; Matsuya, M.; Udoh, K. *J. Dent. Mater.* **2001**, *20*, 305–314.
95. Schiff, N.; Grosgogeat, B.; Lissac, M.; Dalard, F. *Biomaterials* **2002**, *23*, 1995–2002.
96. Huang, H. H. *Biomaterials* **2002**, *23*, 59–63.
97. Fernandez Lorenzo de Mele, M.; Cortizo, M. C. *J. Appl. Electrochem.* **2000**, *30*, 95–100.
98. Nakagawa, N.; Matono, Y.; Matsuya, S.; Udoh, K.; Ishikawa, K. *Biomaterials* **2005**, *26*, 2239–2246.
99. Yokoyama, K.; Ogawa, T.; Asaoka, K.; Sakai, J. *Mat. Sci. Eng. A* **2004**, *384*, 19–25.
100. Yokoyama, K.; Ogawa, T.; Asaoka, K.; Sakai, J. *J. Alloys Compds.* **2005**, *400*, 227–233.
101. Yokayama, K.; Ogawa, T.; Asaoka, K.; Sakai, J. *Mat. Sci. Eng. A* **2006**, *419*, 122–130.
102. Schutz, R. W.; Grauman, J. S. *Mater. Perform.* **1986**, *25*(4), 35–42.
103. Thomas, D. E.; Bomberger, H. B. *Mater. Perform.* **1983**, *22*(11), 29–36.
104. Mandry, M. J.; Rosenblatt, G. *J. Electrochem. Soc.* **1972**, *119*, 20.
105. Wilhelmsen, W.; Grande, A. P. *Electrochim. Acta* **1987**, *32*, 1469–1474.
106. Schutz, R. W.; Porter, R. L.; Horrigan, J. M. *Corrosion* **2000**, *56*, 1170–1179.
107. Paton, N. E.; Williams, J. C. In *Hydrogen in Metals*; Bernstein, I. M., Thompson, A. W., Eds.; American Society for Metals: New York, NY, 1974; pp 409–431.
108. Wasz, M. L.; Ko, C. C.; Brotzen, F. R.; McLellan, R. B. *Scripta Metall.* **1990**, *24*, 2043.
109. Sundaram, P. A.; Wessel, E.; Clemens, H.; Kestler, H.; Ennis, P. J.; Quadakkers, W. J.; Singheiser, L. *Acta Mater.* **2000**, *48*, 1005–1019.
110. Christ, H. J.; Decker, M.; Zeitler, S. *Metall. Mater. Trans. A* **2000**, *31*, 1507–1517.
111. Phillips, I. I.; Poole, P.; Shreir, L. L. *Corros. Sci.* **1972**, *12*, 855.
112. Phillips, I. I.; Poole, P.; Shreir, L. L. *Corros. Sci.* **1974**, *14*, 533.
113. Yan, L.; Ramamurthy, S.; Noel, J. J.; Shoesmith, D. W. *Electrochim. Acta* **2006**, *52*, 1169–1181.
114. Fukuzuka, T.; Shimogori, K.; Satoh, H. In *Titanium'80, Science and Technology*; Proceedings of the Fourth International Conference on Titanium Kyoto: Japan, May 19–20, 1980; pp 2695–2703.
115. Shimogori, K.; Satoh, H.; Kamikubo, F. In *Titanium, Science and Technology*; Proceedings of the Fifth International Conference on Titanium, Munich, Germany, Sept. 10–14, 1984; Lutjering, G., Zwicker, U., Bunk, W., Eds.; 1985; pp 1111–1118.
116. Glass, R. S. *Electrochim. Acta* **1983**, *28*, 1507–1513.
117. Prussner, K.; Decker, M.; Christ, H. J. *Adv. Eng. Mater.* **2002**, *4*, 308–312.
118. Okada, T. *Electrochim. Acta* **1983**, *28*, 1113–1120.
119. Yan, L. Ph.D. Thesis, University of Western Ontario, London, Ontario, Canada, 2007.
120. Dyer, C. K.; Leach, J. S. L. *Electrochim. Acta.* **1978**, *23*, 1387–1394.
121. Weber, M. F.; Shumacker, L. C.; Dignam, M. J. *J. Electrochem. Soc.* **1982**, *129*, 2022–2028.
122. Ohtsuka, T.; Masuda, M.; Sato, N. *J. Electrochem. Soc.* **1987**, *134*, 2406–2410.
123. Tun, Z.; Noel, J. J.; Shoesmith, D. W. *J. Electrochem. Soc.* **1999**, *146*, 988–994.
124. Murai, T.; Ishikawa, M.; Miura, C. *Corros. Eng.* **1977**, *26*, 177–183.
125. Noel, J. J.; Bailey, M. G.; Crosthwaite, J. P.; Ikeda, B. M.; Ryan, S. R.; Shoesmith, D. W. Hydrogen absorption by grade-2 titanium, Atomic Energy of Canada Limited Report, AECL-11608, 1996.
126. Hodgkeiss, T.; McIver, A.; Chong, P. Y. *Desalination* **1987**, *66*, 147–170.
127. Tomari, H.; Masugata, T.; Shimogori, K.; Nishimura, T.; Wada, R.; Taniguchi, N. *Zairyo-to-Kankyo* **1999**, *48*, 807–814.
128. Seiersten, M.; Eggen, T. G.; Lunde, L.; Rogne, T. In Proceedings of the 21st International Conference on Offshore Mechanics and Arctic Engineering, June 23–28, Oslo, Norway 2002; pp 493–498.
129. Lunde, L.; Nyborg, R. In *Engineering Solutions to Industrial Corrosion Problems*; NACE International: Houston, TX, 1993; Paper No. 5.
130. Lee, J. I.; Chung, P.; Tsai, C. H. In *CORROSION86*; NACE International: Houston, TX, 1986; Paper No. 259.
131. Venkataraman, G.; Goolsby, A. D. In *CORROSION96*; NACE International: Houston, TX, 1996; Paper No. 554.
132. Gartland, P. O.; Bjørnais, F.; Schutz, R. W. In *CORROSION97*; NACE International: Houston, TX, 1997; Paper No. 477.
133. Covington, L. C. *Corrosion* **1979**, *35*, 378–382.
134. Shoesmith, D. W.; Ikeda, B. M. The resistance of titanium to pitting, microbially induced corrosion and corrosion in unsaturated conditions, Atomic Energy of Canada Limited Report, AECL-11709, COG-96-557-I, 1997.
135. Hua, F.; Mon, K.; Pasupathi, P.; Gordon, G. M.; Shoesmith, D. W. In *CORROSION04*; NACE International: Houston, TX, 2004; Paper No. 04689.
136. Schutz, R. W. *Mater. Perform.* **1991**, *30*, 58–61.
137. Little, B. J.; Wagner, P. A.; Ray, R. I. In *CORROSION93*; NACE International: Houston, TX, 1993; Paper No. 308.
138. Dexter, S. C.; Zhang, H. J. In *Proceedings of the 11th International Corrosion Congress, Florence, Italy;* Associazone Italiana di Metallurgia: Milan, Italy, 1990; pp 333–340.
139. Mansfeld, F.; Tsai, R.; Shih, H.; Little, B. J.; Ray, R.; Wagner, P. In *CORROSION90*; NACE International: Houston, TX, 1990; Paper No. 109.
140. Mansfeld, F.; Tsai, R.; Shih, H.; Little, B. J.; Ray, R.; Wagner, P. *Corros. Sci.* **1992**, *33*, 445–446.
141. Mansfeld, F.; Liu, G.; Xiao, H.; Tsai, C. H.; Little, B. J. *Corros. Sci.* **1994**, *36*, 2063–2095.
142. Mansfeld, F.; Little, B. J. *Corros. Sci.* **1991**, *32*, 247–272.
143. Little, B. J.; Wagner, P. A.; Ray, R. I. In *CORROSION92*; NACE International: Houston, TX, 1992; Paper No. 173.
144. Noel, J. J.; Shoesmith, D. W. In *Proceedings of the NACE 2001 Research Topical Symposium, March 2001*; Frankel, G. S., Scully, J. R., Eds.; NACE International: Houston, TX, 2001; pp 65–102.
145. He, X.; Noel, J. J.; Shoesmith, D. W. *J. Electrochem. Soc.* **2002**, *149*, B440–B449.
146. He, X. Ph.D. Thesis, University of Western Ontario: London, Ontario, Canada, 2003.
147. He, X.; Noel, J. J.; Shoesmith, D. W. *Corros. Sci.* **2005**, *47*, 1177–1195.
148. He, X.; Noel, J. J.; Shoesmith, D. W. J. *ASTM Int.* **2008**, *5*(8). Available online at http://www.astm.org.

149. Schutz, R. W. In *CORROSION91*; NACE International: Houston, TX, 1991; Paper No. 162.
150. Bergman, D. D.; Grauman, J. S. In *Titanium'92, Science and Technology*; Froes, F. H., Caplan, I., Eds.; The Minerals, Metals, and Materials Society: Warrendale, PA, 1993; pp 2193–2200.
151. Hollis, A. C.; Scully, J. C. *Corros. Sci.* **1993**, *34*, 821.
152. Kolman, D. S.; Scully, J. R. *Metall. Mater. Trans. A* **1997**, *28A*(12), 2645–2656.
153. Gordon, G. M. *Corrosion* **2002**, *58*, 811–825.
154. Andresen, P. L.; Emigh, P. W.; Young, L. M.; Gordon, G. M. In *CORROSION01*; NACE International: Houston, TX, 2001, Paper No. 01130.
155. Wasz, M. L.; Ko, C. C.; Brotzen, F. R.; McLellan, R. B. *Scripta Metall.* **1990**, *24*, 2043.
156. Clarke, C. F.; Hardie, D.; Ikeda, B. M. *Corros. Sci.* **1994**, *36*, 487–509.
157. Clarke, C. F.; Hardie, D.; Ikeda, B. M. Hydrogen induced cracking of grade-2 titanium, Atomic Energy of Canada Limited Report, AECL-11284, 1995.
158. Shoesmith, D. W.; Noel, J. J.; Hardie, D.; Ikeda, B. M. *Corros. Rev.* **2000**, *18*, 331–359.
159. Hardie, D.; Ouyang, S. *Corros. Sci.* **1999**, *41*, 155–177.
160. Hua, F.; Mon, K.; Pasupathi, P.; Gordon, G. M.; Shoesmith, D. W. In *CORROSION05*; NACE International: Houston, TX, 2005; Paper No. 05582.
161. Hua, F.; Mon, K.; Pasupathi, P.; Gordon, G. M.; Shoesmith, D. W. *J. Metals* **2005**, *57*(1), 20–26.
162. Qin, Z.; Shoesmith, D. W. *Mater. Res. Soc. Symp. Proc.* **2007**, *985*, 467.
163. Qin, Z.; Shoesmith, D. W. *J. Nucl. Mater.* **2008**, *379*(1), 169–173.
164. Ikeda, B. M.; Shoesmith, D. W. Industrial experience with titanium, Atomic Energy of Canada Limited Report, AECL-11750, COG-97-4-I, 1997.
165. Leyens, C.; Peters, M. Eds. *Titanium and Titanium Alloys: Fundamentals and Applications*; Wiley-VCH: Weinheim, Germany, 2003; pp 233–497.
166. Boyer, R. R. *Mater. Sci. Eng. A* **1996**, *213*, 103–114.
167. Lütjering, G.; Williams, J. C. In *Engineering Materials and Processes*; Derby, B., Ed.; Springer: Berlin, 2007.
168. Titanium Metals Corporation (Timet) Corrosion resistance of titanium. Available online at http://www.timet.can/pdfs/corrosion.pdf.
169. Van Noort, R. *J. Mater. Sci* **1987**, *22*, 3801–3811.
170. Hansen, D. C. *Interface* **2008**, *17*, 31–34.
171. Shih, C. C.; Lin, S. J.; Chung, K. B.; Chen, Y. L.; Su, Y. Y. *J. Biomed. Mater. Res.* **2000**, *52*, 323–332.
172. Schmutz, P.; Quach-Vu, N. C.; Gerber, I. *Interface* **2008**, *17*, 35–39.
173. Black, J.; Shenk, H.; Boninc; Rostocker, W. R.; Schajowicz, F.; Galante, J. O. *J. Bone Joint Surg.* **1990**, *72*, 126–130.
174. Jacobs, J. J.; L Gilbert, J.; Urban, R. M. *J. Bone Joint Surg.* **1998**, *80-A*, 268–282.
175. Wang, K. *Mater. Sci. Eng. A* **1996**, *213*, 134–137.
176. Okazaki, Y.; Ito, Y.; Kyo, K.; Tateishi, T. *Mater. Sci. Eng. A* **1996**, *213*, 138–147.
177. Niinomi, M.; Kuroda, D.; Fukunaga, K. I.; Morinaga, M.; Kato, Y.; Yashiro, Y.; Suzuki, A. *Mater. Sci. Eng. A* **1999**, *263*, 193–199.
178. Kuphasuk, C.; Oshida, Y.; Andres, C. J.; Hovijitra, S. T.; Barco, M. T.; Brown, D. T. *J. Prosthet. Dent.* **2001**, *85*, 195–202.
179. Johnson, L. H.; King, F. Canister options for the disposal of spent fuel, Nagra, Switzerland, Technical Report 02–11, 2002.
180. Johnson, L. H.; Tait, J. C.; Shoesmith, D. W.; Crosthwaite, J. L.; Gray, M. N. The disposal of Canada's nuclear fuel waste: Engineered barriers alternatives, Atomic Energy of Canada Limited Report, AECL–10718, COG-93-8, 1994.
181. Shoesmith, D. W.; King, F. The effects of gamma radiation on the corrosion of candidate materials for the fabrication of nuclear waste packages, Atomic Energy of Canada Limited Report, AECL-1199, 1999.

3.11 Corrosion of Lead and its Alloys

S. B. Lyon
Corrosion and Protection Center, School of Materials, University of Manchester, Manchester M13 9PL, UK

This article is a revision of the Third Edition article 4.3 by P. C. Frost, E. Littauer and H. C. Wesson, volume 1, pp 4:76–4:97,

3.11.1 Introduction

3.11.1.1 History and Production

Lead was one of the metals known in antiquity; there is evidence of lead production dating back to before the early Bronze Age, with a lead figurine from Upper Egypt dated to approximately 3000 BC.[1] However, at that time lead does not appear to have been greatly prized as it is soft and easily tarnishes. Indeed, early lead ores seem to have been smelted mainly in order to obtain the silver, with which it frequently occurs. However, lead production grew very significantly during the Roman period, where it was useful in its own right for a number of purposes, including plumbing (water transport, water tanks, etc.) and kitchenware and drinking vessels (despite the knowledge, even in antiquity, that lead is generally harmful to human health).

Lead ores comprise mainly sulfide mineralization with smaller amounts of carbonate and sulfate.

Historically, lead was mined on its own (in the United Kingdom, Derbyshire and Leadhills in Southern Scotland were historic sources). Modern ores frequently occur along with zinc, and other species (silver, copper, gold, antimony, bismuth, etc.) in considerably lesser amounts. Lead sulfide (galena) is easily smelted by roasting in air to produce lead oxide, then by carbothermic reduction, which traditionally used charcoal but now uses coke, in a blast furnace.

Lead is currently produced in Australia, China, the United States, Canada, Mexico, and Peru. Western Europe produces about 8% of the total world ore production of around 3 million tonnes (2007), mainly from Sweden, but also Ireland and Spain. Lead is amongst the most recyclable of all metals and has by far the highest recycling rate, primarily from batteries and also from usage in the building trade. Secondary (i.e., recycled) sources of lead generally account, in developed economies, for more than 70% of lead usage.

3.11.1.2 Physical Properties

Lead is characterized by its relatively high density (in comparison to other engineering materials), its extremely low hardness and strength, and its favorable electrochemical properties, including its good resistance to corrosion.[1,2] However, it should be noted that lead is by no means the most dense element; for example, tungsten and tantalum are significantly more dense. Table 1 provides a summary of some physical properties in comparison with other materials.

The density of lead provides it with useful properties in respect of the attenuation of phonon vibrations and electromagnetic waves. Thus, the mass attenuation coefficient for lead is relatively high, and also the neutron absorption cross-section for lead is small, which makes lead effective for the radiation shielding of X-rays, γ-rays, and neutrons. In addition, the softness and high mass of lead effectively damps the propagation of sound waves.

3.11.1.3 Applications

Traditionally, lead as a metal has a number of uses driven by its general resistance to corrosion, as well as its electrochemical properties in rechargeable lead–acid batteries. The main uses of metallic lead are[2]

1. *Lead–acid batteries*: this currently accounts for over 50% and up to 90% of use in certain countries; most lead used in this way is recovered and recycled into the secondary lead market.
2. *Construction*: the main application in construction is for waterproofing flashings and roofing of historic buildings, as well as architectural detailing; the traditional use in water pipes and water storage has now vanished; lead from construction also has a high recycling rate.
3. *Chemical industry*: lead lining of vessels was traditionally used in the chemical industry, particularly in the production of sulfuric acid; however, these uses have now almost vanished.
4. *Metal joining*: lead is (with tin) a key component of solder used to join copper (piping, heat exchangers, etc.) and steels, and for electrical contacts; however, lead-free solders are now widely used in the water and electronics industry.
5. *Munitions*: lead is traditionally used in the manufacture of ammunition, although depleted uranium and tungsten, which are both significantly more dense than lead, are used in high performance (e.g., armor piercing) rounds; however for sporting purposes nontoxic alternatives exist and are increasingly being used.
6. *Dense metals*: lead is used for radiation shielding, for sound dampening, and for balancing of machinery; weights used in sporting applications

Table 1 Physical properties of lead compared with some other common metals

	Pb	*Sn*	*W*	*Cu*	*Fe*
Atomic number	82	50	74	29	26
Atomic weight (g)	207.19	118.69	183.84	63.55	55.85
Density (g cm^{-3})	11.34	7.3	19.3	8.96	7.87
UTS, 99.9% pure (MPa)	12–15	20–30	950–1000	120–170	100–200
Melting point (K)	601	505	3680	1358	1810
Boiling point (K)	2020	2540	5830	2816	3130
Electrical conductivity $\times 10^6$ (Ω^{-1} cm^{-1})	0.048	0.079	0.189	0.596	0.099
Thermal conductivity (W cm^{-1} K^{-1})	0.35	0.73	1.74	4.01	0.238
Linear expansion coefficient $\times 10^{-6}$	29.0	23.5	–	16.5	12.2
Crystal structure (room temperature)	fcc	bct	bcc	fcc	bcc

(such as fishing weights) are being phased out in favor of nontoxic alternatives.

7. *Cable sheathing*: the first electrical cables were sheathed with lead to protect the cable from moisture ingress. For undersea cables, especially high-voltage power transmission lines, there is still no adequate alternative; thus, properly applied lead sheathing has zero water and water vapor transmission.
8. *Alloying*: lead is used as an addition in a number of alloys, including solders, pewter, bearing alloys, etc.; it also may be added to other materials (such as copper alloys and steels) to improve machinability, although alternatives are now available.
9. *Anodes*: by virtue of its relative chemical stability and easy passivation, lead is used as an insoluble anode in many electroplating processes (e.g., for chromium); traditionally, it was also used as a nonconsumable anode in cathodic protection systems, but this application area is decreasing as alternatives now exist.
10. *Fusible alloys*: eutectic alloys containing lead with bismuth, tin, cadmium, and indium are used as low melting point fuses and plugs in certain applications such as sprinkler systems, etc.

3.11.1.4 Alloying

Apart from tin, indium, and bismuth, lead has extremely limited solid solubility for most elements at room temperature, although solubility can increase somewhat at higher temperatures.[3] Thus, most lead alloys consist of primary lead grains either with second phase particles (which may be intermetallic compounds), or with a eutectic mixture, decorating the grain boundaries. Because of the very poor mechanical properties of high-purity lead, alloying is almost always essential in order to achieve acceptable performance. Most commercial lead alloys contain a few tenths of a percent of alloying elements, with strengthening caused by precipitation or by the presence of a eutectic; many alloys are age-hardenable. The main classes of alloy listed below with composition ranges presented in Table 2:

1. *Lead–antimony (+ tin, arsenic)*: the traditional alloy used for batteries, ammunition, sheet, and chemical plant; still very widely used, but the battery application is increasingly being replaced with lead–calcium.
2. *Lead–calcium (+ tin, aluminum)*: increasingly replacing lead–antimony alloys, particularly in battery applications, as they have very low hydrogen evolution characteristics and can therefore be sealed. Lead–calcium–tin is used for electrowinning anodes.
3. *Lead–tin (+ silver, antimony)*: used for jointing alloys (solders) and bearings.
4. *Lead–copper*: used generally for sheet products and linings; also for cable sheathing and in chemical plant.
5. *Lead–silver*: used for anode materials and higher temperature solders.

Table 2 Compositions of typical lead alloys

Alloy type	*Specification*	*Application*	*Composition*
Pb-Sb		Battery grids	1–3% Sb + 0.5–1% S, Se and Cu
		Ammunition	0.5–8% Sb + 0.02–3% As
	BS EN 12548	Cable sheaths	0.5–1% Sb
		Anodes	6–10% Sb + 0.5–1% As
	BS EN 12659	Chemical lead	<0.06% impurities
	BS ISO 4381	Bearings	9–15% Sb + 1–20% Sn
Pb–Ca		Battery grids	0.03–0.07% Ca; +0.03% Al and 0.3% Sn
		Cable sheath/splices	0.04% Ca
		Anodes	0.03–0.09% Ca; + up to 0.3% Sn
Pb–Sn	BS EN ISO 9453	Solders	2–70% Sn; + up to 2% Sb
Pb–Cu	BS ISO 4999	Terne plate	15–20% Sn
	BS EN 12588	Construction (sheet)	0.03–0.06% Cu
Pb–Ag		Battery grids	0.005–0.05% Ag
		Solder	1–6% Ag
		Anodes	0.25–2% Ag; + up to 1% Sn or up to 6% Sb
Pb–Te	BS 3909	Nuclear/radiation	0.06% Te
	BS EN 50307	Cable sheaths	0.035–0.1% Te; +0.03–0.08% Cu

Source: Pregaman, D. R. In *Ullman's Encyclopedia of Industrial Chemistry*; Wiley: New York, 2005.

6. *Lead–tellurium (+ copper)*: because of its low alloy content, used for radiation shielding and, with copper, is a cable sheathing alloy.

3.11.1.5 Mechanical Properties

3.11.1.5.1 Lead

Unalloyed lead has relatively poor mechanical properties,[2,4] thus, in addition to a low ultimate tensile strength (<12 MPa), it has a very low yield stress (<4 MPa); these are considerably lower than tin, for example. The low melting point of lead means that, like tin, it undergoes recrystallization and grain growth at room temperature and is susceptible to creep at stresses above ~2 MPa (~15% of the UTS), which is very low indeed. Thus, while lead of purity in excess of 99.99% is commercially available (BS EN 12659), it is not specified unless its superior corrosion resistance is required. Lead is also susceptible to fatigue, particularly due to thermal cycling, and this is a key failure mechanism in pure and alloyed lead. **Table 3** provides typical mechanical properties for pure lead as well as a range of common lead alloys.

3.11.1.5.2 Lead alloys

Of the elements commonly found in lead alloys, zinc and bismuth aggravate corrosion in most circumstances, while additions of copper, tellurium, antimony, nickel, silver, tin, arsenic, and calcium affect corrosion resistance only slightly, or may even improve it depending on the service conditions. Alloying elements that are of increasing importance are calcium, especially in maintenance-free battery alloys and selenium or sulfur, together with copper as grain refiners (nucleants), in low antimony battery alloys. Other elements of interest are indium and silver in anodes,[5] aluminum in batteries (to control calcium losses),[6] and selenium in chemical lead as a grain refiner.[7]

In Europe, lead alloy designations are specified in ISO TR 7003, "Unified format for the designation of metals," in the format PBnnnA. The designate 'PB' is the chemical symbol for lead, the three digits 'nnn' define specific alloy compositions, while the 'A' designates the application: 'R' for pure lead, 'K' for cable, 'A' for battery alloys, and 'M' for miscellaneous alloys.

Historically, lead for use in chemical plant was specified in BS 334, which defines compositions for five types of lead: A, B1, B2, B3, and C. This standard has now been superseded by BS EN 12659, "Lead and lead alloys," which specifies the composition of effectively pure lead (formally type A). This is because satisfactory alternative materials exist such that lead is now rarely, if ever, specified in chemical plant. Type A lead should only be used in a vibration-free environment and where the superior corrosion resistance is of paramount importance. Historically, for general chemical plant use, type B1 (copper–lead) is to be preferred on account of its much greater structural stability, especially at elevated temperatures. Type B2 (copper–tellurium–lead) has extremely good fatigue resistance, which is retained to a greater extent at elevated temperatures, than does type B1. The main effect of tellurium is to form a fine-grained uniform grain structure, to enhance work hardening, and to delay recrystallization. The silver content in type B3 also delays recrystallization and promotes a large-grained stable structure, which is creep resistant. Type C (antimony–lead) is used for valves, pump bodies, and fatigue-resistant applications, but is not suitable for use at temperatures above 60 °C owing to a rapid increase in creep rate, or in sulfuric acid concentrations above 60%.

BS EN 12548, "Lead alloy ingots for electric cable sheathing and for sleeves," gives compositional requirements for a range of lead alloys for this application.

Table 3 Mechanical properties of selected lead and lead alloys

Material	*Yield Stress (MPa)*	*UTS (MPa)*	*Elongation (%)*	*Fatigue limit (MPa)*	*Creep failure at 20 MPa (h)*
99.99% Pb	3.5	12.2	55	2.7	–
0.06% Cu	9.0	17.5	55	4.9	–
0.06% Ca	24.3	27.9	30	9.0	10
0.5% Sn	27.9	41.8	15	–	30
0.08% Ca + 1% Sn	46.0	59.7	15	–	850
1% Sb	19.3	37.9	20		
2% Sb	24.1	46.9	15		
2.75% Sb	55.2	65.5	10		
6% Sb	71.0	73.8	8		

Source: Pregaman, D. R. In *Ullman's Encyclopedia of Industrial Chemistry*; Wiley: New York, 2005.

The main types are PB001K (formally type B), containing 0.85% antimony; PB021K (formally type E), containing 0.2% Sb and 0.4% Sn; and PB012K (formally 1/2C), containing 0.2% Sn and 0.07% Cd. Type B is suitable for use in environments where severe vibration is expected, while type E is relatively resistant to vibration compared with type 1/2C. The performance of these materials is generally adequate in underground or marine environments.

BS EN 12588, "Rolled sheet lead for building purposes," lays down requirements for composition, structure, thickness, freedom from defects, width and length, and marking. The specified copper content stabilizes the structure of the material, conferring resistance to thermal fatigue cracking caused by grain growth and thermal cycling.

Other UK, European, or worldwide specification standards exist for specific applications, for example, radiation shielding, soft solders, and bearing alloys. However, there are no standards for battery alloys as many of these are proprietary to specific battery manufacturers.

3.11.2 Electrochemistry

3.11.2.1 Thermodynamics

Pourbaix *et al.*[8] studied the Pb–H_2O and Pb–H_2O–X systems, where X is a nonmetal, and have established the domains of thermodynamic stability of lead, lead cations and anions, and insoluble compounds of lead. **Figure 1** shows the Pb–H_2O system in the absence of complexing agents such as acetic acid. Lead can be seen to be a relatively noble metal from pH > 5, but dissolves to form Pb^{2+} species at lower pH and the plumbite oxyanion at pH > 10.5. This is due to the amphoteric nature of lead and is a significant factor in actual environments. Also, passivation at high potential, due to the formation of PbO_2, is evident across the whole pH domain.

In regions where the dissolution of lead is possible, according to the thermodynamics, the rate of corrosion may be very slow. This is because the overpotential for hydrogen evolution on lead is very high in 1 M H_2SO_4, 10^{-12} A cm^{-2} with a Tafel slope of 0.125 mV per decade current, indicating that a 1-electron transfer reaction is rate controlling.[9] Corrosion in near-neutral environments generally results in passivation, with the development of insoluble salt film corrosion products. In strong alkali, the corrosion is more rapid with the formation of plumbite ions.[10] Consequently, in acidic or moderately alkaline solutions, free from complexing agents (particularly organic acids), the corrosion of lead is generally negligible.

In contrast with the Pb–H_2O system, in the presence of significant concentration of sulfate ion, the

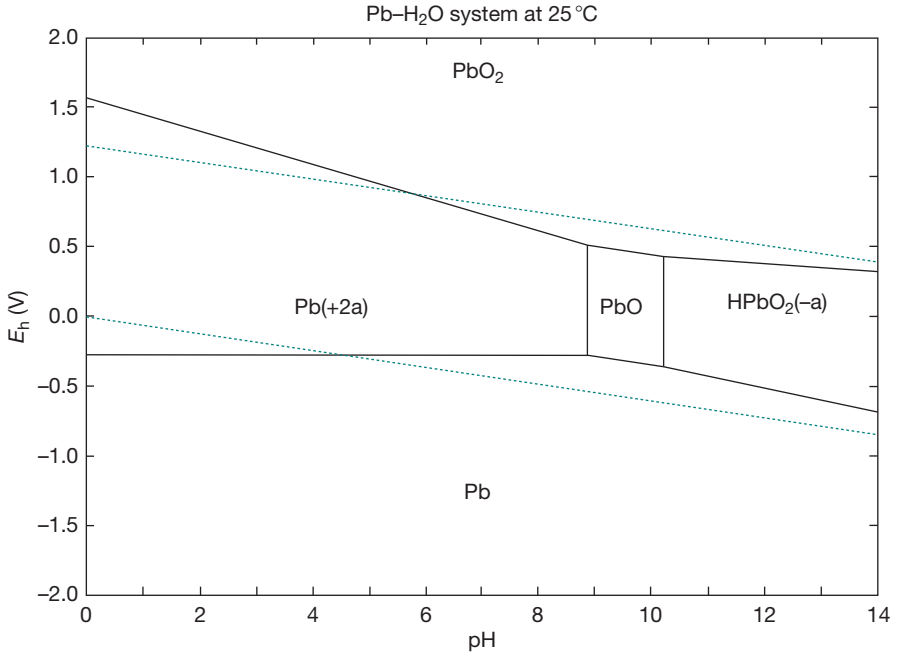

Figure 1 Pourbaix diagram for lead at a dissolved total metal ion concentration of 10^{-5} M.

zone of thermodynamic stability of $PbSO_4$ expands, and lead now passivates by the formation of a salt film of lead sulfate, which is the basis of lead's low corrosion rate in sulfuric acid (**Figure 2**).

In similar way, lead forms a series of relatively insoluble compounds, many of which are strongly adherent to the metal surface. Thus, in conditions where a stable continuous film can form, further reaction is often prevented or greatly reduced. The generally good corrosion resistance of lead results, therefore, from the formation of relatively thick protective films of corrosion product.

3.11.2.2 Dissolution

The standard electrode potential, E^0: $Pb^{2+}/Pb = -0.126\,V$,[11] shows that lead is thermodynamically unstable in acid solutions, but stable in neutral solutions. In acid conditions, the exchange current density for the hydrogen evolution reaction on lead is very small ($\sim 10^{-12}\,A\,cm^{-2}$), but, at higher pH, control of corrosion is usually due to physical blocking of local anodes (from alloying additions and intermetallic compounds, which generally have higher exchange current densities) by virtue of insoluble lead salts that frequently form protective films. At $pH > 11$, lead will corrode freely at low anodic overpotentials dissolving as the $HPbO_2^-$ species. However, at higher potentials, it will passivate, again forming PbO_2. Lead may thus be used as an insoluble anode effectively throughout the entire pH range; an extremely useful characteristic. In summary, the corrosion rate of lead in an environment is frequently not controlled by the electrochemical processes but by the chemical dissolution rate of the corrosion product film.

Under strong cathodic polarization, disintegration can occur with lead, observable as a gray cloud of fine metal particles; this is a significant phenomenon in the application of lead to electrowinning (metal plating) anodes. Hydrogen evolved on the surface of the lead can be absorbed if the current density is sufficiently high,[12] and above this level, the formation of lead hydride may occur, which leads to severe disintegration.[13]

3.11.2.3 Oxidation and Passivation

Lead is characterized by a series of anodic corrosion products, which give a film or coating that effectively insulates the metal physically from the electrolyte, for example: $PbSO_4$, $PbCl_2$, Pb_3O_4, $PbCrO_4$, PbO, PbO_2, $2PbCO_3{\cdot}Pb(OH)_2$; of which $PbSO_4$ and PbO_2 are the most important, as they play a part in batteries and anodes. Lead carbonate and lead sulfate are

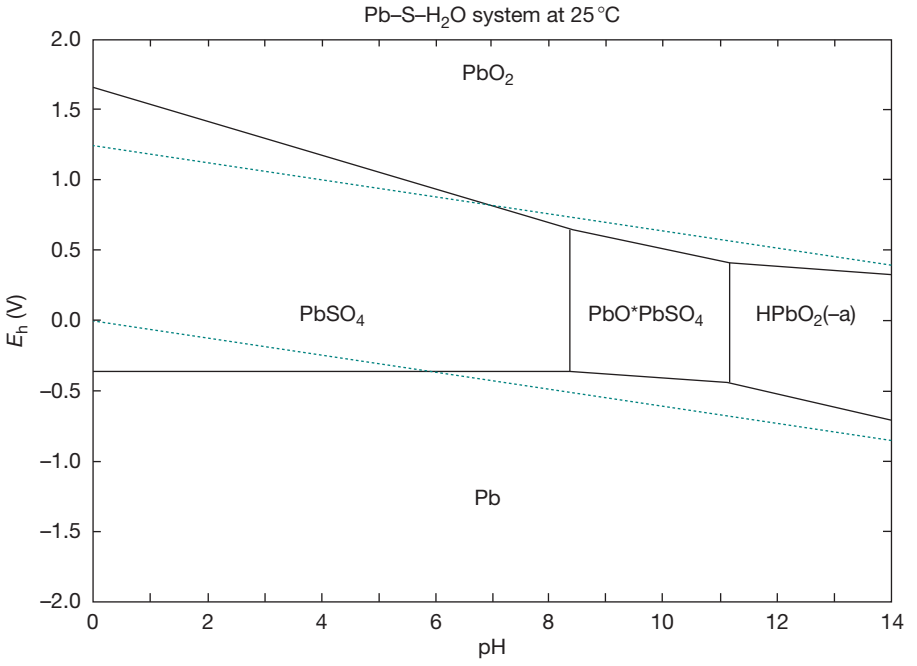

Figure 2 Pourbaix diagram for lead–sulfur in 1 M sulfate ion concentration and a dissolved total metal ion concentration of 10^{-5} M.

particularly important also in atmospheric passivation and chemical industry applications.

In aqueous electrolytes, the anodic behavior of lead varies greatly, depending on the conditions prevailing. Extensive reviews of the aqueous electrochemistry of lead, including its anodic behavior, have been produced, for example, by Kuhn in 1979,[14] and much of this is still valid. The vast majority of historic and current research is concerned with the behavior of lead in sulfuric acid and this is understandable, given that the main application is still in lead–acid batteries. More recently, research has been concerned increasingly with environmental concerns, including lead removal from contaminated locations and the possible application of lead as a barrier material in nuclear waste disposal; these specific issues are dealt with in more detail later.

The dry oxidation of lead was studied in oxygen pressures from 10^{-2} to 1000 torr and at temperatures between −90 and 150 °C.[15] Over several weeks, the oxide grew to a limiting thickness of about 10 nm. Ellipsometry and Auger electron spectroscopy confirmed that the oxide was PbO and that the growth law conformed to the Cabrerra–Mott model (high-field ion conduction). X-ray diffraction data confirmed that the oxide was epitaxial to the lead, but that it was highly strained and that recrystallization of the lead substrate promoted oxide growth.

Passivation of lead in sulfuric acid is caused by the potential-dependent, and generally reversible, formation of PbO, $PbSO_4$, and PbO_2. However, the reactions and transformations are complex and difficult to characterize.[16] At potentials just above the reversible potential for lead oxidation, a dense layer of PbO can form together with porous $PbSO_4$;[17,18] the growth of PbO formed in this way is controlled by the rate of oxygen anion transport through the oxide. At higher potentials, PbO and $PbSO_4$ transform to PbO_2, which occurs in one of the two nonstoichiometric polymorphs, both with a slight oxygen deficiency. Lead anodic corrosion proceeds in two stages in sulfuric acid. Initially, Pb is oxidized to tetragonal PbO, as mentioned earlier; then, in the second stage, this is oxidized to PbO_2. If this process is performed in solid state, α-PbO_2 forms; however, β-PbO_2 can be formed by a dissolution–precipitation mechanism.[19,20] The oxide species are O^{2-} anionic conductors; additionally, there is evidence from studies in batteries that $PbSO_4$ is a Pb^{2+} cationic conductor.[21]

Passivation of lead also occurs in a range of other media, the most important of which is carbonate/bicarbonate as these equilibria are commonly encountered in natural environments.[22] The passivation sequence on anodic polarization is similar to that in sulfuric acid except for the formation of lead carbonate instead of lead sulfate. Thus, Pb may be directly oxidized to PbO or $Pb(OH)_2$, which then reacts with CO_2 (in the atmosphere) or bicarbonate/carbonate ions (in solution) to form protective $PbCO_3$; at higher potentials, PbO_2 is formed. The rate of growth of the passive carbonate film is dependant on the concentration of carbonate in solution. However, unlike in sulfuric acid, the passivation process in carbonate media is essentially irreversible. Although pitting in sulfuric acid is possible (e.g., by perchlorate ions),[23] it is not the common degradation mechanism. However, in carbonate media, pitting is observed with a number of species in solution, including perchlorate[24] and nitrate.[25]

In summary, lead is passive at higher potentials at all pH, forming lead dioxide, which is a defect anion conductor. At intermediate potentials and in solutions of near-neutral to acid pH, lead generally passivates by formation of a salt film characteristic of the solution, for example, $PbSO_4$ in solutions of sulfuric acid. In such cases, the corrosion rate of lead tends to be controlled by the chemical dissolution of the corrosion product (salt film) and not by the potential. At intermediate potentials and high pH, lead will tend to dissolve forming the plumbite ion $HPbO_2^-$. In strong alkali (1 M NaOH), formation of $Pb(OH)_2$ occurs at less positive potentials, which transforms to PbO according to a nucleation and growth mechanism under diffusion control.[10]

3.11.2.4 Corrosion Products

The nature (composition and morphology) of the corrosion product on lead will very frequently enable a good interpretation of the environment in which the material was exposed. However, note that lead dioxide cannot form under ordinary environmental conditions and that other metals cannot polarize lead sufficiently for it to form. Lead dioxide corrosion products can, therefore, only be produced by external polarization, either deliberately (as in a battery or anode) or accidentally (e.g., via stray currents).

From an inspection of the more common compounds of lead, it will be seen that, in many environments, the corrosion product will be relatively insoluble (**Table 4**). Often, however, compact protective films are prevented from forming on the surface of the metal. The nature of the film is influenced by the mode of crystallization, and in the case of the

Table 4 Solubility of lead compounds

Compounds of lead	*Formula*	*Solubility at 25 °C (g dm^{-3})*
Acetate	$(CH_3COO)_2Pb$	550
Formate	$(CHOO)_2Pb$	16
Nitrate	$Pb(NO_3)_2$	600
Chloride	$PbCl_2$	1×10^{-4}
Hydroxide	$Pb(OH)_2$	4×10^{-15}
Carbonate	$PbCO_3$	3.3×10^{-14}
Basic carbonate	$2PbCO_3Pb(OH)_2$	3.3×10^{-14}
Sulfate	$PbSO_4$	1×10^{-8}
Sulfide	PbS	3.4×10^{-28}
Phosphate	$Pb_3(PO_4)_2$	10^{-55}
Oxide	PbO	Insoluble
Dioxide	PbO_2	Insoluble

Source: Weast, R. C., Ed. *Handbook of Chemistry and Physics*, 57th ed.; CRC Press: Boca Raton, FL, 1989; pp B68–B146.

lower oxides, for example, frequently little protection is afforded. Lead dioxide often forms a good adherent film, especially when it is produced from a sulfate film or other adherent compounds during anodizing. Concentrated hydrochloric acid gradually dissolves it to form hexachloroplumbic acid, and with alkalis, plumbites are formed. With sparingly soluble salts of lead, the compactness of the deposits is likely to be strongly influenced by the concentration of the relevant anion; with low concentrations tending to result in imperfect coatings.

3.11.2.5 Galvanic Corrosion

Lead is relatively noble compared with most other metals in common use, apart from copper, and therefore, there is normally little concern about its galvanic corrosion as it will usually be the cathode in a coupled system. Where it is anodic, it will often not corrode significantly due to the formation of protective corrosion product films. However, increases in temperature may cause changes in the porosity of the protective film, or a phase change that, consequently, reduces its protective function. For example, at 75 °C, lead was found to be anodic to steel in seawater and groundwater because of a polarity reversal.[26] However, the expected order of potentials was restored if the water also contained a Bentonite clay suspension.

There are continuing concerns regarding galvanic corrosion involving lead in drinking water systems, where lead-containing solders are traditionally used (but are now being phased out). Particularly, in plumbo-solvent soft waters, lead is leached out from solders in measurable quantities that may be harmful to health.[27] Clearly, the best solution to this problem is not to use lead; however, for the large numbers of historic properties where lead is still present in pipework, inhibition of this form of attack, for example, using silicates or phosphonates, is possible.[28] However, the ratio of chloride to sulfate is critical in controlling the leach rate of lead, and water utilities need to take note of this also in order to minimize the lead solubility of the water supply.[29]

3.11.3 Corrosion

3.11.3.1 Atmospheric Corrosion

Lead has been (and especially in historic and prestige properties, still is) used for roofing, gutters, flashings, downspouts, etc. and exhibits excellent resistance to air (dry or humid) and rain water, producing, after an initial period of time, an attractive patina. Initially, an oxide (PbO) is formed, which then converts by reaction with atmospheric carbon dioxide to plumbonacrite ($Pb_5O(OH)_2(CO_3)_2$) and hydrocerrusite ($Pb_3(OH)_2(CO_3)_2$).[30] In atmospheres containing sulfur dioxide from industrial pollution, the general sequence of corrosion product (patina) formation is: lead oxide → basic lead carbonate → normal lead carbonate → normal lead sulfite → normal lead sulfate.[31] Lead is found to be reactive to common atmospheric gases, NO_x, SO_2, CO_2, as well as the vapors of carboxylic acids.[32] As noted earlier, outdoor exposures were found to produce anglesite ($PbSO_4$) and/or cerussite ($PbCO_3$) while indoor exposures often produced lead carboxylates, due to higher levels of organic acid vapors from wood and wood products. Excluding the carboxylates, these corrosion products have a low solubility and are protective; however, they can produce a white flocculant 'run-off' in wet weather, which can stain surrounding surfaces in the very early stages of exposure.[33]

In marine environments, the initial oxide film reacts with sodium chloride when wet to produce basic lead chloride, which may result in corrosion of adjacent materials such as aluminum.[34] In such environments, the patina stabilizes, but takes approximately twice as long as in other atmospheric environments. A common treatment for new lead is a resin-based patination oil, which suppresses the formation of basic carbonates, allowing the slow controlled growth of a strongly adherent normal carbonate patina from the outset.[35]

Because of increasing concerns about lead in the environment, corresponding concerns regarding the release of lead from buildings are also evident. Thus,

lead ions can be introduced into the biosphere via corrosion and subsequent run-off of Pb^{2+} species, primarily from the solubility of cerrusite (lead carbonate), hydrocerrusite (lead hydroxy carbonate), and anglesite (lead sulfate) in rainwater. After an initial induction period, the measured release rate for lead ions was found to be 10^{-5} moles of Pb per liter, or precipitation run-off per square meter of lead surface (i.e., 2.1 mg dm^{-3}) in both marine and rural locations,[35] which corresponds to a corrosion rate of about 0.3 μm $year^{-1}$ in these atmospheres.

It has been known for centuries that certain species of wood are 'more aggressive' to lead than are others, and this is now understood to be caused by the breakdown of cellulose species in the timber to volatile organic compounds (VOCs), especially acetic acid.[36] These can be liberated by new wood, especially oak, and also by varnishes, glues, urea formaldehyde, plastics, fabrics, and drying-oil paints, which can liberate fumes for a considerable time after application. Acetic acid in the 100–200 ppb range strongly accelerates the corrosion of lead, giving a corrosion product containing lead acetate–oxide–hydrate ($Pb_3O_2(CH_3COO)_2H_2O$) as well as cerrusite and hydrocerrusite.[37] The corrosion rate was found to be independent of relative humidity from 45% to 95% RH. This effect of VOCs on lead corrosion is significant not only in the context of buildings, but also in museums for display of historic artifacts.[38] However, the use of fatty acid soaps, such as sodium decanoate, successfully provides 99.9% inhibition to corrosion, by the formation of lead soaps, which are well known as corrosion inhibitors.[39]

3.11.3.2 Water

3.11.3.2.1 Distilled and condensed water

In distilled water free from dissolved gases, corrosion is slight though significant; however, the rate of corrosion is increased by the presence of oxygen. Small amounts of dissolved oxygen and carbon dioxide cause rapid attack because the formation of a continuous protective film of lead carbonate does not occur. At moderate CO_2 concentrations, passivation of the lead surface occurs because of $PbCO_3$ formation, but in high-CO_2 contents, corrosion is increased because of the formation of soluble lead bicarbonate.[40]

Condensation corrosion is a common cause of failure in lead-work on buildings. Trapped water is evaporated from and condensed on the underside of the lead during thermal cycling in the environment. This repeated condensation causes the production of lead oxide and lead hydroxide, which migrates away from the surface, leaving it unpassivated. Subsequent reaction with CO_2 in the atmosphere produces copious quantities of basic lead carbonate, resulting in blistering, perforation, and finally, disintegration of the lead.[41] Adequate ventilation and adherence to codes of practice are essential to prevent this.[42] Lead sheet can also crack through thermal fatigue, and hence, admit water into a building structure. This is a consequence of over-fixing the lead, using sheets which are too large, or of using lead containing insufficient copper, and can be eliminated by correct installation.

3.11.3.2.2 Natural waters

The European Union directive on the reduction of hazardous materials[43] stipulates that lead is no longer permitted for use in water supply, either as pipework or in solders. Where it is encountered in old buildings, its replacement is strongly recommended. However, because of the long life of existing installations, water may be conveyed through existing lead pipes, or pipes secured using lead-containing solders, for years to come. This may not be hazardous if the waters contain sufficient carbonate, sulfate, or silicate, and are alkaline. The current UK limit for lead in cold water drawn from a water supply tap is 25 ppb (the US limit is lower at 15 ppb); anything above these levels is actionable. Soft waters invariably dissolve lead to some extent, and raised levels of organic acids will render even harder supply waters plumbosolvent.[44] Thus, water treatments to reduce lead solubility are required.

Lead corrodes slightly in most supply waters dependent primarily on the solution pH. The presence of oxygen and oxidizers in the aqueous medium affects the corrosion resistance of the metal more in acidic waters.[45] The most common treatments given to water are to increase the pH (reduce acidity) and remove organic acids; this is easily carried out by flocculation (e.g., with aluminum sulfate) and alkalization (e.g., with calcium hydroxide or carbonate), which will encourage the formation of a protective carbonate scale.[46] Silicate and orthophosphate treatments reduce lead solubility; however, the common use of zinc orthophosphate to control corrosion of steel and cast iron water mains may increase lead corrosion rates.[47,48] In more saline waters, including seawater, lead usually has a good corrosion performance owing to the formation of the normal passive film of hydrocerrusite ($Pb_3(OH)_2(CO_3)_2$) together with Pb(OH)Cl and $PbCl_2$ carbonate–chloride

double salts;[49] however, corrosion rates are linked to the activity of Cl^- ions, particularly in flowing solution.[50]

3.11.3.3 Buried Structures

3.11.3.3.1 Stray-current corrosion

Stray currents are a source of damage to all buried metal structures, and lead pipes and cable sheaths are particularly susceptible. Although lead can corrode under cathodic (alkaline) conditions, it is generally the anodic sites on the pipe or cable sheath that are attacked. Lead is considered to be endangered if the current density is more than $25\,mA\,m^{-2}$. This is influenced by the conductivity of the soil, which is largely determined by the moisture content, but may be affected by salting of roads in winter. Nonmetallic links in pipework may break electrical continuity. This will produce more numerous corrosion sites, but they are frequently less intense.[51] The surface will normally be covered with a mostly whitish corrosion deposit associated with either a smooth pitted surface or a more general rough etched appearance.[40] The corrosion product may comprise oxides, carbonates, hydroxides, and $PbCl_2{\cdot}Pb(OH)_2$ and $PbCl_2{\cdot}6PbO{\cdot}2H_2O$ have additionally been identified. Stray alternating current can also markedly increase corrosion rates,[52] and the use of lead pipes for electrical grounding has resulted in serious corrosion.[51] Electrolytic corrosion may also occur on the inside of cable sheaths by the passage of current from the cable sheath to the wire.[51] No protective coating is fully effective, but many give good protection with modern systems using polymers.[53]

3.11.3.3.2 Underground corrosion

Lead has a long history of use underground in buried structures; historically for water supply, more recently for lead sheathed electrical cables. Corrosion is promoted by stray currents, local inhomogeneities in the lead, galvanic corrosion with another metal, and the environment of the soil.[40] Thus, soils may differ in water content, degree of aeration, or the presence of various chemicals or bacteria, and these can cause local or extensive corrosion of lead. Historically, extensive long-term tests have been conducted on lead in soils, and these data are still valid.[54,55] The worst combination of soils is wet clay and cinders (ashes from coal combustion). The carbon in the cinder acts as an efficient cathode and severe anodic corrosion takes place in the clay environment. Moisture held in the clay permits the passage of relatively high currents. Anodic corrosion can occur when cables are in contact with dissimilar metals, such as steel support racks or copper bonding ribbon. A new (clean) section of cable may also become anodic to an old (passivated) cable and can then corrode.

Sandy soils and loams of high permeability are less aggressive because water tends to be mobile, thereby reducing concentration cells, and frequently drains readily to allow free movement of oxygen, thus reducing the effect of differential aeration cells. Where air circulates freely, a stable patina is often formed. Very large-grained soils are normally good for the reasons aforementioned, but under certain conditions, severe localized pitting can be caused by differential aeration (e.g., caused by differing degrees of soil density and compaction). Soils of low permeability, such as clays and silts, tend to be most corrosive; however, if the soil becomes deaerated the corrosion rate may fall; under such environments, microbial effects, due to sulfate reducing bacteria, often become important and corrosion can then become severe. Trenches are often lined before cable laying and backfilled after laying, with materials such as sand and crushed chalk, in order to encourage good drainage and ensure a consistent and benign local environment.

Sulfates, silicates, carbonates, colloids, and certain organic compounds in soils act as inhibitors if evenly distributed.[40] Nitrates tend to promote corrosion, especially in acid soil waters, due to cathodic depolarization and to the formation of soluble nitrates. Alkaline soils can cause serious corrosion with the formation of the plumbite anion, which decomposes to give PbO. Organic acids and carbon dioxide from rotting organic matter also have a strong corrosive action. Pitting corrosion in most groundwater/soil environments does not occur in the traditional meaning of the term; however, areas of nonuniform, general attack did occur, resulting in pitted surface morphologies.[56]

Calcium hydroxide leached from incompletely cured concrete causes serious corrosion of lead. This is because carbon dioxide reacts with the lime solution to form calcium carbonate, which is practically insoluble. Carbonate ions are therefore not available to form a passive film on the surface of the lead.[40] Typically, thick layers of PbO are formed, which may show seasonal rings of litharge (tetragonal PbO) and massicot (orthorhombic PbO).[57]

To prevent underground corrosion, lead was traditionally protected with coatings of tar, bitumen, resin, etc.; recently, however, polymeric materials (such as polyvinyl chloride, polypropylene, etc.) are

preferred. No coating is wholly effective unless they completely insulate the metal from corrosive agents and stray currents. The most successful method of protection for lead cables is cathodic protection. It is effective at a potential of $E^\circ = -0.8$ V or about 0.1 V more negative than its equilibrium potential in the soil in question;[58] both impressed currents or sacrificial anodes have been used. Excessively negative potentials can increase the pH of the environment, thus causing corrosion.

Sulfate-reducing bacteria in soils can produce metal sulfides and H_2S, which results in the formation of conductive lead sulfide and increased corrosion rates;[59] deep pits containing a black mass of lead sulfide have also been observed. Other microorganisms may also be involved in the corrosion of lead in soil, including other bacteria and fungi.[60]

Interest in lead as a possible barrier material for use in underground repositories for nuclear waste has prompted a number of studies. Repository environments with static groundwater would have very low oxygen contents and high ionic strengths and, under these conditions, lead would corrode at an unsuitably high rate. However, if the repository is flooded and oxygen levels increase, then lead might be acceptable.[61] Mass loss tests, supported by electrochemical polarization experiments, were carried out in natural and simulated groundwater, and in a range of specific salt solutions.[62] Corrosion rates in aerated conditions varied between 1–3 μm year^{-1} in groundwater (which is acceptable) to over 600 μm year^{-1} in sodium acetate and over 380 μm year^{-1} in sodium nitrate (which is very high and unacceptable). Corrosion rates in bentonite clay suspensions likely to be used as repository backfill were 10–15 μm year^{-1} and deemed to be acceptable.

3.11.3.4 Acids

3.11.3.4.1 Mineral acids

Traditionally, sulfuric acid was made, stored, and conveyed in lead; this is because its corrosion resistance at moderate temperatures and over almost all the concentration range of the acid is excellent, provided that the protective sulfate film is not disrupted. Rupture of the sulfate film may be caused by erosion as a result of high-velocity liquids and gases containing acid spray. In such an environment, acid-resistant brick is often used with a liner of lead in between the brick and the (usually steel) vessel. Thermal cycling may also disrupt the film by thermal fatigue. The corrosion rate of lead is generally less than 125 μm year^{-1}, below about 55% concentration up to its boiling point (130 °C), while acid concentrations to 80% have similar corrosion rates below 100 °C. Above an acid concentration of 85%, the corrosion rate of lead increases to unacceptable values.[62] Lead is no longer used for this service in industry, its place having been taken by passive alloys such as tantalum, zirconium, specialist stainless steels, and nickel-based alloys.[63]

Nitric acid readily attacks lead if dilute, and the metal should not even be used for handling nitrate or nitrite species, except at extreme dilutions and preferably with a passivating reagent such as a sulfate, which will confer some protection. Corrosion decreases to a minimum at 65–70% HNO_3, and lead has been used for storage of nitric acid in the cold at this concentration.[40] Hydrochloric acid should generally be regarded as aggressive to lead and its use cannot be recommended, although a satisfactory life has been obtained with acid of up to 30% concentration at ambient temperature and 20% concentration at 100 °C.[40] Resistance of lead to corrosion by HCl is presumably due to the formation of a protective film of lead chloride, which is only slightly soluble at these concentrations combined with its high overpotential for hydrogen evolution. In mixed hydrochloric and hydrofluoric acids (e.g., used for pickling steel) the behavior of lead is unreliable unless the lead is initially passivated in hydrofluoric acid first.

The remaining use of lead in industrial processes is as an anode in electrowinning and as an inert anode in electroplating, and for these applications, there are few economic alternatives. Lead has good resistance to phosphoric and chromic acids (e.g., in chromium plating), and at high current densities, will tend to passivate anyway with the formation of lead dioxide.

3.11.3.4.2 Organic acids

Lead is attacked by most organic acids, which produce soluble lead salts, particularly in the presence of air or other organic oxidants. Aqueous acetic acid, solutions containing acetates, and acetic acid vapor all rapidly corrode lead and should be avoided if possible. During corrosion, the protective film is dissolved yielding lead salts of the organic acid. These are susceptible to rapid carbonation in the presence of CO_2 and water, forming basic lead carbonate, which, in these circumstances, does not form a passive film.

Studies of the electrochemical behavior of lead at 25 °C in acetic, lactic (0.01–1.0 M), oxalic, and tartaric (0.01–0.15 M) acid solutions demonstrated that

lead is readily soluble both in acetic and lactic acid solutions up to 2000 mV.[64] In these acids, anodic dissolution appears to be under charge transfer control, with lactic acid more aggressive than acetic acid with lead passivating at higher potentials. However, in oxalic and tartaric acid solutions a dependence on the acid concentration is evident. Thus, above a certain specific concentration, an anodic current peak is followed by a reduction in current associated with the formation of a passivation salt film that consisting of the oxalate or tartrate species, respectively. As noted above, corrosion by organic acids is important in the construction sector and also in the conservation of historic artifacts.

3.11.3.5 Lubrication Oils

White metal (tin–lead) bearings do not normally fail due to corrosion, but where this has occurred, it has been associated with the generation of acidity in the lubricant, the production of peroxides, and the presence of air. Peroxides appear to be the controlling factor, but corrosion is also reduced in the absence of air. The corrosion product generally consists of basic lead salts of organic acids.[65] The presence of residual organic acids is thought to be the main cause of the corrosion of terne (lead) plated steel when used as fuel tanks.

3.11.3.6 Miscellaneous Environments

As can be seen from the Pourbaix diagram, lead has no stable passive species at pH > 10–11, and hence, lead is not particularly resistant to dilute alkalis, and will dissolve freely as the plumbite oxyanion. Where free access to carbon dioxide is available, a passivating salt film of lead carbonate may form. However, lead is susceptible to lime drips from fresh concrete and cement mortar, which will tend to disrupt the lead carbonate film formation. Lead can tolerate concentrated alkalis such as KOH to 50% and up to 60 °C and NaOH to 30% and 25 °C, although it is explicitly not used for this purpose.

Lead is not generally attacked rapidly by solutions that contain anions, where the lead salt is sparingly soluble, and hence, where lead can passivate by the formation of a salt film. Thus, only nitrates and, to a lesser extent chlorides, are corrosive. The presence of nitrate tends to pit lead, for example, in carbonate solution.[22] In sodium chloride, the corrosion rate increases with concentration to a maximum in 0.05 M solution, then decreases because of the formation of a relatively porous film $PbCl_2$. Control of the cyclic voltammetry conditions allowed the development of a relatively thick and more protective layer.[66] In potassium bromide, adherent deposits are formed, and the corrosion rate increases with concentration. The attack in potassium iodide is slow in concentrations up to 0.1 M, but in concentrated solutions rapid attack occurs, probably owing to the formation of soluble $KPbI_3$. In dilute potassium nitrate solutions (0.001 M and below) the corrosion product is yellow and is probably a mixture of $Pb(OH)_2$ and PbO, which is poorly adherent. At higher concentrations, the corrosion product is more adherent and corrosion is somewhat reduced.[67]

3.11.4 Specific Applications

3.11.4.1 Lead Anodes

Anodes for electroplating and for electrolysis of brine are frequently made of lead and lead alloys. This is because the formation of a passive film of lead dioxide at high anodic potentials where conventional passive alloys, such as chromium containing materials, would be destroyed by transpassive dissolution. Nevertheless, there is generally a very slow continued corrosion, which leads to thickening of the PbO_2 film. The resulting stresses caused by growth of the oxide layer can cause it to crack and disbond, releasing PbO_2 particles into the electrolyte. Alloying elements are frequently added for strength and to stabilize the film; rolled or extruded alloys are generally found to be more resistant to this form of degradation than are cast alloys.

Lead–silver (1–2% Ag) anodes for cathodic protection may be used in brine and seawater applications for cathodic protection of ships and dockside structures[68,69] at current densities of up to 120 A m^{-2}, although in many applications these have now been superseded with platinum-doped titanium or niobium alloys, which can operate at still higher current densities.

Lead–silver, lead–tin, lead–calcium–tin, lead–calcium–silver, and lead–tin–silver are all used for electrowinning, which is generally carried out using sulfuric-acid-based electrolytes. These alloys have replaced the more traditional lead–antimony compositions due to requirements of higher purity in the deposits. In all electrowinning applications, it is essential to keep the potential of the anode well above the $PbO_2/PbSO_4$ equilibrium potential, otherwise rapid corrosion will occur.[69] Electrochemical

studies of electrowinning anodes have been extensively studied and are focused on (a) reduction of anode corrosion rate, (b) reduction of (lead and other metal) contamination in the deposit, and (c) improved current efficiency.

For example, the efficiency and corrosion resistance of calcium- and silver-containing alloys appears to depend on the nature of the PbO_2 passive layer and its electronic and ionic conductivity.[70] The corrosion rate and current efficiency of anodes can be improved significantly by the incorporation of minor amounts of foreign species in the electrolyte. Thus, preconditioning of anodes in a fluoride solution prior to use can result in a compact and more protective PbF_2/PbO_2 bilayer that is more corrosion resistant.[71]

The corrosion rates for lead–silver anode corrosion rates in zinc electrowinning solutions were studied at a range of current densities from 2500 to 10 000 A m^{-2}. Increases in acid concentration and temperature caused increases in corrosion rate, whereas in the absence of bath additions, the rate was independent of current density.[72] Chloride ions increased the corrosion rate, while fluoride preconditioning reduced it, but only in the presence of manganese. The presence of small concentrations of cobalt and manganese ions can reduce the corrosion rate of electrowinning anodes considerably. The effect appears to be related to an increase in the oxygen evolution kinetics that reduces cell overvoltage and causes less disruption of the PbO_2 passive layer.[73]

Traditional chromium plating uses lead–tin or lead–antimony alloys as the anode material, although coated passive metal anodes (e.g., platinized Ti, Zr, Nb, and Ta) have recently been advocated.[74] Lead anodes offer processing advantages in that they can be formed or cast to conform to the surface to be plated, and hence give an even current density and uniform coverage of coating. The electrochemistry of anodes containing tin, antimony, and silver have been studied in electrolytes similar to chrome plating baths. In chromic acid, a passive film of $PbCrO_4$ forms at very low overpotentials, and the subsequent formation of PbO_2 is masked by oxygen evolution. The effects of alloying additions were found to be minor, although antimony raises the passive current substantially and silver reduces the overpotential of oxygen evolution by about 0.2 V.[75] As for electrowinning anodes, the quiescent (nonpolarized) corrosion rate can be very high and it is recommended that anodes are connected at all times. It has been found that 0.5 g l^{-1} of magnesium fluosilicate suppresses corrosion without affecting the plating process.[76]

3.11.4.2 Lead–Acid Battery

Lead–acid batteries comprise by far the single most important worldwide application for lead. The technology of lead–acid batteries is still under constant improvement and is technically still very much relevant;[77] this section briefly discusses very general aspects of the technology. Lead–acid batteries typically consist of lead alloy supports, which carry an electrochemically active mass, the composition of which differs between positive and negative plates, and with the state of charge of the battery. Failure normally occurs in the positive grids of a battery. The main cause of failure is loss of contact between the grid and the active mass because of 'grid growth,' which is caused by the change in volume of the active material during the charge/discharge cycle, and by corrosion of the metal surface, which can be accelerated by stress. Batteries for automotive, electric vehicle, standby services, etc., all have different characteristics and requirements, which are met by battery grid design and choice of alloy.[78,79]

Traditionally, battery grids have been made from lead with 6–14% antimony, with a small amount of arsenic. High antimony alloys have a significant electrochemical disadvantage, that is, they reduce the overpotential for hydrogen evolution on the lead, leading to electrolysis of the electrolyte (to hydrogen and oxygen). Thus, batteries using traditional materials require regular maintenance (topping-up) via additions of distilled water. While alloys in the region of 5–6% antimony are still used in some industrial, deep discharge, and traction applications, high antimony contents have been largely replaced in automotive batteries by complex low antimony or antimony-free lead–calcium–(tin) alloys. Modern automotive batteries now use lead–calcium-based alloys that do not require topping up (provided they are operated within their electrical design parameters). This reduction in antimony content has been made possible by the introduction of additions of solidification nucleants, such as selenium and sulfur, which promote fine-grain structure. It is also increasingly common to find different alloys used in the positive and negative grids and optimized for these applications.

High antimony alloys exhibit high strength, good castability, and give good deep cycling performance. The latter requires that the active mass has good adhesion to the metal, is structurally stable during cycling, and does not passivate. Antimony reduces shedding of active material from the cells, produces a surface film of greater porosity, which becomes more

porous during cycling, promoting stability of the active mass. It has also been shown that $PbSO_4$ is more reluctant to nucleate on antimonial lead.[80] Although corrosion rates may appear quite high, attack is normally of a general nature, which allows a satisfactory service life. This is because the eutectic is preferentially corroded, which reduces intergranular corrosion. Antimony reduces the oxygen overpotential on the positive grid, while Sb^{5+} ions migrate from the positive grid to the negative and be reduced to metallic antimony.[81] This reduces the hydrogen overpotential, leading to excessive gassing, consuming water from the electrolyte, reducing charge efficiency, and liberating stibine (SbH_3). During overcharge, antimony increases the rate of formation of the inner corrosion layer on the positive grid.

Low maintenance batteries, which only require the addition of water infrequently in the second half of their service life, use low antimony alloys that typically contain less than 3% antimony, with some alloys containing as little as 0.6%. The most commonly used alloys have 1.3–1.8% Sb. They always contain As to assist hardening, and a nucleating agent such as Se or S with Cu. These are necessary because the coarse dendritic structure is prone to porosity and hot cracking during casting. The addition of nucleating agents gives a fine-grained structure with good corrosion resistance. Tin is often added to increase fluidity in casting alloys.

Lead–calcium–(tin) alloys are used in maintenance-free automotive starting, lighting, ignition (SLI) batteries, in stationary batteries, and some traction batteries. It is essential that the correct calcium content and a suitable calcium–tin ratio is used. In the binary lead–calcium alloys, a fine-grained structure with serrated grain boundaries is produced by a discontinuous precipitation reaction.[82] The addition of tin changes the nature of the precipitation reactions to give two areas of stability. One is with high calcium–low tin and the other is in the region below 1.8% tin and less than 0.07% calcium. Batteries made from these alloys have a much reduced rate of self-discharge compared with antimonial alloys, thus giving a longer shelf-life, and maintain a high discharge voltage throughout their life.

3.11.4.3 Reactor Coolants

Lead-based liquid metal coolants (using either liquid lead or liquid lead–bismuth eutectic) were first used in a nuclear reactor in the 1960s by the Soviets as an advanced, high power density, submarine propulsion plant. Reactors designed using such coolants have some compelling advantages (e.g., operation at atmospheric pressure, boiling point greatly in excess of the reactor operating temperature, relative nonreactivity to water and air compared with liquid sodium) and comprise a candidate 'Generation IV' fast neutron reactor system as well as a candidate coolant system for fusion reactors. However, lead alloys are significantly more corrosive to constructional materials (e.g., steels) than is liquid sodium. This is due to dissolved oxygen in the lead that reacts with the containing material, as well as liquid metal embrittlement.[83,84] To avoid excessive oxidation of structural alloys, such as martensitic steels, it is necessary to control the oxygen activity to below 10^{-24} atm, and this can be monitored by the use of electrochemical probes.[85]

References

1. Thornton, I.; Rautiu, R.; Brush, S. *Lead – The Facts*; International Lead Association, 2001.
2. Blasket, D. R.; Boxall, D. *Lead and Its Alloys*; Ellis Horwood, 1990.
3. *Smithell's Metal Handbook*, 7th ed.
4. Guruswamy, S. *Engineering Properties and Applications of Lead Alloys*; CRC Press, 1999.
5. Hine, F.; Ogata, Y.; Yasuda, M. *Bull. Electrochemist.* **1988**, *4*, 61–65.
6. Prengaman, R. E. In *Structure Control of Non-antimonial Lead Alloys via Alloy Additions, Heat Treatment and Cold Working*; Proceedings of the 7th International Lead Conference, Lead Development Association: Madrid, 1983.
7. Heubner, U.; Reinert, M. In *Development of Improved Lead Materials for Chemical Plant*; Proceedings of the 7th International Lead Conference, Lead Development Association: Madrid, London, 1983.
8. Delahay, P.; Pourbaix, M.; Van Rysselbergh, P. *J. Electrochem. Soc.* **1951**, *98*, 57.
9. O'M Bockris, J.; Reddy, A. K. *Modern Electrochemistry;* Plenum, 1986; Vol. 2, Table 10.12.
10. Birss, V. I.; Sheralier, M. T. *J. Electrochem. Soc.* **1987**, *134*, 802–808, 1594–1600.
11. Lingane, J. *J. Am. Chem. Soc.* **1938**, *60*, 724–725.
12. Ives, D. J. G.; Smith, F. R. *Trans. Faraday Soc.* **1967**, *63*(1), 217–233.
13. Salzberg, H. W. *J. Electrochem. Soc.* **1953**, *100*, 146–151.
14. Kuhn, A. T. Ed. *The Electrochemistry of Lead*; Academic Press: London, 1979.
15. Eldridge, J. M.; Dong, D. W. *Surf. Sci.* **1973**, *40*, 512–530, 531–544.
16. Bullock, K. R. *J. Electroanalyt. Chem.* **1987**, *222*, 347–366.
17. Ruetschi, P. *J. Electrochem. Soc.* **1973**, *120*, 331–336.
18. Pavlov, D. *Electrochim. Acta* **1978**, *23*, 845–854.
19. Pavlov, D.; Rogachev, T. *Electrochim. Acta* **1978**, *23*, 1237–1242.
20. Fletcher, S.; Matthews, O. B. *J. Electroanalyt. Chemist.* **1981**, *126*, 131–144.
21. Hall, S. B.; Wright, G. A. *Corros. Sci.* **1990**, *31*, 709–714.
22. Abd El Aal, E. E.; Abd El Wanees, S.; Abd El Aal, A. *J. Mater. Sci.* **1993**, *28*, 2607–2614.

23. Ahlberg, E.; Berghult, B. *Electrochim. Acta* **1991**, *36*, 197–201.
24. Abd El Aal, E. E. *Anti-Corros. Meth. Mater.* **2001**, *48*, 116–125.
25. Amin, M. A.; Rehim, S. S. A. *Electrochim. Acta* **2003**, *49*, 2415–2424.
26. Semino, C. J.; Burkart, A. L.; Garciía, M. E.; Cassibba, R. *J. Nucl. Mater.* **1996**, *238*, 198–204.
27. Subramanian, K. S.; Sastri, V. S.; Elboujdaini, M.; Connor, J. W.; Davey, A. B. C. *Water Res.* **1995**, *29*, 1827–1836.
28. Sastri, V. S.; Subramanian, K. S.; Elboujdaini, M.; Perumareddi, J. R. *Corros. Eng. Sci. Technol.* **2006**, *41*, 249–254.
29. Edwards, M.; Triantafyllidou, S. *J. Am. Water Works Assoc.* **2007**, *99*, 96–109.
30. Olby, J. K. *J. Inorg. Nucl. Chemist* **1966**, *28*, 2507.
31. Tranter, G. C. *Br. Corros. J.* **1976**, *11*, 222.
32. Graedel, T. E. *J. Electrochem. Soc.* **1994**, *141*, 922–927.
33. Cook, A. R.; Smith, R. In *Atmospheric Corrosion*; Ailor, W. H., Ed.; Wiley: New York, 1982.
34. Hill, R. H.; Frost, P. C.; Smith, R. In *Corrosion of Aluminium in Contact with Lead in Atmospheric Environments*; Proceedings of the 7th International Lead Conference, Lead Development Association: London, 1983.
35. Matthes, S. A.; Cramer, S. D.; Covino, B. S., Jr.; Bullard, S. J.; Holcomb, G. R. In *Outdoor Atmospheric Corrosion*; Townsend, H. E., Ed.; ASTM Special Technical Publication, 2002, Vol. 1421, pp 265–274.
36. Echavarriía, A. V.; Echeverriía, F. E.; Arroyave, C.; Cano, E.; Bastidas, J. M. *Corros. Rev.* **2003**, *21*, 395–413.
37. Niklasson, A.; Johansson, L.-G.; Svensson, J.-E. *Corros. Sci.* **2008**, *50*, 3031–3037.
38. Tétreault, J.; Sirois, J.; Stamatopoulou, E. *Stud. Conservat.* **1998**, *43*, 17–32.
39. Rocca, E.; Rapin, C.; Mirambet, F. *Corros. Sci.* **2004**, *46*, 653–665.
40. Hofmann, W. *Lead and Lead Alloys Properties and Technology*; Springer-Verlag: London, 1970; English Translation by Lead Development Association.
41. Hill, R. H.; Frost, P. C.; Smith, R. In *Various Aspects of Weathering and Corrosion of Lead in Building Applications*; Proceedings of the 8th International Lead Conference Lead Development Association: London, 1985.
42. *Rolled Lead Sheet – The Complete Manual*; Lead Sheet Association, 2007.
43. *Reduction of Hazardous Substances*; European Commission Directive, 2002/95/EC.
44. Miles, G. *J. Soc. Chem. Indust.* **1948**, *67*, 10–13.
45. Badawy, W. A.; Al-Kharafi, F. M. *Corros. Prevent. Contr.* **1999**, *46*, 13–22.
46. Boffardi, B. P.; Sherbondi, A. M. In *Control of Lead Corrosion by Chemical Treatment*; Proceedings of 'Corrosion 1991' NACE: USA, 1991; Paper 445.
47. Patterson, J. W.; O'Brien, J. E. *J. Am. Water Works Assoc.* **1979**, *71*, 264–271.
48. Edwards, M.; McNeill, L. S. *J. Am. Water Works Assoc.* **2002**, *94*, 79–90.
49. Beccaria, A. M.; Mor, E. D.; Bruno, G.; Poggi, G. *Werkstoffe Korros.* **1982**, *33*, 416–420.
50. Beccaria, A. M.; Mor, E. D.; Bruno, G.; Poggi, G. *Br. Corros. J.* **1982**, *17*(2), 87–91.
51. Glander, F.; Glander, W. *Zeitschrift Metallkunde* **1953**, *44*, 97–101.
52. Costa, J. M.; Hoar, T. P. *Corros. Sci.* **1962**, *2*, 269–274.
53. Dyba, J.; Goodwin, F. In *New Developments in Lead-Sheathed Cables;* Proceedings IEEE International Symposium on Electrical Insulation, USA, 1998.
54. Romanoff, M. *Underground Corrosion*; National Bureau of Standards, 1957; publication #579.
55. Robson, W. W.; Taylor, A. R. Some experiments in the mechanism of corrosion of lead pipes in soils. Report MM/19/54. Associated Lead Manufacturers Ltd., 1954.
56. Joerg, E. A.; Devereux, O. F. *Corrosion* **1996**, *52*, 953–957.
57. Wolf, E. F.; Bonilla, C. F. *Trans. Electrochem. Soc.* **1941**, *79*, 307.
58. Compton, K. G. *Corrosion*; **1956**, 12, 553–60.
59. Schmeling, E. L.; Roschenbleck, B. *Werkstoffe Korros.* **1961**, 12, 215–23.
60. Pintado, J. L.; Montero, F. *Int. Biodeter. Biodegrad.* **1992**, *29*, 357–365.
61. Goodwin, F. E. *Corros. Prev. Contr.* **1985**, *32*(2), 21–24.
62. Cassibba, R. O.; Fernandez, S. *J. Nucl. Mater.* **1989**, *161*, 93–101.
63. Gaverick, L. Ed. *Corrosion in the Petroleum Industry*; ASM International, 1994.
64. Abd-El Rehim, S. S.; Amin, N. H.; Ali, L. I.; Mohamed, N. F. *J. Chem. Tech. Biotechnol.* **1998**, *72*, 197–201.
65. Wilson, B. S.; Garner, F. H. *J. Inst. Petroleum*; **1951**, 37, 225–38.
66. El-Halim, A. M. A.; Fawzy, M. H.; Saty, A. *J. Electroanal. Chem.* **1991**, *316*, 275–292.
67. Vaivads, A.; Liepina, L. *Latvijas PSR Zinatnu Akademijas Vestis* **1954**, *8*, 119–129.
68. Barnard, K. N.; Christie, G. L.; Gage, D. G. *Corrosion* **1959**, *15*, 581–586.
69. Lander, J. J. *J. Electrochem. Soc.* **1956**, *103*, 1–8.
70. Kozin, L. F.; Kozin, V. F. *Protection Metals* **1997**, *33*, 131–136, 549–555.
71. Ramachandran, P.; Balakrishnan, K. *Bull. Electrochem.* **1996**, *12*, 352–354.
72. Newnham, R. H. *J. Appl. Electrochem.* **1992**, *22*, 116–124.
73. Cachet, C.; Le Pape-Rérolle, C.; Wiart, R. *J. Appl. Electrochem.* **1999**, *29*, 813–820.
74. Pavlović, M. G.; Dekanski, G. *J. Solid State Electrochem.* **1997**, *1*, 208–214.
75. McBurney, M. J. P.; Gabe, D. R. *Surf. Technol.* **1979**, *9*, 253–266.
76. Carter, V. E.; Campbell, H. S. *Metal Finishing J.*; **1962**, 8, 103–7.
77. Kiehne, H. A., Ed. *Battery Technology Handbook*; CRC Press, 2003.
78. Berndt, D. INTELEC, Proceedings of the International Telecommunications Energy Conference **2005**; pp 269–275.
79. Garche, J. *Phys. Chem. Chem. Phys.* **2001**, *3*, 356–367.
80. Webster, S.; Mitchell, P. J.; Hampson, N. A.; Dyson, J. I. *J. Electrochem. Soc.* **1986**, *133*, 133–137, 137–139.
81. Dawson, J. L.; Wilkinson, J.; Gillibrand, M. I. In *Power Sources 3*, Proceedings of the 7th International Symposium in Non-mechanical Electrical Power Sources; Brighton, UK, Collins, D. H., Ed., Oriel Press: Newcastle-upon-Tyne,1970; pp 1–9.
82. Caillerie, J. L.; Albert, L. *J. Power Sources* **1997**, *67*, 279–281.
83. Tortorelli, P. F.; Chopra, O. K. *J. Nucl. Mater.* **1981**, *103*, 621–632.
84. Fazio, C.; Benamati, G.; Martini, C.; Palombarini, G. *J. Nucl. Mater.* **2001**, *296*, 243–248.
85. Li, N. *J. Nucl. Mater.* **2002**, *300*, 73–81.

Relevant Websites

www.ilzro.org – International Lead-Zinc Research Organisation.
www.ila-lead.org – International Lead Association.

3.12 Corrosion of Tin and its Alloys

S. B. Lyon
Corrosion and Protection Centre, School of Materials, The University of Manchester, Oxford Road, Manchester, M13 9PL, UK

This article is a revision of the Third Edition article 4.6 by S. C. Britton, volume 1, pp 4:157–4:167,

Glossary

Allotropy The existence of two or more different forms (allotropes) of the same element that are bonded in a different manner; allotropes are thus different structural modifications of an element.

Gray tin The low-temperature allotrope of tin having a cubic structure that is stable below ~13 °C. Note that the transformation from white tin to gray tin is sluggish and generally does not proceed significantly until the temperature is well below 0 °C.

White tin The high temperature allotrope of tin having a body centered tetragonal structure that is stable above ~13 °C.

Abbreviations

AES Auger electron spectroscopy
SHE Standard hydrogen electrode
XPS X-ray photoelectron spectroscopy

3.12.1 Introduction

3.12.1.1 Physical Properties

The element tin is located in Group VI of the periodic table, lying above lead, with which it shares many properties. Tin, like lead, is one of the metals known from antiquity and highly prized for its ability to harden copper, forming bronze. There is evidence that tin was mined in the United Kingdom in

Cornwall from the early bronze age (2100–1500 BC). Certainly, by Roman times, tin from the western edge of Europe (mainly Cornwall and Spain) was traded widely throughout the known world. Tin ore resources are not widely distributed and production is mainly from two forms: (1) hard rock, typified by the Cornish deposits and similar ore bodies in Bolivia and Queensland; and (2) alluvial (placer) deposits, typified by the southeast Asian ore field stretching from Indonesia and Malaysia to Thailand.

Tin is allotropic with the normal, metallic (β) form being body-centered tetragonal above the transformation temperature, that is, ~13.2 °C.[1] The lower temperature allotrope, α or 'gray' tin, is cubic and forms with a significant volume change that tends to result in the disintegration of the material. However, the transformation is kinetically sluggish, although it can be encouraged by mechanical deformation and delayed, or effectively suppressed to lower temperatures, by impurities such as antimony, lead, and bismuth.[2] Gray tin normally appears as nodules of a friable material on the surface of the metallic form and resembles a corrosion product. Thus, the transformation is often not readily distinguishable from corrosion.[3] The transformation mechanism has been studied by high-resolution electron microscopy in order to obtain the lattice orientation relationship between the two allotropes.[4] Thus, the (011) plane of gray tin is parallel to the (001) plane of white tin, and the [211] direction of gray tin is nearly parallel to the [010] direction of white tin. This evidence supports a model for the α-to-β transformation that is partly martensitic and partly diffusional.

The use of unalloyed tin is restricted by its low melting point (232 °C) and by its low tensile strength (15 MPa). On the other hand, its melting point, and its ability to 'wet' other metals (often by the formation of intermetallic compounds), facilitates its use as solder (for metal joining) and as a coating (for corrosion protection), while its softness and high ductility make it suitable for cold working and for bearing applications. Given its relatively low melting point, tin recrystallizes readily at room temperatures, and therefore, the effects of mechanical working are slight and arise from the differences in grain size and not from the effects of work hardening. The formation of tin whiskers is also thought to be a consequence of its low melting point, which results in the growth of fine threadlike structures, typically ~1–2 μm in diameter, with growth rates of up to millimeters per month under appropriate conditions.[5,6]

Given increasing health and safety concerns that lay severe limits on the use of lead in materials, there has been, for some time, a legislative driver for the development of essentially lead-free tin alloys. This has reintroduced problems relating to the formation of gray tin (at lower temperatures) and tin whiskers that were generally absent in lead-containing materials. For example, in the electronic industry, where tin-based solders are now widely used, whisker growth, in particular, can cause problems such as short-circuiting.[7]

3.12.1.2 Applications

The industrial use of tin is limited by its low strength and very limited solubility for most elements at room temperature. However, tin is essential in a number of alloys where it is a minor constituent (e.g., in copper–tin bronzes) and also where it is the major component (e.g., in pewter). The most important forms in which tin is used are

1. tin of more than 99% purity for specialist applications;
2. tin hardened by additions of 1–2% Cu or Sb;
3. pewter with 90–95% Sn, 4–8% Sb, and 1–2% Cu;
4. coatings for other metals, which may be pure tin or tin plus a codeposited species;
5. soft solders with tin and lead in all proportions;
6. lead-free soft solders with >90% Sn and additions of silver, copper, bismuth, indium, or zinc;
7. bearing metals 'high tin' and 'head lead' with a wide range of proportions of tin, antimony, copper, and lead, or with tin (5–30%) in aluminum;
8. diecasting alloys containing 70–80% Sn with antimony, copper, and lead, either one of them or a combination.

The corrosion behavior of tin and tin alloys, whatever their form, is basically similar, except in the case of solders and bearing metals where the wide composition range and special duties of the materials give particular issues. The impurities likely to be present in nominally pure tin are unlikely to affect its corrosion resistance, except for minor effects on the rate of oxidation in air. Low aluminum contents, however, may result in a severe intergranular attack by water; the addition of antimony counteracts this effect. Although 0.1% magnesium appears to be tolerable, larger amounts produce effects similar to those of aluminum.[8]

Apart from the special uses in solders and bearings metal already referred to, and as coatings, tin and its alloys find employment where we can take advantage

of their physical properties and their fair resistance to tarnish and corrosion in near-neutral environments. Tin has traditionally been used in many food-grade applications, although such applications nowadays increasingly use cheaper materials, such as stainless steels and polymers. Tin pipe can be used to condense steam for high-purity distilled water, as a conveyor of beer and soft drinks, especially in coils through cooling media, and, in a larger size, as organ pipes. Some pharmaceutical and food products are packed in collapsible tin tubes, and tinfoil coverings are used on cork wads for jar and bottle closures. The tin alloy pewter is most valued for the decorative forms into which it is easily worked or cast, but it is also used for making drinking vessels and dishes.

3.12.2 Electrochemistry

3.12.2.1 Thermodynamics

The Pourbaix diagram for tin, Figure 1, refers only to solutions in which the formation of soluble tin complexes (e.g., with citric acid) does not occur. Tin is a slightly active metal with its domain of stability below that of the hydrogen equilibrium; in theory, it will corrode in acid, evolving hydrogen gas. It is more noble than iron and nickel, but slightly less noble than lead, although in practice, passivity will alter this sequence. Tin shows a wide range of passivity because of the stability of tin (IV) oxide, SnO_2, which is stable at a lower pH than is PbO. However, tin will dissolve as Sn^{2+} ions at $pH < 2$ and as the corresponding (II)- or (IV)-valent oxy-anion species at $pH > 11$. Note, however, that in regions where, as shown in the diagram, the dissolution of tin is possible, the rate of corrosion may be very low. This is because the overpotential for hydrogen evolution on tin is high, particularly in acid solution. Thus, in a range of concentrations of H_2SO_4,[9] the exchange current for the hydrogen evolution reaction was found to be 10^{-11} A cm^{-2} with a Tafel slope of 0.118 mV per decade current, indicating that a one-electron transfer reaction was rate controlling. In KOH solutions,[10] the exchange current was higher, 3×10^{-6} A cm^{-2}, while the Tafel slope was similar to that in acid, 0.120 mV per decade current. Consequently, in alkaline or moderately acid solutions free from oxygen or oxidizing agents, the corrosion of pure tin may be barely detectable unless the tin is in contact with another metal that has a lower overpotential (higher exchange current density) for hydrogen evolution.

The passivity of tin in the middle pH range (i.e., between 3 and 10), its solubility in acids or alkalis (modified by the high hydrogen overpotential), and the formation of complex ions (especially with organic acids) are the bases of its general corrosion behavior. Other properties that have influenced the selection of tin for particular purposes are the

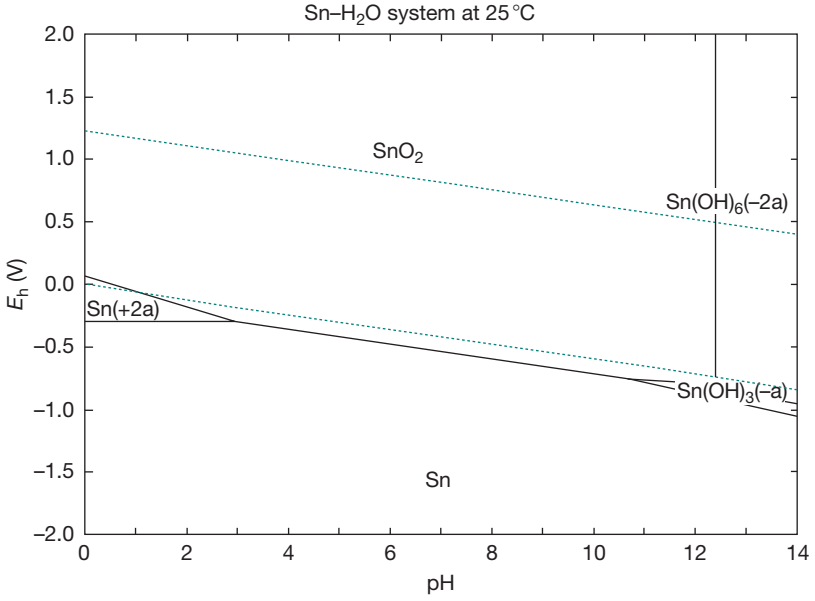

Figure 1 Pourbaix (*E*–pH) diagram for tin in water at a dissolved concentration of 10^{-5} M tin species. Reproduced from HSC: Chemistry, version 6.12, Outotec Research Oy, Finland, 2007.

low toxicity of tin salts (that permit the use of tin in food-grade applications) and the absence of catalytic promotion of oxidation processes that may cause changes in oils or other neutral media affecting their quality or producing corrosive acids.

3.12.2.2 Dissolution

The electrochemistry of tin was extensively reviewed by Stirrup and Hampson in 1977.[11] As can be seen from the Pourbaix diagram, tin shows passivity by virtue of the formation of Sn(IV) oxide (SnO_2), over an extended pH range from about 3 to above 10. Also, as previously indicated, the dissolution kinetics are slow, especially in acid, by virtue of a low exchange current density for hydrogen evolution.

At potentials just above its reversible value, tin dissolves under anodic polarization in acids initially as stannous ion (Sn^{2+}). In 4–8 M sulfuric acid, this reaction has a Tafel slope of close to 40 mV per decade current, indicating a two-electron transfer reaction with a probable bisulfate ion intermediate.[12] The stannous ion is unstable in water at most values of pH (except in acid concentrations typically >1 M), and at low concentrations, is hydrolyzed giving a number of species, depending on pH: $SnOH^+$, $Sn(OH)_2$, $Sn(OH)_3^-$, etc.; at higher tin concentrations, the complex species $Sn_2(OH)_2^{2+}$ and $Sn(OH)_4^{2+}$ are prevalent.[13] The hydroxide complexes are well known to react with halides to give a number of Sn(II) hydroxy–halide complexes; however, these are only present in solution when the halide concentration is $>10^{-3}$ M and at pH values <4. In alkaline conditions, tin initially dissolves as stannite ion, $Sn(OH)_3^-$, which is subject to the same speciation as a function of pH, as indicated earlier.

At higher potentials, Sn(II) is universally oxidized to Sn(IV) species. There are very little experimental data on this reaction; however, Sn(II) to Sn(IV) oxidation was studied in strong sulfuric acid and found to have first-order kinetics with respect to the dissolved species; an increase in H^+ ion concentration decreased the reaction rate, while an increase in SO_4^{2-} had the opposite effect.

3.12.2.3 Passivation

Over the majority of the pH range, the passive film is generally assumed to consist of $Sn(OH)_4$ or SnO_2; however, in view of its very low solubility, data for the speciation of tin (IV) oxides and hydroxides in aqueous environments are very sparse. Indeed, the formation of SnO_2 as a passive film is one of the reasons for the excellent corrosion resistance of tin in noncomplexing aqueous environments.

In 4–8 M sulfuric acid, passivity is consistent with thin films of stannous oxide (SnO); SnO_2 only formed at significantly more positive potentials.[12] Passive films on tin corroded at the open circuit potentials in 6.7 M nitric acid, 5.7 M hydrochloric acid, and 9 M sulfuric acid were analyzed using Mössbauer spectroscopy and found to consist of hydrated SnO_2, $Sn_4(OH)_6Cl_2$, and $SnSO_4$, respectively.[14]

Passive films on tin were studied using infrared and surface-enhanced Raman spectroscopy.[15] In 0.1 M NaOH solution, $Sn(OH)_4$ was found to dominate, and further exposure to dry air was found to dehydrate the film to SnO_2, with the evidence of only a small amount of SnO. The passive film on 0.15 M NaCl solution (near-neutral) was found to consist only of $Sn(OH)_4$. However, angle-resolved X-ray photoelectron spectroscopy (XPS) was used to develop a model for the passive film on tin in 0.1 M KOH, and it was found that tin hydroxide was present only in the outer layers of the film. The inner layer consisted of SnO_2, with the evidence of SnO adjacent to the metal–oxide interface.[16] This appears to be consistent with results from phosphate buffer solutions (pH 4.3) where $Sn(OH)_4$ was found along with a reduced species, either $Sn(OH)_2$ or SnO, at the metal–oxide interface.[15] An electrochemical study of the anodic oxidation of tin was performed in carbonate–bicarbonate buffer solution at pH 8.9. From −0.1 to 1.2 V (SCE), tin exhibited an essentially potential-independent, steady-state, passive current, which was found to be independent of flow conditions.[17] The results indicate that the anodic film grows according to the Mott–Cabrera model and is an oxygen ion conductor. Finally, the electrochemical passivation of tin was studied in citric acid buffer at pH 6.[18] Prepassivation was found to occur along with Sn(II) and Sn(IV) species, while full passivation was associated with Sn(IV) species only. The results indicated that, although the initial film formed coincided mainly with $Sn(OH)_4$, this transformed at longer periods of time to the more thermodynamically stable SnO_2 species.

In summary, tin is found to passivate in aqueous environments from below pH 1 to above pH 12, forming an oxide film that consists of $Sn(OH)_4$ or SnO_2. The latter oxide, which is more stable, may form either initially or transform gradually with time from the hydroxide. It is likely that a thin layer of Sn(II) species is stable at the interface between the passive film and the metal, although films consisting

predominantly of Sn(II) species are not observed except in high concentrations of the reducing acid.

3.12.3 Corrosion and Oxidation

3.12.3.1 Atmospheric Corrosion

3.12.3.1.1 Oxidation in dry air

Oxidation of tin in dry air is slow; the metal remains bright and interference colors are not developed below ~180 °C. On a rolled tin surface heated in air,[19,20] the thickness of the oxide grew according to the logarithmic law at temperatures of up to ~160 °C and according to the parabolic law at higher temperatures, for which the oxide was identified as SnO. For electropolished tin heated in oxygen at pressures of 130 N m^{-2} and above, three stages of oxidation were observed at temperatures of up to 220 °C:[21–24]

1. an initial sigmoid growth curve during nucleation;
2. a logarithmic growth curve when cavities acted as diffusion barriers;
3. erratic behavior caused by random film rupture.

The oxide formed was identified as SnO at temperatures down to 75 °C. However, a mixture of SnO and SnO_2 is formed in dry air at lower temperatures, and in humid air, at temperatures of at least 100 °C.[25] The electrochemical reduction analysis on tin oxidized in dry air at 125 and 150 °C confirmed the presence of SnO with a thin surface layer of SnO_2.[26,27] Small additions, for example, 0.1%, of indium, zinc, or phosphorus reduce the rate of oxidation, and the addition of antimony, thallium, or bismuth accelerates it.[24]

3.12.3.1.2 Corrosion in humid air

In the absence of polluting gases or dusts, increasing relative humidity tends to increase the rate of oxidation[28] and may cause the development of interference colors. In an ordinary atmosphere, some corrosion product may be formed over time. However, tin products are not hygroscopic, and tin is not attacked at relative humidities of below 100% unless the dust falling on the surface is hygroscopic, or impurities in the metal are able to form a hygroscopic product. Indoors, in an unpolluted laboratory atmosphere, a gray film, increasing in weight linearly with time (4 mg m^{-2} day^{-1}), is formed, while in sheltered exposure (no rain) outdoors, the corrosion rate declined with time. The reflectivity of the surface is slowly lost if it is left untouched, but may be preserved by regular washing; in one experiment, when the surface was washed at intervals of 3 weeks, a water wash was adequate for 6 weeks, and although the use of soap was necessary thereafter, almost a complete preservation of reflectivity was achieved.

The impurities ordinarily present in the atmosphere do not appreciably affect the character of corrosion. No tarnishing effect is exerted by hydrogen sulfide, sulfur dioxide, and other acids in low concentrations, including formic, acetic, and other organic acids, which, when evolved from wood or insulating materials, are very often destructive to metals other than tin, in the confined spaces of electrical equipment or of packages. Chlorides accelerate corrosion and tend to form a white corrosion product containing oxychloride. The presence of some impurities, notably zinc, in the metal may cause tarnishing and a loss of brightness in atmospheres containing SO_2.[29] The corrosion rate of electroplated tin on nickel in the presence of sub-ppm amounts of either SO_2 or NO_x did not increase. However, a synergetic effect was found with both pollutants where the corrosion rate was increased significantly.

The atmospheric pollution prevailing in special industrial or laboratory locations may induce more severe corrosion, for example, the vapors from concentrated hydrochloric or acetic acid will etch tin, and moist sulfur dioxide will produce a sulfide tarnish, as will hydrogen sulfide at temperatures of above ~100 °C, and halogens attack tin readily.

When tin is fully exposed out of doors, corrosion is uniform, and the rate falls only slightly with time. The metal becomes dull and accumulates a compact layer of pale gray product, mainly stannous oxide. Rates observed during exposures in the United States for periods of up to 20 years were 1.3–1.8 μm $year^{-1}$ in industrial atmospheres (i.e., mainly polluted with sulfur dioxide), 1.8–2.8 μm $year^{-1}$ in marine atmospheres (i.e., mainly polluted with sea-salt), and less than 0.5 μm $year^{-1}$ in rural atmospheres (i.e., relatively unpolluted).[30]

3.12.3.1.3 Atmospheric corrosion products

The corrosion of tin in various humid atmospheres has been examined using a number of surface analytical techniques, including XPS and Auger electron spectroscopy (AES).[25,31,32] While it is difficult to resolve the peaks of the oxide from those of the hydroxide, and hence, to establish their degree of surface hydration, there is a general agreement that both SnO and SnO_2 may be present depending on the temperature of exposure.

In atmospheres polluted with >100 ppm nitrogen dioxide, tin nitrate was reported to form at 30–35%

RH.[33] In a mixed atmosphere containing more representative atmospheric conditions (40 ppb H_2S, 350 ppb SO_2, 500 ppb NO_2, and 3 ppb Cl_2) at 81% RH, only tin oxides were found.[34] An XPS study on the films formed in SO_2 and NO_x found only oxide species in SO_2, but a mixture of oxides and nitrates with NO_x. No synergy was noted between at-ppm concentrations of SO_2 and NO_x at 85% RH.[35]

3.12.3.2 Corrosion in Acid

3.12.3.2.1 Mineral acids

As the high overvoltage restricts hydrogen evolution, corrosion in organic acids or dilute nonoxidizing mineral acids is generally controlled by the rate of supply of oxygen.[2,3] In solutions of acid open to air, with specimens of size 50×20 mm completely immersed, corrosion rates were, in a range of 0.1 M organic acids, 400–500 g m^{-2} day^{-1}, and in 0.1 M hydrochloric or sulfuric acids, 600 g m^{-2} day^{-1}. In the absence of oxygen, the rates in the two mineral acids were 100–150 g m^{-2} day^{-1}, while they were negligible in the organic acids. Phosphoric acid forms a protective layer, and even in the presence of air, the corrosion rate is only ~20 g m^{-2} day^{-1}. Nitric acid corrodes tin freely even in the absence of oxygen; however, chromic acid forms a protective film. This film, which contains chromic oxide and tin oxides, will, after withdrawal from the acid, give some degree of protection against mildly corrosive conditions. Thus, hot solutions of chromic acid, alone or mixed with phosphoric acid, may be used as passivating media.

3.12.3.2.2 Organic acids

Tin forms complex ions with many organic acids, including those commonly found in fruits (citric, oxalic, malic). This action has important effects on the galvanic behavior of tin. The normal electrode potential of tin is −0.136 V, but the reduction of stannous ion activity resulting from the formation of complexes may depress the corrosion potential to make tin anodic to iron.[36]

The attack of tin by oxalic, citric, and tartaric acids was found to be under the anodic control of the Sn^{2+} salts in solution in oxygen-free conditions.[37] In a study of tin contaminated by up to 1200 ppm Sb, it was demonstrated[38] that the modified surface chemistry catalyzed the hydrogen evolution reaction in deaerated citric acid solution. Tin was found to corrode more rapidly in tartaric acid because of the reduction in the hydrogen overpotential; passivation was caused by a film of tin hydroxide or oxide.[39]

3.12.3.3 Corrosion in Near-neutral Conditions

Pure tin is completely resistant to distilled water, hot or cold. Local corrosion occurs in salt solutions that do not form insoluble compounds with stannous ions (e.g., chloride, bromide, sulfate, nitrate), but is unlikely in solutions giving stable precipitates (e.g., borate, monohydrogen phosphate, bicarbonate, iodide).[40] In all solutions, oxide film growth occurs and the potential of the metal rises. Any local dissolution may not begin for several days, but once it has begun, it will continue, its presence being manifested at first by small black spots and later by small pits. The movement of the solution tends to prevent pitting; stagnation, especially in crevices where the tin touches another solid surface, favors its progress. Contact with a more noble metal such as copper or nickel increases the number and intensity of pits; contact with metals such as aluminum and zinc gives cathodic protection.

As indicated earlier, the bicarbonate ion inhibits the process, which does not occur, therefore, in many supply waters; attack is most likely in waters that, by nature or as a result of treatment, have a low bicarbonate content and relatively high chloride, sulfate, or nitrate content. The number of points of attack increases with the concentration of aggressive anions, and ultimately, slow general corrosion may occur.

During the exposure of 99.75% tin to seawater for 4 years, a corrosion rate of 0.0023 mm $year^{-1}$ was observed.[41] Corrosion in soil usually produces slow general corrosion with the production of crusts of oxides and basic salts. For example, the production of the significant quantities of the metastable corrosion product romarchite (SnO) is commonly seen when studying pewter corrosion products from marine archaeological sites,[42] but is never seen, except transiently or as a thin interfacial phase, in passive films and atmospheric corrosion products.

3.12.3.4 Corrosion by Alkalis

The Pourbaix diagram indicates the possibility of attack by solutions of pH values above ~10.5, but the position of this limit is influenced by temperature, by the constitution of the solution, and by the surface condition of the metal. Corrosion will ensue if the surface oxide is significantly soluble, which will occur increasingly beyond pH 12.

Once corrosion begins, its rate is governed by the oxygen supply and temperature and is not greatly affected by the character of the alkali. Rates of attack

for specimens completely immersed in still solutions open to air are ~600 g m^{-2} day^{-1} at 30 °C and 1000 g m^{-2} day^{-1} at 70 °C. In intermittent immersion such as is experienced in the cleaning of tinned ware by alkaline detergents, however, the rate of corrosion is affected by the nature and concentration of the solution, as these affect the time required for the removal of the oxide film at each fresh immersion.[43] Saturated ammonia solutions do not attack tin, possibly because of the negligible oxygen content, but more dilute solutions behave like those of other alkalis of comparable pH. In aerated alkaline conditions, 0.01–1 M NaOH, corrosion of tin was confirmed to be under cathodic control, and additions of other species, apart from chromate, were found to make little difference to the corrosion rate.[44]

The removal of oxygen from an alkaline solution, as by the addition of sodium sulfite, can prevent corrosion unless the tin is in contact with another metal, such as steel, from which hydrogen can be evolved. Additions of oxidizing agents in small amounts stimulate corrosion, but sufficiently large additions produce passivity. Alkaline chromate solutions in the passivating range produce a film containing chromium oxide, which has some protective value.[19,45]

3.12.3.5 Corrosion in Foodstuffs

Sulfide solutions, sulfurous acid, and some foodstuffs containing organic sulfur compounds produce stains of sulfide, but the rate of loss of metal is low.[2,3] Milk and milk products are usually without action, although local corrosion has been known to occur in dairy equipment. Beer initially dissolves a trace of tin and this may be sufficient to cause a haze in the liquor, but any corrosion usually slows to an insignificant rate after some time.

In general, near-neutral aqueous products are without action except for possible sulfide staining, or when there are dissolved salts present, some local corrosion. The slight acidity, which may develop in solutions of some organic compounds such as formaldehyde or alcohols can be tolerated. Many organic liquids, including oils (essential, animal, vegetable, or mineral), alcohols, fatty acids, chlorinated hydrocarbons, and aliphatic esters, are without action. The absence of any catalytic action of tin on oxidative changes is helpful in this respect. When, however, mineral acidity can arise, as with the chlorinated hydrocarbons containing water, there may be some corrosion, especially at elevated temperature.

Table 1 Standard reduction potentials and galvanic series compared with tin

Standard reduction potentials (vs. SHE)	*Practical galvanic series in sea water*
$Cu^{2+} + 2e^- \Rightarrow Cu$: +0.34 V	Graphite
$Pb^{2+} + 2e^- \Rightarrow Pb$: −0.12 V	Passive stainless steels
$Sn^{2+} + 2e^- \Rightarrow Sn$: −0.14 V	Copper alloys
$Ni^{2+} + 2e^- \Rightarrow Ni$: −0.25 V	Tin (and tin-rich solders)
$Fe^{2+} + 2e^- \Rightarrow Fe$: −0.44 V	Lead (and lead–tin solders)
$Zn^{2+} + 2e^- \Rightarrow Zn$: −0.76 V	Steel and cast iron
$Al^{3+} + 3e^- \Rightarrow Al$: −1.67 V	Aluminum
$Mg^{2+} + 2e^- \Rightarrow Mg$: −2.37 V	Zinc
	Magnesium

3.12.3.6 Galvanic Corrosion

As indicated from the galvanic series, tin is less noble than copper and stainless steels, but more noble than most other elements in common use (**Table 1**). However, tin is usually ineffective as a sacrificial anode because of its very low self-corrosion rate, and generally, may be safely used in contact with most materials.[46] However, in the presence of species such as citric acid, which can form complex ions, tin will activate with its equilibrium potential moving to more negative values. This effect is important in the corrosion protection of steel cans with tinplate.

3.12.4 Applications

3.12.4.1 Tin Coatings

Interested readers are directed to the dedicated section on tin coatings elsewhere in this volume; only brief comments are provided here. Tin coatings may be applied either by hot-dipping from molten metal or by electroplating from either acid or alkaline solutions[2,3] or by metal spraying.[47] Also, tin may be codeposited during electroplating with a range of other elements such as nickel, cobalt, copper, and zinc, each of which gives rise to a particular property. Tin-plated steel is extremely widely used in the food and beverage canning industry as a container and relies on both the low corrosion rate of tin (can exterior) and the common potential reversal to steel in the presence of natural complexing agents (can interior). In practice, because of the high cost of tin, it is essential to use as thin a layer as possible. Thus, the corrosion protection afforded by the tin is usually supported by internal and external lacquering (organic coating) of the can, and it is therefore, the

organically coated tin that provides the full corrosion protection system for the steel substrate.

The thinnest tin coatings are most efficiently applied by electroplating; where this is likely to give pinholes, surface melt reflowing may be used to improve the performance. Where thicker coatings are required, usually for specialist applications, for example, hot dipping or metal spraying can be used. For example, traditional copper cooking utensils are frequently internally coated with tin to several tens of microns in thickness to prevent the interaction of copper with foods that can lead to the development of taints. The advantage of this process is that when the tin wears off, it can be easily replaced by redipping. Hot-dipped (and sprayed) coatings take advantage of the formation of tin–iron or tin–copper intermetallic species for excellent adhesion of the coating.

3.12.4.2 Solders

Alloys of tin with lead and/or a number of other elements comprise a class of jointing materials known as solders. Solders are used for cost-effective and efficient jointing of many materials, most commonly for copper alloys (e.g., heat exchangers) and steels (e.g., cans). Solders are generally characterized by their ability to flow across or 'wet' the metal to be jointed; such wetting is usually accomplished by the formation of intermetallic compounds between the solder and the substrate. Thus, tin forms Cu_6Sn_5 and Cu_3Sn with copper alloys[48] and FeSn, Fe_3Sn, and $FeSn_2$ with steel.[49] The mechanical properties of these intermetallic species are critical; thus, they provide a metallurgical bonding between the jointed materials, but must not form brittle phases. Many types of tin-based solders are available, for example, Sn–Pb (traditional solders with compositions from 60/40, 50/50, 40/60 depending on use), Sn–Zn (for jointing aluminum), and Sn–Ag (lead-free solder for general use). In particular, for health reasons, there is an increasing use of low-lead, or lead-free solders, especially for joints in water supply systems and in food canning. These environmental concerns are now making the electronics industry also move to lead-free formulations.

Effective soldering requires a clean surface, free of contamination such as greases, oils, and water and the removal of the normal air-formed oxide on the material that is to be jointed. Typically, this is carried out initially by mechanical abrasion or solvent cleaning with the final removal of the tenacious surface oxide via a 'flux'. A flux is, by its nature, corrosive, and hence, careful selection of the flux material is necessary. Otherwise, corrosion in service will be promoted locally.[50] It is, however, possible to select fluxes that are active when hot, but give noncorrosive residues when cold, for example, solid organic acids. If it is necessary to use more vigorous materials, such as zinc chloride, any residues must be fully removed. By the nature of their use as a jointing material, solders are usually presented to a corrosive environment as a small area within a much larger area of another metal. Thus, if the solder is anodic to the metal it joins, and if the corroding medium has good electrical conductivity, damaging corrosion is possible due to the unfavorable (small anode versus large cathode) anode-to-cathode area ratio.

Traditional lead–tin solders are anodic to copper, but soldered joints in copper pipes have been widely used without trouble for cold supply waters; possibly, corrosion is restricted by the deposition of cathodic carbonate scales and the formation of insoluble lead compounds. Hot supply waters tend to be more aggressive, but are likely to still give satisfactory service. However, electrolytes of sufficiently high conductivity, such as seawater, will cause corrosion of soldered joints in copper and copper alloys. In automotive radiators, antifreeze solutions have been alleged to cause corrosion, possibly because materials such as ethylene glycol sometimes detach protective deposits. Sodium nitrite, valuable as a corrosion inhibitor for other metals in a radiator, tends to attack solders, but sodium benzoate is safe, and in addition, protects the soldered joint against the action of nitrites.[51]

In environments in which tin is less readily corroded than lead, corrosion resistance of the alloy decreases as the lead content increases; the decrease may, in some circumstances, be sharp at a particular composition. In the more corrosive media, a sharp increase of corrosion rate is observed as the lead content increases beyond 30%. However, in waters with low contents of dissolved salts, the corrosion rate increases slowly with lead content up to ~70% and then rises more steeply. Selective dissolution of tin has been reported to occur in prolonged contact of solders with solutions of anionic surface active agents.[52]

In view of the known tendency for lead to be released in supply waters from conventional soldered joints,[53] there is an accelerating trend away from the use of lead-containing solders in contact with potable water, which is also being driven by legislation.[54] The effects of galvanic corrosion of one of the substitute alloys (Sn–3Ag) in contact with a number of other metals, including copper, have therefore been studied.[55]

3.12.4.3 Tin Interconnections

Tin-based jointing alloys (solders) are the materials of choice for connections and interconnections in the electronics industry. Traditionally, a eutectic tin–lead (67Sn–33Pb) alloy has been used, but the legislative driver for the removal of lead has also affected this sector, which has now effectively moved to encompass the use of lead-free solders. The performance characteristics of electronic connectors is dominated by (1) local galvanic corrosion between different metals, either in contact or as a coating and influenced by applied direct currents; (2) the corrosion of the soldering alloy, which is controlled largely by the presence of residues from various manufacturing and assembly operations; (3) fretting forms of corrosion damage induced by repeated making and breaking of electrical contacts; and (4) the formation of metal whiskers of tin that tend to be produced as a result of applied stress and voltage. All of these phenomena can lead to either a reduction of performance or an outright failure via a variety of mechanisms,[55] the most important of which are increases in the contact resistance with time and short-circuit current paths between contacts because of corrosion products, soldering residues (i.e., fluxes), and whiskers of tin.

Many lead-free solders are based on Sn–Ag–Cu formulations, with Sn–3.5Ag, Sn–0.7Cu, and Sn–3.8Ag–0.7Cu widely in use because of their good mechanical and wetting properties. In 3.5% sodium chloride solution, lead-free solders show an improved corrosion resistance compared with Sn–Pb solder because of lower active currents and lower passive current densities and that the Sn–Ag material was the most resistant.[56] The contact resistance and fretting corrosion resistance of lead-free solders were measured as a function of time.[57] In this case, the contact resistance of the conventional eutectic solder fell more quickly than the lead-free solder; however, the fretting corrosion resistance of Sn–Ag materials was generally improved. The lead-free solders performed significantly better than did the lead-containing solders after steam aging at 93 °C, 100% RH and after mixed flowing gas testing (in 200 ppb NO_2, 10 ppb H_2S, 10 ppb Cl_2) at 30 °C and 70% RH.

There is, therefore, good evidence that the general and fretting corrosion behavior, and consequent contact resistance changes with time, of lead-free solders is at least as good as, and often better than, traditional tin–lead eutectic solders. However, lead-free solders have a greatly increased tendency for the formation of thin filamentary whiskers of tin, which may lead to failure by short-circuit. Tin whisker formation has been known for many years and was originally thought to be driven primarily by electromigration between two contacts or conductive tracks.[58,59] More recently, however, it has become clear that most whisker growth is a process driven by relief of stresses[60] (i.e., from plating or from contact forces), although electromigration may play a role in more extreme conditions.[61]

3.12.4.4 Bearing Metals

There are several classes of tin-containing bearing alloys for use in lubricating conditions: high-tin alloys (substantially lead-free), bearing alloys containing increasing amounts of lead, and aluminum tin alloys; each class may have minor elements (e.g., antimony, indium) added to promote, for example, intermetallic formation. The corrosion of tin-rich white metal bearings is rare, and consequently, detailed studies of the phenomenon are not extensive in the literature. High-tin alloys are relatively resistant to corrosion in the organic acids that tend to be formed during the degradation of lubricating fluids and the tin salts that form have antioxidant capability. Where corrosion of tin-rich bearings has occurred, it is invariably associated with water ingress.[62] For example, 500 ppm water has been shown to be sufficient to cause corrosion, especially in conjunction with chlorine-based high-pressure additives in the oil.[63]

When free access of salt water to a bearing is possible, the tin–lead 'Babbitt' alloys are not suitable, since they are cathodic to steel shafts. For underwater bearings, alloys with 70% Sn, 1.5% Cu, and the balance Zn, are traditionally used; the possible dissolution of zinc gives cathodic protection to the shaft, although the more easily replaced bearing suffers some corrosion.

References

1. Raynor, G. V.; Smith, R. W. *Proc. R. Soc.* **1958**, *244*, 101–109.
2. Britton, S. C. International Tin Research Institute, Report no. 501, 1975.
3. Hedges, E. S. *Tin and Its Alloys*; Edward Arnold: London, 1960.
4. Ojima, K.; Takasaki, A. *Philos. Mag. Lett.* **1993**, *68*(4), 237–244.
5. Britton, S. C.; Clarke, M. *Trans. Inst. Met. Finish.* **1963**, *40*, 205.
6. Britton, S. C. *Trans. Inst. Met. Finish.* **1974**, *52*(3), 95–102.
7. Langan, J. P. Proceedings of the AESF Annual Technical Conference **1993**; pp 689–691.

8. HSC: Chemistry, version 6.12, Outotec Research Oy, Finland, 2007.
9. Quintin, M.; Hagymas, G. J. *J. Chim. Phys.* **1964**, *61*(4), 541–547.
10. Ross, T. K.; Firoiu, C. *Electrochim. Acta* **1963**, *8*, 877.
11. Stirrup, B. N.; Hampson, N. A. *Surf. Technol.* **1977**, *5*, 429–462.
12. Laitinen, T.; Salmi, K.; Sundholm, G.; Viinikka, P.; Yli-Pentti, A. *Electrochim. Acta* **1992**, *37*(10), 1797–1803.
13. Séby, F.; Potin-Gautier, M.; Giffault, E.; Donard, O. F. X. *Geochim. Cosmochim. Acta* **2001**, *65*, 3041–3053.
14. Shibuya, M.; Endo, K.; Sano, H. *Bull. Chem. Soc. Jpn.* **1978**, *51*(5), 1363–1367.
15. Huang, B. X.; Tornatore, P.; Ying-Sing Li. *Electrochim. Acta* **2000**, *46*, 671–679.
16. Keller, P.; Strehblow, H. H. *Z. Phys. Chem.* **2005**, *219*(11), 1481–1488.
17. Gervasi, C. A.; Alvarez, P. E. *Corros. Sci.* **2005**, *47*, 69–78.
18. Seruga, M.; Metiko-Hukovi, M.; Valla, T.; Milun, M.; Hoffschultz, H.; Wandelt, K. *J. Electroanal. Chem.* **1996**, *407*, 83–89.
19. Britton, S. C.; Bright, K. *Metallurgia* **1957**, *56*, 163–168.
20. Trillat, J. J.; Tertian, L.; Britton, S. C. *Métaux Corros. Ind.* **1957**, *32*, 475–481.
21. Boggs, W. E.; Kachik, R. H.; Pellissier, G. E. *J. Electrochem. Soc.* **1961**, *108*, 6–12.
22. Boggs, W. E.; Trozzo, P. S.; Pellissier, G. E. *J. Electrochem. Soc.* **1961**, *108*, 13–24.
23. Boggs, W. E. *J. Electrochem. Soc.* **1961**, *108*, 124–129.
24. Boggs, W. E.; Kachik, R. H.; Pellissier, G. E. *J. Electrochem. Soc.* **1963**, *110*, 4–11.
25. Okamoto, Y.; Carter, W. J.; Hercules, D. M. *Appl. Spectrosc.* **1979**, *33*(3), 287.
26. Hillman, D. D.; Chumbley, L. S. *Sold. Surf. Mount. Technol.* **2006**, *18*, 31–41.
27. Britton, S. C.; Sherlock, J. C. *Br. Corros. J.* **1974**, *9*, 96–102.
28. Kenworthy, L. *Trans. Faraday Soc.* **1935**, *31*, 1331.
29. Zakipour, S.; Leygraf, C.; Portnoff, G. *J. Electrochem. Soc.* **1986**, *133*, 873–876.
30. Hiers, G. O.; Minarcik, E. J. Symposium on the Atmospheric Corrosion of Non-ferrous Metals, American Society for Testing and Materials, Special Technical Publication #175,1956, 135.
31. Ansell, R. O.; Dickinson, T.; Povey, A. F.; Sherwood, P. M. A. *J. Electrochem. Soc.* **1977**, *124*, 1360–1364.
32. Lau, C. L.; Wertheim, J. *Vac. Sci. Technol.* **1978**, *15*, 622–624.
33. Tompkins, H. G. *Surf. Sci.* **1973**, *39*, 143.
34. Brusic, V.; DiMilia, D. D.; MacInnes, R. *Corrosion* **1991**, *47*, 509–518.
35. Sasaki, T.; Kanagawa, R.; Ohtsuka, T.; Miura, K. *Corros. Sci.* **2003**, *45*, 847–854.
36. Willey, A. R. *Br. Corros. J.* **1972**, *7*, 29–35.
37. Gouda, V. K.; Rizkalla, E. N.; Abd-el-Wahab, S.; Ibrahim, E. M. *Corros. Sci.* **1981**, *21*, 1–15.
38. Leidheiser, H.; Rauch, A. F.; Ibrahim, E. M.; Granata, R. D. *J. Electrochem. Soc.* **1982**, *129*, 1651–1658.
39. Abd El Rehim, S. S.; Zaky, A. M.; Mohamed, N. F. *J. Alloys Compd.* **2006**, *424*, 88–92.
40. Hoar, T. P. *Trans. Faraday Soc.* **1937**, *33*, 1152–1167.
41. Friends, J. N. *J. Inst. Met.* **1928**, *32*, 449–454.
42. Dunkie, S. E.; Craig, J. R.; Lusardi, W. R. *Geoarchaeology* **2004**, *19*, 531–552.
43. Britton, S. C.; Michael, D. G. *J. Appl. Chem.* **1955**, *5*, 402–413.
44. Costa, J. M.; Culler, J. R. *Corros. Sci.* **1976**, *16*, 587–590.
45. Britton, S. C.; Angles, R. M. *J. Appl. Chem.* **1954**, *4*, 351–364.
46. Hoar, T. P. *Trans. Faraday Soc.* **1934**, *30*, 472–482.
47. Vourlias, G.; Pistofidis, N.; Stergioudis, G.; Polychroniadis, E. K. *J. Alloys Compd.* **2006**, *416*, 183–187.
48. Parent, J. O. G.; Chung, D. D. L.; Bernstein, I. M. *J. Mater. Sci.* **1988**, *23*, 2564–2572.
49. Crichton, T. J.; Farr, J. P. G. *Trans. Inst. Met. Finish.* **2004**, *82*, 169–173.
50. Costas, L. P. *Weld. J.* **1982**, *61*, 320–326.
51. Wormwell, F.; Mercer, A. D.; Ison, H. C. K. *J. Appl. Chem.* **1953**, *3*, 22–27, 133–144.
52. Watts, C. *Eng. Mater. Des.* **1961**, *4*(11), 740.
53. Subramanian, K. S.; Sastri, V. S.; Elboujdaini, M.; Connor, J. W.; Davey, A. B. C. *Water Res.* **1995**, *29*, 1827–1836.
54. Linder, M.; Mattson, E. Proceedings of the 7th Scandinavian Corrosion Congress, Trondheim **1975**; pp 19–35.
55. Guttenplan, J. D.; Violette, D. R. *Mater. Perform.* **1980**, *29*(4), 76–81.
56. Li, D.; Conway, P. P.; Liu, C. *Corros. Sci.* **2008**, *50*(4), 995–1004.
57. Wu Ji; Pecht, M. G. *IEEE Trans. Compon. Packag. Technol.* **2006**, *29*, 402–410.
58. Berry, R. W.; Bouton, G. M.; Ellis, W. C.; Engling, D. E. *Appl. Phys. Lett.* **1966**, *9*, 263–265.
59. Vardaman, E. J. *Circ. Assemb.* **2004**, *15*, 22–23.
60. Galyon, G. T.; Palmer, L. *IEEE Trans. Electron. Packag. Manuf.* **2005**, *28*, 17–30.
61. Liu, S. H.; Chen, C.; Liu, P. C.; Chou, T. *J. Appl. Phys.* **2004**, *95*, 7742–7747.
62. Bryce, J. G.; Roehner, T. G. *Trans. Inst. Mar. Eng.* **1961**, *73*, 377.
63. Hiley, R. W. *Trans. Inst. Mar. Eng.* **1979**, *91*(2), 52–66.

Relevant Websites

www.itri.co.uk – The International Tin Research Institute.

3.13 Corrosion of Zinc and its Alloys

F. E. Goodwin
International Lead Zinc Research Organization, Inc., 1822 East NC Highway 54, Suite 120, Durham, NC, USA

This article is a revision of the Third Edition article 4.7 by A. R. L. Chivers and F. C. Porter, volume 1, pp 4:168–4:183,

Glossary

White rust A porous layer of zinc oxide and hydroxide build up on zinc coatings after storage in poorly ventilated conditions.

Abbreviations

ASTM American Society for Testing and Materials
BISRA British Iron and Steel Research Association
GOB Good ordinary brand (reference to zinc purity)
HG High grade (reference to zinc purity)
ISO International organization for standardization
ISO CORRAG International organization for standardization-collaborative atmospheric exposure program
SHG Special high grade (reference to zinc purity)
ZA Zinc aluminum

3.13.1 Introduction

3.13.1.1 History

Despite its frequent occurrence with lead, zinc (boiling point 907 °C) was not known to the ancient world as it was generally lost during smelting by evaporation. Thus, the earliest reports of metallic zinc date only from the fifteenth century in China, while in

Europe zinc was not recognized as a separate element until the eighteenth century when small smelting works were first set up for its production. Its earliest use was in alloying, especially with copper (to produce brass), although its compounds were also used for medicinal purposes (e.g., calamine, $ZnCO_3$) and as pigments. Significant European production of zinc commenced from the early eighteenth century. Prior to the discovery of significant lead–zinc sulfide mineralization (e.g., at Broken Hill in Australia), the principal ore source was zinc carbonate (calamine) found throughout Europe and also in the United Kingdom. Final stimulus for the mass production of zinc did not arrive until the dual discoveries of galvanizing for steel and zinc sheet production in the mid-nineteenth century.

3.13.1.2 Production and Usage

The excellent resistance of zinc to corrosion under natural conditions is largely responsible for the many and varied applications of the metal. In fact, half of the world consumption of zinc is in the form of coatings for the protection of steel from corrosion. Zinc is produced and sold according to standard specifications. Three principal grades are recognized by international standards organizations such as ISO, where the zinc specifications are set forth in ISO 752, and the various national standards organizations such as ASTM (Standard Specification B6). The great majority of zinc sold today is made by the electrolytic process, to a purity of 99.99% zinc, and is commonly referred to as special high grade (SHG) zinc. A lower purity grade termed high grade (HG) has a minimum zinc content of 99.9%; the old standard grade, containing 98.0% minimum zinc, is commonly termed Prime Western or good ordinary brand (GOB) zinc. Common impurities in all three grades are lead, cadmium, and iron. Grades with higher purities than SHG are available but are not referred to in the national or international standard specifications.

Zinc in coatings used to protect steel articles coated after fabrication is generally SHG or GOB zinc, although coatings with minor additions of nickel and tin (added during the galvanizing process) can be used to control the reactivity of the steel. Zinc coatings used in continuous coating of sheet and wire are almost always SHG alloyed with aluminum at various levels around 0.15%, 5%, and 55% Al. Additions of magnesium up to 3% can also be made. Further details on zinc coatings and their performance are described elsewhere.

Zinc casting alloys account for about 20% of annual zinc usage. These alloys are commonly alloyed with 4% aluminum to improve castability and strength. Smaller quantities of zinc alloys containing 8, 12, or 27% aluminum, termed ZA alloys, are also utilized. Die castings can be made readily on account of the low melting points and the good flow properties of zinc alloys. Continuous casting is also used, mainly for production of hollow cylinders for bearing materials but also as stock for machining of zinc shapes.

Another 6% of zinc production is sold in semimanufactured form including rolled zinc roofing, anodes, and dry cell battery cans. Its malleability and ductility make it possible to produce zinc in sheet, strip, and plate form by rolling and as rod and wire by extrusion. Rolled zinc in sheet and strip form is a well-established roofing material, particularly in parts of France and northern Europe. A small amount of copper, up to 1.5%, is added to these alloys to improve creep strength. Brass (discussed in the section on copper alloys) and zinc chemicals (chiefly oxide) make up the balance of major zinc uses.

3.13.2 Physical and Mechanical Properties

The bluish-white form of the unalloyed metal is familiar. It is moderately hard and quite malleable at normal temperatures. The tensile strength and impact resistance of the unalloyed metal, although greater than that of tin or lead, are low, so unalloyed zinc is not to be regarded as a structural metal. The main consequence of using unalloyed zinc in applications subject to prolonged loading is the occurrence of creep deformation. Although brittle at room temperature, pure zinc can be rolled and otherwise formed at about 100 °C.

The physical and mechanical properties of pure zinc are given in **Table 1**. A detailed description of the physical and mechanical properties of zinc alloys for cast and wrought zinc products is given in **Table 1**.[1]

Factors influencing the physical and mechanical properties of zinc pressure diecasting alloys are their composition and the cooling rate after casting. Modern zinc pressure diecastings are made with wall thickness between about 0.75 and 3 mm. Such thin sections, coupled with the high cooling rate of the metal die, results in very uniform microstructures. A very fine distribution of zinc-rich and aluminum rich phases is observed regardless of composition.

Table 1 Mechanical and physical properties of pure zinc

Property	
Tensile strength (cast)	28 MN m^{-2} (4000 psi)
(rolled – with grain)	
(99.95% zinc soft temper)	126 MN m^{-2} (18 000 psi)
(98.0% zinc hard temper)	246 MN m^{-2} (35 000 psi)
Elongation (rolled – with grain)	
(99.95% zinc soft temper)	6%
(98.0% zinc hard temper)	5%
Modulus of elasticity	7×10^4 MN m^{-2} (1×10^7 psi)
Brinell hardness, 500 kg load for 30 s	30
Impact resistance	
(pressed zinc, elongation = 30%)	6.5–9 J cm^{-2} (26–35 ft-lbs in^{-2})
Surface tension – liquid (450 °C)	0.755 N m^{-1}
Surface tension – liquid (419.5 °C)	0.782 N m^{-1}
Viscosity-liquid (419.5 °C)	0.00385 N m^{-1}
Velocity of sound (20 °C)	3.67 km s^{-1}
Coefficient of friction	
(rolled zinc v rolled zinc)	0.21
Hardness	2.5 mohs

Source: Porter, F. C. *Zinc Handbook*; Marcel Dekker: New York, 1991.

Gravity cast zinc–aluminum alloys cool at slower rates, allowing coarser microstructures to be produced. However, the average grain size is still of the order of 1 μm, meaning that galvanic effects between the zinc-rich and aluminum-rich constituents of the microstructure are not observed in practice.

Rolled zinc for architecture and other outdoor uses is generally on the basis of the use of zinc–copper–titanium alloys, where the maximum levels of copper and titanium are 1.5% and 0.15%, respectively. However, the relatively high creep strength attainable in this family of alloys can be realized only if the correct mechanical and thermal treatments have been used. A fine-grained, uniformly corroding sheet product can be obtained.

3.13.3 Corrosion Properties

Both zinc and zinc alloys have excellent resistance to corrosion in the atmosphere and in most natural waters, particularly if the waters are scale-forming. The property which gives zinc this valuable corrosion resistance is its ability to form a protective layer consisting of zinc oxide and hydroxide, or of various basic salts, depending on the nature of the environment. When the protective layers have formed and completely covered the surface of the metal, the corrosion proceeds at a greatly reduced rate.

3.13.3.1 Protective Layers on Zinc

In dry air, a film of zinc oxide is initially formed by the influence of atmospheric oxygen, but this is soon converted to zinc hydroxide, basic zinc carbonate, and other basic salts by water, carbon dioxide and chemical impurities present in the atmosphere. It is possible to form many zinc compounds during the process of corrosion of zinc, particularly in tap water. In atmospheric exposures also, the reactions are complex, but a simplified summary is given in **Table 2**.

Below about 200 °C, the initially formed thin film grows very slowly, is invisible and very adherent. This initially formed layer influences the corrosion resistance of the zinc throughout its life. If the film becomes too thick, it is liable to break away or become porous, when, of course, it ceases to provide protection. Moreover, zinc corrosion products occupy a larger volume than the zinc from which they originated and, as the layer thickens, strains are set up which lead to the production of fissures and cracks.

Factors influencing the formation of protective layers are the local pH and the presence of acidic pollutants in the environment. Zinc forms an amphoteric oxide and therefore, the formation of protective layers is slowed by both acidic and alkaline conditions.

Vernon[2] claims that in outdoor atmospheres the corrosion products consist largely of zinc oxide, hydroxide and combined water, but they also contain zinc sulfide, zinc sulfate, and zinc carbonate. The corrosion products can be complex and the manner in which they develop into passive films is described in great detail by Zhang.[3] **Figure 1** shows how the corrosion rate of zinc varies with the pH[4] and it will be seen from this that the attack is most severe at pH values below 6 and above 12.5, while within this range the corrosion is very slow. The actual rates of corrosion shown in **Figure 1** are not of direct relevance, being from aqueous solutions; however the general shape of the curve has been confirmed for many environments.[5]

The electrochemical properties of zinc also have a large bearing on its corrosion behavior. Zinc is more active than the hydrogen equilibrium potential and most other metals commonly encountered, except magnesium and aluminum, but including those found

Table 2 Zinc corrosion reactions in different atmospheres (schematic)

Type of atmosphere	*Attacking substances*	*Corrosion products composition*	*Relative solubility in water*	*Corrosion rate*
Rural	$O_2 + H_2O + CO_2$	$ZnO \rightarrow Zn(OH)_2 \rightarrow 2ZnCO_3 \cdot 3Zn(OH)_2$	Very low	Very low
Marine	$O_2 + H_2O + CO_2 +$	$ZnO \rightarrow Zn(OH)_2 \rightarrow 2ZnCO_3 \cdot 3Zn(OH)_2 \rightarrow$	Moderate	Low
	$+ Cl$	$\left\{\frac{ZnCl_2 \cdot 4Zn(OH)_2}{ZnCl_2 \cdot 6Zn(OH)_2}\right. + \left\{\frac{Zn_3OCl_4}{Zn_4OCl_6}\right.$		
Urban and Industrial	$O_2 + H_2O + + CO_2 + + SO_2$	$ZnO \rightarrow Zn(OH)_2 \rightarrow 2ZnCO_3 \cdot 3Zn(OH)_2 \rightarrow \rightarrow ZnS + ZnSO_3 + ZnSO_4$	Good	High

CO_2 has been included as an attacking substance because it participates in the formation of corrosion products. However, CO_2 is also necessary to form stable films.
Source: Thomas, R. *Rust Prevention by Hot Dip Galvanizing*; Nordic Galv. Assoc.: Stockholm, Sweden, 1980; 32 pp.

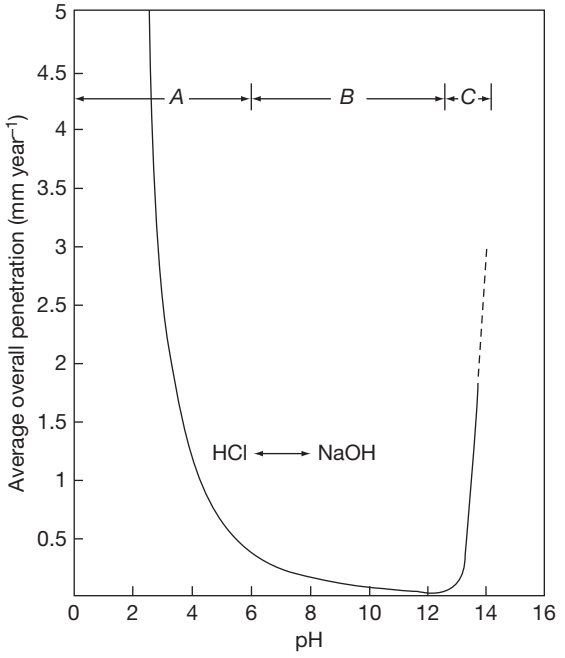

Figure 1 Effect of pH on the rate of corrosion of zinc: (a) rapid corrosion, (b) stable film – low corrosion rate, (c) rapid corrosion. Reproduced from Roetheli, B. E., Cox, G. L.; Littreal, W. B. *Metals and Alloys* **1932**, *3*, 73.

in the less pure forms of zinc. This means that when zinc is in contact with these metals sacrificial electrochemical action (galvanic corrosion) can take place, with zinc forming the anode. Contact with other metals and impurities can therefore cause zinc to corrode rapidly and it is important to avoid intermetallic contacts with metals such as copper, tin, iron or nickel, under immersion in water. On the other hand, the overvoltage for hydrogen evolution on zinc is high, and this can, in some circumstances, lead to a reduction in the corrosion rate, although under normal atmospheric conditions oxygen is generally present in sufficient concentration to act as a cathode reactant.

The severity of bimetallic corrosion is dependent on the ratio of the areas of metals in contact, the duration of wetness, and the conductivity of the electrolyte. For example, other things being equal, seawater, a highly conducting solution, gives rise to more severe bimetallic corrosion than most fresh waters that are of lower conductivity. A film of moisture condensed from the air or rainwater can dissolve contaminants and provide conditions conducive to bimetallic corrosion. Moreover, contaminants already present on the metal surface, such as fingerprints or residues of processing solutions, may absorb moisture from the atmosphere that, although humid, has not actually reached the dew point.

3.13.3.2 Atmospheric Corrosion

3.13.3.2.1 General properties

In dry air, the stability of zinc is remarkable and is conferred by the development of insoluble basic carbonate films after the initially formed oxide layer is exposed to the usual carbon dioxide-containing atmosphere. Once this protective layer of zinc is complete, further attack is negligible. Even under normal urban conditions, such as those in London, zinc sheet, 0.8 mm thick, has been found to have an

effective life of 40 years or more when used as a roof covering and no repair has been needed except for mechanical damage.

Two factors accelerate zinc corrosion in the atmosphere: the duration and frequency of moisture contact and the extent of atmospheric pollution. When moisture is present the initial corrosion product is zinc hydroxide, which is then converted by the action of carbon dioxide to a basic zinc carbonate of composition similar to $ZnCO_3 \cdot 3Zn(OH)_2$.[6] In very damp conditions, unprotected zinc sometimes forms a loose and more conspicuous form of corrosion product known as 'wet storage stain' or 'white rust.'

Industrial atmospheres usually accelerate the corrosion of zinc. When heavy mists and dews occur in these atmospheres, they are contaminated with considerable amounts of acidic substances such as sulfur dioxide and the film of moisture covering the metal can be quite acidic and can have a pH as low as 3. The formation of basic protective films is prevented when zinc is attacked by acidic moisture. Under these conditions the zinc is dissolved but, as the corrosion proceeds, the pH rises, and when it has reached a sufficiently high level basic salts are once more formed and provide further protection for the metal. These usually contain the basic carbonate but may sometimes contain a basic sulfate. As soon as the pH of the moisture film falls again, owing to the dissolution of acidic gases, the protective film dissolves and renewed attack on the metal occurs. Hudson and Stanners[7] conducted tests at various locations in order to determine the effect of atmospheric pollution on the rate of corrosion of steel and zinc. Their figures for zinc are given in **Table 3** and clearly show the effect which industrial contamination has on the corrosion rate. The effect can vary with the direction of the prevailing wind or the ease with which deposits can remain on the surface. Goodwin[8] reported that in acidic atmospheres the increase in corrosion is principally caused by dry deposition of sulfur dioxide and to a lesser extent by acid rain.

In areas near the sea coast, the rates of corrosion may be increased somewhat by the sea spray containing soluble chlorides, but the rates are still much lower than those prevailing in heavily polluted industrial areas. The white corrosion product which is sometimes found under these conditions probably consists of the basic chloride $4Zn(OH)_2 \cdot ZnCl_2$.[6] Chlorides have far less effect than sulfur compounds on the corrosion rate of zinc, but removal of salt deposits by washing is highly beneficial. The effect of chlorides is most harmful when it is combined with sulfurous contamination such as in coastal industrial areas. The effect of sea spray is very different in temperate and tropical areas, in addition to any temperature or humidity effects. Temperate seawater and spray contain higher portions of magnesium salts than those in tropical conditions; these salts help inhibit the corrosion of zinc.

Anderson,[9] reporting on a series of 20-year exposure tests carried out by the ASTM, quotes the average rates of corrosion for various types of environment which are given in **Table 4**.

These results clearly demonstrate; (a) the effect of moisture in increasing the corrosion rate six times in the rural areas compared with the arid areas, and (b) the considerable increase of attack in the industrial areas. Anderson considers that the principal features that control the rate of corrosion of zinc are; (a) the frequency of rainfall and dew fall, (b) the acidity of the atmosphere, and (c) the rate of drying. In situations where the drying of zinc is retarded, corrosion is found to be most severe, for example,

Table 3 Atmospheric corrosion of zinc in various parts of the United Kingdom

Site	*Degree of pollution*	*Standard pollution*[a]	*Corrosion rate (mm year^{-1})*	
			Zinc	*Steel*
Godalming	Slight	0.23	0.001 07	0.042 5
Teddington		0.82	0.002 11	0.063 3
Hornchurch	Moderate	0.92	0.003 24	0.062 7
London (Victoria Park)		1.28	0.004 45	0.075 6
Barking (Greatfield Park)	Heavy	1.60	0.008 43	0.075 0
Salford (Ladywell)		2.31	0.008 43	0.105
Sheffield (Hunshelf Bank)	Severe	3.58	0.012 9	0.107
Billingham (Council Offices)		5.24	0.012 5	0.180

[a]Calculated on weight (mg) of SO_3 absorbed per day by 1 dm^2 on lead dioxide.

the bottom strand of a galvanized wire fence, which is shielded from the sun by grass and weeds.

Ambler[10] has attempted to find a relationship between the corrosion of zinc and iron and atmospheric salinity in the United Kingdom. This followed previous tests in Nigeria,[11] when it was concluded that the governing factor in the corrosion of steel and zinc was airborne salt and that there was a relationship between corrosion and the distance from the sea. In the United Kingdom, however, no such relationship was found to exist and the governing factor in the corrosion of zinc in the atmosphere is confirmed to be the amount of sulfur dioxide pollution.

Environmental concerns have led to studies that have measured the release rate of zinc from rolled zinc sheet during atmospheric exposure. These sheets were exposed either in new conditions or after prior outdoor exposure for durations up to 62 years, at three locations, Stockholm (urban), Olen, Belgium (industrial), and Hoboken, Belgium (urban-highly industrial), for 1 year. **Figure 2** shows both the corrosion rates and the zinc runoff rates as a function of atmospheric sulfur dioxide concentration. The runoff rate is observed to be considerably lower than the corrosion rate, and the corrosion rate was independent of the age of the preweathered panel, depending only upon the sulfur dioxide concentration of the atmosphere.[12] After release from the panel, most dissolved zinc quickly combines with the cations in the soil or water, leaving very little available for interaction with living forms.[13]

Table 4 Further examples of atmospheric corrosion rates for zinc

Atmosphere	*Corrosion rate (mm year^{-1})*
Industrial	0.006 4
Sea Coast	0.001 5
Rural	0.001 1
Arid	0.000 18

Source: Anderson, E. A. Am. Soc. Test. Mater. Special Publication No. 175, June 1955.

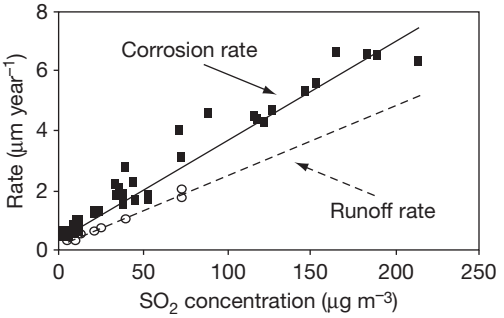

Figure 2 Experimental values and regressions (lines) for corrosion rates (squares) and runoff rates (circles) of zinc. Reproduced from Odnevall Wallinder, I., *et al. Corros. Sci.* **1988**, *40*(11), 1977–1982.

3.13.3.2.2 White rust

When condensation occurs on a fresh zinc surface, as may easily happen during storage in an environment with restricted circulation in which the temperature varies periodically, zinc is generally attacked by the oxygen dissolved in the water, owing to differential aeration between the edges and the centers of the drops. In this form of corrosion, a porous layer of zinc oxide and zinc hydroxide builds up. If the supply of air to the surface is restricted, insufficient carbon dioxide is supplied for the normal formation of a protective zinc carbonate layer. The resulting corrosion product, termed white rust or wet storage stain, is voluminous and porous, and adheres only loosely to the zinc surface. Consequently, it does not protect the zinc against corrosion, which can therefore proceed so long as there is moisture on the zinc surface.

This type of corrosion can take place on any new surface of zinc and is best prevented by storing the metal in a dry, airy place until a protective layer has been formed. Zinc, which has been properly aged in this way, is safe against white-rust formation. Various methods are employed to prevent white rust. Passivation treatments (e.g., chromate or phosphate) are widely used for zinc-plated articles and for galvanized sheet, and occasionally for zinc die castings. Fatty substances, such as oils or lanolin, are sometimes used to protect larger items. Light build-up of white rust can be removed by swabbing with dilute ammonia solution, for example: 19 ml ammonia, 6 g ammonium chloride, 6 g ammonium carbonate, and 71 ml tap water. The area should be well-ventilated and protective goggles should be worn by the operator.

3.13.3.3 Aqueous Corrosion

3.13.3.3.1 Corrosion of zinc in natural waters

Fundamentally, the rate of zinc corrosion depends upon the type, quantity and mode of corrosion products. When zinc is immersed in distilled water containing dissolved oxygen, a protective film, probably

consisting of zinc hydroxide, is slowly formed and this extends over nearly the whole surface. At certain points the metal seems to remain uncovered and local attack continues, resulting in pitting. This may be quite serious and can lead to the rapid penetration of a zinc sheet. The attack does not spread over the whole surface of the zinc but is confined to these small local areas, although similar pits are liable to appear at points in a vertical line directly below the seat of the original corrosion. It has been suggested that the areas attacked occur where particles of corrosion product have fallen and are resting on the surface, shielding it from oxygen. The point thus shielded becomes anodic and suffers corrosion. If oxygen replenishment is made uniform over the whole surface, for example, by 'whirling'[9] a zinc plate, pitting is avoided and the protective film of zinc hydroxide is found over the entire surface. However, too much agitation can sweep away corrosion products before they can become protective. The corrosion rate of zinc in distilled water ranges between 15 and 150 μm year^{-1} and depends strongly on the amount of dissolved oxygen and carbon dioxide.[3] Corrosion data are shown in **Table 5**.

The factors affecting zinc corrosion in distilled water – oxygen, carbon dioxide content, and agitation – also affect corrosion of zinc by natural waters. Natural waters all contain dissolved salts to a certain extent and these tend to form a scale on the surface of the metal. As such scales have a protective affect it is to be expected that corrosion will be less severe in natural, particularly hard, water. This is in fact true and it is often found that distilled water is more corrosive than natural waters. Whether the water is scale forming or not is determined by calculating the Langlier saturation index, a relationship involving concentrations of carbon dioxide, calcium bicarbonate and calcium carbonate together with pH described elsewhere in this handbook. The effect of free carbon dioxide in a hard tap water and in equal mixtures of hard water and low conductivity water is shown in **Figure 3**.

The effect of pH on the corrosion of zinc has already been mentioned. In the range of pH values from 5.5 to 12, zinc is quite stable and as most natural waters come within this range, little difficulty is encountered in respect of pH. If the pH is below the value at which the water is in equilibrium with calcium carbonate, the calcium carbonate will tend to dissolve rather than form a scale. The same effect is produced in the presence of considerable amounts of carbon dioxide, which also favors the dissolution of

Table 5 Effect of oxygen on the corrosion of zinc in distilled water

Test condition[a]	*Temperature (°C)*	*Corrosion rate*[b] *(μm year^{-1})*
Boiled distilled water; specimens immersed in sealed flasks	Room	25.4
Boiled distilled water; specimens immersed in sealed flasks	40	48.3
Boiled distilled water; specimens immersed in sealed flasks	65	83.8
Oxygen bubbled slowly through the water	Room	218.4
Oxygen bubbled slowly through the water	40	348.0
Oxygen bubbled slowly through the water	65	315.0

[a]High grade zinc specimens, in duplicate, immersed for 7 days.
[b]The corrosion rate was calculated after removal of corrosion products.
Source: Anderson, E. A.; Reinhard, C. E. In *Corrosion Handbook*; Uhlig, H. H., Ed.; Wiley: New York, 1948.

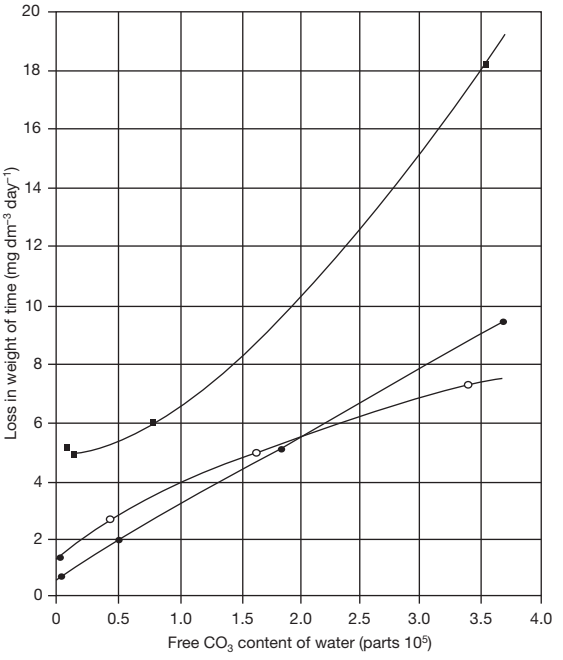

Figure 3 Effect of free carbon dioxide on the corrosion of zinc in different waters: (■) conductivity water; (○) hard water; (●) equal mixture of hard and conductivity water. Reproduced from Kenworthy, L.; Sith, M. D. *J. Inst. Met.* **1944**, *70*, 463–489, with permission from Maney Publishing.

calcium carbonate. In addition, it is important to note that small amounts of metallic impurities (particularly copper) in the water can cause quite severe corrosion and as little as 0.05 ppm of copper in a domestic water system can be a source of considerable trouble with galvanized tanks and pipes. The copper deposits as small cathodic particles on the zinc surface and thereby accelerates localized pitting corrosion.

3.13.3.3.2 Corrosion in seawater

Seawater contains considerable amounts of soluble salts, particularly sodium chloride, which is present in concentrations from 1 to 25%. The North Sea, for example, contains about 3% sodium chloride, 0.47% magnesium sulfate, 0.2% magnesium chloride, and 0.1% calcium chloride. The carbon dioxide content is about 0.0005–0.01% and the pH is between 7.6 and 8.1. The high chloride content would tend to increase the rate of corrosion and this usually takes the form of pitting under these conditions. The corrosive influence of the chloride ions is, however, inhibited by the presence of magnesium and calcium ions by virtue of the formation of a protective layer of magnesium and calcium salts (calcareous scale). Typical corrosion rates of zinc range from 25 μm year^{-1} in the tropics to half that in temperate seas such as the North Atlantic. In tidal areas, where zinc surfaces are immersed twice daily, or areas washed by waves, the corrosion rate is typically twice that of completely immersed zinc.

The effect of the magnesium salts has been clearly demonstrated by Schikorr.[14] Zinc immersed in a solution containing 30 g dm^{-3} of sodium chloride showed a weight loss of 198 g m^{-2} after 14 days. When the solution contained in addition 12 g dm^{-3} of magnesium chloride, the loss in weight was only 4 g m^{-2} after the same period. Artificial seawater was also tested and gave a weight loss of 5 g m^{-2}.

Zinc roofs are quite satisfactory at the coast, where they receive a large amount of saltwater spray, and many British piers have been covered with sheet zinc, which has lasted 50 years and more. Most of the zinc actually immersed in seawater is in the form of zinc coatings, the behavior of which is discussed elsewhere. Experience with these coatings has proved the value of zinc in seawater compared with many other metals in this environment.[15]

3.13.3.3.3 The effect of temperature

It is found that temperature has a marked effect on the rate at which zinc corrodes in water. The corrosion rate in distilled water reaches a maximum in the temperature range 65–75 °C, Figure 4.

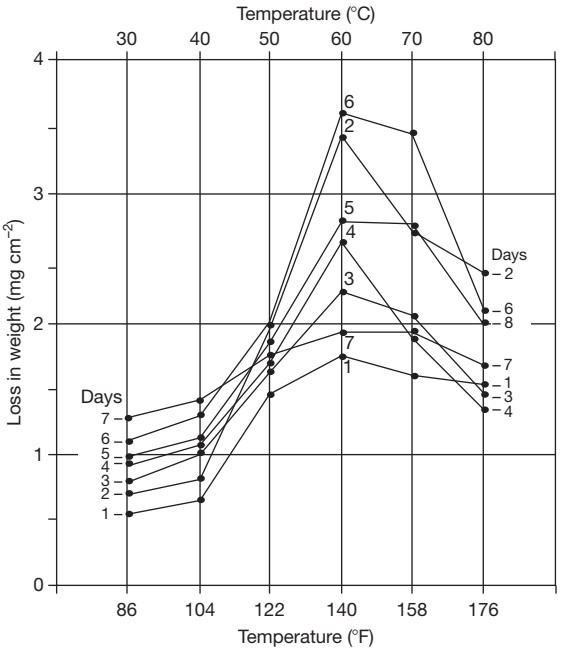

Figure 4 Effect of temperature on the corrosion rate of zinc sheet in distilled water. Reproduced from Maconachie, J. E. *Trans. Electrochem. Soc.* **1934**, *66*, 213–221.

This variation in the corrosion rate with temperature is attributed to changes in the nature of the protective film. At lower temperatures the film is found to be very adherent and gelatinous, while at temperatures around 50 °C it becomes distinctly granular in character and much less adherent. Above 75 °C it again tends to become more adherent and assumes a very compact and dense form. It is believed that the granular coating formed at temperatures around 70 °C is more porous than the others and permits greater access of the dissolved oxygen to the metal. Casting alloys are considerably more corrosion resistant in water than pure zinc because they contain aluminum. Figure 5 shows the effect of temperature on corrosion of three casting alloys with 8%, 12%, and 27% aluminum. The temperature where maximum corrosion rates are observed is 60 °C.

3.13.3.4 Soil Corrosion

The factors influencing the corrosion of metals in soil are more numerous than those prevailing in air or water and the electrochemical effects are more pronounced. Moreover, soils vary widely in their composition and

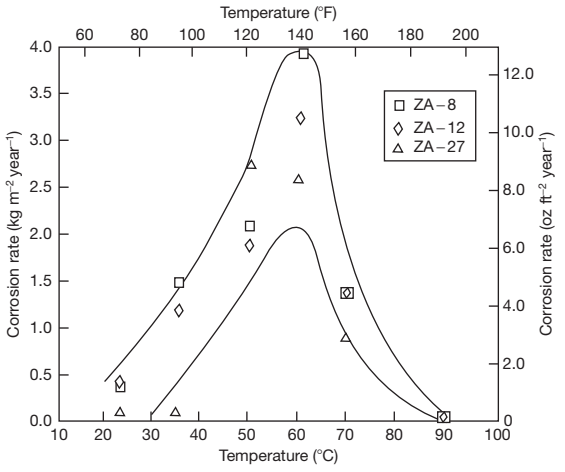

Figure 5 Effect of temperature on the corrosion rate of ZA alloys in tap water, 30–45 day tests. Reproduced from Belisle, S.; Dufresne, R. In International Symposium on Zinc–Aluminum (ZA) Casting Alloys, Toronto, Canada; Canadian Institute of Mining and Metallurgy: Montreal, 1987; pp 109–126.

behavior even over very short distances. Many chemical elements are present in soils, but the ones influencing zinc corrosion behavior are those which are soluble in water, notably base-forming elements such as sodium, potassium, calcium and magnesium. Acid-forming groups such as carbonate, bicarbonate, chloride, nitrate, and sulfate are equally important to consider. The electrical resistivity of soils also strongly influences zinc corrosion rates and is determined by the nature and concentration of the ions formed by chemical salts dissolved in the soil moisture. Moreover, zinc corrosion rates are influenced by physical properties of soils that determine their permeability to air and water. Because of the wide variety of possible soil conditions, it is difficult to obtain reliable data. It is evident, however, that zinc has considerable resistance to corrosion when buried and the severest attack is caused by soils, which are acidic or contain large amounts of soluble salts. A general guideline is that a 600 g m^{-2} galvanized coating on steel will provide protection for 10–20 years in inorganic oxidizing soils but half of this time in inorganic reducing soils.

In tests carried out by the National Bureau of Standards in the United States (now the National Institute of Standards and Technology)[16] specimens of copper alloys, lead, zinc, and zinc alloys were buried at a number of different sites for periods varying from 11 to 14 years. The soils tested covered a pH range from 2.6 to 9.4 and resistivities ranged from 60 to 17 800 Ω cm. The weight losses and maximum depths of pitting were recorded and the results indicated that the most severe corrosion occurred in soils of poor aeration having high acid and soluble-salt contents. Details are shown in **Table 6**.

Although there was no significant difference in weight loss between rolled zinc and zinc alloys, the maximum penetration of the alloys definitely appeared to be greater than that of rolled zinc. BISRA tests on galvanized steel pipe buried for five years at five different sites are described by Hudson and Acock.[17] The galvanized pipes resisted corrosion rather better than steel at all sites. Galvanized pipes of small diameter are frequently used to provide underground water services in farms and similar establishments, and little trouble is experienced.

3.13.3.5 Corrosion Resistance of Zinc in Chemical Environments

3.13.3.5.1 Acids and alkalis

Zinc dissolves in liquids whose pH is below about 5 and above 12.5. Many acids have pH levels below 5 and therefore will attack zinc, while only the stronger solutions of most alkalis would cause any corrosion. Zinc dissolves in caustic soda solution to form zincate ions, that is, ZnO_2^{2-}. Many other factors including agitation, aeration, temperature, polarization, and in some cases the presence of inhibitors may considerably influence the corrosion rate of zinc.

Owing to the high overpotential for hydrogen evolution pure zinc is attacked only very slowly by dilute sulfuric and hydrochloric acids, but impure zinc dissolves quite readily, evolving hydrogen. Thus, when ordinary commercial zinc is placed in a dilute acid it immediately starts to corrode, at first relatively slowly. As corrosion proceeds the impurities present are reprecipitated as a black metallic sponge which may further accelerate the reaction owing to the increased surface area of low overpotential cathodic sites, for example, copper. Some metallic impurities, notably aluminum, retard the corrosion of zinc by acids. This is due to the production of highly protective films. Other metals, such as tin and lead, retard the corrosion initially but after a few hours they are deposited as a metallic sponge, resulting in corrosion as rapid as with ordinary zinc.

Zinc is widely used in contact with many milder chemicals such as detergents and agricultural chemicals. In most cases, zinc or zinc-coated steel comes in contact with these chemicals during handling, packaging and storage.

Table 6 Corrosion of rolled zinc in various soils in the United States

		Average metal loss (μm year^{-1}) and maximum pit depth (mm) after burial for years stated[b]							
Soil type	*Metal*[a]	*Loss after 2.1 years*	*Maximum pit depth*	*Loss after 4 years*	*Maximum pit depth*	*Loss after 9 years*	*Maximum pit depth*	*Loss after 12.7 years*	*Maximum pit depth*
Inorganic oxidizing acid soils									
Cecil clay loam	P	4	0.25	6	0.25	5	0.33	7	0.43
	A	7	0.38	6	0.56	5	0.66	10	0.79
Hagerstown loam	P	8	0.81	6	0.64	3	0.33	4	0.41
	A	9	0.89	7	0.69	4	0.40	5	0.51
Susquehanna Clay	P	12	0.23	13	0.23	6	0.30	6	0.23
	A	9	0.30	7	0.41	4	0.48	6	0.81
Inorganic oxidizing alkaline soils									
Chino silt loam	P	10	0.76	8	0.91	7	1.42	6	1.42
	A	26	0.56	9	0.41	10	0.84	9	1.29
Mojave fine – gravelly loam	P	34	0.64	28	0.71	4	1.12	18	0.86
	A	79	2.41	54	P	7	0.91	17	P
Inorganic reducing acid soils									
Sharkey clay	P	10	0.30	11	0.20	5	0.36	7	0.36
	A	11	0.36	13	0.71	6	0.91	9	0.94
Acadia Clay	P	40	0.76			22	0.71		
	A	57	0.84			26	1.32		
Inorganic reducing alkaline soils									
Docas clay	P	14	0.41	6	0.46	7	2.01	7	0.53
	A	28	0.46	29	0.51	13	1.14	13	1.32

Continued

Table 6 Continued

Soil type	Metal[a]	Average metal loss (μm year^{-1}) and maximum pit depth (mm) after burial for years stated[b]							
		Loss after 2.1 years	Maximum pit depth	Loss after 4 years	Maximum pit depth	Loss after 9 years	Maximum pit depth	Loss after 12.7 years	Maximum pit depth
Merced silt loam	P	34	1.42	17	2.59+	17	2.13	D	P
	A	44	0.86	25	2.03+	9	0.97	D	P
Lake Charles	P	22	0.25	36	0.66	21	0.74	30	1.35
clay	A	48	0.64	57	0.76	32	1.42	33	2.21
Organic reducing acid soils									
Carlisle muck	P	14	<0.15	18	0.25	22	0.56	15	0.46
	A	20	0.30	18	0.91	20	2.44	18	2.51
Tidal marsh	P	24	0.66	24	0.86	9	0.64	14	1.09
	A	20	0.30	16	0.61	16	0.86	15	1.19
Muck	P	67	0.97	54	1.68	35	1.47	25	1.27
	A	81	2.74+	72	P	38	P	35	P
Rifle peat	P	93	1.35	110	2.54	D	P	D	P
	A	164	1.88	172	P	D	P	D	P
Cinders									
Cinders	P	93	2.72+	130	2.99+	D	P	D	P
	A	232	1.48	150	P	D	P	D	P

[a]P = High Grade zinc (58 × 300 × 4 mm) sheet; A = Alloy (4.0%Al + 1.0%Cu) sheet (112 C 170 × 3 mm).
[b]P, perforated; D, specimen destroyed; +, one specimen perforated. Results are usually averaged of two specimens.
Source
Romanoff, M. Underground Corrosion, U.S. Government Printing Office, for National Bureau of Standards, Washington, DC, Circular 579, 1957; 227 pp.

3.13.3.5.2 Salt solutions

When a zinc sheet is immersed in a solution of a salt, such as potassium chloride or potassium sulfate, corrosion usually starts at a number of points on the surface of the metal, probably where there are defects or impurities present. From these it spreads downwards in streams, if the plate is vertical. Corrosion will start at a scratch or abrasion made on the surface but it is observed that it does not necessarily occur at all such places. In the case of potassium chloride (or sodium chloride) the corrosion spreads downwards and outwards to cover a parabolic area. Evans[18] explains this in terms of the dissolution of the protective layer of zinc oxide by zinc chloride to form a basic zinc chloride, which remains in solution.

Feitknecht[19] has examined the corrosion products of zinc in sodium chloride solutions in detail. The compound on the inactive areas was found to be mainly zinc oxide. When the concentration of sodium chloride was greater than 0.1 M, basic zinc chlorides were found on the corroded parts. At lower concentrations a loose powdery form of a crystalline zinc hydroxide appeared. A close examination of the corroded areas revealed craters, which appeared to contain alternate layers and concentric rings of basic chlorides and hydroxides. Two basic zinc chlorides were identified, namely $6Zn(OH)_2{\cdot}ZnCl_2$ and $4Zn(OH)_2{\cdot}ZnCl_2$. These basic salts and the crystalline zinc hydroxides were found to have layer structures similar in general to the layer structure attributed to the basic zinc carbonate which forms dense adherent films and appears to play such an important role in the corrosion resistance of zinc against the atmosphere. The presence of different reaction products in the actual corroded areas leads to the view that, in addition to action between the major anodic and cathodic areas as a whole, there is also a local interaction between smaller anodic and cathodic elements.

3.13.3.5.3 Organic chemicals

Most organic liquids, other than the stronger acids, attack zinc only slowly. Zinc is therefore suitable for storage tanks for liquid hydrocarbons such as motor fuels, for phenols and for trichlorethylene degreasers. Particular care must be taken to exclude moisture, because corrosion at the interface between moisture and hydrocarbon fuels may be considerable. Zinc or zinc-coated vessels are not recommended for use in contact with acid foodstuffs, but are regularly used for dry foods. Zinc is essential in the human diet; the typical recommended daily allowance is 15 mg.

3.13.3.6 Cathodic Protection by Zinc Anodes

Zinc should give a potential of −1.05 V versus $Cu/CuSO_4$ and should have a driving potential of about −0.25 V with respect to cathodically protected steel. Zinc is therefore sufficiently negative to act as a sacrificial anode and its first use for such purposes was on the copper-sheathed hulls of warships more than a century ago. The first attempts to fit zinc anodes to steel hulls, however, were a complete failure, for the sole reason that it had not been realized that the purity of the zinc was of paramount importance. The presence of even small amounts of certain impurities leads to the formation of dense adherent films, which cause the anodes to become inactive.

The major harmful impurity is iron and by keeping the iron content to less than 15 ppm it became possible to produce perfectly satisfactory anodes of zinc.[20,21] Alternatively the effect of the iron can be neutralized by alloying the zinc with certain metals, among which aluminum and silicon or cadmium have been found to be particularly effective. However such alloyed anodes are susceptible to intercrystalline corrosion particularly above 50 °C and for such temperatures the purer anodes are preferable. The presence of cadmium causes the corrosion product to fall away evenly, leaving an active surface.

Zinc alloy anodes are generally very efficient, owing to their nonpolarizing characteristics and to the absence of parasitic reactions when buried or immersed. Therefore, as zinc's 'self-corrosion' is very small, the anode's high efficiency of 85–95% holds throughout the current-density range, whereas the efficiency of magnesium, about 50–55% at high current densities, may fall to only 30% at low current densities. The use of these zinc alloys for reference electrodes to monitor some hull-protection schemes or as permanent reference cells located along pipelines, underlines their nonpolarizing characteristics. The electrochemical equivalent of zinc indicates that 10.5 kg should give 1 A year^{-1}, but in practice this amount of charge is given by about 11–12 kg of zinc compared with 7.7–9 kg of magnesium. As the cost of zinc is relatively low, zinc anodes are found to be very economical. Moreover, as zinc is fairly dense, the volume consumption is about three times lower than that for magnesium and the dimensions of the zinc anode are correspondingly smaller.

The driving potential of zinc to cathodically protected steel is 200–250 mV and this is considerably lower than the 700 mV given by magnesium. While

this value is ideal in seawater or other electrolytes of low resistivity, the use of zinc is not always practicable in environments of higher electrical resistance. For example, it is not likely to be of much use for protecting large underground systems in a high resistivity soil, but on the other hand it proves to be of value for smaller underground units, such as storage tanks, situated in soils of resistivity below about 3000 Ω cm. Olive,[22] for instance, in the United States, discussed the application of zinc anodes for protecting underground equipment at gasoline filling stations. Larger installations, which employ a considerable number of zinc anodes, are the protective schemes for the steel gas mains in Houston and New Orleans.[23] Of a total of some 1200 galvanic anodes in New Orleans about 1000 are of zinc. This is a good example of a case where a system of zinc anodes can be used to protect a large underground installation under the right soil conditions. Zinc is used quite widely for the protection of bare service pipes of small diameter and is receiving increased acceptance for the protection of large-diameter coated pipes in built-up areas in order to minimize interference on adjacent mains. It is also used for protecting galvanized cold-water tanks.

Where the use of zinc anodes is practicable, the low driving potential is a great advantage as the resistance of the steel to be cathodically protected is the controlling resistance and the current output of the anode varies with the requirements of the cathode. Thus it can be said that zinc anodes are largely self-governing.

By far the largest use of zinc anodes is in seawater for the protection of ships' hulls and of North Sea pipelines and drilling rigs. The high conductivity of the seawater and the excellent natural resistance of zinc to corrosion make it very effective in this application. Many examples of trials with zinc anodes on ships can be quoted and the US Navy has done much work in this respect. One example is a paper by Carson,[21] describing zinc anodes attached directly to the hull, which were found to have a life of 8–10 years. This paper also gives the results of tests carried out at the Pacific Naval Laboratory, showing the effect of various impurities in the zinc. Carson looks into the economics of zinc alloy anodes and concludes that for small and medium hull sizes, for example, 1400 m^2 wetted hull area, zinc alloy anodes are more economical than the most competitive alternative systems available and have the additional advantages of more even current distribution, minimum risk of paint-stripping, and maintenance-free long life. For larger hull areas zinc alloy anodes are at least as economic as many alternative systems.

Zinc anodes are made in a variety of shapes and sizes, ranging in weight from 2.25 to 11 kg and in shape from cylindrical rods to rectangular bars. When used underground they are usually placed in a backfill, consisting of gypsum, sodium sulfate and clay, which may be added loose, shipped in a bag around the anode, or obtained in cast form.

The use of zinc anodes together with protection of steel by paint or polymer coatings has been found to confer great advantages of longevity. Even the best types of paint or polymer coatings are porous, so corrosion of the underlying metals must ultimately occur. This may take several years with the best coatings, but the corrosion ultimately destroys the adhesion between the metal and coating so that rapid deterioration takes place. The use of zinc anodes in conjunction with a protective coating greatly improves service life. The corrosion which undermines the coating is prevented and the coating remains firmly attached to give its maximum life. At the same time, the consumption of zinc is reduced dramatically, typically by a factor of 10, because much less steel is exposed and needs protection; a zinc consumption of less than 1.2 kg A^{-1} $year^{-1}$ (i.e., about 0.12 kg $year^{-1}$ m^{-2} of surface to be protected) is a reasonable estimate. The combination of coating and cathodic protection can therefore prove most economical.

3.13.3.7 Zinc–Aluminum (ZA) Casting Alloy Corrosion

3.13.3.7.1 Behavior of the ZA alloys in aerated water from pH 2.0 to 13.0

As part of an International Lead Zinc Research Organization Programme, the corrosion behavior of the ZA casting alloys has been studied at the Noranda Research Center in Canada.[24] Air was bubbled continuously through distilled water flowing through the corrosion cells, its pH being controlled by additions of hydrochloric acid or sodium hydroxide. The temperature was 22 ± 2 °C. Pure zinc sheet was included for comparison. The results are on the basis of immersion times of 4–15 days and show that ZA27 undergoes little attack between pH 6 and 11.5, as does pure zinc. At pH 4.0 there was preferential attack of the decomposed b-phase, whereas at pH 12.8 there was selective dissolution of the aluminum-rich primary dendrites leaving a sponge-like surface. The samples were gravity cast plates.

3.13.3.7.2 Behavior of ZA alloys in neutral salt spray

The ASTM B 117 neutral salt spray test was used with pure zinc and the 4% aluminum diecasting alloy. They were observed to be corroded slightly more than ZA8 and ZA12 during up to 600 h exposure; after longer periods the difference diminished. ZA27 corroded at about one-third the rate of the other alloys, probably because attack occurs on the zinc rich matrix, while ZA27 contains a significantly larger amount of the aluminum-rich phase and behaves like the aluminum die-casting alloy 380 also included in the test.[24]

3.13.3.7.3 Behavior of the ZA alloys at a waste water plant

Gravity die cast ZA alloy test plates and 99.99% pure rolled zinc samples were exposed at a waste water treatment plant in Detroit, MI, USA. The results after one year are summarized in Table 7.[20] High corrosion rates were observed in these sedimentation tanks; by contrast steels with a zinc coating thickness of 85 μm in similar locations in the United Kingdom were found to have substantial residual zinc after 7 years exposure.[20] The Michigan experience showed that the ZA alloys may be better than pure zinc in, for example, the secondary sedimentation tank, but additional protection should be provided unless there is satisfactory performance in a comparable water sample.

Table 7 Corrosion results from 1 year at Detroit, USA Wastewater Treatment Plant

Exposure site	*Sample*	*Corrosion rate ($g\,m^{-2}\,year^{-1}$)*
Atmospheric – Indoor		
Bar screen (high H_2S concentration and humidity)	Zinc	1
	ZA8	2
	ZA12	1
	ZA27	1
Atmospheric – Outdoor		
Primary sedimentation tank (relatively high H_2S and humidity)	Zinc	8–12
	ZA8	9
	ZA12	9
	ZA27	4
Secondary sedimentation tank (relatively high H_2S and humidity)	Zinc	9
	ZA8	10
	ZA12	10
	ZA27	9
Immersed		
Primary sedimentation tank (wastewater with low O_2 containing phosphorus precipitants and coagulants)	Zinc	1239–1601
	ZA8	625
	ZA12	2181
	ZA27	1209
Secondary sedimentation tank (oxygenated wastewater containing microorganisms)	Zinc	857–1174
	ZA8	324
	ZA12	352
	ZA27	253

A corrosion rate of $g\,m^{-2}\,year^{-1}$ corresponds to a uniform depth of penetration between 50 and 60 μm for the ZA alloys.
Visual examination of the immersed samples showed that ZA8 suffered moderate, uniform corrosion in both tanks. ZA12 showed extensive localized corrosion in the primary tank but slight uniform corrosion with localized corrosion at several spots in the secondary tank. ZA27 suffered extensive localized corrosion over most of the surface in the primary tank but only slight uniform corrosion with several very small pits dispersed all over the surface in the secondary tank.
Source: Progress reports Nos. 9 and 10, Project ZM-287 International Lead Zinc Research Organization, Durham, NC 27713-3210, USA.

3.13.3.8 Intergranular Corrosion

Zinc of high purity is not susceptible to intergranular corrosion. However, this type of corrosion has been observed on zinc alloys in all common environments; the presence of alloying elements, aluminum in particular, is required to cause intergranular corrosion. With aluminum, intergranular corrosion is observed in the composition range 0.03–50% and is most severe at 0.2% because of the precipitation of aluminum-rich precipitates at zinc grain boundaries. The presence of other impurities, especially lead, cadmium and tin, greatly accelerates intergranular corrosion rates in zinc-aluminum alloys; however, maintaining the limits of these impurities within the SHG zinc specification prevents this. Heat treatment tends to increase grain boundary segregation in zinc casting alloys and therefore increases susceptibility to intergranular corrosion. Intergranular corrosion is most severe at higher temperatures and in moist, alkaline environments, especially above a pH level of 10.

3.13.4 Recent Developments

The most important recent development is the availability of computer-based prediction methods for zinc corrosion rates, particularly in atmospheric exposures. Traditionally, corrosion rates, and therefore service lives, have been estimated by using a generalized value for each type of atmosphere: rural, industrial, urban and marine. The certainty of prediction has recently been greatly improved by development of a prediction technique based on neural network modeling and assembly of a database relating zinc corrosion rate to the most important primary variables: annual average rainfall, temperature, relative humidity, sulfur dioxide deposition, sea salt deposition and time of

exposure[25]; 47 sets of data, representing different environments, were used to train the model. The correlation coefficient was greatly improved in comparison with past models; the average error of prediction is $(36 \pm 13)\%$ at 95% confidence interval. The major source of error is believed to be factors other than the six that contribute to corrosion performance in this model. Nevertheless, the accuracy is improved in comparison to the ISO CORRAG model[26,27] and various published regression models.[28–31] The model is available at the internet site http://www.galvinfo.com

Alloys with higher contents of aluminum continue to grow in importance, especially for casting using metal or graphite moulds. Up to about 15% aluminum, the materials are non-sparking and can be used in mines. The corrosion behavior of the zinc–aluminum casting alloys can, for practical purposes, be considered as similar to that of pure zinc, even a factor of two in corrosion rate would be of little significance in a solid product. This is to be contrasted with both the behavior and significance of zinc–aluminum alloys when produced as coatings. In this latter case, the production process is designed to give inherently corrosion-resistant structures and only limited corrosion attack can be tolerated because the coating is thin. With castings, the only corrosion criterion is that harmful impurities such as lead, tin and cadmium, which could cause intercrystalline corrosion, should be below specified and low levels; the difference in levels of general corrosion is unlikely to affect the choice of alloy.

The general corrosion rates of zinc and zinc alloys in practice often have been shown to be much less than in simulated conditions; this is because many naturally occurring substances act as inhibitors. **Figure 1** is a good example of this. The diagram is valuable for the qualitative relationship among acid, neutral and alkaline conditions but, in practice, the corrosion rates are usually very much lower than that indicated by the pH because of the effect of other dissolved constituents and the barrier effect of corrosion products. Seawater around the British Isles is much less corrosive to zinc than tropical seawater.

It should be noted that the atmospheric corrosion data in **Table 3** are related to historic environments. Current use in the industrial areas listed with acidic pollution would show much lower corrosion rates as the corrosion of zinc in the atmosphere is essentially related to the SO_2 content (and the time of wetness) and in many countries the sulfurous pollution has been greatly reduced in the past 30 years. Zinc also benefits from rainwater washing to remove corrosive poultices; therefore, although initial corrosion rates are usually not very different on upper and lower surfaces, the latter tend, with time, to become encrusted with corrosion products and deposits, and these are not always protective.

References

1. Porter, F. C. *Zinc Handbook*; Marcel Dekker: New York, 1991.
2. Vernon, W. H. J. *Trans. Faraday Soc.* **1927**, *22*, 113.
3. Zhang, X. G. *Corrosion and Electrochemistry of Zinc*; Plenum: New York, 1996.
4. Roetheli, B. E.; Cox, G. L.; Littreal, W. B. *Metals and Alloys* **1932**, *3*, 73.
5. Belisle, S.; Dufresne, R. In International Symposium on Zinc–Aluminum (ZA) Casting Alloys, Toronto, Canada; Canadian Institute of Mining and Metallurgy: Montreal, 1987; pp 109–126.
6. Morriset, P. *Zinc Alliages* **1959**, *20*, 15.
7. Hudson, J. C.; Stanners, J. F. *J. Appl. Chem.* **1953**, *3*, 86.
8. Goodwin, F. E. In Proceedings of the 16th International General Galvanizing Conference; European General Galvanizing Association: Caterham UK.
9. Anderson, E. A. Am. Soc. Test. Mater. Special Publication No. 175, June 1955.
10. Ambler, H. R. *J. Appl. Chem.* **1960**, *10*, 213.
11. Ambler, H. R.; Bain, A. A. *J. Appl. Chem.* **1955**, *5*, 437.
12. Odnevall Wallinder, I.; Verbiest, P.; He, W.; Leygraf, C. *Corros. Sci.* **1988**, *40*(11), 1977–1982.
13. Brix, K. V. In Proceedings of the 6th International Conference on Zinc and Zinc Alloy Coated Steel Sheets (Galvatech'04), Chicago, USA; AIST: Warrendale, PA, 2004; pp 815–827.
14. Schikorr, G. *Z. Metallk.* **1940**, *32*, 314.
15. Hudson, J. C.; Banfield, T. A. *J. Iron Steel Inst.* **1946**, *154*, 229.
16. Denison, I. A.; Romanoff, M. *J. Res. Nat. Bur. Stand.* **1950**, *44*, 259.
17. Hudson, J. C.; Acock, G. P. Tests on the Corrosion of Buried Iron and Steel Pipes, Iron and Steel Inst. Special Report No. 45, 1953.
18. Evans, U. R. *The Corrosion and Oxidation of Metals*; Edward Arnold: London, 1960.
19. Feitknecht, W. *Chem. Ind. (Rev.)* **1959**, *36*, 1102.
20. Crennell, J. J.; Wheeler, W. C. *G. J. Appl. Chem.* **1958**, *8*, 571; **1956**, *6*, 415.
21. Carson, J. A. H. *Corrosion* **1960**, *16*, 99.
22. Olive, M. J. *Corrosion* **1960**, *16*, 9.
23. Trouard, S. E. *Corrosion* **1957**, *13*, 21.
24. Progress reports Nos. 9 and 10, Project ZM-287 International Lead Zinc Research Organization, Durham, NC 27713-3210, USA.
25. Zhang, X. G.; Goodwin, F. E. In Proceedings of the 5th International Conference on Zinc and Zinc Alloy Coated Steel Sheets (Galvatech'01), Brussels; Belgium Verlag Stahleisen: Dusseldorf, Germany, 2001; pp 311–316.
26. International Standard, ISO 9223, 1992, International Standards Organization, Geneva, Switzerland.
27. King, G. A. *Corros. Mater.* **1998**, *23*, 88.
28. Knotkova, D.; Boschek, P.; Kreislova, K. *ASTM STP 39*; ASTM: Conshohocken, PA, 1995; p 38.
29. Feliu, S.; Morcillo, M.; Feliu, S., Jr. *Corros. Sci.* **1993**, *34*, 403.
30. Feliu, S.; Morcillo, M.; Feliu, S., Jr. *Corros. Sci.* **1993**, *34*, 415.
31. NeuralShell 2, 4th ed.; Ward System Group Inc.: Frederick, MD, 1996.

Further Reading

Revie, R. W. *Uhlig's Corrosion Handbook*; 2th ed.; Wiley: New York, 2000.
Porter, F. C. *Corrosion Resistance of Zinc and Zinc Alloys*; Marcel Dekker: New York, 1994.
Zhang, X. G. *Corrosion and Electrochemistry of Zinc*; Plenum: New York, 1996.
ASM Handbook: Corrosion; ASM International: Materials Park, OH, 2005; Vol. 13B.
Baboian, R. *Corrosion Tests and Standards – Application and Interpretation*, ASTM Manual Series MNL 201995; ASTM: Conshohocken, PA, 2004.
Townsend, H. E. *Outdoor Atmospheric Corrosion*, ASTM STP 1421; ASTM: Conshohocken, PA, 2002.
ILZRO Engineering Properties of Zinc Alloys, 3rd ed.; ILZRO: Durham, NC, 1989; revised, p 116.
ASTM Symposia on Corrosion Behaviour, ASTM STP 175, 290, 435, 646; ASTM: Philadelphia, 1956, 1959, 1968, 1978.
Slunder, C. J.; Boyd, W. K. *Zinc: Its Corrosion Resistance*, 2nd ed., ILZRO: Durham, NC, 1983.

Relevant Websites

www.zincinfocentre.org – Zinc Development Association/Zinc Information Centre.
www.zincworld.org – International Zinc Association.

3.15 Corrosion of Tantalum and Niobium and their Alloys

S. B. Lyon
Corrosion and Protection Centre, School of Materials, The University of Manchester, Oxford Road, Manchester M13 9PL, UK

3.15.1 Introduction

3.15.1.1 Historical Information

Niobium was the first of this pair of elements to be discovered in 1801 when an English chemist, Charles Hatchett, analyzed a specimen of an unknown mineral that had been brought back from America to London.[1] He found evidence that it contained a new element and named it 'columbium' in homage to its original source. A year later, Anders Ekeberg of the University of Uppsala, analyzed a different mineral, this time originating from Ytterby in Sweden and isolated another previously unknown element. He called his discovery 'tantalum' (after Tantalus, son of the Greek god Jupiter, who was sentenced to eternal frustration); isolating the element had obviously been an extremely difficult task.

Columbium and tantalum were assumed to be the same element for over 35 years until, in 1844, their individual valence states were uniquely identified; columbium had both +3 and +5 states while tantalum exhibited only a +5 state. In order to avoid misunderstanding, columbium was renamed 'niobium' (after Niobe, daughter of Tantalus) inadvertently creating over 100 years of dispute between metallurgists (who stuck to the name columbium) and chemists (who

preferred niobium). However, in 1949, the International Union of Pure and Applied Chemistry ruled that niobium was the official usage, although it is still sometimes referred to by its original name, especially in North America.

3.15.1.2 Occurrence and Production

Current primary sources of tantalum and niobium occur separately with the largest single source of tantalum in the world found in West Australia with additional resources in Canada, China, Brazil, and central Africa; it also occurs in small but significant quantities as a by-product of alluvial tin operations, for example, from southeast Asia.[1] The primary ore 'tantalite' is similar in composition to columbite and is an iron–manganese tantalum oxide ($Fe + MnTa_2O_6$). Regarding niobium, the world's largest deposit is in Brazil with a pyrochlore mineralization ($Na + CaNb_2O_6$); reserves here are sufficient to last over 400 years at current production rates. Columbite-tantalite ('coltan'), a mineral with a ratio of Nb_2O_5:Ta_2O_5 ranging from 10:1 to 13:1, occurs in Brazil, Nigeria, and Australia as well as other countries in central Africa.

The extraction and refining of both the metals is determined by the need to separate the elements from each other. The final product is generally the oxide (Ta_2O_5 or Nb_2O_5) but the extraction and refining process involves mineral concentration, dissolution as complex fluorides and solvent extraction or liquid ion exchange. Tantalum and niobium industrial chemicals are generally produced from the oxides, or occasionally from an intermediary fluoride while the metals are derived from their corresponding precursors by thermal reduction using a reactive metal such as sodium or aluminum. The metallic powders can then be used directly for electronic applications (e.g., capacitors), which, in the case of tantalum, amounts to a significant volume (>50%) of the market. Metal powders are processed further under vacuum using electric-arc or electron-beam melting into ingots for the production of pure material or alloys. Multiple remelting may be required to provide the desired level of metallic purity.

3.15.1.3 Physical Properties

Tantalum and niobium are immediately below vanadium in the same group of the periodic table and, hence, share many general properties. They are characterized by their exceptionally high melting points (respectively the fourth and sixth highest melting points of all the elements) and extremely high corrosion resistance due to very stable passive oxide films.[2,3] Like molybdenum and tungsten, they have body-centered cubic structures but, unlike them, their ductile to brittle transitions are well below room temperature (−150 °C for niobium, −200 °C for tantalum; both influenced by impurity content) and they have considerably lower strengths. Consequently, they have excellent ductility and can be easily formed and worked. However, both materials start to oxidize at significant rates above around 200–300 °C and thus require protection at high temperatures, either by the use of coatings, or by keeping them in a protective atmosphere. Niobium has very similar properties, in general, to tantalum but has the advantage of being about half the density (i.e., twice the volume for the same mass) as well as cheaper. The physical properties of tantalum and niobium are similar to their adjacent colleagues in the periodic table, tungsten and molybdenum, respectively (**Table 1**).

3.15.1.4 Mechanical Properties and Alloying

Commercially pure annealed niobium and tantalum have relatively good mechanical properties with, depending on the level of impurities, strengths similar to, or somewhat less than, annealed austenitic stainless steel (**Table 2**). However, they have low

Table 1 Selected physical properties of tantalum, niobium, molybdenum, and tantalum[3]

	Tantalum (Ta)	*Tungsten (W)*	*Niobium (Nb)*	*Molybdenum (Mo)*
Atomic number	73	74	41	42
Atomic weight (g)	180.95	183.84	92.91	95.95
Density ($g\,cm^{-3}$)	16.6	19.3	8.55	10.2
Melting point (K)	3287	3680	2740	2890
Boiling point (K)	5731	5830	5017	4920
Electrical conductivity ($\times 10^6\,\Omega^{-1}\,cm^{-1}$)	0.0761	0.189	0.0693	0.187
Thermal conductivity ($W\,cm^{-1}\,K^{-1}$)	0.575	1.74	0.537	1.38
Crystal structure	bcc	bcc	bcc	bcc

Table 2 Room temperature mechanical properties of annealed tantalum and niobium compared with molybdenum and stainless steel[4,5]

Property	*Tantalum*	*Niobium*	*Molybdenum*	*Austenitic steel (321)*
Density ($g\,cm^{-3}$)	16.6	8.55	10.2	8.0
Ultimate tensile strength (MPa)	280	125	415	620
Yield stress (MPa)	170	75	300	210
Elongation (%)	50	25	35	45
Young's modulus (GPa)	180	100	330	200
Shear modulus (GPa)	69	37.5	120	86
Poisson's ratio	0.35	0.38	0.32	0.29
Specific strength ($MPa\,g^{-1}\,cm^{-3}$)	16.9	14.6	40.7	77.5
Specific modulus ($GPa\,g^{-1}\,cm^{-3}$)	10.8	11.7	32.3	25

work-hardening rates (so, the yield stress does not increase to particularly high values after work hardening) and relatively low specific modulus. Despite being refractory metals, they have somewhat disappointing strengths at high temperatures compared with, for example, molybdenum and tungsten and, without alloying, the room temperature values are not maintained much beyond about 500–600 °C. This is not a practical constraint for aqueous corrosion applications. Both metals (and their alloys) are increasingly susceptible to oxidation above around 300 °C and must be protected in some way. Alloying (e.g., with tungsten, zirconium, etc.) increases the room- and high temperature strengths considerably but at the expense of ductility.

Both metals form a full range of solid solutions with each other resulting in properties that are generally intermediate between the two metals alone. The main commercial solid solution alloy is Ta–40Nb, which has mechanical and corrosion properties slightly lower than unalloyed tantalum but at lower cost. Tantalum may also be alloyed with tungsten ('Tantaloy'); Ta–2.5W, Ta–7.5W, and Ta–10W being the most common commercial alloys (**Table 3**). More complex systems are based on Ta–8W compositions; for example, T-111: Ta–8W–2Hf, and ASTAR 811C: Ta–8W–1Re–0.7Hf–0.025C (which is precipitation hardened). These alloys are designed principally for high strength maintained to reasonably high temperatures; oxidation protection is required and they are not generally used for corrosion applications. Other alloys include those with molybdenum and titanium (Ta–10Ti); the latter being useful for anode applications, as it is less dense (and cheaper) than unalloyed tantalum.

The mechanical properties and corrosion resistance of niobium are somewhat less than tantalum; however, the material is considerably cheaper. Many niobium alloys were developed to optimize their high temperature properties and these include Nb–10Hf–1Ti (C103), Nb–10W–2.5Zr (Cb–752), and Nb–10W–10Hf–0.1Y (C129Y); these alloys also require protection from high temperature oxidation when in use. However, unalloyed niobium is often specified for corrosion-resistant applications; where a higher strength material is required, Nb–1Zr can be substituted with little or no loss of corrosion resistance.

Table 3 Room temperature mechanical properties of some tantalum and niobium alloys[4,5]

Alloy	*UTS (MPa)*	*YS (MPa)*	*Elongation (%)*
Ta–2.5W	380	240	30
Ta–10W	620	480	30
Ta–40Nb	310	210	40
Nb–1Zr	195	125	20
Nb–10W–2.5Zr (Cb-752)	510	380	20
Nb–10Hf–1Ti (C103)	380	260	20
Nb–10Hf–10W–0.1Y (C129Y)	550	410	20

3.15.1.5 Fabrication

Owing to the high melting point and reactivity of tantalum and niobium with oxygen and nitrogen at high temperatures, which prevents conventional consolidation by melting and casting in air, the materials are normally vacuum-sintered, vacuum-arc melted, or electron-beam melted from compacted powder.[4,5] Vacuum sintering yields metal of fine grain, whereas electron-beam melting yields softer coarse-grained metal which requires cold forging prior to rolling. Metal produced by all three techniques will absorb considerable cold work (up to 90% reduction in area) before annealing is necessary; typically 1 h at 1200 °C

(in a vacuum or inert gas shielded furnace) gives full recrystallization. Both tantalum and niobium are weldable using tungsten-electrode inert gas (TIG), resistance, electron-beam (EB) and plasma-arc welding. However, welding is ideally carried out in an inert-gas chamber to avoid reaction with the atmosphere. Material thinner than 0.5 mm cannot readily be TIG or plasma-arc welded and resistance welding may be used, either in air or under water. EB welding gives the best results and generally produces a contamination-free narrow weld and heat affected zone, irrespective of material thickness.

Niobium and tantalum possess excellent room-temperature fabrication characteristics, similar to copper, and compatible with all conventional production practices. Large reductions (up to 90%) in recrystallized material can be achieved without intermediate process annealing. Secondary fabrication operations such as stamping, drawing, spinning, or forming into complex shapes can be performed at room temperature. Intermediate anneals are dependent on the amount of work involved. In tube drawing or deep drawing, annealed material should be used initially with reductions of up to 60–80%, and multiple draws possible, before reannealing.

All conventional machining techniques may be used with the proviso that niobium and tantalum have strong tendencies to gall, tear, and adhere (weld) to the cutting tool. This makes tool design and selection of machining lubricant very important. Carbide, coated carbide, and high-speed tools may all be successfully used with water-soluble cutting oils; lathe operations can also use soluble oil emulsions. Tools should be kept sharp with steep rake angles and fast deep cuts preferred. In practice, most machining procedures that give a satisfactory result with soft copper will generally also give good results with tantalum and niobium.

3.15.1.6 Applications

The majority of tantalum is used in electronic applications (capacitors, etc.) with another large percentage utilized in fine chemicals for a variety of purposes. Likewise, the vast majority of niobium is used as alloying additions to steels. However, although only a small minority of either element is used as a primary metal or alloy in its own right, they are generally used in critical applications in corrosion control where few other choices exist (**Tables 4** and **5**).

3.15.1.7 Economics and Availability

There are sufficient worldwide reserves of both tantalum and niobium to last several hundred years at the current consumption rates. The price of these materials is subject to significant market fluctuation depending upon market demand and mine supply. However, tantalum is significantly more costly than niobium with a traditional spread of about 4–5 times. For example, at the end of 2008, the consumer price for recycled niobium was US$ 55–60 kg^{-1}, and for tantalum US$ 250–260 kg^{-1} (by contrast, for molybdenum it was US$ 35–40 kg^{-1} and for platinum $30 000–40 000 kg^{-1}).

Table 4 Applications for tantalum[6]

Tantalum product	*Application*	*Technical attributes/benefits*
Tantalum carbide and nitride	Cutting tools and tool coatings	Increased high temperature deformation, control of grain growth, high hardness
Tantalum oxide	Optical lenses	High index of refraction
Tantalum powder	Capacitors	High dielectric constant, excellent temperature stability, small size
Tantalum and tantalum alloy fabricated products	Sputtering targets	Thin coatings of tantalum, tantalum oxide or nitride coatings to semi-conductors
	Chemical process equipment	Superior corrosion resistance, passivity at high anodic potentials
	Cathodic protection anodes	
	Prosthetic devices, hips, plates in the skull Suture clips, fasteners, fixings	Attack by body fluids is non-existent.
	High temperature applications	Melting point is 2996 °C, but protective atmosphere or high vacuum required.
Tantalum alloy additions	High temperature alloys for air- and land-based turbines (e.g., jet engines)	High temperature reliability and strength, resistance to corrosion by hot gases.

Table 5 Applications for niobium[6]

Niobium product	*Application*	*Technical attributes/benefits*
Ferro-niobium (~60%Nb)	Niobium additive to 'high strength low alloy' steel	Imparts a doubling of strength and toughness because of grain refining
Niobium oxide	Optical lenses, non-reflective coatings	High index of refraction, high dielectric constant
Niobium powder	Capacitors for electronic circuits	High dielectric constant, stability of oxide dielectric
Niobium carbide and nitride	Cutting tools and tool coatings	High temperature deformation, controls grain growth, high hardness
Niobium and niobium alloy fabricated products	Sputtering targets for coatings Cathode protection anodes Chemical processing equipment	Superior corrosion resistance, passivity at high anodic potentials
Niobium–1% zirconium alloy	Sodium vapor lamps Chemical-processing equipment	Corrosion resistance, gettering of oxygen, resistance to embrittlement
Ferro-niobium and nickel–niobium	Additions to turbine blade alloys for air- and land-based gas turbines	Increase in high temperature resistance and corrosion resistance, oxidation resistance, improved creep resistance, reduced erosion at high temperatures
Niobium–titanium; Niobium–tin	Superconducting wires for high-field magnets and resulting applications	Superconductivity at cryogenic temperatures

The relatively high cost of tantalum is a significant limiting factor in its use, especially since much of the corrosion performance can be obtained from niobium. Nevertheless, its mechanical properties, which are typically more than twice that of niobium, can compensate to a large extent for the cost difference and are critical in some applications. Where thin linings are used, the long life and high reliability of tantalum equipment can more than offset its higher initial cost. In many applications, tantalum and niobium (or their alloys) are increasingly specified as either complete replacements for noble metals, or as stable substrates for noble metal coatings, at considerably lower cost for essentially equivalent performance.

3.15.2 Electrochemistry

3.15.2.1 Thermodynamics

Tantalum and niobium have remarkably similar electrochemistry that is characterized by their passivity over almost the entire range of pH and potential. Thus, although both metals are more active than zinc, for example, the stability of the passive oxide film against almost all corrosive agents (except fluoride) is remarkable. The only significant difference between the elements, which forms the industrial basis for their separation, is that tantalum displays generally only one oxidation state (+5), while niobium has multiple oxidation states (+2, +4, and +5). This difference is reflected in the *E*–pH (Pourbaix) diagrams shown in **Figures 1** and **2**, which are otherwise notable for their lack of complexity. Thus, niobium should theoretically passivate at intermediate potentials with, successively, NbO, NbO_2, and Nb_2O_5 while tantalum forms just Ta_2O_5.

As mentioned above, the metals are relatively susceptible to fluoride which destroys oxide passivity and must therefore be avoided. Also, although not shown on these diagrams, the +5 oxyanions, niobate (NbO_3^-) and tantalate (TaO_3^-), are stable in strong alkali, which can lead to dissolution of the passive film and activation of the metals under these conditions.

3.15.2.2 Hydride Formation

Both tantalum and niobium have high solubility and diffusivity for hydrogen. Thus, reducing conditions (i.e., under either a significant partial pressure of hydrogen gas or electrochemical cathodic polarization) will inevitably cause hydrogen embrittlement of Nb/Ta metals and their alloys; predominantly because of hydride formation.[7] Significant amount of hydrogen can be absorbed into solid solution, up to several percent[8] and two hydride phases are known, Ta/NbH (β-hydride, generally substoichiometric) and Ta/NbH_2 (γ-hydride, close to stoichiometric); thermochemical phase diagrams have been constructed to demonstrate their regions of phase stability as a function of temperature and hydrogen pressure.[9] Hydride formation from solid solution is accompanied

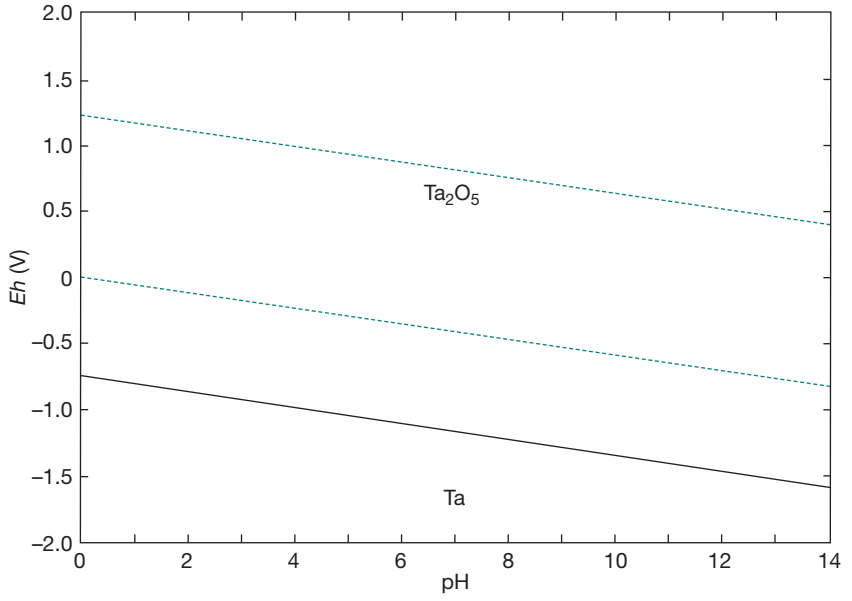

Figure 1 *E*–pH diagram for tantalum at a dissolved metal ion concentration of 10^{-5} M.[3]

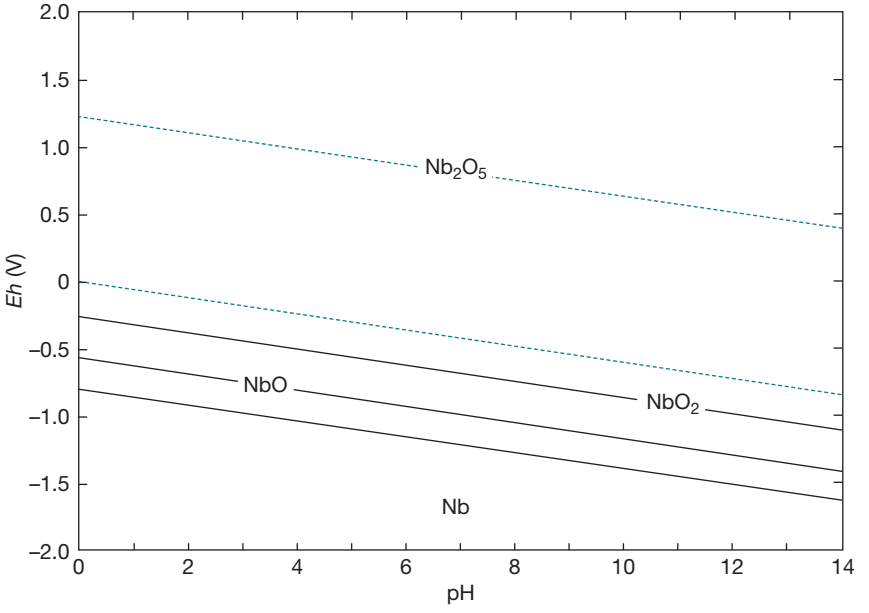

Figure 2 *E*–pH diagram for niobium at a dissolved metal ion concentration of 10^{-5} M.[3]

by significant local strain that causes cracking of the hydride phases and, hence, generation of a population of defects thus lowering the fracture toughness;[10,11] this comprises the main mechanism for embrittlement.

Despite the rapid diffusion rate of hydrogen in the bcc metals ($\approx 10^{-9}\,m^2\,s^{-1}$ at 298 K,[12]) the observed rate of hydride formation is sluggish. The kinetics of hydride formation appears to be limited by the presence of the passive oxide film, which acts as a barrier to hydrogen entry. Alloying significantly increases the rate of hydrogen entry (presumably by disrupting the passive film in some way) and this effect can be utilized for hydrogen storage or for hydrogen permeation membranes.[13] Mechanical deformation of the

alloy (presumably with local cracking of the passive film) can also lead to enhanced hydrogen uptake.[14] Both tantalum and niobium act as cathodes when in contact with almost all other metallic conductors and will, in appropriate environments, become severely embrittled because of hydrogen generation, a situation that should definitely be avoided.

3.15.3 Corrosion Processes

3.15.3.1 Anodizing

The formation of oxide films on tantalum and niobium can be accomplished by direct electrochemical oxidation, generally, either at constant voltage or at constant current. Thus, tantalum and niobium are part of the family of 'valve metals' (including aluminum, tungsten, titanium, zirconium, and hafnium) that form oxides of increasing thickness under increasing anodic polarization. This process is possible because of the thermodynamic stability of the relevant oxides, Ta_2O_5 and Nb_2O_5 (in particular, their insolubility in the electrolytes used and their lack of higher oxidation states). Like all other anodic oxides, they tend to be noncrystalline and incorporate species from the electrolyte into the films during their growth. Indeed, the properties of the formed oxide films can vary considerably as a function of electrolyte used in the anodizing process.

There is great interest in (and indeed applications for) the use of tantalum and niobium in electronic capacitors. This is because the dielectric constants of tantalum and niobium oxides are, respectively, about three and six times higher than anodic alumina, which is the traditional material used for electrolytic capacitors (Table 6). This implies that capacitors of equivalent values (in farads) can be made with smaller volumes, a critical factor in miniaturization of electronic circuitry. Traditionally, it is anodized tantalum that has been used for capacitor applications, predominantly because it has the required electrical properties (thermal stability and low loss at high frequencies). Anodized niobium shows considerably poorer electrical properties despite the favorable factors of its dielectric constant, greater availability and lower cost. This is because, during anodizing, as well as forming the preferred Nb_2O_5, suboxides of NbO and NbO_2 may also form, and these are, respectively, conducting and semiconducting.[15] In recent years, however, there has been a greater understanding of the formation of the anodic film on niobium, as well as novel methods of forming dielectric materials, for example, by atomic layer epitaxy.[16] Consequently, reliable niobium-based capacitors are now becoming available in the market.

Table 6 Electrical properties of various anodic oxides[17,18]

Metal	*Oxide growth ratio (nm V^{-1})*	*Dielectric constant (at 1 kHz)*	*Electrolyte*
Tantalum	3.65	33	0.26 M borate + glycol
Niobium	2.33	60	glycol
Tantalum	3.87	29	0.7 M sulphuric acid
Niobium	2.56	65	0.5 M boric acid +
Aluminium	1.2	9	0.05 M sodium borate

The oxide growth ratio as a function of voltage for anodic film formation is also shown in Table 6. As can be seen, these values can vary considerably from metal to metal and depend on anodizing solution and electrical conditions. The oxide growth ratio derives from a complex interaction of parameters and is principally governed by the densities of metal and oxide, the electric field that is required for the species in the oxide film to migrate, and the efficiency of the film-forming process.

In general, for an anodic oxide film to grow, ions must migrate within the oxide under the influence of the applied voltage (i.e., at a field strength $\approx$100 MV m^{-1}). The current is carried both by anions (e.g., O^{2-}) that migrate inwards and by cations (e.g., Nb^{5+}) that migrate outwards.[19] When outwardly migrating cations reach the oxide–solution interface either they may react with the electrolyte, forming more oxide and thus thickening the film, or they may dissolve in the electrolyte, contributing to loss of current efficiency in film formation. Thus, an electrolyte in which the cations have a high solubility is likely to result in lowered film-formation efficiency. At the oxide–solution interface, the electrolyte may generate oxygen gas, further reducing current efficiency. Finally, the field at the oxide–solution interface encourages incorporation of anions from the solution into the film. Thus, anodic films on niobium and tantalum inevitably incorporate a greater or lesser quantity of anion species from the electrolyte concentrated in the film at the oxide–electrolyte interface.[20]

Generally, anodic films on tantalum are of the barrier type, relatively featureless and reminiscent of barrier films on aluminum.[21] The ionic transport

numbers of tantalum and aluminum have been studied in mixed oxides spanning the composition range. Tantalum ions (Ta^{5+}) are shown to migrate more slowly than Al^{3+} ions, which is consistent with the respective metal–oxygen bond energies, Ta^{5+}–O being higher than Al^{3+}–O. In addition, the cation transport number for tantalum is lower (0.24)[22] than that for aluminum (0.41).[19] The situation of niobium is complicated by the presence (depending on the formation conditions) of additional Nb^{2+} and Nb^{4+} species in the oxide,[23] which are detrimental to its performance in capacitor applications. Nevertheless, the general overview is very similar. Thus, electrolyte species (including phosphate but not chloride) incorporate into the film during anodizing.[24] However, recent work has demonstrated a profound difference with niobium in alkaline electrolytes. Thus, in phosphoric acid at pH 2 the transport number for Nb^{5+} ions is 0.26 which is similar to that for tantalum.[25] However, when the pH is adjusted with ammonium hydroxide to pH 10, the transport number falls to 0.02 and the dielectric constant rises to more than 80 (from 44 at pH 2). It is thought that this change is due to the relative changes in the incorporation of anionic species into the film, specifically phosphate at low pH and a nitrogen species at high pH.

3.15.3.2 Passivity, Corrosion, and Localized Corrosion

As predicted from the Pourbaix diagram, the excellent corrosion resistance of tantalum and niobium is due to the presence of tenacious passive oxide films on the respective metals. Indeed, unalloyed tantalum is indubitably the 'most passive' of all metals just below rhodium and above gold in the Pourbaix practical nobility table. Compared with tantalum, niobium is significantly less passive; however, this is merely relative as niobium is still considerably more corrosion resistant than most other materials. Both the metals spontaneously passivate in almost all environments below 100 °C at atmospheric pressure, except those of low water activity and those containing fluoride, the latter being the metals' (almost only) Achilles heel.

It is extremely difficult to locate literature data on the electrochemistry of dissolution for tantalum or niobium other than in extreme conditions; one must therefore presume that the metals are passive (with consequently low corrosion rates) in most environments. Tantalum is spontaneously passive, with an extremely low corrosion rate in all mineral acids (except HF), at all concentrations and at all temperatures below 100 °C. It is used to condense and concentrate sulfuric acid and exhibits passivity in this medium at a much higher temperature. The corrosion resistance of niobium is generally inferior to that of tantalum, with alloys of niobium and tantalum being intermediate in performance.[26,27]

Recently, the corrosion of niobium has been re-evaluated in sulfuric (20, 40, and 80%) and hydrochloric (20 and 38%) acids at room temperature, 75 and 95 °C.[28] The metal was found to remain passive under all conditions, but with variations in the passive current density corresponding to changes in the mass-loss (corrosion) rate. Minor pitting was observed only in sulfuric acid at concentrations of 20% and 40%. It was suggested that dissolution of the passive oxide was via a $Nb(OH)_4^+$ species, for which species thermodynamic data had recently been obtained.

The pitting (breakdown) potentials of niobium have been investigated in 0.1 M halide solutions.[29] In chloride and iodide up to about 150 V, no pitting or breakdown was observed, and the metal formed an anodic film. In bromide, the breakdown voltage was only 42 V with some slight pitting observed. Likewise, the corrosion behavior of tantalum and niobium was studied in concentrated HBr solution at 25 and 100 °C and, under oxidizing conditions (with added bromine) or reducing conditions (with bubbled hydrogen gas).[30] Tantalum was found to passivate under all conditions studied while niobium corroded slowly at 100 °C with pits of around 5 μm evident. Under reducing conditions, niobium gradually began to corrode actively with hydrogen evolution, while under oxidizing conditions it passivated. Tantalum is thus remarkable in its resistance to pitting corrosion by chloride, bromide and iodide species, and niobium is scarcely far behind.

In contrast to their corrosion resistance in acids, niobium and tantalum corrode at significant rates in strong alkali. Thus, niobium is spontaneously active in NaOH at concentrations greater than 10% and at temperatures above 25 °C.[31] Corrosion leads to the formation of the niobate species, NbO_3^-, with the corrosion rate increasing with concentration and time. Tantalum was found to be significantly more resistant than niobium and remained passive in 10% NaOH up to 75 °C and in 15% NaOH up to 50 °C.[32] At higher concentrations and temperatures, the passive film on tantalum dissolved slowly, forming a

polytantalate species. Tantalum–niobium alloys were found to be intermediate in behavior.[33]

3.15.3.3 Gaseous Environments

3.15.3.3.1 Oxidation in air

Tantalum and niobium are not resistant to oxidation at high temperatures in air. Reaction with both oxygen and nitrogen occurs; in air, reaction is increasingly rapid for both materials above about 500 °C, leading to catastrophic failure. Thus, these metals and their dilute alloys can only be used in high temperature conditions either in a protective (or nonaggressive) environment, or if coated to prevent reaction with the gaseous environment.

Both metals have significant solubility for oxygen and were found to obey Henry's Law for oxygen solubility between 600 and 1100 °C. At 850 °C, oxygen dissolved at up to 2.3 at.% in pure tantalum and 1.3 at.% in niobium; an alloy of Ta–25% Nb dissolved up to 3.4 at.%.[34] The volumetric expansion on proceeding from metal to oxide (Pilling–Bedworth ratio) is among the largest of the engineering alloys: 2.5 and 2.7 for tantalum oxide and niobium oxide, respectively. This can be compared with 2.1 for chromium oxide, 1.65 for nickel oxide and 1.3 for aluminum oxide. This implies that the oxides form under a considerable compressive stress and, indeed, the oxide scales are generally poorly adherent and greatly influenced by specimen geometry.[35] Oxidation rates at even modest temperatures are high and neither alloy is recommended for use in air above 250–300 °C.

For tantalum, initial oxidation is delayed until the equilibrium solubility for oxygen in the metal has been achieved (which is usually rapid). Afterwards, the oxidation process at temperatures below around 400 °C follows a parabolic rate law, thus indicating diffusion-controlled kinetics across the growing oxide film. For thin oxides, in this regime the oxide is relatively protective. Above 500 °C, oxidation proceeds following a linear rate law; in this regime, the oxide is clearly not protective and indeed oxidation will inevitably become catastrophically rapid as the temperature increases. At temperatures in excess of 1000 °C, the metal will effectively burn in pure oxygen.[36] The scale formed in tantalum consists of pure Ta_2O_5; as there is no stable lower oxidation state, there is no other stable oxide. Thicker scales on tantalum tend to comprise parallel layers interspaced with lines of small voids. There is strong evidence that these voids nucleate over metastable suboxide platelets within a thin, oxygen-saturated layer in the metal immediately under the scale.[37]

Niobium, like tantalum, reacts measurably with oxygen at relatively low temperatures (200 °C) although reaction does not become rapid until above about 400 °C. Niobium is influenced, like tantalum, by the dissolution of oxygen in the metal and by the formation of large compressive stresses in the oxide during scale growth. Again, like tantalum, the oxidation kinetics below about 350 °C are parabolic with thinner oxides relatively protective. Above 400 °C, oxidation is initially linear or paralinear and proceeds at a relatively slow rate; however, after a period of time (decreasing with increasing temperature) breakaway oxidation sets in and the oxidation rate increases markedly up to about 600 °C, then decreases substantially.[38] The scale formed mainly comprises Nb_2O_5 with the metastable suboxide also present in the metal just beneath the metal–scale interface (as for tantalum). However, unlike tantalum, Nb_2O_5 increasingly intrudes into the metal from the scale disrupting the formation of the suboxides and causing the rapid breakaway oxidation evident in niobium (and absent in tantalum).[39] The formation of NbO_2 beneath the main scale of Nb_2O_5 at temperatures above around 600 °C is thought to be the major mechanism behind the decrease in the oxidation rate at this temperature.

Wider application of both alloys would result from improving their oxidation resistance. However, owing to the high cost and density of tantalum, much of the research and industrial effort in improving high temperature oxidation resistance focuses on niobium. There are basically two possible methods for achieving this goal: alloying and application of a protective coating. Extensive early work on binary, ternary, and quaternary alloys of niobium with tantalum, tungsten, titanium, and zirconium was performed and it is indeed possible to reduce considerably the oxidation rate of niobium; for example, in Nb–W–Ti alloys.[40] However, in nonoptimized alloys the oxidation rate is still too rapid to be useful and, furthermore, the alloys are required to have satisfactory high temperature mechanical properties (strength and creep resistance).

More recent alloy developments have involved complex alloys containing titanium, aluminum, chromium, silicon, and hafnium (with other minor elements).[41] Although such alloys have somewhat poorer oxidation resistance at lower temperatures,

at temperatures above 1000 °C the oxidation resistance is comparable to or better than nickel-based superalloys. The requirement of good strength and creep resistance is obtained by alloying to promote the formation of intermetallics; either aluminides (up to 1200 °C) or silicides (up to 1500 °C). Thus, alloys such as Nb–30Ti–9Cr–11Al–11Si show an oxidation rate at 1200 °C of 2–3 $\mu m\,h^{-1}$, compared with unalloyed Nb ($\gg 125\,\mu m\,h^{-1}$) and nickel superalloys ($20\,\mu m\,h^{-1}$), while having acceptable strength and creep resistance[42]; room temperature fracture toughness, however, remains low.

The alternative method for improving high temperature oxidation resistance is to form adherent, dense and protective coatings on the metal surface. They also need to have excellent oxidation resistance as well as providing an effective diffusion barrier for oxygen (and other species) from the coating into the alloy. Coatings based on the development of single or multiple layers of aluminum, molybdenum and niobium silicide have successfully demonstrated oxidation resistance at temperatures of 1300 °C.[43–45] Such coatings may be applied by pack cementation, chemical or physical vapor deposition and thermal spraying.

3.15.3.3.2 Other gaseous environments

The reaction of tantalum and niobium with hydrogen to form hydrides has been discussed above and can occur both electrochemically and from the gas phase. Both materials can react with hydrogen at significant rates even at room temperature, for example, by mechanical action.[46] There has, indeed, been considerable interest in the properties of tantalum and, particularly, niobium for hydrogen storage applications. Thermodynamic data predicts the formation of both the mono- and di-hydride phases, which have been confirmed by observation.[47] Hydriding is used commercially as a method to produce powders of niobium and tantalum and their alloys.[48] Since the metals are generally cathodic to other metals, galvanic coupling must be avoided to restrict the possibility of hydrogen embrittlement.

Although tantalum and niobium also react to form nitrides, in air the dominant reaction will be the formation of the oxide. This is because, first, the kinetics of oxidation are much more rapid and, secondly, the nitrides are themselves are thermodynamically unstable with respect to oxidation.[49] However, in a predominantly nitrogen atmospheric, both tantalum and niobium will nitride at temperatures above about 400 °C with parabolic kinetics forming a scale of, respectively, TaN or NbN; in some circumstances the sub-nitride Ta_2N or Nb_2N may also form.[50] Interest in nitriding derives from the extreme hardness of the materials and their potential use as hard finishes for cutting tools, etc, using physical vapor deposition.

Neither tantalum nor niobium are attacked to any great extent by dry or wet chlorine, bromine or iodine liquids or vapors below about 200–250 °C. Tantalum is also virtually uncorroded by HBr and HCl below 370 °C, attack starting at about 375 and 410 °C, respectively. However, as mentioned previously, neither metal has any significant resistance to fluorine or HF.

3.15.3.4 Aqueous Environments

3.15.3.4.1 Mineral acids

Extensive tests were carried out on the corrosion rates of tantalum and niobium in various highly aggressive media by Bishop in the early 1960s[51] and there is no reason to doubt the data today. Tantalum is essentially resistant to corrosion in nitric acid at all concentrations and temperatures. The corrosion rate in 70% acid at 270 °C is only about $100\,\mu m\,year^{-1}$, which is lower than zirconium and it does not have the latter's sensitivity to halide or metal ion contamination. Niobium is only marginally less resistant to tantalum in nitric acid. Corrosion in other oxidizing acids (e.g., chromic, perchloric) is minimal at all concentrations and temperatures.

Tantalum resists hydrochloric acid at all concentrations up to 190 °C. However, above 25% HCl at 190 °C, the corrosion rate of tantalum (and niobium) rises rapidly (**Figure 3**) and entry of hydrogen will cause embrittlement. Tantalum is also resistant to hydrochloric acid mixtures even in the presence of sulfuric acid and its salts in all proportions and at concentrations up to boiling point. It is not corroded by phosphoric acid at concentrations up to 85% and temperatures up to 200 °C, provided fluoride ion contamination often found in commercial acid does not exceed 5 ppm. It is essentially completely resistant to perchloric acid, chromic acid, hypochlorous acid, hydrobromic acid, hydriodic acid and most organic acids provided they do not contain fluorides, fluorine or free sulfur trioxide.

Tantalum is resistant to 98% sulfuric acid up to at least 160 °C and even higher temperatures at lower concentrations. Practically, it may be used up to 200 °C in all concentrations and 225–250 °C at concentrations between 80 and 90%. Tantalum is attacked by sulfur trioxide at ambient conditions at

rates higher than 1 mm year^{-1} and fuming sulfuric acid, containing sulfur trioxide, attacks tantalum at room temperature as do hydrofluoric and fluorosilicic acids.

Niobium is resistant to mineral acids at lower concentrations and temperatures, especially under oxidizing conditions. **Figures 3** and **4** show the corrosion behavior of niobium and tantalum in laboratory tests in various concentrations of sulfuric, hydrochloric acids and phosphoric acid. It has excellent resistance to nitric acid, the rate of attack in 70% acid at 250 °C being only 250 μm year^{-1}. In dilute sulfurous acid at 100 °C, the corrosion rate is below 15 μm year^{-1}, but in concentrated acid at the same temperature it is greater than 250 μm year^{-1}.

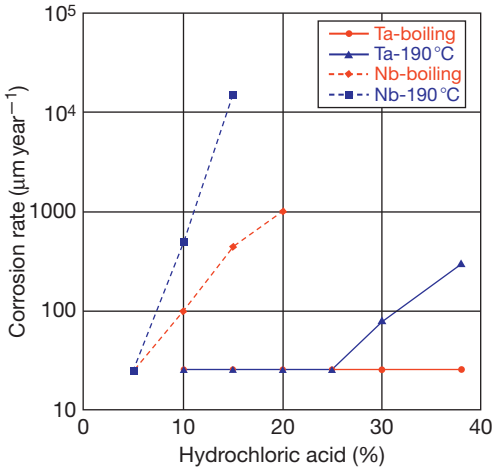

Figure 3 Corrosion rates for tantalum and niobium in HCl (25 μm year^{-1} was the lower limit of measurement and, where this value is indicated, corrosion rates were generally less than this value; in most cases, considerably so).[53]

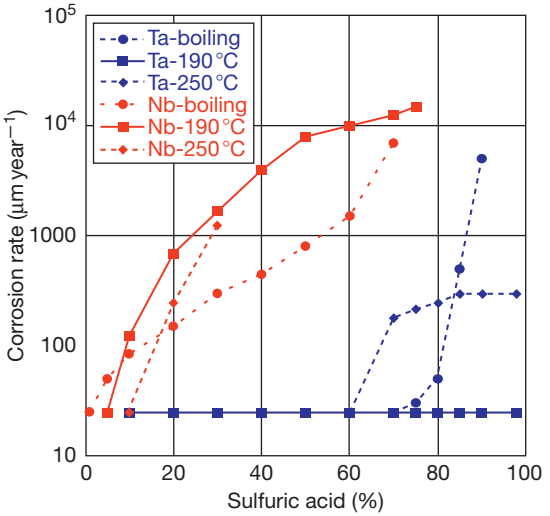

Figure 4 Corrosion rates of tantalum and niobium in H_2SO_4 (25 μm year^{-1} was the lower limit of measurement and, where this value is indicated, corrosion rates were generally less than this value; in most cases, considerably so).[53]

In view of the cost of tantalum, and the overall inferior corrosion resistance for critical applications offered by niobium, there is interest in exploring the performance of alloys of tantalum with other elements. The most commercially developed alloys are Ta–Nb materials although Ta–W, Ta–Mo as well as ternary and quaternary alloys of titanium and zirconium where tantalum or niobium (β-phase stabilizers) are significant components. Robin and coworkers have extensively investigated the entire composition range of Ta–Nb alloys in sulfuric, hydrochloric and phosphoric acids,[52,53] and confirmed the earlier results of Bishop while generating isocorrosion curves for the range of alloys in these environments.

In sulfuric acid, the corrosion rates increase with temperature and acid concentration but decrease with time because of slow oxide growth. The addition of tantalum improves the corrosion resistance of niobium with corrosion rates of Ta–Nb alloys intermediate between niobium and tantalum; the corrosion mechanism in the alloys included selective dealloying of niobium. Anodizing of the alloys reduced the short-term corrosion rates but made no difference to the long-term rates. Similar comments apply to exposures in hydrochloric and phosphoric acid except that the alloy with composition Ta–40Nb was confirmed as extremely corrosion resistant with performance similar to tantalum and Ta–W alloys show increased resistance to hydrogen embrittlement.

3.15.3.4.2 Alkalis

Neither tantalum nor niobium has satisfactory corrosion resistance in alkaline solution with the passive oxide films dissolving at varying rates depending on the concentration and temperature of the environment (**Table 7**). Corrosion thus occurs by continuous reformation of the passive film; no pitting is seen. Damage to tantalum equipment has been experienced unexpectedly when strong alkaline solutions are used during cleaning and maintenance.

Tantalum is attacked, even at room temperature, by concentrated alkaline solutions. However, tantalum is fairly resistant to dilute alkaline solutions. In one long-term exposure test in a paper mill, tantalum suffered no attack in a solution with a pH of 10. In contrast, niobium is not resistant to alkalis even

Table 7 Corrosion rates of tantalum and niobium in some alkaline media[54]

Material	*Alkali*	*Temperature (°C)*	*Corrosion rate (μm year^{-1})*	*Embrittlement*
Tantalum	NaOH (5%)	98	3–4	No
	NaOH (10%)	20	0.25	No
	NaOH (10%)	98	8–10	No
	NaOH (50%)	38–57	>1000	Yes
	NaOH (50%)	120	>1000	Yes
	NaOH (73%)	113–129	>1000	Yes
Niobium	NaOH (1%)	98	>750	Yes
	NaOH (5%)	98	>1200	Yes
	NaOH (10%)	98	>2000	Yes
Tantalum	KOH (5%)	100	<80	Yes
	KOH (10%)	Boiling	<120	Yes
	KOH (40%)	27	>1000	Yes
	KOH (50%)	100	>1000	Yes
Niobium	KOH (1%)	98	600	Slightly
	KOH (5%)	98	>2500	Yes
	Na_2CO_3 (10%)	98	>1500	Yes
	K_2CO_3 (10%)	98	>1500	Yes
	Na_2PO_4 (25%)	98	>1300	Yes
	Na_2S (10%)	98	90	No

in dilute solution or in weak alkali (e.g., Na_2CO_3) and suffers rapid attack with severe hydrogen embrittlement occurring at higher temperatures of exposure.

3.15.3.4.3 Hydrogen embrittlement and galvanic interactions

As indicated previously, a galvanic couple in which tantalum or niobium is the cathode can prove disastrous because of embrittlement. On the other hand, if either material is the anode they generally passivate so readily in most environments that no damage occurs, and the galvanic current drops to a very low value. Haissinksky[55] studied couples of tantalum with platinum, silver, copper, bismuth, antimony, molybdenum, nickel, lead, tin, zinc, and aluminum in 0.1 N H_2SO_4. Except when tantalum was coupled to zinc or aluminum, it was the more negative member (anode) of the couple. However, the galvanic current rapidly decreased as the tantalum passivated. In hydrofluoric acid, tantalum was again more positive than zinc and aluminum, but more negative than platinum, silver, copper, antimony, nickel, and lead. However, in this environment high steady-state currents were observed because tantalum corrodes rather than passivates in fluoride solutions.

Time is an important factor in determining whether tantalum will be damaged by galvanic effects[56] as illustrated in Table 8. However, such data provides only guidance. In practice, it would be dangerous to depend on laboratory tests only to provide information as to whether tantalum is negative in a given galvanic couple situation. Niobium behaves similarly and if it is cathodic in a galvanic couple the results can prove disastrous because of hydrogen embrittlement. If niobium is the anode in such a couple, it anodizes so readily that no damage occurs and the galvanic current drops to a very low value because of the formation of an anodic oxide film.

Hydrogen embrittlement of these materials may be avoided completely by polarizing the metals anodically (anodic protection). In such cases, the passive film will thicken or at least be maintained. An effective technique is to couple the metal to a material with a very high exchange current density for hydrogen evolution; essentially, a platinum group metal (e.g., platinum, palladium, ruthenium, etc.). This method can also work by surface ion implantation, for example, with platinum,[57] or by the introduction of some platinum species into the environment, where it will deposit onto the exposed surfaces. Another method is to use alloying, typically with rhenium, tungsten or molybdenum.[58] These are believed to function either by doping the passive film and so favorably changing the charge carrier density (so, it is less conductive), or by changing the hydrogen solubility and hydride nucleation mechanism in the alloy.

3.15.3.4.4 Fluorides

Neither tantalum nor niobium has any significant corrosion resistance to fluorine, hydrofluoric acid or indeed environments containing even relatively low concentrations of fluoride. For example, in

Table 8 Electrochemical potential of tantalum in the indicated solution with respect to various metals[56]

Time after immersion (s)	*Coupled metal*	*Potential of tantalum (mV)*		
		3% NaCl	1% HCl	1% NaOH
30	Hastelloy B	−34	−30	−105
3600	Hastelloy B	+3	+1	−5
30	Hastelloy C	−50	−70	−135
3600	Hastelloy C	−3	−3	−5
30	Nickel	−65	−35	−180
3600	Nickel	−3	0	−5
30	Lead	−2	+50	−10
3600	Lead	+60	+55	+30
30	Aluminum	+130	+275	+620
3600	Aluminum	+230	+210	+510
30	304 stainless	−50		
3600	304 stainless	−3		

concentrated nitric acid at 50 °C no significant increase in the corrosion rate for tantalum was observed.[59] However, at 13 ppm fluoride the corrosion rate increased 2–3 times, and above this level increasingly so. Ta–40Nb alloy corroded about 10 times faster than unalloyed tantalum under all conditions studied. Apart from strong alkali, fluoride-containing environments are the only conditions where tantalum and niobium would be expected to corrode at significant rates at ambient temperatures. This is because the passive oxide films are dissolved to form fluoro and oxyfluoro complexes. It is perhaps not surprising that this would occur, since reaction with fluoride forms the basis of the industrial process for purification and separation of the elements.

3.15.3.4.5 Aqueous salts

Tantalum and niobium have excellent resistance to virtually all salt solutions under virtually all conditions of concentration and temperature, including: chlorides, sulfates, nitrates and salts of organic acids, provided (a) they do not contain fluorides, fluorine, and free sulfur trioxide, or (b) hydrolyze to produce strong alkalis.

3.15.3.5 Liquid Metals

Significant interest lies in the use of refractory metals for two main applications: as a constructional material for molten metal die casting and in applications (particularly relating to nuclear) where molten metal coolants might be used. The high cost of niobium and tantalum precludes their use as die materials and, in any case, (unlike molybdenum, which is the preferred die material) they have limited resistance to molten zinc above 450 °C.[60]

Molten metals have many advantages as nuclear reactor coolants. Thus, they have very high heat transfer capability with no change in phase and can operate at atmospheric pressure (unlike water–steam systems, for example). Applications that have been considered (and even implemented in some cases) include: fission reactor coolants, fusion reactor coolants/deuterium breeder blankets and spallation neutron targets (where a high-intensity particle beam from an accelerator impacts upon a heavy metal target, generating a high-intensity neutron source. The liquid metal systems that have been considered include: mercury, gallium, lead, lead–bismuth eutectic, sodium, sodium–potassium eutectic, and lithium.

The degradation of a metallic container material in a liquid metal environment depends upon a number of factors and can manifest in two main ways: dissolution of the container material (or its protective oxide) into the molten environment, embrittlement (liquid metal embrittlement) of the container material with the environment. The mechanisms for liquid metal embrittlement remain complex and unclear, and often depend upon the container–environment combination; however, reaction of the container material with impurities (e.g., dissolved oxygen) in the molten metal and formation of destructive or protective intermetallic compounds between the container material and the environment appear to be among the important factors.[61]

Considerable research was carried out in the 1950s by the then US Atomic Energy Commission[62] on the corrosion resistance of materials in liquid metals, particularly in regard to fast fission reactor coolants and this work is summarized as follows. Liquid bismuth was found to have little action on

tantalum at temperatures below 1000 °C but caused some intergranular attack above this temperature; with no detrimental effects on stress rupture properties up to 815 °C. Niobium was also resistant to bismuth at lower temperatures (up to 560 °C) and it suffered some degree of embrittlement at 815 °C. In molten gallium, tantalum was resistant up to 450 °C, but poor above 600 °C. Niobium was slightly less resistant than tantalum, showing good resistance at 400 °C but poor resistance above 450 °C. Both tantalum and niobium were resistant to liquid lead at least up to 815 °C, possessed good resistance to molten lithium up to 1000 °C and in mercury vapor up to 600 °C. Liquid sodium, potassium or their alloys had little effect on either tantalum or niobium up to 1000 °C if oxygen free. However, in the presence of significant dissolved oxygen, the liquid metals could become corrosive at lower temperatures.

More recent work has shed light on the critical importance of the dissolved impurity levels (particularly oxygen) in the molten metal and also the proposed containment materials. Tantalum exhibited essentially no reaction in liquid lead under oxidizing conditions at 600 °C for 100 h.[63] In liquid sodium or potassium, reaction with the passive oxide layers on niobium and tantalum form ternary oxides whose solubility contribute to the overall corrosion rates. Nitride, carbide and hydride formation is also seen with the corresponding dissolved species.[64] In liquid lithium, however, the oxides on tantalum and niobium are unstable and are reduced to the metal. Additionally, liquid metal embrittlement by lithium, in the form of metal penetration along grain boundaries, occurs when the oxygen levels exceed 400 or 100 ppm in niobium or tantalum respectively.[65]

3.15.3.6 Organic Compounds

In general, tantalum is completely resistant to organic compounds and may be used in almost all conditions. However, in environments of low water activity niobium and tantalum show evidence of pitting corrosion (in methanol)[66] and even dissolution (bromine in acetone).[67]

3.15.4 Industrial Applications

3.15.4.1 Chemical Process Equipment

Tantalum and niobium and their alloys find significant use in process equipment in very corrosive duties that arise in metal pickling, chemicals/petrochemicals manufacture, oil refining and other operations or in processes that can tolerate only limited metal ion contamination such as pharmaceuticals manufacture. Typical applications include reaction and separation equipment, heaters and heat exchangers, piping and valves, thermowells and rupture discs. The relatively high costs and excellent corrosion resistances of the alloys dictate/permit the use of relatively thin, typically 0.5–1.00 mm sections for heat exchange or as clad/loose linings on cheaper substrates, usually steels, for pressure containment. A common application is in heat exchangers (evaporators and coolers) for the concentration, handling and reconcentration of sulfuric, nitric, hydrohalide and mixed acids. However, the alloys cannot be used in HF or HF-containing fluids, which include commercial, pure phosphoric acid.

3.15.4.2 Anodes

Both tantalum and niobium have exceptionally high positive breakdown potentials for pitting corrosion and significant oxygen evolution in chloride environments (>150 V for tantalum and >100 V for niobium in seawater). Thus, they are both ideal substrates either on their own, or as substrates for platinum group metals as nonconsumable anodes and are used in all fluoride-free environments, although niobium is preferred because of its lower cost.

Applications for impressed current anodes include all those where nonconsumable impressed current anode might be specified, for example, in sea and brackish water, brines, concrete and soils. However, platinized niobium anodes are particularly suitable (compared with platinized titanium) for use in high-resistance environments where large positive driving voltages are required to deliver reasonable currents. They are often used, therefore, in deep well ground beds in order to protect long lengths of buried pipe. Although driving potentials up to about 100 V may be used, crevice corrosion can occur at lower driving voltages in the range 20–40 V especially in the presence of impurities such as copper and iron, and under deposits or in mud.[68]

In similar manner, both tantalum and niobium have been explored for use as nonconsumable long-life anodes for electrowinning, electroplating, and oxygen evolution applications.[69,70]

3.15.4.3 Medical and *In Vivo* Applications

Tantalum and niobium are very stable passive metals and are completely inert to body fluids and tissues.

In particular, bone and tissue do not recede from tantalum, which makes it attractive as an implant material for the human body. Tantalum's comparatively low strength precludes its use as a structural (i.e., joint) implant although it is, for example, used for bone-support plates. However, its electrical properties are such that tantalum (or anodized tantalum) is used extensively for capacitively coupled electrodes for muscle or nerve stimulation.[71] Its high density provides radioopacity and it has uses as a marker on other larger implant components, where tantalum is usually deposited as a surface layer.

References

1. Tantalum and Niobium International Study Center. Historical information, occurrence and production Available at www.tanb.org.
2. Smallwood, R. E. Ed. *Refractory Metals and their Industrial Applications*; ASTM Special Technical Publication, 1982; Vol. 849.
3. *HSC: Chemistry – V6.12 (Thermochemical Database)*; Outotec Research Oy: Finland, 2007.
4. Allegheny Technologies. Niobium technical data sheet from ATI Wah Chung. Available at www.wahchang.com.
5. Cabot Corporation. Tantalum and niobium technical data sheets. Available at www.cabot.com.
6. Tantalum and Niobium International Study Center. Applications of niobium and tantalum. Available at www.tanb.org.
7. Maeland, A. J.; Libowitz, G. G.; Lynch, J. F.; Rak, G. *J. Less-common Metals* **1984**, *104*, 133–139.
8. Westlake, D. G.; Miller, J. F. *J. Less-common Metals* **1979**, *65*, 139–154.
9. Oates, W. A.; Kuji, T.; Flangan, T. B. *J. Less-common Metals* **1985**, *105*, 333–338.
10. Matsui, H.; Yoshikawa, N.; Koiwa, M. *Acta Metall.* **1987**, *35*, 413–426.
11. Gahr, S.; Grossbeck, M. L.; Birnbaum, H. K. *Acta Metall.* **1977**, *25*, 125–134, 135–147.
12. Viilkl, J.; Alefeld, G. In *Diffusion in Solids: Recent Developments*; Nowick, A. S., Burton, J. J., Eds.; Academic Press: New York, 1974.
13. Rothenberger, K. S.; Howard, B. H.; Killmeyer, R. P.; Cugini, A. V.; Enick, R. M.; Bustamante, F.; Ciocco, M. V.; Buxbaum, R. E. *J. Membr. Sci.* **2003**, *218*, 19–37.
14. Clauss, A.; Forestier, H. *Les Compt. Rendus l'Académie Sci. Paris* **1958**, *246*, 3241–3243.
15. Olszta, M. J.; Dickey, E. C. *Microsc. Microanal.* **2008**, *14*, 451–458.
16. Kukli, K.; Ritala, M.; Leskelä, M. *J. Electrochem. Soc.* **2001**, *148*, F35–F41.
17. Kover, F.; Musselin, M. J. *Thin Solid Films* **1968**, *2*, 211–238.
18. Skeldon, P.; Shimizu, K.; Thompson, G. E.; Wood, G. C. *Surf. Interf. Anal.* **1983**, *5*, 252–263.
19. Brown, F.; Mackintosh, W. D. *J. Electrochem. Soc.* **1973**, *120*, 1096–1120.
20. Randall, J. J., Jr.; Bernard, W. J.; Wilkinson, R. R. *Electrochim. Acta* **1965**, *10*, 183–201.
21. Chung, S.; Thompson, G. E.; Wood, G. C.; Drake, M. P. *Chemtronics* **1987**, *2*, 98–100.
22. Pringle, J. P. S. *J. Electrochem. Soc.* **1974**, *120*, 1391–1400.
23. Magnussen, N.; Quinones, L.; Dufner, D. C.; Cocke, D. L.; Schweikert, E. A.; Patnaik, B. K.; Barros Leite, C. V.; Baptista, G. B. *Chem. Mater.* **1989**, *1*, 220–225.
24. Li, Y.-M.; Young, L. *J. Electrochem. Soc.* **2000**, *147*, 1344–1348.
25. Ono, S.; Kuramochi, K.; Asoh, H. *Corros. Sci.* **2009**, doi: 10.1016/j.corsci.2008.11.027.
26. Robin, A. *Int. J. Refract. Metals Hard Mater.* **1997**, *15*, 317–323.
27. Robin, A.; Rosa, J. L. *Int. J. Refract. Metals Hard Mater.* **2000**, *18*, 13–21.
28. Asselin, E.; Ahmed, T. M.; Alfantazi, A. *Corros. Sci.* **2003**, *49*, 694–710.
29. Lavanya, A.; Anjaneyulu, Ch. *Bull. Electrochem.* **2002**, *18*, 317–320.
30. Uehara, I.; Sakai, T.; Ishikawa, H.; Takenaka, H. *Corrosion* **1989**, *45*, 548–553.
31. Robin, A. *J. Appl. Electrochem.* **2004**, *34*, 623–629.
32. Robin, A. *J. Appl. Electrochem.* **2003**, *33*, 37–42.
33. Robin, A. *Corros. Eng. Sci. Technol.* **2003**, *40*, 51–56.
34. Lauf, R.; Altstetter, C. *Scr. Metall.* **1977**, *11*, 983–985.
35. Stringer, J. *J. Less-common Met.* **1968**, *16*, 55–64.
36. Cowgill, M. G.; Stringer, J. *J. Less-common Met.* **1960**, *2*, 233–240.
37. Stringer, J. *J. Less-common Met.* **1966**, *11*, 111–118.
38. McLintock, C. H.; Stringer, J. *J. Less-common Met.* **1963**, *5*, 278–294.
39. Taylor, A.; Stringer, J. *J. Less-common Met.* **1975**, *39*, 143–159.
40. Miller, G. L.; Cox, F. G. *J. Less-common Met.* **1960**, *2*, 207–222.
41. Briant, C. L. *J. Eng. Mater. Technol.* **2000**, *122*, 338–341.
42. Subramanian, P. R.; Mindiratta, M. G.; Demiduk, D. M. *J. Met.* **1996**, *48*, 33–38.
43. Dzyadykevich, Yu. V. *Powder Metall. Met. Ceram.* **1986**, *25*, 38–43.
44. Majumdar, S.; Sengupta, P.; Kale, G. B.; Sharma, I. G. *Surf. Coat. Technol.* **2006**, *200*, 3713–3718.
45. Vilasi, M.; Francois, M.; Podor, R.; Steinmetz, J. *J. Alloys Compd.* **1998**, *264*, 244–251.
46. Dunlap, R. A.; Small, D. A.; Mackay, G. R. *J. Mater. Sci. Lett.* **1999**, *18*, 881–883.
47. Esayed, A. Y.; Northwood, D. O. *Int. J. Hydrogen Energy* **1992**, *17*, 41–52.
48. Candioto, K. C. G.; Nunes, C. A. *Int. J. Refract. Metals Hard Mater.* **2006**, *24*, 413–417.
49. Strafford, K. N. *Corros. Sci.* **1979**, *19*, 49–62.
50. Prokoshkin, D. A.; Voronova, T. A.; Gorbova, A. S.; Kashirtsev, V. N. *Met. Sci. Heat Treat.* **1984**, *26*, 357–360.
51. Bishop, C. R. *Corrosion* **1963**, *19*, 308t–314t.
52. Robin, A. *Int. J. Refract. Metals Hard Mater.* **1997**, *15*, 317–323.
53. Robin, A.; Rosa, J. L. *Int. J. Refract. Metals Hard Mater.* **2000**, *18*, 13–21.
54. Tingley, I. I.; Rogers, R. R. *Corrosion* **1965**, *21*, 132.
55. Haissinsky, M. *Metaux Corros.* **1948**, *23*, 15–18.
56. Wehrmann, R. Corrosionomics; Fansteel Metallurgical Corp., Sept. 1956.
57. Ensinger, W.; Wolf, G. K. *Surf. Coat. Technol.* **1992**, *51*, 41–44.
58. Gypen, L. A.; Brabers, M.; Deruyttere, A. *Werkstoffe Korrosion* **1984**, *35*, 37–46.
59. Klas, W.; Herpers, U.; Michel, R.; Reich, M.; Droste, R.; Holm, R.; Horn, E.-M.; Mueller, G. *Werkstoffe Korrosion* **1991**, *42*, 570–575.
60. Hodge, W.; Evans, R. M.; Haskins, F. *J. Met.* **1955**, *7*, 824–832.

61. Joseph, B.; Picat, M.; Barbiera, F. *Eur. J. Appl. Phys.* **1999**, *5*, 19–31.
62. Miller, E. C. *Liquid Metals Handbook*; Atomic Energy Commission, Navy Department: Washington, DC, 1952; Chapter 4, pp 144–183.
63. Loewen, E. P.; Ballinger, R. G.; Lim, J. *Nucl. Technol.* **2004**, *147*, 436–456.
64. Barker, M. G. *Revue Int. Hautes Temperatures Refractaires* **1979**, *16*, 237–243.
65. Klueh, R. L. *Metall. Trans.* **1974**, *5*, 875–879.
66. Ramgopal, T. *Corrosion* **2005**, *61*, 757–765.
67. Kamada, K.; Mukai, M.; Matsumoto, Y. *Electrochim. Acta* **2004**, *49*, 321–327.
68. Hayfield, P. C. S. *Mater. Perform.* **1981**, *20*, 9–15.
69. Skomoroski, R. M.; Baboian, R.; Zobbi, R. G.; Camp, E. K. *Plating* **1973**, *60*, 1115–1119.
70. Cardarelli, F.; Taxil, P.; Savall, A.; Comninellis, Ch.; Manoli, G.; Leclerc, O. *J. Appl. Electrochem.* **1998**, *28*, 245–250.
71. Donaldson, P. E. K. *Med. Biol. Eng.* **1974**, *12*, 131–135.

Further Reading

Corrosion Handbook; ASM International, 2008; Vol. 13B.

3.16 Corrosion of Tungsten and its Alloys

S. B. Lyon
Corrosion and Protection Centre, School of Materials, The University of Manchester, Oxford Road, Manchester M13 9PL, UK

Glossary

Oxide dispersion strengthened A method of strengthening or hardening alloys by dispersing a fine (micron-size) oxide throughout the structure usually by processing the material via powder route. This acts both to pin dislocations (and hence harden the material) and also to pin grain boundaries (and hence limit grain growth and reduce creep at high temperatures).

3.16.1 Occurrence and Production

Tungsten is a relatively rare element in nature with soil abundance similar to molybdenum. It is mined predominantly as wolframite (iron manganese tungstate) or scheelite (calcium tungstate) both containing above 70% of tungsten. Due to the high melting point of tungsten, routes to the production of tungsten powder are essential. Thus in processing, and after gravity concentration, most ores are converted to a form in which they can be reduced to the metal. This is generally carried out by initial leaching of the ore to produce tungstic acid followed by conversion to ammonium paratungstate, calcining to tungsten oxide (WO_3) and then reduction in hydrogen at 800–1000 °C to produce commercially pure tungsten powder.[1]

3.16.1.1 General Properties

Tungsten is a transition element in the third row of the periodic table, the elements immediately above tungsten (in Group 6B) being molybdenum and chromium with which tungsten shares many similarities in chemistry (oxidation states from 2 to 6) and metallurgy (body-centered cubic lattice). Tungsten has the highest melting point (3410 °C) – more than any metal – while its vaporization point (5550 °C) is second only to that of rhenium. Excluding actinides, its density (19.3 $Mg\,m^{-3}$) is the fifth greatest of the elements, being equivalent to gold and only slightly less than the adjacent elements rhenium, osmium, iridium, and platinum.[2]

Commercially pure tungsten has relatively high ultimate tensile strength (1000 MPa at 25 °C dropping to 250 MPa at 1500 °C) and elastic modulus (410 GPa at 25 °C, dropping to 360 GPa at 1500 °C).

Thus, a significant fraction of the room temperature mechanical properties are retained at high temperatures.[3] Tungsten also has relatively high thermal and electrical conductivity (about one-third of copper).[2] Tungsten oxidizes relatively easily at elevated temperatures, reacting with both oxygen and nitrogen to form oxides and nitrides; these are generally nonprotective above 300°C. Thus, the processing of and the applications for tungsten must take care to avoid reaction, for example, by use of inert gas or reducing gas blanketing, or necessarily must remove oxides that form after processing.[1] Electrochemically, tungsten is rather similar to molybdenum, dissolving as tungstate ions at pH greater than about 5. However, it does have an extended stability regime for WO_3 (compared with MoO_3) and therefore tungsten has reasonable stability (is passive) in acidic solutions. Indeed, tungsten, as one of the so-called 'valve metals,' may be anodized (e.g., in sulfuric acid) to form a stable, relatively protective film of tungsten oxide.[4]

3.16.1.2 Fabrication

There are no refractory materials that can contain molten tungsten; consequently powder metallurgical routes are invariably used in the initial processing of tungsten. Thus, tungsten (and any alloying components) in powder form are generally hydrostatically pressed into billets to a green density of 55–60%. Such billets are then sintered by direct resistance electric arc or electron beam heating to 2500–3000°C in order to increase the density to above 90% and preferably above 93%, in order to permit further mechanical processing.

During processing, care must be taken to avoid pick-up of oxygen, nitrogen, and carbon from the environment. These elements will form, respectively, oxides, nitrides, and carbides generally residing at grain boundaries, which will cause embrittlement of the material and importantly, reduce ductility and limit mechanical working. Typical impurities after powder processing are: carbon – 0.04%, oxygen – 0.023%, and nitrogen – 0.002%. Vacuum arc remelting can significantly lower these values to 0.03%, 0.004%, and 0.001%, respectively.[3]

Tungsten, as a body-centered cubic metal, undergoes a ductile–brittle transition that is a function of temperature, sample dimensions and also impurity levels and alloying content. Generally, this occurs well above room temperature and for commercially pure tungsten (99.95%) the transition temperature is 300–500°C. However, this transition temperature can be reduced by prior mechanical deformation such that at small section sizes it is possible to successfully undertake wire drawing, extrusion, etc. at room or slightly elevated temperatures. Typically, sintered tungsten billets are initially forged or swaged above the recrystallization temperature at 1600–1700°C in a reducing atmosphere in order to densify them and, by this way, the ductile-to-brittle transition temperature can be reduced to below 100°C. The lowered processing temperature permits easier operation of sheet rolling and wire drawing, although, due to the high intrinsic yield stress of tungsten, working forces are necessarily significantly larger than for other materials. The ductility of tungsten is significant above its ductile-to-brittle transition temperature with a reduction of area of about 20% at 100°C and over 60% at 1000°C.[1]

3.16.1.3 Applications

The greatest use (50–55%) of tungsten is as tungsten carbide (WC and W_2C) in the form of metal matrix composite materials such as 'cemented' carbide machine tools, hard coatings, etc. Corrosion of cemented carbides, of course, does not involve corrosion of the WC particles themselves, but of the cobalt or cobalt–chromium metallic binder. Other uses are in alloying of carbon steel (15–20%) for various purposes, in particular for 'high-speed' tool steels, also containing WC. Tungsten is also used as an alloying addition to stainless steels (e.g., for enhanced resistance to chloride) and in high temperature nickel-based superalloys. A further quantity is used in the fine chemicals and electronics industry. Only about 15% of tungsten is used in the metallic form.[5]

The main uses of tungsten metal invoke its unique properties of high melting point, high density and intrinsically high strength, and elastic modulus at high temperature. The classical high melting point application is, of course, as incandescent filaments in lighting with other common uses including electric arc electrodes (in welding, arc lamps, etc.), electrical contact materials for relays, etc., and in electron-emitting (thermionic) materials for vacuum valves, etc. An unusual application where the high strength and high melting point of tungsten are both useful is in rocketry components. Regarding high density materials, the main civil applications include yacht keels, moveable ballast in racing cars and aircraft (where the competitive material in both cases is depleted uranium), in sports materials for weight trimming (e.g., professional darts, golf clubs, etc.),

and for radiation shielding where it can be used in significantly thinner sections than the traditional lead materials and is effectively nontoxic in handling.

A new application that is being developed is for military materiel (i.e., high kinetic energy projectiles) where the current use of depleted uranium on the battlefield has, self-evidently, been found to cause serious, and lingering, toxicological and radiation hazards. Although the use of tungsten in this application is not without its own toxicological problems, the immediate and long-term health risks are of a significantly lower order of magnitude compared to uranium. Tungsten also has a generally very low solid solubility with most metallic elements and it has been proposed that this property may be exploited in future (Generation IV) liquid metal fast neutron reactors for power generation.

3.16.1.4 Alloys

Tungsten is commonly alloyed to reduce the inevitable decrease in mechanical properties as the temperature is raised, to limit grain growth at high temperatures, and to control thermionic electron emissivity. Alloying is invariably undertaken by powder metallurgical routes and, by this method, it is also easy to incorporate ceramic powders, for example, as oxide dispersion strengthened (ODS) materials.[1]

Tungsten has significant solid solution miscibility only with a few other elements, the most important of which are molybdenum (where a series of alloys up to 50% Mo are in use) and rhenium, which is totally miscible with tungsten and where alloys of up to 25% are useful (Table 1). Interestingly, solid solution alloying with molybdenum reduces the mechanical properties while alloying with rhenium increases the yield stress by up to 15% and significantly increases the alloy recrystallization temperature; it also lowers the ductile-to-brittle transition temperature such that the alloy with 25% Re is fully ductile at room temperature. Unfortunately, the very high cost and limited availability of rhenium limits the significant use of these latter materials.

The high temperature mechanical properties of tungsten and solid solution tungsten alloys may be improved by oxide dispersion hardening. Typically, thoria (especially for electrical applications due to increased electron emissivity) is preferred as it has the best high temperature stability. For incandescent lamp filaments, potassium oxide is frequently used as a dispersant. On processing, this decomposes to produce numerous tiny bubbles in the structure that pin grain boundaries thus restricting grain growth.[6] The final class of alloys essentially comprises tungsten grains embedded within a binder phase (e.g., W with Ni/Cu/Fe/Mo as binder).

Table 1 Chemical composition of selected tungsten alloys[7]

Alloy	*Composition (wt)*
Commercial purity alloys	
W – powder processed	0.04% C, 0.023% O, 0.002% N
W – vacuum arc remelted	0.03% C, 0.004% O, 0.001% N
Oxide dispersed alloys	
Thoria dispersed tungsten	As above+1–2% ThO_2
Solid solution alloys	
W–Mo	10–50% Mo
W–Re	3–5% and 25% Re
Binder phase alloys	
W–Ni–Cu and W–Ni–Fe	Usually in grades of 90%, 93%, 95%, and 97% W, balance of Ni+Cu or Ni+Fe

3.16.2 Corrosion

3.16.2.1 Electrochemistry

3.16.2.1.1 Thermodynamics

Tungsten is a base metal with its domain of thermodynamic stability lying completely below that of water (Figure 1). However, it is significantly more noble than molybdenum and particularly chromium, elements that are above tungsten in the same group (VI) of the periodic table. Tungsten tends to dissolve in near neutral to alkaline solutions to tungstate species in association with an alkali metal cation; other cations tend to produce insoluble tungstates. Tungsten has domains of passivity associated with WO_2 and WO_3 with the latter material having low solubility and being stable to further oxidation. This characteristic allows tungsten to be anodized successfully, for example in sulfuric acid, and hence the metal belongs to the family of 'valve metals.' Tungsten forms many relatively insoluble complexes, including chloride ions. Its alloying effects are similar to that of molybdenum in that it is added to stainless steels and other alloys to increase the resistance to chloride-induced localized corrosion.[5]

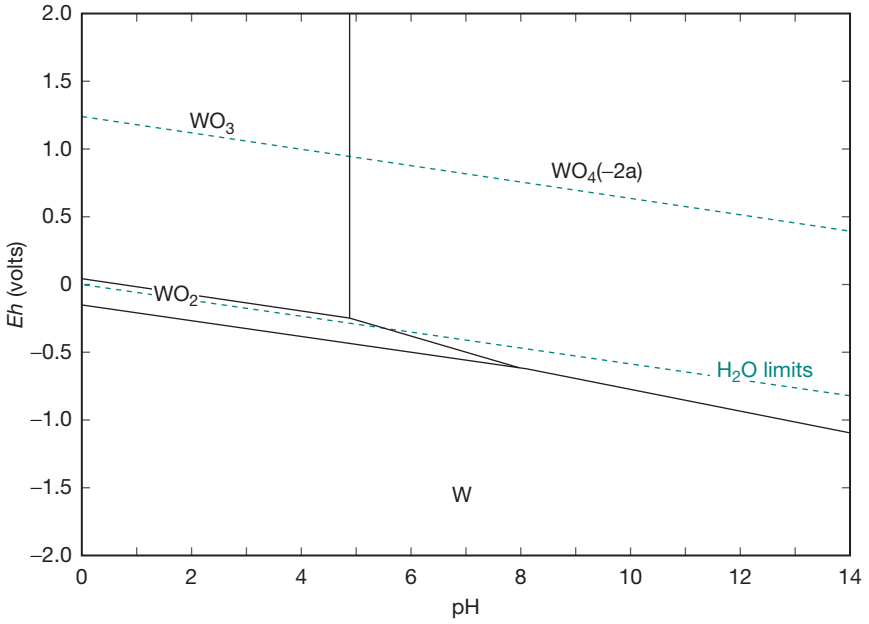

Figure 1 Pourbaix diagram for tungsten at a metal ion concentration of 10^{-5} M. Reproduced from *HSC: Chemistry*, version 6.12, Outotec Research Oy: Finland, 2007.

3.16.2.1.2 Anodic dissolution of tungsten

As implied by the Pourbaix diagram, there are no simple aquo-cations of tungsten; rather tungsten dissolves generally as a tungstate (WO_4^{2-}) above about pH 5, or as tungstic acid (H_2WO_4) at very low pH. In alkaline solutions above about pH 12, the dissolution kinetics have been found to be Tafel in nature with smooth dissolution to dissolved tungstate anion. The rate limiting step apparently involves a one-electron transfer process (Tafel slope$\approx$120 mV per decade) and has first order kinetics with respect to hydroxide ion concentration.[8] This no doubt masks a complex, step-wise, dissolution mechanism. Controlled dissolution of tungsten is an important process in the semiconductor industry where efficient planarization of tungsten chip layer interconnects is required.[9]

In contrast, below pH 5, tungsten forms a passive anodic oxide film of WO_2 (at intermediate voltages) or WO_3 (more commonly). Under galvanostatic anodization, voltages can reach up to 120–150 V at currents between 2 and 16 A m^{-2}. However, the resultant anodic film requires a relatively high (compared with other valve metals) current density to maintain it and this is thought to be due to the significantly higher solubility of the amorphous film compared to crystalline WO_3.[10] The dissolution of anodically-formed tungsten oxide in 0.1 M sulfuric acid occurs under first-order reaction kinetics via hydration to tungstic acid and is significantly more soluble if higher formation currents are used initially.[11]

3.16.2.2 Corrosion Processes

3.16.2.2.1 Oxide removal/cleaning

As noted above, it is necessary to carry out many fabrication operations, especially of heavy sectioned material, at temperatures in excess of 1000 °C. Under these conditions, and unless a protective atmosphere is used, the surface of the tungsten will become covered in an oxide scale. The thickness and tenacity of the oxide depends on the temperature used for the fabrication operation. Thick oxide scales may be removed in a molten mixture of 90% sodium hydroxide and 10% sodium nitrite at 400 °C for a few seconds. This attacks tungsten oxide rapidly and care should be taken during this process, in particular the material must be dry, otherwise splashing could occur. On removal the component should be allowed to cool in air before washing the retained salt in hot water. Alternatively, thick oxide layers may be removed by a mechanical abrasion, for example abrasive blasting. Thinner tungsten oxide scales may be removed by immersion in mixed acid etch solutions, for example: nitric acid+HF+water at 1:1:1 ratio.

Lightly oxidized tungsten can be cleaned by heating in 10% caustic soda solution at about 80°C followed by rinsing in water and then dilute hydrochloric acid solution (10%) to neutralize the remaining caustic before finally rinsing in water and drying.[1]

3.16.2.2.2 Aqueous corrosion of tungsten and its alloys

Generally, the aqueous corrosion of commercially pure (and oxide dispersed) tungsten depends upon the pH, with passivity expected below pH 5 and active dissolution above pH 5. In practice, the air-formed film on tungsten oxide provides significant protection against dissolution to mildly alkaline conditions (pH ≈ 8) while the dissolution kinetics at pH 12 imply a corrosion rate of about 20–30 μm year^{-1}, that is, about one-tenth of iron. Thus, commercially pure tungsten is passive or corrodes relatively slowly in most aqueous conditions except in strong alkali at pH>12.[12]

Tungsten is generally more active than most common alloying additions except iron, against which it is slightly noble under alkaline conditions. Thus, tungsten might be expected to act sacrificially under immersed aqueous conditions and this has been confirmed in the corrosion of alloys containing copper in the binder phase which suffer from preferential corrosion of the tungsten grains. However, metal bonded tungsten alloys using a Ni–Fe binder phase are generally found to be somewhat more active than tungsten. This may be due to the solubility of tungsten into this phase (in contrast tungsten has negligible miscibility in copper-containing binder phases) and also due to the protective nature of the air-formed passive film on tungsten.[12]

Amorphous alloys of tungsten with niobium, tantalum, zirconium, and chromium, at concentrations from 15 to 50%, have been prepared by DC magnetron sputtering and the corrosion of these materials has been studied in hydrochloric acid at 1–12 M. Under these conditions, the deposited films are non-equilibrium, amorphous, and spontaneously passive. Also, generally such alloys have exceptionally low passive current densities.[13]

3.16.2.2.3 Electrochemical planarization of electronic interconnects

Electronic integrated circuits frequently comprise deposition of electronic components on multiple layers. Thus, current microprocessors have 7–9 layers and it seems likely that this figure will increase. Copper is used as the electrical connection strips within each layer while tungsten plugs are used as the interlayer connections. A critical process after tungsten deposition is 'planarization,' which is designed to reflatten the wafer prior to formation of the next semiconductor layer. The process, more properly known as chemomechanical polishing, is essentially a controlled erosion–corrosion process. There are many proprietary solution mixtures that are used but their common feature is that they contain a mild oxidizing agent designed to dissolve the tungsten while leaving the silicon wafer untouched.[9]

3.16.2.2.4 Dissolvable implants

There is a significant application for dissolvable body implants in certain applications. For example, stents are often used to secure blood vessels, etc. in the body from, for example, embolisms. While most of such stents are permanent, some are temporary and there is an advantage if they gradually dissolve (i.e., corrode) in the body. Clearly, such materials need to be nontoxic and magnesium alloys are a clear material of choice in such an application. Unfortunately, the corrosion rate of magnesium alloys is generally rather high, they corrode with release of hydrogen gas and they are difficult to locate in X-rays. In view of this, research is currently underway on the use of tungsten stents which are thought to be relatively or completely nontoxic.[14]

3.16.2.2.5 High temperature oxidation and corrosion

Tungsten begins to oxidize significantly above about 300°C in dry air forming a WO_3 scale that grows under parabolic kinetics. Marker studies demonstrate that the growth kinetics are by inwards diffusion of oxygen anions through the anion vacancies in a scale with distinct oxygen sub-stoichiometry (i.e., WO_{3-x}). The Pilling–Bedworth ratio for WO_3 is 3.3, which implies that a protective scale is expected but that the growth stresses are relatively large. In view of this, oxide spallation might be expected and, indeed, this occurs rather readily under thermal cycling.[15,16] In contrast to its behavior in dry air, the oxidation of tungsten in steam is characterized by the formation, above about 800°C, of relatively volatile tungstic acid (H_2WO_4) – or more accurately hydrated tungsten oxide ($WO_3 \cdot H_2O$). Under these conditions, oxidation occurs by linear kinetics and the metal 'evaporates' at a rate controlled by the mass transport of water vapor. This process is rapid with rates of up to 1–2 mg cm^{-2} h^{-1} at 800°C.[17]

Compared with air, tungsten corrodes more rapidly in carburizing and sulfidizing environments at

high temperature, however, its performance in a chloridizing environment is considerably better than most other high temperature materials and significantly improved molybdenum.[18] In view of this tungsten is added to several alloys to improve the resistance to environments containing chlorine. The chlorination kinetics are similar to those of molybdenum, but considerably slower. Mass changes are linear with time implying that a protective scale does not form. Also, the reaction rate order with respect to the partial pressure of chlorine is about one-half, which implies that the reaction is under chemical rate control with respect to dissociation of chlorine molecules.[19]

3.16.2.2.6 Corrosion in liquid metals

Several next generation (Generation IV) nuclear reactor concepts include fast neutron reactor technologies based on liquid metal coolants. These include, for example, the sodium-cooled fast reactor and the lead–bismuth cooled fast reactor. Further, fusion reactor concepts include deuterium fuel breeding using molten lithium or lead–lithium alloys. Finally, specialist applications in nuclear science (e.g., spallation neutron targets, liquid metal ion sources) require the use of molten metals and, hence, containment of such materials is critical.

In view of the limited or zero miscibility of tungsten with many other materials its corrosion performance has been studied in most of these applications. Thus, the corrosion of tungsten in lead and lead–bismuth eutectic was excellent at 600 °C with no apparent wetting of the metal and no degradation detected after 100 h exposure.[20] Likewise, no degradation of tungsten was evident in liquid lead–lithium eutectic at 800 °C. Finally, in liquid sodium minimal signs of corrosion were evident on polished tungsten at 600 °C after 1500 h of exposure.[21] These results indicate that tungsten clearly has excellent resistance at a wide range of liquid metals and, although it cannot be used as a structural material due to cost and resource limitations, it will find application in critical niche areas.

References

1. Yih, S. W. H.; Wang, C. T. *Tungsten Sources, Metallurgy, Properties, and Applications*; Plenum Press: New York, 1979.
2. Lide, D. R. Ed. *CRC Handbook of Chemistry and Physics*, 86th ed.; Taylor & Francis: USA, 2005.
3. Gregor, M.; Čížek, L.; Widomska, M. *J. Mater. Process. Technol.* **2004**, *157–158*, 683–687.
4. Pourbaix, M. *NACE* **1974**, 281–285.
5. International Tungsten Industry Association, Rue Père Eudore Devroye 245, 1150 Brussels, Belgium. http://www.itia.org.uk/.
6. Matweb: Online materials information resource. http://www.matweb.com/.
7. Schade, P. *Int. J. Refract. Met. Hard Mater.* **2002**, *20*, 301–309.
8. Kelsey, G. S. *J. Electrochem. Soc.* **1977**, *124*, 814–819.
9. Seo, Y.-J.; Kim, N.-H.; Lee, W.-S. *Mater. Lett.* **2006**, *60*, 1192–1197.
10. Ammar, I. A.; Salim, R. *Corros. Sci.* **1971**, *11*, 591–609.
11. El-Basiouny, M. S.; Hassan, S. A.; Hefny, M. M. *Corros. Sci.* **1980**, *20*, 909–917.
12. Ogundipe, A.; Greenberg, B.; Braida, W.; Christodoulatos, C.; Dermatas, D. *Corros. Sci.* **2006**, *48*, 3281–3297.
13. Bhattarai, J.; Akiyama, E.; Habazaki, H.; Kawashima, A.; Asami, K.; Hashimoto, K. *Corros. Sci.* **1998**, *40*, 1897–1914.
14. Peuster, M.; Fink, C.; von Schakenburg, C. *Biomaterials* **2003**, *24*, 4057–4061.
15. Royce, R. E.; Roberts, E. F. I. *Corros. Sci.* **1969**, *9*, 357–361.
16. Sikka, V. K.; Rose, C. J. *Corros. Sci.* **1980**, *20*, 1201–1209.
17. Greene, G. A.; Finfrock, C. C. *Exp. Therm. Fluid Sci.* **2001**, *25*, 87–99.
18. Prescott, R.; Stott, F. H.; Elliott, P. *Corros. Sci.* **1981**, *29*, 465–475.
19. Landsberg, A.; Hoatson, C. L.; Block, F. E. *J. Electrochem. Soc.* **1971**, *118*, 1331–1336.
20. Loewen, E. P.; Ballinger, R. G.; Lim, J. *Nucl. Technol.* **2004**, *147*, 436–456.
21. Xu, Y.-L.; Long, B.; Xu, Y.-C.; Li, H.-Q. *J. Nucl. Mater.* **2005**, *343*, 360–365.
22. *HSC: Chemistry*, version 6.12, Outotec Research Oy: Finaland, 2007.

Further Reading

Lassner, E.; Schubert, W.-D. *Tungsten: Properties, Chemistry, Technology of the Element, Alloys, and Chemical Compounds*; Kluwer Academic/Plenum: New York, 1999.

3.17 Corrosion of Molybdenum and its Alloys

S. B. Lyon
Corrosion and Protection Centre, School of Materials, The University of Manchester, Oxford Road, Manchester M13 9PL, UK

3.17.1 Occurrence and Production

Molybdenum, which with tungsten is below chromium in Group VI of the periodic table, was not discovered as an element until the latter part of the eighteenth century, around the same time as tungsten. Molybdenum and tungsten are relatively rare elements in nature with similar soil abundances and many chemical similarities. Molybdenum assumed industrial significance during the First World War when a shortage of tungsten caused molybdenum to be used as a substitute in alloy steels.

Molybdenum occurs as the primary ore molybdenite (MoS_2) and also in association with other sulfide mineralizations, particularly copper. The original resources for the primary ore are in the United States, China, and in the Russian Federation, while the majority of molybdenum is now produced as a by-product of copper mining in Chile, Canada, and elsewhere. The current (2006) production of molybdenum amounts to 195 000 tonnes while the estimated global reserves amount to 19 million tonnes giving about 100 years supply at current consumption rates.[1]

Molybdenite is concentrated, from either primary or by-product sources, by froth floatation and then roasted to produce technical grades of molybdenum oxide (MoO_3), from which ferro-molybdenum (for alloying with steel) is produced using an iron thermite reaction. Further purification of MoO_3 is carried out in a similar manner to tungsten, that is, by chemical purification via an ammonium molybdate intermediate and then reprecipitation of purified MoO_3. Pure molybdenum metal and its alloys are

produced via powder metallurgy routes and the metal powder is obtained by direct reduction of purified MoO_3 using hydrogen. MoS_2, which is used as a lubricious additive, is usually obtained directly by purification of molybdenite.[2]

3.17.2 General

3.17.2.1 Physical Properties

Molybdenum shares many of its industrially useful properties with tungsten, but it has the advantage of being more readily available and can be much more easily processed due to its lower melting point. Table 1 compares its physical properties with other selected materials. It has excellent electrical and thermal conductivity, only slightly less than tungsten, but has the advantage of being about half the density. Molybdenum has also one of the lowest linear expansion coefficients of any metal from room temperature to above 1000 °C, which makes its use in glass-to-metal seals and in electronic components important. In addition, its thermal conductivity and linear expansion coefficient are quite close to silicon and also, given its relatively good electrical conductivity (31% of copper), molybdenum finds use as a chip packaging and interconnect material.

3.17.2.2 Mechanical Properties

Like tungsten, molybdenum retains significant mechanical properties at high temperatures and, hence, is useful in a number of specialist applications although it needs to be protected from significant oxidation above about 300–400 °C. Like all body centred cubic metals, molybdenum has a ductile-to-brittle transition which is usually at or slightly above room temperature. However, thin sections are generally sufficiently ductile to be formed at ambient temperatures; thicker sections require an increased temperature to avoid cracking. Commercially pure molybdenum has a relatively high yield and the ultimate tensile strength, the values of which are affected by the presence of impurities such as carbon or oxygen. Table 2 compares some typical mechanical properties for tungsten and molybdenum where it is evident that molybdenum has a further significant advantage in terms of its relatively high specific modulus (stiffness).

Table 1 Physical properties of molybdenum compared with other elements[3]

	Mo	*W*	*Re*	*Cu*
Atomic number	42	74	75	29
Atomic weight (g)	95.95	183.84	186.21	63.55
Density (g cm^{-3})	10.2	19.3	21.1	8.96
Melting point (K)	2890	3680	3450	1358
Boiling point (K)	4920	5830	5870	2816
Electrical conductivity ($\times 10^6\ \Omega^{-1}\ cm^{-1}$)	0.187	0.189	0.054	0.596
Thermal conductivity (W $cm^{-1}\ K^{-1}$)	1.38	1.74	0.479	4.01
Linear expansion coefficient ($\times 10^{-6}$)	4.8	–	4.5	16.5
Crystal structure	bcc	bcc	hcp	fcc

Table 2 Typical mechanical properties of commercially pure annealed molybdenum compared with other annealed high temperature materials[4–6]

	Molybdenum (at 25 °C/1200 °C)	*Tungsten (at 25 °C)*	*AISI-321 (at 25 °C)*	*Waspalloy (at 25 °C)*
Density (g cm^{-3})	10.2/10.1	19.3	8.0	8.2
Elastic modulus (GPa)	330/240	420	200	230
Ultimate tensile strength (MPa)	550/140	980	620	1330
Yield stress (MPa)	350/–	750	210	910
Elongation at failure	35%/–	<5%	45%	27%
Specific modulus (GPa $g^{-1}\ cm^{-3}$)	31.4/23.7	21.8	25.0	28.0
Specific strength (MPa $g^{-1}\ cm^{-3}$)	53.9/13.9	51.8	27.5	162.8

At ambient temperatures the yield strength of molybdenum is similar to normalized low-alloy steel and significantly higher than that of austenitic stainless steel. However, while the low-alloy steels are limited to use at service temperatures of about 550 °C and stainless steels to about 870 °C, unalloyed molybdenum retains useful strength up to 1200 °C (in appropriate protective atmospheres).

3.17.2.3 Applications

Molybdenum has a wide variety of industrial applications: as an alloying ingredient in low alloy and stainless steels, in combined forms as an industrial chemical or catalyst, and as a functional metal or alloy. In aqueous environments, molybdenum corrodes at a relatively low rate, generally considerably slower than iron. It is also relatively resistant to acid corrosion and has exceptional resistance to corrosion in hydrochloric acid. Although normally it shows passivity, molybdenum is subject to transpassive oxidation at most pH to a soluble (molybdate) species in aqueous conditions. However, molybdenum is useful in many specialist industry applications especially under mildly oxidizing to reducing conditions. In gaseous atmospheres, molybdenum oxidizes at modestly elevated temperatures in oxidizing environments to form the volatile species MoO_3. Thus, the metal is thermodynamically unstable under oxidizing conditions, both aqueous and at high temperature. Without adequate protection, care must therefore be taken to avoid temperatures above about 400 °C in oxidizing gaseous environments.

About one-half of the demand for metallic molybdenum (usually as ferro-molybdenum) is as an alloying addition to carbon steels where it delays the onset of the pearlite transformation and forms strengthening carbide phases in preference to iron.[1] Thus, molybdenum, in concentrations in the range 0.1–1%, is part of the portfolio of alloying additions to steels (e.g., including chromium, molybdenum, vanadium, tungsten, and nickel) that perform this general function. Compared with plain carbon–manganese steels, molybdenum-containing steels have increased strength and creep resistance, at elevated working temperatures.[7] At higher concentrations, that is, above 1% and up to 8%, molybdenum is a critical addition to many grades of steel tool, steel grades that resist softening at high temperatures where it functions by precipitation of alloy carbides 'high speed steels.'[7] However, the presence of molybdenum (in quantities up to several percent) has relatively minor effects on the corrosion resistance of the ferrous based alloy.

An important secondary use is that about one-quarter of the demand[1] is used as an alloying addition to corrosion resistant alloys such as stainless steels and nickel–chromium alloys. In these applications, molybdenum strongly influences the localized corrosion resistance. Thus, modification of 18Cr–10Ni austenitic stainless steel (i.e., AISI304L) by the addition of at least 2% Mo, results in an alloy (AISI316L) that has substantially improved pitting and crevice corrosion resistance (and lower critical current density for passivation). Further additions of molybdenum (with appropriate metallurgical balancing) give additional improvements.

Molybdenum is also used in much smaller quantities as an alloying addition to titanium (as a beta phase stabilizer) and in high temperature nickel-based superalloys. However, the main applications for unalloyed molybdenum (or molybdenum-based alloys), about 20–25% of the demand, take advantage of its good retention of strength at elevated temperature (up to 1800 °C), its relatively high thermal and electrical conductivity, its low thermal expansion coefficient, its high melting point, its generally good compatibility with molten glasses and ceramics, and its generally low wettability for molten metals. Thus, key applications for molybdenum metal and its alloys include:

- electrical industry (i.e., high current switch contacts, etc.),
- electronic industry (i.e., chip-level interconnects, etc.),
- hot working tools for metal forming,
- dies for molten metal casting especially of zinc (Mo–30W),
- corrosion resistant coatings (for specific chemical processes),
- corrosion resistant equipment for specialist chemical manufacture,
- seals and plugs in glass-lined vessels,
- equipment for glass manufacture: furnaces, crucibles, and stirrers,
- high temperature furnaces and associated components,
- glass-to-metal seals,
- heat shielding in engine parts and in rocketry,
- halide processes for metal purification (e.g., Van Aarkel process for Ti and Zr).

3.17.2.4 Fabrication

Due to the high melting point of molybdenum, powder processing methods are normally applied whereby

the metal powder is sintered after isostatic pressing typically in the temperature range 1650–1900 °C. Additional arc or electron-beam remelting may then be used to further consolidate ingots; however, care must be taken to avoid excessive grain growth. As implied above, the fabrication of molybdenum and its alloys is largely dictated by its ductile–brittle transition temperature. Although many metal forming operations, for example, on thin sheet and wire less than about 0.5 mm in thickness, can be carried out at room temperature it is cautionary to raise the working temperature of the work piece and die slightly (e.g., 50–200 °C). Thicker sections will require commensurately higher working temperatures; however, above about 550 °C molybdenum starts to oxidize at a considerable rate thus protective atmospheres of hydrogen (e.g., cracked ammonia) are required for significant metal-working of sections above about 650 °C.[2]

All normal fabrication routes can be used to produce molybdenum components, such as metal spinning, flow turning, deep drawing, and pressing. Specific fabrication temperatures are given[8] for various forming processes, including roll forming. Ingots of molybdenum produced either by sintering or by arc-melting are readily forged after heating to about 1500 °C (with appropriate protection against oxidation). Swaging or hot rolling to reduce the ingot size is performed while it is hot, commencing at about 1300 °C and falling as the ductility of the metal improves to about 700 °C. As the metal thickness decreases, the rolling temperature can also be decreased. Sheet rolling is generally performed at room temperature (or slightly warm) with intermediate anneals at 700–1000 °C. The typical annealing temperature range for full stress-relief of cold worked material lies in the range 870–980 °C. Commercially pure molybdenum may be recrystallised at around 1150–1200 °C; for alloyed molybdenum this temperature generally is increased.

Molybdenum alloys may be machined by any of the standard methods such as milling, turning, drilling, boring, grinding, shaping, threading, and tapping (**Table 3**). However, the low coefficient of expansion of molybdenum makes it necessary to keep the tool cool when drilling in order to prevent seizure or possible cracking of the metal or tool. Drilling is normally carried out dry but swarf can be carried out with suitable cutting oils. When milling, cutters must be kept sharp and a copious amount of coolant be provided.

It is possible to weld molybdenum using a TIG inert gas-shielded arc-welding process although this is generally more successful on vacuum arc remelted material. When welding, a heat-affected zone is unavoidable and grain growth must be anticipated. These characteristics always give a weld with less ductility than the parent material and no method of welding is entirely satisfactory particularly if the joint is to be stressed. Resistance spot and seam welding is

Table 3 Some commercially produced molybdenum alloys[2]

Material	*Composition*	*Recrystallization temperature*	*Applications*
Commercial purity: Mo	0.01–0.04% C, <0.02 Fe, <0.01% Ni, Si, <0.003% O, N	1100 °C	Furnace components, windings, etc., glass-metal seals
Clad alloys:			Electrical switch, contact
Mo–Cu	15, 30% Cu	–	materials, electronic
Mo–Ag	35, 50% Ag	–	packaging
Substitutional:			
Mo–W	20–30% W	1200 °C	Molten metal casting
Mo–Re	25–45% Re	1300 °C	Cryogenic ductility
Carbide strengthened:			
TZM	0.5% Ti, 0.08% Zr, 0.03% C	1400 °C	Hot work tooling, dies, glass
TZC	1.2% Ti, 0.3% Zr, 0.1% C	1550 °C	manufacture, spinnerets,
MHC	1.2% Zr, 0.05% C	1550 °C	heating electrodes, etc.
ZHM	0.4% Zr, 1.2% Hf, 0.12% C	1550 °C	
HWM-25	25%W, 1.0% Hf, 0.07% C	1650 °C	
Oxide dispersed:			
PSZ	0.5% ZrO_2	1250 °C	Furnace components and
MH	0.015% K, 0.03% Si	1800 °C	elements from 1800 to 2000 °C
KW	0.02% K, 0.03% Si, 0.1% Al	1800 °C	
MLR	0.7% La_2O_3	1800 °C	
MY	0.55% Y_2O_3	1300 °C	

used to join thin sections particularly for electrical and electronic applications. Molybdenum may be brazed using a flame torch and furnace brazing techniques. Small components may also be soldered although they require preplating, usually with nickel.

3.17.2.5 Alloys

Molybdenum has sufficient strength to be useful in its commercially pure form. However, as it is not possible to strengthen molybdenum by heat treatment, work hardening is the only viable method of increasing strength in commercially pure material. Like tungsten, molybdenum has poor solubility for most other elements (which is useful for applications involving molten metals); however, solid solution alloys with up to 30% tungsten and 45% rhenium are successfully used. Carbide precipitate and oxide dispersion hardened alloys are also effective with the second phase particles effective in preventing excessive grain growth at very high temperatures.

3.17.3 Aqueous Corrosion

3.17.3.1 Electrochemistry

3.17.3.1.1 Thermodynamics

Molybdenum is a relatively base metal, similar to iron, with its domain of thermodynamic stability lying completely below that of water (Figure 1). However, it is significantly more noble than chromium and slightly more so than tungsten. Molybdenum has a partial domain of passivity associated with the formation of MoO_2 across the whole pH range, but is unstable to oxidation from the Mo(IV) to the Mo(VI) state (i.e., it is transpassive) at higher potentials. Thus, molybdenum dissolves at more positive potentials as an oxyanion of molybdic acid depending upon the pH; that is, as $MoO_3{\cdot}H_2O$ (more properly molybdic acid H_2MoO_4) at low pH, as the hydrogen molybdate anion between pH 3 and 5, and as the molybdate anion above about pH 5–6. Molybdenum tends to form less soluble compounds with species such as sulfur and chlorine. For example, the *E*–pH diagram containing 0.1 M sulfur species shows a large domain of stability for MoS_2 at more negative potentials (Figure 2).

Generally, in aqueous conditions, molybdenum and its alloys are effectively passive and show considerably lower corrosion rates than iron (e.g., see Table 4).

3.17.3.1.2 Anodic behavior and passivation

The main electrochemical interest in molybdenum arises because of its profound influence on the localized corrosion of stainless steels. Several theories exist for this effect. For example, it has been proposed that the presence of high valency Mo in the chromia passive film reduces the density of cationic charge carriers thus increasing the breakdown potential.[9]

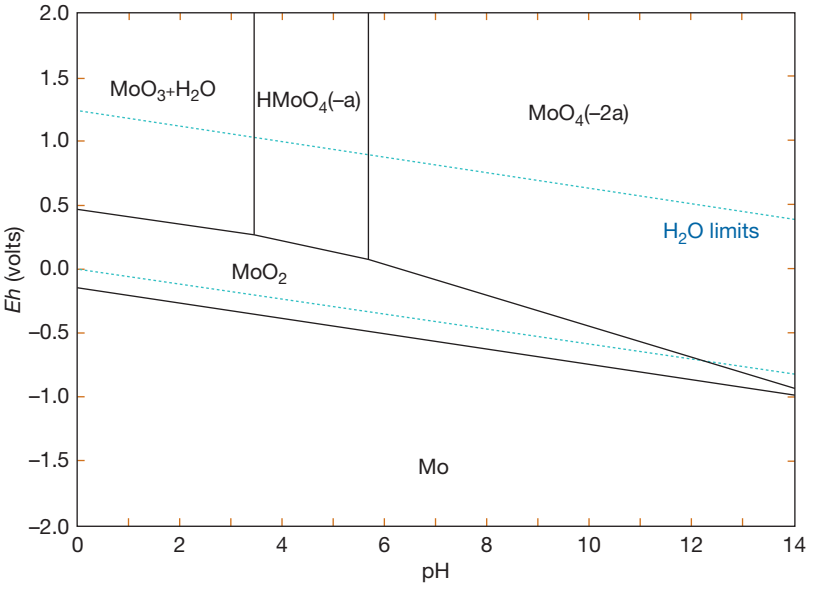

Figure 1 *E*–pH diagram at 25 °C and at a molybdenum ion concentration of 10^{-5} M.[3]

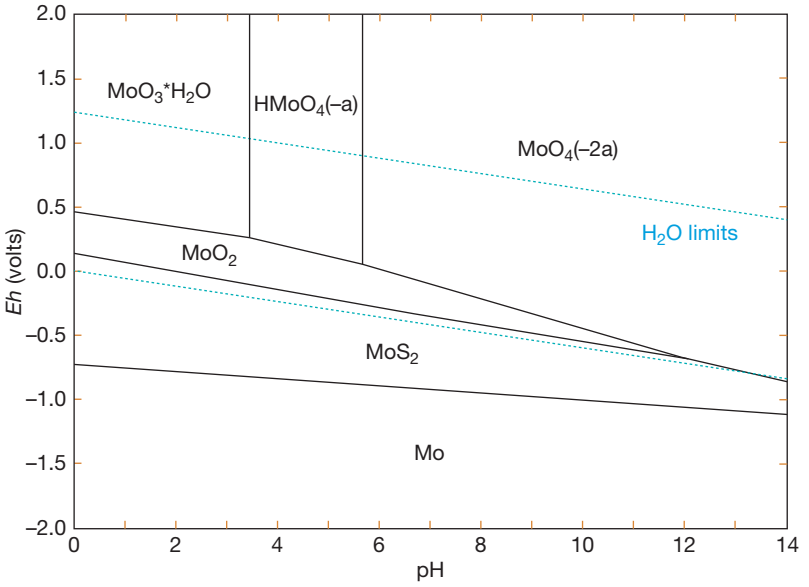

Figure 2 *E*–pH diagram at 25 °C and at Mo ion and S ion concentrations of 10^{-5} and 0.1 M respectively.[3]

Table 4 Corrosion rates in selected aqueous solutions – 6 day tests [20,21]

Environment (25–35 °C)	*Corrosion rate: aerated (mm year^{-1})*	*Corrosion rate: deaerated (mm year^{-1})*
Acids		
HCl: 1–35%	0.03–0.06	–
H_2SO_4: 1–30%	0.5–10	–
H_3PO_4: 1–30%	0.5–0.3	–
Salts		
NaCl (3%)	0.01	0
NH_4Cl (20%)	0.005	0
$FeCl_3$ (20%)	41	34
$CuCl_2$ (20%)	19	6.5
Alkalis		
NH_3 (0.35%)	0.14	0
NH_3 (29%)	0.02	0
NaOCl (10%)	11	–
NaOH (1%)	0.4	0
NaOH (10%)	0.1	0.025

Other notable theories include: adsorption of molybdate in the outer reaches of the film producing a cation-selective membrane (i.e., reducing chloride ion penetration),[10] local enrichment at actively dissolving sites reducing the local dissolution kinetics,[11] and the reduced solubility of molybdenum chloride and sulphate species affecting pit solution chemistry.[12] However, no general consensus is evident from this data and it is possible that a variety of mechanisms may operate in synergy.

Regarding the anodic behavior of pure molybdenum metal, the Pourbaix diagram implies that molybdenum is passive at intermediate potentials, with the formation of molybdenum dioxide, and that it is subject to transpassive dissolution at more positive potentials. It is generally accepted that molybdenum exhibits passivity over the majority of the pH range; however, the exact nature of this passivity is still in some doubt. The most generally accepted model, consistent with the thermodynamic diagram, is that the passive film consists of MoO_2 which dissolves to a higher valency species at more positive potentials with a higher valence oxide, MoO_3, present under alkaline conditions.[13] For example, in 0.1 M HCl, X-ray photoelectron spectroscopy (XPS) evidence shows that a film is present on molybdenum that consists of an inner MoO_2 region and an outer layer of $MoO(OH)_2$.[8,14] Also, electrochemical impedance spectroscopy (EIS) evidence is consistent with the presence of a passive film at all pH between 1 and 13.[15–17] However, since the anodic polarization curve, for example in sulfuric acid, shows no anodic peak but rather progresses immediately to a potential independent region, some workers have argued that at low pH there is no macroscopic passive film but rather a chemisorbed, strongly-bound oxygen layer.[18] There is general agreement, however, that molybdenum corrodes by transpassive dissolution at all pH at relatively higher potentials, dissolving, most probably via a Mo(V) intermediate state.[19]

3.17.3.2 Corrosion Processes

3.17.3.2.1 General corrosion

Arc cast (or arc remelted) molybdenum has greater corrosion resistance than the powder metallurgical product, especially in large sections, which is probably due to the decreased porosity of the cast variety. Components that have been metal sprayed (clad) with molybdenum have considerably worse corrosion resistance than the bulk material, again due to the porosity of the coating. However, where techniques (such as high velocity oxy fuel (HVOF)) can produce dense coatings, the corrosion resistance should improve and cladding of materials such as steel should then become viable. Table 4 gives corrosion rates in a selection of environments.

In contrast to most other passive metals, molybdenum is relatively unaffected by the presence of halide ions and is consequently relatively resistant to most localized corrosion processes. Molybdenum thus has generally excellent performance in nonoxidizing acid to near-neutral environments (containing halides or otherwise) and particularly in hydrohalide acids (e.g., HCl). However, in neutral-to-alkaline conditions, where molybdenum oxyanions become more stable, dissolution of molybdenum increases. Thus, it is only moderately resistant to aerated solutions of ammonium hydroxide and has fair resistance in 1–10% sodium hydroxide. Molybdenum is significantly less resistant to corrosion in organic acids such as acetic and formic (at 10%, the corrosion rate being 0.2–0.3 mm $year^{-1}$), and in 0.25% benzoic acid (0.25 mm $year^{-1}$) at 100 °C. Combinations of inorganic and organic acids generally lead to increased corrosion rates, for example, addition of 5% sulfuric to 10% acetic acid triples the corrosion rate from 0.33 to about 1 mm $year^{-1}$.[20]

Oxidizing conditions severely reduce molybdenum's corrosion resistance, and aeration causes a significant increase in corrosion. It is therefore rapidly attacked by oxidizing acids such as nitric acid, and by reducing acids containing oxidizers such as HNO_3, $FeCl_3$, $CuCl_2$, etc. Also, mercuric chloride causes an intense form of pitting corrosion. It is severely corroded in sodium hypochlorite solutions.

3.17.3.2.2 Galvanic corrosion

In seawater (and presumably most other environments) molybdenum is found to be effectively protected by coupling to aluminum, steel, and magnesium.[19] However, contact with copper is more problematic and may slightly increase or decrease its corrosion rate in neutral chloride media, but act protectively in acid reducing media. In sodium hydroxide solution, molybdenum acts sacrificially to protect steel and, hence, Mo coatings on steel or cast iron are not always effective in alkaline conditions, especially when significantly porous. Coupling of molybdenum to stainless steels in most environments has no effect on the corrosion rate of either material.

3.17.3.2.3 High temperature water

Refractory and dense materials such as molybdenum, tungsten, and rhenium, are candidates for use in nuclear applications. For nuclear fusion reactor concepts in particular, dense refractory alloys that are resistant to liquid metals and that have good thermal conductivity are essential for efficient heat transfer. Similar requirements are evident in nuclear science applications such as spallation neutron sources. In all such cases, water cooling is likely to be important. To this end, a study of the corrosion of various candidate alloys was undertaken in high temperature pressurized water up to 320 °C.[22]

In flowing, high temperature water containing 400 ppb dissolved oxygen at pH 6–7, molybdenum and its alloys were found to have significantly better corrosion resistance than tungsten and its alloys. Up to 260 °C, neither material is corroded significantly ($<$50 μm $year^{-1}$ for tungsten and ~25 μm $year^{-1}$ for molybdenum). However, at 320 °C the corrosion rate of tungsten increased significantly to over 200 μm $year^{-1}$ while that of molybdenum was about 4 times lower (~50 μm $year^{-1}$). Alloying with rhenium had a detrimental effect on the high temperature corrosion resistance for both alloys, resulting in grain boundary attack with corrosion rates rising to over 1 mm $year^{-1}$ in the case of W–Re alloys.[22]

3.17.3.2.4 Corrosion of molybdenum alloys

The general and galvanic corrosion behavior of both the TZM and Mo–30W alloy are generally at least equal or sometimes superior to that of unalloyed molybdenum in many aqueous solutions of acids, bases and salts apart from strongly oxidizing environments such as in nitric acid.[23]

Sintered and amorphous molybdenum alloys containing significant amounts of tantalum, titanium, chromium and niobium have all been found to offer excellent resistance to strong reducing acids such as hot concentrated hydrochloric, sulfuric, phosphoric, oxalic and formic. For example, a sintered Ti–40Mo alloy corrodes between 1000 and 10 000 times more

slowly than Ti in boiling 35% hydrochloric acid although the corrosion rate in neutral conditions was unaffected.[24] Likewise, binary amorphous Mo–Cr, Mo–Nb, and Mo–Ta alloys all show spontaneous passivity in 12 M HCl with overall corrosion rates, in all cases, significantly less than the individual alloy components.[25]

Ti–15Mo alloys are of interest for prosthetic and replacement body implants (e.g., joints replacements and dental implants) because their relatively low elastic modulus matches better than that of bone. Further advantages include the excellent corrosion resistance of the alloy in body fluids, the relatively low toxicity of molybdenum and, for dental implants, resistance to fluoride.[26,27]

3.17.4 High Temperature Corrosion

3.17.4.1 Gaseous Environments

3.17.4.1.1 Oxidation

Molybdenum begins to oxidize significantly in air at about 300 °C. Oxidation becomes rapid at 500 °C and the rate of attack is very rapid by 1200 °C.[28] Below about 400 °C an adherent relatively stable MoO_2 scale is formed and oxidation proceeds according to the parabolic law under diffusion controlled transport through the growing scale. However, MoO_2 is unstable to further oxidation to MoO_3, which has a significant vapor pressure. Above 500 °C, the vapor pressure of MoO_3 becomes increasingly significant and at some higher temperature, depending on the total partial pressure of oxygen, the rate of evaporation of MoO_3 equals its rate of formation. At this point the volatilization rate becomes extremely rapid following linear kinetics. This sequence is summarized in Table 5.

The formation of molten MoO_3 above 802 °C results in a sudden increase in the oxidation rate because the rate of diffusion of oxygen through a liquid phase is considerably higher than through the solid phases present at lower temperatures. Also, for molybdenum-containing alloys where Mo is less than 50 wt%, the molten oxide can act as a flux for other potentially protective oxide species.[29] Note that the sequence of oxidation is consistent with the thermodynamic properties of the oxides. The activation energy for molybdenum oxidation to MoO_3 in the chemical rate-controlled region was found to be 82 kJ mol^{-1} at all temperatures above about 550 °C. At temperatures above around 1100 °C, samples were required to be as small as possible in order to provide enhanced diffusion and, hence, eliminate gas-phase effects. The reaction rate between molybdenum and oxygen in this regime is among the highest measured of all elements and significantly greater than that for tungsten.[27] At exceptionally high temperatures, typically less than 1900 °C and depending on pressure, MoO_3 dissociates to MoO_2, which then immediately combusts producing a flame.[30]

Secondary ion mass spectrometry (SIMS) has been performed on molybdenum oxide scales of thickness 10–12 μm after oxidation at 500 °C in order to analyze the distribution of MoO_2 and MoO_3, and the thicknesses of these layers, in the scale.[31] The majority of the scale (>90%) was found to consist of MoO_2 with only a comparatively thin region, less than 0.5 μm in thickness, corresponding to MoO_3 and located at the oxide–gas interface

3.17.4.1.2 Sulphidation

There is considerable interest in the corrosion of molybdenum in sulfidizing environments containing H_2S or SO_2/SO_3. This is in part due to the beneficial

Table 5 Oxidation sequence for molybdenum as a function of temperature[27]

Oxidation class	*Reaction conditions*	*Oxidation phenomena*	*Rate-controlling process*
1	Below 450 °C	Adherent solid oxide films or scales form	Diffusion control of metal or oxygen through oxide
2	450–800 °C	Solid oxide scales form but MoO_3 volatilizes with lower pressures favoring evaporation	Oxide scales not protective – chemical control via interfacial reaction.
3	802 °C – a transition temperature governed by gas-phase mass transport	Liquid MoO_3 is stable, but volatilizes as soon as oxide forms	Chemical reaction at metal interface with liquid oxide/gas.
4	Above transition temperature	Oxide volatilizes as fast as it forms	Gas-phase transport of oxygen to metal interface.

effect of molybdenum alloying additions for some alloys in reducing hot corrosion in these environments[32] and in part due to the manufacture of MoS_2 catalysts, for example by sulfidation of Mo-containing alloys, which are used in the hydrodesulfurization of petroleum fuels.[33]

Below about 600–700 °C, molybdenum undergoes relatively slow sulfidation, forming MoS_2. Appreciable reaction rates commence only above about 700 °C where an adherent and generally protective scale of MoS_2 forms by inwards diffusion of sulfur with parabolic reaction kinetics.[34] A change in the sulfidation rate after an initial period has been found to be the result of the formation of an inner layer of Mo_2S_3.[35] Sulfidation occurs in any environment containing significant partial pressure of sulfur, such as sulfur vapor, and also in gas mixtures containing sulfur species such as H_2S or SO_2.

The extremely low defect density of MoS_2, coupled with its relatively high melting point, is the main reason why molybdenum is resistant to sulfidation. In contrast, the sulfides of most other functional metals are highly defective and have low melting points (e.g., $Fe_{1-x}S$) and thus offer effectively no protective barrier. In view of this, doping of the sulfide scale is important and controls the sulfidation rate. Thus, in H_2/H_2S gas mixtures the sulfidation rate of molybdenum is increased with increasing hydrogen partial pressure and this may be explained by hydride doping of MoS_2.[36] Likewise, doping of lithium into the scale can increase the sulfidation rate by up to 10^4 times.[37]

3.17.4.1.3 Other environments

Carburization of molybdenum proceeds at high temperatures in vacuum when in contact with graphite components. Reaction only becomes significant above about 1200 °C when a layer of Mo_2C is formed on the metal surface. This is thought to grow by diffusion of carbon across the layer and is found to thicken with parabolic kinetics. This behavior is similar to that of tungsten but the molybdenum carbide layer grows faster than that for tungsten carbide. The formation of the continuous surface carbide layer in these materials slows their whole-scale carburization and embrittlement under these conditions.[38]

Molybdenum is nitrided in environments containing nitrogen (such as cracked ammonia) at temperatures 800–1200 °C with the formation of a continuous Mo_2N layer under approximate parabolic growth kinetics. Below 800 °C, the reaction is too slow to measure while above 1200 °C Mo_2N starts to decompose. Unlike with carburization, the reaction layer does not appear to provide protection against nitriding of the underlying material, which is likely to become extensively embrittled above around 1000 °C.[39]

In halogenating environments, molybdenum has significantly worse corrosion performance compared with tungsten[40] and the latter is a preferred alloying addition to improve the resistance to environments containing chlorine. The chlorination kinetics are similar to tungsten but considerably faster and no protective scale forms.[41]

3.17.4.2 Fused Materials

3.17.4.2.1 Liquid metals

Like tungsten, molybdenum has a relatively low solubility in many molten metals and this has inspired research on the use of molybdenum as a container, or as a process component, in liquid metal environments, particularly in molten metal die casting, and for the nuclear industry (liquid metal cooled fission reactors and fusion reactor concepts). Thus, like tungsten, molybdenum has excellent resistance to molten lead and lead–bismuth alloys.[42] In liquid sodium, molybdenum appears to be unaffected by the dissolved oxygen content but is dependent on dissolved carbon resulting in the formation of a Mo_2C corrosion product layer. This compares with tungsten, which is dependent on the mass transport of dissolved oxygen in forming ternary layers of oxide.[43] Molybdenum has significant advantages (high temperature strength, etc) in dies for hot metal working and for molten metal dies. In particular, the Mo–30W alloy is extremely resistant to molten zinc and this material is used extensively for zinc dies and as a container/crucible for molten zinc.[44]

3.17.4.2.2 Molten glasses

Molybdenum has good resistance to corrosion/degradation in most molten glasses except those containing lead oxide, which acts as an effective flux. Of course, molybdenum is still susceptible to oxidation above about 400 °C, unless protected by an appropriate gas atmosphere or by a coating. Further information on protective coatings is given below, however, traditionally physical cladding with platinum, or electrodeposition of dense, protective platinum coatings have been used and are effective. The corrosion resistance of molybdenum disilicide in molten glass is also of interest as this material is frequently used as a heating element for temperatures up to 1800 °C in air (due to the formation of protective layers of silica).

Additionally, direct electrical resistance heating of molten glass using molybdenum electrodes is often used (molten glass is an ionic conductor).

The corrosion resistance of molybdenum and molybdenum disilicide in molten soda-glass was studied at 1565 °C over a period of 48 h.[45] Molybdenum was found to have the best corrosion resistance forming a film of MoO_2 that was about 15 µm thick with a total recession loss over the testing period equivalent to about 110 µm. The oxide film on molybdenum was found to be cracked and this clearly allowed additional reaction beneath the film and further corrosion. On $MoSi_2$, no protective layer was formed with a loss of recession equivalent to over 315 µm. In all cases the corrosion rate was found to be related to the amount of dissolved oxygen in the glass. In contrast, molten borosilicate (E) glass under similar conditions is a much less aggressive environment, with no significant corrosion of molybdenum noted and considerably less attack on $MoSi_2$.[46]

3.17.4.3 Protection

The inability of molybdenum to withstand oxidizing conditions at even moderate temperatures has led to many investigations of the means of reducing the oxidation rate. Alloying has not been successful since the loss of key high temperature mechanical properties are unacceptable. Thus, protective coatings appear to be the most effective option. A number of coatings have been developed for molybdenum. At intermediate temperatures, up to about 900–1000 °C, molybdenum can effectively be protected against oxidation by cladding, by thermal sprayed coatings or by electroplating, for example with chromium–nickel.[47]

At higher temperatures, most protective strategies are based on siliconizing, that is, the formation of a coating of molybdenum disilicide. Such coatings generally have similar oxidation resistance to $MoSi_2$ heating elements up to about 1700 °C. Simple silicide coatings may be formed on molybdenum using a variety of methods, for example using gas-phase diffusion (i.e., cementation) processes. This predominantly forms the favored phase $MoSi_2$, however, after the cementation process is completed and during high temperature service, silicon can further diffuse into the molybdenum substrate forming the less protective Mo_5Si_3 phase. The service life of the coated alloy depends on the initial thickness of the $MoSi_2$ layer, whether it remains uncracked as also the temperature of operation, as the coating is slowly consumed by oxidation to silica.[48] More sophisticated coatings, used especially in the glass industry, are based on Si–B–C formulations and these can give more reliable operation to about 1450 °C.[49]

References

1. Imgrund, H.; Kinsman, N. *Stainless Steel World,* 20–31 September 2007.
2. International Molybdenum Association, Molybdenum and Applications of Molybdenum and Its Alloys. Available at http://www.imoa.info/.
3. *HSC: Chemistry, V6.12 (Thermochemical Database);* Outotec Research Oy: Finland, 2007.
4. Suppliers data via MATWEB. Available at http://www.matweb.com/
5. Stoloff, N. S. In *Superalloys II: High Temperature Materials for Aerospace and Industrial Power*; Sims, C. T., Stoloff, N. S., Hagel, W. C., Eds.; Wiley: USA, 1987; pp 61–96.
6. Gupta, C. K. In *Extractive Metallurgy of Molybdenum;* CRC Press, 1992; Chapter 1.
7. Brandes, E. A.; Brook, G. B. *Smithells Metals Reference Book,* 7th ed. Butterworth-Heinemann, 1994; Table 22–47.
8. Czarnecki, E. G.; Stacey, J. T.; Zimmerman, D. K. In *Refractory Metals and Alloys*; Semchyshen, M., Perlmutter, I., Eds.; Interscience Publishers: New York, 1963; Vol. 2.
9. Urquidi-Macdonald, M.; Macdonald, D. D. *J. Electrochem. Soc.* **1989**, *136*, 961–967.
10. Clayton, C. C.; Lu, Y. C. *J. Electrochem. Soc.* **1986**, *133*, 2465.
11. Newman, R. C. *Corros. Sci.* **1985**, *25*, 331–350.
12. Schneider, A.; Kuron, D.; Hofman, S.; Kirchheim, R. *Corros. Sci.* **1990**, *31*, 191.
13. Hull, M. N. *Electroanal. Chem. Interf. Electrochem.* **1972**, *38*, 143–157.
14. Halada, G. P.; Clayton, C. R.; Herman, H.; Sampath, S.; Tiwari, R. *J. Electrochem. Soc.* **1995**, *142*, 74.
15. Badawy, W. A.; Al-Khara, F. M. *Electrochim. Acta* **1998**, *44*, 693–702.
16. Gad-Allah, A. G.; Abd El-Rahman, H. A. *J. Appl. Electrochem.* **1988**, *18*, 441–446.
17. De Rosa, L.; Tomachuk, C. R.; Springer, J.; Mitton, D. B.; Saiello, S.; Bellucci, F. *Mater. Corros.* **2004**, *55*, 602–609.
18. Pozdeeva, A. A.; Antonovskaya, E. I.; Sukhotin, A. M. *Corros. Sci.* **1966**, *6*, 149–158.
19. Itagaki, M.; Suzuki, T.; Watanabe, K. *Electrochim. Acta* **1997**, *42*, 1081.
20. 'Acherman, W. L.; Carter, J. P.; Kenahan, C. B.; Schlain, D. *Corrosion properties of molybdenum, tungsten, vanadium and their alloys, Report Investigations No. 6, US Bureau of Mines* **1966**, p 715.
21. Bishop, C. R. *Corrosion* **1963**, *19*, 308t–314t.
22. Ishijima, Y.; Kakiuchi, K.; Furuya, T.; Kurishita, H.; Hasegawa, M.; Igarashi, T.; Kawai, M. *J. Nucl. Mater.* **2002**, *307–311*, 1369–1374.
23. Ackerman, W. L.; Carter, J. P.; Schlain, D. *Corrosion properties of the TZM and Mo–30W alloy, US Bureau of Mines Report No. 7* **1969**, p 196.
24. Nakahara, K.; Tokumoto, K.; Sakaguchi, S.; Hayashi, Y. *J. Jpn. Soc. Powder Powder Metall.* **1997**, *44*, 241–246.
25. Park, P. Y.; Akiyama, E.; Habazaki, H.; Kawashima, A.; Asami, K.; Hashimoto, K. *Corros. Sci.* **1996**, *38*, 1731–1750.
26. Kumar, S.; Narayanan, T. S. N. S. *J. Dent.* **2008**, *36*, 500–507.

27. Karthega, M.; Raman, V.; Rajendran, N. *Acta Biomater.* **2007**, *3*, 1019–1023.
28. Gulbranson, E. A.; Andrew, K. F.; Brassart, F. A. *J. Electrochem. Soc.* **1962**, *110*, 952–959.
29. Brenner, S. S. *J. Electrochem. Soc.* **1955**, *102*, 16–21.
30. Bartlett, R. W. *J. Electrochem. Soc.* **1964**, *113*, 744–746.
31. Gritscha, M.; Piplitsa, K.; Hutter, H.; Wilhartitz, P.; Wildner, H.; Martinz, H. P. *Surf. Sci.* **2000**, *454–456*, 284–288.
32. Strafford, K. N.; Winstanley, G. R.; Harrison, J. M. *Werkstoffe Korrosion* **1974**, *25*, 487.
33. Vissers, J. P. R.; De Beer, V. H. J.; Prins, R. *J. Chem. Soc., Faraday Trans. 1: Phys. Chem. Cond. Phases* **1987**, *83*, 2145–2155.
34. Gerlach, J.; Hamell, H. J. *Metall* **1969**, *23*, 1006–1011.
35. Lee, B. S.; Rapp, R. *J. Electrochem. Soc.* **1984**, *131*, 2998–3006.
36. Cheung, W. H.; Young, D. J. *Oxid. Met.* **1991**, *36*, 15–25.
37. Grzesik, Z.; Migdalska, M.; Mrowec, S. *High Temp. Mater. Processes* **2007**, *26*, 355–363.
38. Martinz, H. P.; Prandini, K.; Kock, W.; Sporer, D. *Mater. Corros.* **1998**, *49*, 246–251.
39. Martinz, H. P.; Prandini, K. *Int. J. Refract. Met. Hard Mater.* **1993/1994**, *12*, 179–186.
40. Prescott, R.; Stott, F. H.; Elliott, P. *Corros. Sci.* **1981**, *29*, 465–475.
41. Landsberg, A.; Hoatson, C. L.; Block, F. E. *J. Electrochem. Soc.* **1971**, *118*, 1331–1336.
42. Loewen, E. P.; Ballinger, R. G.; Lim, J. *Nucl. Technol.* **2004**, *147*, 436–456.
43. Barker, M. G.; Morris, C. W. *J. Less-Common Met.* **1976**, *44*, 169–176.
44. Burman, R. In *Refractory Metals and Their Industrial Applications*; Smallwood, R. E., Ed.; ASTM STP, 1982; Vol. 849, pp 3–17.
45. Kamakshi Sundamn, S.; Hsu, J.-Y.; Speyer, R. F. *J. Am. Ceram. Soc.* **1994**, *77*, 1613–1623.
46. Kamakshi Sundamn, S.; Hsu, J.-Y.; Speyer, R. F. *J. Am. Ceram. Soc.* **1995**, *78*, 1940–1946.
47. Couch, D. E.; Shapiro, H.; Taylor, J. K.; Brenner, A. *J. Electrochem. Soc.* **1958**, *105*, 450–456.
48. Wang, Y.; Li, Y.; Hu, X. *J. Mater. Sci. Technol.* **2001**, *17*, 479–481.
49. Martinz, H. P.; Nigg, B.; Matej, J.; Sulik, M.; Larcher, H.; Hoffmann, A. *Int. J. Refract. Met. Hard Mater.* **2006**, *24*, 283–291.

3.14 Corrosion of Zirconium and its Alloys

T.-L. Yau
12103 SE High Creek Road, Happy Valley, OR 97086-4729, USA

Glossary

Widmanstätten A metallurgical structure showing a characteristic cross-hatched appearance due to the grains is formed along the preferred crystallographic planes.

Zircaloy One of a group of alloys used as a nuclear fuel cladding material in light water reactors, thus taking advantage of the relatively low neutron capture cross section and relatively high corrosion resistance of zirconium.

Abbreviations

CPI Chemical process industry
DHC Delayed hydride cracking
HAZ Heat affected zone
NHE Normal hydrogen electrode
SCC Stress corrosion cracking

3.14.1 Introduction

Zirconium belongs to Group IVb of the period table being in the second row, beneath titanium and above hafnium. It has similar (but not identical) metallurgical and chemical properties to titanium and may be described as refractory (since their melting points are above the range of iron, cobalt, and nickel), reactive (since they are highly active and have, consequently, extremely negative equilibrium potentials), and corrosion resistant (since, by virtue of their passivity, they resist attack in many highly corrosive environments). Zirconium and titanium have similar corrosion properties; thus, both metals are excellent for handling seawater, while chromium-containing passive alloys (i.e., stainless steels) are susceptible to localized corrosion in seawater.[1] Moreover, both metals are susceptible to environments of low water activity and are attacked, for example, by halide-containing methanolic solutions; such attack being preventable by the addition of small quantities of water as an inhibitor.[2,3]

Zirconium and titanium are also sister metals of distinctive contrast.[4] The common perception is that zirconium is more suitable than titanium in handling reducing environments (such as hydrochloric and dilute sulfuric acids) than oxidizing environments (such as ferric chloride). Although there is some truth to this perception, it is not always true. Thus, in chloride-free and highly oxidizing environments (e.g., nitric acid), zirconium is often more corrosion resistant than titanium; mistakes can be made when such differences are ignored.

Historically, while the development of titanium resulted from the ever-increasing demands of the aerospace industry, the demand for zirconium arose from the nuclear industry.[5] For this latter application, a suitable structural material to clad nuclear fuel must have good corrosion–oxidation resistance, resistance to irradiation damage, adequate mechanical properties, and

transparency to thermal neutrons. Properly alloyed zirconium meets these requirements. After zirconium became available outside nuclear submarine programs in 1958, research on developing additional applications for zirconium has grown. So, in addition to fuel cladding material for water-cooled nuclear reactors, zirconium began to find uses in the chemical process industry because of its excellent resistance to a broad range of corrosives. Zirconium is also used in specialist surgical tools and instruments and is a highly beneficial alloying addition to iron-, copper-, magnesium-, aluminum-, molybdenum-, and titanium-based alloys. Zirconium is useful as a getter because of its ability to combine with gases at elevated temperatures. Along with niobium, zirconium is superconductive at low temperatures and is used to make superconductive magnets.

3.14.1.1 General Characteristics

3.14.1.1.1 Alloy categories

There are two major applications for zirconium and its alloys: nuclear and nonnuclear. Both of these use alloys with low levels of alloying additions and are, thus, based on the alpha microstructure (i.e., the hexagonal close packed lattice) with dilute additions of solid solution strengthening and alpha stabilizing elements like oxygen and tin. However, in niobium-containing alloys, there is the presence of some niobium-rich second phase particles of the body-centered cubic (beta) lattice.

One of the major differences between nuclear and nonnuclear zirconium alloys is in hafnium content. Nuclear grades of zirconium alloys are virtually free of hafnium (not greater than 100 ppm). Hafnium has an enormous effect on absorbing thermal neutrons, which is critical for nuclear applications and is, therefore, suitable for nuclear reactor control rods that are required to absorb excess neutrons in order to control the uranium fission process. On the other hand, nonnuclear grades of zirconium may contain up to 4.5% hafnium. Hafnium has only a minor effect on zirconium's mechanical and chemical properties.

3.14.1.1.2 Physical and mechanical properties

Zirconium is a lustrous, grayish white, ductile metal whose typical physical and mechanical properties are listed in Tables 1 and 2, respectively. For engineering purposes, there are three interesting features of zirconium. First, the density of zirconium is lower than those of iron- and nickel-based stainless alloys. Second, zirconium has a low coefficient of thermal expansion (the coefficient of thermal expansion of zirconium is about two-thirds that of titanium, about one-third that of type 316 stainless steel, and about one-half that of nickel-copper alloys). Third, zirconium has a thermal conductivity ($22\,W\,m^{-1}\,K^{-1}$), which is about 30% greater than that of stainless alloys ($16\,W\,m^{-1}\,K^{-1}$). These features allow zirconium to be fabricated into compact, efficient equipment, for example as heat exchangers in aggressive environments.

Zircaloy-2, Zircaloy-4, and the niobium-containing alloys are nuclear grades. Zircaloy-2 and Zircaloy-4 contain about 1.5% tin but are different in iron and nickel contents. Thus, Zircaloy-4 has more iron but no nickel in order to minimize hydrogen pick-up. Both alloys are popular in water-moderated reactors, such as boiling water and pressurized water reactors. The Zr–2.5Nb alloy is used in heavy water moderated reactors, such as Canada Deuterium Uranium (CANDU) reactors.

Table 1 Physical properties of zirconium, titanium, hafnium, and iron

	Zirconium	*Titanium*	*Hafnium*	*304L*
Atomic number	40	22	72	26
Relative atomic mass	91.22	47.87	178.49	55.85
Lattice structure	hcp < 1140 K bcc > 1140 K	hcp < 1060 K bcc > 1060 K	hcp < 2050 K bcc > 2050 K	bcc < 1180 K fcc > 1180 K
Melting point (K)	2125	1943	4876	1809
Density ($Mg\,m^{-3}$)	6.49	4.5	13.1	7.86
Young's modulus (GPa)	68	116	78	211
Electrical conductivity $(\Omega\,cm)^{-1}$	0.0236×10^{-6}	0.0234×10^{-6}	0.0312×10^{-6}	0.0993×10^{-6}
Thermal conductivity ($W\,m^{-1}\,K^{-1}$)	22.7	21.9	23	80.2
Thermal expansion (K^{-1})	5.7×10^{-6}	8.6×10^{-6}	5.9×10^{-6}	11.8×10^{-6}
Thermal neutron capture cross-section (m^2)	1.8×10^{-29}	–	1.05×10^{-26}	–

hcp, hexagonal close packed; bcc, body centered cubic; fcc, face centred cubic.

Table 2 Nuclear and nonnuclear grades of zirconium alloys

	Composition (wt%)									
Alloy design (UNS #)	*Zr + Hf (min)*	*Hf (max)*	*Sn*	*Nb*	*Fe*	*Cr*	*Ni*	*Fe + Cr*	*Fe + Cr + Ni*	*O (max)*
Nuclear grades										
Zircaloy-2 (R60802)	–	0.01	1.20–1.70	–	0.07–0.2	0.05–0.15	0.03–0.08	–	0.18–0.38	–
Zircaloy-4 (R60804)	–	0.01	1.20–1.70	–	0.18–0.24	0.07–0.13	–	0.28–0.37	–	–
Zr-2.5Nb (R60901)	–	0.01	–	2.40–2.80	–	–	–	–	–	–
Nonnuclear wrought grades										
Zr700 (R60700)	99.2	4.5	–	–	–	–	–	0.2 (max)	–	0.10
Zr702 (R60702)	99.2	4.5	–	–	–	–	–	0.2 (max)	–	0.16
Zr704 (R60704)	97.5	4.5	1.0–2.0	–	–	–	–	0.2–0.4	–	0.18
Zr705 (R60705)	95.5	4.5	–	2.0–3.0	–	–	–	0.2 (max)	–	0.18
Zr706 (R60706)	95.5	4.5	–	2.0–3.0	–	–	–	0.2 (max)	–	0.16
Nonnuclear casting grades										
Zr702C	98.8	4.5	–	–	–	–	–	0.3 (max)	–	0.25
Zr704C	97.1	4.5	1.0–2.0	–	–	–	–	0.3 (max)	–	0.3
Zr705C	95.1	4.5	–	2.0–3.0	–	–	–	0.3 (max)	–	0.3

Zr700, Zr702, Zr704, Zr705, and Zr706 are nonnuclear grades for wrought materials. Zr702C, Zr704C, and Zr705C are nonnuclear grades for casting materials. Zr700 is an alloy with an oxygen content of less than 1000 ppm which has improved bondability in explosive cladding applications and deep drawing applications. Zr702 is commercially pure zirconium and is most popular for corrosion resistant applications. Zr705 is preferred when strength is an important factor.

Moreover, because recyclable material is generated from fabrication of nuclear fuel cladding, a major impurity in nonnuclear alloys is tin, which is not shown in **Table 2**. The use of recycled materials lowers the cost of nonnuclear alloys and keeps mechanical properties consistent. The elevated tin content may affect zirconium's corrosion properties in certain environments. Also, since there is not enough demand in nonnuclear applications to support the production of Zr704, in nonnuclear applications, Zr704 may be effectively Zircaloy-2 or Zircaloy-4.

Zirconium and hafnium form a solid solution at all concentrations. However, the presence of small amounts of hafnium in zirconium does not significantly affect mechanical or chemical properties other than the thermal neutron cross-section. The counterparts of nuclear and nonnuclear grades of zirconium alloys are interchangeable in mechanical properties. However, specification requirements for nuclear materials are more extensive than those for nonnuclear materials. Mechanical requirements only for nonnuclear alloys are given in **Tables 3** and **4**. It can be seen that Zr705 is the strongest alloy with improved formability.

Additional typical property data are given in **Table 5** and in **Figures 1** and **2**. **Table 5** shows that the fatigue limits of zirconium alloys are very notch sensitive. **Figure 1** shows that the tensile strengths of zirconium alloys decrease quickly with increasing temperature. **Figure 2** indicates that Zr702 and Zr705 creep at low temperatures and stresses. These are important factors to consider in the application of zirconium equipment, particularly at elevated temperatures.

Table 3 ASTM requirements for the room temperature mechanical properties of zirconium alloys

Alloy	*UTS (MPa)*	*YS (MPa)*	*Elongation (%)*	*Bend test radius*
Zr700	380 (max.)	305 (max.)	20	5T
Zr702	380	205	16	5T
Zr704	415	240	14	5T
Zr705	550	380	16	3T
Zr706	510	345	20	2.5T

Bend tests are not applicable to material more than 4.75-mm thick. T is the thickness of the bend test specimen.

Table 4 ASME mechanical requirements for Zr702 and Zr705 used for unfired pressure vessels

Material form and condition	*ASME number*	*Alloy grade*	*UTS (min) (MPa)*	*YS (min) (MPa)*	*Maximum allowable stress in tension for metal temperatures not exceeding °C (MPa)*							
					−30 to 40	*65*	*125*	*175*	*225*	*275*	*325*	*375*
Plate, sheet, strip	SB 551	702	380	205	108	104	84.3	70.1	58.7	47.9	40.3	35.5
		705	550	380	158	144	119	105	94.7	86.8	81.2	77.6
Seamless tubing	SB 523	702	380	205	108	104	84.3	70.1	58.7	47.9	40.3	35.5
		705	550	380	158	144	119	105	94.7	86.8	81.2	77.6
Welded tubing[a]	SB 523	702	380	205	92.4	122	71.4	59.7	49.4	40.7	34.1	30.9
		705	550	380	134	88.4	101	89.5	80.8	73.9	68.9	66
Forgings	SB 493	702	380	205	108	104	84.3	70.1	58.7	47.9	40.3	35.5
		705	550	380	158	144	119	105	94.7	69.4	81.2	77.6
Bar	SB 550	702	380	205	108	104	84.3	70.1	58.7	47.9	40.3	35.5
		705	550	380	158	144	119	105	94.7	86.8	81.2	77.6
Seamless pipe	SB 658	702	380	205	108	104	104	70.1	58.7	47.9	40.3	35.5
		705	550	380	158	144	119	105	94.7	86.8	81.2	77.6
Welded pipe[a]	SB 658	702	380	205	92.4	122	71.4	59.7	49.4	40.7	34.1	30.9
		705	550	380	134	88.4	101	89.5	80.8	73.9	68.9	66

[a]0.85 factor used for welded product.

Table 5 The 10^7 fatigue limits for zirconium alloys

Alloy	*Fatigue limit (MPa)*	
	Smooth	*Notched*
Iodide Zr	145	55
Zircaloys or Zr 705 (annealed 2 h at 732 °C)	283	55
Zr–2.5% Nb (Aged 4 h at 566 °C)	290	55

3.14.1.1.3 Microstructure

Typical microstructures for the parent metal, heat-affected zone (HAZ), and weld metal of annealed zirconium alloys are shown in Figures 3–5. Zr702 is effectively an unalloyed grade (apart from some oxygen) and exhibits an equiaxed alpha structure as shown in Figure 3(a). Most elements have very low solubility in zirconium with oxygen, titanium, hafnium, and scandium the few exceptions. Zirconium

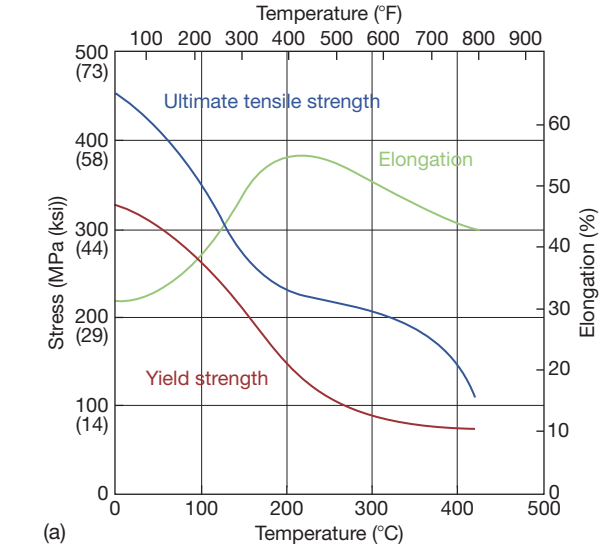

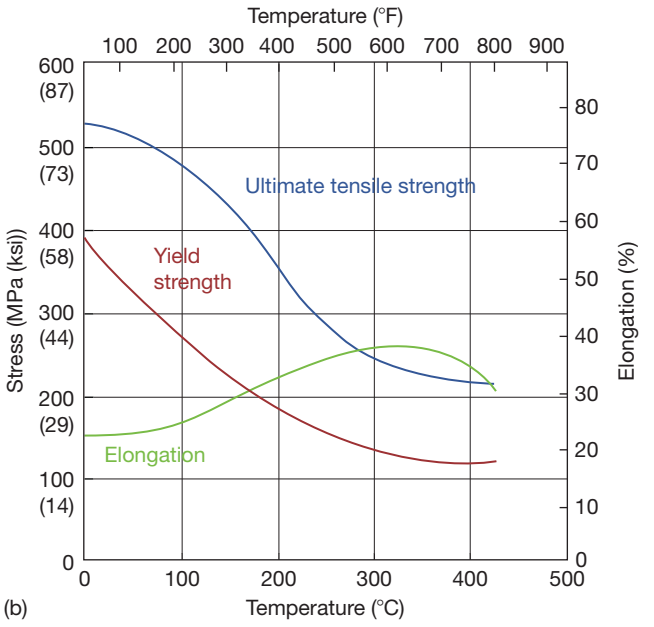

Figure 1 (Continued)

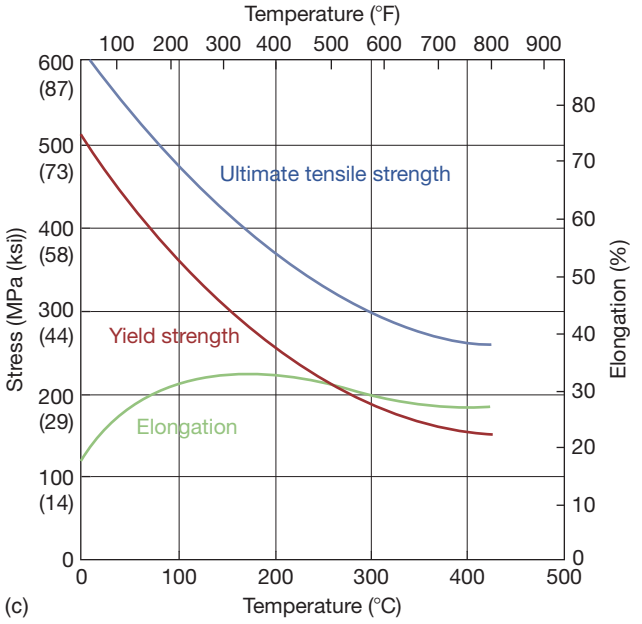

Figure 1 Tensile properties vs. temperature curves for zirconium alloys: (a) Zr702, (b) Zr704, and (c) Zr705.

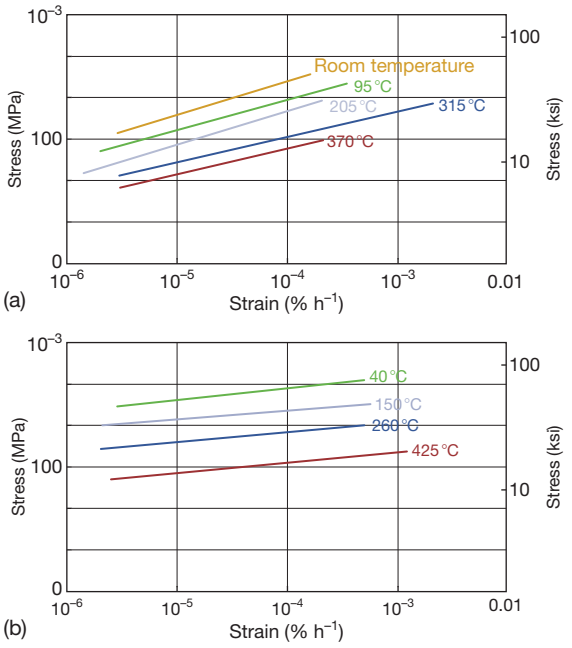

Figure 2 Minimum creep rate vs. stress curve for zirconium alloys: (a) Zr702 and (b) Zr705.

tends to react with many elements to form intermetallic compounds during the production stage, and one of these (and also a major impurity) is iron. Consequently, the most visible second-phase particles in **Figure 3(a)** are Zr–Fe compounds. There may also be fine chromium and nickel particles incorporated into these compounds that are well distributed in the alpha structure.

With few grain-boundary pinning precipitates in Zr702, grains in the HAZ grow to much larger sizes generally with an acicular structure (**Figure 3(b)**) while the weld metal itself exhibits a Widmanstätten structure as shown in **Figure 3(c)**. Welding has a great effect on the morphology of second-phase particles, and this affects the corrosion of zirconium in certain conditions. Like Zr702, Zircaloys or Zr704 exhibit an equiaxed alpha structure in the parent metal (**Figure 4(a)**), a pronounced acicular alpha structure in the HAZ (**Figure 4(b)**), and a Widmanstätten structure in the weld metal (**Figure 4(c)**).

Zr705 exhibits a two-phase structure. It has much finer grain than that of the alpha alloys as shown in **Figure 5**. It contains both the alpha zirconium phase and the beta niobium phase in the parent metal (**Figure 5(a)**). The HAZ has a mild change in structure as shown in **Figure 5(b)**. The weld metal has a fine acicular structure of alpha zirconium and beta niobium (**Figure 5(c)**).

3.14.1.2 Chemical and Corrosion Properties

Zirconium is a highly reactive metal, as evidenced by its standard potential of −1.53 V versus the normal hydrogen electrode (NHE) at 25 °C. For comparison,

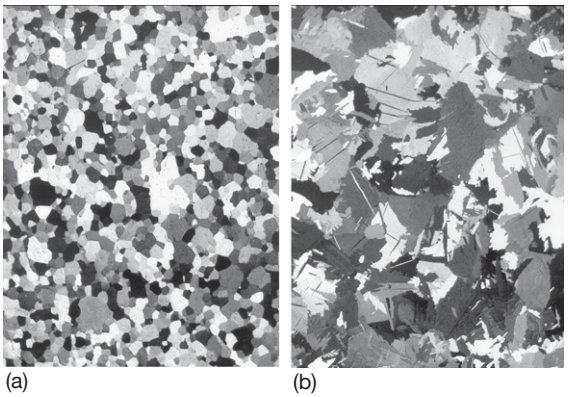

Figure 3 Microstructure of Zr702: (a) parent metal of Zr702, (b) HAZ of Zr702, and (c) weld metal of Zr702.

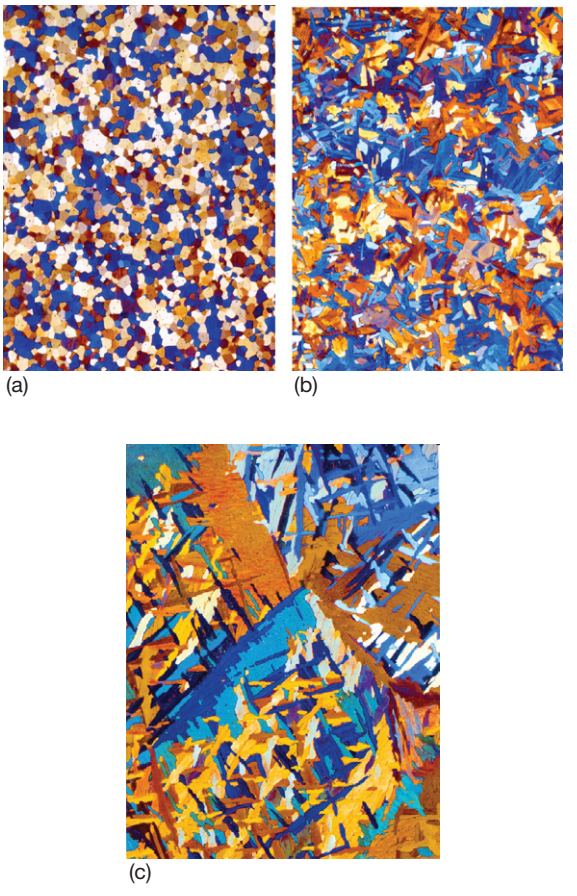

Figure 4 Microstructure of zircaloy-4 or Zr704: (a) parent metal of zircaloy-4 or Zr704, (b) HAZ of zircaloy-4 or Zr704, and (c) weld metal of zircaloy-4 or Zr704.

the potentials for titanium, chromium, iron, and nickel are −1.53, −0.74, −0.44, and −0.25 V, respectively. Zirconium owes its high corrosion resistance to its strong affinity for oxygen. In an oxygen-containing medium such as air, water, or carbon dioxide, zirconium spontaneously reacts with oxygen at ambient temperature and below to form an adherent, protective oxide film on its surface. This film is self-healing and protects the base metal from chemical and mechanical attack at temperatures up to about 350 °C. As a result, zirconium resists attack in most acids, salt solutions, alkaline solutions, and organic media. Zirconium is particularly suitable for handling reducing acids in which most passive alloys have great difficulty in forming passive films. However, in more extreme conditions, such as hydrofluoric acid, hot concentrated sulfuric acid, and certain dry organic halides, a passive oxide cannot readily form and, hence, zirconium is not suitable for handling these media.

In addition, zirconium is susceptible to localized corrosion, such as pitting and SCC in chloride solutions under oxidizing conditions. However, zirconium is not susceptible to crevice corrosion in chloride solutions since the condition in a crevice is often reducing. However, zirconium is susceptible to crevice corrosion in fluoride solutions and sulfuric acid. Examples of review articles on the corrosion of zirconium are given.[6,7]

3.14.1.3 Manufacture

3.14.1.3.1 Fabrication

Corrosion failures of zirconium equipment can often be prevented by using alternate choices or methods of design, fabrication (including welding), or by specific heat treatment processes and techniques. Final

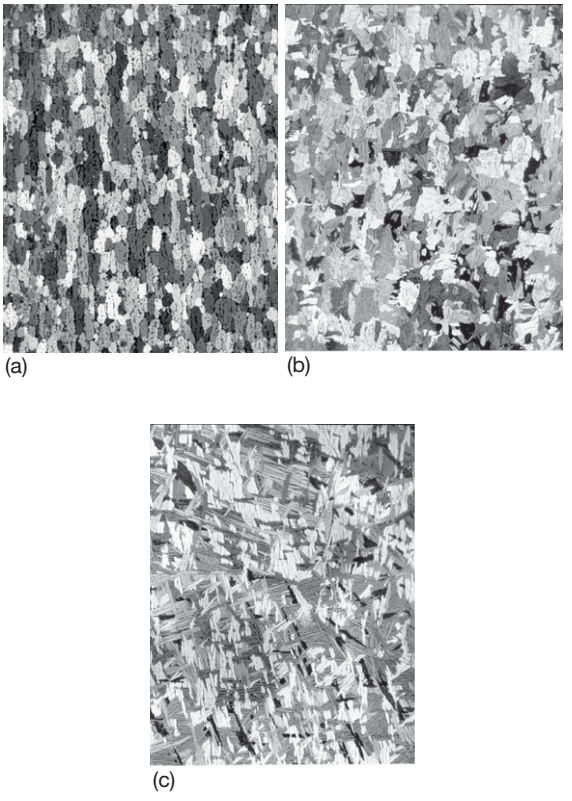

Figure 5 Microstructure of the Zr–2.5Nb alloy or Zr705: (a) parent metal of the Zr–2.5Nb alloy or Zr705, (b) HAZ of the Zr–2.5Nb alloy or Zr705, and (c) weld metal of the Zr–2.5Nb alloy or Zr705.

surface treatment methods can also be applied to modify a surface finish or remove impurities from a surface for improved corrosion resistance. During standard fabrication processes, the surface of the material can become embedded with particles that may affect the corrosion resistance of the zirconium. Since zirconium is relatively a soft metal, abrasive grinding stones may embed aluminum oxide or silicon carbide particles in the material surface causing preferred sites for the initiation of localized corrosion. Abrasive grinding operations performed on zirconium should, therefore, be followed by conditioning with a clean stainless steel brush, clean draw file, or rotary carbide burr to remove any abrasive particles embedded on the surface. If the final part is blasted for a cosmetic appearance, steel shot blast should not be used because the shot will embed into the material surface causing potential localized corrosion failures, especially if used in an acidic chloride environment. However, if the use of steel shot cannot be avoided, then it must be followed by acid pickling or chemical cleaning to remove embedded iron particles.

If other alloys are fabricated near the zirconium vessel, potential sources for embedded particles include grinding and weld spatter of foreign material. For this reason, it is recommended that the zirconium equipment not be welded and fabricated in an area where other materials are being ground, welded, or torch cut. If a zirconium vessel is fabricated in a bay where other materials are being fabricated, then the area should be surrounded by protective barriers and kept clean. Any weld spatter should be removed by stainless steel brushing, grit or glass bead blasting, or light grinding.

It is recommended that hydrostatic expansion be performed when zirconium tubes are expanded into a tubesheet prior to welding. This minimizes the potential for embedded particles on the ID of the tube surface caused during roller expansion as a result of improperly cleaned roller expansion tooling. Corrosion failures in halogen acid environments have been identified where roller expansion of tubes was used. Embedded particles may cause localized pitting attack of the tubes and eventual penetration of the tube wall. For halogen acid applications, all final equipment surfaces exposed to the corrosive environment should be free of iron contamination.

Any tooling used for the fabrication of zirconium should be thoroughly cleaned to remove any contamination left by previous materials. Tooling used for welding or conditioning, such as grinding stones, wire brushes, draw files, etc., should be dedicated for zirconium only. If this tooling has been used previously on other materials, the materials may contaminate the zirconium surface. It is recommended that color coding of the ancillary tooling (files, grinding stones, wire brushes, etc.) be implemented to minimize the potential for cross contamination.

3.14.1.3.2 Problems arising from handling

When zirconium is handled or moved using a forklift and/or lifting straps, protective coverings should be used to prevent the steel from being smeared into the zirconium metal surface. Forklift blades and steel straps will also cause scratches, scrapes, and surface defects that could be detrimental when it is exposed to subsequent forming operations and to certain corrosive environments. To minimize pickup of steel and other metal particles, it is recommended whenever possible to cover the forming dies with a protective covering such as leather, rubber, or some other types of noncontaminating material. This will also minimize the potential for surface damage caused by the steel tooling.

3.14.1.3.3 Welding

Generally, zirconium welds exhibit similar corrosion resistance to nonwelded areas except when used at the higher concentrations of sulfuric acid (see corrosion resistance of Zr in Section 3.14.3.3.1). Improper welding processes, however, can affect the mechanical and corrosion properties of zirconium. Interstitial element pickup, such as hydrogen, nitrogen, oxygen, and carbon in welds will generally not increase the corrosion rate of zirconium. These interstitials may, however, reduce the ductility of the metal and cause premature mechanical failures. Nitrogen contamination caused by plasma cutting with nitrogen gas may increase the corrosion rate of zirconium in nitric acid environments. If any type of cutting operation performed (e.g., oxyacetylene, plasma, laser, etc.) is used, the HAZ should be removed by grinding or machining prior to welding. Water jet cutting should be used for the cutting of zirconium, where possible, to avoid the potential for contamination caused by the heat input. The water jet cut should also be conditioned because this process utilizes an abrasive (i.e., garnet, etc.), which will embed into the zirconium surface.

3.14.1.3.4 Heat treatment

Improper heat treatment can result in damage to zirconium in a way which could be deleterious to corrosion resistance. Zirconium can be damaged during heat treatment if the material is placed in a nonoxidizing (i.e., reducing) atmosphere. An atmosphere with excess hydrogen (or with sufficient cathodic polarization) will cause the zirconium to absorb hydrogen and may affect the corrosion resistance of the zirconium. Before heat treatment, the zirconium vessel must be thoroughly cleaned of any surface impurities to prevent contamination during elevated temperature annealing.

When zirconium is cold formed and then heated into the full annealing temperature range, critical grain growth may occur. The grain structure will enlarge in the areas where 2–10% strain energy or cold work has been placed. Cold work of this degree can occur in some cases where plate has been brake press formed into pipe or elbows. On many occasions, formed pipe should be stress relieved at 550 °C for 30 min per 25 mm of thickness. This heat treatment will relieve the stresses caused by forming and welding. If the material is heated to the annealing range of 650–790 °C, the cold worked areas with 2–10% work will recrystallize forming very large grains surrounded by fine grains (i.e., unworked areas). These areas can be either on the outer metal surface, which is in tension, or on the inner surface, which is in compression and will have large grains with large grain boundaries. These very large areas of accelerated grain growth may be more susceptible to intergranular attack in the higher concentrations of sulfuric acid and should be avoided.

3.14.1.3.5 Chemical cleaning

If zirconium equipment is to be used in halogen acids, it is recommended that it has to be cleaned chemically to remove any embedded iron during fabrication. This process should be done by a company experienced in the cleaning of a reactive metal. Smooth and clean surfaces will have the optimum corrosion resistance where rough surfaces are more likely to have surface imperfections, which could initiate premature corrosion attack, especially in the more severe environments. Before any equipment is placed in any corrosive media, it should be cleaned thoroughly to remove oils, grease, paint, and other surface debris.

3.14.2 Corrosion

3.14.2.1 Oxide Films

Zirconium behaves much like other passive metals, such as titanium, iron, and chromium, relying on passive oxide films for corrosion resistance. However, zirconium is unique in several aspects in the formation and properties of its oxide film. First, the growth of the zirconium oxide film entirely results from the migration of the O^{2-} ion.[8] That is, a new layer of oxide film continues to form at the metal–oxide interface. The first layer will form spontaneously because of the reactive nature of zirconium and its strong affinity (reactivity and solubility) for oxygen. Additional layers will form at much reduced and decreasing rates resulting from the protective power of the first and additional layers. This also implies that zirconium can conveniently heal any damage done at the metal–oxide interface, provided that the damage is done in an oxygen-containing environment. Very often, there is a thin layer of protective oxide film at the interface even if or when the outer layer is porous and not so protective.

Second, the oxide film on zirconium is most likely ZrO_2. The existence of oxygen derivatives of zirconium in valence states other than four may be possible but is doubtful.[9] However, the passive films on most passive metals can be oxides in valency of various states. For example, the oxide film on titanium

can be the most protective TiO_2 film formed in oxidizing media, or a much less protective film as TiO, Ti_2O_3, and their mixture formed in reducing media. Third, ZrO_2 is a compound that is closer to insulators than to semiconductors. The chemical bonding between zirconium and oxygen is very strong and the transport of current through the film becomes increasingly difficult as the film grows. However, as for many passive alloys, the protective film is unreliable in the presence of flaws on the surface.

Accepting ZrO_2 as the compound for the passive film on zirconium does not lead to a total agreement among researchers. After all, ZrO_2 has three different crystalline structures: cubic (c), tetragonal (t), and monoclinic (m). Normally, c, t, and m ZrO_2 are stable at temperatures between 2680 and 2370 °C, between 2370 and 1240 °C, and below 1240 °C, respectively. Burgers *et al.*[10] reports the film formed on zirconium during anodic polarization in a phosphoric solution to be monoclinic (m) ZrO_2, identical to the natural zirconium ore 'baddeleyite'. However, according to Charlesby,[11] the anodic film is cubic (c) ZrO_2 in the case of polarization in 0.1 N HNO_3; in dilute H_2SO_4 or a borate solution, the film is primarily amorphous, but contains some cubic ZrO_2. Cox[12] has stated that the passive film formed on H_2SO_4 is predominantly the cubic structure with traces of the monoclinic structure.

The oxide film formed on zirconium alloys in water and steam is just as complicated. The oxide scales are known to be predominately monoclinic ZrO_2; however, it has been shown that the oxide layer is under high compressive stress, which may stabilize the oxide in its tetragonal form.[13,14] Studies by Raman spectroscopy and X-ray diffraction have shown that the oxide is a mixture of both (t) and (m) ZrO_2 structures.[15,16] Godlewski *et al.*,[15] using tapered samples, have shown that in Zircaloy-4 and Zr–1% Nb alloys, ~40% of the oxide film near the oxide–metal interface has (t) structure and the proportion of (t) decreases to ~15% as the distance from the interface increases beyond ~600 nm. Using the reflection high energy electron diffraction technique on the Zr–2.5% Nb alloy, Khatamian and Lalonde[17] detected a mixture of nearly (c), (t), and (m) structures for films of 200-nm thick or less and the (m) structure for the outer layers of films thicker than 800 nm.

It appears that protective oxide films can, therefore, be (m), (t), (c), or their mixtures. It would be incorrect to assume that zirconium and its alloys have, for example, (t) ZrO_2 to be corrosion and oxidation resistant. After all, to form, for example, (t) ZrO_2 at a temperature between 1240 and 2370 °C cannot protect zirconium. All three forms of zirconium oxide are about equally inert. Which one forms on zirconium's surface depends on temperature, alloying elements, environmental composition, and the state of stress in the film. Regardless of its structure, as long as the film is compact and adherent, it is protective.

3.14.2.2 Effects of Water

Water is the essential ingredient in aqueous corrosion of most metals and alloys. The presence of water in many environments makes them much more corrosive to common metals. However, with few exceptions, water is zirconium's best friend. For example, a major reason for using zirconium in the nuclear industry (apart from its low neutron capture cross section) is its excellent resistance to water and steam. This capability even extends into highly reducing conditions such as hydrochloric and dilute sulfuric acids. However, zirconium may become vulnerable in certain water-free environments, for example, organic solutions. Without water, zirconium is not able to repair any damage made to the protective film. Hence, the reactive nature of zirconium will be exposed to corrosive attack; the addition of small amounts of water may stop this.

Exceptions include the presence of water in chlorine and fluorine that makes them corrosive to zirconium. Unlike titanium, zirconium resists attack by dry chlorine (titanium may even ignite in dry chlorine). However, zirconium is susceptible to local attack in wet chlorine, which can be regarded as an oxidizing chloride solution (i.e., containing chloride and hypochlorite). Water-containing fluorine is corrosive to both titanium and zirconium.

3.14.2.3 Effects of Temperature

Zirconium is regarded as both a reactive and refractory metal because of its high melting point of 1852 °C. However, zirconium is not suitable for high temperature applications because of its reactivity. Zirconium reacts with many metallic and nonmetallic elements at elevated temperatures, that is why zirconium needs a clean surface and argon shielding in welding. Heat treatments may be done in air, but only with a clean surface. For example, to leave a fingerprint on zirconium's surface, this may result in local breakaway oxidation as demonstrated in **Figure 6**.

Zirconium may be used for long-term service generally only when the temperature is 350 °C or lower. For example, the corrosion rate of zirconium changes

little in nitric acid and dilute sulfuric acid as the temperature increases within zirconium's limit. With increasing temperature, the corrosion rate of zirconium may increase but so does the film formation rate. The net change remains small. Of course, in noncompatible media, such as hydrofluoric acid and concentrated sulfuric acid, the corrosion rate of zirconium increases rapidly with increasing temperature.

3.14.2.4 Effects of pH

Thermodynamically, zirconium behaves like most passive metals in acidic and alkaline solutions as shown in Figure 7.[9] Zirconium dioxide or hydrated zirconium dioxide dissolves as ZrO^{2+} when the pH is less than or equal to 3.5 and as Zr^{4+} when the pH is less than about 1. Dissolution as ZrO^{2+} is expected to be much slower than as Zr^{4+}. Zirconium dioxide retains most of its protective capability until the pH is less than 1 and above 13. In fact, zirconium is one of the few metals that exhibit excellent corrosion resistance over such a wide range of pH and, hence, zirconium equipment can be used in processes that cycle between strong acids and strong alkalis. In this aspect, zirconium is better than other high-performance materials, such as titanium, tantalum, glass, and polytetrafluoroethylene (PTFE), which are generally poor in strong alkalis.

The pH has some effect on the solubility of the oxide film on zirconium, but the effect is not dramatic. Practically, the corrosion resistance of zirconium has little dependence on pH over a wide range.[18] Zirconium dioxide is virtually insoluble in neutral water. It dissolves slightly as the pH increases or decreases as long as pH is not extreme. Slight dissolution conditions for zirconium oxides may have some beneficial effects that are discussed later.

However, pH change may alter the corrosive nature of impurities in a solution. Two important impurities to be considered are ferric ion and fluoride ion. Ferric ion is a common, well-known oxidizing ion that induces pitting on metals and alloys in halide

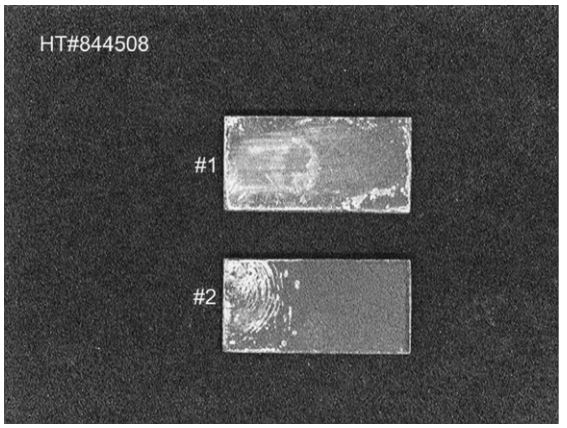

Figure 6 Effect of finger print on zirconium after heating at 760 °C for 30 min.

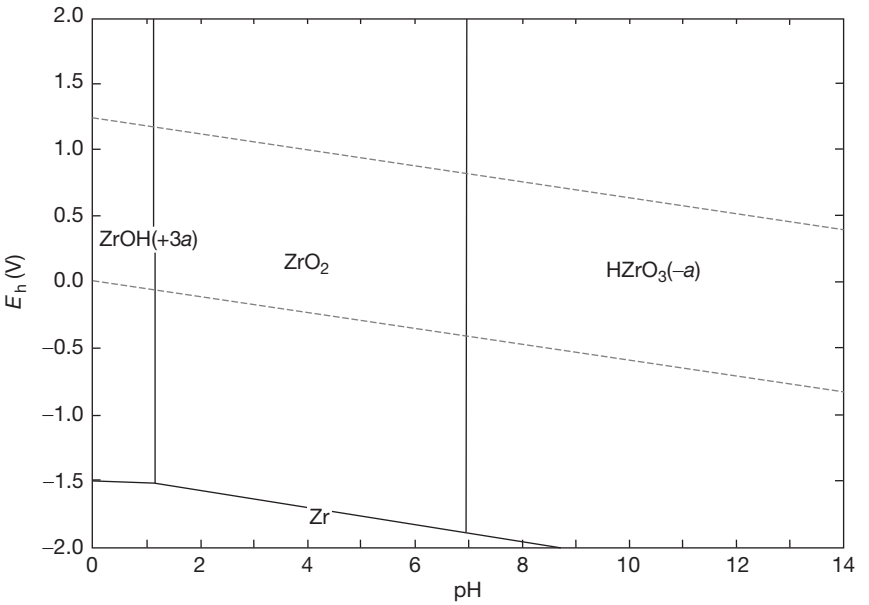

Figure 7 The potential–pH diagram of zirconium in water at 25 °C for a dissolved metal ion concentration of 10^{-5} M.

solutions. Fluoride ion has the capability to interfere with oxide formation even at low temperatures. Normally, ferric ion exits in solutions when the pH is less than or equal to 2.5 and when the solution potential exceeds 0.771 V versus NHE.[9] In a nonaerated acid, iron corrodes to yield ferrous ions that are too reducing to induce pitting on most metals and alloys. Ferrous ion tends to become ferric ion in the presence of oxygen. Zirconium resists pitting in iron-containing chloride solutions when the pH is 3 or greater.[19] To control the pitting of zirconium in copper-containing chloride solutions, the pH needs to be 5 or greater.[20]

Furthermore, the corrosivity of fluoride solutions may change dramatically with changing pH. Zirconium is totally defenseless in hydrofluoric acid (HF) at all concentration and temperature as it forms soluble zirconium complex ions in the acid. Although zirconium is not suitable for handling HF solutions, it has some resistance to certain fluoride solutions, such as calcium and sodium fluorides, provided the pH is sufficiently high and the temperature is sufficiently low. The corrosion rate of zirconium in saturated calcium fluoride at pH 5 and 90 °C is close to zero ($<0.025\ \text{mm year}^{-1}$). However, although the corrosion rate of zirconium in saturated sodium fluoride (at pH 7.4) is also effectively zero at 28 °C, it is more than $1270\ \mu\text{m year}^{-1}$ at 90 °C. One major difference between calcium and sodium fluorides is their solubility in water. At room temperature, the solubility of calcium and sodium fluorides are 2 and 4300 ppm, respectively. Hot solutions with a lot of dissolved fluoride ions are potentially corrosive to zirconium. However, the concentration of dissolved fluoride ions is not always proportional to the concentration of the added fluoride salt.

Thermodynamically, hydrofluoric acid exists when the pH is less than or equal to about 3.2.[9] The solution then becomes increasingly corrosive to zirconium, regardless of temperature, with decreasing pH. Therefore, zirconium is not recommended for handling fluoride-containing acids, unless the fluoride ions are effectively removed by complexing.[21] It is important to be aware that there may be overlooked sources of fluoride in particular processes.[22] For example, technical grade phosphoric acid can contain over 1000 ppm of fluoride ion (not necessarily indicated in the specification). Food grade phosphoric acid clearly gives the minimum fluoride content, typically, <5 ppm. Other overlooked sources include contaminated waters, recycled acids, fluxes, and fluorinated compounds.

3.14.2.5 Localized Corrosion

3.14.2.5.1 Pitting corrosion

Like most passive metals and alloys, zirconium is susceptible to pitting in all halide solutions except fluoride solutions[23] where it is vulnerable to general corrosion. For zirconium, the susceptibility to pitting is greatest in chloride solutions and decreases as the halide ion becomes heavier. This is the reverse order in the case for titanium, which is highly resistant to pitting in chloride solution but is vulnerable to pitting in iodide solutions.

The pitting potentials of zirconium in 1 N solutions of Cl^-, Br^-, and I^- are +380, +660, and +910 mV NHE, respectively. These potentials decrease gradually with increasing concentration and decrease rapidly in concentrated halide solutions.[24] Other factors, such as pH,[24] temperature,[24] alloying element,[25] and film quality,[26] also affect pitting potential under certain conditions. The major concern for zirconium is pitting in chloride solutions. **Figure 8** illustrates the electrochemical behavior of zirconium and stainless steel. In chloride-free solutions, zirconium is more corrosion resistant than stainless steel and most other passive alloys. However, in chloride-containing solutions, zirconium's advantage disappears in oxidizing conditions. Thus, although zirconium may have a slightly higher pitting potential than stainless steel in chloride solutions, it pits at a much higher rate than stainless steel under a constant potential condition.

Zirconium does not pit in most chloride solutions, such as seawater and underground fluids, because its corrosion potential is often lower than the pitting potential.[27,28] The presence of oxidizing ions, such as ferric and cupric ions, in acidic chloride solutions may increase the corrosion potential to exceed the pitting potential, therefore, pitting may occur. Pitting may also occur when there is an applied anodic potential or when zirconium is coupled with a more noble material, such as graphite or platinum. Nitrate and sulfate ion can inhibit the pitting of zirconium under certain conditions.[20,29,30] Corrosion control measures for pitting and other types of corrosion will be discussed in a later section.

3.14.2.5.2 Crevice corrosion

In chloride solutions, zirconium is among the most resistant of metals to crevice corrosion. Zirconium is not subject to crevice corrosion even in low-pH chloride solutions or chlorine gas. This can be rationalized by the common model proposed for

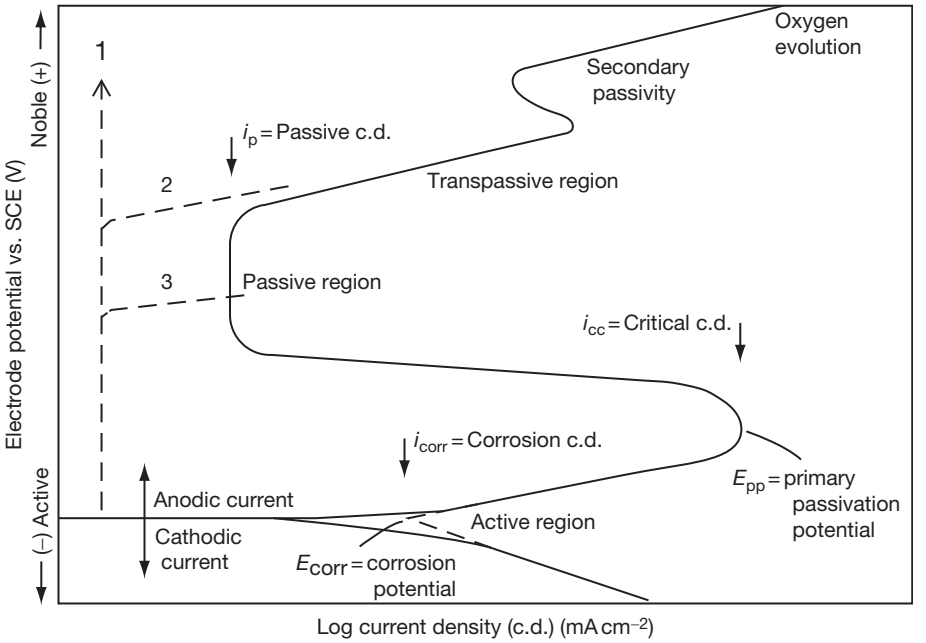

Figure 8 The electrochemical behavior of stainless steel and zirconium in (1) chloride-free dilute solutions, (2) chloride-free concentrated solutions, and (3) chloride-containing solutions. Solid line: Common features found in stainless. Dotted line: Common features found in zirconium.

crevice corrosion. In the initial stage of crevice corrosion, metal dissolution and oxygen reduction occur uniformly over the entire surface, including the interior of the crevice. After a short interval, the oxygen within the crevice is depleted because of its confinement, so oxygen reduction ceases within the crevice while metal dissolution continues. This tends to produce an excess of positive charge in the solution, which is necessarily balanced by the migration of negative chloride ions into the crevice. At the same time, positively charged ions, such as Fe^{3+}, stay outside the crevice. Similar to the pitting process, metal chloride dissociates into an insoluble hydroxide and a free acid ($H^+ + Cl^-$). In addition, the condition within crevices is too reducing to have ferric ions. These changes are actually favorable for zirconium. Consequently, zirconium is not susceptible to crevice corrosion in chloride solutions.

To follow the same model, zirconium would be susceptible to crevice corrosion in fluoride solutions. Crevice corrosion at the contact between zirconium and PTFE would be a special case. PTFE is an inert material and releases few fluoride ions when it is produced by the pressurized process for making virgin materials. It can also be produced from recycled materials by remelting. Recycled PTFE is not as stable as virgin PTFE and may release large amounts of fluorides. Crevice corrosion of zirconium under PTFE gaskets has occurred several times in acids when recycled PTFE or a less stable type of fluoropolymer had been used.

Furthermore, zirconium is susceptible to crevice corrosion in dilute sulfuric acid when the acid is allowed to concentrate within the crevice.

3.14.2.5.3 *Intergranular corrosion*

Zirconium alloys poorly with most elements and is miscible only with titanium, hafnium, and scandium. Thus, most elements have very low solubility in zirconium and form intermetallic compounds as second phase precipitates. Iron is the major, most visible impurity in zirconium, and zirconium–iron compounds are the most important to consider. Depending on thermomechanical history, zirconium–iron compounds distribute in zirconium in several ways.[31] Mill products typically have the uniform distribution of fine particles. Grain boundaries also are favorite sites for these particles to precipitate. More importantly, these particles tend to be spheroidal under the annealed condition. These particles can become elongated in the HAZ and the weld metal under the as-welded condition as shown in **Figure 9(a)** and **9(b)**. When there are sufficient elongated particles, they tend to form interconnected networks and are,

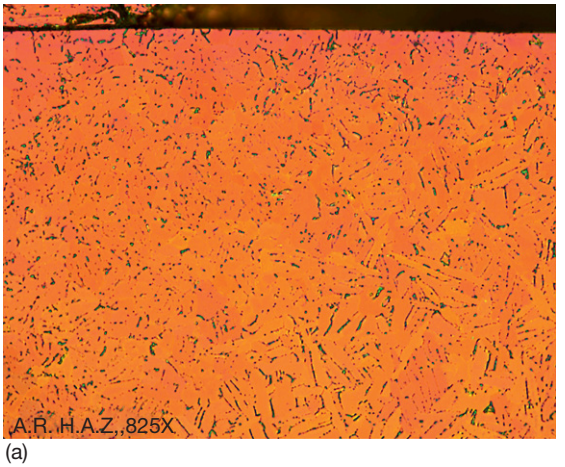

(a)

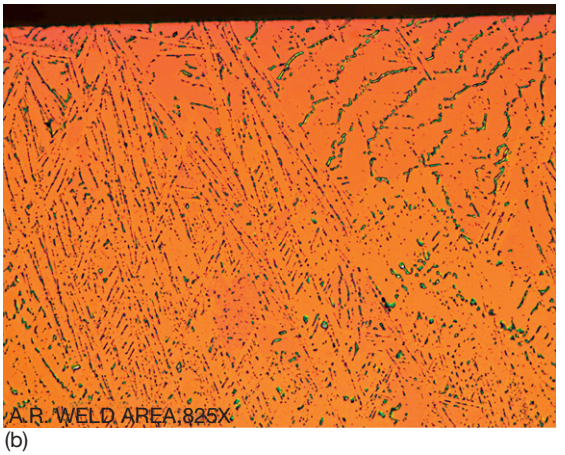

(b)

Figure 9 (a) The HAZ of as-welded Zr702 and (b) the weld metal of as-welded Zr702.

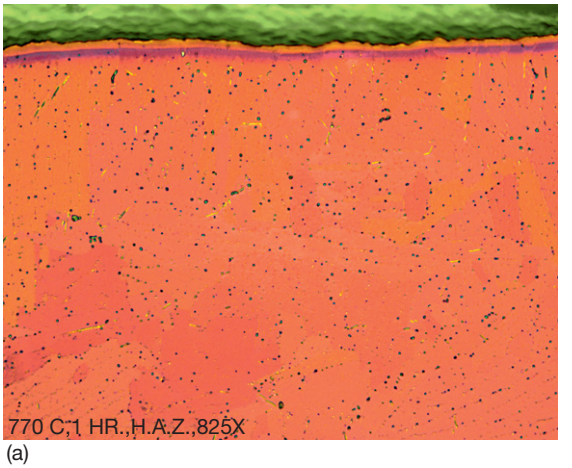

(a)

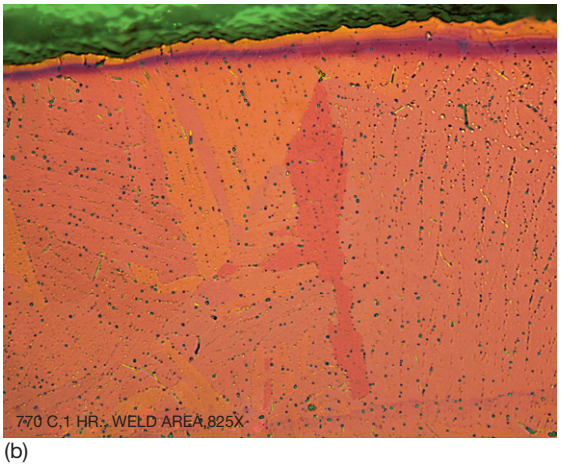

(b)

Figure 10 (a) The HAZ of heat-treated Zr702 and (b) the weld metal of heat-treated Zr702.

therefore, not as corrosion resistant as zirconium in most environments. Consequently, the HAZ and the weld metal are susceptible to intergranular corrosion in media such as concentrated sulfuric and hydrochloric acids.

Heat treatment can be used to modify the morphology of the second-phase particles in the HAZ and the weld metal. Heating at 770 °C is effective as shown in **Figure 10**. After heat treatment, elongated particles become spheroidal similar to those in the parent metal. The resistance of zirconium to intergranular corrosion is, therefore, greatly improved.

3.14.2.5.4 Stress corrosion cracking

Zirconium and its alloys resist stress-corrosion cracking (SCC) in many environments, such as NaCl, $MgCl_2$, NaOH, and H_2S, which are strong SCC-inducing agents on common metals and alloys. Thus, zirconium service failures resulting from SCC are few in chemical applications. The high SCC resistance of zirconium can be attributed to its high repassivation rate. In the presence of water or oxygen, any breakdown in the surface oxide film is quickly healed. The environments known to cause SCC of zirconium include $FeCl_3$, $CuCl_2$, halogen, or halide-containing methanol and certain other organics, concentrated HNO_3, liquid mercury or caesium,[32] and 64–69% H_2SO_4.[33] Control measures for the SCC of zirconium include:

- avoiding high sustained tensile stresses;
- modifying the environment, for example, changing pH, concentration, or adding an inhibitor;
- maintaining a high-quality surface film, that is, one low in impurities, defects, and mechanical damage;

- applying a small cathodic potential or coupling with a more active material;
- insulating the contact between zirconium and a noble material, such as graphite and platinum;
- shot peening.

3.14.2.5.5 Delayed hydride cracking

Hydrogen is well known for its capability to cause damage in many metals and alloys. In titanium and zirconium, which form brittle hydrides, failure can occur by two embrittlement processes. One process is a reduction in the fracture toughness of the metal due to the presence of a high concentration of hydride platelets that have their in-plane dimensions in the crack growth direction. The second process is delayed hydrided cracking (DHC), which is the result of a mechanism of crack initiation and slow propagation.[34]

In DHC, hydrogen diffusion in the metal is required. Gradients of concentration, temperature, and stress are all important factors in controlling diffusivity as given in the general diffusion equation:

$$\mathcal{J} = \frac{DC_x}{RT}\left[RT\frac{\mathrm{d}\ln C_x}{\mathrm{d}x} + \frac{Q^*\mathrm{d}T}{T\ \mathrm{d}x} - \frac{V^*\mathrm{d}\sigma}{3\ \mathrm{d}x}\right]$$

where $\mathcal{J}$ is the hydrogen flux; D, the diffusivity of hydrogen at any point x; C_x, the concentration of hydrogen at any point x; R, the gas constant; T, the temperature; Q^*, the heat of transport of hydrogen in metal; V^*, the volume of transport of hydrogen in metal; and σ is the tensile stress (a compressive stress would have a negative value).

That is, hydrogen is driven by three forces to an area of lower concentration, colder temperature, and higher tensile stresses. Since DHC may occur at low temperatures in a matrix of uniformly distributed hydrogen, its mechanism is believed to be as follows: stress gradients at stress concentration sites attract hydrogen, resulting in local hydride precipitation, growth, and reorientation. When the growing hydride reaches some critical size, the hydride either cleaves or the hydride–matrix interface opens up to nucleate a crack. Once a crack has nucleated, propagation occurs by repeating the same process at the crack tip and, as such, is a discontinuous process. It should be noted that the formation of hydrides is not a necessary requirement for this mechanism to operate, as is the case in delayed hydrogen embrittlement in high-strength steels.

Stress and stress gradient are two necessary requirements for DHC to occur and, fortunately, they are controllable. High stresses without gradients will not induce DHC. Hydrogen cannot move when high stresses are uniformly distributed in the structure. High-stress gradients are needed to move hydrogen but cannot be created without high stresses. High stresses are also required in fracturing hydride.

Stress relieving is one of the most effective measures in preventing DHC. It takes considerable time for hydrogen to reach the highly stressed area and to precipitate out as hydride platelets. Furthermore, the platelets must grow large enough for cracking to occur. Depending on many factors, it sometimes takes 2 years for DHC to happen, but 5 weeks after welding is the shortest known period for Zr705 to suffer DHC at room temperature. This provides a base for the Boiler and Pressure Vessel Code of the ASME (Section VIII, Division 1, Subsection C, UNF-56, (d), 1992, p.183) to add the following guideline:

> Within 14 days after welding, all products of zirconium Grade R60705 shall be heat-treated at (538–593 °C) for a minimum of 1 h for thicknesses up to 1 in. (25.4 mm) plus ½ h for each additional inch of thickness. Above 800 °F (427 °C), cooling shall be done in a closed furnace or cooling chamber at a rate not greater than 500 °F h^{-1} (260 °C h^{-1}) divided by the maximum metal thickness of the shell or head plate in inches but in no case more than 500 °F h^{-1}. From 800 °F, the vessel may be cooled in still air.

3.14.2.6 Galvanic Corrosion

With the naturally occurring oxide film, zirconium often assumes a noble potential in most environments. As an example, the galvanic series in seawater is close to the nobility of noble materials. Since zirconium is more corrosion resistant than most materials in a wide range of corrosives, zirconium is likely the cathode in most cases. The material in contact with zirconium could corrode at a much faster rate. The risk for zirconium is absorption (as cathode) and, hence, hydrogen embrittlement.

However, in incompatible environments, such as hydrofluoric acid and concentrated sulfuric acid, zirconium may assume an active potential. Moreover, zirconium may be activated at vulnerable sites when it is in contact with a noble material in chloride solutions. Graphite and carbides in the powder form can be very effective in promoting galvanic corrosion on zirconium since a small amount of powder may produce a very large cathodic area. The effect of coupling with graphite on the corrosion of zirconium in boiling 20% HCl is shown in **Table 6**.[20] It is

Table 6 Effect of graphite-coupling on the corrosion of zirconium in boiling 20% HCl after 4 weeks of exposure

Specimen area (cm^2)		*Area ratio graphite/ zirconium*	*Corrosion rate, mm year^{-1} (mpy)*
Graphite	*Zirconium*		
–	31.0	0	0.013 (0.51)
5.9	31.0	0.19	0.013 (0.51)
24.8	5.0	4.96	0.0173 (0.68)[a]
27.0	2.5	10.8	0.239 (9.4)[a]

[a]Localized corrosion.

evident that the effect can be dramatic when the surface area of graphite is significantly larger than that of zirconium.

The effect of galvanic coupling to carbon-based materials is common in chemical equipment due to their popularity and the availability of various forms. Carbon-based materials are used as structural materials, gaskets, additives to lubricants, etc. Galvanic effects induced by carbon-based materials should be appraised not just for zirconium but also for other common metals and alloys.

3.14.2.7 Microbiologically Influenced Corrosion

Microbiologically induced or influenced corrosion (MIC) occurs as a result of the presence and metabolism of living organisms in the corrosion environment or on the corroded material. Regardless of the mechanism, MIC can cause large damage to process equipment when natural waters are used in hydrostatic tests or as cooling fluids. However, results of long-term tests in natural waters indicate that zirconium is immune to MIC.

The organisms of greatest concern are sulfate-reducing bacteria. Metabolic processes may produce corrosives, such as sulfuric acid, inorganic or organic sulfides, and organic acids. Common metals and alloys have a high affinity for sulfur and its compounds. As a result, metabolic products simply make it too corrosive for common metals and alloys. Conversely, zirconium has little affinity for sulfur and its compounds. Zirconium resists attack by most inorganic and organic acids as well. Metabolic products are not corrosive to zirconium. In addition, changes in oxygen potential, salt concentration, pH, etc. from organisms do not degrade zirconium's corrosion resistance. Cathodic depolarization associated with anaerobic growth is unfavorable to certain metals and alloys but not to zirconium.

3.14.2.8 Erosion–Corrosion

Erosion is defined as accelerated corrosion resulting from the conjoint action of corrosion and erosion in the presence of a moving corrosive fluid. This type of attack is highly dependent on fluid flow-rate and corrosivity. It is particularly prevalent in areas where high local turbulence, impingement, or cavitation of the fluid may occur on metal surfaces. Solids that are suspended in fluid may result in abrasion, which may also drastically accelerate metal removal.

In compatible environments, zirconium forms a hard, tenacious ZrO_2 surface film that provides an excellent barrier to erosion–corrosion. Also, zirconium can quickly repair damage done to the film in environments containing oxygen. Consequently, zirconium can withstand many corrosives at high flow rates. To study this, a corrosion test loop was constructed to investigate the effects of flow rate and heat flux on the corrosion of zirconium tube specimens.[35] No effect was detected when the test conditions were 50% sulfuric acid at 166 °C flowing at 2.1 m s^{-1}.

Many passive alloys have the difficulty of forming protective films on their surfaces in sulfuric acid, and they are, therefore, vulnerable to erosion–corrosion in the acid. This is demonstrated in **Figure 11**.[36] In a sulfuric acid-based mixture, the corrosion of zirconium is insensitive to increasing rotation speed up to 10 000 rpm. On the other hand, corrosion of Alloy C-276 increases continuously from low speed to high speed under the same test conditions.

3.14.2.9 Fretting Corrosion

Fretting corrosion results from the combined effects of wear and corrosion and takes place when vibration contact is made at the interface of tight-fitting, highly loaded surfaces, such as between the leaves of a spring or in rolling contact bearings. Factors affecting fretting corrosion include contact load, amplitude, frequency, temperature, and corrosivity of the environment.

Fretting corrosion is a concern for zirconium, since zirconium is a soft and reactive metal. It occurs when zirconium's protective oxide film is mechanically damaged or removed. Measures should be taken to control fretting corrosion. Fretting corrosion on zirconium may be avoided by proper design and fabrication, or through the addition of a heavy oxide coating to combat mechanical effects. This coating drastically reduces friction and prevents the removal of the protective oxide layer.

3.14.2.10 Surface Condition

Corrosion is a surface phenomenon, so surface condition is an important factor in the corrosion of metals and alloys. It plays an important role not just in the initiation but also in the propagation of localized corrosion. The corrosion resistance of zirconium is not affected by common surface features such as scratch and heat tint, but may be degraded by embedded particles such as iron and silicon carbide in oxidizing chloride solutions. As indicated in **Figure 12**, zirconium with different surface conditions has a wide range of rest potential in a hydrochloric acid solution.[20] The potential of pickled zirconium is low and stays low. The potential of zirconium with SiC abraded surface increases quickly to reach the breakdown potential. In chloride solutions, it is preferred for zirconium to have a low potential that is below the breakdown potential. Pitting is therefore avoided. Zirconium with a clean, smooth surface is expected to have the optimum resistance to localized corrosion including pitting, SCC, and DHC.

3.14.2.11 Tin in zirconium

Zircaloy recycling is a major source for zirconium in making zirconium alloys and it can be noted that there may be more than 2000 ppm tin in Zr702 without violating the chemical requirements given in **Table 2**.

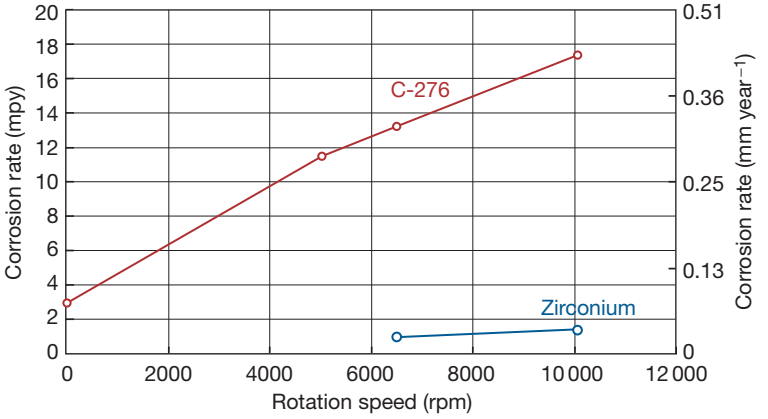

Figure 11 Results of rotating cylinder electrode tests in a mixture of sulfuric acid, organic acids, and water at 100 °C.

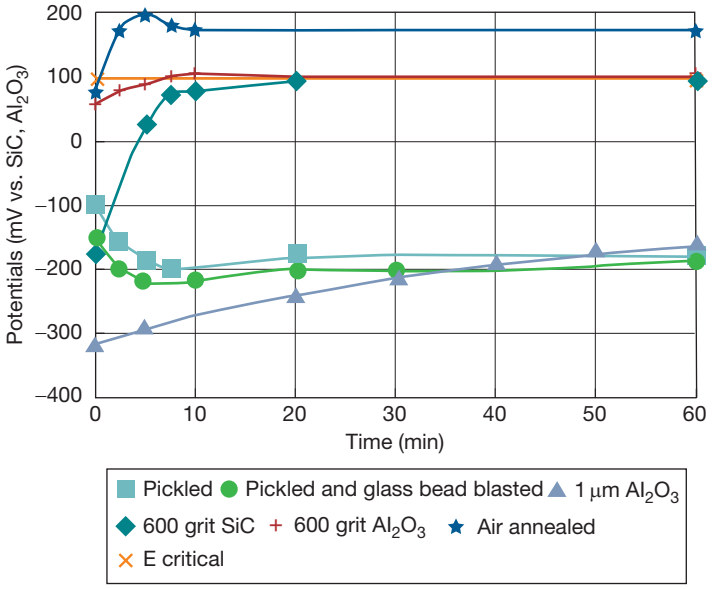

Figure 12 Surface effect on the rest potential of Zr702 in 10% HCl + 500 ppm ferric ion at 30 °C.

Advantages of utilizing Zircaloy recycle include consistent mechanical properties, improved corrosion–oxidation resistance in water and steam, and reduction in cost and material conservation. Small amounts of tin may be beneficial or acceptable for Zr702. However, there are cases to implicate that zirconium with a sufficiently high tin content has degraded corrosion resistance in certain environments. Zircaloys have a mechanical strength advantage over Zr702 and, hence, have been used in the manufacture of fittings for corrosive applications. Zircaloy fittings have failed in hot glacial acetic acid after 3 weeks to 5 months of service.[37] Zr702 and Zr705 are known to be highly compatible with acetic acid. Thus, the failures of Zircoloy can be attributed to the high tin content (~1.4%) in the alloys.

The zircaloy family of materials was developed for improved corrosion properties in high pressure water and steam primarily as a cladding material for nuclear fuel. Tin additions to zirconium were originally intended to offset the harmful effects of impurities like nitrogen where they were often higher than 40 ppm. However, the nitrogen content of the present zircaloy materials is much lower, and higher levels of tin can be more harmful than beneficial in this circumstance. Thus, the corrosion resistance of zircaloy-4 in 400 °C steam improves with decreasing tin content from 1.41 to 0.09%.[38] It should be noted that the test temperature was much higher than the operating temperature of zirconium equipment in nuclear reactor (pressurized water) environments (285–350 °C). This effect of tin is expected to decrease with decreasing temperature.

Results of 28-day tests show that the presence of greater than 3000 ppm tin is much more critical to zirconium in boiling sulfuric acid than in boiling acetic, hydrochloric, and nitric acids. The critical tin content in zirconium for sulfuric acid service seems to be between 2000 and 3000 ppm.[39] However, the distribution of tin in zirconium is not uniform. To take the fluctuation into consideration, the target point for the tin content in Zr702 should be set at 1500 ppm, if 2000 ppm proves to be the limit for the alloy in sulfuric acid service.[39] Recently generated data seem to support this recommendation.[40]

3.14.3 Corrosive Environments

3.14.3.1 Pressurized Water and Steam

Due to its passivity, zirconium is suitable for nuclear applications since water-cooled reactors operate with oxygen or hydrogen charged coolant at temperatures from 286 to 350 °C. The corrosion and oxidation of unalloyed zirconium in high temperature water and steam are irregular; that is, oxide growth is not generally self-limiting. This behavior is related to variations in the impurity content of the metal with nitrogen and carbon impurities particularly harmful. The oxidation rate of unalloyed zirconium increases markedly when nitrogen and carbon concentrations exceed 40 and 300 ppm, respectively.[41,42] The irregular behavior of unalloyed zirconium has stimulated alloy development programs. Zircaloy-2, zircaloy-4, Zr–2.5Nb, and Zr–1Nb ('Zirlo') are the most important alloys developed for nuclear applications because they are more reliable and predicable for use in hot water and steam, in addition to being stronger.

During oxidation at elevated temperatures, zirconium alloys initially form a tightly adherent oxide film at a rate that is at first quasicubic but, after an initial period, undergoes a transition to linear behavior. Unlike the white, porous oxide films on unalloyed zirconium, the oxide film on zircaloy-2 remains dark and adherent throughout transition and in the post-transition region. Zircaloy-4 differs in composition from zircaloy-2 by having a slightly higher iron content but no nickel. Both variations are intended for reducing hydrogen pickup during corrosion but with minimal effect on overall corrosion resistance during reactor operation. Hydrogen pickup detrimentally influences fuel cladding performance with regard to hydride formation. For example, in water at 360 °C, the hydrogen pickup for zircaloy-4 is about 25% of the theoretical quantity, or less than half of that for zircaloy-2. In addition, hydrogen pickup for zircaloy-4 is less sensitive to hydrogen overpressure than that for zircaloy-2. For both alloys, hydrogen pickup is greatly reduced when dissolved oxygen is present in the medium.[41]

The Zr–2.5Nb alloy is considered somewhat less resistant to corrosion than the zircaloys with exceptions. Nevertheless, the Zr–2.5Nb alloy is suitable for many applications, such as pressure tubes in the primary loops of some reactors. Furthermore, the corrosion resistance of the Zr–2.5Nb alloy can be substantially improved by heat treatments.[42,43] In addition, the Zr–2.5Nb alloy is superior to Zircaloys in steam at temperatures above 400 °C.[43]

3.14.3.2 Other Aqueous Systems

3.14.3.2.1 Cooling waters

Unalloyed zirconium does not seem to have irregular behavior in cooling waters, such as the towns water, river water, or potable water, that are used as the

cooling media in the chemical process industry. Such waters have much higher levels of impurities than water used in the nuclear reactors. The highest temperature in such heat exchangers is around 300 °C, and the longest lifetime is more than 20 years; zirconium has generally performed well in these waters.

The major difference between pure water in nuclear reactors and common cooling waters is their corrosivity. There is also the important factor of the effect of neutron flux on the oxidation process, which is likely to accelerate corrosion by increasing lattice diffusion. However, in the chemical process industry zirconium heat exchangers can have a long and satisfactory life. For example, two zirconium heat exchangers were retired from a urea plant after continual service for 20 years. The tubes looked like new and were used to build yet another heat exchanger. The watersides of the tubes were covered with very thin oxide films without any sign of breakaway oxidation after 20 year's use.

3.14.3.2.2 Salt solutions

Zirconium has excellent corrosion resistance to seawater, brackish water, and polluted water. Zirconium's advantages in salt waters include its insensitivity to variation in factors like chloride concentration, pH, temperature, velocity, crevice, and sulfur-containing organisms. The effects of pH on iron-ions-containing salt water were discussed earlier. Results of certain field and laboratory tests are summarized as follows.[28]

Zr702 specimens with or without a crevice attachment were placed in the Pacific Ocean at Newport, OR, for up to 129 days. All welded and nonwelded specimens exhibited nil corrosion rates. Marine biofouling was observed; however, no attack was found beneath the marine organisms or within the crevices. Laboratory tests were performed on specimens of Zr702 and Zr704 in boiling seawater for 275 days and in 200 °C pressurized seawater for 29 days. Both alloys resisted general corrosion, pitting, and crevice corrosion.

U-bend specimens, with or without steel coupling, of Zr702, nickel-containing Zr704 or zircaloy-2, and nickel-free Zr704 or zircaloy-4, were tested in boiling seawater for 365 days as shown in Table 7. No cracking was observed during the test period. Overstressing of the tested U-bends indicated that all specimens, except one, remained ductile. The exception was the welded nickel-containing Zr704 with steel coupling which showed some hydrogen and oxygen absorption. Chemical analyses and metallographic examinations on other U-bends did not reveal any evidence of hydrogen absorption and hydride formation. Results of chemical analyses are given in. These results support that the presence of nickel in zirconium promotes hydrogen pick-up.

Table 7 Chemical analyses for hydrogen and oxygen (ppm) of tested U-bends in boiling seawater for 365 days

Metal	*Hydrogen*	*Oxygen*
Nonwelded Zr702 U bend with steel coupling	6	1350
Nonwelded Zr704 (Ni-containing) U bend with steel coupling	8	1480
Nonwelded Zr704 (Ni-free) U bend with steel coupling	9	1440
Welded Zr702 U bend with steel coupling	8	1250
Welded Zr704 U bend (Ni-containing) with steel	450	5000
Welded Zr704 (Ni-free) U bend with steel coupling	5	1480

Zirconium resists most salt solutions, which include halogen, nitrate, carbonate, and sulfate.[59,60] Corrosion rates are typically very low at temperatures at least up the boiling point. Solutions of strong oxidizing chloride salts, such as ferric and cupric chlorides, are examples of the few exceptions. Zirconium is considerably more resistant to chloride SCC than are stainless steels.[32] For example, U-bends of Zr702 do not fail in boiling 42% magnesium chloride. Another attractive property of zirconium is its high resistance to crevice corrosion. Zirconium is not subject to crevice corrosion even in acidic chloride solutions at elevated temperatures. No attack was observed on zirconium in a salt spray environment.[67]

3.14.3.2.3 Sulfur compounds

Sulfur and its compounds are highly corrosive to common metals. They are often present in underground fluids, such as oil, natural gas, and geothermal fluids. Though zirconium is a reactive metal, it has little affinity for sulfur. Consequently, zirconium has excellent corrosion resistance to sulfur and its compounds. It requires a high temperature, around 700–900 °C, for zirconium to react with sulfur vapor or hydrogen sulfide to yield a number of sulfides. Moreover, there is no instance of zirconium–sulfur bonds forming in aqueous systems.[44,45] Practically, therefore, zirconium is immune to sulfide stress cracking (SSC).

3.14.3.3 Inorganic Acids

3.14.3.3.1 Sulfuric acid

Sulfuric acid is the most important acid for use in the manufacture of many chemicals. For example, the

acid is used as a dehydrating agent, an oxidizing agent, an absorbent, a catalyst, a reagent in chemical syntheses, and much more. These highly versatile capabilities can be attributed to the complicated nature of this acid. Sulfuric acid is a corrosive with a continuously changing character. It changes from the reducing nature of dilute acid to the oxidizing nature of concentrated acid. The reactivity of sulfur compounds and the difficulty of forming protective oxide films under reducing condition make common passive metals vulnerable to corrosion in dilute acid. In fact, hot, dilute acid is a pickling solution for steel and stainless steel. Solutions become increasingly oxidizing at or above 65%. The usefulness of passive metals and alloys depends strongly on acid concentration, temperature, aeration, and other impurities.

Zirconium and its alloys are straightforward in their corrosion resistance to sulfuric acid as shown in **Figures 13–15**.[48] Published data for zirconium before the establishment of Zr702 were collected to construct **Figure 13(a)**. Corrosion data generated at the Wah Chang company were used to construct **Figures 13(b), 14,** and **15** for ASTM grades. It should be noted that isocorrosion curves are normally constructed based on short-term results of laboratory tests conducted under well-controlled conditions. The curves should be used to understand the corrosion behavior of the alloys rather than to predict the performance of the alloys in actual service. There are many factors affecting the performance of the alloys. The factors include impurities in the alloys and environments, equipment design and fabrication, operating conditions, and maintenance.

Zirconium and its alloys resist attack by sulfuric acid at all concentrations up to 70%. The major difference among these grades is in the near boiling region when the acid concentration is greater than 60%. In this region, Zr702 outperforms Zr704 and Zr705. In 70–80% sulfuric acid, the corrosion resistance of zirconium and its alloys depends strongly on temperature. In higher concentrations, the corrosion rate of zirconium and its alloys increases rapidly with concentration due to the formation of nonprotective zirconium sulfate film.

There are three regions in **Figure 13(a)** that are attractive for using zirconium in sulfuric acid services. The first region is dilute sulfuric acid, $\leq$10%, at elevated temperatures. In this region, the temperature limit for zirconium is well above 200 °C. The second region is hot 10–45% sulfuric acid, where zirconium is highly stable in the passive state. Zirconium can tolerate lots of oxidizing impurities and some chlorides. The third region is 45–70% sulfuric acid where zirconium stays corrosion resistant when factors like acid concentration and impurities are controlled within zirconium's limitations.

The corrosion behavior of zirconium can be further examined from electrochemical measurements. The anodic polarization curves of zirconium in 4.9–72.5% sulfuric acid at near-boiling temperatures are shown in **Figure 16**. As indicated in **Figure 16**, zirconium experiences a passive-to-transpassive transition in sulfuric acid with an increasing potential. Zirconium does not have the active region in sulfuric acid as is the case with common metals and alloys.

As indicated in **Figure 16**, zirconium has very high transpassive (breakdown) potentials in dilute sulfuric acid. This indicates that zirconium can tolerate large amounts of oxidizing agents, such as ferric and nitrate ions in dilute sulfuric acid. For example, there is no effect on zirconium in steel pickling application even after a few percent of iron dissolves in dilute sulfuric acid, provided that chlorides are not present in significant amounts.

In >20% sulfuric acid, the breakdown potential of zirconium decreases noticeably with increasing concentration. Looking at **Figure 16** closely, still there is a visible passive region for zirconium in 65% sulfuric acid. This means zirconium can tolerate some amounts of strong oxidizing agents in $\leq$65% sulfuric acid.[47] In >65% sulfuric acid, zirconium becomes sensitive to the presence of oxidizing agents. **Figure 17** illustrates the effect of the presence of 200 ppm of various oxidizing agents on zirconium in >65% sulfuric acid.

The acid concentration limit is very important when zirconium is used to process sulfuric acid in the marginal concentration region, such as 60% or more. In less than 65% sulfuric acid, although the vapor is almost entirely water, the concentration shows little change in a pressurized system. However, acid concentration can change significantly because, for example, of the imperfect sealing of a system. Acid concentration can easily change in a vacuum system because the water vapor is continuously removed.

When the acid concentration limit is exceeded, zirconium may corrode rapidly. Under certain conditions, a pyrophoric surface layer may be formed on zirconium. The pyrophoric surface layer on zirconium formed in 77.5% sulfuric acid +200 ppm ferric ion at 80 °C consisted of γ-hydride, zirconium sulfate, and fine metallic particles. The combination of γ-hydride and metallic particles is suggested to be responsible for the pyrophoricity.[48] Treating in hot steam can be used to eliminate this tendency.

As shown in **Figures 13(b), 14,** and **15**, the resistance of zirconium in >55% sulfuric acid is

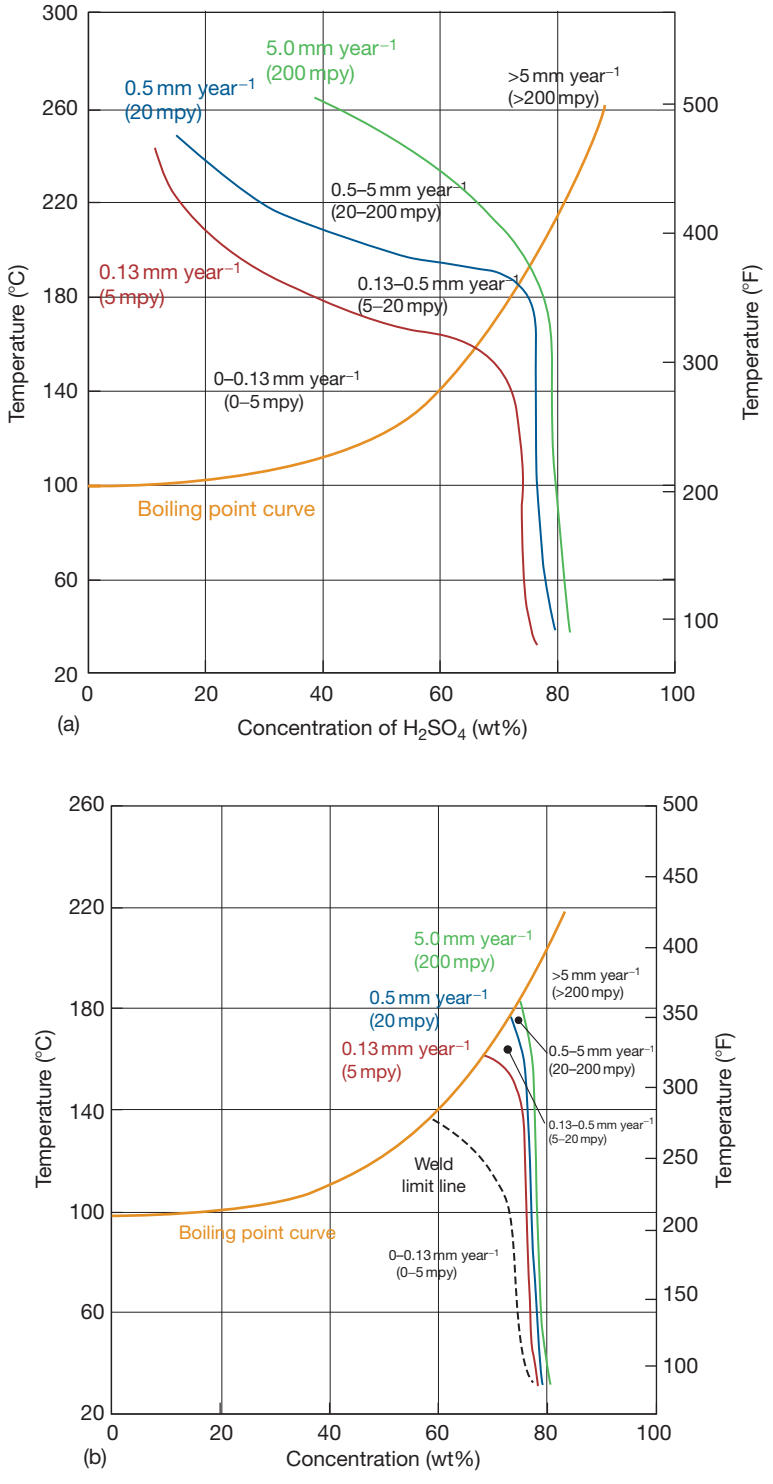

Figure 13 The isocorrosion diagram of (a) zirconium in sulfuric acid and (b) Zr702 in sulfuric acid.

somewhat degraded resulting from welding. Zirconium weld metal may corrode preferentially and can be attributed to the morphology of the second-phase particles as previously discussed. Heat treatment at 775 ± 15 °C for 1 h per 25 mm of thickness can be used to restore the corrosion resistance of weld metal.

The presence of chlorides in sulfuric acid does not degrade zirconium's resistance unless oxidizing ions

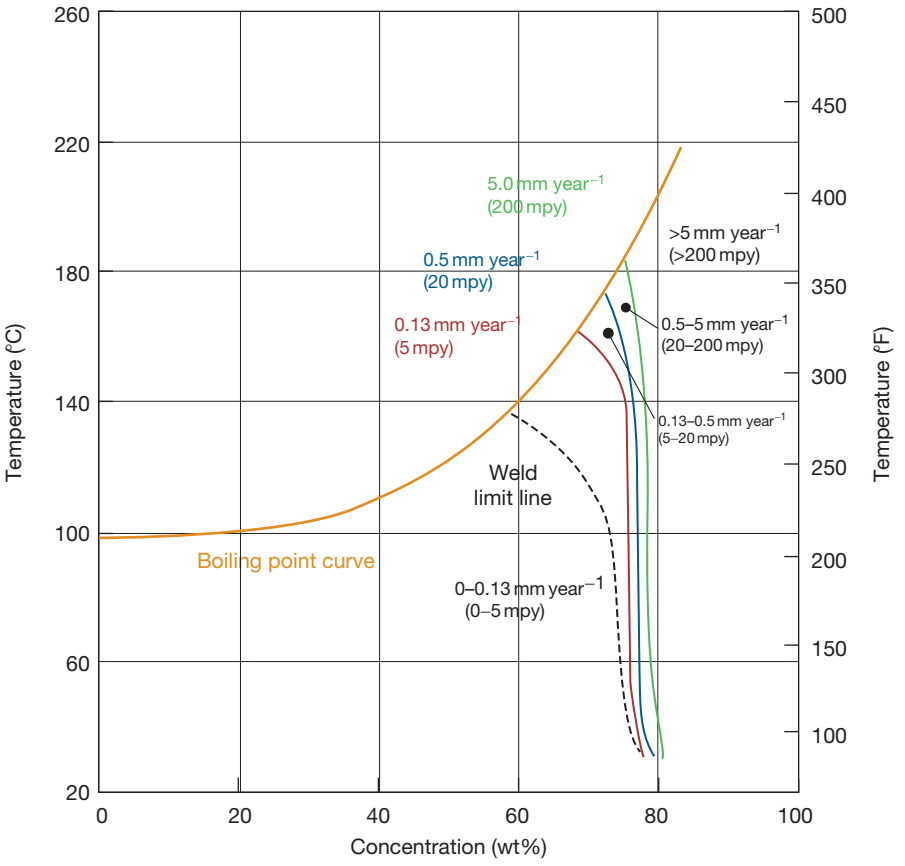

Figure 14 The isocorrosion diagram of Zr704 in sulfuric acid.

are also present. When heavy metal ions and halide ions coexist in sulfuric acid, the optimum acid concentration range for zirconium is 60–65%. Sulfate ion possesses a mild inhibitive effect on the pitting of zirconium in chloride solutions. In ≤1% chloride solution, a minimum $[SO_4^{2-}]/[Cl^-]$ ratio of ≥42 is needed for inhibition.[20] The more sulfate ions in the solution, the more oxidizing ion zirconium can tolerate before pitting occurs. **Figure 18** can be used as a guide when chloride ions and oxidizing ions coexist.

3.14.3.3.2 Halogen acids

Zirconium resists attack by most halides, including halogen acids. Exceptions include hydrofluoric acid and oxidizing chloride solutions. It has been discussed that surface condition greatly affects the corrosion of zirconium in oxidizing chloride solutions. Zirconium has some corrosion resistance in certain fluorides when the pH is high enough. For example, small amounts of fluorides in city or ground water have little effect on zirconium's corrosion resistance. However, a few ppm hydrofluoric acid will noticeably increase the general corrosion of zirconium. Nevertheless, zirconium and its alloys have very limited usefulness in fluoride-containing solutions. The concern is general corrosion but not pitting. Zirconium and its alloys exhibit low corrosion rates in fluoride solutions only when the temperature is low enough, and the pH is high enough. They are totally defenseless in HF-containing solutions. At room temperature, hydrofluoric acid exists when the pH is less than 3.18. The effect of pH on the corrosion of zirconium in fluoride-containing solutions is shown in **Table 8**.[49]

It should be noted that there are overlooked sources for fluorides.[21,22] Overlooked sources include recycled chemicals and PTFE. For example, recycled sulfuric acid may contain more than 100 ppm fluoride ions.[21] When zirconium equipment faces fluoride-containing acids, inhibitors that form strong fluoride complexes should be added for protection.[21] Useful inhibitors include zirconium sponge, soluble zirconium chemicals, and phosphorous pentoxide. **Table 9** gives results of the effects of certain inhibitors on zirconium's corrosion in fluoride-containing solutions.

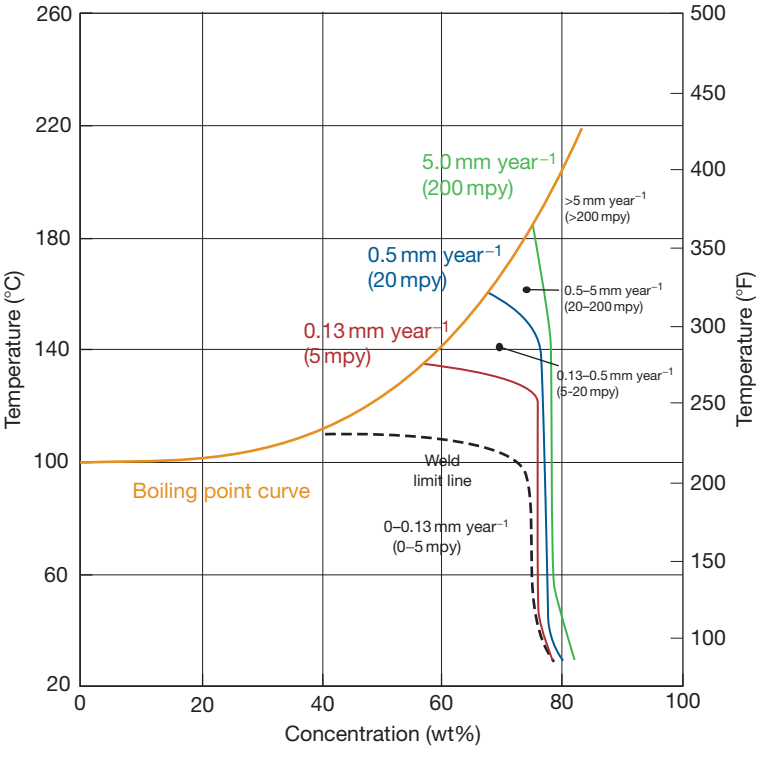

Figure 15 The isocorrosion diagram of Zr705 in sulfuric acid.

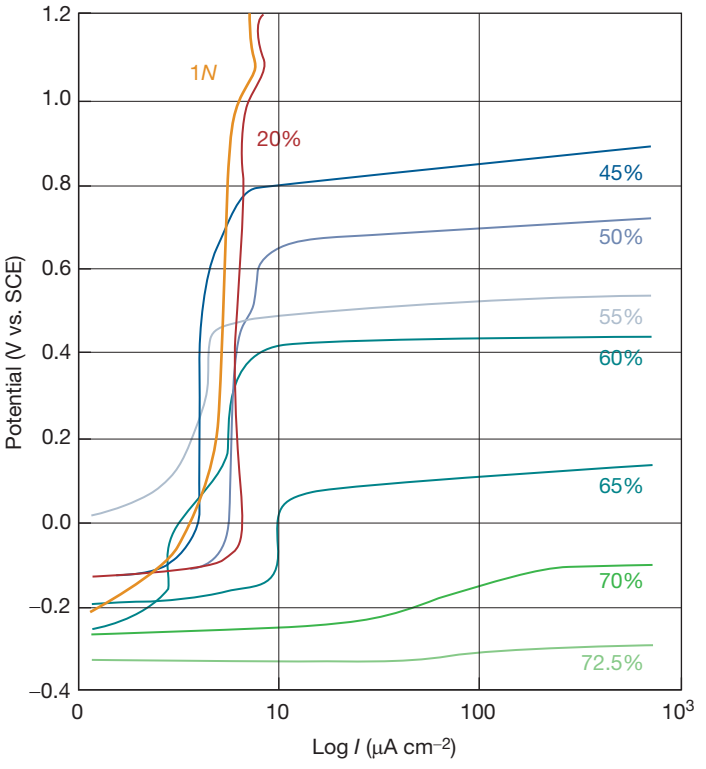

Figure 16 Anodic polarization curves for Zr702 in sulfuric acid at near boiling temperature.

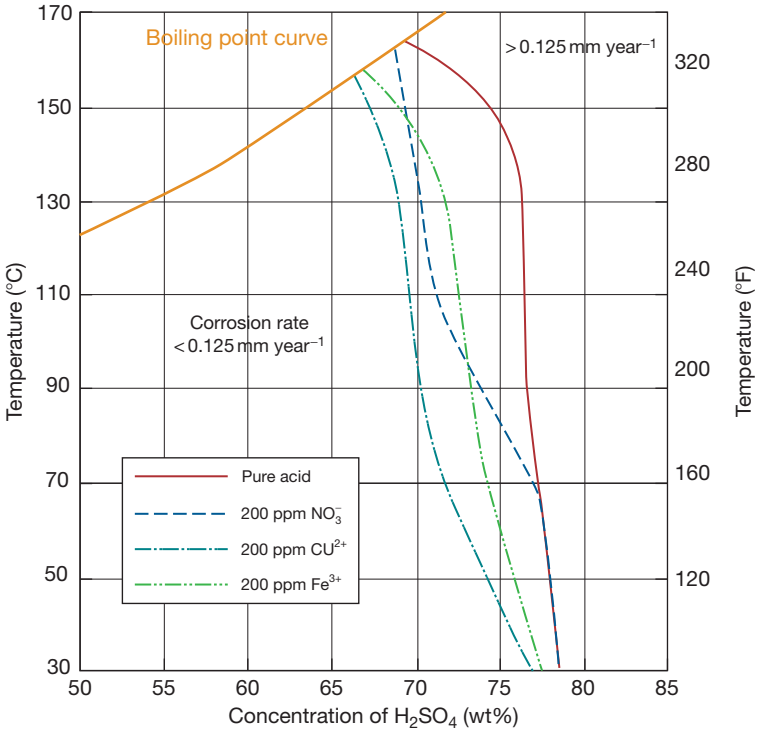

Figure 17 Effect of various oxidizing ions on the 0.125-mm year^{-1} isocorrosion line for Zr702 in sulfuric acid.

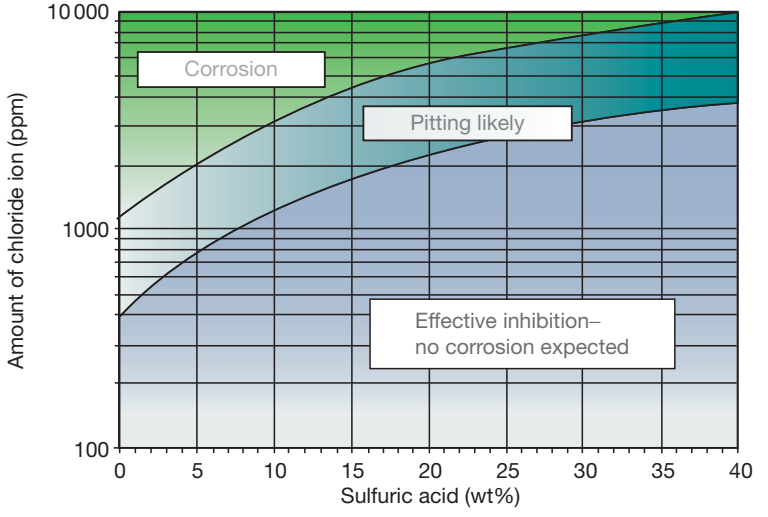

Figure 18 Chloride allowable for Zr702 in sulfuric acid in oxidizing condition.

Unlike titanium and tantalum, the corrosion resistance of zirconium in halides increases in the order of chloride, bromide, and iodide. Unless the condition is oxidizing, zirconium is very corrosion resistant in chloride solutions, including strong hydrochloric acid. Oxidizing conditions include the presence of oxidizing agents, coupling with a noble material, and applied anodic potential. In the absence of oxidizing conditions, zirconium is one of the most corrosion resistant metals to hydrochloric acid. As shown in **Figure 19**, zirconium is totally resistant to attack in all concentrations of hydrochloric acid. Normally, stainless alloys can be considered only for handling very dilute and/or low-temperature hydrochloric

Table 8 Corrosion of Zr702 in fluoride-containing solutions at 80 °C after four 1-day cycles

Solution (ppm)						
$CaCl_2$ (%)	*$MgCl_2$ (%)*	*F (as NaF)*	*F (as CaF_2)*	*P_2O_5*	*pH*	*Corrosion rate, mm year^{-1} (mpy)*
0.2	0.1	200	100	–	1	8.79 (346)
0.2	0.1	200	100	–	3	0.17 (6.69)
0.2	0.1	200	100	1200	1	3.54 (139.4)
0.2	0.1	–	300	–	1	8.79 (346)
0.2	0.1	–	300	1200	1	0.39 (15.4)
2.0	1.0	200	2800	–	1	2.87 (113)
2.0	1.0	200	2800	–	3	0.01 (0.39)
2.0	1.0	200	2800	800	1	0.13 (5.1)
2.0	1.0	–	300	–	1	3.71 (146)
2.0	1.0	–	300	1200	1	0.01 (0.39)
6.6	3.3	200	9800	–	1	1.92 (75.6)
6.6	3.3	200	9800	–	3	0.01 (0.39)
6.6	3.3	200	9800	800	1	0 (0)
6.6	3.3	–	300	–	1	1.02 (40)
6.6	3.3	–	300	1200	1	0.02 (0.78)

Table 9 Effect of zirconium sponge or phosphorous pentoxide on the corrosion of Zr702 in fluoride-containing solutions

Medium	*Inhibitor*	*Temp. (°C)*	*Corrosion rate, mm year^{-1} (mpy)*
7.2% AlF_3 + 0.5% HF	None	90	>25.4 (>1000)
7.2% AlF_3 + 0.5% HF	16% Zr Sponge	90	<0.025 (<1.0)
0.2%$CaCl_2$ + 0.1% $MgCl_2$ + 620 ppm CaF_2; pH = 1	None	80	8.89 (350)
0.2%$CaCl_2$ + 0.1% $MgCl_2$ + 620 ppm CaF_2; pH = 1	1200 ppm P_2O_5	80	0.38 (15)
2%$CaCl_2$ + 1% $MgCl_2$ + 620 ppm CaF_2; pH = 1	None	80	3.8 (150)
2%$CaCl_2$ + 1% $MgCl_2$ + 620 ppm CaF_2; pH = 1	1200 ppm P_2O_5	80	<0.025 (<1.0)
6.6%$CaCl_2$ + 3.3% $MgCl_2$ + 620 ppm CaF_2; pH = 1	None	80	1.0 (40)
6.6%$CaCl_2$ + 3.3% $MgCl_2$ + 620 ppm CaF_2; pH = 1	1200 ppm P_2O_5	80	<0.025 (<1.0)
90% HNO3 + 200 ppm HF	None	25	>25.4 (>1000)
90% HNO3 + 200 ppm HF	800 ppm Zr sponge	25	0.254 (1.0)

acid. Zirconium would outperform stainless alloys in hydrochloric acid. Moreover, zirconium is not as susceptible to hydrogen embrittlement in hydrochloric acid as tantalum.

Although hydrochloric acid is strongly reducing, the anodic polarization curves of zirconium still do not have an active region as exhibited in Figure 20. However, Figure 20 shows that zirconium may suffer pitting and/or SCC when it is anodically polarized to a potential at or exceeding the pitting potentials. The same types of corrosion problems can be developed in hydrochloric acid when strong oxidizing agents are present. Figure 21 illustrates the detrimental effect of ferric ions in 20% HCl at 100 °C. The presence of ferric ions polarizes the zirconium surface to a potential exceeding the pitting potential. Thus, local breakdown of the passive surface at preferred sites occurs, and a condition develops that favors pitting and/or SCC. Maintaining zirconium at a potential in its passive region, which is arbitrarily set at 50–100 mV below the corrosion potential, can counteract the detrimental effects resulting from the presence of ferric ions.

3.14.3.3.3 Nitric acid

Because of its passivating power, nitric acid is considered to be compatible with passive alloys. However, nitric acid becomes highly corrosive when its temperature is high or when impurities, such as heavy-metal ions, are present. The passivating power favors the formation of oxide films but may also cause the passive films to break down.

Zirconium is considerably more suitable than most passive alloys for handling nitric acid, particularly when the acid is hot, impure, and/or variable in concentration. The excellent corrosion resistance of zirconium in nitric acid has been recognized for more than 30 years.[50–52] Below the boiling point and at 98% nitric acid, and up to 250 °C and at 70% nitric

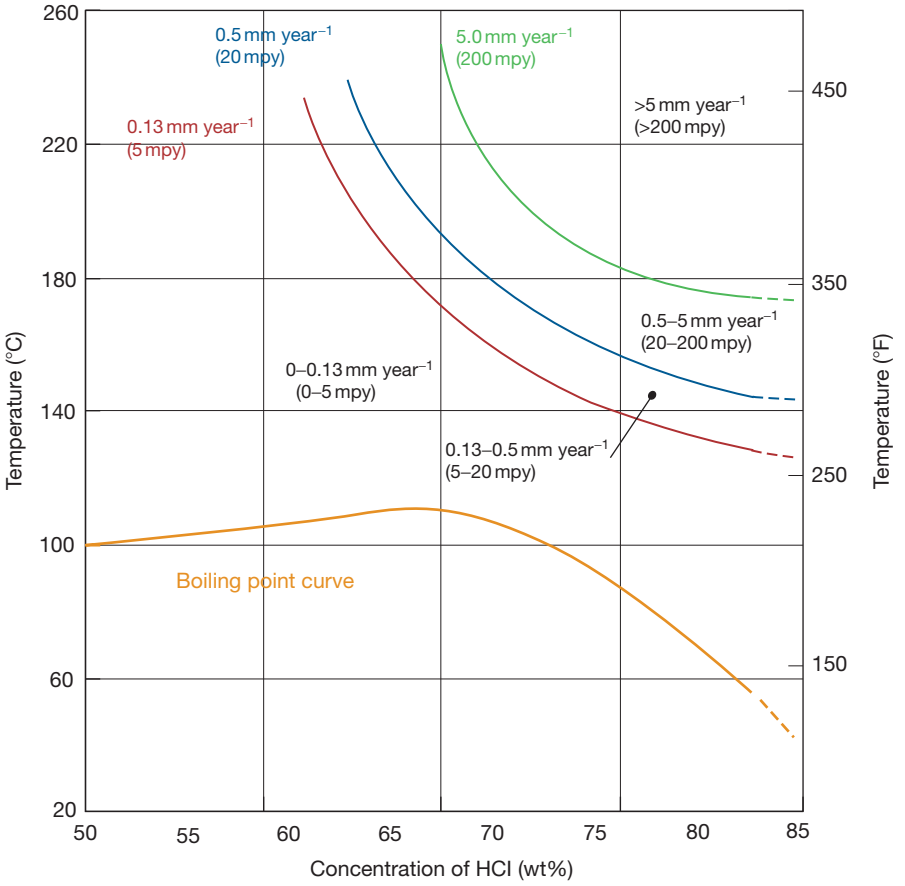

Figure 19 The isocorrosion diagram of Zr702 in hydrochloric acid.

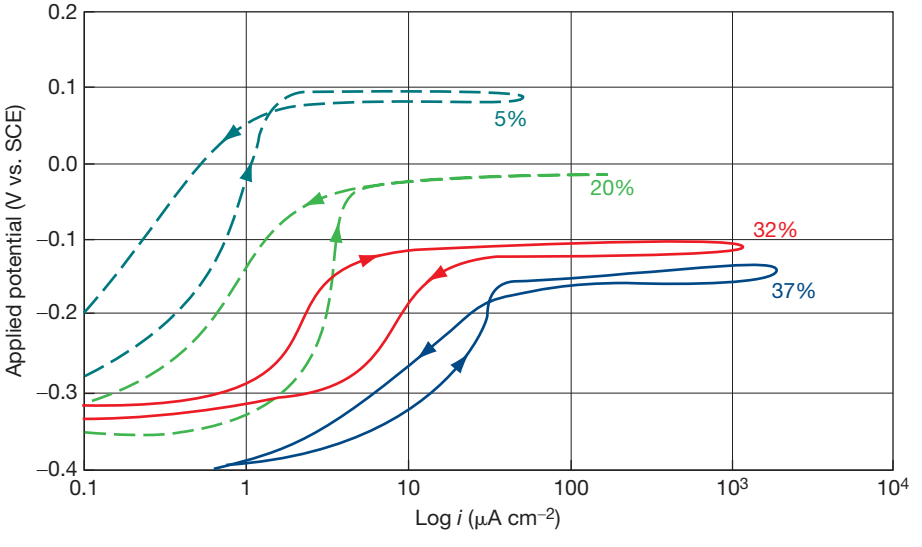

Figure 20 Anodic polarization curves for Zr702 in hydrochloric acid at near boiling temperature.

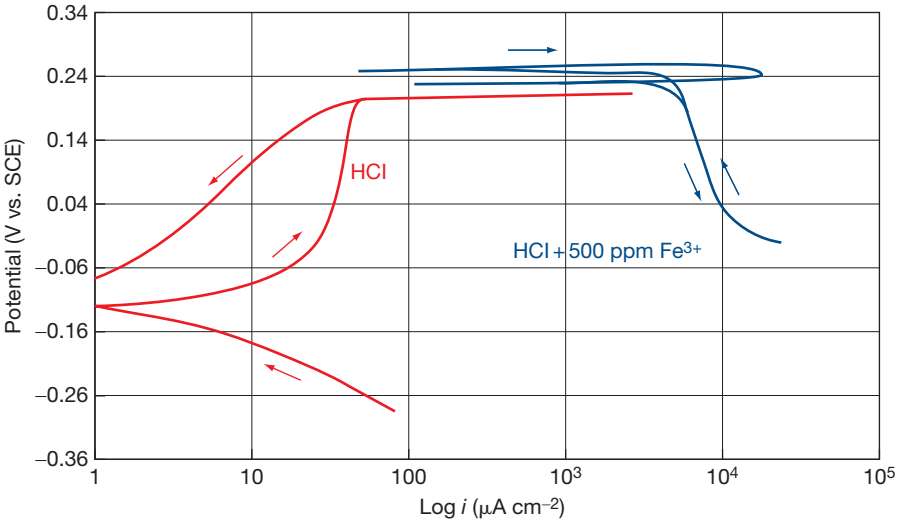

Figure 21 Effect of 500-ppm ferric ions on the anodic polarization of Zr702 in 20% hydrochloric acid at 100 °C.

acid, the corrosion rate of zirconium is less than 0.13 mm year^{-1} as shown in **Figure 22**.

Zirconium is normally susceptible to pitting in acidic oxidizing chloride solutions. However, nitrate ion is also an inhibitor for the pitting of zirconium because of its passivating power. The minimum $[NO_3^-]/[Cl^-]$ molar ratio required to inhibit pitting of zirconium is between 1[30,51,52] and 5.[53] Results of tests indicate that zirconium's resistance is not degraded in up to 70% nitric acid with dissolved 1% ferric chloride, 1% sodium chloride, 1% seawater, 1% ferric ion, or 1% stainless steel at 204 °C.[54] Still, the presence of an appreciable amount of HCl should be avoided since zirconium is not resistant to aqua regia.

The polarization curves of zirconium in nitric acid are shown in **Figure 23**. Again, zirconium has the passive-to-transpassive transition similar to that which occurs in sulfuric acid. However, corrosion potentials are noble because of the oxidizing nature of nitric acid. As indicated in the above test results, common oxidizing agents, such as ferric ions, do not affect the corrosion resistance of zirconium in nitric acid. The polarization curves do suggest that, zirconium may be susceptible to SCC in concentrated nitric acid. This is shown by the low passive-to-transpassive potential. This is consistent with the observation of SCC in U-bend specimens in greater than 70% nitric acid.[55] The slow strain-rate technique reveals zirconium's susceptibility to SCC in less than 70% nitric acid.[56] Results of C-ring tests indicate that zirconium specimens will have a long life when they are stressed below the yield point.[55] Avoiding high-sustained tensile stresses is effective in controlling the SCC of zirconium.[57]

Additional concerns include the accumulation of chlorine gas in the vapor phase and the presence of fluorides. Chlorine gas may be generated by the oxidation of chlorides by nitric acid. Areas that can trap chlorine gas should be avoided for zirconium equipment when chlorides are present in nitric acid. Fluorinated materials should be carefully applied and may be overlooked sources for fluorides.

3.14.3.3.4 Phosphoric acid

Phosphoric acid is less corrosive than other mineral acids. Many materials demonstrate useful resistance in phosphoric acid at least at low temperatures. Corrosion rates often increase with temperature and impurities in the acid. **Figure 24** shows that zirconium resists attack in phosphoric acid at concentrations up to 55% and temperatures exceeding the boiling point. Above 55% phosphoric acid, the corrosion rate of zirconium increases with temperature. The most interesting area for zirconium would be dilute acid at elevated temperatures. **Figure 25** gives the anodic polarization curves of zirconium in phosphoric acid at near-boiling temperatures. As concentration increases, the passive range diminishes gradually, and the passive current increases progressively. It appears that zirconium passivates more slowly in phosphoric acid than in other mineral acids.

If phosphoric acid contains more than a trace of fluoride ions, attack on zirconium may occur. Because

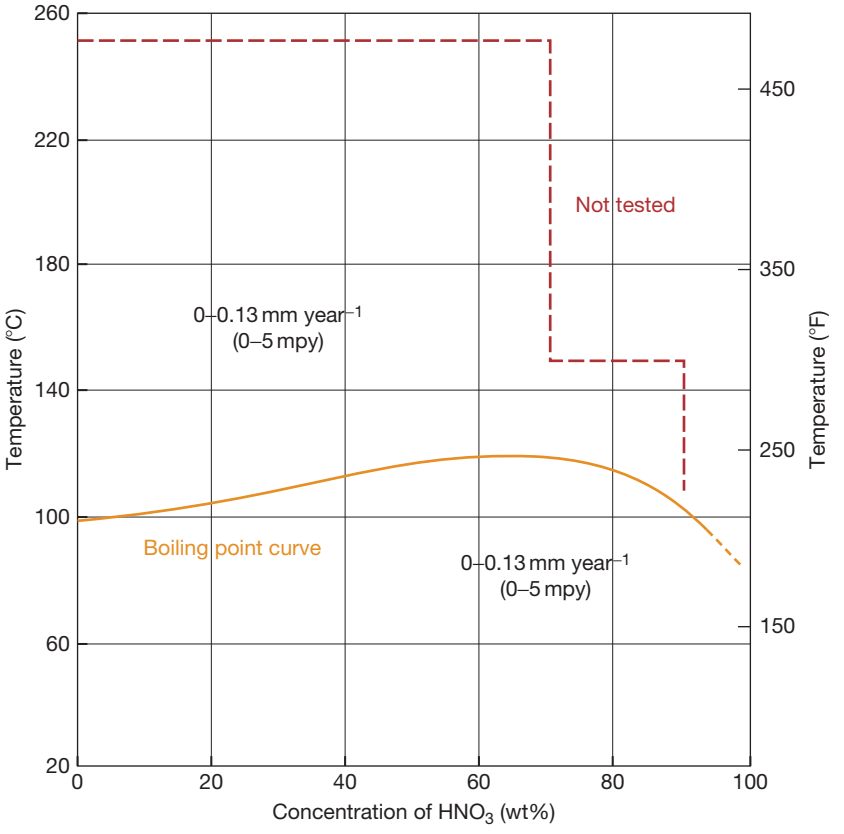

Figure 22 The isocorrosion diagram of Zr702 in nitric acid.

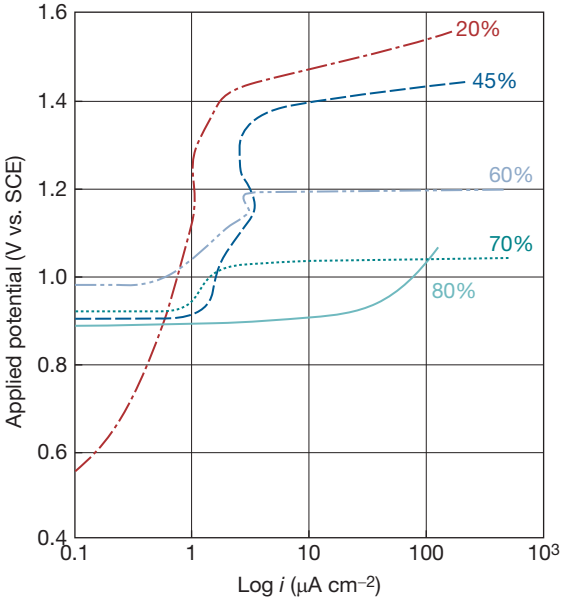

Figure 23 Anodic polarization curves for Zr702 in nitric acid at near boiling temperature.

fluoride compounds are often present in phosphoric acid, the acid specification is important when zirconium equipment is involved. For example, food grades contain little fluoride ion, while technical grades may contain tens to thousands ppm fluoride ions.

3.14.3.3.5 Other inorganic acids

Zirconium resists chromic acid up to 30% at temperatures to 100 °C[58] but it is not suitable for handling certain chrome-plating solutions that contain fluoride catalysts. Zirconium is also resistant to certain mixed acids that include sulfuric–nitric, sulfuric–hydrochloric, and phosphoric–nitric mixtures. The sulfuric acid concentration must be below 70%.[51,52,59,60] Zirconium is aggressively attacked in 1:3 volume mixtures of nitric and hydrochloric acids (aqua regia). In the volume mixture, zirconium is attacked more slowly than in the aqua regia.[51,52] In mixtures greater than the 3:1 ratio, zirconium becomes resistant. Data for some mixed acid systems are given in **Table 10**.

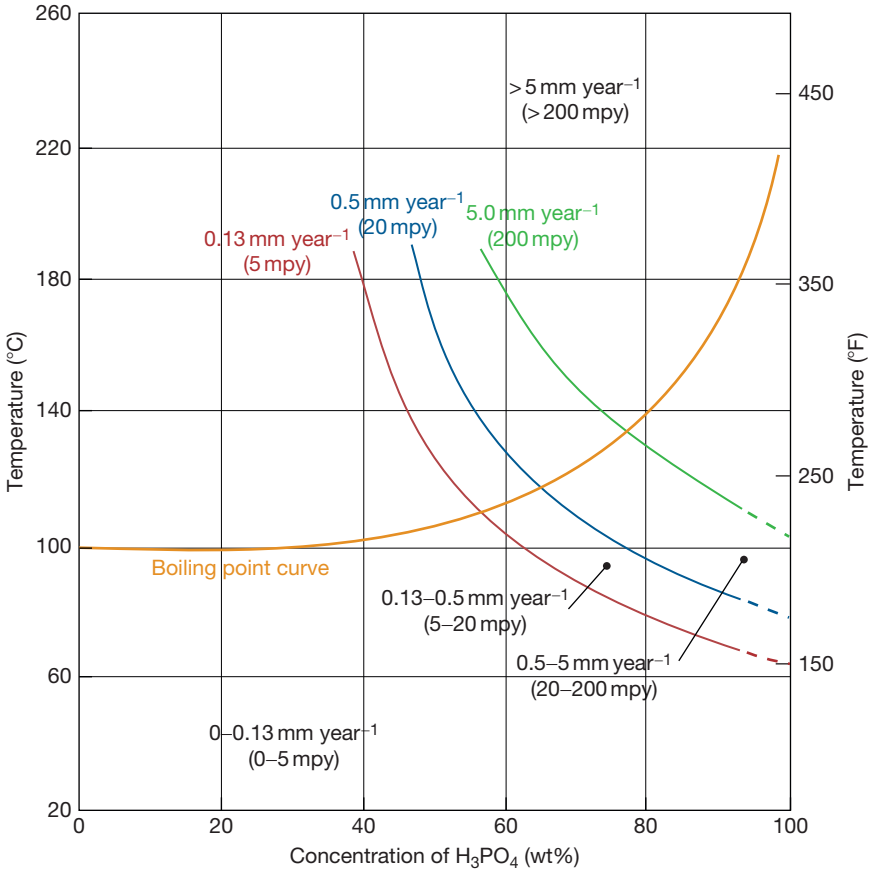

Figure 24 The isocorrosion diagram of Zr702 in phosphoric acid.

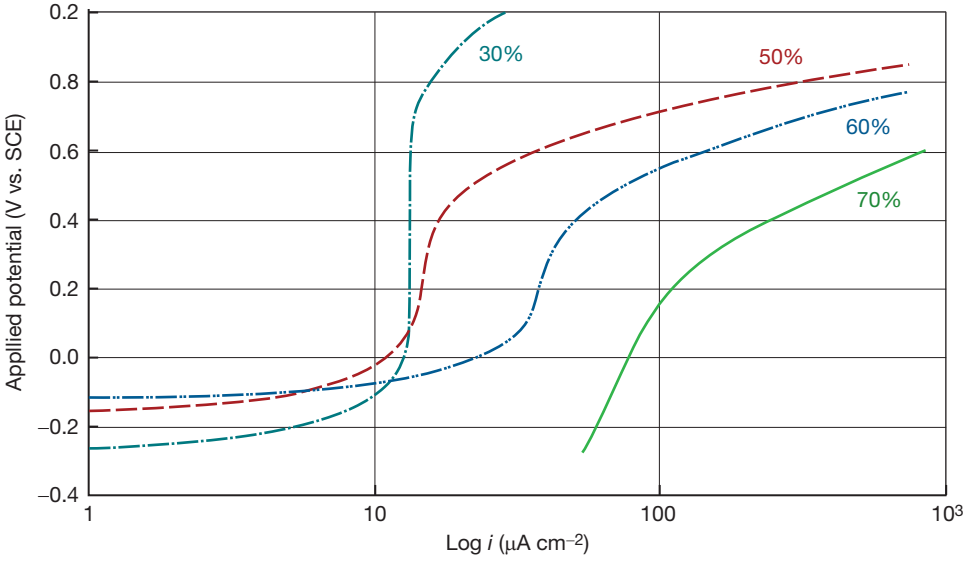

Figure 25 Anodic polarization curves for Zr702 in phosphoric acid at near boiling temperature.

Table 10 Corrosion of zirconium in certain mixed acids

Test Solution (wt%)		*Temperature (°C)*	*Corrosion rate, mm year^{-1} (mpy)*
1% H_2SO_4	99% HNO_3	RT, 100	0.001 (0.06)
10% H_2SO_4	90% HNO_3	RT, 100	WG
14% H_2SO_4	14% HNO_3	Boiling	0.002 (0.1)
25% H_2SO_4	75% HNO_3	100	3.9 (150)
50% H_2SO_4	50% HNO_3	RT	0.016 (0.63)
68% H_2SO_4	5% HNO_3	Boiling	50.8 (2000)
68% H_2SO_4	1% HNO_3	Boiling	0.28 (11)
75% H_2SO_4	25% HNO_3	RT	6.6 (260)
88% H_3PO_4	0.5% HNO_3	RT	0.0 (0.0)
88% H_3PO_4	5% HNO_3	RT	WG
Aqua Regia	–	RT	Dissolved
20% HCl	20% HNO_3	RT	Dissolved
10% HCl	10% HNO_3	RT	Dissolved
7.5% H_2SO_4	19% HCl	Boiling	0.012 (0.5)
34% H_2SO_4	17% HCl	Boiling	0.008 (0.3)
40% H_2SO_4	14% HCl	Boiling	0.005 (0.2)
56% H_2SO_4	10% HCl	Boiling	0.05 (2.0)
60% H_2SO_4	1.5% HCl	Boiling	0.025 (1.0)
69% H_2SO_4	1.5% HCl	Boiling	0.12 (5.0)
69% H_2SO_4	4% HCl	Boiling	0.38 (15.0)
72% H_2SO_4	1.5% HCl	Boiling	0.51 (20.0)

WG, weight gain.

3.14.3.4 Other Aqueous Environments

3.14.3.4.1 Hydrogen peroxide

Hydrogen peroxide is a unique and most important covalent peroxide. Many of its physical properties resemble those of water. However, chemically, it is very much different from water. It is not as stable as water. It decomposes into water and oxygen upon heating or in the presence of numerous catalysts, particularly salts of such metals as iron, copper, manganese, nickel, or chromium. Explosion may occur resulting from catalytic decomposition. Often small amounts of stabilizers, for example, tin salts and phosphates, are needed to suppress peroxide decomposition.

Hydrogen peroxide can be corrosive even to highly corrosion resistant metals and alloys such as titanium. In fact, titanium is one of the worst materials for handling hydrogen peroxide solutions. One reason is that hydrogen peroxide has the capability of forming peroxide complex compounds by attacking metals and alloys. These compounds may be soluble and are not as protective as oxide films.

Zirconium is regarded as one of the best materials for hydrogen peroxide service.[61,62] Its corrosion resistance in this medium is excellent. It does not produce active ions to catalytically decompose hydrogen peroxide. It has few problems for use in the production of hydrogen peroxide since it is essential to keep impurities out of process streams.

Nevertheless, zirconium is susceptible to pitting in oxidizing chloride solutions, and hydrogen peroxide is an oxidizer. Zirconium may pit in hydrogen peroxide solutions even when drops of hydrochloric acid are added for acidification.[63] It should be noted that zirconium is fully compatible with other acidic peroxide solutions when acids such as sulfuric acid are added.

3.14.3.4.2 Alkaline solutions

Zirconium resists attack in most alkalis, which include sodium hydroxide, potassium hydroxide, calcium hydroxide, and ammonium hydroxide.[58,64,65] This makes zirconium distinctly different from some other high performance materials, such as titanium, tantalum, glass, graphite, and PTFE, which are attacked by strong alkaline solutions.

U-bends of Zr702 were tested in boiling 50% sodium hydroxide. During the test period, the concentration changed from 50% to about 85%, and temperature increased from 150 to 300 °C. The PTFE washers and tubes used to make the U-bends dissolved. However, the zirconium U-bends remained ductile and did not show any cracks after 20 days.

Coupons of Zr702 were tested in white liquor, paper-pulping solution, which contains sodium hydroxide and sodium sulfide, at 125, 175, and 225 °C. All coupons had corrosion rates of less than

0.025 mm year^{-1}. In the same solution, graphite and glass both corroded at 100 °C. Zr702 also exhibited resistance to SCC in simulated white liquor.[66]

3.14.3.4.3 Urea

Zirconium has been recognized as the most corrosion-resistant metal for urea-synthesis service.[68,69] Stainless alloys corrode in urea-synthesis conditions at rates exceeding 2 mm year^{-1}.[68] Even silver has a high corrosion rate at 0.76 mm year^{-1}. Although titanium does not corrode much, it exhibits several problems, such as erosion[69] and hydrogen embrittlement.[70]

One of the earliest applications of zirconium was in the production of urea. Certain zirconium vessels and heat exchangers have been in service for more than 30 years and show no signs of corrosion. However, the high corrosion rates of stainless steels are greatly reduced when oxygen is added to the process stream. Oxygen or air injection has become popular as the corrosion control measure in urea plants. The advantage of zirconium has been overlooked for many years.

In recent years, zirconium is making a comeback. The driving force for the renewed interest in zirconium is the concern about the presence of heavy metals in fertilizers. Stainless steel equipment still corrodes somewhat even with the oxygen injection measure. To protect the environment, permissible levels for the presence of heavy metal salts in fertilizers are being tightened. The corrosion resistance and nontoxicity of zirconium cannot be ignored in achieving new environmental standards.

3.14.3.5 Organic Acids

3.14.3.5.1 Acetic acid

The importance of acetic acid in the organic chemistry industry is comparable to that of sulfuric acid in the inorganic chemistry industry. Acetic acid can effectively acidify aqueous solutions, increasing their corrosivity. It is not highly corrosive at low temperatures. Many materials, including wood, rubber, aluminum, copper, stainless steels, and titanium, have been used in acetic acid service with different degrees of success. Corrosion problems arise due to variations in acid concentration, temperature, solution impurities or catalysts, and heat transfer.[71]

For over 40 years, zirconium has been recognized as one of the most versatile materials for acetic acid service.[71–74] Zirconium shows nil corrosion rates (<0.025 mm year^{-1}) in most acetic acid media at temperatures up to at least 260 °C. In fact, acetate ions have a mildly inhibitive effect on the localized corrosion of zirconium in halide solutions. Conditions that lead to corrosion are few. They include very dry acid (<650 ppm water) and the presence of copper ions in the acid.[75]

Zirconium has become an important material for the production of acetic acid through the reaction of methanol and carbon monoxide. This technology has been studied for more than 40 years. It could be commercialized in the 1970s only when the corrosion problems of structural materials were managed. In this technology, the reaction must proceed at a high temperature (at or greater than 150 °C) and a high pressure (3.3–6.6 MPa) in the presence of a halide as the catalyst. Process equipment must be made of highly corrosion-resistant materials. Zr702 and Zr705 are often used to construct process equipment, such as reactors, columns, heat exchangers, pumps, valves, piping systems, trays, and packings.

When various alloys were evaluated in acetic acid environments, zirconium was identified as the most corrosion resistant.[72,73] Nevertheless, in certain tests, zirconium exhibited pitting and high corrosion rates in mixtures of acetic acid and acetic anhydride when copper ions were present. Copper ions seem to play a catalytic role in the corrosion process. It is undesirable, therefore, for zirconium equipment to be exposed to acetic acid contaminated with copper ions. Copper ions may come from corrosion of upstream equipment made of copper-containing alloys and may also be added as catalysts in certain processes.

3.14.3.5.2 Formic acid

Formic acid is more easily ionized than acetic acid. Therefore, formic acid is expected to be more corrosive than acetic acid. Indeed, formic acid attacks many common metals and alloys. Steel corrodes rapidly in this acid at all concentrations, even at ambient temperatures. Stainless alloys have some serious limitations. Type 304 stainless steel resists only 1–2% formic acid at boiling. Type 316 stainless steel is attacked by hot formic acid in the intermediate concentrations. Nickel-based alloys may corrode at high rates in the acid with the presence of certain impurities like halides and under heat-transfer conditions. Titanium and its alloys are not consistent due to factors such as aeration and water content. Compared to the mentioned alloys, zirconium is versatile and corrosion resistant in most formic acid solutions.[76]

Zirconium has played a key role in the commercialization of the Leonard–Kemira process.[77,78] In this process, CO gas contacts methanol in the presence of a catalyst to form methyl formate in a reactor.

The methyl formate is hydrolyzed in the presence of a catalyst to yield formic acid and methanol, which are separated by distillation. The methanol is recycled in the first stage of the process. Factors such as elevated temperatures and pressures and the presence of water and catalyst make common materials, including glass lining, resin and plastic coatings, and stainless alloys inadequate as structural materials for this process. Zirconium proves to be the most economical structural material for use in the main equipment for this process.

3.14.3.6 Other Organic Environments

Zirconium has excellent corrosion resistance in most organic environments. Exceptions are certain halide-containing organic solutions (e.g., impure methanol) and organic halides (e.g., dichloroacetic and trichloroacetic acids). Zirconium has been extensively tested in organic-cooled reactors where the coolant consists of mixtures of high-boiling aromatic hydrocarbons, for example, terphenyls.[79] These coolants are non-corrosive to zirconium. However, early experiments in the organic coolants indicated that hydriding was a major concern. It was found that chlorine as an impurity in the coolants was the reason for hydriding. Elimination of the chlorine and maintenance of a good surface oxide film by ensuring the presence of some water (>50 ppm) alleviates the hydriding problem. Indeed, the combination of a lack of water and the presence of halogens or halides is the common reason for zirconium to corrode in organic environments. For example, addition of some water suppresses zirconium's susceptibility to SCC in alcohol solutions with halides.[80–82]

On the one hand, zirconium shows excellent corrosion resistance in many chlorinated carbon compounds, such as carbon tetrachloride and dichlorobenzene at temperatures up to 200 °C. On the other hand, zirconium is poor in certain chlorinated organic chemicals, such as acetyl halides, even at ambient temperatures. It is well known that certain organic halides are very corrosive to metals in the absence of water and oxygen. Metals can directly incorporate into these compounds to form intermetallic compounds. The reactions were investigated extensively by Grignard during the early 1900s. Today, organometallic halides are termed 'Grignard' reagents. Unsaturated organic compounds and alkyl, aryl, and vinyl halides are commonly used to react with metals in the preparation of organometallic compounds. They are potentially corrosive to metals, including zirconium. From the corrosion point of view, organic halides can be classified into three groups, that is, water soluble, water insoluble, and water incompatible.

Water-soluble halides, such as aniline hydrochloride, chloroacetic acid, and tetrachloroethane, are not corrosive to zirconium. More active halides, such as dichloroacetic and trichloroacetic acids, are corrosive to zirconium. Corrosion rates of zirconium in these two acids at boiling are greater than 500 and 1250 μm $year^{-1}$ respectively. Water addition and stress relieving could be effective in controlling the corrosion of zirconium in water-soluble halides. Water-insoluble halides, such as trichloroethylene and dichlorobenzene, are not corrosive to zirconium, which is to be expected because of their stability. They do not dissolve in water, and they can be physically mixed together with water. Water-incompatible halides, such as acetyl chloride, may be highly corrosive to zirconium. They are not just unstable, but also react violently with water. There is no chance for water to be present in this type of halides, which are the most undesirable organic compounds for zirconium to handle.

3.14.4 High Temperature Degradation

3.14.4.1 Oxidation and Hot Corrosion

Zirconium forms a visible oxide film in air at about 200 °C. The oxidation rate becomes high enough to produce a loose, white scale on zirconium at temperatures above 540 °C. At temperatures above 700 °C, zirconium can absorb oxygen and become embrittled after prolonged exposure.

Zirconium reacts more slowly with nitrogen than with oxygen since it has a higher affinity for oxygen than for nitrogen. Also, a layer of oxide film normally protects zirconium from reacting with nitrogen. However, once nitrogen penetrates through the oxide layer, it diffuses into the metal faster than oxygen. Clean zirconium starts the nitriding reaction in ultrapure nitrogen at about 900 °C. Temperatures of 1300 °C are needed to fully nitride zirconium. The nitriding rate can be enhanced by the presence of oxygen in the nitrogen or on the metal surface.

The oxide film on zirconium provides an effective barrier to hydrogen absorption up to 760 °C, provided that small amounts of oxygen are also present in hydrogen for healing damaged spots in the oxide film. In an all-hydrogen atmosphere, hydrogen absorption will begin at a much lower temperature,

that is, 310 °C. Zirconium will ultimately become embrittled by forming zirconium hydrides. Hydrogen can be removed from zirconium by prolonged vacuum annealing at temperatures above 760 °C.

The corrosion and oxidation of zirconium and its alloys in steam are of special interest to nuclear power applications. The alloys can be exposed for prolonged period without pronounced attack at temperatures up to 425 °C. In the 360 °C steam, up to 350 ppm chloride and iodide ions, 100 ppm fluoride ions, and 10 000 ppm sulfate ions are acceptable for zirconium in general applications but not in nuclear power applications.

Zirconium is stable in ammonia up to about 1000 °C, in most gases (carbon monoxide, carbon dioxide, and sulfur dioxide) up to about 300–400 °C, and in dry halogens up to about 200 °C. At elevated temperatures, zirconium forms volatile halides. The corrosion resistance of zirconium in wet chlorine depends on surface condition. Zirconium is susceptible to pitting in wet chlorine unless it has been properly cleaned.

3.14.4.2 Molten Salts and Metals

Zirconium resists attack in some molten salts. It is very resistant to corrosion by molten sodium hydroxide to temperatures above 1000 °C and is also fairly resistant to potassium hydroxide. The oxidation properties of zirconium in nitrate salts are similar to those in air. Zirconium also resists some types of molten metals, but the corrosion resistance is affected by trace impurities such as oxygen, hydrogen, or nitrogen.[83] It has a corrosion rate less than 25 μm year^{-1} in liquid lead to 600 °C, lithium to 800 °C, mercury to 100 °C, and sodium to 600 °C. The molten metals known to attack zirconium include aluminum, zinc, bismuth, and magnesium.

3.14.5 Corrosion Protection

3.14.5.1 Protective Film Formation

Zirconium oxide, which forms on zirconium's surface, is among the most insoluble compounds in a broad range of corrosives. This film, although very thin, provides excellent protection for zirconium from corrosion in most media. When the film is mechanically damaged, it will regenerate itself. For corrosion resistance, there is no need to thicken the film before zirconium equipment is placed in a corrosive medium. However, it is desirable to preoxidize zirconium for meeting heavy mechanical duties. Properly oxidized zirconium has a much-improved performance against sliding forces, although it can be damaged by striking action. Oxidized zirconium pump shafts are an example of common applications. Bolts and nuts are often oxidized for the purpose of preventing galling. Several methods for forming thick layers of oxide films are available. They include anodizing, autoclaving in hot water or steam, oxidation in air or oxygen, and formation in molten salts.

Anodizing forms a very thin film (<0.5 μm). The surface of zirconium with anodized films appears in different colors that vary through the entire spectrum. The thickness of the film is in the range of the wavelengths of visible light. Consequently, because of interference of this light, only certain wavelengths are selectively reflected through the film from the zirconium metal underneath. Nevertheless, the film is formed at ambient temperatures and does not adhere to the underlying metal as well as thermally produced films. Anodized films may look beautiful but have very limited capability to protect the metal from mechanical damage.

Autoclaving in hot water or steam is a common practice for determining 'corrosion resistance' in the nuclear industry. In this method, the uniform film of high integrity is formed in pressurized (19 MPa) deionized water at 360 °C for 14 days or in high purity steam (10 MPa) at 400 °C for 1–3 days. In addition to improving corrosion resistance, the rate of hydrogen absorption is greatly reduced.

Oxidation in air or oxygen under well-controlled conditions can produce high quality films on zirconium. The formed films serve as an excellent bearing surface against a variety of materials. For example, a layer of black film forms on a cleaned zirconium component in air at 550 °C for 4–6 h[84] or in a fluidized bed using oxygen during the oxide formation period but using an inert gas during the heating and cooling periods.[85] The resultant oxide layer is approximately 5 and 20 μm, respectively. It is equivalent to sapphire in hardness and is diffusion bonded to the base metal. The oxide layer can be damaged by a striking force, but it serves as an excellent surface for sliding contact.

Film formation in molten salts is useful for small components. In this process, a zirconium subject is treated in fused sodium cyanide containing 1–3% sodium carbonate, or in a eutectic mixture of sodium and potassium chlorides with 5% sodium carbonate.[86] Treatment is carried out at a temperature ranging from 600 to 800 °C for up to 50 h. The thickness of

oxide film formed by this method is 20–30 µm. This film greatly improves resistance to abrasion and galling over thick oxide films grown by many other methods.

3.14.5.2 Surface Conditioning

Figure 11 shows the effect of surface condition on the rest potential of zirconium in 10% HCl + 500 ppm Fe^{3+} at 30 °C. Air annealing yields rest potentials nobler than the pitting potential, E_{crit}, due to the formed thick oxide during annealing. This does not mean that pitting will occur if the film quality is good. This does put thick oxide coated materials in a position vulnerable to pitting, particularly when there is an anodically applied potential. Surfaces abraded with either 600 grit SiC or Al_2O_3 cloth reach the pitting potential quickly and have short pit initiation times. This can be attributed to the presence of embedded particles resulting from rough polishing. Pickled and finely polished surfaces have rest potentials below the pitting potential. They are very resistant to pitting even in oxidizing chloride solutions. This can be attributed to surface homogeneity that favors general corrosion but not localized corrosion. Results of immersion tests indicate that pickled zirconium performs well in boiling 10% $FeCl_3$ and in ClO_2.[20,87] It is well known that zirconium with a normal surface finish is unsuitable for handling these solutions.

3.14.5.3 Electrochemical Protection

Zirconium exhibits a passive-to-transpassive transition with increasing potential in all mineral acids except hydrofluoric acid.[88] The commonly observed active node, as shown in Figure 8 for many metal–acid systems, is not observed for zirconium. Consequently, zirconium performs well in most reducing media. This can be attributed to zirconium's ability to take oxygen from water to form a stable passive film. Most passive alloys would need some oxidizing agent, such as the presence of oxygen, for them to form passive films. In fact, zirconium is one of the best metals for handling reducing media. On the other hand, zirconium may experience corrosion problems, such as pitting and SCC, under oxidizing conditions. These problems can be controlled by converting the oxidizing condition to a more reducing condition by various means.

Potentiostatically, by impressing a potential that is arbitrarily 50–100 mV below its corrosion potential, zirconium becomes corrosion resistant in oxidizing chloride solutions.[89] Tables 11 and 12 demonstrate the benefits of electrochemical protection in controlling pitting and SCC. Table 11 shows that the general corrosion rates of unprotected zirconium in oxidizing chloride solutions may be low. However, the penetration rates are much higher than the general corrosion rate. Electrochemical protection eliminates this local attack. As indicated in Table 12, unprotected U bends of welded zirconium cracked in all but one case shortly after exposure. Protected U bends resisted cracking for the 32-day test interval in all but one acid concentration. Thus, electrochemical protection offers an improvement to the corrosion properties of zirconium in oxidizing chloride solutions.

This technique is also applicable to control the SCC of zirconium in concentrated nitric acid.[57] Because of the strong oxidizing power of the acid, zirconium exhibits a noble corrosion potential. Also, there is a large difference between the corrosion potential and the critical potential to cause SCC. It is desirable to control the potential of zirconium a few hundred millivolts below the corrosion potential or at 740 mV NHE.

3.14.5.4 Other Measures

Ferric and cupric ions are the common oxidizing agents experienced in the CPI. Cupric ion is more

Table 11 Corrosion rate of zirconium in 500 ppm Fe^{3+} solution after 32 days

Environment	*Acidity*	*Temp. (°C)*	*Penetration rate, mm year^{-1} (mpy)*	
			Unprotected	*Protected*
10% HCl	3 N	60	0.18 (7.1)	<0.003 (<0.12)
		120	1.30 (51.2)	<0.003 (<0.12)
Spent acid (15% Cl)	5 N	65	0.91 (35.8)	<0.003 (<0.12)
		80	0.91 (35.8)	<0.003 (<0.12)
20% HCl	6 N	60	0.09 (3.5)	<0.003 (<0.12)
		107	1.50 (59)	<0.003 (<0.12)

Table 12 Time to failure of welded zirconium U bends in 500 ppm Fe^{3+} solution after 32 days

Environment	*Acidity*	*Temp. (°C)*	*Time to failure (days)*	
			Unprotected	*Protected*
10% HCl	3 N	60	<0.1	NF[a]
		120	<0.1	NF
Spent acid (15% Cl)	5 N	65	<0.3	NF
20% HCl	6 N	60	NF	NF
		107	<0.1	NF
28% HCl	9 N	60	2	NF
		94	<0.1	NF
32% HCl	10 N	53	1	32
		77	<0.1	20
37% HCl	12 N	30	<0.3	NF
		53	1	NF

[a]NF: no failure.

Table 13 Test results of zirconium (as-received condition) in boiling 500 ppm Cu^{2+} containing NaCl solutions after seven 1-day runs

Average corrosion rate, mm year^{-1} (mpy)

No.	*% NaCl*	*pH*	*Nonwelded coupons*	*Welded Coupons*
1.	3.5	1	0.05 (1.97)[a]	0.60 (23.6)[a]
2.	25	1	0.04 (1.57)	0.55 (21.7)[a]
3.	3.5	4.8	0.01 (0.39)[a]	0.60 (23.6)[a]
4.	25	4.0	0.03 (1.18)	0.56 (22)[a]
5.	3.5	5.0	0.02 (0.78)	0.64 (25)[a]
6.	25	5.0	Nil	Nil
7.	3.5	6.0	Nil	Nil
8.	25	6.0	Nil	Nil
9.	3.5	7.5	Nil	Nil
10.	25	7.5	Nil	Nil

[a]Pitting.

detrimental than ferric ion in promoting the general corrosion and pitting of zirconium in acidic chloride solutions. Tables 13 and 14 demonstrate the effect of pH, welding, and heat treatment on the corrosion of zirconium in cupric ion-containing solutions. The corrosion problems of zirconium in these solutions can be controlled by adjusting the pH to 6 or higher (Table 13) or by high temperature heat treatment (Table 14). In ferric ion-containing solutions, it is sufficient to adjust the pH to 3 or higher.

Various inhibitors, such as nitrate, sulfate, and stannous ions, can be used to control the pitting of zirconium in chloride solutions.[20] Furthermore, the solution potential of an oxidizing solution can be lowered when a small amount of hydrofluoric acid is added.[20,57] Therefore, hydrofluoric acid can be used to control pitting and SCC of zirconium in

Table 14 Effects of heat treatment on the corrosion of zirconium (sand-blasted and pickled) in boiling NaCl + $CuCl_2$ solutions after seven 1-day runs

Average corrosion rate, mm year^{-1} (mpy)

No.	*Metal*	*Condition*	*35% NaCl + 500 ppm Cu^{2+}*	*25% NaCl + 500 ppm Cu^{2+}*
1.	Nonwelded	As conditioned	0.01 (0.39)[a]	0.025 (0.98)[a]
2.	Welded	As conditioned	0.01 (0.39)[a]	0.033 (1.3)[a]
3.	Welded	760°C/AC	<0.003 (0.12)[a]	0.006 (0.24)[a]
4.	Welded	760°C/WQ	<0.003 (0.12)[a]	0.004 (0.16)[a]
5.	Welded	871°C/AC	0.003 (0.12)	0.006 (0.24)[a]
6.	Welded	871°C/WQ	0.003 (0.12)	0.004 (0.16)[a]
7.	Welded	982°C/AC	0.005 (0.20)	0.007 (0.27)
8.	Welded	982°C/WQ	0.005 (0.20)	0.007 (0.27)

[a]Pitting AC, air-cooled; WQ, water-quenched.

oxidizing solutions, such as concentrated nitric acid and ferric chloride solutions. Since hydrofluoric acid is very corrosive to zirconium, the corrosivity of this acid can be neutralized by adding a complexing agent, such as zirconium sponge or zirconium compounds.

Tensile stresses provide a driving force for not just SCC but also for other types of corrosion to occur. Lowering residual stresses by a stress-relieving treatment is useful in controlling pitting as well.

3.14.6 Industrial Applications

For more than 40 years, many corrosive applications have been developed for zirconium and its alloys. Zirconium and its alloys are being used as structural materials in fabricating columns, reactors, heat exchangers, vaporizers, pumps, piping systems, valves, and agitators for the chemical process industry. The chemical process industry recognized the advantages of zirconium for solving corrosion problems from zirconium's inception.

3.14.6.1 Processes Using Sulfuric Acid

Zirconium is used for the manufacture of H_2O_2 by the electrolysis of acid sulfates. This production process is extremely corrosive and, at one time, graphite equipment was standard for this process. FMC's plant in Vancouver, WA, found that zirconium was superior to graphite and used zirconium equipment to produce up to 90% H_2O_2. The average maintenance-free life of the heat exchanger was 10 years; graphite exchangers failed after 12–18 months of service. The graphite equipment failure was attributed to the leaching of the binder from the graphite by the 35% H_2SO_4 feed, which created a porous condition and ultimately caused failure.

The experience of zirconium in peroxide production led to the replacement of the graphite heat exchangers with zirconium shell and tube exchangers in the manufacturing of acrylic films and fibers. In this application, the H_2SO_4 concentration was as high as 60% at 150 °C. Another major application in H_2SO_4 concerns the manufacture of methyl methacrylate. The system at Rohm and Haas' plant in Deer Park, Texas, includes pressure vessels, columns, heat exchangers, piping systems, pumps, and valves all made from zirconium. A zirconium unit, which was built more than 20 years ago, is still in service.

Zirconium is also widely used for column internals and reboilers in the manufacture of butyl alcohol. The operating conditions are 60–65% H_2SO_4 at temperatures to boiling and slightly above. Zirconium may corrode under upset conditions of elevated concentrations and when such impurities as Fe^{3+} are present. Zirconium has been used in H_2SO_4 recovery and in recycle systems in which fluorides are not present, and the acid concentration does not exceed 65%. A major application for zirconium is in iron and steel pickling, using hot 5–40% H_2SO_4.

Rayon is a manmade textile fiber, and most of today's rayon is made by the viscose process. Equipment made of graphite was popular for use in the H_2SO_4-affected areas of this process, yet is vulnerable to breakdowns. Avtex Fiber, Inc. began experimenting with zirconium equipment in 1970. Zirconium's excellent performance prompted Avtex to convert more pieces of equipment to zirconium, which included 10 acid evaporators, 14 shell- and tube heat exchangers, and 12 bayonet heat exchangers. In addition to dramatically reducing maintenance costs and downtime, the zirconium equipment improved operating efficiency and lowered overall energy costs.

Hydroxyacetic acid (HAA), also known as glycolic acid, can be produced in a synthetic process other than being extracted from natural sources. Under high pressure (30–90 MPa) and temperature (160–200 °C), formaldehyde reacts with carbon monoxide and water in the presence of an acidic catalyst, such as sulfuric acid, to form HAA. Dupont could not rely on a silver lining for reliable service in this process as silver showed poor erosion resistance in the piping system. There were cases of blowouts in the piping due to failure of the lining. By the mid-1980s, zirconium lining was evaluated when other materials, such as glass, ceramic, stainless alloys, and titanium were found unsuitable. Zirconium is well known for its corrosion resistance in weak sulfuric acid at temperatures up to and above 260 °C. An 8-month field test at Dupont indicated that a zirconium tube would not corrode in the most severe service section of the process. Zirconium's excellent resistance to erosion is also apparent and consequently, Dupont replaced silver lining with zirconium lining in piping sections more than 5 years ago. It was estimated that zirconium lining would last at least three times as long as silver lining.

3.14.6.2 Processes Using Halogen Acids

Zirconium has many applications in HCl, such as the production of concentrated HCl and polymers. Zirconium heat exchangers, pumps, and agitators have been used for more than 15 years in an azo dye

coupling reaction. In addition to being very corrosion resistant in this medium, zirconium does not plate out undesirable salts that would change the color and stability of the dyes.

Lactic acid is commercially produced either by fermentation or by synthesis. The synthetic process is based on lactonitrile, which is prepared by reacting acetaldehyde with hydrogen cyanide at up to 200 °C. Lactonitrile is then hydrolyzed in the presence of HCl to yield lactic acid. In the HCl-affected areas, suitable materials are limited. Glass-lined materials are prone to breakdowns. Stainless alloys corrode and introduce toxic materials to the process stream. Titanium and its alloys are susceptible to crevice corrosion in hot chloride solutions. Zirconium is ideal for this process. Since lactic acid is produced as a fine chemical, contamination has to be prevented in all areas. Oxidizing HCl conditions resulting from the presence of ferric or cupric ions are avoided. Moreover, zirconium is highly resistant to crevice corrosion in chloride solutions. Since the 1970s, zirconium equipment has provided excellent service in lactic acid production.

Other applications in HCl include the breaking down of cellulose in the food industry and the polymerization of ethylene chloride, which is carried out in HCl and chlorinated solvents.

Zirconium and its alloys have been identified to offer the best prospects from a cost standpoint as materials for an HI decomposer in hydrogen production. They resist attack by HI media (gas or liquid) from room temperature to 300 °C. Most stainless alloys have adequate corrosion resistance to HI only at low temperatures.

3.14.6.3 Processes Using Nitric Acid

There is an increasing interest in the use of zirconium for HNO_3 service. For example, because of the high degree of concern over safety, zirconium is chosen as the major structural material for the critical equipment used to reprocess spent nuclear fuels.

In most HNO_3 service, stainless steel has been the workhorse for decades. The excellent compatibility between zirconium and HNO_3 was not thought to be needed. This situation changed when nitric acid producers started to modernize their technology in the late 1970s. Conventionally, HNO_3 is manufactured by oxidation of ammonia with air over platinum catalysts. The resulting nitric oxide is further oxidized into nitrogen dioxide and then absorbed in water to form HNO_3. Acid of up to 65% concentration is produced by this process. Higher concentration acid is produced by distilling the dilute acid with a dehydrating agent. Before the l970s, dual-pressure processes were the dominant means of HNO_3 production. A typical dual-pressure process operates the converter at about 500 kPa and the absorber at about 1100 kPa. In the late 1970s, Weatherly, Inc. introduced a high mono-pressure process which operates at 1300–1500 kPa. The advantages of this new process include:

- greater productivity due to higher operating pressure;
- smaller equipment resulting in a lower capital cost;
- higher energy recovery capabilities.

The new process was first tried in 1979 when Mississippi Chemical in Yazoo City, MS, retrofit their existing plant with a new compressor system to increase pressure for greater productivity and energy efficiency. It was at this point that severe corrosion problems were discovered. Prior to the upgrade, the cooler condenser was constructed of type 304L stainless steel tubesheets and type 329 stainless steel tubes. Under the previous operating conditions, the cooler condenser had experienced some corrosion, which was managed by plugging tubes and replacing the unit every 3 to 4 years. Shortly after the upgrade, with an operating temperature and pressure of 200 °C and 1035 kPa, 10% of the type 329 stainless steel tubes were found to be leaking. This condenser was replaced with a unit using type 310L stainless steel, which had to be replaced after 13 months of operation. The original condenser with new tubes of improved grade 329 stainless steel was replaced by the 310L unit. Mississippi Chemical began looking for alternatives.

In an attempt to find a solution to this problem, autoclave tests were conducted on many newer types of stainless steels and zirconium in solutions up to 204 °C and at concentrations up to 65%. Clearly, zirconium was the only suitable material for the mono-pressure process. Corrosion rates of zirconium coupons were consistently below 25 μm $year^{-1}$. The next step was to test zirconium tubes in service. Several tubes were installed into a rebuilt stainless steel condenser. They were destructively examined after 13 months and showed no signs of corrosion. Zirconium tubes were then placed in another condenser for 1 year. Once again, there were no signs of corrosion.

Consequently, Mississippi Chemical replaced its stainless steel cooler condenser with one constructed

from zirconium tubes and zirconium/304L stainless steel explosion-bonded tubesheets. This unit contains more than 18 km of zirconium tubing. In service since 1984, the zirconium unit has already outperformed the stainless steel predecessors. Thereafter, several zirconium cooler condensers have been built for other HNO_3 producers.

Mono-pressure plants are not the only ones to use zirconium as a solution to corrosion problems. Certain plants use a distillation process to increase the acid concentration. The acid is passed through a reboiler and enters a distillation column to drive off water for concentrating the acid. In 1982, Union Chemicals replaced the bottom portion of each of two distillation columns and the tube bundles of each of two reboilers. The lower parts of the columns had been constructed originally with type 304L stainless steel that experienced corrosion problems. Titanium was tried, but also failed. While glass-lined steel did not have the corrosion problems experienced by type 304L stainless steel and titanium, the maintenance costs were found to be unacceptable. Zirconium provides significantly improved corrosion resistance without adding maintenance costs. Zirconium also solved corrosion problems in the reboilers. Prior to the installation of zirconium tube bundles, both 304L and titanium tube bundles had failed in less than 18 months of operation.

With proper design and fabrication, zirconium's susceptibility to SCC can be suppressed in highly concentrated HNO_3. For example, an Israeli chemical plant uses zirconium tubes in a U-tube cooler that processes bleached HNO_3 at concentrations between 98.5 and 99%. The unit cools the acid from 70–75°C to 35–40 °C. Previously, U-tube coolers were made from aluminum, which failed in 2–12 weeks. The zirconium unit has been in service for more than 2 years, operating 24 h a day, 6 days a week.

3.14.7 Safety

Zirconium is low in toxicity and is not known to be a carcinogen. The permissible exposure limit for zirconium set by various health agencies is 5 mg m^{-3}. For comparison, the limit for iron is 1 mg m^{-3}. One major concern is zirconium's reactivity. Under most conditions, the reactivity works toward zirconium's advantage. This reactivity allows zirconium to react spontaneously with oxygen to form a protective film, which suppresses its reactivity. Consequently, zirconium can be safely used under most conditions. Nevertheless, unsafe situations may develop when this reactive nature is overlooked.

Heat of formation for zirconium dioxide at 25 °C is 1101.3 kJ mol^{-1}. It is potently exothermic. The generated heat can be easily absorbed by a large piece of zirconium. After the oxide film is formed, the oxidation rate will decrease quickly and pose no problems. However, when the heat is generated at a very small area, ignition may occur. Care should be exercised in handling fine materials including powder, sponge, machine chips, and thin foils. Ignition of fine materials will result in a very rapid, high temperature fire, which can be extinguished by using dry salt or sand. Attempts to extinguish a large zirconium fire with water will only result in scavenging of the oxygen atoms in the water molecules by the burning zirconium, leaving the hydrogen molecules to act as additional fuel or explosion source. These very large fires should be allowed to burn out by themselves.

It is normally safe to handle a large piece of zirconium. Still, ignition may occur when this piece experiences an enhanced oxidation reaction in a confined space. Under this condition, generated heat cannot easily dissipate, leading to escalated oxidation reaction and ignition becomes possible.

Furthermore, when zirconium's corrosion resistance is grossly exceeded in certain environments, pyrophoric films may form on its surface.[48] These environments include concentrated sulfuric acid and ferric chloride-containing solutions that may induce massive localized corrosion. Consequently, the solid surface is broken down into tiny pieces that contain corrosion products and unreacted zirconium particles. When unreacted particles are fine enough, ignition may occur. This pyrophoricity can be neutralized by treating it with steam.[48] Unreacted particles will oxidize in steam to become stable oxide or cover with a thick layer of oxide film. Treating time is about 20 min when the steam temperature is 250 °C. A longer time is needed when a lower temperature steam is used.

3.14.8 Future Possibilities

Trends in the CPI may offer some clues for zirconium's applications in coming years. They include improving product quality, developing new technologies, and assuring safety and environmental protection.

In compatible environments, zirconium yields few zirconium ions, which are colorless and

biocompatible. Zirconium becomes attractive for producers who do not just want to make a product, but want to make a product of high quality without undesirable impurities. The presence of undesirable impurities may affect the product's performance or may be harmful to the environment. The use of zirconium in the urea production is an example. Another example is the use of zirconium in the production of phenolic resins.[75] Purely from the viewpoint of mechanical integrity, iron-based alloys are suitable structural materials. However, in order to make phenolic resins for high-end uses, the products need to be colorless and very low in impurities. Then, zirconium becomes the necessary choice. If this trend continues, zirconium should find more applications in the food, the electronic, and the pharmaceutical industries.

There is the increasing demand for energy and the effort in reducing greenhouse gases. Many technologies are being developed to produce renewable energy. As indicated in the section of halide-containing processes, zirconium looks promising for the production of hydrogen from the decomposition of HI. In certain ethanol processes, the hydrolysis of starch into glucose is accomplished rapidly by treatment with dilute sulfuric acid at elevated temperature. High performance alloys like zirconium are needed for this type of processes.

Moreover, safer, advanced nuclear reactors have been developed. There is a renewed interest in nuclear energy. Many new nuclear power plants are being built and planned. Demand for zirconium in this arena will certainly rise and with it demand for optimized alloys that permit longer service and, consequently, higher utilization of the available uranium fuel.

Finally, developments in nanotechnology create new materials and corrosion challenges. Certain nanodevices process small amounts of corrosives through relatively large areas of corroding surfaces. Alloys of low corrosion rates may be unsuitable as structural materials. Zirconium could be a good match for certain nanodevices.

References

1. McIntyre, D. R. *Chem. Eng.* **1980**, April 7, 107.
2. Proceedings of Seminars on Accelerated Crack Propagation of titanium in Methanol, Halogenated Hydrocarbons and Other Solutions, March 6, Battelle's Defense Metals Information Center, 1967.
3. Mori, K.; Takamura, A.; Shimose, T. *Corrosion* **1966**, *2*, 29.
4. Yau, T. L. *Werkst. Korros.* **1992**, *43*, 358.
5. Rickover, H. G.; Geiger, L. D.; Lustman, B. History of the development of zirconium alloys for use in nuclear reactors, U.S. Energy Research and Development Administration, Division of Naval Reactors; TID-26740, U.S. GPO: Washington, DC, 1975.
6. Yau, T. L. *Corrosion Engineering Handbook*; Marcel Dekker: NY, 1996; p 195.
7. Yau, T. L.; Sutherlin, R. C. *Corrosion: Materials; ASM Handbook*; ASM International: Materials Park, OH, 2005; Vol. 13B, p 300.
8. Whitton, J. L. *J. Electrochem. Soc.* **1968**, *115*, 58.
9. Pourbaix, M. *Atlas of Electrochemical Equilibria in Aqueous Solutions*; Pergamon Press, 1966; p 223.
10. Burgers, W. G.; Claassen, A.; Zernike, J. *Z. Phys.* **1932**, *74*, 593.
11. Charlesby, A. *Acta Metall.* **1953**, *1*, 340–347.
12. Cox, B. *J. Electrochem. Soc.* **1970**, *117*, 654–663.
13. Bradhurst, H.; Heuer, P. M. *J. Nucl. Mater.* **1970**, *37*, 35–47.
14. Roy, C.; David, G. *J. Nucl. Mater.* **1970**, *37*, 71–81.
15. Godlewski, J.; Gros, J. P.; Lambertin, M.; Wadier, J. F.; Weidinger, H. In *ASTM STP;* ASTM: West Conshohocken, PA, 1991; Vol. 1132, p 416.
16. Godlewski, J. In *ASTM STP;* ASTM: West Conshohocken, PA, 1994; Vol. 1245, p 663.
17. Khatamian, D.; Lalonde, S. D. *J. Nucl. Mater.* **1997**, *245*(1), 10–16.
18. Brown, M. L.; Walton, G. N. *J. Nucl. Mater.* **1975**, *58*, 321–335.
19. Yau, T. L. *Corrosion* **1982**, *38*(12), 615.
20. Yau, T. L.; Maguire, M. A. *Advances in Localized Corrosion*; NACE: Houston, TX, 1990; p 311.
21. Yau, T. L. *Outlook* **1988**, *9*(4), 4.
22. Yau, T. L.; Holmes, D. R. Fluorides from overlooked sources, Paper presented at Wah Chang's Corrosion Applications Conference, 7–12 September 2003, Coeur d'Alene: ID.
23. Kolotyrkin, Y. M. First International Congress on Metallic Corrosion, London; Butterworths: London, 1962; p 10.
24. Maguire, M. In *ASTM STP;* ASTM: West Conshohocken, PA, 1984; Vol. 830, p 175.
25. Cragnolino, G.; Galvele, J. R. *Passivity of Metals*; The Electrochemical Society, 1974; pp 1053–1057.
26. Shibato, T.; Ameer, M. A. M. *Corros. Sci.* **1992**, *33*, 1633–1643.
27. Yau, T. L. Corrosion 84; NACE: Houston, TX, 1984; Paper no. 140.
28. Yau, T. L. Corrosion 83; NACE: Houston, TX, 1983; Paper no. 26.
29. Jangg, G.; Webster, R. T.; Simon, M. *Werkst. Korros.* **1978**, *29*, 16.
30. Maraghini, M.; Adams, G. G.; Russelberghe, P. V. J. *J. Electrochem. Soc.* **1954**, *101*, 400.
31. Yau, T. L.; Webster, R. T. *Corrosion* **1983**, *39*, 218.
32. Yau, T. L. In *Stress-Corrosion Cracking: Materials Performance and Evaluation*; Jones, R. H., Ed.; ASM, 1992; p 299.
33. Fitzgerald, B. J.; Yau, T. L. In 12th International Corrosion Congress, Houston, TX, 19–24 September 1993; Paper no. 092.
34. Yau, T. L.; Webster, R. T. Corrosion/95; NACE: Houston, TX, 1995; Paper no. 250.
35. Yau, T. L.; Webster, R. T. In *ASTM STP;* ASTM: West Conshohocken, PA, 1985; Vol. 866, pp 36–47.
36. Nelson, J. G. In Private communication, 28 April 2000.
37. Haffpauir, R.; Hsieh, J.; Coles, M.; Wong, C. 1997 Zirconium – Organics Conference Proceedings; Wah Chang 1998; p 29.

38. Takeda, K.; Anada, H. In *ASTM STP;* ASTM: West Conshohocken, PA, 2000; Vol. 1354, p 592.
39. Yau, T. L. Corrosion Solutions Conference Proceedings; Wah Chang 2001; p 255.
40. Holmes, D. R. Tin in zirconium 702 – Effect in sulfuric acid applications, Paper presented at Wah Chang's Corrosion Applications Conference, 7–12 September 2003, Coeur d'Alene, ID.
41. Kass, S. *Corrosion of Zirconium Alloys,* ASTM; ASTM: West Conshohocken, PA, 1964; Vol. 368, p 3.
42. Thomas, D. E. In *Metallurgy of Zirconium*; Lustman, B., Kerze, F., Jr., Eds.; McGraw-Hill: New York, 1955.
43. Dalgaard, S. B. Proceedings of the Conference on Corrosion Reactor Materials; International Atomic Energy Association 1962; Vol. 2, p 159.
44. Latimer, W. M. *The Oxidation States of the Elements and Their Potentials in Aqueous Solutions*; Prentice-Hall: Englewood Cliffs, NJ, 1952; p 270.
45. Blumenthal, W. B. *Zirconium Compounds*; National Lead Co., TAM Division, 1969.
46. Knittel, D. R.; Webster, R. T. *ASTM STP;* ASTM: West Conshohocken, PA, 1981; Vol. 728, p 191.
47. Yau, T. L. *ASTM STP;* ASTM: West Conshohocken, PA, 1984; Vol. 830, p 203.
48. Yau, T. L. *ASTM STP;* ASTM: West Conshohocken, PA, 1984; Vol. 830, p 124.
49. Yau, T. L. *Corrosion in Desulfurization Systems*; NACE: Houston, TX, 1984.
50. Bishop, C. R. *Corrosion* **1963**, *19*, 308t.
51. Andreeva, V. V.; Glukhova, A. I. *J. Appl. Chem.* **1961**, *11*, 390.
52. Andreeva, V. V.; Glukhova, A. I. *J. Appl. Chem.* **1962**, *12*, 457.
53. Maraghini, M.; Adams, G. G.; Russelberghe, P. V. J. *J. Electrochem. Soc.* **1954**, *101*, 400.
54. Yau, T. L. *ASTM STP;* ASTM: West Conshohocken, PA, 1986; Vol. 917, p 57.
55. Yau, T. L. *Corrosion* **1983**, *39*, 167.
56. Beavers, J. A.; Griess, J. C.; Boyd, W. K. *Corrosion* **1981**, *36*, 292.
57. Yau, T. L. *Corrosion* **1988**, *44*, 745.
58. Shetlon, S. M. U.S. Bureau of Mines Bull. **1956**, 561.
59. Golden, L. B.; Lane, I. R., Jr.; Acherman, W. L. *Ind. Eng. Chem.* **1952**, *44*, 1930.
60. Golden, L. B.; Lane, I. R., Jr.; Acherman, W. L. *Ind. Eng. Chem.* **1953**, *45*, 782.
61. Bloom, R., Jr.; Weeks, L. E.; Raleigh, C. W. *Corrosion* **1960**, *16*, 164t.
62. Yau, T. L. *Outlook, Wah Chang* **1991**, *12*(1), 3.
63. Yau, T. L. *TAPPI J.* **1991**, *74*(3), 155.
64. Gegner, P. L.; Wilson, W. L. *Corrosion* **1959**, *15*, 341t.
65. Graighead, C. M.; Smith, L. A.; Jaffee, R. I. *Screen tests on metals and alloys in contact with sodium hydroxide at 1000 and 1500°F,* U.S. Energy Commission Report BMI-707, Battelle Memorial Institute, November 1951.
66. Yau, T. L. *Mater. Perform.* **1993**, *32*(6), 65.
67. Golden, L. B. *Zirconium and Zirconium Alloys*; ASM, 1953.
68. McDowell, D. W. *Chem. Eng.* **1974**, *26*, 96.
69. Miola, C.; Richter, H. *Werkst. Korros.* **1992**, *43*, 396.
70. Krystow, P. E. *Chem. Eng. Prog.* **1971**, *67*(4), 59.
71. Corrosion Resistance of Nickel-Containing Alloys in Organic Acids and Related Compound, Publication Number 1285, NiDI, Toronto, Canada 1979.
72. Togano, H.; Osato, K. *Boshoku Gijutsu* **1961**, *10*(13), 529.
73. Shimose, T.; Takamura, A.; Segawa, S. *Boshoku Gijutsu* **1966**, *15*(2), 49.
74. Yau, T. L. *Outlook, Wah Chang* **1987**, *8*(3), 2.
75. Yau, T. L. *J. Test. Eval.* **1996**, *24*(2), 110.
76. Yau, T. L. *Outlook, Wah Chang* **1988**, *9*(3), 6.
77. Leonard, J. D. Eur. patent 5,998, 12 December 1979.
78. Kemira specifies zircadyne 702 for use in a formic acid application, *Outlook* **1990**, *11*(1), 1.
79. Cox, B. In *Advances in Corrosion Science and Technology;* Plenum Press: New York, NY, 1976; Vol. 5, p 173.
80. Mori, K.; Takamura, A.; Shimose, T. *Corrosion* **1966**, *22*, 29.
81. De, P. K.; Elayaperumal, K.; Balschandra, J. *Corros. Sci.* **1971**, *11*, 579.
82. Cox, B. Reports AECL-3551, 3612, and 3799, Atomic Energy of Canada Ltd. 1970/1971 or 3551 (1970); 3612 (1970) and 3799 (1971).
83. Koenig, R. F. Corrosion of zirconium and its alloys in liquid metals, U.S. Atomic Energy Commission Report No. KAPL-982, 1 October 1953.
84. Watson, R. D. Oxidized zirconium as a bearing material in water lubricated mechanism, Report CRE-996, Atomic Energy of Canada, 1960.
85. Kemp, W. E. *Outlook, Wah Chang* **1990**, *11*(2), 4.
86. Haygarth, J.; Fenwick, L. *Thin Solid Films* **1984**, *118*, 351.
87. Fahey, J.; Holmes, D. R.; Yau, T. L *Corrosion* **1997**, *53*(1), 54.
88. Magurie, M. A.; Yau, T. L. *Corrosion 86*; NACE: Houston, TX, 1986; Paper no. 265.
89. Yau, T. L.; Magurie, M. A. *Corrosion* **1984**, *40*, 289; **1985**, *41*, 397.

3.18 Corrosion of Beryllium and its Alloys

R. S. Lillard
Los Alamos National Laboratory, Los Alamos, NM, USA

3.18.1 Metallurgy

Beryllium is a light metal (1.85 g cm^{-3}) with a hexagonal close-packed structure (axial ratio 1.568). Table 1 displays the composition of S200D Be versus S200F two common grades of Be (Brush Wellman), both of which are fabricated from powder materials. The main difference between these grades of Be is the concentrations of BeO, iron, and aluminum (Al). Both grades are manufactured by comminuting vacuum cast ingots, followed by grinding or milling to produce powder.[1] In this process, a thin oxide layer forms around the Be powder particles, resulting in a high BeO content and resultant BeO inclusions that form after hot isostatic pressing. The grain sizes of these two grades of Be are on the order of 10–40 μm, which is characteristic of powder products as the BeO particles pin grain boundaries and retard grain growth.

The most notable of its mechanical properties is its low ductility at room temperature. Deformation at room temperature is restricted to slip on the basal plane, which takes place only to a very limited extent. Consequently, at room temperature, beryllium is, by normal standards, a brittle metal, exhibiting only ~2–4% tensile elongation. Mechanical deformation increases this by the development of preferred orientation, but only in the direction of working and at the expense of ductility in other directions. Ductility also increases very markedly at temperatures above ~300 °C with alternative slip on the (1010) prismatic planes. In consequence, all mechanical working of beryllium is carried out at elevated temperatures. It has not yet been resolved whether the brittleness of beryllium is intrinsic or results from its impurities. Solid solubility of other metals in Be is very low and, to date, it has not been possible to overcome the brittleness problem by alloying.

3.18.2 Extraction and Fabrication

Beryllium is extracted from the main source mineral, the aluminosilicate beryl, by conversion to the hydroxide and then through either the fluoride or the chloride to the final metal. If the fluoride is used, it is reduced to beryllium in magnesium by a Kroll-type reaction. The raw metal takes the form of 'pebble' and contains much residual halides and magnesium. With the chloride, on the other hand, the pure metal is extracted by electrolysis of a mixture of fused beryllium chloride and sodium chloride. The raw beryllium that results is dendritic in character and contains residual chloride.

Before further processing, the raw metal must be purified. Various methods of leaching have been tried on a laboratory scale, but in practice, the method usually adopted is vacuum induction melting. The ingot so produced is then converted to powder by reducing it to chips/turnings, followed by grinding.

Table 1 Typical Be S200D and Be S200F chemistries

Constituents	*S200F*	*S200D*
Beryllium	≈98.5	≈98.0
Beryllium oxide (BeO)	≤1.5	≤2.0
Aluminum	0.10	0.16
Carbon	0.15	0.15
Iron	0.13	0.18
Magnesium	0.08	0.08
Silicon	0.06	0.08
Other metallic impurities	0.04	0.04

All values are given in weight percent.

On a laboratory scale, the grinding is generally done by ball milling; while in production, milling is carried out between beryllium-faced plates.

The particle size of powder most often used for consolidation is 200 mesh (74 mm sieve aperture), and the most widely practiced method of consolidation is hot pressing *in vacuo*.

Setting aside the necessity for hot working and the toxicity issue, the fabrication of consolidated beryllium generally follows normal lines; rolling, extrusion, drawing, forging, etc. have all been successfully carried out. It is interesting to note that because of the high chemical activity of beryllium, allied to the method of consolidation from powder, the usual grade of metal contains ~1–2% of beryllium oxide as described earlier. It could therefore, be considered almost a mild cermet rather than a conventional pure metal. Specifications for typical chemical composition are detailed in **Table 1**.

3.18.3 Aqueous Corrosion Behavior

3.18.3.1 Commercial Grades of Be

The initial studies of the breakdown of passivity in beryllium focused on those environments expected to be generated in the early 'development reactors' where beryllium was used as a neutron reflector, and are not available in the general literature.[2] In these studies, beryllium was exposed to various concentrations of hydrogen peroxide (a water radiolysis product) as a function of solution pH and temperature. At the end of exposure periods, coupons were evaluated for pit density and penetration depth. The effect of coupling beryllium to aluminum and stainless steels on corrosion rate was also investigated. Although beryllium corrosion rates were high in some of the simulated environments, service lifetimes of beryllium reflectors exposed to high-purity, low-temperature, irradiated water were reported to be good.[3]

At this point, it is worth noting that the Be ion exists only in the Be(II) oxidation state; however, early literature, sometimes incorrectly, reported a Be(I) oxidation state.[4] These reports were later discredited. Sheth used weight loss to study the anodic dissolution of Be in numerous solution, including halides (F^-, Cl^-, ...), sulfates, and phosphates.[5] Thus, reports of the existence of a Be(I) oxidation state can be explained by Sheth's observation of metal disintegration, unoxidized loss of metal that skewed correlations between charge passed and weight loss data.

In general, early literature on other forms of beryllium corrosion is limited. Although some polarization studies of beryllium in chloride and sulfate environments have been conducted,[6] other investigations focused on weight loss[7] and visual observation[3,8] to evaluate susceptibility to corrosion. Levy found that beryllium is susceptible to pitting attack in chloride at its open circuit potential (OCP) and uniform attack (i.e., '...a thick, dark anodic film...') in $NaNO_3$ solution.[6] Similar observations were made by Prochko.[8] Additional studies by Stonehouse and Beaver used humidity cabinet experiments to evaluate the susceptibility of beryllium to corrosion from surface residue deposited during machining.[3]

Other investigations have focused on the corrosion associated with beryllium carbides. One of the primary impurities in historic grades of beryllium is carbon, 0.2 wt% or more, which results in the formation of second-phase particles (Be_2C). In the presence of water, these carbides react quickly to form BeO ($\Delta G = -581$ kJ mol^{-1})

$$Be_2C + 2H_2O \rightarrow 2BeO + CH_4 \qquad [1]$$

as discussed by Mueller.[9] It may be noted, however, that the relative surface concentration of carbides is low and once the carbide has been consumed by this reaction with water, no further role of carbides is expected.

Gulbrandsen *et al.* studied the passivity of Be in phosphoric acid, oxalic acid, phosphate, borate, carbonate buffer solutions, and sodium hydroxide to characterize the passive current density over a pH of 1–15.[10] It was shown that a minimum in passive current density for beryllium occurs near pH 11 and increases logarithmically in more acidic and alkaline solutions. Moreover, it was also observed for any one solution pH that the passive current density is a function of ionic strength. However, Gulbrandsen did not address the formation of soluble oxalic and phosphoric beryllium complexes that form in some of

the solutions used. This may account for their observation of steady-state passive currents below the thermodynamic limit of pH 2.

More recently, Hill *et al.* studied the passivity and break down of 98.5% pure Be.[11] The solutions used were sulfuric acid adjusted to a solution pH of 1 and 2, 0.25 M boric acid (pH = 4.6), 0.05 M sodium borate/0.5 M boric acid (pH = 7.2), 0.025 M sodium borate/0.05 M sodium hydroxide (pH = 10.7), and sodium hydroxide adjusted to a solution pH of 12.5. A summary of the corrosion current densities and passive current densities as a function of pH is presented in **Figure 1**. Below pH 2, Be exhibited active dissolution at all applied anodic potentials. In solution pH 2–12.5, it was shown that Be exhibits passive anodic behavior at potentials between the OCP and 0.6 V versus saturated calomel electrode (SCE). Anodic polarization above 0.6 V SCE in the pH range of 2–12.5 led to an abrupt increase in the passive current density, followed by oxygen evolution. This abrupt increase was attributed to a change in the specific resistivity of the passive film, as determined by electrochemical impedance spectroscopy (EIS). EIS experiments were also used to show that the oxide growth rate on Be is 6.4 Å V^{-1} over the potential range of 0–4 V. At higher anodization potentials, the growth rate appeared to be somewhat lower likely due to an increase in oxide conductivity.

Breakdown of passivity was studied in chloride and fluoride solutions. In chloride, the attack was found to be localized. Typical potentiodynamic polarization curves for S200D beryllium in deaerated NaCl solutions ranging in concentration from 10^{-4} to 1 M Cl^- are presented in **Figure 2**. For Cl^- concentrations below 1 M, the anodic polarization of the sample was characterized by a region of passivity followed by a logarithmic increase in the current density, which corresponded to the onset of pitting corrosion. In deaerated 1 M Cl^-, pitting at the OCP was observed. The voltage that corresponded to the onset of pitting corrosion, E_{pit}, was found to decrease logarithmically with increasing chloride concentration according to the relationship

$$E_{pit} = -0.067\log[Cl^-] - 1.01 \qquad [2]$$

where E_{pit} is in volts versus SCE and $[Cl^-]$ is the concentration of chloride in molarity (**Figure 3**). As seen in this relationship, a −0.067 V change in the pitting potential per decade of chloride concentration was observed. A similar relationship between E_{pit} and chloride concentration has been noted for pure aluminum (Al); however, the relationship between the pitting potential of Al in Cl^- concentration is −0.091 V per decade $[Cl^-]$. For 18Cr–8Ni stainless steel, the pitting potential has been found to vary by −0.088 V per decade $[Cl^-]$. Thus, the pitting potentials of Al and stainless steel are more sensitive to changes in chloride concentration than are those of Be. In addition, as defined by the *y*-intercept in eqn. [1], for any one chloride concentration, E_{pit} for Be is more negative than those of Al and stainless steel.

Hill *et al.* also investigated the breakdown of passivity in sodium fluoride (NaF) solutions ranging in concentration from 10^{-1} to 10^{-4} M F^-. At a

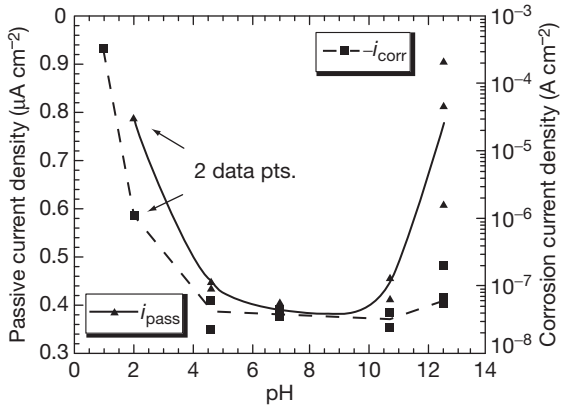

Figure 1 Passive current density, i_{pass}, and corrosion current density, i_{corr}, as a function of solution pH. A minimum in i_{pass} and i_{corr} exists between a pH of 4.5 and 10.7. Reproduced from Hill, M. A.; Butt, D. P.; Lillard, R. S. *J. Electrochem. Soc.* **1998,** *145*, 2799, with permission from The Electrochemical Society.

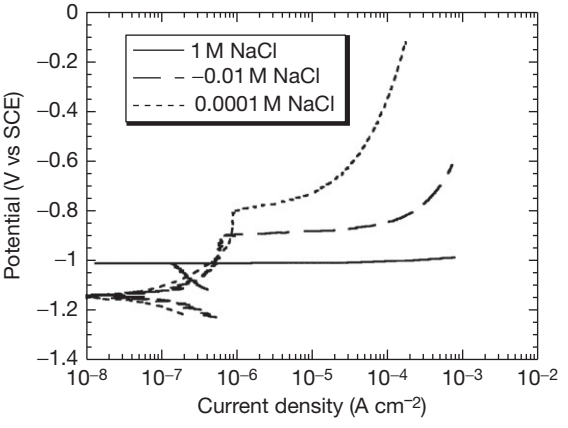

Figure 2 Beryllium polarization curves as a function of chloride concentration showing a decrease in pitting potential with an increase in chloride concentration. Reproduced from Hill, M. A.; Butt, D. P.; Lillard, R. S. *J. Electrochem. Soc.* **1998**, 145, 2799, with permission from The Electrochemical Society.

F^- concentration of 10^{-4} M, the anodic polarization of the sample was characterized by a region of passivity followed by a logarithmic increase in the current density which corresponded to the onset of pitting corrosion. The pitting potential was found to be −0.742 V SCE. In comparison, for 10^{-4} M Cl^-, the pitting potential was −0.773 V SCE. Pitting type corrosion was also observed for 10^{-3} M F^-; however, no region of passivity was observed upon anodic polarization. While at the lower fluoride concentrations the breakdown of passivity was localized, at the higher fluoride concentrations (10^{-1} to 10^{-2} M) beryllium was susceptible to uniform attack.

3.18.3.2 High-Purity Be

Lillard investigated the factors influencing the transition from metastable to stable pitting high-purity single crystal beryllium.[12] The goal of that work was to determine the relationship between physical bulk metal properties, such as crystallographic orientation of the surface, and the critical pitting environments in terms of ohmic and mass transport models on the breakdown of passivity. To accomplish this, electrodes were fabricated from one zone-refined Be single crystal (99.99% Be via ion coupled plasma (ICP) analysis) that was sectioned using electrical discharge machining (EDM). Experiments were conducted on the following surfaces: (0001) the basal plane, (10–10) a Type-I prism plane, and (11–20) a Type-II prism plane. The solutions used in this study were sulfuric acid adjusted to a pH of 2 and near-neutral 0.01 M sodium chloride.

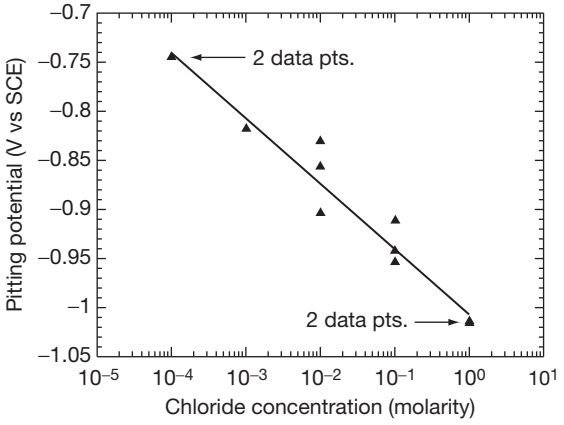

Figure 3 Pitting potential as a function of chloride concentration displaying a logarithmic relationship between E_{pit} and [Cl^-]. Reproduced from Hill, M. A.; Butt, D. P.; Lillard, R. S. *J. Electrochem. Soc*. **1998**, 145, 2799, with permission from The Electrochemical Society.

A summary of the critical parameters from the potentiodynamic polarization data for the three orientations investigated is presented in **Table 2**. E_{pit} was found to decrease with electrode orientation in the order (0001) > (10 −10) > (11–20). The scatter in E_{pit} for each orientation was moderate, and in only one case did the potential regions overlap; the maximum E_{pit} for the (11–20) surface was 0.01 V greater than the minimum E_{pit} for the (10–10) surface. Post-exposure observation found that the corrosion pits were not hemispherical, rather, they were highly crystallographic in nature (**Figure 4**). Corrosion pits on the surfaces of prism planes (10–10) and (11–20) were characterized by interiors that had crystallographically oriented, parallel plates of unattacked material. In comparison, the morphology of the corrosion pits in polycrystalline Be are also characterized by parallel plates of unattacked Be, separated by trenches of similar size and shape (**Figure 5**). Similar morphologies were also observed by Straumanis in polycrystaline Be.[13] The orientation dependence of pit propagation in single crystal and polycrystalline Be was explained within the context of the metal–metal bond strength as a function of surface orientation.[14] Using the calculations of the electron density distribution, it was proposed that crystallographic pits propagate preferentially at ledges/steps that

Table 2 Critical parameters from potentiodynamic polarization curves for Be single crystals in 0.01 M NaCl as a function of surface orientation

Surface orientation	E_{corr} *(V vs SCE)*	i_{pass} *(A cm^{-2})*	E_{pit} *(V vs SCE)*
S200D polycrystalline	−1.15, $\sigma = 0.03$	6.1×10^{-7}, $\sigma = 0.4\times10^{-7}$	−0.862, $\sigma = 0.030$
(0001)	−1.28, $\sigma = 0.20$	1.1×10^{-7}, $\sigma = 0.16\times10^{-7}$	−0.644, $\sigma = 0.035$
(10–10)	−1.39, $\sigma = 0.12$	1.8×10^{-7}, $\sigma = 0.23\times10^{-7}$	−0.732, $\sigma = 0.027$
(11–20)	−1.28, $\sigma = 0.08$	1.3×10^{-7}, $\sigma = 0.34\times10^{-7}$	−0.800, $\sigma = 0.047$

The data from polycrystalline S200D grade Be (98.5% Be) from Stonehouse is also presented.

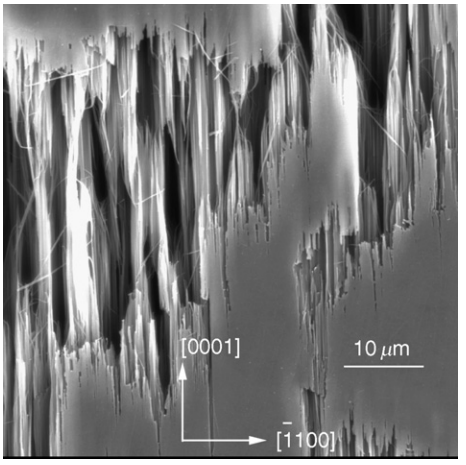

Figure 4 SEM micrograph of typical corrosion pits in the (11–20) surface of Be after potentiodynamic polarization above the pitting potential in 0.01 M NaCl. Orientation of the lamlella (and pit walls) was parallel to the [0001] direction and normal to the (11–20) surface. Reproduced from Lillard, R. S. *J. Electrochem. Soc.* **2001**, *148*, B1, with permission from The Electrochemical Society.

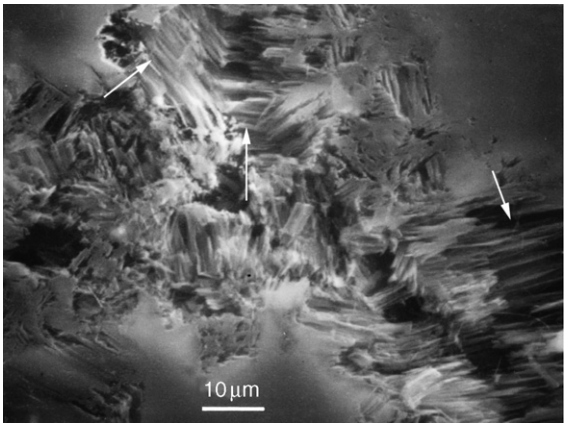

Figure 5 SEM micrograph of corrosion pits in S200D grade (powder pressed) Be showing orientation of pit walls and parallel plates of unattacked Be lamella (normal to arrows) left behind after pit propagation. The size of any one set of parallel plates is consistent with the grain size of this material (~10–40 μm). Reproduced from Lillard, R. S. *J. Electrochem. Soc.* **2001**, *148*, B1, with permission from The Electrochemical Society.

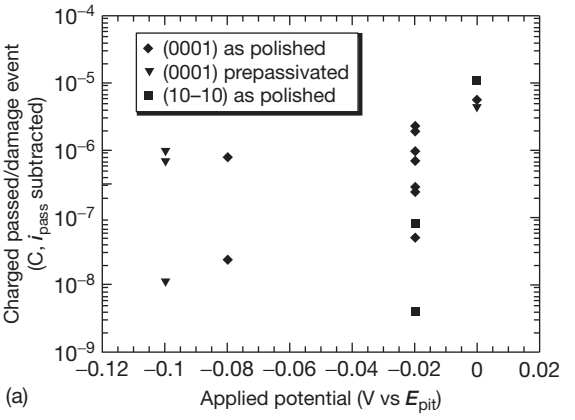

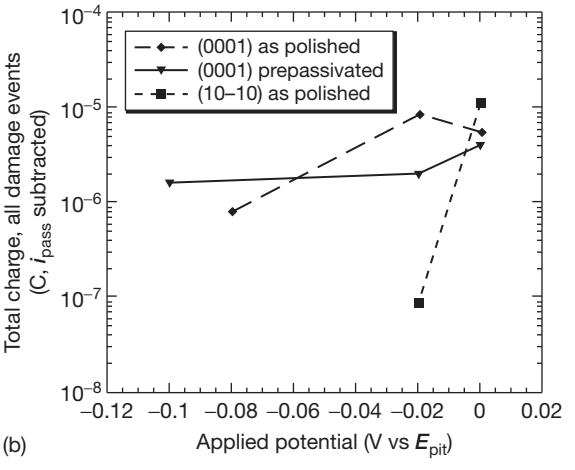

Figure 6 (a) A summary of the damage events; charge passed per event versus applied anodic potential (vs E_{pit}) for the (0001) and the (10–10) surfaces in 0.01 M NaCl solution. (b) A summary of the damage events; total charge passed during all damage events versus applied anodic potential (vs E_{pit}) for the same surfaces in shown in (a). Only damage events that repassivated were considered in these plots. Reproduced from Lillard, R. S. *J. Electrochem. Soc.* **2001**, *148*, B1, with permission from The Electrochemical Society.

expose susceptible lattice positions by removing atoms of lowest bond strength.

At potentials more positive than the repassivation potential, E_{rp}, a unique type of current transient was observed in the current/time data collected during potentiostatic experiments. This type of transient was always associated with a large amount of charge passed and visible damage on the electrode surface. The average charge passed, peak charge passed, and total number for damage transients increased with increasing anodic potential for each surface orientation are shown in **Figure 6**. From these results, it was concluded that the transition from metastable to stable pitting is governed by surface damage, and more likely, a bulk property of the metal such as surface energy/metal bond strength.

3.18.3.3 Galvanic Effects – The Influence of Be Inclusions

As discussed in Sections 3.18.1 and 3.18.2, commercially available beryllium is generally a powder-processed material. In addition to the relatively high BeO content, most impurity concentrations in commercial beryllium exceed the solubility limit and produce precipitates. The precipitates that form generally are present as both binary and ternary intermetallic phases with Be. Of the possible intermetallics that may form in the commercial grades of Be, $FeBe_5$, $TiBe_{11}$, and $FeAlBe_4$ have been observed on fracture surfaces,[15] although the galvanic relationships between these precipitates and the Be matrix were not defined. These galvanic relationships impact on environmental fracture models from the standpoint of crack tip chemistry and potential, as well as localized corrosion models, from either a cathodic reduction or anodic site chemistry standpoint. In addition, they play an important role in the localized corrosion of Be.[11,16]

To enhance the understanding of the mechanisms of localized corrosion and stress corrosion cracking in commercial grades of beryllium, Hill *et al.* initiated a study of the galvanic relationships between Be and the single phase particles.[17] The beryllides studied were $TiBe_{12}$, $FeAlBe_4$, and δ-phase iron beryllide $FeBe_5$ (nominal composition $FeBe_{12}$, crystallographically $FeBe_5$). They were prepared by arc-melting and casting high-purity elemental material. The solutions studied were of sulfuric acid adjusted to a pH of 2, 0.05 M sodium borate/0.5 M boric acid (pH = 7.2), 0.025 M sodium borate, and sodium hydroxide adjusted to a pH of 10.5 and sodium hydroxide adjusted to a solution pH of 12.5.

In a pH range of 7.2–12.5, all of the beryllides exhibited passive behavior. Most notably, a transpassive region was noted in the Fe-containing beryllides at a solution pH of 7.2. With respect to the pH 2 solution, active dissolution of all beryllides was observed at this pH. This was confirmed by post-exposure examinations of the samples, which revealed a large quantity of damage.

A summary plot of OCP values for each beryllide along with that of commercially pure Be is shown in Figure 7 as a function of pH. These data were collected after 48 h of immersion and represent steady-state OCP values. This plot is useful in that it allows one to determine the galvanic relationships between second phase particles in a Be matrix. For example, with respect to $FeAlBe_4$, the OCP is more negative than that of beryllium in the pH range of 2.0–10.5. Thus, from a mixed potential standpoint, when coupled in commercial Be under these conditions, the $FeAlBe_4$ may act as a site for active dissolution. This finding was confirmed experimentally in galvanic couple tests.

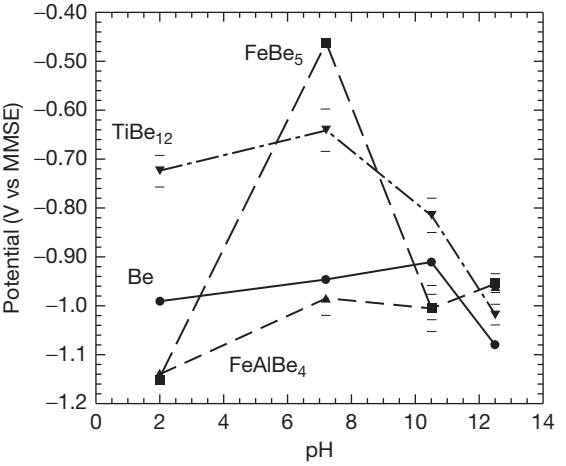

Figure 7 A summary plot of OCP for $FeBe_5$, $FeAlBe_4$, and $TiBe_{12}$ as a function of solution pH. Data were collected after 48 h of immersion and represent steady-state OCP values. Reproduced from Hill, M. A.; Hanrahan, R. J.; Haertling, C. L.; Schulze, R. K.; Lillard, R. S. *Corrosion* **2003**, *59*, 424, with permission from NACE International.

3.18.3.4 Environmental Fracture

Reports on environmental fracture of Be are limited. The first reported work on the stress-corrosion cracking of beryllium related to its use in water containing 0.005 M hydrogen peroxide at pH 6–6.5 and at ~90 °C.[18] Although some pitting occurred in these exposure, there was no evidence of stress corrosion, even though the tests employed extruded metal stressed at up to 90% of the yield stress. Later work included stress corrosion studies of Be tensile bars' exposure to synthetic seawater.[19] In that environment, time to failure decreased from ~2350 h at an applied stress of 1220 psi to 40 h at an applied stress of 40 000 psi. Further, crack initiation appeared to be related to localized corrosion of the sample. Electron microscopy of the fracture surfaces found the crack habit to be transgranular in character. Subsequent work by the same group studied the influence of applied current, anodic and cathodic, on time to failure.[20] As might be anticipated, applied anodic currents promoted pitting attack and decreased time to failure. However, applied cathodic currents reduced pitting attack and eliminated environmental fracture altogether.

3.18.3.5 Corrosion Control

From what has already been indicated, it will be apparent that the use of beryllium in most commercial environments involving moisture will require some form of surface protection to mitigate pitting corrosion. Corrosion control measures range from painting[21] to Zn galvanizing.[22] In addition to those studies, Paine and Stonehouse[23] used a high temperature silicone-based paint on beryllium heat-sinks for aircraft brakes. They also studied cathodic protection in fresh- and saltwater solutions via manganese plating on the steel parts that were mated to Be. Other work on cathodic protection includes the stress corrosion study in aerated synthetic seawater described in **Section 3.18.3.4**. There, an impressed cathodic potential was used to protect Be from localized attack by chlorides.[20]

Booker examined the application of chromate conversion coatings (CCCs) to mitigate Be corrosion in chloride environments.[24] As the coating bath composition was not specified in that paper, one can only presume that these coatings were based on Alodine® (a nitric acid-based solution containing $NaF/KBF_4/K_2ZrF_6/K_3Fe(CN)_6$). Chromium deposition (and ultimately corrosion protection) was greatly dependent on the manner in which the sample was cleaned and etched. To obtain the best performance, it was necessary to etch the samples in a nitric acid–hydrofluoric acid solution just prior to coating. The need for this F^- base etch has been confirmed in our laboratory. Samples prepared in this manner were described by Booker as having satisfactory performance in high humidity and salt spray exposures. A similar investigation of CCCs was reported by Levy.[6]

The use of anodization to control Be corrosion has been somewhat problematic. Kerr reported on the anodization of Be in an aqueous solution of 10% nitric acid containing 200 g l^{-1} CrO_3 (chromic acid).[25] In that work, samples were anodized at a constant current density of 0.03 A cm^{-2}. Although films as thick as 0.35 mm were grown in this solution, when the limiting voltage was reached, the current remained constant with time. Thus, it was concluded that for Be, there is no voltage-dependent limiting oxide thickness as is the case for other valve metals such as aluminum, zirconium, and tantalum. In an attempt to overcome this difficulty, Kerr explored the use of an ammoniacal glycol solution (25 g l^{-1} NH_3 in ethylene glycol), which has been used successfully to grow compact insulating films on aluminum. For current densities of 1.9 mA cm^{-2}, limiting thicknesses were formed on Be. However, as was the case in chromic acid, the current remained roughly constant with time and it was concluded that the films formed in this solution were not insulating. Subsequently, Hill has shown that the specific resistivity of the oxide on Be decreases with increasing applied potential and undergoes a transition at ~2 V versus NHE.[11] This was attributed to a change from a compact to a more porous film though this behavior may owe to other factors such as the incorporation of unoxidized metal into the film. Levine has also reported on anodic films grown in ammoniacal glycol solution and nitric acid solutions containing chromic acid.[26] Similarly, films grown in nitric acid were always crystalline, while those grown in ethylene glycol were amorphous. Levine reported current potential relationships similar to Kerr, indicating that these films were not insulating. Shetata has reportedly been able to overcome this problem by growing films on Be in near-neutral ethylene glycol saturate with sodium phosphate dibasic and sodium sulfate.[27] For constant current densities in the order of 2–3 mA cm^{-2}, samples anodized in this solution quickly reached limiting voltages of 50 V (<30 s) and, correspondingly, decreasing current density with time. Films grown on Be in this manner were insulating and are of the order of 5 μm thick. Unfortunately, we have not been able to reproduce these results in our own laboratory.

3.18.4 High Temperature Oxidation of Be and the Beryllides

3.18.4.1 Beryllium

Early high temperature oxidation studies of Be focused on dry and moist oxygen environments. Gulbransen examined the reaction of Be (Brush) with dry oxygen (0.76–7.6 cm O_2) over the temperature range of 350– 950 °C.[28] At lower temperatures (below 825 °C) and high O_2 pressures (7.6 cm O_2), the oxidation rate appeared to fit a logarithmic or inverse logarithmic law, while at higher temperatures, the rates appeared to by parabolic (**Figure 8**). Weight gain data (W) as a function of time (t) were fit to a parabolic rate law, $W^2 = Kt + C$, where K is the parabolic rate constant. Below 650 °C, K increased from 0.93×10^{-16} cm^2 s^{-1} at 350 °C to 5.4×10^{-15} cm^2 s^{-1}; at 950 °C, K was equal to 1.0×10^{-12} cm^2 s^{-1}.

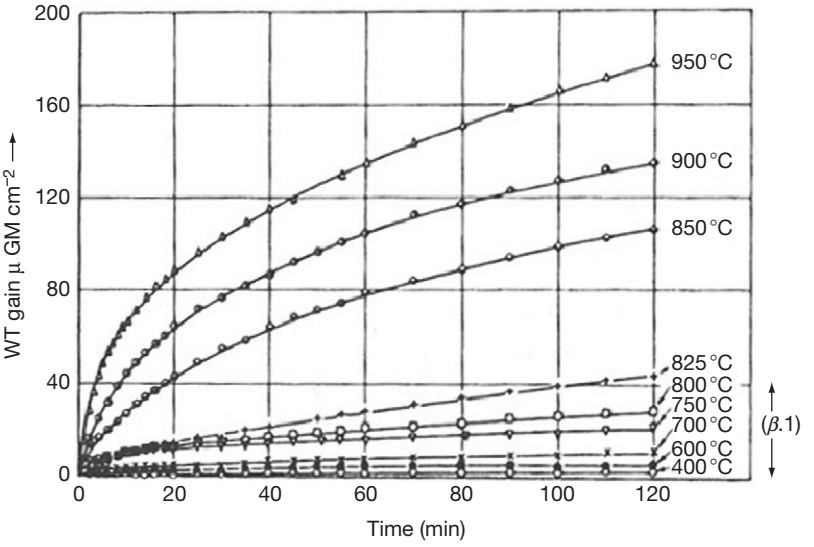

Figure 8 The influence of temperature on the oxidation rate of Be in dry O_2 at a pressure of 7.6 cm. Reproduced from Gulbransen, E. A.; Andrew, K. F. *J. Electrochem. Soc.* **1950**, *97*, 383, with permission from The Electrochemical Society.[28]

Arrhenius plots of log K versus $1/T$ identified two activation energies for oxidation; below 750 °C, the activation energy was equal to 8.5 kcal mol^{-1}, while above 750 °C, the activation energy was 50.5 kcal mol^{-1} (**Figure 9**). Similar activation energies in the high temperature range were observed in the later work by Cubicciotti.[29] For Pechiney flake Be (referred to as 'French-flake' being produced in France), Be in 10-cm dry O_2 and temperatures below 650 °C, Alymore found higher oxidation rates and at temperatures greater than 650 °C with breakaway oxidation observed.[30] Similar trends were found by Ervin, who concluded that the first stage of Be (Brush/NMC) oxidation is a protective diffusion controlled process (Be vacancies).[31] He further concluded that the formation of pits at accumulation sites of vacancies at the metal–oxide interface in this stage lead to a second, catastrophic stage of oxidation. To date, there is no clear explanation of discrepancy between the Gulbransen–Cubicciotti observations of passive behavior and low oxidation rates in the range of 350–950 °C and the works of Alymore–Ervin that found breakaway oxidation above 650 °C. For example, one investigator did not use powder product as compared with results from pressed disc or flake nor were there clear distinction between vendors (Brush versus Pechiney flake).

With respect to the addition of H_2O, Alymore investigated oxidation rates for Be in moist O_2

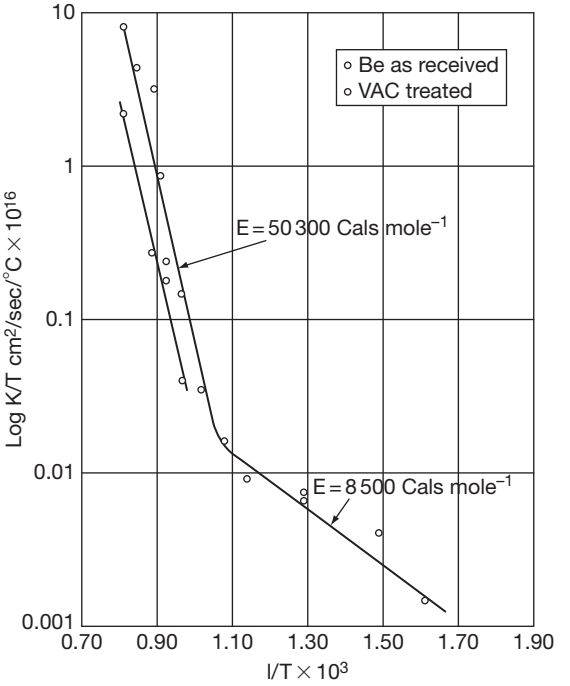

Figure 9 Arrhenius plot from data in **Figure 8** showing the parabolic rate constant as a function of inverse temperature (K). Two unique behaviors, and thus activation energies, are observed above and below ~750 °C (1020 K, $1/T = 0.00098$). Reproduced from Gulbransen, E. A.; Andrew, K. F. *J. Electrochem. Soc.* **1950**, *97*, 383, with permission from The Electrochemical Society.

(10 cm O_2, 1.2 cm H_2O) and water vapor.[32] In 1.2-cm H_2O and temperatures below 650 °C, oxidation rates were logarithmic/parabolic. After 300 h of exposure, the weight gains were of the order of 20 μg cm^{-2}. Above 650 °C, breakaway oxidation was observed. In water vapor below 650 °C, rates were again logarithmic/parabolic and relatively low, less than 50 μg cm^{-2}. Above 650 °C, breakaway oxidation was again observed.

The possible use of beryllium in nuclear engineering and in the aircraft industry encouraged considerable investigation into its oxidation characteristics in carbon dioxide and carbon monoxide (dry and moist) at temperatures of up to 1000 °C. For Pechiney-flake Be, Gregg found that the oxidation of Be in dry CO_2 (pressure of 10 cm) was logarithmic at temperatures equal to and below 550 °C and inverse logarithmic between 600 and 750 °C for exposure times up to 300 h (**Figure 10**).[33] They proposed that film thickening occurs via the outward diffusion of Be^{2+} to react with chemisorbed carbon dioxide at the gas–oxide interface where the following reactions take place to form oxide and carbide species.

$$2Be + CO_2 \Rightarrow 2BeO + C \qquad [3]$$

$$2Be + C \Rightarrow Be_2C \qquad [4]$$

In moist CO_2 (total CO_2 pressure of 10 cm, with 1.2-cm partial pressure H_2O) at temperature equal to and below 650 °C, results were similar to those in dry CO_2. However, at temperatures greater than 650 °C, breakaway oxidation was observed (**Figure 11**).[34] Radiotracer experiments in moist CO_2 found the build up of gas in the exposure vessel, which led the authors to conclude that water was reacting with the BeC to form methane:

$$Be_2C + 2H_2O \Rightarrow BeO + CH_4 \qquad [5]$$

Unfortunately, no conclusions concerning the mechanism of the breakaway oxidation were reported. Similar rate constants and threshold temperatures were found by Menzies for flake as well as Brush sheet and powder products in 300 psig CO_2/300 ppm H_2O for longer exposure periods (up to 8000 h).[35] Higgins investigated Be–CO_2–H_2O systems at higher temperatures and higher water content and found similar thresholds.[36] Raine and Robinson found that small additions of calcium greatly improved the resistance of Be to breakaway oxidation.[37] Further, it was found that the addition of Ca modified the pressure dependence of the corrosion reaction in CO_2.

In dry carbon monoxide, Gregg found that the oxidation rates were greater by at least a factor of 10 than those observed in dry CO_2; however, the transition temperatures from logarithmic to inverse logarithmic behavior that were reported in that study were similar to those reported by Gulbransen (**Figure 8**).[38] In this environment, the possible reactions are

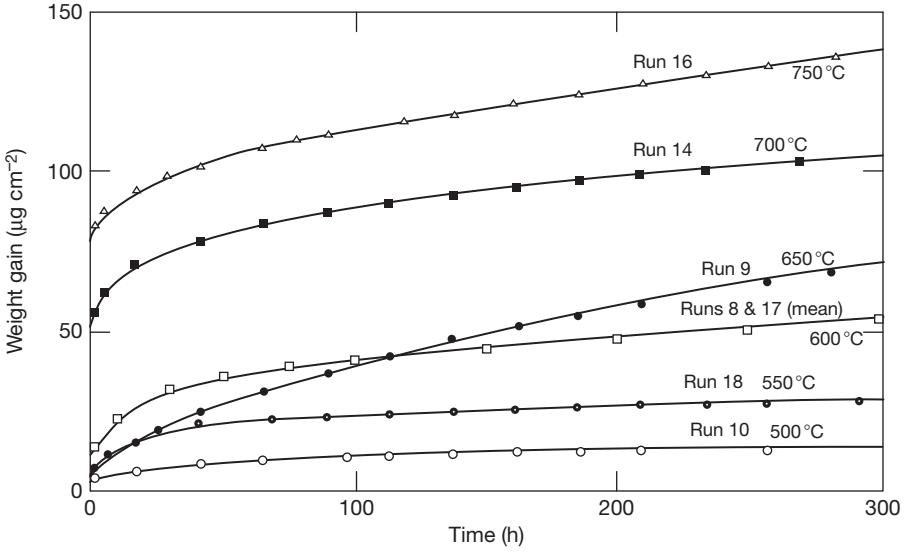

Figure 10 Oxidation of Be as a function of temperature in dry CO_2 at pressure of 10 cm. Reproduced from Gregg, S. J.; Hussey, R. J.; Jepson, W. B. *J. Nucl. Mater.* **1961**, *3*, 175, with permission from Elsevier.[33]

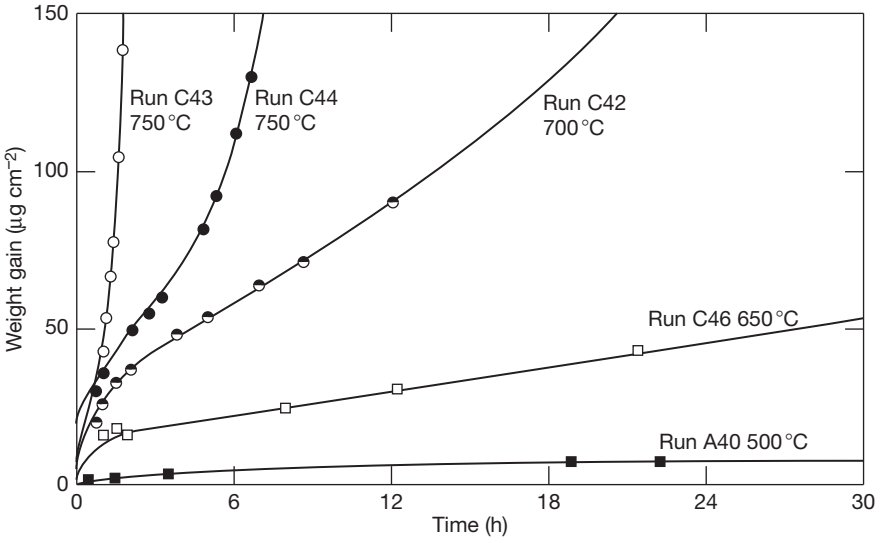

Figure 11 Oxidation of Be as a function of temperature in moist CO_2 at a total pressure of 10 cm with 1.2-cm partial pressure H_2O. Reproduced from Gregg, S. J.; Hussey, R. J.; Jepson, W. B. *J. Nucl. Mater.* **1961**, *4*, 46, with permission from Elsevier.

$$Be + CO \Rightarrow BeO + C \quad [6]$$

$$3Be + CO \Rightarrow BeO + Be_2C \quad [7]$$

The higher oxidation rates observed in CO were attributed to a nonprotective reaction product that spalls from the sample. It was proposed that the lower ratio of BeO to C production in CO oxidation (eqn. [6]), as compared with CO_2 oxidation (eqn. [3]), results in excessive C (or Be_2C) incorporation, and thus, a less protective film. Subsequent selected-area transmission electron microscope diffraction patterns by Scott confirmed that BeC_2 was in fact incorporated into the oxide during oxidation in CO.[39] Subsequent work on these alloys by Scott found that calcium acted to reduce oxidation rates by decreasing the extent of intergranular oxidation of the metal.[40]

3.18.4.2 Beryllides

Beryllium intermetallics are currently being considered as replacement materials for beryllium in demonstration fusion reactors. Although beryllium is commonly used as a neutron multiplier in the fusion blanket, its melting point is low (1285 °C) and the ITER demonstration reactor requires temperature in the 600–900 °C range. Possible replacements include beryllium–copper such as CuNiBe and $TiBe_2$. These two intermetallics are representatives of the Laves phases group C14 and C15. Phases in these groups include $CrBe_2$, $NbBe_2$, $TaBe_2$, and VBe_2 and have been the subject of limited oxidation studies. Paine *et al.* tested the above phases in dry air for 100 h at temperatures up to 1426 °C.[41] Each was shown to have good oxidation resistance under these test conditions. However, the study was heavily biased toward the highest melting point compounds, of which $TiBe_2$ is one, and therefore, many phases were not examined because they did not appear promising for service above 1371 °C. In a separate study, Alves *et al.* investigated Ti beryllides, Be–5% Ti ($Be_{12}Ti$), and Be–7% Ti, which was a two-phase system consisting of $Be_{12}Ti$ surrounded by Be.[42] From surface analytical experiment (X-ray emission and RBS) of samples oxidized at 800 °C for 1–4 h, it was found that the oxidation in the two-phase system was faster than in $Be_{12}Ti$.

By far, the largest amount of information on any beryllide relates to $ZrBe_{13}$ and other zirconium-based beryllides. In experiments on powders, Ervin and Nakata found a protective BeO on $ZrBe_{13}$ and $NbBe_{12}$ between 900 and 1500° C.[43] The oxidation rate for $ZrBe_{13}$ in 0.1-atm oxygen was parabolic and is presented in **Figure 12**. In comparison, the rates reported by Paine were much higher for air. Paine reported that the oxidation rate for $ZrBe_{13}$ in dry air (at 1537 °C) was 10 mg cm^{-2} after 100 h and 6 mg cm^{-2} for moist air after the same period.[41] The temperature dependence of the rate constants

from the Ervin data is shown in Figure 13 as an Arrhenius plot. As seen in this figure, two activation energies for oxidation (Q) were observed. In the range of 1100–1400 °C, Q was determined to be 5.6×10^4 J, while in the range between 1400–1500 °C, Q was determined to be 21.5×10^4 J. Similar results were found for $NbBe_{12}$; however, for $NbBe_{12}$, Q was constant over the entire temperature range examined and determined to be equal to 13.0×10^4 J. Ervin and Nakata reported accelerating oxidation of $ZrBe_{13}$ at lower temperatures in 0.1 atm oxygen (Figure 14), while $NbBe_{13}$ was immune to this phenomenon. This observation was attributed to "fracture and disintegration of the metal phase causing a continual increase in the exposed metal surface area." This phenomenon is known as pest and has been reported by several other authors.[44–48] Chou *et al.* reported that the susceptibility of $ZrBe_{13}$ to pest is increased in the presence of moist air, although this finding is not uniform amongst other authors investigating Zr-based beryllides. In addition, Chou concluded that the formation of BeO-rich wiskers is important in the pest mechanism of beryllides, but did not report how they might form or why they cause disintegration.

The influence of Be additions on the high temperature oxidation of NiAl and TiAl-based intermetallics has been investigated by Hanrahan.[49] In TGA studies conducted from 800 to 1200 °C for 16 h in air, Be-modified NiAl containing 1, 2, or 5 at.% Be exhibited lower weight gain and comparable or slower oxidation rates than the pure binary material. In addition, the reaction kinetics in these

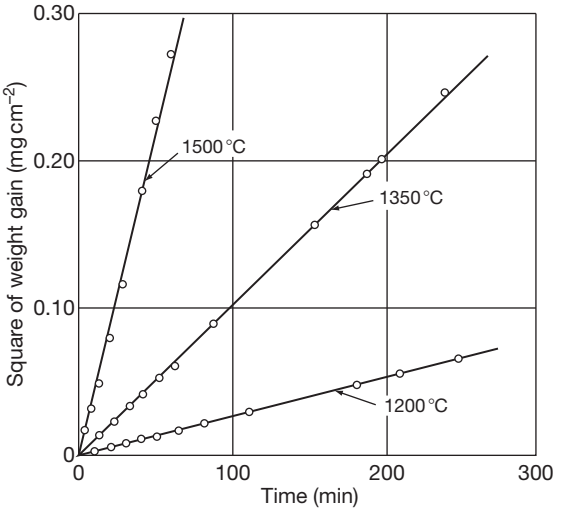

Figure 12 Oxidation of $ZrBe_{13}$ as a function of temperature in 0.1 atm O_2. Reproduced from Ervin G., Jr.; Nakata, M. M. *J. Electrochem. Soc.* **1963**, *110*, 1103, with permission from The Electrochemical Society.

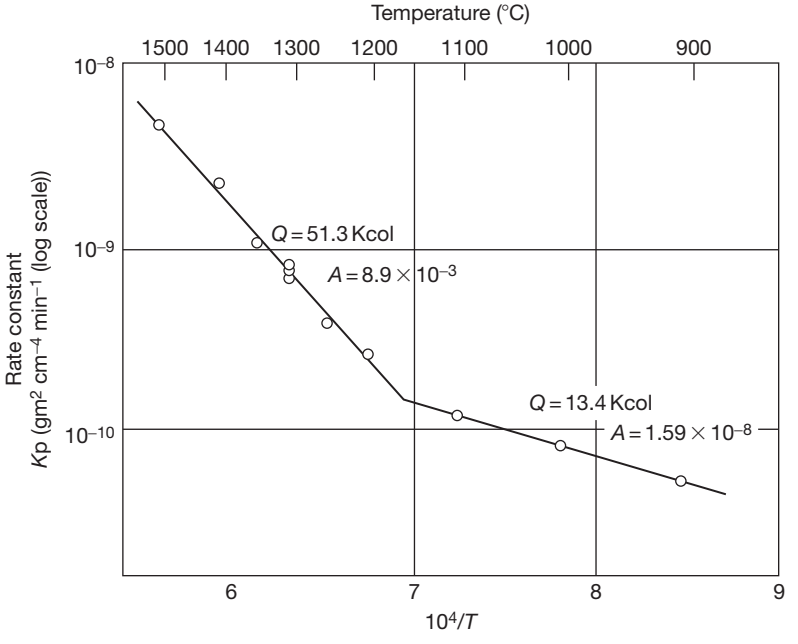

Figure 13 Arrhenius plot from data in 5.4.2.1 showing the parabolic rate constant as a function of inverse temperature (K) for $ZrBe_{13}$ in 0.1 atm O_2. Reproduced from Ervin G., Jr.; Nakata, M. M. *J. Electrochem. Soc.* **1963**, *110*, 1103, with permission from The Electrochemical Society.

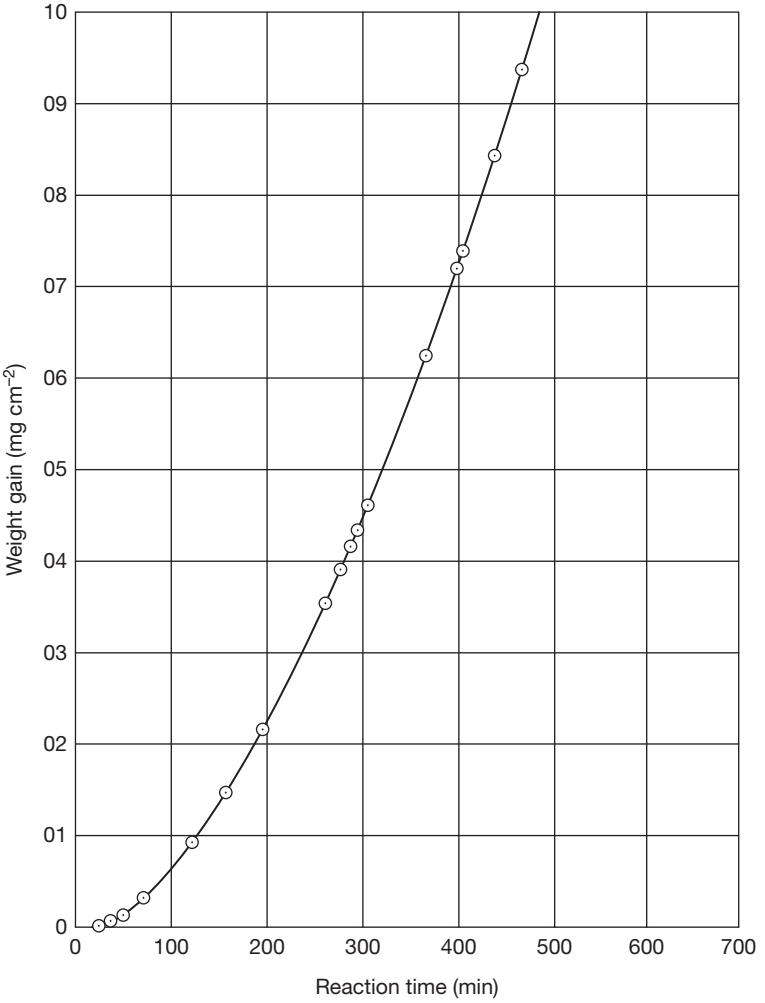

Figure 14 Low-temperature (600–700 °C) oxidation of $ZrBe_{13}$ in 0.1-atm O_2. Reproduced from Ervin G., Jr.; Nakata, M. M. *J. Electrochem. Soc.* **1963**, *110*, 1103, with permission from The Electrochemical Society.

experiments were equal to or slower than in NiAl. The surfaces of the Be-modified specimens showed minimal topography, with no evidence of the usual transient alumina phases grown on binary NiAl in this temperature range. From X-ray diffraction and surface analysis, it was found that oxidation did not result in formation of BeO at any of the temperatures. Rather, the presence of layers of Al_2O_3 and ternary oxide phases, primarily $BeO{\cdot}Al_2O_3$ (chrysoberyl), were observed. It was proposed that the formation of this phase prevents the growth of the transient alumina phases. Thus, lower weight gains and slower reaction kinetics were observed due to the rapid formation of the chrysoberyl phase followed by nucleation of α-alumina at the scale–metal interface, rather than the formation of transient alumina phases often observed to form on NiAl. In other studies, Be additions to Ti–Al–Cr-based alloys at 800 °C and 1000 °C in dry air resulted in the formation of a protective $BeAl_2O_4$ spinel phase.[50] In moist air, only Ti–Al–Cr–Be alloys with a high Cr content (10–15 at.%) formed the protective $Be{\cdot}Al_2O_4$ scale.

References

1. Stonehouse, A. J. *J. Vac. Sci. Technol. A* **1986**, *4*, 1163.
2. English, J. L. Interim Report on the Corrosion of Beryllium in Simulated Cooling Water for the Proposed Development Reactor, ORNL-298, Oak Ridge National Laboratory, March,1949.
3. Stonehouse, A. J.; Beaver, W. W. Corrosion and Protection of Beryllium Metal, BBC-TR 335: The Brush Beryllium Co., 1963.

4. Aida, H.; Elboin, I.; Garreau, M. *J. Electrochem. Soc.* **1971**, *118*, 243.
5. Sheth, K. G.; Johnson, J. W.; James, W. I. *Corros. Sci.* **1969**, *9*, 135.
6. Levy, D. J. The Electrolytic Polarization of Beryllium, LMSC-6-90-61-75,; Lockheed Missiles and Space Division, Sunnyvale, CA, 1961.
7. Miller, P. D.; Boyd, W. K. Corrosion of Beryllium, DMIC Report 242, Defense Metals Information Center, Battelle Memorial Institute, Columbus, 1961.
8. Prochko, R. J.; Myers, J. R.; Saxer, R. K. *Mater. Prot.* **1966**, *5*, 39.
9. Mueller, J. J.; Adolphson, D. R. In *Beryllium Science and Technology*; Floyd, D. R., Lowe, J. N., Eds.; Plenum Press: New York, 1979; Vol. 2, 417.
10. Gulbrandsen, E.; Johansen, A. M. J. *Corros. Sci.* **1994**, *36*, 1523.
11. Hill, M. A.; Butt, D. P.; Lillard, R. S. *J. Electrochem. Soc.* **1998**, *145*, 2799.
12. Lillard, R. S. *J. Electrochem. Soc.* **2001**, *148*, B1.
13. Straumanis, M. E.; Mathis, D. L. *J. Electrochem. Soc.* **1962**, *109*, 434.
14. Lillard, R. S. *Electrochem. Solid-State Lett.* **2003**, *6*, B29.
15. Cotton, J. D.; Field, R. D. *Metall. Trans. A* **1997**, *28*, 673.
16. Venugopal, A.; MacDonald, D. D.; Varma, R. *J. Electrochem. Soc.* **2000**, *147*, 3673.
17. Hill, M. A.; Hanrahan, R. J.; Haertling, C. L.; Schulze, R. K.; Lillard, R. S. *Corrosion* **2003**, *59*, 424.
18. Logan, H. L.; Hessing, H. Summarising Report on Stress Corrosion of Beryllium, NBS-6, Nat. Bur. Stand., Washington, 1955.
19. Miller, R. A.; Myers, J. R.; Saxer, R. K. *Corrosion* **1967**, *23*, 11.
20. King, T. T.; Myers, J. R. *Corrosion* **1969**, *25*, 349.
21. Terlo, G.; Ya, A. D. 628185, Department of Navy, 1966.
22. Beach, J. G.; Faust, C. L. *J. Electrochem. Soc.* **1953**, *100*, 276.
23. Paine, R. M.; Stonehouse, A. J. Corrosion/77, 1977, Paper No 26.
24. Booker, J.; Stonehouse, A. J. *Mater. Prot.* **1969**, *8*, 43.
25. Kerr, I. S.; Wilman, H. *J. Inst. Met.* **1955**, *84*, 379.
26. Levin, M. L. *Trans. Faraday Soc.* **1958**, *54*, 935.
27. Shetata, M. T.; Kelly, R. *J. Electrochem. Soc.* **1975**, *122*, 1359.
28. Gulbransen, E. A.; Andrew, K. F. *J. Electrochem. Soc.* **1950**, *97*, 383.
29. Cubicciotti, D. *J. Amer. Chem. Soc.* **1950**, *72*, 2084.
30. Alymore, D. W.; Gregg, S. J.; Jepson, W. B. *J. Nucl. Mater.* **1960**, *2*, 169.
31. Ervin, G.; Mackay, T. L. *J. Nucl. Mater.* **1964**, *12*, 30.
32. Alymore, D. W.; Gregg, S. J.; Jepson, W. B. *J. Nucl. Mater.* **1961**, *3*, 190.
33. Gregg, S. J.; Hussey, R. J.; Jepson, W. B. *J. Nucl. Mater.* **1961**, *3*, 175.
34. Gregg, S. J.; Hussey, R. J.; Jepson, W. B. *J. Nucl. Mater.* **1961**, *4*, 46.
35. Menzies, I. A. *Corros. Sci.* **1962**, *3*, 35.
36. Higgins, J. K.; Antill, J. E. *J. Nucl. Mater.* **1962**, *5*, 67.
37. Raine, T.; Robinson, J. A. *J. Nucl. Mater.* **1962**, *5*, 341.
38. Gregg, S. J.; Hussey, R. J.; Jepson, W. B. *J. Nucl. Mater.* **1960**, *2*, 225.
39. Scott, V. D. *Nature* **1960**, *186*, 466.
40. Scott, V. D.; Ranzetta, G. V. T. *J. Nucl. Mater.* **1963**, *9*, 277.
41. Paine, R. M.; Stonehouse, A. J.; Beaver, W. W. *Corrosion* **1964**, *20*, 307t.
42. Alves, E.; Alves, L. C.; Franco, N.; da Silva, M. R.; Paul, A. *Mater. Nucl. Sys.* **2007**, *159*, 233.
43. Ervin, G.; Nakata, M. M. *J. Electrochem. Soc.* **1963**, *110*, 1103.
44. Chou, T. C.; Nieh, T. G.; Wadsworth, J. *Scripta Metallurgica* **1992**, *27*, 897.
45. Aitken, E. A.; Smith, J. P. *J. Nucl. Mater.* **1962**, *6*, 119.
46. Lewis, J. R. *J. Met.* **1961**, *13*, 829.
47. Paine, R. M.; Stonehouse, A. J.; Beaver, W. W. In *Nuclear Metallurgy*, International Symposium on Compounds of Interest in Nuclear Reactor Technology; Waber, J. T., Chiotti, P., Miner, W. N., Eds.; AIME: Ann Arbor, 1964; Vol. 10, 495.
48. West Brook, J. H.; Wood, D. L. *J. Nucl. Mater.* **1964**, *12*, 208.
49. Hanrahan Jr, R. J.; Butt, D. P.; Chen, K. C.; Taylor, T. N.; Maggiore, C. J.; Thoma, D. J. Proceedings of the TMS Annual Meeting, 28 Feb.–4 March 1999, San Diego, CA, USA; pp 305–315.
50. Hanrahan, R. J., Jr.; Chen, K. C.; Brady, M. P. Proceedings of the Electrochemical Society 193rd Meeting of the Electrochemical Society; May 3–8, 1998; San Diego, CA; 458.

3.19 Corrosion of Uranium and its Alloys

S. B. Lyon
Corrosion and Protection Centre, School of Materials, University of Manchester, Oxford Road, Manchester M13 9PL, UK

This article is a revision of the Third Edition article 5.6 by J. E. Antill and R. A. Jarman, volume 1, pp 5:78–5:86,

Abbreviations

DU Depleted uranium
PVD Physical vapor deposition
RH Relative humidity
SCE Standard calomel electrode
UTS Ultimate tensile strength
YS Yield stress

Symbols

E_{corr} Corrosion potential

3.19.1 Introduction

3.19.1.1 Background

Uranium is a naturally occurring, and naturally radioactive, element whose predominant commercial interest lies in the ability of the ^{235}U isotope to undergo nuclear fission with consequent release of large amounts of energy. Uranium metal was first prepared in 1841 by Peligot using reduction of anhydrous UCl_4 with potassium. Uranium is an f-block element and a member of the actinide family that has similar, but not identical, chemistry with other elements in its series. Its radioactive nature was not appreciated until 1891 when Becquerel first detected it; however, natural uranium is only mildly radioactive, emitting relatively low-energy α and β radiation, while material that has been depleted in ^{235}U can be 30–40% less radioactive than natural uranium.

The main health and safety concern with uranium is its chemical toxicity as a heavy metal, rather than its natural radioactivity, which is relatively easily contained. Prior to the discovery of its fissionable nature in 1938 by Hahn and Strassman, it was used in a number of small-scale applications, predominantly because it imparts an attractive orange color to pottery glazes and a characteristic yellow-green color to glass. Uranium is not a particularly rare element and occurs in greater abundance than, for example, mercury, silver, cadmium, and tungsten and has a similar abundance to molybdenum.[1]

3.19.1.2 Applications

The fissionable isotope ^{235}U comprises about 0.7% of natural isotopic abundance with the majority of the balance consisting of ^{238}U; ^{234}U is also naturally present, but in tiny amounts. By far, the major use of uranium is currently as a nuclear fuel in which the ^{235}U percentage generally requires enrichment over the natural level, commercial light-water reactors typically being designed to operate with 3–5% of ^{235}U. The energy released during nuclear fission is approximately 200 MeV per atom or about 80 GJ g^{-1} (^{235}U); this is approximately equivalent to 2.7 tons of coal or 13.7 barrels of oil. At 33% thermal efficiency, a 1000 MW electrical generating station consumes about 1 ton of ^{235}U per year (compared with about 3 000 000 tons of coal per year). Interestingly, coal contains trace quantities of uranium (and thorium, another radioactive element) at levels from 1 to 10 ppm. Thus, a 1000 MW coal-fired power station typically releases between 3 and 30 tons of uranium + thorium into the environment every year of operation: comparable in mass (although very considerably less so in radioactivity) to spent nuclear fuel.

Other applications include those where uranium's exceptional density (19.05 Mg m^{-3}) is advantageous; these include ballast and counterweights in aircraft and yachts, radiation shielding in medicine and industrial radiography, as well as military uses in defensive armor plating and high-kinetic energy armor-piercing ammunition. Commonly, depleted uranium (DU; typically <0.25% ^{235}U, with a radiation level about 40% less than natural uranium) is used as it is a relatively cheap and abundant material with no other significant applications (the world inventory of DU is said to be over 1 million tons).

3.19.1.3 Metallurgy and Alloying

Uranium, unusually for a metallic element, has a room-temperature structure that is orthorhombic (α-U) below about 670 °C, tetragonal (β-U) from 670 to 770 °C, and body-centered cubic (γ-U) above about 770 °C. The orthorhombic structure implies significant anisotropy in physical properties, and few alloying elements have significant, if any, room-temperature solubility. The mechanical properties of uranium are more akin to those of tungsten than of gold. Thus, cast commercial-purity uranium has yield and ultimate tensile strengths of, respectively, 200–250 and 600–700 MPa, comparable to austenitic stainless steels, with a ductility of about 25%. It has a ductile to brittle transition at about 0 °C, where its impact strength and fracture toughness fall significantly.

The most common alloys of uranium are titanium (~0.75% Ti), niobium (~2–7% Nb), and molybdenum (up to 10% Mo). The alloys are hardenable by solid-solution heat treatment in the γ-phase region, then by quenching and aging to form second-phase particles. Room-temperature aged titanium-containing alloy has a yield stress (YS) of up to 600 MPa and ultimate tensile strength (UTS) of 1200 MPa, which can be increased to over 1200 and 1800 MPa respectively, with negligible ductility by aging at 500 °C. The niobium-containing alloy has lower strength but improved ductility after aging. **Table 1** gives property data for some of the more common uranium alloys. In view of these relatively attractive mechanical properties, it has been mooted that uranium might constitute a valuable structural material for specific applications although the dual attributes of its mild radioactivity and relatively poor corrosion resistance are large barriers to any significant adoption.[1]

Table 1 Properties of some uranium alloys; vacuum-annealed to ensure low hydrogen content

Alloy	*Processing*	*YS (MPa)*	*UTS (MPa)*	*Elongation (%)*	*Corrosion resistance*
Unalloyed U	Cast and β-quenched	295	700	22	Poor
Unalloyed U	α-Rolled	270	720	31	Poor
U–0.75Ti	γ-Quenched	650	1310	31	Fair
U–0.75Ti	γ-Quenched, aged 450 °C, 6 h	1210	1660	<2	Fair
U–2.0Mo	γ-Quenched, aged 550 °C, 5 h	675	1110	23	Poor
U–2.3Nb	γ-Quenched, aged 600 °C, 5 h	545	1060	28	Fair
U–4.5Nb	γ-Quenched, aged 260 °C, 16 h	900	1190	10	Acceptable
U–6.0Nb	γ-Quenched	160	825	21	Good
U–10Mo	γ-Quenched	900	930	9	Good
U–7.5Nb–2.5Zr	γ-Quenched	540	850	23	Good

Argonne National Laboratory, USA: Depleted Uranium and Uranium Alloy Properties, published at: web.ead.anl.gov/uranium/guide/ucompound/propertiesu/brochure.cfm[2]

3.19.2 Aqueous Corrosion

3.19.2.1 Thermodynamics

Uranium is an extremely active element and has a complex chemistry, showing all oxidation states from +2 to +6. In the absence of hydride formation, the Pourbaix diagram, **Figure 1**, shows a significant domain of passivity due to the formation of UO_2 as well as other, more complex, oxides. Importantly, thermodynamics predict that the passive oxide UO_2 is susceptible to further oxidation (transpassive dissolution) at both low and high pH, forming soluble uranium species of valency 6; it also transforms to hydrated UO_3 at intermediate pH. These reactions occur at a slow rate in humid air and, consequently, UO_2 is not generally protective and the corrosion resistance of unalloyed uranium is poor. Where hydride formation is included in the thermodynamic diagram (**Figure 2**), UH_3 formation is seen also to be stable, although in the presence of humid air the hydride forms only transiently further reacting to UO_2 and water. Thus, in order to handle uranium without significant degradation, a dry-nitrogen glove-box atmosphere is required. Hydride formation can give rise to severe embrittlement and stress corrosion cracking phenomena, and finely divided uranium can spontaneously ignite and burn pyrophorically.

3.19.2.2 Water

As predicted from the thermodynamic diagram, uranium reacts with water to form uranium dioxide, hydrogen, and uranium hydride. However, the hydride usually has only an ephemeral existence and reacts itself with water to form uranium dioxide and hydrogen. Reaction rates decrease with pH below 2, and it has been suggested that the solid products form by the inward diffusion of hydroxyl ions through the oxide.[3] The oxide is produced mainly as a nonadherent powder, and a linear rate law is obeyed.

Autoclave tests have demonstrated that the rate constant increases markedly with temperature up to at least 300 °C (**Figure 3**).[4] The corrosion rate is also influenced by dissolved gases in the water. In particular, the presence of dissolved oxygen decreases substantially the reaction rate[4] but makes the metal susceptible to crevice corrosion and pitting attack. The inhibition is most marked at lower temperatures, at which the oxygen solubility is highest and the hydrogen product is not sufficient to reduce the oxygen content locally. The oxygen could exert its influence by being adsorbed preferentially on the oxide[5] or by removing the disruptive influence of the formation of uranium hydride. An alternative view of such 'hydrogen effects' relates them to changes in the

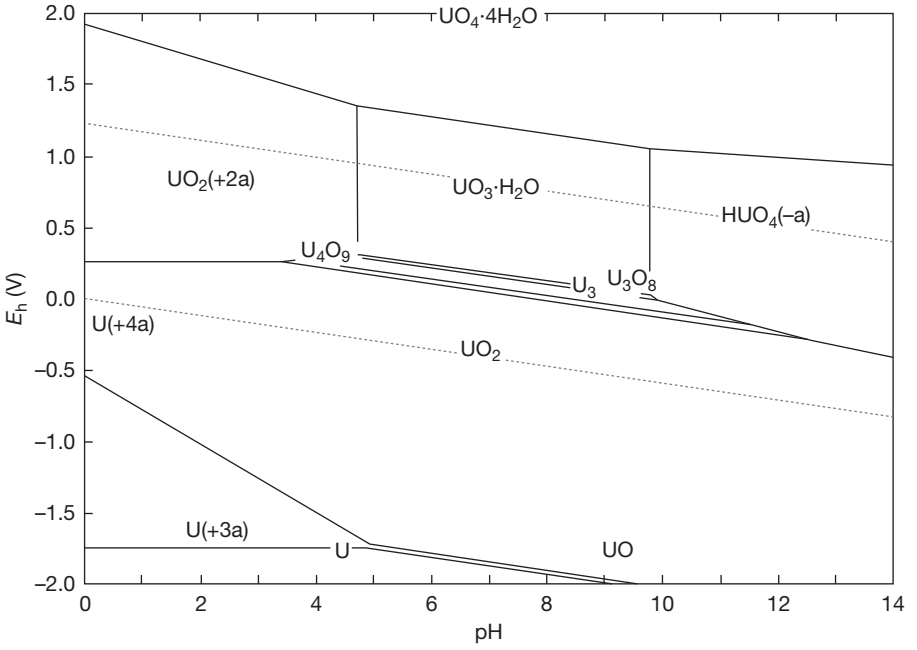

Figure 1 Pourbaix diagram for uranium (with hydride absent) at a metal ion concentration of 10^{-5} M. Calculated with HSC: Chemistry, version 6.12; Outotec Research Oy: Finland, 2007.

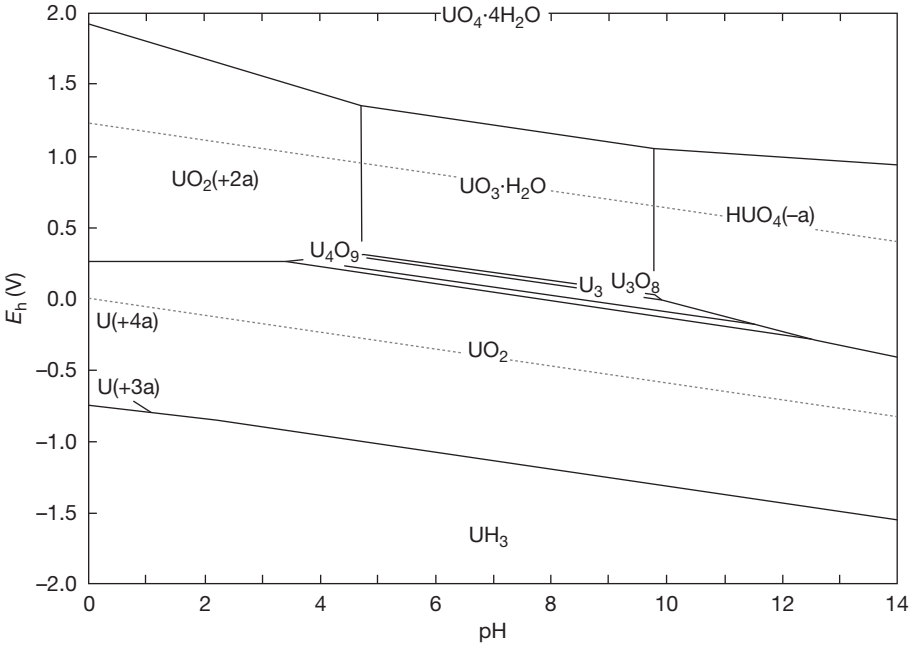

Figure 2 Pourbaix diagram for uranium (hydride present) at a metal ion concentration of 10^{-5} M. Calculated with HSC: Chemistry, version 6.12; Outotec Research Oy: Finland, 2007.

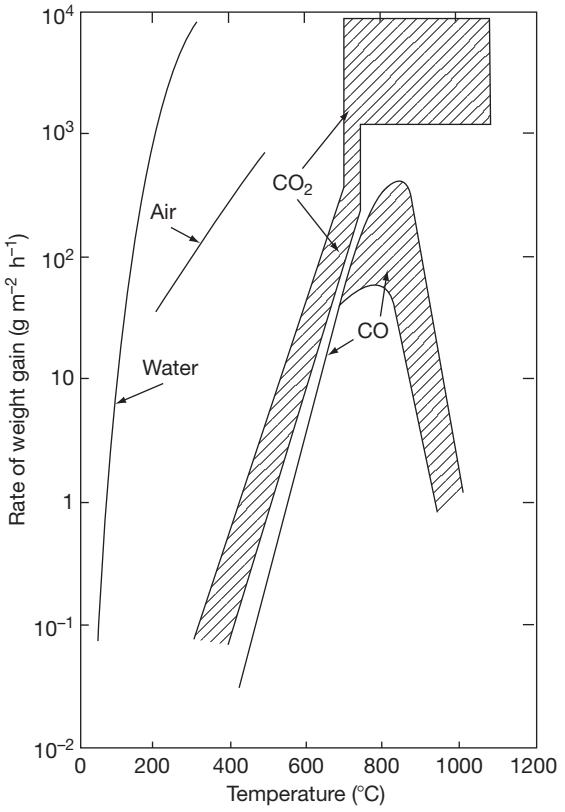

Figure 3 Oxidation rates of uranium in distilled water, air, CO_2, and CO as a function of temperature.

electrical properties of the oxide detected by impedance measurements during corrosion.[6]

Peretrukhin *et al.* studied the corrosion of uranium and its dilute alloys (<0.5% of Zr, Nb, and Ru) in water and bicarbonate aqueous solutions together with the effect of radiolytically generated hydrogen peroxide. No significant difference in corrosion rates for the alloys was found. Regarding the corrosion mechanism, U(III) was found to be rather unstable in neutral solutions and significant precipitation of $U(OH)_3$ occurred; no significant quantities of hydride or soluble U(III) species were found.[7]

The atmospheric oxidation kinetics for U(IV) to U(VI) were also studied,[7] where it was shown that U(IV) oxidation by atmospheric oxygen in the pH range 1.5–4.0 resulted in first-order kinetics with respect to uranium. Notably, an induction period for uranium (IV) accumulation was evident, after which the reaction accelerated. The reaction mechanisms differed in the two media: in weakly acid solutions, after the initial appearance of U(VI), evidence for disproportionation of the U(V) intermediate was found. Of mechanistic importance is the formation of a copolymer of U(IV) and U(VI), which at pH $\geq$ 4 prevents formation of U(V) and limits the oxidation rate. In the presence of hydrogen peroxide, the metallic uranium surface became transpassive and the corrosion rate increased by at least an order of magnitude.

Mechanical failure, which may be associated with stress corrosion as well as hydrogen pickup, has been observed for specimens of uranium[8] and various quenched alloys. For at least the alloys, it is enhanced by chloride ions[9] and is inhibited by cathodic polarization.[10] At higher temperatures, the only resistant metallic materials based upon uranium are alloys containing appreciable amounts of the γ-phase stabilizing elements, molybdenum, niobium, and zirconium,[4] the silicide U_3Si,[11] and the aluminides. However, the alloys, as distinct from the intermetallic compounds, tend to fail suddenly by disintegration after long periods of exposure, possibly because of internal hydride formation.

The corrosion of DU metal in deaerated groundwater (similar to that at the proposed Yucca mountain nuclear waste repository in the United States) was studied at 90 °C with a view to investigate the rate and products of corrosion: that is, UO_2, UO_{2+x}, UH_3, and H_2.[12] After exposure over an 81-day period, X-ray powder diffraction revealed the presence of UO_2 and higher oxides: that is, UO_{2+x}; however, no hydride was detected. The corrosion rate of the uranium metal in the water at 90 °C was determined by measuring the evolution of hydrogen gas, and this revealed a corrosion rate of 1.42 mg cm^{-2} h^{-1}. This value agreed extremely well with a published Arrenhius-type expression for the corrosion rate of uranium metal in water that had been obtained from a compilation of experimental data[13]:

$$\ln k = 22.34 - \frac{7989}{T}$$

where T is the absolute temperature (K) and k is the corrosion rate (mg cm^{-2} h^{-1}).

3.19.2.3 Atmospheric Corrosion

Uranium tarnishes readily in the atmosphere at room temperature. Electropolishing inhibits the process, while etching in nitric acid activates the surface. Uranium dioxide and hydrated UO_3 are the principal solid products, although uranium hydride may have a transitory existence. The corrosion is enhanced by water vapor and hence is governed by the humidity conditions.[14] However, the presence of oxygen markedly inhibits attack by water vapor.[5] Danon *et al.* undertook a desorption study of the surface chemistry of chemisorbed species on atmospherically oxidized uranium.[15] The main identified species included water (in different binding forms) and hydrogen. The latter originates from the water–uranium oxidation reaction, which produces uranium dioxide and two types of hydrogen: a near-surface hydride and a surface-chemisorbed form that desorbs at a lower temperature than the hydride. Water was found to be bound in four forms: (a) a reversibly chemisorbed molecule, (b) tightly bound water molecules, (c) strongly bounded hydroxyl groups and, the most stable (d) a complex water–carboxylate. Hydrogen desorption was also studied, with two main peaks found, one being ascribed to the desorption of lattice hydrogen and the higher temperature peak being related to the decomposition of hydrides.

The corrosion of uranium in water vapor was studied between 50 and 90 °C and from 32% to 86% RH using thermogravimetry.[16] The results show three stages in the uranium–water oxidation reaction. Thus, a rapid initial reaction is followed by a reducing rate and, in the third stage, the corrosion reaction proceeds linearly with an activation energy of about 43 kJ mol^{-1} at 74.7% RH.

3.19.2.4 Effects of Water Radiolysis

The effect of α-radiolysis of water on the corrosion potential of UO_2 has been measured where the cell construction allowed the source to be brought within 30 mm of the UO_2 electrode.[17] Oxidizing conditions were provided at the UO_2 surface, and over a period of 30 h, the main process occurring appeared to be the catalytic decomposition of H_2O_2 to H_2O and ½O_2 with some oxidation of the UO_2. The oxidation of uranium by water was studied by Fuller *et al.*[18] using infrared and sorption analysis. Oxidation occurred in cycles forming laminar layers of oxide that tend to spall off because of the strain at the oxide–metal interface. The reaction rate is directly proportional to the amount of adsorbed water on the oxide product, and transport was rapid through the open hydrous product. Dehydration of the hydrous oxide irreversibly forms a more inert oxide which cannot be rehydrated to the degree that prevails in the original hydrous product by uranium oxidation with water. An anomalous temperature dependence was observed for the oxidation of oxycarbide layers on the surface of uranium metal.[19] Normally, oxidation or corrosion reactions are expected to proceed more rapidly as water temperature increases, but the removal of the outermost atomic layers of carbon from uranium oxycarbide by oxygen reproducibly proceeds at a much faster rate at 25 °C than at 280 °C.

The kinetics of UO_2 fuel oxidation by the products of γ radiolysis of water have been studied by Sunder *et al.* as a function of absorbed dose rate.[20] The radical species formed during water radiolysis are much more effective in promoting UO_2 oxidation

than molecular oxidants, howsoever formed. Thus, UO_2 oxidation during γ radiolysis of water occurs in two stages: (a) the formation of a thin layer of UO_{2+x} (of composition close to $UO_{2.33}$); and (b) the subsequent oxidative dissolution of this surface layer to produce soluble U(VI) species and secondary phases, probably hydrated schoepite ($UO_3{\cdot}xH_2O$), on the UO_2 substrate. The first stage occurs in the potential range $-500\,\text{mV} < E_{\text{corr}} < -100\,\text{mV}$ (versus SCE). The second stage starts around $E_{\text{corr}} \sim -100\,\text{mV}$ and eventually achieves steady state at a value of E_{corr} determined by the γ dose.

3.19.2.5 Galvanic Corrosion

Galvanic corrosion reports have emerged from two sources. In the first,[21] the chemical compatibility of uranium carbides and Cr–Fe–Ni alloys was discussed. Evaluation was by thermodynamic modeling and experimental phase studies. Two reaction temperatures (700 and 1000 °C) were used to simulate normal and overtemperature operation of advanced liquid metal fast-breeder reactor fuel-cladding couples. In the second, McIntyre *et al.*[22] coupled depleted U–0.75% Ti to aluminum, magnesium, or mild steel in synthetic seawater. The galvanic current was monitored with time. Gravimetric measurements, polarization resistance measurements, and galvanic currents were monitored over extended periods of time in order to detect changes in galvanic corrosion behavior. Good agreement was obtained for corrosion rates determined electrochemically and those obtained from gravimetric methods.

Galvanic corrosion is also important in metallic coatings applied as protective barriers in uranium. For example, electroplated nickel is an excellent corrosion-resistant barrier; however, when it is subject to localized attack (i.e., pitting), corrosion of uranium occurs at the coating–substrate interface.[23] Rapid failure of the coating tends to ensue because of the volume increase caused by development of uranium corrosion products that causes undermining and cracking of the coating.

3.19.2.6 Stress Corrosion Cracking

Uranium alloys are susceptible to stress corrosion cracking (SCC) and knowledge of the surface stresses involved are essential. In an uncoated U–Ti alloy, these have been found to be relatively large and compressive at 365 MPa, but the presence of nickel or zinc coatings led to much smaller compressive stress.[24] The stress corrosion behavior of U–7.5Nb–2.5Zr in oxygen and hydrogen gases over a temperature range of −20 to 100 °C under pressures varying from 0.3×10^{-6} to 0.15 MPa has been analyzed using a fracture mechanics approach.[25] SCC mapping and cracking kinetics were determined as functions of stress intensity factor, temperature, and pressure. It was found that the mechanism responsible for SCC varied with the experimental conditions used.

Powell and his coworkers have explored the hydrogen embrittlement problem associated with uranium alloys.[26,27] Looking at the internal hydrogen embrittlement of γ-stabilized uranium alloys (i.e., containing Mo, Nb), they found that the tensile ductility decreased only slightly with increasing hydrogen content up to a critical hydrogen concentration, above which the tensile ductility dropped to nearly zero.[26] The critical hydrogen content for the ductility loss increased with increasing hydrogen solubility in the alloy. The fracture surfaces were not characteristic of those found under conditions of SCC. Hydrogen embrittlement of U–5.7Nb alloy showed enhanced microvoid coalescence fracture with loss of tensile ductility for hydrogen concentrations less than 23 mg hydrogen per gram of metal, the alloy having been solution-annealed at 800 °C and water-quenched.[27] However, specimens with 36 mg hydrogen per gram of metal had much lower ductilities and exhibited a new, possibly hydride, phase which was associated with brittle transgranular fracture when this phase has a lenticular morphology extending well across the parent metal grains.

The interactions between aqueous corrosion and mechanical deformation in uranium and alloys involve complex processes of mechanical damage. Various mechanisms are possible for the observed reduction in ductility/fracture toughness during corrosion, including SCC (e.g., via brittle film fracture or film-induced cleavage), hydrogen embrittlement (e.g., via classical mechanisms or by hydride formation), as well as others. Bussiba *et al.*[28] undertook a series of mechanical tests in order to determine the influence of specific mechanisms on the performance of lean uranium alloys (U–0.1Cr and U–0.75Ti) in water and at controlled levels (30, 40, and 80%) of RH. Crack growth rates of between 10^{-5} and $10^{-9}\,\text{m s}^{-1}$ were determined at a stress intensity corresponding to $16\,\text{MPa m}^{1/2}$. Cracking appeared to operate discontinuously with trigger events corresponding to acoustic noise generation. In all conditions (i.e., humid air or immersion), surface hydride formation was observed; however, their role in the fracture process could not be confirmed. However,

the rather rapid crack growth velocities seem to imply a triggering mechanism that involves hydrogen embrittlement.

3.19.3 Gases at High Temperatures

3.19.3.1 Carbon Dioxide and Carbon Monoxide

The solid corrosion products resulting from reaction with carbon dioxide and carbon monoxide are uranium dioxide, uranium carbides, and carbon.[29] The major reaction with carbon dioxide results in the formation of carbon monoxide and UO_2:

$$U + CO_2 \rightleftarrows UO_2 + 2CO$$

Uranium can also form the carbide with an overall reaction:

$$2U + CO_2 \rightleftarrows UC + UO_2$$

The formation of uranium carbide must involve carbon transfer from the gas phase and probably occurs via reactions of carbon monoxide with the metal through pores of the oxide scale. This transfer could occur by direct reaction or via the thermal decomposition of the gas to produce carbon dioxide, which may then react subsequently with uranium, thus forming the carbide:

$$2CO \rightleftarrows C + CO_2$$

Diffusion studies on UO_2 demonstrate that oxygen ions are the major diffusing species in the oxide and, therefore, that the oxide grows by the inward passage of oxygen.[30] Volume changes associated with the oxidation lead to large stresses in the oxide and subsequently to the formation of solid products in the form of powders and/or cracked porous scales.

At the temperatures of interest, a linear rate law is quickly established, and the rate-determining step is believed, in general, to be diffusion of oxygen ions through a thin layer of adherent oxide of constant average thickness at a given temperature. For carbon dioxide, the rate constant (**Figure 3**) increases steadily with temperature until there is a sudden increase in rate, together with some selfheating from the high heat of reaction, at or near the β–γ phase transition in the metal (780 °C); at higher temperatures there is little or no dependence of reaction rate on temperature up to 1000 °C. The majority of the oxide forms as either a nonadherent powder (the particle size of which increases with temperature) or, at the highest temperatures, as a cracked adherent scale. The formation of scale accounts for the lack of temperature dependence for the rate constant at the highest temperatures and could result either from sintering of the oxide or, more probably, from the growth stresses being relieved by plastic deformation of the oxide and/or the underlying metal, rather than rupture of the oxide. At the highest temperatures, the rate-determining step might be gaseous diffusion through the porous scale.[31] The presence of small amounts of water vapor (greater than 100 ppm) and oxygen (greater than 10 ppm) enhances the attack significantly at the lower temperatures of 400–500 °C,[29] and under these conditions preferential attack is frequently observed at carbide inclusions in the metal.[32] Major alloy additions of silicon (greater than 3.8%) impair oxidation resistance at all temperatures, whereas additions of copper (1%), titanium (5–10%), and molybdenum (10–15%) decrease the rates, but only at the higher temperatures.[33] The beneficial influence of copper is associated with the enrichment of the element at the metal–oxide interface as the UCu_5 phase.[34] The mechanisms responsible for the effects of the other alloying elements have not been firmly established, but can be attributed to changes in the physical defects and thicknesses of the adherent oxide and, hence, in its protective properties.

The oxidation rates in carbon monoxide (**Figure 3**) are less than those for carbon dioxide. They increase steadily with temperature up to 800 °C but then decrease markedly by a factor of 100 up to 1000 °C. The decrease in rate can be attributed to the dissociation of carbon dioxide at higher temperatures and to its consequently low partial pressures.

3.19.3.2 Air

Thermal oxidation of uranium dioxide proceeds in air and results ultimately in the formation of U_3O_8 at temperatures above 200–300 °C. The lower oxides may also be formed as intermediaries and at lower temperatures. The volume change associated with formation of U_3O_8 is greater than for uranium dioxide and, as with carbon dioxide, leads to a linear rate law being established. This gives significantly more rapid oxidation kinetics[35] by comparison with the behavior in carbon dioxide (**Figure 3**). The rapid reaction rate, coupled with the large enthalpy or reaction, leads to an appreciable selfheating of specimens and an associated increase in reaction rate. In this situation, the supply of oxygen from the air can be rate-determining. The susceptibility of the metal to selfheating increases with the surface area-to-volume ratio of components, and powders may spontaneously ignite at room temperature.[36] However, large blocks

of metal are not normally liable to selfheating until 400–600 °C and then need an external heat source to maintain the situation. Alloy additions of molybdenum (5–15%) markedly reduce reaction rates.[10,37] Minor additions of other elements may either enhance or reduce the susceptibility to ignition[38] (e.g., aluminum or copper, respectively).

3.19.3.3 Steam

The mechanisms of corrosion by steam are similar to those for water up to 450 °C, but at higher temperatures are more closely related to the behavior in carbon dioxide. Studies at 100 °C have demonstrated that uranium hydride is produced during direct reaction of the water vapor with the metal and not by a secondary reaction with the hydrogen product. Also, at 100 °C it has been shown that the hydride is more resistant than the metal.[3] Inhibition with oxygen reduces the evolution of hydrogen and does not involve reaction of the oxygen with the uranium.[6] Above 450 °C, the hydride is not stable and hydrogen is released directly to the gas phase. Also, the cohesion and protection provided by the uranium dioxide increase with the formation of a dense scale, at least for short times at the highest temperatures. As a consequence, the extent of reaction after a period greater than 100 min is at a maximum at 300–400 °C with a rate of weight gain of $10^3\,g\,m^{-2}\,h^{-1}$. The reaction rate increases only slowly with temperature from 500 to 1200 °C, although one piece of work reported a marked increase in attack near the β–γ transition in the metal,[39] analogous to that obtained in carbon dioxide. A parabolic rate law has been found to apply at temperatures of 500–1200 °C for periods of 30 min to 6 h,[40] although another work indicates that this law is established for only 1–2 h above 880 °C and that a linear law generally applies.[39] It follows that for a period of 1–2 h, the extent of corrosion in steam straddles that for carbon dioxide, being greater at temperatures less than 700 °C and comparable or less at higher temperatures.

The oxidation rates of uranium in steam were measured between 200 and 550 °C. Arrhenius-type behavior was observed below 300–350 °C, with activation energies of 47 kJ mol^{-1} for U foil below 350 °C and 58 kJ mol^{-1} for U bar below 300 °C.[41] However, a significant rate reduction was observed at higher temperatures. In all cases, the oxidation products were uraninite-structured UO_{2-x} compounds. Nonadherent oxide layers were formed on bar samples below ~300 °C, but became increasingly adherent at higher temperatures. Similarly, the oxide layers on foil samples below ~350 °C had highly porous cellular structures, whereas the layers formed at higher temperatures were significantly denser. For both materials, the fall in oxidation rate above 300–350 °C was attributed to reduced steam ingress to the underlying metal caused by the increasingly protective surface oxide.

Oxidation of UO_2 by pure steam at pressures of 7 and 70 atm and 500 and 600 °C was measured using thermogravimetry.[42] Linear kinetics were observed, which varied as the square root of the steam pressure, and is consistent with initial rates extrapolated from higher temperature experiments in 1-atm steam. At temperatures characteristic of normal operation of defective fuel rods, the rate of hydrogen production by thermal oxidation of the fuel in steam is small compared to that due to cladding corrosion. The presence of H_2 in the steam was found to have much greater influence on reducing the rate of oxidation UO_2 than on oxidation of cladding.

An experimental study of UO_2 oxidation in pure steam and in $H_2O/Ar/H_2$ mixtures was conducted using a thermal balance at 1 atm in the temperature range 1000–1350 °C.[43] Two surface reaction models were assumed. A phenomenological model assumes that the reaction rate is proportional to the difference between the [O] in the solid and the equilibrium pO_2 in the ambient gas. The results show that this model is a poor fit for oxidation in steam, but is good for $H_2O/Ar/H_2$ mixtures. A mechanistic model, based on the assumption that the rate-controlling step was water dissociation at the solid surface, provides a very good fit to all the data. Thus, as long as the pressure is 1 atm, either model can be used to predict nuclear fuel oxidation in severe loss of coolant accidents because the ambient gas invariably contains hydrogen produced by Zircaloy corrosion. However, the kinetics of oxidation in high-pressure steam–hydrogen mixtures are still uncertain. Evidence of uranium volatilization and preferential etching at the grain boundaries at high temperatures were observed.

3.19.4 Corrosion Processes

3.19.4.1 Protective Coatings

Uranium may be anodized in ethylene glycol containing ammonia and this produces oxide films that are predominantly uranium dioxide in composition[44] and which show considerable resistance to atmospheric corrosion. During film formation at constant current, the voltage rises steeply to a plateau giving predominantly crystalline films. After reaching a

second voltage plateau, the films are largely amorphous. The rate of oxidation during the initial voltage rise, assuming maximum current efficiency, is between 1.6 and 2.0 nm V^{-1}.

Metallic and organic-based coatings have been developed to protect uranium from oxidation at low and high temperatures. The work on metallic coatings has covered intermetallic compounds and solid solutions of uranium with aluminum, zirconium, copper, niobium, nickel, and chromium.[45] Aluminum- and zirconium-based coatings[46,47] can be particularly effective in reducing attack over an extended range of temperature. Also, nickel plating can provide protection against atmospheric corrosion.[48] Work on organic coatings has demonstrated that they can enhance resistance to atmospheric corrosion.[49,50] This behavior is attributed to the loss of the inhibiting action of oxygen due to water vapor permeating the coatings more readily than oxygen.

Aluminum, zinc, magnesium, Al–Zn, Al–Mg, nickel, titanium, TiN, and Al/TiN coatings have all been applied by the arc plasma physical vapor deposition (PVD) technique to a DU alloy for corrosion protection assessment.[51] The as-deposited specimens were examined by scanning electron microscopy for surface morphology and tested for adhesion. Electrochemical polarization tests and immersion tests were conducted in aerated 3.5 wt% NaCl solution. Results of electrochemical polarization in 3.5% NaCl solution and observations after long-term exposure tests indicated that both Al–Zn and Al–Mg alloys appear to be the best sacrificial coating materials for improving the corrosion resistance of DU–0.75 Ti.

The effect of various oxyanions (MoO_4^{2-}, PO_4^{3-}, VO_4^{3-}, MnO_4^{-}, SiO_4^{4-}, and WO_4^{2-}) on the corrosion inhibition of U–0.75Ti alloy in nitric acid has been studied.[52] Results indicate that chemical or electrochemical activation of the uranium in 0.1 M HNO_3 + 0.025 M molybdate can lead to the formation of a rudimentary conversion coating. Building on this finding, molybdenum oxide-based coatings were formed on U–0.75Ti alloy[53] using nitric acid in order to activate the metal surface. Successful coatings were produced of the order of 650 nm in thickness. After aging, the coated samples showed an ennobled potential of around 400 mV and a reduced corrosion current density of around 10 times.

3.19.4.2 Irradiation Effects

The behavior of irradiated uranium has been studied mainly with respect to the release of fission products during oxidation at high temperatures.[54] The fission products most readily released to the gas phase are krypton, xenon, iodine, tellurium, and ruthenium. The release can approach 80–100%. For ruthenium, it is dependent upon the environment and only significant in the presence of oxygen to form volatile oxides of ruthenium.

Studies of the influence of irradiation on the kinetics of oxidation have been confined to postirradiation work. In general, prior irradiation increases reactivity, although there are considerable inconsistencies in the enhancements obtained.[17,54,55] The effects can be derived from an increased surface area associated with the swelling voids produced in the metal by the irradiation, and can also probably arise to a lesser extent from chemical effects of the fission products.

The postirradiation examination of two uranium aluminide fuel plates exposed to aqueous corrosion showed failure due to pinhole corrosion during irradiation to about 76% of the maximum burn-up limit.[56] It was thought that the cladding failed by pitting corrosion initiated at preexisting pits at a hot spot. Fuel plate material was washed out through these pinholes due to aqueous corrosion and erosion. Egert[57] also looked at corrosion of coated uranium and found corrosion occurring at defects present in the coating. An equation was derived to predict the extent of substrate corrosion, given the number of defects per unit area and knowledge of the corrosion kinetics of the substrate.

3.19.4.3 Corrosion and Dissolution of UO_2

As noted earlier, uranium dioxide is susceptible to transpassive dissolution to soluble uranium species at low and high pH and at sufficiently high potentials caused by the presence of oxygen in air, or of strongly oxidizing peroxide or radical species formed as a result of water radiolysis. At intermediate potentials, UO_2 may be oxidized to UO_{2+x} or hydrated UO_3. In order to suppress this oxidation, the effects of dissolved hydrogen on the aqueous corrosion of uranium dioxide (UO_2) under nuclear waste disposal conditions were studied.[58] Measurements of the corrosion potential (E_{corr}) indicate that the oxidation of dissolved hydrogen on noble-metal particles polarizes the UO_2 nuclear fuel surface to reducing potentials (−300 to −400 mV vs. SCE); that is, to E_{corr} values more negative than those observed under anoxic (argon-purged) conditions (−200 mV vs. SCE). Thus, noble-metal particles incorporated within UO_2 act catalytically to oxidize H_2. It is the galvanic coupling of these

particles to the UO_2 matrix that lowers the corrosion potential, thereby preventing oxidation of the fuel surface.

3.19.4.4 Uranium in the Environment

Corrosion of anthropogenic uranium in natural environments is not well understood, but is important for determining potential health risks and mobility in the environment. Buck *et al.* conducted studies of a site in the southwestern United States containing DU that has been weathering for approximately 22 years.[59] The main products of corrosion were found to be schoepite ($((UO_2)_4O(OH)_6{\cdot}6(H_2O))$) and meta-schoepite ($(UO_3{\cdot}2(H_2O))$), and occur on their own, mixed with clay/silt aggregates, or as coatings upon soil grains. It appeared from this study that local soil geomorphology and chemistry at this site limit uranium mobility and decreases potential health risks. However, changes in land use and/or climate could increase uranium mobility.

There is considerable concern over the use of dense kinetic energy projectiles containing DU in the battlefield and the consequent spread of uranium into the environment. The degradation of a DU penetrator shot in battle in Western Kosovo in 1999 and collected from there in June 2001was studied.[60] Corrosion products on the surface were confirmed as UO_2, with the possible presence of other more oxidized uranium forms, such as U_3O_8 and $UO_3{\cdot}2(H_2O)$. Raman spectra from the surface shows evidence for mobile UO_2^{2+} uranyl ions. It can be concluded, therefore, that such projectiles will, in the environment, progressively release mobile uranium species.

In the United Kingdom, the testing of armor-piercing DU 'penetrators' has resulted in the deposition of DU in the sediments of the Solway Firth. Handley-Sidhu *et al.* undertook an investigation of this material by simulating Solway Firth sediments under variable conditions of salinity to study the impact of the corroding DU on the environment, including the microbial population.[61] Under suboxic conditions, the average corrosion rates were $0.056\,g\,cm^{-2}\,year^{-1}$, implying that complete corrosion of a 120-mm penetrator would take approximately 540 years. Under sulfate-reducing conditions, corrosion ceased because of passivation of the surface. Corroding DU resulted in more reducing conditions and decreased microbial diversity as indicated by DNA sequencing and phylogenetic analysis. Since few uranium species were measured in the sediments adjacent to the DU projectiles, it must be assumed that U was transported into the surrounding environment through dissolution of U(VI), with subsequent interactions resulting in the formation of secondary uranium species in the sediment.

References

1. The Encyclopedia of the Earth: Uranium (published at www.eoearth.org/article/uranium).
2. Argonne National Laboratory, USA: Depleted Uranium and Uranium Alloy Properties, published at: web.ead.anl.gov/uranium/guide/ucompound/propertiesu/brochure.cfm.
3. McD Baker, M.; Less, L. N.; Orman, S. *Trans. Faraday Soc.* **1966**, *62*(2), 513.
4. Wanklyn, J. N.; Jones, P. J. *J. Nucl. Mater.* **1962**, *6*, 291.
5. McD Baker, M.; Less, L. N.; Orman, S. *Trans. Faraday Soc.* **1966**, *62*(2), 525.
6. Leach, J. S. L. *J. Inst. Met.* **1959**, *88*, 24.
7. Peretrukhin, V. F.; Maslennikov, A. G.; Tsivadze, A. Yu.; Delegard, C. H.; Yusov, A. B.; Shilov, V. P.; Bessonov, A. A.; Bulatov, G. S. *Protect. Met.* **2008**, *44*(3), 211–232.
8. Hughes, A. N.; Orman, S.; Pictor, G. *Corros. Sci.* **1970**, *10*, 239.
9. Magnani, N. J. *J. Nucl. Mater.* **1972**, *42*, 271.
10. McLaughlin, B. D. *J. Nucl. Mater.* **1972**, *43*, 343.
11. Bourns, W. T. Corrosion Testing of Uranium Silicide Fuel Specimens, AECL-2, 1968; p 718.
12. Fonnesbeck, J. E. *Corros. Eng. Sci. Technol.* **2003**, *38*(1), 51–56.
13. Hilton, B. ''Review of oxidation rates of DOE spent nuclear fuel: Part 1: metallic fuel,'' Report ANL– 00/24, Argonne National Laboratory, Idaho Falls, ID, USA, 2000.
14. Waber, J. T. ''A Review of the Corrosion Behaviour of Uranium,'' Report LA-2035, Los Alamos Scientific Laboratory, Los Alamos, NM, December 1958.
15. Danon, A.; Koresh, J. E.; Mintz, M. H. *Langmuir* **1999**, *15*(18), 5913–5920.
16. Xiong, B.-T.; Meng, D.-Q.; Yang, W.-C.; Luo, W.-H.; Zhang, G.-F.; Lu, Y.-J. *Yuanzineng Kexue Jishu/Atomic Energy Sci. Technol.* **2005**, *39*(3), 226–231.
17. Bailey, M. G.; Johnson, L. H.; Shoesmith, D. W. *Corros. Sci.* **1985**, *25*, 233.
18. Fuller, E. C.; Fuller, E. L., Jr.; Smyrl, N. R.; Condon, J. B.; Eage, M. H. *J. Nucl. Mater.* **1984**, *120*, 174.
19. Ellis, W. P. *Surf. Sci.* **1981**, *109*, L567.
20. Sunder, S.; Shoesmith, D. W.; Christensen, H.; Miller, N. H. *J. Nucl. Mater.* **1992**, *190C*, 78–86.
21. Beahm, E. C.; Culpepper, C. A. *Nucl. Technol.* **1981**, *54*, 215.
22. McIntyre, J. F.; Lefeave, E. P.; Musselman, K. A. *Corrosion* **1988**, *44*, 502.
23. Wang, Q.-F.; Ye, H.; Zhang, P.-C.; Lang, D.-M.; Wang, X.-H.; Wang, J.-Y. *Yuanzineng Kexue Jishu/Atomic Energy Sci. Technol.* **2005**, *39*(1), 44–48.
24. Sha, W.; Wang, Y.-H. *J. Less Common Met.* **1989**, *146*, 179.
25. Lepoutre, D.; Nomine, A. M.; Miannay, D. *J. Less Common Met.* **1986**, *121*, 521.
26. Powell, G. L.; Kroger, J. W.; Bennet, R. K. *Corrosion* **1976**, *32*, 9.
27. Powell, G. L.; Northcutt, W. G. *J. Nucl. Mater.* **1985**, *132*, 47.
28. Bussiba, A.; Alush, H.; Katz, Y. *Mater. Sci. Res. Int.* **1997**, *3*(4), 244–251.

29. Pearce, R. J.; Whittle, I.; Hilton, D. A. *J. Nucl. Mater.* **1969**, *33*, 1.
30. Belle, J. *J. Nucl. Mater.* **1969**, *30*, 3.
31. Pearce, R. J. *J. Nucl. Mater.* **1970**, *34*, 332.
32. Hayfield, P. C. S.; Graham, R. L.; Ramshaw, G. In Institute of Metals Symposium on Uranium and Graphite, 1962; Paper no. 5.
33. Antill, J. E.; Peakall, K. A. *Less Common Metals* **1961**, *3*, 239.
34. Antill, J. E.; Peakall, K. A. *J. Electrochem. Soc.* **1963**, *110*, 1146.
35. Baker, L.; Bingle, J. D. *J. Nucl. Mater.* **1966**, *20*, 11.
36. Baker, L.; Schnizlein, J. G.; Bingle, J. D. *J. Nucl. Mater.* **1966**, *20*, 22.
37. Isaacs, J. W.; Wanklyn, J. N. *AERE R-3* **1960**, 559.
38. Schnizlein, J. G.; Baker, L.; Bingle, J. D. *J. Nucl. Mater.* **1966**, *20*, 39.
39. Hopkinson, B. E. *J. Electrochem. Soc.* **1959**, *106*, 102.
40. Wilson, R. E.; Martin, P. *ANL* **1962**, *6*, 569.
41. Hayward, P. J.; Evans, D. G.; Taylor, P.; George, I. M.; Duclos, A. M. *J. Nucl. Mater.* **1994**, *217*(1–2), 82–92.
42. Olander, D. R.; Soo Kim, Y.; Wang, W.-E.; Yagnik, S. K. *J. Nucl. Mater.* **1999**, *270*(1), 11–20.
43. Abrefah, J.; Braid, A. D.; Wang, W.; Khalil, Y.; Olander, D. R. *J. Nucl. Mater.* **1994**, *208*(1–2), 98–110.
44. Flint, O.; Polling, J. J.; Charlesby, A. *Acta Metall.* **1954**, *2* (5), 696–712.
45. Buddery, J. H.; Clark, M. E.; Pearce, R. J.; Stobbs, J. J. *J. Nucl. Mater.* **1946**, *13*, 169.
46. Baque, P.; Koch, P.; Dominget, R.; Darras, R. *CEA-R-3* 638.
47. Pearce, R. J.; Giles, R. D.; Tavender, L. E. *J. Nucl. Mater.* **1967**, *24*, 129.
48. Orman, S.; Owen, L. W.; Picton, G. *Corros. Sci.* **1972**, *12*, 35.
49. Orman, S. *Atom* **1969**, *150*, 93.
50. Orman, S.; Walker, P. *J. Oil Colour Chem. Assoc.* **1965**, *48*, 233.
51. Chang, F.; Levy, M.; Jackman, B.; Nowak, W. B. *Surf. Coating. Tech.* **1989**, *39–40*(1–3 Pt 2), 721–731.
52. Roeper, D. F.; Chidambaram, D.; Clayton, C. R.; Halada, G. P. *Electrochim. Acta* **2005**, *50*(18), 3622–3633.
53. Roeper, D. F.; Chidambaram, D.; Clayton, C. R.; Halada, G. P. *Electrochim. Acta* **2005**, *51*(3), 545–552.
54. Parker, G. W.; Creek, G. E.; Barton, C. J.; Martin, W. J.; Lorenz, R. A. Oak Ridge National Laboratory Report ORNL-3981, 1967.
55. Fischer, D. F.; Schnizlein, J. G. *J. Nucl. Mater.* **1968**, *28*, 124.
56. Vinjami, K.; Hobbins, R. R. *Nucl. Tech.* **1983**, *62*, 145.
57. Egert, C. M. *Corrosion* **1988**, *44*, 36.
58. Broczkowski, M. E.; Zhu, R.; Ding, Z.; Noel, J. J.; Shoesmith, D. W. *Mater. Res. Soc. Symp. Proc.* **2006**, *932*, 449–456.
59. Buck, B. J.; Brock, A. L.; Johnson, W. H.; Ulery, A. L.; *Soil Sediment Contam.* **2004**, *13*(6), 545–561.
60. Mellini, M.; Riccobono, F. *Chemosphere* **2005**, *60*(9), 1246–1252.
61. Handley-Sidhu, S.; Worsfold, P. J.; Boothman, C.; Lloyd, J. R.; Alvarez, R.; Livens, F. R.; Vaughan, D. J.; Keith-Roach, M. J. *Environ. Sci. Technol.* **2009**, *43*(2), 350–355.

Relevant Websites

www.world-nuclear.org – World Nuclear Organization, London UK.

3.20 Corrosion of Amorphous and Nanograined Alloys

H. Habazaki
Graduate School of Engineering, Hokkaido University, N13-W8, Kita-ku, Sapporo 060-8628, Japan

Glossary

Sputter deposition Sputter deposition is a physical vapor deposition (PVD) method of depositing thin films by sputtering, that is, ejecting material from a target or source, which then deposits onto a substrate – for example, a silicon wafer.

Amorphous alloy An amorphous alloy is a metallic material with a disordered atomic-scale structure. In contrast to most metals, which are crystalline and therefore have a highly ordered arrangement of atoms, amorphous alloys are noncrystalline.

X-ray photoelectron spectroscopy (XPS) XPS is a quantitative spectroscopic technique that measures the elemental composition, empirical formula, chemical state, and electronic state of the elements that exist within a material. XPS spectra are obtained by irradiating a material with a beam of aluminum or magnesium X-rays while simultaneously measuring the kinetic energy (KE) and number of electrons that escape from the top 1–10 nm of material being analyzed.

Rutherford backscattering spectroscopy (RBS) RBS is an analytical technique used in materials science. Sometimes referred to as high-energy ion scattering (HEIS) spectroscopy, RBS is used to determine the structure and composition of materials by measuring the backscattering of a beam of high energy ions impinging on a sample.

Abbreviations

RBS Rutherford backscattering spectroscopy
XPS X-ray photoelectron spectroscopy

3.20.1 Corrosion of Amorphous Alloys

Amorphous alloys have been attracting much attention as a new class of metallic materials with excellent physical, mechanical, and chemical properties since their introduction in the late 1960s. The corrosion resistance of amorphous alloys is remarkable and some amorphous alloys are immune even to concentrated hydrochloric acids. Much interest has also been seen in amorphous alloy electrode materials due to their superior electrocatalytic properties as well as high durability, originating from high corrosion resistance. The synergistic effect of various alloying elements homogeneously mixed at the atomic level, in addition to the structurally metastable nature, contributes to the superior chemical properties.

It was believed until the late 1980s that rapid quenching with a quenching rate of more than $\sim 10^5$ K s^{-1} is

required to develop amorphous alloys. During this period, amorphous alloys were produced mostly by melt-spinning and physical vapor deposition (PVD) methods, including sputter deposition. Laser treatment of the alloy surface, as well as ion implantation, was used to develop amorphous alloy surfaces on bulk metallic substrates. In the late 1980s, amorphous alloys with extremely high glass-forming ability were discovered, and bulk amorphous alloys, usually referred to as bulk metallic glasses, are now available in many alloy systems by a conventional casting process. Extremely high glass-forming ability is attained in multicomponent alloy systems with large atomic size ratios of more than 12% and with negative heats of mixing. The discovery of bulk metallic glasses has eliminated the size limitation of amorphous alloys, and their practical importance has been significantly enhanced. Here, corrosion behavior of a range of amorphous alloys, including bulk metallic glasses, is outlined, together with nanocrystalline metallic materials. Interest has also been shown in nanocrystalline alloys due to their enhanced mechanical strength. The influence of nanocrystalline precipitates in an amorphous matrix on corrosion behavior of amorphous alloys will also be discussed here.

3.20.1.1 Examples of Corrosion-resistant Amorphous Alloys

Great interest in the corrosion resistance of amorphous alloys was initiated by the early work of Hashimoto and coworkers, which revealed the very high corrosion resistance of iron–metalloid alloys containing chromium even in aggressive hydrochloric acid solutions.[1,2] Results of corrosion tests for the amorphous Fe–10 at.% Cr–13 at.% P–7 at.% C alloy (alloy composition hereafter denoted as Fe–10Cr–13P–7C) and crystalline type-304 stainless steel are shown in **Figure 1**.[1] The melt-spun amorphous Fe–10Cr–13P–7C alloy reveals no measurable corrosion even in 1 mol dm^{-3} HCl solution, while the corrosion rate of type-304 stainless steel increases with the increase in the concentration of HCl, greater than 10 mm s^{-1} in 1 mol dm^{-3} HCl solution. The amorphous Fe–10Cr–13P–7C alloy is spontaneously passive in HCl solution, and anodic polarization of this alloy does not induce pitting corrosion. The corrosion resistance of Fe–Cr–metalloid alloys was further improved by the addition of molybdenum.[3–6] Amorphous alloys containing sufficient amounts of both chromium and molybdenum were spontaneously passive even in concentrated HCl solution at elevated temperatures.[6]

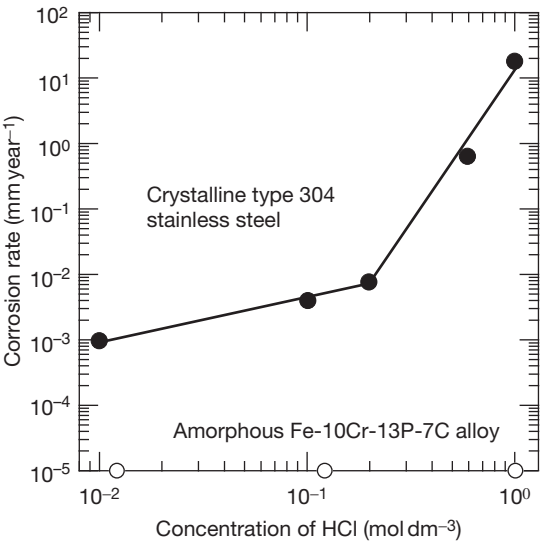

Figure 1 Example of the greatly enhanced corrosion resistance in 1 mol dm^{-3} hydrochloric acid at room temperature of a Fe-based metallic glass (Fe–10Cr–13P–7C) compared to a crystalline, type-304 stainless steel alloy (Fe–18Cr–8Ni).[1]

In addition to Fe-based amorphous alloys, corrosion-resistant nickel-based amorphous alloys were discovered in the late 1980s. Amorphous Ni-based alloys containing 20 at.% or more tantalum were immune to corrosion in boiling 9 mol dm^{-3} HNO_3 solution and maintained metallic luster.[7] Ni–Nb alloys containing 40–60 at.% niobium were also highly corrosion-resistant; their corrosion rates were as low as ~1 μm $year^{-1}$ in boiling 9 mol dm^{-3} HNO_3 solution. Amorphous Ni–Nb and Ni–Nb–Cr alloys were spontaneously passive in 0.1 mol dm^{-3} H_2SO_4 solution, but transpassive dissolution occurred at high anodic potentials.[8] The amorphous Nb-valve metal alloys were also highly corrosion-resistant in hot concentrated phosphoric acid solution as well as in boiling sodium hydroxide solution.[9,10] The addition of small amounts of phosphorus enhances its glass-forming ability as well as its corrosion resistance.[11–16] The role of phosphorus in improving the corrosion resistance of amorphous alloys will be described later.

Most of these corrosion studies were performed using melt-spun amorphous alloy ribbons. In the late 1980s PVD methods, including sputter deposition, were introduced to produce corrosion-resistant amorphous alloys. One of the successful applications of this technique is an aluminum alloy system. The solid solubility of many alloying elements in aluminum at equilibrium is very limited, usually less than a

few atomic percent. None of the existing commercial aluminum alloys have good resistance against localized corrosion. Amorphous Al alloys containing supersaturated alloying elements, including molybdenum, tungsten, chromium, copper, and tantalum, show markedly improved pitting corrosion resistance.[17–27] Some amorphous Al alloys display good corrosion resistance even in hydrochloric acid solutions.[28–30] An example of improved pitting potential by the addition of molybdenum and tungsten is shown in **Figure 2**. The pitting potential of crystalline high-purity aluminum is ~−0.7 V versus SCE in a borate buffer solution containing 0.1 mol dm^{-3} NaCl. The addition of molybdenum ennobles pitting potential by more than one volt, with the addition of tungsten shifting the potential in a more positive direction.[22]

Amorphous alloys with ideally high corrosion resistance, consisting only of corrosion-resistant elements, were developed in the 1990s. Sputter-deposited Cr–X, Mo–X and W–X alloys, in which X denotes Ti, Zr, Nb, or Ta, were shown to be spontaneously passive in concentrated hydrochloric acid.[31–44] The extremely high stability of homogeneous double oxyhydroxides of Cr^{3+} and valve metal cations is responsible for the extraordinary corrosion resistance of Cr-valve metal alloys.[45–48]

Intensive studies have recently been conducted on the corrosion behavior of bulk metallic glasses due to their wide range of potential applications. Bulk metallic glasses with extremely high corrosion resistance even in hydrochloric acid solutions have also been developed in Fe-based and Ni-based alloy systems. Bulk metallic glasses of Fe–Cr–Mo–C–B with and without phosphorus were synthesized over a wide composition range by copper mold casting, and showed high corrosion resistance in concentrated hydrochloric acid with corrosion rates in the range of 10^3 to 10^2 mm $year^{-1}$.[49] Bulk Ni-based glasses, containing Nb, Ta, Cr, and Mo in addition to phosphorus, are resistant in concentrated hydrochloric acid.[50,51]

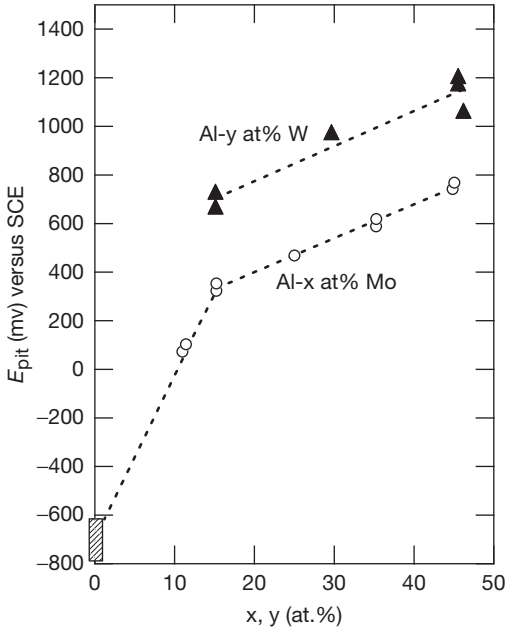

Figure 2 Pitting potentials of sputter-deposited Al–Mo and Al–W alloys, as well as high purity aluminum, in a borate buffer solution containing 0.1 mol dm^{-3} NaCl.[24]

3.20.1.2 Mechanism of Extremely High Corrosion Resistance

It was believed that extremely high corrosion resistance of some amorphous alloys is a consequence of the rapid formation of uniform passive films without weak points and with a high concentration of corrosion-resistant alloying element species in the thin passive films. As mentioned above, some amorphous alloys are immune even in concentrated hydrochloric acid. Such excellent corrosion resistance is not achieved by practical crystalline metals and alloys. Single-phase amorphous alloys are structurally and compositionally homogeneous, free from metallurgical heterogeneities such as grain boundaries, second phases, precipitates, inclusions, and segregations. In crystalline alloys, corrosion is often initiated preferentially at such heterogeneous sites. The compositionally uniform nature of amorphous alloys is a key to the coverage of the entire surface of a metallic substrate by a highly protective thin passive film to protect the alloy from severe corrosive attack.

The rapid formation of a highly protective passive film on amorphous alloys was demonstrated in an iron–chromium alloy system.[52] The high corrosion resistance of chromium-containing crystalline and amorphous alloys is attributed to the formation of passive films highly enriched in trivalent chromium species. For instance, immersion of amorphous Fe–10Cr–13P–7C alloy in 1 mol dm^{-3} HCl solution for 1 week gives rise to the formation of a passive film consisting exclusively of hydrated chromium oxyhydroxide, $CrO_x(OH)_{3-2x}$.[53] Although chromium-enriched passive films are formed on both crystalline and amorphous chromium-containing alloys, enrichment is more significant for amorphous alloys, contributing to the better corrosion resistance of amorphous alloys. **Table 1** shows the concentrations of Cr^{3+} ions in the passive films formed on chromium-containing

Table 1 Cationic fractions of Cr^{3+} ions in passive films formed on amorphous chromium-containing alloys and stainless steels in 1 mol dm^{-3} HCl solution[52]

Alloys	*Cationic fraction of Cr^{3+} ions in passive films*	*Passivation process*
Amorphous alloys		
Fe–10Cr–13P–7C	0.97	Spontaneous passivation
Fe–3Cr–2Mo–13P–7C	0.57	Anodic polarization
Co–10Cr–20P	0.95	Spontaneous passivation
Ni–10Cr–20P	0.87	Spontaneous passivation
Ferric stainless steels		
Fe–30Cr(–2Mo)	0.75	Anodic polarization
Fe–19Cr(–2Mo)	0.58	Anodic polarization

amorphous and crystalline alloys in 1 mol dm^{-3} HCl solution.[52] Crystalline ferritic stainless steels are passivated by anodic polarization, and the cationic concentrations of chromium species in the passive films are 75 and 58 at.% for Fe–30 at.% Cr and Fe–19 at.% Cr, respectively. For amorphous alloys, enrichment of chromium in passive films is more significant, although the contents of chromium in the alloys are lower than those in the crystalline alloys. For the amorphous Fe–10Cr–13P–7C alloy, which shows spontaneous passivation in 1 mol dm^{-3} HCl solution, the cationic percentage of chromium is 97 at.% in the passive film and only 3 at.% of cations are Fe^{2+} and Fe^{3+} ions. The concentration of chromium in the passive film formed on amorphous Fe–3Cr–2Mo–13P–C alloy is comparable to that in the passive film formed on crystalline Cr–19Cr steel. Thus, remarkable enrichment of chromium in the passive film is possible for amorphous alloys even if the chromium content in the alloy is as low as a few atomic percent. Amorphous alloys are metastable and hence surface reactivity is high. High reactivity of alloy surface leads to rapid dissolution of unnecessary alloying constituents, assisting the fast and significant enrichment of chromium species to form a stable and highly protective passive film.

Amorphous alloys are not always corrosion-resistant. The presence of a corrosion-resistant element is essential for improved corrosion resistance. In the absence of a corrosion-resistant element, amorphization increases the reactivity of the metal surface,

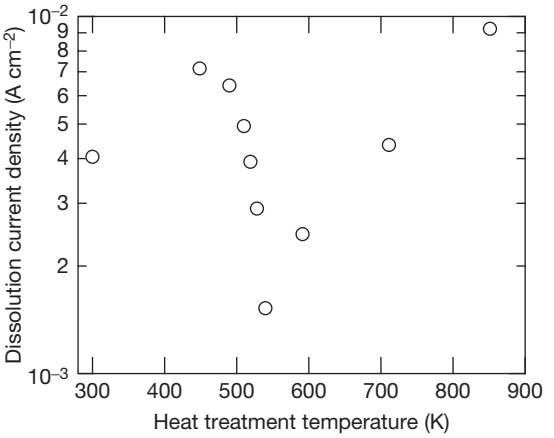

Figure 3 Anodic dissolution rate of amorphous Co–25B alloy at −0.3 V versus SCE in a solution of pH 1.8 containing 0.5 mol dm^{-3} Na_2SO_4. After heat treatment at several temperatures.[54]

resulting in the occurrence of more aggressive corrosion. For instance, active dissolution rates of amorphous Fe–Cr–P–C alloys are larger than those of crystalline alloys with similar composition.[54] During annealing of amorphous Co–25 at.% B alloy, the alloy crystallizes to a Co_3B phase. The Co_3B phase decomposes to Co_2B and Co by further annealing at higher temperatures. **Figure 3** shows the anodic dissolution current density of the Co–25 at.% B alloy at −0.3 V versus SCE in 0.5 mol dm^{-3} Na_2SO_4 (pH 1.8) after annealing at various temperatures.[55] The dissolution rate of the amorphous Co–25 at.% B alloy decreases due to crystallization to Co_3B, indicating higher reactivity of the amorphous surface than that of the crystalline counterpart. Increased dissolution rate again above 623 K is associated with the chemical heterogeneity produced by decomposition of Co_3B to Co_2B and Co.

Another important point for the improved corrosion resistance of amorphous alloys is linked to the fact that amorphous alloys are able to form supersaturated solid solutions containing one or more alloying elements. In amorphous alloys, corrosion-resistant elements can be added uniformly, exceeding the solubility limit at equilibrium. The solid solubility of an alloying element in aluminum is usually less than a few percent. Practical Al alloys consist of an fcc Al phase and an intermetallic compound phase, with concentration of alloying element in the fcc matrix phase remaining low. Thus, the pitting corrosion resistance is not highly enhanced by alloying. However, if the sputter deposition technique is applied for the preparation of aluminum alloys,

a single-phase aluminum alloy supersaturated with an alloying element can be produced in an almost entire composition range and amorphous structure is obtained in a wide composition range.[28] The pitting corrosion resistance of sputter-deposited Al–Mo and Al–W metastable solid solution alloys in a chloride-containing neutral solution increases significantly with an increase in alloying element content, as shown in **Figure 2**.[22] Corrosion rates of a range of sputter-deposited Al-early transition metal alloys in 1 mol dm^{-3} HCl solution also greatly decreases with an increase in content of the alloying element.[28] The improved corrosion resistance of aluminum alloys supersaturated with an alloying element is attributed primarily to the formation of passive films containing corrosion-resistant elements.[28,56–58] Compositions of passive films formed by anodic polarization were examined by X-ray photoelectron spectroscopy (XPS). Based on the results of analysis, it has been proposed that MoO_4^{2-}, CrOOH, Ta_2O_5, or ZrO_2 present in passive films inhibits the adsorption of chloride ions and increase resistance to pit initiation in chloride-containing neutral solutions.

However, there are also some reports that passive films on solid solution aluminum alloys, including Al–W alloys, are practically free from alloying element species,[59–61] although pitting potential greatly ennobles with increase in content of the alloying element. The improved corrosion resistance of aluminum alloys has also been discussed in terms of local dissolution kinetics; alloying improves pitting resistance through a reduction in the ability of pits to maintain the critical local environment necessary for growth.[62]

A systematic study has been undertaken using transmission electron microscopy and Rutherford backscattering spectroscopy (RBS) to elucidate the growth process of anodic films on single-phase aluminum alloys. During anodizing of most dilute aluminum alloys, only aluminum is oxidized initially at the alloy–film interface, forming an alumina film free from alloying element species.[63] The alloying element is accumulated in a thin alloy layer, ~1–2 nm thick, immediately beneath the anodic film. Once the average composition of the enriched alloy layer reaches a critical level, the alloying element is oxidized and incorporated into the oxide film, with the average composition of the enriched layer maintaining the critical level.[64] It has been proposed that in the enriched alloy layer, clusters of the alloying element or the alloying element-rich clusters are developed (**Figure 4**). The critical level of enrichment is dependent upon the alloying element. There is a good correlation between the critical amount of alloying element in the enriched alloy layer and the Gibbs free energy per equivalent of the formation of alloying element oxide (**Figure 5**).[63] An element with larger Gibbs free energy per equivalent for formation of oxide, that is, a nobler element, has more significant enrichment. No enrichment of an alloying element occurs when the alloying element has a Gibbs free energy per equivalent for formation of oxide similar to or less than that of Al_2O_3. In addition to the growth of anodic films at high current efficiency, preferential oxidation of aluminum and accumulation of an alloying element at the alloy surface also occur during chemical etching of aluminum alloys in alkaline solutions, chemical polishing, and electropolishing.[65,66] In neutral chloride-containing solutions, the dissolution rate of the passive film on aluminum alloys is considerably low unless localized attack occurs. Thus passive films free from alloying element species have been detected by surface analysis., Dissolution of alloy results in accumulation of the alloying element at the alloy surface once local breakdown of passive film occurs. Thus, finally, the passive film containing corrosion-resistant alloying element species may be developed, probably inhibiting the growth of pits.

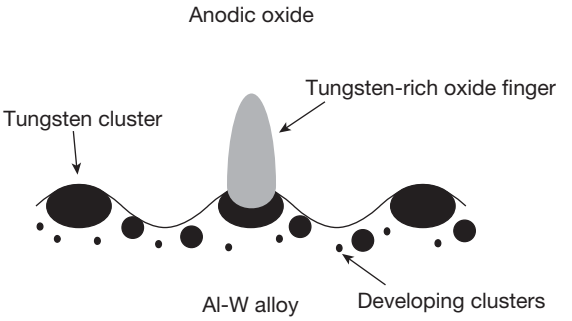

Figure 4 Schematic illustration showing development of tungsten clusters in the enriched alloy layer, ~2 nm thick, immediately beneath the anodic film, and subsequent oxidation of the cluster with a critical size on a dilute Al–W alloy.

3.20.1.3 Role of Alloying Elements in Improving Corrosion Resistance

3.20.1.3.1 Phosphorus

Amorphous alloys are classified as metal–metal and metal–metalloid alloy systems. Metalloid elements, such as boron, carbon, silicon, and phosphorus, are added primarily for enhancing glass-forming ability.

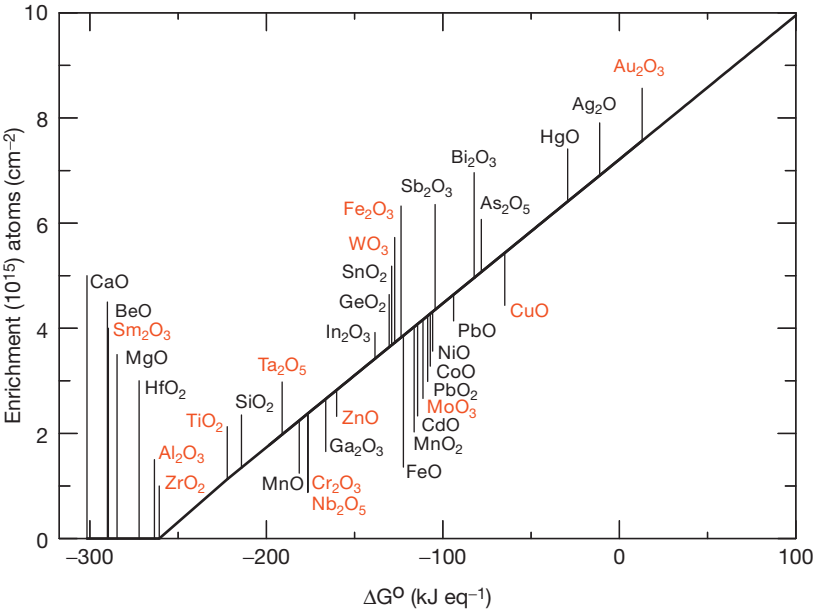

Figure 5 The steady-state enrichment of the alloy predicted for anodizing of binary aluminum alloys, containing ~1–5 at.% alloying element. Predictions are obtained using the relationship between enrichment and Gibbs free energy per equivalent for formation of the alloying element oxide derived from experimental results for a limited range of alloys anodized at 50 A m^{-2} at 298 K.

Among such metalloid elements, phosphorus is particularly beneficial in enhancing corrosion resistance, although it is known that phosphorus segregates at the grain boundaries of stainless steels and induces intergranular corrosion and stress-corrosion cracking of stainless steels. Amorphous Fe–Cr–13Si–7B and Fe–Cr–20B alloys in 9 mol dm^{-3} H_2SO_4 solution dissolve actively and their corrosion rates increase with increasing chromium content. In contrast, the corrosion rates of amorphous Fe–Cr–13P–7C and Fe–Cr–13P–7B alloys in the same solution decrease markedly with the addition of more than 7 at.% chromium.[67] For Ni-based amorphous alloys, the addition of phosphorus reduces the corrosion rate in hydrochloric acid even if a passivating element is absent. The amorphous Ni–20P alloy shows a low corrosion rate of less than 0.1 mm $year^{-1}$ even in concentrated HCl solution, in which nickel metal dissolves aggressively.[68] Marked decrease in the corrosion rate has been found with the addition of only small amounts of phosphorus to amorphous Ni–Ta alloys; the addition of 2 at.% phosphorus decreases the corrosion rate by more than four orders of magnitude in boiling 6 mol dm^{-3} HCl solution.[7]

The high corrosion resistance of amorphous Ni–P alloys in acid solutions is not associated with oxide-based passivity. The alloys do not reveal a clear active–passive transition, and the anodic current density increases gradually with anodic potential.[69–71] The corrosion rate of the amorphous Ni–19P alloy is not dependent upon the concentration of HCl-unusual behavior for oxide-based passivity.[72] Chemical passivity by adsorption of hypophosphite ions was proposed on the basis of results of XPS analysis of Ni–P alloy specimens polarized anodically in deaerated HCl and H_2SO_4 solutions.[69] In addition to hypophosphite ions, enrichment of elemental phosphorus as a consequence of preferential dissolution of nickel was found by XPS analysis. Kinetic analysis of anodic dissolution of the amorphous Ni–P alloy in HCl solution revealed that the dissolution current density follows Fick's second law (**Figure 6**), thus being diffusion-controlled.[73] An explanation of these results is that the elemental phosphorus layer formed by selective dissolution of nickel acts as a diffusion barrier for dissolution of nickel, reducing the dissolution rate of the alloy. The elemental phosphorus layer has high cathodic activity for proton and oxygen reduction. Thus, the formation of an elemental phosphorus layer shifts the corrosion potential in the noble direction as a consequence of the enhancement of cathodic activity and suppression of anodic dissolution. When a passivating element, such as chromium, is present, ennoblement of the corrosion potential promotes

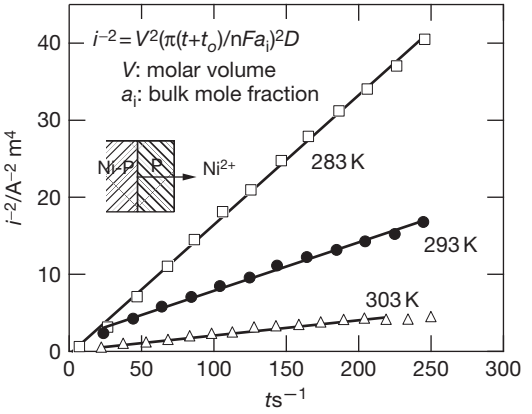

Figure 6 Reciprocal of square of current density i for dissolution of nickel from a melt-spun amorphous Ni–19P alloy specimen at 100 mV versus SCE in 1 mol dm^{-3} HCl at three different temperature as a function of time t.[73]

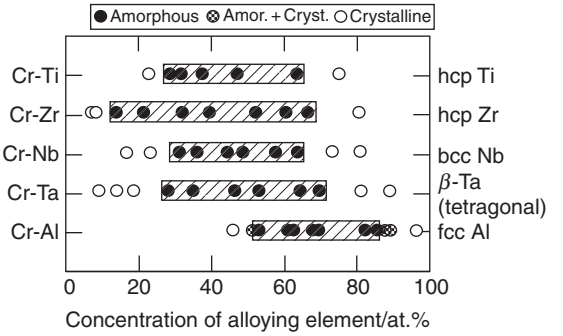

Figure 7 Structures of sputter-deposited Cr-valve metals alloys identified by X-ray diffraction.

passivation. This may be the reason why many amorphous alloys containing a passivating element and phosphorus, including amorphous Ni–Cr–P and Fe–Cr–P–C alloys, are spontaneously passive even in concentrated acid solutions.

In these studies, the chemical state of phosphorus species has been analyzed by XPS. Special attention must be paid to the characterization of passive films by XPS. Exposure of the specimen surface to air during transfer of the specimen from the electrochemical cell to the spectrometer often changes the chemical state of species in passive films. For instance, surface elemental phosphorus changes to phosphate species.[74] The chemical state of molybdenum in passive films on molybdenum-containing corrosion-resistant alloys also changes from Mo^{4+} to Mo^{6+} species during exposure to air. For precise identification of the chemical species in passive films by XPS, exposure of specimens to air before introduction into the spectrometer must be avoided.

3.20.1.3.2 Synergy of corrosion-resistant elements

It is well known that the addition of molybdenum to stainless steels improves localized corrosion in chloride-containing solutions. Molybdenum also reduces active dissolution rates of stainless steels in acid solutions. Even for amorphous alloys, the addition of molybdenum markedly improves the corrosion resistance of chromium-containing amorphous alloys.[5,75,76] In the active dissolution potential region of chromium, molybdenum is passive, forming stable tetravalent molybdenum species. Such stable molybdenum species reduce the active dissolution rates of stainless steels and chromium-containing amorphous alloys. In addition to active dissolution rates, the stability of the passivity of stainless steels and amorphous alloys is enhanced by the addition of molybdenum. Because molybdenum dissolves transpassively as molybdate ions in the passive potential region of the alloys, the composition of passive films on molybdenum-containing alloys is often not greatly different from that on molybdenum-free counterparts. There are several reports on the role of molybdenum in enhancing the stability of a passive state.[4,77,78] The precise role of molybdenum in enhancing passivity is still a subject of controversy.

Ideal corrosion-resistant materials should be alloys consisting only of corrosion-resistant elements. Such alloys have been prepared by a magnetron sputtering method, and, interestingly, it has been revealed that the alloys show superior corrosion resistance to that of each alloy-constituting metal. **Figure 7** shows structures of sputter-deposited chromium-valve metal alloys identified by X-ray diffraction.[31–33] The alloys show an amorphous single-phase structure in a wide composition range. Even crystalline alloys are single phase. Their corrosion rates in 6 mol dm^{-3} HCl and 12 mol dm^{-3} HCl solution are shown in **Figure 8**. In 6 mol dm^{-3} HCl solution, chromium and titanium metals dissolve actively, but binary Cr–Ti alloys are spontaneously passive and show extremely low corrosion rates, several orders of magnitude lower than those of the alloy-constituting elements.[33] The binary amorphous Cr–Zr alloys also reveal low corrosion rates in the 6 mol dm^{-3} HCl solution, the rates decreasing with increasing chromium content.[32] The binary amorphous Cr–Ta alloys are immune even in 12 mol dm^{-3} HCl solution at 303 K in a wide composition range. Corrosion resistance of binary Cr–Nb alloys is also better than that of

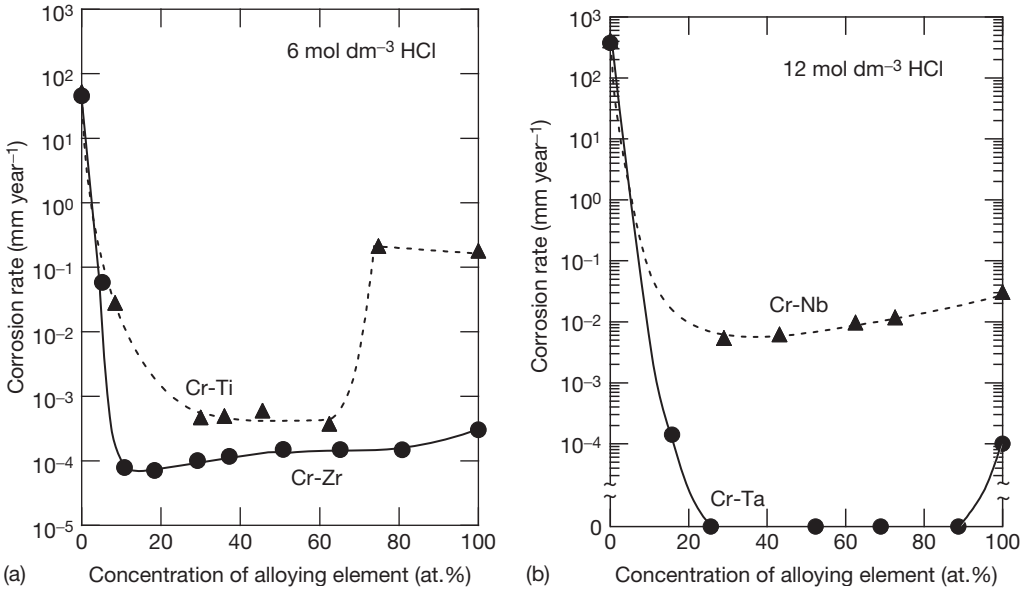

Figure 8 Corrosion rates of sputter-deposited (a) Cr–Ti and Cr–Zr alloys in 6 mol dm^{-3} HCl solutions and (b) Cr–Nb and Cr–Ta alloys in 12 mol dm^{-3} HCl solution at 303 K.[31–33]

chromium and niobium metals.[31] Again, corrosion rates decrease with increasing chromium content.

Such excellent corrosion resistance of amorphous Cr-valve metal alloys was interpreted from XPS analyses of passive films; passive films consisting of double oxyhydroxides containing chromium and valve metal cations are remarkably protective in concentrated hydrochloric acids.[45–48] The formation of uniform double oxyhydroxides was identified from the shift of peak binding energies of photoelectrons of each cation. Similarly, Mo-valve metal alloys and W-valve metal alloys prepared by magnetron sputtering reveal high corrosion resistance in concentrated HCl solution. Their corrosion resistance is better than that of the corresponding alloy-constituting metals.[36–40,42,79]

3.20.1.4 Corrosion Behavior of Bulk Metallic Glasses

The discovery in the late 1980s of amorphous alloys with extremely high glass-forming ability has eliminated the shape limitation of amorphous alloys, and a wide variety of applications are now being considered. As described in the review paper by Inoue,[80] a range of bulk metallic glasses, including Zr-based, Ti-based, Fe-based, Ni-based, Mg-based, and Ln-based alloys, have so far been developed by conventional casting and water cooling processes. The high glass-forming ability of these bulk metallic glasses is associated with the stabilization of supercooled liquids. In metallic alloys, diffusion rates of alloy-constituting elements in their liquid phase are generally very fast at high temperatures just below the melting point. Due to high diffusivity, phase transformation occurs from supercooled liquid to a crystalline phase within a very short time of less than 10^{-5} s. In multicomponent alloy systems forming bulk metallic glasses, diffusivity is suppressed, stabilizing the supercooled liquid state. Bulk metallic glasses are therefore obtained even with a slow cooling rate of 1 K s^{-1} from liquids. Such metallic glasses with high glass-forming ability reveal in reality a wide temperature range of supercooled liquid region below the crystallization temperature.

Since bulk metallic glasses possess superior mechanical and physical properties, they have potential engineering importance. Thus, the corrosion behavior of bulk metallic glasses in potential service environments needs to be elucidated. Tailoring of extremely corrosion-resistant bulk metallic glasses may allow us to use metallic materials in aggressive environments, in which crystalline metallic materials cannot be used because of corrosion.

3.20.1.4.1 Zr-based bulk metallic glasses

Zr-based bulk metallic glasses have been the most extensively studied glassy alloys. Because of their excellent mechanical properties of high tensile

strength, low Young's modulus, and large elastic elongation limit, Zr–Al–Cu–Ni bulk metallic glasses have been commercialized as golf clubs and pressure sensors. Good corrosion resistance of Zr–Al–Cu–Ni alloys was reported in chloride-free solutions in a wide pH range.[81,82] Their corrosion behavior is similar to that of zirconium metal. Zirconium is one of the valve metals, showing spontaneous passivation and high corrosion resistance in chloride-free acid, neutral, and alkaline solutions.[83] The passive film formed on Zr–Al–Cu–Ni alloys consists mainly of zirconium oxide with a small fraction of aluminum cation. For the Zr–Ti–Nb–Cu–Ni–Al alloy, it was revealed that in 0.5 mol dm^{-3} H_2SO_4 and 1 mol dm^{-3} HNO_3 solutions, the fully amorphous alloy showed better passivation stability than nanocrystalline, quasicrystalline, and crystalline ones with the same composition.[84]

In contrast to their high corrosion resistance in chloride-free solutions, Zr-based metallic glasses suffer pitting corrosion in chloride-containing solutions. The pitting occurs because of the existence of micrometer-sized crystalline inclusions.[82] Inclusions develop during casting at a slow cooling rate, being induced by oxygen in the casting atmosphere; bulk Zr–Al–Cu–Ni alloys containing higher oxygen content develop large fractions of crystalline inclusions.[81] The shape and size of the crystalline inclusions as well as their concentration are largely dependent upon the alloy composition, oxygen content, and cooling rate. The pitting is initiated preferentially at the interface between the amorphous matrix and a crystalline inclusion.

In addition to the reduced fraction of crystalline inclusions, modification of alloy composition is effective in improving pitting corrosion resistance. The addition of 5 at.% of titanium or niobium to Zr–30Cu–10Al–5Ni bulk metallic glass greatly reduces the pitting susceptibility in 0.05 mol dm^{-3} NaCl solution.[85] The pitting corrosion resistance of melt-spun Zr–20Cu–10Al–10Ni alloy is enhanced by substituting zirconium with niobium up to 20 at.%.[86] The corrosion rate of the Zr-based alloy in 1 mol dm^{-3} HCl solution decreases significantly with increasing niobium content. In 3% NaCl solution, the addition of niobium greatly shifts the pitting potential of the alloy in the positive direction.

Zr-based bulk metallic glasses have also attracted attention as biomaterials because of suitable mechanical properties as well as biocompatibility.[87] The bulk metallic glass of Zr–17.9Cu–14.6Ni–10Al–5Ti, commonly known as Vitreloy 105, possesses a low modulus that is close to that of bone, as well as high elastic limit and superior strength. An unusual collection of mechanical properties of the bulk metallic glass would be advantageous in various biomedical applications.

As a part of investigations of the biocompatibility of Zr-based bulk metallic glasses, their corrosion behavior has been examined in artificial body fluids.[87–90] It has been found that pitting corrosion occurs on Zr-based metallic glasses in phosphate-buffered saline environments by anodic polarization. However, the susceptibility of pitting is not so high, particularly at low chloride concentrations. The corrosion behavior of the Vitreloy 105 bulk metallic glass has been compared with that of common biomaterials of 316L stainless steel, Ti–6Al–4V, and CoCrMo alloys in a phosphate-buffered saline solution.[87] The corrosion rate of the Zr-based bulk metallic glass was lower than that of 316L stainless steel, being comparable with the corrosion rates of Ti–6Al–4V and CoCrMo alloys. Furthermore, bulk metallic glass showed better localized corrosion resistance than 316L stainless steel. The combined mechanical and electrochemical properties of Zr-based bulk metallic glasses indicate their potential as a new generation of biomaterials.

3.20.1.4.2 Corrosion-resistant bulk metallic glasses

It has been demonstrated that bulk forms of iron-based and nickel-based metallic glasses containing sufficient amounts of corrosion-resistant elements show excellent corrosion resistance in aggressive acid solutions. Corrosion-resistant rod-shaped Ni-based alloys, including Ni–5Cr–5Ta–3Mo–16P–4B, Ni–15Cr–10Mo–16P–4B, Ni–(10–15)Cr–5Ta–16P–4B and Ni–$(40-x)$Nb–xTa–(3–5)P alloys, of 1–2 mm in diameter were successfully prepared by copper mold casting.[51,91,92] These alloys are spontaneously passive in 6 mol dm^{-3} HCl solution, showing very low corrosion rates. The corrosion resistance of bulk metallic glasses is comparable to that of metal-spun thin ribbons of the same composition. Thus, the cooling rate does not influence the corrosion behavior of metallic glasses. To obtain sufficient glass-forming ability to form bulk metallic glasses, large amounts of corrosion-resistant elements cannot be added to alloys. However, the combined addition of two or three corrosion-resistant elements to nickel-based and iron-based alloys provides excellent corrosion resistance. The combination of chromium, tantalum, and molybdenum is effective for enhancing corrosion resistance.[50,92]

A bulk form of corrosion-resistant metallic glasses was also successfully prepared by sheath-rolling consolidation of encased amorphous alloy powders. The Ni–10Cr–5Nb–16P–4B metallic glass shows a wide temperature range of supercooled liquid region (more than 50 K) below crystallization. Alloy powders prepared by a gas atomization technique were encased in a stainless steel tube and then heated to temperature of the supercooled liquid region. Sheath-rolling at this temperature produced a bulk metallic glass plate. The potential application of the sheath-rolled and copper-mold cast Ni–10Cr–5Nb–16P–4B bulk metallic glass in an exhaust gas chimney of a waste incinerator has been pointed out.[93] In the environment at 423 K and 463 K, severe corrosion attack occurred on type-316L stainless steel and Alloy B due to dew-point corrosion, whereas bulk metallic glass retained its metallic luster and showed no detectable corrosion weight change for 20 days. Superior corrosion resistance of iron-based bulk metallic glasses containing chromium and molybdenum has also been reported. The availability of corrosion-resistant bulk metallic glasses opens up their applications to very aggressive environments, in which conventional crystalline metallic materials cannot be used due to severe corrosion.

3.20.1.5 Corrosion Behavior of Nanocrystalline Alloys

3.20.1.5.1 Nanocrystalline-precipitated amorphous alloys

It is likely that precipitation of crystalline phases in an amorphous alloy matrix containing corrosion-resistant elements is detrimental to its corrosion resistance because of the increased chemical heterogeneity. It is known that amorphous alloys containing corrosion-resistant elements show higher corrosion resistance than fully crystallized alloys with the same composition. This is, however, not always true when nanocrystalline phases are precipitated in an amorphous matrix phase. In certain amorphous Al alloys and Zr alloys,[94–99] it has been demonstrated that good resistance of fully amorphous alloys to localized pitting corrosion is not deteriorated or improved by nanocrystalline precipitation. Nanocrystalline precipitates can be introduced in an amorphous phase by heat treatment of fully amorphous alloys or by utilizing a slow cooling rate during the fabrication of amorphous alloys from the liquid state. The latter condition is required to develop bulk metallic glasses such that they often contain nanocrystalline precipitates in an amorphous matrix. Thus an understanding of the influence of nanocrystalline precipitates on corrosion behavior is a crucial issue for the practical application of bulk metallic glasses. Furthermore, nanocrystalline-amorphous alloys have attracted attention since they show improved mechanical strength.[100] The crystallization behavior of amorphous alloys is dependent upon alloy composition. For aluminum-rich amorphous alloys, including Al–5Fe–5Gd, Al–8.7Ni–4.3Y, and Al–3Co–7Ce alloys, solute-lean fcc-Al phase nanocrystals are primarily precipitated in an amorphous matrix during heat treatment. Such amorphous–nanocrystalline alloys maintain high pitting potential in chloride-containing solutions comparable to that of fully amorphous alloys, though fully crystallized alloys show considerably low pitting potential.[95–99] For the Al–5Fe–5Gd alloy, even ennobled pitting potential in 0.6 mol dm^{-3} NaCl solution by precipitation of 10–15 nm sized nanocrystals has been reported (**Figure 9**).[98] Ennoblement of pitting potential is also observed for amorphous Zr–Cr alloys; precipitation of hcp Zr nanocrystals of less than 20 nm shifts the pitting potential in the positive direction in 6 mol dm^{-3} HCl solution.[94] Ennoblement of the pitting potential is explained by the enrichment of the solute in the amorphous matrix. Precipitation of nanocrystalline Zr induces enrichment of chromium in the amorphous phase, making the matrix phase more pitting-resistant. The presence of a critical size of nanocrystals, that is, 20 nm, in improving localized corrosion resistance has also been pointed out. Below the critical size, a chromium-enriched highly

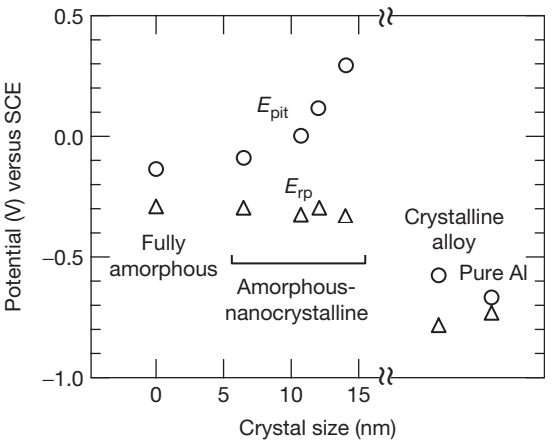

Figure 9 Pitting and repassivation potentials for Al–5Fe–5Gd in deaerated 0.6 mol dm^{-3} NaCl. Pitting and repassivation potentials of pure Al are shown for comparison. Scan rate 0.1 mV s^{-1}.[98]

protective passive film can cover the entire alloy surface, but preferential dissolution of a less corrosion-resistant phase occurs when the size of the precipitates exceeds the critical size.

There are also examples of precipitation of nanocrystals less than 10 nm size in amorphous matrix being detrimental in terms of corrosion. The copper-mold cast Ni–10Cr–5Ta–16P–4B bulk metallic glass contains an fcc nickel phase of 2–3 nm in size in the amorphous matrix, showing higher anodic dissolution current than that of fully amorphous alloy ribbon in potentiodynamic polarization curves.[91] Smaller sizes of the fcc Ni precipitates have lower detrimental effect. Sputter-deposited Cr–Nb alloys are spontaneously passive in 6 and 12 mol dm^{-3} HCl solutions. The as-deposited alloys crystallize to a two-phase mixture of bcc Cr and Cr_2Nb, Cr_2Nb and niobium-rich amorphous phase, Cr_2Nb and bcc Nb, or chromium-rich amorphous phase and bcc Nb, depending upon alloy composition and heat treatment conditions. The Cr_2Nb phase has high corrosion resistance, similar to that of the amorphous single phase alloy. The formation of nanocrystalline bcc Cr and bcc Nb phases increases initial passive current density. However, the steady state passive current density is as low as that of the as-deposited alloy, as the amorphous or Cr_2Nb matrix phase maintains high corrosion resistance. Thus, the formation of soluble nanocrystals in corrosion-resistant matrix phases increases the initial dissolution rate but not always the steady-state anodic dissolution rate.

3.20.1.5.2 Nanocrystallization of conventional crystalline corrosion-resistant materials

Finally, it may be worth mentioning that nanocrystallization of conventional corrosion-resistant materials such as stainless steel, markedly improves the susceptibility for localized corrosion without changing the alloy composition. Using a conventional type-304 stainless steel target, nanocrystalline stainless steel films have been prepared by sputter deposition.[101,102] The pitting potential of nanocrystalline films with grain size of 25 nm is ~850 mV more positive than that of conventional bulk material of the same composition, even though enrichment of chromium in the air-formed oxide is lower for nanocrystalline films.[101] Sputter-deposited films have a bcc structure. Improved pitting corrosion resistance may not be related to structural transformation from the fcc phase of bulk material to the bcc phase of nanocrystalline films, because the pitting potential of ferritic bulk stainless steel containing 18% Cr is even lower than that of austenitic stainless steel with the same Cr content.

It is well accepted that pitting corrosion of stainless steel in chloride-containing environments is usually initiated at manganese sulfide particles in the steel. A recent study also suggests the possibility that pitting is triggered by an attack on chromium-depleted zones around the manganese sulfide particles.[103] In stainless steel films prepared by sputter deposition that produces single-phase materials dissolving most alloying and impurity elements, the chemical heterogeneity of the steel surface should be neglected. By using a process that forms nanograined metastable materials with reduced chemical heterogeneity, corrosion resistance can be improved remarkably without changing chemical compositions, even if there is a high concentration of impurity elements that are generally detrimental to corrosion.[102]

References

1. Naka, M.; Hashimoto, K.; Masumoto, T. *J. Jpn. Inst. Met.* **1974**, *38*, 835–841.
2. Naka, M.; Hashimoto, K.; Masumoto, T. *Corrosion* **1976**, *32*, 146–152.
3. Hashimoto, K.; Asami, K.; Naka, M.; Masumoto, T. *Sci. Rep. Res. Inst., Tohoku Univ., Ser. A* **1979**, *27*, 237–245.
4. Hashimoto, K.; Asami, K.; Teramoto, K. *Corros. Sci.* **1979**, *19*, 3–14.
5. Asami, K.; Naka, M.; Hashimoto, K.; Masumoto, T. *J. Electrochem. Soc.* **1980**, *127*, 2130–2138.
6. Hashimoto, K.; Kobayashi, K.; Asami, K.; Masumoto, T. *Metallic Corrosion*, Proceedings of the Eighth International Congress on Metal Corrosion, Mainz, Germany, 6–11 Sept; DECHEMA, Frankfurt am Main, Germany, 1981; pp 70–75.
7. Shimamura, K.; Kawashima, A.; Asami, K.; Hashimoto, K. *Sci. Rep. Res. Inst. Tohoku Univ. Ser. A* **1986**, *33*, 196–210.
8. Singh, I. B.; Misra, R. D. K.; Chaudhary, R. S.; Akhtar, D. *Mater. Sci. Eng.* **1987**, *92*, 173–178.
9. Mitsuhashi, A.; Kawashima, A.; Asami, K.; Hashimoto, K. In *Corrosion, Electrochemistry and Catalysis of Metallic Glasses*, Proceedings of the Symposium of the Elctrochemical Society, Honolulu, USA, 1987; Diegle, R. B., Hashimoto, K., Eds.; The Electrochemical Society: Pennington, NJ, USA, 1988; pp 191–200.
10. Shimamura, K.; Miura, K.; Kawashima, A.; Asami, K.; Hashimoto, K. *Sci. Rep. Res. Inst., Tohoku Univ., Ser. A* **1988**, *34*, 107–117.
11. Mitsuhashi, A.; Kawashima, A.; Asami, K.; Hashimoto, K. *Boshoku Gijutsu* **1988**, *37*, 3–8.
12. Lee, H. J.; Akiyama, E.; Habazaki, H.; Kawashima, A.; Asami, K.; Hashimoto, K. *Corros. Sci.* **1995**, *37*, 1313–1324.
13. Lee, H. J.; Akiyama, E.; Habazaki, H.; Kawashima, A.; Asami, K.; Hashimoto, K. *Corros. Sci.* **1995**, *37*, 321–330.
14. Lee, H. J.; Akiyama, E.; Habazaki, H.; Kawashima, A.; Asami, K.; Hashimoto, K. *Mater. Trans., Jim* **1996**, *37*, 383–388.

15. Lee, H. J.; Akiyama, E.; Habazaki, H.; Kawashima, A.; Asami, K.; Hashimoto, K. *Corros. Sci.* **1996**, *38*, 469–485.
16. Lee, H. J.; Akiyama, E.; Habazaki, H.; Kawashima, A.; Asami, K.; Hashimoto, K. *Corros. Sci.* **1996**, *38*, 1269–1279.
17. Kim, Y.; Buchheit, R. G. *Electrochim. Acta* **2007**, *52*, 2437–2446.
18. Janik-Czachor, M.; Jaskiewicz, A.; Kedzierzawski, P.; Werner, Z. *Mater. Sci. Eng. A* **2003**, *358*, 171–177.
19. Principe, E. L.; Shaw, B. A.; Davis, G. D. *Corrosion* **2003**, *59*, 295–313.
20. Metikos-Hukovic, M.; Radic, N.; Grubac, Z.; Tonejcv, A. *Electrochim. Acta* **2002**, *47*, 2387–2397.
21. Bockris, J. O.; Kang, Y. K. *J. Solid State Electrochem.* **1997**, *1*, 17–35.
22. Wolowik, A.; JanikCzachor, M.; Werner, Z. *Mater. Chem. Phys.* **1997**, *49*, 164–168.
23. Davis, G. D.; Shaw, B. A.; Rees, B. J.; Pecile, C. A. *Surf. Interf. Anal.* **1995**, *23*, 609–617.
24. Moffat, T. P.; Stafford, G. R.; Hall, D. E. *J. Electrochem. Soc.* **1993**, *140*, 2779–2786.
25. Bockris, J. O.; Minevski, L. V. *J. Electroanal. Chem.* **1993**, *349*, 375–414.
26. Davis, G. D.; Shaw, B. A.; Rees, B. J.; Ferry, M. *J. Electrochem. Soc.* **1993**, *140*, 951–959.
27. Davis, G. D.; Moshier, W. C.; Long, G. G.; Black, D. R. *J. Electrochem. Soc.* **1991**, *138*, 3194–3199.
28. Yoshioka, H.; Yan, O.; Habazaki, H.; Kawashima, A.; Asami, K.; Hashimoto, K. *Corros. Sci.* **1990**, *31*, 349–354.
29. Yoshioka, H.; Habazaki, H.; Kawashima, A.; Asami, K.; Hashimoto, K. *Electrochim. Acta* **1991**, *36*, 1227–1233.
30. Yoshioka, H.; Habazaki, H.; Kawashima, A.; Asami, K.; Hashimoto, K. *Corros. Sci.* **1991**, *32*, 313–325.
31. Kim, J. H.; Akiyama, E.; Habazaki, H.; Kawashima, A.; Asami, K.; Hashimoto, K. *Corros. Sci.* **1993**, *34*, 1947–1955.
32. Kim, J. H.; Akiyama, E.; Habazaki, H.; Kawashima, A.; Asami, K.; Hashimoto, K. *Corros. Sci.* **1993**, *34*, 1817–1827.
33. Kim, J. H.; Akiyama, E.; Yoshioka, H.; Habazaki, H.; Kawashima, A.; Asami, K.; Hashimoto, K. *Corros. Sci.* **1993**, *34*, 975–987.
34. Kim, J. H.; Akiyama, E.; Habazaki, H.; Kawashima, A.; Asami, K.; Hashimoto, K. *Corros. Sci.* **1994**, *36*, 511–523.
35. Bhattarai, J.; Akiyama, E.; Kawashima, A.; Asami, K.; Hashimoto, K. *Corros. Sci.* **1995**, *37*, 2071–2086.
36. Park, P. Y.; Akiyama, E.; Habazaki, H.; Kawashima, A.; Asami, K.; Hashimoto, K. *Corros. Sci.* **1996**, *38*, 1649–1667.
37. Park, P. Y.; Akiyama, E.; Habazaki, H.; Kawashima, A.; Asami, K.; Hashimoto, K. *Corros. Sci.* **1996**, *38*, 1731–1750.
38. Park, P. Y.; Akiyama, E.; Kawashima, A.; Asami, K.; Hashimoto, K. *Corros. Sci.* **1996**, *38*, 397–411.
39. Bhattarai, J.; Akiyama, E.; Habazaki, H.; Kawashima, A.; Asami, K.; Hashimoto, K. *Corros. Sci.* **1997**, *40*, 19–42.
40. Bhattarai, J.; Akiyama, E.; Habazaki, H.; Kawashima, A.; Asami, K.; Hashimoto, K. *Corros. Sci.* **1997**, *39*, 355–375.
41. Bhattarai, J.; Akiyama, E.; Habazaki, H.; Kawashima, A.; Asami, K.; Hashimoto, K. *Corros. Sci.* **1998**, *40*, 1897–1914.
42. Bhattarai, J.; Akiyama, E.; Habazaki, H.; Kawashima, A.; Asami, K.; Hashimoto, K. *Corros. Sci.* **1998**, *40*, 757–779.
43. Bhattarai, J.; Akiyama, E.; Habazaki, H.; Kawashima, A.; Asami, K.; Hashimoto, K. *Corros. Sci.* **1998**, *40*, 155–175.
44. Bhattarai, J.; Akiyama, E.; Habazaki, H.; Kawashima, A.; Asami, K.; Hashimoto, K. *Corros. Sci.* **1998**, *40*, 19–42.
45. Li, X. Y.; Akiyama, E.; Habazaki, H.; Kawashima, A.; Asami, K.; Hashimoto, K. *Corros. Sci.* **1997**, *39*, 1365–1380.
46. Li, X. Y.; Akiyama, E.; Habazaki, H.; Kawashima, A.; Asami, K.; Hashimoto, K. *Corros. Sci.* **1997**, *39*, 935–948.
47. Li, X. Y.; Akiyama, E.; Habazaki, H.; Kawashima, A.; Asami, K.; Hashimoto, K. *Corros. Sci.* **1998**, *40*, 1587–1604.
48. Li, X. Y.; Akiyama, E.; Habazaki, H.; Kawashima, A.; Asami, K.; Hashimoto, K. *Corros. Sci.* **1998**, *40*, 821–838.
49. Pang, S. J.; Zhang, T.; Asami, K.; Inoue, A. *Acta Mater.* **2002**, *50*, 489–497.
50. Katagiri, H.; Meguro, S.; Yamasaki, M.; Habazaki, H.; Sato, T.; Kawashima, A.; Asami, K.; Hashimoto, K. *Corros. Sci.* **2001**, *43*, 183–191.
51. Kawashima, A.; Habazaki, H.; Hashimoto, K. *Mater. Sci. Eng. A* **2001**, *304*, 753–757.
52. Hashimoto, K. In *Passivity of Metals and Semiconductors*; Froment, M., Ed.; Elsevier: Amsterdam, 1983; 235. Proceedings of the Fifth International Symposium, Bombannes, France, May 30-June 3.
53. Asami, K.; Hashimoto, K.; Masumoto, T.; Shimodaira, S. *Corros. Sci.* **1976**, *16*, 909–914.
54. Hashimoto, K.; Osada, K.; Masumoto, T.; Shimodaira, S. *Corros. Sci.* **1976**, *16*, 71–76.
55. Huerta, D.; Heusler, K. E. *J. Non-Cryst. Solids* **1983**, *56*, 261–266.
56. Davis, G. D.; Moshier, W. C.; Fritz, T. L.; Cote, G. O. *J. Electrochem. Soc.* **1990**, *137*, 422–427.
57. Moshier, W. C.; Davis, G. D.; Cote, G. O. *J. Electrochem. Soc.* **1989**, *136*, 356–362.
58. Moshier, W. C.; Davis, G. D.; Ahearn, J. S.; Hough, H. F. *J. Electrochem. Soc.* **1986**, *133*, 1063–1064.
59. Shaw, B. A.; Davis, G. D.; Fritz, T. L.; Rees, B. J.; Moshier, W. C. *J. Electrochem. Soc.* **1991**, *138*, 3288–3295.
60. Janik-Czachor, M.; Wolowik, A.; Szummer, A.; Lublinska, K.; Hofmann, S.; Kraus, K. *Electrochim. Acta* **1998**, *43*, 875–882.
61. Wolowik, A.; Janik-Czachor, M. *Mater. Sci. Eng. A* **1999**, *267*, 301–306.
62. Frankel, G. S.; Newman, R. C.; Jahnes, C. V.; Russak, M. A. *J. Electrochem. Soc.* **1993**, *140*, 2192–2197.
63. Habazaki, H.; Shimizu, K.; Skeldon, P.; Thompson, G. E.; Wood, G. C.; Zhou, X. *Trans. Inst. Met. Finish.* **1997**, *75*, 18–23.
64. Habazaki, H.; Shimizu, K.; Skeldon, P.; Thompson, G. E.; Wood, G. C. *Philos. Mag. B* **1996**, *73*, 445–460.
65. Liu, Y.; Colin, F.; Skeldon, P.; Thompson, G. E.; Zhou, X.; Habazaki, H.; Shimizu, K. *Corros. Sci.* **2003**, *45*, 1539–1544.
66. Zhou, X.; Thompson, G. E.; Habazaki, H.; Shimizu, K.; Skeldon, P.; Wood, G. C. *Thin Solid Films* **1997**, *293*, 327–332.
67. Im, B. M.; Akiyama, E.; Habazaki, H.; Kawashima, A.; Asami, K.; Hashimoto, K. *Corros. Sci.* **1993**, *34*, 1829–1839.
68. Zhang, B. P.; Kawashima, A.; Asami, K.; Hashimoto, K. *Boshoku Gijutsu* **1989**, *38*, 384–389.
69. Diegle, R. B.; Sorensen, N. R.; Clayton, C. R.; Helfand, M. A.; Yu, Y. C. *J. Electrochem. Soc.* **1988**, *135*, 1085–1092.
70. Diegle, R. B.; Sorensen, N. R.; Clayton, C. R.; Helfand, M. A. In *Corrosion, Electrochemistry and Catalysis of Metallic Glasses*; Diegle, R. B., Hashimoto, K., Eds.; The Electrochemical Society, Pennington, NJ, USA, 1988; pp 80–103. Proceedings of the Symposium of the Elctrochemical Society, Honolulu, USA, 1987.
71. Krolikowski, A.; Karbownicka, B.; Jaklewicz, O. *Electrochim. Acta* **2006**, *51*, 6120–6127.

72. Zhang, B. P.; Habazaki, H.; Kawashima, A.; Asami, K.; Hashimoto, K. *Corros. Sci.* **1992**, *33*, 667–679.
73. Habazaki, H.; Ding, S. Q.; Kawashima, A.; Asami, K.; Hashimoto, K.; Inoue, A.; Masumoto, T. *Corros. Sci.* **1989**, *29*, 1319–1328.
74. Zhang, B. P.; Habazaki, H.; Kawashima, A.; Asami, K.; Hashimoto, K. *Corros. Sci.* **1992**, *33*, 103–112.
75. Habazaki, H.; Kawashima, A.; Asami, K.; Hashimoto, K. *Mater. Sci. Eng. A* **1991**, *134*, 1033–1036.
76. Habazaki, H.; Kawashima, A.; Asami, K.; Hashimoto, K. *Corros. Sci.* **1992**, *33*, 225–236.
77. Sugimoto, K.; Sawada, Y. *Corros. Sci.* **1977**, *17*, 425–437.
78. Clayton, C. R.; Lu, Y. C. *Corros. Sci.* **1989**, *29*, 881–898.
79. Bhattarai, J.; Akiyama, E.; Habazaki, H.; Kawashima, A.; Asami, K.; Hashimoto, K. *Corros. Sci.* **1998**, *40*, 155–175.
80. Inoue, A. *Proc. Jpn. Acad. Ser. B* **2005**, *81*, 156–171.
81. Gebert, A.; Buchholz, K.; Leonhard, A.; Mummert, K.; Eckert, J.; Schultz, L. *Mater. Sci. Eng. A* **1999**, *267*, 294–300.
82. Gebert, A.; Mummert, K.; Eckert, J.; Schultz, L.; Inoue, A. *Mater. Corros.* **1997**, *48*, 293–297.
83. Pringle, J. P. S. *Electrochem. Acta* **1980**, *25*, 1420–1437.
84. Mudali, U. K.; Scudino, S.; Kühn, U.; Eckert, J.; Gebert, A. *Scr. Mater.* **1994**, *50*, 1379.
85. Raju, V. R.; Kuhn, U.; Wolff, U.; Schneider, F.; Eckert, J.; Reiche, R.; Gebert, A. *Mater. Lett.* **2002**, *57*, 173–177.
86. Pang, S. J.; Zhang, T.; Kimura, H.; Asami, K.; Inoue, A. *Mater. Trans. JIM* **2000**, *41*, 1490–1494.
87. Morrison, M. L.; Buchanan, R. A.; Leon, R. V.; Liu, C. T.; Green, B. A.; Liaw, P. K.; Horton, J. A. *J. Biomed. Mater. Res. A* **2005**, *74A*, 430–438.
88. Hiromoto, S.; Tsai, A. P.; Sumita, M.; Hanawa, T. *Mater. Trans.* **2002**, *43*, 3112–3117.
89. Hiromoto, S.; Asami, K.; Tsai, A. P.; Hanawa, T. *Mater. Trans.* **2002**, *43*, 261–266.
90. Hiromoto, S.; Tsai, A. P.; Sumita, M.; Hanawa, T. *Corros. Sci.* **2000**, *42*, 1651–1660.
91. Habazaki, H.; Sato, T.; Kawashima, A.; Asami, K.; Hashimoto, K. *Mater. Sci. Eng. A* **2001**, *304*, 696–700.
92. Katagiri, H.; Meguro, S.; Yamasaki, M.; Habazaki, H.; Sato, T.; Kawashima, A.; Asami, K.; Hashimoto, K. *Corros. Sci.* **2001**, *43*, 171–182.
93. Hashimoto, K.; Katagiri, H.; Habazaki, H.; Yamasaki, M.; Kawashima, A.; Izumiya, K.; Ukai, H.; Asami, K.; Meguro, S. *Mater. Sci. Forum* **2001**, *377*, 1–8.
94. Mehmood, M.; Zhang, B. P.; Akiyama, E.; Habazaki, H.; Kawashima, A.; Asami, K.; Hashimoto, K. *Corros. Sci.* **1998**, *40*, 1–17.
95. Sweitzer, J. E.; Scully, J. R.; Bley, R. A.; Hsu, J. W. P. *Electrochem. Solid State Lett.* **1999**, *2*, 267–270.
96. Sweitzer, J. E.; Shiflet, G. J.; Scully, J. R. *Electrochim. Acta* **2003**, *48*, 1223–1234.
97. Lucente, A. M.; Scully, J. R. *Electrochem. Solid State Lett.* **2007**, *10*, C39–C43.
98. Lucente, A. M.; Scully, J. R. *Corros. Sci.* **2007**, *49*, 2351–2361.
99. Goldman, M. E.; Unlu, N.; Shiflet, G. J.; Scully, J. R. *Electrochem. Solid State Lett.* **2005**, *8*, B1–B5.
100. Choi, G. S.; Kim, Y. H.; Cho, H. K.; Inoue, A.; Masumoto, T. *Scr. Met. Mater.* **1995**, *33*, 1301–1306.
101. Inturi, R. B.; Szklarskasmialowska, Z. *Corrosion* **1992**, *48*, 398–403.
102. Fujimoto, S.; Hayashida, H.; Shibata, T. *Mater. Sci. Eng. A* **1999**, *267*, 314–318.
103. Ryan, M. P.; Williams, D. E.; Chater, R. J.; Hutton, B. M.; McPhail, D. S. *Nature* **2002**, *415*, 770–774.

3.21 Corrosion of Noble Metals

S. B. Lyon
Corrosion and Protection Centre, School of Materials, The University of Manchester, Oxford Road, Manchester M13 9PL, UK

This article is a revision of the Third Edition article 6.1 by G. W. Walkiden and R. A. Jarman, volume 1, pp 6:3–6:27,

Glossary

Noble metal A metal generally characterized by having relatively positive potentials and low corrosion rates when immersed in an aqueous environment by virtue of its relative thermodynamic stability with respect to its simple hydrated ions in solution (and not solely by its passivity).

PGMs The platinum group of metals that comprises: platinum, palladium, rhodium, ruthenium, osmium and iridium; or (PGM) a single element of that group.

Sterling silver An alloy containing at least 92.5% silver plus other (unspecified) alloying additions, commonly copper. In the United Kingdom, this level of purity is the minimum standard guaranteed by hallmark.

Troy ounce A historic unit of measurement common in medieval Europe and said to derive from the city of Troyes, France; approximately equal to 31.1 g. Currently used in the weighing, trading, and description of precious metals and jewels.

3.21.1 Introduction

The group of noble metals comprises adjacent elements from the second and third row of the transition metals and from groups 8b (platinum group metals – PGMs) and 1b (silver and gold) of the periodic table. They are characterized by their exceptional resistance to corrosive attack by a wide range of liquid and gaseous substances and their relative stability at high temperatures, conditions under which base metals would be rapidly oxidized. This resistance to chemical and oxidative attack arises principally from the inherent, high thermodynamic stability of the noble metals. Apart from gold (which does not form an oxide in aqueous media), in other noble metals a thin film of adsorbed oxygen or oxide may form under oxidizing or anodic conditions, which can enhance their corrosion resistance via passivity. In some materials, for example silver in halide solutions, salt films can accomplish a similar passivation effect.

Their high initial cost, combined with a mechanical strength which is generally inferior to that of the base metals, results in only a limited number of corrosion-related applications for the noble metals, and they are as used only as sheaths, linings, or coatings, for example, electrodeposits. However, noble metals have some critical applications, for example, equipment for fine chemical and pharmaceutical production, for fiber drawing, in the glass industry, and for crystal growth.

Silver is produced in a number of countries, generally as a by-product from mining other materials, particularly lead, zinc, copper, nickel, and gold, although some significant primary mines operate in Australia, Mexico, and Russia. (Basic information regarding physical and mechanical properties, application, and production of the noble metals were obtained from the references listed.) The largest producers are in Latin America (e.g., Peru, Mexico, Chile), while China, Australia, and Eastern Europe also produce significant quantities. Gold is mined as a primary product in a number of countries (e.g., South Africa, Australia, Ghana), but is also produced as a secondary product from other mining operations (e.g., Peru, Indonesia). By far, the majority (>80%) of the PGMs are produced from primary resources in South Africa and Russia, with lesser amounts from secondary resources. **Table 1** shows estimated supply and demand figures for all the noble metals. Note the relatively small volumes of material recovered. In years of excess of supply over demand, stocks are built-up, which are then released when demand exceeds supply. This is demonstrated for ruthenium demand in 2006. Noble metals are subject to large fluctuations in price according to market demands.

3.21.2 Properties

Although in the majority of their applications the choice of noble metals is determined by their chemical property rather than by their physical and mechanical properties, some consideration of the latter is necessary. Therefore, important physical and mechanical properties are reported in **Tables 2** and **3**.

3.21.2.1 Silver and Gold

Silver in the fully annealed state is a soft, ductile metal, which is easily fabricated into the very wide range of forms employed in industry by the normal metal-working techniques such as drawing, spinning, rolling, etc. Silver work-hardens appreciably during fabrication. The mechanical strength of silver is markedly affected by an increase in temperature and falls to about 25% of the initial value of cold, hard-worked silver when the metal is heated to just over 200 °C. Silver has the highest electrical and thermal conductivities of all

Table 1 Estimated supply/demand and average prices for noble metals in 2006

Metal	*Supply (tons)*	*Demand (tons)*	*Volume (m^3)*	*Average Price ($/oz: $/kg)*	*$/kg*
Silver	26 900	–	2569	11.5	370
Gold	3 400	–	176	635	20 450
Platinum	218	218	9.18	1140	36 650
Palladium	259	213	21.6	320	10 290
Rhodium	27.1	27.6	1.98	4550	146 300
Ruthenium	26 (est.)	41.5	3.11	195	6 200
Iridium	–	3.94	0.174	350	11 250
Osmium	–	<0.1	<0.004 5	–	–

Basic information regarding physical and mechanical properties, application, and production of the noble metals were obtained from the references listed.
Source: Matthey, J. *Platinum Metals Market Review*; 2007.

Table 2 Physical properties of the noble metals

Property	*Ag*	*Au*	*Ru*	*Rh*	*Pd*	*Os*	*Ir*	*Pt*
Atomic number	47	79	44	45	46	76	77	78
Relative atomic mass	107.9	196.9	101.1	102.9	106.4	190.2	192.2	195.1
Room temperature structure	fcc	fcc	hcp	fcc	fcc	hcp	fcc	fcc
Density (mg m^{-3})	10.49	19.32	12.45	12.41	12.02	22.61	22.65	21.45
Melting point (K)	1234	1337.6	2523	2236	1825	3300	2716	2045
Boiling point (K)	2438	3130	4423	3970	3237	5285	4701	4100
Resistivity ($\times 10^{-6}\,\Omega$ cm)	1.59	2.06	6.80	4.33	9.93	8.12	4.71	9.85
Thermal conductivity (W m^{-1} K^{-1})	419	311	105	150	76	87	148	73

Source: The PGM database. Available at: www.platinummetalsreview.com/jmpgm/
HSC 6.1: Thermochemical Database; Outotec, 2007.

Table 3 Room temperature mechanical properties of the noble metals and some alloys

Metal (annealed)	*Melting point (K)*	*Proof stress at 0.2% (MPa)*	*Ultimate tensile strength (MPa)*	*Elongation (%)*	*Young's modulus (GPa)*
Silver	1234	40	180	60	82
Gold	1337.6	30	120	70	72
Ruthenium	2523	370	430	3	420
Rhodium	2236	80	700	15	315
Palladium	1825	50	190	40	115
Osmium	3300	Brittle	Brittle	Brittle	555
Iridium	2716	235	1100	10	515
Platinum	2045	45	150	40	170
+5% Rhodium	2098	55	210	35	170
+10% Rhodium	2123	65	310	35	180
+20% Rhodium	2173	80	480	30	215
+30% Rhodium	2193	95	510	30	–
+40% Rhodium	2213	100	580	30	–
Pt–10Rh + dispersed ZrO_2	2123	240	355	30	190

Source: The PGM database. Available at: www.platinummetalsreview.com/jmpgm/

the metals, and these properties are sometimes utilized for specialist applications. Silver is available in several grades, including fine silver, the normal commercial product containing a minimum of 99.95% silver, and chemically pure silver containing a minimum of 99.99% silver, used for catalytic and special purposes where the presence of certain trace impurities may adversely affect its resistance to corrosion.

Silver is available in many standard forms – sheet, strip, foil of thicknesses down to 0.013 mm, rod, wire down to 0.013 mm diameter, gauze, tubes, bimetal as silver-clad copper or phosphor-bronze, and many others. It is easily fabricated by the normal techniques of rolling, spinning, drawing, etc., and readily binds to itself by fusion-welding using argon-arc welding. Flame welding may be used, but the resulting welds are often not as satisfactory, owing to the possibility of oxygen absorption while the metal is molten, followed by embrittlement by hydrogen. Fine silver filler rods may be used, and hammering the weld fillet down to the contour of the surrounding metal produces a very strong joint.

Gold is an extremely soft and ductile metal and exhibits little work hardening during deformation. Applications of gold are almost entirely restricted to thin linings or electrodeposits on base-metal equipment. It is available for industrial purposes in a grade containing a minimum of 99.9% gold in a wide range of forms – sheet, foil, tube, wire, etc. It is easily fabricated, and when it is being joined to itself, it may be fusion-welded with an oxy-hydrogen flame or hammer-welded at temperatures well below the melting point.

3.21.2.2 Platinum Group Metals

Pure platinum is soft, ductile, and easily fabricated, although its mechanical properties are affected by the degree of cold working and the presence of impurities or alloying constituents. In its applications, it is frequently alloyed with other PGMs; the melting points of its alloys with Rh, Ir, Os, and Ru being higher than the parent metal, those with Pd being lower. In most cases, the strength, rigidity, hardness, and resistance to corrosion are improved by alloying. Contamination with certain base metals (e.g., iron), however, can lead to embrittlement and failure of platinum and its alloys and, for example, if steel tongs are used to handle platinum at high temperatures, then they should be platinum-tipped to avoid iron pick-up.

The PGMs have a range of often unique properties that find critical use in a number of key applications, for example, in automotive catalysts, chemical catalysts, electronics, and jewelry; however, such applications are outside the scope of this chapter. Apart from palladium, the other PGMs are seldom used in isolation for corrosion-resistant applications, mainly because of their cost and availability. Palladium has very similar properties to platinum but is less corrosion resistant. Its remarkable ability to absorb large quantities of hydrogen is used in hydrogen permeation membranes and in similar applications such as solid-state hydrogen reference electrodes. Iridium and osmium are characterized by their extreme densities, their high melting points, and their low ductility and high hardness, which are sometimes utilized in specialist corrosion and wear-resistant applications for hard alloys: for example, the traditional use of iridium–osmium tipped fountain pens and precision pivots and bearings. Rhodium, ruthenium, and iridium are used as alloying additions to platinum in order to improve the mechanical and physical properties. Iridium is used in specialist equipment for fine crystal growth (e.g., in electronics), especially from 1600 to 1900 °C. Both iridium and osmium form oxides that are volatile at modest temperatures, which, in the case of osmium, forms and volatilizes at room temperature.

Platinum is available as sheet, foil down to 0.0064 mm thick, tube, rod, wire down to 0.0064 mm diameter, wire down to 0.001 mm diameter, and clad on thin sections of base metals, for example, copper, nickel, Inconel, etc. Platinum, palladium, and the normal alloys of platinum used in industry are easily workable by the normal techniques of spinning, drawing, rolling, etc. To present a chemically clean surface of platinum and its alloys after fabrication, they may be pickled in hot concentrated hydrochloric acid to remove traces of iron and other contaminants; this is important for certain catalytic and high temperature applications. In rolling or drawing thin sections of platinum, care must be taken to ensure that no dirt or other particles are worked into the metal, as these may later be chemically or electrolytically removed, leaving defects in the platinum.

When platinum or its alloys are joined, properties of the weld or solder must be such that it is no less corrosion- or oxidation-resistant for the application in question than the parent metal. Platinum and its alloys are readily joined to themselves and to certain base metals, for example, iron, nickel, and copper. The principal methods for joining platinum are as follows

1. Fusion welding, using a platinum or alloy filler rod of the same composition as the parent metal and a shielded electric arc or an oxy-hydrogen flame (an oxy-acetylene flame may cause carbon pick-up by the molten metal). The weld fillets are then cold hammered to the contours of the surrounding metal to provide a strong joint.
2. Platinum and rhodium–platinum alloys when cleaned are readily hammer-welded to themselves and to each other at temperatures in the range 800–1000 °C. The welds so produced are completely homogeneous.

3. Fine gold, copper, silver–palladium, or platinum–palladium–gold–copper alloys may be used to solder platinum to itself and to its alloys, or to steels, nickel, etc. No fluxes are used, and soft solders should not be employed.

3.21.2.2.1 Platinum–rhodium

Rhodium alloys readily with platinum in all proportions, although the workability of the resulting alloy decreases rapidly with increasing rhodium content. Alloys containing up to about 40% rhodium, however, are workable and find numerous applications. Alloys that contain more than 40% rhodium, while very difficult to fabricate, are almost immune from attack by oxidizing acids. The Pt–10Rh alloy is particularly resistant to attack by free wet chlorine such as that produced by the combustion of halogenated organic vapors.

The resistance of rhodium–platinum alloys to corrosion is about the same as, or slightly better than, that of pure platinum, but they are much more stable at high temperatures. They have excellent resistance to creep above 1000 °C, a factor which largely determines their extensive use in the glass industry, where continuous temperatures sometimes exceeding 1500 °C are encountered. Rhodium additions to platinum reduce appreciably the volatilization of pure platinum at high temperatures.

3.21.2.2.2 Alloys of platinum with other PGMs

Iridium alloys with platinum in all proportions and alloys containing up to about 40% iridium are workable, although considerably harder than pure platinum. The creep resistance of iridium–platinum alloys is better than that of rhodium–platinum alloys at temperatures below 500 °C. Their stability at high temperatures, however, is lower, owing to the higher rate of formation of a volatile iridium oxide. Additions of ruthenium increase the hardness of platinum substantially, but the limit of workability is reached at about 15% ruthenium. Apart from a somewhat greater tendency to oxide formation at temperatures above 800 °C, the resistance to corrosion of ruthenium–platinum alloys is comparable with that of iridium–platinum alloys of similar composition.

3.21.2.2.3 Dispersion strengthened alloys

Platinum–rhodium alloys are used extensively in high temperature applications for crucibles and related equipment, especially in the glass industry. The increasing cost of rhodium and platinum provides a strong driver to reduce overall costs, and this has led to the development of a range of oxide dispersion strengthened alloys and composite alloys using, for example, platinum coatings on palladium cores.[1] The most common formulation is of zirconia-dispersed Pt–10Rh alloy[2] with somewhat higher room temperature strength than Pt–10Rh and 2–3 times the creep rupture properties of Pt–40Rh at 1400 °C (Table 3).

3.21.3 Thermodynamic Behavior

The behavior of the noble metals (indeed all metals) in different environments is determined by three principal factors:

1. their relative thermodynamic stability (nobility);
2. the formation of passive protective films;
3. their tendency to form complex ions in solution.

In the absence of species that form soluble complex ions, the noble metals are extremely resistant to corrosion by aqueous solutions of alkalis, salts, and acids. However, the resistance of silver to oxidizing acids is generally lower than that of the other noble metals, while in halogen acids, it forms a protective film of insoluble halide. Silver also differs from the other noble metals in forming a sulfide tarnish film in the presence of reduced sulfur compounds. Where complexing species are present and they stabilize the metal ions in solution (e.g., cyanide) the noble metals will corrode.

3.21.3.1 Silver

Silver, with a standard electrode potential $E_{Ag+/Ag} = 0.79\,V$, is exceeded in nobility only by gold and the PGMs. The Pourbaix diagram for silver (Figure 1) shows that at potentials below about 0.4 V and in the absence of complexing ions, silver is immune to attack over almost the whole pH range.

The situation is different in the presence of complexing agents, such as cyanide, or with species with which silver forms an insoluble salt, such as chloride. Thus, the presence of halides (with the exception of fluoride) substantially increases the zone of passivity, because of the formation of halide salt films as passivation layers;[1] at 25 °C, the solubility product of AgCl is 1.7×10^{-10}, of AgBr is 5.0×10^{-13}, and AgI is 8.5×10^{-17}; AgF is soluble. Silver will also passivate in solutions containing sulfate. However, in the presence of sulfide, silver can form Ag_2S tarnish films, even in the absence of air.

Silver, therefore, is thermodynamically stable in reducing acids, for example, hydrochloric acid, acetic

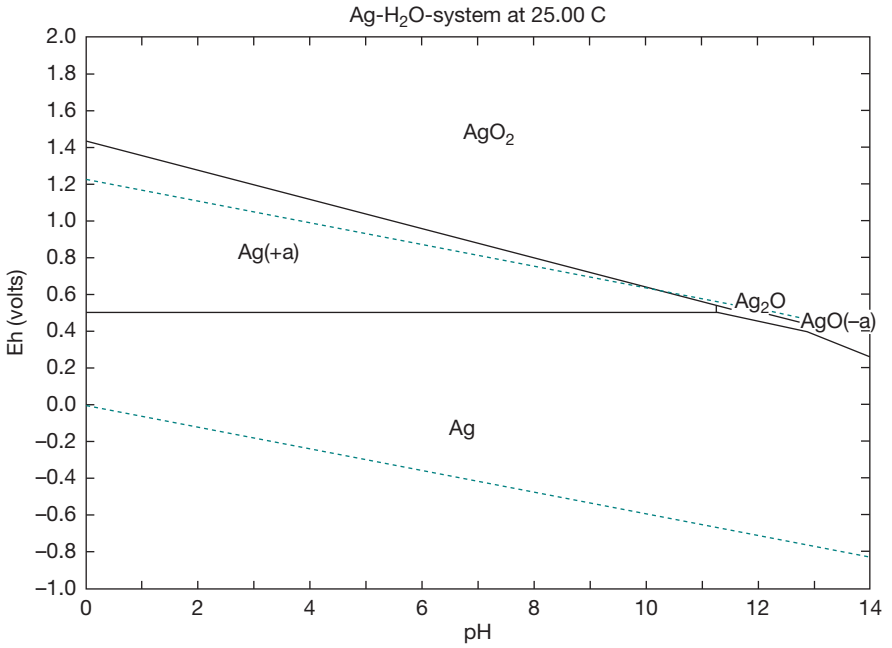

Figure 1 Pourbaix (*E*–pH) diagram for silver at a metal ion concentration of 10^{-5} M. Reproduced from *HSC 6.1: Thermochemical Database*; Outotec, 2007.

acid, phosphoric acid, provided oxidizing substances are absent. Oxidizing acids, for example, nitric acid, hot sulfuric acid at concentrations exceeding 80%, and reducing acids containing oxidizing agents will be corrosive to silver, and the diagram shows that an extensive zone of corrosion occurs at elevated potentials in the acid region. When silver is passivated by a halide film, as is formed for example in hydrochloric acid, the film is tenacious, self-healing, and highly insoluble. However, such films are easily reduced, for example, by galvanic coupling to a less noble metal such as zinc, aluminum, and passive stainless steels and nickel-based alloys. In such instances, silver will continuously corrode. In highly alkaline solution, silver corrodes only within a narrow region of potential, provided complexants and oxidants are absent. It is thus suitable to handle aqueous solutions of sodium or potassium hydroxides at all concentrations; it is also unaffected by fused alkalis.

3.21.3.2 Gold

The high resistance of gold to attack by a very wide range of corrosive media results from its exceptional thermodynamic stability in aqueous conditions. The Pourbaix diagram for gold (**Figure 2**) shows immunity from attack over the whole range of pH values and, uniquely, gold's zone of thermodynamic stability includes the entire region of water stability; thus, it is immune from corrosion in aerated water. Gold, however, is easily complexed, and its solubility in hydrochloric acid containing an oxidizing agent (e.g., nitric acid) results from a combination of high redox potential and the formation of chloroauro complex ions ($AuCl_4^-$). The unstable Au^+ ion and the easily reducible Au^{3+} ion also readily form stable complexes. Gold is unaffected in alkaline solutions, but in the presence of cyanides the soluble $Au(CN)_2^-$ ion is readily formed by air oxidation. This reaction forms the basis for the extraction of gold from its ores on an industrial scale.

3.21.3.3 Platinum Group Metals

All the six PGMs are highly resistant to corrosion by most acids, alkalis, and other chemicals. As may be seen from the potential–pH diagram (**Figure 3**), platinum is immune to attack at almost all pH levels, although it will corrode slowly in aqua regia (concentrated hydrochloric acid + nitric acid). It should also be noted that platinum is significantly less noble than gold and is covered by an oxide film in air (unlike gold, which is oxide free).

Platinum is unaffected by most organic compounds, although some compounds may catalytically decompose or become oxidized on a platinum surface at

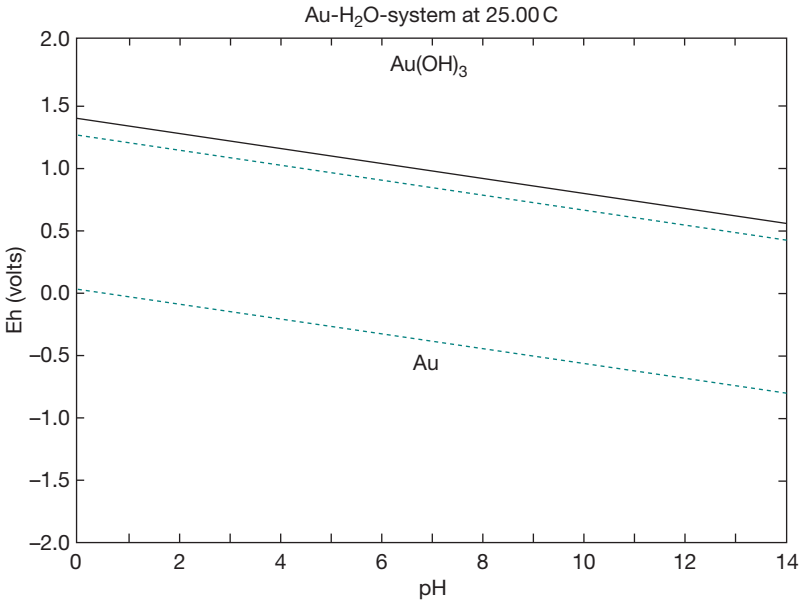

Figure 2 Pourbaix diagram for gold at a metal ion concentration of 10^{-5} M. Reproduced from *HSC 6.1: Thermochemical Database*; Outotec, 2007.

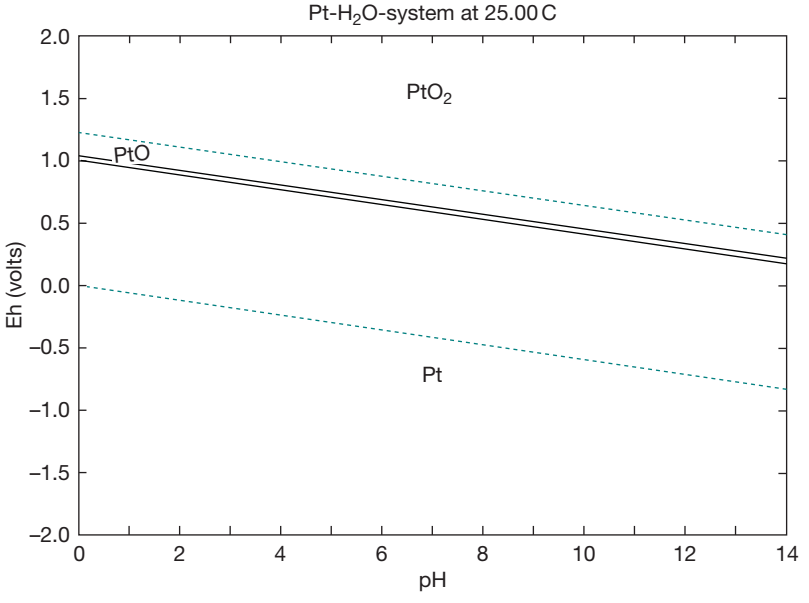

Figure 3 Pourbaix diagram for platinum at a metal ion concentration of 10^{-5} M. Reproduced from *HSC 6.1: Thermochemical Database*; Outotec, 2007.

elevated temperatures, resulting in an etched appearance of the metal.

Compared with platinum, palladium is significantly less noble, as can be seen from its Pourbaix diagram (**Figure 4**), where an extended passive oxide region is notable (PdO) and simple Pd^{2+} aquo-ions are stable at low pH and high potential (compare with platinum). However, palladium is relatively stable in the presence of aqueous solutions of all pH values with the exception of strong oxidizing agents and complexing substances. Nonoxidizing acids, for example, acetic, oxalic, hydrofluoric, and sulfuric acids, have no effect on the metal at ordinary temperatures. Strongly oxidizing acids, however, for example, hydrochloric acid containing nitric acid, rapidly attack palladium. Dilute nitric acid attacks palladium only slowly, but the metal

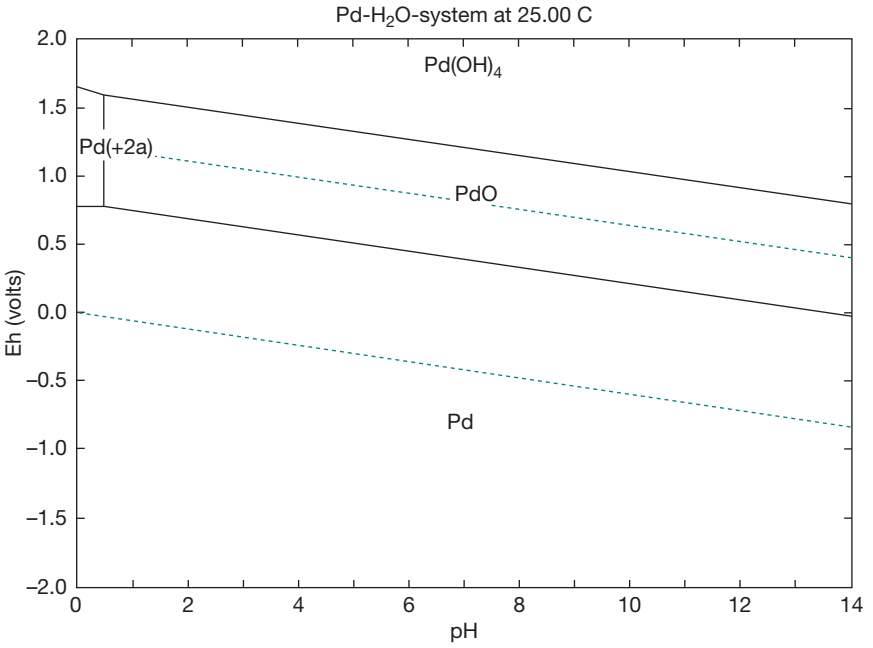

Figure 4 Pourbaix diagram for palladium at a metal ion concentration of 10^{-5} M. Reproduced from *HSC 6.1: Thermochemical Database*; Outotec, 2007.

is rapidly corroded by the concentrated acid. Alloys of palladium with platinum, however, retain most of the corrosion resistance of platinum. In ordinary atmospheres, palladium is resistant to tarnish, but some discoloration due to sulfide-film formation may take place in industrial atmospheres containing sulfur dioxide. Alkaline solutions, even in the presence of oxidizing agents, are without significant effect.

The resistance of rhodium and iridium to chemical attack is very similar to that of platinum, although with a wider domain of stability, particularly, at low pH in oxidizing solution. Additions of rhodium or iridium to platinum generally raise the overall corrosion resistance of the alloy to a very wide range of reagents. Like the other noble metals, in the absence of complexing agents both rhodium and iridium are stable in aqueous solutions at all pH values. Both metals are unattacked by alkalis, acids or oxidizing agents in aqueous solution, although oxidizing molten salts (e.g., potassium nitrate) are more corrosive. Iridium, in particular, has excellent resistance to fused lead oxide, silicates, and molten copper and iron at temperatures up to 1500 °C.

Ruthenium and osmium are decidedly less noble than the other four elements in the platinum group. Both exist in numerous valency states and very readily form complexes. Ruthenium is not attacked by water or noncomplexing acids, but is easily corroded by oxidizing alkaline solutions, such as peroxides and alkaline hypochlorites. Osmium forms a volatile (and toxic) oxide at room temperature in air, and hence, should be handled with care.

3.21.4 Corrosion and Electrochemistry

There is great interest in the electrochemistry of the noble metals; many of them having scientifically interesting and sometimes unique properties that can result in commercially useful attributes, for example, in electrocatalysis. However, it is impossible to provide a fully comprehensive review in this section and it is not even attempted. Thus, the general electrochemistry of the materials is only superficially considered here. From the perspective of corrosion, one of the most interesting and potentially valuable effects is the substantial reduction in the corrosion rate of passive alloys (i.e., stainless steels) as a consequence of the addition of small amounts of noble metal. For further detailed information the reader is referred to the separate chapter on cathodic modification of stainless steels and titanium.

3.21.4.1 Silver

3.21.4.1.1 Anodic processes

Silver generally corrodes anodically below the reversible oxygen potential, unless an insoluble

oxide or salt is formed. When silver is used as an anode in sulfuric acid solutions, its behavior shows an analogy with that of lead. Silver sulfate, Ag_2SO_4, is first formed, and this acts as a passive film.[3] When the potential is raised the sulfate is oxidized to AgO, which may be cathodically reduced back to Ag_2SO_4 at a potential lower than that required for its initial formation. When made anodic in nitrate solutions, silver generally dissolves quantitatively as Ag^+, and this forms the basis of the electrorefining techniques widely used in the industry. Similar considerations apply to the anodic behavior of silver in cyanide solutions, where silver forms a cyanide complex. In chloride solutions, silver anodes become covered with a layer of silver chloride.[4] The anodic oxidation and reduction of silver in alkaline solutions is of interest in battery applications, and a few percent of alloying additions of palladium or gold improve the capacity of silver oxide electrodes.[5]

Silver is not generally resistant to sulfidizing environments, as is commonly demonstrated by the atmospheric tarnishing of silver (see below), generally the formation of a sulfide film of varying thickness. The aqueous corrosion of silver in sulfide solution was studied using electrochemical and analytical methods in order to elucidate the mechanisms.[6] Under anodic polarization, silver initially forms Ag_2S, which is then further oxidized to Ag_2O at higher potentials. The limiting anodic current density was found to be proportional to the sulfide concentration in solution, and this was thought to be due to diffusion of SH^- ion to the silver surface. The reaction rate increased as the pH increased, which is consistent with the change in speciation of SH^- ion in solution; little effect on corrosion rate was found with dissolved oxygen content. X-ray diffraction and Raman spectroscopy indicated the formation of Ag_2S as the main reaction product.

3.21.4.1.2 Atmospheric corrosion and tarnishing

Silver is traditionally used decoratively and functionally in fine cutlery and tableware and is valued for its high luster and long life. It has also been widely used in electrical contact applications because of its high conductivity. Although silver is stable to oxidation, it forms a tarnish film in atmospheres containing inorganic or organic sulfur species and chlorides. This dulls the surface and detracts from appearance; the film also increases contact resistances. Atmospheric levels below 0.1 ppm of H_2S, SO_2, and HCl are sufficient to tarnish silver at measurable growth rates. Dry nitrogen atmospheres stops tarnish film growth, which suggests that the process is electrochemical and occurs in a thin adsorbed water layer on the metal surface and requires air as oxidant.[7] Long chain organic molecules containing sulfur were also found to strongly interact with silver surfaces, giving tarnish films of similar composition to those found in H_2S.[8]

The sulfidation of silver was studied in a tubular reactor, with well-controlled mass transfer characteristics. In dry air, H_2S slowly reacted with silver at a constant rate, independent of the flow. The mechanism is surface controlled, and was found to involve atmospheric oxygen; the rate being increased significantly in the presence of an alternative oxidant (NO_x). In humid air, corrosion was over 1000 times faster, with the kinetics now controlled by mass transfer of H_2S in the gas phase.[9] In a series of comprehensive studies, the effect of carbon oxysulfides (COS) was also investigated and it was concluded that the sulfidation of silver by COS was at least as significant as by H_2S; the detailed mechanisms of film growth were also determined.[10]

Significant research effort has been expended on preventing (or at least reducing) the kinetics of the tarnishing process. These apply one of three strategies: coating the silver, alloying the silver, or use of a tarnish (corrosion) inhibitor. In the electronics sector, electroplating with gold is commonly used in order to limit corrosion of contacts and consequent increase in contact resistance, and is generally a successful solution. However, if the excellent appearance of decorative silver is required, gold plating (i.e., a gilt finish) is not acceptable.

A number of treatments have been considered for tarnish protection, including palladium or rhodium plating (importantly the latter causes very little color change on silver), tarnish inhibitors incorporated into commercial polishes (commonly using organic thiols),[11] treatments with lacquers or plasma-polymerized coatings, and formation of self-assembled monolayers.[12] In a comparative evaluation of their performance, the commercial tarnish inhibitors were found not to provide significant protection, while the most effective treatment was an organic lacquer, followed by rhodium plating and the self-assembled monolayer treatment.[13]

The search for a tarnish-resistant silver alloy has been ongoing for at least 70 years with, until recently, comparatively little success. Although alloys of silver that substitute some of the copper content for palladium, nickel, zinc, or tin do tarnish more slowly than standard sterling silver,[14] they have no compelling advantage. Novel formulations for decorative silver alloys are constrained by the need to stay

within the purity level for hallmarked sterling silver (i.e., more that 92.5% silver content). Until recently, no novel alloy had significant proven advantages in this application. However, an alloy containing germanium has been shown to be relatively resistant to sulfide tarnishing, and is now marketed as 'Argentium.'[15] The improved surface properties are due to preferential oxidation of germanium, resulting in a continuous protective oxide layer, and the high diffusivity of germanium, which permits the layer to be reestablished rapidly if damaged.

3.21.4.2 Gold

3.21.4.2.1 Anodic processes

Gold is thermodynamically stable to corrosion in ordinary aerated noncomplexing environments, and, of course, it neither tarnishes in the atmosphere nor in biological fluids. It is, therefore, ideal for applications in the decorative, medical and dental (*in vivo*), and electrical (contacts and connectors) areas. It is also used extensively (as is platinum) as a nonreactive electrode substrate for laboratory electrochemical studies of redox reactions of species in solution, however, such applications are not within the scope of this discussion.

The anodic oxidation of gold itself is of interest (indeed it is among the most studied of oxidation processes), as it can elucidate generic mechanisms for film formation and metal dissolution under anodic dissolution. In general terms, on anodic polarization in noncomplexing electrolytes, for example, sulfate, perchlorate, hydroxide, etc., gold will reversibly passivate by forming an oxide/hydroxide film above about +1.4 V (SHE) at pH 0. Thus, in sulfuric acid gold dissolves transiently to the Au(I) species but rapidly passives forming a film of hydroxide,[16] containing Au(III) species consisting generally of $Au(OH)_3$. Evidence for lower oxides is no longer convincing. Conway's extensive and thorough review describes in detail the adsorption and oxidation on noble metal surfaces.[17] Unlike conventional corrosion, anodic oxidation on gold proceeds predominantly by surface chemical processes, involving submonolayer adsorption of hydroxide and oxide species (hydroxide electrolytes) that eventually grow by coalescence and thickening, eventually forming a macroscopic multilayer hydrous oxide film, probably by field assisted ion migration. In the presence of other anions, a competitive chemisorption with, for example, HSO_4^-, ClO_4^-, Cl^-, occurs, which inhibits the onset of surface oxidation. Studies using scanning tunneling microscopy (STM) and atomic force microscopy (AFM) on single-crystal gold surfaces has shown the development of single-atom dimensioned pits, and have demonstrated that atomic rearrangement (or dissolution) is more difficult from atom terraces than from edges.[18]

In solutions where gold forms a soluble complex ion, gold may dissolve or may passivate (depending on the concentration of the complexing ion and the potential). On anodic polarization in acidic chloride solutions, gold initially dissolves, due to formation of the $AuCl_4^-$ ion, at potentials greater than about +1.3 V (SHE, pH = 0), depending on the chloride ion concentration; no evidence is seen for dissolution in the Au(I) state. At higher potentials greater than about +1.6 V, gold passivates forming an oxide film.[19] In alkaline cyanide solutions (pH = 13), which are of obvious interest for gold extraction and in electroplating, dissolution proceeds above about −0.66 V (SHE) by competitive adsorption of the cyanide ion on gold, followed stepwise by single-electron transfer and then adsorption of another cyanide ion, leading to the formation of the $Au(CN)_2^-$ ion. No convincing evidence for formation of the Au(III) state, $Au(CN)_4^-$, is found at higher potentials, instead passivation terminates dissolution at potentials above about +0.38 V (SHE, pH = 13) due to formation of an $Au(OH)_3$ film.[20]

In addition to cyanide and chloride, gold forms complexes with a number of other common species in acid or alkaline conditions, including thiosulfate, thiocyanate, thiourea, sulfite, bromide, and iodide. The anodic dissolution of gold in these environments was reviewed by Nicol in 1980.[21] In view of the toxicity of cyanide, there is obvious interest in using alternative leaching agents for gold recovery, and thiourea, thiocyanate, and bromide processes have been considered. Of more academic interest is the surface chemistry and electrochemistry of gold in the presence of sulfur-containing species, where many detailed studies have been carried out; however, these are beyond the scope of this section.

3.21.4.2.2 Gold extraction

Since the late nineteenth century, most recovery of gold from crushed ore has been via the MacArthur–Forrest cyanidation process. This utilizes the stability of the gold cyanide complex ion ($Au(CN)_2^-$: $K = 10^{-38}$) to dissolve gold, which may then be recovered by electrodeposition or via zinc dust (Merrill–Crowe process).[22,23] The principle dissolution reaction is given by Elsener's equation:

$$4Au + 8CN^- + O_2 + 2H_2O \leftrightarrows 4Au(CN)_2^- + 4OH^-$$

For the sake of efficient extraction and to minimize loss of cyanide as volatile HCN, the leaching is done ideally at pH close to 10.5. The cyanidation process requires an oxidant to be present (usually dissolved oxygen), and the efficiency of extraction is reduced if insufficient oxidant is present. Other factors that reduce leaching efficiency (present in so-called 'refractory' ores) include the presence of sulfides, copper, iron, and zinc. Pretreatment of crushed ores is often required as is the use of additional oxidants (chemical or biological – i.e., sulfur oxidizing bacteria).

Once leached, the gold has to be recovered from the relatively dilute cyanide solution. One of the largest gains in efficiency of gold recovery from more dilute cyanide liquors is the absorption of the gold complex on activated carbon, and a variety of processes are in use, for example, the carbon-in-pulp process.[22] For cyanide processes, there is also the considerable problem of cyanide disposal. To counter this, various other processes have been considered, with some in active development. These include the use of bromine, chlorine, thiourea, and thiosulfate. Although these have advantages, much research needs to be done to optimize them. Currently, therefore, the cyanide process is generally still the most economical.

3.21.4.2.3 Dealloying and nanoporous materials

Dealloying as a corrosion phenomenon has been known for over 100 years, the classical case being dezincification (i.e., selective dissolution of zinc from brass leaving a copper-rich, mechanically weak, layer). Dealloying typically occurs in an alloy where at least two of the components have relatively well-separated equilibrium potentials in the environment. In such cases, where the alloy is polarized between these values, the less noble component of the alloy is selectively dissolved, leaving the remaining more noble component. This mechanism invariably produces layers that have profoundly altered mechanical properties usually of very low fracture toughness (i.e., they are brittle). These have been found to have profound influence on many stress-corrosion cracking processes in alloys.[24,25] Although it was not called such, and the mechanism was not then known, dealloying was first developed as a process to produce porous nickel (by selective dissolution of aluminum from a nickel–aluminum alloy – Raney nickel), which is used a catalyst in various chemical processes.[26]

Selective dissolution in, for example, Cu–Au and Ag–Au alloys has been well studied in order to determine generic aspects of the dealloying mechanism in these and other more commercially important alloys. Increasingly, controlled dealloying is being used in its own right to produce tailored nanoporous gold substrates for chemical sensing and catalytic applications. The ordered intermetallic alloy Cu_3Au is an excellent template to study dealloying phenomena. At low overpotentials for copper dissolution, scanning tunneling microscopy has demonstrated 2-dimensional clustering of gold, while at higher overpotentials the surface is mostly covered by gold and effectively passivates in two dimensions, although small regions of material continue to dissolve generating 3-dimensional roughness and porosity.[27] Above a threshold potential, global surface roughening occurs, which is strongly influenced by adsorption of species such as sulfate, chloride, and alkyl-thiols on the surface of the gold atoms. This process has been modeled using a continuum model such that porosity during dealloying develops on a length scale that is characteristic of the surface aggregation (diffusion) of the noble metal atoms.[28]

The formation of nanoporosity in $Ag_{0.7}Au_{0.3}$ and $Ag_{0.65}Au_{0.35}$ alloys during dealloying in perchloric acid has been studied. Without halide addition, the pores were of the order of 8 nm, while with chloride, bromide, and iodide, the pore size changed, respectively, to 17, 16, and 67 nm. This coarsening can be interpreted as an increase in surface mobility of the gold atoms in the presence of halides.[29] Gold substrates with tailored nanostructures can thus be prepared by controlled electrochemical dealloying. Although development is still required, in particular, to resist coarsening of the porosity during application, nanoporous gold substrates have many potential applications, for example, in electrocatalysis,[30] fuel cells,[31] and chemical and biochemical sensing.[32]

3.21.4.3 Platinum Group Metals

3.21.4.3.1 Anodic processes

The PGMs are characterized by their intrinsic thermodynamic stability and in this they are similar to gold. The key difference between them is that gold remains oxide-free in aerated noncomplexing aqueous environments; however, the PGMs are predicted to retain an oxide film that contributes to their passivity. The PGMs have many important properties and applications in catalysis, which are beyond the scope of this section.

For many years, it was assumed that platinum and other PGMs were oxide-free in air and in aerated

solutions; however, the advent of rapid cyclic sweep voltammetry techniques has allowed the elucidation of the redox processes between platinum and oxygen, and this research was reviewed extensively by Conway in 1995.[17] After initial adsorption of oxygen-containing species, a place exchange mechanism takes place between Pt and O to effectively develop a 2-dimensional and then a 3-dimensional oxide film. Oxygen adsorption, reduction, and place exchange occur via a variety of steps, with the rate-determining processes for each part of the mechanism determined; however, a full discussion is well beyond the scope of this chapter. Like gold oxide, formation on, and dissolution of, platinum occurs as a function of crystallography. On low-index surfaces, oxide formation passivates the surfaces more easily, resulting in lower dissolution rates at higher potentials, while nanofaceted surfaces dissolve more rapidly, which is the evidence that atomic edges and corners are the main locations of dissolution.[33] Perhaps the most interesting finding is that although like gold, anion adsorption plays a role, it appears to be much less important, which reflects the increased stability of PGMs to complexing species such as halides, cyanides, etc.

PGMs are, therefore, extremely resistant to dissolution in almost all aqueous environments under almost all conditions. For example, and in contrast to gold and silver, high pressures and temperatures are required for the dissolution of platinum in cyanide to occur at significant rates. Table 4 shows the corrosion resistance of the PGMs in various environments; importantly, PGMs are one of the few non-polymeric materials that can successfully handle fluorides and HF without significant problems.

Table 4 Corrosion resistance of PGMs in various environments

Environment	*Ru*	*Rh*	*Pd*	*Os*	*Ir*	*Pt*
HF (40%, 20 °C)	A	A	A	A	A	A
HCl (36%, 100 °C)	A	A	B	A	A	B
H_2SO_4 (96%, 100 °C)	A	B	C	A	A	A
HNO_3 (62%, 100 °C)	A	A	D	D	A	A
$HCl + HNO_3$ (aqua regia, 100 °C)	A	A	D	D	A	D
H_3PO_4 (100 °C)	A	A	B	D	A	A
$HClO_4$ (100 °C)			C			A
KCN (100 °C)			D			C
NaOCl (100 °C)	D	B	C	D		A

A – No attack; B – Minor attack but can be used; C – Major attack and cannot be used; D – Rapid attack.
Source: Darling, A. S. In *Electronic Design Materials*; Waller, W. F., Ed.; Macmillan, 1971; Chapter 3.

3.21.4.3.2 Platinum extraction and secondary recovery

As noted earlier, ambient temperature and pressure cyanide leaching is not effective for the recovery of PGMs from crushed ore bodies. Thus, after mining and concentration by gravity and/or froth flotation, the materials are smelted on a copper–nickel matte (sulfide-rich intermediate), which is further separated into copper and nickel anode materials and are purified electrolytically. The PGMs remain within the (insoluble) anode slime and were traditionally recovered using wet chemical methods, including sequential precipitation. Current technology uses a liquid–liquid solvent extraction technique that is more efficient, offering enhanced recovery and lower cost.[34]

Efficient secondary recovery of PGMs from, for example, vehicle exhaust catalysts, and recovery and separation from other metals from, for example, electronic circuit boards, is critical for their sustainable use. In such cases, higher temperatures and pressures, as well as more corrosive solutions, can be used. Several leaching processes have been proposed, the majority using strong hydrochloric acid containing an oxidant (i.e., aqua regia)[35,36] at high temperature and pressure leaching with cyanide.[37,38] The pressure cyanide processes are better developed and can, under ideal conditions, extract over 95% of the platinum and palladium and about 85–90% of rhodium.

3.21.4.3.3 Cathodic processes: Hydrogen evolution

The PGMs are well-known for their outstanding electrocatalytic activity, especially for the evolution of hydrogen. The exchange current density for the overall hydrogen evolution reaction

$$2H^+ + 2e^- \leftrightarrows H_2(g)$$

varies by about 10 orders of magnitude from mercury and lead to platinum (Table 5).

The large exchange current density of PGMs implies a correspondingly low overpotential for hydrogen evolution. This property finds extensive applications in electrocatalysis in general, and in hydrogen storage and release, hydride batteries, and fuel cells, where nanosized PGM particles are used, to increase surface area and to reduce the quantity of expensive material used. An important application is noble metal alloying of passive metals (stainless steels and titanium), where small amounts (0.2%) of noble metals (typically Pt, Pd, or Ru) causes spontaneous passivation in acids by increasing the cathodic rate of hydrogen evolution.

Table 5 Exchange current densities for the evolution of hydrogen on various metals in various environments

Environment	*Metal*	*Exchange current density, i_o ($A\,cm^{-2}$)*
1 M H_2SO_4 at 20 °C	Palladium	$10^{3.0}$
	Platinum	$10^{3.1}$
	Rhodium	$10^{3.6}$
	Iridium	$10^{3.7}$
	Nickel	$10^{5.2}$
	Gold	$10^{5.4}$
	Titanium	$10^{8.2}$
	Aluminium	$10^{-10.0}$
	Lead	$10^{12.0}$
	Mercury	$10^{12.3}$
0.1 M HCl at 20 °C	Platinum	$10^{-2.6}$
	Palladium	$10^{-3.2}$
	Silver	$10^{-5.6}$
	Gold	$10^{-5.6}$
	Iron	$10^{-6.0}$
	Nickel	$10^{-6.0}$
	Copper	$10^{-6.8}$
	Lead	$10^{-13.2}$

Source: Parsons, R. *Handbook of Electrochemical Constants*; Butterworths, 1959.
Bockris, J. O. M.; Reddy, A. K. N. *Modern Electrochemistry*, 2nd ed.; Springer, 1998.

The PGMs are somewhat susceptible to a reduction in their catalytic activity as a consequence of 'poisoning' with other surface active species, including metallic impurities with lower exchange current density, which will tend to plate out onto cathodically polarized surfaces.[39] On the other hand, noble metal oxides, in particular, ruthenium and iridium oxide, are almost as effective cathodic electrocatalysts as platinum and palladium; they are almost immune to poisoning by metal ions in solution.[40,41]

3.21.5 High temperature Properties

3.21.5.1 Silver and Gold

Owing to their relatively low melting points and mechanical strengths, silver and gold find very few applications at elevated temperatures. Silver below its melting point has considerable resistance to oxide-film formation, but molten silver dissolves appreciable quantities of oxygen, which precipitates as silver oxide or bubbles dispersed throughout the metal when the metal solidifies. Gold is not subject to oxide-film formation at any temperature up to its melting point, but may be covered by a thin adsorbed layer of oxygen. The absence of an oxide film enables gold to be pressure-welded at room temperatures.

3.21.5.2 Platinum Group Metals

The excellent resistance of platinum, rhodium, and iridium to oxidation at high temperatures finds numerous applications in technology, in particular, in the form of platinum-based alloys. Osmium and ruthenium form volatile oxides and are therefore not suitable for high temperature use on their own.

Platinum, while it does not form a measurable oxide film, is covered by thin adsorbed layer of oxygen,[42] which volatilizes at an increasing rate as its temperature rises above 1000 °C, via a volatile metastable oxide.[43] In the presence of flowing oxygen or air, the rate of volatilization is considerably increased. Rhodium, iridium, and palladium exhibit oxide-film formation, at a temperature as low as 600 °C.[44] However, palladium oxide dissociates above 870 °C, the metal then appearing bright up to its melting point. Absorption of oxygen without film formation occurs, however, and palladium increases in weight. Platinum looses more mass via this volatilization mechanism compared with rhodium and iridium, from 900 to 1200 °C, but their volatilities are about the same at temperatures around 1300 °C. However, below 1100 °C, alloys of platinum with rhodium and palladium loose less mass than do pure platinum, but palladium–platinum alloys absorb oxygen detrimentally. Rhodium–platinum alloys at high temperatures show no preferential loss of either metal, and are widely used. Iridium–platinum alloys show greater loss of weight on heating in air, because of the greater rate of oxidation of iridium and the higher volatility of the oxide of this metal. Iridium is thus lost preferentially from iridium–platinum alloys. Selected properties of the PGM oxides are shown in **Table 6**.

Volatilization of platinum and its alloys at high operating temperatures may be substantially reduced by avoiding contact with air or oxygen, especially if the environment is flowing, for example, due to convection currents. This may be achieved by completely embedding the metal in high-purity alumina refractory; flame-sprayed coatings, for example, are effective in preventing free circulation of air over the metal. Only alumina that is largely free from silica and other oxides that are more easily reduced can be used, otherwise contamination and embrittlement of the platinum may result from partial reduction of such oxides.

Grain growth of platinum and its alloys when operating continuously at high temperatures is often responsible for failure of the metal, resulting from weaknesses developed by large intercrystal boundaries. This defect may be largely eliminated by the use of

Table 6 Selected properties of PGM oxides

Oxide	*Molar Mass*	*Density*	*Pilling–Bedworth ratio*	*Properties at high temperature*
RuO_2	133.1	6.97	2.31	Dissociates at 930–950 °C
RuO_4	165.1		–	Sublimes at 40 °C
RhO	118.9			Dissociates above 1000 °C
Rh_2O_3	253.8	8.2	1.87	Dissociates above 1100 °C
PdO	122.7	8.31	1.66	Dissociates above 870 °C
OsO_2	222.2	11.29	2.33	Dissociates at 650 °C
OsO_4	254.2	4.95	6.09	Boils without decomposition at 131 °C
IrO_2	224.2	11.69	2.24	Decomposes at 400 °C
PtO	211.1	14.9	1.56	Dissociates above 1100 °C
Pt_3O_4	649.3	8.89	2.68	Decomposes when heated
PtO_2	227.3	10	2.63	Thermally unstable

Source: Savitskii, E. M. *Physical Metallurgy of Platinum Group Metals*; Elsevier, 1979.

sintered metal produced by powder-metallurgical techniques, or by the incorporation of a small amount of a refractory oxide, carbide, or nitride in powder form in the body of the metal, such as zirconia-dispersed platinum–rhodium alloys.[44]

3.21.6 Selected Applications

3.21.6.1 Chemical Process Equipment

3.21.6.1.1 Linings

Traditionally, noble metal linings were used in chemical and pharmaceutical production as linings for steel and copper equipment and occasionally as vessels, condensers, and other equipment. However, such uses have generally been superseded either by more cost-effective coating materials (e.g., tantalum, glass lining), or alternative construction materials (e.g., stainless steel, graphite).

Linings may be of two types: either loose or bonded. Loose linings provide good contact between vessel and lining – adequate for good heat transfer – but are not suitable to be used in reduced pressure as the gap between vessel and lining will expand causing the lining to fail. Traditionally, silver linings for chemical plant were used particularly for highly alkaline environments in which silver has excellent performance; where used, silver linings are generally 0.5–1 mm thick. Solid silver construction, 1–2.5 mm thick, may be employed for condenser coils, distillation heads, etc. Traditional bonded silver linings for mild steel or copper vessels are generally soldered *in situ* onto the walls of the vessel using a tin–silver solder. Such soft-soldered linings should not exceed 200 °C for their maximum continuous operating temperature. However, bonded linings are suitable for operation under vacuum conditions, and provide excellent heat-transfer characteristics.

Platinum, rhodium–platinum, and iridium–platinum alloys are employed in line and sheath autoclaves,[45] reaction vessels and tubes, calorimeters,[46] and a range of other laboratory and commercial equipment.[47] Linings are generally 0.13–0.38 mm thick, and for certain applications coextruded platinum-lined nickel-based alloys (Inconel 625), or other metal reactor or cooling tubes are fabricated. In such cases, the platinum is bonded to the base metal, but in all other instances platinum linings are of the 'loose' type.

3.21.6.1.2 Bursting discs

Bursting discs are a simple and effective (fail-safe) protection against overpressurization in a closed system. The protection of pressure vessels containing corrosive materials presents a special problem for the selection of bursting discs as bursting discs should not corrode (and hence weaken) until they are required to fracture under an overpressure. For this reason, corrosion resistant, high reliability bursting discs have been traditionally fabricated from noble metals,[48] although other cost-effective alternatives now exist (e.g., tantalum or niobium). The recommended maximum temperatures for continuous use are 80 °C for gold, 150 °C for silver, 300 °C for palladium, and 450 °C for platinum.

3.21.6.1.3 Spinnerets

The spinning of viscose rayon for the production of yarn, tire cord, and staple fiber involves the extrusion of an alkaline solution of cellulose into an acid bath. The orifices through which individual fibers are extruded are often extremely small – down to

30 μm or less in diameter – and their dimensional accuracy must be maintained to a very high degree for long periods, while operating in two highly corrosive media simultaneously. Platinum–gold alloys are the traditional material of construction for rayon spinnerets, in particular, Au–30Pt + 0.5Rh as a grain-refining additive. This alloy has greater hardness, which permits a high polish to be produced in a scratch-resistant exit face, while the small grain size ensures that the holes produced have a high grade of uniform circularity. Other noble metal alloys for spinneret construction include rhodium–platinum, iridium–platinum, iridium–rhodium–platinum, ruthenium–platinum, ruthenium–palladium, and platinum–palladium. The use of these alloys in this application is being superseded by the introduction of tantalum, which has comparable corrosion resistance at lower cost.[49]

3.21.6.2 High temperature Materials

3.21.6.2.1 Molten glasses and salts

A principal application of PGM metals is in the production of fine, optical glasses and glass fibers; platinum-alloy crucibles and spinnerets are generally resistant to molten glasses at temperatures from 1200 to 1500 °C, with continuous operation at 1400 °C. Traditionally, Pt–Rh alloys were used for this purpose with typically 10% Rh added to improve high temperature creep-rupture performance and to reduce evaporation loss. Useful gains in creep-rupture properties can be made using zirconia-dispersed materials, either of pure platinum or of Pt–10Rh alloy.[2] Materials may be used as sheet for fabricated metal crucibles, as thin foil liners for covering ceramic (i.e., alumina) crucibles, and as flame-sprayed coatings[50] on a ceramic substrate. Also, flame-sprayed or plasma-evaporated alumina coatings can be used to protect PGM materials from evaporation losses at high operation temperatures.[51]

Platinum is generally highly resistant to air-saturated oxide glasses because of the formation of a thin stable layer of oxide that passivates the metal.[52] Stressing during immersion in molten glass (and hence cracking the passive oxide) greatly increases the dissolution rate of the metal in the glass.[53] Under reducing conditions, for example, nonoxide glasses and/or with an inert gas atmosphere, platinum is much less resistant to molten glass, with increased dissolution and additional reaction to form embrittling intermetallic compounds.[54] Where platinum cannot be used, or where even higher temperatures are required (1500–2000 °C), iridium crucibles can be used.[55]

Platinum crucible materials are also generally suitable for containing molten salts over similar temperature ranges as for molten glass. However, salts that can easily form complex ions with platinum will cause its corrosion; also, coupling to other metals can result in enhanced dissolution if it encourages the formation of the complex ionic species in the melt.[56] Platinum and iridium crucibles and equipment are extensively used in single crystal growth production from molten precursors.

3.21.6.2.2 Metal joining

Solders and brazes (although the distinction is not clear, solders are useful for 'lower' temperatures, while brazes are suitable for 'higher' temperatures) are widely used materials for metal joining. Their key characteristics are that

1. their melting point is lower than the parent material to be joined;
2. a metallurgical bond, usually by intermetallic development or interdiffusion, is formed between the solder and the parent material.

One common formulation of a tin-based lead-free solder contains several percent silver and is more corrosion resistant than the material it replaces. For use in higher temperature, silver-based brazing alloys are widely used. In both cases, galvanic corrosion of the parent (joined) material should be considered as the joining alloy is commonly significantly more noble. Thus, where silver brazing alloys are used to join stainless steel, a narrow zone of corrosion on the stainless steel often occurs on subsequent exposure in tap water.[57]

PGM brazing alloys, commonly containing palladium with alloying additions, including gold, silver, nickel, copper, are also utilized. They have significant advantages, including high temperature strength and stability as well as corrosion resistance, and have been used to join stainless steels,[58] nickel-based superalloys,[59] and other refractory materials, with minimal corrosion problems. Their low vapor pressure gives them advantages in high vacuum systems, and their low toxicity (if nickel-free) gives them advantages as a dental brazing alloy.[60]

3.21.6.2.3 Furnace windings

Rhodium–platinum alloys containing up to 40% Rh have been traditionally used in the form of wire or

ribbon in electrical resistance windings for furnaces to operate continuously at temperatures up to 1750 °C. Such windings are usually completely embedded in a layer of high-grade alumina cement or flame-sprayed alumina to prevent volatilization losses from the metal due to the free circulation of air over its surface. However, these types of furnace windings have been largely superseded by molybdenum disilicide materials, which are resistant in air at a similar temperature. For reducing (hydrogen) atmospheres, Pt–Rh alloy windings are still useful, although molybdenum metal windings may also be used at considerably lower cost.

3.21.6.2.4 Temperature measurement

Until 1968, platinum–rhodium thermocouples (type S) were used as the standard interpolating thermometer in IPTS-68 (International Practical Temperature Scale of 1968) because of their good thermal stability. However, the present temperature scale ITS-90 (International Temperature Scale of 1990) now uses a Standard Platinum Resistance Thermometer.[61] The particular advantages of PGM materials in temperature measurement are, of course, their excellent stability to oxidation and corrosion. Thus, platinum resistance thermometers offer a more reliable temperature measurement than the traditional thermocouples up to around 600–650 °C and are unaffected by the environment. At higher temperatures, Pt/Pt–10Rh (type S) or Pt/Pt–13Rh (type R) thermocouples may be used for accurate temperature measurement in essentially all atmospheres up to 1450 °C. Both types of thermocouple have a short-term stability, typically better than 0.5 °C, with a long-term reproducibility of better than 2.0 °C. For higher temperatures up to 1800 °C, Pt–6Rh/Pt–30Rh (type B) thermocouples can be used.

3.21.6.2.5 Gas turbine applications

Improvements to gas turbine operating efficiency require an increase in the gas temperature of the turbine and combustion chamber. Since most gas turbine materials are now optimized more for their high temperature strength and creep resistance, their hot corrosion and oxidation resistance has become relatively poorer. Platinum aluminide coatings have been developed, which, in combination with other coating types, offer improved performance for nickel-based superalloys.[62] Platinum, by substituting for nickel in the aluminide, eliminates chromium-rich precipitates from the outer coating layer and limits the diffusion of refractory transition elements such as molybdenum, vanadium, and tungsten into the outer coating layer.[63]

3.21.6.3 Dental and Medical Applications

3.21.6.3.1 Dental restorations

Generally, the noble metals, particularly gold, have excellent biocompatibility, and the use of gold and gold–palladium alloys in dental restorations is very common. However, they are too soft to be used on their own and require alloying (typically with copper, silver, and palladium, plus other minor components), and this increases corrosion susceptibility. There are a number of classification schemes for these alloys: First, based on their strength, and second, on their metal content. There are numerous alloys, many proprietary and many designed for specific aspects of the dental restoration task; the main classes are listed in Table 7.

The oral environment is corrosive and materials for use must be correspondingly corrosion resistant; thus, the general corrosion of dental alloys is of interest partly with a view to increase the service life of implants and partly for biocompatibility. The main issues are

1. tarnishing and discoloration, usually caused by foods and drinks that contain sulfur;[64]
2. galvanic corrosion between adjoining oral alloys of differing composition;[65]
3. galvanic corrosion caused by microsegregation of alloy components at grain boundaries or in the interdendritic regions in cast materials.

Failure modes exhibited include generation of expansive corrosion products causing disbonding of the implant, general thinning of the material, and cracking.

Table 7 Classification for dental alloys

	Yield stress (MPa)	*Elongation (%)*
Type I	<140	18
Type II	140–200	18
Type III	200–340	12
Type IV	>340	10
	Typical composition	
High noble	Au > 40% + total noble metals > 60%	
Noble	Total noble metals > 25%	
Base	Total noble metals < 25%	

Source: Wataha, J. C. *J. Prosth. Dent.* **2002**, *87*, 351–363.

Conventional mercury amalgam restorations are typically anodic to noble and more noble alloys and will corrode preferentially[66] and can lead to cracking. Therefore, care has to be taken in mixing restorative alloy materials. For example, cracking of gold crowns has been observed as a consequence of intergranular–interdendritic corrosion in association with corrosion of an underlying mercury-based amalgam alloy.[67] Electrochemical and corrosion tests in ammonium and sodium sulfide solutions, as a simulation of the oral environment, has demonstrated that the tarnishing is particularly related to the silver and copper contents of the alloys.[68] Generally, as might be expected, the higher the noble metal content of the alloy used, the more the corrosion resistant;[69] hence, selection of the correct restorative alloy is a balance between mechanical and other required properties and corrosion resistance.[70]

3.21.6.3.2 *Medical sensing and electrodes*

Unalloyed noble metal (or high noble metal content) body implants are used for a number of purposes, with generally few or no corrosion issues arising. Reference above has been made to the production of nanoporous gold electrodes of exceptionally high surface area. These have a number of potential applications in medical sensing; for example, insulin determination.

Noble metals, particularly platinum and platinum alloys, find use as electrode materials for *in vivo* nerve stimulation (e.g., heart, neural, auditory electrode implants, etc.). The applied potentials used are generally transient in nature (i.e., a pulse waveform), and significant corrosion of electrode materials can be observed. For example, Pt, Au, Rh, Ir, Pt–10Ir, and Pt–10Rh electrodes were severely corroded under a bipolar current pulse of $1\,A\,cm^{-2}$, while Rh was moderately attacked. At $0.1\,A\,cm^{-2}$, Au, Rh, and Ir were resistant to corrosion.[71] However, although examination of heart pacemaker electrodes has shown evidence of corrosion in all cases, in no case had this resulted in the failure of the implant.[72]

3.21.6.4 Electrical Contact Materials

High reliability electrical contacts are frequently plated with noble metals (Ag, Au, Pd, etc.) in order to limit any corrosion and consequent increase in contact resistance with time. This is because uncoated copper contact materials are particularly susceptible to corrosion and contact failure mechanisms involving vibration (e.g., in motor vehicles), giving rise to wear-fretting effects in addition to corrosion.

Silver coatings are liable to grow intrusive whiskers in sulfidizing, and to a lesser extent in chloridizing environments, although much less than copper or tin. The main environmental driver is the presence of hydrogen sulfide at or above 200 ppb, which can be reached, for example, in pulp and paper processing,[73] where significant failures have occurred.

Gold alloys and gold coatings are also extensively used for electrical contacts, especially in the electronics industry. Corrosion failure mechanisms are associated with the growth of gold shorts from cathodic conductors, especially where chloride ions are present. On anodically biased conductors, a voluminous reaction product of $Au(OH)_3$ is produced by anodizing.[74,75]

3.21.6.5 Anodes

3.21.6.5.1 *Dimensionally stable anodes*

Nonconsumable anode materials are used extensively in electroplating, electrowinning, chlorine production, and water electrolysis (oxygen evolution) and have traditionally variously utilized silver, lead, magnetite, graphite, and noble metals. Of these, chlorine production by electrolysis of brine is among the most energy intensive and industrially important.

For chlorine evolution, platinum generally shows very low rates of attack, and platinum anodes can be used for both cathodic protection in seawater and for chlorine production at low overvoltage.[76] This attribute takes advantage of using platinum-coated titanium or niobium substrate materials; the substrates are stable to the conditions of electrolysis, while the electrode reaction (e.g., chlorine evolution) occurs on the platinum surface. At low current densities, the platinum can be corroded, especially at low pH; however, at high current densities, passivation of the platinum occurs and corrosion reduces considerably. However, the corrosion rate of platinum can be much higher if an alternating current component is present, as this tends to thicken the passive film. Rhodium and iridium are as resistant to anodic corrosion as platinum, but are more resistant to the influence of alternating currents.

The single most important advance in anodes for chlorine evolution is in the replacement of noble metal coatings on stable substrates with oxide coatings using ruthenium modified by iridium ('mixed metal oxides').[77] These provide efficient production of chlorine at low overvoltage, with no corrosion, provided the overpotential is kept below a critical value.[78] Such anodes are called 'dimensionally stable'

because, in principle, they do not need replacement throughout the life of the plant, provided they are operated within the correct parameters.[79] They are also responsible for a reduction of about 20% in the energy usage per unit of chlorine production.

Given the success of noble metal oxide-doped anodes in chlorine evolution, they are being trialed in a number of other applications that would benefit from improved electrocatalysis.

3.21.6.5.2 Cathodic protection

Although there are a wide range of possible anode systems for impressed current cathodic protection, noble metal-coated titanium mesh anodes have been used for many years in a wide variety of applications, including protection of reinforcement steel in concrete and cathodic protection systems in seawater (e.g., for vessels, etc.). In severe environments, or where the system requires a high driving voltage, platinum-coated niobium anodes are used because of the increased stability of niobium (compared with titanium) to chlorides. More recently, the use of noble metal oxide-coated electrodes has also become increasingly important, with their advantages of higher current density and increased lifetime under polarization.[80]

References

1. Rowe, M. S.; Heywood, A. E. *Mater. Des.* **1984**, *5*, 30–33.
2. McGrath, R. B.; Badcock, G. C. *Platinum Met. Rev.* **1987**, *31*, 8–11.
3. Jones, P.; Thirsk, H. R. *Trans. Faraday Soc.* **1954**, *50*, 732–739.
4. Altukhov, V. K.; Shatalov, V. G. *Sov. Electrochem.* **1998**, *23*, 912–915.
5. Grozdić, T. D.; Stojić, D. L. *J. Power Sources* **1999**, *79*, 1–8.
6. Lee, J. I.; Howard, S. M.; Keller, J. J.; Cross, W.; Han, K. N. *Metall. Mater. Trans. B* **2001**, *32*, 895–901.
7. Rice, D. W.; Peterson, P.; Rigby, E. B.; Phipps, P. B. P.; Cappell, R. J.; Tremoureux, R. *J. Electrochem. Soc.* **1981**, *128*, 275–284.
8. Sinclair, J. D. *J. Electrochem. Soc.* **1982**, *129*, 33–40.
9. Volpe, L.; Peterson, P. J. *Corros. Sci.* **1998**, *29*, 1179–1187, 1189–1196.
10. Graedel, T. E. *J. Electrochem. Soc.* **1992**, *139*, 1963–1970.
11. Kartlucke, D.; Scholz, R. R.; Funk, M. J.; Baumgartner, M. E. *Galvanotechnik* **1992**, *83*, 1918–1926.
12. Burleigh, T. D.; Gu, Y.; Donahey, G.; Vida, M.; Waldeck, D. H. *Corrosion* **2001**, *57*, 1066–1074.
13. McEwan, J. J.; Scott, M.; Goodwin, F. E. In Proceedings of the South African Institute of Mining and Metallurgy, 8th International Corrosion Conference, Johannesburg 2006.
14. Ray, K. W.; Baker, W. N. *Indust. Eng. Chem.* **1932**, *24*, 778–781.
15. Johns, P. G.; Davis, S. In Proceedings of the 31st International Precious Metals Institute Conference 2007.
16. Jirsa, F.; Buryanek, O. Z. *Z. Elektrochem. Angew. Physik. Chem.* **1923**, *29*, 126–135.
17. Conway, B. E. *Prog. Surf. Sci.* **1995**, *49*, 331–452.
18. Schneeweiss, M. A.; Kolb, D. M.; Liu, D.; Mandler, D. *Can. J. Chem.* **1997**, *75*, 1703–1709.
19. Ye, S.; Ishibashi, C.; Shimazu, K.; Uosaki, K. *J. Electrochem. Soc.* **1998**, *145*, 1614–1623.
20. Kirk, D. W.; Foulkes, F. R.; Graydon, W. F. *J. Electrochem. Soc.* **1978**, *125*, 1436–1443; *J. Electrochem. Soc.* **1979**, *126*, 2287–2288.
21. Nicol, M. J. *Gold Bull.* **1980**, *13*, 46–55, 105–111.
22. Marsden, J. O.; House, C. I. *The Chemistry of Gold Extraction*; Society of Mining Engineers, 2006.
23. Prasad, M. S.; Mensah-Biney, R.; Pizarro, R. S. *Miner. Eng.* **1991**, *4*, 1257–1277.
24. Sieradzki, K.; Kim, J. S.; Cole, A. T.; Newman, R. C. *J. Electrochem. Soc.* **1987**, *134*, 1635–1639.
25. Newman, R. C.; Corderman, R. R.; Sieradzki, K. *Br. Corros. J.* **1989**, *24*, 143–148.
26. Raney, M. US Patent 1,628,190, 1927.
27. Moffat, T. P.; Fan, F.-R. F.; Bard, A. J. *J. Electrochem. Soc.* **1991**, *138*, 3224–3235.
28. Erlebacher, J.; Aziz, M. J.; Karma, A.; Dimitrov, N.; Sieradzki, K. *Nature* **2001**, *410*, 450–453.
29. Dursun, A.; Pugh, D. V.; Corcoran, S. G. *J. Electrochem. Soc.* **2003**, *150*, B355–B360.
30. Jia, F.; Yu, C.; Ai, Z.; Zhang, L. *Chem. Mater.* **2007**, *19*, 3648–3653.
31. Zhang, J.; Liu, P.; Ma, H.; Ding, Y. *J. Phys. Chem. C* **2007**, *111*, 10382–10388.
32. Hu, K.; Lan, D.; Li, X.; Zhang, S. *Anal. Chem.* **2008**, *80*, 9124–9130.
33. Komanicky, V.; Chang, K. C.; Menzel, A.; Markovic, N. M.; You, H.; Wang, X.; Myers, D. *J. Electrochem. Soc.* **2006**, *153*, B446–B451.
34. Charlesworth, P. *Platinum Met. Rev.* **1981**, *25*, 106–112.
35. Tyson, D. R.; Bautista, R. G. *Separ. Sci. Technol.* **1985**, *22*, 1149–1167.
36. Gaita, R.; Al-Bazi, S. J. *Talanta* **1995**, *42*, 249–255.
37. Kuczynski, R. J.; Atkinson, G. B.; Dolinar, W. J. In Proceedings of the TMS Fall Meeting, 1995; pp 527–541.
38. Chen, J.; Huang, K. *Hydrometallurgy* **2006**, *82*, 164–171.
39. Savadogo, O.; Amuzgar, K.; Piron, D. L. *Int. J. Hydrogen Energy* **1990**, *15*, 783–788.
40. Blouin, M.; Guay, D. *J. Electrochem. Soc.* **1997**, *144*, 573–581.
41. Kötz, E. R.; Stucki, S. *J. Appl. Electrochem.* **1987**, *17*, 1190–1197.
42. Andreeva, V. V.; Shishakov, N. A. *J. Appl. Chem.* **1961**, *11*, 388–389.
43. Alcock, C. B.; Hooper, G. W. *Proc. R. Soc. A* **1960**, *254*, 551–561.
44. Raub, E.; Plate, W. Z. *Z. Metall.* **1957**, *48*, 529–539.
45. Ziemniak, S. E.; Guilmette, P. A.; Turcotte, R. A.; Tunison, H. M. *Corros. Sci.* **2008**, *50*, 449–462.
46. Bailey, J. J.; Gehring, D. G. *Anal. Chem.* **1961**, *33*, 1760–1762.
47. Rowe, M. S.; Heywood, A. E. *Platinum Met. Rev.* **1984**, *28*, 7–12.
48. Barrell, J. D. *Platinum Met. Rev.* **1982**, *26*, 13–15.
49. Butyagin, P. A.; Baksheev, I. P.; Zakharova, R. I. *Fibre Chem.* **1997**, *29*, 251–252.
50. Coupland, D. R. *Platinum Met. Rev.* **1993**, *37*, 62–70.
51. Panfilov, P.; Bochegov, A.; Yermakov, A. *Platinum Met. Rev.* **2004**, *48*, 47–55.
52. Le Haret, P. *Glass* **2003**, *80*, 345.

53. Rytvin, E. I.; Medovoi, L. A. *Mater. Sci.* **1976**, *11*, 488–490.
54. Rapin, C.; Vilasi, M.; Podor, R.; Carton, A.; Gaillard-Allemand, B.; Berthod, P.; Steinmetz, P. *Mater. Sci. Forum* **2004**, 461–464, 1125–1132.
55. Couderc, C.; Williams, P.; Coupland, D.; Matthey, J. *Glass* **2007**, *84*, 24–27.
56. Hara, M.; Shinata, Y.; Hashimoto, S. *Corros. Sci.* **1997**, *39*, 627–638.
57. Steffens, H.-D.; Wielage, B.; Brandl, W. *Welding J.* **1989**, *68*, 151–157.
58. Leinenbach, C.; Gelder, N.; Bissig, V.; Gattiker, F.; Klotz, U. E. *Sci. Technol. Welding Joining* **2007**, *12*, 708–717.
59. Bose, D.; Datta, A.; Rabinkin, A.; De Cristofaro, N. J. *Welding J.* **1989**, *65*, 23–29.
60. Bessing, C.; Bergman, M.; Sjögren, M. *Swed. Dent. J.* **1991**, *15*, 7–14.
61. Preston-Thomas, H. *Metrologia* **1990**, *27*, 3, 107.
62. Wing, R. G.; McGill, I. R. *Platinum Met. Rev.* **1981**, *25*, 94–105.
63. Tawancy, H. M.; Abbas, N. M.; Rhys-Jones, T. N. *Surf. Coat. Technol.* **1991**, *49*, 1–7.
64. Laub, L. W.; Stanford, J. V. *Gold Bull.* **1981**, *14*, 13–18.
65. Holland, R. I. *Eur. J. Oral Sci.* **1980**, *88*, 269–272.
66. Karov, J.; Hinberg, I. *J. Oral Rehabil.* **2001**, *28*, 212–219.
67. Odén, A.; Tullberg, M. *Acta Odontol. Scand.* **1985**, *43*, 15–17.
68. Angelini, E.; Zucchi, F. *Surf. Technol.* **1984**, *21*, 179–191.
69. Meyer, J.-M.; Reclaru, L. *J. Mater. Sci. Mater. Med.* **1995**, *6*, 534–540.
70. Upadhyay, D.; Panchal, M. A.; Dubey, R. S.; Srivastava, V. K. *Mater. Sci. Eng. A* **2006**, *432*, 1–11.
71. Johnson, P. F.; Hench, L. L. *Brain Behav. Evol.* **1977**, *14*, 23–45.
72. Parsonnet, V. P.; Villanueva, A.; Driller, J.; Bernstein, A. D. *Pacing Clin. Electrophysiol.* **1991**, *4*, 289–296.
73. Chudnovsky, B. H. In Proceedings of the Annual Holm Conference on Electrical Contacts, 2001, pp 140–150.
74. Frankenthal, R. P.; Becker, W. H. *J. Electrochem. Soc.* **1979**, *126*, 1718.
75. Frankenthal, J. P.; Kruger, J. *Gold Bull.* **1985**, *18*, 46.
76. Conway, B. E.; Novak, D. M. *J. Electroanal. Chem.* **1979**, *99*, 133–156.
77. Burke, L. D.; O'Neill, J. F. *J. Electroanal. Chem.* **1979**, *101*, 341–349.
78. Consonni, V.; Trasatti, S.; Pollak, F.; O'Grady, W. E. *J. Electroanal. Chem.* **1987**, *228*, 393–406.
79. Trasatti, S. *Electrochim. Acta* **2000**, *45*, 2377–2385.
80. Kroon, D. H.; Ernes, L. M. *Mater. Perform.* **2007**, *46*, 26–29.

Further Reading

Cotton, S. A. *Chemistry of Precious Metals*; Springer, 1997.

The Silver Institute, Information resource about silver. www.silverinstitute.org

The Gold Institute, Information resource about gold. www.gold.org

Gold Bulletin, Current and back issues of this journal are freely available online at www.goldbulletin.org

Platinum Metals Review, Current and back issues of this journal are freely available online at www.platinummetalsreview.com

The PGM Database, Comprehensive physical, metallurgical and chemical data on the platinum group metals and their alloys available as a searchable online database and linked off the Platinum Metal Review homepage and also from: www.noble.matthey.com

Corrosion Handbook; ASM International, 2008; Vol. 13B.

3.22 Corrosion of Passive Alloys: The Effect of Noble Metal Additions

J. H. Potgieter
School of Chemical and Metallurgical Engineering, University of the Witwatersrand, Johannesburg, South Africa

Abbreviations

SCE Saturated calomel electrode
SHE Standard hydrogen electrode

Symbols

i_p passive current density
i_{cr} critical current density
i_{co} corrosion current density
i_{cath} current density of cathodic process
i_{tr} transpassive current density
E_{co} corrosion potential
E_p passivation potential
E_O^A anodic potential of base metal or alloy
E_O^C potential of cathodic component
E_{tr} transpassive potential

3.22.1 Introduction

Pt-group metals (PGMs), together with silver and gold, constitute the group known as noble metals. These metals find wide application in a number of different fields, such as catalysts, fuel cells and metal winning electrodes, dental alloys, and even semiconductors. The focus of this chapter will be limited to the addition of PGMs, and in some cases silver and gold, to Cr-based stainless steel alloys used in process industries where prevailing reducing acid conditions create major challenges for the corrosion resistance of equipment construction materials, and failures as a result of corrosion can create serious safety hazards and cause substantial maintenance and production losses. It will also not consider PGM-based alloys in which the majority of alloying elements consist of the PGM, although these alloys are becoming increasingly important for high temperature corrosion resistant applications. Two excellent reviews appeared recently[1,2] describing the manufacturing of such alloys, as well as their physical, mechanical, and corrosion properties.

Owing to the very specialized nature of the topic under discussion, it is not surprising that research on the addition of noble metals to alloys for the improvement of corrosion resistance, or cathodic alloying of materials, has not been widely investigated or described in literature. Another reason might be that the major producers of the PGMs used in the enhancement of corrosion resistance, namely Pd (Pd) and Ru (Ru), have traditionally been South Africa and Russia (old USSR), and they are the obvious beneficiaries of an increased demand for their produce should this approach of adding PGMs to stainless steels markedly increase the demand for the elements in question. It seems that research work on this was mainly done by the Tomashov's group (in Russia), Higginson and others at Mintek (Council for Mineral Technology, South Africa), the University of the Witwatersrand in collaboration with Mintek, and Tjong and coworkers in Hong Kong. As a result, there has been little discussion of the topic in the literature, and no comprehensive review paper on the subject appeared to date. The present review, therefore, covers previous work carried out by various groups from different laboratories and, in addition, discusses some more recent results from the past two decades. Furthermore, this review will be restricted to aqueous corrosion in reducing acid media, and will not specifically consider high temperature corrosion resistance of cathodically modified stainless steels. Conclusions are drawn from earlier results, and possible areas for future research are outlined.

3.22.2 Cathodic Modification and Passivation

During the course of the past 50 years, a number of papers concerning the application of cathodic modification and the corrosion behavior of cathodically modified alloys have been published, especially by the Tomashov group in Russia. However, none of these provides a comprehensive description of the electrochemistry of the cathodic modification phenomenon and of the mechanisms involved. One of the purposes of this review, therefore, is to present in detail all aspects concerning the electrochemistry of cathodic modification. The practical applications of cathodic modification in different alloy systems, and the corrosion behavior of cathodically modified alloys in different acidic media, will be dealt with later in the review.

An examination of the mechanisms of corrosion processes by Tomashov[3] indicates that there are four possible ways in which corrosion-resistant alloys can be produced and the resistance of alloys against electrochemical attack increased, namely:

- an increase in the degree of thermodynamic stability;
- retardation of the kinetics of the cathodic processes;
- retardation of the kinetics of the anodic processes; and
- the production of stable passivating oxide layers.

The thermodynamic stability of commercial steels can be increased in only a limited number of cases, for example, Cr-containing steel can be alloyed with a nickel or molybdenum.[3,4] Cathodic reactions can be retarded in two ways: by the elimination of active cathodic impurities, such as iron or copper in zinc, from alloys and by the increase of overvoltage of the cathodic process, for example, by the alloying of manganese or zinc to magnesium alloys, and of arsenic or antimony to steel. Stable passivating oxide layers can be obtained by adding Cr, which is thermodynamically less stable than iron, to iron to produce stainless steel which owes its corrosion resistance to the formation of passivating oxide layers on the surface of the steel. Retarded cathodic reactions can change the polarization curves as shown in **Figure 1**.

The anodic reaction can be retarded as a result of an increase in the ability of the alloy to be passivated. This can be done in various ways, including the alloying of iron, nickel and ferronickel steels with Cr, or the introduction of active cathodes into the alloy, for example, the alloying of stainless steels and titanium with PGMs. The latter technique is known as cathodic modification.

3.22.3 Origin of Cathodic Modification

Cathodic modification is not widely known and practiced outside USSR, but it is by no means a new discovery or concept. As early as 1911, Monnartz[5] reported that the rapid corrosion of Fe–Cr alloys in certain acids can be prevented either by the winding of a Pt wire around the sample used in the corrosion test, or by the alloying of the steel with Pt. Nobody seems to have shown much interest in this discovery until Tomashov *et al.*[6] first confirmed it in 1948, and then further developed the concept of 'cathodic alloying' in their work on stainless steels and titanium and its alloys. Other contributions have been made mainly by Stern and coworkers[7–11] and Cotton.[12–15]

In principle, passivity can be induced in a base metal or an alloy by the addition of a noble metal (one of the PGMs, gold, or silver) having a high cathodic exchange current density, provided that the passive region of the base alloy extends to potentials that are more negative than the redox potential of the environment. This is schematically represented in **Figure 2**, in which line A represents the cathodic polarization curve for the metal and B, the cathodically modified alloy. Hence, for metals and alloys that exhibit stable passivity at potentials sufficiently more negative than the existing hydrogen potential in the system, spontaneous passivation will be possible in the absence of any substance or compound more oxidizing than hydrogen ions. The effect of cathodic modification should therefore be most pronounced in nonoxidizing acid environments, for example, deaerated hydrochloric and sulfuric acids.

This conclusion has been confirmed by Greene *et al.*[11] who found that, while addition of PGMs to Cr

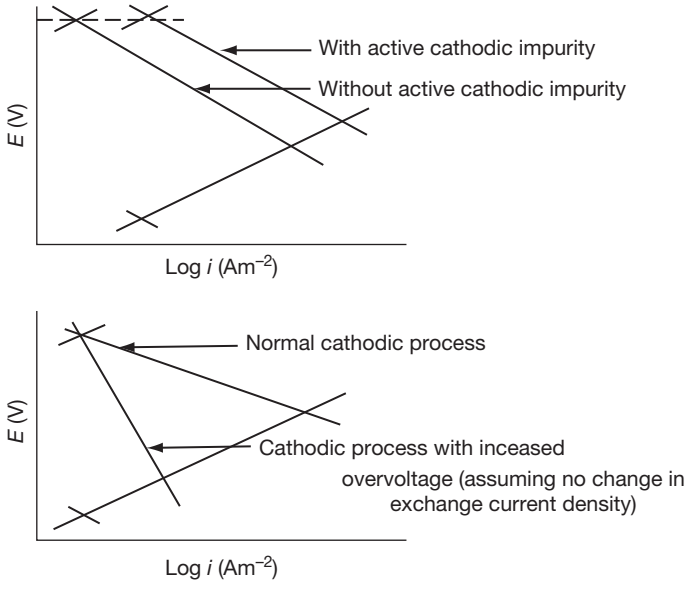

Figure 1 Schematic representation of ways in which cathodic reactions can be retarded.

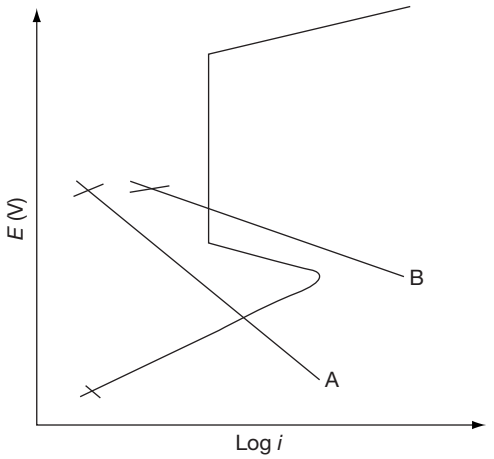

Figure 2 Schematic illustration of the effect of cathodic modification. A is the cathodic polarization curve for the parent metal, while B is the cathodic polarization curve for the cathodically modified alloy.

in nonoxidizing acids (hydrochloric and sulfuric acids) improved its corrosion resistance, they had a detrimental effect in oxidizing acid (nitric acid) because the oxidizing acid increased the potential to a value in the transpassive range.

3.22.4 Requirements for Cathodic Modification

The basic conditions required for successful cathodic alloying can be summarized as follows[3]:

- The base alloy must have a small critical current density (i_{cr}) that will be easily exceeded by the current of the hydrogen cathodic reaction on the added noble metal at the given passivation potential (E_p).
- The passivation potential (E_p) of the base metal must be sufficiently negative to allow the cathodic component that has been introduced to change the corrosion potential (E_{co}) of the alloy to a value in the passive range that is more positive than (E_p) but less positive than the potential associated with the onset of tranpassive processes (E_{tr}).
- The transpassive potential (E_{tr}) of the base alloy should be sufficiently electropositive to allow a wide passive range.

Furthermore, the cathodic alloying component should itself satisfy certain basic conditions[3]: it should have a higher exchange current density i_0 (and lower overvoltage) for the cathodic process of hydrogen evolution than the base metal or the alloy, and it should be corrosion resistant under the given conditions. In nonoxidizing acids (such as sulfuric and hydrochloric acids), the conditions requiring a sufficiently negative passivation potential are satisfied by stainless steels, Cr-based alloys and titanium-based alloys, while the PGMs have the necessary high exchange current density, i_0 (and low overvoltage), for hydrogen evolution.

3.22.5 Principle of Cathodic Modification

Figure 3 presents schematic diagrams of the four distinct states that can be displayed by a system with an active–passive transition. The different states depend upon the relative efficiency of the cathodic process (or processes) in each case.

3.22.5.1 Active State

When the rate of the cathodic process is relatively low (as shown by the solid line in Figure 3(a)), the system will be in the active state. The metal or alloy undergoes stable active dissolution at a potential of E_{co} with a current density of i_{co}, and the following conditions prevail:

$$E_O^A < E_{co} < E_p \text{ and } i_{cath}(E_p) < i_{cr}$$

The active state is established spontaneously. Hence, if an external perturbation causes the system to move momentarily into the passive potential range, the active state will be spontaneously reestablished.

3.22.5.2 Active–Passive State

For a higher, intermediate rate of the cathodic process (as shown by the solid line in Figure 3(b)), there are three possible conditions for the system. These conditions are given at the three points A, B, and C at which the cathodic line and anodic curve intersect.

At potential C (E_p), anodic dissolution of the metal or alloy occurs at a relatively high corrosion rate. At potential B ($\sim E_p$), the system is in an unstable state rarely observed in practice. At potential A ($> E_p$), the system is in the passive state, and the corrosion rate is very low. If the system is perturbed, the different conditions of the active-passive state will not be spontaneously reestablished.

3.22.5.3 Passive State

For a high rate of the cathodic process (as shown by the solid line in Figure 3(c)), the anodic and cathodic

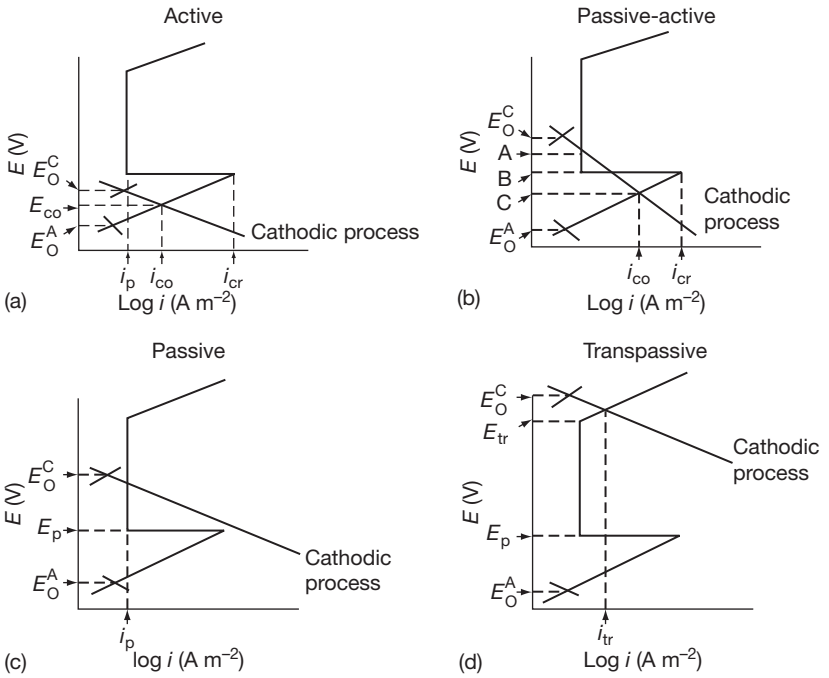

Figure 3 Different active–passive status in an alloy system.

curves intersect at only one point. The system is in a stable, passive state. The following conditions prevail:

$$E_O^C > E_p \text{ and } i_{cath}(E_p) < i_{cr}$$

The rate of metal or alloy dissolution is very low and is equal to the passive current density i_p. The passive state is also spontaneously stable, which means if the passivity is momentarily disturbed, the passive state will be spontaneously reestablished.

This kind of system is typical of cathodically modified Cr, stainless steel, and titanium alloys in nonoxidizing acid environments. The Cr, stainless steel, and titanium alloys all have passivation potentials more negative than the evolution potential of hydrogen in acidic media. When a PGM is added to any of these alloys, a large increase in the rate of hydrogen evolution will occur, which is large enough to move the corrosion potential of the cathodically modified alloy in the region of stable passivity. Spontaneous passivation of the alloy will therefore be the result.

3.22.5.4 Transpassive State

For a very high rate of the cathodic process (as shown by the solid line in **Figure 3(d)**), or in highly oxidizing environments, it is possible that $E_O^C > E_{tr}$. At this high potential, the metal or alloy will have a higher rate of dissolution than it will at potentials in the passive range, and considerable corrosion can take place.

A comprehensive study by Stern and Wissenberg[8] on the effect of various PGMs and other noble metals in causing the spontaneous passivation of titanium in boiling dilute sulfuric and hydrochloric acids showed that the increase in corrosion resistance of the titanium depends on the concentration of the PGMs added and also that alloying additions of as little as 0.1% (by mass) resulted in a pronounced improvement in corrosion resistance. They found that the effect of the various alloying elements in improving the corrosion resistance of an alloy generally decreased in the order:

$$\text{Ir} > \text{Rh} > \text{Ru} > \text{Pt} > \text{Pd} > \text{Os} > \text{Au} > \text{Re}$$

According to the available comparable data, there seems to be a reasonable parallel between the hydrogen exchange current densities and the extent to which additions of the various PGMs improve corrosion resistance, although a close examination shows that exceptions do occur, and that this agreement is not conclusive.[16]

The relatively high exchange current density of Pd indicates that it should be an effective alloying element in conferring stable passivity. Although equivalent data under these conditions are not available for Ru, it is widely considered to be a more effective cathode for hydrogen evolution than is Pd. It should therefore be a fairly effective cathodic modifying agent. Streicher[17] tested Pd, Pt, iridium, osmium, rhodium, and Ru as cathodic additives to ferritic

stainless steels, and showed that Ru additions (0.2%) indeed produced better corrosion resistance than did Pd additions (0.2%). Higginson[18] also confirmed that Ru confers better corrosion resistance on ferritic stainless steels than does Pd. The commercial titanium alloy Ti–0.2% Pd containing 0.2% Pd which was developed by the Tomashov group proves that cathodically modified alloys can be economically viable corrosion resistant materials for severe reducing conditions.

3.22.6 Mechanism of Cathodic Modification

Upon formation of the alloy, it is conceivable that the atoms of each alloying component maintain their electrochemical individuality. Consequently, although it is a solid solution, the surface of the alloy is electrochemically heterogeneous at an atomic level, and the atoms of the solid solution do not possess identical corrosion resistance. It seems that the PGMs can inhibit corrosion in two ways, namely;

- by acting as a catalyst for hydrogen evolution (and thus increasing the efficiency of the cathodic process); and
- by inhibiting the anodic dissolutions of the metal or alloy to which they are added.

As a result of the initial interaction of the different atoms of the alloy with the corrosive media, there is a rearrangement of atoms at the alloy surface resulting in a redistribution of the PGM on the surface of the alloy, before passivity is established.[19,20] Three separate mechanisms have been proposed[18] to account for the distribution process, namely:

- dissolution of the PGMs followed by diffusion through the electrolyte and, secondarily, electrochemical deposition of the noble metal on the alloy surface;
- volume diffusion (from the bulk alloy) of the PGM atoms; and
- surface diffusion of the PGM atoms.

The dissolution–deposition model was proposed in some early research into the cathodic modifications of titanium alloys.[15] Diffusion of the PGM ions (or complexes) through the electrolyte to the surface of the alloy could easily occur at a sufficient rate to account for the observed redistribution. However, it is impossible for the PGMs to be oxidized in the potential range associated with the dissolution of the cathodically modified alloy, and this fact is a major obstacle, providing a fundamental objection to this mechanism.

The volume-diffusion and surface-diffusion mechanisms do not involve dissolution of the PGM, although the latter model does not preclude the possibility of partial solvation of PGM atoms. However, the difficulty initially associated with these mechanisms was that the diffusion rates associated with similar processes were not high enough to account for the redistribution of PGM atoms at relatively low temperatures. This objection remains valid for the volume-diffusion mechanism.

The important feature of the surface-diffusion mechanism concerns the nature of the surface undergoing anodic dissolution. In recent years, an increasing amount of evidence has emerged which favors the surface-diffusion mechanism in alloying systems that undergo selective dissolution. Forty and Durkin[21] showed that, for silver alloys containing 10 at.% gold, the surface diffusion of the more noble component of the alloy (gold) is responsible for substantial reordering of the surface during anodic dissolution in nitric acid. Pickering[22] classified the polarization curves of alloys in terms of their tendency towards selective dissolution and the surface enrichment of the more noble metal. He also pointed out that the morphology of cathodically modified alloys should be that of a solid planar surface enriched in the noble metal. Work by Tomashov *et al.*[23,24] on cathodically modified alloys has also provided evidence in favor of a surface-diffusion mechanism.

A surface undergoing anodic dissolution is an extremely disturbed surface because selective dissolution causes a high concentration of defects in the surface. This, in turn, can cause rapid diffusion of the atoms of the noble-metal component to the surface of the alloy. Normally, diffusion coefficients associated with surface diffusion are considerably higher than those for volume diffusion, particularly at ambient temperature. A diffusion coefficient of 10^{-2} cm^2 s^{-1}[25] which is estimated for Cr atoms from a surface analysis of a ferro-Cr alloy undergoing dissolution in a 0.1 M solution of hydrochloric acid, is several orders of magnitude higher than the diffusion coefficients required for volume–bulk diffusion, and proves that the observed redistribution rates in cathodically modified alloys can be accounted for by a surface-diffusion mechanism.

It therefore seems that the most important results of noble metal additions to Cr, stainless steel, and other alloys are:

a. Cathodic modification can increase the corrosion resistance of materials in nonoxidizing acids by increasing the potential to a value that is in the passive potential range.
b. During anodic dissolution, noble-metal atoms are redistributed on the surface of the alloy, probably by a surface-diffusion mechanism.

3.22.7 Cathodic Modification of Cr and Cr-Based Alloys

Since 1948, both Tomashov *et al.*[6] and Stern *et al.*[8] have proved that the tendency to passivation and the corrosion resistance of Cr in a nonoxidizing acid environment can be increased by the addition of small amounts of PGMs to these alloys.[6,8,11,26–30] Alloying with these cathodic additives causes dramatic improvements in corrosion resistance, and does not reduce the low-temperature plasticity of the Cr. It therefore opens up extensive possibilities for the use of these alloys in new industrial applications.

3.22.7.1 Effect of the Addition of Noble Metals

3.22.7.1.1 Cathodic modification

Greene *et al.*[11] conducted a comprehensive investigation into the influence of small additions of various PGMs, as well as some other noble metals, on the corrosion resistance of Cr in both nonoxidizing acids (hydrochloric, sulfuric) and an oxidizing acid (nitric). The tests carried out for the determination of the loss in mass in boiling sulfuric acid (5–98%), in hydrochloric acid (5–15%), and in nitric acid (65%) showed that an addition of as little as 0.1% PGMs to Cr (Cr–0.1% Pt) could cause a decrease in the corrosion rate of the Cr by a factor 10^5 or more. Each of the alloying additions improved the corrosion resistance in nonoxidizing environments, whereas several of the PGMs, particularly Pt and Ru, actually accelerated corrosion in nitric acid, which is a highly oxidizing environment. This phenomenon can be explained by the fact that the corrosion potential of Cr in a boiling solution of 65% nitric acid is very noble, and is very close to the beginning of its transpassive region. Alloying with an inert element having a large exchange-current density for the reduction of nitric acid can shift the existing high positive potential of the alloy into the transpassive region, resulting in an increased dissolution of the metal. In electrochemical tests carried out at room temperature, a decrease in the critical anodic current density for passivation was found in all the Cr alloys containing noble elements, except those containing rhenium, silver and gold. The decreasing order of effectiveness of the various alloying additions in causing corrosion resistance in sulfuric and hydrochloric acids is as follows:

$$\mathrm{Ir} > \mathrm{Rh} > \mathrm{Ru} > \mathrm{Pt} > \mathrm{Pd} > \mathrm{Os} > \mathrm{Au} > \mathrm{Re} > \mathrm{Cu} > \mathrm{Ag}$$

This can be correlated with the hydrogen-overvoltage behavior of these elements.

The corrosion of ductile Cr alloyed with Ru, osmium, iridium, Pt, Pd, and rhenium in solutions of 5–60% sulfuric acid at various temperatures has been described by Tomashov *et al.* in various papers.[27–30] Tomashov[3] found that Cr that has no cathodic additives (PGMs) corrodes at a high rate, while cathodically modified alloys self-passivate easily, and their corrosion resistance is several orders of magnitude higher than that of pure Cr. An increase in the concentration of the alloying component also increases the stability of the passive state.

A detailed study of Cr–Pd (0.1–0.4%) and Cr–Pt (0.1–0.4%) alloys in a 50% solution of sulfuric acid at 98 °C[30] revealed that the addition of small amounts of nitrate ions (0.02% NO_3^- or 0.2 g dm^{-3} NO_3^-), which serve as an oxidizing agent, considerably increased the stability of the passive state in this aggressive condition. On the other hand, concentrations of up to 10 mg dm^{-3} of chloride ions in solutions of 40% sulfuric acid at 65 °C delayed the onset of self-passivation, and also narrowed the range of the passivation region for ductile Cr–0.3% Ru, and Cr–0.4% Ru alloys.[6] Work by Kato and Sakaki[31] on Cr with Pd and Ru additions, confirmed the beneficial effect of both on the increased corrosion resistance of the Cr in sulfuric acid, as well as the fact that Ru is more effective than Pd in this regard.

3.22.7.1.2 Kinetic effect

Tomashov *et al.*[27,29,32,33] investigated the effect of PGMs on the active dissolution of ductile Cr in sulfuric acid. Results of the dissolution kinetics of ductile Cr alloyed with Ru, iridium, Pd, and Pt (0.1–0.4%) in a solution of 40% sulfuric acid at 65 °C and at a fixed potential of −175 mV (SHE) show that the PGM alloying elements decrease the anodic dissolution rate of Cr, and also that the corrosion resistance of the alloy depends on the concentration and nature of the alloying addition.

Investigations of the Cr–PGM alloys by electron microscopy after active corrosion had taken place showed that the accumulating PGMs formed separate islets rather than a homogeneous layer on the surface of the alloy. It is presumed that the dissolution of Cr from the Cr–PGM alloy occurs by means of successive transfer into the solution of the atoms that are at the corners and edges of the crystal lattice and those that have an enhanced activity. If these sectors of the crystal lattice are blocked by more corrosion-resistant PGM atoms, anodic dissolution of the Cr atoms that lie on the flat steps of the alloy lattice and that bind more firmly to it will take place less readily. The PGM atoms gradually lose their bonding with the neighboring Cr atoms, and remain on the surface in the form of adsorbed atoms are adatoms.[32–34] The further surface diffusion of such adatoms results in the formation of microcrystals of pure PGMs, which are metals that preserve the electric contact with the substrate alloy.[32,33] Thus, with an increase in the PGM content of the alloy, more active surface centers are blocked by the added PGM atoms, and the rate of Cr solution from the alloy in the active state decreases. While Tomashov *et al.*[32–34] do not preclude the possibility of the partial solvation of the PGM atoms, they conclude that the changing distribution of the PGM metal occurs mainly as a result of a surface diffusion mechanism.

The retardation of the anodic dissolution of Cr by all the PGM additives seems to occur as a result of the operation of two mechanisms. The dominant mechanism is a blocking mechanism, in which the PGMs (as adatoms) block the active sites in the crystal lattice of Cr, thus preventing corrosion as described earlier. A lesser effect was also observed to occur as a result of a 'screening' mechanism, in which a layer of the PGM adatoms and trapped hydrogen in the pores between the cathodic component particles partly screen the surface of the alloy, causing a decrease in the active anodic surface and in corrosion.

3.22.8 Cathodic Modification of Stainless Steels

3.22.8.1 Addition of Noble Metals to Fe–Cr Stainless Steels

The Tomashov group has made the main contribution to the knowledge of corrosion resistance of Fe–Cr alloys cathodically modified with noble metals in various acid media at different concentrations and temperatures.

In the 1960s, Tomashov[35] demonstrated the beneficial effect of the addition of Pt, Pd, rhenium, and copper to Fe–27% Cr alloys in 20–30% sulfuric acid at between 10 and 25 °C. Even small additions (less than 0.5%) of Pt, Pd, and rhenium reduced the corrosion in the Fe–27% Cr alloy by as much as 99.85%.[17] With its higher hydrogen overvoltage, copper is less effective as a cathodic additive. The addition of 0.2% Pd to Fe–18% Cr in 20% sulfuric acid of 20 °C resulted in a large increase in the corrosion resistance of the Fe–Cr alloy. Under these conditions, the corrosion resistance of Fe–18% Cr–0.2% Pd is comparable with that of an Fe–18% Cr–3% Mo alloy. When 0.2% Pd was added to Fe–25% Cr in 30% sulfuric acid at 20 °C, the alloy became even more corrosion resistant than Fe–25% Cr steels with additions of either 3% molybdenum or 6% nickel. The higher corrosion resistance of an Fe–18% Cr–3% Mo–0.2% Pd steel when compared to that of Fe–18% Cr–0.2% Pd and Fe–18% Cr–3% Mo steels illustrated, for the first time, the synergistic beneficial effect of the simultaneous additions of molybdenum and Pd to an alloy. This effect was later confirmed by Biefer[36] and Higginson.[18]

After demonstrating the cathodic modification effect in Fe–Cr stainless steels, the Tomashov group discovered that the effect of cathodic additions was enhanced with an increasing Cr content (above 25%) in an alloy.[37] Investigations carried out on Fe–Cr alloys with varying Cr contents (25–100%) to which 0.2% Pd was added indicated that Fe–40% Cr–0.2% Pd had the optimum passivation characteristics in 10–50% sulfuric acid and 1% hydrochloric acid at 100 °C. Under these conditions, the Fe–40% Cr–0.2% Pd alloy required the minimum time for self-passivation and displayed the minimum corrosion in the passive range, as well as a small critical current density and a highly negative passivation potential. The addition of 0.2% Pd to the Fe–40% Cr steel caused a dramatic decrease of a factor of 2×10^5 in the corrosion rate in a boiling solution of 40% sulfuric acid. The remarkable corrosion resistance of the Fe–40% Cr–0.2% Pd alloy when compared to that of other alloys can be clearly seen from **Table 1**.

Although the effect of the addition of Pd in improving the corrosion resistance is much less in hydrochloric acid, the corrosion rate in the passive state is still reduced by a factor of ~100. The alloy was found to have high corrosion rates in a solution of hydrochloric acid at concentrations of more than 1%.

This extraordinary corrosion resistance in sulfuric acid was confirmed by Higginson,[18] who found that

Table 1 Corrosion rate (CR) of some acid-resistant alloys in 40% sulfuric acid at 100 °C

Alloy	*CR (mm year^{-1})*
Fe–40% Cr	~10 000[37]; ~5 000[38] (10% acid)
Fe–23% Cr–28% Ni–3% Mo	3[37]
Hastelloy A, B	0.2[37]
C	0.3[37]
Ti–30% Mo	0.18[37]
Fe–40% Cr–0.2% Pd	0.05[37]
Fe–40% Cr–0.2% Ru	0.03[38]
Fe–29% Cr–4% Mo–2% Ni	~ 8000[39]
Fe–29% Cr–4% Mo–2% Ni–0.2% Ru	12.93[39]

an improvement was obtained in the corrosion rate of a factor of $(1–5) \times 10^4$ for Fe–40% Cr–0.2% Pd and Fe–40% Cr–0.2% Ru alloys compared to that of Fe–40% Cr in a boiling solution of 10% sulfuric acid. The alloy containing Ru was more resistant than the alloy containing Pd. The greater effect of the Ru was explained on the basis that it is a more effective cathode for the evolution of hydrogen than is Pd. A similar investigation conducted by Howarth[40] indicated that no improvement in corrosion resistance is gained by the use of Pt rather than Ru for purposes of cathodic modification. Higginson[18] also observed that the critical time and charge density for spontaneous passivation of Fe–40% Cr–Ru alloys depends on the concentration of Ru in the alloy, and the kind of acid (hydrochloric or sulfuric) in which the corrosion takes place.

Work by Potgieter and van Bennekom[41] indicated that although the optimum Cr concentration for maximum corrosion resistance in Fe–Cr–0.2% Pd alloys was 40% Cr, there was no difference in the corrosion resistance of an Fe–40% Cr–0.2% Ru and an Fe–30% Cr–0.2% Ru alloy. This implies that in Ru containing alloys, the maximum Cr content can be restricted to 30% by mass, which means that it can be produced commercially in the same way as the patented Fe–28Cr–4% Mo superferritic stainless steel. It also means huge gains in the physical and mechanical properties of the alloy, as Fe–40% Cr alloys are very brittle and difficult to form. A later work by Wolff *et al.*[42] indicated that further additions of 5% Al to Fe–35/40% Cr–0.2% Ru not only improved the high temperature hot corrosion resistance at elevated temperatures, but also aqueous corrosion resistance against sulfuric acid solutions of 10% at room temperature. The Fe–40% Cr and Fe–35% Cr–5% Al alloys corroded actively in 10% sulfuric acid, while the alloys containing 0.2% Ru additions passivate spontaneously, with the one containing the Al having the lowest corrosion rate. However, this latter alloy of Fe–35% Cr–5% Al had inferior pitting corrosion resistance compared to the Fe–40% Cr one in a 3.5% NaCl solution. Once again it was observed that the addition of 0.2% Ru to both the alloys increased their pitting resistance in the salt solution.

Detailed investigations were carried out by Tomashov[43] on Fe–25% Cr steels alloyed with 0.3% and 2.0% Pd and Ru in 5–50% sulfuric acid and 1 and 5% hydrochloric acid at 50–100 °C. It was found that the general and pitting corrosion resistance was higher in the alloys containing Ru than in the alloys containing Pd.

These results were attributed to several factors:

- Ru reduces the overvoltage of cathodic hydrogen generation more effectively than does Pd, thereby increasing the efficiency of the cathodic process.
- Ru, unlike Pd, reduces the rate of anodic dissolution by reducing the critical current density required for passivation, especially in media containing chloride ions. This observation was confirmed by both Biefer[36] and Higginson.[18]
- Ru is susceptible to the adsorption of oxygen and the formation of phase oxides, and thus enters the composition of the hydroxide and oxide layers formed on the surface of the steel, while Pd remains as a separate metallic phase in the surface layer.
- Because the passivating oxide layers on the steel contain Ru as well as Cr, the resistance of the steel to the activating effect of chloride ions increases. Thus, Ru does not impair the resistance to pitting corrosion, but Pd does impair this resistance.

An electron microscopy investigation[23] into the accumulation of Pd on the surface of Fe–25% Cr–(0.1–0.5%) Pd in 10% sulfuric acid at 25–100 °C revealed that the size and amount of accumulated particles on the surface of the alloy depend not only on the initial concentration of the Pd in the alloy, but also on the temperature at which active dissolution takes place. The size and distribution of the accumulated Pd particles are explained on the basis of the theory of Erdey-Gruz and Volmer, which states that nuclei of crystallization arise at a definite supersaturation of adsorbed atoms on the surface of the alloy. An increase in the concentration of the Pd should therefore result in both an increase in the number of nuclei

and decrease in the particle size. Higginson[18] confirmed this in a study of the accumulation of Ru on Fe–40% Cr–(0.1–0.2%) Ru alloys corroding in 0.5 M sulfuric acid (4.9%) and 0.5 M hydrochloric acid (1.8%). He also found that a greater amount of accumulation occurred in a solution of hydrochloric acid than in sulfuric acid, apparently as a result of the adsorption of chloride ions, which increases the surface diffusion rate of Ru atoms during anodic dissolution.

Tjong[44] investigated the corrosion behavior of an Fe–24% Cr alloy with sputter-deposited Pd thin films on the surface in 0.5 M HCl solutions at room temperature, and found that prolonged corrosion protection against active dissolution in the hydrochloric acid medium is due to the formation of a sufficiently thick Pd-enriched surface layer containing Fe–Cr. Auger analysis of the passive surface revealed that a thick Cr oxide layer form with and on the Pd-enriched surface, thus confirming the earlier work by Tomashov described above.[3,23] Recent work by Tjong and Chu[45] investigated the same parent alloy, but this time with Ru ion implanted on the surface, and in sulfuric acid. They found that the basic alloy with Ru does not passivate in the 0.5-M sulfuric acid solution, whereas the one containing ion-implanted Ru atoms does. Furthermore, XPS analysis of the passivated surface showed that Ru is incorporated as Ru^{4+} species in the hydrated Cr oxyhydroxide passive film formed on the Ru-implanted Fe–24% Cr alloy, which is once again in agreement with the results from Tomashov[3] discussed above.

Biefer[36] assessed the influence of several transition metals, as well as additions of Pd and rhenium in different concentrations to type 430 ferritic stainless steel (17% Cr) in 0.5-M sulfuric acid at ambient temperature (24 °C). The results indicate that the addition of 0.46% Pd to 430 stainless steel resulted in spontaneous passivation, but insufficient levels of Pd (0.06–0.26%) increased the active corrosion rate by a factor of as high as 10.

It was found that in 1-M hydrochloric acid (3.6%), the additions of Pd to steel 430 were strongly deleterious, and increased the corrosion rate from a factor of 10 to a factor of 30. Further, it was observed that Pd was deleterious to the pitting corrosion of ferritic stainless steels. However, at levels of 0.99% Pd, 430 stainless steel appears to have a superior corrosion resistance even to that of highly alloyed austenitic stainless steels in concentrated sulfuric acid at high temperatures.

Although Tomashov[35] concluded that the addition of 0.2% Pd to Fe–18% Cr steel was sufficient to result in spontaneous passivation in 20% sulfuric acid at 20 °C, Biefer[36] found that type 430 stainless steel with an addition of 0.26% Pd did not passivate spontaneously in 0.5 M sulfuric acid at 24 °C. A probable reason for this discrepancy is the presence of relatively high amounts of carbon and impurities in the 430 stainless steel. Lizlovs and Bond[46] showed, in measurements of anodic polarization, that the performance of a standard type-430 steel was surpassed by that of a 17% Cr steel of high purity.

3.22.8.2 Addition of Noble Metals to Fe–Cr–Mo Stainless Steels

Tomashov *et al.*[47–49] investigated the corrosion characteristics of several Fe–Cr stainless steels containing molybdenum (2–3%) and Pd (0.1–0.5%) in sulfuric acid (1–80%) at temperatures varying from 10 °C to boiling point (about 100 °C). The results indicated that, when molybdenum is added to an Fe–25% Cr steel containing 0.3% Pd, the concentration and temperature ranges in which the steels self-passivate in sulfuric acid are narrowed.

According to them, the simultaneous alloying of Fe–24% Cr with molybdenum and Pd leads to a marked increase in the stability of the passive film in sulfuric acid, because molybdenum is incorporated in the passivating film on the steel, resulting in a more protective surface layer.[48] The shrinkage of the region of passive behavior was also confirmed by Agarwala and Biefer[50] in their investigation of type-430 stainless steel, especially at high concentrations of sulfuric acid. They found that type-430 steels with additions of 3% Mo–0.5% Pd and 2% Mo–1% Pd had comparatively large regions of spontaneous passivity in sulfuric acid up to concentrations of 25% at temperatures near boiling point. They even passivated in the presence of 2–3% sodium chloride in sulfuric acid solutions at 24 °C, thus showing much more resistance to chlorides than steels that contain only Pd.

The Tomashov group[49] showed further that Fe–18% Cr–2% Mo alloyed with 0.3% Pd self-passivates, is corrosion resistant in 1–40% sulfuric acid at between 10 and 100 °C and has a lower corrosion rate than commercial Fe–18% Cr–10% Ni stainless steel under the same conditions.

Streicher[17,51] also investigated the effect of additions of PGMs to an Fe–Cr–Mo alloy. Without these additions, the rate of attack on an Fe–28.5%Cr–4% Mo alloy in a 10% solution of boiling sulfuric acid

was found to be ~52 000 mm year^{-1}. Each of the six added PGMs, when present in excess of a certain minimum amount that varied from 0.005 to 0.2%, passivated the Fe–28.5% Cr–4% Mo alloy in 10% boiling sulfuric acid. The minimum concentration of PGMs required to passivate the base alloy decreased with an increase in the Cr content. Additions of a PGM at a concentration lower than the required to produce passivity actually increased the corrosion rate as compared to that of Fe–28.5% Cr–4% Mo. This was also observed by Biefer[36] for Fe–17% Cr (type 430 steel). Scheers *et al.*[52] and McEwan *et al.*[53] found that Fe–29% Cr–4% Mo–2% Ni with small amounts of Ru also performed excellently in phosphoric acid solutions, and that Ru greatly enhances the corrosion resistance of the base alloy. Further work by Potgieter *et al.*[39] on these Fe–29% Cr–4% Mo–2% Ni alloys with various levels of Ru and silver additions, as well as a partial copper substitution for Ni, confirmed that excellent corrosion resistance can be achieved against sulfuric acid solutions as concentrated as 30–40% at boiling point with decreases in corrosion rates by a factor of 10^2 to 10^3. A level of at least 0.2% Ru is required for a worthwhile and significant corrosion resistance improvement, and silver additions, even in much larger concentrations than Ru, are not as effective as Ru to improve corrosion resistance of the base alloy. Substitution of half of the Ni with a similar amount of Cu does not seem to have a major beneficial or detrimental effect, except in severely aggressive conditions (40% H_2SO_4 at boiling point), where the effect is decidedly detrimental. This is shown in **Table 2**, which also includes a value of a duplex stainless steel discussed further on in this report.

The observation made by both Tomashov *et al.*[48] and Agarwala and Biefer[50] that the simultaneous presence of Pd and molybdenum in Fe–Cr steels promotes more stable passivity than the presence of each individual element alone was confirmed by both Streicher[17,51] and Higginson.[18] Higginson found that Fe–40% Cr that had been alloyed with both 1.8% molybdenum and 0.1% Ru passivated far more quickly in sulfuric acid (0.5 M) than did an Fe–40% Cr–0.1% Ru alloy. According to Tomashov *et al.*[48] this is true not only for solutions of sulfuric acid, but also for solutions of dilute hydrochloric acid (1–3%). However, Higginson[18] showed that the addition of 0.1% Ru to an Fe–40% Cr–1.8% Mo steel could not cause the spontaneous passivation of the alloy to occur in a solution of 0.5 M hydrochloric acid. The fact that Tomashov *et al.*[48] could achieve spontaneous passivation while Higginson could not, can be attributed to different conditions in their respective investigations.

The addition of molybdenum has different effects on the corrosion resistance of Cr steels in the active state in solutions of sulfuric and hydrochloric acid. In solutions of sulfuric acid, the presence of molybdenum reduces the corrosion rate, but in solutions of hydrochloric acid, it increases the rate. The corrosion potential in both acids of steel containing molybdenum is more positive than that of steel without molybdenum. This fact can be explained if it is assumed that molybdenum not only retards anodic dissolution, but also increases the effectiveness of the cathode process owing to the reduced overvoltage of hydrogen on molybdenum. The predominant action of molybdenum on the anodic process appears in solutions of sulfuric acid but, in hydrochloric acid, where passivation is hindered by the presence of chloride ions, it is mainly the cathodic influence of molybdenum that prevails. This leads to a marked increase in the rate of dissolution of steel, because the

Table 2 Corrosion roles of a superferritic SS with various Ru and Ag additives in boiling sulfuric acid solutions

Alloy	*[H_2SO_4] %*			
	10	20	30	40
Fe–29% Cr–4% Mo–2% Ni–0% Ru	0.008 3	1.733	1.884	–
Fe–29% Cr–4% Mo–2% Ni–0.05% Ru	0.001 2	0.020 5	1.004 4	4687
Fe–29% Cr–4% Mo–2% Ni–0.10% Ru	0.000 8	0.003 1	0.421 9	4099
Fe–29% Cr–4% Mo–2% Ni–0.20% Ru	0.000 6	0.002 7	0.064 5	12.93
Fe–29% Cr–4% Mo–1% Ni–1% Cu–0.20% Ru	0.015 2	0.051 8	0.089 2	3550
Fe–29% Cr–4% Mo–0.20% Ru	0.230 0			
Fe–29% Cr–3% Mo–14% Ni–0.20% Ru	0.000			
Fe–29% Cr–4% Mo–2% Ni–0.1% Ag	0.022 7	3.719		
Fe–29% Cr–4% Mo–2% Ni–0.5% Ag	0.033 3	1.560		
Fe–29% Cr–4% Mo–2% Ni–1.0% Ag	0.118 3	0.472 6		

effectiveness of the cathodic process on molybdenum in hydrochloric acid is insufficient to bring the steel into the passivated state. The simultaneous presence of Pd and molybdenum in steel produces a more effective cathodic process[48] and could possibly lead to passivation. Thus, in sulfuric acid molybdenum affects not only the cathodic process (together with PGMs), but also retards the anodic process. The combined influence of molybdenum and PGMs on the anodic and cathodic processes of Fe–Cr stainless steel in sulfuric acid is summarized schematically in **Figure 4**.

Streicher[51] also carried out investigations into the pitting corrosion of Fe–28% Cr–4% Mo alloys to which PGMs in several halide media had been added.

The results show clearly that Pd destroys the pitting resistance in all of the three pitting solutions tests, while rhodium impairs the resistance in ferric chloride and the bromine–bromide solution. None of the other four PGMs had any influence on the pitting resistance in these media, except for Pt, which caused failure in the bromine-bromide solution. No mechanism was suggested as an explanation for these observations. Streicher concluded that, of the six PGMs only iridium, osmium, and Ru can be used to produce the passivity of stainless steels in sulfuric acid without impairing their resistance to pitting corrosion in oxidizing chloride and bromide environments. Recent investigations by Sherif El-Sayed *et al.*[54] on the behavior of Fe–Cr–Ni–Mo–(0–0.3% Ru) in chloride media confirmed the beneficial effect of Ru on the pitting corrosion resistance of stainless steels.

As far as organic media are concerned, it was found[35] that the addition of 0.1% Pd to Fe–25% Cr in a solution of 50% formic acid at 100 °C decreased the corrosion rate of steel by a factor of approximately 60. An Fe–25% Cr–3% Mo steel is stable under these conditions, both with and without Pd.

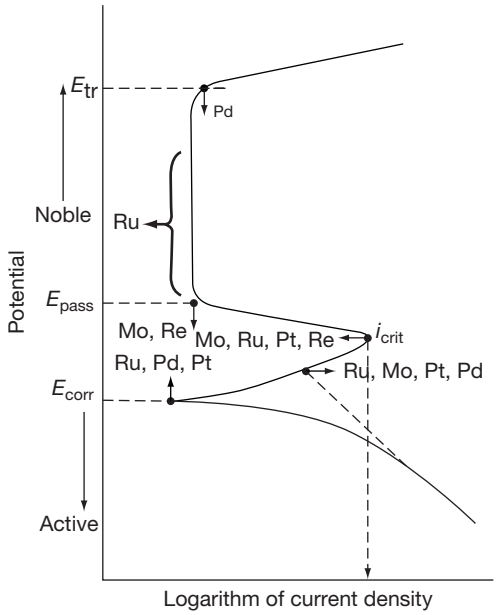

Figure 4 Summary of the effects of alloying additions on the polarization characteristics of Fe–Cr stainless steel in sulfuric acid.

3.22.9 Cathodic Modification of Fe–Cr–Ni Stainless Steels

Although the effect of cathodic alloying additives on Fe–Cr–Ni stainless steels is not as dramatic as for Fe–Cr steels, it can nevertheless bring about marked improvement in the corrosion resistance of Fe–Cr–Ni alloys, especially in fairly aggressive conditions.[55]

3.22.9.1 Addition of Noble Metals to Fe–Cr–Ni Stainless Steels

The addition of 0.1–0.5% Pt, 0.1–0.9% Pd and 1.2% Cu to Fe–18% Cr–9% Ni (an austenitic stainless steel) in 20–40% sulfuric acid at 20 °C reduced the corrosion of the Fe–Cr–Ni alloy by as much as 99.85%.[17,56] The results also indicated that the effectiveness of the alloying additions increased in the order Cu < Pd < Pt.

An electrochemical investigation into the alloying of Fe–25% Cr–6% Ni steel with Pd[57] (0.1%, 0.2%, and 0.5%) showed that the corrosion rate is reduced by more than an order of magnitude in 20% sulfuric acid at 100 °C over that for steel without Pd. However, steels containing Pd (0.1–0.5%) do not reach the stable passive region, and continue to dissolve at a considerable rate. The corrosion rate of Fe–25% Cr–6% Ni–0.5% Pd in a solution of 10% sulfuric acid at 100 °C is lower by a factor of 4 compared with the steel without any Pd.

Tomashov[35] also demonstrated that the addition of 0.2% Pd to an Fe–18% Cr–10% Ni alloy greatly reduced the corrosion of this austenitic stainless steel. The substitution of part of the nickel by manganese (Fe–18% Cr–2% Ni–8% Mn) produced an austenitic stainless steel with a corrosion performance that was not nearly as good as that of a steel with 10% nickel. The alloying of this manganese substituted steel with 0.2% Pd rectified this impaired corrosion resistance, and resulted in a steel with similar

corrosion characteristics to that of an Fe–18% Cr–10% Ni–0.2% Pd alloy.

A recent study by Peled and Itzhak[58] into the effect of silver, Pd, and gold on the corrosion behavior of hot-pressed and sintered type 316 stainless steel in 0.5-M sulfuric acid at 25 °C indicated that the corrosion resistance of the base alloy could be dramatically improved by additions of noble metals Silver concentrations of less than or equal to 1% improved the corrosion resistance of the sintered stainless steel only for limited periods of exposure. Pt additions of about 2% were found to be sufficient to preserve the sintered stainless steel in the passive state. However, high Pt contents (about 5%) resulted in a tendency for the passive layer to break down. Samples containing additions of gold at various concentrations (1–5%) exhibited clear anodic active-passive transitions with a wide range of passivation. The addition of 5% gold to the sintered stainless steel caused the alloy to remain passive.

An interesting beneficial synergistic effect between nickel and Ru was noticed by Streicher.[51] Lower concentrations of Ru (0.1%) and nickel (0.1%) were needed to passivated Fe–28% Cr–4% Mo in a 10% solution of boiling sulfuric acid than the concentrations of either Ru (0.2%) or nickel (0.25%) that were needed when they were used alone. Although it seemed that Higginson[18] was unaware of that since he neither confirmed nor disproved it; he nonetheless found that the addition of 1% nickel to a Fe–40% Cr–0.1% Ru alloy resulted in an increase in the time needed for the occurrence of spontaneous passivation in 0.5 M sulfuric acid. He also concluded that the inhibition of the anodic dissolution reaction in sulfuric acid was much greater for the alloy containing both nickel and Ru than for that containing only 0.1% Ru. The alloying of Fe–40% Cr–0.1% Ru with 1% nickel also caused spontaneous passivation to occur approximately seven times faster in 0.5 M hydrochloric acid than for the Fe–40% Cr–0.1% Ru alloy. Thus, while an addition of 1% nickel to Fe–40% Cr–0.1% Ru was advantageous and lowered the passivation time in hydrochloric acid, the same did not apply when sulfuric acid was used since the passivation time increased. This synergistic effect between Ni and Ru was also confirmed by Potgieter and Kincer[38] in sulfuric acid, in their work on Fe–40% Cr–Ni–Ru alloys in 0.5 M hydrochloric and sulfuric acids. Their results indicated that less expensive Ni can be substituted for Ru to improve corrosion resistance effectively in sulfuric acid, but not in hydrochloric acid.

As far as organic acid media are concerned, work by the Tomashov group[35,55] indicated that an Fe–25% Cr–6% Ni–0.1% Pd alloy in a solution of 50% formic acid at 100 °C had a significantly reduced rate of corrosion when compared with the alloy without Pd. An alloy of 26% Cr–0.5% Ni to which noble metals had been added (0.5% Pt and 0.5–1.0% Pd) could withstand solutions of 50% formic acid and 10% oxalic acid at 100 °C for better than a similar alloy without the additions of any noble metals.

3.22.9.2 Addition of Noble Metals to Fe–Cr–Ni–Mo and Fe–Cr–Mn–Ni Stainless Steels

Investigations by Tomashov *et al.*[35,55,59,60] into the corrosion resistance of nitrided stainless steels revealed than an addition of 3% molybdenum to Fe–25% Cr–6% Ni steel in a solution of 30% sulfuric acid at 20 °C produced a sufficiently stable alloy in which the further addition of Pd (0.1%) did not result in any significant improvement in the corrosion resistance.[55] This occurs as a result of the fact that molybdenum not only retards the anodic dissolution of steel, but also promotes the cathodic evolution of hydrogen. Passivation is thus caused by the increased effectiveness of the cathodic process as well as the inhibition of the anodic process.

The work of the Tomashov group also showed that highly nitrided (0.7–0.9%) Fe–25% Cr–3% Ni–2% Mo–Mn stainless steels to which 0.1–0.5% Pd had been added had a very high corrosion resistance in mildly aggressive conditions, such as in solutions of 20–40% sulfuric acid at 20–100 °C, as well as in solutions of 1–3% hydrochloric acid at 20–50 °C.[59] However, at least 0.2% Pd is needed for self-passivation and high corrosion resistance to occur under more aggressive conditions (2% or higher hydrochloric acid at 50 °C or higher and 30% or more sulfuric acid at 50 °C or higher).[55] In mildly aggressive media, the corrosion resistance of the steel depends on the ability of the molybdenum to cause self-passivation as a result of the increased effectiveness of the cathodic process and inhibition of the anodic process. The simultaneous addition of Pd and molybdenum in a stainless steel broadens the region of self-passivation of the steel. The favorable influence of Pd on the corrosion resistance of stainless steel is due primarily to the cathodic modification of the steel and, in the presence of molybdenum, to its beneficial effect on the stability of the passive state.

Results also indicated that Fe–25% Cr–6% Ni–3% Mo–0.2% Pd that does not contain nitrogen could not be passivated in a solution of hydrochloric acid. Only a high nitrogen content (0.5% or more) leads to an increase in the corrosion resistance and self-passivation of these alloys in solutions of dilute hydrochloric acid (2–5% hydrochloric acid at 50 °C).[60] The positive influence of nitrogen occurs as a result of its influence on the structure of steel. A high nitrogen content creates a more homogeneous austenitic structure, and thus prevents the partitioning of Cr, molybdenum, and nickel in a two-phase austenitic–ferritic structure. Steel containing Pd but no nitrogen cannot be passivated in solutions of hydrochloric acid, apparently owing to the heterogeneity of the structure, which contains ~40% ferrite. The presence of appreciable amounts of both austenite and ferrite phases in the alloy, which cause a galvanic interaction between the two electrochemically different phases, is possibly responsible for this observed corrosion behavior.

Work carried out by Tjong[61] on Fe–24Cr–6V–Ru (0–0.2%) and Potgieter[62] on Fe–22% Cr–5% Ni–3% Mo–(0–0.3%)Ru and having a very low nitrogen content, showed that in these ferritic steels Ru has a major beneficial effect in increasing the corrosion resistance of the base alloy towards attack by 1 M H_2SO_4 solutions. The effect increases by increasing the Ru contents, and the Ru in all cases caused a shift in the open-circuit corrosion potential towards more noble values. Under conditions of active–passive transition behavior, Ru additions also lowered the critical current density required for passivation and lowered the cathodic Tafel slope.

Tomashov *et al.*[59] proved that Fe–Cr–Ni–Mn and Fe–Cr–Mn alloys containing 0.5% Pd self-passivated, and had a high corrosion resistance in solutions of 20% sulfuric acid at 100 °C. However the steels containing only 0.2% Pd did not self-passivate in solutions of 2 and 3% hydrochloric acid at 25 °C, and had a low resistance to corrosion. Manganese shifts the complete passivation potential of Fe–Cr steel to values that are more positive, but to be a lesser degree than nickel. The beneficial effect obtained when Cr steels are alloyed with nickel and manganese can be ascribed to the fact that they cause a smaller shift in potential to the positive direction upon complete passivation than occurs when they are alloyed with nickel alone. The further addition of nickel to Cr–Mn steels also lowers the critical current density at the onset of passivation. This permits better self-passivation, and a higher corrosion resistance upon cathodic alloying.

3.22.9.3 Galvanic Coupling in Fe–Cr–Ni Stainless Steels

Bianchi *et al.*[63] investigated the galvanic coupling of different stainless steels with sheet Pt in various non-oxidizing acid solutions at various concentrations and temperatures. For example, it was found that, in an aerated solution of 38% sulfuric acid at 25 °C, types 316, 304, and 430 (a ferritic alloy) stainless steel resisted corrosion when the ratio of the area of Pt to that of the stainless steel was 1, 10, and 100, respectively. This acquired corrosion resistance was attributed to the anodic protection of the stainless steels by Pt, which is a more efficient cathode for the reduction of oxygen. This greater efficiency of Pt for the reduction of oxygen shifted the potential of the stainless steel to a value in the passive range, thereby enhancing the resistance to corrosion. The same effect is observed when Pt is alloyed with steel, and is known as a cathodic modification of the stainless steel by the PGM. The galvanic coupling of two austenitic stainless steels, AISI 304 (18% Cr–8% Ni) and AISI 316 (18% Cr–8% Ni–2% Mo) with Pt, was studied electrochemically by Kabi *et al.*[64] in solutions of 2 and 5 M sulfuric acid at 28 °C. They confirmed that galvanic coupling with Pt enhanced the corrosion resistance of both steels, since the critical current density was lowered at the onset of passivation, as was the passivating current density. The corrosion potential of both alloys also shifted to a more positive value.

3.22.10 Cathodic Modification of Duplex Stainless Steels

The development of the duplex stainless steels (steels containing a ferrite–austenite mixture) was first reported by Bain and Griffiths[65] as early as 1927. Duplex stainless steels combine the advantages of ferritic and austenitic stainless steels and, although a large amount of data has been collected and published about duplex stainless steels, very little work has been reported in the literature about the addition of noble metals to these steels.

It appears that Tomashov's is the only group that has carried out any work on the influence of the addition of noble metals on duplex stainless steels. Furthermore, it appears that their work on the addition of Pd to duplex stainless steels was purely incidental, their main thrust having been focused on the investigation of the effect of Pd on the corrosion characteristics of

highly nitrided austenitic stainless steel (some containing molybdenum as well) in non-oxidizing acid solutions. The occurrence of two phases (ferrite and austenite) in some highly nitrided austenitic stainless steels also led to investigations of duplex stainless steels that were alloyed with Pd.[59]

In one of the investigations by the Tomashov group[60] into the corrosion resistance of Fe–Cr–Ni stainless steels in hydrochloric acid, two duplex stainless steels were produced with low levels of nitrogen (0.03% or more). The Fe–25% Cr–6% Ni–3% Mo alloy contained 30% ferritic phase, while the Fe–25% Cr–6% Ni–3% Mo–0.2% Pd alloy contained 40% ferrite phase. Both steels were found to corrode actively in a solution of 3% hydrochloric acid at 50 °C.

A higher corrosion rate was found in the duplex steel containing Pd because, in conditions in which the steel does not self-passivate and in which it corrodes with the evolution of hydrogen, the presence of an effective cathodic additive with a low hydrogen overvoltage enhances the cathodic reaction and increases the corrosion rate.

This investigation showed that duplex stainless steels containing Pd cannot be passivated in a solution of up to 3% hydrochloric acid at 50 °C because of the heterogeneity of its structure. Both Cr and molybdenum are powerful ferrite stabilizers, while nickel is primarily an austenite stabilizer. Therefore, the distribution of the different components in the two phases differs by several percentage points as a result of partitioning. The austenitic phase, being depleted of Cr and molybdenum and enriched with nickel, experienced difficulty in achieving passivation.

In another paper on the corrosion resistance of highly nitrided austenitic stainless steels alloyed with Pd, Tomashov *et al.*[59] produced some duplex stainless steels that typically consisted of 18–25% Cr, 7–11% Mn, ~2% Mo, and nearly 1% N, with a varying ferrite content of 36–50%. These steels were additionally alloyed with 0.1–0.5% Pd. No nickel was present in any of theses alloys.

Corrosion tests conducted in solutions of 20–50% sulfuric acid at 20–100 °C indicated that all the duplex alloys containing Pd initially corroded intensively after immersion and activation before they became self-passivated. The time required for self-passivation decreased with an increase in both the Pd content of the steel and an increase in temperature, but increased with an increase in the concentration of acid (20–40% sulfuric acid). In a solution of 20% sulfuric acid at 100 °C, only the steels containing 0.4% and 0.5% Pd self-passivated. This investigation also showed that duplex stainless steels containing Pd had a greater corrosion resistance in 2–3% hydrochloric acid at 20–50 °C than did similar cathodically modified austenitic stainless steels.

Potgieter[66] carried out an extensive investigation into the corrosion behavior of different stainless steel groups cathodically modified with Ru in sulfuric acid solutions at various temperatures. Three groups of low nitrogen duplex stainless steels were investigated, namely Fe–22% Cr–3% Mo, Fe–29% Cr–3% Mo, and Fe–35% Cr–3% Mo, with sufficient amounts of Ni added to each group (9.14% and 18% respectively) to ensure a fully duplex structure containing approximately equal amounts of austenite and ferrite in each case after suitable heat treatment. Varying amounts of Ru, namely 0.1–0.3%, were added to each of the base alloys in each group, yielding a total of twelve alloys. One of the reasons for the selection of the three groups was to determine whether the effect of the Ru in inhibiting corrosion would become more enhanced with an increasing Cr content in the alloy, as was the case with the ferritic and superferritic stainless steel. The choice of Ru was motivated by two factors, that is, the fact that is was more effective than Pd, and the huge excess being produced in South Africa for which there is currently no alternative applications. The compositions of the various alloys are given in **Table 3**.

The results obtained from mass loss tests indicated that significant decreases in the corrosion rates of duplex alloys could be obtained by the addition of small amounts of Ru to the base alloys. The increase in the corrosion resistance was the most

Table 3 Chemical composition (%m/m) of the duplex stainless steels investigated

Alloy	*Cr*	*Ni*	*Mo*	*Ru*
377	22.0	9.07	2.81	–
378	22.1	9.20	2.89	0.14
379	22.4	9.14	2.82	0.22
380	22.4	9.24	2.92	0.28
413	28.5	14.4	2.70	–
414	28.4	14.0	2.70	0.06
398	29.6	14.3	2.73	0.17
399	30.1	14.8	2.88	0.28
400	34.7	18.6	2.72	–
416	33.9	17.4	2.60	0.15
448	35.0	18.8	2.50	0.23
446	34.5	18.5	2.80	0.28

For each alloy the balance of the composition is made up of Fe.

pronounced in the alloy group with the lowest Cr and nickel content. Electrochemical measurements indicated that the corrosion potentials of all the alloys containing Ru were raised to more noble values in sulfuric acid solutions. Under conditions where the alloys passivated spontaneously, a decrease in cathodic Tafel slopes occurred. When the alloys were actively corroding, Ru additions decreased the critical as well as the passive current densities of all three groups of alloys. Increasing acid concentrations and temperatures were found to increase the corrosion rates, critical current densities and passive current densities of all the alloys investigated. At the same time a lowering in the corrosion potential occurred for each individual alloy with increasing severity of the corrosive environment. In contrast to commercial duplex stainless steel, where the potential of the specimen with respect to the environment determines the phase that would preferentially corrode, only the ferrite phase corroded preferentially in these low nitrogen duplex alloys through a range of active to passive potentials investigated.

The effect of the various acid concentrations and temperatures used in the investigation on the different duplex stainless steel group can best be described by the compiled isocorrosion curves presented in Figure 5. Areas to the left and below each curve indicate the conditions where stable (spontaneous) passivation occurs, while areas to the right and above each curve indicate active corroding conditions. The beneficial effects of increased Cr and nickel additions in improving the corrosion resistance between each of the groups of duplex stainless steels are clearly visible, while the beneficial effect of increasing Ru additions in each group can also be easily distinguished.

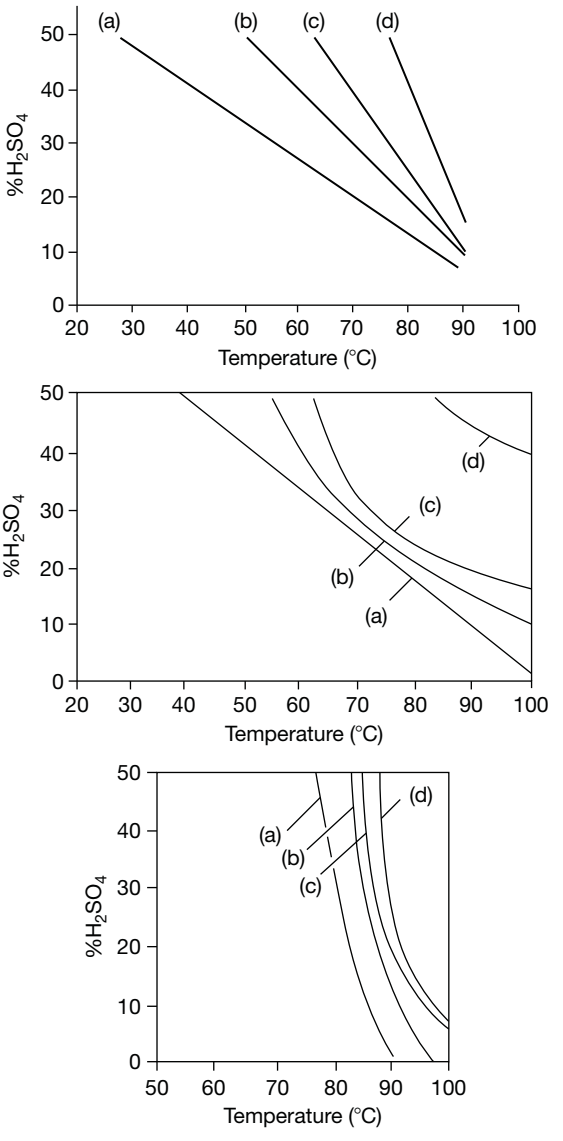

Figure 5 Isocorrosion curves of different duplex stainless steel group with varying Ru concentrations (i) 22% Cr–9% Ni–3% Mo (a = 0% Ru; b = 0.1% Ru; c = 0.2% Ru; d = = 0.3% Ru); (ii) 29% Cr–13% Ni–3% Mo (a = 0% Ru; b = 0.1% Ru; c = 0.2% Ru; d = 0.3% Ru); and (iii) 35% Cr–17% Ni–3% Mo (a = 0% Ru; b = 0.1% Ru; c = 0.2% Ru; d = 0.3% Ru).

3.22.11 Surface Alloying with PGMs

Unlike bulk alloying, which requires the introduction of a considerable amount of a noble-metal component to obtain a protective effect, surface alloying seems to be a more economical way to achieve the same purpose. It is therefore not surprising that a fair amount of research has been conducted to establish the corrosion resistance of various alloys with PGM surface coatings.

3.22.11.1 Cathodically Modified Cr Coatings

Tomashov *et al.*[67] showed that the corrosion resistance of electrolytic Cr plating could be substantially increased in solutions of nonoxidizing acids when Cr and Pd were deposited layer by layer. Small additions of Pd (1–3%) significantly increased the corrosion resistance of Cr coatings in solutions of 20% sulfuric acid and 5–10% hydrochloric acid. The sequence of alternating Cr and Pd layers, as well as subsequent heat treatment (annealing) after plating, also influenced the corrosion characteristics.

3.22.11.2 Surface Alloying in Fe–Cr Alloys

When Fe–27% Cr is surface alloyed with Pd (0.1–0.5 μm) by an electroplated coating followed by annealing, it acquires a high resistance to corrosion in solutions of 20% sulfuric acid at 100 °C.[68–70] While steel that does not contain Pd was nonresistant, the corrosion rate in the coated steel decreased by several orders of magnitude. The annealing of the samples did not hinder the corrosion resistance, despite the diffusion of a considerable amount of Pd into the base metal. In milder conditions, the introduction of less Pd into the surface layer is even sufficient to prevent corrosion. It was calculated[69] that the minimum amount of Pd that is necessary per unit surface area to impart corrosion resistance is about 0.1 g m^{-2}, which corresponds to mean Pd layer thickness of ~10 nm.

The electrospark method of coating[68–70] yields similar results for corrosion resistance in Fe–27% Cr, and may offer a convenient method for increasing the corrosion resistance of large structures that cannot be electroplated with Pd in baths.

Agarwala and Biefer[50] agree with the Tomashov group that the surface deposition of Pd appears to be a relatively inexpensive way of obtaining good corrosion resistance in stainless steels. They found that the deposition of Pd from a Pd chloride solution onto type 430 stainless steel and type 430 stainless steel plus 2% molybdenum cause the specimens to passivate spontaneously when exposed to 0.5-M sulfuric acid. The molybdenum-bearing steel was more readily passivated than the molybdenum-free steel. They concluded that this behavior supports statements that Pd enriched the surface of an alloy during the initial period of corrosion.

3.22.11.3 Surface Alloying Fe–Cr–Ni Stainless Steel

Work on the cathodic alloying of Fe–Cr–Ni stainless steel surfaces was first carried out by Bianchi *et al.*[71] who electroplated a Fe–19% Cr–11% Ni alloy with Pt. They concluded that, even with a Pt coverage of as low as 20 mg m^{-2}, the Pt provides efficient protection of the stainless steel in solutions of concentration up to 75% H_2SO_4 at 25 °C. They attributed this greater corrosion resistance of the stainless steel to two factors. First, Pt is a more efficient cathode for the reduction of oxygen than is stainless steel and, second, the selective deposition of Pt in the form of small round particles (~0.01 μm in diameter) blocked the most active sites of the stainless steel surface. Electron microscopy was carried out on thin-film samples, and provided evidence for the selective electrodeposition of Pt at emerging dislocations and grain boundaries.

Tomashov *et al.*[68,72] investigated this possibility using two different methods of applying Pd to the surface of an Fe–18% Cr–10% Ni alloy, namely electrolytic plating, and electrospark alloying. The Fe–18% Cr–10% Ni alloy with electrolytically deposited coatings of Pd (0.1–5 μm) acquire high corrosion resistance in a solution of 20% sulfuric acid at 100 °C. Under less aggressive conditions, even less Pd is required in the surface layer to protect the steel from corrosion. When the Fe–18% Cr–10% Ni stainless steel was modified by electrospark alloying, stable passivity was once again obtained. When an Fe–40% Cr–0.2% Pd alloy was used for the coating, the concentration of Pd on the surface of the Fe–18% Cr–10% Ni steel was ~1%, which increased to between 12 and 18% as self-passivation was established. It was found that spark alloying with this combined Cr and Pd alloying addition produced better resistance against corrosion than that obtained when alloying was carried out with Pd alone. However, electrolytic deposition produced a smoother more continuous coating than was produced by spark alloying.

In acid solutions (20% H_2SO_4 at 100 °C), the simultaneous presence of a specimen of carbon steel, which dissolves with the evolution of hydrogen, causes the potential of the specimen coated with Pd (1 μm) to shift towards a more negative value, and causes the stainless steel to dissolve actively. This situation arises irrespective of whether or not there is contact between the carbon steel and the stainless steel coated with Pd.

Potgieter and van Bennekom[73] investigated the corrosion behavior of 316 austenitic stainless steel electrolytically plated with silver and heat treated to diffuse the silver into the material in various sulfuric acid solutions at temperatures of 25, 45, and 75 °C. **Table 4** gives an indication of the performance of the base and plated alloys in the various H_2SO_4 solutions. As can be expected, the best corrosion resistance was observed in the solutions at 25 °C, while the most severe corrosion occurred in the solutions at 75 °C. The silver plated alloy by far outperformed the unplated base alloy under all test conditions, and caused a marked improvement in corrosion resistance. Furthermore, silver has the advantage that it is substantially cheaper than Ru, almost by a factor of 10.

Potgieter *et al.*[74] investigated the effect of Ru evaporated by an electron beam onto an Fe–22% Cr–9% Ni–3% Mo duplex stainless steel on the corrosion

Table 4 Electrochemical parameters of surface alloyed and nonsurface alloyed 316 SS at 25 °C

H_2SO_4 (%)	*Nonalloyed with Ag*		*Surface alloyed with Ag*			
	i_{crit} (A cm^{-2})	i_{corr} (A cm^{-2})	E_{corr} (mV)	i_{crit} (A cm^{-2})	i_{corr} (A cm^{-2})	E_{corr} (mV)
1	37.1	12.84		21.1	6.18	
10		28.48	102		11.15	264
20	87.4	37.41	−310	42.6	13.43	285
30	99.6	90.91	−120	63.3	24.30	280

Table 5 Main features of the influence of noble metal additions on the corrosion resistance of various alloy systems

Alloy system	H_2SO_4	HCl
Ductile chromium	5–98% at boiling point	5–15% at boiling point
	0.1% PGM additions cause a decrease in the corrosion rate by a factor of 10^5 or more	
	Decreasing order of effectiveness of PGMs: Ir > Rh > Ru > Pt > Pd > Os.	
Ferritic stainless steels	20–30% at 25 °C. Additions of <0.5% PGMs decrease the corrosion rate by as much as 99.85%	
	Synergistic beneficial effect on corrosion rate if both a PGM and Mo are present in an alloy.	
	Effect of PGM on corrosion rate increase with increasing chromium content (above 25% in an alloy).	
	Fe–40% Cr–0.2% Pd even more resistant than Hastelloy alloys in	
	10–50% at boiling point	1% at boiling point
	Ru a better cathodic additive than Pd. Insufficient cathodic additive accelerates corrosion	
	Behaviour of PGM alloyed ferritic SSs different in H_sSO_4 and HCl media.	
Austenitic stainless steels	Effect of PGM additions not as dramatic as for ferritic stainless steels, but increase corrosion resistance nonetheless, especially in fairly aggressive conditions. Synergistic beneficial effect on corrosion rate if both a PGM and nickel are present in an alloy.	
	Also possible to enhance corrosion resistance by galvanic coupling with Pt.	
Duplex stainless steel		3% at 50 °C.
		Alloys with low nitrogen content corrode actively even with PGM additions.
	20–50% at 20–100 °C	2–3% at 20–50 °C
	PGM additions (0.5%) cause self-passivation	Highly nitrided manganese substituted duplex SSs with PGM additives more resistant than similar cathodically modified austenitic SS

resistance of the alloy in 10% H_2SO_4, and compared it with that of a bulk alloyed sample containing 0.2% Ru. It was found that the two alloys performed similarly and that both had improved corrosion resistance compared to the base alloy without any Ru addition to it.

The main features of the influence of noble-metal additions on the corrosion resistance of the various alloy systems are summarized in Table 5.

3.22.12 Summary of the Effect of PGMs and other Noble Metals on the Corrosion Resistance of Cr-Based Alloys

From the above discussion, it can be concluded that cathodic alloying additives (PGMs) greatly increase the corrosion resistance of Cr in nonoxidizing acid environments. The processes of active dissolution and passivation of cathodically modified Cr can be satisfactorily interpreted from a comparison of the different electrochemical processes; the anodic process on Cr, and the process on the cathodic component. It is also evident that the corrosion resistance of Fe–Cr stainless steels can be significantly increased in nonoxidizing media over a large range of concentrations and temperatures by small additions (0.5% or less) of PGMs. The amount of PGMs needed to produce passivity in Fe–Cr alloys can be decreased by an increase in the Cr content. When molybdenum is also present in the base alloy, a further beneficial synergistic effect between molybdenum and the PGMs can decrease the concentration of the PGMs needed for stable passivity even further. The pitting corrosion resistance of Fe–Cr–Mo steels can be impaired by some of the PGMs. The use of various methods for surface alloying has also proved

successful in reducing high corrosion rates, and similar results to those achieved by use of bulk alloying can be achieved in increasing the resistance to corrosion. However, long-term assessment has to be carried out on surface alloying before any conclusive judgment can be reached.

Similarly, the alloying of multicomponent stainless steels with Pd can also lead to a significant increase in the corrosion resistance of such steels especially in more aggressive environments. However, the corrosion resistance of these steels also depends, to a large extent, on the presence and combination of other components, for example, molybdenum, manganese, and nitrogen.

The work carried out by Tomashov *et al.*[59,60] provides some insight into the corrosion behavior of cathodically modified duplex stainless steels. The effect of the addition of Ru on the corrosion mechanism and the corrosion of each phase in duplex stainless steels were further investigated by Potgieter,[66] who found that the increase in corrosion resistance was the most pronounced in the alloy group with the lowest Cr and Ni content. Furthermore, it was shown that the Ru additions lowered the cathodic Tafel slopes, the critical current densities required for passivation and only the ferritic phases underwent preferential dissolution under conditions of active corrosion.

Evidence indicates that, for all cathodically modified alloys of titanium, stainless steel, and Cr, there is an enrichment of the PGMs on the surface of the alloy at the onset of passivation. It seems that, in all cases, the enrichment of the surface of the alloy during the corrosion process can be explained as being due to a diffusion mechanism.

3.22.13 The Nature of the Passive Film on Cathodically Modified Alloys

There are various ways in which the corrosion resistance of an alloy can be improved. The formation of stable oxide layers constitutes one such method. Stainless steels owe their corrosion resistance largely to the formation of passivating oxide layers on the surface of the alloys. However, the effect of PGMs and/or their incorporation in stainless steels on the composition of the passive surface layer has not yet received much attention.

Initially, there is an atmospheric oxide film present on the surface of the cathodically modified alloy.[75] Auger analyses have indicated that the composition and structure of the passive film on some cathodically modified alloys are similar to those on other stainless steels.[76] It is accepted that the less noble components of stainless steel, for example Cr and iron, oxidize the fastest during the initial stage of active dissolution, thus leaving the noble metal atoms originally present in solid solution as adatoms on the surface of the alloy. Since the noble metal atoms do not oxidize at the low potentials normally encountered during active dissolution, they accumulate on the surface of the alloy. Once a sufficient quantity has accumulated, it can cause spontaneous passivation of the alloy to occur. Although there is ample evidence from various sources[11,23,32,55,75–77] that there is an accumulation of the cathodic component, present in solid solution in the alloy, on the surface of the alloy during the first few minutes of active dissolution, before the passive state is established, very little is known about the nature of the passive film itself, and only a few investigations have been carried out.

3.22.14 Russian Studies

Tomashov *et al.*[60] concluded that, in the absence of preliminary etching, Pd which is originally present in solid solution in the alloy, is incorporated into the passive film formed on a Fe–25% Cr–6% Ni–3% Mo–N–0.2% Pd alloy after exposure in HCl, but that in the case of preliminary etching in the active region, Pd accumulates on the surface of the alloy in the form of an independent phase. Furthermore, it seems that Pd increases the stability of the passive film. It was also found that the simultaneous presence of Pd and molybdenum in an Fe–25% Cr–2% Mo–0.3% Pd alloy in nonoxidizing acids promotes more stable passivity than do either Pd or molybdenum alone.[48] This is attributed to the direct influence of molybdenum on the anodic process, as well as the assumption that molybdenum was incorporated in the passivating film on the steel.

Tomashov *et al.*[77] also determined that an Fe–25% Cr alloy to which Ru is added, passivated easier in 5–50% H_2SO_4 and 1–5% HCl at 50–100 °C than did a similar alloy with an equal Pd content.

Electron microscopy indicated that the surface layer on the Fe–25% Cr–2% Pd alloy consisted mainly of a chromic oxide (Cr_2O_2) film with metallic Pd precipitates, while no metallic Ru particles were detected in the chromic oxide film on the surface of the Fe–25% Cr–2% Ru alloy. On this basis it was concluded that one of the reasons for the better resistance of the Ru-containing alloy as

compared to the Pd-containing one, was due to the fact that a large fraction of the accumulated Ru was not present in the form of an independent phase, but was included in the composition of hydroxide and oxide layers that had formed on the surface of the alloy, thereby increasing the resistance of these layers.

A detailed electron microscopy study, by Tomashov *et al.*[23] of the accumulation of Pd on the surface of an Fe–25% Cr steel during active corrosion in H_2SO_4 revealed that the particle size of the accumulated Pd depends on the temperature at which dissolution took place, as well as on the Pd concentration in the steel. This was confirmed by Higginson *et al.*,[76] who also found that the concentrations of Ru were higher on the passive surfaces of Fe–40% Cr–0.1% Ru alloys than on the passive surfaces of Fe–40% Cr–0.2% Ru. He furthermore established that the accumulation of Ru on the surfaces of Fe–40% Cr–(0.1–0.2%) Ru also depended on the kind of acid in which corrosion took place.

The composition and morphology of the passive surfaces of the cathodically modified alloys studied by Higginson *et al.*[76] are those predicted by Pickering[22] in his review of selective dissolution for alloys containing low concentrations of the noble metal. These results in addition confirm that the chloride ion tends to produce a coarser distribution, thus supporting the suggestion that the chloride ion increases the rate of surface diffusion of Ru during selective dissolution.

3.22.15 The Fe–40% Cr–PGM System

Although Higginson *et al.*[76] detected Ru with Auger analysis in the Fe–40% Cr–(0.1–0.2%) Ru alloy after spontaneous passivation in 0.5 M HCl and in the Fe–40% Cr–0.1% Ru alloy after spontaneous passivation in 0.5 M H_2SO_4, they only concluded that the enrichment in Ru occurred at the metal oxide film interface, without elaborating on the possible inclusion of the Ru in the passive film. Finer detail about the precise nature of the passive film on Fe–40% Cr–Ru alloys was obtained in a study by Tjong.[61] Tjong confirmed observations by Higginson *et al.*[76] that more Ru is present on the surface of the Fe–40% Cr–0.1% Ru alloy after spontaneous passivation in 0.5 M HCl than in the case of the alloy containing 0.2% Ru and ascribes this to the fact that active dissolution preceding passivation of the 0.1% Ru alloy in 0.5 M HCl is faster than that of the Fe–40% Cr–0.2% Ru alloy. As a result, larger amounts of Ru adatoms are accumulated on the surface of the alloy containing 0.1% Ru than on that of the alloy containing 0.2% Ru. In both alloys passivating spontaneously in 0.5 M HCl, considerable enrichment of Cr as well as Ru occurs in the passive films. Tjong[61] estimated that the thickness of the passive film on the Fe–40% Cr–0.2% Ru alloy, after spontaneous passivation in 0.5 M HCl, was ~3.2 nm.

Tjong[61] also agrees with Higginson *et al.* [76] that Ru is only incorporated in the passive film of the Fe–40% Cr–0.1% Ru alloy after spontaneous passivation in 0.5 M H_2SO_4 and could not be detected for the Fe–40% Cr–0.2% Ru under similar conditions. However, when X-ray photoelectron spectroscopy (XPS) was used, the presence of Ru in the passive film on Fe–40% Cr–0.2% Ru after passivation in 0.5 M H_2SO_4 was detected in the form of Ru^{4+}. Tjong[61] concluded that it is likely that both Ru hydroxide as well as RuO_2 may be present in the passive film. It was pointed out earlier by Tomashov *et al.* [77] that in Cr steel containing Ru, that the Ru tends to be incorporated into the hydroxide or oxide layers formed on the Cr steel. The presence of Ru^{4+} was also detected in the passive films formed on Fe–40% Cr–0.1% Ru after exposure to 0.5 M H_2SO_4 and both Fe–40% Cr–0.1% Ru and 0.2Ru after spontaneous passivation in 0.5 M HCl. Tjong[61] thus proved that Cr and Ru are both incorporated in the passive films formed spontaneously on the Fe–40% Cr–0.1% Ru and Fe–40% Cr–0.2% Ru alloys in both hydrochloric and sulfuric acid solutions as Ru^{4+} and Cr^{3+} species. Further evidence for the incorporation of Ru into the passive film as Ru^{2+} species, comes from the work of Kato and Sakaki[31] who investigated the passivation of Cr–Ru materials in sulfuric acid with AES and XPS.

In another study of the Fe–40% Cr alloy system, Tjong[78] found a remarkable difference in the nature of the passive films formed on an Fe–40% Cr–0.2% Pd alloy that passivated spontaneously and under potentiostatic control in 0.5 M HCl at 25 °C. A comparison of the AES composition depth profiles as well as in the [Cr]/[Cr] + [Fe] concentration ratios with sputtering time reveals that there is a marked difference in the composition of the passive films formed under different conditions. The passive film on the Fe–40% Cr–0.2% Pd alloy that underwent spontaneous passivation in 0.5 M HCl was estimated to be 2.4 nm thick and was enriched in Pd relative to Cr. The enrichment of Pd was responsible for the occurrence of spontaneous passivation. In the passive film formed on this same

alloy under potentiostatic control at 220 mV for 40 min, strong enrichment in Cr was found. No Pd was incorporated into this passive film. XPS measurements on both passive surfaces indicated that the Pd is present in the spontaneously passivated film as Pd^{2+}, whereas Cr is present as Cr^{3+}. This is a significant finding which indicates that there is a difference in the type of oxide formed by different PGMs when spontaneous passivation of Fe–40% Cr–0.2%PGM alloys occur in 0.5 M HCl.

In another investigation[79] of the passivation of Fe–40% Cr–(0.1–0.2)% Pt alloy in 0.5 M HCl at 25 °C, Tjong[79] found that the passive film that formed on these alloys is extremely thin, that is, ~1.6 nm. Although Auger spectra did not detect the presence of Pt in the passive surfaces of the Fe–40Cr–Pt system, XPS measurements revealed the existence of the Pt-passivating species and the fact that the surface film contains two Pt species, that is, Pt^{2+} and Pt^{0} (metallic Pt).

3.22.16 Other Quaternary and Ternary Fe–Cr Alloys with PGMs

Tjong[80] also investigated the passivation characteristics of an FeCrNiMoRu ferritic stainless steel containing 22% Cr, 5% Ni, 3% Mo, and 0–0.3% Ru in 0.5 M HCl at 25 °C. XPS analysis of the passive film on the FeCrNiMo alloy containing 0.3% Ru after spontaneous passivation in 0.5 M HCl showed the presence of three molybdenum species, namely Mo^{0}, Mo^{4+}, and Mo^{6+}, in the passive film. The presence of molybdenum in the spontaneously formed passive film indicated that the film is thin enough to allow escape of photoelectrons ejected from the substrate alloy through the film. It was also found that nickel and Ru were absent and did not accumulate in the passive film.

Auger and XPS analyses on passivated films on Fe–24% Cr containing sputter-deposited Pd and exposed to 0.5-M HCl, revealed that a thick Cr oxide layer formed on the Pd enriched surface of the alloy.[44] XPS analysis of a similar base alloy containing ion implanted Ru after exposure to 0.5 M H_2SO_4 showed that Ru is incorporated as Ru^{4+} in the passive film formed on the alloy.

Studies by Potgieter *et al.*[81] and Baradlai *et al.*[82] on Fe–22% Cr–9% Ni–3% Mo–(0–0.3%) Ru alloys spontaneously passivated in 1–20% sulfuric and 1–2% hydrochloric acid with *in situ* radiotracer methods, AES and XPS analyses, indicate a strong bisulphate/sulphate accumulation on the alloys' surfaces that is related to the redistribution of the main alloying elements (Cr, Ni, Mo), as well as Ru, in the surface oxide films formed on the steels. The steel containing 0.3% Ru which passivated spontaneously in the HCl showed a significant enrichment of Mo. Cr seems to be mostly present as Cr_2O_3 (deeper region) or $Cr(OH)_3$ (outermost range). Various types of iron oxides (Fe_3O_4, Fe_2O_3 and FeO(OH)) were also observed. The Fe_3O_4 and Cr_2O_3 contents were higher in the samples containing Ru than in those without it. Another investigation by the same group[83] using ordinary type-316 stainless steel and a 316 alloy containing 0.5% Ru, shows that after exposing it to HCl and H_2SO_4, selective dissolution of the less noble components occur first, while the majority of the surface defect sites are occupied by Cr, Ni, Mo, and Ru species. The enhanced protection and stability of the passive layers on the 316 + 0.5% Ru are most likely related to the changes in the chemical state and redistribution of these alloying elements on the surface. Myburg *et al.*[84] compared the surface composition of passive layers of an Fe–22% Cr–9% Ni–3% Mo with and without 0.3% Ru after passivation in 0.1 M HCl and 1 M H_2SO_4 with each other after AES and XPS analyses, and concluded that the passive film of the alloy having a Ru addition contained more Cr_2O_3 and Fe^{2+} than $Cr(OH)_3$ and Fe^{3+}, than was found for the alloy without Ru. Their observations correlated with the fact that Ru and Ni act as blocking agents and therefore increase the probability to form a stable passive layer.

Olefjord and Elstrom[85] have reported that the beneficial effect of nickel is not connected with the occurrence of this metal in the passive film. Instead the accumulation of nickel in the underlying alloy surface decreases the dissolution rate in the active condition and thereby enhances the formation of the anodic passive film.[86] It has been pointed out previously by Tomashov *et al.*[87] that Ru blocks lattice point defects during active dissolution and thereby decreases the dissolution rate of Cr from the active sites. It is believed that molybdenum exhibits similar blocking characteristics. It is therefore clear that Mo, Ni, and Ru are competing species in promoting self-passivation. The absence of Ru from the XPS spectra can be explained by taking into account the fact that the molybdenum concentration is ~10 times higher than that of the Ru. Therefore, the molybdenum adatoms presumably blocked the majority of the active surface sites prior to passivation, while only a small number of defect sites are blocked by Ru adatoms. After spontaneous passivation the molybdenum adatoms were incorporated into the film as Mo^{4+} and

Mo^{6+} species. The XPS measurements also showed that the outermost zone of the passive film that formed on the spontaneously passivated FeCrNiMo alloy with 0.3% Ru consists of Cr and molybdenum hydroxides.

In another investigation on the corrosion behavior of a Fe–24% Cr–6% V alloy containing various amounts of Ru (0.12–0.35%), Tjong[88] concluded from the Auger spectrum that Ru was absent in the passive film on the alloy that passivated spontaneously in 5% HCl solution at 25 °C. This was in contrast to what was found for a spontaneously passivated Fe–40% Cr–0.2% Ru alloy in 0.5 M HCl, where Ru was detected in the passive film. However, the Auger spectrum does show the presence of both Cr and vanadium in the spontaneously formed passive film. It therefore seems that the presence of Ru in the passive film not only depends on experimental conditions, but also on the alloy composition and the presence of other alloying elements.

According to Tjong,[88] the absence of Ru in the spontaneously formed passive film on the Fe–25% Cr–6% V–0.35% Ru alloy can be explained in terms of the competition between vanadium and Ru in blocking the surface-defect sites of the lattice. Because the concentration of vanadium is about 20 times greater than that of Ru, most of the surface defect sites are blocked by vanadium rather than Ru. It was also found that both Cr and vanadium were enriched in the passive film formed on this alloy. The thickness of the passive film was estimated to be approximately 1.8 nm.

Peled and Itzhak[89] investigated the nature of the passive films on hot pressed and sintered 316 stainless steel containing Cu, Au, Pd, and Pt additions of various concentrations after spontaneous passivation occurred in 0.5 M H_2SO_4. Auger spectroscopy indicated a maximum in the molybdenum concentrations at a depth of about 0.6 nm in all the passive steel samples, regardless of the composition. These observations mean that molybdenum is accumulated in the passive film. Furthermore, it was found that the oxide-film thickness of passive samples containing Au, Pd, and Pt was about 12–15 nm as compared to about 2–3 nm for passive sintered 316 stainless steel. This was ascribed to the low cathodic overpotential of Au, Pd, and Pt which enhance hydrogen evolution in the cathodic areas and promote the creation of a passive oxide layer in the anodic areas, thus resulting in a thicker oxide film. However, marked enrichment of copper was found on the surface of the passive, Cu-containing, sintered stainless steel samples after exposure to H_2SO_4, while only a slight surface enrichment of the noble alloying elements was observed in the passive samples containing Au, Pd, and Pt.

3.22.17 Summary of the Current Observations about the State of Passive Film Compositions on Cathodically Modified Alloys

The following statements can be made to summarize the current state of knowledge regarding passive films formed in reducing acid media:

i. Accumulation of PGMS originally present in solid solution in the alloy occurs on the surface of the alloy during the initial dissolution period.
ii. Alloying elements such as Mo, V, and Ni can compete with the PGMs in blocking active surface sites during the initial stage of the corrosion process. This might result in the PGMs not being detected in the formed passive film, especially if the concentration of the other alloying elements is significantly higher ($>10\times$) than that of the PGMs.
iii. The amount, particle size, and morphology of the accumulated PGM on the surface alloy depend on the temperature at which the dissolution occurs as well as the medium in which it is taking place. Greater amounts of PGMs are found on surfaces of alloys that corroded in HCl than on those that were placed in H_2SO_4. This is attributed to increased surface-diffusion rates of the PGM adatoms in the presence of Cl^- ions. Another factor that influences the accumulation of PGMs on the alloy surface is its initial concentration in the alloy. In alloys with lower PGM concentrations, active dissolution occurs faster and results in more adatoms accumulated on the final passive surface.
iv. There is a difference in the passive films formed spontaneously and those formed under potentiostatic control. In the former case the PGM is incorporated in the passive film as an oxide, while in the latter case it is not, and is only present in an accumulated metallic form.
v. Different PGMs form different types of oxides on passivated surfaces. Ru occurs as Ru^{4+} in the passive film after spontaneous passivation in H_sSO_4 and HCl, while Pd is incorporated into the passive film as Pd^{2+} after spontaneous passivation of the same base alloy in HCl, or occurs in

the Pd^0 form on the surface. Pt can occur in both the Pt^{2+} and Pt^0 states in the passive film.

vi. Determinations of the thicknesses of the passive films formed on cathodically modified stainless steels were carried out on a limited number of ferritic stainless steels that passivated spontaneously in HCl. Vast opportunities exist to extend this kind of investigations to other stainless steels in the same or different media (e.g., in H_2SO_4) under a variety of conditions. Such an endeavor would shed more light on the role of PGMs and other alloying elements in enhancing the corrosion resistance of cathodically modified alloys.

3.22.18 Noble Metal Corrosion Resistance in Reducing Acids

Before closing this chapter, it is necessary to briefly take cognizance of the corrosion resistance of pure PGMs and other noble metals under reducing conditions (typically in hydrochloric and sulfuric acid solutions) to complete the description and understanding of their effects in various alloying systems exposed to such reducing acid conditions. The interest in recent times and the latest information is a result of renewed interest in the use of PGMs and their respective alloy or oxides combinations in various anode configurations for the chlorine–alkali industry for the electrolytic manufacture of chlorine, as well as the use of PGMs in fuel cell applications.

3.22.18.1 Hydrochloric Acid

Kuhn and Wright[90] quoted evidence that the electrochemical behavior of platinum (Pt) in strong hydrochloric acid solutions can be ascribed to a $PtCl_6$ corrosion product that changes to $PtCl_4$ after passivation. Other sources quoted by Kodera *et al.*[91] confirmed that in the presence of Cl^- ions, Pt dissolves as the $PtCl_4^{2-}$ or $PtCl_6^{2-}$ complex. Apparently the specific adsorption of chloride ions on the electrode surface begins immediately after hydrogen desorption. In the same report it is mentioned that iridium (Ir) resist corrosion more than Pt and that it dissolved as $IrCl_6^{3-}$ and $IrCl_6^{2-}$ if the HCl concentration in solution is stronger than 3 M. Ru corrodes more readily than Pt and Ir, and Llopis and coworkers[92,93] have found that RuO_4 was formed on ruthenium (Ru) electrodes which partially dissolved, presumably as H_2RuO_5, during anodic CV sweeps in hydrochloric acid solutions.

Sandenbergh and van der Lingen[94] calculated Pourbaix diagrams for Pd–Cl–H_2O and Ru–Cl–H_2O systems with 250 g l^{-1} HCl using Stabcal software with the NBS and Uncritical databases and found that Ru should only oxidize (corrode) at potentials more positive than 0.347 V (vs. SHE) or 0.106 V (vs. SCE), while for Pd the values should be more positive than 0.180 V (vs. SHE) or −0.061 V (vs. SCE). Their experimental results were in excellent agreement with these theoretical predictions, thus lending credibility to their reported values of 3.6×10^{-6} and 2.8×10^{-3} A cm^{-2} for the exchange current densities of Ru and Pd in 25% (m/m) HCl, respectively. These authors cautioned though that the values that were obtained are dependent on prior exposure time and surface enrichment of the alloying elements and should not be interpreted as steady state data.

3.22.18.2 Sulfuric Acid

Pourbaix's diagram predicts that Pt metal will dissolve as Pt^{2+} during anodic polarization in strong acid solutions. In sulfuric or nitric acid solution the electrolyte enhances the passivation of Pt, especially in 0.5–5 M solutions, and the extent of corrosion seems to be dependent on the formed platinum oxide,[91] which is presumably PtO.[90] In more concentrated sulfuric acid solutions of 14–18 M, sulfur deposition seems to occur on the Pt electrode surface by cathodic polarization, which induces Pt corrosion under anodic polarization. The corrosion mechanism is thus different in dilute and concentrated sulfuric acid solutions, something which has also been observed in terms of nickel's behavior as an alloying element in stainless steels.[95] In an effort to understand and improve the dissolution behavior of Pt in polymer electrolyte fuel cells (PEFCs), Mitsushima *et al.*[96] reported a solubility of Pt of 3×10^{-6} M at 25 °C in 1 M H_2SO_4 which increases with higher temperatures and increasing acid concentration. They postulated that platinum solubility in an oxygen-containing atmosphere would occur according to the dissolution reaction:

$$PtO_2 + H^+ + H_2O = Pt(OH)_3^+$$

Ota *et al.*[97] reported a dissolution rate of 5 μg A^{-1} h^{-1} for Pt in 1 M H_2SO_4 at 40 °C and the formation of a monolayer of platinum oxide, probably PtO, when Pt is anodized under mild conditions. It was found that the corrosion of Pt is always lower in

sulfuric acid solutions than in hydrochloric acid solutions of similar concentration, because the sulphate anions do not coordinate with the dissolved Pt ions in the way the chloride ions form chlorocomplexes referred to earlier.

In sulfuric acid solution Ru can passivate due to the formation of RuO_4.[92] Lezna *et al.*[98] reported electrochemical evidence which indicated that the O-layer formation and reduction of Ru in sulfuric acid depend on the range over which the potential is cycled. The anodic reaction initiated when the potential exceeds the equilibrium potential of 0.455 V for the reaction:

$$Ru = Ru^{2+} + 2e^{-}$$

yields the equivalent of a monolayer of probably a mixture of oxygen-containing species such as Ru_2O, Ru(OH), or $RuO{\cdot}H_2O$ during the first stage of the electrooxidation process. This can change to Ru_2O_3 and RuO_2 as the potential is increased to 1.4–1.5 V (vs. SCE). Although no specific formula is given for it, a formal oxide of Ir begins to form at about the potential of oxygen evolution in 0.5 M H_2SO_4, and this oxide is only reduced in the hydrogen adsorption and evolution region.[92,93]

According to Pourbaix[99] the standard potentials for several noble metals dissolving are 0.80 V for Rh/Rh^{3+}, 0.99 V for Pd/Pd^{2+}, 1.19 V for Pt/Pt^{2+} and 1.50 V for Au/Au^{3+} versus RHE. Rand and Woods[100] reported similar values in their investigating on the dissolution of Pt, Pd, Rh, and Au electrodes in 1-M sulfuric acid solutions at 25 °C and emphasized that the amount of metal dissolved during a potential sweep (e.g., as in CV) will depend both on the nature and pretreatment of the electrode, on the experimental conditions, any stirring of the solution and the surface's structure. Their work supported a direct anodic dissolution mechanism of the noble metals according to the general reaction:

$$M = M^{n+} + ne^{-}$$

and the amounts of dissolved metals analyzed in solution correlated well with their electrochemical measurements and other reported values in the literature. It should be kept in mind that all the postulated oxide species formed on the surfaces of PGMs and noble metals during oxidation/corrosion were based on electrochemical data and little evidence could be found of surface analytical measurements to support the electrochemical data.

3.22.19 Final Conclusions

Despite the work during the last 50–60 years in this field, there are still a number of unanswered questions, and matters to be resolved. It is clear that the effects of cathodic modification in enhancing corrosion resistance are definitely more dramatic in ferritic stainless steels than in austenitic or duplex stainless steels. If Pd is replaced by Ru, then the maximum Cr content at which the largest decrease in the corrosion rate in superferritic (Fe–40% Cr) alloys is observed, can be lowered by at least 10%, which can have enormous cost and workability advantages. Because surface alloying seem to be equally efficient to bulk alloying in increasing the corrosion resistance of various stainless steels, it is definitely a more cost effective option to exploit in terms of practical applications of cathodically modified stainless steels for process equipment manufacture. However, it is not clear if cathodically modified stainless steels will always remain too expensive for uses other than those where safety hazards are the overriding concern and everything else is therefore of secondary importance.

References

1. Cornish, L. A.; Süss, R.; Watson, A.; Preussner, J.; Prins, S. N.; Wenderoth, M., Völkl, R., Glatzel, U. *J. SAIMM* **2007**, *107*, 713–724.
2. Cornish, L. A.; Süss, R.; Völkl, R.; Wenderoth, M.; Vorberg, S.; Fischer, B.; Glatzel, U.; Douglas, A.; Chown, L. H.; Murakumo, T.; Preussner, J.; Lupton, D.; Glaner, L.; Maledi, N. B.; Potgieter, J. H.; Sephton, M.; Williams, G. *J. SAIMM* **2007**, *107*, 697–711.
3. Tomashov, N. D. *Prot. Met.* **1986**, *22*, 679.
4. Tomashov, N. D. *Corrosion* **1958**, *14*, 229.
5. Monnart, P. *Metallurgie* **1911**, *8*, 161.
6. Tomashov, N. D.; Sinelschtschikova, G. P. Vedineeva, M. A. *Ber. Akad. D. Wissenschaft (Dokl. Akad. Nauk SSSR) (Moscow 1962)* Bd. **1948**, *1*, 105–108.
7. Stern, M. *J. Electrochem. Soc.* **1958**, *105*, 638.
8. Stern, M.; Wissenberg, H. *J. Electrochem. Soc.* **1959**, *106*, 751–764.
9. Stern, M.; Bishop, C. R. *Prepr. Am. Soc. Metals* **1959**, *51*, 165; *ASM* **1960**, *52*, 239.
10. Stern, M.; Bishop, C. R. *Trans. ASM* 1961, 54.
11. Greene, N. D.; Bishop, C. R.; Stern, M. *J. Electrochem. Soc.* **1961**, *108*, 836–841.
12. Cotton, J. B. *Chem. Ind.* **1958**, *68–9*, 492; *Werkstoffe und Korrosion* **1960**, *1*, 152.
13. Cotton, J. B. *Chem. Eng.* **1960**, *67*, 166.
14. Cotton, J. B. *Chem. Eng.* **1959**, *66*, 200.
15. Cotton, J. B. *Ber. 111. Int. Congr. Metallic Corr. Moscow,* **1966**, 54.
16. Bockris, J. O. M.; Bonciocat, N.; Guthmann, F. *An Introduction to Electrochemical Science*; Sykeham Publishers: London, 1974; 72.
17. Streicher, M. A. *Platin. Met. Rev.* **1977**, *21*, 51–55.

18. Higginson, A. Ph.D Thesis, University of Manchester (UMIST), Manchester, U.K, 1987.
19. Tomashov, N. D. *Prot. Met.* **1967**, *3*, 3; **1986**, *22*, 679.
20. Tomashov, N. D. *Prot. Met.* **1981**, *17*, 11.
21. Forty, A. B.; Durkin, J. A. *Philos. Mag.* **1980**, *42*, 295.
22. Pickering, H. W. *Corros. Sci.* **1983**, *23*, 1107–1120.
23. Tomashov, N. D.; Chernova, G. P.; Volkov, L. N.; Yakharov, A. P.; Sheshenina, Y. E. *Prot. Met.* **1973**, *9*, 289–292.
24. Tomoshov, N. D.; Chernova, G. P.; Ustinkskii, E. N.; Chalykh, A. E.; Ilin, M. I.; Matveev, V. V.; Rubitsov, A. E. *Prot. Met.* **1984**, *20*, 158.
25. Brox, B.; Olejford, I. In Proceedings of the Stainless Steel 84 Conference, Institute of Metals: London, 1985; 134.
26. Tomashov, N. D.; Chernova, G. P. *Passivity and Protection of Metals Against Corrosion*; Nauka: Moscow, 1965; pp 89–97.Translated from Russian by B.H. Tytell, Plenum Press, New York, 1967.
27. Tomashov, N. D.; Chernova, G. P.; Ustinskii, E. N. *Platin. Met. Rev.* **1979**, *23*, 143–149.
28. Tomashov, N. D.; Chernova, G. P.; Trevilov, V. I.; Ratinski, A. N.; Poryadchenko, N. E.; Savranski, E. F.; Ustinskii, E. N. *Prot. Met.* **1980**, *16*, 208–213.
29. Tomashov, N. D.; Chernova, G. P.; Ustinskii, E. N. *Prot. Met.* **1980**, *16*, 452–455.
30. Tomashov, N. D.; Chernova, G. P.; Trevilov, V. I.; Ratinski, A. N.; Poryadchenko, N. E.; Savranski, E. F.; Ustinskii, E. N. *Prot. Met.* **1983**, *19*, 89–93.
31. Kato, M.; Sakaki, T. *J. Jpn. Inst. Met.* **1993**, *57*(4), 410–416.
32. Tomashov, N. D.; Chernova, G. P.; Ustinskii, E. N. *Prot. Met.* **1981**, *17*, 325–330.
33. Tomashov, N. D.; Chernova, G. P.; Ustinskii, E. N. *Corrosion* **1984**, *40*, 134–138.
34. Tomashov, N. D.; Chernova, G. P.; Ustinskii, E. N.; Chalykh, A. E.; Il'in, M. I.; Matveev, V. V.; Rubstov, A. E. *Prot. Met.* **1984**, *20*, 158–162.
35. Tomashov, N. D. *Werkstoffe Korrosion* **1967**, *8*, 694–707.
36. Biefer, G. J. *Can. Metall. Q.* **1970**, *9*, 537–550.
37. Tomashov, N. D.; Chernova, G. P. *Prot. Met.* **1975**, *11*, 379–384.
38. Potgieter, J. H.; Kincer, M. U. *S. Afr. J. Chem* **1991**, *44*, 47–50.
39. Potgieter, J. H.; Machio, C. N.; Olubambi, P. A.; Sherif, E. M. In Proceedings Eurocorr 2007, Freiburg in Breisgau, Germany 9–13 Sept 2007.
40. Howarth, D. Unpublished results, Randburg, Council for Mineral Technology, 1987.
41. Potgieter, J. H.; Van Bennekom, A. *Can. Metall. Q.* **1995**, *34*, 143–146.
42. Wolff, I. M.; Iorio, L. E.; Rumpf, T.; Scheers, P. V. T.; Potgieter, J. H. *Mater. Sci. Eng. A* **1998**, *241*(1–2), 264–276.
43. Tomashov, N. D.; Chernova, G. P.; Chigirinskaya, L. A.; Nasedkina, E. A. *Prot. Met.* **1986**, *22*, 704–710.
44. Tjong, S. C. *Appl. Surf. Sci.* **1991**, *51*, 157–164.
45. Tjong, S. C.; Chu, P. K. *Surf. Coat. Technol.* **2007**, *201*, 6781–6784.
46. Lizlovs, E. A.; Bond, A. P. *J. Electrochem. Soc.* **1969**, *116*, 574.
47. Tomashov, N. D.; Chernova, G. P.; Markova, O. N. *Prot. Met.* **1973**, *9*, 616–618.
48. Tomashov, N. D.; Chernova, G. P.; Golovanenko, S. A.; Ul'yanin, E. A.; Goronkova, A. D. *Prot. Met.* **1980**, *16*, 83–89.
49. Tomashov, N. D.; Chernova, G. P.; Ryabchenkov, A. V.; Gerasimov, V. I.; Aksenova, L. I.; Agakishiev, O. D.; Chigirinkskaya, L. A. *Prot. Met.* **1985**, *21*, 155–159.
50. Agarwala, V. S.; Biefer, G. J. *Corrosion* **1972**, *28*, 64–74.
51. Streicher, M. A. *Corrosion* **1974**, *30*, 77–91.
52. Scheers, P. V. T.; McEwan, J. J.; Knight, D. *Corros. Coat.* **1994**, 1–4.
53. McEwan, J. J.; Knight, D.; Scheers, P. V. T. *Proceedings of the XVth CMMI Congress; SAIMM* **1994**; Vol. 2, pp 151–155.
54. Sherif El-Sayed, M.; Potgieter, J. H.; Comins, J. D.; Cornish, L. A.; Olubambi, P. A.; Machio, C. N. In Proceedings Eurocorr 2007, 9–13 Sept, Freiburg in Breisgau, Germany 2007.
55. Tomashov, N. D.; Chernova, G. P. Chigirinskaya, L. A. *Corrosion* **1978**, *34*, 445–446.
56. Hoar, T. P. *Platin. Met. Rev.* **1958**, *2*, 117–119.
57. Tomashov, N. D.; Chernova, G. P.; Volkov, L. N. *Prot. Met.* **1970**, *6*, 388–390.
58. Peled, P.; Itzhak, D. *Corros. Sci.* **1988**, *28*, 1019–1028.
59. Tomashov, N. D.; Chernova, G. P.; Lakomskii, V. I.; Torkhov, G. F.; Chigirinkskaya, L. A.; Slyshankova, V. A. *Prot. Met.* **1977**, *13*, 6–11.
60. Chernova, G. P.; Chigirinskaya, L. A.; Tomashov, N. D. *Prot. Met.* **1980**, *16*, 1–5.
61. Tjong, S. C. *Appl. Surf. Sci.* **1990**, *44*, 7–15.
62. Potgieter, J. H. *J. Mater. Sci. Lett.* **1996**, *15*, 1408–1411.
63. Bianchi, G.; Barosi, A.; Trasatti, S. *Electrochim. Acta* **1965**, *10*, 83–95.
64. Kabi, C.; Mukherjee, K. P.; Rastogi, M. C. *J. Electochem. Soc. India* **1985**, *34*, 256–260.
65. Bain, E. C.; Griffith, W. E. *Trans. Metall. Soc. AIME* **1927**, *75*, 166–213.
66. Potgieter, J. H. *S. Afr. J. Chem.* **1993**, *46*(3/4), 58–64.
67. Tomashov, N. D.; Chernova, G. P.; Fedoseeva, T. A. *Prot. Met.* **1976**, *12*, 1–3.
68. Tomashov, N. D.; Chernova, G. P.; Fedoseeva, T. A.; Kornienko, L. P. *Prot. Met.* **1981**, *17*, 406–411.
69. Tomashov, N. D.; Chernova, G. P.; Reshetnikov, S. M.; Fedoseeva, T. A.; Vdovin, S. F.; Kornienko, L. P. *Prot. Met.* **1979**, *15*, 525–528.
70. Tomashov, N. D.; Chernova, G. P.; Fedoseeva *Corrosion* **1980**, *36*, 201–27.
71. Bianchi, G.; Camona, G. A.; Fiori, G.; Mazza, F. *Corros. Sci.* **1968**, *8*, 751–757.
72. Tomashov, N. D.; Chernova, G. P.; Fedoseeva, T. A.; Kornienko, L. P. *Surf. Technol.* **1981**, *13*, 241–256.
73. Van Bennekom, A.; Potgieter, J. H. *Surf. Eng.* **2001**, *17*(1), 71–74.
74. Potgieter, J. H.; Wentzel, E.; Myburg, G. *Surf. Eng.* **1992**, *8*(4), 289–292.
75. Tomashov, N. D.; Chernova, G. P.; Ustinski, E. N. *Platin. Met. Rev.* **1979**, *23*, 147.
76. Higginson, A.; Newman, R. C.; Proctor, R. P. M. *Corros. Sci.* **1989**, *29*, 1293–1318.
77. Tomashov, N. D.; Chernova, G. P.; Chigirinskaya, L. A.; Nasedkina, E. A. *Prot. Met.* **1986**, *22*, 704–720.
78. Tjong, S. C. *Surf. Coat. Technol.* **1982**, *38*, 46–52.
79. Tjong, S. C. *Appl. Surf. Sci.* **1990**, *45*, 301–318.
80. Tjong, S. C. *Werkstoffe Korrosion* **1989**, *40*, 729–734.
81. Potgieter, J. H.; Barnard, G.; Myburg, G.; Varga, K.; Baradlai, P.; Tomesanyi, L. *J. Appl. Electrochem.* **1996**, *26*, 1103–1110.
82. Baradlai, P.; Potgieter, J. H.; Barnard, W. O.; Tomcsanyi, L.; Varga, K. *Mater. Sci. Forum* **1995**, *185–188*, 759–768.
83. Varga, K.; Baradlai, P.; Barnard, W. O.; Myburg, G.; Halmos, P.; Potgieter, J. H. *Electrochim. Acta* **1997**, *42*(1), 25–35.
84. Myburg, G.; Varga, K.; Barnard, W. O.; Baradlai, P.; Tomcsanyi, L.; Potgieter, J. H.; Louw, C. W.; van Staden, M. J. *Appl. Surf. Sci.* **1998**, *136*, 29–35.

85. Olefjord, I.; Elfstrom, B. O. *Corrosion* **1982**, *38*, 46–52.
86. Olefjord, I.; Brox, B.; Jelvestam, U. *J. Electrochem. Soc.* **1985**, *132*, 2854–61.
87. Tomashov, N. D.; Chernova, G. P.; Ustinski, E. N. *Corrosion* **1984**, *40*, 134–8.
88. Tjong, S. C. *ISIJ* **1990**, *30*, 397–402.
89. Peled, P.; Itzhak, D. *Corros. Sci.* **1991**, *32*, 83–90.
90. Kuhn, A. T.; Wright, P. M. *Electroanal. Chem. Interf. Electrochem.* **1973**, *41*, 329–349.
91. Kodera, F.; Kuwahara, Y.; Nakazawa, A.; Umeda, M. *J. Power Sources* **2007**, *172*, 698–703.
92. Llopis, L.; Tordesillas, I. M.; Alfayate, J. M. *Electrochim. Acta* **1966**, *11*, 623–632.
93. Llopis, L.; Vazquez, M. *Electrochim. Acta* **1966**, *11*, 633–640.
94. Sandenbergh, R. F.; Van der Lingen, E. *Corros. Sci.* **2005**, *47*, 3300–3311.
95. Potgieter, J. H.; Olubambi, P. A.; Machio, C. N.; Cornish, L.; Sherif, E. S. M. *Corros. Sci.* **2008**, *50*, 2572–2579.
96. Mitsushima, M.; Koizumi, Y.; Uzuka, S.; Ota, K. I. *Electrochim. Acta* **2008**, *54*, 455–460.
97. Ota, K. I.; Nishigori, S.; Kamiya, N. *J. Electroanal. Chem.* **1988**, *257*, 205–215.
98. Lezna, R. O.; De Tacconi, N. R.; Arvia, A. J. *J. Electroanal. Chem.* **1983**, *151*, 193–207.
99. Pourbaix, M. *Atlas of Electrochemical Equilibria in Aqueous Solution*; Pergamon Press: Oxford, 1966.
100. Rand, D. A. J.; Woods, R. *Electroanal.Chem. Interf. Electrochem.* **1972**, *35*, 209–218.

3.24 Degradation of Carbon and Graphite

S. B. Lyon
Corrosion and Protection Centre, School of Materials, The University of Manchester, Oxford Road, Manchester M13 9PL, UK

Glossary

Exfoliation The process of separation or shedding of layers of a structure, caused by mechanical abrasion, or particularly intercalation within a structure, resulting in the disruption of the bonding forces between 2-dimensional sheets of a material, such as graphite.

Fullerene A generic molecular structure for carbon, comprising linked polygonal sheets that build into a 3-dimensional structure such as a tube or ball and which resembles the geodesic dome structures originally designed by the architect Buckminster Fuller, after whom such structures are named.

Intercalation An ionic or molecular process that comprises the entry, or exchange, of species into a 2- or 3-dimensional lattice structure, for example, between the 2-D-layered sheets that constitute graphite. Such entry often results in significant changes in physical or chemical properties of the structure.

3.24.1 Technical Carbon and Graphite

3.24.1.1 Introduction

Natural flake graphite was known in ancient times as a mineral with well described properties, albeit in small volumes. However, the material became of technical interest only when an electric resistance furnace, capable of graphitization of carbonaceous materials and production of materials in large dimensions, was developed by Acheson in 1895.[1] Currently, only a few mines supply natural graphite, the main producing countries being China, Ukraine, Brazil, Russia, and Canada, although many mines produce

the less-valuable amorphous material in small volumes and not the more-valuable flake graphite. In the United Kingdom, a small graphite mine near Kendal was the basis of the Lakeland pencil manufacturing industry.

Baked carbon and industrial graphite can be manufactured from almost any form of carbonaceous precursor that leaves a carbon-rich material when heated in the absence of air. The main difference between the two substances is that graphitization requires furnace baking for much longer periods at higher temperatures and is therefore considerably more costly. However, its properties, for example, electrical conductivity, high temperature strength, etc., are greatly superior to baked carbon. In view of the limited natural resources, the main carbon precursors for carbon and graphite manufacture are generally cokes derived either from petroleum or coal, the former giving the highest purity and lowest ash content.

Carbon atoms can coordinate in several different ways with adjacent atoms. Thus, in the sp^3 form, carbon is tetragonally coordinated in 3 dimensions, while in the sp^2 form, carbon is trigonal planar.[2] Although carbon is obviously most abundant in nature in the form of various coals (largely, amorphous carbon containing various amounts of volatile materials and ash), this key difference in bonding is well exhibited in carbon's naturally occurring allotropes: graphite (sp^2 bonding in 2-D macromolecular sheets), and most appealingly, diamond (sp^3 bonding in 3-D macromolecules). In recent years, however, it has also been recognized that carbon can form a multitude of polymeric-like structures and macromolecules based particularly on sp^2 bonding, for example, fullerenes.

3.24.1.2 Baked Carbon

At atmospheric pressure, carbon does not melt, but sublimes at very high temperatures (above 4000 °C). It can, therefore, only be manufactured using conventional ceramic processing routes. Thus, the precursor material (e.g., coal-derived coke) is initially ground to a desired particle size range, and then a clay-like green compact is formed with petroleum pitch or coal tar as binder. This is then formed into a final or near-net shape compact typically by extrusion, die-molding, or isostatic pressing. Significant anisotropy may be developed during such compact formation, especially with extruded materials. Also, the considerable shrinkage that will take place during heating has to be taken into account in the initial dimensions of the green compact. After formation, the green compact is then baked in a pyrolysis furnace (i.e., with the exclusion of air) in order to eliminate oxidation and to ensure the carbonization of the pitch binder and the removal of volatile species by diffusion. During this process, it is important to limit the initial heating rate and temperature in order to ensure dimensional stability of the material. Depending on the application and the precursor, the initial pyrolysis temperatures are typically from 200 to 500 °C, with a final baking temperature of 650–900 °C. To avoid excessive cracking and porosity, large dimensioned samples require slow heating and cooling with furnace cycles of tens of days possible.

Carbon products from a single baking cycle are usually relatively porous (15–25 % porosity). Thus, although there are some uses for porous carbons (e.g., for the infiltration of copper for carbon brushes in electric motors, etc.), such products are, more generally, subjected to repeated cycles of pitch infiltration and baking in order to reduce porosity to desired levels (**Figure 1**).

3.24.1.3 Industrial Graphite

Baked carbon precursors may be graphitized by further heat treatment, using direct resistance heating with water-cooled electrodes. This further improves the mechanical and electrical properties of the material and also reduces the ash and volatile content. However, additional shrinkage takes place during the graphitization process. Initially, the temperature is raised to between 900 and 1200 °C where any residual pitch filler is fully carbonized. Thereafter, the temperature is raised in stages: from 1500 to 2000 °C, residual impurities such as hydrogen and sulfur are volatilized; above 2200 °C, a significant graphite crystallization commences; above 2600 °C, the graphite crystallite growth predominates; finally, at ~3000 °C, the electrical and mechanical properties become optimal. At this point, the residual impurity content (mostly as nonvolatile metal-containing ashes) should be below 1000 ppm, which is sufficient for the majority of purposes. Prolonged treatment at higher temperatures can further reduce this value to 200–300 ppm. The total cycle time of heating and cooling may take several tens of days.

Normally, the levels of residual impurity after high temperature graphitization are adequate for most purposes. However, very high-purity grades such as nuclear graphite require further lower-temperature thermal treatment using halogens, or

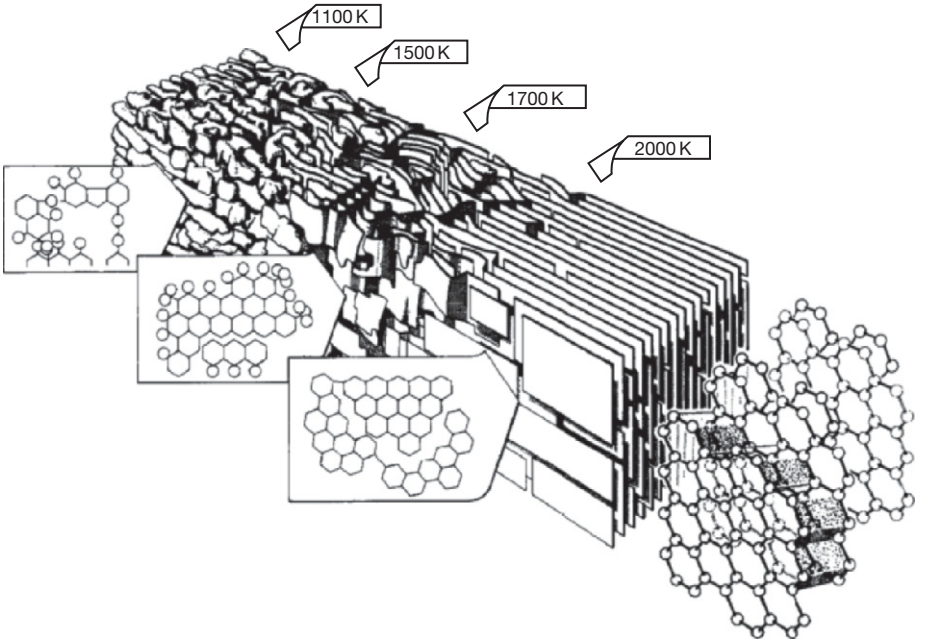

Figure 1 Schematic diagram showing the progressive graphitization of carbon. Reproduced from Marsh, H. *Carbon* 1991, *29*, 703–704, with permission from Elsevier Publications.[3]

more commonly, halogen-containing compounds (e.g., carbon tetrachloride) in order to convert residual metal species to volatile halides. In this way, the residual impurity level can be reduced to below 1 ppm.

3.24.1.4 Glassy Carbon

Vitreous or glassy carbon is important because of its low reactivity (high corrosion resistance). These are generally produced by the pyrolytic decomposition of thermoset polymer resins (e.g., phenolic resins), with or without fiber reinforcement (e.g., by cellulose or rayon).[4] Carbonization occurs in the solid phase, and there is no significant crystallite growth or porosity development even at graphitizing temperatures. The production of this type of carbon requires moderate and carefully controlled baking rates, because large volumetric contractions occur (~50%) and considerable volumes of volatiles are emitted.

3.24.1.5 Pyrolytic Graphite

Carbon may be directly deposited on a heated substrate by the decomposition of hydrocarbons such as methane, benzene, or acetylene. The reaction conditions determine how the deposition occurs (i.e., surface or gas phase polymerization), but it is essential to avoid soot formation in the gas. The structure of pyrolytic graphite can be varied from randomly oriented (i.e., essentially isotropic and nanocrystalline) to highly oriented material of near theoretical density. The high anisotropy of this latter material leads to markedly different properties in directions parallel and perpendicular to the graphite planes. This feature is an advantage particularly in heat transfer applications where high conductivity in one or two directions is desired to be combined with poor conductivity in a third direction.

3.24.1.6 Carbon Fiber and Carbon Composites

Carbon fibers essentially comprise long bundles of linked graphite plates in a highly oriented crystal structure layered parallel to the fiber axis. This results in extreme anisotropy, with elastic moduli of up to 200–400 GPa on-axis versus only 35 GPa off-axis. Carbon fibers can be manufactured from several different precursor fibers, such as polyacrylonitrile, rayon, etc., and by high temperature pyrolysis with or without pretensioning, usually in a two-stage process with initial carbonization at ~1500 °C followed by graphitization at ~3000 °C. In such ways, the properties of the resulting fibers can be varied somewhat to emphasize

either high strength (2000–5000 MPa) or high stiffness (200–400 GPa). Given the range of densities for carbon fibers (1.7–1.85 g cm^{-3}), they have outstanding specific strength and stiffness characteristics.

Carbon fibers may be used with a variety of matrix phases, including polymer composites (e.g., epoxy–carbon) and carbon–carbon composites (fiber-reinforced graphite). The latter can be made via vapor deposition routes; however, these are generally slow and costly. Alternatively, methods involving fibers can be impregnated into a thermoset resin (e.g., phenolic) or petroleum pitch, followed by further pyrolysis steps.

3.24.1.7 Other Forms of Carbon: Fullerenes and Carbon Nanostructures

Until 1985, carbon was thought to exist only in two allotropes: diamond and graphite. This changed when, using mass spectroscopy, an entirely new form of carbon was found in which the atoms are arranged in closed structures. The original discovery, for which the Nobel Prize for Chemistry was awarded in 1996, was for the isolation and the identification of the C_{60} molecule, which is shaped like a soccer ball (i.e., consisting of alternating pentagons and hexagons). Such closed-shaped molecules are named fullerenes because of their resemblance to the geodesic domes first constructed by the architect R. Buckminster Fuller. Since 1985, many additional fullerene molecules have been identified, and furthermore, several additional molecular shapes, often based on rolled up sheets of graphite, have been identified, for example, carbon nanotubes. Many of these materials have interesting electrical and other characteristics, and there is hope that they will eventually outgrow the laboratory and become industrially useful.

3.24.1.8 Final Manufacture and Surface Finishing

Baked carbon and industrial graphite are both fully machinable with the use of conventional tools, although carbide or diamond-tipped tools are preferable especially when cutting lower-porosity glassy carbon because of its higher hardness. Additional treatments that seal the surface and/or internal porosity are also often used. These include, for example, sealing/impregnation with organic materials such as phenolic resins or Polytetrafluoroethene (PTFE) (although this will limit the application temperature to below ~200 °C) and a final impregnation with pitch followed by a low-temperature pyrolysis process. High temperature degradation (usually by oxidation) may be reduced by impregnation with inorganic salts, such as borates and phosphates, which melt at operating temperatures, sealing the pores. All forms of carbon may be coated with, for example, silicon carbide, silicon nitride, or high-density pyrolytic graphite by chemical vapor deposition. Such treatments can provide greatly improved oxidation and chemical (wet corrosion) resistance.

3.24.2 General Characteristics

Carbon and graphite have a number of useful and even unique properties that may be summarized as follows:

- retention of modulus, strength, and erosion resistance to very high temperatures (up to 3200 °C in nonoxidizing atmospheres);
- low coefficient of thermal expansion and high thermal conductivity (25% of copper), giving rise to excellent thermal shock resistance;
- high corrosion resistance and a wide resistance to chemical attack except to strongly oxidizing species;
- significant electrical conductivity especially in fully graphitized materials;
- low friction and self-lubrication in graphitized grades;
- controllable porosity, giving a spectrum of structures from dense, hard materials to nanoporous materials with very high surface area;
- efficient moderation of fast neutrons and scattering of thermal (i.e., slow) neutrons, coupled with a low-absorption cross section for both thermal and fast neutrons in high-purity grades

The physical properties of a number of grades of carbon are summarized in **Table 1**. It should be noted, however, that the material properties will vary over a wide range depending upon the original source of carbon (e.g., natural graphite, petroleum coke, or coked coal), the original powder size prior to sintering, the binder used (e.g., petroleum pitch, coal tar, etc.), and the temperature and time of heat treatment, including the number of cycles of pitch infiltration and recarbonization. Also, depending on the initial morphology of the input carbon source

Table 1 Typical properties of carbon and graphite materials[5]

Property	*Baked carbon*	*Industrial graphite*	*Glassy carbon*	*Pyrolytic graphite*
Bulk density (mg m^{-3})	1.65–1.8	1.7–1.9	1.3–1.5	2.1–2.2
Nominal porosity (%)	15–20%	9–18%	25–30%	<1%
Compressive strength (MPa)				–
Modulus of elasticity (GPa)	8–14	10–15	12–20	28–31
Tensile strength (MPa)	0.007–0.016			8–12 *//c* 110 *//ab*
Coefficient of thermal expansion (K^{-1})	3.5–5.5 × 10^{-6}			15–25 *//c* −1–1 *//ab*
Thermal conductivity (W m^{-1} K^{-1})	30–100	100–200	4–10	1–3 *//c* 190–390 *//ab*
Electrical conductivity (Ω^{-1} m^{-1})	200–1000			300–1000 *//c* 20 000–25 000 *//ab*
Ash content	<0.2%	<0.1%	1–2%	<1 ppm

(e.g., natural flake graphite), materials produced by extrusion and related processes may retain significant anisotropy in the final manufactured product. Thus, one purpose in using the increasing grinding of the input carbon source is to produce small particle sizes that reduce or eliminate this anisotropy.

Carbon and graphite are unusual in that (in the absence of oxidative degradation) their strength and Young's modulus generally increase with temperature. Thus, the tensile strength of industrial graphite is about twice the room temperature value at 2500 °C, while its modulus is ~40% higher. Fully dense (pyrolytic) graphite generally has outstanding high temperature properties, especially if isotropic (i.e., essentially containing randomly oriented nanocrystallites). More normally, however, its properties are highly directional and vary within the graphite basal plane (*ab*-direction) and across the planes (*c*-direction). This variation is due to the large difference in interatomic distance between in-plane atoms and out-of-plane atoms. This directionality of properties can be utilized for advantage in certain applications, for example, where good heat transfer in one direction is required to be coupled with poor heat transfer in another direction (Figure 2).

The oxidation of carbon and graphite materials leads to the formation of gaseous products (i.e., CO and/or CO_2) and results in a rapid decrease in properties, especially strength. These reactions begin to become significant above ~350 °C, but can be controlled by reducing or eliminating the porosity of the materials, in which case slow reaction will occur only on the surface of the material, leading to a steady loss of thickness. In the absence of oxidation, the dimensional stability of carbon and graphite materials is excellent, provided their final heat treatment temperature is not exceeded. If this occurs, then additional graphitization may take place, leading to shrinkage.

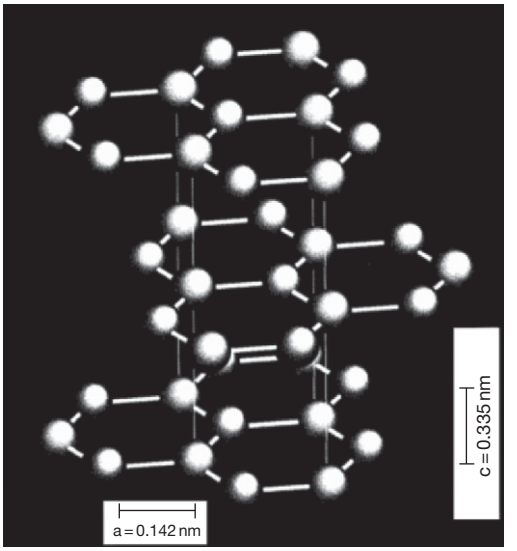

Figure 2 Schematic diagram showing the atomic structure of graphite. Reproduced from European Carbon and Graphite Association, Avenue de Broqueville 12, B-1150 Bruxelles, with permission from Elsevier Publications.

3.24.3 Applications

Carbon is relatively inert chemically and thus may be used in all its forms under a variety of corrosive conditions. Many applications depend upon the acceptable electrical and excellent heat conductivity

of carbon and graphite and upon the unique retention of significant strength at very high temperatures. Thus, current major uses include

- carbon anodes in the Hall–Heroult aluminum cell and in electric arc furnaces such as for steel production and remelting; this is by far the greatest tonnage usage;
- heat exchangers, gaskets, seals, etc. for use in the chemical industry;
- furnace linings (e.g., in the iron blast furnace) as well as other high temperature furnace components, including crucibles;
- resistive and inductive susceptor elements in furnace and related specialist activities (e.g., graphite tube furnaces for atomic absorption spectroscopy);
- dies for optical glass fiber drawing and related operations;
- reaction vessels, crucibles, and supports in the electronics industry for Si wafer and especially for III–V semiconductor manufacture;
- heat transfer in brake blocks and other friction components, as well as low friction bearing materials, seals, etc. in the automotive and aerospace industries;
- conductive brushes for slip rings and commutator components in electric motors, etc;
- neutron moderator and reflector materials in the nuclear industry;
- heat-resisting components in aerospace and rocketry;
- biomedical applications (carbon is fully biocompatible);
- Electrodes for conventional batteries and ultra-high surface area electrodes for lithium ion cells and supercapacitors.
- electrodes in electrolysis cells (e.g., chloralkali production) and cathodic protection anodes, etc.

3.24.4 Degradation of Carbon and Graphite

3.24.4.1 Aqueous Corrosion

In aqueous conditions and at room temperature, carbon is thermodynamically unstable to direct oxidization to carbon dioxide, the bicarbonate ion, or the carbonate ion, depending upon the pH, and to direct reduction to methane at all pH. In practice, these reactions are severely kinetically hindered, and apart from oxidation at pH below ~1, occur at negligible rates at all pH up to 100 °C. The only significant aqueous oxidation processes occur in strongly oxidizing environments such as concentrated nitric acid, perchloric acid, chromic acid, and chromates, or at highly oxidizing (positive) potentials. Thus, at pH 0 and under appropriate conditions, carbon will slowly form carbon dioxide at potentials more positive than ~0.45 V on the hydrogen electrode scale (SHE). This implies that carbon/graphite is a relatively noble element – indeed, it is slightly more noble than copper. Therefore, while coupling graphite components to other metals, this important factor should be taken into account.

Most degradation of industrial graphite under aqueous conditions occurs not as a result of oxidation, but as a consequence of the reaction within pores of the material, for example, with residual impurities or binder phases, causing initially localized mechanical damage, but ultimately macroscopic mechanical failure of the component. Alternatively, where chemical species (e.g., chloride ion) can intercalate between the graphite layers, thus causing exfoliation, degradation is greatly increased.

3.24.4.2 Aqueous Environments

The performance of glassy carbon electrodes in sulfuric acid under anodic polarization has been examined at room temperature as a function of acid concentration and anodic current density.[6] It was found that the dominant process of mass removal was via a mechanical mechanism with initial selective oxidative attack in regions of apparent lower density. This appeared to result in a mechanical stress, thus giving rise to local spallation. The formation of CO_2 as the oxidative product was also confirmed. Degradation did not occur below the potential for oxygen evolution, but above this value was approximately linear with applied anodic current density and with acid concentration up to 4 M H_2SO_4. A degraded surface film, ~2–4 μm in thickness, formed after passage of ~80 000 C m^{-2}.

The corrosion of industrial graphite was examined in 30% (5.5 M) phosphoric acid at 25 and 80 °C.[7] Under free corrosion conditions in air, the electrochemical potential fell in the range 0.59–0.62 V (SHE), which is somewhat greater than the theoretical value of 0.45 V. Potentiodynamic polarization implied the presence of a surface film, most likely of adsorbed oxygen and hydroxide species. Secondary ion mass spectrometry confirmed this hypothesis and also demonstrated significant penetration of phosphorus within the graphite, either as an

intercalated species, or more likely, adsorbed onto internal porosity (Figure 3).

The mass-loss rates for carbon electrolysis anodes used in brines for chlorine production were examined as a function of temperature, current density, and NaCl concentration.[8] The mass-loss rate was found to decrease with increase in chloride concentration and increase with temperature. The maximum degradation rate was at approximately neutral pH, the rate falling off by a factor of 2–3 under acid (pH 1) and alkaline (pH 11) conditions; at neutral pH, the degradation rate was found to be a function of current density. The degradation mechanism occurred via the reaction of an adsorbed chloride–graphite intermediate. Significant reductions in degradation rate were achieved as the overall porosity of the anodes decreased, and particularly, when the average pore size decreased below ~5 μm.

The oxidation of high-purity (nuclear) graphite was studied in nitric acid at temperatures between 275 and 300 °C and at 100–120 bar pressure.[9] Under these extreme conditions, graphite is smoothly oxidized to carbon dioxide, while the nitric acid is reduced to nitrogen. Average reaction rates from 0.4 to 1 mol h^{-1} were obtained under these conditions.

The corrosion of small graphite tube furnaces, used in atomic adsorption spectroscopy, was studied primarily in order to ascertain the effect of their degradation on the accuracy of analysis.[10] However, it was found that the order of acid reactivity followed the trend: $HNO_3 < HF < HCl < HClO_4$. This was explained by two tendencies: first, the ability of the aggressive species to intercalate between the graphite sheets, and second, the ability of the species to oxidize the graphite. Thus, hydrochloric acid, which is nonoxidizing but which can intercalate easily because of the small size of the chloride ion, is more aggressive than nitric acid, resulting in mechanical damage (exfoliation) to the graphite.

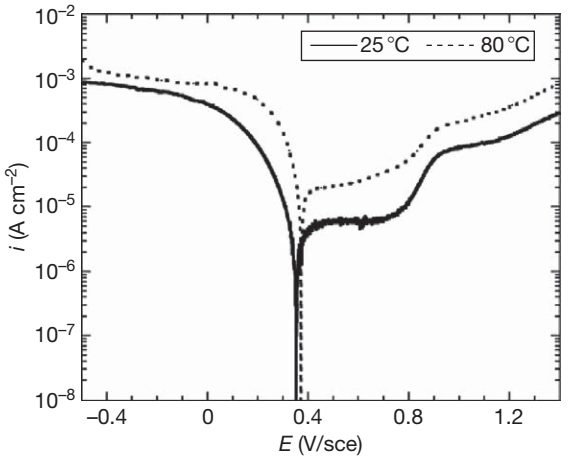

Figure 3 Potentiodynamic polarization of graphite in phosphoric acid. Reproduced from Guenbour, A.; Kebkab, N.; Bellaouchou, A.; Iken, H.; Boulif, R.; BenBachir, A. *Appl. Surf. Sci.* **2006**, *252*, 8710–8715, with permission from the European Carbon and Graphite Association (page 4 on presentation: ''The element C''.

The electrochemical degradation of glass-like carbon (GC), diamond-like carbon (DLC), and highly ordered pyrolytic graphite (HOPG) were studied in nitric–hydrofluoric acid mixtures at 50 °C.[11] Under repeated potential cycling within the range for water stability, small pits became apparent on the GC electrode and the HOPG electrode became severely roughened. However, a few, if any, morphological changes were evident on the DLC electrode. The heavy degradation of the HOPG electrode was ascribed to the oxidation of intercalated species and the consequent exfoliation of the graphite sheets.

The stability of graphite-reinforced epoxy-composite materials was studied under both galvanic coupling (i.e., where the graphite was a net cathode) and anodic polarization in order to understand electrochemically induced degradation processes. When the composite was connected to sacrificial anode materials in seawater, it suffered a significant (30%) reduction in strength over 140 days' exposure.[12] This was found to be due to the degradation of the graphite–epoxy bond probably via a similar mechanism to cathodic disbondment of organic coatings. Under anodic polarization, significant damage was apparent even at comparatively low current densities of 1 μA cm^{-2}. This was ascribed to direct oxidation of the graphite fibers at local potentials above the oxygen evolution reaction.[13] Consequently, care has to be taken when using carbon fiber reinforcement composite materials where they may become electrochemically polarized.

In summary, all forms of technically important carbon may be degraded in aqueous conditions by two main mechanisms: electrochemical oxidation under anodic polarization (or chemical oxidation using a strong oxidizing agent) and the intercalation of small species between the graphite sheets with consequent swelling leading to the exfoliation of the sheets. Both of these processes may be greatly reduced in extent by use of dense materials of low overall porosity and/or with pore sizes in the micron range.

3.24.4.3 Galvanic Corrosion

Since carbon/graphite is relatively noble, care has to be taken to ensure its galvanic compatibility with metals in which it is in contact. Thus, graphite is cathodic to most common metals such as steels, and particularly, the light metals aluminum and magnesium. Indeed, early aluminum airframes, which were commonly marked out for cutting using graphite pencils, suffered from corrosion along the residual pencil marks.[14] Also, a cathodic residue of carbon, deposited from lubrication oils during tube drawing, is responsible for the pitting of copper tubing in some natural drinking supply waters. Thus, the general assumption should be that electrical contact between carbon/graphite and other metals under aqueous corrosion conditions should generally be avoided.

As an example, the galvanic corrosion behavior of graphite fiber-reinforced epoxy composites coupled to a series of materials (aluminum alloys AA2024, 7075, and 5052, stainless steels AISI301, 302, 321, 15-5PH, and 17-7PH, carbon steel AISI4340, nickel–aluminum–bronze, and titanium Ti–6Al–4V) was studied.[15] The graphite composite was found to be cathodic in 3.5% NaCl to all of the alloys studied. Relatively high galvanic currents were evident when coupled to all aluminum alloys and to the carbon steel: the corrosion in these cases was effectively limited by cathodic oxygen reduction at the graphite cathode. Dealloying was evident for the nickel–aluminum–bronze material, and hence, coupling this material to graphite is also not recommended. Of the passive alloys, minor pitting was observed for the lower grades of stainless steel, while only titanium was deemed to be wholly safe.

Although graphitic materials are not generally recommended where oxygen reduction is the dominant cathodic process, they are relatively widely used as gasket materials in a crevice situation: where oxygen depletion would be expected. Under these conditions, the electrochemical potential of the graphite will become significantly depressed tending to that of the hydrogen evolution reaction. The likelihood of crevice attack with graphite gaskets was explored by experiment and modeling[16] where it was predicted that, in nonchlorinated seawater, graphite is likely to become anodic to duplex stainless steels, and hence protective, in a tight crevice because of oxygen depletion. However, for lower grades such as AISI316, where initiation is due to micropitting, such protection would not be effective.

3.24.4.4 High Temperature Oxidation

Carbon is largely nonreactive in air or oxygen at temperatures below ~350 °C. However, above 400 °C the rate of reaction increases significantly. The principle oxidants are air (i.e., O_2), steam (H_2O), and carbon dioxide (CO_2), the main reaction equilibria being:

$$C + O_2 \rightleftarrows CO_2 \quad [1]$$

$$C + CO_2 \rightleftarrows 2CO \quad [2]$$

$$C + H_2O \rightleftarrows CO + H_2 \quad [3]$$

The CO_2 shift reaction [2] and the water gas reaction [3] are both thermodynamically unfavorable below ~700 °C, but start to become kinetically significant above ~750 °C. The kinetic reactivity[17] differs greatly as a function of the material's porosity, its residual ash content (i.e., on the presence of oxidative catalysts, such as metallic impurities), and interestingly, also on the form of carbon. Studies of the thermal stability of diamond, graphite, carbon black, C_{60} and C_{70} fullerenes, and carbon nanotubes were carried out by thermal gravimetric analysis in nitrogen and air.[18] In nitrogen, the low molecular weight materials (i.e., the fullerenes and the carbon black) started to sublime above ~300–400 °C; however, graphite and diamond showed mass losses of less than 3% up to 900 °C. In flowing air, the onset temperatures for the reaction of C_{70} and C_{60} fullerenes were ~430 °C and 530 °C, respectively. Carbon black commenced reaction at ~505 °C, graphite showing significant mass losses above ~610 °C. The carbon nanotube structures were most resistant, with an onset temperature of 820 °C, while diamond had an onset temperature of 800 °C. However, once reaction commenced, oxidation was found to progress rapidly (**Figure 4**).

Thus, the kinetics of oxidation of different forms of carbon are clearly very different at lower temperatures. However, as the oxidation temperature increases, the surface reactivity becomes less rate-limiting, and above 800 °C, the oxidation rate is determined by mass transfer in the gas phase.[19] For example, the reaction of nuclear graphite with air was found to follow three regimes as a function of temperature.[20] In the lowest temperature range from 400 to 600 °C, the reaction exhibited the highest activation energy (~160 kJ mol^{-1}) and was chemical reaction rate controlled. In the intermediate range from 600 to 800 °C, the activation energy fell to 72 kJ mol^{-1}, with the reaction kinetics controlled by

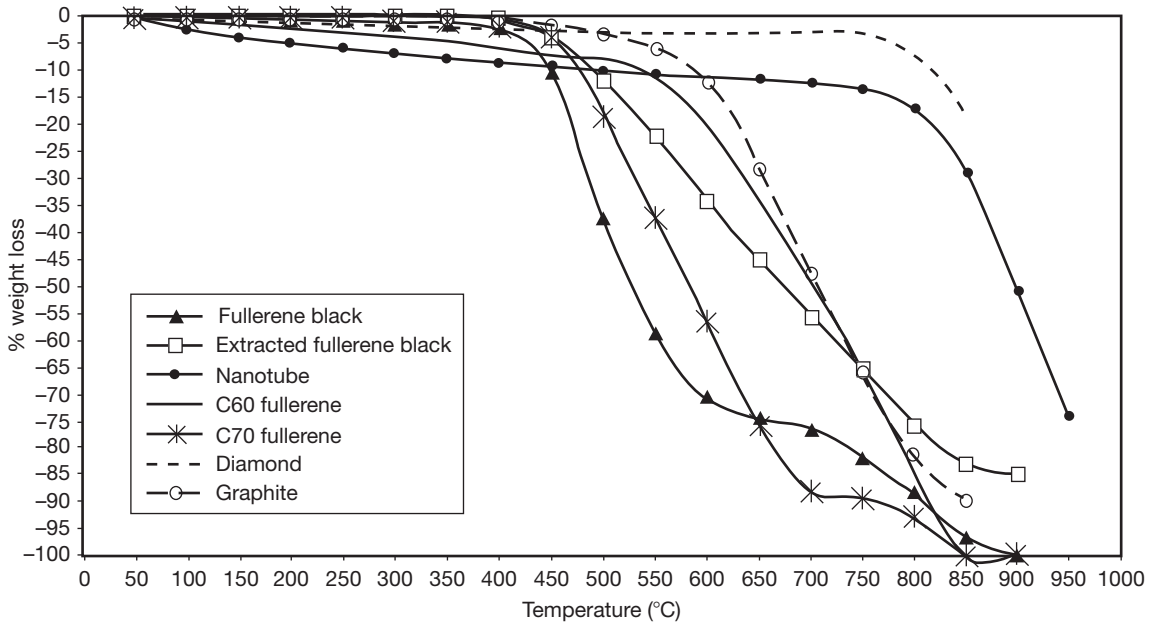

Figure 4 Thermal gravimetric analysis on carbon materials in flowing air at 20 °C min^{-1}. Reproduced from Cataldo, F. *Fullerenes, Nanotubes and Carbon Nanostruct*. **2002**, *10*, 293–311, with permission from Taylor and Francis.

the diffusion of reactant and products within the pores in the material. Above 800 °C, the activation energy was low-to-negligible, the rate-controlling step in the oxidation process being boundary diffusion in the bulk gas phase.

3.24.4.5 High Temperature Environments

Carbon will react directly at high temperatures with many nonmetallic elements such as sulfur and halogens and with metallic elements that can dissolve significant quantities of carbon (e.g., iron). The layered structure of graphite is also susceptible to intercalation with a range of species both ionic and molecular (e.g., from molten salts), leading to the disruption and the exfoliation of the graphite layers.[21] This phenomenon is critical in the use of graphite intercalation electrodes in Li-ion rechargeable cells in room temperature molten salts.[22]

Many molten metals will dissolve significant quantities of carbon, iron being the most obvious example of this. Notwithstanding this factor, carbon refractory materials are a critical component of many smelting and purification processes particularly for their outstanding resistance to thermal shock. For example, the hot-air zone of the iron blast furnace (i.e., close to the tuyeres or hot air nozzles) is an extreme environment requiring high temperature stability with resistance to hot gas erosion and large temperature fluctuations. In view of this, carbon refractories, often impregnated with oxide materials such as zirconia to improve abrasion and erosion resistance, are the materials of choice.[23]

3.24.4.6 Protection against Degradation

For high temperature use, it is normal to protect carbon from oxidation, as relatively small mass losses (e.g., 5–10%) have been found to result in losses of mechanical properties of up to 50%.[19] Alternative gas atmospheres such as H_2 or N_2 are most easily used; however, at temperatures above ~1500–1600 °C, hydrogen will react to form methane, while nitrogen will react at temperatures above ~1700 °C to form cyanogen. Thus, at very high temperatures, inert gas atmospheres, such as argon or helium, are essential. Careful matching of the grade of carbon or graphite to the application, for example by the selection of low porosity (high density) grades, will also help to limit degradation rates both at high temperature and in aqueous conditions.

There has long been a search for coating methods to protect carbon from high temperature degradation, which is predominantly an oxidation problem. Such coatings should match the thermal expansion properties of carbon (to avoid spallation on thermal cycling), should adhere well, should have a low permeability to oxygen, and clearly, should not

themselves degrade/oxidize under the conditions of operation. Coatings that are molten at the operating temperature (i.e., glazes) are obviously resistant to cracking and are self-healing.[24] The most successful of such glazes are based on boron oxide (B_2O_3), which melts at ~500 °C and starts to volatilize significantly above 1200 °C, although their upper limit of operation is ~900 °C when their permeability to oxygen starts to become significant.[25] Phosphorus-type glazes may also be used successfully in a similar manner.[26]

Above ~900 °C, single layer coatings become increasingly ineffective and multilayer coatings are required. Many types of oxide, carbide, and nitride coatings have been applied with a view to limiting oxidation. The most successful are those based on silicon carbide either in conjunction with boron oxide (i.e., as self-healing agent)[24] or in functional coatings with graded thermal expansion coefficients matched to the substrate.[27] Coatings can be formed using a variety of methods, including sol–gel, pack cementation, and chemical or physical vapor deposition. Silicon carbide is successful, partly because it oxidizes to silicon oxide; however, the upper temperature limit for SiO_2 is ~1700–1800 °C when its vapor pressure starts to become significant; thus, in practice, the practical temperature limit is ~1650 °C. Above 1800–2000 °C, nonoxide ceramics become increasingly susceptible to oxidation and many oxide ceramics are not stable to carbothermic reduction. However, for specialist uses, such as rocketry components, which require only a few minutes' or hours' operation at maximum temperature, coatings such as hafnium and zirconium carbides and borides have been implemented successfully.

3.24.5 Nuclear Graphite

3.24.5.1 Radiation Damage

The main purpose of graphite in a fission reactor is to slow ('thermalize') fast neutrons, which are emitted during fission, so that they can be recaptured by heavy nuclei in order to maintain the fission chain reaction. Graphite can also act to reflect slow neutrons back into the reactor core, thus improving neutron usage and may find use in a similar role in future fusion reactor systems. To accomplish this goal satisfactorily, nuclear graphite has exceptionally low impurity levels, that is, below a few parts per million. This is because elemental impurities will unacceptably increase the neutron capture cross-section of the graphite. Apart from this difference in purity, the microstructures of nuclear grades of graphite are essentially similar to other graphite grades except that they generally have lower porosity resulting in improved mechanical properties.

Fast neutrons typically emerge from a fission event with a mean energy of ~2 MeV (a velocity of 15 000 km s^{-1}). This needs to be reduced to ~1 km s^{-1} (~50–100 eV), which is approximately in equilibrium with the surrounding temperature, and hence, these neutrons are known as 'thermal.'[28] Radiation damage in graphite thus occurs as a result of inelastic scattering between the neutrons and carbon atoms that result in the displacement of the carbon from their preferred lattice positions. An incoming neutron will typically require between 500 and 1000 of such scattering events, and travel ~500 nm (i.e., significant in terms of the lattice spacing), before it is in thermal equilibrium; this results in a significant displacement of the carbon atoms, and consequently, a significant storage of energy (Wigner energy) in the form of an unstable lattice. For room temperature irradiation of graphite, this energy can reach over 20 MJ kg^{-1}. This is easily more than sufficient, when released in an uncontrolled manner, to raise the temperature of the material spontaneously by several hundred degrees. Graphite-moderated power reactors, however, generally operate at temperatures that are sufficiently high to result in a continuous thermal annealing of the graphite such that the storage of Wigner energy is insignificant.

Neutron irradiation of graphite also results in significant dimensional changes as a consequence of the difference between inelastic scattering within (*ab*-direction) and between (*c*-direction) the graphite layers.[28] Thus, in single crystal graphite, there is a significant expansion in the between-plane direction and a slight contraction in the in-plane direction. In macroscopic graphite, this results in an initial shrinkage of components, but an ultimate expansion of component sizes giving rise to a significant stress generation.[29] Both these factors have to be taken into account in reactor designs. The physical properties of graphite also change as a result of irradiation.[30] In particular, irradiation induces creep within the graphite and also reduces the elastic modulus of the material in the *c*-direction by ~6%. Also produced are many radiation-induced dislocation structures with the graphite, which disrupts normal lattice vibrations, and hence, the thermal conductivity of irradiated graphite is reduced substantially (by up to two orders of magnitude).

3.24.5.2 Enhanced Radiolytic Oxidation

In graphite-moderated, carbon dioxide-cooled nuclear power reactors, γ-irradiation modifies the chemistry of the reaction between graphite and CO_2. This takes the form of a radiolytic decomposition[31] of carbon dioxide to carbon monoxide and an oxygen radical as follows:

$$CO_2 \rightleftarrows CO + O^{\bullet}$$

Although this decomposition is only transient because of the back reaction, the generation of gas-phase oxygen radicals (and related oxidizing species) is significant enough to comprise the major in-reactor oxidative degradation process for nuclear graphite. As the oxidation of small amounts of graphite can lead to relatively large reductions in mechanical properties, it is important to limit this process as much as possible. In practice, this is achieved in a number of ways. First, the addition of 1–1.5% of carbon monoxide into the coolant tends to scavenge the oxygen radicals produced in the gas-phase, although this process becomes less efficient above 1.5% CO. Thus, in order to maintain long-term integrity of the graphite moderator core, smaller amounts of methane and hydrogen are also added. The former decomposes within the graphite structure to form a sacrificial carbon layer, while the addition of hydrogen limits significant carbon deposition on the fuel rods (which would reduce the reactor efficiency).

References

1. Acheson, E.G. U.S. Patent 542982, 1985; U.S. Patent 568 323, 1896.
2. Morgan, P. *Carbon Fibres and Their Composites*; CRC Press, 2005; Chapter 2.
3. Marsh, H. *Carbon* **1991**, *29*, 703–704.
4. Chekanova, V. D.; Fialkov, A. S. *Russ. Chem. Rev.* **1971**, *40*, 413–428.
5. European Carbon and Graphite Association, Avenue de Broqueville 12, B-1150 Bruxelles.
6. Neffe, S. *Carbon* **1988**, *26*, 687–692.
7. Guenbour, A.; Kebkab, N.; Bellaouchou, A.; Iken, H.; Boulif, R.; BenBachir, A. *Appl. Surf. Sci.* **2006**, *252*, 8710–8715.
8. Rabah, M. A.; Nassif, N.; Abdul Azim, A. *Carbon* **1991**, *29*, 165–171.
9. Farrell, J. P.; Haas, P. A. *Ind. Eng. Chem.* **1967**, *6*, 277–280.
10. Rohr, U.; Ortner, H. M.; Schlemmer, G.; Weinbruch, S.; Welz, B. *Spectrochim. Acta B* **1999**, *54*, 699–718.
11. Swain, G. M. *J. Electrochem. Soc.* **1994**, *141*, 3382–3393.
12. Sloan, F. E.; Talbot, J. B. *Corrosion* **1992**, *48*, 830–838.
13. Sloan, F. E.; Talbot, J. B. *Corrosion* **1992**, *48*, 1020–1026.
14. Dr. Brian Johnson, UMIST, Personal communication.
15. Bellucci, F. *Corrosion* **1992**, *48*, 281–291.
16. Turnbull, A. *Corrosion* **1999**, *55*, 206–212.
17. McKee, D. W. In *Chemistry and Physics of Carbon*; Walker, P. L., Thrower, P. A., Eds.; Marcel Dekker: New York, 1980; Vol. 16.
18. Cataldo, F. *Fullerenes, Nanotubes and Carbon Nanostruct.* **2002**, *10*, 293–311.
19. Pickup, I. M.; McEnaney, B.; Cooke, R. G. *Carbon* **1985**, *24*, 535–543.
20. Xiaowei, L.; Jean-Charles, R.; Suyuan, Y. *Nucl. Eng. Des.* **2004**, *227*, 273–280.
21. Wang, Z. D.; Inagaki, M. *J. Mater. Chem.* **1992**, *2*, 629–632.
22. Doughty, D. H. *Soc. Adv. Mater. Process Eng. J.* **1996**, *32*, 75–81.
23. Vernilli, F. Jr.; Justus, S. M.; Silva, S. N.; Mazine, A.; Baldo, J. B.; Longo, E.; Varela, J. A. *Mater. Corros* **2005**, *56*, 475–480.
24. de Castro, D.; McEnaney, B. *Corros. Sci.* **1992**, *33*, 527–542.
25. McKee, D. W.; Spiro, C. L.; Lamby, E. J. *Carbon* **1984**, *22*, 507–511.
26. McKee, D. W.; Spiro, C. L.; Lamby, E. J. *Carbon* **1984**, *22*, 285–290.
27. Kwon, O. S.; Hong, S. H.; Kim, H. *J. Eur. Ceram. Soc.* **2002**, *23*, 3119–3124.
28. Telling, R. H.; Heggie, M. I. *Philos. Mag.* **2007**, *87*, 4717–4846.
29. Li, H.; Fok, A. S. L.; Marsden, B. J. *J. Nucl. Mater.* **2008**, *372*, 164–170.
30. Tanabe, T.; Maruyama, T.; Iseki, M.; Niwase, K.; Atsumi, H. *Fusion Eng. Des.* **1995**, *29*, 428–434.
31. Best, J. V.; Stephen, W. J.; Wickham, A. J. *Prog. Nucl. Energy* **1985**, *16*, 127–178.

Further Reading

European Carbon and Graphite Association, Avenue de Broqueville 12, B-1150 Bruxelles, http://www.carbonandgraphite.org

Ishikawa, T.; Nagaoki, T. *Recent Carbon Technology*; JEC Press, 1983.

Pierson, H. O. Ed. *Handbook of Carbon, Graphite, Diamonds and Fullerenes: Processing, Properties and Applications*; Applied Science: New York, 1994.

3.23 Corrosion of Metal Matrix Composites

L. H. Hihara
Department of Mechanical Engineering, Holmes Hall 302, College of Engineering, University of Hawaii at Manoa, 2540 Dole St., Honolulu, HI, USA

Abbreviations

B MF Boron monofilament
B_{MF}^{E} B_{MF} electrode with MF ends exposed
B_{MF}^{S} B_{MF} electrode with MF circumferential surface exposed
CD Current density
HP Hot-pressed
MMC Metal–matrix composite
SC Semiconductor
SiC MF Silicon carbide monofilament
SiC_{MF}^{E} SiC_{MF} electrode with MF ends exposed
SiC_{MF}^{S} SiC_{MF} electrode with MF circumferential surface exposed

Symbols

^{E} Electrode with fiber or MF ends exposed (e.g., SiC_{MF}^{E})
$E_{APPLIED}$ Applied potential
E_{pit} Pitting potential

E_{GALV} Galvanic couple potential
g Gaseous state
Gr Graphite
Gr^E Gr electrode with fiber ends exposed
i Current density
i_a Anodic current density
i_c Cathodic current density
i_{CORR} Corrosion current density
i_{GALV} Galvanic current density
l Liquid state
s Solid state
^{S} Electrode with fiber or MF circumferential surface exposed (e.g., SiC_{MF}^S)
t Thickness
V_{SCE} Volts versus a calomel electrode
x_C or X_C Cathodic area fraction
ρ resistivity

3.23.1 Introduction

Metal–matrix composites (MMCs) are metals that are reinforced with either continuous or discontinuous constituents usually in the form of fibers (F), monofilaments (MF), particles (P), whiskers (W), or short fibers (SF). The reinforcements can be metals (e.g., tungsten), nonmetals (e.g., carbon, silicon), or ceramics (e.g., silicon carbide, boron carbide, or alumina). The selection of the matrix metal and reinforcement constituent is usually based on how well the combination interacts to achieve the desired properties. MMCs are usually stiff, strong, and lightweight, but they are also engineered for other properties. Reinforcements have been used in MMCs to increase stiffness,[1] strength,[1] thermal conductivity,[2] neutron shielding, and vibration damping capacity; and to reduce weight,[1] thermal expansion,[3] friction,[4] and wear.[5] Some, but not all, MMC properties are governed by the rule of mixtures.[6] Although MMCs have properties more useful than those of their individual constituents, resistance to corrosion is usually sacrificed. The corrosion behavior of MMCs is often significantly different from that of their monolithic matrix alloys because of the presence of the reinforcements that alter the microstructure, electrochemical properties, and corrosion morphology.

The different types, typical applications, corrosion characteristics, and corrosion protection of MMCs will be summarized below.

3.23.2 Types of MMCs

A variety of MMCs have been developed with matrices such as aluminum, magnesium, lead, depleted uranium, stainless steel, titanium, copper, and zinc. Only MMCs with aluminum matrices, however, are extensively available.[3] Reinforcement constituents for MMCs include boron (B), graphite (Gr), silicon (Si), silicon carbide (SiC), boron carbide (B_4C), titanium diboride (TiB_2), alumina (Al_2O_3), mica, quartz, tungsten, yttria, and zircon. The reinforcement constituents usually range from 10 to 60 vol.%.

In this chapter, the MMC types will be denoted as matrix type/reinforcement composition/vol.% reinforcement type. Hence, aluminum/Al_2O_3/50 P MMC denotes an aluminum matrix MMC reinforced with 50 vol.% of Al_2O_3 particles.

3.23.2.1 Continuous-Reinforced MMCs

Continuous-reinforced (CR) MMCs are reinforced with continuous fibers or MF generally resulting in anisotropic properties, with substantial enhancements in the longitudinal direction of the reinforcement. The reinforcement diameter generally varies from 10 μm for fibers (**Figure 1(a)**) to 150 μm for MF (**Figure 1(b)**). Continuous reinforcements are usually much more

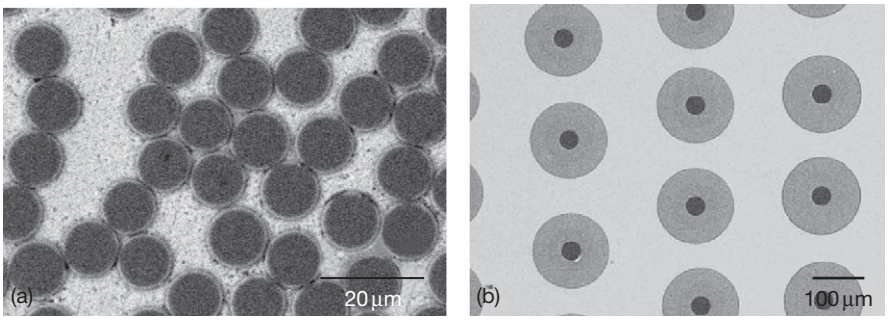

Figure 1 Micrographs of (a) pure Al/Al_2O_3/50 F MMC (courtesy of J. Zhu) and (b) Ti–6Al–4V/SiC/MF MMC (courtesy of R. Srinivasan).

expensive than their discontinuous counterparts. Fabrication costs of CR MMCs are also higher than that of discontinuous-reinforced (DR) MMCs.

3.23.2.2 Discontinuous-Reinforced MMCs

DR MMCs are reinforced with particles, whiskers, or SF, and generally have isotropic properties and lower material and fabrication costs as compared to CR MMCs. Enhancements in properties of DR MMCs, however, are usually modest in comparison to CR MMCs. Reinforcement volume percents range from ~15 to 25% for structural MMCs (**Figure 2(a)**), and greater than 30% for MMCs used in electronic packaging (**Figure 2(b)**). Uniform particle and particle-size distribution are preferred in structural MMCs for optimal mechanical properties. In electronic-grade MMCs, the particle and particle-size distribution may not be uniform in order to maximize the reinforcement volume fraction. The high reinforcement loading in electronic-grade MMCs is necessary to reduce the coefficient of thermal expansion (CTE) to levels closer to that of electronic materials such as silicon and gallium arsenide.

3.23.3 MMC Applications

MMCs are being used in the aerospace, automotive, electronics, utilities, sports, and defence industries.

3.23.3.1 Examples of Applications for CF MMCs

Aluminum/B/MF MMCs have been used for structural tubes in the space shuttle, resulting in 44% reduction in weight over aluminum alloys in the original design.[7] Aluminum/Gr/F MMCs, which have unique properties such as negative to near-zero CTE, have been used as antenna booms in the Hubble Space Telescope.[3] In the automotive industry, $Al/Al_2O_3/F$ MMCs have been used to replace cast iron components. $Al/Al_2O_3/F$ MMCs with low weight, high temperature tensile and fatigue strengths, low thermal conductivity and expansion, and superior wear resistance are used in engine blocks, pistons, and cylinder heads.[8] Other types of $Al/Al_2O_3/F$ MMCs with low weight, high strength, and high damping capacity are used for automotive push rods, resulting in increased horsepower generation.[9] These $Al/Al_2O_3/F$ MMCs are also used as load-carrying core wires in high-current capacity and low-sag aluminum conductor cables (**Figure 3**). The $Al/Al_2O_3/F$ MMCs core wires impart desirable properties to the cable such as high strength at ambient and elevated temperatures, low CTE, and lightweight.

3.23.3.2 Examples of Applications for DR MMCs

Aluminum/SiC/20 P MMCs were used to replace aluminum tubes in the catamaran 'Stars and Stripes '88,' resulting in 20 wt% savings in comparison with monolithic aluminum.[3] Aluminum/Si/43 P MMCs, which are machinable, lightweight, and possess a low CTE, are used for electronic packaging (**Figure 4(a)**). For thermal management applications, copper-matrix MMCs are reinforced with milled graphite fibers that have negative CTEs and thermal conductivities exceeding that of copper. Accordingly, the resulting Cu/Gr MMCs have lower CTEs and higher thermal conductivity than copper.[10] In the automotive sector, DR MMCs are used for engine

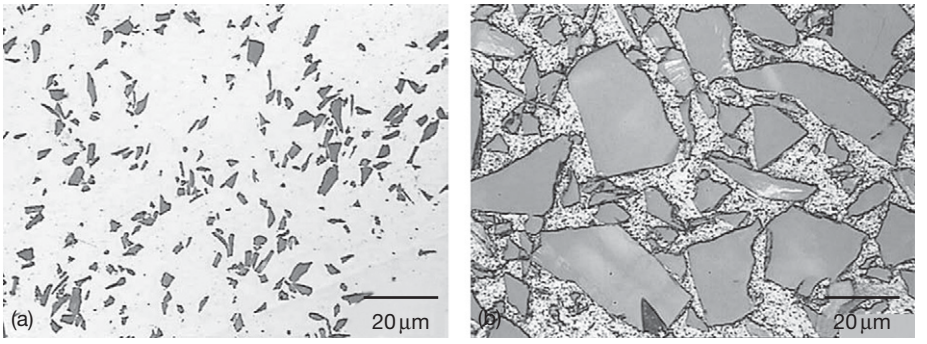

Figure 2 Micrographs of (a) Al 6092/SiC/10 P-T6 MMC and (b) Al 6092 /SiC/50 P-T6 MMC. Courtesy of G. Hawthorn.

pistons, piston connection rods, rear wheel driveshafts, break calipers, cylinder liners, push rods, rocker arms, and valve guides.[11] DR MMCs are also used in the sports industry for high-performance bicycle frames and components, golf clubs, and baseball bats.[11] In the aircraft industry, examples of DR MMCs' used are fan exit guide vanes in turbine engines, ventral fins, helicopter blade sleeves (**Figure 4(b)**), and fuel access covers.[12] Other potential emerging applications for DR MMCs are shoes for tracked vehicles and lightweight armor.

3.23.4 Corrosion Characteristics

The presence of the reinforcements and the processing associated with MMC fabrication can lead to accelerated corrosion of the metal matrix. Special concerns regarding corrosion become important in MMCs as compared to the corrosion of the monolithic matrix alloys. Accelerated corrosion in MMCs may originate from electrochemical, chemical, and physical interaction between MMC constituents because of their intrinsic properties or those induced by processing. Galvanic interaction between the reinforcement, matrix, and interphases can accelerate corrosion. Interphases and reinforcements may undergo chemical degradation, which is not electrochemical in nature. The microstructure of MMCs can influence corrosion by inducing segregation, intermetallic formation, and dislocation generation. Processing deficiencies may result in unexpected forms of corrosion.

The parameters affecting MMC corrosion that will be discussed are (1) electrochemical effects related to the primary MMC constituents; (2) electrochemical effects of the interphases; (3) chemical degradation in MMCs; and (4) secondary effects caused by the microstructure and processing. Corrosion in selected environments and corrosion protection will also be covered.

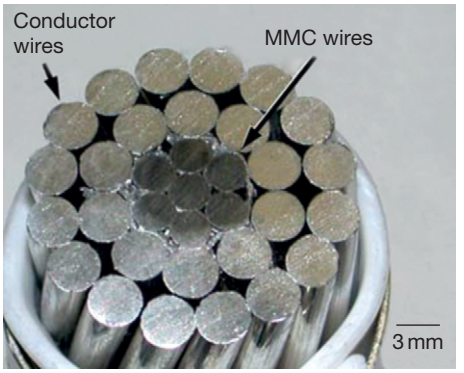

Figure 3 Aluminum conductor composite reinforced cable specimen. Notice the seven inner Al/Al_2O_3/F MMC core wires.

3.23.4.1 Electrochemical Effects Related to the Primary MMC Constituents

Galvanic corrosion between the matrix and reinforcements is one of the primary concerns regarding the corrosion behavior of MMCs. Depending on the electrochemical properties of the MMC constituents, the galvanic corrosion rate can be controlled by either the anodic or cathodic reaction, or by both. Anodic control prevails when the cathodic reaction is depolarized (**Figure 5(a)**); cathodic control prevails when the anodic reaction is depolarized (**Figure 5(b)**); and there is mixed control when both the anodic and cathodic reactions polarize (**Figure 5(c)**).[13] For a galvanic couple with equal matrix and reinforcement

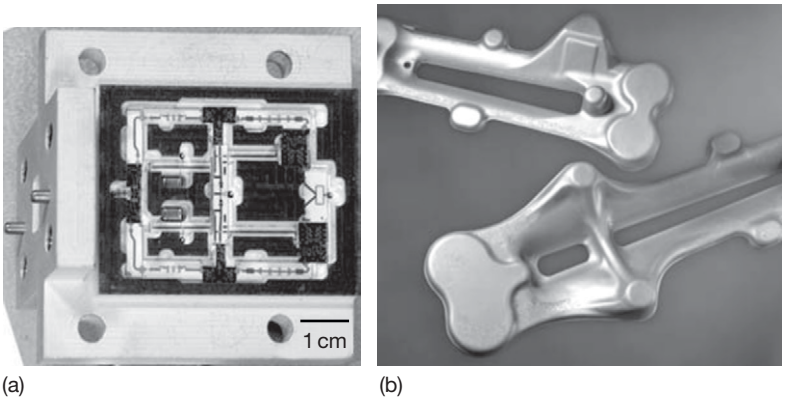

(a) (b)

Figure 4 (a) Pure Al/Si/43 P MMC electronic package, and (b) 2009 Al/SiC/15 P-T4 helicopter blade sleeves (courtesy of DWA Aluminum Composites).

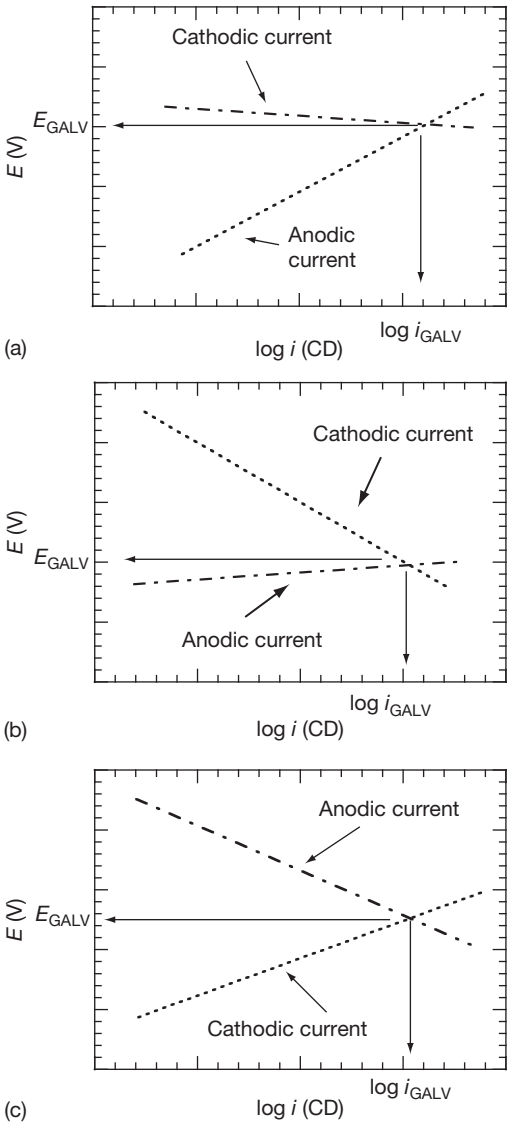

Figure 5 Polarization diagrams showing (a) anodic control, (b) cathodic control, and (c) mixed control in galvanic corrosion.

area fractions, the intersection of the anodic polarization curve of the matrix metal and the cathodic polarization curve of the reinforcement indicates the magnitude of the galvanic corrosion current density (i_{GALV}) (**Figure 6**). Hence, the degree of galvanic corrosion depends on the environment, matrix alloy, reinforcement electrochemistry, resistivity, and area fraction.

3.23.4.1.1 Environment

The environment has a significant effect on galvanic corrosion rates. The two most primary factors are usually dissolved-oxygen content and electrolyte composition (e.g., presence of aggressive ions).

In deaerated environments, the governing cathodic reaction for corrosion is hydrogen evolution:

$$2H_2O + 2e^- = H_2 + 2OH^- \quad [1]$$

In aerated solutions, oxygen reduction can also operate, and generally results in higher corrosion rates:

$$O_2 + 2H_2O + 4e^- = 4OH^- \quad [2]$$

For example, if pure magnesium is coupled to an equal area of SiC MF with the ends exposed (SiC_{MF}^{E}), the galvanic corrosion rate between Mg and SiC_{MF}^{E} would increase by ~4 times if the solution is oxygenated (**Figure 6**). Interestingly, the normal corrosion rate of uncoupled pure magnesium does not significantly change in the presence of dissolved oxygen[14] since hydrogen evolution is the governing cathodic reaction for magnesium, as exemplified in **Figure 6**. Hence, it is important to recognize that the corrosion behavior and trends of the MMC could be significantly different than that of the monolithic matrix alloy.

The presence of aggressive ions can greatly increase the corrosion rate, especially for alloys to lose passivity. For example, the galvanic corrosion rate between a passive metal matrix and conductive reinforcements would be limited to the passive current density (CD), as demonstrated with the polarization diagram Al 6061-T6 plotted with those of various reinforcements in aerated chloride-free 0.5 M Na_2SO_4 (**Figure 7**). In the presence of aggressive ions that breakdown passivity, the galvanic corrosion rates can dramatically increase (**Figure 7**). Using Al 6061-T6 coupled to an equal area of P100 graphite fibers with the ends exposed (Gr^{E}) as an example, the galvanic corrosion rate increases ~300 times in aerated 3.15 wt% NaCl as compared to that in aerated 0.5 M Na_2SO_4 (**Figure 7**).

3.23.4.1.2 Matrix metal

Galvanic corrosion in MMCs reinforced with conductive, noble reinforcements is a concern in environments in which the matrix metal corrodes actively. For example, for MMCs reinforced with an equal area fraction of graphite fibers, i_{GALV} in aerated 3.15 wt% NaCl (**Figure 8**) would be only 5×10^{-7} A cm^{-2} for Ti–15V–3Cr–3Sn–3Al (Ti-15-3), 1.5 orders of magnitude larger for pure copper (10^{-5} A cm^{-2}), and 3 orders of magnitude larger for Al 6061-T6 (3×10^{-4} A cm^{-2}). The passivity of Ti-15-3 prevents i_{GALV} from exceeding the passive-CD (**Figure 8**).

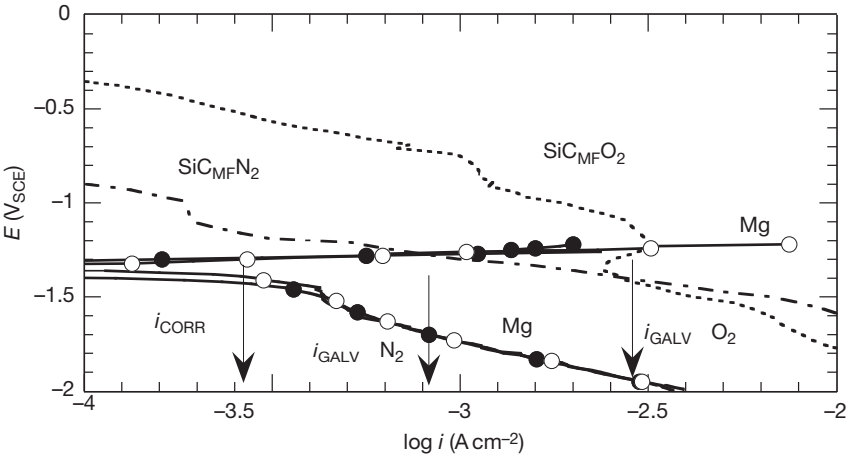

Figure 6 A collection of anodic and cathodic polarization curves of Mg (99.95%) exposed to aerated (open circles) or deaerated (solid circles) 0.5 $NaNO_3$ at 30 °C, and cathodic polarization curves of SiC_{MF}^{E}[15] exposed to deaerated or aerated 0.5 $NaNO_3$ at 30 °C. Scan rate = 0.1 mV s^{-1}. Superscript E denotes MF ends were exposed.

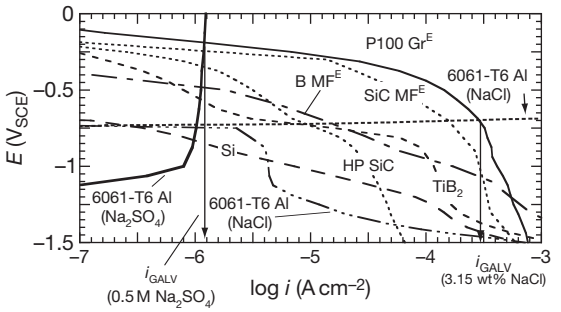

Figure 7 A collection of anodic polarization diagrams of Al 6061-T6[16] exposed to aerated 0.5 M Na_2SO_4 or 3.15 wt% NaCl at 30 °C, and cathodic polarization diagrams of P100 Gr^{E},[16] hot-pressed (HP) SiC,[16] SiC_{MF}^{E},[15] and Si,[17] TiB_2, and B_{MF}^{E} exposed to aerated 3.15 wt% NaCl at 30 °C. Scan rate = 0.1 mV s^{-1}.

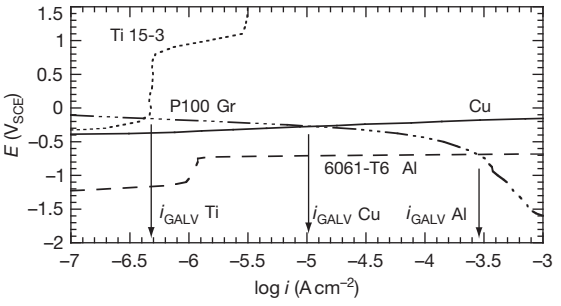

Figure 8 Anodic polarization diagrams of Ti 15-3,[18,19] pure Cu (99.999%), and Al 6061-T6[16] in deaerated 3.15 wt% NaCl at 30 °C. Cathodic polarization diagram of P100 Gr fibers[16] in aerated 3.15 wt% NaCl at 30 °C. Scan rate = 0.1 mV s^{-1}.

In the case of pure copper, i_{GALV} is about 1 order of magnitude less than the normal copper corrosion CD (10^{-4} A cm^{-2}) in the aerated 3.15 wt% NaCl; hence, galvanic action would increase corrosion of copper, but not significantly.

3.23.4.1.3 Reinforcement electrochemistry

In cases where galvanic corrosion is under cathodic control, the type of reinforcement may have a significant effect on the rate of galvanic corrosion. For example, in aluminum MMCs, the galvanic corrosion rates between Al 6061-T6 and various reinforcements ranked from the highest to lowest in aerated 3.15 wt% NaCl is as follows (**Figure 9**): P100 Gr > carbon-cored SiC_{MF}^{E} with ends exposed > tungsten-cored B_{MF}^{E} with ends exposed > hot-pressed (HP) SiC > Si. It should also be noted that ceramic reinforcements may vary in purity and structure, and some reinforcements are in themselves composites. This leads to interesting electrochemical behavior. For example, SiC MFs have carbon-rich outer layers and carbon cores, and their polarization diagrams have a stronger resemblance to P100 Gr^{E} than to HP SiC. The orientation of reinforcements may also affect electrochemical behavior. SiC MFs have carbon cores and B MFs have tungsten cores. The polarization behavior of the circumferential surface of the MFs are different compared with the behavior of the ends of the MFs that expose the carbon and tungsten cores (**Figure 9** compares cathodic curves for SiC MF^{S} versus SiC MF^{E}, and B MF^{S} versus B MF^{E}).

Therefore, the composition of the reinforcement is important to the extent that it affects the kinetics of hydrogen evolution and oxygen reduction.

For reinforcements of very high resistivity, galvanic corrosion can also be limited by a large ohmic drop through reinforcement.

3.23.4.1.4 Reinforcement photoelectrochemistry

If the MMC reinforcements or constituents are semiconductors (SCs), galvanic currents between the matrix metal and SC could be suppressed or accelerated depending on whether the SC is n-type or p-type, respectively.[22]

n-Type SCs

An n-type semiconductor is photoanodic, and under illumination promotes photooxidation reactions. One such reaction is the oxidation of water. In the presence of moisture and illumination on MMCs that contain n-type SCs, photogenerated electrons could polarize the MMC to more negative potentials inducing cathodic protection (**Figure 10**).[22] While the MMC is under illumination, E_{corr} shifts from E_{corr} (dark) to E_{corr} (illum), and the dissolution from the matrix decreases from i_{matrix} (dark) to i_{matrix} (illum). Accordingly, during anodic polarization of Al 6092/Al_2O_3/20 P-T6 MMCs that were immersed in air-exposed 0.5 M Na_2SO_4 solutions, anodic current densities increased sharply during illumination which were attributed to photoanodic currents generated by water oxidation on TiO_2 particles that were likely introduced with the Al_2O_3 reinforcements.[23] The open-circuit potentials also decreased upon illumination. In these MMCs exposed to outdoors, corrosion films were also thinner on the topside of specimens exposed to sunlight as compared with the backside of the specimens not exposed to sunlight.[24] Interestingly, MMCs containing p-type SCs had thicker corrosion films on the sunlit surfaces as opposed to the shaded surfaces.[24]

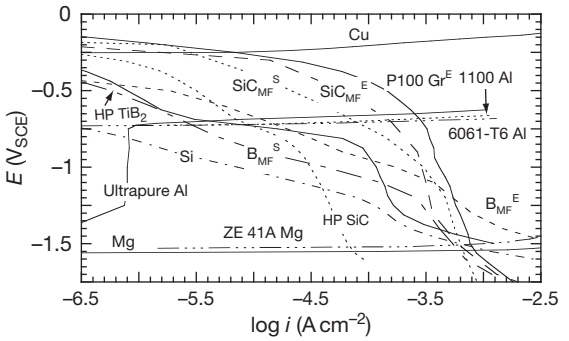

Figure 9 A collection of anodic polarization diagrams of ultrapure Al (99.999%),[16] Al 1100,[17] and Al 6061-T6,[16] and cathodic polarization diagrams of P100 Gr^E,[16] HP SiC,[16] $SiC_{MF}{}^E$,[20] $SiC_{MF}{}^S$,[20] Si,[17] $B_{MF}{}^E$,[21] and $B_{MF}{}^S$ [21] exposed to aerated 3.15 wt% NaCl at 30 °C. Scan rate = 0.1 mV s^{-1}.

p-Type SCs

A p-type SC is photocathodic and under illumination promotes photoreduction reactions. Depending on the electrolyte conditions, proton or oxygen reduction may be enhanced at the p-type semiconductor. In the presence of moisture and illumination on MMCs that contain p-type SCs, photoreduction causes cathodic current to increase, raising the corrosion potential and corrosion rates (**Figure 11**).[22] While the MMC is under illumination, E_{corr} shifts positive from E_{corr} (dark) to E_{corr} (illum), and the dissolution from the matrix increases from i_{matrix} (dark) to i_{matrix} (illum). Accordingly, during cathodic polarization of pure Al/Si/43 P MMCs[25] and various Al 6092/SiC/P-T6 MMCs[22] that were immersed in air-exposed 0.5 M Na_2SO_4 solutions, cathodic current densities increased sharply during illumination, which were attributed to photocathodic currents on

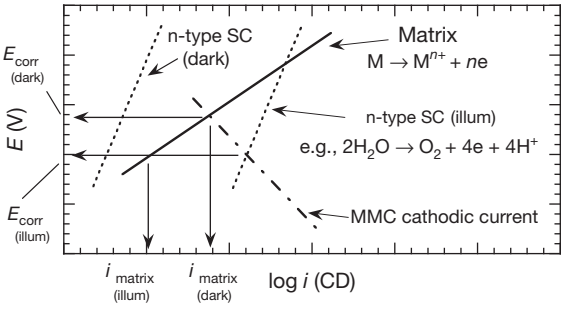

Figure 10 Polarization diagrams showing the effect of an illuminated n-type semiconductor (SC) on the corrosion current density (CD) of the MMC matrix.

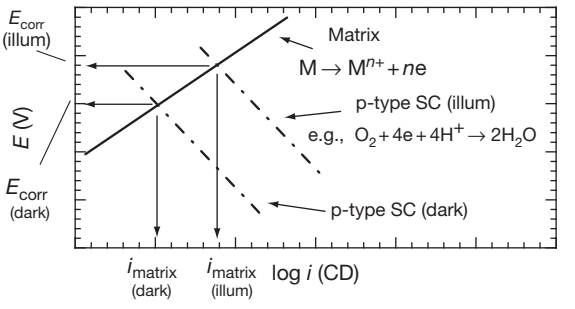

Figure 11 Polarization diagrams showing the effect of an illuminated p-type SC on the corrosion CD of the MMC matrix.

the Si or SiC particles. The open-circuit potentials also increased upon illumination.[22] In these MMCs exposed to outdoors, corrosion films were also thicker on the sunlit surfaces as opposed to the shaded surfaces.[24]

3.23.4.1.5 Reinforcement resistivity

Reinforcement materials generally fall into the categories: insulators, SCs, or conductors (**Table 1**). For reinforcements that are insulators, galvanic corrosion is not possible. For SCs, the degree of galvanic corrosion will be restricted by the magnitude of ohmic losses through the reinforcements. This is demonstrated[21] by plotting (**Figure 12**) the cathodic curve derived from the hydrogen evolution on P100 Gr[26] exposed to aerated 3.15 wt% NaCl at 30 °C and incorporating a term for hypothetical ohmic losses through the electrode (eqn [3]).

$$E_{\mathrm{APPLIED}}(V_{\mathrm{SCE}}) = -0.67 - 0.081 \times \log i + i\rho t \qquad [3]$$

The ohmic loss term $i\rho t$ corresponds to a planar electrode having a thickness t and resistivity ρ, and one-dimensional current flow through the thickness. Equation [3] was plotted for various resistivity values and an electrode thickness of 5 μm with that of anodic polarization diagrams of copper, Al 6061-T6, ZE 41A Mg, and pure magnesium in 3.15 wt% NaCl. Notice the effect of ohmic losses on the cathodic polarization diagrams and decreasing galvanic current densities as the reinforcement resistivities increase (**Figure 12**). For example, i_{GALV} of Al 6061-T6 is $\sim 10^{-4}\,\mathrm{A\,cm^{-2}}$ for an ohmic loss IR_1 resulting from a reinforcement resistivity of $10^{7}\,\Omega\,\mathrm{cm}$. The value of i_{GALV} reduces to $\sim 10^{-7}\,\mathrm{A\,cm^{-2}}$ when the ohmic loss is increased to IR_2 by a reinforcement resistivity of $10^{10}\,\Omega\,\mathrm{cm}$. The effect of reinforcement resistivity on the galvanic corrosion rate is also dependent on the type of matrix metal. The limiting effect on galvanic corrosion rates on copper only manifests at very high reinforcement resistivities (e.g., $>10^{7}\,\Omega\,\mathrm{cm}$ in **Figure 12**); whereas, effects are seen on Al 6061-T6, ZE 41A Mg, and magnesium at lower resistivities. Note that the i_{GALV} values correspond to galvanic couples having equal anode and cathode areas.

Figure 12 is based on a fixed electrode thickness, but note that the critical resistivity to limit the galvanic corrosion rate below a particular level is also dependent on the thickness of the reinforcement since the ohmic loss is equal to $i\rho t$. Hence, if ohmic losses are to limit galvanic corrosion, reinforcements having higher resistivity are needed as the thickness or particle size of the reinforcement decreases. For example, to maintain an ohmic drop of 0.5 V at a galvanic CD of $10^{-4}\,\mathrm{A\,cm^{-2}}$, a 50-μm particle would need a resistivity of $10^{6}\,\Omega\,\mathrm{cm}$; whereas, a 5-μm particle would need a resistivity of $10^{7}\,\Omega\,\mathrm{cm}$ to achieve the same ohmic loss. If the reinforcements that are used in MMCs are not of high purity, resistivities may drop significantly allowing galvanic corrosion to ensue. For example, Al/SiC MMCs are fabricated from both high-purity green SiC and lower-purity black SiC, depending on the application. The resistivity of SiC may vary by ~18 orders of magnitude depending on its purity.[27] Boron MFs are more conductive than pure boron due to tungsten and tungsten borides in the core.[28] In fact, many

Table 1 Resistivities of reinforcement materials

Material	*Resistivity (Ω cm)*	*Temperature (°C)*	*Notes*	*Ref.*
Al_2O_3	$>10^{14}$	30	99.7% Al_2O_3	29
Mica	10^{13}–10^{17}	–	Muscovite $KAl_3Si_3O_{10}(OH)_2$	30
SiC	10^{-5}–10^{13}	–	Function of purity	27
B	6.7×10^{5}	25	Pure	31
B_4C	10^{0}			32
Si	10^{-2}–10^{5}	–	Function of purity	29
P100 Gr fiber	2.5×10^{-4}	–	Thornel	33
P55S Gr fiber	7.5×10^{-4}	–	Thornel	33
$SiC_{MF}{}^{E}$	4×10^{-2}	25	The superscript 'E' indicates that electrical contact was made with the end of the MF exposing the core; the 'S' indicates that electrical contact was made with only the MF circumferential surface (excluding the core). SiC MFs have carbon cores and B MFs have tungsten cores.	21
$SiC_{MF}{}^{S}$	2×10^{-2}	25		
$B_{MF}{}^{E}$	2×10^{-1}	25		
$B_{MF}{}^{S}$	5×10^{-1}	25		

reinforcement materials have resistivities that are not high enough to stifle galvanic corrosion. The resistivities of some reinforcement materials are shown in Table 1. The treatment above for the ohmic losses through reinforcement particles should only be considered as an approximation since one-dimensional current flow was assumed. In the actual case, the ohmic drop through the edges of the particle could be much less than through the thickness. The galvanic corrosion rate can also significantly increase as the area fraction of the reinforcements increases.

3.23.4.1.6 Reinforcement area fraction

The galvanic corrosion rate generally increases with the area fraction of the reinforcement. This is demonstrated (Figure 13) using the anodic polarization diagrams of copper, Al 1100, Al 6061-T6, pure magnesium (99.95% metallic purity), and ZE 41A Mg, and the cathodic polarization diagram of P100 Gr.[16] The cathodic curve for P100 Gr^E shifts to higher currents as its area fraction is increased, causing the galvanic current with the various metals and alloys to increase. Since the galvanic couples are predominately under cathodic control, the catchment area principle[34] can be used to determine i_{GALV} as a function of the area fraction of the cathodic reinforcement.[16]

$$i_{GALV} = i_C(X_C/1 - X_C) \quad [4]$$

The parameter i_{GALV} is the dissolution CD of the matrix (i.e., i_{GALV}/anode area); i_C is the CD of the cathode; X_C is the area fraction of the cathode; and $(1 - X_C)$ is the area fraction of the anode. The value of i_C can be set equal to the CD of the cathodic constituents at the galvanic couple potential. For example, the galvanic couple potentials of ultrapure aluminum, Al 1100, and Al 6061-T6 couple to various reinforcements are coincident with the pitting potentials of the aluminum alloys (i.e., $\sim -0.75\ V_{SCE}$). Hence, the values of i_C for a variety of reinforcements were read at $\sim -0.75\ V_{SCE}$ from Figure 7. By plotting eqn [4], a graph (Figure 14) was generated from which i_{GALV} of ultrapure aluminum, Al 1100, or Al 6061-T6 can be obtained as a function of the area fraction of P100 Gr^E, SiC MF^E, B MF^E, HP SiC, and Si with exposure to aerated 3.15 wt% NaCl at 30 °C.[21] Figure 14 shows that to sustain a galvanic corrosion rate equal to the normal corrosion rate of Al 6061-T6, it would take less than 0.05 area fraction of P100 Gr^E or SiC MF^E, between 0.2 and 0.3 area fraction of B MF^E and HP SiC, and more

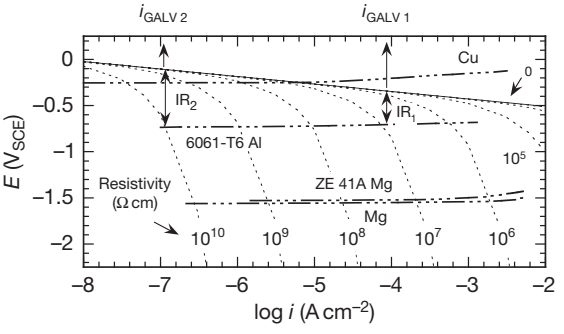

Figure 12 Plots of the Tafel equation for oxygen reduction on P100 Gr^E incorporating the effect of hypothetical ohmic losses based on various resistivities eqn [3] in aerated 3.15 wt% NaCl at 30 °C.[21] The anodic polarization diagrams of Cu, Al 6061-T6,[16] pure Mg, and ZE 41A Mg are also shown. The pure Mg and ZE41A Mg diagrams correspond to oxygenated solutions. Scan rate = 0.1 mV s^{-1}.

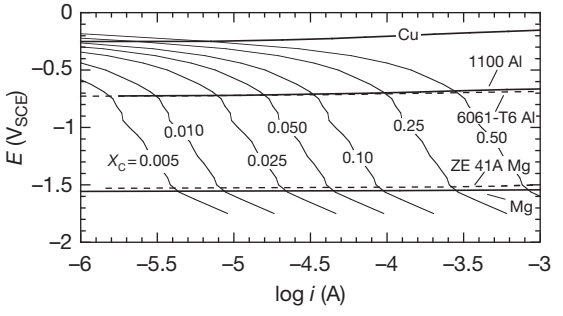

Figure 13 Anodic polarization diagrams of Cu, Al 1100, Al 6061-T6, Mg, and ZE 41A Mg, and cathodic polarization diagrams of P100 Gr^E[16] showing the effect of the P100 Gr^E area fraction X_C on the galvanic current in aerated 3.15 wt% NaCl at 30 °C. Scan rate = 0.1 mV s^{-1}.[21] The electrode area of the anodic diagrams corresponds to 1 cm^2.

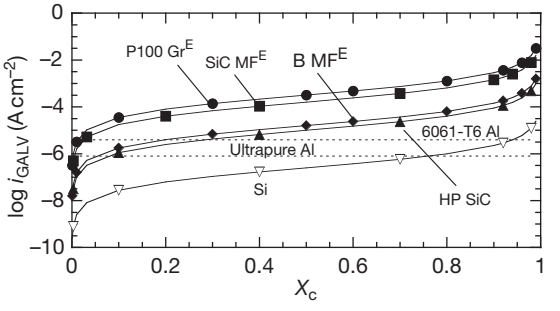

Figure 14 Graphs showing the galvanic corrosion current density i_{GALV} of ultrapure Al (99.999%), Al 1100, or Al 6061-T6 as a function of the area fraction X_C of P100 Gr^E, SiC MF^E, B MF^E, HP SiC, and Si for exposure to aerated 3.15 wt% NaCl at 30 °C. The horizontal dashed lines represent the normal corrosion rates of ultrapure Al and Al 6061-T6. Reproduced from Hihara, L. H. *Corros. Rev.* **1997**, *15*(3–4), 361.

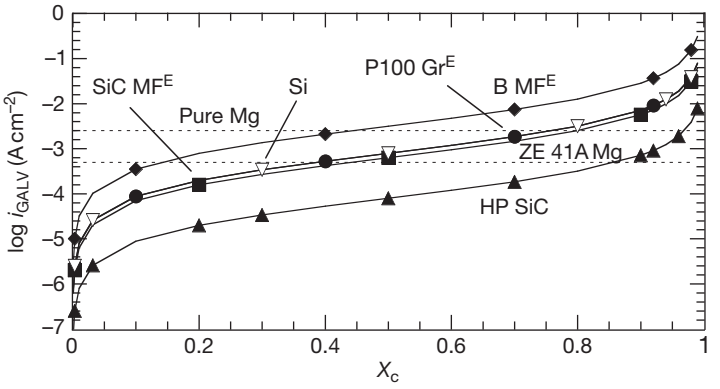

Figure 15 Graphs showing the galvanic corrosion current density i_{GALV} of pure Mg and ZE 41A Mg as a function of the area fraction X_C of P100 Gr^E, SiC MF^E, B MF^E, HP SiC, and Si for exposure to aerated 3.15 wt% NaCl at 30 °C. The horizontal dashed lines represent the normal corrosion rates of pure Mg and ZE 41A Mg.

than 0.9 area fraction of Si. It should be noted that for those reinforcements for which i_C was read in the diffusion-limited regime for oxygen reduction, galvanic corrosion rates could increase with additional convection. A similar figure was developed for pure magnesium and ZE 41A Mg (Figure 15).

The above discussion did not take into consideration the distribution of the anodic and cathodic current densities over the MMC microstructure. In some cases, for very low levels of conductive particles, localized corrosion can be induced by solution alkalinization, as will be discussed below.

3.23.4.1.7 Microstructure

The physical presence of the reinforcements also greatly affects MMC corrosion. The reinforcements, which are usually inert in comparison to the matrix, are often left in relief as the matrix corrodes leaving behind a network of fissures that trap corrosion products and exacerbate corrosion (Figure 16). The initiation and propagation of corrosion sites are generally influenced by the electrical resistivity and volume fraction of the MMC constituents, including the reinforcements, interphases, and intermetallics. The corrosion behavior of MMCs in the open-circuit condition can be quite different from what might be expected based on anodic polarization diagrams of the MMCs. For example, in near-neutral 0.5 M Na_2SO_4 solutions, various aluminum MMCs passivate (Figure 17)[35,36] during anodic polarization, but in the open-circuit condition, the same MMCs are susceptible to localized corrosion. The localized corrosion in the open-circuit condition is caused by the development of localized anodic and cathodic

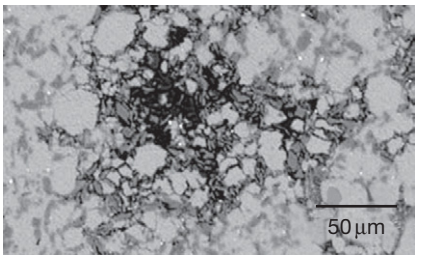

Figure 16 SEM micrograph of region of localized corrosion on Al 6092/SiC/20 P-T6 MMC exposed for 24h in aerated 0.5 M Na_2SO_4 at 30 °C in the open-circuit condition. Micrograph courtesy of H. Ding.

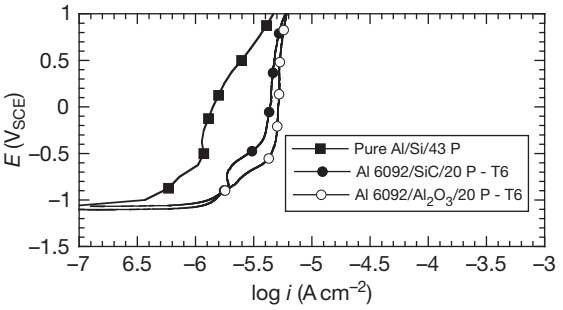

Figure 17 Anodic polarization curves of various Al MMCs exposed to 0.5 M Na_2SO_4 at 30 °C. Scan rates are 1 mV s^{-1} (Al 6092-T6 MMCs) and 0.1 mV s^{-1} (pure Al/Si/43 P MMC).

sites. The alkalinity in cathodic regions and acidity in anodic regions are accentuated by the formation of microcrevices in the network of reinforcement particles in relief. In the case of Al MMCs, aluminum loses its passivity in both the acidic and alkaline environments because of the amphoteric nature of aluminum oxide.

When an MMC is exposed to an electrolyte in the open-circuit condition, the sum of anodic current I_a is equal to the sum of cathodic current I_c:

$$I_a = I_c \quad [5]$$

Hence, the anodic and cathodic current densities are related by eqn [6],[35]

$$i_c = i_a \frac{(1 - x_c)}{x_c} \quad [6]$$

where i_c and i_a are the cathodic and anodic current densities, respectively, and x_c is the area fraction of cathodic constituents, here assumed to be conductive reinforcement, interphase, or intermetallic particles.

From eqn [6], the cathodic CD over cathodic constituents in the MMC microstructure can be approximated if the anodic CD of the matrix i_a, and the area fraction of cathodic constituents x_c are known. Experimental results on Al MMCs have indicated that the corrosion initiation sites depended on the amount of electrically conductive cathodic constituents that are present in the MMC microstructure. If the area fraction of cathodic constituents were low, corrosion initiated around the cathodic constituents because of solution alkalinization; if the area fraction of cathodic constituents were high, corrosion initiation appeared more random around the reinforcement constituents.

Equation [6] was used to calculate the cathodic CD (**Table 2**) emanating from cathodic sites based on the area fraction x_c, and the assumption that the passive CD of the aluminum matrix was $\sim 4 \times 10^{-6}$ A cm^{-2}, based on the passive CD of various Al 6092-T6 MMCs (**Figure 17**). This passive CD should also be approximately equal to the initial anodic CD i_a of the Al matrix in the MMC at the open-circuit potential, prior to the development of significant pH gradients.

Low content of cathodic constituents

When the amount of cathodic sites is relatively low, cathodic current densities become concentrated over the few cathodic sites resulting in hydroxide ion buildup. If the matrix material is not stable at high pH levels, localized corrosion can result. **Table 2** shows the values of i_c as a function of x_c, assuming a value for i_a to be equal to 4×10^{-6} A cm^{-2}, which is an estimate of the passive CD of an Al 6092-T6 matrix.

Table 2 Values[a] of i_c as a function of x_c

i_c (A cm^{-2})	x_c
4×10^{-3}	0.001
4×10^{-4}	0.01
1×10^{-4}	0.04
4×10^{-5}	0.1
2×10^{-5}	0.2
9×10^{-6}	0.3
4×10^{-6}	0.5

[a] i_c values correspond to $i_a = 4 \times 10^{-6}$ A cm^{-2}.

When values of x_c become less than $\sim$0.04 (**Table 2**), the cathodic current densities begin to exceed 10^{-4} A cm^{-2}, which can lead to solution alkalinization by oxygen reduction and hydrogen evolution. Cathodic current densities of the order of 10^{-4} A cm^{-2} causes phenolphthalein dye in 0.5 M Na_2SO_4 solutions to transform from clear to red for electrodes in quiescent solutions. The color change of phenolphthalein occurs in a pH range from 8.3 to 9.8. Aluminum corrosion rates increase exponentially when the pH exceeds $\sim$8.[37] Hence, corrosion can be expected around cathodic constituents if their area fractions are low.

Accordingly, corrosion was observed on an Al 6092/Al_2O_3/20 P-T6 MMCs around intermetallic particles (**Figure 18**) in 0.5 M Na_2SO_4, in which Al passivates during anodic polarization.

In these MMCs, the Al_2O_3 particles are insulators and cannot serve as cathodes; however, several types of particles, including titanium suboxides with compositions close to that of Ti_6O, Ti_3O, Ti_2O, and TiO; TiO_2 (likely doped); Ti–Zr–Al containing oxides; and Fe–Si–Al intermetallics[23] were found. Of these particles, the titanium suboxides, TiO_2, and the Fe–Si–Al intermetallics supported significant cathodic activity.[23] The area fraction of the non-Al_2O_3 particles in the MMCs was estimated to be of the order of 0.01 using image analysis.[35] Hence, if the area fraction of the cathodic constituents was less than 0.01, cathodic current densities in excess of 10^{-4} A cm^{-2} could result in significant solution alkalinization and corrosion.

The scanning vibrating electrode technique (SVET) and scanning ion-selective electrode technique (SIET) revealed that localized corrosion over Al 6092/Al_2O_3/20 P-T6 MMCs immersed in 0.5 M Na_2SO_4 was coinciding with that in alkaline, cathodic regions.[38]

The type of corrosion discussed above was suppressed in pH 7 buffered solutions. Only staining was observed around the intermetallics (**Figure 19**).

High content of cathodic constituents

MMCs that contain relatively high levels of cathodic sites should generally be more immune to corrosion

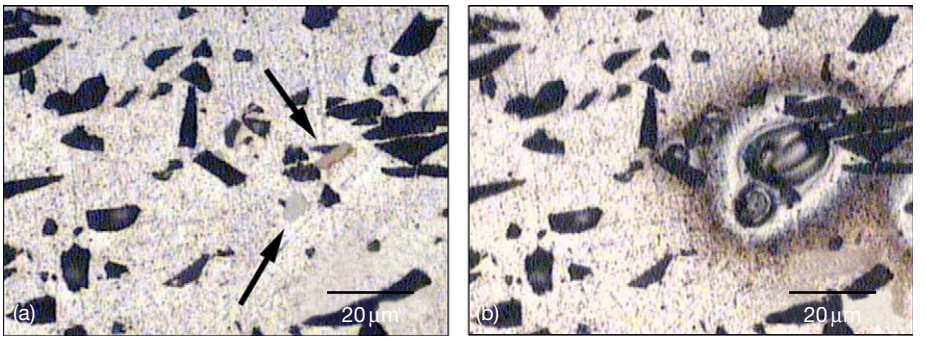

Figure 18 Virgin Al 6092/Al_2O_3/20 P-T6 MMC (a) and after 2 days of immersion (b) in air-exposed 0.5 M Na_2SO_4 at 30 °C. Intermetallic particles appear as light gray, and Al_2O_3 appears as near black.

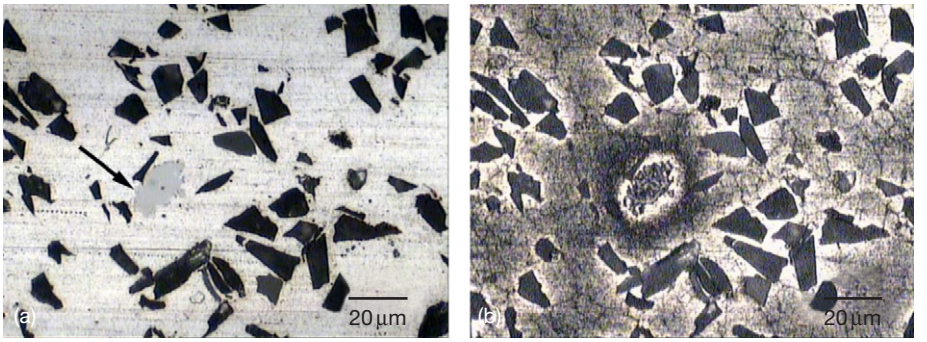

Figure 19 Al 6092/Al_2O_3/20 P-T6 MMC in the virgin state (a) and after immersion for 17 days in air-exposed pH 7 buffered solution at 30 °C (b). Notice staining of the matrix around the intermetallic particle, but lack of localized corrosion.

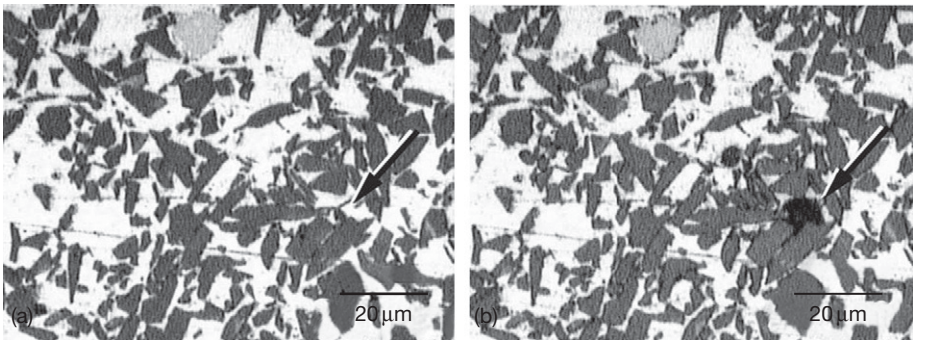

Figure 20 Al 6092/SiC/40 P-T6 MMC in the virgin state (a) and after immersion for 2 days (b) in air-exposed 0.5 M Na_2SO_4 at 30 °C.

initiation caused by extensive hydroxide ion buildup around the cathodic constituents, since the cathodic current is dispersed over more sites.

For example, in Al MMCs that are exposed to Na_2SO_4 solutions in which the Al matrix passivates, the cathodic current densities are estimated to be relatively low (i.e., $\leq 4 \times 10^{-5}$ A cm^{-2}) (**Table 2**) for x_c greater than ~0.1. Accordingly, corrosion initiation sites on Al 6092-T6 MMCs reinforced with semiconductive SiC (**Figure 20**) and B_4C (greater than 10 vol. %) were different in appearance from the alkali-induced corrosion around intermetallics (**Figure 18**) in the Al 6092/Al_2O_3/20 P-T6 MMC.[35]

One possible source of the corrosion initiation sites on the Al 6092-T6 MMCs reinforced with SiC or B_4C could be the formation of crevices at SiC–Al

or B_4C–Al interfaces by the hydrolysis of Al_4C_3, which is a reaction product of SiC and Al[39], and B_4C and Al.[40] Al_4C_3 readily hydrolyses upon contact with moisture and could leave fissures in the SiC–aluminum and B_4C–aluminum interface (see **Section 3.23.4.3**).

Once a crevice is formed at the particle-matrix interface, crevice corrosion can ensue. If the reinforcement particles are electrically conductive, they can serve as cathodic sites for hydrogen and/or oxygen reduction. As a result, for Al MMCs, the environment in the crevice will become acidic:

$$Al \rightarrow Al^{3+} + 3e^- \quad [7]$$

$$Al^{3+} + \frac{3}{2}H_2O \rightarrow \frac{1}{2}Al_2O_3 + 3H^+ \quad [8]$$

The acidified solution in the crevice can breakdown passivity because of the amphoteric nature of Al_2O_3 and exacerbate corrosion. Eventually, corrosion spreads and encompasses adjacent particles forming a network of microcrevices caused by reinforcement particles in relief (**Figures 21**). The solution above the network of microcrevices has been measured to be acidic in the initial stages of growth.[38] The region around the centralized anodic region becomes alkaline because of the reduction of oxygen in surrounding regions.[38]

3.23.4.2 Electrochemical Effects of the Interphases

During the fabrication processing of MMCs, reactions between the reinforcement and matrix may lead to the formation of an interphase at the reinforcement–matrix interface. The presence of the interphase may lead to corrosion behavior different from what might be expected based on virgin MMC constituents. For example, Pohlman[41] could not measure galvanic currents between virgin B MFs and Al 2024 or Al 6061 in 3.5% NaCl solutions, indicating that galvanic corrosion between aluminum matrices and B MFs should be negligible. In actual Al/B/MF MMCs, however, galvanic corrosion takes place between the aluminum matrix and the aluminum boride interphase on the surface layers of the B MFs.[41] Pohlman measured galvanic currents between the aluminum alloys and B MFs that were extracted from the matrix. A 4-μm-thick layer of aluminum boride enveloped the extracted B MFs. Galvanic currents measured between the aluminum alloys and aluminum boride were similar to those between the alloys and the extracted B MFs. When the layer of aluminum boride was removed from the extracted B MFs, the galvanic current ceased, which indicated that the aluminum boride interphase was necessary for galvanic corrosion.

3.23.4.3 Chemical Degradation in MMCs

MMCs may also degrade by chemical reactions that cannot be directly assessed by electrochemical measurements. Interphases and reinforcement phases may undergo chemical degradation which cannot be detected, for example, with the aid of anodic polarization. In aluminum MMCs, the hydrolysis of the Al_4C_3 interphase is one such example. Aluminum carbide degradation can affect Al/Gr, Al/SiC, and Al/B_4C MMCs. Reinforcement phases may also experience degradation. For example, mica particles have been reported to undergo exfoliation in Al/mica MMCs.

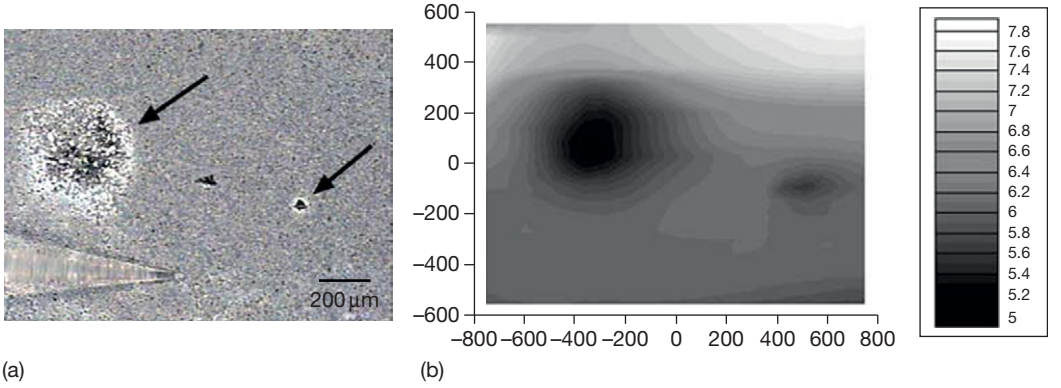

Figure 21 Al 6092/SiC/20 P–T6 MMC in air-exposed 0.5 M Na_2SO_4 (a), and pH profile over the specimen (b). Notice acidification of localized corrosion sites, and the alkalinization of surrounding cathodic sites.

3.23.4.3.1 Aluminum carbide hydrolysis

Aluminum carbide forms by the reaction of aluminum and carbon,[42]

$$4Al(l) + 3C(s) = Al_4C_3(s) \quad [9]$$

and its formation is substantial in Al/Gr MMCs during processing if temperatures are significantly higher than the liquidus temperature. At lower temperatures, Al_4C_3 formation can be controlled.[43]

Aluminum carbide also forms by the reaction of aluminum and SiC,

$$4Al(l) + 3SiC(s) = Al_4C_3(s) + 3Si(s) \quad [10]$$

and has been found at SiC–Al interfaces if the Si activity in liquid aluminum is low.[39]

The formation of Al_4C_3 by the reaction of Al and B_4C is reported to occur rapidly at 900 °C. In addition, many other Al–B–C compounds are known to form.[40]

In the presence of moisture, Al_4C_3 hydrolyzes to liberate methane gas by the reaction

$$Al_4C_3(s) + 12H_2O(l) = 4Al(OH)_3(s) + 3CH_4(g) \quad [11]$$

Methane evolution has been detected from Al/Gr MMCs containing Al_4C_3.[44,45] The rate of Al_4C_3 hydrolysis was measured to be ~1% per hour for HP Al_4C_3 (78% of theoretical density and porous) exposed to pure water at 30 °C.[26] Buonanno[45] reported that Al_4C_3 hydrolysis in Al/Gr MMCs leaves fissures at fiber–matrix interfaces. The hydrolysis of Al_4C_3, therefore, could result in rapid penetration into the MMC microstructures through fiber–matrix interfaces, and lead to the formation of microcrevices at reinforcement–matrix interfaces.

3.23.4.3.2 Mica degradation

Muscovite mica $KAl_3Si_3O_{10}(OH)_2$ particles of ~70 μm in size[46] have been used in Al MMCs developed for potential use in applications where good antifriction, seizure resistance, and high-damping capacity are required.[47] During exposure to nondeaerated 3.5 wt% NaCl solutions, the mica particles appeared to have absorbed moisture, swelled, and then exfoliated.[48]

3.23.4.4 Secondary Effects

The presence of the reinforcement phases in the MMCs may alter the microstructural features in the matrix material in ways that are nonexistent in the monolithic matrix alloys. Two examples that are discussed here are the formation of intermetallic phases around reinforcements by solute rejection during solidification,[49] and the mismatch in the CTE between reinforcements and matrices that can lead to dislocation generation,[50] which potentially could lead to higher corrosion in some metals.[51]

3.23.4.4.1 Intermetallics

Intermetallics may have potentials and corrosion resistance different from that of the matrix. **Table 3** shows corrosion potentials, pitting potentials, and normal corrosion current densities of various metals and intermetallics.[52] Noble and inert intermetallics may induce galvanic corrosion of the matrix; whereas, active intermetallics may go into dissolution and leave fissures or crevices.

In Al/Al_2O_3 MMCs, Al_8Mg_5 and Mg_2Si, intermetallics provided corrosion paths along fiber–matrix interfaces.[53] Pits in Al/Al_2O_3 MMCs exposed to NaCl solutions containing H_2O_2 were attributed to the dissolution of $MgAl_3$, which is rapidly attacked at low potentials.[54] In Al/mica MMCs, a dendritic

Table 3 Corrosion data[a] of intermetallics

Constituent	E_{corr} (mV_{SCE})	E_{pit} (mV_{SCE})	i_{corr} ($A\,cm^{-2}$)
Cu (99.9)	−232	−30	1.8×10^{-6}
Si (99.9995)	−441	–	–
Cr (99.0)	−506	297	–
Al_3Fe	−539	106	2.1×10^{-6}
Al_7Cu_2Fe	−551	−448	6.3×10^{-6}
$Al_{20}Cu_2Mn_3$	−565	−428	3.4×10^{-7}
Al–4%Cu	−602	−406	2.3×10^{-6}
Al_3Ti	−603	−225	5.6×10^{-7}
Al_2Cu	−665	−544	7.3×10^{-6}
Al–2% Cu	−672	−471	1.3×10^{-6}
Al_3Zr	−776	−275	2.5×10^{-6}
Al_6Mn	−779	−755	6.3×10^{-6}
$Al_{12}Mn_3Si$	−810	−621	1.7×10^{-6}
Al (99.9999)	−823	−610	3.9×10^{-6}
Al_2CuMg	−883	80	2.0×10^{-6}
Mg (AlCu)	−943	−2	2.3×10^{-5}
7075-T651 Al	−965	−739	1.1×10^{-6}
Zn (99.99)	−1000	–	1.2×10^{-6}
$Al_{32}Zn_{49}$	−1004	–	1.4×10^{-5}
Mg_2Al_3	−1013	−846	4.8×10^{-6}
$MgZn_2$	−1029	–	8.4×10^{-5}
Mn (99.9)	−1323	–	–
Mg_2Si	−1538	–	7.7×10^{-6}
Mg (99.9)	−1586	−1391	5.5×10^{-6}

[a]Aerated, pH 6, 0.1 M NaCl.
Source: Data from Birbilis, N.; Buchheit, R. G. *J. Electrochem. Soc.* **2005**, *152*(4), B140–B151.

phase, which was probably Mg_2Al_3 or Al_8Mg_5, and spheroidized $CuMgAl_2$ were preferentially attacked in nondeaerated 3.5 wt% NaCl.[55]

3.23.4.4.2 Dislocation density

The high strengths of particulate MMCs in comparison to their monolithic alloys are generated by high dislocation densities caused by a mismatch in the CTE between reinforcement and matrix, and heating and cooling histories.[50] Since cold working, which is the result of generating high dislocation densities, is known to change the corrosion behavior of metals such as steel[51] and aluminum,[56] the corrosion behavior of MMCs may also be affected by high dislocation densities.[21] It has been suggested that corrosion near the SiC–Al interface in Al/SiC MMCs could be caused by high dislocation density because of a mismatch of the CTE between SiC and Al.[57,58]

3.23.4.4.3 MMC processing

Processing-induced corrosion is not inherently caused by the primary components of the MMC system, but results from processing deficiencies. The corrosion of diffusion bonds in Al/B MMCs and corrosion due to microstructural chlorides in some Al/Gr MMCs are two examples.

Low-integrity diffusion bonds

The open-circuit potentials of Al MMCs reinforced with B MFs were active as that of their monolithic matrix alloys in aerated NaCl solutions,[59,60] which were not expected since B MFs had open-circuit potentials that were noble to that of the monolithic matrix alloy. On the basis of the mixed-potential theory, it was expected that the MMCs would equilibrate at potentials between that of the noble B MF and the monolithic matrix alloy. To investigate the origin of this discrepancy, Bakulin *et al.*,[60] measured the open-circuit potentials of HP stacks of aluminum foil processed in the same way as the MMC (but without the B MFs), and found that the HP aluminum stacks were active as that of the monolithic alloy as well as the MMCs. The only difference between the HP stacks of aluminum foil and the monolithic aluminum was crevices in the diffusion bonds between adjacent foils which served as additional anodic sites.

Microstructural chlorides

Some types of Al 6061/Gr/50 F-T6 MMCs were found to have been contaminated with microstructural chlorides during processing[61] by the Ti–B vapor deposit method[62] that utilizes $TiCl_4$ and BCl_3 gases. The presence of microstructural chlorides in the Al/Gr MMCs was confirmed during microstructural analyses, and the effect of the chlorides was evident in anodic polarization diagrams.[63] These MMCs are pitted at $\sim -0.6\,V_{SCE}$ in 0.5 M Na_2SO_4[63]; whereas, both the matrix alloy and other types of Al/Gr MMCs are processed by pressure infiltration without the use of chlorides passivate in 0.5 M Na_2SO_4.[45] The residual microstructural chlorides also make these MMCs inherently unstable, and as a result, some specimens have suffered from corrosion initiating subcutaneously beneath monolithic Al skins after long storage in laboratory air (**Figure 22**). This type of subcutaneous corrosion has also been observed in a similar type of Mg/Gr MMC (**Figure 23**).

3.23.4.5 Corrosion in Environments

A comprehensive study of Al 6092-T6 MMCs reinforced with black SiC (5, 10, 20, 40, and 50 vol%), green (high purity) SiC (50 vol%), B_4C (20 vol%), and Al_2O_3 (20 vol%) has been examined in a battery of immersion, humidity-chamber exposure, and outdoor exposure tests.[64] The wide range of reinforcement types and testing conditions allows trends in corrosion behavior to be made and will be

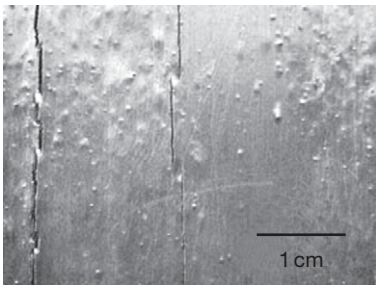

Figure 22 Subcutaneous corrosion in Al/Gr MMC with over 10 years exposure in laboratory air.

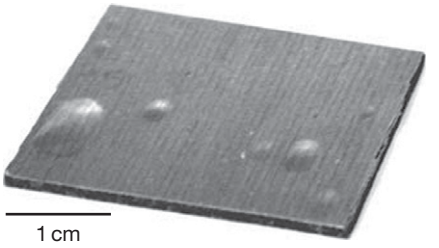

Figure 23 Mg/Gr MMC showing subcutaneous corrosion after more than 15 years in storage.

highlighted here. Since galvanic corrosion between the Al 6092-T6 matrix and reinforcement particles depends on the ability of the particle to conduct electricity, the electronic resistivities of the particle should have an effect on the corrosion behavior. The resistivity of B_4C is $\sim 10^0\,\Omega$ cm,[32] that of SiC ranges from $\sim 10^{-5}$ to $10^{13}\,\Omega$ cm depending on its purity,[27] and that of Al_2O_3 is $10^{14}\,\Omega$ cm.[29] The green SiC possessing high electrical resistivity should be less likely to promote galvanic corrosion of the aluminum matrix as compared to black SiC, which is of lower purity and resistivity.

3.23.4.5.1 Immersion exposure

Immersion studies were conducted for 90 days in 3.15 wt% NaCl, ASTM seawater, real seawater, 0.5 M Na_2SO_4, and ultrapure 18 Ω cm water exposed to air at 30 °C. The dimensions of the specimens were ~2.54 cm × 2.54 cm × 0.25 cm. Specimens in triplicate were examined, but data correspond to results from two specimens for each testing condition (**Figure 24**). The third specimen was reserved for further surface analyses.

Corrosion rates were generally highest for the MMCs immersed in 3.15 wt% NaCl. The rates were much lower in ASTM seawater because of the formation of a film on the MMC surfaces, which was likely composed of Al–Mg hydrotalcite-like compounds.[65] The film may have impeded the diffusion of dissloved oxygen to cathodic regions limiting the corrosion rate. For most of the specimens, the corrosion rates in Na_2SO_4 were similar to those in NaCl. Although Al MMCs generally passivate in Na_2SO_4 solutions during anodic polarization, they corrode in the open-circuit condition because of the formation of localized acidic and alkaline regions (see **Section 3.23.4.1.7**).

Most of the trends observed in the corrosion rate versus the reinforcement composition and type indicated that the level of galvanic corrosion between the matrix and reinforcements increases as the reinforcement electrical resistivity decreases, and as the reinforcement content increases. For the MMCs with 20 vol% of particulates, the corrosion rates were generally highest for that reinforced with B_4C, followed by that with black SiC, and least for that with Al_2O_3. Of the three types of reinforcements, the B_4C has the lowest electrical resistivity, and Al_2O_3 has the highest. For the MMCs reinforced with 5, 10, 20, 40, and 50 vol% black SiC, the corrosion rates also generally increased as the volume fraction increased. For the MMCs reinforced with 50% black or green SiC, corrosion rates were higher for those that were reinforced with the lower purity, more conductive, black SiC in ASTM seawater and 0.5 M Na_2SO_4. It was expected that this trend would also be observed for the 3.15 wt% NaCl solution, but the results in this solution were skewed because of crevice and localized corrosion on one of the MMCs reinforced with the higher-purity, less-conductive, green SiC. A crevice formed on the specimen because of contact with the specimen holder, and a highly localized corrosion

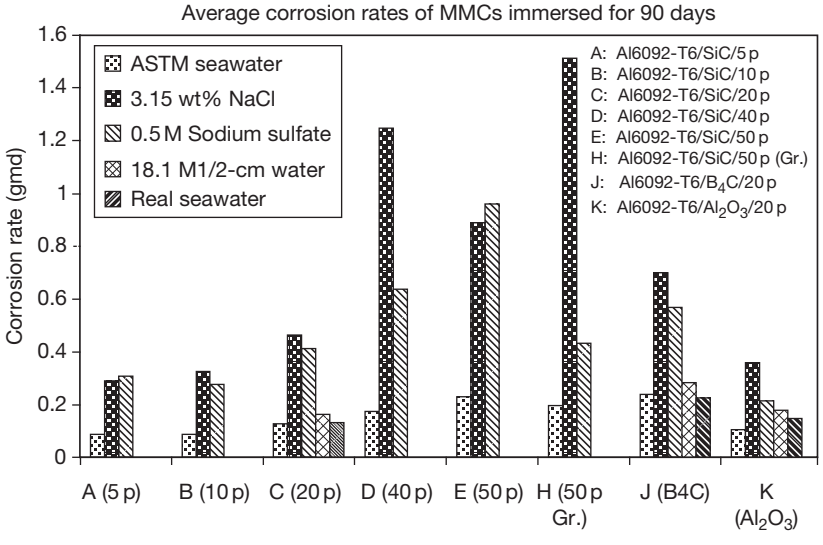

Figure 24 Corrosion rates of Al 6092-T6 MMCs under immersion conditions in air-exposed solutions for 90 days at 30 °C. Reproduced from Hawthorn G. A. MS Thesis, University of Hawaii at Manoa, Honolulu, 2004.

site formed in a region of high plastic deformation where the specimen was stamped for identification.

3.23.4.5.2 Humidity chamber exposure

Humidity chamber studies were conducted for 90 days at 85% RH (relative humidity) and 30 °C. The dimensions of specimens were ~2.54 cm × 2.54 cm × 0.25 cm. The specimens were treated in 3.15 wt% NaCl, ASTM seawater, actual seawater, and 0.5 M Na_2SO_4 by immersion in the electrolyte for 1 min, air-dried, and then placed in the humidity chamber. Specimens in triplicate were examined, but data correspond to results from two specimens for each testing condition (**Figure 25**). The third specimen was reserved for further surface analyses.

The corrosion rates of specimens treated with ASTM seawater were generally comparable to or exceed those treated with NaCl, as the hydrotalcite-like films cannot form in the absence of an electrolyte. The specimens treated with Na_2SO_4 generally had the lowest corrosion rates. Corrosion rates also generally increased for the MMCs reinforced with black SiC as the SiC content increased. For the MMCs reinforced with 50 vol% SiC, corrosion rates were lower for those having the high-purity, higher resistivity, and green SiC.

3.23.4.5.3 Outdoor exposure

The MMC specimens were exposed to six outdoor sites. The specimens were ~9 cm in diameter and 2.5 mm in thickness. Specimens in triplicate were examined, but data correspond to results from two specimens for each testing condition (**Figure 26**). The third specimen was reserved for further surface analyses.

The test sites were industrial (Campbell Industrial Park), agricultural (Ewa Nui), arid (Waipahu), marine (Kahuku and Coconut Island sites), and rain forest (Lyon Arboretum). Weather and environmental data are provided for the 180-day exposure period (**Table 4**).

Some trends are clearly visible in the corrosion data (**Figure 26**). The corrosion rates of the MMCs reinforced with black SiC generally increased with an increase in volume fraction of the reinforcement. This would be expected due to galvanic action between the black SiC and aluminum matrix. For the MMC reinforced with 50 vol% SiC, those having the black SiC corroded at higher rates than those reinforced with the high-purity, higher-resistivity, and green SiC. For the three types of MMCs with 20 vol% particulates, those reinforced with B_4C generally corroded at a higher rate than those reinforced with less-conductive SiC or Al_2O_3.

The highest corrosion rates were generally observed at the Manoa (very wet), Coconut Island (marine), and Kahuku (marine) test sites. The high corrosion rate at Manoa is likely due to persistent rain since chloride levels are negligible at that site.

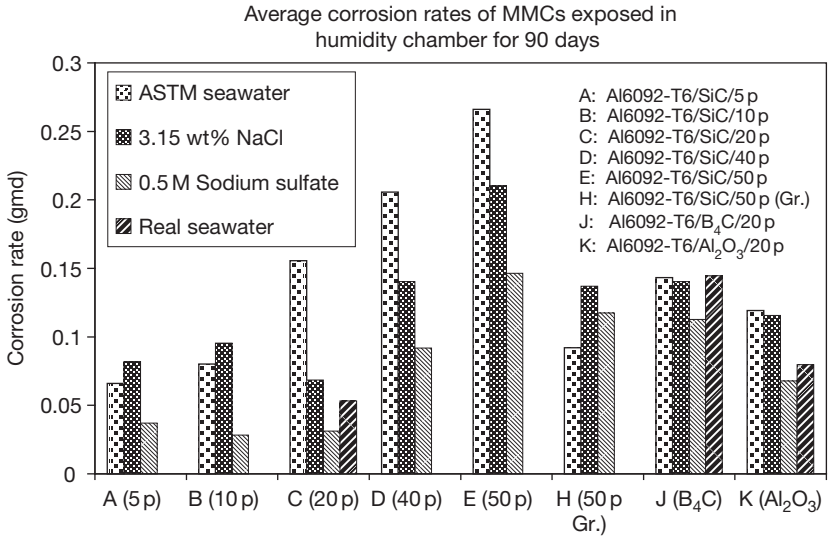

Figure 25 Corrosion rates of Al 6092-T6 MMCs treated with various salts and exposed to 85% RH for 90 days at 30 °C. Reproduced from Hawthorn G. A. MS Thesis, University of Hawaii at Manoa, Honolulu, 2004.

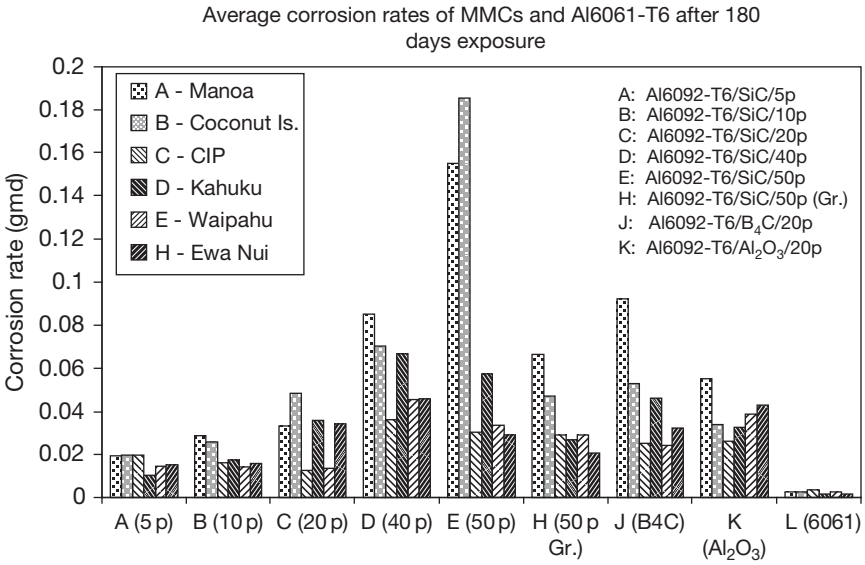

Figure 26 Corrosion rates of Al 6092-T6 MMCs exposed to outdoor test sites for 180 days. Reproduced from Hawthorn G. A. MS Thesis, University of Hawaii at Manoa, Honolulu, 2004.

Table 4 Weather and atmospheric data for 180-day exposure at test sites

Test site	*Avg. temp (°C)*	*Rain (cm)*	*% of exposure time when TOW = 0*[a]	*% of exposure time when TOW = 15*[a]	*Avg. Cl^- deposition rate ($mg\,m^{-2}\,day^{-1}$)*	*Avg. humidity (%RH)*
Manoa	22.9	357.9	60.6	26.4	–[b]	83.1
Coconut Is.	25.8	65.0	54.8	9.2	58.3	74.9
Campbell	27.2	45.5	66.5	4.6	24.4	63.2
Kahuku	25.6	132.1	59.6	15.1	89.9	73.4
Waipahu	26.3	79.0	80.3	7.1	10.7	66.9
Ewa Nui	25.9	82.6	77.6	6.5	9.4	67.4

[a]A TOW sensor value of zero indicates that the specimens are dry and a value of 15 indicates that the specimens are wet.
[b]Below detectable level of 7.0.
Source: Hawthorn, G. A. MS Thesis, University of Hawaii at Manoa, Honolulu, 2004.

3.23.5 Corrosion Protection of MMCs

Corrosion of metals can be prevented with the use of protective coatings and inhibitors. The type of coating (e.g., impervious, inhibitive, or cathodically protective) will depend on the application; for example, immersion or atmospheric exposure. For MMCs, however, a proven coating system for the matrix alloy may not be suitable. Poor adhesion and wettability between the coating and reinforcement or differences in the electrochemical properties of the alloy and the MMC may render a good coating system for the ineffectiveness of alloy for the MMC. Other coating techniques such as anodization could also be ineffective or even deleterious to the MMC. Various studies on the corrosion protection of MMCs utilizing organic coatings, inorganic coatings, anodization, chemical conversion coatings, and inhibitors have been summarized elsewhere.[66]

3.23.6 Conclusions

The corrosion of MMCs is significantly more complicated and less predictable than that of their monolithic alloys. MMC systems that consist of active metal matrices and noble reinforcements have inherent galvanic corrosion problems. Some systems, such as those containing aluminum and carbon, may also be susceptible to interphase formation of the deleterious Al_4C_3, which hydrolyses in the presence of moisture. Other complications arise when reinforcements are

SCs, which have electrical resitivities that can span orders of magnitude and are sensitive to impurity levels. In addition, impurities in semiconducting reinforcements may cause them to become n-type or p-type which can lead to photo-induced corrosion or even beneficial photoinduced cathodic protection. The presence of the reinforcements may also influence the formation of intermetallics and the generation of dislocations, which also affect corrosion behavior. These additional concerns make designing and utilizing MMCs a significant, but worthy, engineering challenge. Many of the extraordinary mechanical and physical properties of MMCs cannot be achieved with conventional metal alloys. Standardization of MMC constituents (e.g., purity levels in reinforcements) and the stringent control of processing temperatures and histories could help develop MMCs with more predictable corrosion behavior.

References

1. Weeton, J. W.; Peters, D. M.; Thomas, K. L. *Guide to Composite Materials*; American Society for Metals: Metals Park, OH, 1987; pp 2–2.
2. Park, G. B.; Foster, D. A. International Technical Conference Proceedings, SUR/FIN'90, Boston, MA, July, 1990; American Electroplaters and Surface Finishers Society: Boston, MA, 1990; pp 1349–1369.
3. Harrigan, W. C. J. *Metal Matrix Composites: Processing and Interfaces*; Academic Press, 1991; pp 1–16.
4. Liu, Y.; Rohatgi, P. K.; Ray, S.; Barr, T. L. In Conference Proceedings, ICCM/8, 1991; Tsai, S. W., Springer, G. S., Eds.; Society for the Advancement of Material and Process Engineering (SAMPE), 1991; p 20H.
5. Lim, T.; Lee, C. S.; Kim, Y. H.; Han, K. S. In Conference Proceedings, ICCM/8, 1991; Tsai, S. W., Springer, G. S., Eds.; Society for the Advancement of Material and Process Engineering (SAMPE), 1991; pp 20E.
6. Ashby, M. F.; Jones, D. R. H. *Engineering Materials*, 2nd ed; Butterworth Heinemann, 1998; Vol. 2.
7. Buck, M. E.; Suplinskas, R. J. In *Engineered Materials Handbook on Composites;* ASM International: Metals Park, Ohio, 1987; Vol. 1, pp 851–857.
8. Saffil Saffil. www.saffil.com (May).
9. 3M Metal Matrix Composites, www.3m.com/market/industrial/mmc/www.3m.com/market/industrial/mmc/ (May).
10. FiberNide, http://fibernide.com/copper.html October 2007.
11. DWA Technologies Inc., http://dwatechnologies.com/ October 2007.
12. ALMMC Aluminum Metal–Matrix Composites Consortium, www.almmc.com
13. Wesley, W. A.; Brown, R. H. *The Corrosion Handbook*, 1st ed; Uhlig, H. H., Ed.; Wiley: New York, 1948; pp 481–495.
14. Uhlig, H. H.; Revie, R. W. *Corrosion and Corrosion Control*, 3rd ed; Wiley: New York, 1985; p 354.
15. Hihara, L. H.; Kondepudi, P. K. *Corros. Sci.* **1994**, *36*, 1585–1595.
16. Hihara, L. H.; Latanision, R. M. *Corrosion* **1992**, *48*(7), 546–552.
17. Lin, Z. J. M.S. Thesis, University of Hawaii at Manoa, Honolulu, 1995.
18. Tamirisa, C. M.S. Thesis, University of Hawaii at Manoa, Honolulu, HI, 1993.
19. Hihara, L. H.; Tamirisa, C. *Mater. Sci. Eng. A* **1995**, *198*, 119–125.
20. Hihara, L. H.; Latanision, R. M. *Int. Mater. Rev.* **1994**, *39*, 245.
21. Hihara, L. H. *Corros. Rev.* **1997**, *15*(3–4), 361.
22. Ding, H.; Hihara, L. H. In 212th ECS Meeting, Washington, DC, October 7–12, 2007, Washington, DC, 2007.
23. Ding, H.; Hihara, L. H. In 212th ECS Meeting, Washington, DC, October 7–12, 2007, Washington, DC, 2007.
24. Adler, R. P. I.; Snoha, D. J.; Hawthorn, G.; Hihara, L. H. In *Characterization of Environmentally Exposed Aluminum Metal Matrix Composite Corrosion Products as a Function of Volume Fraction and Reinforcement Specie, paper 067029*; Tri Serice Corrosion Conference, Orlando, Florida, 2005; Beatty, J., Adler, R. P. I., Eds., Orlando, Florida, 2005.
25. Ding, H.; Hihara, L. H. *J. Electrochem. Soc.* **2008**, *155*(5).
26. Hihara, L. H. Ph.D. Thesis, Massachusetts Institute of Technology, Cambridge, MA, 1989.
27. Ichinose, N. *Introduction to Fine Ceramics*; John Wiley and Sons, 1987; p 50–52.
28. Tsirlin, A. M. In *Strong Fibres (Handbook of Composites)*; Watt, W., Perov, B. V., Eds.; Elsevier Science Publishers, 1985; Vol. 1, pp 155–199.
29. Bolz, R. E.; Tuve, G. L. *CRC Handbook of Tables for Applied Engineering Science*, 2nd ed.; CRC Press: Boca Raton, FL, 1973; pp 262–264.
30. Clauser, H. R. *The Encyclopedia of Engineering Materials and Processes*; Reinhold Publishing Corporation, 1963; p 429.
31. Greenwood, N. N.; Earnshaw, A. *Chemistry of the Elements*; Pergamon Press, 1984.
32. Yamada, S.; Hirao, K.; Yamauchi, Y.; Kanzaki, S. *Ceram. Int.* **2003**, *29*, 299.
33. Weeton, J. W.; Peters, D. M.; Thomas, K. L. *Guide to Composite Materials*; American Society for Metals: Metals Park, OH, 1987; pp 5–10.
34. Evans, U. R. *Metallic Corrosion, Passivity and Protection*; Edward Arnold and Co.: London, 1937; pp 513–516.
35. Hihara, L. H.; Devarajan, T. S.; Ding, H.; Hawthorn, G. A. In *Corrosion Initiation and Propagation in Particulate Aluminum-Matrix Composites,* Tri-Service Corrosion Conference, Orlando, Florida, November 14–18, 2005; Orlando, Florida.
36. Hihara, L. H.; Lin, Z. J. In Seventh Japan International SAMPE Symposium and Exhibition: Tokyo, Japan, 1999.
37. Deltombe, E.; Vanleugenhaghe, C.; Pourbaix, M. In *Atlas of Electrochemical Equilibria in Aqueous Solutions*; Pourbaix, M., Ed.; National Association of Corrosion Engineers: Houston, TX, 1974; pp 168–176.
38. Ding, H.; Hihara, L. H. *J. Electrochem. Soc.* **2005**, *152*, 4.
39. Iseki, T.; Kameda, T.; Maruyama, T. *J. Mater. Sci.* **1984**, *19*, 1692–1698.
40. Grytsiv, A.; Rogl, P. In *Light Metal Systems. Part 1: Selected Systems from Ag–Al–Cu to Al–Cu–Er*; Springer: Berlin Heidelberg, 2004; p 11A1.
41. Pohlman, S. L. *Corrosion* **1978**, *34*, 156–159.
42. Becher, H. J. In *Handbook of Preparative Inorganic Chemistry*, 2nd ed.; Brauer, G., Ed., Academic Press, 1963; Vol. 1, p 832.
43. Kendall, E. G. In *Metal Matrix Composites*; Kreider, K. G., Ed.; Academic Press: New York, 1974; Vol. 4, pp 319–397.
44. Portnoi, K. I.; Timofeeva, N. I.; Zambolotskii, A. A.; Sakovich, V. N.; Trefilov, B. F.; Levinskaya, M. K.; Polyak, N. N. *Poroshkovaya Metallurgiya* **1981**, *218*(2), 45–49.

45. Buonanno, M. A. Ph.D. Thesis, Massachusetts Institute of Technology, Cambridge, MA, 1992.
46. Deonath, S. K.; Bhat, R. T.; Rohatgi, P. K. *J. Mater. Sci.* **1980**, *15*, 1241–1251.
47. Rohatgi, P. K.; Asthana, R.; Das, S. *Int. Mater. Rev.* **1986**, *31*, 115.
48. Deonath, S. K.; Namboodhiri, T. K. *Composites* **1988**, *19*, 237–243.
49. Mortensen, A.; Cornie, J. A.; Flemings, J. *J. Met.* **1988**, *40*, 12.
50. Arsenault, R. J. In *Metal Matrix Composites: Mechanisms and Properties*; Everett, R. K., Arsenault, R. J., Eds.; Academic Press: New York, 1991; pp 79.
51. Uhlig, H. H.; Revie, R. W. *Corrosion and Corrosion Control*, 3rd ed., Wiley: New York, 1985; p 123.
52. Birbilis, N.; Buchheit, R. G. *J. Electrochem. Soc.* **2005**, *152* (4), B140–B151.
53. Bruun, N. K.; Nielsen, K. In *Metal Matrix Composites-Processing, Microstructure and Properties*, 12th Riso International Symposium on Materials and Science, 1991; Hansen, Ed., 1991; pp 257–264.
54. Yang, J. Y.; Metzger, M. In *Extended Abstracts*; The Electrochemical Society: Denver, CO, 1981; Vol. 81-2, Abstract no. 115.
55. Deonath, S. K.; Namboodhiri, T. K. *Corros. Sci.* **1989**, *29*, 1215–1229.
56. Butler, G.; Ison, H. C. K. In *Corrosion and Its Prevention in Waters*; Robert, E., Ed.; Krieger Publishing: New York, 1978; p 149.
57. Ahmad, Z.; Paulette, P. T.; Aleem, B. J. A. *J. Mater. Sci.* **2000**, *35*, 2573–2579.
58. Yao, H.-Y.; Zhu, R.-Z. *Corrosion* **1998**, *54*(7), 499–503.
59. Sedriks, A. J.; Green, J. A.; Novak, D. L. *Metall. Trans.* **1971**, *2*, 871–875.
60. Bakulin, A. V.; Ivanov, V. V.; Kuchkin, V. V. *Zaschita Metallov* **1978**, *14*(1), 102–104.
61. Hihara, L. H.; Latanision, R. M. *Mater. Sci. Eng.* **1990**, *A126*, 231–234.
62. Harrigan, W. C. J.; Flowers, R. H. In *Failure Modes in Composites*; Cornie, J. A., Crossman, F. W., Eds.; The Metallurgical Society of AIME: Warrendale, PA, 1979; Vol. IV, pp 319–335.
63. Hihara, L. H.; Latanision, R. M. *Corrosion* **1991**, *47*, 335–341.
64. Hawthorn, G. A. MS Thesis, University of Hawaii at Manoa, Honolulu, 2004.
65. Ding, H.; Hawthorn, G. A.; Hihara, L. H. *ECS Trans.* **2008**, *26*(24), 29.
66. Hihara, L. H. In *ASM Handbook, Corrosion: Materials*; Cramer, S. D., Covino, J., Eds.; ASM International: Materials Park, OH, 2005; Vol. 13B, pp 538–539.

Further Reading

Aylor, D. M. In *Metals Handbook, 9th ed.; Corrosion*; ASM International: Metals Park, Ohio, 1987; pp 859–863.
Jones, R. H. In *Environmental Effects on Engineered Materials*; Jones, R. H., Ed.; Marcel Dekker, 2001; pp 379–390.
Lucas, K. A.; Clarke, H. *Corrosion of Aluminum-Based Metal Matrix Composites*; Research Studies Press: England, Wiley: New York, 1993.
Trzaskoma, P. P. In *Metal Matrix Composites: Mechanisms and Properties*; Everett, R. K., Arsenault, R. J., Eds.; Academic Press, 1991; pp 383–404.

3.25 Degradation of Engineering Ceramics

R. Morrell
National Physical Laboratory, Teddington, Middlesex TW11 0LW, UK; Institut für Strucktur-und Funktionskeramik, Montanuniversität Leoben, A8700 Leoben, Austria

Glossary

Advanced (advanced technical, fine) ceramic A highly engineered, high-performance, predominantly nonmetallic, inorganic, ceramic material having specific functional attributes (*Note:* US – advanced ceramic; Europe – advanced technical ceramic; Japan (English term) – fine ceramic; Germany – Hochleistungskeramik).

Ceramic An inorganic, nonmetallic material consolidated by the action of heat.

Chemical porcelain A ceramic material manufactured principally from clays, feldspars and quartz, and/or alumina, and generally of low iron content.

Chemical stoneware A ceramic material manufactured principally from clays, feldspars and quartz, and/or alumina, designed to retain dimensions during firing, and manufactured in large pieces.

Chemical vapor deposition (CVD) Method of producing a coating on a body (and more rarely a solid object on a mandrel) by reaction between gases at high temperature, for example, $SiCl_4 + CH_4$, producing SiC.

Corrodant Substance causing corrosion.

Delayed failure The sudden failure of a ceramic component without detectable creep as a result of subcritical crack growth under stress.

Flexural strength The fracture stress of a defined beam test-piece loaded in flexure and computed as the nominal tensile surface stress; usually applied to ceramic and other brittle materials.

Glass-ceramic A material fabricated as a glass which is then subjected to a controlled crystallization (devitrification) process to give a fine-grained microstructure with desired properties.

Hardmetal A metal/ceramic composite material comprising typically a hard ceramic phase with a metallic binder phase. Examples: WC/Co, WC/Ni, TiC/Fe.

High-alumina ceramic An advanced ceramic material comprising principally a compound of aluminium and oxygen with or without other minor components to aid densification or control properties.

Hydration The formation of a hydroxide material, especially at the corrosion interface of a material, especially a ceramic.

Mullite A ceramic phase comprising a compound of alumina and silica.

Nonoxide ceramic An advanced ceramic material comprising principally borides, carbides, nitrides, or silicides, for example, silicon nitride, molybdenum disilicide.

Reaction bonding A process for ceramic manufacture in which a ceramic bond between grains is produced *in situ* by chemical reaction between relevant species, for example, between silicon and nitrogen to produce silicon nitride.

Subcritical crack growth The process of crack extension over time without complete failure.

TZP (tetragonal zirconia polycrystals) A zirconia ceramic, typically, but not exclusively, partially stabilized with yttria (hence Y-TZP) and with submicrometer grain size to retain principally the tetragonal phase of zirconia, resulting in high strength.

Zirconia ceramic An advanced technical ceramic material comprising principally a compound of zirconium and oxygen with or without other minor components to provide phase stabilization, to aid densification or to control properties.

Abbreviations

CBN Cubic boron nitride
CVD Chemical vapor deposition
HBN Hexagonal born nitride
PTFE Polytetrafluoroethylene
TZP Tetragonal zirconia polycrystal

3.25.1 Ceramic Materials as Engineering Products

3.25.1.1 Ceramic Materials and Applications

For many years, ceramic materials have formed a vital part of the palette of materials available for engineers, but with the principal disadvantage that they are brittle and may not be available in particularly large sizes. In former times, the choice was limited to porcelain-like products, which could be made for items such as pestles, mortars, mills, and chemical plant tower packings. Such materials generally have good resistance to being attacked by aqueous solutions up to 100 °C. Their principal advantage is that they produce no corrosion scale layers and no obvious metallic contamination of the process for which they are used. However, such materials are not particularly strong and/or wear resistant. Over the last half-century, the development of a wider range of harder and stronger materials for general engineering applications has greatly widened the field of applications from a corrosion

perspective. Such newer products have improved the performance of a wide range of existing devices compared with the use of metallic components, and have enabled new applications and processes to be developed, upon which the entire world now relies.

3.25.1.2 Mechanical and Thermal Limitations

The main disadvantage of ceramic materials is that they are, in engineers' terms, brittle. They generally show linear elastic behavior to fracture, which occurs at strains of less than 0.5%, usually less than 0.1%. They therefore have to be treated with care from the design and application point of view. There must be an avoidance of stress concentrations that initiate fracture, which means that the designer should change his/her mindset, throw away his/her metallic designs with all their in-built assumptions, and start from scratch with chunky designs, which minimize stresses and thus maximize reliability. Failures in trials often result from poor or inappropriate design and a failure to understand stress concentrations and thermal gradients, as much as from attempting to use an inappropriate material.

A further consequence of brittleness is a limitation to thermal stress and thermal shock resistance. Steep temperature gradients or sudden changes of surface temperature, particularly downshock, can result in internal stresses, which are not relaxed by plastic deformation processes, but which can cause rapid failure. The larger the item, the more it is prone to thermal stress failure. Care is needed in the choice of material to withstand thermal shock. In general, for dense, fine-grained materials, thermal stress is reduced and thermal shock resistance is improved with reductions in thermal expansion coefficient and elastic modulus, and with increases in thermal conductivity and strength. Materials that have larger grain sizes, perhaps some open porosity, and lower elastic modulus, such as many refractory products, may show better thermal shock resistance than do finer-grained, denser, stronger materials, because the elastic energy developed is less, and damage takes the form of microcracking rather than macrocracking. Changing the material to maximize thermal shock resistance may have limitations in terms of resistance to corrosive attack. Therefore, care in material selection has to be taken. Unless parts are of thin sections, where concerns about thermal stress are less, it may be better to design the whole function to restrict thermal stressing occurring while retaining the corrosion resistance of the material of choice.

3.25.2 Microstructure and Corrosion Processes

3.25.2.1 Role of Microstructure

Ceramic materials are typically made by a powder route, with a high temperature consolidation process to form the final microstructure. This process may be *via* solid state diffusion or sintering, or *via* a liquid phase mechanism, or *via* a combination of the two. In many cases, it leaves a continuous second phase, often of a glassy or partially crystallized nature, running between the grains. This is a key aspect of ceramic microstructures that needs to be considered from the point of view of corrosion. It means that not only the base crystalline phase or phases, but also the secondary, often unspecified, continuous phase, has to be resistant to corrosion in the medium under consideration.

An example of this is the series of materials known as high-alumina ceramics. By itself, high-purity alumina powder requires a high sintering temperature, and particularly expensive raw materials. Usually, a small amount of MgO is added to control grain growth during sintering, and this tends to segregate to grain boundaries along with any residual impurities such as sodium. For control of electrical properties such as dielectric loss, small additions of silica are made to create a glassy phase. Reductions in firing temperature can be achieved by adding additional components such as CaO. Although the alumina grains themselves are corrosion resistant, the resulting continuous grain boundary phase may not be, especially in acid media where the material can be penetrated through this phase without necessarily any change in dimensions or appearance. Such penetration can be disastrous for strength, wear, and erosion resistance, as well as for any process containment. Thus, although there may be claims that might seem to indicate that high-alumina ceramics have generically good corrosion resistance, which would be borne out for high-purity materials, it is not generally the case. Materials have to be chosen for their individual fitness for purpose, balanced against the ability to make the size and shape required. Often, it is necessary to undertake a test under the specific conditions of anticipated use to prove that they have the required corrosion resistance.

The majority of ceramic materials contain some residual porosity as a result of the process route

used in their fabrication. For engineering purposes, selected materials should be specified as being 'impervious,' in which case the pores are individual, and mostly not connected to each other. Liquids cannot penetrate the material except by dissolving a continuous phase. In some cases, this porosity is 'open,' that is, it is accessible from the exterior of the body, and there is a large accessible internal surface area that is subject to corrosive attack. With some materials, notably with chemical porcelains and stonewares, the integrity of the item may rely on an intact, impervious skin, which, if broken, permits corrodants to access the more-porous bulk.

Further details concerning individual material types are found in later sections.

3.25.2.2 Corrosion Processes

While corrosion of metallic alloys involves the dissolution or oxidation/hydroxylation of metal atoms at the surface, usually with electrolytic drivers, oxide ceramics are already oxides, and are usually quite stable against further hydration except under hydrothermal conditions (temperatures of 300–500 °C and pressures of 10s or 100s of atmospheres). They may possess a surface monolayer of hydroxide, but typically, this is stable. Removal of material from such a surface by aqueous environments requires chemical dissolution of the ceramic structure itself. In materials such as high-purity, single-phase alumina or silicon carbide, this is difficult; hence the corrosion resistance.

Some single-phase products have only moderate corrosion resistance in acidic or alkaline environments, notably those that are based primarily on alkaline or acidic oxides. Thus, magnesium and calcium silicates and some aluminosilicates tend not to be acid resistant, while silica and highly siliceous glasses tend to be relatively resistant to acids, but are attacked by strongly alkaline environments.

In structures with corrosion-resistant primary grains and secondary phases such as glasses, attack may be much more rapid, especially if the glassy network is highly disrupted by locally high levels of alkaline and alkaline earth ions. Acidic environments can much more readily attack this glassy phase. It is quickly leached of its alkaline ions, leaving a porous siliceous gel acting as a diffusion medium for the corroding species. Another example is of the free silicon phase in some versions of silicon carbide ceramics. The result is that the material can be penetrated down the grain boundaries without the generation of any surface layers and without loss of dimensions.

In nonoxide ceramics, which are free from oxide phases, the first step to dissolution is oxidation or hydration. In silicon carbide and silicon nitride, the surface comprises a protective layer of silica. To progressively remove material, not only does this layer have to be removed, requiring a strongly alkaline condition, but also the underlying material then has to be oxidized. Only certain corrodant conditions will achieve this, hence the corrosion resistance of such materials. In some cases, the material oxidizes or hydrates readily. An example is the soft, crystallographically hexagonal form (HBN) of boron nitride. The oxide product is boric oxide, which readily reacts with water. Once hydration occurs at a significant rate, dissolution is continuous, and there is no protective skin.

The majority of commonly available ceramics for structural purposes are not electrically conducting to any significant extent at temperatures up to 500 °C. Consequently, they do not suffer from electrolytic effects, and hence from corrosion processes that involve this type of process. Only in materials that are electronically or ionically conducting, one might see such effects. With a few exceptions (e.g., siliconized silicon carbide), such materials are generally not employed for corrosion-resisting functions. However, an interesting example of a study of electrolytic corrosion of titanium-based ceramics and ceramic composites (TiN, Ti(C,N), TiB_2) in seawater has been made by Lavrenko *et al.*[1] They showed that the rate of corrosion was three or four orders of magnitude less than in the majority of metallic materials, and that the process was dominated by the formation of a TiO_2-based layer, which was analyzed in detail.

3.25.2.3 Subcritical Crack Growth

It is well established that the strength of many types of ceramic materials is determined by small defects or 'flaws,' which can be located in the bulk or at the surface. The combination of the largest flaw and the most highly stressed location determines the short-term strength. If such flaws are accessible to the external environment, the strength may be controlled by that environment through its effect on the process of breaking atomic bonds at the tips of stressed flaws. The net effect of this 'subcritical crack growth' is that both the short-term strength and the lifetime under steady applied stress are reduced.

The key element in this process is the presence of water, or more exactly, OH^- ions at the crack tip. The effect is accelerated by high temperature, and is influenced by pH. Glasses are the most susceptible of materials, followed by oxide-based ceramics and nonoxide-based materials with oxidic continuous secondary phases. Nonoxides that are inert to water, such as some silicon carbides, show very little effect.

The susceptibility of materials to this effect can be determined either by conducting strength tests at a wide range of stressing rates (four or more orders of magnitude), or by undertaking crack growth experiments on long-crack fracture toughness test-pieces. The information derived may be of importance for applications in which the actual bulk corrosion rates are very low or negligible, but the material is highly stressed.

3.25.2.4 Corrosion/Erosion

There is a strong synergistic effect of corrosion and wear or erosion. There are two principal processes:

- The enhanced reaction between the medium and the ceramic surface, brought about by raised local temperature and the simultaneous removal of the reaction product;
- The undercutting of surface grains by the corrodant penetrating grain boundaries, followed by the mechanical removal of grains.

The first mechanism occurs in dense materials in which the grain boundaries are not preferentially penetrated. An example is in silicon carbide or silicon nitride subjected to sliding wear against a similar counterface. In these cases, the wear process enhances hydration of the surface to silica, which is progressively removed through the sliding process. The rate may be low, but is the principal damage mechanism in sliding seal wear. The second mechanism is when the rate-determining factors are chemical penetration and grain loosening.

3.25.3 Testing Procedures and Standards

3.25.3.1 Standards

Testing standards for aqueous-based corrosion performance are generally flexible in corrodant conditions and duration to allow for a very wide range of potential applications in which particular conditions may arise. For example, ASTM C 650 for ceramic tile permits any corroding substance of application relevance, advises against the use of HF because of its obvious rapid attack on any silicate-based material, and suggests that a general indication of respectively acid or alkali resistance can be obtained by the use of 10% HCl or 10% KOH at room temperature for 24 h. This standard uses visual color and texture change as the main indicator of attack, preferred to the measurement of change of gloss or mass change. A similar test is available as EN ISO 10545-13 (superseding EN 106 and EN 122) for both unglazed and glazed tiles, using visual assessment of changes in surface appearance, and for glazed tiles, a 'pencil' test for the roughening of a glazed surface. The test duration is rather more extended than in ASTM C 650.

A test with a specific purpose in mind is described in BS4789 for alumina and beryllia ceramics for vacuum envelopes. It involves boiling in concentrated nitric acid (sp. gr. 1.42), followed by washing in water, then dilute ammonia, and again in water. The test-pieces are then conditioned by heating to 1200 °C for 30 min before weighing and calculation of mass loss. There is also a requirement to inspect for local cracking and spalling. The original intention behind this test was to determine whether the ceramic materials could withstand the removal of metallizing by acid digestion, followed by reprocessing at high temperature, and still maintain integrity and vacuum-tightness. This test originated from work reported by Binns.[2] Experience has shown that it is indeed very effective in identifying those materials that can be rapidly penetrated by acids.

A more general procedure is listed in CEN EN 12923-1. This provides guidance on the use of various criteria in deciding the extent of corrosive attack under any aqueous-based conditions. It provides options for characterization microstructurally, by mass change, dimension change, hardness change, flexural strength change, and by analysis of species dissolved into the reactant.

ISO 17092 provides methods for acid and alkali attack based on standardized HCl and NaOH solutions that are similar in principle to ASTM C 650, but intended for engineering type materials.

ISO 6474 (alumina) and ISO 13356 (zirconia) specifying ceramics for human body implantation such as in orthopedics require evidence that there is no change in strength after immersion in a simulated body fluid (saline, bovine serum, or the like) as one of the criteria for acceptability.

ASTM C 1368 and EN 843-3 provide methods for studying subcritical crack growth in an optional medium, which can include corrosive liquids. It is based on flexural strength testing at a series of rates over at least four orders of magnitude in loading or straining rate. The variation of mean strength with stressing or straining rate is used to compute the subcritical crack growth exponent *n*. This method is typically limited to tests of a few hours' duration, and therefore, if longer durations of exposure (and slower rates of attack) are relevant, the alternative method is dead-load 'delayed failure' testing, but this method has only been standardized so far in ASTM C 1576.

3.25.3.2 Procedures

3.25.3.2.1 Equipment

In conducting corrosion tests in highly corroding media, it is necessary to consider carefully the containment vessels, and whether they themselves will be corroded to an extent that may affect the outcome of the test. Borosilicate glass vessels are usually perfectly adequate for acid tests at ambient pressure, but may have limited life under alkali tests. Test-pieces can be suspended in baskets or from wires, but should be separate from each other and should not rest on the bottom of the vessel to avoid erosion or damage, notably during boiling tests.

In the modern era, the safest way of undertaking aggressive corrosion tests is to use polytetrafluoroethylene (PTFE)-lined digestion bombs placed in an oven at the relevant temperature. Tests at temperatures of up to 200 °C can usually be undertaken without damaging the PTFE, giving pressures of up to 10 atm dictated by the certified maximum for the vessel. The advantage is the small volume of corrodant being handled, especially if it is subsequently being analyzed for dissolved species. The disadvantage is the limited volume of corrodant that can be employed, which might lead to exhaustion, and the fact that it is static within the vessel, which can lead to some areas of corrosion shielding.

It is sometimes necessary to understand the performance of materials in the presence of combined corrosion and erosion or abrasion. Such tests are certainly relevant to plant operation where fluids and possibly abrasive debris are being circulated, but are more difficult to set up in a meaningful way and to control in the laboratory. Cox and Morrell[3] describe a method of acidic and alkaline slurry erosion based on a spinning disc, applied to alumina ceramics for chemical plant pipeline use. Wear of baffles intended to induce turbulence to avoid laminar flow films, coupled with changes in dimensions of the test discs led to some nonlinearity of conditions. Nevertheless, differences between different materials and corrodants were adequately demonstrated.

Standardized abrasive wear testing of hard materials is typically undertaken in rotating wheel experiments using loose abrasive, which becomes trapped between the wheel and the test-piece. Examples are ASTM B 611 (hard metals, steel wheel, brown alumina grit in water), ASTM G 65 (general applications, rubber edged wheel, sand, dry), and the light wear ball-cratering test (CEN EN 1071-6 intended for ceramic coatings). With suitable precautions, these tests can also be used with acidic or alkaline environments, which can be fed along with the abrasive. This approach can be used to study the synergistic effect of simultaneous corrosion and abrasion.

3.25.3.2.2 Assessment techniques

Mass change

Measurements of mass change following corrosion can be misleading with ceramics. This type of test works well for materials that are uniformly dissolved, but if there is grain boundary penetration, corrosion products can be variably trapped in the developed porosity. Washing and drying, even refiring to high temperature, does not necessarily remove them all. It is even possible to obtain a mass gain despite clear penetration, which is clearly misleading if candidate materials are ranked solely using mass change. It is recommended that mass change tests are always used in conjunction with a test that is not influenced by residual corrosion products.

Change of cross-section

This test has the same limitations and problems as with testing metallic materials. It may not provide a particularly relevant result on ceramics under aqueous corrosion conditions, because generally size changes are very small if the primary phases are not attacked, and of course, penetration is not characterized. In some cases, the method may have value, where there is clear loss in section, for example, when corrosion is combined with erosion or wear.

The most reliable method is usually the preparation of a cross-section and its dimensioning using a measuring microscope.

Dye penetration

This is an extremely useful test. Test-pieces are simply immersed for an hour or two in a suitable dye solution after corrosion and washing. After washing in solvent, the greater retention of dye compared with uncorroded material is an initial indicator of some penetration, which can be confirmed by sectioning or fracturing the test item. If the corrosion tests have been conducted on flexural strength test bars (see the following section), the depth of penetration is easily seen after fracture.

Flexural strength

For smaller-sized parts, which may suffer a risk of fracture in the intended application, knowledge of any reduction in strength as a result of corrosion can be important. Such tests are normally performed on standardized flexural strength test-pieces, typically >45 mm × 4 mm × 3 mm tested in four-point flexure (ASTM C 1161, CEN EN 843-1, ISO 14704) for advanced technical ceramics. It is recommended that at least 10 test-pieces are used for any one corrosive condition, as well as for the uncorroded reference state, in order to allow for the typical spread of strengths typically obtained with brittle materials.

Change of surface texture

The roughening or pitting of a ceramic surface can occur in corrosion, and this can be characterized using conventional roughness measurement techniques. Caution is needed with the texture characterization of ceramic surfaces in general, and the guidance given in EN 623-4 is intended to encourage good and relevant practice.

Hardness

Surfaces that suffer penetration lose apparent hardness. They may even become soft enough to be scratched or chipped using a knife, while micro- or macrohardness tests can be used to quantify such an effect (see EN 843-4, ISO 14706). The method is appropriate for small penetration depths, up to say 20–50 μm, which might not reveal themselves as changes in strength, but not for larger depths where the test may become meaningless.

Chemical changes to the corrodant

Chemical analysis of the corrodant after the test can offer an insight into which species in a multicomponent material are being preferentially removed. Very sensitive techniques are available.

General comments

Care should be taken to ensure that any loose or precipitated material is fully accounted for. Material can be dissolved and reprecipitated elsewhere, including the vessel walls and sample suspension system. An example of what can be achieved and some of the pitfalls are given by Öhman *et al.*,[4] who studied the leaching of high-purity alumina by sodium bicarbonate buffered water. They determined that in this case, gravimetric methods of determining material loss give significantly greater values than determined by using a fluoroscopic method of analyzing the corrodant solution. An analysis of solution equilibrium calculations showed that precipitation was unlikely, but far more likely was the development of a surface skin by a hydration/reprecipitation mechanism, which when dried out for test-piece weighing gave a friable surface, which was readily lost.

3.25.3.3 Testing Standards

Following are the standards providing testing methods relevant to various varieties of ceramics:

EN 12923-1:2006 Advanced technical ceramics – Monolithic ceramics – Part 1: General practice for undertaking corrosion tests (Generic standard for technical and engineering materials providing procedures for determining attack, appropriate for any reagent.)

ISO 17092:2005 Fine ceramics (advanced ceramics, advanced technical ceramics) – Determination of corrosion resistance of monolithic ceramics in acid and alkaline solution. (Testing in 6 N H_2SO_4 and NaOH boiling solutions for 24 h with attack criteria being mass loss, dimension changes, and loss of mechanical strength.)

EN ISO 10545-13:1997 Ceramic tiles – Part 13: Determination of chemical resistance. (A variety of test solutions permitted, including ammonium chloride (representing household cleaning products), sodium hypochlorite (swimming pools), HCl, citric acid, KOH, and lactic acid (foodstuffs), used for 24 h on glazed surfaces. Criteria based on visual inspection, reflectivity, and 'pencil' test.)

EN 993-16:1995 Methods of test for dense shaped refractory products. Determination of resistance to sulfuric acid

ISO 28706-4 Vitreous and porcelain enamels. Determination of resistance to chemical corrosion. Part 1: Determination of resistance to chemical corrosion by acids at room temperature.

Part 2: Determination of resistance to chemical corrosion by boiling acids, neutral liquids, and/or their vapors.
Part 3: Determination of resistance to chemical corrosion by alkaline liquids, using a hexagonal vessel
Part 4: Determination of resistance to chemical corrosion by alkaline liquids, using a cylindrical vessel

3.25.4 Performance of Specific Material Types

3.25.4.1 Oxide-Based Materials

3.25.4.1.1 Porcelains and aluminosilicates

The longevity of many silica-based materials, including earthenware, porcelains, and even some glasses, in wet environments is eminently demonstrated by archaeological evidence. Most clay-based materials comprise crystalline phases such as quartz, cristobalite, and mullite embedded in a glassy matrix produced by melting mineral phases containing alkalis and alkaline earth species. The solubility of such glasses in water is limited, and while the attack does slowly occurs by a leaching/hydration process, it does not restrict their use in many applications. In fact, they will also withstand some aggressive, aqueous environments, such as strong acid and alkaline solutions.

For applications in the kitchen and the laboratory, so-called 'chemical porcelains' with very low or zero open porosity without glazes have been in use for many years, particularly in the pharmaceutical industry, and are not radically different in structure from materials used for electrical insulators. They have been employed in a range of applications, the most commonly known one being pestles and mortars, up to some moderate-sized items for use as one-piece corrosion and abrasion-resistant linings. However, one of the limitations of such materials is their manufacture in large pieces. The shrinkage obtained on firing makes shape and dimension control difficult. One long-standing route around this problem is to restrict the shrinkage by adding prefired refractory particulates to the clay mix. However, this allows porosity to be developed, and often a product will only remain impervious if the surface skin, which effectively seals the bulk microstructure, remains intact. Such materials, often called 'chemical stoneware,' can be made in the large pieces required for chemical tower packing, and still remain the preferred option for large-sale use. Similar materials are used for corrosion-resistant hygienic tiling of surfaces.

In addition, similar materials are available in brick form for building structural chemical plant linings. Varieties are available with microstructures appropriate for acid or alkali resistance. These would be grouted with appropriate acid- or alkaline-resistant cements, which although not as corrosion resistant as the bricks, survive sufficiently for the vessel to survive and prevent corrosion of external steelwork. The scientific literature on such materials is very limited, but Charlebois[5] has described a number of such applications, including sulfite digesters in the paper industry, sodium chlorate tanks, and tanks for HCl leaching of TiO_2 ore.

Bennett[6] reports on sulfuric acid testing of four aluminosilicate brick materials made from different sources of red shale or fireclay, but all show rather higher rates of attack than SiC, silica, carbon, or alumina, minimum rates being obtained with carbon and alumina.

Marcus and Ahrens[7] show that highly siliceous materials (fused silica glass, sintered mullite, and sintered clay/zircon) have rather lower corrosion rates in concentrated phosphoric acid at 204 °C than many nonsiliceous oxides (alumina, beryllia, spinel), cordierite ($2MgO{\cdot}2Al_2O_3{\cdot}5SiO_2$) showing intermediate behavior.

3.25.4.1.2 Alumina

The ceramic family most commonly employed for engineering components is that based on aluminum oxide (alumina, Al_2O_3), being generally stronger, harder, and more abrasion resistant than porcelains. There is a huge spectrum of types of alumina ceramic depending on their intended engineering function. Containing more than 80% by mass of Al_2O_3, but more typically in excess of 95%, they usually have additional components added to control the sintering process, to reduce the sintering temperature, or to modify the final properties. It is probably true to say that no two alumina ceramics from different sources are the same in all respects, but some generalizations may be helpful (more details can be found in Morrell[8]):

1. High-purity alumina without additions does not sinter well and tends to suffer from exaggerated grain growth. Such materials tend to be used only for crucibles.
2. High-purity alumina with small controlled amounts of MgO or Y_2O_3 when in ultrafine powder form can be sintered to full density with control of grain

size. Such products include biomedical implants (fine-grained) or translucent lamp envelopes (medium-coarse grained).

3. Aluminas of lesser purity (sometimes called 'debased' alumina) used for lower value-added products, for example, in electronics, usually have deliberate additions of MgO, SiO_2, and CaO. This produces a distinct secondary glassy phase, which can act as a sink for impurities such as alkalis, and thereby control dielectric properties, especially loss tangent.
4. Alumina ceramics for general engineering may be similar to those for electrical purposes in terms of compositions; indeed often, a given product is treated as multifunctional. Others, such as those sintered using MnO and TiO_2, which produce a low-temperature eutectic liquid during firing, tend to have applications restricted to mechanical ones. More generally, if strength and wear/erosion resistance is an important feature, products tend to be of finer grain size than used for many electrical applications.
5. While the majority of aluminas are highly resistant to corrosion in high pH or neutral solutions, only a few products are designed for resistance to aqueous corrosion at low pH. This requires control of the nature of the secondary phase composition.

There is an extensive literature on corrosion resistance. Thermodynamically, Al_2O_3 is not stable in water, but is attacked only very slowly. Öhman *et al.*[4] evaluated the rate of attack of simulated groundwater on a high-purity alumina hot-pressed material substantially free from secondary phases. The buffered sodium bicarbonate solution used gave pH 8.5. In tests of up to 90 days' duration and at temperatures in the range 40 °C–100 °C, depths of corrosion determined by mass loss and fluoroscopic analysis for aluminum in the corrodant solution were of the order of only a few nanometers. As mentioned earlier, the factor of 5 discrepancy between the two analysis methods was ascribed to the development of a hydrated surface skin, which was readily lost when dried. A similar very thin deposited layer was found by Real *et al.*[9] in tests on a similar sintered material boiled for 2 weeks in 5% salt solution. This treatment did not significantly affect the strength or the apparent hardness of the material.

One of the first systematic studies of corrosion resistance was made on a fairly high-purity crucible material, conducted by Jaeger and Kraseman.[10] Attack by various acidic and alkaline solutions at 95 °C for 3 days was very significant for HF and HF/H_2SO_4 and for strong (1:2) NaOH solution. For many other acids, attack was slow.

Table 1 Corrosion resistance of alumina ceramics[11]

Body no.	Composition (wt%)				Mass loss, 50% HNO_3, RT, 18 h (mg cm^{-2})
	Al_2O_3	CaO	MgO	SiO_2	
1	94.1	1.8	0.7	3.4	7.0
2	94.7	1.7	1.2	2.4	5.0
3	95.2	1.0	0.7	3.1	3.5
4	95.8	0.6	0.7	3.0	0.6
5	94.7	0.6	0.7	3.4	0.2
6	94.7	0.6	1.1	3.7	0.1
7	96.6	–	1.3	2.2	0.04

Richards[11] reported the corrosion resistance of experimental 'debased' alumina ceramics in HNO_3 as a function of secondary phase composition. From the data provided (**Table 1**), it can be seen that the mass loss rate can vary by more than a factor of 100, depending on the ratio of $MgO:CaO:SiO_2$. It can be concluded that the best resistance is achieved when the ratio of alkaline earths to silica in the secondary phase is small, and when the amount of CaO is minimized. Commercial products are available that are free from CaO for maximized resistance to acidic corrosion, but have a disadvantage that they tend to have lower toughness because of an increased thermal expansion mismatch between the alumina grains and the secondary phase.

These findings are supported by the work undertaken at NPL during the 1970s.[12, 13] A variety of alumina ceramics of between 95% and 99.8% were tested in H_2SO_4 (10%, v/v, boiling, 72 h), HCl (20%, w/v, boiling, 72 h), HNO_3 (35%, w/v, boiling, 72 h), HF (40% solution, 20 °C, 72 h), and KOH (10%, w/v, boiling, 72 h). The criteria used were weight loss and spalling tendency on reheating to 1000 °C (**Figure 1**), dye penetration (**Figure 2**), strength loss, and hardness loss. The principal results are shown in **Table 2**.

A summary of some of the conclusions is as follows:

1. A translucent high-purity alumina was found to be resistant to all acids with no detectable weight loss, dye penetration, or tendency to spall.
2. A number of refractory or electrical aluminas (up to 99.7% Al_2O_3) were badly attacked in all acids, and some pitted badly or disintegrated when reheated indicating the presence of trapped corrosion products. There were significant losses in strength and hardness, indicating the development

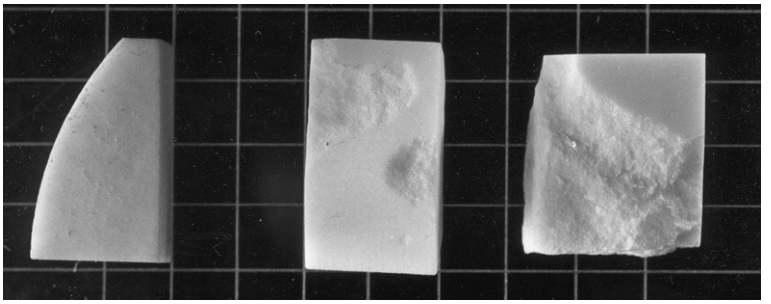

Figure 1 The entrapment of corrosion products within the surface of corroded alumina ceramics produces spalling on reheating to 1000 °C. Exposure to HF for 72 h at room temperature; left to right: Materials C, G, and K (see **Table 2**, Ref. 14). Reproduced with permission of HMSO through National Physical Laboratory.

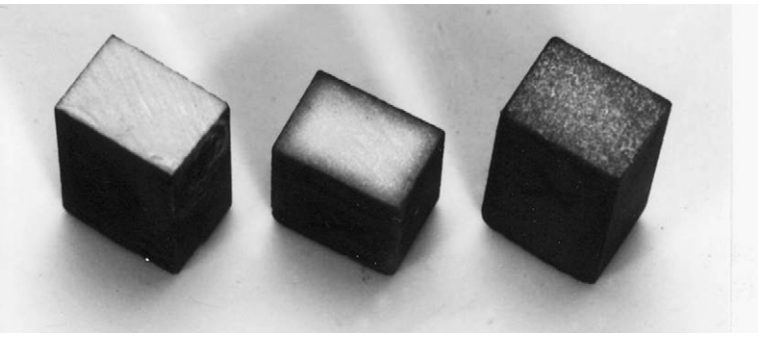

Figure 2 Fracture surfaces of test-bars after 72 h immersion in boiling H_2SO_4 followed by dye impregnation, showing a range of degrees of attack.[13,14] Reproduced with permission of HMSO through National Physical Laboratory.

Table 2 Corrosion tests on high-alumina ceramics[12–14]

Material	*Al_2O_3 (%)*[a]	*Mass loss (mg cm^{-2})*					*Flexural strength after exposure (% of original)*				
		HCl	*HNO_3*	*H_2SO_4*	*HF*	*KOH*	*HCl*	*HNO_3*	*H_2SO_4*	*HF*	*KOH*
A[c]	99.8	0	0	–	0	0					
B[c]	(96)	6.4	2.5	3.6	–	<0.1					
C[b]	99.8	1.5	1.0	1.0	0.05	−1.0	34			48	
D[b]	99.4	D	PP	D	D	<0.1					
E[b]	99.2	D	D	0.65	0.76	0					
F[b]	99.6	D	0.3	D	P	0					
G[b]	99.6	P	S	S	SS	0					
H[d]	94.6	0.07	0.06	0.08	15	0.77	91	95	92	45	58
I[c]	97.5	SS	PP	2.5	D	<0.1	44	51	58	25	97
J[c]	99.1	0.25	P	0.35	0.66	<0.1	65	73	76	21	86
K[c]	99.5	P	D	S	D	<0.1	26	27	27	34	84

[a]By XRF analysis except (–);
[b]*Refractory grades;*
[c]Engineering grades;
[d]'Acid-resisting' grade.
Appearances after heating to 1000 °C: P = surface pits, PP = bad pitting, S = surface spalling, SS = severe spalling, D = disintegrated.

of a porous layer, but without any significant loss in dimensions.

3. A 95% material claimed to be acid resistant was found to be so compared with most others, except in HF, which attacks the siliceous phase. In this material, most of the CaO is replaced by MgO, and the SiO_2 content raised to provide a relatively corrosion-resistant intergranular glassy phase.
4. Alumina itself is slowly dissolved by strong alkalis, but there is much less preferential penetration

through any intergranular phase, resulting in a progressive removal of the surface rather than the penetration seen with acids. Strength as measured in a flexural test on small test-pieces, which preferentially stresses the corroded surface, tends to be better maintained than in acids.

Later work at NPL[3] evaluated the effects of combined corrosion and erosion in acids and alkalis on a small range of alumina ceramics. Three alumina ceramics were employed, two fine-grained, of nominal 99.5%, and one coarse-grained, of nominal 97.5% alumina. Tests were made on discs spinning in a heated corrosive liquid, with and without SiC as a hard particle erodant, as well as on test-bars suspended in the liquid. All the three materials were significantly penetrated by acidic solutions, HCl being the most aggressive. The 97.5% alumina was attacked much faster than were the 99.5% materials, but these showed significant differences in behavior. **Figure 3** shows the change in flexural strength measured at room temperature for different corrodant types. Immersion in KOH solution produced the least effect. There were very minor changes in both mass and strength as a result of immersion in water.

The addition of 5% (v/v) SiC grit to acidic corrodants in these tests resulted in an acceleration in the rate of mass loss by a factor of between 2 and 4 compared with tests in liquid only. This is explained by the fact that the removal of the secondary phase renders the remaining material rather weaker and more readily eroded. By comparison, the erosion rate in KOH solution was only slightly faster than that in water at the same temperature, indicating that the microstructure is not weakened in the same way.

Engell and Jakobsen[15] have reviewed corrosion mechanisms in alumina ceramics used for liquid pump parts, including brown-colored versions incorporating MnO and TiO_2 as low-temperature liquid phase formers. Tests were run for up to 5000 h at 90 °C at pH 5.5, 9, and 12 buffered by NaOH. **Figure 4** summarizes some of their results. The rates of attack increase with increasing pH over this range, but there are significant variations between the materials.

Genthe and Hausner[16] studied single-crystal sapphire and ruby, and high-purity hot-pressed aluminas with and without MgO and Cr_2O_3 dopants. The dissolution rates in HCl and H_2SO_4 (180 °C, 168 h) were minimal for single-crystal materials, but greater for polycrystalline ones, which was attributed to the preferential removal of the grain boundary phase. In H_2SO_4/H_3PO_4 mixtures, attack rates were significantly higher owing to the dissolution of alumina itself, although increasing amounts of Cr_2O_3 tended to suppress this process.

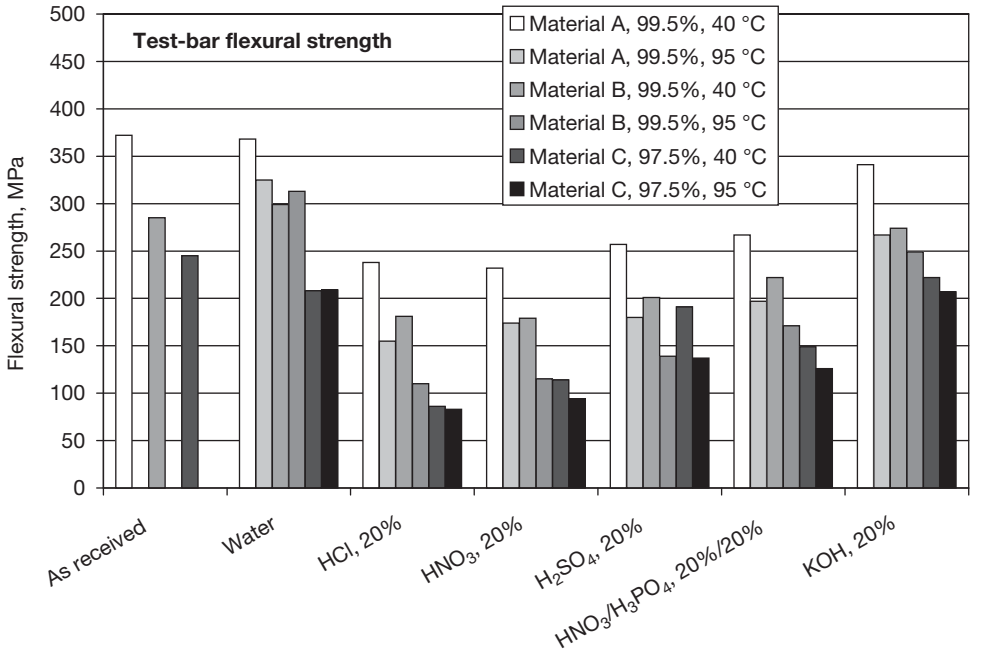

Figure 3 Loss in strength of test-bars immersed in flowing liquid for 23 h in various corrodants (data from Ref. 3).

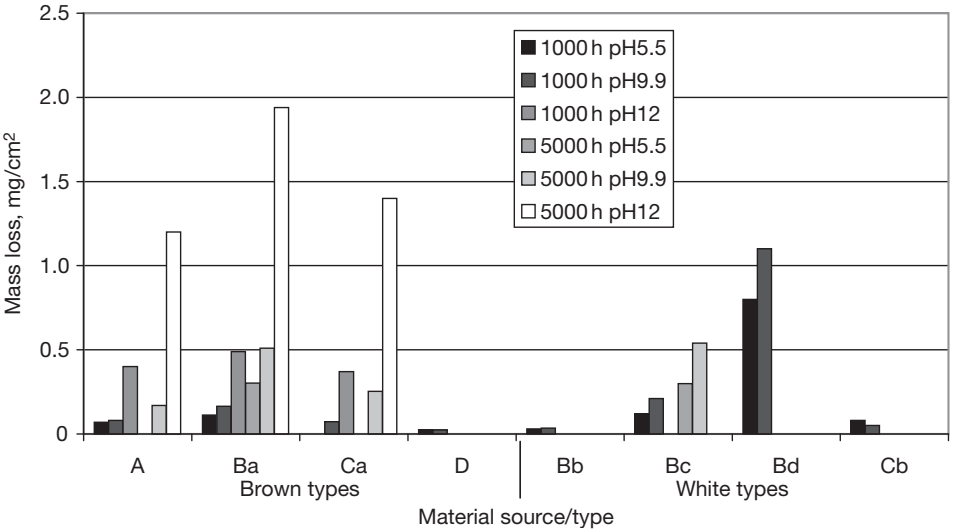

Figure 4 Corrosion test results from Ref. 15 at 90 °C on brown and white alumina ceramics from different manufacturers. (*Note:* not all combinations were tested.)

Mikeska *et al.*[17] report that all alumina ceramics, including those of nominally very high purity, other than single-crystal sapphire are very significantly attacked by HF at 90 °C as a result of grain boundary phases, the effect being worst with high levels of silica in the secondary phase. Fang *et al.*[18] show that an 85% alumina is rapidly penetrated by a 1% HF + 5% HCl solution at room temperature, to leave a porous layer that was readily eroded in a subsequent wet sand erosion test.

Tests on 94% and 99% aluminas in concentrated (96%) phosphoric acid have been reported by Marcus and Ahrens.[7] At room temperature, the dissolution rate was minimal over a period of a month, but at 204 °C, the higher-purity material was attacked faster with a dissolution rate equivalent to 450 mm year^{-1}, compared with 35 mm year^{-1} for the 94% material. This is likely to be a result of a slower reaction with the continuous glassy phase than with alumina itself.

Sato *et al.*[19] tested two aluminas at 150–200 °C in 0.1 M to 25 M NaOH. A 93% alumina material was attacked several times faster than was a 99.5% alumina, primarily by dissolution of the secondary phase. Small test-pieces (3 × 4 × 20 mm) were essentially consumed by the 25 M solution within a day at 200 °C and within 5 days at 160 °C.

This wide range of performance implies that although alumina ceramics generally show good resistance to weak and neutral solutions, great care must be taken to select the most appropriate product if aggressively acidic service conditions are intended. Materials not designed for acid resistance may be penetrated much faster than might be expected.

Dailly *et al.*[20] evaluated the stress-corrosion behavior of several types of electrical substrate alumina ceramic in air and in Ringer's solution (saline, appropriate for biomedical environments), using the double torsion plate method. In this method, the test-piece is rapidly loaded, and then the machine crosshead is stopped and the stress relaxation monitored as the crack progresses along the length of the plate. The crack velocity was determined from the relaxation rate. In all the cases, the crack velocity exponent (n in the relationship $v = AK_I^n$ where v is the crack velocity, K_I is the stress intensity factor, and A is a constant) was in the range 17–30, indicating the clear existence of subcritical crack growth. This value was lower in saline than in moist air, that is, the material becomes more susceptible to crack growth. The results given do not provide a clear indication of what features of the composition, especially the relative proportions of the secondary components, control the behavior, but the authors suggest that the presence of MgO is disadvantageous. Byrne *et al.*[21] used the same technique on a variety of materials and found significant differences in crack growth in strong acids and alkalis. Barinov *et al.*[22] report similar large changes in n with different pH values for one alumina, but not another, using the method of flexural strength testing over a very wide range of testing rates.

Circumstantial evidence from *in vitro* and *in vivo* failures of highly loaded alumina femoral

components suggests that high-purity materials are not immune to the phenomenon, although Ferber and Brown[23] have found that the values of n are higher.

3.25.4.1.3 Zirconia

Material types

Zirconia in its pure form undergoes two solid-state phase transformations on cooling from the melt (cubic–tetragonal–monoclinic), making the production of useful ceramic materials impossible. Structural stabilization is required. To stabilize the cubic form, MgO, CaO, or Y_2O_3 can be used in sufficient quantity; such products are known as *stabilized zirconia*. Such materials find uses as crucibles and oxygen sensors, but are not particularly strong or tough.

Developments in the 1970s were made with partially stabilized materials that enabled much stronger tougher products to be made. With MgO additions, a ceramic shape sintered in the cubic phase field is subjected to a programmed cooling schedule in which a fine-scale tetragonal phase precipitate is developed inside the large cubic grains (~30 μm). The destructive martensitic-like conversion of the tetragonal phase to the monoclinic phase with significantly lower density is avoided by constraint of the cubic phase and by retaining a small precipitate size. Such products are known as *transformation toughened partially stabilized zirconia*, but often just 'partially stabilized zirconia.' Mixed stabilizers are sometimes used instead of just MgO.

An alternative approach is with yttria additions, most commonly with 3 mol%. In this case, a very fine powder (<100 nm) is prepared at which size scale tetragonal zirconia is stable to below room temperature. This is sintered to a dense ceramic at a relatively low temperature (~1450 °C) in order to avoid excessive grain growth. Such materials typically have a grain size of ~0.5 μm, which is mostly the tetragonal phase, although the surface layer may contain some monoclinic phase. Such products are known as *tetragonal zirconia polycrystals* or more commonly as 'TZP.' When the stabilizer is yttria ('Y-TZP'), this product has a high strength, and a wide range of applications, including biomedical devices such as hip joints, but has a limited performance at raised temperature because of an increased risk of progressive transformation from the surface. To circumvent this problem, alternative or mixed stabilizers have been proposed.[24] Research has been conducted on the use of other lanthanides, such as scandia, but such materials are primarily intended for oxygen ion conduction and are not generally commercially available.

The principle of transformation suppression in tetragonal ZrO_2 is also used to improve the strength of other ceramic materials, notably alumina.

Stabilized zirconia

Compared with TZP materials (see the later sections), cubic stabilized zirconia (CSZ) has been considered to be more stable to hydrothermal degradation. However, as shown by Guo and He,[25] an 8Y–ZrO_2 material typical of that used for oxygen ion sensors showed precipitation of the monoclinic phase after exposure to 0.026 atm. water vapor pressure at 250 °C, and some tendency to cracking, but with an increase in electrical conductivity.

Lay[14] reports significant rates of attack by boiling acid solutions on a CaO-stabilized material, especially H_2SO_4, but no attack by 80 °C solution of KOH. 6Y-CSZ and 8Y-CSZ are reported to be highly corrosion resistant, especially in neutral or alkaline solutions.[26]

Transformation toughened partially stabilized materials

Sato *et al.*[27] report that an MgO partially stabilized material does not undergo tetragonal-to-monoclinic transformation in 1 M HCl and 1 M sodium acetate–acetic acid pH 3 solution at up to 140 °C for up to 40 days, but some transformation and a loss of strength occurred when exposed to water at above 200 °C, Mg^{2+} ions being detected in solution.

Fang *et al.*[18] report on corrosion testing of a UK origin material, partially stabilized with MgO and Y_2O_3 and containing some SiO_2, in an HF/HCl solution, simulating an oil pipeline cleaning solution. They noted that HF tended to attack the grain-boundary silica, while HCl attack tended to leach the yttrium and to destabilize and dissolve the zirconia grains. The process was thought to be such that the surface of the material was progressively removed with no significant influence on strength or erosion rate in a subsequent sand jet wet erosion test.

Mikeska *et al.*[17] report a corrosion penetration rate >100 mm year^{-1} in HF at 90 °C.

Y-TZP, Ce-TZP, and Ce–Y-TZP

There is extensive literature on the problem of destabilization of Y-TZP in water or steam in the temperature range 150–400 °C, but there is no conclusive explanation. The most likely process is the diffusion of water into the ceramic, annihilating oxygen vacancies, releasing yttrium ions, and leaving the zirconia

grains with insufficient stabilization.[28–31] It has been suggested that the impurity content of the material affects this process, changing the level of stability,[32–37] but the exact mechanisms have not been conclusively determined. The net result is the expansile growth of groups of monoclinic zirconia grains on the surface, giving small raised regions that can be plucked out leaving a pit.[31] In the short term, such pits do not necessarily affect the strength of the material, but eventually macrocracking can occur.

Researchers usually characterize the process using X-ray diffraction and report the percentage of monoclinic phase at the surface. Using this approach, it has been shown that there is a nucleation delay for the process, of length determined by temperature, which has allowed prediction of rates at temperatures as low as 37 °C (orthopedic applications at human body temperature[32]). The process has also been found to be surface preparation dependent. Grinding the surface of this material caused some transformation to occur, often considered to be beneficial by creating high surface residual compressive stresses. Subsequent rates of transformation of such surfaces are different from those of as-fired surfaces, as illustrated in **Figure 5**. Other recent literature on this problem includes Refs. 29, 31, 39, and 40.

Bastide *et al.*[24] determined that the material containing 1 mol% Y_2O_3 and 7 mol% CeO_2 was stable at well below room temperature, was not quite as strong as 3 mol% Y-TZP, but possessed a good strength retention after exposure to steam at up to 300 °C up to 2000 h. Similar results have been reported.[41,42] However, this product is not yet commercially available. Another route to improving the stability has been shown to be carbonitriding the surface in a ZrN + C bed at high temperature.[43] In contrast, Sc_2O_3 stabilization has been found not to be effective in restricting hydrothermal transformation.[44]

In more severe chemical environments, Shojai and Mantyla[45] report that 3Y-TZP zirconia ceramic membranes lost weight in both acid and alkaline solutions at room temperature, but suggest that the material did not transform at a significantly enhanced rate compared with exposure to water.

For 3Y-TZP, Mikeska *et al.*[17] report a corrosion penetration rate >100 mm year^{-1} in HF at 90 °C.

Kritzer *et al.*[46] report on corrosion tests on a Ce-TZP, using HF and HBr at 24 MPa pressure at 500 °C. Some intergranular attack was noted, HF being less corrosive than HBr, but no weight loss or phase transformation was found.

Kalin *et al.*[47] describe Y-TZP ball on alumina disc wear test experiments, in which the rate of wear of the balls in the severe wear condition is pH-controlled. A low pH of 0.9 resulted in much lower friction and milder wear than did high pH values where the formation of distinct tribolayers led to grain fracture, rough surfaces, and high friction coefficients.

Composites with ZrO_2

Hisamori and Mimura[48] studied the role of Y–ZrO_2 additions to alumina, and found that with optimized amounts of the addition, there were some small improvements in average strength after exposure to deionized water at 200 °C and 1.59 MPa pressure,

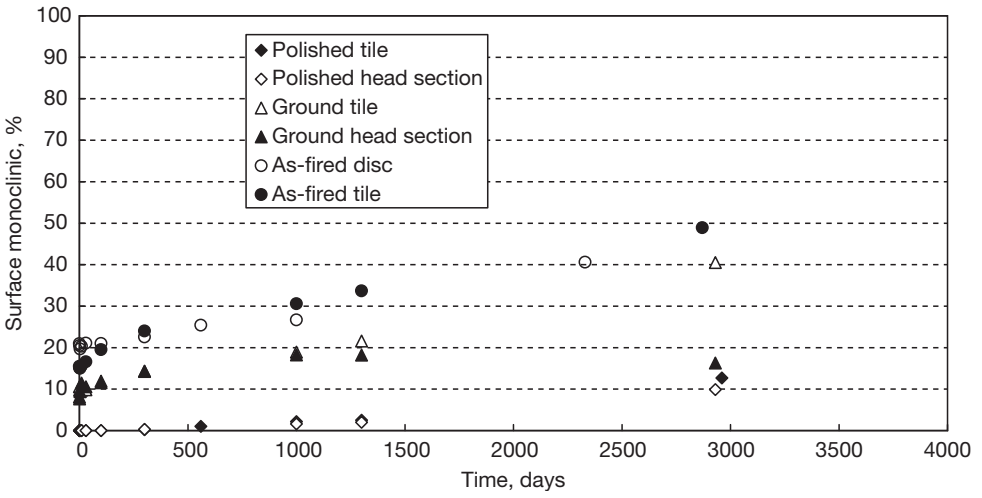

Figure 5 The transformation of Zyranox® Y–TZP material formed as flat tiles and as ceramic femoral heads as a function of time of exposure to simulated body fluid at 37 °C.[38]

although it was unclear why this should be the case. Microstructural analysis of the surface of the test-pieces showed that the presence of zirconia induced pitting with associated microcracks that might be associated with the transformation of surface-connected or near-surface zirconia grains. Herrmann *et al.*[49] demonstrate similar microstructural effects, and show that the corrosion rate under such conditions is higher than in pure alumina. Material made by Hirano and Inada[50] and by Nakanishi *et al.*[51] showed no change in monoclinic content after high temperature aging in water.

Thompson and Rawlings[52] identified structural changes in such a material when subjected to HCl attack. In medium- to long-term tests at room temperature, microcracking was associated with the leaching of yttria from the zirconia phase, and this eventually led to macrocracking. There was increased transformation of near-surface zirconia from the tetragonal to the monoclinic form. There was also a progressive loss in strength, compared with an initial drop and then a plateauing of the strength of the same alumina without reinforcement.

3.25.4.1.4 Other oxide ceramics

Mullite – Yoshio *et al.*[53] studied water attack at 300 °C and 8.6 MPa pressure on various synthetic mullite materials, and found that the mechanism of attack was dissolution of silica and the formation of a hydrated layer of boehmite (AlOOH). The composition of the mullite and the processing route adopted affect the results.

3.25.4.1.5 Glasses and glass-ceramics

Glasses

The majority of technical glasses are based on a network-forming oxide (such as silica, boric oxide, phosphoric oxide, etc.) modified with a range of other oxides. Of these, the silicate glasses are the more corrosion resistant, while the others tend to be readily attacked by water. In general, the greater the proportion of the network-modifying components in glasses, the less resistant they are to corrosion, because the remaining silicate network is more readily broken up, and the modifiers are more easily removed. Thus, many specialized glasses that are designed with specific control on expansion coefficients and glass transformation temperatures, for example, for sealing applications, tend to have a lesser ability to resist corrosion than does even window or bottle glass.

The ability of corrosive solutions to attack glasses thus depends primarily on glass composition and corrodant pH. Under near-neutral conditions, silicate glasses are very slowly hydrated at the surface, the surface being depleted of network modifying ions, such as Ca and Na by ion exchange. Silica itself is almost insoluble in water, except at elevated temperature and pressure. Good corrosion resistance is reported for high-silica, some borosilicate (e.g., Pyrex®), aluminosilicate, and high-lead compositions. Soda–lime, alkali–lead, lead borosilicate, and low-melting borosilicate sealing glasses have less good properties, while high-alkali, calcium aluminate, phosphate, and borate glasses have poor properties.

Under strongly acid conditions, network-modifying species are removed more readily, but the adequate stability of glass at room temperature is well demonstrated by the use of ordinary soda–lime glass containers for the long-term storage of mineral acids. Similarly, sodium borosilicate glasses are widely used for chemical processing in the laboratory and in chemical plant, but have the advantage of improved thermal shock resistance because of their lower expansion coefficients. High-silica glasses have the best acid resistance, while softer sealing glasses can be very rapidly attacked in mineral acids. An exception to this behavior is with HF, which attacks the silicate network, producing SiF_4, so that many glass etchants and cleaning solutions contain HF as a primary component.[54] Glasses with a high CaO content are the most resistant to HF because of the formation of insoluble CaF_2, which impedes the corrosion process.

Attack by strongly alkaline solutions is often more rapid than attack by mineral acids, because these actually dissolve the silicate network. Many dishwasher detergents are mildly alkaline, and over time can destroy the surface of glassware or glazed chinaware. The rate of corrosion is less composition dependent than with acid corrosion, aluminosilicate and special alkali-resistant compositions faring the best.

At higher temperatures, glasses become much less stable toward water-based corrodants. The surface layer can become like a sponge as the network modifiers are leached out. This has been exploited in the Vycor® process[55] for making high-silica glass; a sodium borosilicate glass is heat treated to cause two-phase separation to give interpenetrating silica-rich and silica-poor phases, the latter being readily removed by acids. A second heat treatment is used to densify the porous body.

Glass-ceramics

Glass-ceramics are produced by the homogeneous nucleation and crystallization (sometimes known as 'devitrification') of special glass compositions.[56] This process allows the exploitation of glass-making to form ceramic and ceramic-glass shapes that have special characteristics not readily achievable by conventional ceramic sintering routes. There is a huge variety of compositional types for different purposes. Some examples include

Lithium aluminosilicates:	Low and near-zero expansion coefficients, for thermally shock-resistant cookware and cooker hobs (e.g., Pyroceram®), and for optical components such as telescope mirrors (e.g., Zerodur®) Photosensitive glasses, which after heat treatment can be selectively etched
Magnesium aluminosilicates:	Medium-to-low expansion coefficients, for electronic substrates, heat exchangers, high temperature uses
Lithium zinc silicates:	Medium-to-high expansion coefficients, for glass-metal sealing, lead throughs, etc.
Fluorine–silicates:	These devitrify to fluorine-based micas to give machinability, for example, Macor®, for prototype work, including dental ceramics.

The first two types listed have also been used for the fabrication of fiber-reinforced ceramic composites, using silicon carbide fibers and a hot-pressing route to manufacture.

In general, glass-ceramics are seldom optimized for aqueous-based corrosion resistance, and tend to be attacked faster than the parent glass. The baseline glass composition is devised to permit processing as a glass, while permitting control over the devitrification. Therefore, the microstructure generally comprises intended crystalline silicate phase assemblage plus a residual glassy phase. Like glasses, all will be rapidly attacked by HF, but in other common chemical species behavior will be very much composition dependent. Some examples of recent studies of corrosion behavior are given in Refs. 57–59.

Data on the corrosion resistance of Macor® machinable glass-ceramic are shown in **Figure 6**, taken from the manufacturer's brochure.[60] Compared with other oxide ceramics and glasses, the material appears to be significantly attacked by water. It is possible that the leaching of fluorine ions from the fluorine-based mica phase creates HF in solution. This results in accelerating attack on the silicate phases if the HF is not removed by solvent replacement.

Some examples of stress-corrosion effects in water are given in Refs. 61–65.

3.25.4.2 Nonoxide-Based Materials

3.25.4.2.1 Silicon carbides

Material types

Silicon carbides are among the most acid resistant of ceramics at up to 100 °C, but the behavior differs among the different types available for use in engineering and chemical applications:

1. Reaction-bonded silicon carbide is made by infiltration of silicon into a SiC/C mass, a process which forms bonding SiC and leaves a generally interpenetrating, continuous silicon phase filling the pore space. The principal advantage of this process route is the minimal size change that occurs.
2. Sintered silicon carbide is made by a high temperature sintering process, producing either a dense or a porous, nominally single-phase material. The material can be either α-SiC (hexagonal structure) or β-SiC (cubic structure). There is usually some residual porosity.
3. Liquid-phase sintered silicon carbide is made by employing additions of typically yttria and alumina to form a liquid phase at the sintering temperature. This phase solidifies to a continuous second phase.

In addition, for special purposes, other microstructural modifications can be employed, including the addition of graphite flakes for the reduction of friction in sliding seals, and the deliberate generation of closed porosity to act as a liquid reservoir, also for seals.

Reaction-bonded silicon carbides

Tests at NPL have shown no significant mass loss or penetration of several types of reaction-bonded SiC for a range of acids. The most aggressive was boiling orthophosphoric acid, in which a mass loss of 0.3 mg cm^{-2} was obtained in 30 min.[12] Similar results are cited by Marcus and Ahrens.[7] The only acid combination to produce much more rapid attack is HF/HNO_3, which attacks the residual silicon phase by the dual process of oxidizing the surface to silica and the latter's immediate removal by HF. This combination can be used to remove completely any residual silicon, but it leaves a weakened, open-porous

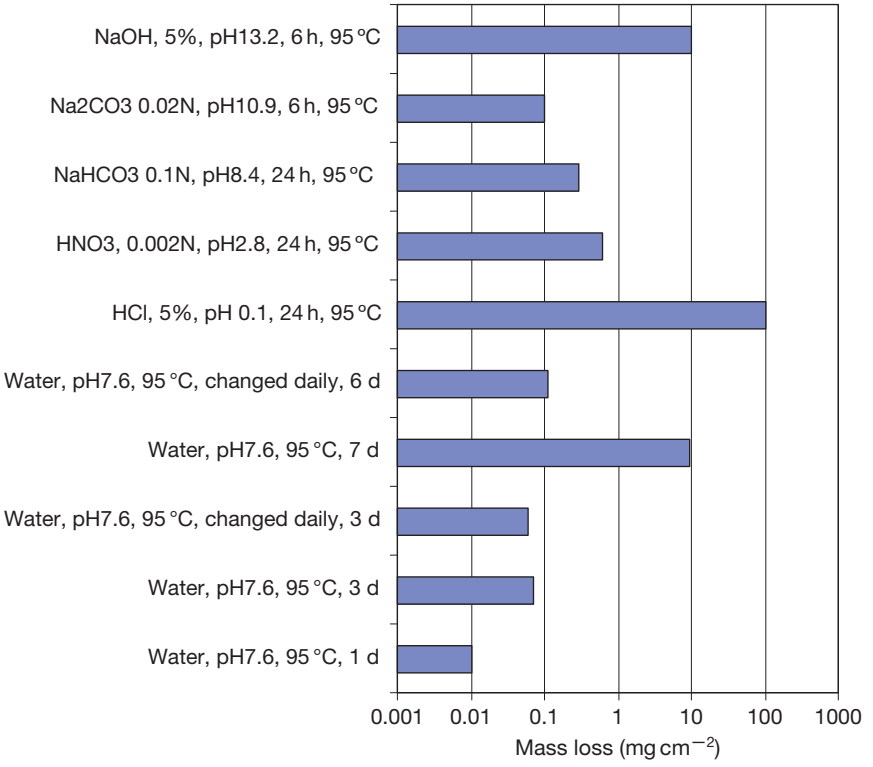

Figure 6 Corrosion test results on Macor® machinable glass-ceramic.[60]

material. In contrast, Fang *et al.*[18] show that an HF/HCl mixture at room temperature produces only a very slow attack rate. Strong alkalis, as exemplified by tests using 10% KOH at 80 °C for 168 h, also attack the material by direct rapid dissolution of the silicon phase, 30 mg cm^{-2} mass loss being obtained.

At higher temperatures, hydrothermal conditions result in oxidation and the removal of the oxide. Thus in steam at 220 °C (20 bar) for 24 h, a mass loss of 1.9 mg cm^{-2} was obtained. More recently, more extreme conditions have been evaluated on three materials with different free Si contents in water at 360 °C for 7 days.[66] The rate of mass loss increased with increasing Si content, the Si phase being leached away by water oxidation and by dissolution as silicic acid. The rate increased further when an initially alkaline solution (pH 9) was used, rather than pH 6 of deionized water.

Mikeska *et al.*[17] used 20 M HF at 90 °C and found a significant rate of penetration by the removal of the silicon phase through the formation of H_2SiF_6.

Sintered silicon carbides

In this form, silicon carbide is one of the most resistant of all ceramics to both acidic and basic aqueous-based corrosion, and finds a wide range of applications, including components in paper-making plant, cement plants, and heat exchangers.

In water, sintered silicon carbide is quite stable up to ~400 °C, but at higher temperatures, hydrothermal decomposition can take place at the surface by the following reactions (Yoshimura *et al.*[67] working with powders):

$$SiC + 2H_2O \rightarrow SiO_2 + CH_4 \quad \text{or}$$
$$SiC + 4H_2O \rightarrow SiO_2 + CO_2 + 4H_2$$

The authors suggest that water diffuses faster than oxygen through the thin protective surface layer of amorphous silica that is always present, accelerating the reaction compared with the oxidation rate in dry air. The silica is progressively dissolved allowing further oxidation to occur. At lower temperatures, the removal of the silica by abrasive or sliding wear processes exposes fresh surface, which oxidizes, and this defines the rate of surface removal.

Acid attack on a sintered material (B and C sintering acids) has been shown by Genthe *et al.*[68] to be minimal at 240 °C, 168 h for HCl, HNO_3, and HF, but significant in an HNO_3/HF mixture

($\sim$270 mg cm^{-2}) as a result of a combined oxidation and dissolution effect.

Marcus and Ahrens[17] have evaluated two forms of porous sintered SiC in 96% H_3PO_4 at 204 °C, and found minimal rates of attack.

The alkaline corrosion resistance of two forms of sintered silicon carbide has been examined by Sato *et al.*[69] They found that there was sensibly no attack by up to 25 M NaOH held at up to $\sim$200 °C for 3 days. Above this temperature and up to 300 °C, there was still no attack, provided that there was no free oxygen, but in the presence of oxygen, attack became significant, the surface layer of the material becoming penetrated and minor grain boundary phases being removed, leading to a significant loss in strength. This process greatly increases the exposed surface area of silicon carbide, which is then attacked *via* a hydrolysis type reaction given earlier, the silica being dissolved by the alkaline solution. The authors fitted a shrinking core model to the depth of penetration observed.

Liquid phase sintered silicon carbides

Liquid phase sintering is a recent development for SiC compared with the other process methods, and has been exploited in an attempt to improve strength and toughness of a SiC-based material. Like the situation with silicon nitride (explained later), it involves the use of additives such as alumina and yttria to promote densification at high temperature, and leaves these components as a grain boundary phase on completion of the process. The corrosion resistance of this type of product has not been widely studied, but it is likely to be poorer than the solid-state sintered version with some penetration likely in strong acids and strong alkalis.

Chemical vapor deposited (CVD) SiC

Generally, one would expect CVD SiC to behave similar to the sintered versions. Kim *et al.*[70] have studied the behavior of CVD SiC in water at 360 °C in comparison with sintered material, and found that the former performed better. Under these conditions, slow grain-boundary attack occurred, leading to an initially parabolic weight loss with time, but after some days resulting in the loosening of surface grains with a step increase in mass loss.

Mikeska *et al.*[17] showed that this material has excellent resistance to HF at 90 °C, and recommended its use as a coating to protect other forms of SiC that corrode down grain boundaries.

Other SiC composites

The corrosion properties of particulate composite materials based on SiC/TiC mixtures with alumina as a sintering aid have been studied[68] using a range of acids. It was established that the attack rates were very low in concentrated HCl ($\leq$4 mg cm^{-2} after 168 h at 210 or 240 °C), most of the attack being surface removal of TiC. An HF and HNO_3 mixture proved to attack an order of magnitude faster, probably because the SiC phase was also removed, while an HF/HNO_3 mixture attacked yet another order of magnitude faster at only 100 °C in 24 h because of the synergistic effects oxidizing the SiC and removing the SiO_2 formed.

3.25.4.2.2 Silicon nitrides

Material types

Like SiC, there are several routes by which silicon nitride materials can be produced. The first materials were produced by *hot-pressing* with, typically, MgO, and although this method has been extensively used and data on test materials have been widely reported in the literature, this method is nowadays rarely used for technical products because of the cost and a lack of shaping flexibility. The other widely researched early method was *reaction bonding*, in which a preform of powdered silicon was converted to silicon nitride by heating in nitrogen. This material has open porosity, and therefore, is seldom employed for its corrosion resistance except as a crucible material for high temperature melts. In recent decades, the focus has switched to *sintering* the material using additions such as alumina and yttria, although a whole range of more exotic sintering aids has been explored with the aim of maximizing high temperature performance, particularly oxidation and creep resistance. The sintering process is relatively complex, and usually requires an overpressure of nitrogen in order to suppress high temperature dissociation, known as *gas-pressure sintering*. An alternative process is to first use the reaction bonding process at $\sim$1350–1400 °C on a silicon-based shape containing sintering aids, and then to raise the temperature to $\geq$1750 °C to induce the sintering process. Such products are usually termed *sintered reaction-bonded* silicon nitride. The lowest closed porosity levels in any sintered products, and hence the highest densities, often require *hot isostatic pressing*. Sometimes this is done as part of the primary fabrication route, and sometimes as a second operation. Some versions of sintered silicon nitride have optimized fracture

toughness through the development of elongated silicon nitride grains; products of this type are typically used for corrosion-resistant rolling bearings.

The term 'sialon' is used for materials in which the composition is adjusted such that a solid solution between alumina and silicon nitride is produced as the primary phase. The secondary phases contain sintering aids, and thus such products can be considered as rather similar to sintered silicon nitrides in most respects, including corrosion resistance. There is no defined boundary between the two types.

Silicon nitride in its purest state can be prepared by chemical vapor deposition, but is not widely available. Because of the absence of secondary phases, this material has better corrosion resistance than do materials containing secondary phases to aid sintering.

Composites between silicon nitride and other nonoxides have been developed, with additions of BN, TiB_2, TiN, $MoSi_2$, but these are outside the scope of this chapter.

Sintered silicon nitrides

Perhaps the most detailed published ambient pressure study is that of Okada and Yoshimura,[71] who evaluated a dense gas-pressure sintered silicon nitride in boiling sulfuric acid. This material contained secondary components alumina and yttria, which form a grain-boundary phase that is, for the most part, continuous. Flexural strength and mass loss were determined as a function of time at a range of boiling acid concentrations. It was found that in a 1 h test, pH 3 solution boiling at 103 °C created the biggest loss in strength and mass, with higher concentrations have a lesser effect. In prolonged exposure, there was a progressive loss of mass and of nominal flexural strength, the latter attributable to the development of a weakened porous surface skin. After 72 h exposure to 6 N sulfuric acid at 105 °C, the strength had dropped from an initial level of 888 ± 57 MPa to 445 ± 45 MPa. Some of this drop may be attributable to the removal of residual stresses due to machining the original test-pieces. The surface layer thickness, as a measure of penetration rate, increased from 100 μm after 24 h to more than 250 μm after 72 h, approximating to a rate of $\sim$3 μm h^{-1} after an initial transient, but without loss of physical cross-section. The mechanism of corrosion is not discussed, but is likely to be a simple dissolution process of the yttria part of the secondary phase, while the silicon nitride itself is not significantly attacked. This type of attack has also been reported by Lin *et al.*[72] and is likely to be found in most commercial products with alumina and yttria as the sintering aids. Similar attack processes have been found for a material with yttria and lanthana as the sintering aids.[73] Products with alternative rare-earth additions rather than yttria are likely to be more corrosion resistant. Fang *et al.*[18] show that a sintered sialon material with a glassy second phase is reasonably resistant to corrosion by a 1% HF + 5% HCl solution.

Sato *et al.*[74] tested a series of hot isostatically pressed silicon nitrides containing Y_2O_3 and Al_2O_3 sintering aids in 1 M HCl at 70 °C for 50–240 h. Analysis of the test solution showed that Al and Y dissolved preferentially from the grain boundary phase, and that retained strength progressively reduced with ageing time. It was further found that when the solution concentration was less than 1 M, the corrosion rate was controlled by the reaction at the surface, and when greater than 5 M, the rate was determined by diffusion through the corrosion product layer. In a material containing no additives, no attack occurred.

Sato *et al.*[75] have compared the rates of attack of a 25 M NaOH solution at 150–200 °C for 3 days on hot-pressed and sintered silicon nitrides of similar composition, both containing Al_2O_3 and Y_2O_3 as densification aids. It was found that the rate of attack in terms of mass loss was low at 150 °C, but at higher temperatures, the sintered material with 5.2 wt% additions was attacked more rapidly than was the hot-pressed material with 4.7 wt% additions. This was ascribed to the preferential dissolution of silica. However, the hot-pressed material lost strength in a more catastrophic way with a total weight loss greater than in the sintered material, although the reasons for this are not entirely clear.

Sato *et al.*[76] have reported experiments on three materials with differing grain boundary phase compositions, conducted under neutral hydrothermal conditions (200–300 °C) for 3 days. A white deposit developed on the surface of the material, which was found to contain hydrated silica and grain boundary phases of alumina and yttria. The material in which this phase remained glassy appeared to perform better than those in which it is partially crystallized. Strength was found to drop from an initial 630 MPa toward 400 MPa.

Reaction-bonded silicon nitride

Being open-porous, this material is not widely used for liquid environments at low temperature, and therefore, few data are reported, but if substantially

free from impurities, it will, like hot-pressed and some sintered versions, show good corrosion resistance to acids. Marcus and Ahrens[7] report minimal rates of attack in H_3PO_4 at 204 °C.

3.25.4.2.3 Boron nitrides

Material types

Boron nitride exists in two forms: the crystallographically cubic form (CBN) is akin to diamond in properties, while the hexagonal form (HBN) is akin to graphite. CBN is difficult to densify, but is made in monolithic form as a cutting tool and die material. In contrast, HBN is available as a hot-pressed, machinable form for general applications, and via a vapor phase route, when it is usually termed 'pyrolytic.'

CBN

CBN is widely claimed to be corrosion resistant, but no specific information is available at this time. The binder phase employed to aid the compaction process is likely to control performance.

HBN

Corrosion performance is limited by a hydration process that converts BN to boric acid with the release of nitrogen. Oda and Yoshio[77,78] have shown that the rate of attack on a solid material under hydrothermal conditions (150–300 °C, 1–10 days) is related to crystal orientation, because the oriented grains in pyrolytic material are attacked more slowly than the more randomly orientated hot-pressed material, as shown by micrographic evidence. **Figure 7** shows their results for the linear portions of the trends of mass loss as function of time, ignoring an initial transient. The activation energy for the hydrolysis process was computed as 60 kJ mol^{-1}, based on equivalent tests on powdered material.

Moderate rates of attack by both acids and alkalis were found in NPL tests at 140 °C/23 h. Marcus and Ahrens[7] report moderate rates of attack at 204 °C in H_3PO_4.

3.25.4.2.4 Specialist materials

AlN – Young and Duh[79] report that corrosion rates at room temperature in alkaline solutions are much faster than in neutral or acid solutions as a result of a catalyzed hydration process with the formation of aluminates as intermediaries. Marcus and Ahrens[7] report rapid dissolution in H_3PO_4 at 204 °C.

TiC – Genthe *et al.*[68] have tested hot-pressed material, and shown some slow acid attack in HCl and HF, but rapid attack in HNO_3 and HF–HNO_3 mixture.

TiB_2 – Monticelli *et al.*[80] demonstrate that hot-pressed material with 1.5% Ni behaves like a passive metal in 3.5% salt solution at 25–65 °C, with the formation of a corrosion-resistant TiO_2 layer on the surface. However, tests at NPL have shown that hot-pressed material is rapidly attacked by acids at 140 °C/23 h, especially HCl, but is very resistant to KOH solutions. Marcus and Ahrens[7] showed that a hot-pressed material was attacked faster than a sintered material in H_3PO_4 at 204 °C.

$MoSi_2$ – Marcus and Ahrens[7] report slow attack by H_3PO_4 at 204 °C.

B_4C – NPL tests have shown negligible attack by acids and alkalis at 140 °C/23 h on a hot-pressed material, except an HNO_3 + H_3PO_4 mixture, which gave slight attack. Mikeska *et al.*[17] report minimal

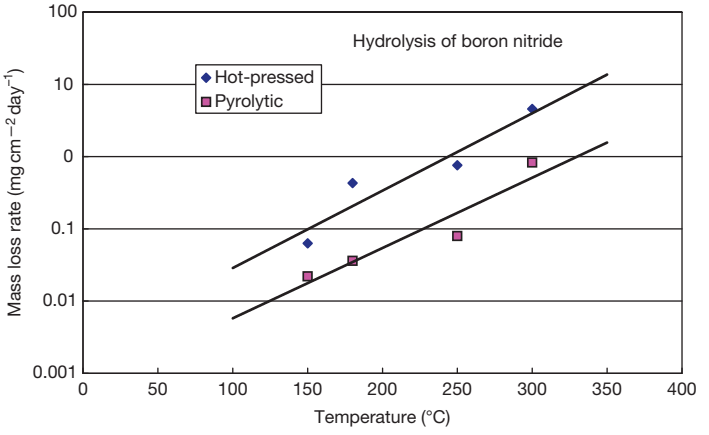

Figure 7 Hydrolysis of dense boron nitride as a function of temperature.[77,78]

attack by HF at 90 °C. Marcus and Ahrens[7] report negligible attack rates by H_3PO_4 at 204 °C.

Pure WC, CaF_2, MgF_2 show excellent resistance to HF at 90 °C.[17]

3.25.4.3 Comparative Attack Rates

From the foregoing, it will be appreciated that the performance of any one material is highly dependent not only on its composition and microstructure, but also on the conditions to which it is subjected and how the effects of corrosion are measured. It is therefore particularly difficult to give a clear appreciation of the comparative performance of the huge range of materials now available. There are relatively few sources of directly comparative numerical data over a wide range of products. Some appreciation can be obtained from unpublished NPL work[13] given in **Figure 8**.

3.25.5 Some Specific Applications Requiring Corrosion Resistance

3.25.5.1 Chemical Process Vessels

There has been a long history of the use of technical ceramics for chemical process vessels, both as the lining and as furniture inside them. If the vessels are limited in dimensions to typically 500 mm or less, they can be made from monolithic shells of dense, chemically resistant porcelain, which provide a long life except perhaps with the most aggressive of reagents. Examples include digesters and ball mills. If the vessels are larger, a lining of chemically resistant brickwork is required, usually bedded into a chemically resistant mortar. The mortar may be the life-limiting factor, but despite this, successful applications have been achieved for many years. A review of such applications may be found in Charlebois.[5]

Furniture, such as so-called 'tower packing,' is often made from a chemically resistant stoneware, a product much coarser in texture than porcelain, but with similar properties, provided that the as-fired surface skin remains intact. This skin acts as a glaze, which seals access to internal porosity. In some aggressive environments, their successful application may be reliant on preservation of the skin. More expensive options rely on alumina ceramics, but these tend to be available only in rather smaller pieces. Other applications reliant on alumina include filter plates, filters, nozzles, pipe linings, etc.

In the laboratory, chemical porcelains continue to be used for pestles, mortars, and other corrosion-resistant parts for chemical handling. Low thermal expansion glass-ceramics are used for hot-plate and stirrer plate units, minimizing the risks of corrosion from common chemicals. Similar materials are used in the kitchen for cookware and for cooker hobs.

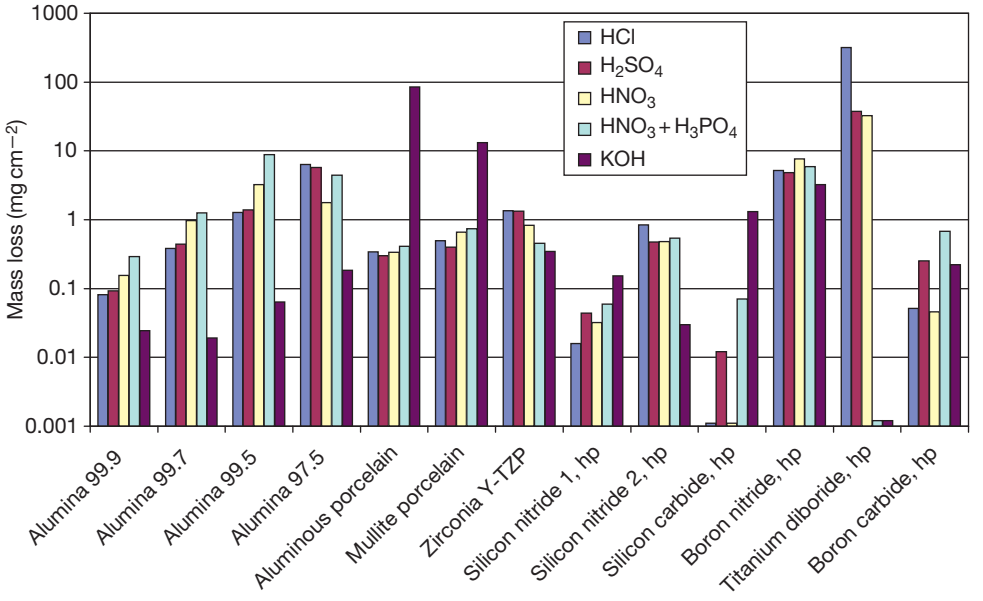

Figure 8 Comparative rates of mass loss after exposure in PTFE-lined digestion bombs to various 20% by volume solutions at 140 °C for 23 h.

3.25.5.2 Rotating Seals

Rotating seal faces for pumps are usually made from a hard material such as a ceramic and an abradable material, often carbon or graphite based. Alumina ceramics are the most commonly employed hard faces for water and organic liquid-based media, and have demonstrably long lives in the absence of excessive abrasion or very high or very low pH. Examples include central heating pumps, light-duty chemical process pumps, and food processing pumps. Where there is additional loading, such as abrasive particles, a harder material is usually employed, such as silicon carbide. For vehicular water cooling pumps, silicon nitride has been widely used because of its better strength and thermal shock resistance compared with alumina.

For highly acidic conditions, secondary phases in alumina limit corrosion/abrasion performance and silicon carbide-based materials are often employed.

Silicon carbide is also often the material of choice in gas bearings and gas pump seals.

3.25.5.3 Flow-meter Bodies

Flow-meters for highly corrosive chemical plant circuits based on electroconduction are typically made from alumina ceramics. Insulated electrodes can be sealed through the wall to provide the sensing circuit, and provided that the right choice of material is made, the life can be much longer than that of the attached pipework.

3.25.5.4 Food Processing

The linings of food processing equipment can often, with advantage, be made from alumina ceramics, which resist corrosion from food acids as well as abrasion. Food is not contaminated in the same way as it might be with metallic linings such as stainless steel. The key requirement is that the materials withstand typical chlorinated steam cleaning processes, which can be more aggressive than the food itself. Materials with good resistance to hydrochloric acid at elevated temperatures are required.

3.25.5.5 Valves

Seal faces for valves, including shower mixers, quarter-turn faucets, gas valves, etc., are typically made from pairs of alumina ceramics plates with flat lapped faces. These resist corrosion from normal water supplies to elevated temperature, and have a long, corrosion-free life that is usually limited only by risks of mechanical damage from the metallic components used to operate them, or from the deposition of lime-scale, which can jam them, or lead to excessive wear.

Corrosion-resistant ball valves used for chemical plant are also made typically up to 150 mm diameter. The choice of material for this application is critical, as in the case of flow-meters.

3.25.5.6 Medical

The human body places unusually corrosive conditions on materials used for implants, but because of their corrosion resistance, ceramics are successfully being employed for both dentistry and orthopedics. In the mouth, glassy porcelains are used for individual tooth crowns, and the literature contains increasing number of reports of the use of machinable glass–ceramics for forming tooth shapes, and of zirconia (Y-TZP type) for prosthetic bridges. For orthopedics, the combination of strength and corrosion resistance of, particularly, alumina is exploited for balls and cups for hip replacement. Zirconia (Y-TZP type) has also been used, and offers higher mechanical strength, but as described earlier, there are some potential limitations of phase stability at body temperature. Increasingly, alumina–zirconia composite materials are being employed to overcome the instability problem, and silicon nitride is on the horizon, already widely employed for rolling bearing balls.

Other corrosion-resistant ceramics used in the body include glassy carbons for heart valves, and hydroxyapatite as a fully biocompatible ceramic, which can be used as a coating on metallic components to enhance oseointegration, or as a free-standing material to assist in bone reconstruction. Bioglasses and bioglass-ceramics also have specialized applications in which reaction with the body is deliberately exploited in their function.

3.25.6 Selecting the Right Material

It is hard to predict performance, and, therefore, it is important when selecting ceramic materials for corrosion-resisting applications to undertake some relevant testing to check potential performance, unless there is direct previous experience with a particular type of product. Often, ceramic materials are not specifically optimized for applications

requiring corrosion resistance, and may contain species that are readily removed. Simple ranking tests will provide a guide, as in **Figure 8**.

In addition, there are other factors which may dictate material choice, including price, availability in the shape and dimensions required, aspects of mechanical performance, and aspects of joining to other components. For those not experienced with the use for ceramic components, specialist advice should be sought.

References

1. Lavrenko, V. A.; Panasyuk, A. D.; Desmaison-Brut, M.; Schvets, V. A.; Desmaison, J. *J. Eur. Ceram. Soc.* **2005**, *25*, 1813–1818.
2. Binns, D. B. *The Use of Ceramics in Valves;* British Ceramic Research Association Special Publication no. 48, **1965**, p 157.
3. Cox, J. M.; Morrell, R. *Brit. Ceram. Proc.* **1989**, *43*, 29–40.
4. Öhman, L. O.; Ingri, N.; Tegman, R. *Bull. Amer. Ceram. Soc.* **1982**, *61*(5), 567–571 and 581.
5. Charlebois, G. W. *Mater. Perform.* **1991**, *3*, 71–75.
6. Bennett, J. P. Corrosion resistance of selected ceramic materials to sulfuric acid, Report of Investigations 9011; US Bureau of Mines, 1986.
7. Marcus, L.; Ahrens, R. L. *Bull. Amer. Ceram. Soc.* **1981**, *60*(4), 490–493.
8. Morrell, R. *Handbook of Properties of Technical and Engineering Ceramics. Part 2, Data Reviews, Section 1, High-Alumina Ceramics*; HMSO: London, 1987.
9. Real, M.; Cooper, D. R.; Morrell, R.; Rawlings, R.; Weightman, B.; Davidge, R. W. *J. Phys. Coll.* **1986**, *C1*(2), C1-763–C1-766.
10. Jaeger, G.; Kraseman, R. *Werkstoffe Korrosion* **1952**, *3*(11), 401–415.
11. Richards, G. *Trans. Br. Ceram. Soc.* **1981**, *80*(4), 120–124.
12. Lay, L. A. *The Resistance of Ceramics to Chemical Attack*; NPL Report CHEM 96; National Physical Laboratory: Teddington, Middlesex, UK, 1979.
13. Lay, L. A. Unpublished NPL results, 1980.
14. Lay, L. A. *Corrosion Resistance of Technical Ceramics*, 2nd ed.; HMSO: London, 1991.
15. Engell, J.; Jakobsen, P. *Danish Materials Society Yearbook* 1990, pp 89–112.
16. Genthe, W.; Hausner, H. *Euroceramics* **1989**, *3*, 3.463–3.467.
17. Mikeska, K. R.; Bennison, S. J.; Grise, S. L. *J. Am. Ceram. Soc.* **2000**, *83*(5), 1160–1164.
18. Fang, Q.; Sidky, P. S.; Hocking, M. G. *Corros. Sci.* **1997**, *39*(3), 511–527.
19. Sato, T.; Sato, S.; Okuwaki, A.; Tanaka, S. *J. Am. Ceram. Soc.* **1991**, *74*(12), 3081–3084.
20. Dailly, D. F.; Hastings, G. W.; Lach, S. *Proc. Br. Ceram. Soc.* **1981**, *31*, 191–200.
21. Byrne, W. P.; Hanney, M. J.; Morrell, R. *Proc. Br. Ceram. Soc.* **1982**, *32*, 303–314.
22. Barinov, S. M.; Fateeva, L. V.; Ivanov N.V.; Orlov, S. V.; Shevchenko, V. Ja. *Scripta Mater.* **1998**, *38*(6), 975–980.
23. Ferber, M. K.; Brown, S. D. *J. Am. Ceram. Soc.* **1980**, *63*, 424–429.
24. Bastide, B.; Canale, P.; Odier, P. *J. Eur. Ceram. Soc.* **1989**, *5*, 289–293.
25. Guo, X.; He, J. *Acta Mater.* **2003**, *51*(17), 5123–5130.
26. Kawakubo, T.; Hirayama, H.; Kaneko, T. *J. Soc. Mater. Sci. Jpn.* **1990**, *39*(438), 312–317.
27. Sato, T.; Endo, T.; Shimada, M.; Mitsudome, T.; Otabe, N. *J. Mater. Sci.* **1991**, *26*(5), 1346–1350.
28. Ohmichi, N.; Kamioka, K.; Ueda, K.; Matsui, K.; Ohgai, M. *J. Jpn. Ceram. Soc.* **1999**, *107*(2), 128–133.
29. Yasuda, K.; Arai, S.; Itoh, M.; Wada, K. *J. Mater. Sci.* **1999**, *34*(15), 3597–3604.
30. Pecharromán, C.; Bartolomé, J. F.; Requena J., Moya, J. S.; Deville, S.; Chevalier, J.; Fantozzi, G.; Torrecillas, R. *Adv. Mater.* **2003**, *15*(6), 507–511.
31. Ikeda, J.; Pezzotti, G.; Iwamoto, M.; Ueno, M. *Key Eng. Mater.* **2007**, *330–332*(2), 1203–1206.
32. Chevalier, J. *Biomaterials* **2006**, *27*(4), 535–543.
33. Chevalier, J.; Gremillard, L.; Deville, S. *Ann. Rev. Mater. Res.* **2007**, *37*, 1–32.
34. Chevalier, J. J.; Deville, S.; Münch, E.; Jullian, R.; Lair, F. *Biomaterials* **2004**, *25*(24), 5539–5545.
35. Butt, D. P.; Payyapilly, J. J. *J. Nucl. Mater.* **2007**, *360*(2), 92–98.
36. Gremillard, L.; Chevalier, J.; Epicier, T.; Fantozzi, G. *J. Am. Ceram. Soc.* **2002**, *85*(2), 401–407.
37. Takigawa, Y.; Naka, Y.; Higashi, K. In *Proceedings of Conference Materials in Clinical Applications VII Trans Tech: Zürich, Switzerland, 2006; pp 106–111.*
38. Murray, M.; Stuart, J.; Morrell, R. In *Performance Evaluation of Zirconia Femoral Heads*; Proceedings of the Conference on Engineers Meet the Surgeons; Inst. Mechanical Engineers: London, 2002.
39. Lance, M. J.; Vogel, E. M.; Reith, L. A.; Cannon, W. R. *J. Am. Ceram. Soc.* **2001**, *84*(11), 2731–2733.
40. Kosmac, T.; Dakskobler, A.; Oblack, C.; Jevnikar, P. *Int. J. Appl. Ceram. Technol.* **2007**, *4*(2), 164–174.
41. Lin, J. D.; Duh, J. G.; Lo, C. L. *Mater. Chem. Phys.* **2003**, *77*(3), 808–818.
42. Hernandez, M. T.; Jurado, J. R.; Duran, P.; Fierro, J. L. G. *J. Am. Ceram. Soc.* **1991**, *74*(6), 1254–1258.
43. Zhao, Z.; Liu, C.; Northwood, D. O. *Ceram. Eng. Sci. Proc.* **2001**, *22*(4), 59–66.
44. Basu, D.; Das Gupta, A.; Basu, M. K.; Sarkar, B. K. *J. Eur. Ceram. Soc.* **1996**, *16*(6), 613–617.
45. Shojai, F.; Mantyla, T. A. *J. Am. Ceram. Soc.* **2001**, *21*(1), 37–44.
46. Kritzer, P.; Schacht, M.; Dinjus, E. *Mater. Corros.* **1999**, *50*(9), 505–516.
47. Kalin, M.; Dražič, G.; Novak, S.; Vižintin, J. *J. Eur. Ceram. Soc.* **2006**, *26*, 223–232.
48. Hisamori, N.; Kimura, Y. *J. Soc. Mater. Sci. Jpn.* **1999**, *48*(3), 275–281.
49. Herrmann, M.; Seipel, B.; Schilm, J.; Nickel, K. G.; Michael, G.; Krell, A. *J. Eur. Ceram. Soc.* **2005**, *25*(10), 1805–1812.
50. Hirano, M.; Inada, H. *J. Mater. Sci.* **1991**, *26*(18), 5047–5052.
51. Nakanishi, T.; Sasaki, M.; Ikeda, J.; Mijaji, F.; Kondo, M. *Key Eng. Mater.* **2007**, *330–332*, Part 2, 1267–1270.
52. Thompson, I.; Rawlings, R. D. *J. Mater. Sci.* **1992**, *27*, 2823–2830.
53. Yoshio, T.; Oda, K.; Suemasu, T.; Kohno, A. *J. Jpn. Ceram. Soc.* **1992**, *100*(5), 668–674.
54. Holland, L. *The Properties of Glass Surfaces*; Chapman and Hall: London, 1964.
55. Hood, H. P.; Nordberg, M. E. British Patent 2,221,709, 1934.
56. McMillan, P. W. *Glass-Ceramics*, 2nd ed.; Academic Press: London, 1979.
57. Salama, S. N.; Salman, S. M. *J. Eur. Ceram. Soc.* **1994**, *13*(6), 521–528.

58. Demirkesen, E.; Göller, G. *Ceram. Int.* **2003**, *29*(4), 463–469.
59. Livingston, F. E.; Adams, P. M.; Helvajian, H. *Appl. Phys. A: Mater. Sci. Eng.* **2007**, *89*(1), 97–107.
60. Corning Inc., Company brochure on Macor.
61. Li, C. G.; Si, W. J.; Zhang, W. F. *Key Eng. Mater.* **2007**, *336–338*(part 3), 2429–2431.
62. Hiratsuka, A.; Yoshikawa, A.; Ogwara, K.; Adachi, K. *Mater. Sci. Forum,* **2003**, *426–429*, 4471–4476.
63. Studart, A. R.; Filser, F.; Kocher, P.; Gaukler, L. J. *Biomaterials* **2007**, *28*(17), 2695–2705.
64. Teixeira, E. C.; Piascik, J. R.; Stoner, B. R.; Thompson, J. Y. *J. Mater. Sci. – Mater. Med.* **2007**, *18*(6), 1219–1224.
65. Qiao, G. J.; Wang, Y. L.; Jin, Z. H.; Zhou, H. J. *Int. J. Fatigue* **1996**, *18*(8), 523–527.
66. Kim, W. J.; Hwang, H. S.; Park, J. Y. *J. Mater. Sci. Lett.* **2002**, *21*, 733–735.
67. Yoshimura, M.; Kase, J.; Somiya, S. *J. Mater. Res.* **1986**, *1*(1), 100–103.
68. Genthe, W.; Robayie, J. K.; Hausner, H. *cfi/Ber. Deut. Ker. Ges.* **1991**, *68*(6), 262–265.
69. Sato, T.; Taura, K.; Okuwaki, A. *Brit. Ceram. Trans. J.* **1992**, *91*, 181–185.
70. Kim, W. J.; Hwang, H. S.; Park, J. Y.; Ryu, W. S. *J. Mater. Sci. Lett.* **2003**, *22*, 581–584.
71. Okada, A.; Yoshimura, M. *Key. Eng. Mater.* **1996**, *113*, 227–236.
72. Lin, C. H.; Komeya, K.; Meguro, T.; Tatami, J.; Abe, Y.; Komatsu, M. *J. Jpn. Ceram. Soc.* **2003**, *111*(7), 452–456.
73. Monteverde, F.; Mingazzi, C.; Giogi, M.; Bellosi, A. *Corros. Sci.* **2001**, *43*(10), 1851–1863.
74. Sato, T.; Tokunaga, Y.; Endo, T.; Shimada, M.; Komeya, K.; Komatsu, M.; Kameda, T. *J. Am. Ceram. Soc.* **1988**, *71*(12), 1074–1079.
75. Sato, T.; Sato, S.; Tamura, K.; Okuwaki, A. *Br. Ceram. Trans. J.* **1992**, *91*, 117–120.
76. Sato, T.; Murakami, T.; Endo, T.; Shimada, M.; Komeya, K.; Kameda, T.; Komatsu, M. *J. Mater. Sci.* **1991**, *26*, 1749–1754.
77. Oda, K.; Yoshio, T. *Nippon Seramikkusu Kyokai Gakujutsu Ronbunshi* **1989**, *97*(9), 903–910.
78. Oda, K.; Yoshio, T. *J. Jpn. Ceram. Soc.* **1993**, *101*(8), 855–859.
79. Young, C. D.; Duh, J. G. *J. Mater. Sci.* **1995**, *30*(1), 185–195.
80. Monticelli, C.; Frignani, A.; Bellosi, A.; Brunoro, G.; Trabanelli, G. *Corros. Sci.* **2001**, *43*(5), 979–992.

3.26 Degradation of Glass and Glass Ceramics

S. Oliver and B. A. Proctor
Pilkington Ltd., St. Helens WA10 3TT, UK
C. A. May
School of Engineering, University of Greenwich, London SE10 9LS, UK

This article is a revision of the Third Edition article 18.2 by D. S. Oliver and B. A. Proctor, volume 2, pp 18:9–18:26,

Glossary

Glass A solid material that is characterized by lack of crystallinity; that is, with short-range but not long-range order.

Glass-ceramic An initially glassy material that, when heat-treated, forms a crystalline phase such that the material, on cooling, comprises a composite containing the crystalline phase surrounded by the remaining glassy material; such materials generally have enhanced mechanical properties compared to either a typical glass or a typical ceramic of similar composition.

Network former A compound such as silica (SiO_2) that, when cooled at a sufficient rate, will on its own form a glass.

Network modifier A compound such as soda (NaO) or calcia (CaO) that will not form a glass on cooling and, when combined with a network former, will disrupt network bonds.

Static fatigue The process of delayed fracture below the normal facture stress of a glass that results from cracks growing from flaws on the glass surface, usually exacerbated by the presence of moisture or humidity.

Vitreous The glass-like state of a material that might otherwise crystallize (e.g., vitreous silica is the glassy state of the compound SiO_2, while quartz is one of the crystalline phases of the same compound).

3.26.1 Introduction

One of the most important properties of commercial glasses is their great resistance to corrosion; any chemical laboratory apparatus, window, or windscreen provides an excellent illustration. Windows remain virtually unchanged for centuries, resisting the influences of atmosphere and radiation. A vast range of products may be safely stored in glass for decades at ordinary temperatures, and the fact that glass can be used with alkaline, neutral, and acid environments allows the same equipment to be used for a variety of processes.

The principal difficulty associated with the use of glass equipment is the fact that glass fractures rather than deforms on severe impact. Thus, although it may be toughened by thermal treatment or ion exchange, glass remains a material that has intrinsically a relatively low value of facture toughness and small critical flaw size. Glass is also more prone than metals to damage by thermal shock, although this difficulty can be largely avoided by the use of low-expansion glass formulations. Finally, the size of glassware that can readily be fabricated is sometimes below the needs of a particular process.

3.26.2 Commercial Glasses

The term glass defines a family of materials that exhibit as wide a range of differences among themselves as exists among metals and alloys. The great variety of physical and chemical properties available arises from the possibility of including almost all the stable oxides, sulfides, halides, etc. throughout the periodic table in different glass formulations. Many branches of the family, for example, those borates, silicates, and phosphates which are water-soluble, are of little interest in the present context. It is, however, worth bearing in mind that glasses can be designed to combine particular physical properties with good chemical resistance.

For most of the commercial oxide glass families, silica (SiO_2) is the main ingredient. However, lower melting points and greater flexibility of properties are achieved with the addition of other oxides and modifiers. Depending upon the choice of these additional constituents, glasses are classified into groups, including fused silica, soda–lime glasses, leaded glasses, aluminosilicate glasses, borosilicate glasses, etc. A cross section of some commercial glass compositions is given in Table 1.[1]

Fused silica is a general classification within which is a range of varieties and types of material with differences in purity, transmission, and grade. This type of glass may be used up to 900 °C in continuous service; it resists attack by a great many chemical reagents, rapid attack occurring only in hydrofluoric acid and concentrated alkali solutions.

Container glass is suitable for the storage of beverages, medicines, cosmetics, household products, and a wide range of laboratory reagents.

Tubing glass is suitable for general laboratory use and chemical apparatus construction, though neutral or hard borosilicate are preferred for more severe conditions, these representing the most resistant glasses available in bulk form.

Neutral glasses are generally less resistant than the hard borosilicate type, but are more easily melted

Table 1 Typical glass compositions

	1	*2*	*3*	*4*	*5*	*6*	*7*	*8*	*9*	*10*	*11*
SiO_2	100%	72.7%	72.8%	71.4%	71.5%	80.3%	57.2%	67.5%	54.2%	63.6%	57.1%
Al_2O_3	–	1.1%	1.7%	2.2%	5.5%	2.8%	1.0%	4.8%	14.3%	2.9%	4.6%
B_2O_3	–	–	–	–	10.0%	12.3%	–	–	8.3%	5.0%	11.8%
MgO	–	3.8%	–	3.9%	–	–	–	–	4.5%	3.2%	–
CaO	–	8.4%	10.5%	4.6%	0.2%	–	–	0.1%	17.7%	7.3%	0.4%
BaO	–	–	–	0.8%	3.0%	–	–	12.0%	–	2.6%	–
Na_2O	–	13.1%	14.5%	15.0%	8.0%	4.0%	4.0%	7.2%	0.6%	14.5%	14.2%
K_2O	–	0.5%	–	1.7%	1.2%	0.4%	8.5%	6.9%	0.1%	0.6%	0.8%
ZrO_2	–	–	–	–	–	–	–	–	–	–	3.8%
TiO_2	–	–	–	–	–	–	–	–	–	–	7.5%
PbO	–	–	–	–	–	–	29.0%	–	–	–	–
Li_2O	–	–	–	–	–	–	–	0.5%	–	–	–
Others	–	0.4%	0.5%	0.4%	0.6%	0.2%	0.3%	0.3%	0.3%	0.3%	0.4%

1, fused silica; 2, window glass; 3, container glass; 4, fluorescent tubing; 5, neutral glass; 6, hard borosilicate; 7, lead glass; 8, TV tube and screen; 9, textile glass fiber; 10, glass wool insulation; 11, superfine glass wool.

and shaped. They are formulated so that the pH of aqueous solutions is unaffected by contact with the glass, making it particularly suitable in pharmaceutical use for the storage of pH-sensitive drugs.

Borosilicate glasses are, in terms of different types available, the most versatile types of glass produced. In general, borosilicate glasses are grouped into five types: low-expansion glass, low electrical-loss glass, materials for seals to metals, glasses for laboratory apparatus, and optical-grade glasses, including those with enhanced transmission beyond the visible spectrum. The example given, that is, hard borosilicate glass, is typically used for ovenware, laboratory apparatus, etc., and combines low expansion and high chemical resistivity with chemical stability. These types of glasses generally require high fabrication temperatures compared with soft soda glasses.

Electronic grade glasses are used in cathode ray tube screens and similar applications, and contain higher quantities of heavy elements (e.g., lead, barium, etc.) in order to absorb radiation. These glasses do not operate under severe corrosion conditions, but surfaces must not leach excessive alkali under damp conditions or electrical breakdown can occur.

Glass fibers present particular problems in corrosive environments because of their very high surface/volume ratios. Glasses for electrical insulation are generally formulated from alkali-free aluminoborosilicate glasses (generally known as E-glass) and are frequently specified as containing less than 1% alkali (Na_2O and K_2O). This type of glass is also used extensively for the reinforcement of plastics where its high resistance to moisture attack ensures a durable product.

Glass wools are used for less demanding applications and generally contain some alkali to aid in processing. Superfine wool contains zirconia and titania to enhance the chemical resistance while retaining the properties necessary for economic fine fiber formation.

3.26.3 Physical Properties

3.26.3.1 Structure

Glass has been defined as 'an inorganic product of fusion which has cooled to a rigid condition without crystallizing.' The atomic structure of glasses is more closely related to liquids than to crystals. The properties of glasses are manifestations of this structure, being governed in particular by the random liquid-like disposition of the network-forming ions (commonly Si^{4+} and B^{3+}); the presence of mobile, interstitial alkali ions; and the 'single-molecule' nature of the lattice. The bonding within the atomic network is partly covalent and partly ionic. Thus, the network bonds are highly directional with a range of interbond angles, bond lengths, and bond energies; the bonding electrons are restricted to particular energy levels within the bonds. The network-modifying ions (commonly alkali and alkaline-earth ions) are ionically bound to the network although the field strength and diameter of the alkali ions allow them some mobility as a function of temperature.

The random nature of the glass structure imparts a range of bond energies in the network, and hence a characteristic feature of glasses is a continuous

softening over a range of temperature, a continuous viscosity/temperature curve, and the absence of a true melting point. For convenience in comparing the viscosity behavior of different glasses, arbitrary temperatures at which the glass has specific viscosities are often quoted.[2] The Littleton softening point[3] is most commonly used. At this temperature, the glass has a viscosity of $10^{6.6}$ Pa s.

The glass transition temperature T_g corresponds to a viscosity between 10^{12} and 10^{13} Pa s depending on the definition and on the method of measurement. Glass behaves as a Newtonian liquid at temperatures well above the glass transition. It is this behavior that prevents the necking generally observed during plastic deformation of metals and which allows glass to be easily formed into such a large number of useful configurations.

In practice, an important range of viscosities are those from 10^{11} to $10^{13.5}$ Pa s, known as the annealing range. The annealing point and the strain point are generally taken as the temperatures at which the glass has a viscosity of $10^{12.4}$ and $10^{13.6}$ Pa s, respectively. Within this range, the glass is effectively a solid, but internal stresses can be relieved within a practical time scale. Rapid cooling of glass articles through the annealing range eventually results in permanent and sometimes catastrophic thermal stresses. However, it is possible to cool the glass relatively quickly from the lower end of the annealing range.

The structural features are reflected in the characteristic properties of inorganic glasses and bring about a broad overall similarity in behavior as summarized below. Values for the physical properties of the glasses listed in Table 1 are given in Table 2.

3.26.3.2 The Nature of the Glass Surface

It is widely accepted that the composition of the surface of a glass is different from that of its interior. Alkali loss during forming, grinding, polishing, and surface treatments affects the structure of the surface, but a more basic difference is brought about by the effect of the unbalanced force fields at the surface on the ions within the glass.

Glass is composed of glass-forming cations (e.g., B^{3+}, Si^{4+}, P^{5+}) surrounded by polyhedra of oxygen ions in the form of triangles or tetrahedra. Two types of oxygen ions exist: bridging and nonbridging. The former, bonded to two network-forming ions, link polyhedra, and the latter, bonded to one network-forming ion only, carry an excess negative charge. To compensate for this, charged cations of low positive charge and large size (e.g., Na^+, K^+, Ca^{2+}) are located within the structure. Silicon may be substituted by other cations of large positive charge and small size; these are collectively known as network formers.

The difference in size and field strength between ions is reflected in the polarizabilities of each ion and their final position relative to the glass surface. Since the force field is unbalanced, ions of low polarizability will remain near the surface and ions of higher polarizability will move towards the interior of the glass. A strong feature of chemical reactions associated with the surface is the need to screen adequately (and not merely to neutralize) those cations that have strong electric fields. If the unbalanced field is removed by the presence of materials, liquid, adsorbed vapor, or solid in contact with the glass, there is sufficient mobility within the glass surface zone for it to revert to a more normal structure by the diffusion of ions towards the surface.

3.26.3.3 Thermal Expansion

Glasses having coefficients of linear thermal expansion of from 5×10^{-7} to over 10^{-5} K^{-1} are available. However, high-expansion glass compositions do not

Table 2 Physical property data for the glasses of compositions listed in Table 1[1]

	1	*2*	*3*	*4*	*5*	*6*	*7*	*8*	*9*	*10*	*11*
Density (mg m^{-3})	2.2	2.49	2.46	2.49	2.42	2.24	3.03	2.62	2.58	2.57	2.54
Strain point (°C)	987	520	490	495	518	515	–	448	616	–	–
Annealing point (°C)	1082	545	540	524	565	565	–	470	657	–	–
Littleton softening point (°C)	1594	735	720	705	780	820	631	670	843	688	710
Resistivity (Ω m at 20 °C)	10^{15}	10^{13}	–	10^{15}	10^{15}	–	–	–	–	–	–
Dielectric constant (at 1 kHz)	3.8	7.4	–	7.8	–	5.1	7	–	–	–	–
tan δ (at 1 MHz)	small	–	–	0.008	–	0.02	0.001	–	–	–	–
Refractive index	1.48	1.52	–	1.51	1.49	1.47	1.56	1.51	1.55	–	–
Thermal conductivity (W m^{-2} K^{-1})	1.38	1.05	1.02	1.04	1.04	1.13	0.84	1.01	0.97	–	–
Thermal expansion ($\times 10^7$ K^{-1})	5.4	79.3	87	85.5	50	33	84	85.5	49	83	–
Specific heat (J kg^{-1})	775	987	821	833	819	794	–	733	796	–	–
Young's modulus (GPa)	7.3	7.4	–	–	–	6.3	5.75	7.4	7.2	–	–

generally have long-term chemical durability. Glass-ceramic materials, on the other hand, are remarkable for the very wide range of thermal expansion coefficients that can be obtained. At one extreme, materials having negative coefficients are available, while for other compositions very high positive coefficients can be obtained. Between these two extremes, there exist glass-ceramics having thermal expansion coefficients practically equal to zero and others whose expansion coefficients are similar to those of ordinary glasses or ceramics or to those of certain metals and alloys and, hence, allow thermal compatibility. This range of expansion coefficients is allied with good chemical durability.

3.26.4 Mechanical Properties

Characteristically, glasses are susceptible to brittle fracture under tension but tend to have significantly higher compressive strengths. The ionic and directional nature of the bonds and the localization of bonding electrons to pairs of atoms preclude bond exchange. This, coupled with the random nature of the atomic lattice, that is, the absence of close-packed planes, makes gross slip or plastic flow extremely difficult.

3.26.4.1 Strength

If flaws and stress concentrators, which emphasize the brittle nature of glass, can be avoided, then a glass article behaves as though its strength is governed by the high interatomic bond strength. Glasses are therefore inherently very strong materials, theoretically capable of exhibiting a tensile strength of about 7 GPa. In practice however, surface flaws act as stress concentrators under tensile loading, and commercial glasses in bulk show a mean strength in tension of only about 40 MPa. The statistical variation of strength about this figure makes it desirable to allow a substantial safety margin and to design using a figure of about 7 MPa.[4]

The strength of glass can be increased to about 200 MPa by commercial (generally thermal) toughening processes. The use of such glasses is not possible, however, at elevated temperatures since resoftening will occur. Undamaged commercial glass fibers display strengths of about 2 GPa, which is dependent upon surface protection, given usually by organic coatings. Removal of the coating results in a marked decrease in strength due to the introduction of small surface flaws.

3.26.4.2 Elastic Modulus

Up to the fracture stress, glass behaves, for most practical purposes, as an elastic solid at ordinary temperatures. Most silicate-based commercial glasses display an elastic modulus of about 70 GPa, that is, about one-third the value for steel. If stress is applied at temperatures near the annealing range, then delayed elastic effects will be observed and viscous flow may lead to permanent deformation.

The brittle nature of glasses at normal temperatures makes them inappropriate for use in locations where severe impacts are likely to be encountered. In the design of pipelines or other equipment, it is possible to use normal engineering assembly techniques provided that suitable gaskets or cushioning are provided at joints and supports and that care is taken in tightening bolts to avoid unequal or localized stresses.

3.26.4.3 Thermal Shock Resistance

The ability of a glass article to withstand sudden changes of temperature depends primarily on its thermal expansion coefficient, its thickness, and its design. For articles of identical shape, a low-expansion glass (such as a commercial borosilicate) will withstand appreciably greater temperature shocks than will glass of a higher expansion coefficient. Thermal shock-resistance testing is usually carried out by transferring the articles from a hot environment to a cold vessel containing water at a predetermined temperature.[5] In general, transitions from a hot to a cold environment are more likely to produce failure than those in the opposite direction since they tend to induce tensile stresses at the surface.

3.26.5 Chemical Properties

3.26.5.1 Degradation

Technical glasses are now used so extensively and in such widely varying circumstances that it is necessary to be as accurate as possible in describing their chemical properties. The deterioration of individual glasses is dependent on composition, manufacture, and use and, unless the degradation processes are accelerated, may be observable only after very long periods of time. A typical figure for the corrosion rate of an ordinary soda–lime–silica glass would be less than 10 $\mu m\ year^{-1}$. The effect is accelerated when the exposure takes place at higher temperatures, for example, in boiling

Table 3 The corrosion resistance for commercial glasses listed in Table 1

	Glass				
	1	*2*	*3*	*6*	*7*
Water	A	B	B	A-B	B-C
Acid	A	B	B	A-B	B-C
Weathering	A	C	C	A-B	B-C

A, essentially resistant; B, possibility of degradation; C, certain degradation.[1]

water or in an autoclave. Table 3 compares the corrosion resistance of some commercial glasses.

One of the most commonly used measures of durability, that is, loss of sodium from the glass, is important to the pharmaceutical and chemical industries, but other changes such as loss of surface quality, are of equal importance for optical and window glasses. The properties of a wide range of technical glasses are well catalogued,[5–7] but the data are often inadequate when considering a particular application and where possible nonstandard 'whole article' tests are advisable.

3.26.5.2 Glass Durability Tests

In selecting a glass for chemical durability, regard must be paid to the temperature and concentration of the corrosive agent, length of exposure, ratio of reagent volume to surface exposed, and mechanical operating conditions. Guidelines on the durability of many commercial glasses in some attacking media are available from standard durability tests. There are two types of durability tests for glassware: 'grain' or 'powder' tests and 'whole article' tests.

3.26.5.2.1 Grain tests

In these tests, samples of glass crushed and graded to a specified sieve size are exposed under standard conditions of time and temperature to the attacking medium. The temperatures commonly used are 98 °C (water bath) and 121 °C (autoclave) and the attacking media are water, acid, and alkali. The amounts of a particular glass constituent (usually soda or total alkali) removed from a standard weight in a given time are determined. Various standard test methods have been established.[8–11] However, variability is found between different laboratories, and using a particular grain test has shown considerable divergence, and it appears that to obtain consistent results very close adherence to the details of the standard procedures is necessary.[12]

3.26.5.2.2 Whole-article tests

Grain tests are open to the criticism that they do not necessarily reflect the behavior of the finished product in service, and hence various tests on complete glass articles have been developed. These are normally carried out under accelerated conditions, and on completion various relevant factors are determined, such as loss in weight, alkali or other constituents extracted, the weight of soluble and insoluble materials in the extract, and an assessment of surface condition. Analytical microscopy and other surface analytical tools can be of great assistance in determining mechanisms.

Whole-article tests are particularly useful in the evaluation of window and optical glasses. Various tests have been proposed for window glass, but no standards exist. The usual procedure is to subject the glass to an accelerated humidity/temperature weathering cycle and to assess the surface conditions after a given period of treatment. The degree of haze formation has been suggested as a method of measuring surface damage, but generally visual comparison with a standard is used. Figure 1 illustrates the application of such a test to various optical glasses.

Many optical glasses are much less resistant to attack than are container and window glasses, and less severe tests are necessary. A commonly used method is to immerse specimens in either dilute nitric acid or standard acetate solution (pH 4.6) for specified periods at room temperature, and then to examine the surfaces.

Glass fibers present a particular problem in that the resistance of the base glass is unlikely to be representative of the performance of the final product. Generally, empirical methods are used to test the glass fibers *in situ* in a composite material: for example, the fibers are made up into rods or rings with the appropriate partly polymerized plastic; the composites are then cured under specified conditions; and the breaking strength is determined after various exposures to water or steam.

3.26.6 Mechanisms of Glass Corrosion

3.26.6.1 General Properties

Glass surfaces may react with corrosive agents in one or a combination of the following ways:

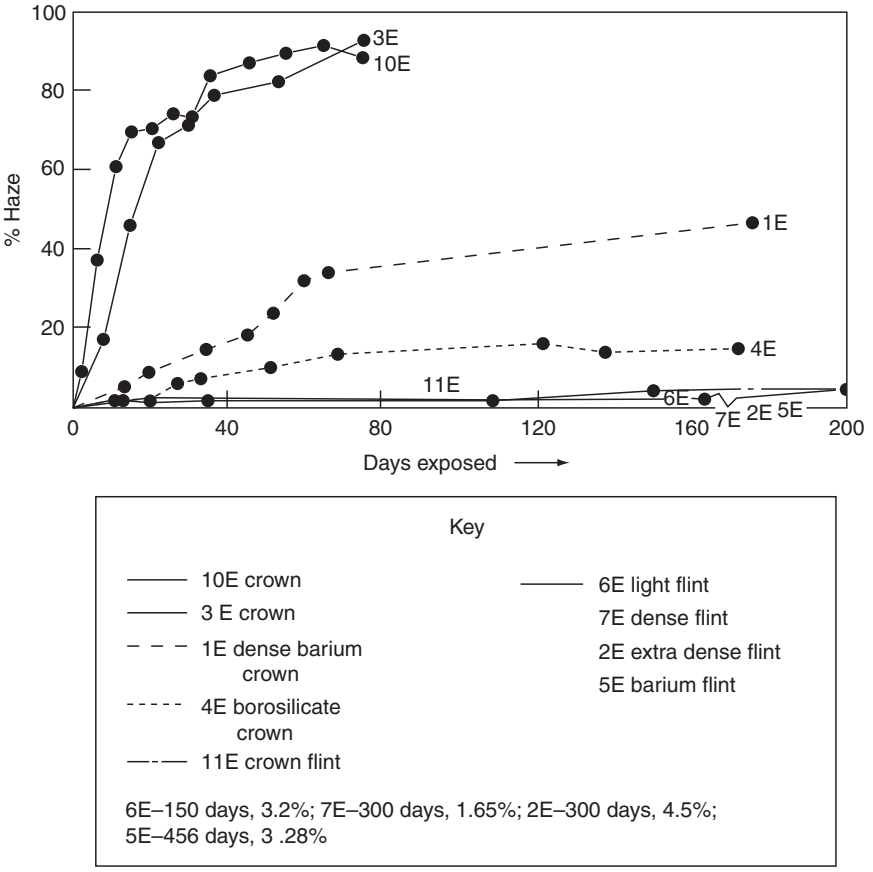

Figure 1 Comparison of optical glasses after exposure to an alkaline solution. Simpson, H. E. *J. Soc. Glass Technol.* **1953**, *37*, 249; *J. Am. Ceram. Soc.* **1953**, *36*, 143–146.[13]

a. by forming new compounds on the surface;
b. by selectively losing material from a leached porous layer;
c. by continuous dissolution leaving a freshly exposed surface.

Important effects on glass durability in aqueous conditions, due to the interrelation between glass composition and environmental pH, have been reviewed by Doremus[14] and Adams.[15] To some extent, durability can be predicted on thermodynamic grounds.[16,17] In general, additions of CaO (calcia) and Al_2O_3 (alumina) to a basic alkali silicate glass confer water resistance; additions of zirconium, lanthanum, tin, and chromium oxides improve alkali resistance; and reducing the levels of boron, aluminum, or lead oxides, in glasses where they are present, improves acid resistance. Predictions of the effects of added oxides on glass durability should, however, be treated with caution. Structural factors, such as occurrence of phase separation, coordination state, mixed alkali effect, and/or kinetic effects resulting from the presence or absence of insoluble reaction product layers on the glass surface, can influence durability to a significant extent.

More generally, Valez *et al.*[18] have reviewed the corrosion behavior of silicate and borate glasses in contact with alkali metals and molten salts, as well as in aqueous conditions.

Another important aspect of glass corrosion behavior that should be emphasized is the effect of applied stresses. Glass is subject to stress-enhanced corrosion, which is often described as static fatigue. Under a continuously applied stress, and in the presence of normal environmental moisture (or other more aggressive corrosion conditions), cracks may grow from flaws on the glass surface and this can lead to delayed failure at stresses below the strength level that is measured in a short-term loading test.[17,19] As a consequence, common silicate glasses are usually expected to have a

load-bearing capacity at one-quarter to one-third the short-term strength when continuously loaded over some 50 years in the normal atmosphere.

3.26.6.2 Corrosion Mechanisms

There is no serious challenge to the view that the alkali or alkaline-earth ions are removed from glass in water by an ion exchange process in which H^+ ions diffuse into the glass to preserve the electrical neutrality of the system. However, only under certain circumstances can the rate-controlling process be directly related to the diffusion of sodium in the glass. Most glass/corrosive agent systems are treated as unique cases, since in addition to the concentration of the attacking agent, temperature, rate of flow, and reaction time contribute to what is observed. General chemical principles of electrophilic and nucleophilic types of general attack can be applied to glasses.[20] The first is considered as an attack on nonbridging oxygen atoms by reagents with an electron deficiency and the second as an attack on bridging oxygens by reagents with an electron excess.

For the most common series of corrosive agents – water, steam, acids, alkalis, and salts – the hydrolytic processes peculiar to each determine the mechanism of attack. Thus, under the right circumstances, hydrolytic attack on bridging oxygen atoms can occur, which is an irreversible reaction resulting in permanent damage to the glass network. The corrosion process is modified by the physical state of the surface. Grinding and polishing processes, in particular, leave the structure with a degree of roughness and residual stress; all can contribute to accelerated corrosion.

3.26.6.3 The Action of Water and Acids

During attack, the alkali and alkaline-earth network-modifying ions are exchanged by H^+ or H_3O^+ from an acid solution. In some glasses the exchange process can go to completion causing only a small degree of network damage. In water, the exchange process proceeds at a very much slower rate relative to the acid conditions, and some attack of the network is possible as a result of the presence of alkali ions from the glass moving into solution. This is most pronounced when glass is attacked by steam at high temperature and where there is no mechanism for the removal of alkali from the hydrolyzed zone. Acid solutions mitigate this form of attack by neutralizing the alkali as it is formed.

The attack of most glasses in water and acid is diffusion controlled, and the thickness of the porous layer formed on the glass surface consequently depends on the square root of the time. There is ample evidence that the diffusion of alkali ions and basic oxides is thermally activated, suggesting that diffusion occurs either through small pores or through a compact body. The reacted zone is porous and can be further modified by attack and dissolution, if alkali is still present, or by further polymerization. Consolidation of the structure generally requires thermal treatment.

3.26.6.4 Attack by Alkali Solution, Hydrofluoric Acid, and Phosphoric Acid

A common feature of these corrosive agents is their ability to disrupt the network. This process is not encumbered by the formation of porous layers, and the amount of leached matter is linearly dependent on time. Consequently, the extent of attack by strong alkali is usually far greater than either acid or water attack. Both HF and H_3PO_4 form compounds of silicon as a result of attack on the network: silicon fluoride from hydrofluoric acid and silicyl phosphate from phosphoric acid.

3.26.6.5 Chemical Attack by Other Agents

If the hydrogen ion concentration is sufficiently high, the glass loses a substantial amount of weight by leaching, but these reactions are dependent on the nature of the ions in solution. Certain salts, especially those of Zn, Al, and Be, if present as trace amounts, can have a beneficial effect by poisoning the process and limiting the occurrence of leaching.

3.26.6.6 Cleaning of Glass

There is no universally ideal technique for either cleaning glass or avoiding contamination of the surface. In the most severe circumstances of corrosion, the only methods capable of restoring an acceptable surface finish consist of grinding and polishing or removing the contamination and corroded layers by strong etching agents such as hydrofluoric acid. Less severe conditions may respond to treatment by various detergent solutions or organic solvents, these being considerably aided by ultrasonic vibration. Manual washing or ultrasonic cleaning can be used to remove massive dirt accumulations. Vapor solvent degreasing processes, for example using isopropyl alcohol, has minimal corrosive action on the glass.

To restore old stocks of corroded glass, treatment in hot 1% sodium hydroxide solution followed by

rinsing in 5% hydrochloric acid and a final rinse in pure water at room temperature is recommended.[21]

3.26.6.7 Applications

Over recent years, a number of new applications of glasses have grown out of increased understanding and control of glass corrosion behavior. Conventional silicate and borosilicate glasses are subject to severe corrosive attack in highly alkaline solutions (pH 12–13.5), such as those found in Portland cement, and there is rapid and drastic loss of strength in fibers formed from soda or borosilicate compositions. To counter this, alkali-resistant glass fibers have been developed from silicate glass compositions and containing about 16 wt% of zirconia[22,23] and these have formed the basis for development of a range of glass-fiber reinforced cement (GRC) materials, analogous to glass-fiber reinforced plastics (GRP). In the GRP field, it has been shown that E-glass borosilicate fibers are prone to strength loss and stress corrosion in acidic environments[24,25] – this in turn led to the development of an acid-resistant version of E-glass for use in such conditions.

3.26.7 Vitreous Silica

Vitreous silica, also referred to as quartz glass, fused quartz, or fused silica, is a material of considerable importance, possessing a unique combination of high softening temperature, excellent resistance to chemical attack, and high transparency. Its general, physical, and mechanical characteristics are common to all glasses, the difference being that the high purity (>98.7% SiO_2) maximizes the durability, fusion temperature, and volume stability. The general superiority of the properties of fused silica over conventional glasses is well illustrated in **Table 1**. It has excellent high temperature properties in excess of 1000 °C, high resistivity, high chemical stability, and excellent thermal shock resistance due to its low coefficient of expansion. However, the high softening point makes it much more difficult to fabricate than conventional glasses.

3.26.7.1 Manufacturing

The raw materials for the production of vitreous silica are either high-purity rock crystal from which the transparent form is produced, or vein quartz (high-grade glass sand) from which impurities have been removed by acid leaching. The persistence of liquid and gaseous inclusions is partly responsible for the translucency of cheaper forms of vitreous silica. Ground quartz is melted at around 2000 °C by induction heating in a graphite crucible. Even at this temperature, the melt viscosity is so high (10^5–10^6 Pa s) that trapped gas bubbles do not float to the melt surface and can only be removed by vacuum treatment. At high temperature, the SiO_2 partly dissociates to the monoxide SiO, which is volatile.

Vitreous silica produced by this route contains small amounts of impurities such as Fe, Cr, Al, and Ca. These may be removed by reaction to form volatile metal chlorides, whereupon the remaining $SiCl_4$ can be hydrolyzed in a flame to produce fine molten droplets of SiO_2 which then deposit on a cold base; impurity levels below 10^{-7}% can be reached in this process and are essential in applications such as optical fibers.

3.26.7.2 Structure and Physical Properties

3.26.7.2.1 Polymorphism of silica

Although vitreous silica is nominally a homogeneous isotropic amorphous material, and should normally remain so during its service life, it is in fact in a metastable condition. The tendency to revert to crystalline forms with attendant deterioration in mechanical durability places severe limitations on the range of applications. **Figure 2** illustrates the polymorphic forms of silica, and the dimensional changes accompanying each transition.

Changes from one polymorphic form of crystalline SiO_2 to another, as from tridymite to quartz at temperatures below 870 °C and to cristoballite above 1470 °C, involve the breaking of Si–O bonds. High energies are required for these 'reconstructive' changes, and changes from one form to another require very long periods for completion. On the other hand, inversions from high- to low-temperature forms of quartz or cristoballite involve only changes in the angles between adjoining SiO_4 tetrahedra, and these 'displacive' transformations are accomplished almost instantaneously. The accompanying volume changes lead to disruption of ware containing significant amounts of quartz or cristoballite.

3.26.7.2.2 Thermal expansion

The coefficient of thermal expansion of vitreous silica is very small (5.4×10^{-7} over the range 0–1000 °C), about one-sixth that of porcelain. It is thus highly resistant to thermal shock.

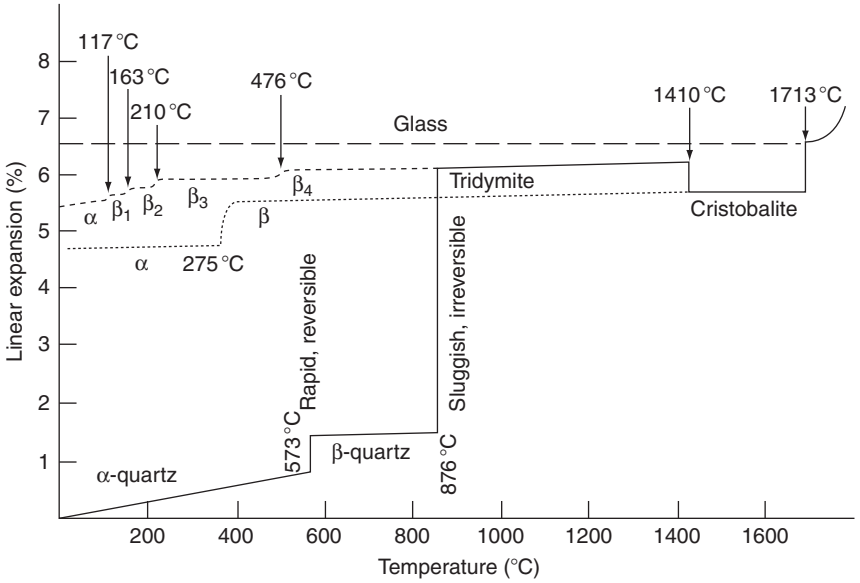

Figure 2 Polymorphism and dimensional changes in silica as a function of temperature.

3.26.7.2.3 Heat resistance

Being a glass, vitreous silica softens progressively as it approaches its melting point of 1713 °C. The maximum recommended working temperature is 1050 °C in an oxidizing atmosphere, though it may be taken to 1350 °C for short periods. Surface devitrification to cristoballite occurs above this temperature. This causes some loss of transparency, but chemical and mechanical durability are unaffected provided the temperature does not fall below the β–α inversion temperature (275 °C), which would lead to the initiation of cracks. It should be noted that devitrification is accelerated by traces of alkali–metal compounds, particularly potassium and lithium salts, sodium tungstate, and ammonium fluoride. Devitrification is also enhanced by water vapor and oxygen, but inhibited by neutral or reducing atmospheres.

3.26.7.2.4 Thermal conductivity

The thermal conductivity of fused silica is low ($1.38\ W\ m^{-2}\ K^{-1}$). The transparent form passes infrared radiation with little loss up to wavelengths of 3.5 μm.

3.26.7.2.5 Electrical characteristics

The insulating properties of glass are excellent. At ordinary temperatures, the resistivity of the translucent form is $10^{15}\ \Omega\ m$, and it is capable of withstanding high-frequency discharges at high voltages. See also **Table 1** for data on other physical properties and for comparison with other glasses.

3.26.7.3 Resistance to Chemical Attack

Most glasses suffer chemical attack and deterioration due to ion exchange of sodium ions to form a highly alkaline solution, which subsequently attacks the network. As network-modifying oxides are absent from fused silica, this mode of attack does not occur. Hence fused silica is highly resistant to most aqueous solutions, even aqua regia at elevated temperatures having no effect. Reagents that attack the network silica directly, such as strong alkalis and fluorides, cause serious damage and are therefore to be avoided.

3.26.7.3.1 Boiling water and steam

There is limited reaction with water and steam at moderate temperatures and pressures. However, silica is slightly soluble up to around 6 ppm. However, at temperatures in the range 400–500 °C and pressures of the order of 3.5 MPa the solubility rises to 0.14% for the translucent form and 0.035% for the transparent.

3.26.7.3.2 Fluorine, hydrofluoric acid, and alkaline solutions

Silica is susceptible to attack by all three reagents, the rate of corrosion increasing with temperature and concentration. Although 5% caustic soda solution can be contained in fused silica at room temperature, attack becomes significant at pH values greater than 9, as shown in **Figure 3**.

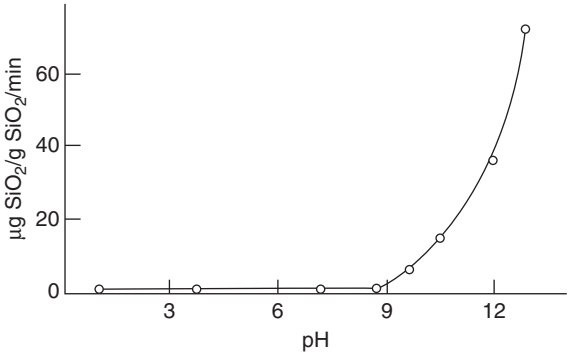

Figure 3 Effect of pH on the rate of silica extraction from vitreous silica powder at 80 °C. Reproduced from El-Shamy, T. M. M.; Douglas, R. W. *J. Am. Ceram. Soc.* **1967**, *50*, 1–7.

The essential step in the dissolution reaction of silica is the breaking of a siloxane bond Si–O–Si. This bond, although strong, is polar, and may be represented as ($Si^{\delta+}$–$O^{\delta-}$). The excess positive charge associated with the silicon atom makes it susceptible to attack by nucleophilic reagents such as the hydroxide ion, which attaches itself to the silicon, rupturing the network at that point. The attack by HF on silica is thought to proceed by a similar mechanism in which there is simultaneous nucleophilic and electrophilic attack on the network silicon and oxygen atoms, respectively. It should be pointed out the H^+ ion cannot effect disruption of the siloxane bond without the simultaneous action of the F^- ion. Consequently, sulfuric and nitric acids do not initiate attack even at temperatures up to 1000 °C.

Sodium fluoride also attacks silica, as do sodium metaphosphate and sodium polyphosphate, and to a lesser extent sodium carbonate and sodium cyanide. Attack is particularly vigorous for fused alkalis, alkali halides, and phosphates.

3.26.7.3.3 Basic oxides

As an acidic oxide, SiO_2 is resistant to attack by other acidic oxides, but has a tendency towards fluxing by basic oxides. An indication of the likelihood of reaction can be obtained by reference to the appropriate binary phase equilibrium diagram. The lowest temperature for liquid formation in silica oxide binary systems is shown below:

Oxide	Al_2O_3	BeO	CaO	MgO	ThO_2	TiO_2	ZrO_2
Eutectic (°C)	1546	1670	1436	1543	1700	1540	1675

3.26.7.3.4 Metals

Silica is decomposed only by those metals that have a high thermodynamic affinity for oxygen. On this basis, molten sodium should be compatible with silica:

$$2Na(1) + 1/2SiO_2(s) = Na_2O + 1/2Si(s)\ \Delta G = 73 kJmol^{-1}$$

Although the equilibrium levels of the reaction products are very small, both can dissolve in liquid sodium; also sodium oxide can form compounds with silica. As a consequence, the reaction moves to the right, leading to further reduction of silica. Nevertheless, vitreous silica crucibles have been used successfully for containing molten antimony (850 °C), copper (1210 °C), gallium (1100 °C), germanium (1100 °C), lead (500 °C), and tin (900 °C).

In accordance with the free energy predictions, silica is readily attacked by molten aluminum, lithium, magnesium, and calcium.

3.26.7.4 Applications of Vitreous Silica

The high thermal and electrical resistance of vitreous silica, and its imperviousness to chemical attack, make it suitable for a wide range of applications. These include chemical and physical laboratory apparatus, tubes and muffles for gas and electric furnaces (including vacuum furnaces), pyrometers, insulators for high-frequency and high-tension electrical work, mercury-vapor and hydrogen-discharge lamps, high-vacuum apparatus, plants (complete or partial) for chemical and related industries, equipment for the manufacture of pure chemicals, tubes, chimneys and radiants for the gas- and electric-heating industries, component material in refractory and ceramic mixtures, etc.

It is used for pipes to carry hot gases and acids and in acid distillation units, condensing coils, S-bend coolers, hydrochloric acid cooling and absorption systems, nitrating pots, and cascade basin concentrators for sulfuric acid. The resistance of vitreous silica to most acids is also utilized in the manufacture of electric immersion heaters and plate heaters for acidic liquors in chemical processes and electroplating baths. Vitreous silica wool is used for filtration of acidic liquids and filtering hot gases. The resistance of vitreous silica to water and steam at normal temperatures and pressures makes it applicable in the production of pure water for the manufacture of highly purified chemicals. Because of its thermal properties, it is used for the construction of muffles of oval cross section used for the bright-annealing of metal strip and wires. Special products include transparent vitreosil components, which are ideal

Table 4 Property data for some glass-ceramics

	A	*B*	*C*	*D*	*E*
Compositional type	Lithium aluminosilicate	Lithium aluminosilicate	Potassium magnesiasilicate	Lithium aluminosilicate	Lithium aluminosilicate
Density ($mg\,m^{-3}$)	2.55	2.5	2.53	2.5	2.5
Thermal expansion coefficient ($\times 10^{-7}\,K^{-1}$)	6	12.7	97	4.2	–3
Transition point (°C)	820	–	–	–	–
Softening point (°C)	950	–	–	1250	–
Service limit (°C)	800	1000	1500	–	810
Bend strength (MPa)	120	180	88	110	130

A: 'Heatron-T', B: 'Neoceram-15', C: 'Corning 9650' (machinable), D: 'Pyroceram 9608', E: 'Hercuvit'.

for continuous measurement in corrosive atmospheres, and quick-immersion thermocouple protection sheaths for rapid temperature measurement.

3.26.8 Glass Ceramics

3.26.8.1 Definition and Properties

Glass-ceramics are a family of materials that are polycrystalline in nature and are formed from the liquid or glassy state. A glass-ceramic article is made by the heat treatment of a vitreous body in two stages:

1. *Nucleation:* The glass is held at a temperature below its softening point for a period of minutes or hours to allow nuclei to develop.
2. *Crystallization:* The temperature of the nucleated glass is raised to just below the softening point when crystals form and grow around the nuclei.

Ideally the product is a fine-grained ceramic containing interlocking crystal grains of sizes ranging from less than 10 nm in transparent glass-ceramics to several micrometers, with a residual, usually small, glass content. The behavior of the material is largely determined by the choice of the crystalline phase; by suitable choice, a range of useful properties has been obtained.

As a class of materials, glass-ceramics have the following general characteristics:

1. Impervious, with moderate densities similar to those of glasses.
2. Improved facture toughness compared with glass or ceramic materials.
3. Relatively high tensile strengths (a consequence of item 2).
4. Stiff, elastic (Hookean) limited-to-zero plasticity.
5. Considerable hardness and resistance to abrasion.
6. Chemical stability and resistance to corrosion.
7. Resistance to medium-high temperatures (higher temperatures than most glasses but lower than the refractory oxides) and low thermal conductivity.
8. Resistance to the passage of electrical current.

Special characteristics can be developed in individual materials depending on the cations present and their arrangement relative to each other and to the oxygen anions. The most important of these characteristics is low, medium, or high reversible thermal expansion. The properties of some commercially available glass-ceramics are summarized in Table 4.

3.26.8.2 Chemical Durability of Glass-Ceramics

While the chemical behavior of a glass-ceramic is strongly influenced by the chemical composition of the parent glass, several different crystalline compounds together with a residual glass phase are likely to be present. The relative resistances of these phases to attack by water or other reagents will determine the chemical stability. In general, a glass that exhibits poor chemical stability is unlikely to give rise to a glass-ceramic of high stability. To this extent, the factors that govern the stability of glass-ceramics can be equated to those that determine the chemical stability of glasses.

In most cases, glass-ceramics possess good chemical stability and certainly compare favorably in this respect with other ceramic materials. Table 5 summarizes manufacturers' data for chemical attack on the materials listed in Table 4.

Certain types of glass-ceramic have good resistance to attack by corrosive chemical reagents. Low-expansion glass-ceramics derived from lithium aluminosilicate glasses are only slightly inferior to

Table 5 Chemical resistance data for the glass-ceramics listed in Table 4

	A	*B*	*C*	*D*	*E*
Powder method					
Water solubility (mg Na_2O/mg sample)	0.29	0.8	128	0.1–0.3	0.12
Acid solubility (mass loss in %)	0.06	3.5	5	0.02–0.1	0.2
Alkali solubility (mass loss in %)	0.13				4
Surface method	0				
H_2O (90 °C, 24 h) (mass loss in mg cm^{-2})	0.13				
5% HCl (90 °C, 24 h) (mass loss in mg cm^{-2})	0.04				
5% NaOH (90 °C, 24 h) (mass loss in mg cm^{-2})					

borosilicate chemically resistant glass with regard to attack by strong acids and are somewhat more resistant to attack by alkaline solutions. Materials derived from magnesium aluminosilicate glass compositions are slightly less resistant to attack by strong acids and alkalis than are chemically resistant borosilicate glasses. Even at high temperatures, these types of glass-ceramic retain resistance to attack by corrosive gases. For certain applications, it is important that the glass-ceramic should be unaffected by contact with reducing gases at high temperatures. In such cases, the composition must not include any oxides such as lead, which are easily reduced to the metal.

References

1. Oliver, S.; Proctor, B. A.; May, C. A. In *Shreir's Corrosion*, 3rd ed.; Butterworth-Heinemann, 1994; Chapter 18.3.
2. Cole, H. *Viscosity–Temperature Relations in Glass: 1. Viscosity in Glass;* International Commission on Glass, 1970.
3. ASTM Method C338-93: Standard Method of Test for Softening Point of Glass; American Society for Testing and Materials, 2008.
4. BS 2598-4:1980, ISO 4704:1977 – Glass plant, pipeline and fittings: Specification for glass plant components.
5. BS 3517:1991, ISO 718:1990 – Methods for thermal shock tests on laboratory glassware.
6. Volf, M. B. Technical Glasses; Pitman: London, 1961.
7. Wessel, H. *Silikattechnik* **1967**, *18*, 205–211; **1968**, *19*, 6–10.
8. ASTM Method C 225-68: Standard Methods of Test for Resistance of Glass Containers to Chemical Attack.
9. DIN 12116:2001: Testing of glass – Resistance to attack by a boiling aqueous solution of hydrochloric acid – Method of test and classification; DIN EN 12122:2005: Chemicals used for treatment of water intended for human consumption – Ammonia solution.
10. BS 3473 Parts 1–5: Chemical resistance of glass used in the production of laboratory glassware, 1991.
11. ISO 695:1991: Glass – Resistance to attack by a boiling aqueous solution of mixed alkali – Method of test and classification; ISO 719:1985: Glass – hydrolytic resistance of glass grains at 98 °C – Method of test and classification.
12. Wiegel, E. *Glastechnische Berichte* **1956**, *29*, 137–144.
13. Simpson, H. E. *J. Soc. Glass Technol.* **1953**, *37*, 249; *J. Am. Ceram. Soc.* **1953**, *36*, 143–146.
14. Doremus, R. H. *Treatise Mater. Sci. Technol.* **1979**, *17*, 41–67.
15. Adams, P. B. *J. Non-Cryst. Solids* **1984**, *67*, 193–205.
16. Paul, A. *J. Mater. Sci* **1977**, *12*, 2246–2268.
17. Newton, R. G.; Paul, A. *Glass Technol.* **1980**, *21*(6), 307–309.
18. Velez, M. H.; Uhlmann, D. R.; Tuller, H. L. *Rev. Latinoamericana Metall. Mater*; **1982**, *11*(1).
19. Kurkjian, C. R. Ed. *Strength of Inorganic Glass*; NATO Conference Series VI, *Materials Science,* Vol. 11; Plenum Press: New York, 1985.
20. Budd, S. M. *Phys. Chem. Glasses* **1961**, *2*, 111–114; Budd, S.M.; Frackiewicz, J. *Phys. Chem. Glasses* **1961**, *2*, 115–118.
21. Tichane, R. M. *Am. Ceram. Soc. Bull.* **1963**, *42*, 441.
22. Majumdar, A. J.; Ryder, J. F. *Glass Technol.* **1968**, *9*(3), 78–84.
23. Proctor, B. A.; Yale, B. *Philos. Trans. Roy. Soc. London A* **1980**, *294*, 427–436.
24. Metcalfe, A. G.; Gulden Mary, E.; Schmitz, G. K. *Glass Technol* **1971**, *12*, 15–23.
25. Torp, S.; Arvesen, R. In 34th Annual Technical Conference, Reinforced Plastics/Composites Institute, SPI, 1979; Session 13-D.

Further Reading

Clark, D. E.; Zoitos, B. K. *Corrosion of Glass, Ceramics and Ceramic Superconductors;* William Andrew Publishing/Noyes, 1992.
Doremus, R. H. *Glass Science,* 2nd ed., Wiley, 1994.
Lewis, M. H. *Glasses and Glass-Ceramics;* Chapman and Hall, 1989.
Shelby, J. H. *Introduction to Glass Science and Technology,* 2nd ed.; Royal Society of Chemistry, 2005.
Varshneya, A. K. *Fundamentals of Inorganic Glasses;* Academic Press, 1993.

Relevant Websites

www.sgt.org – Society of Glass Technology
www.ceramics.org – Glass and Optical Materials Division of The American Ceramic Society

3.27 Degradation of Glass Linings and Coatings

G. Schäfer
Pfaudler Werke GmbH, Pfaudlerstrasse, D-68723 Schwetzingen, Germany

Glossary

Adhesion (enamel-basis metal) Amount of the force required to separate a coating from its basis metal and the area of the corresponding surface.

Blister Defect that appears as a localized bubble under the surface of the fired vitreous enamel.

CIP Cleaning in place – standard procedure in chemical plants to avoid or remove surface contaminations or settlements. Normally carried out after several production batches. pH and temperature are often just the opposite of the regular production conditions.

Cover coat Vitreous enamel with specific chemical and/or esthetic properties as the final coat.

Crazing Defect resembling a network of fine hairline cracks in a coating.

Fishscaling Small half-moon shaped defects occurring in the vitreous enamelled surface. Can occur immediately on cooling or after some time has elapsed following firing. This defect originates from supersaturation of the substrate with hydrogen (acquired during firing), which explosively fractures the

enamel coating because of the pressure that has accumulated with time at the enamel–steel interface.

Ground coat Vitreous enamel, containing adherence-promoting agents and applied directly to the substrate to function as an intermediate bonding layer between the substrate and the cover coat.

Scale Oxide formed on the surface of a metal during heating at elevated temperatures.

Spark test High-voltage electrical test in which a spark is used to detect discontinuity in coating. Applied voltages can be as high as 20 kV.

Technical enamel/vitreous enamel Product formed by the heating of an inorganic mixture, to a temperature just high enough for fritting, or uniform fusion to occur. It is designed for application to metallic surfaces for protective, functional, and/or aesthetic purposes, and specifically will exhibit cubic thermal expansion of between 150 and $450 \times 10^{-7}\ K^{-1}$, in the temperature range 20–100° C, the actual value varying specifically with the type of substrate and the field of application.

Abbreviations

ORP Oxidation/reduction potential

APAVE Association des propriétaires d'appareils à vapeur et électriquest

ASME American Society of Mechanical Engineers

ISO International Organization for Standardization

WWG World Wide Glass: Pfaudler trademark for a high chemically inert vitreous enamel

PPG Pfaudler Pharma Glass: Trademark for a specially designed glass with both very high acidic and alkaline resisitivity

PTFE Polytetrafluorethylene

3.27.1 Introduction

While glass can provide many of the desirable features of an almost ideal inert material, manufacturing difficulties and safety considerations prevent its use in large-scale dimensions for chemical process equipment, and mechanical considerations would, in any case, make it necessary to treat any such equipment with great care.

The high chemical resistance, and the nontoxic, nonflammable, nonflavorable, and thermal resistant properties of glass, can, however, be combined with the mechanical strength of metals by covering metal surfaces exposed to corrosive media with a layer of suitable glass. It thus becomes feasible to produce large-scale storage or transport tanks or to run large-scale reactors under high overpressures and extended temperature profiles. Reaction vessels, storage tanks, all-glass-lined pump smoke stacks, distillation columns, etc. can all be made of glass-lined equipment.

The principal advantage of glass linings is the increased size as well as the mechanical and thermal strength that are possible compared with all-glass equipment and the flexibility of operation with different chemicals compared with all-metal equipment. The increased heat transmission, in comparison with glass equipment, can also be an advantage.

The principal disadvantages are the loss of transparency and the potential vulnerability of the lining to mechanical damage unless sensible precautions are taken in handling, installation, and service. A variety of metals can be protected in this way, including copper, gold, stainless steel, titanium, and aluminum, but by far the most extensive use is for carbon steel based equipment.

The actual size of glass-lined equipment varies from 4 l autoclaves up to storage tanks that exceed a size of 120 000 l. The pressure regime under service can range from vacuum up to 25 bars in standard operation processes. Because of the often severe application properties run in glass-lined equipment, the sensor probes used to monitor production processes have to be made of glass or of glass-lined parts. These include acidity (pH) and potential (ORP-redox) probes, temperature sensors, conductivity measurements, and also glass-lined radar probes as well as oscillating sensing forks for fluid level measurement.

3.27.2 Manufacturing of Glass-Lined Steel Equipment

3.27.2.1 Glass Formulations

Glass frits used in vitreous enamels may contain as many as 20 components, though these may be classified in three functional categories: glass formers (SiO_2 and B_2O_3, which constitute the random network of the glass), the dioxides (ZrO_2, CeO_2, and TiO_2, which all enhance alkali resistance and are

also opacifiers), and the alkali and alkaline earths (which lower fusion temperature and increase the expansion coefficient). While high alkali (e.g., sodium, potassium) content lowers resistance to acid attack, adequate amounts are required to dissolve the oxides on the surface of the steel. Alkaline earth elements (e.g., calcium, barium), on the contrary, increases the chemical resistivity up to a certain extent. A kind of 'mixed alkali effect' additionally enhances the properties of the enamel by creating nanosized local stress inside the glass matrix thereby reducing the amount of easily dissolvable species. A relatively infusible ground-coat frit becomes supersaturated in iron oxide, which eventually crystallizes in the enamel, a defect known as 'copper heading.' Compromise is necessary, as too fluid a ground-coat results in over-rapid reaction and 'burning off,' precipitating the chipping of the enamel coating later on. Ground-coat frits contain much more boron oxide than the enamels used for the cover coat. Additions of alumina can be used to control viscosity, surface smoothness, and mechanical hardness of the glass.

Depending on the field of application, specific chemical, surface, and manufacturing properties of the enamel are required, resulting in compositions most appropriate for the area of the specific subject. This results in two different composition schemes 'A' and 'B' for technical enamels and enamels for domestic appliances respectively, which are schematically shown in the composition triangle in **Figure 1**. **Table 1** lists the oxides most often used for glass making. A high silica-to-boric oxide ratio composition is used for industrial enamels in reaction vessels and in hot water tanks where the higher firing temperature is required for improved chemical and thermal resistance.

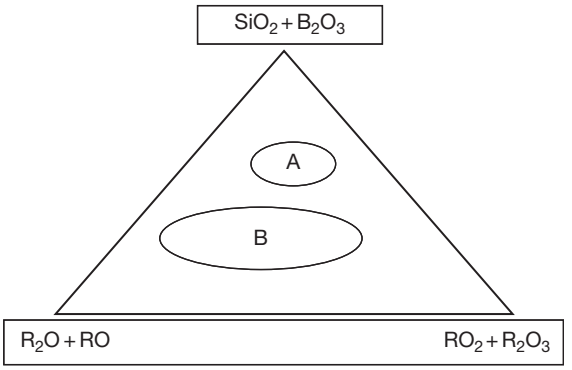

Figure 1 Area 'A' represents the chemical composition of technical enamels, 'B' shows the much wider area of enamels used for domestic appliances, such as cookware, burner cups, fridges, ovens, bath tubs, architectural panels, etc.

3.27.2.2 Glass Preparation

Most of the manufacturers of glass-lined equipment have their own glass formulations, although frit manufacturers also sell appropriate frits. In most cases, the chemical constitution has not been disclosed, but the more successful types are borosilicates containing high amounts of silicate (>55 wt%), aluminum, and alkaline earth oxides than do the typical heat-resistant borosilicates.

In formulations for ground coating the steel, the glass composition contains more cobalt and manganese oxide than do ordinary glasses to enable a better adhesion to the plain steel surface and to form a chemical bond between the metal and the glass. The thermal expansion coefficients of the glasses are of the order of $(8–9) \times 10^{-6}\,K^{-1}$ for this application, but vary for other metallic substrates. The disparity between these figures and the higher expansion coefficient of the steel, which is in the order of $14 \times 10^{-6}\,K^{-1}$, is quite deliberate and results in the development of compressive stresses in the glass layer after processing (i.e., after cooling from the sintering temperature). The stress developed gives more resistance to thermal shock or external stresses than if the expansion coefficient of the glass and steel were accurately matched.

The raw materials required to produce the particular glass composition are thoroughly mixed and melted at temperatures above 1300 °C. The melt is normally quenched directly into cold water, but often quenching is carried out using cooled copper-based rolling blades. While the directly quenched melts produce irregularly shaped, cracked particles, the rollers form disc-like shapes.

Both types of frits are ground in the same way, either dry to form powders or wet-milled with clay and quartz added to form a viscous slip. It can be applied to steel by spraying or dipping, depending on the shape, size, and design of the structure.

Table 1 Oxides used in glass manufacture

Glass former	*Glass modifier R_2O*	*Glass modifier RO*	*Glass former RO_2, R_2O_3*	*Adhesion promoter*
SiO_2	Li_2O	MgO	TiO_2	CaF_2
B_2O_3	Na_2O	CaO	ZrO_2	MnO_2
	K_2O	SrO	SnO_2	CoO
		BaO	Fe_2O_3	NiO
		ZnO	Al_2O_3	

3.27.2.3 Metal Preparation

A low-carbon (<0.2% C) steel is usually used in the manufacturing of chemical process reactors or storage tanks, distillation columns, and the like; the steel quality is defined in several standards,[1–3] which include also the minimum and maximum content of other constituents than that of iron, and stipulate surface standards prior to the lining process. For other parts of the reactor, such as nozzle parts, pipes, etc., specific requirements are defined in various EN standards.[4,5]

These requirements contain the maximum content and diffusivity of hydrogen, amount of slacks, and define test methods for estimating the propensity for defects such as fishscaling, blistering, crazing, scaling, and poor adhesion. Cast iron is frequently used in equipment such as valve bodies and pipe unions. It should be of good quality, close-grained gray iron, free from blow-holes, cavities, and porosity. Repair of such defects by filling is not permissible in the reactor field.

Conventional welding techniques are used in production and assembly of the steel body, but special precautions must be taken to ensure that the weld metal is of a similar composition to the base metal. Moisture-free electrodes must be used.[6–8] According to the assigned production place, the equipment has to fulfill different local requirements, which are all specified in technical rules.[2]

3.27.2.4 Certifications

This knowledge about industrial enamel and the glass lining process is the basis of the European glass lining industry. It is used to manufacture highly sophisticated products according to ISO 9001, APAVE, ASME, Druckgeräterichtlinie, China Code, etc., which are certified regularly by external audits of the manufacturers.

The design and dimensioning of a specific vessel results from customer requests and should be in accordance to the local laws and standards. **Table 2** lists some of them.

All these regulations define how a vessel has to be designed and also how the required quality has to be controlled. They assess criteria for welding and lay down instructions that define accompanying material tests to ascertain the overall quality of a vessel. All these instructions increase the amount of testing enormously, and make the production more costly, but ensure a safe running of a chemical plant where they are applied to. In the end, they lead to the international reputation of equipment manufactured in Europe (**Table 3**).

Table 2 List of technical rules to define good manufacturing procedures used for manufactured products related to chemical industry

AD 2000 Merkblatt HP-0	*ATEX 94/9/EG*	*DIN EN 729-2*
DGRL97/23/EG	ASME R	TRD 201
SVTI	ASME NB	CODAP
UIC	ASME U	DIN 6700-2
AQSIQ	DIN ISO 9001:2000	

Typically, a completed steel assembly is examined in detail by ultrasonic and X-ray detection to check for defects likely to impair serviceability. It is then often normalized above 860 °C to relieve stresses arising from fabrication and to reduce hydrogen content. The heat treatment also has the advantage of burning off organic contamination and carbon residues localized near the steel surface. After cooling, the vessel is sand-blasted either with silica grit or steel shot to remove the scale formed during the normalization procedure and promote mechanical keying of the glass ground-layer to be applied (by roughening the surface). Degreasing and chemical descaling is no longer used for large-scale equipment because of the risk of hydrogen uptake and consequent fishscaling and also for environmental restrictions.

Important points in vessel design are

1. The metal thickness should be as uniform as possible throughout, avoiding heavy bosses, lucks, or brackets.
2. Sharp edges must be avoided under all circumstances, the minimum radius recommended for all curved surfaces is ~8 mm, at complex-shaped parts, and with smaller dimensions, radii can be as small as 3 mm. The risk of sudden shaling increases as the radius decreased. Therefore, for such parts, thickness limitations are defined.
3. The risk of distortion on firing is greater if the design includes numerous apertures in the vessel or its cover.
4. The minimum metal thickness must take into consideration that the mechanical strength of steel decreases sharply during heating. Several standards[9] define maximum tolerances for deviations from the original design.

Table 3 List of technical standards which define technical requirements and material flow and documentation procedures for manufactured products related to chemical industry

EN 14483-1 to 5	Defines physical and chemical properties of glass coatings. Describes testing devices and procedures
EN 14430	Defines spark testing devices and technical spec for glass linings
EN 15159-1 to 2	Technical delivery conditions, min spec of glass linings and vessels defined
CODAP	French standards, include welding procedures, heat treatment and material flow until delivery of glass-lined devices
Swiss standard	Swiss standards, include welding procedures, heat treatment and material flow until delivery of glass-lined devices

3.27.2.5 Lining Process

The first coat consists of a ground-coat, which is sprayed as the first layer in the form of a wet slip. After drying, it is normally fired at temperatures above 900 °C. The alternative, directly dusting hot parts with dry powder, has diminished completely. After inspection, either a second ground-coat or several cover coats are applied directly. Each coating allows a buildup of ~0.3–0.5 mm of glass, which means that an average of 4–6 coats are required to build up a desired glass thickness of 1.5–2 mm.

Each coat is dried thoroughly and is fired according to a firing program, especially designed for each part. Cover coats are fired between 780 and 850 °C, depending on the size of the part, glass type, and coat number. To avoid thermal-induced stresses within the glass lining, slow cooling is most appropriate for a high standard of quality. Inadequate cooling rates lead to a number of severe defects,[10] which are not accepted by customers.

To avoid any kind of defect, for example, blisters, bubbles, scale, etc., visual inspection and spark testing at 20 kV after each coat reveals the integrity of the coating. To ensure pore-free quality, small defects are ground and refilled with cover coat slip, blisters are ground down to the steel, and, by using special patch grounds in combination with cover coats slips locally, a homogeneous and sound layer of glass can be built up again.

3.27.3 Properties of Glass on Steel

3.27.3.1 Mechanical Properties

With a properly formulated glass and correct firing, the lining withstands stresses up to the elastic limit of steel without breaking. Impacts sufficiently severe to dent steel will probably cause fractures in the lining. The hardness and abrasion-resistance of the lining exceeds the properties of all-glass equipment, and a smooth and easily cleaned surface is produced during firing. The combined effect of mechanical keying of the glass to the metal and the chemical bonding developed between glass and steel results in very high adhesive strength.[11] Thus, at room temperature, the typical bond strength of glass to steel can be greater than 100 MPa, the fracture toughness is $\sim 70\,\mathrm{MPa\,m^{-1/2}}$ and compressive strength reaches 800 MPa.

3.27.3.2 Thermal Properties

The thermal shock resistance of glass-lined equipment, that is, the safe limit of the temperature difference between the glass surface of the vessel and any charge introduced varies to some extent according to general operation conditions. Minimum values are defined in the EN standard 15159-2. To fulfill the requirements of chemically inert industrial enamel, a value of at least 190 °C is required. Modern industrial vitreous enamels are much better and can withstand even sudden temperature changes of 220 °C, on defined standardized test plates.

For reactors, a maximum temperature difference of 140 °C, according to EN 15159-3, is allowed. This value is very close to the thermal shock borderline of steel, where a sudden temperature difference leads to plastic deformation of the steel substrate, causing severe cracking in the glass.

Plant operation temperatures vary nowadays from −150 up to 280 °C, with the maximum operating temperature limited by the corrosivity of the liquid in contact with the enamel. The heat transfer coefficient for heating in glass-lined equipment is of the order of $400\,\mathrm{W\,m^{-2}\,K^{-1}}$ but can be increased by agitation. For cooling, corresponding figures would be[12] $280\,\mathrm{W\,m^{-2}\,K^{-1}}$. The numerical values depend on the thickness of the glass coating, increasing with decreasing glass thickness, and the figures quoted represent the behavior of an average coating of 1.4 mm in thickness.

3.27.3.3 Chemical Properties

The general pattern of chemical durability of glass linings is higher than for all-glass equipment. Water absorption is negligible, chemical resistance is very high to all acids except hydrofluoric acid and at high temperatures and concentrations of phosphoric acid. Attack by water is measurable only with great difficulty, leading to deviations caused largely by quality of the used water. Almost all organic solvents produce no measurable effect, and strong alkaline solutions (e.g., 20 wt% NaOH) are satisfactorily handled up to at least 60 °C; above that temperature, there might be appreciable reaction. For most types of chemicals, corrosion of the enamel can be assessed by measuring the loss in thickness either in weight per unit area and time or by directly calculating thickness loss when exposed to the liquid.[13]

Conditions in service vary widely. Many cold liquids (milk, ketchup, and beverages) have little corrosive action, and the chosen glass lining need not be very acid-resistant. By contrast, very often base chemicals are produced, which need high temperatures and strong inorganic acids often under high pressure for processing; glasses, therefore, have to be extremely chemically resistant. Further needs are high durability against leaching effects. Thus, the modern semiconductor industry asks for impurity concentrations of their products (pigments, LCD crystals) at the ppb level. Only a few of the modern industrial enamels fulfill these exacting requirements. In the life-science industry, normally acid-based reactions are carried out, but cleaning in place (CIP) often requires the use of strong alkaline solutions at high temperatures, so the resistance to caustic attack needs to be much higher than in the past.

3.27.3.4 Testing Methods

Investigations recently carried out on the leaching effects during corrosion tests showed that the time used for running the tests has a significant influence on the achieved results. Excessive time periods lead to an increase in dissolved glass constituents, which then again further hinder corrosion of the glass. This inhibition effect, described by the mass balance equation, is an ongoing process of glass corrosion. New EN standards with drastically increased concentrations of corrosive media and reduced reaction times especially for alkaline testing have overcome these effects and now lead to better and reproducible data.[14] The values hold for both immersion and vapor-phased conditions, depending on the media used (**Table 4**).

The effect of temperature on alkaline corrosion is illustrated by data from Pfaudler.[11] There are various glass compositions in service, and it is important to ensure that the lining is appropriate for the particular process to be carried out. An example of the behavior of two different technical enamels compared with borosilicate and lime glass is shown in **Table 5**. This table gives some resistance data with regard to typical acids and alkalis, all data measured according to EN 14483-1–5.[13,14]

Table 4 The durability of several materials against chemical attack

Material	*Acidic solutions*			*Alkaline solutions*		
	HCl (20%)	*H_2SO_4 (60%)*	*HNO_3 (25%)*	*NaOH (5%)*	*Na_2CO_3 (10%)*	*NH_3 (1%)*
WWG	0.039 (108 °C)	0.1 (160 °C)	0.1 (135 °C)	0.51 (80 °C)	0.10 (56 °C)	0.1 (82 °C)
PPG	0.046 (108 °C)	0.1 (160 °C)	0.1 (135 °C)	0.32 (80 °C)	0.10 (63 °C)	0.1 (92 °C)
Borosilicate glass	0.056 (108 °C)	No data available	No data available	1.2–4.1 (80 °C)	No data available	0.29 (80 °C)
Soda lime glass	0.245 (108 °C)	No data available	No data available	1.57 (80 °C)	No data available	No data available
Hastelloy C4 2.4610	0.51 (62 °C)	0.1 (50 °C)	0.125 (60 °C)	No data available	0.05 (135 °C)	No data available
Stainless steel 1.4571	Dissolves fast	≫10 (100 °C)	0.1 (124 °C)	Stress corrosion cracking	No data available	No data available
Carbon steel 1.0488	Dissolves fast	Dissolves fast	1 (20 °C)	Stress corrosion cracking	2.2 (20 °C)	No data available

The numbers indicate thickness loss in (mm $year^{-1}$).
Data for WWG, PPG, borosilicate, and soda lime glass are from Schäfer,[15] hastelloy from Dechema-Werkstoff Tabelle,[16] stainless and carbon steel from ''Key to Steel'' Handbook.[17]

Table 5 Comparative corrosion tests between borosilicate glass, soda lime glass, and technical enamels

Material (glass or enamel)	*Chemical corrosion tests – comparison of technical enamel and glass*			
	Acid resistivity EN 14483-1 (mm year^{-1})	*Acid resistivity EN 51174 (mm year^{-1})*	*Alkaline resistivity DIN 2743 (mm year^{-1})*	*Alkaline resistivity EN 14483-5 (mm year^{-1})*
	20% HCl, 108 °C, 168 h	20% HCl, 140 °C, 24 h	0.1 M NaOH (0.4%), 80 °C, 24 h	1N NaOH (4%), 80 °C, 48 h
WWG[a]	0.038–0.043	0.20–0.24	0.27–0.3	0.48
PPG[a]	0.046–0 05	0.22	0.13–0.2	0.32–035
Duran 8330	From 0.245 (1 d) to 0.06 (5d)	0.385	0.848–1.615	1.23–4.13
AR glass[b]	0.056	0.313	1.18	1.57

[a]WWG and PPG are trademarks of technical enamels produced by Robbins and Myers Inc.
[b]AR Glass: Sodium–calcium silicate glass (soda lime glass).
Source: Lorentz, *R. Werkst. Korr*. **1982**, *33*, 247.

3.27.3.5 Surface Properties

For several applications, the smoothness of the glass surface is the most important factor, making glass more attractive than stainless steel vessels, for example. Polymer producers ask for very smooth surfaces with nonstick behavior, thereby improving the cleanability of the enameled reactor walls compared with stainless steel ones. Even if the thermal properties of a glass-lined reactor are worse than those of stainless steel, because of higher sticking rates of polymer particles on stainless steel, glass-lined reactors achieve at least similar performance rates during service.

3.27.3.6 Enamel Behavior in Service

Enamels, although resistant to many alkalis, are not necessarily completely resistant. Thus, weight loss from enameled iron test pieces has been related to resistance to detergent attacks, but field assessment of the effect of alkaline materials upon enamel does not always agree with accelerated laboratory tests. In such a case, the fitting of a glass-lined test piece into the vessel is required. The production test can last for several weeks, allowing a realistic calculation of the durability of the glass. Often, large differences between enamels occur depending on their chemical composition. Often, also minor changes in the production process have a drastic influence and increase on the performance of a glass lining. As an example, addition of caustic soda above 80 °C is often used to neutralize a product.

If the addition is done solely through a nozzle at the upper bottom, no fast mixing between the two liquids occurs, which would corrode the glass within a distinct zone near the edge of the liquid level. By using a dip pipe for the addition of the caustic soda, complete mixing and dilution occurs immediately, drastically reducing the chemical attack and also improving the performance of the process.

3.27.3.7 General Aspects of Glass Enamel Corrosion

Evidence (about the interaction of liquids with glass surfaces) has come from the results of research work in developing corrosion-resistant glass compositions and there is now better understanding of the mode of chemical attack on glass. Reaction on the surface occurs through ion exchange, dissolution, and absorption. Signs of these reactions are a dimming of gloss, thin film interference colors, and surface-roughening on general degradation. In the beginning, the corrosion becomes apparent as a loss of gloss, but there is no direct correlation between gloss and chemical degradation by ongoing attack. Continued penetration of the glass structure by some ions could lead to its decomposition. The thickness of the ion-exchanged surface layer is related to the durability of the glass and initial reactions are rapid.[18,19] An intermediate phase is formed whose structure, thickness, and durability depends on the glass composition as well as the temperature and pH of the attacking/reacting liquid.[20]

The borosilicate glasses on coated steel contain silica and alkali metal oxides and the reactions can be considered as involving silicate networks. Attacks begin as an interaction between silicate lattice ions and protons from the liquid with the consequent leaching of monovalent and divalent ions.

3.27.3.8 Attack by Water

No enamel or glass is thermodynamically stable against attack by water. The durability is caused by

the diffusivity of alkali ions inside the silica network. This can generally be described by a diffusion kinetics and thus follows a $\sqrt{t}$-relationship. Initially, there is the replacement of an alkali ion in the glass by a proton (H) from the water,

$$-\mathrm{Si}-\mathrm{ONa}+\mathrm{HOH}=-\mathrm{Si}-\mathrm{OH}+\mathrm{Na}^{+}+\mathrm{OH}^{-} \quad [1]$$

The released hydroxyl ion shifts the pH of the solution and interacts with the siloxane bond in the vitreous network

$$-\mathrm{Si}-\mathrm{O}-\mathrm{Si}-+\mathrm{OH}^{-}=-\mathrm{Si}-\mathrm{OH}+-\mathrm{Si}-\mathrm{O}^{-} \quad [2]$$

This open oxygen interacts with a water molecule to form dissolved silicic acid

$$-\mathrm{Si}-\mathrm{O}^{-}+2\mathrm{HOH}=\mathrm{H_2SiO_3}+2\mathrm{OH}^{-} \quad [3]$$

The resulting hydroxyl ion is available for further reaction in reaction [2]. As the hydrogen ions replace alkali (R) ions, a surface film forms, which has properties different from the solid glass. This film swells, acting as a barrier to further diffusion of ions into and out of the bulk material, thus inhibiting further attack. If this layer dries out, the thin films produce characteristic, iridescent interference colors. Depending on the chemical durability of the glass, the mechanism of attack varies. Highly chemical-resistant enamels withstand the OH^- attack, and corrosion is mainly caused by ion exchange and proton interaction. This leads to the general equation

$$-\mathrm{Si}-\mathrm{ONa}+\mathrm{HOH}=\mathrm{H_2SiO_4}+\mathrm{Na}^{+}+\mathrm{OH}^{-} \quad [4]$$

3.27.3.9 Attack by Alkaline Solutions

With the migration of alkali ions (R^+) into the leachant, attack is no longer solely by water. If R^+ is sodium, the attack on the glass is

$$-\mathrm{Si}-\mathrm{O}-\mathrm{Si}-+\mathrm{Na}^{+}\mathrm{OH}^{-} = -\mathrm{Si}-\mathrm{OH}+-\mathrm{Si}-\mathrm{O}-\mathrm{Na} \quad [5]$$

Alkaline ions in solution increase the pH with two consequences. The rate of silica extraction increases with rise in pH value above 8–9 and the rate of alkali exchange is reduced. However, as the higher alkalinity favors dissolution of silica, further alkali is released by the lattice. The quantity of alkali extracted can be used as a measure of the resistance of the glass to attack.

3.27.3.10 Attack by Acid

3.27.3.10.1 Mineral acids

The mode of attack with mineral acids is similar to that by water, namely at the site of siloxane bond –Si–O–Si–. Hydrochloric, sulfuric, and nitric acids all attack through similar mechanisms. Phosphoric acid, when almost water-free, is no more corrosive than the other mineral acids. However, diluted phosphoric acid forms polyanionic networks that are good complexing agents and increase the leaching of monovalent and divalent cations from the vitreous network (via the formation of alkaline and alkaline earth silicyl phosphates).

3.27.3.10.2 Organic acids

Some glasses are more prone to attack by organic acids than by other acids with a lower pH value. These acids form complex ions in solution, which increase the glass solubility. Many vitreous enamels contain larger divalent cations in their network, specifically Ca, Sr, and Ba ions reduce ion diffusivity in the lining.

3.27.3.11 Further Possibilities of Corrosive Attack on Glass

3.27.3.11.1 Attack by complex formation

Chelating agents sequester polyvalent cations and, if present in a corrosive liquid, can increase the rate of attack on the glass. The cations Mg^{2+}, Ca^{2+}, Al^{3+}, Zr^{4+}, and Ti^{4+} are known to stabilize the siliceous surface film and so aid corrosion resistance, but in the presence of say, ethylenediaminetetraacetic acid (EDTA), with which these ions interact, this protective action is increasingly nullified as the ions are removed from the silicate surface. Complexes are formed between Si^{4+} and some organic acids, notably gallic acid and tannic acid.

3.27.3.11.2 Attack by fluorides

All silicates are severely attacked by hydrofluoric acid and its constituents with F^- ion acting as a catalyst. Only the form of the silica network influences to some extent the reaction rate.

$$(\mathrm{SiO_2})_{\text{glass lining}}+6\mathrm{HF}=\mathrm{H_2SiF_6}+\mathrm{H_2O} \quad [6]$$

$$\mathrm{H_2SiF_6}+\mathrm{H_2O}=(\mathrm{SiO_2})_{\text{dissolved}}+6\mathrm{HF} \quad [7]$$

Although neutralization reduces the rate of fluoride attack, no inhibition of this process is so far known.

3.27.3.12 Inhibition of Corrosion Attack

The reaction routes of chemical attack aforementioned also open the possibility for inhibiting the attack on glass by altering the chemical equilibrium to favor the reactant (glass) side of the equations. Thus, appropriate chemical additions can reduce the glass dissolution rate considerably. This holds especially for attack of protons on glass where the addition of dissolved SiO_2 into the process fluid shifts the equilibrium constant towards a higher stability of the vitreous glass matrix. Formally, reaction [8] is used to calculate the amount of dissolved SiO_2 necessary to stabilize the lining.

$$\begin{aligned} &\mathrm{Na-O-Si-ONa} + 2\mathrm{HOH} \\ &= \mathrm{H_2SiO_3} + 2(\mathrm{Na^+} + \mathrm{OH^-}) \end{aligned} \quad [8]$$

Equilibrium is achieved when the dissolution concentration of the main constituent SiO_2 reaches saturation level. $[H_2SiO_3]_{diss}$ describes the amount of dissolved SiO_2, $[Na_2SiO_3]_{glass}$ stands for the glass matrix containing alkaline ions.

$$K = \frac{[\mathrm{H_2SiO_4}]_{diss}[\mathrm{NaOH}]^2}{[\mathrm{Na_2SiO_4}]_{glass}[\mathrm{H_2O^2}]} \quad [9]$$

The addition of a small amount (normally 100–300 ppm) of SiO_2, according to eqn [9], shifts the equilibrium towards the reactant side and therefore hinders glass corrosion.

3.27.3.13 Effect of Leaching – Temperature Dependence

The quantity of alkali extracted from a glass matrix in a fixed time increases with increasing temperature. Depending on the composition of the glass coating and the alkali present (ions of different size behave differently) the amount leached approximately doubles for each 10 °C rise in temperature. This temperature dependence can be expressed by the equation (Arrhenius):

$$A = B\exp(-\Delta E/RT) \quad [10]$$

where A is the specific reaction rate changing with temperature, B is a constant, R is the gas constant, T is the absolute temperature, and ΔE the activation energy for the process of alkali removal from the glass. Alkali extraction is always associated with changes in pH and such changes depend on the quantities of alkali and silica released. For details, see the mechanism of water attack. Where glass linings are exposed to water or steam at temperatures above 160 °C and/or at extreme pH values, the plant manufacturers should be consulted.

3.27.4 Damage Monitoring and Analysis

3.27.4.1 *In Situ* Sensing Technology

Glass damage or corrosion may be monitored by applying a low voltage to the coated metallic substrate and recording the resulting current, which must necessarily flow from any damaged parts of the coating that significantly expose the metallic substrate. Provided that a history of the plant process and the type of insulating material used on the equipment installed is known, this can provide a record of the percentage of damaged (or unharmed) coating. Three methods are used to monitor glass defects, which have no need of additional installed test samples: Low DC voltage method that measures the overall ohmic resistance of a vessel[21]; electrochemical noise analysis that records and analyses the frequency-dependant noise spectrum of a vessel[22]; potentiometric decomposition analysis that measures the electrochemical potential of steel in a conductive solution.[23,24]

All three methods require at least some electrical conductivity of the solution, and all use the vessel (i.e., metallic substrate) as one of the working electrodes.

1. Simple voltage–current measurements are restricted by the specific conductivity of the liquid (must be high enough – works normally in all water-based liquids) and all installed parts demonstrate insulating behavior. A defect is recorded if the current exceeds a previously defined level. The method can lead to a large number of false alarms and, as such, is often not so useful (with the monitoring equipment being shut down).

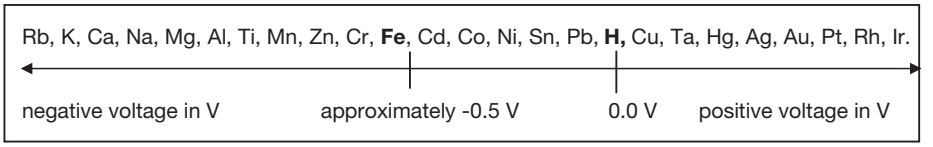

2. Electrochemical noise analysis records the frequency spectrum (from mHz up to a few kHz) on the sample and looks for deviations from historic records that can indicate ongoing corrosion. However, the noise spectrum can often change drastically depending on the process conditions where this does not imply defect formation. Interpretation is thus quite difficult and automatic computation does not work well. Often the onset of corrosion is unseen or misinterpreted.
3. The potentiometric decomposition analysis overcomes these limitations. Recent developments allow the monitoring of glass defects also if metal parts such as nickel-based inlet tubes or graphite-filled polytetrafluorethylene (PTFE) linings or metal-based distillation columns are used. The method is based on the EMF build-up by an electrochemical cell. It makes use of the specific electrochemical potential of each element which is unique among all types of solutions and compositions, pH values, or temperatures.

The potentiometric method is based on the definition of electrochemical potentials, where the zero point is defined as the standard hydrogen electrode of potential equal to 0 V at 25 °C at 1 bar pressure of hydrogen and a solution that is 1 molar in proton concentration. Noble metals produce positive potentials, base metals negative ones.

Advantages of the method include ease of adjustment to a computer-based monitoring system, short time cycles (within minutes), and relative lack of dependence on changes in pH, temperature, or composition of the solutions.

3.27.4.2 Repairs to Enamel Damage

Repair cements are quite satisfactory and economical for mild chemical service over lengthy periods. For severe chemical service, enameled areas up to 120 mm in diameter can be repaired by specialists with tantalum plugs, discs, and PTFE gaskets. These materials have a similar chemical resistance to that of glass. Larger areas of damage or corrosion need special glass-lined plates (covers) fixed with several studs and cement.

Complete reenameling of equipment is feasible, but is often accompanied by a microstructural changes in the metal, and for this reason, it is limited to 4–5 times. With each reenameling distortion becomes larger and the process may consequently be uneconomical. For this reason, a complete inspection of a vessel is required to allow a decision as to whether reenameling or a new vessel is the more economical alternative.

3.27.4.3 Recent Developments

The traditional method of producing glass-lined vessels involves stages of annealing, degreasing, shot blasting, acid pickling, followed by application of up to two ground coats and five cover coats, each with a separate firing. Tighter legislation and higher energy costs have lead to the development of processes in which one or more of these stages may be omitted. These advances are achieved through greater understanding and control of glass composition, and by adopting more sophisticated powder-handling techniques. This includes statistical methods of running a vessel mixture of various shapes, dimensions, and different coats-to-finish in one furnace run.

The more demanding the requirements of customers using enameled vessels for their production, the finer the resolution of analytical instruments being developed and the lower the permitted amounts of dissolved glass constituents in the products. These implications are requested especially by life-science companies and the semiconductor industry, as they call for decreases in the allowed level of leached impurities to almost 1 ppb. Mainly, impurity levels of transition metal oxides reduce the yield of product drastically, making it impossible to produce them in the qualities demanded. Typical examples are enantioselective oxidation reactions of proteins, manufacturing of LCD crystals, and photoresistant chemicals for the chip industry. This has led to the development of new enamels that consists only of biologically nontoxic metal oxides and that therefore remove CoO, NiO, MnO, Fe_2O_3, SnO_2, ZnO, Cr_2O_3, SrO, and BaO from the glass compositions.

References

1. DGRL 97/23/EG.
2. ASME R, ASME Boiler and Pressure Vessel Code, R – Stamp.
3. EN 10028-1: Flat products made of steel for pressure purposes – general requirements.
4. EN 15711: Vitreous and porcelain enamels – glass lined flanged steel pipes and flanged steel fittings – quality requirements.
5. EN10209: Cold rolled low carbon steel flat products for vitreous enamelling – technical delivery conditions.
6. EN 12536: Welding consumables – rods for gas welding of nonalloy and creep resisting steels.
7. EN ISO 15607_2004-03: Specification and approval of welding procedures for metallic materials Part 1: General rules for fusion welding.
8. EN287-1: Qualification test of welders – fusion welding.
9. EN 15159-1: Vitreous and porcelain enamels – glass lined apparatus for process plants – quality requirements.

10. EN 51176-1: Vitreous and porcelain enamels – presentation and characterization of defects Part 1: Enamels for chemical service and vessels.
11. Pfaudler glass linings **614-1e**, Pfaudler Werke GmbH, D-68723 Schwetzingen, Germany, 2007.
12. Reinemuth, J.; Heinzmann, M. *CIT* **2007**, *79*, 53–67.
13. EN 14483-1: Vitreous and porcelain enamels – determination of resistance to chemical corrosion Part 1.
14. EN 14483-5: Vitreous and porcelain enamels – determination of resistance to chemical corrosion Part 5.
15. Schäfer, G. *Mitt. DEV* **2004**, *6*, 90–95.
16. Dechema-Werkstoff Tabelle DECHEMA e.V. Theodor-Heuss-Allee 25, D-60486 Frankfurt am Main.
17. ''Key to Steel'' Handbook, Verlag Stahlschlüssel Wegst GmbH Theodor-Heuss-Str 36, 71672 Marbach a.N., 2001.
18. Lorentz, R. *Werkst. Korr.* **1982**, *33*, 247.
19. Petzold, Pöschmann: Email und Emailliertechnik, Deutscher Verlag für Grundstoffindustrie, 2. Auflage 1992.
20. Gesche, G. *Mitt. VDEfa* **1958**, *6*, 101.
21. Bard, A. J.; Faulkner, L. R. *Electrochemical Methods*; John Wiley, 1980.
22. Göllner, J.; Burkert, A. *Mater. Corros.* **1998**, *49*, 614.
23. Harrison, J. A.; Thirsk, H. R. *Electroanalyt. Chem.* **1971**, *5*, 67–148.
24. Trampert, R. *CAV* **2007**, *3*, 34.

3.28 Degradation of Vitreous Enamel Coatings

T. Curtis
Research and Development Director, Escol Products Ltd, UK

This article is a revision of the Third Edition article 16.1 by N. S. C. Millar and C. Wilson, volume 2, pp 16:3–16:12,

Glossary

Frit A complex of oxides of boron and silicon with alkali and transition metals forming a glass that is suitable for fusing onto a metal, thus forming a vitreous enamel coating.

3.28.1 Nature of Vitreous Enamels

A vitreous enamel coating is, as the name implies, a coating of a glassy substance which has been fused onto the basis metal to give a tightly adherent hard finish, resistant to many abrasive and corrosive materials. The purpose of modern vitreous enamels is twofold, that is, to confer corrosion protection to the metal substrate and at the same time provide permanent color, gloss, and other aesthetic values.

Most of the corrosion resistance, and indeed other properties of the finish, are determined by the composition of the vitreous enameller's raw material *frit*, although other factors can influence them to a minor degree. Frit, for application to sheet and cast iron, is essentially a complex alkali-metal alumino borosilicate and is prepared by smelting together an intimate mixture of refractory materials such as silica, titania, felspar, china clay, etc. at temperatures between 1100 and 1450°C with fluxes exemplified by borax, sodium silicofluoride and nitrates and carbonates of lithium, sodium and potassium. Smelting continues until all the solid matter has inter-reacted to form a molten mass; but unlike true glass, this liquid does contain a degree of bubbles. At this stage the melt is quenched rapidly by either pouring it into water or between water-cooled steel rollers to form 'frit' or 'flake.'

Frit may be milled dry or wet. The long established dry process is used for cast iron baths and for chemical plants. Where possible the preferred process for vitreous enamel application today is dry electrostatic. The frit is milled with low level additions of refractory and/or inorganic pigments together with typically 0.3–0.4% of a silicone. The silicone imparts the required electrical characteristics to the ground frit to enable efficient application of the powder to the metal substrate. This is achieved in cylinders using balls of porcelain, steatite or denser alumina, or with pebbles of flint, to produce a fine powder of predetermined size.

In the more common wet process, frit is milled with water, colloidal clay, opacifier, coloring oxide, refractory and various electrolytes in a ball mill to a closely controlled fineness or coarseness.

Typical frit and mill formulae are given in Table 1. Frits are tailor-made for each application so that the most desired properties are at their maximum in each case and the formulae thus presented must be regarded as examples of general composition.

3.28.2 Metal and Metal Preparation

To obtain a defect-free finish, it is essential that the basis metal is of the correct composition and suitably cleaned.

3.28.2.1 Cast Iron

For cast iron enameling the so-called grey iron is preferred. Its composition varies somewhat, depending upon type and thickness of casting, but falls within the following limits: 3.25–3.60% total C, 2.80–3.20% graphitic C, 2.25–3.00% Si, 0.45–0.65% Mn, 0.60–0.95% P, and 0.05–0.10% S.

The standard method of cleaning cast iron for enameling is by grit or shot blasting, which may be preceded by an annealing operation.

3.28.2.2 Steel

Two general types of sheet steel are in current use, *viz.* cold-rolled mild steel and decarburized steel. A typical analysis for cold-rolled steel is 0.1% C, 0.5% Mn, and 0.04% S. It can be obtained in regular, deep drawing or extra-deep drawing grades. This type of steel is normally used with a ground coat including cobalt and nickel, as shown in Table 1.

Decarburized steel is mild steel that has undergone heat treatment in a controlled atmosphere to reduce carbon content to about 0.005%. White or coloured enamel can then be applied directly to this type of steel without the need for a ground coat layer.

Sheet steel is normally prepared for application of enamel by a sequence of operations including thorough degreasing, acid pickling, and neutralization. A nickel

Table 1 Typical enamel frit compositions (%) and a mill addition

	Chemical plant	*Sheet-iron (ground coats)*			*Sheet iron (white)*	*Sheet iron (acid resistant black)*	*Cast iron (semi-opaque)*
Na_2O	15.8	17.5	21.8	16.0	7.0	16.0	17.5
K_2O	–	–	–	–	5.0	–	3.0
Li_2O	–	–	–	–	1.0	1.0	–
CaO	1.2	–	–	–	–	3.0	–
BaO	–	–	–	5.5	–	6.0	–
CaF_2	3.4	6.0	5.5	4.0	–	2.0	2.0
Na_2SiF_6	–	–	–	–	5.5	2.0	–
Al_2O_3	2.9	5.0	9.0	1.0	2.5	1.0	4.5
B_2O_3	0.9	20.0	18.2	25.0	15.0	7.0	7.5
SiO_2	60.0	50.0	44.0	47.0	46.0	53.0	43.5
TiO_2	15.8	–	–	–	18.0	8.0	13.5
CoO	–	0.4	0.3	0.5	–	0.4	–
NiO	–	0.5	0.6	0.5	–	0.6	–
MnO	–	0.6	0.6	0.5	–	–	–
Sb_2O_5	–	–	–	–	–	–	8.5
	100.0	100.0	100.0	100.0	100.0	100.0	100.0

Sheet iron white mill addition

Frit	100	Grind to fineness of 1 g residue on 200 mesh sieve (50 ml sample)
Water	35–40	
Titania	1	
Clay	2.5	
Bentonite	0.3	
Sodium nitrite	0.05	
Potassium carbonate	0.1	

dip stage is often included to deposit a thin, porous layer of nickel applied at about $1\,g\,m^{-2}$, especially when the conventional ground coat is not used.

3.28.2.3 Enamel Bonding

For effective performance, the enamel must be firmly bonded to the underlying metal and this bond must persist during use. The bond is formed by the molten enamel flowing into 'pits' in the metal, that is, mechanical adhesion, and by solution of the metal in the glass, that is, chemical adhesion. The coefficient of thermal expansion of the enamel in relation to the cast iron or sheet steel and enamel setting temperature determines the stress set up in the coating. As enamel, like glass, is strongest under compression, its thermal expansion should be slightly less than the metal.

3.28.2.4 Enamel Application and Fusion

Vitreous enamel is normally applied to the prepared metal or over a ground coat by spraying or dipping. Alternative wet techniques are used, of which the most common has been electrostatic wet spraying. Electrophoretic deposition from slurry has been found to be highly suitable for some components.

On sheet iron, a ground coat including cobalt and nickel, is generally used, but for mass production (e.g., cookers) use of decarbonized steel and direct application of colors is more common. This involves more complex steel pretreatment.

After drying the applied slurry, the enamel is fused onto sheet steel at about 800–850 °C for about 4–5 min. For cast iron, a longer time and lower temperature are normal.

The old dry process enameling of cast iron (baths etc.) is no longer widely used. The method consisted of sieving finely powdered frit onto preheated casting and inserting it back into a furnace at about 900 °C to produce the smooth finish.

In recent years increasing use has been made of the electrostatic application of a dry powder spray by many manufacturers, who require a limited range of colors. Dry electrostatic finishes are fused at temperatures in the same range as conventional ones.

3.28.3 Properties of Enamel Coatings Affecting Corrosion

3.28.3.1 Mechanical Properties

This group includes surface hardness, that is, scratch and abrasion resistance, adhesion and resistance to chipping, crazing, and impact. All these and other properties depend upon adhesion between the vitreous enamel layer and the metal being good and remaining so.

There is no single test that will give a quantitative assessment of adhesion; all those which have been proposed cause destruction of the test plan. It has already been stated that this property is dependent upon mechanical and chemical bonds between enamel and metal. One must, however, also consider stresses set up at the interface and within the glass itself during cooling after fusion or after a delay.

The coefficient of thermal expansion is primarily determined by frit composition, although mill additions can have a minor influence. As a general rule, superior acid and thermal shock resistance are obtained with low expansion enamel, and the skill of the frit manufacturer is in obtaining good resistance and maintaining a sufficiently high expansion to prevent distortion of the component (pressing or casting). Several workers have produced a set of factors for expansion in relation to the enamel oxides that constitute the frit, which provides a guide to the frit producer. However, as these factors are derived from a study of relatively simple glasses smelted to homogeneity, it must be emphasized that they are only a guide. The effect of substituting certain oxides for others in standard titanium superopaque enamel is given in Table 2. The use of a nickel dip improves adhesion by minimizing iron oxide formation, but it should be noted that some iron oxide formation is necessary to produce enamel/metal adhesion. In the most common methods of testing for adherence to sheet iron, the coated metal is distorted by bending, twisting, or impacting under a falling weight. In the worst cases the enamel is removed leaving the metal bright and shiny, but in all others a dark-colored coating remains with slivers of fractured enamel adhering to a greater or lesser degree. With cast

Table 2 Effect of frit ingredients on enamel expansion

Constituent varied	*Expansion change*
Increase alkali metal	Increase
Replace Na_2O by Li_2O	Increase
Replace Na_2O by K_2O	Decrease
Increase fluorine	Decrease
Increase B_2O_3	Decrease
Replace SiO_2 by TiO_2	Increase
Increase TiO_2	Slight increase
Replace SiO_2 by Al_2O_3	Slight increase
Introduce P_2O_5	Slight increase
Introduce BaO	Increase
Increase SiO_2	Decrease

iron enameling it is not possible to distort the metal and in this case an assessment of adhesion is obtained by dropping a weight on to the enamel surface and examining for fractures. Erroneous results can be obtained in that often thicker enamel coatings appear to be better bonded and resistant to impact, whereas in fact the converse is true. Provided the bond is adequate, this test really gives an indication of the strength of the enamel itself.

According to Andrews[1] a typical sheet iron ground coat has a tensile strength of about 10 kg mm^{-2}. In small cross-sections, however, the tensile strength of glass is improved and fine threads, for example, as in glass fiber, are quite strong. Enamels under compression are 15–20 times stronger than an equal thickness under tension.

The hardness of an enamel surface is an important property for such items as enameled sink units, domestic appliances, and washing machine tubs which have to withstand abrasive action of buttons, etc. On Moh's scale, most enamels have a hardness of up to 6 (orthoclase). There are two types of hardness of importance to users of enamel, *viz.* surface and subsurface. The former is more important for domestic uses when one considers the scratching action of cutlery, pans, etc. whereas subsurface hardness is the prime factor in prolonging the life of enameled scoops, buckets, etc. in such applications as elevators or conveyors of coal and other minerals.

Of the several methods of measuring this property, those specified by the Porcelain Enamel Institute and the Institute of Vitreous Enamellers are the best known and most reliable. Both consist of abrading a weighed enamel panel with standard silica or other abrasive suspended in water and kept moving on an oscillating table with stainless steel balls. The loss in weight is measured periodically and a graph of time versus weight loss indicates both the surface and subsurface abrasion resistance. Pedder[2] has quoted relative weight loss figures for different types of enamel. They are shown in Table 3.

Fine bubbles uniformly distributed throughout the coat improve elasticity and thus mill additions and under and over firing influence this property. The greatest effect on elasticity is enamel thickness and most developments are aimed at obtaining a satisfactory finish with minimum thickness.

Table 3 Comparison of abrasion resistance of different enamels[a]

Types of enamel	*Average loss in weight (g)*[b]
Acid resisting titania based	56×10^{-4}
Acid resisting non-titania	342×10^{-4}
Antimony white cover coat	582×10^{-4}
High refractory enamel	129×10^{-4}
Plate glass	70×10^{-4}

[a]Data from Pedder.[2]
[b]Overall figure for tests under standardized conditions for each grade of enamel.

3.28.3.2 Thermal Properties

These properties are made use of in many applications ranging from domestic cookers to linings which must withstand heat from jet engines. There is simple heat resistance, that is, the ability of the enamel to protect the underlying metal from prolonged heat and also thermal shock resistance, which is the ability to resist sudden changes in temperature without failure occurring in the coating. These thermal properties depend upon the relative coefficient of thermal expansion of enamel and metal, enamel setting point, adhesion, enamel thickness, and geometry of the shape to which the finish is applied.

It is obvious that adhesion must be good in order to prevent rupture at the enamel/metal interface during heating and cooling. Thick coatings are liable to spall when subjected to thermal change due to the differential strain set up within the enamel layer itself, caused by poor heat conductivity of the glass. Thus again thin coatings are desirable.

Compressive forces on enamel applied to a convex surface are less than when a concave surface is coated, and it is therefore apparent that the sharper the radius of the metal, the weaker the enamel applied to it will be. This fact is also relevant to mechanical damage.

Thermal shock resistance is important for gas cookers, pan supports and hotplates where spillage is liable to occur; but in oven interiors heat resistance is more relevant.

The softening point of conventional cast and sheet iron enamels is about 500 °C, but special compositions are obtainable, which operate successfully at 600 °C. Other more specialized enamels withstand service conditions ranging from being in excess of dull red heat, for example, as obtained in fire backs, to those capable of enduring short exposure to temperatures of around 1000 °C, for example, in jet tubes, after burners, etc.

3.28.3.3 Chemical Resistance

That examples of glass and glazes manufactured many centuries ago still exist is an indication of the

good resistance of such ceramics to abrasion, acids, alkalis, atmosphere, etc.

In this section, chemical resistance will be divided into three parts, *viz.* acid, alkali (including detergents), and water (including atmosphere). Normally enamel is formulated to withstand one of the corrosive agents more specifically than another, although vitreous enamel as a general finish has good 'all round' resistance, with few exceptions such as hydrofluoric acid and fused or hot concentrated solutions of caustic soda or potash.

3.28.3.3.1 Acid resistance

This property is best appreciated when the glass structure is understood. Most enamel frits are complex alkali metal borosilicates and can be visualized as a network of SiO_4 tetrahedra and BO_3 triangular configurations containing alkali metals such as lithium, sodium and potassium or alkaline earth metals, especially calcium and barium, in the network interstices.

Fused silica may be regarded as the ultimate from the acid resistance aspect but because of its high softening point and low thermal expansion, it cannot be applied to a metal in the usual manner. Rupturing or distorting this almost regular SiO_4 lattice makes the structure more fluid. Thus to reduce its softening point B_2O_3 is introduced whereby some of the Si–O bonds are broken and an irregular network is formed. Further distortion of the network is obtained by introducing alkali and alkaline earth metals into the lattice. If fluorine is included in the frit, more bonds are broken; in this case an oxygen atom (–O–) linking two silicon or boron atoms is replaced by a fluorine atom (F–) – which, being monovalent, cannot join two Si or B atoms and hence causes bond rupture. A study of relevant phase diagrams and eutectics proves useful in formulating low firing enamels.

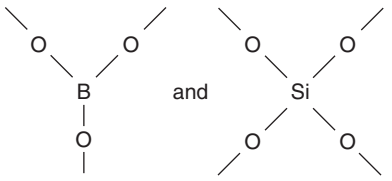

Thus all frit ingredients act as either network formers or modifiers and with the principal exception of silica, titania, and zirconia, all cause diminution in acid resistance. The reacting acid causes an exchange between metal ions in the network modifier of the glass and hydrogen ions from the acid. This naturally occurs at the enamel surface, but as the etching or leaching reaction proceeds, a resulting thin layer of silica-rich material inhibits further reaction. Thus acid attack is dependent upon enamel composition and pH, with time and temperature playing a part. Sodium oxide and boric acid are both leached out by acid attack, and it has been found that the Na_2O/B_2O_3 ratio is constant for any enamel and is dependent upon enamel composition.

An increase in titania content of the frit acts in a similar way to increasing silica in enhancing acid resistance with the added advantage that the coefficient of expansion is also raised slightly and the glass viscosity is not increased as much as by the equivalent SiO_2 increment. This only applies to the titania remaining in solution in the glass and does not necessarily hold when the frit is supersaturated with TiO_2, which occurs with the modern opaque sheet iron covercoats when some of the pigment recrystallizes and causes opacification on cooling from the firing process.

In formulating holloware enamels, the degree of acid resistance required is less than for chemical plant, for example, reaction vessels. Consequently the RO_2 (SiO_2 and TiO_2) is lower, thus permitting increased quantities of fluxes to be fired at lower temperatures and having superior chip resistance. Conversely, chemical plant enamels are higher in silica and dissolved titania and require harder firing. An example of such an enamel is shown in **Table 1**.

The acid resistance required for domestic appliances varies with the particular component, for example, the oven interior of a gas cooker necessitates higher resistance than the outer sides – the former being at least Class A using 2% sulfuric acid while the latter can have a lower grading based on less aggressive citric acid tests. These tests are detailed in EN 14483-1:2004.

The enamel mill addition, degree of firing, and furnace atmosphere all affect acid resistance. An increase in clay and alkaline electrolyte detracts from this property and underfiring also has an adverse effect. The use of organic suspending agents is thus preferable to clays, from this aspect, but other factors must also be considered. Similarly replacement of 1% milling clay by 0.25% of the more colloidal bentonite is beneficial. Large additions of quartz at the mill improve heat resistance, and, provided the firing temperature is increased to dissolve a sufficient quantity of this silica in the glass, acid resistance is also enhanced.

In the glass-bottle industry bottles can be cooled in a dilute SO_2/SO_3 atmosphere to increase chemical resistance. A similar effect has been noted with

vitreous enamel. It has been postulated that a thin layer of –OH groups or $–OH–H_2O$ (hydronium) ions is adsorbed on the surface of fired enamel. These ions are transformed into $–OSO_2$ or $–OSO_3$ in the presence of oxides of sulfur which are more resistant to further acid attack. It is known that the acid resistance of a recently fired enamel improves with ageing, probably due to enamel reaction with SO_2/SO_3 in the atmosphere and it is quite common for the grading to improve from Class A to Class AA (EN 14483-1:2004).

In enamels for chemical plant such as autoclaves, it is not only the degree of acid resistance which is important but also the freedom of the finish from minute flaws detectable by high frequency spark testing or chemical methods. Chemical methods depend upon a color change when the reagent such as ammonium thiocyanate reacts with the iron exposed at the bottom of the pinhole or flaw in the finish. Alternatively, an electric cell can be formed via the exposed iron in the flaw and detected chemically.

In general, strong mineral acids are more severe in their attack on enamel than weak organic acids. Vargin[3] has stated that the severity of action of organic acids on enamel increases with the increase in the dissociation constant of the acid. Temperature plays a major part in acid resistance – the nearer the boiling point the greater the rate of attack. It is more significant than acid concentration.

It is recognized that vitreous enamel possesses good acid resistance, but an exception is hydrofluoric acid. This is due to the relative ease of reaction between this acid and the silica (which is the largest constituent in the frit) to form silicon tetrafluoride. This reaction is made use of in some 'de-enameling' plants.

3.28.3.3.2 Alkali and detergent resistance

The usual method of de-enameling sheet iron is by immersion in fused or hot strong aqueous solutions of caustic soda where the silica network is broken down to form sodium silicate. However, in spite of this fact, enamels are capable of withstanding detergents and mild alkalis and this finish is often used very successfully in washing machines, baths, sink units, etc. where alkaline conditions prevail. Such enamels are usually higher in alumina than acid-resisting enamel and often contains zirconia in the frit. Other elements which aid alkali resistance are barium, calcium, lead, and zinc, and their function in this context is to increase the bond with the essentially silica network and form insoluble silicates which act as a protective coating slowing down the formation of soluble sodium silicate. The necessity for alkali resistance is relatively limited when compared with detergent resistance and it has been shown that while these two properties are similar, a finish resistant to one is not necessarily a resistant to the other.

The Institute of Vitreous Enamellers produced a report on detergent resistance in 1959[5] and the following facts are brought out:

1. Semi-opaque acid-resistant titania enamel and alkali-resistant frit generally have good detergent resistance whereas non-acid-resistant sign enamel and $Al_2O_3/B_2O_3/P_2O_5$-based finishes have poor resistance.
2. Initially, detergent attack is accompanied by a deposit on the enamel surface which can be abraded off resulting in an apparently unaffected glossy appearance. This contrasts with acid attack when a progressive weight loss occurs and original gloss cannot be restored once it has been lost or diminished. After more prolonged detergent attack it is not possible to restore the original high gloss.
3. The rate of attack is very dependent upon temperature. At boiling temperature it is several times greater than that at room temperature.
4. An increase in milling clay has a marked effect on improving this property.
5. Increased detergent concentration, coarser grinding of the frit, and nonstandard firing all cause minor deterioration in resistance.

In the design of an enamel for a washing machine tub, detergent resistance alone is not sufficient and the enamel must also be capable of withstanding the possible abrasive action of buttons, zip fasteners, etc.

3.28.3.3.3 Resistance to water and atmosphere

These properties are of particular importance in enameled signs, architectural panels, cooking utensils, and hospital ware subjected to repeated sterilization. That such enameled signs as 'Stephen's Inks', etc. are still in existence and in good condition after many years of outside exposure coupled with the fact that the use of vitreous enamel as a finish for architectural panels is growing, are ready pointers to the good water and atmospheric resistance of enamel. Enameled hospital utensils such as kidney bowls score over organic finishes because of ease of sterilization and also because they are less accommodating to germs, bacteria, etc. on account of their lower electrostatic type attraction for such microbes.

Action of water on enamel is in many ways similar to that of acids in that the network modifier is the weak link and through hydrolysis can be removed from the glass system resulting in loss of gloss and porous surface. As with acids and alkalis, attack on the glass by water can be continued in extreme cases, by an attack on the inorganic coloring matter initially liberated or made more active. In an enclosed system the soluble salts first leached out from the enamel by water become in turn the corrosive element and further attack is dependent upon the pH of such a salt, or, for example, on the Na_2O/B_2O_3 ratio.

Introduction of divalent calcium and barium oxides into frits in preference to monovalent sodium and potassium generally increases water resistance. Further, oxides of tetravalent and pentavalent metals have a favorable effect on the resistance of glasses and enamel to water. The influence of B_2O_3 and fluorine in the frit on chemical resistance is variable and is dependent upon the content and balance of the frit constituents, but they usually cause diminution in resistance. In general, mill-added clay, silica, and opacifier increase water resistance provided the firing or fusing of the enamel is at the optimum.

As is expected, atmospheric resistance is related to water and the acid formed from CO_2, SO_2, SO_3, etc. The action of ultraviolet light has no apparent effect on vitreous enamel unlike the case with organic finishes.

There is good correlation between atmospheric and acid resistance, and this fact is helpful to manufacturers of architectural panels as they can easily and quickly determine the latter property and do not have to carry out lengthy exposures to relatively unpolluted air. An exception, however, occurs with reds and yellows where strict correlation is not always true, and in these cases a test based upon exposure to a saturated copper sulfate solution under illumination by a white fluorescent light has been advocated.

In the main the comments recorded in this section apply to enamel fused onto sheet and cast iron. Enamel is, however, applied to aluminum, stainless steel, copper, and noble metals on account of its aesthetic value and also to confer durability to the base metal. With low melting point metals such as aluminum it is obvious that superb resistance to chemicals is not as feasible as in the case of iron as the base. Nevertheless, such metals are vitreous enameled in growing quantities and sold, indicating that the range of color and durability obtained is superior to that possible with alternative finishes.

It can justly be claimed that vitreous enamel coating applied to sheet or cast iron (or indeed any other metal) will confer to the basic shape color, gloss, texture, and high degree of resistance to corrosive influences.

References

1. Andrews, A. I. *Porcelain Enamels*; Gerrard Press, Champaign, IL.
2. Pedder, J. W. G. *Inst. Vit. Enam.* **1959**, *9*(9).
3. Vargin, V. V. Ed. *Technology of Enamels*; Maclaren & Sons Ltd., 1967; pp 31, 78.
4. Krauter, J. C.; Kraaijveld, Th. B. *Inst. Vit. Enam.* **1970**, *21*(2).
5. I.V.E. Technical Sub-committee Report, *Bull. Inst. Vit. Enam.* **1960**, *10*, 285.

3.29 Degradation of Ceramic Masonry Linings

D. I. Hughes
Hanson Building Products, Accrington Nori Factory, Accrington, Lancashire BB5 6NR, UK

Abbreviations

ASTM American Society for Testing and Materials
BS British Standard
PTFE Polytetrafluoroethylene
PVDF Polyvinylidene fluoride
PVC Polyvinyl chloride
SSPC Steel Structures Painting Council

3.29.1 Introduction

Ceramic materials have been used for many years as linings to process equipments, chimneys, and chemical resistant flooring. The materials utilized have been both man-made and naturally occurring. By using ceramics, the engineer is employing a material which offers excellent corrosion resistance, abrasion and impact resistance, as well as (generally) an excellent thermal barrier.

Chemical resistant masonry is generally emplaced to act as a barrier to prevent corrosion of a substrate, which is most commonly steel but may also be any suitable structural material such as concrete or glass reinforced plastic. The protection system, therefore, acts effectively as a lining that generally comprises multiple layers supported by a shell (i.e., the substrate) that provides strength and rigidity. The lining system that prevents corrosive chemicals from reaching the shell generally consists of a membrane and one or more layers of chemical resistant bricks, bonded with a chemical resistant mortar. The three products used in chemical resistant construction are therefore:

1. chemically inert ceramic products such as brick, stone or blocks,
2. chemically resistant mortars,
3. chemically resistant membranes

Traditional ceramic materials are usually derived from clays and are thus based on silicate/silica chemistry. They can be classified into structural ceramics, such as pottery, porcelain, refractories, glasses, etc.; and inorganic binders such as cements, gypsum, etc. Most of these materials consist of crystallographic grains of one or more phases that are bound together by another phase that is commonly glassy and melts at the sintering temperature for the material.

That corrosion/degradation of ceramics and glasses does occur is incontrovertible. However, it is important to remember that, unlike in metals, it is a chemical dissolution process and not an electrochemical process. Thus, the dominant controlling mechanisms for the degradation of ceramic materials are the rate of the surface chemical reactions and the rate of diffusion of reacting species to and from the surface.

3.29.2 Ceramic Masonry Linings

3.29.2.1 Chemically Resistant Bricks

3.29.2.1.1 Acid-resistant brick

The man-made chemical resistant ceramic products generally offered are of two types, categorized by the raw materials from which they were manufactured:

- red shale acid-resistant products
- fireclay acid-resistant products

These products, often referred to as 'acid brick,' are visually identified by their respective colors of red and off-white. Historically the red shale products have been favored by British and North American manufacturers. The fire clay products are manufactured often as a refractory by-product. Their properties are dependant upon the structure of the raw material and the manufacturing methods. Both products are manufactured from clays containing low levels of acid soluble components. By firing at relatively high temperatures and by prolonging the firing time these products become partially vitrified throughout the entire body of the brick. This produces a strong brick with low water absorption, which is practically chemically inert (Table 1).

The performance of these ceramic products is very similar although differences exist due to their relative density and porosity. The red shale product being a highly vitrified dense bodied ceramic is excellent in applications covering a wide range of acid concentrations and temperatures. Red shale bricks have a surface porosity of practically zero percent, preventing penetration of chemicals into the body of the ceramic avoiding chemical spalling. The fireclay materials that have lower levels of flux within the clay generally fire to lower degrees of vitrification and hence exhibit higher porosity. As a result fireclay bricks unfortunately are susceptible to chemical spalling, as their relatively high porosity extends throughout the body of the brick. Chemical spalling is the

Table 1 Typical physical properties of red shale and fireclay bricks

Property	*Test method*	*Red shale*	*Fireclay*
Density (Mg cm^{-3})	ASTM C 20	2.45	2.15
Water absorption (%)	ASTM C 20	2	5
Apparent porosity (%)	ASTM C 20	5	11
Cold crushing strength (MPa)	ASTM C 133	>150	>80
Acid solubility (%)	ASTM C 279	7	6
Thermal spalling (no. of cycles at 450 °C)	DIN 51068	5	10

result of crystallization of salts that have penetrated the brick. The crystal growth weakens the structure of the brick causing it to fracture. The thermal spalling resistance of red shale is lower than that of the fireclay product. The fireclay products being more open bodied give improved thermal spalling resistance. They are often used in 'refractory' applications. Thermal spalling is not a problem normally encountered in liquid phases, where temperatures are generally below 150 °C. Due to its low porosity the red shale product usually conforms to the standard Type III in ASTM C 279. The fireclay product is described as meeting Type II in ASTM C 279.

Both products are manufactured in a variety of different shapes. The shapes can be specifically manufactured to suit the complex arrangements often found in chemical reaction vessels. The two products are used in similar applications; the choice between them generally made purely on economic considerations.

3.29.2.1.2 High-density fireclay

This material is similar to the low density fireclay, however, the density is increased to 2.3 $Mg\,m^{-3}$ and the porosity lowered to 5%. As a result the cold crushing strength is improved as is the acid solubility. The somewhat improved performance over the two previously mentioned products is offset by a considerable increase in cost.

3.29.2.1.3 Carbon/graphite

Carbon brick is used in conditions where shock resistance is of prime importance. Due to their much higher porosity and lower coefficients of expansion these materials are capable of withstanding thermal and pressure shock to a much higher degree than those products previously mentioned. Carbon brick can be used to absorb surface stresses in brick linings which would otherwise cause compressive failure of red shale or fireclay bricks. Carbon brick also exhibits resistance to attack by both strong alkali and hydrofluoric acid.

Carbon brick is generally derived either from coking coal or from petroleum coke. The petroleum cokes offer a higher purity containing very low levels of ash. Often clays are used as binding agents during brick manufacture. The nature of the ash and binding agent must be considered when specifying carbon brick types as they will alter the chemical resistance of the brick. In particular the resistance to strong alkali and hydrofluoric acid can be adversely affected by the composition of the ash or binding agent. Carbon brick is generally stable to very high temperatures in the absence of an oxidizing atmosphere. However, in air the temperature limit for carbon brick is 350 °C, above which the carbon brick will be destroyed by oxidation to carbon dioxide (Table 2).

3.29.2.1.4 Silicon carbide

Silicon carbide brick is made from SiC (80–90%) normally nitride bonded with Si_3N_4. This relatively high porosity material gives good thermal spalling resistance along with a general high chemical resistance. The bricks and special shapes made from this product can be used at high temperatures where high abrasion resistance is required (although alumina brick can offer a slightly higher abrasion resistance) (Table 3).

3.29.2.1.5 Foamed glass

Foamed borosilicate glass or aluminosilicate glass is formed into blocks which have zero percent water absorption. This is a highly efficient impermeable insulating material with good chemical resistance to all acids, except hydrofluoric acid. This product cannot be used in the presence of alkali solutions. Foamed glass offers a very good thermal barrier having a particularly low thermal conductivity. Foamed glass blocks are available in a variety of different shapes and grades. The grading of the product is related to its density. Foamed glass blocks can be easily cut with a 'wood' saw. The application of this material is limited by its extremely low crushing strength and abrasion resistance (Table 4).

Table 2 Typical physical properties of carbon bricks

Property	*Petroleum-derived coke*	*Coal-derived coke*
Bulk density ($Mg\,m^{-3}$)	1.50	1.60
Apparent porosity (%)	25	19
Cold crushing strength (MPa)	40	80
Modulus of elasticity (GPa)	12	10
Tensile strength (MPa)	6	7
Coefficient of linear thermal expansion (K^{-1})	3.5×10^{-6}	5.4×10^{-6}
Thermal conductivity (25 °C–400 °C) ($W\,m^{-1}\,K^{-1}$)	4–6	4–4.5
Upper temperature limit (in air) (°C)	350	350
Ash content (%)	<1.0	6.6

Table 3 Typical physical properties of nitride-bonded silicon carbide bricks

Property	*Value*
Bulk density ($Mg\,m^{-3}$)	2.63
Apparent porosity (%)	16
Modulus of rupture (MPa)	38
Cold crushing strength (MPa)	165
Abrasion resistance – BS1902 (cm^3)	30
Thermal conductivity at 200 °C ($W\,m^{-1}\,K^{-1}$)	20

Table 4 Typical physical properties of foamed glass

Property	*Test method*	*Value*
Specific weight (± 10% tolerance)	C165	$0.12\,Mg\,m^{-3}$
Thermal conductivity (± 10%)	C203	$0.038\,W\,m^{-1}\,K^{-1}$
At 0 °C		$0.040\,W\,m^{-1}\,K^{-1}$
At 10 °C		
Compressive strength (average at break point)	C 240-85	700 kPa
Flexural strength	C 303	400 kPa
Flexural modulus of elasticity	C 518	800 MPa
Coefficient of thermal expansion	E 96	$9 \times 10^{-6}\,K^{-1}$
Specific heat	E 136	$0.84\,kJ\,kg^{-1}\,K^{-1}$
Thermal diffusivity	ISO8302	$4.2 \times 10^{-7}\,cm^2\,s^{-1}$

3.29.2.1.6 Alumina

Fine grain, high grade alumina shapes are manufactured from an exceptionally pure, uniformly controlled alpha aluminum oxide and are engineered to be one of the best wear resistant materials available to counteract fine particle abrasion. Preengineering and advanced processing techniques enable the manufacture of alumina products in a variety of geometries from simple to complex shapes. Grid support beams and packing internals for sulfuric acid towers are normally manufactured from high alumina clays (Table 5).

3.29.2.1.7 Porcelain

Similar to high alumina brick, porcelain is an extremely dense material manufactured from high alumina content materials (85%). Its zero water absorption and excellent chemical resistance can be put to use where it is important to maintain product purity. The density of this product generally exceeds $2.45\,Mg\,m^{-3}$.

3.29.2.1.8 Silica

High silica content bricks (>98%) can be used for a wide range of very high concentration acids. Their use must be avoided in the presence of hydrofluoric acid and strong alkali. They are available as both a high density product and also as a low density silica product. The low density product combines excellent chemical resistance with good thermal insulating properties (Table 6).

Table 5 Typical physical properties of sintered alumina

Property	*Value*
Bulk density ($Mg\,m^{-3}$)	2.52
Alumina content (wt%)	>90
Water absorption (%)	0
Gas permeability (%)	0
Compressive strength (GPa)	1.77
Young's modulus (GPa)	270
Thermal conductivity ($W\,m^{-1}\,K^{-1}$)	18
Thermal expansion (K^{-1})	8.30×10^{-6}
Vickers hardness (GPa)	9.00

Table 6 Typical physical properties of silica bricks

Product	*Low density*	*High density*
Bulk density ($Mg\,m^{-3}$)	0.80	1.90
Crushing strength (MPa)	4	51
Modulus of rupture (MPa)	1	15
Thermal conductivity ($W\,m^{-1}\,K^{-1}$)		
At 100 °C	0.175	0.645
At 250 °C	0.195	0.700
At 400 °C	0.215	0.725

3.29.2.1.9 Cast basalt

Basalt rock is quarried, crushed, and then melted and poured into moulds. Extremely complex shapes can be manufactured. This product offers excellent chemical resistance and abrasion resistance. It is used for lining bunkers, hoppers, and chutes carrying abrasive chemicals (Table 7).

3.29.2.1.10 Granite

Granite has been used for centuries as a chemical resistant block. Simply cut to shape from deposits of granite rock this product can be used in a variety of different chemical and abrasion resistant applications. The properties of granite can vary immensely from one source to another. Large shaped granite blocks have found use throughout the steel industry as 'skid blocks' in steel pickling tanks (Table 8).

3.29.2.1.11 Refractory bricks

A large range of refractory bricks are manufactured throughout the world. They are occasionally used in chemical resistant linings acting normally as an

Table 7 Typical physical properties of cast basalt rock

Property	*Value*
Density (Mg m^{-3})	2.9
Mohs hardness	>8
Compressive strength (MPa)	>450
Water absorption (%)	0

Table 8 Typical physical properties of granite block

Property	*Value*
Nominal composition (%)	
SiO_2	>70.0
Al_2O_3	<18.0
K_2O, Na_2O	<10.0
TiO_2	<1.0
Fe_2O_3	<2.0
CaO, MgO	<2.5
Bulk density BS1902 (Mg m^{-3})	>2.40
Water absorption BS3921 (%)	<1
Cold crushing strength ISO 179.3:N12 (MPa)	>200
Modulus of rupture (MPa)	>25

insulating brick behind the 'true' chemical resistant brick. The manufacturers do not list chemical resistance amongst the properties of these products. Their physical properties vary greatly from one product to the other. When designing chemical resistant linings using these products their selection should consider the following points: (1) the type of chemicals likely to contact the product should not damage the product. Higher temperatures can increase the chemical solubility of the product. (2) The compressive stress that the brick will experience must be below the compressive strength of the brick. (3) The thermal conductivity and brick thickness should be as much as needed to give the required temperature drop. The products used most commonly in chemical resistant construction include the following:

Insulating firebricks are manufactured from low iron silica/alumina clays. They have properties of low density and high porosity. Having high porosity makes them unsuitable in applications where total immersion in liquid chemicals is a probable condition. Their temperature range can extend to 1000 °C.

Mullite bricks are manufactured from clays having a preponderance of alumina over silica. Hence, the fired bricks contain little free alumina. The partial vitrification produces a brick offering good chemical resistance and high compressive strength. These bricks can be used in low duty chemical resistant applications when 'acid brick' is not available.

3.29.2.2 Mortars

3.29.2.2.1 Silicate-based mortars

In chemical resistant masonry construction the choice of mortar is determined by the chemical and thermal conditions of the process. Care must be taken when using these mortars, as deviation from the manufacturers mixing instructions and recommendations regarding their use can result in a mortar with poor strength and chemical resistance.

These mortars consist of sodium or potassium silicate liquid mixed with a silica filler. The hardening process is accelerated by the use of a catalyst, for example, polyphosphate, silicofluoride, amines, and lead oxide. The advantage of polyphosphate hardened mortars is a low fluid absorption (2% for sodium polyphosphate). Potassium silicate mortars, utilizing silicofluorides must be washed with weak acid as part of the curing process. This also assists in lowering the fluid absorption.

These mortars have excellent chemical resistance to low and high concentration acids. Their temperature limit is 800 °C. A disadvantage of these mortars is their high porosity >12%. They are not suitable for contact with hydrofluoric acid and alkali solutions. Potassium silicate mortar is the most widely used. The use of sodium silicate mortar has declined due to its relatively high water solubility. With the addition of suitably graded fillers the potassium silicate mortar can be modified to produce a potassium silicate concrete that can be cast in a similar manner to Portland cement (**Table 9**).

3.29.2.2.2 Synthetic and natural resins

Furane resin

Furane resin mortars have found wide popularity in the United Kingdom and North America due to their excellent chemical resistance and ease of use. This is the standard mortar for low sulfuric acid concentration (<70%) applications in vessel linings and flooring. They consist of furane resin liquid mixed with filler. The fillers available are silica, graphite or carbon. The normal filler is silica. For hydrofluoric acid and hot concentrated alkaline conditions carbon filled grades of furane mortar should be used. The carbon filled variety of this mortar is the mortar of choice when bonding carbon brick. The cheaper silica filled furane resin mortar should always be used when bonding acid brick. Furane mortars offer good erosion resistance and a service temperature of up to 200 °C. Some specialist furane mortars can withstand temperatures up to 300 °C (**Table 10**).

Table 9 Typical physical properties of potassium silicate mortar

Property	*Value*
Density ($Mg\,m^{-3}$)	>1.85
Tensile strength (MPa)	3.5
Compressive strength (MPa)	>21
Modulus of rupture (MPa)	10
Coefficient of expansion (K^{-1})	15×10^{-6}
Water absorption (%)	15
Temperature limit (°C)	800
Conformance	ASTM C 466

Table 10 Typical physical properties of silica filled furane mortar

Property	*Value*
Tensile strength (MPa)	4
Compressive strength (MPa)	38
Flexural strength (MPa)	17.5
Bond strength (MPa)	1.5
Density ($Mg\,m^{-3}$)	1.985
Water absorption (%)	0.2
Temperature limit (°C)	200
Conformance	ASTM C 395

Modified phenolic resin

Phenolic mortars offer chemical resistance over a wide range of both acid and alkali conditions. A choice of either carbon or silica based fillers are available. Being phenol based, care must be taken when using these mortars. In recent years the safety precautions required when using this mortar have resulted in a reduction in its use. Graphite filler and a double hardener system permit this mortar to be utilized in prestressing brickwork which places the brick lining in permanent compression. The porosity of these mortars is extremely low. They exhibit a good degree of erosion resistance and have a maximum service temperature of 190 °C (Table 11).

Epoxy resin

Epoxy resin mortars are supplied as a two- or multicomponent system. The chemical resistance of these mortars is good. They can be used to withstand medium strength acid and alkali. They exhibit extremely high bond strength between brick and steel. Epoxy mortars are limited by a maximum temperature of 90 °C. Epoxy resins have found extensive use as monolithic screed coatings for concrete in flooring applications (Table 12).

Table 11 Typical physical properties of phenolic resin mortar

Property	*Value*
Tensile strength (MPa)	3
Compressive strength (MPa)	44
Bond strength (MPa)	1.2
Density ($Mg\,m^{-3}$)	2
Water absorption (%)	0.3
Temperature limit (°C)	190
Conformance	ASTM C 395

Table 12 Typical physical properties of epoxy resin mortar

Property	*Value*
Tensile strength (MPa)	7
Compressive strength (MPa)	52
Bond strength (MPa)	2.0
Density ($Mg\,cm^{-3}$)	2
Water absorption (%)	0.3
Temperature limit (°C)	90
Conformance	ASTM C 395

Polyester resin

This family of mortars includes bisphenols, chlorinated polyester and vinylester based products. These mortars offer good resistance to acid, especially oxidizing acids. They have poor resistance to organic solvents with the exception of acetic acid. Epoxy mortars have better resistance to organic solvents. The bond strength is equivalent to epoxy. The compressive strength of polyester mortar is the highest of all resin based mortars (65 MPa).

3.29.3 Chemically Resistant Membranes

The membrane is the final line in defense for the shell and the first material in the system to be applied during installation. The membrane should, where possible, be impervious. Its selection, however, is often determined by temperature and chemical resistance considerations.

3.29.3.1 Asphalt/epoxy Mastic

A nonrigid material is applied directly to the vessel shell. The degree of flexibility is generally governed by the amount of epoxy and hardener that is used in the mix. Asphalt and bitumen are often used on their own as a membrane for chemical resistant floors.

Table 13 Typical physical properties of PTFE sheet

Property	*Value*
Density ASTM D 792 ($Mg\,m^{-3}$)	2.1–2.2
Water absorption ASTM D 570 (%)	<0.01
Tensile strength ASTM D 638–D 1708 (MPa)	25–30
Elongation ASTM D 638–D 1708 (%)	250–400
Tensile modulus ASTM D 638–D 1708 (MPa)	750
Flexural modulus ASTM D 638–D 1708 (MPa)	44–52
Coefficient of linear expansion ASTM D 696 (K^{-1})	$10–15 \times 10^{-5}$
Thermal conductivity ASTM C177 ($W\,m^{-1}\,K^{-1}$)	0.2–0.45

Table 14 Typical physical properties of Hypalon sheet

Property	*Value*
Breaking strength ASTM D751 (N)	500
Tongue tear ASTM D751 (N)	250
Temperature resistance (high) ASTM D2136 (°C)	160
Water absorption (%)	3.0
Density (for black unreinforced) BS903 ($Mg\,m^{-3}$)	1.6
Thermal expansion coefficient ASTM C864 (K^{-1})	20×10^{-5}
Thermal conductivity ($W\,m^{-1}\,K^{-1}$)	0.11
DC electrical resistivity at 125 °C (Ω cm)	2.3×10^{11}

3.29.3.2 Ceramic Paper/Potassium Silicate

The ceramic paper (high purity chemical resistant paper made from aluminosilicate refractory fibres) is soaked in sodium silicate and pasted onto the substrate in sheets (similar to applying wallpaper), forming an impervious membrane. This membrane is often used in high strength acid applications. Temperature resistance is excellent.

3.29.3.3 Fluorocarbons

Fluorocarbons, such as PTFE and PVDF, offer excellent chemical resistance and thermal resistance up to 250 °C and are applied usually in sheet form. Given their intrinsic 'nonstick' surfaces, their use is limited by the performance of the bonding agent either epoxy or asphaltic mastic. Often the surface of the sheet is 'etched,' to improve bonding. The sheet thickness is often very thin: 0.125 or 0.25 mm (Table 13).

3.29.3.4 Lead

For best performance, this excellent membrane should be homogeneously applied. In service, temperatures must be kept below 70 °C to avoid creep. A lack of personnel with the necessary installation skills has led to a reduction in the use of lead as a membrane.

3.29.3.5 Thermoplastic

Sheets of a thermoplastic material such as Hypalon (chlorosulfonated polyethylene) may be applied to the shell with adhesive. Being a thermoplastic material the joints may be welded and the sheets are often reinforced with a polyester scrim. This membrane is nonrigid and has an upper limit of sulfuric acid concentration of 70%. It may be used as a membrane for both vessel and flooring applications (Table 14).

3.29.3.6 Glass Fiber Reinforced Resins

These are rigid membranes. The glass fiber reinforces furane, phenolic, or epoxy based compounds to reduce the susceptibility to hairline cracks.

3.29.3.7 Rubber

Either hard or soft rubbers, both natural and synthetic can be used as membranes behind acid bricks. They are not suitable for high acid concentrations and have temperature limitations of 90 °C. Petroleum products can damage butyl rubber. PVC can be used in the presence of oxidizing chemicals. There are numerous types of rubber available; the most popular being bromobutyl, chlorobutyl, and neoprene. These products are often combined to produce calendered sheets which are frequently used to protect steel substrates. A bromobutyl/neoprene rubber sheet membrane (neoprene as the backing sheet to give improved bond strength) has found great success in lining vessels for the metallurgical industry (Table 15).

3.29.4 Design and Construction of Ceramic Masonry Linings

Ceramic masonry lining systems are utilized extensively to prevent corrosion of vessel shell materials, chimney shell materials and concrete floors. This is an extremely complex subject which cannot be effectively dealt with in this publication. The following guidelines will be of use to the engineer involved in the design of ceramic masonry corrosion resistant linings. The engineer is recommended to approach

Table 15 Typical physical properties of BIIR/CR rubber sheet

Property	*Value*
Tensile strength (MPa)	≥ 7
Elongation at break (%)	≥ 350
Hardness (Shore A)	50 ± 5
Rebound resilience (%)	≥ 10
Abrasion (mm^3)	< 225
Density ($Mg\,cm^{-3}$)	1.26 ± 0.02
Bonding strength on steel ($N\,mm^{-1}$)	> 4
Electrical resistance (Ω)	> 108
Test voltage	> 10
Max. continuous operating temperature (°C)	< 90
Thermal conductivity ($W\,m^{-1}\,K^{-1}$)	0.28

the ceramic product manufacturer, the membrane manufacturer, the mortar manufacturer and the specialist installer for advice regarding ceramic lining design.

3.29.4.1 Vessel Linings

A multitude of different structures may require lining after specification. The most important fact to be remembered when designing ceramic lined structures is that the most likely form of failure is tension or shear. Ceramic lined units must, therefore, be designed to make the most of the excellent properties of compressive *strength* shown in ceramics and avoid possible tensile failure of the lining.

General process parameters will determine the type of mortar, membrane and ceramic material to be utilized. Once these have been specified the thickness and number of layers of brick must be determined. Temperature gradients must be calculated in order to check the membrane and substrate temperatures thus avoiding excursions beyond material performance limits. Stress–strain calculations can be performed to determine the structural integrity of the lining system.

Vessels are generally cylindrical, offering curved surfaces to be brick lined. This is an ideal situation, provided the thermal expansion of the shell is kept under control when the brickwork will be placed into compression during operation. Circular bricks should be used against curved surfaces. The use of thin tiles as backing courses and square bricks on tapered joints is not recommended due to the difficulty of transferring the stress evenly. This 'cheap' design which has been adopted recently by some manufacturers/installers is prone to movement resulting in shear which causes cracking of the mortar joints and tiles.

The bases of vessels are often flat. A superior base design is a dished base lined with at least two layers of brick, generally radial end arch bricks installed in concentric circles or radial stretchers installed in a cruciform arrangement. If a flat base is a necessity then multiple layers of bricks must be utilized if lifting of the lining is to be avoided.

Great care must be taken in designing the ceramic brick elements used in forming nozzles and manholes. The use of special shaped ceramic units for this application is highly recommended. Forming nozzles by cutting standard bricks during installation can only be successful provided an extremely skilled craftsman performs the work.

A number of specialist vessels may require supports for packed beds. Due to their excellent corrosion resistance ceramic products are utilized to form support structures for tower packing in sulfuric acid plant drying and absorption towers. Two designs are currently available:

(i) support wall and beams
(ii) self supporting dome

The first method has an extremely successful track record. The use of the self supporting dome, however, has led to gas channeling at a number of installations, especially on larger diameter towers. The ceramic product is a most effective product for this structure. The design choice is left with the engineer.

To optimize the corrosion resistance of the lining it is essential that the ceramic masonry lining is installed by experts following strict guidelines issued by the manufacturers of the lining components. The guides will cover a number of important areas, including vessel shell construction and preparation, material storage, mixing of products, installation technique for the membrane, mortar and brick, the curing process and inspection. The following general guide is the basis for all ceramic masonry lining systems.

3.29.4.1.1 Fabrication of suitable steel vessels

All welded joints shall be continuous and ground smooth to a minimum of 3 mm radius for convex corners and to a minimum of 6 mm radius for concave corners. All surfaces shall be free of weld splatter of foreign material. Voids, gaps, holes, pockets, or undercut welds are not permitted. Vessels should be fabricated to an appropriate constructional code, for example: PD5500 (UK), GOST (Russia), ASME VIII (USA), AD2000 (Germany), ODAP2000 (France).

3.29.4.1.2 Storage of materials

Where possible, all materials to be used in the brick lining shall be stored in such areas and under such cover as to prevent water from entering any of the packages or from soaking the brick. In addition, for 16–24 h before use, all materials shall be maintained at temperatures not below 16 °C (in cold weather) or above 32 °C (in hot weather). If the materials have become damp (e.g., during transportation) then they must be thoroughly dried with blown dry air before use.

3.29.4.1.3 Surface preparation

Prior to applying the membrane, the contractor shall prepare the surface to be lined in accordance with SSPC-SP10 or SA 2½; blast cleaning should be carried out using silica grit to ensure that the surface is free of all rust and foreign matter. Following cleaning, all dust and silica shall be removed. The surfaces to be lined shall be fully dry and, if necessary, dried to achieve this.

3.29.4.1.4 Application of a membrane

The membrane must be applied before the steel surface develops a visible rust film. Any rusted surface must be cleaned again. Spot cleaning may be done by wire brushing followed by solvent cleaning. The membrane is installed in accordance with the manufacturer's recommendations. For sheet rubber membranes, this operation may require specialist rubber lining labor.

3.29.4.1.5 Mortar

The mortar shall be mechanically mixed in the ratio quoted on the manufacturer's specification sheet. No water or other foreign matter or unauthorized fillers, extenders or fluids shall be added to the mix. Mixing equipment shall be clean at the start of mixing and all surplus or unused mortar shall be removed between batches to prevent excessive inter-batch contamination and retempering of spent mortar.

In general, the mortar shall be completely free of lumps, dried mortar particles and foreign material. The mortar shall be capable of being spread uniformly over a brick surface without dragging. When the set of the mortar has advanced to the point that it will no longer wet the brick properly, no more of that batch shall be used and the balance shall be discarded.

3.29.4.1.6 Brick laying

All cutting of brick shall be done with a brick saw outside the vessels to prevent chips and small particles from falling on the membrane backing. After cutting, all brick shall be fully air dried, wiped with an absorbent cloth and mortared into position when dry.

All joints shall be full and tight, the brick double buttered (i.e., all brick surfaces in mortar joints or against vessel membrane shall be buttered on both surfaces) and pressed firmly in place. All bricks shall be laid with a sliding motion to eliminate the possibility of air pockets and shall be firmly pressed into place and tapped until all surplus mortar is forced out of joints. Any excess mortar must be cut off cleanly with a trowel before initial set takes place. This mortar may be used to butter brick surfaces. Excessive waste of mortar must be avoided.

Large joints are unacceptable. The mason should aim for 3–4 mm joints. The width of mortar will be checked by an inspector. The top surface of brick shall not be coated with mortar until the next course of brick is placed. At the start of brickwork each day, all surplus mortar projecting from end joints of brickwork laid on the previous day shall be struck off the area on which the new brickwork is to be applied. Joints between courses and layers shall be staggered for maximum strength and to eliminate the possibility of straight line penetration from the interior directly to the vessel wall.

The brick lining subcontractor shall maintain proper material and internal air temperatures, and provide for full cure time as required by the mortar manufacturer. No bricks shall be laid when the temperature is less than 3 °C above the dewpoint and during winter time, all work areas shall be kept at a minimum temperature of 21 °C day and night until the mortar has set. No excessive moisture is acceptable (such as condensation on the steel plate in the vessel) where bricks are being installed. Condensation may be prevented by portable heaters (preferably electric) inside the vessels. Any brickwork less than 5 days old which has been wetted shall be replaced. Care should be taken to prevent condensation on or behind the brickwork from blowers or other devices used for heating.

The following is a guide to hardening time for potassium silicate mortar:

Temperature (°C)	*Time (days)*
10	10
16	8
21	6
27	4

In order to develop the optimum mortar strength, the curing shall be a minimum of 6 days or the above guide time, whichever is longer. After the completion of curing, the joints (when using potassium silicate mortar) shall be washed with 10% sulfuric acid to protect the surface against moisture or high humidity damage, unless the equipment is being placed immediately into acid service. Please note that acid washing of potassium silicate mortar is a vital part of the curing process and must not be omitted. Furane based mortars do not require acid washing.

All waste materials, spoiled and unused brick and mortar, water and cleaning materials shall be kept away from all acid proof masonry until it is cured.

3.29.4.1.7 Inspection and quality control

Work areas (mixing, brick cutting and installation areas) shall be maintained sufficiently clean so that foreign matter is not introduced into the lining system. Adequate lighting shall be maintained in the vessel during installation work to enable a sound lining to be obtained in accordance with this standard. The work will be inspected by the client's inspector at the following stages:

1. before the application of membrane, to ensure that all metal surfaces are clean and dry;
2. after the application of membrane, to ensure that complete coverage has been achieved;
3. during the laying of brick, to ensure that the specified conditions are followed.

Lining installations which are not in accordance with the specification or in which injurious defects, improper application, or excessive repairs are indicated shall be subject to rejection. A full inspection report shall be submitted to the manufacturer prior to the equipment being placed in service.

3.29.4.2 Linings to Flooring, Pits, and Trenches

Ceramic masonry lining systems have been successfully utilized to protect floors, pits, and trenches from the action of corrosive chemicals for many decades. Just as with vessel lining systems the total package consists of the three main components – membrane, brick, and mortar. The specification of the three component is entirely dependant upon the process conditions; taking careful consideration of the chemical types, temperatures and exposure times. Correct product specification, design and installation technique will produce a corrosion resistant lining which will maintain many years of trouble free service. The lining offers not only corrosion resistance but also thermal resistance, abrasion resistance and impact resistance. The use of an acid brick system will permit heavy loading such as those experienced in chemical tanker loading bays.

For the majority of applications an asphalt/epoxy membrane, acid brick and furane mortar are used for the lining system. The membrane and mortar can be altered to suit specific process conditions. For high concentration acids Hypalon sheet membrane is often specified. In the presence of hot alkali or hydrofluoric acid carbon bricks may substitute acid bricks.

Both acid brick and acid tile are used for masonry lining systems. A tile is recognized internationally as a masonry unit with a thickness of 30 mm or less. Tiles are available in most of the materials mentioned previously for brick products. Their corrosion resistance is material and manufacturing method dependant. The choice between brick or tile is primarily one of determining the appropriate thickness of the masonry unit for the application. The thickness of the masonry unit must be sufficient to offer structural stability, mechanical protection and thermal protection.

It is worth stating, again, that ceramic masonry lining systems offer excellent performance provided they are placed in *compression*. Tensile and shear stresses are unacceptable. It is therefore essential that the substrate to which the ceramic masonry lining is to be applied has sufficient strength and rigidity to support the lining under all anticipated loads. In order to achieve sufficient rigidity it is recommended that the floor, pit or trench be constructed from reinforced concrete. The use of sheet steel, wood or concrete blocks as a substrate is unadvisable.

Concrete floors generally contain expansion and construction joints to permit movement. These joints must be mated to similar joints in the ceramic masonry lining. The joints are a potential source of leakage and therefore serious corrosion to the underlying substrate. The positioning of the joints, the material used for the joints and the design of joints is important if the integrity of the floor is to be maintained. The manufacturers should be consulted over the design of chemical resistant expansion joints.

There a number of corrosion resistant expansion joint materials available. The type of compression/expansion must be considered when specifying the joint material. Many joint materials deform under compression and then protrude from the joint. This would be totally unacceptable in enclosed joints, which may be employed in multi layer brickwork

systems. In a single layer brickwork system the protruding joint may be cut off. A brief list of the corrosion resistant expansion joint material, currently available, is as follows:

Plasticized PVC	Polyurethane foam	Natural rubber
Ceramic blanket	Silicone sealants	Teflon felt
Polyester foam	Flexible epoxy	Carbon sponge

Flexible epoxy has the best overall chemical resistance combined with a temperature resistance of 75 °C. For precise details of expansion joint corrosion and temperature resistance the manufacturer should be consulted.

3.29.4.3 Linings to Chimneys

Combustion processes invariably produce acid gases. In order to reduce energy wastage in power stations the flue gas temperatures have been steadily reduced over the last four decades. Flue gas desulfurization has also led to a reduction in flue gas temperatures. It is now commonplace to have flue gas temperatures below 90 °C, which is below the sulfuric acid and water dewpoints. As a result, acid condenses on the inside of the chimney causing corrosion of the flue liner and, hence, precautions against this occurrence have to be taken.

Ceramic masonry chimney linings serve as a chemical and abrasion resistant barrier against gases, liquids, and solids thereby protecting the chimney shell (windshield). There are generally three distinct lining systems for concrete or steel windshields:

- full height, free standing flues;
- multilevel flues (as single or multiflue systems);
- full height linings as an integral component of the windshield.

Lining materials are carefully chosen to suit the flue gas conditions. Nonmetallic lining materials include acid brick, foamed glass block, synthetic rubber and glass fiber reinforced resins.

Flues constructed entirely of acid brick and chemical resistant mortars (normally potassium silicate) have an excellent proven track record. They are the only nonmetallic material capable of withstanding high temperature gases and a wide variety of corrosive chemicals. As free standing brickwork elements, unconstrained by an outer shell, the brick flues have a tendency to exhibit tensile failure, when operated at elevated temperatures. Large cracks in the brick flues are evidence of this type of failure. The use of interlocking bricks and high bond strength mortars has reduced the incidence of stress cracks in brick flues. With the advent of chimneys operating with low temperature flue gases, tensile failure is no longer a problem and the brick flues can give an extremely long trouble free service.

The key benefits of acid brick flues are:

- durability,
- suitability for use in FGD and non-FGD systems,
- cost effective,
- long service life,
- excellent track record.

A large number of chimneys, throughout the world, have been built either entirely of steel or a concrete windshield with steel flues. The production of acid condensates in the flue gases, due to lower flue gas temperatures causing serious corrosion problems in these chimneys. Most of these chimneys now require the installation of a corrosion protective lining. Due to loading limitations on the foundations, the large weight of acid brick and mortar precludes this product as a viable solution. Foamed glass blocks bedded and jointed in chemical resistant mortars offer a suitable answer to the problem of corrosion prevention. The foamed glass block combines light weight with excellent acid resistance and thermal insulation properties. The choice of chemical resistant mortar is dependant upon the flue gas conditions. The mortar can also be used as the membrane applied to the steel shell, behind the foamed glass blocks.

Further Readings

McCauley, R. A. Ed. *Corrosion of Ceramic and Composite Materials*, 2nd ed.; CRC Press, 2004.
Sheppard, W. L. Ed. *Corrosion and Chemical Resistant Masonry Materials Handbook*; William Andrew, 1986.
Bennet, J. P. In *Corrosion of Glass, Ceramics and Ceramic Superconductors*; Clark, D. E., Zoitos, B. K., Eds.; Noyes Publications, 1992; Chapter 15.

3.30 Degradation of Cement and Concrete

P. Lambert, R. Brueckner, and C. Atkins
Materials & Corrosion Engineering, Spring Bank House, 33 Stamford Street, Altrincham WA14 1ES, UK

Symbols

A Aluminum oxide
C Calcium oxide
$C_{(x)}$ Concentration
C_o Surface concentration
c Number of ions per unit volume
D_c Diffusion coefficient ($m^2\ s^{-1}$)
e Electron charge
F Iron oxide
F(x) Flux
$f_{ck,cyl}$ Minimum characteristic cylinder strength ($N\ mm^{-2}$)
$f_{ck,cu}$ Minimum characteristic cube strength ($N\ mm^{-2}$)
k Boltzmann constant
$\bar{N}$ NaO_2-equivalent
S Silicon oxide
T Absolute temperature (K)
t Time (s)
w/c Water–cement ratio
x Distance from the exposed face (m)
X_d Depth of chloride penetration (m)
Z Valency
σ Conductivity ($\Omega^{-1}\ m^{-1}$)

Abbreviations

AFm Tricalcium-aluminate-ferrite-monosulfate
AFt Tricalcium-aluminate-ferrite-trisulfate
ASR Alkali silica reaction
BRE Building Research Establishment
C–A–H Calcium aluminate hydrate
C–S–H Calcium silicate hydrate
DEF Delayed ettringite formation
GGBS Ground granulated blast furnace slag
HAC High alumina cement
IStructE Institute of Structural Engineers
OPC Ordinary Portland cement
PFA Pulverized fuel ash
pH Potentio hydrogenii
SRPC Sulfate resisting Portland cement
TEG Thaumasite Expert Group
TF Thaumasite formation
TSA Thaumasite form of sulfate attack

3.30.1 The Chemistry of Cement

3.30.1.1 Cement Types

EN 197-1:2000 defines cement as "a hydraulic binder, i.e., a finely ground inorganic material which, when mixed with water, forms a paste which sets and hardens by means of hydration reactions and processes and which, after hardening, retains its strength and stability even under water." The hardening of cement is mainly a result of the hydration of calcium silicates and, to a lesser extent, of aluminates.

Portland cement consists of cement clinker and various other constituents, which determine its classification. These additional constituents can be granulated blast furnace slag, natural and industrial pozzolanic materials, burnt shale, limestone, silica fume, and calcium sulfate, which are added during the manufacture to control setting. EN 197-1:2000 covers 27 common cement products, which are grouped into five main cement types as follows:

CEM I – Portland cement
CEM II – Portland–composite cement
CEM III – Blast furnace cement
CEM IV – Pozzolanic cement
CEM V – Composite cement

3.30.1.2 Compounds Present in Portland Cement

Ordinary Portland cement (OPC) is made up of the compounds listed in Table 1. The abbreviations are in the standard cement chemist's notation: C = calcium

Table 1 Compounds present in anhydrous cement

Cement component	*Abbreviation*	*% in OPC*	*Hardening rate*
Tricalcium silicate	C_3S	>50	Rapid
Dicalcium silicate	C_2S	<20	Slow
Tricalcium aluminate	C_3A	<10	Rapid
Tetracalcium aluminoferrite	C_4AF	<10	Extremely slow

oxide, S = silicon oxide, A = aluminum oxide, and F = iron oxide.

It is, however, more customary to express the composition of cements in terms of oxide analysis, that is, CaO, SiO_2, Al_2O_3, Fe_2O_3, NaO_2, and so on. From this it is possible to calculate the so-called 'Bogue compositions' shown in Table 1. The following equations are based on solving certain simultaneous equations and were first derived by Bogue.

For the system C_3S–C_2S–C_3A–C_4AF:

$$C_3S = 4.01710CaO - 7.6024SiO_2 - 1.4297Fe_2O_3 - 6.7187Al_2O_3(-2.852SO_3)$$

$$C_2S = 8.6024SiO_2 + 1.0785Fe_2O_3 + 5.0683Al_2O_3 - 3.0710CaO$$

$$C_3A = 2.6504Al_2O_3 - 1.6920Fe_2O_3$$

$$C_4AF = 3.0432Fe_2O_3$$

The equations were produced by assuming that all the Fe_2O_3 reacts with Al_2O_3 and CaO to form the C_4AF, the remaining Al_2O_3 reacts with CaO to form the C_3A. The CaO then reacts with the SiO_2 to form C_2S and any CaO left reacts with the C_2S to form C_3S.

It should be recognized that in commercial manufacture, equilibrium conditions are unlikely to be achieved. Coarse particles may not be completely converted because some of the reactions occurring in manufacture are between liquid and solid phases and also resolution during cooling of previously crystallized phases may not be complete. Component parts may be embedded in each other where the liquid may not be able to act upon them or the liquid may crystallize independently without the formation of equilibrium products. The minor components of cements such as sodium, potassium, and magnesium oxides will also have an effect. Despite the aforementioned problems, the ability to produce a simplified equation for the composition of the cement from its constituent parts has obvious benefits for the cement industry and also for scientific research.

3.30.2 The Hydration of OPC

3.30.2.1 The Silicates

There is an empirical character to the information available with respect to the hydrolysis of the calcium silicates because of a wide variation in water contents and lime–silica ratios between component parts of the system. Also, products of the same composition can be represented by several phases, and it is difficult to prepare large crystals representative of those produced during cement hydration because the hydrates are in the form of gels.[1] In general, the reactions are considered to be as follows:

$$3CaO \cdot SiO_2 + 3H_2O \rightarrow 2CaO \cdot SiO_2 \cdot 2H_2O + Ca(OH)_2$$

$$2(3CaO \cdot SiO_2) + 6H_2O \rightarrow 3CaO \cdot 2SiO_2 \cdot 3H_2O + 3Ca(OH)_2$$

$$2CaO \cdot SiO_2 + 2H_2O \rightarrow 2CaO \cdot SiO_2 \cdot H_2O$$

$$2(2CaO \cdot SiO_2) + 4H_2O \rightarrow 3CaO \cdot 2SiO_2 \cdot 3H_2O + Ca(OH)_2$$

It is worth noting that Joisel[2] reports that there is no stoichiometrically defined hydrate of calcium silicate, and as a consequence, during hydration, intermediate compositions may exist locally between C_2SH_2 and CH. Taylor[3] states that the composition of calcium, silica, and water varies between CS(aq.) and C_3S_2(aq.) without significant change in the X-ray diffraction pattern. It is the C–S–H that imparts the cementing action in concrete, derived from surface forces interacting over the large surface area of the C–S–H.

The rate of early hydration of silicates is controlled by the rate of dissolution of calcium and hydroxide ions into a liquid phase from the C–S–H layer produced around the cement grains.[4]

There is some debate whether or not the calcium silicate hydrate binds chlorides. Ramachandran[5] investigated the hydration of tricalcium silicate supplied by the Portland Cement Association in the presence of calcium chloride, using various techniques and concluded that there is evidence for the presence of various states of chloride. Ramachandran attributed this to two mechanisms: one due to the positively charged surface of the C–S–H adsorbing

negatively charged chloride ions and the second being the formation of some interlayer chloride, which was irremovable by leaching with ethyl alcohol but could be removed by leaching with water. Water molecules are more readily able to access the finer pores than does ethyl alcohol because of their smaller size. He added that the chloride ions incorporated into the C–S–H are not mobile enough in water to cause corrosion in reinforced systems.

Lambert *et al.*[6] used tricalcium silicate produced by firing a mixture of calcium oxalate, alumina, and magnesia to produce Jeffrey's Alite[7] ($C_{54}S_{16}AM$), which is reported to be a reasonable approximation of C_3S. They reported, using pore water extraction to monitor the pore solution, that when the chlorides are added as sodium chloride no binding takes place. This is supported by the fact that the pH remained at ~12.5, which is the pH of saturated calcium hydroxide, which agreed with work done on microsilica binding using sodium chloride.[8]

3.30.2.2 Tricalcium Aluminate

Tricalcium aluminate is reported to preferentially react with calcium sulfate as follows:[9]

$$3CaO \cdot Al_2O_3 + 3CaSO_4 \cdot 2H_2O + 30H_2O \rightarrow$$

Tricalciumaluminate

$$3CaO \cdot Al_2O_3 \cdot 3CaSO_4 \cdot 32H_2O$$

Ettringite

The term 'ettringite' has come into use in a generic sense to represent the calcium aluminate or ferrite trisubstituted hydrates (AFt) formed as a result of the reaction of tricalcium aluminate hydrating with gypsum and water.

If chlorides are present, the tricalcium aluminate mainly reacts with the sulfates present first to form the chloroaluminate, $3CaO{\cdot}Al_2O_3{\cdot}CaCl_2{\cdot}10H_2O$, more commonly known as Friedel's salt.[10] It is worth noting that the formation of Friedel's salt will only take place if anhydrous tricalcium aluminate is present, and therefore, it would be expected that diffused chlorides will only be bound to a small extent. When tricalcium aluminate is hydrated in the presence of both gypsum and calcium chloride, a small amount of chloroaluminate is formed immediately, but the main consumption of chlorides begins only after the supply of sulfate ions is exhausted.

3.30.2.3 Tetracalcium Aluminoferrite

Tetracalcium aluminoferrite hydration is not well understood,[11] but is generally regarded as similar to the hydration of tricalcium aluminate under comparable conditions. $Fe(OH)_3$ gel, AFt, $C_2(A,F)H_8$, $C_4(A,F)H_{13}$, and $Al(OH)_3$ gel have also been observed. C_4AF has a general formula of $2CaO{\cdot}(Al_2O_3)_x(Fe_2O_3)_{(1-x)}$ where x is between 0 and 0.7. In most Portland cements x is usually 0.5.[12]

Ettringite is also produced and will undergo the same series of subsequent reactions as that formed during the tricalcium aluminate hydration. A chloroferroaluminate phase produced by the hydration of tetracalcium aluminoferrite in the presence of calcium chloride and analogous to Friedel's salt has also been identified.[13]

3.30.3 Stages in Cement Hydration

There are three main stages in the hydration of OPC.

3.30.3.1 The First Stage

When OPC is mixed with water, a rapid reaction takes place, which forms a supersaturated solution. After this rapid period of initial hydration lasting less than 15 min, a period of very slow hydration lasting for several hours called the dormant or induction period occurs. There are four main theories for the cause of this period.

The first is that a layer of hydration products precipitate over the surface of the cement grains. After a period of time this splits, either by pressure caused by the formation of hydration products under this protective layer[14] or by osmotic pressure building up under the surface of the grain[15] and hydration commences again. The second theory states that hydration only starts when an initial hydrate of low permeability converts into one of a higher permeability[16] and therefore is similar to the first. The third proposes that the induction period ends because of calcium hydroxide crystallizing into solution, and thus forming nuclei that act as seed crystals for further calcium hydroxide, thereby allowing hydration of the silicates to proceed.[17]

The final theory reports that the induction period exists due to a potential barrier corresponding to a critical size of calcium silicate hydrate (C–S–H) nuclei.[18]According to this theory, C–S–H is initially only formed on imperfect preferential sites on the

surface of calcium silicates. Only after the hydrate nuclei reach a critical size does hydration extend to other parts of the surface and hence hydration accelerates.

The first theory is the simplest and has some evidence for its validity. Jennings and Pratt[19] concluded that, as hydration at the end of the dormant period is characterized by hollow spines growing out of the grains, this suggests that a membrane has ruptured and the interior of the grains flows out through these spines and hydrates on contact with the exterior solution. However, they also state that the environment of the experiment was artificial because it was at a water solids ratio of 20, and therefore, the procedure may be flawed although fibers such as those that were created in the experiment have been found in cement in practical situations. They suggest that when cement comes into contact with water, the calcium quickly passes into solution and a silica-rich layer forms a gelatinous coating containing alumina. This coating allows the passage of ions such as sulfates, potassium, and calcium along with water but not aluminum and silicon ions.

Odler and Dörr[20] studied the hydration of tricalcium silicate and concluded that the fourth theory was more accurate in this application. Addition of 'seed crystals' of calcium hydroxide did not affect the induction period, but the addition of prehydrated tricalcium silicate had a marked effect, thus discounting the third theory. They also stated that the preinduction period was controlled by the concentration of calcium hydroxide in the solution, and hence discounted the precipitation theory.

The time of inception and the duration of the dormant period depend mainly on the water–cement ratio, fineness of the cement, and its composition. The cement paste at this stage appears to be a suspension of fine powder in water. Odler and Dörr[21] state that the amount of tricalcium silicate that hydrates in the preinduction period can be altered by experimental procedure and the presence of defects in the crystalline lattice. The tricalcium silicate anneals with time, resulting in a lower number of lattice defects, resulting in an extension of the dormant period, thus further discounting the precipitation theory and supporting the final one.

During the dormant period a certain amount of sedimentation takes place, known as bleeding. This is undesirable because the water rises to the surface carrying fine cement particles with it, resulting in the formation of a high water–cement ratio slurry on the surface, called laitance, which has a low strength. This causes problems when trying to continue construction up a column or wall and should be removed before casting continues. Also, flow channels of low cement content, and therefore low strength, can occur in the body of concrete structures. In reinforced concrete structures, this bleeding can cause voids beneath the reinforcement, which are reported to be sites for potential corrosion attack.[22]

3.30.3.2 The Second Stage

The growth of plastic strength begins after the end of the dormant phase and can be divided into two stages. At the end of the dormant phase a period of hydration takes place, known as 'setting,' which lasts to about 30% of the total hydration. During this stage, the cement loses its plasticity and the cement paste becomes hard. Coagulation of the structure takes place and is characterized by the presence of a three-dimensional network formed by disordered coupling of the finest particles in the disperse phase through thin layers of the dispersion medium, resulting in a network low in strength. In this stage, crystallization only occurs in the form of individual crystallites, mainly in the form of calcium hydroxide and sulfoaluminate.

The onset of this phase is known as the initial set, and the end of the set, marked by the total loss of plasticity, is known as the final set.

3.30.3.3 The Third Stage

After the final set, the hydration process slows down and the 'hardening period' begins, during which the cement gains most of its mechanical strength. In this stage, more intense crystal formation is accompanied by crystal bonding, forming a strong crystalline network. Subsequent strength development comes from the growth of hydrated calcium silicate crystalline structure as crystals are formed from the supersaturated solution. The rate of this stage is controlled by diffusion through the cement matrix. If mechanical deformation is applied at the onset of this stage, it is usually detrimental to its ultimate strength.

3.30.3.4 Admixed Chlorides and the Rate of Hydration

Calcium chloride falls into the category of accelerating admixtures and, being a low-priced industrial by-product, was extensively used. In 1977, however, due to the increased risk of corrosion of reinforcement

steel, the use of chloride-based accelerators was prohibited in all reinforced or prestressed concrete in the United Kingdom.

Accelerators increase the initial rate of chemical reaction between the cement and the water so that the concrete stiffens, hardens, and develops strength more rapidly. This is a benefit because it allows the earlier striking (i.e., removal) of formwork. They have a negligible effect on workability and 28-day strengths are rarely affected. The addition of small amounts (<1 mass%) of calcium chloride sometimes retards the set; however, this effect is very variable. Larger amounts produce an acceleration, and amounts over 3% have been known to cause a flash set. Sodium chloride produces a less pronounced change in the rate of hydration and the effect is more erratic, sometimes accelerating, sometimes retarding.

3.30.3.5 Summary of the Hydration of Cement

The hydration products of the silicates are basically a calcium silicate hydrate gel of varying morphology and composition between $1 < C/S < 2$ and calcium hydroxide. Contained within this gel are areas where iron, sulfate, and aluminum ions have been adsorbed into the lattice. It is probable that some chlorides can also be absorbed in this way. Chlorides may also form complexes with hydrating calcium silicates. Specific information about the calcium silicate hydrates is hard to obtain because they are poorly crystalline, which leads to difficulty in analysis. Also, variations occur throughout the cement matrix, which are time dependant because of the nature of the solid solutions formed.

Aluminate hydrates also form solid solutions, leading to time-dependant variations as compounds migrate through the matrix. Chlorides are predominantly bound to the aluminate compounds by the formation of Friedel's salt. The hydration products of the aluminoferrites are similar to those of the aluminates with iron substituting for aluminum in varying quantities.

The hydration of cement takes place in three stages. A period of rapid hydration occurs as water is added to the anhydrous cement. After about 15 min this stops and a period of little activity takes place, known as the dormant period. This lasts for about 3–4 h, after which hydration recommences. The end of the dormant period is thought to be caused by the break down of some protective membrane of hydration products covering the surface of the cement grains or by the transformation of a hydrate to a more porous form or by the volume of hydrates on the surface of the grain reaching a critical mass. The post dormant phase of hydration is known as the setting period, when crystallites of calcium hydroxide and sulfoaluminate are known to form. Eventually, the hydration products build up and this causes the process to become diffusion controlled. It is during this hardening period that the cement gains its mechanical strength.

3.30.4 High Alumina Cement

High alumina cement (HAC), as the name suggests, contains a large proportion of alumina; typically about 40% each of alumina and lime with around 15% of ferrous and ferric oxides, plus 5% silica.

HAC was developed as an alternative to OPC because of its increased resistance to sulfate attack, and in this respect, it performs well. This resistance to sulfate attack is due to the absence of $Ca(OH)_2$ in hydrated HAC and also due to the protective influence of the relatively inert alumina gel formed during hydration. HAC is not attacked by CO_2 dissolved in pure water, and while it is not acid resisting, it can tolerate very dilute solutions of acids (pH > ~4) found in industrial effluents but not hydrochloric, hydrofluoric, or nitric acids.

Another positive feature of HAC is its very high rate of strength development. About 80% of its ultimate strength is reached in 24 h, and even at 6–8 h the concrete is strong enough for the side formwork to be struck and for the preparation for further concreting to take place. It is for this attribute that it became popular for the production of precast beams used in floor and roofing systems in the late 1960s and early 1970s.

Because a number of high profile catastrophic failures occurred in the early 1970s, the suitability of HAC concrete for use in structural components has been of concern. The Building Research Establishment (BRE) subsequently carried out a major investigation[23] and identified that HAC is subject to a process known as conversion.

Conversion occurs due to the primary hydrates present in the material being chemically unstable. The conversion process involves a change in the mineralogy of the cement, which becomes increasingly porous and friable with age and also loses alkalinity. Under conditions where the overall dimensions of the body are constant, as is the case in set

cement paste, conversion results in an increase of porosity of the paste.

The strength of hydrated cement paste or of concrete is very strongly affected by its porosity; a porosity of just 5% can reduce the strength by more than 30%. As a result, conversion markedly reduces the strength of HAC. Also, the increased porosity means the concrete is more susceptible to other forms of attack such as alkali, sulfate attack, or carbonation.

As the concrete becomes more porous, it allows easier movement of oxygen and water as well as aggressive species like chloride ions. This, combined with the loss of alkalinity, can result in the increased possibility of reinforcement corrosion, which can also cause deterioration of the concrete. This deterioration is accelerated by the presence of excess water, for example, from leakages, condensation, or groundwater.

The effects of conversion on the strength of beams depend on the original strength and quality of concrete used. In some cases, the increase in porosity has been reported to allow moisture to react with unhydrated cement particles and produce an increase in strength. In other cases, significant strength reduction can take place.

3.30.5 Pozzolanic Materials

A number of materials are available that can be used to partly replace the cement content of a concrete mix, saving cement and usually providing additional benefits in terms of performance and durability; these include blast furnace slag, fly ash, metakaolin, and natural volcanic ashes. Such materials, whether natural or human-made, have been thermally modified to produce potentially reactive compounds of silica and alumina.

The first hydraulic cements based on pozzolanic materials date back to Roman times. These were materials that reacted with lime water to produce a hardened mass and employed the volcanic ash obtained from the slopes of Mount Vesuvius, in the vicinity of the Italian town of Pozzuoli from which the term Pozzolanic originates. The term is now commonly used to represent any material that reacts with alkaline water to harden. There are a number of industrial by-products that are used in this way to replace a proportion of the cement used in concrete.

There are typically two main benefits. The first is a reduction in cost, as the by-products are typically cheaper than the cement they replace. The second is a perceived enhancement in the properties of the concrete produced. This can take the form of increased resistance to aggressive materials, enhanced strength, or slower curing (which for large concrete pours is a benefit as the heat generated is reduced and consequently the risk of thermal-induced cracking when the concrete cools). There is a further potential benefit with regards to sustainability, as there is less cement used and it consumes what would otherwise be an industrial by-product.

3.30.5.1 Ground Granulated Blast Furnace Slag

Typically up to 70% of the cement used in a mix can be replaced with ground granulated blast furnace slag (GGBS). This means that a relatively standard concrete mix containing 300 kg of cement per cubic meter of concrete would contain 90 kg of OPC and 210 kg of GGBS. The benefits of GGBS are typically a reduced heat of hydration for large pours, and an increase in the overall durability of the concrete. This is both due to an increased resistance to the effects of aggressive chemicals on the concrete and due to a reduced rate of passage for aggressive species such as chlorides into the concrete.

The reduced heat of hydration produces a slower strength gain and a longer setting time. This means that the concrete may require more careful placement and curing techniques to minimize the risk of plastic cracking problems. The slower hydration may also produce substandard strength gain, resulting in a difficulty in achieving a target strength (the common method used to assess the quality control of concrete on a construction site). Some cases have been found where a portion the GGBS did not hydrate, but this is rare.

3.30.5.2 Pulverized Fuel Ash

Pulverized fuel ash or fly ash (PFA) is a by-product of coal-fired power stations and can achieve similar effects to GGBS, that is, an increase in durability and a reduction in heat of hydration, with a risk of plastic cracking problems because of difficult curing. The replacement quantities are lower than GGBS (typically up to 35%).

3.30.5.3 Silica Fume

Silica fume, also known as microsilica and nanosilica, is a highly reactive pozzolanic filler, which is used to achieve high strength and dense concrete. Silica

fume is a by-product of the manufacture of silicon and ferrosilicon alloys from high-purity quartz and coal in a submerged-arc electric furnace. The SiO_2 content is generally in the range between 80 and 98 mass%. The process produces a very fine material, which has a high pozzolanic reactivity. The silica particles react with the calcium hydroxide of the cement paste and form calcium silicate hydrates. The hydrates fill the space between the cement hydration products, and in particular, the weaker calcium hydroxide interface around aggregate particles increases the strength and density of the concrete. Contrary to the other cement replacements, the use of silica fume leads to a more rapid hydration and typically higher strengths.

3.30.5.4 Inert Fillers

Fillers are very finely ground materials, which have a similar particle size to Portland cement. Fillers, such as limestone or quartz powder, are inert or quasiinert materials, which mainly improve the density and stability of the cement paste. The workability, permeability, bleeding, or cracking tendency are also improved. Inert fillers do not contribute to the hydration; however, limestone powder can be beneficial for the hydration. It is able to form monoaluminate carbonate hydrates and supports the formation of ettringite.[24]

Modern UK and European Portland cements (CEM I), BS EN 197-1:2004, are permitted to contain up to 5% limestone filler as a minor addition. This can lead to a higher susceptibility to thaumasite formation because of a considerable internal source of carbonate ions.[25]

3.30.6 Concrete

Concrete has been an important construction material for more than the last 100 years. Concrete is a three-phase system consisting of cement, aggregate, and water. Nowadays, concrete is usually a five-phase system because of the addition of additives and admixtures for property improvements and cost reduction. The binder compounds cement and additives are discussed in Sections 3.30.1.1 and 3.30.5, respectively.

3.30.6.1 Aggregate

Aggregates occupy more than 75% of the volume of concrete and hence form one main indicator of the strength. The properties of aggregate characterize the performance of concrete. According to the density of aggregate, concrete is divided into three groups of lightweight ($400-<2000\,kg\,m^{-3}$), normal ($2000-2800\,kg\,m^{-3}$), and heavyweight concrete ($\geq 2800\,kg\,m^{-3}$).

Aggregate is a cheap compound in relation to cement. Hence, it is desired to use as much aggregate as possible, but with the restriction to achieve a durable concrete. Aggregate influences physical, chemical, and thermal characteristics and may affect the durability. Beside the economic factors, aggregate is used to increase the concrete's stability, that is, reduction of shrinkage, to decrease the susceptibility to chemical attack due to the reduction of susceptible cement paste, and to decrease thermal effects. Cement paste is susceptible to shrinkage-induced cracking, carbonation, sulfate attack, and mechanical attack such as erosion and fire. However, aggregate can cause concrete deterioration such as alkali–silica reaction, frost attack, and in the case of salt contamination, corrosion may be initiated. Organic impurities may affect the hydration, and coating of fine particles such clay may reduce the bond.

To obtain good quality concrete, the compactness of the aggregate bulk has to be high, that is, to follow certain particle size distributions. This is mainly achieved using at least two size groups: fine (0–5 mm) and coarse (>5 mm) particles. The fine particles are also referred to as sand.

Another point of division of aggregate is based on their source. There are natural and industrial manufactured aggregates. Industrial products are mainly light- and heavyweight aggregates. Examples of natural aggregates are basalt, granite, limestone, quartz, and gabbro.

The strength of natural occurring aggregates is mostly higher than the cement paste; therefore, the weakest part within the concrete system is the cement paste, and in particular, the interface between cement paste and aggregate. The strength of cement correlates well with the concrete strength of a three-phase system. On the other hand, lightweight aggregates have a lower strength than do the cement paste. There are three different crack patterns that relate to the strength relation between aggregate and cement paste in concrete. Concrete under stress may crack either within the cement paste or along the aggregate–paste interface or through the cement paste and aggregate particle or within the aggregate materials.

3.30.6.2 Water

Water is the third main phase within the concrete system, beside cement and aggregates. Water is essential for the formation of the strength giving hydrates within the cement paste such as the C–S–H phases. Hydration of cement is discussed in **Section 3.30.3**. The effects of the quantity of water, the water–cement ratio, on the strength are discussed in **Section 3.30.6.5**.

Natural occurring water and recycled water from concrete production can be used. The suitability depends on secondary substances in the water. Impurities may affect the hydration and consequently the strength of concrete. Organic substances should not be present. Seawater should not be used in reinforced concrete. The use of recycled water is specified in EN 1008. The usable amount of recycled water depends on the actual density showing the percentage of fine particles. Recycled water should not be used in concrete with air entrainment.

3.30.6.3 Admixtures

Admixtures are an additional ingredient of concrete. They are used to improve fresh concrete properties, such as workability and bleeding behavior, combined with an increase in strength and durability.

BS EN 934-2:2001 defines admixtures as "materials which are added during the mixing process of concrete in a quantity not more than 5% by mass of the cement content of the concrete, to modify the properties of the mix in the fresh and/or hardened state." They are mainly based on chemicals. Admixtures can be classified according to their function in

- water reducing/plasticizing,
- high range water reducing/superplasticizing,
- water retaining,
- air entraining,
- set accelerating,
- hardening accelerating,
- set retarding,
- water resisting,
- set retarding/water reducing/plasticizing,
- set retarding/high range water reducing/superplasticizing, and
- set accelerating/water reducing/plasticizing admixture.

The application of admixtures should always be in accordance to the manufacturers' guidance. The dosages should be within the recommended range because of the high sensitivity of concrete to the admixture.

Plasticizers are used to reduce the water–cement ratio in order to gain early and high-strength concrete with increased durability. Air entraining admixtures are used to increase the freeze–thaw resistance. Accelerating admixtures are commonly used in the precast sector and for cold weather concreting, whereas retarding admixtures are used to counteract the effects of hot weather on hydration.

Admixtures are a relative expensive component of concrete, however, the positive effects, such as increased workability and durability, can reduce total costs.

3.30.6.4 Concreting

Concrete should be mixed so that a homogenous mix is ready for transport and placement. The time between first contact of cement and water and final placing is limited to 90 min. The temperature of the concrete when placed is also limited so that the concrete temperature should be in the range of 5–30 °C. Concreting should be suspended when the air temperature is 3 °C and falling. The temperature of concrete placed in hot weather conditions can be reduced using cooled aggregates, ice as water replacement, or special curing methods to prevent excessive core and surface temperatures.

The placed concrete should be properly vibrated so that the reinforcement is enclosed and air voids (<1 mm) are reduced to less than 2%. However, over-vibration may cause loss of homogeneity because of segregation. The following curing process mainly determines the durability of the concrete. This is of special importance during cold and hot weather concreting. Concrete placed in cold weather should be cured longer to allow for the retardation of the hydration. The temperature gradient between core and surface should be minimized and the concrete should be prevented from freezing during its early stages of hydration. All surfaces should be protected against any weather effects. The rate of hydration increases with increasing temperatures so that special curing measures have to be taken into account in hot weather conditions. These may be cooling systems within the core of the concrete to prevent temperature above 60 °C, protection of the surface against sun, wind, and evaporation, and continuous humidification to achieve high grades of hydration within the surface layer.

Improper curing in cold weather may cause excessive bleeding, increased pore volume due to freezing, plastic cracking and thermal cracking caused by high temperature gradients. Wind and sun may cause extensive surface evaporation, causing a highly porous, less durable surface. Excessive core temperature can cause cracking and thermodynamical changes within the hydration products, causing delayed ettringite formation (DEF).

3.30.6.5 Strength of Concrete

The compressive strength of concrete is the most expressive property to describe the quality, and therefore, the long-term performance of concrete. This characteristic mainly determines the durability and permeability and can primarily be described with the water–cement ratio (w/c ratio). Secondary parameters affecting the concrete strength are aggregate–cement ratio, the properties of the aggregate, including the maximum aggregate size and the degree of compaction. In addition to the strength of concrete, the curing regime is of significant importance to achieve a durable and long-performing concrete structure.

The water–cement ratio is inversely proportional to the strength under the condition that the concrete is well compacted, allowing an air void content of less than 2%. The inverse proportionality is not valid below a w/c ratio of 0.38. The amount of water required for the total theoretical hydration of cement is in the range of 0.26–0.28; however, water is also physically bound within the cement matrix, that is, water is absorbed. A w/c ratio of 0.38 is required for the total hydration, including chemical and physical bond. Below this value, the degree of hydration and compaction decrease causing loss of strength. The increase of the w/c ratio above 0.38 causes the formation of capillarity pores, and hence, a reduction in strength. Water–cement ratios commonly used in the field are in the range of 0.45–0.60 or admixtures are added to achieve workability by low w/c ratios.

The effective water–cement ratio available for the hydration varies to the amount of water added to the mix. Additional water may be supplied by surface moisture of aggregate or water may be withdrawn from the mix because of absorption from the not saturated aggregates.

Various types of pores are present in the hydrated cement matrix, which may affect strength and durability. Gel and shrinkage pores formed during the hydration of cement are a usual compound within the matrix. Capillary pores form above $w/c = 0.38$ by total hydration; however, these pores may form below this value by reduced degree of hydration. The capillary pores are responsible for all transport processes within the concrete. Continuity between the capillary pores should be prevented until a w/c ratio of ~0.45, providing a durable concrete. Air voids formed during the mixing process can have a diameter up to 1 mm. To improve the freeze–thaw resistance artificial air pores can be introduced by using an air entrainment admixture. These pores are round and not connected and have a maximum diameter of 300 μm to allow the freezing water to expand. The last type of porosity is due to compaction voids, which mainly arise from variable workmanship.

The amount of cement within the mix can affect the strength. Very low cement contents and cement contents exceeding about 530 $kg\,m^{-3}$ decrease the performance. High cement contents may cause extensive hydration shrinkage leading to large cracks in the paste. The properties of the aggregates are another secondary parameter, as partly discussed in Section 3.30.6.1. Beside the type of aggregate, the moisture, surface texture, grading, and strength influence the strength of concrete.

Concretes are classified in EN 206-1:2000 according to their compressive strength after 28 days, see Table 2. The classification for lightweight concrete is similar and can be found in EN 206-1:2000.

Table 2 Standard concrete strengths according to EN 206-1:2000

Concrete compressive strength class	*Minimum characteristic cylinder strength* $f_{ck,cyl}$ ($N\,mm^{-2}$)	*Minimum characteristic cube strength* $f_{ck,cube}$ ($N\,mm^{-2}$)
C8/10	8	10
C12/15	12	15
C16/20	16	20
C20/25	20	25
C25/30	25	30
C30/37	30	37
C35/45	35	45
C40/50	40	50
C45/55	45	55
C50/60	50	60
C55/67	55	67
C60/75	60	75
C70/85	70	85
C80/95	80	95
C90/105	90	105
C100/115	100	115

3.30.7 Degradation

3.30.7.1 Cracking

There are many different types of crack that can occur in concrete. The consequences of these can range from purely aesthetic to structurally significant, and care should be taken when assessing them. It should always be borne in mind that concrete will always typically crack, but that cracks may or may not be structurally significant. Cracks may be as a result of the manner in which it performs structurally, as concrete has a low tensile strength. These are discussed in the order they occur, in the following sections.

3.30.7.1.1 Plastic settlement cracking

During concrete hydration, there is a period where it is a solid suspended in a liquid phase. This is known as the plastic stage. If this stage lasts too long, or the mix contains a significant amount of water, the solid particles can settle, see **Figure 1**. Mixes that hydrate slowly, such as those placed in cold weather, or with a high proportion of cement replacements are typically more vulnerable to this type of cracking. This typically manifests itself in the form of cracks immediately over the reinforcement steel, which provides a shorter path for the ingress of potentially aggressive species. If plastic settlement cracks are visible on a new structure, there is a significant possibility that extensive cracking has occurred and the surface should be grit blasted to identify the true extent of the problem before remedial measures are considered.

3.30.7.1.2 Plastic shrinkage cracking

If during hydration water is lost to the atmosphere quicker than it can be replenished from the hydrating concrete, the surface undergoes plastic shrinkage cracking. This typically takes the form of many small cracks over the surface of the structure and can be minimized with careful curing. As with plastic settlement cracking, if this is visible on the surface of concrete, the true extent needs to be identified before embarking on remedial measures. This can be achieved by a light grit blast.

3.30.7.1.3 Early age thermal cracking

As concrete hydrates, it generates heat. If this heat is not adequately controlled, then the concrete will cool after hydration, and as a result, will shrink. This may result in visible cracks forming. For water retaining structures, the basic approach is to limit the width of cracks by having a higher number of smaller cracks.

3.30.7.1.4 Long-term drying shrinkage

Over a significant period of time, concrete tends to shrink as shown in **Figure 2**. This will produce cracks and can be the basis or the allowable movement at structural joints. If the movement does not occur at the joints, there is additional restraint or the joints are incapable of movement, shrinkage cracks may occur. These are typically uniformly spaced across a structure as the concrete tends to shrink in a uniform manner.

3.30.7.2 Corrosion of Steel in Concrete

The single commonest cause of degradation of reinforced concrete is corrosion of the reinforcement. The pore water in concrete is highly alkaline and in a strongly alkaline environment steel is passivated, and does not corrode, by the formation of a stable and adherent oxide coating, thought to be Fe_2O_3. However,

Figure 1 Plastic settlement cracking.

Figure 2 Shrinkage.

this passive film can become unstable due to two mechanisms: those of chloride ion attack and carbonation. This is instigated by either carbon dioxide penetration reducing the pH, or by the presence of chlorides. Once corrosion has initiated, the rust produced is typically insoluble and has a greater volume than the original steel. As a result, tensile stresses develop in the concrete and the cover delaminates. This typically occurs with section losses below that, which are structurally sensitive; however, the falling concrete can pose a significant hazard. In addition, the corrosion may be taking place in an unobservable area, and hence the damage may go unnoticed until significant corrosion has taken place. In addition, the original design may have a limited factor of safety by current standards, and hence any corrosion may be intolerable.

3.30.7.2.1 Chloride attack

Chloride ions are considered to be the major cause of corrosion of reinforcement, see **Figure 3**. The level at which chlorides are generally considered to represent a risk of corrosion is typically greater than 0.4 mass% of cement.

3.30.7.2.2 Sources of chloride ions

The main source of chloride ions is typically from external sources such as deicing salts on roads or from the marine environments, the sea. However, there are situations whereby chlorides can end up in the concrete mix prior to casting of the concrete. Chlorides from this source are known as internal chlorides, and during the hydration of cement, a quantity of these are bound to the cement hydrates. For any particular cement, the relationship is thought to be primarily governed by the ratio of chloride to cement by mass. Internal sources can be from aggregate contamination by using marine-dredged aggregates that have not been washed properly, or by using contaminated water in the mix. Note that in some parts of the world, it is difficult to obtain chloride-free aggregates and chloride-free water. Chlorides have been deliberately added to the mix to control the hydration rate, although this practice has been discouraged.

3.30.7.2.3 Carbonation

Carbonation occurs where carbon dioxide in the atmosphere dissolves in water to form carbonic acid. This reacts with the alkaline concrete and reduces the pH to a value below 10, see **Figure 4**. It has been reported[26] that carbonation also increases the concentration of free chloride in the pore solution by releasing bound chlorides.

As the above processes require some diffusion through the concrete to the steel any factor that influences the rate of these processes also affects the corrosion rate, thus dense well compacted concrete with adequate cover can provide excellent protection to embedded steel and there are oil platforms in the North Sea that have survived 17 years[27] with no observable corrosion of the reinforcement bars taking place. Cement replacements are often used to provide an enhanced durability and resistance to passage of aggressive ions but do require more care in placement or these benefits may not be realized.

3.30.7.2.4 Chloride ion diffusion

As stated above, chloride ion ingress is the major cause of deterioration of reinforced concrete structures. Therefore, knowledge of the nature of diffusion of chloride ions through concrete would be necessary for any structure to have a designed lifetime. Ideally,

Figure 3 Chloride-induced corrosion.

Figure 4 Carbonated concrete sample treated with phenolphthalein indicator (magenta color represents uncarbonated concrete).

it would be possible to calculate a figure for the time taken for chlorides to reach the steel in sufficient quantities to cause depassivation from the mix design and cover. This has led to certain experimental procedures being developed that attempt to model chloride diffusion on a laboratory scale and these methods are outlined below.

Generally, current investigations into this topic can be divided into three types: those using the diffusion cell method, those using immersion into solution, and those using electrical properties of concrete to monitor diffusion, usually resistivity. The first two methods apply laws developed by Adolf Fick in 1858, which govern diffusion on a quantitative basis, to obtain diffusion coefficients for the materials under test; the third infers a diffusion coefficient from the change in the total quantity of ions in the pore solution with time, which manifests itself by an increase in ionic conductivity.

3.30.7.2.5 The diffusion cell

In this type of experiment, slices of cement mortar are taken and inserted into a diffusion cell.[28] Both sides of the cell are filled with either deionized water, saturated calcium hydroxide, or dilute sodium hydroxide, with one side containing chloride ions added in the form of sodium chloride. This method applies Fick's first law after the rate of change of chloride ion concentration in compartment one becomes constant:

$$-\mathcal{J}(x) = \frac{\mathrm{d}C}{\mathrm{d}t} = D_\mathrm{c}\frac{\mathrm{d}C_{(x)}}{\mathrm{d}x}$$

where $\mathcal{J}(x)$ is the flux of x, D_c is the diffusion coefficient ($\mathrm{m^2\,s^{-1}}$), and C is the concentration.

Tests such as this can take a significant length of time to achieve steady state. To avoid this, a direct current voltage can be applied to accelerate the test and calculate the flux of ions from the total current flowing. The problems with this method are that current is used in transporting all ions, not just the chlorides, and also a certain amount of heat is developed.

A modified version of this test was used by Luping and Nilsson,[29] who applied the test to both cement paste and mortar samples of varying water–cement ratios and applied a voltage of 30 V across a 70-mm-long cured samples with solutions of saturated calcium hydroxide and 3% sodium chloride. They compared the results obtained in this manner with conventional diffusion cell data and recorded current and temperature (a rise of only a few degrees after 8 h of testing) and obtained chloride profiles by sectioning the samples after 2 months of testing. The following equation was produced as a method of calculating the diffusion coefficient from the depth of chloride penetration, derived from a combination of electrochemical and ionic diffusion equations.

$$D_\mathrm{c} = 1.189 \times 10^{-11}\,\frac{X_\mathrm{d} - 1.061X_\mathrm{d}^{0.589}}{t}$$

where D_c is the diffusion coefficient ($\mathrm{m^2\,s^{-1}}$), X_d is the depth of chloride penetration (m), and t is the time (s).

This suggests a clearly defined depth of chloride penetration, which is not necessarily the case. As an alternative, Fick's second law can be applied to calculate the diffusion coefficient under non-steady-state conditions.

$$\frac{\delta C}{\delta t} = D_\mathrm{c}\frac{\delta^2 C}{\delta x^2}$$

where D_c is the effective diffusion coefficient ($\mathrm{m^2\,s^{-1}}$).

3.30.7.2.6 Immersion testing

As the name suggests, in this type of diffusion, testing blocks of concrete are taken, all but one of their surfaces are sealed, and the blocks are immersed in a solution. After a time, the blocks are removed and chloride ion profiles are obtained. Sections of the block are taken using either dry drilling or cutting with a diamond saw. The solutions in which the samples are immersed vary considerably from sodium chloride to seawater. For unidirectional diffusion into a semiinfinite medium, an accepted solution to Fick's second law is:

$$C_{(x,t)} = C_\mathrm{o}\left(1 - \mathrm{erf}\,\frac{x}{2\sqrt{D_\mathrm{c}t}}\right)$$

Where $\mathrm{erf}(z) = \frac{2}{\sqrt{\pi_0^z}}\mathrm{e}^{-y^2}\mathrm{d}y$, x is the distance from the exposed face (m), C_o is the surface concentration, and t is the time (s).

3.30.7.2.7 Resistivity measurements

Although not a direct method of measuring diffusivity of ions into concrete, this technique has been applied to infer variations in ionic concentrations in the pore solution. The use of conductivity in concrete as a measure of diffusivity was first suggested by Brace[30] for use in analyzing the properties of rocks. If a material is made up of a solid, insulating phase, with a

liquid phase distributed through it, then diffusion and conductivity are controlled by the same process and are related using the Einstein relationship.

$$\sigma = \frac{e^2}{kT}\sum_j c_j Z_j D_j$$

where σ is the conductivity ($\Omega^{-1}\,m^{-1}$), e is the electron charge, k is the Boltzmann constant, T is the absolute temperature (K), c_j is the number of ions per unit volume of j, Z_j is the valency of j, and D_j is the diffusion coefficient of j.

Buenfeld and Newman [31] continued this work, on the basis that the conductivity of concrete when wet is 5×10^8 times more than that of the dry material, and therefore electrical conductance takes place through the pore water. They point out, however, that the conductance depends entirely on the composition of the pore water solution, and therefore, variations in conductivity could be due to any increase in any ions in the pore solution, or the variations could be due to surface changes in the concrete itself.

3.30.7.2.8 Errors in diffusion experiments

The fundamental purpose of the above experiments is to obtain a value characteristic of the rate of ionic movement of chlorides through concrete. Ideally, it would be then possible to take this figure and apply it in the design stages of a structure to provide an accurate life expectancy.

This approach is flawed for concrete structures as design lives are very long, 120 years for bridges, and over this period of time, the environment can change considerably; for example, consider how much the world has developed over the past 120 years. With design lives of this scale the problem becomes one of adequate maintenance and repair rather than an initial design and build problem, although, of course, the ability to maintain the structure must be designed for.

Accelerated testing for diffusion involves either using thin sections or applying a voltage across the samples to accelerate the ionic flux. The first method must be questioned, because if used as an accelerated test, it may miss important effects that occur later in the life of the sample, as the morphology of the pore structure changes on contact with the solution. The second is additionally unsafe, because in concrete, charge balance is maintained as chloride ions diffuse in by the migration of hydroxide ions (see later). This would not be the case if using an applied voltage, and therefore, too much emphasis may be placed on the diffusion of cations in the process.

Chatterji[32] states that the assumption of constant diffusivity is seldom satisfied, with results suggesting that an increasing or decreasing depth of penetration could be observed depending on history. He adds that the use of a measured diffusion coefficient by any method to calculate the long-term chloride penetration depth is uncalled for and may be misleading.

Theoretically, Fick's second law cannot be used to analyze the chloride ion migration data through cementitious materials, as no account is made for any chemical reactions that take place during the process. Saetta *et al.*[33] reported that temperature, relative humidity, and degree of hydration all have an effect on the effective diffusion coefficients.

3.30.7.2.9 Corrosion ladder

This is a proprietary corrosion sensor developed by Raupach *et al.*[34] to allow monitoring of the indication of potential corrosion problems in new structures. Steel bars are cast parallel to the reinforcement at varying depths from the concrete surface up to and beyond the depth of rebar at strategic places in the structure. The potentials of these are recorded and when they change from a passive state to an active one, it is an indication that the steel has depassivated either due to the presence of chlorides or by carbonation. The occurrence of corrosion can be checked by connecting the mild steel electrodes to the stainless steel. If the mild steel has depassivated, then a current will flow, which can be measured using a zero resistance ammeter.

One possible problem with this method of monitoring is that when the chlorides reach the steel, it starts to corrode, producing voluminous corrosion products, and hence causes the concrete to spall. It is possible that only a small area of the steel has enough chlorides to cause activation and this test may therefore be unrepresentative of the overall state of the structure. In addition to this, very accurate positioning of the steel would be required in a small distance of concrete not greater than 150 mm. The size of the probe may also cause difficulties in areas of high stress, where the presence of the probe may reduce the load-bearing capacity of the section.

3.30.7.2.10 Tests on retrieved samples

The following testing methods all involve taking a sample of concrete. This is done by collecting the dust from a drilled hole and treating this with nitric acid to extract the free and bound chlorides into

solution. This solution is then usually neutralized and a known quantity is taken for testing by an external laboratory. The locations for testing are invariably limited by available time and access, and therefore, care must be taken in assessing the results.

3.30.7.2.11 Chloride ion selective electrodes

As the potential of the silver–silver chloride electrode depends on the chloride ion activity, the temperature, and the standard electrode potential of both the ion selective electrode and the reference electrode (it is compared with), in laboratory tests, the chloride-sensitive electrode is first calibrated in a set of solutions of known concentration. When a plot of potential against the log of chloride concentration is made, a straight line is obtained, and therefore, when the ion-selective electrode is submerged into an unknown solution, the chloride concentration of the solution can easily be calculated from the calibration plot. The potential obtained can be affected by the presence of bromide ions from a marine environment as there is some bromide in seawater. This approach has been used to produce a commercially available probe that has been installed in a number of structures.

3.30.7.3 Alkali-Silica Reaction

Alkali silica reaction (ASR) is a type of the more known 'Alkali-aggregate reaction' and was first reported in the United States by T.A. Stanton in 1940.[35] The reaction between alkali and aggregate as the cause of concrete degradation has been investigated since the early 1920s due to the occurrence of ASR in a dam in California, where opal was used as aggregate. Europe and the United Kingdom generally assumed that ASR was a degradation process which only occurred in North America until first cases were discovered in the early 1970s. Nowadays, ASR is present and recognized throughout the world. The causes of ASR and the protective measures to minimize the risk are well documented.

ASR is a chemical reaction between various forms of silica from the aggregate and alkali hydroxides (NaOH, KOH) from the pore solution in presence of moisture. The alkalis mainly derive from the cement. The reaction product, the alkali–silica gel, is more voluminous than the concrete and, after exceeding the tensile strength of the concrete, forms a distinctive crack pattern, see **Figure 5**. The cracks formed have the appearance of a spider web; however, affected prestressed elements tend to show cracks parallel to the stress direction.

Figure 5 Typical crack pattern of ASR.

The reaction affects the appearance and serviceability of a structure, although generally its structural integrity, particularly the compressive strength, is not affected. However, the formation of cracks can enhance the penetration of various aggressive compounds, leading to acceleration of other types of degradation. ASR is often observed in combination with corrosion and sulfate attack and can be their predecessor.

The reaction can be described in accordance to Wieker *et al.*[36] as follows.

Formation of alkali hydroxides (NaOH, KOH) during cement hydration

$$K_2SO_4 + Ca(OH)_2 \rightarrow CaSO_4 + 2KOH$$
$$NaSO_4 + Ca(OH)_2 \rightarrow CaSO_4 + 2NaOH$$

Water intake and expansion

$$2NaOH + SiO_2 + nH_2O \rightarrow Na_2SiO_3 \cdot nH_2O$$

The reaction can proceed when further water ingress takes place. The gel, an alkali–silica hydrate, is able to react with water and calcium hydroxide to form calcium silicate hydrates and alkali hydroxides, which can form more gel and degrade concrete over a long term.

$$Na_2SiO_3H_2O + Ca(OH)_2 + nH_2O \rightarrow$$
$$CaSiO_3 \cdot nH_2O + 2NaOH$$

This reaction is a definite process because the majority of the alkalis remain in the gel.

The formation of the alkali–silica gel causes swelling[37] and the expansion pressure developed during this process can reach up to 20 N mm^{-2}, exceeding the tensile strength of concrete, which is in the range 2–5 N mm^{-2}.

The reactivity of aggregate depends on the mineralogical structure of the SiO_2 and its proportion of amorphous and other reactive forms of silica. The reaction between SiO_2 and alkalis always occurs; however, this reaction is destructive in the presence of reactive SiO_2. All amorphous and cryptocrystalline SiO_2 minerals can be considered as reactive.[24] These include opal, chalcedony, greywacke, granite, and porphyry. ASR can be prevented when one of the three risk factors, alkalis, reactive SiO_2, and moisture, is minimized or eliminated. Moisture cannot be entirely controlled. The use of reactive aggregates is difficult to exclude because of the regional availability of aggregate. The transportation of nonreactive aggregates is commercially inefficient.

The amount of available alkalis can be controlled during the manufacture of cement so that the NaO_2-equivalent ($\bar{N}$) is less than 0.6,[38] which conforms to a hydroxide ion concentration of around 500 mmol l^{-1}. The use of GGBS, PFA, microsilica, or other pozzolanic material increases this threshold. Alkalis react with the high reactive fine pozzolanic particles during the early stages of the cement hydration before setting. Ca^{2+} ions are bound in reaction products of the pozzolanic material. These two reactions bind the alkalis in insoluble compounds with the cement matrix. Pozzolanas increase the density of the concrete, and hence, reduce the permeability of external and mobility of internal alkalis.

In the case of confirmed ASR degradation in structural elements, there are series of measures to monitor and control ASR. The IStructE[39] described these measures as follows:

- Regular monitoring of the structure to check that deterioration does not reach dangerous proportions. This requires experienced engineering judgment.
- Detailed check on the structural details to establish criticality, in particular, a critical examination of the robustness of the reinforcement detailing.
- Measures to reduce the amount of water available to the structure.
- Limited strengthening of the structure.
- Partial or full demolition followed by rebuilding.

The appropriate measure should be assessed through a series of investigations comprising the documentation of the degradation, a desk study to gain information about the materials used, the type of construction, and the rate of degradation. Destructive investigations should include the retrieval of cores in degraded and sound areas and their assessment in the laboratory. This may include strength tests, petrographic examination, and visual inspection.

3.30.7.4 Sulfate Attack

3.30.7.4.1 Conventional sulfate attack

The damaging influence of sulfates on concrete has been known since 1877, and first investigations were performed by Candlot[40] and Michaelis[41] at the end of the nineteenth century. They identified a complex water-enriched compound in the damaged matrix and described it as

$$3CaO \cdot Al_2O_3 \cdot 3CaSO_4 \cdot 30H_2O$$

Michaelis called the salt formed 'cement bacillus,' and nowadays it is known as 'ettringite,' and this is the main reaction product in various forms of sulfate attack. Several forms of sulfate attack have been identified that affect various phases of the cement hydration products.[42]

Sulfate attack can result in one of two forms of deterioration, the first is due to leaching of the calcium containing phases, particularly portlandite [$Ca(OH)_2$] as shown in **Figure 6**. The second is the more familiar expansive form caused by formation of more voluminous reaction products such as gypsum, monosulfate, and ettringite. The expansive form can

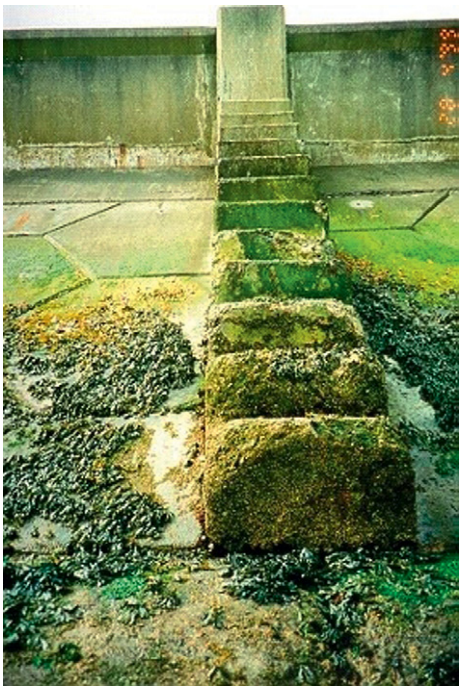

Figure 6 External sulfate attack.

be categorized by the location of the supplied sulfate whether there is an external or internal source.

The main reaction products of sulfate attack are gypsum and/or ettringite, and the reaction mechanism is generally accepted as portlandite transforms into gypsum and calcium aluminate hydrate into ettringite, the latter being the more expansive reaction. These findings allowed the development of sulfate-resisting Portland cement (SRPC-BS 4027-1996), which is mainly characterized by a limited tricalcium aluminate content ($C_3A < 3.5\%$). The low presence of the main ingredient for the deteriorative reaction hinders the formation of the more voluminous reaction products, which is mainly ettringite. Guidelines, such as BS EN 206, BS EN 1992, and BS 8500, have also been produced resulting in the solution to the majority of problems caused by sulfate attack.

3.30.7.4.2 Thaumasite form of sulfate attack

The thaumasite form of sulfate attack differs to the forms described earlier, including the conventional sulfate attack in that the calcium silicate hydrates (C–S–H phases), the main binding agent in all Portland cement binders, is targeted rather than the calcium aluminate hydrates (C–A–H phases) and the highly soluble calcium hydroxide ($Ca(OH)_2$).

Although TSA has been recognized for many years, it did not receive any serious attention from either industry or the research community until the discovery of 10 cases of the thaumasite form of sulfate attack in the foundations of overbridges along the M5 motorway in Gloucestershire in 1998.[43] The seriously attacked columns had been all buried in backfilled Lower Lias Clay and were discovered during strengthening works. In response to this discovery, the UK Government convened the Thaumasite Expert Group (TEG) with "the remit to produce interim advice and guidance on the implications for existing buildings and structures and for the design and specification of new constructions in the UK."

The TEG emphasized that deterioration as a result of the formation of thaumasite has become a separate form of sulfate attack, which has the potential to affect a wide variety of components and a range of building materials. The TEG gave thaumasite two classifications. The first being the 'thaumasite form of sulphate attack' (TSA) where significant damage of the concrete–mortar matrix has occurred as a consequence of replacement of cement hydrates by thaumasite. In this case, the TSA-affected concrete transforms into a soft, mushy mass with a distinctive white coloration. The second classification the 'thaumasite formation' (TF) refers to the occurrence of thaumasite as precipitations in pre-existing voids and cracks without causing deterioration of the host concrete or mortar. However, thaumasite formation can be a precursor of the thaumasite form of sulfate attack and constitute an early stage in the deterioration process, as suggested by Sims and Huntley,[44] who suggested changing the term TF to 'incipient TSA.'

In their report, the TEG recognized two sets of conditions for the formation of TSA in buried concretes, these are four primary and four secondary risk factors. The TEG emphasizes "that all of the four primary risk factors need to be present before significant TSA will occur within a buried Portland cement-based concrete." The primary risk factors are defined as

- a source of sulfates and/or sulfides in the ground;
- a source of carbonate;
- presence of mobile groundwater; and
- low temperatures ($<15\,^{\circ}C$).

The source of silicate, which is also a necessary component, was not included into the risk factors as it is an actual element in all Portland cement-based materials and is mainly present as calcium silicate hydrate phases (C–S–H phases).

The four secondary risk factors are identified by the TEG as

- type and quantity of cement used in concrete;
- quality of concrete mix, compaction;
- changes to ground chemistry and water regime resulting from construction; and
- type, depth and geometry of buried concrete.

On the basis of the findings of the TEG and other researchers, conventional sulfate attack and thaumasite form of sulfate attack have to be considered as two separate forms, which occur in different environments. TSA takes mainly place in low temperatures ($<15\,^{\circ}C$), whereas conventional sulfate attack is predominantly at ambient temperatures of $>15\,^{\circ}C$. However, $15\,^{\circ}C$ cannot be considered as a threshold between both types of attack.

Low temperatures favor the formation of thaumasite where generally less than $15\,^{\circ}C$ is necessary with an optimum value of $\sim 5\,^{\circ}C$. The formation ability increases with the decrease of the temperature, that

is, the lower the temperature the faster the formation of thaumasite.

One reason for the increase in deterioration rate with reduced temperature is solubility. The solubility of carbon dioxide increases with decreasing temperature, leading to about twice the amount of dissolved carbonate in solution at 0 °C than at 25 °C; portlandite is also more soluble at low temperatures, whereas thaumasite is in the order of a hundred times less soluble. From this follows an increased rate of deterioration at low temperatures.[45] On the other hand, lower temperatures lead to a better stability of the six-coordinated $[Si(OH)_6]^{2-}$ groups that are present in the structure of thaumasite. The cut-off point where the mineral formed changes from thaumasite to ettringite should be between 15 and 20 °C. The typical temperature conditions in the ground at foundation depth in the United Kingdom range from about 9 to 12 °C and are therefore in the optimum range of below 15 °C.[46]

The more frequent detection of TSA during the past decade is most probably due to the development of more selective analytical and diagnostic techniques, which are able to differentiate unambiguously between ettringite and thaumasite as well as mixed crystals of both. Crammond[47] suggests that TSA is not a recent phenomenon and has occurred likely in the past, but has not been recognized as such because of several reasons:

- failure to detect thaumasite in standard sulfate resistance tests;
- improved analytical techniques;
- buried concretes rarely inspected;
- postconstruction enhancement of sulfate levels in the ground; and
- changes in the composition of modern cements.

Many other cases of TSA may remain unidentified or have been reported spuriously as 'sulfate attack' caused by ettringite formation because of misidentification due to the structural similarities. Furthermore, the traditional diagnosis 25 years ago was performed using chemical analysis alone, and this method is not able to distinguish between ettringite and thaumasite. Nowadays, the mechanisms of the different types of sulfate attack are well known and the facilities for an unambiguous identification are available.

3.30.7.4.3 Delayed ettringite formation

Ettringite is a hydration product with two faces. The formation of ettringite during the first stage of cement hydration controls the setting time of the paste. Ettringite formation is responsible for the workability of fresh concrete. Ettringite can be destructive when it forms in the hardened cement paste. This degradation process has been mainly observed in heat-treated elements with high strengths and high density exposed to external conditions; however, the formation can also occur in non-heat-treated elements.

The destructive ettringite formation was first observed in a structural element at the beginning of the twentieth century. Ettringite is common hydrate in concrete and the presence does not need to conclude that a deterioration process had occurred.

The effect of increased heat on young concrete can be the formation of delayed ettringite. Causes are heat treatment of concrete elements and extensive heat development in mass concrete or under hot external conditions. Heat treatment of concrete accelerates the hydration and strength gain, respectively, and enables the manufacturer shorter stripping off times for the elements. Hot weather conditions can cause DEF during mixing and hydration as well as in already hardened concrete.

Temperature influences the stability of monosulfate and ettringite. The increase in temperature decreases the stability of both monosulfate and ettringite; however, the rate of the decrease of ettringite is higher, that is, monosulfate is thermodynamically more stable above 90 °C. Alkalis in pore solution reduce this threshold to 50–60 °C.[48] These changes of the stability of ettringite lead to the formation of monosulfate, free available sulfates (Na_2SO_4) in pore solution, and sulfates bound in the C–S–H phases above the critical temperature. Calcium silicate hydrates are able to bind sulfate ions during the hydration. Monosulfate becomes metastable when the temperature drops below the critical threshold.

If the concrete element is exposed to changeable weather conditions, that is, wet–dry cycles, then the sulfate ions in the pore solution and within the C–S–H phases react with the metastable monosulfate and C_3AH_6 to form the more voluminous ettringite. This reaction can cause expansion and cracking within the cement paste. The volume of ettringite is eight times greater than C_3A and 2.3 times greater than monosulfate. Ettringite can also form in pores and is not destructive.

Pozzolanas, latent hydraulic material, and microsilica reduce the susceptibility of concrete to DEF. Heat-treated elements should undergo special procedures, such as initial storage before treatment,

controlled warming, constant heat control, controlled cooling, and an after treatment.

3.30.7.5 Mechanical Damage

3.30.7.5.1 Abrasion/erosion

Abrasion or erosion can be defined as the wearing away of surfaces. It is commonly considered that it requires the action of a hard material on a softer one, but this is not the case. Over a significant period of time, a soft material can slowly wear away a harder one.

Concrete is no exception to this and will be subject to abrasion with time. Typically, it is a very slow process, unless it is subject to other mechanisms discussed later. For conventional reinforced concrete, the abrasion is likely to be of most of the concern if it results in an uneven surface for traffic, or if it significantly reduces cover to the reinforcement. Uneven surfaces often allow puddles of water to form, which can markedly accelerate the abrasion process, see **Figure 7**. When water is trapped while being subject to wheel loading, a significant pressure is exerted in the horizontal plane. This can rapidly lead to undermining of the surrounding surfaces, or opening up of existing defects, leading to increasingly more widespread surface degradation.

3.30.7.5.2 Cavitation

Cavitation occurs when liquids undergo a change in pressure to a point where the pressure in the liquid is below its vapor pressure. This produces bubbles in the liquid, which subsequently collapse and produce shockwaves. This can result in a very aggressive environment and extremely high rates of abrasion. This process is accepted as a mechanism that results in coastal erosion whereby air pockets within water are forced into fissures. The continuing inflow of water results in the collapsing of pockets and a range of shock waves being produced that result in degradation.

3.30.7.5.3 Frost

Frost damage is caused by a simple mechanism. Moisture within the concrete expands as it freezes, and as a result, tensile stresses form near to the surface. This can result in the surface crazing then scaling off, see **Figure 8**. In areas vulnerable to frost, a common approach to controlling the risk of frost action is to include an air entraining admixture. There are a range of products available to achieve this. The use of an air entraining admixture produces a series of evenly dispersed discontinuous pores within the concrete that are relatively uniform in diameter, the majority of which are less than 0.3 mm. This provides two benefits. The first is that the surface absorbency is reduced, because the pores are discontinuous. The second is that they are able to absorb the stresses induced by frost, because the pores remain air filled, and hence, unsaturated.

3.30.7.5.4 Exfoliation

Exfoliation is caused by a similar principle to frost, in that the pore structure becomes filled with a material that subsequently expands, see **Figure 8**. In this case, it is a solution containing soluble salts. As the moisture dries out, the solution becomes more and more concentrated until ultimately the soluble salts recrystallize. The recrystallized salts may be greater in volume than the original solution, and therefore, tensile stresses are imparted into the concrete.

Figure 7 Erosion of concrete by flowing water.

Figure 8 Exfoliation of a seawater outfall.

It should be noted that the surface of concrete that is exposed to the solution may not be the one that suffers from exfoliation. If one face of a concrete surface is adjacent to a highly concentrated solution, and the other is exposed to a drying environment, the salt solution can be drawn a significant distance to the drying face, where the recrystallization takes place. This can be a problem in immersed tunnels. Typically, the solution on the exterior of the tunnel is chloride contaminated and the capillary absorption that takes place will cause corrosion as well as exfoliation.

The first thing to note is that concrete already contains a supersaturated solution of calcium hydroxide. However, calcium salts typically have a relatively low solubility, and therefore, as the moisture dries out, the salts that are precipitated do not have a large volume expansion associated with them. For exfoliation to occur, a more soluble salt is usually present. In many cases in natural environments, this is sodium chloride based, but any highly soluble salt can produce a similar effect.

Coatings or waterproofing for concrete are commonly vapor permeable to prevent osmotic blistering. As a result, this can cause a drying out of the coated concrete. If the concrete is contaminated with a soluble salt, the concentrations in the pores under the coating will increase, until the salts precipitate. This can cause the surface to exfoliate, which can result in coating failure. It should also be noted that solubilities typically increase with temperature. As a result, exfoliation may also occur due to a temperatures change.

To control the risk of exfoliation or frost attack, the basic approach is to either prevent significant salt ingress or prevent drying of the surface. Typically, a coating system would provide protection against salt ingress, but note that a vapor permeable coating can increase drying out of the concrete and may therefore cause exfoliation if the substrate is heavily contaminated.

3.30.7.5.5 Fire

Following the great fire of Chicago in 1871, all iron- and steel-framed structures were coated with a basic form of concrete fire protection. When cement hydrates, it chemically combines with a significant amount of water. In the case of fire, as the temperature increases, the hydrated compounds break down and release the water, thus dissipating heat and energy. This means that while the surface of the concrete may have been subject to high temperatures, the depth of damage may be limited.

After a fire, the appearance of any structure can give the impression of a scene of total destruction. Because of the smoke, everything will be blackened. There will be areas where concrete has cracked and may have spalled. The levels of damage may appear significant but due to concretes ability to dissipate heat, the actual damage may well be recoverable.

If the temperature of the concrete has not exceeded 300 °C on cooling, the residual strength is commonly considered to not be significantly affected.[49] The reduction in strength is often offset by factors that resulted in the concrete having higher strengths than required by the original structural capacity. A word of caution should be raised as it is often assumed that the concrete strength increases with time beyond that required by the design. For older cements, this was the case, as in order to achieve the required strength at 28 days, the ultimate strength needed to be higher. Cements are more finely ground and cement producing companies have improved quality control systems that mean the factors of safety included to ensure the concrete meets the required 28 days strength are now lower. The ultimate strength achieved may not be significantly greater than that obtained at 28 days.

The temperature at which significant structural deterioration occurs coincides with a color change in many concretes, where the material develops a pink hue. This discoloration is due to the presence of ferrous salts in the aggregates, and may not occur if these are not present. It is important to note that this does not apply in every case, and the levels of heat damage and degradation of the cement should be confirmed using petrographic analysis on samples. Where temperatures exceed 500 °C, the strength is usually severely compromised.

References

1. Bernal, J. D. In Proceedings of Symposium on the Chemistry of Cement, London, 1952.
2. Joisel, A. In Proceedings of the 5th International Symposium on the Chemistry of Cement, Tokyo, 1968; Vol. 2, p. 268.
3. Taylor, H. F. W. *J. Chem. Soc.* **1950**, 3682.
4. Kondo, R.; Daimon, M. *J. Am. Ceram. Soc.* **1969**, *58*, 87.
5. Ramachandran, V. S. *Mater. Construct* **1971**, *4*(19), 1.
6. Lambert, P.; Page, C. L.; Short, N. R. *Cement Concr. Res.* **1985**, *15*, 675.
7. Jeffrey, J. W. In Proceedings of the 3rd International Symposium on the Chemistry of Cement, 1952; Cement and Concrete Association: London, 1954; p. 30.

8. Page, C. L.; Vennesland, O. *Mater. Construct.* **1983**, *6*(91), 19.
9. Collepardi, M.; Baldini, G.; Pauri, M.; Corradi, M. *Cement Concr. Res.* **1978**, *8*, 571.
10. Friedel, M. G. *Bull. Soc. France Mineral* **1897**, *20*, 122.
11. Liang, T.; Nanru, Y. *Cement Concr. Res.* **1994**, *24*, 150.
12. Tamas, F. D.; Vertes, A. *Cement Concr. Res.* **1973**, *3*, 575.
13. DeKeyser, W. L.; Tenoutasse, N. In Proceedings of the 5th International Symposium on the Chemistry of Cement, 1968; Vol. II, p. 379.
14. Hansen, W. L. In The 3rd Pacific Area National Meeting of the ASTM, San Francisco, 1959.
15. Powers, T. C. *J. Res. Dev. Lab. Portland Cement Association* **1961**, *3*(1), 47.
16. de Jong, J. G. M.; Stein, H. N.; Stevels, J. M. *J. Appl. Chem.* 1972, *17*, 246.
17. Tadros, M. E.; Skalny, J.; Kalyoncu, R. S. *J. Am. Ceram. Soc.* 1976, *59*, 344.
18. Fujii, K.; Kondo, W. *J. Am. Ceram. Soc.* **1974**, *57*, 492.
19. Jennings, H. M.; Pratt, P. L. *Cement Concr. Res.* **1979**, *9*, 501.
20. Odler, I.; Dörr, H. *Cement Concr. Res.* **1979**, *9*, 277.
21. Odler, I.; Dörr, H. *Cement Concr. Res.* **1981**, *11*, 765.
22. Tremper, B.; Beaton, J. L.; Stratful, R. F. Federal Highway Research Road Bulletin No 182, Washington, DC, 1959; p. 18.
23. BRE Digest 392, Assessment of existing high alumina cement concrete construction in the UK, BRE, UK, March, 1994.
24. Stark, J.; Wicht, B. *Dauerhaftigkeit von Beton – Der Baustoff als Werkstoff (Durability of Concrete)*; Birkhäuser: Basel, 2001 (in German).
25. Department of the Environment, Transport and the Regions. The thaumasite form of sulphate attack: Risks, diagnosis, remedial works and guidance on new construction. Report of the Thaumasite Expert Group, DETR, London January 1999.
26. Kayyali, O. A.; Haque, M. N. *Cement Concr. Res.* **1988**, *18*, 636.
27. Cathodic Protection of Offshore Structure Marine Technology Directorate Publications G0/102.
28. Page, C. L.; Short, N. R.; El-Tarras, A. *Cement Concr. Res.* **1981**, *11*, 395.
29. Luping, T.; Nilsson, L. *Am. Concr. Mater. J.* **1992**, *89*(1), 49.
30. Brace, W. F. *J. Geophys. Res.* **1977**, *82*, 3343.
31. Buenfeld, N. R.; Newman, J. B. *Mag. Concr. Res.* **1984**, *36*, 67.
32. Chatterji, S. *Cement Concr. Res.* **1995**, *25*, 299.
33. Saetta, A. V.; Scotta, R. V.; Vitaliani, R. V. *ACI Mater. J.* **1993**, *90*(5), 441.
34. Raupach, M.; Schiessl, P. In Proceedings of the 6th International Confernce on Structural Faults and Repair; Forde, M.C., Ed,; Engineering Technical Press, 1995; p. 221.
35. Stanton, T. A. In Proceedings of American Society of Civil Engineers 1940, pp. 1781–1811.
36. Wieker, W.; Herr, R.; Huebert, C. *Betonwerk Fertigteil-Technik* 1994, *60*(11), 86–90.
37. Taylor, H. F. W. *Cement Chemistry* , 2nd ed.; Thomas Telford: London, 1997.
38. Locher, F. W.; Sprung, S. Ursache und Wirkungsweise der Alkalireaktion *Betontechnische Berichte 1973*, Duesseldorf: Betonverlag, 1974; pp. 101–123.
39. IStructE Report 62, Structural effects of alkali-silica reaction: technical guidance on appraisal of existing structures, 1992; pp. 48.
40. Candlot, E. *Bull. Soc. Encour. Ind. Nat.* **1890**, *89*, 682–689.
41. Michaelis, W. *Tonindustrie-Zeitung* **1892**, *6*, pp. 105–106.
42. Brown, P. W. *Cement Concr. Compos.* **2002**, *24*, 301–303.
43. Halcrow Group Ltd.: Halcrow Thaumasite Investigation – Final Interpretative Report, 2000.
44. Sims, I.; Huntley, S. A. *Cement Concr. Compos.* **2004**, *26*, 837–844.
45. Collett, G.; Crammond, N. J.; Swamy, R. N.; Sharp, J. H. *Cement Concr. Res.* **2004**, *34*, 1599–1612.
46. Crammond, N. J.; Collett, G. W.; Longworth, T. I. *Cement Concr. Compos.* **2003**, *25*, 1035–1043.
47. Crammond, N. J. *Cement Concr. Compos.* **2003**, *25*, 809–818.
48. Wieker, W.; Huebert, C.; Schubert, H. Untersuchungen zum Einfluss der Alkalien auf die Stabilitaet der Sulfoaluminathydrate in Zementstein und –moerteln bei Warmbehandlung. Schriftenreihe des Institutes fuer Massivbau und Baustofftechnologie, Universitaet Karlsruhe, 1996, pp. 175–186.
49. Concrete Society Technical Report 33, Assessment and repair of fire-damaged concrete structures, Concrete Society, UK, 1990.

3.31 Degradation of Plastics and Polymers

D. J. Hourston
Department of Materials, Loughborough University, UK

This article is a revision of the Third Edition article 18.6 by J. A. Brysdon, volume 2, pp 18:53–18:77, © 2010 Elsevier B.V.

Glossary

Glass transition temperature The temperature at which polymer molecules cease being effectively locked into position and have sufficient rotational energy to be able to coil and uncoil.

Polymer resin A polymerized synthetic or chemically modified natural material, including thermoplastic materials such as polyvinyl chloride and thermosetting materials such as epoxy resins, which are used with other components such as fillers to form plastics.

Thermoplastic A polymeric material (e.g., nylon) which is capable of being repeatedly softened by increases in temperature and hardened by decreases in temperature.

Thermoset/thermosetting A polymeric material (e.g., an epoxy resin) which, upon curing, results in a three-dimensional structure and that decomposes rather than melts upon heating.

Abbreviations

ABS Acrylonitrile butadiene styrene polymers
DSC Differential scanning calorimetry
FEP Flourinated ethylene propylene resins
HIPS High impact polystyrene
MBS Methacrylate butadiene styrene polymers
PBT Polybutylene terephthalate
PEEK Polyetheretherketone
PES Polyether sulfone
PMMA Polymethylmethacrylate
PP Polypropylene
PPO Polyphenylene oxide
PPS Polyphenylene sulfide
PS Polystyrene
PTFE Polytetrafluoroethylene
PVC Polyvinyl chloride
PVdC Polyvinylidene chloride
PVdF Polyvinylidene flouride
SBR Styrene butabiene rubber
SBS Styrene butadiene styrene triblock copolymer

Symbols

ΔG Change in Gibb's free energy
ΔH Change in enthalpy
L Latent heat of vaporisation
P Partial polarity
ΔS Change in entropy
T_g Glass transition temperature
T_m Melting temperature

3.31.1 Introduction

From ancient times, organic materials, such as beeswax, have been used for surface protection of metallic and other artifacts. The nineteenth and especially the twentieth centuries saw huge advances[1,2] in surface coatings for the protection of metals against corrosion. This development continues apace right up to the present day. Some of the drivers of these developments are not only the ever-present desire to improve protection, but also to find materials and systems which are less polluting and which conform with increasingly stringent environment protection legislation. The latter driver has, for example, led to much work on waterborne coatings[3] to replace systems containing organic solvents, which were traditionally simply lost to the atmosphere. It is also the driving force behind the spectacular rise of polymeric materials which has led to the replacement of metals as the structural material in a vast range of manufactured

items. A glance around any room will reveal many plastic items which formerly would have been metallic.

In the past, corrosion control has involved, in the main, the use of metal alloys, protective coatings, inhibitors, etc. Corrosion problems may now often be circumvented by the use of organic polymers in the form of plastics or rubbers.[1] It must, however, be stressed that such polymeric materials are not totally inert to chemicals in their immediate environment, including, possibly, to metallic substrates or contacts.

3.31.2 Definition of 'Plastics'

In this section, both the terms 'polymer' and 'plastic' are encountered. The former is much easier to define than the latter. A polymer, or macromolecule, may be defined as a species with a molar mass much greater than that encountered in common organic substances such as alcohol, petrol, chloroform, etc., and which is comprised of smaller, repetitive molecular units. Although there is no specific definition that can universally define the polymeric (macromolecular) state, a molecular mass of at least several thousand is generally taken as indicating its start. Such polymer molecules may be linear, branched, have a network structure, etc. These different molecular geometries influence the properties of the given polymer very significantly.[4,5]

It is difficult to provide a satisfactory definition of the term 'plastics'. Attempts at reasonably concise definitions tend to include certain materials such as rubbers, adhesives, fibers, glasses and surface coatings which are not usually considered as plastics, and to exclude a number of materials such as bituminous plastics, shellac and polytetrafluorethylene which usually are considered as plastics. In reality, the term becomes defined by common usage rather than by a physical/chemical description. However, in general, it may be said that plastics are usually high-molecular-weight polymers that at some stage in their existence are capable of flow, but may also be brought into a non-fluid form in which they have sufficient toughness and strength to be useful in self-supporting applications. Although they may be self-supporting, this does not exclude the possibility of reinforcing the plastics with fibers, or other fillers, or laminating them with other materials. Sometimes metals are coated with plastics, but usually at a greater thickness than is common with surface coatings such as paint films (which are, of course, also polymers).

The rapid rise of the plastics industry may be attributed to a number of factors. Foremost has been the fact that while many materials of construction have been subjected to continual increase in their price, the development of the petrochemicals industry and economies of scale have, for most of the time, led to reductions in the prices of plastics materials. Thus, with the passage of time, more and more products constructed from traditional materials have become cheaper to produce from plastics. The trend of increased plastics usage seems bound to continue in the foreseeable future, now driven by our ever-increasing ability to make polymer molecules (plastics) with better controlled molecular architectures[6] and by better processing technologies.[7]

Such a growth also requires, of course, that plastics possess properties suitable for the end uses envisaged. It is now possible, by control of synthesis, by chemical modification, by careful control of the relevant processing technology (injection molding, extrusion, etc.) or by the selective use of additives such as fibers, nanofillers, etc., to make products varying widely in their properties. The following is a list of some of the salient properties expected of plastics materials.

1. Tenacity. While some plastics are rigid and others flexible, all commercial materials show a degree of strength and toughness when stressed rapidly, superior to simple crystals and common glass.
2. Low thermal conductivity.
3. Low electrical conductivity.
4. Low heat resistance compared with common metals. The vast majority of plastics will not withstand 100 °C for extended periods and only a very few highly specialized products will withstand temperatures of 400 °C and above.

3.31.3 The Chemical Nature of Plastics

3.31.3.1 Free-Radical Addition Polymerization of Monomers with Double Bonds

In this case, the reactive double bond in a small molecule, such as ethylene or propylene, allows it to join another similar molecule.[5] These small molecules are known as monomer molecules. The chemical equation below shows this process for ethylene. The value of n in the equation can typically exceed 10 000 and can rise above 1 000 000.

$$n\mathrm{CH_2=CH_2} \rightarrow [-\mathrm{CH_2}-\mathrm{CH_2}-]_n$$

Such a molecule is referred to as a polymer, in this case polyethylene. Styrene, propylene, vinyl

chloride, vinyl acetate, and methyl methacrylate are other examples of monomers that can polymerize in this way. Sometimes, two monomers may be reacted together so that residues of both are to be found in the same chain. Such materials are known as copolymers and are exemplified by ethylene–vinyl acetate copolymers and styrene–acrylonitrile copolymers. If there are three such repeat units in a given polymer, it is termed a terpolymer.

3.31.3.2 Step-Growth Polymerization

In this case, reaction between two functional groups occurs, which leads to the production of a polymer and also a small molecule. This is a condensation reaction. A good example of this type of chemistry is the reaction between adipic acid and hexamethylene diamine, which yields nylon-6,6 and water as the small molecule:

$$n\mathrm{HOOC(CH_2)_4COOH} + n\mathrm{H_2N(CH_2)_6NH_2} \rightarrow [-\mathrm{OC(CH_2)_4CONH(CH_2)_6NH}-]_n + 2n\mathrm{H_2O}$$

Most nylons, polyesters, phenolics and a number of other plastics are produced by this route.[8]

3.31.3.3 Rearrangement Polymerization

Here the mechanism resembles step-growth polymerization, but no small molecule is split at each individual reaction step. In the first example, 1,4-butane diol reacts with hexamethylene di-isocyanate to give polyurethane:

$$n\mathrm{HO(CH_2)_4OH} + n\mathrm{OCN(CH_2)_6NCO} \rightarrow [-\mathrm{O(CH_2)_4OOCNH(CH_2)_6NHCO}-]_n$$

In the second, ε-caprolactam, a ring compound opens up to give nylon-6:

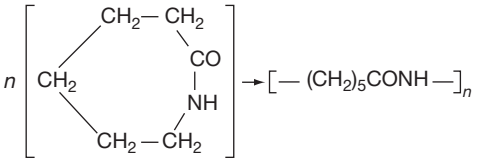

The polymerization of ε-caprolactam is commonly known as a ring-opening polymerization, a technique also used with other cyclic compounds such as ethylene oxide, propylene oxide and tetrahydrofuran.

3.31.3.4 Ionic Polymerization

In the case of ionic polymerization, the growing polymer molecules (commonly referred to as polymer chains) are temporarily terminated by ionic groups, which may be anionic (anionic polymerization) or cationic (cationic polymerization). The major advantage of this type of polymerization is that it offers good control over the resulting molecular architecture.[8]

Polymers may also be obtained from biological sources.[9,10] Cellulose, the principal constituent of cotton and a major constituent of wood, is such a polymer. So also are lignin, chitin from crustacean shells, natural rubber, gutta percha, and proteins. Sand (silica) may be considered as an inorganic polymer. While many of these are unmodified, some, like cellulose, cannot be considered as plastics in their natural state, but if chemically modified, useful plastics materials such as cellulose acetate, celluloid, and ethyl cellulose may be obtained. Natural rubber is clearly the basis of a huge worldwide industry.

3.31.4 The Physical Nature of Plastics

Many polymers, such as polystyrene, consist of long chain-like molecules of high molecular weight. A typical average molecular weight for a polystyrene sample is about 200 000 and since the molecular weight of the monomer is 104 this implies that there are around 2000 repeat units joined together in a typical molecule taken from that sample. It is the case in nearly all plastics that a given sample contains molecules covering a distribution of molecular weights. This distribution, in some cases, may be very wide.[5] Since the backbone carbon–carbon bonds can rotate relatively freely, such molecules are most unlikely to be stretched out, but are more likely to be coiled up into what is referred to as a random-coil conformation.[11]

In the case, for example, of polystyrene, the molecules at room temperature do not have enough rotational energy to twist around the backbone chemical bonds and so, in the mass, the polymer is rigid. On heating above a certain temperature, sufficient energy for such subchain movement is obtained and on application of a shearing stress in processing such as extrusion, the polymer molecules partly uncoil. Chain segments slip past each other and, in the mass, flow occurs. On cessation of stress, slippage ceases, the chains again coil up and, on cooling, the mass again hardens. If desired, the whole process of heating, shearing and cooling may be repeated. Materials that behave in this way are known as

thermoplastics.[7,11] Two points should, however, be noted. Firstly, if cooling is faster than the chain recoiling process, then a frozen-in molecular orientation will result. This can grossly affect the polymer properties, in some cases adversely. Secondly, repeated heating and shearing may be accompanied by changes such as oxidation and polymer degradation, which will limit, in practice, the number of times heating and cooling can be applied on a particular polymer sample. In terms of tonnage, the bulk of plastics produced are thermoplastics, a group that includes the polyethylenes, polypropylene, polystyrene, polyvinyl chloride (PVC), the nylons, polycarbonates and cellulose acetate. There is, however, a second class of materials, the thermosetting plastics.[7,11] They comprise long-chain molecules, similar to a typical thermoplastic molecule, however, as rather smaller molecules. They are formed, often in a mold, into the desired final shape and then subjected to chemical reaction, often by heating, in such a way such that the molecules link with one another to form a cross-linked network as shown in **Figure 1**. As the molecules are now interconnected, they can no longer slide extensively past one another and the material is said to have set, cured or cross-linked. Plastic materials behaving in this way are designated as thermosetting plastics, a term which is also used to include those materials that can be cross-linked with suitable catalysts at room temperature. Important thermosetting plastics include the phenolic resins, melamine–formaldehyde resins, the epoxy resins and unsaturated polyester resins used in glass-reinforced plastics.

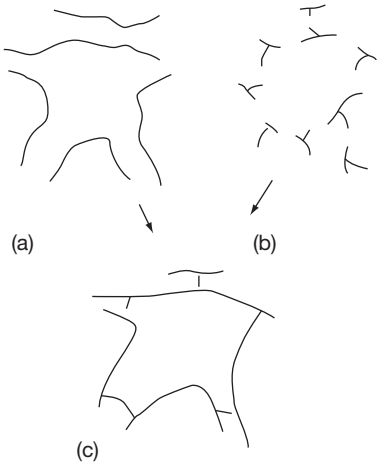

Figure 1 Joining up of (a) long-chain molecules or (b) branched molecules to produce (c) a cross-linked polymer.

3.31.4.1 Thermoplastics

Thermoplastics may be considered in four subclasses: (a) amorphous thermoplastics; (b) rubber-modified amorphous thermoplastics; (c) plasticized amorphous thermoplastics, and (d) crystalline thermoplastics.

3.31.4.1.1 Amorphous thermoplastics

These are made from polymers that have a sufficiently irregular molecular structure to prevent them from crystallizing. Examples of such materials include polystyrene and polymethyl methacrylate. The structural irregularity in these examples arises from the free-radical addition polymerization process used in their synthesis. This results in the repeat unit side groups being present in essentially random configurations,[5] which is sufficient to prevent crystallization.

At very low temperatures, these materials are glass-like and rigid. On heating, a temperature is eventually reached where the material softens. If the polymer is of sufficiently high molecular weight, it becomes rubbery above this temperature. The temperature at which this occurs is known as the glass transition temperature (T_g),[5,11] and is in effect the temperature at which the polymer molecules have sufficient rotational energy to be able to coil and uncoil. As the individual polymer molecules, in their random-coil conformations, interpenetrate each other, the resulting chain entanglements prevent flow. At higher temperatures there are two possibilities. Polymers of moderate molecular weight may achieve such energy that they can flow, while high molecular weight materials may decompose before the flow point is reached. This is shown schematically in **Figure 2**,

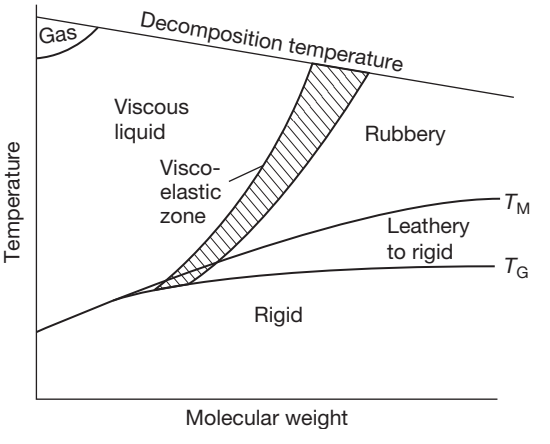

Figure 2 Temperature–molecular weight phase diagram for amorphous polymers.

which indicates the phases in which this type of polymer can occur. It should be stressed that the boundary lines will change position with change of polymer type.

It can be seen that up to a certain molecular weight a polymer may be processed either as a liquid (by injection molding, extrusion, etc.) or as a rubber (by vacuum forming, sheet blowing, hot pressing). In the case of a polymer of much higher molecular weight, it can be seen that it can only be shaped in the rubbery state, and if it is intended to be processed by, say, injection molding, then the molecular weight may first have to be reduced. An important illustration of this is with well-known acrylic materials such as Perspex (polymethyl methacrylate), which can have too high a molecular weight to be injection-molded.

It is possible to make some generalizations about the properties of amorphous thermoplastics.

1. The T_g will determine the maximum temperature of use of the material as a rigid thermoplastic. For amorphous rubbers, the T_g value will determine the minimum temperature of use.
2. Below T_g, most amorphous polymers show a more or less linear stress–strain curve with no yield point. The tensile strengths are typically around 50 MPa, elongation at failure usually less than 10%, and the elastic modulus typically around 2.5 GPa. Since the area under the curve provides a measure of the energy required to rupture the specimen, and since this area is small, such polymers will have a low impact strength (which is closely related to the energy to break) and will break with a brittle fracture.
3. They are generally more permeable to gases than crystalline polymers. This is more so above T_g than below.
4. They usually have a much wider range of solvents than crystalline polymers.

3.31.4.1.2 Rubber-modified amorphous polymers

The brittleness of amorphous polymers has been a hindrance in their commercial development. However, for reasons now substantially understood, the addition of rubbery polymers as dispersed droplets into the glassy polymer can often lead to substantial increases in impact strength,[12] albeit usually at some cost to tensile strength and, in many cases, to transparency.

The most important polymers of this important class are as follows.

1. High-impact polystyrene (a polystyrene modified with a styrene–butadiene rubber (SBR) or a polybutadiene rubber).
2. ABS, which is based on a copolymer of acrylonitrile, butadiene and styrene.
3. Methacrylate–butadiene–styrene polymers (MBS) and related materials, which are chemically similar to ABS but are often available in transparent form.
4. Rubber toughened epoxy resins.
5. High-impact PVC; in this case the impact modifiers are not always rubbers, but the mechanism of their action is probably similar.

3.31.4.1.3 Plasticized amorphous thermoplastics

Certain plastics may be mixed with high boiling temperature, low-volatility liquids to give products of lower T_g. The most important example of this class occurs with PVC, which is often mixed with liquids such as di-*iso*-octyl phthalate, tritolyl phosphate, or other diesters to bring the T_g below room temperature. These liquids work by increasing the free volume in the materials, thereby facilitating the segmental motions that constitute the glass transition process. If their volatility is a problem in a given case, it may be possible to use either a polymeric plasticizer[13] or a chemically bound plasticizer.[14] The resultant plasticized PVC is flexible and to some degree quite rubbery. Other commonly plasticized materials are cellulose acetate and cellulose nitrate.

It is essential to appreciate that such plasticizers may also considerably modify the chemical properties of the plastic material since the plasticizer may be readily extracted by certain chemicals and chemically attacked by others while the base polymer may be unaffected.

3.31.4.1.4 Crystalline thermoplastics

While polymers such as polyethylene and nylon-6,6 do not show any regular external form, which is characteristic of crystals, closer examination reveals that they have many properties common to crystalline materials. They exhibit distinct X-ray diffraction patterns[5] and exhibit specific melting in differential scanning calorimetry (DSC).[5] Although the exact nature of this crystallinity is not fully resolved in some cases, it would appear that polymer segments pass through zones in which molecular arrangement is highly ordered, that is, crystalline. In some ways these zones act like knots, or cross-links, holding the individual molecules of such materials together.

The effect of heating crystalline polymers from low temperatures is more complex than with amorphous polymers. Initially, the material is rigid and hard. As the temperature goes through the T_g, light crystalline materials soften slightly and become leather-like, but highly crystalline materials show relatively little change in properties. Further heating results in the crystals melting, often over quite a wide temperature range, and the polymer becomes rubbery. Whether or not it melts or decomposes first on further increase in temperature will depend on both the particular polymer and its molecular weight.

A typical phase diagram for such polymers is given in **Figure 3**. With such crystalline polymers, the melting point, T_m, replaces the T_g as the factor usually determining the maximum service temperature of thermoplastics and minimum service temperature of rubbers. However, it is more difficult to make generalizations about properties. The following remarks may, however, be pertinent for crystalline polymers.

1. Below T_g, tensile strengths are usually at least as high for crystalline polymers as for amorphous ones. Between T_m and T_g, the strength and rigidity will be very dependent on the degree of crystallinity and to some extent on the molecular weight. Tensile strengths commonly range from below 10 to around 90 MPa.
2. In most cases, crystal densities differ from those of amorphous polymers. This leads to differences in refractive index, which in turn cause scattering of light at boundaries between amorphous and crystalline zones. Such materials are opaque, except in certain instances where the crystal structure can be carefully oriented to prevent such scattering of light.

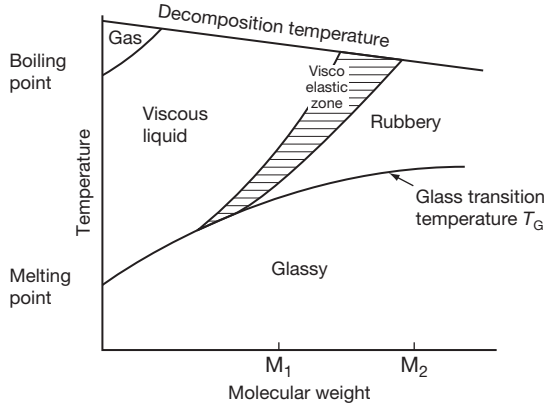

Figure 3 Temperature–molecular weight phase diagram for crystalline polymers.

3. The close molecular packing makes diffusion more difficult than with amorphous polymers compared under similar circumstances, that is, either below T_g, or above T_g but below T_m, of the crystalline polymer.
4. Thermodynamic considerations lead to considerable restriction in the range of solvents available for such polymers.[5,11]

3.31.4.2 Thermosetting Plastics

If glycerol, a trihydric alcohol, reacts with phthalic anhydride, three ester links can be made from each glycerol unit. Continued reaction will eventually cause the molecules to link up in a three-dimensional network in which, theoretically at least, the whole polymer mass becomes one giant molecule.

For reasons of production feasibility, such cross-linked plastics are normally prepared in two stages. In the first stage, either a low-molecular-weight branched polymer or a higher-molecular-weight linear (unbranched) polymer is produced. Such materials are thermoplastic and in most cases soluble in some solvents. At a convenient (later) time, this intermediate is subjected to heat, electromagnetic radiation (such as ultraviolet), or chemical reactants, such that the branched molecules join together, or the linear polymers cross-link, thereby producing an infusible, insoluble material. Since, in the early days of the plastics industry, the cross-linking processes required heat, these materials became known as 'thermosetting plastics.' Today this term is commonly extended to materials which can cross-link at room temperature: for example, many organic coating systems (or paints).

Because thermosetting plastics have an irregular form, they are amorphous, and because of their network structure, they are invariably rigid. They do not dissolve without decomposition, but may swell in appropriate solvents, the amount of swelling decreasing with increasing cross-link density. Well-known thermosetting plastics include the phenolics, urea–formaldehyde and melamine–formaldehyde resins, unsaturated polyesters and epoxy resins.

3.31.4.3 Reinforced Plastics

The mechanical properties of plastic materials may often be considerably enhanced by embedding fibrous materials in the polymer matrix.[15] While such techniques have been applied to thermoplastics, the greatest developments have taken place with the thermosetting plastics. The most common reinforcing materials are

glass and cotton fibres,[16] but many other materials including paper, carbon fiber, inorganic whiskers, particulates including nanoscale particulates,[15] are used. Reinforcing fibers normally have a modulus of elasticity that is substantially greater than the resin, so that under tensile stress much of the load is borne by the fibers. The modulus of the composite is, therefore, intermediate to that of the fiber and of the resin.

In addition to the nature of resin and fiber, the laminate properties also depend on the degree of bonding between the two main components and on the presence of other additives, including entrained air bubbles. Because of this, some parts, fabricated by simple hand build-up techniques, may exhibit strengths no better, or even worse, than unreinforced materials. This problem is often worst with glass fibers, which are, therefore, normally treated with special finishes to improve the resin–glass bond.

The highest mechanical strengths are usually obtained when the fiber is used in fine fabric form, but for many purposes the fibers may be used in mat form, particularly glass fiber. The chemical properties of such laminates are largely determined by the nature of the polymer, but capillary attraction along the fiber–resin interface can occur when some of these interfaces are exposed at a laminate surface. In such circumstances, the resistance of both the reinforcement and the matrix must be considered when assessing the suitability of a laminate for use in chemically demanding situations. For more information, the reader is referred to the article on polymer–matrix composites.

3.31.5 Polymer Orientation

It is not difficult to appreciate that if polymer molecules are aligned, as in **Figure 4(a)**, then a much higher tensile strength will be obtained if a test is carried out in the X–X direction as opposed to the Y–Y direction. It is also not difficult to understand why such a material has lower impact strength than a randomly coiled mass of molecules, **Figure 4(b)**, because of the ease of cleavage of the material parallel to the X–X direction.[15]

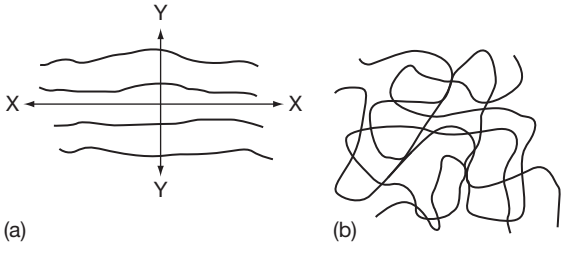

Figure 4 Polymer segment alignment: (a) parallel and (b) random.

Similar remarks may also be made where crystal structures, or fiber reinforcements, are aligned rather than the individual molecules. For fibers and filaments such orientation is desirable, but for solid objects where impact strength is often more important than tensile strength such orientation is usually unwelcome. It can also have further unwanted effects. This arises from the fact that oriented molecules are thermodynamically unstable and will at the first opportunity try to achieve random-coil conformations. Thus, on heating samples up to temperatures near T_g, severe distortion can occur, leading to warped moldings.

Another serious effect, solvent stress cracking,[17] occurs with liquids which are not in themselves solvents but which may wet the polymer surfaces. These facilitate relief of frozen-in stresses by surface cracking, which can be a severe problem in using many injections and blow moldings with specific chemicals. Examples of this are white spirit with polystyrene, carbon tetrachloride with polycarbonates and soaps and silicone oils with low-molecular-weight polyethylenes.

In addition to orientation in one direction (monoaxial orientation), biaxial orientation is possible. This is achieved when the sheet is stretched in two directions, resulting in layering of the molecules. This can increase the impact strength, tensile strength and solvent cracking resistance of polymers, and with crystalline plastics the polymer clarity may also be improved.

3.31.6 The Chemical Properties of Polymers

It is common practice to talk about the chemical resistance of polymers, unaware of the fact that this can mean different things. To avoid this it is probably wiser to differentiate between the following.

1. Resistance of a polymer to chemical attack resulting in breakdown of some covalent bonds and the formation of new ones. This could involve molecular breakdown initiated by heat or radiation, including ultraviolet light.
2. Resistance to dissolution by liquids.
3. Resistance to cracking in aggressive environments.
4. Permeability to gases and liquids.

It is also important to bear in mind that, for specific end uses, polymers are commonly mixed with a number of additives such as plasticizers, stabilizers, antioxidants, fillers, fire retardants, pigments, dyes and other polymers, and that this may well have an important influence on their chemical properties. The following discussion will, however, be confined to pure polymers.

3.31.6.1 Resistance to Chemical Attack

Expressed simply, the resistance of a polymer to chemical attack may be said to be determined by the following factors:

- the nature of the chemical bonds present,
- interactions between chemical groups that occur repeatedly along the molecular chain, and
- the presence of occasional 'weak-links.'

In commercial polymers, there are a rather limited number of chemical bond types to be found and it is possible to make a number of general observations about the chemical reactivity in the following list of examples.[5,8,18]

1. Polyolefins such as polyethylene and polypropylene contain only C–C and C–H bonds and may be considered simply as high-molecular-weight paraffins. Like the simpler paraffins, they are somewhat inert, and their major chemical reaction is a substitution reaction, for example, halogenation. In addition, the branched polyethylenes and all the higher polyolefins contain tertiary carbon atoms which are reactive sites for oxidation. Because of this, it is necessary to add antioxidants to stabilize the polymers against such oxidation. Some polyolefins may be cross-linked by peroxides.
2. Polytetrafluoroethylene (Teflon) contains only C–C and C–F bonds. These are both very stable and the polymer is exceptionally inert.[19] A number of other fluorine-containing polymers are available, which may contain in addition C–H and C–Cl bonds. These are somewhat more reactive, and those containing C–H bonds may be cross-linked by peroxides and certain diamines and diisocyanates.
3. Many polymers, such as the diene rubbers, contain double bonds. These will react with many agents such as oxygen, ozone, hydrogen halides and halogens. Ozone, and in some instances oxygen, will lead to scission of the main chain at the site of the repeat-unit double bond and this will have a catastrophic effect on the molecular weight. The rupture of one such bond per chain will halve the average molecular weight.
4. Ester, amide, and carbonate groups are susceptible to hydrolysis. When such groups are found in the main chain, their hydrolysis will also result in a reduction of molecular weight. Where hydrolysis occurs in a side chain, the effect on molecular weight is usually insignificant. The presence of benzene rings adjacent to these groups may offer some protection against hydrolysis, except where organophilic hydrolyzing agents are employed.
5. Hydroxyl groups are extremely reactive. These occur attached to the backbones, for example, of cellulose and polyvinyl alcohol.
6. Benzene rings in both the backbone structure and on the side groups can be subjected to substitution reactions. Such reactions do not normally cause great changes in the fundamental nature of the polymer. They seldom lead to chain scission or cross-linking. However, the phenolic resins provide an important exception to this.

There are numerous examples of chemical reactions consequent upon chemical groups that occur repeatedly along a chain. In some cases, the reaction occurs randomly between adjacent pairs of groups such as in the reaction between aldehydes and polyvinyl alcohol and of zinc dust with polyvinyl chloride:

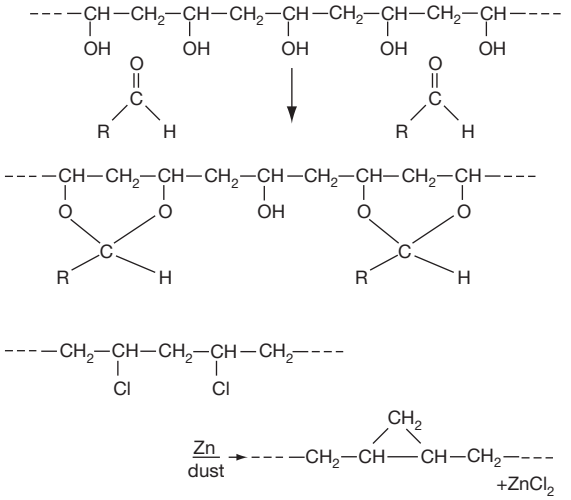

In other instances the reactions appear to occur in sequence down individual chains, for example, in the depolymerization reactions of polyformaldehyde (polyacetal) and polymethyl methacrylate, which are referred to sometimes as unzipping reactions.

In other cases, cyclization reactions can occur such as on heating polyacrylonitrile.

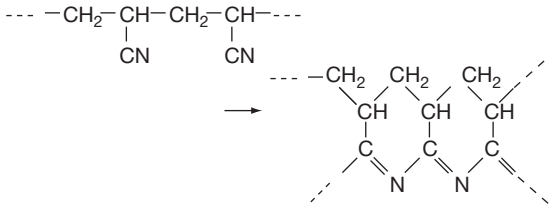

It is commonly found that polymers are less stable, particularly to molecular breakdown at elevated temperatures, than low-molecular-weight compounds containing similar groupings. In part, this may be due to the regular repetition of groups along a chain as discussed above, but more frequently it is due to the presence of weak links along the chain. These may be at the end of the chain (terminal) arising from specific mechanisms of chain initiation and/or termination, or nonterminal, and due to such factors as impurities that become built into the chain, an aberration in the modus operandi of the polymerization process or, perhaps, to branch points.[20]

The combination of weak links and unzipping can be catastrophic and has been a particular problem in the commercial development of some polymers, in particular polyacetals.[21]

3.31.6.2 Polymer Solubility

The solution properties of polymers have been subjected to intensive study, in particular to complex mathematical treatment.[5,22,23] This section will, however, confine the discussion to a qualitative and practical level.[5]

One chemical will be a solvent for another if the molecules are able to co-exist on a molecular scale, that is, the molecules show no tendency to separate. In these circumstances, the two species are said to be compatible. The definition concerns equilibrium properties and gives no indication of the rate of solution, which will depend on other factors such as temperature, the molecular size of the solvent and the size of voids in the solute.

Molecules of two different species will be able to coexist if the force of attraction between different molecules is not less than the forces of attraction between two like molecules of either species. This is shown more clearly by reference to **Figure 5**, which shows two types of molecules A and B. The average forces between the like molecules are F_{AA} and F_{BB}, and the average forces between dissimilar molecules are F_{AB}. If F_{AA} was the largest of these three forces, then the A molecules would tend to congregate or cohere, rejecting the B molecules. A similar phase separation would occur if F_{BB} was the greatest.

It is, therefore, seen that only when $F_{AB} \geq F_{AA}$ and $F_{AB} \geq F_{BB}$ will coexistence or compatibility be possible. Obviously, if it is possible to obtain some measure of these forces, it should be possible to make predictions about polymer solubility. What then is a suitable measure of the forces holding like molecules together? One would expect the latent heat of vaporization, L, to exceed that cohesion energy by an amount corresponding to the work done by evaporation, an amount approximating to RT, where R is the gas constant and T the absolute temperature. Such a diagram of $(L - RT)$ might be a sufficient measure if all of the molecules were of about the same size.

However, it is reasonable to suppose that compatibility should not be greatly affected by molecular size and that the shorter polymer molecules in **Figure 6(a)** should be just as compatible as the longer ones in **Figure 6(b)**, although their theoretical latent heats of vaporization will be greatly different. In such circumstances, a reduced diagram of $(L - RT)/M$ will give a measure of intermolecular energy per unit weight. Similarly, a measure of the intermolecular

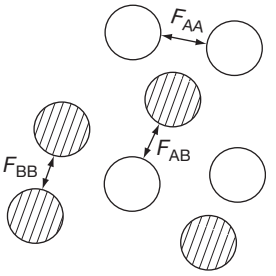

Figure 5 Two different molecular species will be compatible if $F_{AB} \geq F_{AA}$ and $F_{AB} \geq F_{BB}$. In other circumstances the molecules will tend to separate if they have sufficient energy for molecular movement.

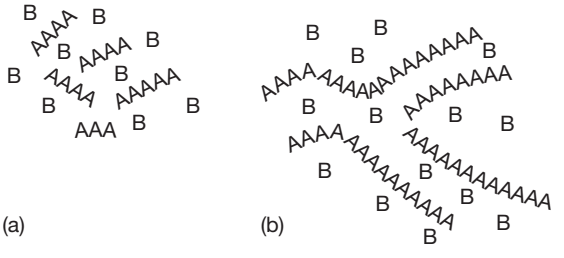

Figure 6 Polymer molecules: (a) short and (b) long.

or cohesion energy per unit volume will be given by the following expression, where D is the density.

$$\frac{L - RT}{M/D}$$

This expression is known as the cohesive energy density[5,24] with units of megapascal. The square root of this expression is more commonly encountered in quantitative studies and is known as the solubility parameter and given the symbol δ.

$$\delta = \sqrt{\frac{L - RT}{M/D}} \text{MPa}^{1/2}$$

The solubility parameter is, thus, an experimentally determinable property, at least for low-molecular-weight materials. In the case of polymers that cannot be vaporized without decomposition, a method of calculating from a knowledge of structural formula has been devised by Small and others.[24,25] It is now possible to provide an estimate of F_{AA} and F_{BB}, but the magnitude of F_{AB} has to be considered separately for each different system.

3.31.6.2.1 Amorphous nonpolar polymers and amorphous nonpolar solvents

It is generally assumed in these circumstances, by analogy with gravitational and electrostatic attractions, that F_{AB} will be equal to the geometric mean of F_{AA} and F_{BB}. Thus, if by definition $F_{AA} > F_{BB}$, then, $F_{AA} > F_{AB} > F_{BB}$. Considering these conditions, it can be seen that compatibility will occur between amorphous nonpolar polymers and solvents only when $F_{AA} = F_{AB} = F_{BB}$; that is, when polymer and solvent have similar solubility parameters (in practice to within about 2 $\text{MPa}^{1/2}$). Reference to the values of δ in Tables 1 and 2 provides examples of this. For example, natural rubber (unvulcanized) ($\delta = 16.5$) is soluble in toluene ($\delta = 18.2$) and carbon tetrachloride ($\delta = 17.5$) but not in ethanol ($\delta = 25.9$). Cellulose diacetate ($\delta = 23.2$) is soluble in acetone ($\delta = 20.4$), but not in methanol ($\delta = 29.6$) or toluene ($\delta = 18.2$). It should be noted that apart from the problem of achieving a molecular level of dispersion, it is not necessary for the solvent to be liquid; it may be an amorphous solid. Such tables are of greatest use with nonpolar materials with values of δ not exceeding 19.4 $\text{MPa}^{1/2}$ and when the polymers are amorphous.

3.31.6.2.2 Crystalline nonpolar polymers and amorphous solvents

Most polymers of regular structure will crystallize if cooled below the melting point, T_m. This is in accordance with the thermodynamic law that a process will occur only if there is a decrease in Gibbs free energy ($-\Delta G$) in going from one state to another. Such a decrease occurs on crystallization as the molecules pack in a regular fashion. Since a process occurs only when it is accompanied by a decrease in free energy, there is no reason why a crystalline nonpolar polymer should dissolve in a solvent at temperatures well below the melting point. However, as the melting point is approached, the $T\Delta S$ term in the equation below increases.

$$\Delta G = \Delta H - T\Delta S$$

Table 1 Solubility parameters (δ) of polymers

Polymer	*δ ($\text{MPa}^{1/2}$)*	*Polymer*	*δ ($\text{MPa}^{1/2}$)*
Polytetrafluorethylene	12.6	Polyethyl acrylate	18.8
Polychlorotrifluoroethylene	14.7	Polysulfide rubber	18.4–19.2
Polydimethyl siloxane	14.9	Polystyrene	18.8
Ethylene–propylene rubber	16.1	Polychloroprene rubber	18.8–19.2
Polyisobutylene	16.1	Polymethyl methacrylate	18.8
Polyethylene	16.3	Polyvinyl acetate	19.2
Polypropylene	16.3	Polyvinyl chloride	19.4
Polyisoprene (natural rubber)	16.5	Bisphenol A polycarbonate	19.4
Polybutadiene	17.1	Polyvinylidene chloride	20.0–24.9
Styrene–butadiene rubber	17.1	Ethylcellulose	17.3–21.0
Poly-*t*-butyl methacrylate	16.9	Cellulose dinitrate	21.5
Poly-*n*-butyl methacrylate	17.7	Polyethylene terephthalate	21.8
Poly-*n*-hexyl methacrylate	17.5	Acetal resins	22.6
Polybutyl acrylate	18.0	Cellulose diacetate	23.1
Polyethyl methacylate	18.4	Nylon 66	27.7
Polymethylphenyl siloxane	18.4	Polymethyl α-cyanoacrylate	28.8
		Polyacrylonitrile	28.8

Table 2 Solubility parameters (δ) and partial polarities (P) of some common solvents

Solvent	δ ($MPa^{1/2}$)	*P*	*Solvent*	δ ($MPa^{1/2}$)	*P*
Dimethylpropane	12.9	0	Chloromethane	19.8	–
2-Methylpropene	13.7	0	Dichloromethane	19.8	–
Hexane	14.9	0	1,2-Dichloroethane	20.0	0
Ethoxyethane	15.1	0.03	Cyclohexane	20.2	–
Octane	15.5	0	Carbon disulfide	20.4	0
Methylcyclohexane	15.9	0	Acetone	20.4	0.69
2-Methylpropanoate	16.1	–	Octanol	21.0	0.04
2,4-Dimethylpentan-3-one	16.3	0.3	Butanenitrile	21.4	0.72
2-Methyl butyl acetate	16.3	–	Hexanol	21.8	0.06
Cyclohexane	16.7	0	2-Butanol	22.0	0.11
2,2-Dichloropropane	16.7	–	Pyridine	22.2	0.17
3-Methyl-1-butyl acetate	16.9	–	Nitroethane	22.6	0.71
Pentylacetate	17.3	0.07	Butanol	23.3	0.10
Tetrachloromethane	17.5	0	Cyclohexanol	23.3	0.08
Hexan-2-one	17.7	0.4	2-propanol	23.4	–
Piperidine	17.7	–	Propanol	24.3	0.15
Xylene	18.0	0	Dimethyl formamide	24.7	0.77
Methoxymethane	18.0	–	Hydrogen cyanide	24.7	–
Toluene	18.2	0	Acetic acid	25.7	0.30
1,2-Dichloropropane	18.4	–	Ethanol	25.9	0.27
Ethyl acetate	18.6	0.17	Formic acid	27.5	–
Benzene	18.8	0	Methanol	29.6	0.39
4,4-Hydroxymethylpentan-2-one	18.8	–	Phenol	29.6	0.06
Trichloromethane	19.0	0.02	Glycerol	33.7	0.47
1,1,2-Trichloroethene	19.0	0	Water	47.7	0.82
Tetrachlorethane	19.2	0.01			
2-Hydroxyethoxyethan-2-ol	19.6	–			

Here, T is the absolute temperature, ΔS the entropy change, and ΔH the enthalpy change. So, with increasing temperature, ΔG can become negative and dissolution can therefore occur.

Hence, at room temperature, there are no solvents for polyethylene, polypropylene, poly-4-methylpentene-1, polyacetal or polytetrafluoroethylene, but at temperatures of about 30 °C below their melting points solvents of similar solubility parameter are effective. It should also be noted that at room temperature swelling may occur in the amorphous zones of the polymer in the presence of solvents of similar solubility parameter.

3.31.6.2.3 Amorphous nonpolar polymers and crystalline solvents

This situation is identical to the previous one, and occurs, for example, when paraffin wax is mixed into rubber above its melting point. On cooling, the paraffin wax tends to crystallize, some of it on the surface of the rubber. Such a bloom is one way of protecting a diene rubber from ozone attack.

3.31.6.2.4 Amorphous polar polymers and solvents

Molecules are held together by one, or more, of four types of forces: dispersion, dipole, induction and hydrogen bonding. In the case of aliphatic hydrocarbons, the so-called dispersion forces predominate. However, many covalent bonds contain dipoles, with one end being partially positively charged and the other partially negatively charged. Such dipoles may interact with dipoles on other molecules and lead to enhancement of the total intermolecular attraction. Molecules that possess dipoles and interact in this way are said to be polar. Many well-known solvents (e.g., water) and polymers (e.g., PVC) are polar, and it is generally considered that for interaction both the solubility parameter and their degrees of polarity should match. This is usually expressed in terms of partial polarity,[24] which expresses the fraction of total forces due to dipole bonds. Some figures for partial polarities (P) for solvents are given in Table 2, but there is a lack of quantitative data on the partial polarities of polymers. A comparison of

polarities has to be made by common sense rather than a quantitative approach. For example, hydrocarbon polymers would be expected to have a negligible polarity and would then be more likely to dissolve in toluene rather than diethyl ketone, although both have similar solubility parameters.

3.31.6.2.5 Crystalline polar polymers and solvents

It has already been pointed out that at temperatures well below their melting point crystalline nonpolar polymers will not interact with solvents, and similar considerations can apply to a large number of polar crystalline polymers. It has, however, been possible to find solvents for some polar, crystalline polymers such as the nylons, polyvinyl chloride and the polycarbonates. This is because of specific interactions between polymer and solvent that may often occur by, for example, hydrogen bonding.

For example, nylon-6,6 will dissolve in formic acid, glacial acetic acid and phenol, solvents that not only have similar solubility parameters but also are capable of acting as proton donors while the carbonyl groups on the nylon act as proton acceptors.

More interesting examples are given with PVC and the polycarbonate of bis-phenol A – both are slightly crystalline polymers. It is noticed here that while dichloromethane is a good solvent and tetrahydrofuran a poor solvent for the polycarbonate, the reverse is true for PVC, yet all four materials have similar solubility parameters. It would seem that the explanation is that a form of hydrogen bonding occurs between the polycarbonate and methylene chloride and between PVC and tetrahydrofuran. In other words, there is a specific interaction between each solvent pair:

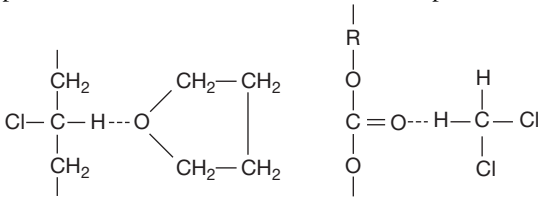

Many studies have been made to assess the propensity to hydrogen bonding of chemical structures.[24] As a result, the following broad generalizations may be made.

1. Proton donors include highly halogenated compounds such as chloroform and pentachlorethane; less halogenated materials are weaker donors.
2. Polar acceptors include, in roughly descending order of strength, amines, ethers, ketones, aldehydes, and esters, with aromatic materials usually being more powerful than aliphatic ones.
3. Some materials such as water, alcohols, carboxylic acids, and primary and secondary amines may be able to act simultaneously as proton donors and acceptors. Cellulose and polyvinyl alcohol are two polymers that also function in this way.
4. A number of solvents such as the hydrocarbons, carbon disulfide and carbon tetrachloride are quite incapable of forming hydrogen bonds.

3.31.6.2.6 Rubbers and thermosetting plastics

Covalently cross-linked rubbers and plastics cannot dissolve without chemical change. They will, however, swell in solvents of similar solubility parameter, the degree of swelling decreasing with increasing cross-link density. The solution properties of the thermoplastic elastomers, which are two-phase materials, are much more complex and dependent on whether or not the rubber phase and the thermoplastic domains are dissolved by the solvent.

3.31.6.3 Resistance to Cracking in Aggressive Environments

It has been found with many rigid plastics materials that, under stresses well below the normal yield stress, cracking occurs in environments where the polymer will be unaffected when free of stress. The mechanism for this stress-cracking phenomenon is not fully understood and, indeed, there may well be different mechanisms in different circumstances. There do, however, appear to be four main types.

- Solvent cracking of amorphous polymers.
- Solvent cracking of crystalline polymers.
- Environmental stress cracking.
- Thermal cracking.

Examples of solvent cracking of amorphous polymers[26] are polystyrene with white spirit, polycarbonate with methanol and polysulfone with ethyl acetate. The propensity to solvent stress cracking is, however, far from predictable, and intending users of a polymer should check on this before use.

In the case of crystalline polymers, it may be that solvents can cause cracking by activity in the amorphous regions of these more complex morphologies. Examples of this are benzene and toluene with polyethylene. In polyethylene, however, a greater problem is that of environmental stress cracking,[17] which

occurs with materials such as soap, alcohols, surfactants and silicone oils. Many of these are highly polar materials that cause no swelling, but are simply absorbed either into, or on to, the polymer. This appears to weaken the surface and allows cracks to propagate from minute flaws. Cracking caused by heat (thermal cracking) appears to act in a similar manner, but in this case oxygen is the aggressive environment, becoming active at 70–80 °C with some polyethylenes.

3.31.6.4 Diffusion

The efficacy of polymers when used to protect metals from corrosive environments is, of course, strongly influenced by their efficiency as barrier materials. When applied to metals by some techniques, such as fluidized-bed coating, there is always the danger of 'macrodiffusion' through pinholes, which are gross imperfections in the surface region and which do not have to be visible to be very much greater than the dimensions of penetrating molecules.

Assuming, however, that the film is continuous, the concern then is with the permeability of the corrosive fluids in the polymer film. This involves both the dissolution of the fluid into the polymer, which will be determined by the conditions discussed previously, and the rate of diffusion of the fluid through the polymer. This has been discussed elsewhere[18,27] in detail, but may be summarized as follows.

1. The lowest diffusion rates occur with crystalline polymers below the T_g, since there is very little space through which diffusing molecules may pass.
2. Amorphous polymers below the T_g have a somewhat higher permeability, but diffusion is still difficult.
3. For amorphous polymers above the T_g, that is, in the flexible and rubbery states, there is more space (free volume) available through which diffusing molecules may pass, and so these materials show comparatively high diffusion rates with low-molecular-weight diffusing fluids.
4. For crystalline polymers between T_g and T_m, the diffusion rate is very dependent on the degree of crystallization.

3.31.7 Review of Commercial Plastics

3.31.7.1 Amorphous Thermoplastics

3.31.7.1.1 Polyvinyl chloride

PVC[28] is one of the two most important plastics in terms of tonnage and shows many properties typical of rigid amorphous thermoplastics. However, PVC is not a truly amorphous polymer in that it has short stereoregular repeat unit sequences which can lead to crystallinity values up to about 10 vol.%. PVC softens at about 70 °C, burns only with difficulty, but is thermally unstable. To reduce this instability, stabilizers are invariably compounded into the polymer.

Being slightly crystalline, there are a few good solvents, the best known of which are nitrobenzene, cyclohexanone, and tetrahydrofuran. When mixed with certain nonvolatile solvents such as some phthalates, adipates, and phosphates, flexible materials are obtained, which are referred to as plasticized PVC.

In order to improve toughness, many rubbers and other soft polymers may be used as additives to modify the compound. Some copolymers based on vinyl chloride are available of which the most important are the vinyl chloride–vinyl acetate materials used in flooring compositions and surface coatings.

3.31.7.1.2 Polystyrene

The volume of expanded polystyrene (PS) produced probably exceeds the total volume production of all other plastics (excluding the polyurethanes). About half the tonnage of polystyrene produced is in the form of high-impact polystyrene (HIPS): a complex blend containing styrene–butadiene rubber or polybutadiene.[7,19] Styrene–acrylonitrile (SAN) has improved heat resistance, oil resistance and slightly better impact strength.

3.31.7.1.3 Acrylonitrile–styrene–butadiene polymers (ABS)

These are complex blends and copolymers of excellent toughness.[7,19]

3.31.7.1.4 Poly(methyl methacrylate)

Poly(methyl methacrylate) (PMMA)[7,19] is used mainly where high light transmission and excellent weathering properties are of greatest importance. This polymer is the most well known of a very wide range of acrylic polymers that find use as rubbers, fibers, plastics, adhesives and surface coatings. The sheet forms (Perspex, Plexiglas, Oroglas) are often of high molecular weight and dissolve only with some difficulty.

3.31.7.1.5 Polyvinyl acetate and derivatives

Polyvinyl acetate is used largely for coating applications,[7,19] but the derivative polyvinyl alcohol will, provided there are some residual acetate groups, dissolve in water. Reaction products of polyvinyl

alcohol with aldehydes such as polyvinyl formal and polyvinyl butyral are also commercially available materials.

3.31.7.1.6 Cellulose-based plastics

These long-established materials[9,10] have limited chemical resistance. Ethyl cellulose is, however, often used in conjunction with mineral oil for hot-melt strippable coatings for protecting metal parts against corrosion and marring during transport and storage.

3.31.7.2 Crystalline Plastics

3.31.7.2.1 Polyethylene

The polyethylenes (high density, low density, linear low density, etc.) are among the largest tonnage polymeric materials produced worldwide.[7,19] They are attacked by only a few chemicals, are not swollen by water or common organic solvents, but are susceptible to environmental stress cracking in the presence of certain detergents, esters, alcohols and silicones. Commercial materials vary in the regularity of their molecular structure, the more regular grades having a higher density and rigidity and lower gas permeability.

3.31.7.2.2 Polypropylene

Polypropylene has similar chemical properties to polyethylene, but is less susceptible to environmental stress cracking. It may also be used at somewhat higher temperatures.[7,19]

3.31.7.2.3 Other polyolefins

A variety of other crystalline polyolefins such as polybutene-1 (improved creep resistance over polyethylene), poly-4-methyl pentene-1 (excellent temperature deformation resistance) and ethylene-vinyl acetate polymers (greater flexibility) are available.[7]

3.31.7.2.4 Polytetrafluorethylene

Polytetrafluorethylene (PTFE) does not absorb water, has no solvents and is almost completely inert to chemical attack, except by molten alkali metals and sodium in liquid ammonia. Furthermore, it does not soften below 320 °C, is electrically inert and has a very low coefficient of friction. It is more expensive than general-purpose plastics, requires special fabrication techniques, is degraded by high-energy radiation and has a low creep resistance.[7,19]

3.31.7.2.5 Other fluorine-containing plastics

These materials[7,19] in general, attempt to compromise between the exceptional end-use properties of PTFE and the greater ease of processing of other thermoplastics. Examples include polychlorotrifluoroethylene, tetrafluoroethylene–hexafluoropropylene copolymers (FEP resins), and polyvinylidene fluoride. Polyvinyl fluoride is available in film form with excellent weathering resistance.

3.31.7.2.6 Polyamides (nylons)

The main types of nylon[7,19] are oil and petrol resistant, but on the other hand susceptible to high water absorption and hydrolysis. There are a few solvents which include phenol and formic acid. Special grades include a water-soluble nylon, amorphous copolymers and low-molecular-weight grades used in conjunction with epoxy resins. Transparent amorphous polyamides are also now available.[7]

3.31.7.2.7 Polyformaldehydes (polyoxymethylenes, polyacetals)

These are physically similar to general-purpose nylons, but with greater stiffness and lower water absorption. There are no common solvents, but swelling occurs in liquids of similar solubility parameter. Poor resistance to ultraviolet light and limited thermal stability are two disadvantages of these materials.[7,19]

3.31.7.2.8 Other polyethers

The chlorine-containing polyether 'Penton' has excellent resistance to mineral acids, strong alkalis and most common solvents.[29] However, it is not recommended for use with oxidizing acids such as fuming nitric acid. Poly-2,6-dimethyl phenylene oxide (PPO) and certain related materials are similar to the nylons, but have superior heat resistance. These polymers are somewhat liable to stress-cracking problems.[7,19] Several polyethers are used as intermediates in the preparation of polyurethane foams, while others such as polyethylene glycol are water soluble.[7]

3.31.7.2.9 Linear polyesters

Polyesters [7,19] may be obtained in a wide variety of forms including rubbers, fibers, films, laminating resins, surface coatings and thermoplastic molding powders. The last named are somewhat similar to the nylons, but are more rigid. Chemical applications are limited because of their sensitivity to alkaline solutions and hot water.

3.31.7.2.10 Polycarbonates and polysulfones

These are tough materials with heat resistance better than most thermoplastics. They are resistant to attack by acids and alcohols, but the polycarbonates are sensitive to alkalis.[7,19]

3.31.7.3 Thermosetting Resins

These materials[7,19] often have better heat resistance than thermoplastics. Thermosetting resins are used in a variety of guises including surface coatings, but as plastics they are most frequently used in molding compositions and laminates. The tensile strength of unfilled rigid thermosetting resins is of the same order as for amorphous thermoplastics, that is, about 55 MPa, but this value may be greatly affected by the choice of fillers. For example, polyester–glass chopped-mat laminates often have tensile strengths in excess of 100 MPa, while values several-fold higher may be achieved by using carbon or boron fibers with epoxy resins. Further increases are becoming possible through the use of nanofillers.

3.31.7.3.1 Phenol–formaldehyde (phenolic) plastics

The chemical resistance is affected by the type of phenol used, cresols giving the best acid resistance, while xylenols are often used to obtain the best alkali resistance. For chemical-resistant applications, the fillers used in the molding powder and in the reinforcing material in laminates should be inorganic, for example, glass. These resins[7,19] are usually dark in color.

3.31.7.3.2 Aminoplastics

In this group, melamine–formaldehyde resins[7,19] with their good heat resistance, scratch resistance, and stain resistance, are usually preferred to urea–formaldehyde resins, where chemical resistance is important. Unlike the phenolics, these materials are not restricted to dark colors.

3.31.7.3.3 Unsaturated polyesters

It is possible to prepare unsaturated polyester-based laminates without application of external heat and pressure, thereby facilitating the manufacture of large objects such as boats using simple equipment. The laminates have somewhat limited chemical resistance, being attacked by many acids, alkalis and organic solvents.[7,19] Glass fiber is the common reinforcing agent, and in some products there is a tendency for capillary action to occur along the fiber bundles. Distilled water, in general, is more active in this respect than aqueous salt solutions, including seawater.

3.31.7.3.4 Epoxy and furan resins

These important materials,[7,19] somewhat more expensive than the polyesters, may also be fabricated without the use of pressure, and at ambient temperatures, if so desired. They are markedly superior to polyesters in chemical resistance, particularly towards alkalis.

3.31.7.3.5 Silicones

This term is given to a wide range of polymers[7,19] including fluids, rubbers and thermosetting resins. Although rather expensive compared to most other plastics, they are particularly noted for their thermal stability and their water repellency.

3.31.7.3.6 Polyurethanes

These are another large class of polymers[7,19,30] that are available in a wide range of forms, including rigid and flexible rubbers, foams, surface coatings and adhesives. The solid polymers, including the rubbers, have particularly good abrasion resistance. The polyurethanes, as a class, are somewhat lacking in resistance to acids and alkalis, and to the prolonged action of water and steam.

3.31.8 Polymers with Enhanced Heat Resistance

Very often, a desirable feature of a plastic material is its low softening point which enables it to be melt-processed at temperatures much lower than those normally used for metals and inorganic glasses. The ever-more sophisticated uses to which plastics materials have been put have, however, led to the demand for newer polymers with improved heat resistance to supplement those materials already available such as PTFE and the polycarbonates. For example, the polyimides (e.g., bismaleimides) are a developing class of polymer with good high temperature properties.[7,19]

Factors that need to be taken into account at high temperatures are the flammability of the polymer, or a compound from it, and the smoke evolution characteristics of the polymer and its degradation compounds. In general, the maximum service temperature for which a polymer may be used in a given application (i.e., prior to serious oxidative degradation, including burning) depends generally on two independent factors.

1. The thermal stability of the polymer, particularly in air.
2. The softening behavior of the polymer.

Polymer thermal stability is largely concerned with chemical reactivity, which may involve oxygen, ultraviolet radiation or depolymerization reactions. The presence of weak links and the possibility of chain reactions involving polymer chains may lead to polymers having lower thermal stability than predicted from studies of low-molecular-weight analogues.

The softening behavior of a thermoplastic material depends to a large extent on the flexibility of the chains and their ability to crystallize. Significant cross-linking of a reasonably stiff-chained polymer will lead to material that is unlikely to soften below its decomposition temperature. Intermediate to the linear and cross-linked polymers are various 'ladder polymers' in which the polymer molecule consists of a pair of more or less parallel chains bridged in a manner analogous to the rungs of a ladder.[31,32]

Resistance to burning depends on many factors. It is, however, to be noted that those polymers that burn only in air enriched with oxygen tend to have high carbon-to-hydrogen ratios and/or may also emit materials during degradation, such as hydrogen chloride, which are inherent flame retardants. Low smoke emission is also often associated with a high carbon-to-hydrogen ratio. **Table 3** gives some collected data for the limiting oxygen index, the minimum percentage of oxygen in an oxygen/nitrogen mixture that will sustain combustion under a specified set of test conditions.

Polyimides, obtained by reacting pyromellitic dianhydride (1,2,4,5-benzenetetracarboxylic anhydride) with aromatic amines, can have ladder-like structures and commercial materials that may be used up to temperatures in excess of 300 °C are available. They are, however, somewhat difficult to process. Thus, the polyamide-imides, which are easier to process but have lower heat resistance, have been developed. One disadvantage of polyimides is their limited resistance to hydrolysis; therefore, they may crack in aqueous environments above 100 °C.[7,19]

The polyether imides show much better hydrolytic stability with little change in tensile strength after exposure to water at 100 °C for 1 year. These materials also show exceptional resistance to mineral acids and are unharmed by most hydrocarbons including gasoline (petrol) and oils.

Although all commercial polysulfones are, in fact, polyethersulfones, the latter term is given to specific polysulfones that have improved heat resistance.

Table 3 Limiting oxygen index data for a variety of polymers (unfilled)

Polymer	*Limiting oxygen index (%)*
Polyacetal	15
Polymethyl methacrylate (Perspex)	17
Polypropylene (PP)	17
Polyethylene (PE)	17
Polybutylene terephthalate (PBT)	18
Polystyrene (PS)	18
Polyethylene terephthalate (PET)	21
Nylon 6	21–34
Nylon 66	21–30
Nylon 11	25–32
Polyphenylene oxide (PPO)	29–35
Acrylonitrile butadiene styrene (ABS)	29–35
Polycarbonate of bisphenol A	26
Polysulfone	30
Polyimide	32
Polyarylate	34
Polyether sulfone (PES)	34–38
Polyether ether ketone (PEEK)	35
Phenol-formaldehyde resin	35
Polyvinyl chloride (PVC)	23–43
Polyvinylidene fluoride (PVdF)	44
Polyamide-imide	42–50
Polyphenylene sulfide (PPS)	44–53
Polyvinylidene chloride (PVdC)	60
Polytetrafluoroethylene (PTFE)	90

Commercial polymers now have values of T_g ranging from 190 to well above 300 °C, but the cost generally increases sharply with T_g.[7,19] Polyether ether ketones (PEEKs)[7,19] are similar to polyethersulfones; however, unlike the polysulfones, these materials are crystalline and have higher maximum service temperatures. They also have better resistance to hydrolysis at elevated temperatures than the polymides. Polyarylates are highly aromatic linear polyesters with relatively high values of T_g (up to 194 °C) and are self-extinguishing.[7,19]

Polyphenylene sulfides,[7,19] when glass-fiber filled, have high temperature ratings, second only to PEEKs among commercial thermoplastics. These materials often have better resistance to environmental stress cracking than the polysulfones and have found use in automotive applications because of their resistance to corrosive engine exhaust gases, ethylene glycol and gasoline.

3.31.9 Thermoplastic Rubbers

These materials[7,19] have characteristics of both rubbers and thermoplastics. At room temperature they

behave like cross-linked rubbers, but at elevated temperatures the cross-links, in the form of separated phases in block copolymers such as SBS (styrene–butadiene–styrene triblock copolymer), or ionic clusters or crystallites, break down and the materials may be processed like a thermoplastic. Unlike truly cross-linked (vulcanized) rubbers, these materials may be capable of dissolution in solvents, although not necessarily at room temperature.

SBS thermoplastic elastomer is a block copolymer consisting of a block of butadiene units end-capped by polystyrene blocks. Below the T_g, the polystyrene blocks from different chains congregate into polystyrene domains, which act as both cross-links and reinforcing fillers. The polymers will dissolve in certain hydrocarbon solvents. Hydrogenated SBS materials have better resistance to ageing.

Thermoplastic polyester rubbers[7,19] are also block copolymers consisting of polyether and polyester sequences. The polyester groups are capable of crystallization and the crystal structures, in this case, act as the physical cross-links. These materials have good hydrocarbon resistance. Similar thermoplastic polyamide rubbers are also available. Thermoplastic polyolefin rubbers are usually blends based on polypropylene and ethylene–propylene rubbers. They are not resistant to hydrocarbons.

References

1. Orr, E. W. *Performance Enhancement in Coatings*; Hanser: Munich, 1998.
2. Marrion, A. R. *The Chemistry and Physics of Coatings*, 2nd ed.; Royal Society of Chemistry: Cambridge, 1994.
3. Glass, J. E. *Technology of Waterborne Coatings*; American Chemical Society: Washington, DC, 1997.
4. Sperling, L. H. *Introduction to Physical Polymer Science*; Wiley: New York, 1986.
5. Cowie, J. M. G.; Arrighi, V. *Polymers: Chemistry & Physics of Modern Materials*, 3rd ed.; CRC Press, 2007.
6. Moad, G.; Solomon, D. H. *The Chemistry of Radical Polymerisation*, 2nd ed.; Elsevier: New York, 2005.
7. Brydson, J. A. *Plastics Materials*, 7th ed.; Elsevier: New York, 1999.
8. Odian, G. *Principles of Polymerisation*; McGraw-Hill: New York, 1970.
9. Kennedy, J. F.; Phillips, G. O.; Wedlock, D. J.; Williams, P. A. *Cellulose and its Derivatives*; Ellis Horwood: Chichester, 1985.
10. Young, R. A.; Rowell, R. M. *Cellulose Structure, Modification and Hydrolysis*; Wiley-Interscience: New York, 1986.
11. Sperling, L. H. *Introduction to Physical Polymer Science*, 2nd ed.; Wiley: New York, 1992.
12. Collyer, A. A. *Rubber Toughened Engineering Plastics*; Chapman & Hall: London, 1994.
13. http://www.dsm.com/en_US/html/drs/polymericplasticizers.htm
14. Wilson, A. S. *Plasticisers Principles and Practice*; The University Press: Cambridge, 1995.
15. Ward, I. M.; Hadley, D. W. *An Introduction to the Mechanical Properties of Solid Polymers*; Wiley: Chichester, 1993.
16. Dyson, R. W. *Engineering Polymers*; Blackie: New York, 1990.
17. Brostow, W.; Corneliussen, R. D. *Failure of Plastics*; Hanser: Munich, 1986.
18. Brydson, J. A. *Plastics Materials*, 5th ed.; Butterworth-Heinemann: London, 1989.
19. Alfredo Campo, E. *Industrial Polymers*; Hanser: Munich, 2008.
20. Singh, B.; Sharma, N. *Polym. Degrad. Stabil.* **2008**, *93*, 561–584.
21. Flynn, J. H. *Handbook of Thermal Analysis and Calorimetry;* Elsevier: Amsterdam, 2002; Vol. 3.
22. Yamakawa, H. *Modern Theory of Polymer Solutions*; Harper & Row: New York, 1971.
23. Richards, E. G. *An Introduction to Physical Properties of Large Molecules in Solution*; Cambridge University Press: Cambridge, 1980.
24. Van Krevelen, D. W. *Properties of Polymers: Their Correlation with Chemical Structure; Their Numerical Estimation and Prediction from Additive Group Contributions*, 3rd ed.; Elsevier: Amsterdam, 1990.
25. Small, P. A. J. *J. Appl. Chem.* **1953**, *3*, 71–78.
26. Andrews, E. H.; Bevan, I. *Mechanics and Mechanism of Environmental Crazing in a Polymeric Glass*; Elsevier: New York, 1972.
27. Crank, J.; Park, J. S. *Diffusion in Polymers*; Academic Press: London/New York, 1968.
28. Grossman, R. F. *Handbook of Vinyl Formulating*, 2nd ed.; Wiley-Interscience: New Jersey, 2008.
29. http://www.gaylordchemical.com/bulletins/bulletin105b/Bulletin105B-15.html
30. Ulrich, H. *Chemistry and Technology of Isocyanates*; Wiley: Chichester, 1996.
31. http://chem.chem.rochester.edu/~chem424/ladder.htm
32. Schluter, A. D.; Offler, M.; Enkelmann, V. *Nature* **1994**, *368*, 831–834.

3.32 Degradation of Polymer Matrix Composites

R. H. Martin
Materials Engineering Research Laboratory Ltd, Wilbury Way, Hitchin SG4 0TW, UK

Glossary

Extrusion A manufacturing process in which a softened blank of plastic material is forced through a shaped die to produce a continuous ribbon of the formed product.

Gelcoat A polymer material that is used to provide a high-quality finish to the visible surface of a fiber reinforced composite material.

Polymer resin A polymerized synthetic or chemically modified natural material including thermoplastic materials such as polyvinyl, and thermosetting materials such as epoxies, that are used with other components such as fillers to form plastics.

Pultrusion A manufacturing process that consists of pulling a fiber reinforcing material through a resin impregnation bath and a shaping die prior to final curing.

Thermoplastic A polymeric material (for example nylon) which, upon curing, forms one- or two-dimensional molecular structures and is capable of being repeatedly softened by increases in temperature and hardened by decreases in temperature.

Thermoset/thermosetting A polymeric material (e.g., epoxy) which, upon curing, results in a three-dimensional structure and decomposes rather than melting upon heating.

Abbreviations

CPI Chemical processing industry
CRA Corrosion resistant alloy
DCB Double cantilever beam
DMA Dynamic mechanical analysis
DSC Differential scanning calorimeter
ECR Corrosion resistant e-glass
ESC Environmental stress cracking/corrosion
FRP Fiber reinforced plastic
FTIR Fourier transform infrared
GC Gas chromatography
GRP Glass reinforced plastic
MS Mass spectroscopy

TGA Thermogravimetric analysis
TMA Thermomechanical analysis
UV Ultraviolet
Vf Fiber volume fraction

Symbols

c Chlorine dioxide concentration (g l^{-1})
t Time (s)
T_g Glass transition temperature
t_{95} Time to reach 95% of original property (s)
B Factor in the presence of deposits
D Diffusion coefficient (m^2 s^{-1})
E_a Activation energy (J mol^{-1})
E_{11} Young's modulus in the fiber direction (GPa)
E_{22} Young's modulus transverse to the fiber direction (GPa)
G_{12} Shear modulus (GPa)
M_t Total mass absorbed at time t (kg)
M_∞ Total mass at equilibrium (kg)
R Universal gas constant (J K^{-1} mol^{-1})
T Temperature (K)
W Rate of weight loss (kg s^{-1})
α Corrosion depth factor
Φ Depth of corrosion (m)

3.32.1 Introduction

In the past, the primary reason for the use of fiber reinforced plastics (FRPs) is because of weight saving for their relative stiffness and strength. As an example, a carbon fiber composite can be five times stronger than 1020 grade steel while having only one-fifth the weight. Aluminum (6061 grade) is much nearer in weight to carbon fiber composite, but the composite can have twice the modulus and up to seven times the strength. A comparison of some properties of metals and composites is shown in **Figure 1**.

A composite, which is generically a material that is made up of two or more distinct (i.e., macroscopic, not microscopic) materials, comes in different configurations but is essentially a plastic material within which there are embedded fibers or particles. The plastic, or more correctly a polymer, is more often termed the matrix or sometimes the resin. The fibers or particles dispersed within the polymer are known as the reinforcement. The reinforcement is generally orders of magnitude stiffer than the matrix, thus resulting in a stiffened plastic. This stiffer reinforcement can either be randomly distributed short fibers or continuous fibers (sometimes in mat form) that are laid in a particular direction within the matrix. The resulting material thus may have different properties in different directions (anisotropic or orthotropic, depending on the lay-up). This characteristic is usually exploited to optimize the design and results in the composite material being tailorable in that its mechanical properties can be formed to meet specific directional loading.

Most engineering materials are essentially isotropic. That is, they have the same properties such as strength and modulus in any direction. There may be 'grain' in some metals because of the manufacturing

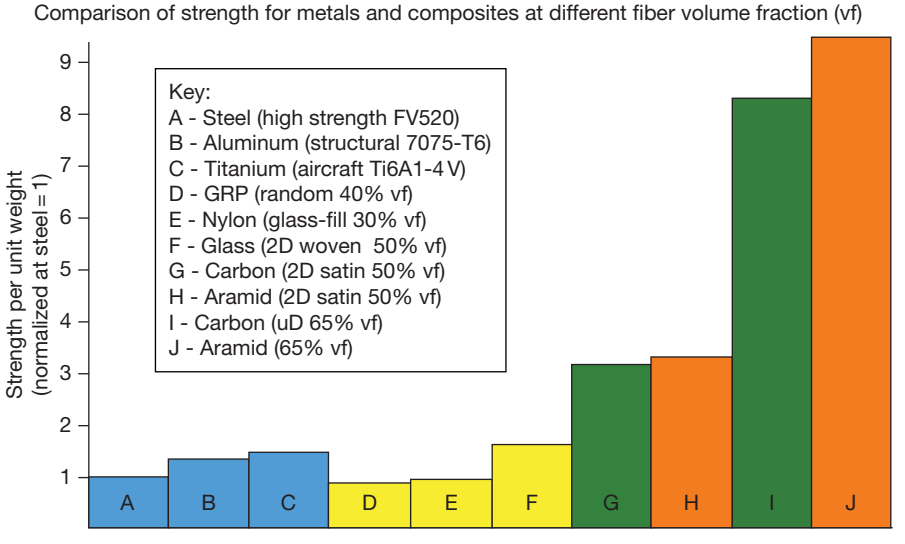

Figure 1 Comparison of specific strength of different metals and FRPs (www.merl-ltd.co.uk).

process, but it is only in critical applications that this matters. Most machining or casting processes do not have to take directional differences into account. Because of the different fiber orientation, mentioned above, most composites will have very different properties in different directions. For example, a carbon FRP may be up to 100 times stronger under tension than it is in shear, and the stiffness may differ in the two directions by similar ratios.

Several different terms have been used by different industries to describe a composite material, and these acronyms have become jargons. More technical descriptions include:

GRP	Glass reinforced plastic (in which the fiber is glass and the resin is any of the polymer resins)
GRE	Glass reinforced epoxy (in which the fiber is glass and the resin is an epoxy)
FRP	Fiber reinforced plastic (in which the fiber may be any of those listed above and the resin is any of the polymer resins)
CFRP	Carbon FRP (in which the fiber is carbon and the resin is any of the polymer resins)
PMC	Polymer matrix composite

None of these terms are incorrect, although some cover a wider range of material classes. FRP is a generic term and will be used throughout this chapter when referring to composite materials generically.

Both thermosetting and thermoplastic polymers can be used for the matrix material, and the most common thermosetting matrix materials include polyester, vinyl ester and epoxy, and bismaleimide for higher-temperature applications. Thermoplastic matrix materials tend to have higher performance ability and include polymers such as polyimide, phenolic, polypropylene, polyetheretherketone (PEEK), and polyphenylene sulfide (PPS).

Another primary benefit of FRPs is their durability in hostile environments, often termed corrosive environments, although in reality, composite materials do not 'corrode.' While the matrix is primarily the binder that transfers the load to the reinforcement, it is also very resilient to environmental attack. The type of resin needs to be carefully selected so that it can withstand the service temperature (high or low) conditions, and it should not be significantly affected within its lifetime by fluids (gases or liquids) with which the FRP will come into contact. Hence, FRPs are used in very corrosive applications such as for acid storage in the chemical processing industry and longevity in marine environments such as in vessels and offshore oil and gas applications. These applications are discussed in more detail in this chapter.

The effect of exposure to various environments such as heat, moisture, solvents, acids, ozone, hydrocarbons, loads, etc., and more importantly a combination of these parameters, may degrade the material's key properties. For load bearing applications, these properties may include stiffness and strength. Cracks may appear and accumulate ultimately leading to failure. For fluid containment applications, cracks may coalesce leading to a leak path for this fluid even though the structure is globally still intact. Despite these safety critical uses, the degradation of an FRP is still not a well understood phenomenon compared to the corrosion of metals.

The reason that the long-term degradation of FRPs is not well understood is because it is a very complex process with many interrelated factors and has led to much ongoing research into the topic. Degradation is often given the generic term 'ageing' that can include the more benign physical ageing effects such as swelling from moisture absorption, that is largely reversible, to the more serious chemical ageing where material properties are permanently (irreversibly) degraded. Additionally, synergistic effects to ageing from mechanical loading, such as creep, need to be considered in isolation (or in addition) to that associated with the environment and often change the rate of degradation. Environmental ageing of FRPs occurs from the surface or edge inwards and requires time to penetrate into the material's center, and the rate of ageing can be directional (like the mechanical properties); further, it is generally dependent on the temperature and stresses. The complexity described above makes predicting ageing around detailed geometries such as stress concentrations nontrivial.

Added to the issue of ageing of FRP materials is the variety of different manufacturing methods available to manufacture components. The reader is pointed toward the works of Jones,[1] Matthews *et al.*,[2] and in ASM Handbook[3] for detailed information on manufacturing. The methods available depend very much on the nature and quality of the component to be manufactured. For the low-end marine industry, uncured resin is poured over chopped glass fibers laid in a mould to form what is often termed 'fiberglass.' A step-up on this approach is known as filament

winding where the fibers are wrapped around a net-shape mandrel, and the resin poured on or the fibers are dipped in the resin before winding. Both methods are low-cost manufacturing techniques and the resin is generally cured at room temperature. Alternative lower-cost manufacturing methods include injecting the resin into a mould or extruding or pultruding the composite profile through a die to form the part desired. Additionally, resin-rich layers, known as gel coats can be put on the outside of the parts for better resistance or appearance. To improve the quality and performance of the resin, vacuum, pressure and temperature are used in a variety of combinations. A vacuum is employed by placing the component in a bag and the vacuum is used to help to pull the resin through the fibers and, more importantly, to remove air and other gases from the final composite part reducing porosity. Pressure is used on the outside of the vacuum bag to help form and consolidate the part again, helping to reduce porosity. Temperature is used for stronger resins to assist in curing and consolidation. The combination of these three manufacturing parameters requires an autoclave and produces a high-quality, high-strength part and is still the manufacturing method of choice for the aerospace industry.

A further difficulty is introduced with the need to predict long-term ageing using short-term testing and analysis. For long-term life prediction based on short-term data, representing the true service history (load, temperature, time, fluid, etc.) for long-term structural life prediction is a vital step to validate any short-term-based predictive methodology. The coupon tests must reflect the effect of ageing on the polymer (i.e., matrix-dominated properties) because the fibers may mask any property loss in the resin. However, fibers can sometimes degrade in some environments quicker than the polymer and additionally the fiber–matrix interface can be attacked and this too must be represented in any accelerated ageing methodology. Further, the chemical bond between the fiber and resin itself (often know as the interface region) can be degraded. All of these degradation methods are important to understand. Loss of fiber properties greatly reduces the strength and stiffness of the FRP laminate because that is their main purpose. Similarly, a break down of the bond between the fiber and the resin leads to the fibers not providing stiffness and strength through transfer of shear between the two. Reduction of properties of the resin is also important because it provides the load transfer between fibers.

It is this shortage of long-term data or of an accelerated ageing methodology to determine the residual properties of a FRP component at any time in its life that still hinders the uptake of FRPs in some applications. However, over the decades when composites have been used, much has been learned, and this chapter addresses some of this work detailing the nature of ageing of composites and the use of composites in certain industry sectors where corrosion or degradation is an issue. This chapter will describe how it is the degradation or ageing of a composite that needs to be understood when these materials are used in hostile environments. This chapter is not intended to be a general introduction to FRPs; there are many publications available for this purpose[1–3] or informative internet-based sites such as The Virtual Composite Material Consultant.[4]

3.32.2 Ageing Mechanisms

The ageing of an FRP comprises an ongoing development of damage that is dependent on the type of polymer matrix, the fiber type and architecture, the fiber volume fraction and the operating conditions of temperature, relative humidity, oxidative attack, solvent infusion, internal moisture concentration, air pressure, mechanical loads, and the time of exposure. These degradation factors are often related and varying. For example, a FRP pipe used to transport hydrocarbons may experience hot oil field fluids internally, ultraviolet (UV) radiation from sunlight, and moisture externally, external loads from supports and other loading. The external temperature may vary between -40 and $+40\,^{\circ}\mathrm{C}$ depending on the location while the internal temperature may be that of the oil at temperatures up to $+100\,^{\circ}\mathrm{C}$. However, a fuselage or wing FRP structure may experience temperature cycles of -55 to $+40\,^{\circ}\mathrm{C}$ between flight and ground with ice, cleaning solutions, moisture, jet fuel, ozone, UV and other environmental conditions, making the determination of residual life a complex procedure. Therefore, ideally these conditions must be represented in any simulation of ageing for predictive purposes to accurately reproduce the degradation mechanisms. In reality, only the key conditions considered to be the more potentially damaging may be investigated. In any test program, it is important to use relevant material or structural properties as an indicator of the state of ageing of the material. This may be the mass change, the glass transition temperature T_g, the crack density, the modulus, strength or a combination of these properties. Therefore, a complete understanding of all the degradation processes should be known or an

assumption made on what is the primary degradation mechanism. The section below describes some of the key degradation mechanisms that individually or combined form the ageing of a composite material.

3.32.2.1 Physical Ageing and Time-Dependent Effects

Polymers, both in their rubbery (above T_g) and in their glassy state (below T_g), are characterized by viscoelasticity, a time-dependent mechanical behavior. The characteristic times of this constitutive behavior are much longer in the glassy state and decrease at temperatures near and above T_g. Typical evidences of viscoelasticity are creep and stress relaxation. Creep is a time-dependent deformation that usually has three stages when under a constant load, rapid primary creep, a steady-state secondary creep rate and a rapid acceleration in the creep rate leading to rupture. Stress relaxation is a related phenomenon where stresses are relieved when under a constant deformation. In composite materials, the stress transfer between the viscoelastic matrix and the elastic reinforcement, or between layers with different fiber directions (laminae) needs to be considered for long-term ageing characterization. For long-term property estimation, especially when considering FRP properties that are more dominated by the resin than the fiber, long-term viscoelastic behavior can be accelerated by adopting the time–temperature superposition principle.[5,6] This principle is based on the premise that the behavior for long time periods at low temperatures corresponds to that for short time periods at higher temperatures. This is because in a polymer, the polymer chains are more mobile and easier to arrange at higher temperature resulting in a higher compliance or lower modulus. The time–temperature superposition principle is evident from the compliance curves in creep experiments (or modulus curves for stress-relaxation experiments) at different temperatures that are related to one another by a simple temperature-dependent shift on the log time scale.

The fundamentals on physical ageing and the dependency of mechanical properties on time and temperature become more pronounced when testing close to the T_g. The T_g itself may well be affected by moisture; lowering T_g, and service temperatures may be close to wet T_g requiring aspects of physical ageing to be a vital part of a durability analysis.

With physical ageing, polymers below their T_g exhibit a time-dependent rearrangement of their structure. The mutual interaction between viscoelasticity and physical ageing imposes the introduction of time–ageing and time–temperature shift factors. Other time-shifting effects may also exist based on the applied stress, moisture condition and other environmental factors. These time-dependent properties and physical ageing has an affect on the material's overall strength and stiffness. Thus, ideally an accelerated ageing analysis needs to include an aspect of physical ageing such that the strength/failure criteria includes time-dependent coefficients and a nonlinear viscoelastic–viscoplastic damage analysis.

For accelerated physical ageing tests, the relationships are obtained from short-term tests using the time-dependent experimental data described above. It is important that no chemical ageing (discussed further below) is included. The typical properties measured depend on the application, but most testing presented in the literature has been on off-axis plies because they give a good representation of matrix-dominated properties.[6] However, the literature often falls short in producing such time-dependent relationships for more useful design properties such as static properties of FRP laminates with or without holes.

3.32.2.2 Hygrothermal Effects

Hygrothermal effects are related to the uptake of water molecules from a humid environment or water in direct contact with the FRP when the component is submerged in water (or other solution). The water is absorbed by the polymer matrix and results in plasticization of the matrix leading to hydrolytic degradation or hydrolysis which lowers the molecular weight and hence mechanical properties of the FRP. The rate of hydrolysis may be accelerated by the application of load or more significantly with elevated temperature and high- or low-pH conditions. In contact with the polymer, low molecular weight liquids are absorbed by and diffuse into the polymer until saturation (equilibrium) is reached. The rate of diffusion and equilibrium are dependent on the chemical structure and morphology, such as the degree of crystallinity of the polymer. For an FRP, these properties are also related to the type of fibers, the volume fraction and the nature of the fiber–matrix interface.

The relationship between time and moisture mass uptake can classically be characterized using simple approaches such as Fick's law, but generally for FRPs, diffusion is more complex with competing factors affecting the rate of diffusion.[7] With time, moisture diffuses into the FRP through the surfaces and there

is a moisture-content concentration gradient through the thickness. Indeed, for some FRPs there may be a different concentration through the edges than through the surfaces. If the moisture content or temperature is cycled, this will lead to local dryness at the surface plies compared to the centre of the laminate. This moisture distribution can lead to significant residual stresses within the laminate that can in turn cause outer ply delamination of blisters.

Short-term hygrothermal effects on FRPs may extend beyond plasticization of the matrix and lead to mechanical damage such as the creation of microvoids, matrix cracking and blistering. These microcracks, in turn, provide fast diffusion paths (for both liquid water and water vapor) and then alter the moisture-absorption characteristics of the laminate.

Long-term exposures may not cause mechanical damage, described above, but the plasticization may well change matrix-dominated mechanical properties such as interlaminar and intralaminar shear modulus and the transverse tensile strength and modulus. Properties like compression modulus and strength are greatly affected by the shear properties of the matrix; hence, under hot and wet conditions compression properties may be severely degraded. The high temperature and humidity exposure of FRPs effectively plasticizes the matrix, more so closer to the T_g of the material which reduces when the material is saturated.

Post-cure reactions, hydrolysis and leaching of products within the FRP coupled with the decrease of T_g when moisture is absorbed, make modeling the effects of moisture complex and warrent further investigation. Such modeling can supply important information to establish the effects of moisture on time–temperature shift factors, by scaling the temperature axis on the basis of T_g change. As a result, Fick's law needs to be extended to model three-dimensional diffusion in anisotropic materials. For FRPs, the value of the diffusion coefficient, D, for the neat polymer needs to be modified to account for the tortuous path created by the presence of the fibers (their size, distribution, aspect ratio, orientation, etc.). Hence, D becomes an anisotropic property that is dependent on fiber direction. In FRP laminates with several layers of different orientation, the different diffusivity in each layer must be considered for the overall laminate. In ideal Fickian behavior, moisture absorption increases linearly with the square root of time for values of $M_t/M_\infty \leq 0.5$ (where M_t is the total amount of moisture absorbed at time t and M_∞ is the total amount absorbed at equilibrium). Time–thickness scaling allows the long-term prediction of absorption in thick laminates from thin-sample measurement, when Fick's law applies. Diffusion can be accelerated by increasing the temperature and follows the Arrhenius relationship eqns [1]

$$D = D_0\left[\exp\left(\frac{-E_a}{RT}\right)\right] \qquad [1]$$

Where E_a is the activation energy of the diffusion rate, R is the universal gas constant, and T is the absolute temperature of the exposure in Kelvin.

As discussed above, Fickian law may not always be demonstrated in composites where, following reaching equilibrium, there can be a slow long-term increase in mass uptake or a decrease in mass or both. The decrease may arise from products leaching from the FRP over time and the increase from a two-stage absorption process where the first is Fickian and the second a relaxation-based phenomenon.[8]

3.32.2.3 Thermooxidative Degradation

While the application of temperature and moisture can have negative effects on the composite, exposure to temperature in an air environment can cause thermooxidative ageing. This ageing mechanism arises from the thermal instability of the polymer and leads to oxidative attack that comprises chain scission, cross-linking, and thermooxidative reactions. Thermal degradation of FRPs, in an inert atmosphere, is exclusively a thermolysis phenomenon, while in air it is dominated by oxidation. Thermolysis is the result of breaking of covalent bonds in the polymer network and, in general, thermal stability of high-performance polymers in an inert atmosphere is very good.[6,8–11] Oxidation is usually characterized in terms of weight loss generally from the surfaces of the laminate. This weight loss is predominantly from the matrix and will penetrate into the laminate at higher temperatures and long exposures. Eventually, microcracks will form leading to a larger reduction in the mechanical properties of the FRP. These weight losses are generally permanent (irreversible) and even a small weight change can be an indication of the onset of damage at the surface. For oxidation to occur at the center of the laminate, the diffusion process must be understood, including the diffusion of oxygen and reactions products throughout the polymer matrix in a similar manner to liquid diffusion discussed above. The pattern of oxidation reactions and subsequent chemical changes depends on the exposure temperature, the resin system, and the oxygen content. Simply

increasing the temperature to accelerate the characterization of oxidation is nontrivial. The changes in mechanical properties postexposure are a function of sample thickness and surface protection as well as the ageing temperature and the material's T_g. Therefore, the examination of the thermooxidative stability of an FRP must include not only the degradation of mechanical properties, but also the failure mechanisms to ensure that they are consistent when comparing two laminates aged at different temperatures in an attempt to accelerate thermooxidative ageing.

3.32.2.4 Chemical Ageing

Chemical ageing follows principles very similar to oxidative ageing but occurs when the environmental fluid is an acid, alkali solvent, or many other fluids to which an FRP may be exposed. These chemicals actually attack the resin, the fiber, or the fiber–matrix interface (or any combination of these three). When the FRP is subjected to exposure to, for example, an acid solution, depending on the concentration of the solution, competing ageing mechanisms may occur. The liquid will first be absorbed in a hygrothermal fashion as described above. In time (dependent on the strength and nature of the chemical involved and the compatibility of the polymer), the material will chemically react with the FRP. This results in an increase in cross-linking density that can severely affect the mechanical properties by densification and increasing the T_g. Also, products may be leached out of the FRP in an irreversible manner. This will result in weight loss and a potential decrease in properties. With further time, actual physical material loss can occur, resulting in a more dramatic change in properties.

In order to perform studies of long-term and accelerated chemical ageing, usually a large test program is required with long periods of time and a selection of parameters (temperature, chemicals, loads). A variety of specimen types is also required to assess the degradation of mechanical properties parameters such as specimen type, lay-up, thickness, material, etc. As with other ageing types, chemical ageing is a diffusion-related phenomenon. Therefore, the use of thick specimens will delay observable changes in mechanical properties although significant surface damage may have occurred. Different lay-ups will affect the interlaminar stresses, which will affect diffusion rates.[12] Additionally, edge effects can play a role and this is often where mechanical failure can initiate. As a result, chemical ageing exposures are often conducted on panels of FRP and mechanical specimens cut from these panels once the ageing is complete. Another approach is to coat the free edges of the test specimens with a resilient coating to prevent unrepresentative edge damage.

An additional approach to characterizing chemical ageing to better understand the change in the polymer is to conduct thermal analysis on the FRP or the matrix. Of all the properties, T_g is the most common one measured using thermal analysis because it is a good indication of physical changes. Methods and approaches to measure T_g vary and all are reasonably well established as standards. These include dynamic mechanical analysis (DMA) that may be performed in torsion or flexure depending on the test apparatus; differential scanning calorimetry (DSC); or thermomechanical analysis (TMA). These methods all raise the temperature of the FRP and look for inflection points of peaks in the property being measured. The DMA tends to be more sensitive than the DSC for materials such as phenolics. Thermogravimetric analysis (TGA) is used to measure the rate of change of weight versus time and temperature in a controlled gas environment. TGA is highly dependent on the available surface of the specimens placed into the test chamber and hence the size of the pieces of materials that are used can effect measurements. It is sometimes useful to identify how the polymer has changed during ageing and other equipments such as Fourier transform infrared (FTIR) spectroscopy and gas chromatography (GC) as well as mass spectroscopy (MS) are used to evaluate the degradation products. These techniques can also be used for thermooxidative ageing.

3.32.2.5 UV and Weathering Degradation

Similar to oxidative ageing, weathering affects the surface of the FRP laminate. Generally, UV ageing affects the appearance of the laminate (particularly color loss) and this degradation in appearance can be considered failure (aesthetically). Often, the change in color has a minor effect on structural performance. Weathering is a combination of ultraviolet radiation, temperature from the sun, oxygen and any ambient moisture such as humidity or precipitation.[13,14] With the use of coatings and additives, the structural performance of FRPs can be maintained and the weathering effects tend to be surface related and appear as:

- fading and darkening;
- yellowing;
- blooming; and
- loss of gloss and chalking.

Yellowing, fading, and darkening are generally due to chemical degradation in the polymer. Blooming can be caused by an additive coming to the surface, whereas loss of gloss is generally caused by erosion of the surface layer. While the loss of surface quality may be considered benign, it can lead to leaks and weakening.

The severity of the ageing due to weathering is strictly dependent on the nature of the climate or the geographical region, for example, tropical, desert, arctic, etc. Predicting the weathering performance of FRPs is carried out both in laboratories using artificial weathering and in long-term experimental field ageing. The latter takes several years and becomes very specific to the material and location selected for the study. The specimens are directly exposed to outdoor conditions at a fixed angle relative to the horizontal and in a fixed direction. To accelerate weathering, the UV radiation is concentrated onto the test specimen using special mirrors. Also, locations with high levels of sunshine, for example, Florida and Arizona are used to compare with longer-duration exposures in regions with less sunshine hours.

There are a larger number of laboratory-based ageing tests along with actual case studies where specimens are exposed to UV radiation from a variety of UV light sources. There are currently three key laboratory methods used for artificial weathering.[14] The carbon arc lamp uses two strong emission bands that peak at 358 and 386 nm which are much more intense than natural sunlight. These have a lower effect than solar radiation on materials that absorb only short-wavelength UV radiation. The xenon arc lamp gives a broad spectrum of light that matches the solar spectrum quite closely. Filters are used to reduce the short-wavelength UV light from these lamps that are not present in sunlight. Fluorescent lamps have special phosphors selected to emit UV light at a particular waveband. Exposure is carried out under controlled conditions of temperature and moisture. With the varied nature of weather, conducting accelerated tests to simulate specific weather exposure for predictive purposes is difficult. As a result, accelerated methods tend to focus on the worst-case weather scenarios and any correlations must be qualitative.

3.32.2.6 Mechanical Degradation

This chapter focuses more on the ageing of FRPs under environmental loads, and, strictly speaking, mechanical degradation is not part of ageing. Nevertheless, it is often a consequence of ageing. Mechanical damage processes such as matrix cracking, delamination, plastic strain, interfacial failure are generally irreversible. In an FRP, some of these damage modes may be seen to be benign or subcritical; however, the damage may accumulate or lead to damage elsewhere by transferring load ultimately leading to failure. The most common mechanical degradation, especially when operating at high temperature, is the formation of cracks in the matrix either within the ply or transverse to the ply. Fatigue, environmental loading, and residual stresses can all promote the onset and accumulation of these cracks. The laminate strength, stiffness, and thermal properties as well as failure modes can be affected by transverse matrix cracking which can also promote higher uptake of moisture deeper in the laminate. The prediction of these failure modes are often parts of a long-term durability assessment, especially under fatigue loads. The reader is directed towards Jones,[1] Mathews and Rawlings,[2] and ASM Handbook,[3] for a description of predicting mechanical failure in FRP laminates.

3.32.2.7 Fire Testing

While the above sections discuss various environmental forms of ageing, FRPs are often, perhaps surprisingly, used in high-risk fire applications. These include the aerospace industry in the event of on-board fires and crashes, marine vessels with very high requirements for resistance to fire, railways, where the fire resistance for underground trains is perhaps the most stringent, and offshore oil and gas requirements. Many of these fire-resistance requirements arise from unfortunate incidents. Glass and carbon fibers do not burn but the resin may well set alight or give off noxious fumes or both. Different resins have different fire resistance to jet fires (where a flame is concentrated on one spot) and pool fires. The combination of low thermal conductivity, resin endotherm effects, structural integrity and coatings mean FRPs can have excellent fire-resistance performance but this does need to be strictly controlled using established small-scale tests to evaluate the combustibility and ignitability. Models based on the energy flux involved in decomposition have been used to predict fire performance of materials.[15] However, no further discussion on fire testing is given in this chapter because it goes beyond the scope of less severe forms of ageing and degradation.

3.32.2.8 Synergistic Effects

Each of the sections above described individual possible ageing mechanisms that may occur to an FRP

laminate. However, an FRP component is a combination of fibers, the fiber–matrix interface, and the polymer matrix that may be subject to long-term ageing of a combination of the above ageing scenarios. Hence, the mechanical properties and fitness for purpose may change through a combination of thermal oxidation, physical ageing, hygrothermal effects, UV exposure, and chemical attack. Therefore, macroscopic changes need to account for the synergies between these ageing mechanisms and any accelerated ageing methodology should really account for these combined factors – a nontrivial task!

3.32.3 Accelerated Ageing

As discussed above, one of the biggest advantages of composite materials is their long life in harsh environments. Ironically, it is this long life and the difficulties in being able to reliably predict the long life that has hindered the uptake of composites. The development of a robust accelerated ageing methodology is a key technology development for FRPs. An accelerated-ageing methodology should accelerate the action of degradation factors without altering the underlying molecular mechanisms of ageing. The analogy that a chicken does not hatch quicker from the egg by boiling the egg applies here. As discussed, the ageing process may cause both reversible and irreversible changes and the accelerated ageing methodology must simulate these processes. The design of an accelerated methodology relies on the knowledge of material properties and their relationship with environmental conditions (temperature, pressure, loads, relative humidity, UV, etc.) and upon the fundamental ageing or damage mechanisms as described in the previous section.

The purpose of accelerated ageing methodology is simply to speed up the accumulation of damage or deformation, potentially leading to failure. This is achieved by establishing relationships between time and various parameters, such as temperature, fluid concentration, load, etc. that can be related back to the in-service conditions. Accelerated testing also aims to determine the material microstructure and damage at the end-of-life or ideally at any time during the life of the component. For most structural applications, the durability and mechanical fatigue are the main degradation processes in which frequency and load are the main acceleration factors used. For FRPs in corrosion applications, exposure temperature is the primary means of accelerating ageing, but other parameters include increasing the concentration of a degradative chemical, applying pressure, or a load. Most accelerated ageing experiments consider a single accelerating factor because it is difficult to test multiple accelerated conditions and understand the synergistic effects as discussed above. The preferred approach is to incrementally subject samples to accelerated conditions. For the approach to be valid, a fundamental understanding of material response and the reversible and irreversible degradation processes is required and needs to be incorporated into the modeling.

An accelerated test methodology must follow the following steps[16]:

(a) identification of the material, including the polymeric matrix and the fiber (including type, volume fraction, orientation, sizing, etc.);
(b) identification of the primary ageing mechanism for the environment, for example, thermooxidation, hydrolysis, UV ageing, etching,. . .;
(c) identification of the physical properties, most important to the application, to be measured in the accelerated ageing test (e.g., mass loss, stress, strength, toughness, leak resistance, color, . . .);
(d) selection of the environmental acceleration of degradation factors such as temperature, time, concentration, etc.;
(e) carry out the accelerated tests under conditions given in (c) and (d);
(f) use theoretical modeling (e.g., Arrhenius relationship, time–temperature superposition, curve-fitting) of the degradation factors; and
(g) validating some of the modeling by performing long-term tests that are representative of in-service conditions.

For accelerated ageing, the synergistic effects of time, pressure, and conditions on FRP degradation should be established. Free space exists between molecular chains to a greater or lesser degree leading to a balance between stiffness and flexibility. However, this same free space can mean that polymers can absorb fluids to which they are exposed, especially those with similar solubility parameters. Such absorption can physically weaken the polymer to provide an effect of ageing. In addition, the fluid might chemically attack the polymer to provide an additional effect. The kinetics of these two ageing effects is governed by; (i) diffusion, and (ii) chemical kinetics, both of which are governed by Arrhenius relationships with regard to the influence of temperature. This characterization is commonly based on

weight loss and, where possible, mechanical property reduction measurements as a function of time and temperature. The rate of weight loss (W) versus time can be modeled by using an Arrhenius relationship, eqns [2].[8]

$$W = A\left[\exp\left(\frac{-E_a}{RT}\right)\right] \qquad [2]$$

where W represents the ratio between the weight loss and the starting weight of the sample and A is an empirical factor. However, because the thermooxidative degradation in an FRP laminate occurs at the surface, the above equation does not necessarily relate to the same reduction in mechanical properties that are dominated by the bulk properties, and not just the surface properties. A good example of this is an interlaminar fracture test such as the double cantilever beam (DCB)[17] where the fracture data are measured from a delamination in the centre of the specimen. During an ageing test, much of this delamination is not exposed to the environment.

There are few published works on experimental work using a change in a specific mechanical property of relevance, say modulus or strength in eqns [3], to allow modeling of the global effect on a component from local ageing degradation at the surface. Chemical kinetics, classically involving concentrations of reactants and products, can employ the fact that for cross-linked polymers, concentration of cross-links is approximately proportional to the modulus or stiffness. Hence, measurements of changes in modulus from ageing can be plotted logarithmically against linear time (for first-order reactions) at each temperature. From a series of such ageing plots at different temperatures, times to attain the same degree of modulus change can be used to develop the Arrhenius plot, eqns [3].

$$\ln\frac{1}{t_{95}} = A\frac{-E_a}{RT} \qquad [3]$$

where t_{95} is the time for a property to reach 95% of its original value (although other values can be used), T is the absolute temperature, R is the universal gas constant (8.314 J deg^{-1} mol^{-1}), A is a constant, and E_a the activation energy. This expression holds well where there is only one degradation mechanism taking place and this is seldom the situation in the chemical processing environments.

The mechanics and chemistry of degradation can be different at higher-temperature exposures to that at lower-temperature exposures. Mass-loss curves can change significantly with temperature because of different mechanism occurring, including removal of volatiles, additional cross-linking, and structural rearrangements of the matrix. Testing at temperatures too close to the T_g gives degradation rates that are nonlinear, making estimates of useful remaining life invalid.

One acceleration method for thermooxidative stability is to increase the temperature and the pressure of the oxygen,[18] thus accelerating the rate of degradation due to oxidation. However, other attempts to accelerate ageing in acids by increasing the acid concentration were less successful, with only small increases in the ageing rate being achieved.[19]

While the above sections have described the current technology and gaps in predictive methodologies, there are FRP components in-service with long duration lives. The approaches used to give some estimation on long-term life include single-point data (properties after a specific set of ageing conditions) and short-term ageing extrapolation. The following section describes some applications where ageing has been considered.

3.32.4 Ageing Associated with Supersonic Flight

Many of the earliest applications of carbon FRPs were in military aircraft where the main ageing mechanisms were hygrothermal. As discussed above, this reduced the modulus of the matrix lowering some mechanical properties. As a result, most aircraft with FRP components use hot wet properties as part of the design allowables. Several aerospace programmes have been concerned with commercial supersonic aircraft to replace the Concorde. Long-term thermooxidative ageing became a key technology development for these aircraft. The first major study on ageing of FRPs for supersonic aircraft was performed by Kerr and Haskins.[20] The materials investigated included carbon- and boron-epoxy and carbon polyimide that were exposed to elevated temperatures for up to 50 000 h. The effect of altitude was also included representing the reduced oxygen levels at high altitudes. The laminates used were typically $[0°/\pm45°]_s$ and temperatures ranging from 122 to 177 °C representing temperatures up to Mach 2.4 flight. The tests performed included tensile, compression, and shear and also tests to study the effects of moisture and creep after the exposures in an attempt to identify the thermooxidative ageing mechanisms. These tests were chosen as those

typically used in an aircraft design process as opposed to those required to identify the effects of ageing.

For some materials, edge cracking and severe property degradation was identified at temperatures of 177 °C after 5000 h of ageing with a 0.1 MPa pressure. This degradation was not noted after 25 000 h at the same temperature but at 0.014 MPa. Degradation was observed for epoxy specimens at times under 5000 h when aged at 177 °C, which was close to the T_g of materials. Degradation was a severe crumbling of the matrix at the specimen surface. Ageing damage was far less at 122 °C after many more hours exposure. This demonstrates that raising the temperature to accelerate ageing may not be a valid approach when the exposure temperature reaches T_g. The polyimide-based specimens had much better thermooxidative stability. At 232 °C, after 50 000 h the tensile properties decreased, although no macroscopic damage to the resin could be observed, although clearly some degradation had occurred from the weight-loss results. In this instance, the selection of a matrix-based mechanical test during the ageing program would perhaps identify matrix degradation after shorter exposure times.

During NASA's High-Speed Research (HSR) programme in the 1990s, studies were conducted that focused mainly on high temperature polymers for a new generation of High-Speed Civil Transport (HSCT) aircraft with a speed target between Mach 2.0 and 2.4 with a design requirement of 60 000–120 000 h. The work in this program focused on new materials' development for high temperature use and included carbon bismaleimides and polyimides.

One of the primary difficulties in characterizing the effects of ageing on changes in structural properties is the correlation of 'ageing'-related data, such as weight loss, to changes in material mechanical properties such as strength, stiffness, and toughness. An investigation in the change of lamina properties (E_{11}, E_{22}, and G_{12}), T_g and weight loss for this programme can be found elsewhere.[20] An IM7/8320 carbon thermoplastic and an IM7/5260 carbon bismaleimide were aged in air-circulating ovens at 125 and 175 °C for 5000 h (representing 10% of the life of proposed life for HSCT). In this time frame, the materials showed little signs of ageing at 125 °C. The IM7/5260 had a 2% weight loss after 5000 h at 175 °C. This corresponded to a 10% decrease in E_{22} and a 2% decrease in G_{12}, but no significant change in T_g or E_{11}.

A test program to evaluate the synergistic effects of stress, temperature, moisture, time, radiation, and oxygen level on the properties of bismaleimide composites was conducted as part of the HSR programme.[10,11,18,21–23] Isothermal ageing as well as thermal cycling, and creep tests were conducted at temperatures up to 250 °C. As for the Kerr and Haskins work, exposure temperatures close to the materials T_g led to very rapid ageing and anomalous effects that made it difficult to develop an accelerated ageing approach.

Martin[17] has investigated the delamination onset under thermal mechanical fatigue with modeling used to predict delamination onset. To verify the methodology, isothermal statics tests were conducted at temperatures of 125 and 175 °C (representing Mach 2 and Mach 2.4 flight, respectively) on quasi-isotropic laminates fabricated from carbon bismaleimide (IM7/5260). Raising the temperature had the effect of decreasing the value of strain energy release rate (G) at the edge by reducing residual thermal stresses. However, the materials fracture toughness was also lower at higher temperatures. The isothermal ageing results of these materials discussed by Kerr *et al.*[20] would need to be incorporated as additional effects of ageing. These would need to be included in addition to the change in properties related to temperature and fatigue.

For aerospace applications, open-hole tension and compression of laminates are important properties for damage tolerance designs. As discussed above, thermooxidative ageing attacks the surface and an investigation was conducted by Morgan *et al.*[22] to determine the influence on isothermal ageing of laminates with a hole drilled before and after ageing and edge cut before and after ageing. Quasi-isotropic laminates fabricated from IM7/5260, IM7/8320, and IM7/K3B a carbon polyimide added to the HSR program were aged at temperatures of 125 and 175 °C (additional exposures at 200 °C were carried out on the IM7/K3B) for periods up to 5000 h. For IM7/5260 and IM7/8320, significant damage was seen on the surfaces and this degraded the stress to cause delamination at the edges but did not affect ultimate strength of the laminate, because of the presence of 0 ° fibers in the loading direction. Removal of these damaged edge by cutting them off brought the edge delamination stress back to the undamaged value demonstrating that thermooxidative ageing begins at the surface. For the K3B laminate, no edge delamination was observed before lamination failure reflecting the higher toughness of this material and hence the better resistance to thermooxidative ageing. Little difference was identified whether the holes were drilled before or after ageing. While there would be some damage to

the matrix within the holes after ageing, the failure is still dominated by the local stress concentration on the 0 ° fibers at the hole.

3.32.5 Ageing in the Oil and Gas Industry

FRPs are key candidate materials for replacing carbon steel in the Oil and Gas Industry because of their good corrosion resistance and light weight. However, this industry is very risk averse and the uptake of these materials has been slow and is directly related to the operational risks for that component. The shortage of long-term performance data of FRPs in oil and gas applications does not aid their uptake. However, the potential improvements in component and system performance using FRPs will ultimately reduce capital and maintenance requirements, and this fact has enabled some usage of composites in the industry.[24,25]

The environments in the oil and gas industry can be very harsh. The fluids with which FRPs might come into contact include those illustrated in Figure 2, along with some of the potential ageing effects. The composition of crude oil varies around the world from well to well. It mainly comprises aliphatic alkanes (hydrocarbons) such as hexane, octane, decane, etc. Aromatic hydrocarbons may also be present and these are known to swell epoxy matrices. The presence of corrosive media such as hydrogen sulfide or even carbon dioxide in water (carbonic acid) can chemically attack the entire composite, especially if a GRP is under load promoting environmental stress cracking/corrosion (ESC). In addition, most oil and gas operations are conducted at high temperatures (up to 200 °C) and at high pressures, helping to accelerate ageing of the material.

The notable uses of FRPs in this industry are in pipeworks, gratings, and blast and fire protection. Apart from hundreds of kilometers of GRP pipe used for transporting hydrocarbon and water lines in the Middle East, FRPs are also being increasingly used to line steel pipes where the FRP provides corrosion protection for the pipe bore by acting as a barrier to the passage of transported fluids. The composite-lined pipe solution is in direct competition with conventional corrosion-resistant alloy (CRA) systems for downhole and flowline/pipeline applications. Statoil Hydro pioneered the use of downhole tubing with composite materials in the North Sea. A Duoline 20 liner was examined after five years of

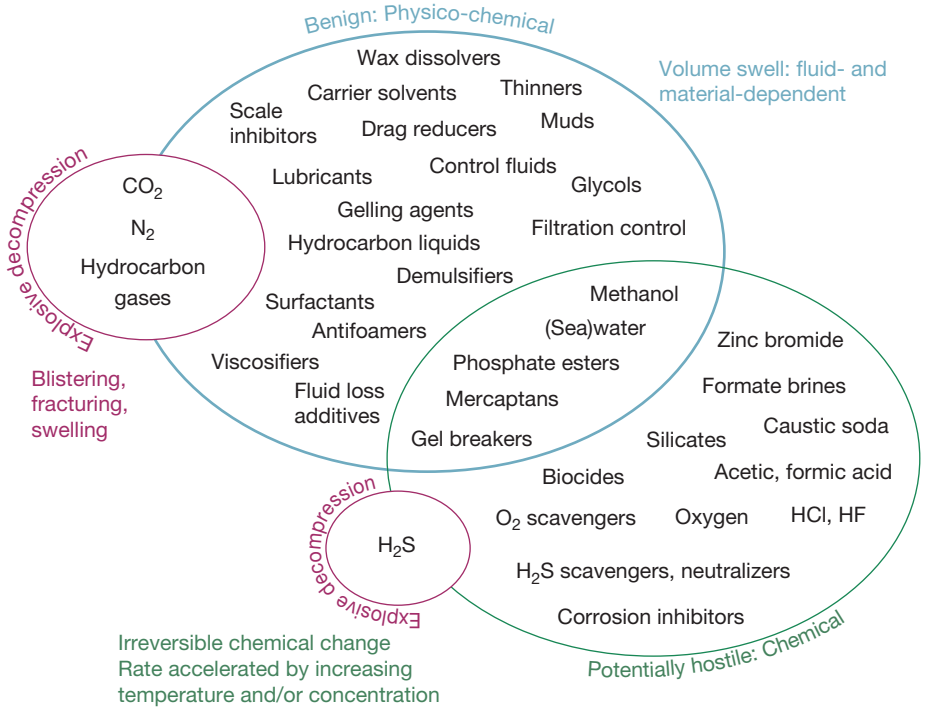

Figure 2 Possible fluids used in the oil and gas industry and their effects on polymers.

service at up to 110 °C and was found to be in excellent condition.[26] The technology has generally been confined to water injection service. A consortium project has been run by Oil States Industries UK to help understand the chemical compatibility of various types of FRP exposed to different oil field fluids, with the aim of obtaining 20-year life.[27] These liners see a variety of hostile media including hydrocarbons at temperatures up to 160 °C, and short exposures to methanol, HCl/HF, and other fluids for cleaning operations. As part of the materials screening tests conducted at MERL, Hitchin, UK, single-point data was generated for specific conditions such as several days at 160 °C in hydrocarbon and brine mix, 8 h of HCL exposure, etc. Several postexposure tests were conducted to ascertain surface degradation, weight change and mechanical property change of the liners. A picture of a glass-epoxy liner exposed to HCl for 8 h shows complete degradation (**Figure 3**).

GRP piping onshore is primarily filament-wound glass-epoxy and it has been successfully installed in 100 km runs in the Middle East for transport of hydrocarbons and other fluids. One of the shortcomings for these pipes is that the corrosion science of metals is much more developed and understood than the ageing and degradation of these materials. International standards exist for the design and installation of such pipework where short-term tests are used to account for such degradation and sufficient safety factors employed. DNV-OS-C501 standard discusses the various effects on mechanical properties under the influence of temperature, moisture and chemicals, and suggests that "... the degradation rates shall be obtained for the actual materials in question..." but gives no method for quantifying these effects in the long term. The ISO 14692 Part 2 Annex D provides information on defining partial factors A1/A2 to account for temperature and chemical resistance, respectively. These factors are used to give knockdowns on properties that were measured at standard temperatures. While values for determining A1 are well established, A2 can be generated for water but is less well identified for other chemicals. The standard makes recommendations of other standards (such as ASTM C 581) that can be used for deriving these factors for other chemicals, although these standards were not specifically written for determining A2 (see **Section 3.32.6**). While these approaches have allowed GRP piping to be specified, it is generally accepted that an improved approach of quantifying such degradation is needed.

Ageing from contact of the transport fluid in these GRP pipes occurs from the surface inwards and requires time to penetrate into the material's centre, as discussed above. The ageing or degradation of an FRP pipe has many stages and it is up to the user to determine at which phase failure is said to have occurred, **Figure 4**. Almost immediately at Stage 1, the fluid will diffuse into the polymer causing immediate physical changes. This is a complex phenomenon for an FRP material in contact with mixed fluids and is discussed further below. In Stage 2, the fluids would have diffused further into the FRP and the inner surface might have begun to chemically age. In Stage 3, the ageing is such that it has caused mechanical damage on the inner surface. Fluid diffusion and chemical ageing continue in Stage 3, but with the presence of cracks the fluid can now penetrate quicker. In Stage 4 diffusion, chemical ageing and mechanical damage has continued, but now the mechanical damage on the inner surface is sufficient for material to be removed. Stage 4 also shows cracks

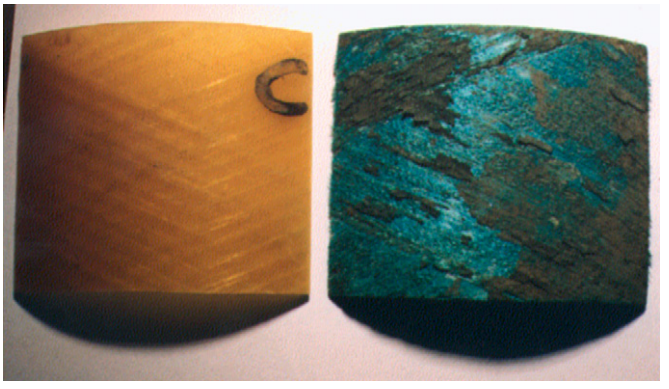

Figure 3 Section of glass-epoxy liner submitted to an HCl exposure. Courtesy of MERL.

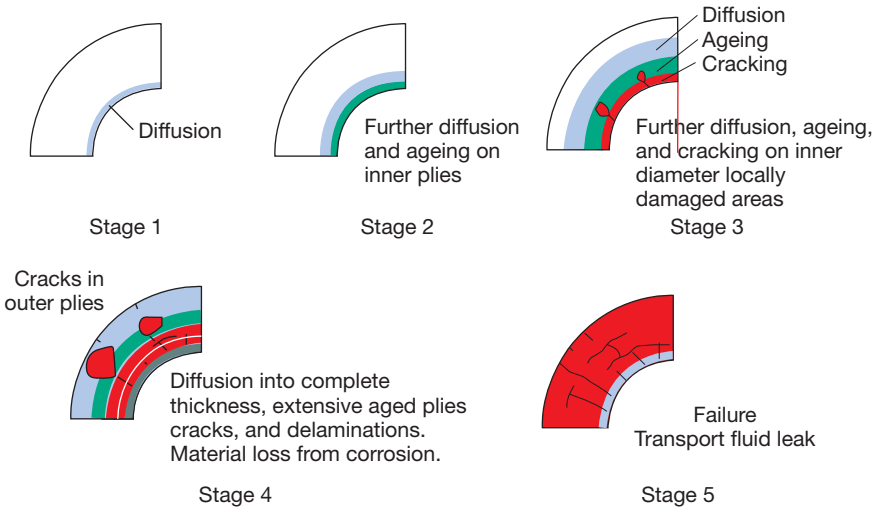

Figure 4 A schematic of GRP degradation when transporting a hostile fluid.

on the outside of the pipe from other damages such as erosion or UV degradation. Stage 5 shows complete damage through the pipe wall and subsequent leaking.

In most pipe designs, 'failure' should be considered as somewhere between Stages 1 and 3 and the influence on strength of the system evaluated to allow for sufficient safety factors (e.g., A2) to be applied.

In order to predict the life of an FRP laminate the following information needs to be known:

- The aged condition of the material and the profile through the thickness. This can be determined by knowing the rate of ageing (physical and chemical) for a given set of conditions (fluid type, temperature profile, time, etc.).
- The key material properties at a given amount of ageing. This depends on what is classed as the residual life of the pipe (see next bullet). The mechanical properties that are used to determine this residual life are those that have to be measured.
- The residual life of the structure with given damage and degradation profile; this is dependent on what is considered as failure for example, leak, global change in stiffness, % loss of material, inner cracking.

The technology for generating the information above does not exist at the time of publication.

The advantages of FRP gratings used offshore are obvious in the improved resistance to corrosion in a sea water environment and their durability and light weight, compare to metallic options, **Figure 5**. The products are generally pultruded glass reinforced,

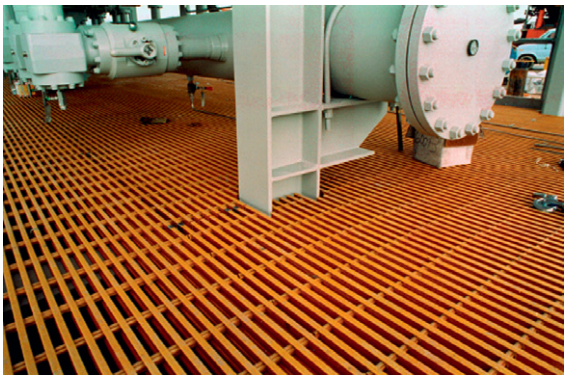

Figure 5 A glass-phenolic grating on the Mars Platform in the Gulf of Mexico, Courtesy of Strongwell.

offering a cost-effective manufacturing method. The use of phenolic resins allows the parts to meet fire-resistance requirements offshore. An important driver for GRP gratings has been the ease of installation compared to steel. The ageing of these materials follows the same aspects as marine composites discussed in **Section 3.32.7** and includes hydrolysis and UV ageing. The fire resistance of these phenolic gratings is also a key reason behind their selection, but fire properties goes beyond the scope of this chapter.

Composites are also being increasingly used to protect subsea structures such as wellheads, and flowlines, protecting them from impact events such as dropped objects and commercial fishing operations. This is an accepted area of use where the perceived risks of adoption are outweighed by the benefits in performance and corrosion resistance. Another example of the use of composites in hostile

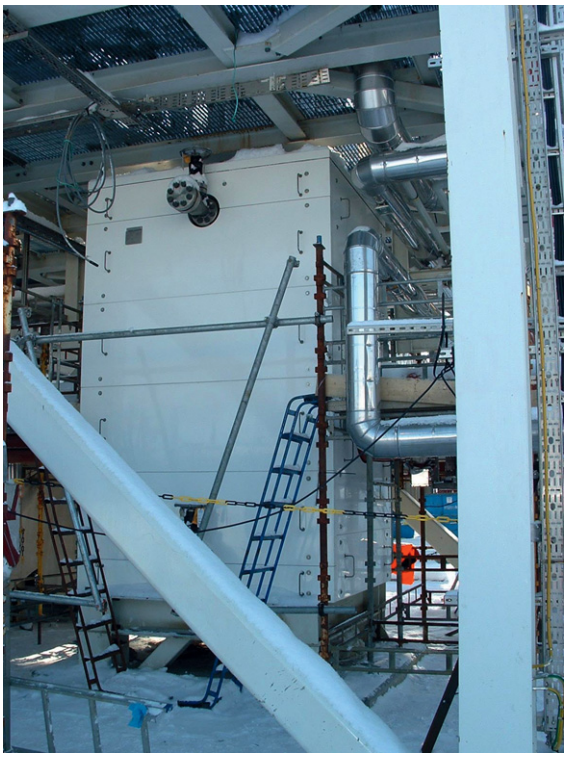

Figure 6 Composite fire-blast protection enclosure. Reproduced with permission from Solvent Composite Systems Ltd.

environments is a ProTek(tm) Jet Fire and Blast protection enclosure manufactured from composite panels by Solent Composite Systems Ltd., Figure 6. This enclosure was installed at the LNG plant in the Arctic town of Hammerfest in northern Norway to protect emergency shutdown equipment. The composite structure resists an explosion pressure equivalent to 7 tonnes per square meter and protects against 90 min exposure to the erosive and heating effects of a hydrocarbon jet fire with a flame temperature of 1150°C resulting from a high pressure gas leak. During this period the equipment temperature does not exceed 65°C. The ageing aspects of long-term water exposure, biofouling, and hydrolysis are covered in Section 3.32.7.

3.32.6 Ageing in the Chemical Processing Industry

In the chemical processing industry (CPI), the environments for equipment such as reactor vessels, storage tanks, scrubbing towers, stacks, piping, valves, etc. may be extremely harsh (Figure 7). In many instances, corrosion-resistant alloys including highly alloyed stainless steel, titanium, and nickel-based alloys have

Figure 7 FRP scrubbing tower. Courtesy of Dow Chemicals.

to be used and even these can corrode in these environments. One solution adopted in this industry is the use of FRPs in manufacturing this equipment.

FRP materials are used to a large extent in plants which manufacture chlorine, chlorate and concentrated acids (e.g., sulfric, hydrochloric, hydrofluoric, nitric) as well as metal chloride solutions (e.g., NaCl, $FeCl_3$, $AlCl_3$, $MgCl_2$, $NiCl_2$).[28] FRPs are now also used in desulfrization plants (flue-gas ducting, scrubbers, etc.) which also have applications in oil and gas production. In many instances, a thermoplastic liner is used in the metallic and FRP pipes to act as a corrosion or permeation barrier, or both. The thermoplastic lining may be PA11, PVC, or PP; or for more aggressive service, PVDF. Because of the environmentally hostile nature of some of the chemicals being transported or stored, failure is unacceptable. However, failures do occur (Figure 8).[29] These failures may not only be very costly, but also present a health and safety risk to the workers at the plant, local residents and environment. The consequences and liability of equipment failure, even minor leaks, are becoming increasingly severe and have resulted in a very strict regulatory climate. Although FRP is often used to solve problems of corrosion on various metallic materials, these materials can still be affected by these fluids.[30]

The types of resins and fibers depend very much on the application being considered. Thermosetting

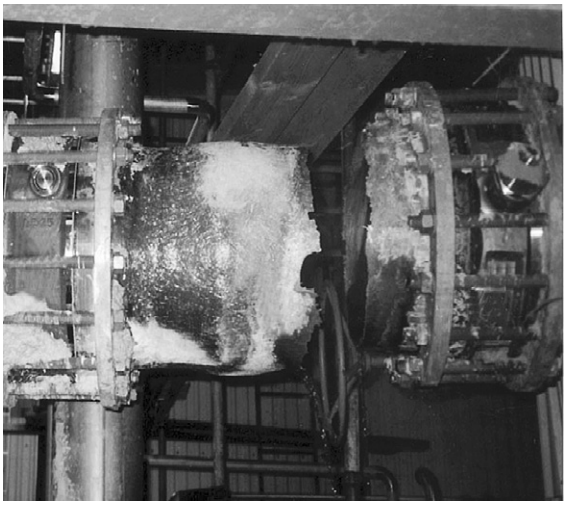

Figure 8 Failure in alkaline aqueous solution at 70 °C. Courtesy of G. Bergman.

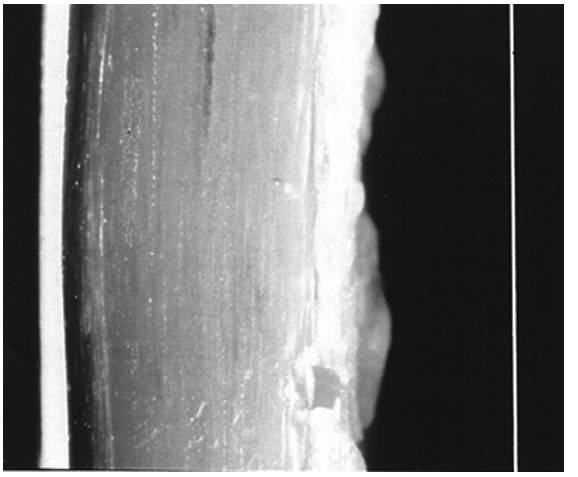

Figure 9 Uniform corrosion in an FRP pipe after 14 years of service. The white line shows the original thickness. Courtesy of G. Bergman.

resins are suitable for large moldings and for filament wound pipes. The most important resin systems used for corrosion protection in the CPI include polyesters, epoxies, bismaleimides, phenolics, and vinyl esters.[28,31] Epoxies have certain advantages, in that they have lower cure shrinkage, adhere better to steel substrates, and offer better chemical resistance than polyesters towards hot alkalis. Vinyl esters are favored because they offer a compromise between epoxies and polyesters, offering good corrosion resistance with moderate relative cost. E-glass fiber is used as the reinforcement for the main structural part with a more chemical resistant fiber such as ECR-glass used in the layer in contact with the corrosive fluid. A protective resin-rich layer is often used on the surface adjacent to the acid.

Prediction methods for FRPs in the CPI must account for chemical ageing and include diffusion, hydrolysis and ultimately cracking, blisters and other damage. Eventually, this degradation may continue and lead to actual material loss from the inside of the vessels (**Figure 9**).[32]

Degradation in FRP composites may be defined as one of any of the following in the exposed surface:

• cracks	• loss of fiber	• etching
• pitting	• softening	• delamination
• thickness change	• blistering	• discoloration
• charring	• leaching	• fiber blossomin
• resin loss		

The published work related to chemical resistance of FRP materials in different environments has focused on immersion testing, rather than the more realistic single-sided exposure. Much of the published data quote only single-point data, for example, "The mass of material X increases by 10% in methanol after 10 days at 60 °C." This information may be misleading because the overall trend may involve a mixture of competing mechanisms as discussed in previous sections. For hybrid materials (e.g., the use of a corrosion-resistant veil), the prediction method must account for the time for the ageing to reach each layer.

Further, FRPs may be subject to step changes in property changes leading to failure such as resin embrittlement. This failure is often termed environmental stress cracking (ESC) and also applies to the glass fibers when undergoing strains in excess of 2% and exposed to even dilute acids.[33] In any long-term evaluation, it is necessary to use diagnostic equipment to ensure that the cause for the change in properties of the FRP is understood.

Estimates of remaining life of FRP equipment in the CPI often rely on periodic visual inspection, intuition, and experience of the inspector. The inspector searches out defects such as blistering, delamination, or signs of leaking. Often a bright light is shone on the opposite side of the laminate to help reveal flaws. The inspector often also checks the condition of the laminate surface with a Barcol indentation tester. Drastic reduction in Barcol readings since the previous inspection indicates degradation. On the basis of these findings, the inspector will judge whether the equipment is still safe to operate and when the next inspection should occur.[30]

3.32.6.1 ASTM Standard for Long-Term Chemical Resistance

Materials are generally approved for long-term usage in the CPI using ASTM C 581 *Standard Practice for Determining Chemical Resistance of Thermosetting Resins Used in Glass-Fiber-Reinforced Structures Intended for Liquid Service*. This standard requires immersion of a material in a fluid at a single temperature. Various properties (Barcol hardness, flexural modulus and strength, and T_g) are determined at intervals normally within one year. If the properties do not decrease by a certain amount, the material may be approved for long-term usage. However, this method does not offer an approach to allow an extrapolation to longer-term usage at varied of temperatures and is therefore little more than a screening test.

To demonstrate the use of ASTM C 581, an FRP laminate that may be used for the linings of tanks and vessels used to store acids was tested.[30] Plaques of materials were immersed in concentrated HCl or H_2SO_4 for 12 months. Periodically, Barcol hardness, mass change, and flexural properties were measured on specimens cut from these plaques. The mass change is shown in **Figure 10**, illustrating that the material shows weight loss early in the exposures and the rate of weight loss begins to reduce as the test progresses. The change in Barcol hardness, shown in **Figure 11**, shows that there is an initial increase in both exposures, indicating that some form of local hardening has occurred. After 6 months' exposure, the hardness begins to decrease, leading to 10–15% from the starting values after 12 months. This indicates that there is more than one ageing mechanism occurring and the resulting change in properties cannot be taken from only the end data point.

3.32.6.2 The Arrhenius Relationship

Using the different test parameters used in ASTM C 581 in the previous section, the feasibility of using an Arrhenius relationship was presented elsewhere.[30] Key to this approach being successful is that the elevated temperature exposures do not cause a change in the ageing mechanisms observed at lower temperatures.

A Derakane 411 vinyl ester resin was tested with two plies of 45g E-Glass chopped-strand mat, with a 0.25-mm C-glass veil. The materials were exposed to 37% HCl at temperatures of 40, 60, and 80 °C. Before and after the exposures, thickness and weight in air and water were measured to determine any changes. Following the ageing and the weighing, suitable specimens were cut from the plaques. Three point-bend tests were conducted and showed that the modulus initially increased before decreasing, whereas at the higher temperatures, the modulus and strength continually decreased, showing a change in mechanism at the different temperatures. The work demonstrated that there is an overall trend from test to test of a property change with exposure time, the rate of which increases with time. It is this general concept that lays foundation for developing accelerated ageing approaches using the Arrhenius equation if a single mechanism is present. The 5 and 10% change of flexural strength were plotted against the reciprocal of the absolute exposure temperature and a straight line fitted. The shorter-term,

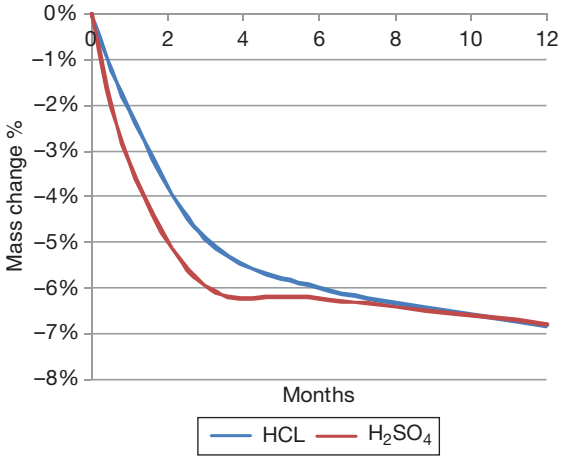

Figure 10 Mass change of an FRP in concentrated acid.

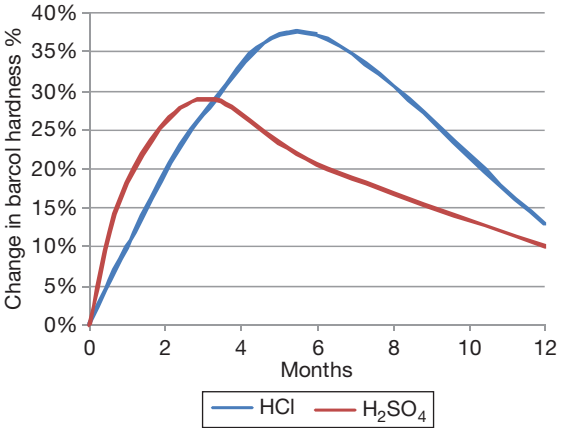

Figure 11 % Change in Barcol hardness of an FRP in concentrated acid.

higher-temperature exposure tests were able to predict the properties at lower-temperature exposures. The energy of activation for this change is in the region of 80 kJ mol^{-1}, which is indicative of chemical ageing. However, an Arrhenius curve cannot be drawn for the modulus because of the initial increase in modulus in the early exposure times, this invalidating this method unless the different mechanisms are separated.

3.32.6.3 Using a Semiempirical Corrosion Approach

Another approach to the long-term ageing of FRPs is to relate the effects of ageing to those of corrosion in metals, because on the macrolevel the results are very similar. Many types of corrosion found in metals can also be found in FRP, such as uniform corrosion (material loss), localized corrosion (pitting), selective corrosion, stress corrosion, corrosion fatigue, erosion corrosion, and layer corrosion (delamination). CFRPs are conductive and galvanic corrosion effects may arise when being coupled to a metal component.

On the basis of the results of corrosion analyses of samples taken from FRP equipment used for different chlorine dioxide environments in various pulp mill applications over a period of 20 years, a semiempirical relationship for uniform corrosion behavior of FRP in chlorine dioxide environments has been established,[32]

$$\Phi = Bt^{\alpha}cA\exp\left(\frac{-E_a}{RT}\right) \qquad [4]$$

where Φ is the depth of corrosion (mm), B is a special factor in case of protective deposits on the surface (usually $B = 0$ or 1), t is the time in service (years), α is a factor which depends on the thickness and degree of degradation of the corroded surface layer (usually α is between 0.5 and 1), c is the concentration of chlorine dioxide (g l^{-1}), A is a material constant which depends on the type of resin, the degree of curing, and the laminate structure, E_a is the activation energy of the rate-controlling step of the corrosion process (kJ mol^{-1}), R is the general gas constant (8.3 J mol^{-1} K), T is the temperature (K).

This expression is not proven for other applications and environments, although the premise should hold.

3.32.7 Ageing in the Marine Industry

One of the more established uses of FRPs with long and chopped fiber resins in marine vessels from small dinghies to racing yachts. A review of marine composites is given elsewhere.[34,35] The FRP materials are mainly E-glass reinforced polyester and epoxy, but with the high-performance vessels carbon fiber composites and a range of sandwich materials are now used. Almost always, a protective outer coating or gelcoat is used to help prevent diffusion and to give a better appearance. There is much experience on the ageing of these materials in this environment. However, similar to the studies in other industries, research studies on ageing for this industry have focused on short-term ageing tests under severe conditions that may have little relationship with in-service use.

Leisure craft or pleasure boats, defined as vessels built for recreational purposes, were one of the first applications of FRPs. The average lifetime of a FRP pleasure boat is 30 years, demonstrating the anticipated long use life of these materials. For commercial vessels including fast ferries, lifeboats, fishing boats, and some military vessels have been made from a conventional GRP material since the 1960s. Some vessels such as mine countermeasure vessels are in excess of 40 m length and the nonmagnetic and conducting properties of the GRP add another advantage to the use of these materials. The low weight of FRP materials make them attractive for submarine use in internal and external structures such as sonar domes.

Woven or chopped glass strand mats in a polyester resin is the typical FRP use in marine applications and much work on ageing of these materials in a sea water environment has been conducted.[36] Higher-end materials, including stitched multiaxial cloth, carbon epoxy are used for the higher end applications where ageing may be less of a concern such as in racing yachts. The document also provides a database of material properties to be used if test data are not available. Typical hull laminate thicknesses vary from 5 mm for pleasure craft up to 150 mm for hulls that must survive underwater explosions. The difference in thickness has an affect on the time to reach equilibrium and hence begin hydrolytic ageing. Manufacturing techniques have been developed over the past 10 years to utilize resin infusion to draw the resin through the dry fibers. This has resulted in the ability to have a higher fiber to resin volume fraction giving thinner laminates with the same strength as the previously used wet lay-up manufacturing methods with lower volume fractions. Sandwich panels comprising a core (foam or balsawood) surrounded by thin layers or skins of FRP are a preferred manufacturing method for large hulls. However, the thin skins, their bonding to the core

and degradation of the core material present further concerns for ageing. As mentioned above, a gelcoat is almost always used and this serves to protect the laminate.

There are a number of different damage modes for marine composites and the gelcoats, including osmosis, blisters, pinholes, wrinkling, debonding/delamination, crazing, etc., can all be considered a form of ageing. Blisters are a particular ageing damage mode in marine environments, where the osmotic pressure is developed between the gelcoat and the FRP. This is built up from products such as glycols leached from the base FRP and can cause local delamination or blisters and is particularly apparent with a gelcoat that is more permeable than the base laminate. The temperature and the composition of the seawater, which varies around the world, are important aspects in consider ageing of marine FRPs as well as the loading from wave load, slamming load, hydrostatic pressure, etc. Antifoul treatments are used on many boats to prevent biofouling or marine growth. These are applied to the gelcoat and may in themselves age the coating.

Conventional marine ageing of a marine FRP follows the same degradation mechanisms as discussed in Section 3.32.2.2. This is physical ageing causing plasticization and swelling (potentially leading to interfacial debonding and delaminations) and chemical ageing such as hydrolysis of the matrix and, in saltwater environments, the fiber and the fiber–matrix interface. Many of the ageing studies are conducted at higher temperatures to reduce the ageing times. A number of case studies are presented in Searle and Summerscales,[36] where an attempt to better understand the changes due to ageing of properties that can be used for design were studied. In one study, weight change was measured along with shear strength and modulus for three GRPs (polyester, vinyl ester, and epoxy, all with the same glass reinforcement). The work demonstrated that the resin and fiber interface within an FRP absorbs water, not just the resin. In the same work, FRP materials were exposed to an accelerated exposure (elevated temperature), and the same panels were exposed to the sea for up to a year. The results suggest that without due attention to the various ageing conditions, the accelerated test will overpredict changes in properties.

For realistic accelerated ageing of marine FRPs, several aspects need to be considered. Virtually, all laminates, as stated above, will have a gelcoat. While not an impermeable layer, it is a resin-rich layer and needs to be considered in ageing analysis. The work in Searle and Summerscales[36] demonstrated that the composition of the water can greatly affect the ageing of the FRP. Seawater will diffuse into polymers slower than distilled water, and ageing exposure using distilled water may be overly conservative. In addition, during ageing, products may leach out of the FRP into the water. These products will themselves change the composition of the water more significantly if small vessels and hence small volumes of water are used. As for other applications, the use of temperature as an ageing accelerator must be used with caution. The increase in temperature can serve to promote further cross-linking in partially cured polyesters and use of ageing temperatures near or above the T_g can cause degradation mechanisms that will never occur at lower temperatures. For true comparisons for sea environments, it is the inclusion of biofilms that will develop, followed by biofouling, resulting in a complete covering. This needs to be considered when conducting weight-gain/loss measurements and the influence of the living matter on the properties of the composites needs to be better understood.

3.32.8 Concluding Remarks

This chapter has described some of the more common forms of ageing of FRPs. Ageing is a summation word for degradation and can include physical changes of the matrix such as swelling or irreversible chemical changes such as hydrolysis or oxidation. The extent of the degradation is very much dependent on the exposure the FRP material will experience including the fluid in contact, time, pressure temperature, load applied, if any, etc. Some attempts have been to develop predictive modeling capability for the long-term durability assessment of FRP components, but this still remains an area for further research. As the use of FRP materials increases and the demands for extended performance grow, so does the need and importance to develop predictive capability for assigning the fitness for the purpose of an FRP structure at any time during its service.

References

1. Jones, R. M. *Mechanics of Composite Materials*; Scripta Book Company: Washington DC, 1975.
2. Matthews, F. L.; Rawlings, R. D. *Composite Materials: Engineering and Science*; Woodhead Publishing: Cambridge, England, 2002.
3. *ASM Handbook, Volume 21 Composite*; ASM International: Ohio, 2001.

4. www.vircon-composites.com
5. Struik, L. C. *Physical Ageing in Amorphous Polymers and Other Materials*; Elsevier Scientific: New York, 1978.
6. Gates, T. In *Ageing of Composites*; Martin, R., Ed.; Woodhead Publishing: Cambridge, England, 2008; Chapter 1.
7. Jones, F. R. In *Reinforced Plastics Durability*; Pritchard, G., Ed.; Woodhead Publishing: Cambridge, England, 1999; Chapter 3.
8. Mensitieri, G.; Iannone, M. In *Ageing of Composites*; Martin, R., Ed.; Woodhead Publishing: Cambridge, England, 2008; Chapter 9.
9. Harris, C. E.; Gates, T. S. Eds. *High Temperature and Environmental Effects on Polymeric Composites*; ASTM STP 1174; American Society for Testing and Materials: Pennsylvania, 1993.
10. Martin, R. H.; Siochi, E. J.; Gates, T. S. In *Proceedings of the American Society for Composites Seventh Technical Conference*, University Park Pennsylvania, 13–15 October 1992; pp 207–217.
11. Tsotsis, T. In *Ageing of Composites*; Martin, R., Ed.; Woodhead Publishing: Cambridge, England, 2008; Chapter 5.
12. Weitsman, Y. *Mech. Phys. Solids* **1987**, *35*(1), 73–93.
13. Layton, J. In *Reinforced Plastics Durability*; Pritchard, G., Ed.; Woodhead Publishing: Cambridge, England, 1999; Chapter 6.
14. Halliwell, S. *Ageing of Composites*; Martin, R., Ed.; Woodhead Publishing: Cambridge, England, 2008; Chapter 15.
15. Dodds, N.; Gibson, G. In *Composite Materials for Offshore Applications*; American Bureau of Shipping, 1999; pp 77–92.
16. Gates, T. S. On the use of accelerated test methods for characterisation of advanced composite materials, NASA TP-2003-212407, May 2003.
17. Martin, R. H. In *High Temperature and Environmental Effects on Polymeric Composites*; ASTM STP, 1174; Harris, C. E., Gates, T. S., Eds.; American Society for Testing and Materials: Pennsylvania, 1993.
18. Tsotsis, T. K.; Lee, S. M. *Compos. Sci. Technol.* **1998**, *58*, 355–368.
19. Hogg, P. J.; Hull, D. In ; Harris, B., Ed.; In *Developments in GRP Technology,* Harris, B., Ed.; Applied Science: London, UK, 1983; Vol. 1, pp 37–90.
20. Kerr, J. R.; Haskins, J. F. Time temperature stress capabilities of composite materials for advanced supersonic technology applications, NASA CR-178272, May 1987.
21. Martin, R. H.; Siochi, E. J.; Gates, T. S. In *7th Technical Conference on Composite Materials*, The Pennsylvania University, American Society for Composites, October 1992.
22. Morgan, R. J.; Shin, E.; Dunn, C.; Fouch, E.; Jurek, B.; Jurek, A. In *Proceedings of the 39th International SAMPE Symposium,* April 1994, pp 1564–1575.
23. Martin, R. H. In *AIAA/ASME/ASCE/AHS/ACE 35th Structures, Structural Dynamics and Materials Conference*, Hilton Head, SC, April 1994; pp 18–20.
24. Martin, R. H. A Technology Gap Review of Composites in the UK Oil and Gas Industry, March 2007www.merl-ltd.co.uk.
25. Frost, S. In *Ageing of Composites*; Martin, R., Ed.; Woodhead Publishing: Cambridge, England, 2008; Chapter 14.
26. Melve, B.; Nice, P. In *Statoil, MERL Oilfield Engineering with Polymers Conference*; London, 2003.
27. http://medlicott.uk.com/bus/osiuk_jip.htm
28. Kelly, P. *Reinforced Plastics Durability*; Pritchard, G., Ed.; Woodhead Publishing: Cambridge England, 1999; Chapter 9.
29. Bergman, G. *Corrosion*; 2004; NACE Paper 04611.
30. Martin, R. H. *Ageing of Composites*; Martin, R., Ed.; Woodhead Publishing: Cambridge England, 2008; Chapter 17.
31. Pritchard, G. In *Advanced Composites*; Elsevier Applied Science, 1989; pp 163–196.
32. Bergman, G. *J. Hazard. Mater.* **2007**, *142*(3), 695–704.
33. French, M. A.; Pritchard, G. *Compos. Sci. Technol.* **1993**, *47*, 257–263.
34. Davies, P.; Choqueuse, D. In *Ageing of Composites*; Martin, R., Ed.; Woodhead Publishing: Cambridge England, 2008; Chapter 12.
35. Choqueuse, D.; Davies, P. In *Ageing of Composites*; Martin, R., Ed.; Woodhead Publishing: Cambridge England, 2008; Chapter 18.
36. Searle, T. J.; Summerscales, J. In *Reinforced Plastics Durability*; Pritchard, G., Ed.; Woodhead Publishing: Cambridge England, 1999; Chapter 7.

3.33 Degradation of Natural Rubber and Synthetic Elastomers

A. bin Samsuri
Department of Polymer Technology, MARA University of Technology (UiTM), 40450 Shah Alam, Selangor, Malaysia

Glossary

Damping Basic property of an elastomer to dampen, absorb or reduce vibrations. High damping elastomers are those having high glass-transition temperature (T_g), which are widely used to isolate vibrations.

Glass-transition temperature (T_g) It denotes the temperature below which the elastomer becomes glassy and brittle, above which it is soft and rubbery. T_g reflects molecular mobility and hence the internal viscosity of the elastomer. High T_g indicates low molecular mobility or high internal viscosity and vice versa.

Heat build-up The amount of heat accumulated in the elastomer when subject to cyclic deformation. It is closely related to hysteresis.

Hysteresis It is a term to denote energy dissipated as heat when the elastomer is subject to cyclic stresses or in a single stress–strain cycle. The area bounded by the extension and retraction curve gives a quantitative measure of hysteresis.

Raw rubber Fresh rubber or an elastomer as received from the supplier.

Scorch It is a rubber technology term to denote the occurrence of a premature crosslink, which is an undesirable feature during the shaping process.

Vulcanizate or vulcanized elastomer Indicates rubber or elastomer that has been vulcanized or cured, and thus, contains network structure or chemical crosslinks.

Abbreviations

ACM Polyacrylic rubber
ASTM American Society for Testing Materials
CED Cohesive energy density
CIIR Chlorinated butyl rubber
CM Cement metal failure
CP Cement primer failure
CR Polychloroprene rubber
CSM Chlorosulfonated polyethylene rubber
DCP Dicumyl peroxide
DOPPD Dioctyl-*p*-phenylenediamines
ECO Copolymer of epichlorohydrin rubber
ENR50 Epoxidized natural rubber (50 mol% epoxidation)
EPM Ethylene propylene rubber
EV Efficient vulcanization
GRG General rubber goods
IHRD International Rubber Hardness Degrees
IIR Isobutylene isoprene (butyl) rubber
IR Synthetic polyisoprene rubber
IRG Industrial rubber goods
ISO International Organization for Standardization
MRB Malaysian Rubber Board
MRPRA Malaysian Rubber Producers Research Association
MS Malaysian standard
NBR Nitrile rubber
NR Natural rubber
PP Polypropylene
PTR Polysulphide rubber
SBR Styrene butadiene rubber
TAC Triallyl cyanurate
TAIC Triallylisosyanurate
TARRC Tun Abdul Razak Research Centre
UiTM Mara University of Technology
UV Ultraviolet light
XNBR Carboxylated nitrile rubber

Symbols

A Cross-sectional area (m^2)
***A*$_o$** Unstrained (original) cross-sectional area (m^2)
B Crack growth constant
c Crack length (mm, m)
***c*$_o$** Natural flaw size (mm, m)
***C*$_o$** Concentration of antiozonant ($mg\,cm^{-2}$)

C_s Concentration of antiozonant at the rubber surface (mg cm^{-2})
D Diffusion coefficient ($m^2\,s^{-1}$)
dc/dt Crack growth rate ($m\,s^{-1}$)
f Force (N)
f_f Frequency (Hz)
h Height (m)
k_c Compression stiffness ($N\,m^{-1}$)
k_s Shear stiffness ($N\,m^{-1}$)
l Half thickness of film sheet (mm, m)
L Length (m)
M Molecular weight ($g\,mol^{-1}$)
M_∞ Total mass of liquid absorbed after an infinite time (g, kg)
M_L Mass of layer per unit area of surface ($g\,mm^{-2}$, $kg\,m^{-2}$)
M_t Total amount of liquid absorbed per unit area after immersion time, t ($g\,mm^{-2}\,s^{1/2}$)
N Number of molecules per unit volume of rubber ($mol\,cm^{-3}$)
N_f Fatigue life (number of cycles of failure) (cycles, kilocycles)
R Molar gas constant (8314 $J\,mol^{-1}\,K^{-1}$)
S Shape factor
T Absolute temperature (K)
t Time (s)
T_g Glass-transition temperature (°C, K)
V_1 Molar volume of solvent (m^3)
v_f Volume fraction of seeding particles present in the rubber
v_r Volume fraction of rubber in the swollen gel
W Width (m)
W_s Strain energy density ($J\,m^{-3}$)
$[X]_{phy.}$ Physically manifested crosslink concentration ($mol\,kg^{-1}$)
δ Solubility parameter $(MPa)^{1/2}$
ΔH Latent heat of vaporization (J)
λ Extension ratio
ρ Density ($kg\,m^{-3}$)
χ Rubber–solvent interaction parameter

3.33.1 Introduction

Natural rubber and elastomers belong to the same group of materials known as high molecular weight polymers. According to the International Organization for Standardization (ISO) rubber vocabulary,[1] an elastomer is a macromolecular material which returns rapidly to approximately its initial dimensions and shape after substantial deformation by a weak stress and release of the stress. However, an elastomer has always been recognized as a synthetic elastic polymer.[1] A polymer is a high molecular weight material having many units of small molecules chemically joined or linked by normal covalent bonds to form long chain molecules. These flexible and soft materials find wide uses in many engineering applications, such as natural rubber (NR) bridge bearings, and earthquake and seismic bearings. Indeed NR has had a sound track record in many engineering applications for over 150 years.[2] Elastomers have some unique properties that metals do not have. These include

- high bulk modulus (2000–3000 MPa) relative to their Young's modulus (0.5–3.0 MPa),
- some inherent damping, and
- large strain deformation.

Rubbers having high bulk modulus hardly change their volume when deformed. In simple words, rubber is incompressible. Like incompressible liquids, it has a Poisson's ratio close to 0.5. If rubber is constrained, to prevent changes in shape, it becomes much stiffer, a feature that is used to full advantage in the design of compression springs. Elastomeric bridge bearings and seismic bearings are examples of products that rely on these properties.

The damping inherent in the elastomer is a very important property as it helps to prevent the amplitude of the vibration of the spring from becoming excessive if resonant frequencies are encountered. Elastomeric products such as vibration isolators and engine mounts rely on the inherent damping properties of the elastomer.

The elastomer undergoes large strain deformation (a few hundred percent) without failure by an applied stress below its breaking stress. This means that it can store much more energy per unit volume than steel. Elastomeric dock fender systems make use of its large stored energy capacity to absorb shocks, blows and the impact exerted by ships.

Some of the merits of elastomeric springs over metal springs are as follows[2]:

- no maintenance is required,
- the energy storage capacity is high,
- with correct design, the rubber spring can provide different stiffness in different directions, or nonlinear load–deflection characteristics,
- a certain amount of misalignment is tolerable as the rubber spring can accommodate this tolerance,
- easier to install,
- hysteresis inherited by the elastomer is able to dampen dangerous resonant vibrations.

Another important property of an elastomer is its strong resistance to inorganic acids, salts, and alkalis. In contrast, acids attack metals. For these reasons, the linings of chemical tanks and pipes, especially those containing caustic solutions, are made from elastomers. The function of the elastomer here is to protect the metal against attack by corrosive chemicals.

Every product has its own life span. The designed lifetime of a product depends on the environmental conditions and the nature of the application. It is very important to choose the materials correctly to meet the intended service conditions and the surrounding environment. The aging process is the determining factor that limits the life span of the product. The term aging is always associated with the degradation or corrosion process as applied to metals, which may take many forms. In metals, corrosion takes place in the form of rusting, which involves oxygen and moisture. In elastomers, the term degradation is preferred to corrosion and covers a wider scope than that of metals. Degradation takes place in the form of oxidation, ozone cracking, flex cracking, liquid absorption and heat aging. Degradation in elastomers is very complex as it involves oxygen, ozone, mechanical strain, heat, trace metals, etc. There are other agencies such as solvents, oils, fuels, hot air (steam) and water, which may degrade elastomers and affect the service life of elastomeric products. A specific section on the degradation of elastomers discusses all these issues again later.

3.33.2 Classifications of Rubber and Elastomers

3.33.2.1 Classification in Terms of Origins

Natural rubber comes from trees known as *Hevea brasiliensis*, and shrubs called guayule. The pictures in **Figure 1** show typical rubber trees grown in the hot tropical climate of Malaysia, and the fresh latex that exudes from the bark of the rubber tree, after tapping with a sharp tapping knife. The fresh latex that exudes from the tree known as field latex contains about 70% water. After removing this large amount of unwanted water, the latex is known as concentrated latex and has about 60% of rubber content. Centrifuging is the preferred method of concentrating field latex because of its efficiency and rapidness compared to creaming and evaporation methods. Apart from latex, natural rubbers are available commercially in standard bale form, weighing about 33.33 kg. These bales of NR are produced specifically to meet certain technical requirements such as minimum dirt content, viscosity consistency, ash content, etc.

Figure 1 Pictures of (a) natural rubber trees (top), (b) NR latex exudes from natural rubber tree (middle), and (c) closer view of NR latex collected in a cup (bottom).

All synthetic elastomers are produced by the polymerization process. The early production of synthetic elastomers such as styrene butadiene rubber (SBR), polychloroprene rubber (CR), and nitrile rubber (NBR) relied on emulsion polymerization. One of the main drawbacks of emulsion polymerization is the lack of uniformity of polymer molecules with respect to stereo regularity. This is due to the

different ways in which diene monomer molecules can react, and it applies to all free radical polymerization processes of diene monomers. However, there was a real breakthrough with the discovery of the Ziegler–Natta catalyst in 1954, which enabled the control of the microstructure of polyisoprene.[3] Synthetic polyisoprene is produced by the solution polymerization process using catalysts of the alkyl lithium types such as trialkyl aluminum/titanium tetrachloride mixtures.[3] The Al/Ti mole ratio is critical for achieving high cis content. Currently, there are about 27 types of rubbers or more commercially available in the market. The choice depends on the nature of application, service conditions and environment.

3.33.2.2 Classification in Terms of Purposes

Elastomers can be classified further either as general-purpose rubbers or as specialty rubbers. General-purpose rubbers are those elastomers that are widely used in the manufacture of tires, industrial rubber goods (IRG), and general rubber goods (GRG). Most of the general-purpose elastomers cannot meet high service temperature and high oil resistance specifications or the combinations of these two requirements. The most common general-purpose rubbers include NR, SBR, CR, NBR, ethylene–propylene–diene rubber (EPDM), and BR. In contrast, specialty rubbers are those elastomers that are tailor made to meet certain specific requirements, such as low temperature flexibility, high swelling resistance towards oil (hydrocarbon, fuel, gasoline, etc.) and very high service temperature or combinations of these requirements. Specialty rubbers include silicone rubber, fluoroleastomers, epicholorohydrin, cholorosulfonated rubber, etc. **Table 1** shows some of the rubbers which belong to these grades and their typical applications.

3.33.2.3 Classification in Accordance with International Organization for Standardization

Elastomers can also be classified according to the ISO 4632/1-1982(E)[4] which provides information about rubber as a material with specifications. They are classified and designated in terms of their performance to heat aging, swelling resistance towards oil and low temperature flexibility. This method of classification is very helpful as it facilitates the purchasers and suppliers to make the correct selection of suitable materials, and avoid wasting time and energy.

These designations are determined by a type based on resistance to heat aging, by a class based on resistance to swelling in oil, and by a group based on low temperature resistance.[4] These classification criteria are used to establish a characteristic material designation consisting of three capital letters, where

- the first letter signifies Type (heat resistance)
- the second letter signifies Class (oil resistance)
- the third letter signifies Group (low temperature resistance).

Tables 2–4 show the heat aging temperature, limits of volume swell and brittleness temperature for establishing Type, Class and Group respectively.[4] Type is determined by the maximum temperature at which heat (air oven) aging for 70 h, in accordance with ISO 188, causes a change in tensile strength of not more than ±30%, a change in elongation at break of not more than −50%, and a change in hardness of not more than ±15 International Rubber Hardness Degrees (IHRD). Class is based on the resistance of the material to swelling in American Society for Testing Materials (ASTM) Oil No. 3, when tested in accordance with ISO 1817. In the test, the immersion time shall be 70 h at a temperature determined in **Table 2**. Group is based on the brittleness temperature of the material when measured in accordance with ISO/R 812.

Thus if an elastomer is designated as BCD, it means that it is classified as Type B, Class C and Group D. This implies that the elastomer resists temperatures up to 100 °C, with volume swelling not exceeding 120% in oil No. 3 and is not brittle at −40 °C.

Most of the general purpose elastomers shown in **Table 1** have poor heat resistance except for ethylene propylene rubber (EPM) as shown in **Figure 2**. EPM can withstand service temperature of about 150 °C as it is categorized as Type D. General purpose elastomers also have poor swelling resistance towards hydrocarbon oil except nitrile rubber (NBR) which is classified as Class H with maximum volume swell of 30%. A majority of the specialty elastomers shown in **Table 1** have both excellent heat resistance and swelling resistance. From the chart shown in **Figure 2**, silicone rubber having both methyl and vinyl substituent groups on the polymer chain (VMQ) has equivalent heat resistant (Type G) with silicone rubber having methyl, vinyl, and fluorine substituent groups on the polymer chain (FVMQ). However, they have different Class with respect to swelling resistance. VMQ belongs to Class E while FVMQ belongs to Class J. Clearly

Table 1 General purpose rubbers and specialty rubbers

General purpose rubbers	*Typical applications*	*Specialty rubbers*	*Typical applications*
Natural rubber (NR)	Mainly for tires, industrial and general rubber goods, bridge and earthquake bearings, bridge expansion joints, etc.	Carboxylated nitrile rubber (XNBR)	Oil resistant hoses, boots, seals and gaskets and other automotive components with very good oxidation resistance
Synthetic polyisoprene (IR)	Tires, sports goods, earthquake rubber bearings, IRG.	Polysulphide rubber (PTR)	Used mainly where good resistance to solvents is required
Styrene butadiene rubber (SBR)	Passenger car tires, IRG, GRG	Polyurethane rubber (AU, EU)	Gaskets, seals, solid tires, and foams
Butyl rubber (IIR)	Tire tubes, tube liners, enclosures, air bags, and curing bladders	Silicone rubber (Si)	Able to withstand a very wide range of service temperatures from −45 to 200 °C. Various grades are available covering a very wide range of applications such as baby teats, catheters, medical applications, wire and cables, electronic components, etc.
Butadiene rubber (BR)	Tires, sports goods	Chlorosulfonated polyethylene rubber (CSM)	Electrical insulator in cable and wire industry, tank lining, colored-stable weather-resistance products, oil resistant hoses and gaskets
Ethylene–propylene–diene rubber (EPDM)	Gaskets, seals, automotive components, IRG, and GRG	Polyacrylic rubber (ACM)	Seals and gaskets for high temperature applications, 180–200 °C
Polychloroprene rubber (CR)	Hoses, rubber bearings, expansion joints, belts, and conveyors	Fluorocarbon rubber (FPM)	Products which are resistant to chemicals, oils and solvents. Able to withstand high service temperatures exceeding 250 °C. Outstanding oxidation and ozone resistance. Flame resistant. Hoses, gaskets and seals for aircraft, jets, and rockets
Nitrile rubber (NBR)	Oil-resistant hoses, seals, O-rings, gaskets	Epichlorohydrin rubber (ECO)	Automotive industry – gasket, seals, hoses to withstand service temperatures above 130 °C

Table 2 Heat aging temperature for establishing Type[4]

	Type									
	A	B	C	D	E	F	G	H	J	K
Test temperature (°C)	70	100	125	150	175	200	225	250	275	300

Table 3 Limits of volume swelling for establishing Class[4]

	Class										
	A	B	C	D	E	F	G	H	J	K	L
Vol. swell max. (%)	No rqmt.	140	120	100	80	60	40	30	20	10	5

Table 4 Limiting brittleness temperatures for establishing Group[4]

	Group						
	A	B	C	D	E	F	G
Limiting brittleness temperature (°C)	0	−10	−25	−40	−55	−75	−85

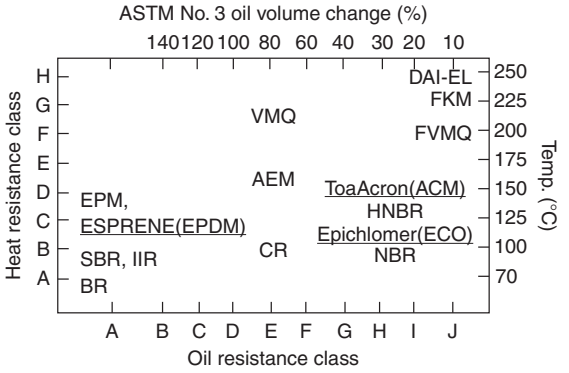

Figure 2 A chart showing type and class of elastomers. Adapted from Hashimoto, K.; Maeda, A.; Hosoya, K.; Todani, Y. *Rubb. Chem. Technol.* **1998,** *70*(3), 449–519, with permission from American Chemical Society.

FVMQ is more resistant to swelling towards the solvent than VMQ grade, as the fluorine atom is highly polar. Figure 3 shows the general chemical structure of silicone rubber with different substituent groups.

The main backbone chain is made of repeating −Si−O− groups while the methyl groups are attached at the side. Both Si–O and Si–CH_3 bonds are thermally stable. This explains why VMQ and FVMQ grades have the same Type of heat resistance, as the main chain backbone is the same for both. The Si–O bond is partially ionic and it is relatively easy to be broken by concentrated acids and alkalis even at room temperature. Another important feature of the chemical structure of silicone rubber is the relatively large bond angle of Si–O (about 140–160°).[7] The intermolecular forces between silicone chains are very low probably because of the large distance between the adjacent chains, as silicone atoms are relatively large. Thus this facilitates ease of chain rotation which accounts for the lowest glass-transition temperature T_g (∼−120 °C) among the commercially available elastomers. The dimethyl rubbers swell more in aliphatic and aromatic hydrocarbons than in acetone and diesters. However, the swelling resistance towards hydrocarbon oil can be enhanced by the replacement of one methyl group on each silicon atom by a more polar group such as trifluropropyl group ($-CH_2CH_2CF_3$), that is, the FVMQ grade.

3.33.3 General Properties of Elastomers

All elastomers have some common properties such as being flexible, tough, relatively impermeable to both water and air, and elastic when vulcanized. One of the unique features of a vulcanized elastomer is its ability to exhibit high elasticity: the elastomer can be stretched to a few hundred percent and recover its original shape and dimensions almost instantaneously when the deforming force is released. For a material to exhibit high elasticity, it must fulfill the following conditions:

- flexible long chain molecules with relatively low molecular interaction forces,
- the long chain molecules must be cross linked (at least 2% cross linked network),
- rubbery above T_g.

The elasticity of an ordinary solid such as metal is associated with its internal energy. In contrast, the elasticity of rubber is entropy driven.

Elastomers are also well known for their good resistance to acids, alkali and chemical solutions. Elastomers have a proven record of accomplishment as the material used for tank lining or related chemical vessels. Beyond these common characteristics, each rubber has its own unique properties depending on the chemical structure as discussed briefly below.

3.33.3.1 Structure–Property Relationship

The effects of chemical structure on some important physical and technological properties are summarized in Table 5.

3.33.3.1.1 Mechanical strength

Tensile strength, tear strength, crack-growth resistance and fatigue life of the vulcanized elastomer depend on the chemical structure and its geometrical configurations. Elastomers having regular microstructure are able to crystallize, and those that have irregular microstructure are amorphous. Figure 4 shows the chemical structure of general-purpose elastomers such

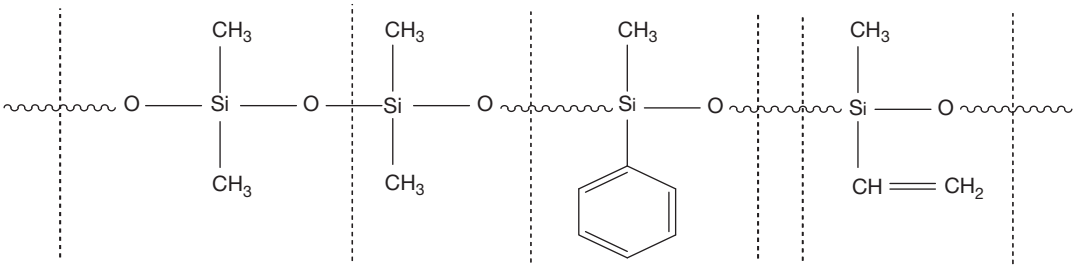

Figure 3 Chemical structure of silicone rubber: MQ grade consists of methyl, PMQ grade consists of benzene rings and VMQ grade consists of vinyl.

Table 5 Influence of chemical structure on physical and technological properties of elastomers

Basic structure	*Technological significance*
1. Nature of carbon–carbon backbone chain (i) Double bonds (ii) Single bonds	Unsaturated elastomers (having double bonds) are capable of being vulcanized with sulfur. Saturated elastomers (having single bonds) cannot be vulcanized with sulfur, but with peroxide. Unsaturated elastomers have poorer ozone cracking resistance and poorer oxidative resistance than saturated elastomers
2. Geometrical configurations	Regular microstructure would favor crystallization. Irregular microstructure leads to amorphous elastomers. The degree of crystallization affects mechanical strength
3. Polarity	Affects the degree of swelling resistance, rubber to metal bond strength, T_g and electrical resistivity
4. Chain flexibility and glass transition temperature, T_g	Affects hysteresis and damping, and other related properties such as resilience, heat build-up, mechanical strengths, etc.
5. Molecular weight distribution	Broad molecular weight distribution provides easier processing than narrow molecular weight distribution

as natural rubber (NR), styrene butadiene rubber (SBR) and polychloroprene rubber (CR).

Natural rubber is 100% *cis*-1,4-polyisoprene indicating that it has regular microstructure, thus enabling it to crystallize. NR will crystallize at low temperatures. Crystallization has its own kinetic; in the case of NR the maximum rate of crystallization occurs at −26 °C.[2,6] When the rubber crystallizes, it hardens progressively and eventually loses its flexibility and rubber-like elasticity. The maximum amount of crystalline region is about 33% in the case of NR. However, if a tensile strain (more than 200%) is applied to NR it crystallizes almost instantaneously even at high temperatures. This phenomenon is known as strain-induced crystallization. Since crystallization is a reversible process, the crystals are completely melted once the applied strain is removed.

Low temperature crystallization brings few disadvantages to NR, particularly when it involves mixing. When NR crystallizes, it becomes very stiff and may cause damage to the mills. To overcome this problem, the common practice is to place the crystallized NR in a hot room (oven) to melt the crystals so that the rubber regains its flexibility. Any unmelted crystals present during the mixing process would interfere with the incorporation and dispersion of the compounding ingredients. In contrast, strain-induced crystallization offers a big advantage in that it helps to enhance the mechanical strength of the rubber. For example, an unfilled or gum NR vulcanizate gives higher tensile strength (23–27 MPa) than unfilled SBR gum vulcanizate (2–3 MPa). Unfilled (gum) vulcanizate refers to a vulcanized rubber containing no filler apart from the compounding ingredients necessary for vulcanization. The crystals that are formed during straining act like a reinforcing filler to enhance the tensile strength. Thus for a noncrystallizing elastomer, it is necessary to incorporate a reinforcing filler into the rubber to enhance its strength.

In addition to the reinforcing filler, the types of chemical crosslink such as polysulfidic(C–S_x–C), monosulfidic (C–S–C), or carbon–carbon (C–C) also affect the strength of the vulcanized elastomer.[8] Polysulfidic crosslinks are weak and labile with lower bond energy than monosulfidic and carbon–carbon links. Polysulfidic crosslinks enhance mechanical strengths such as tensile and tear strengths because these weak and labile crosslinks relieve stresses by 'yielding.'[8]

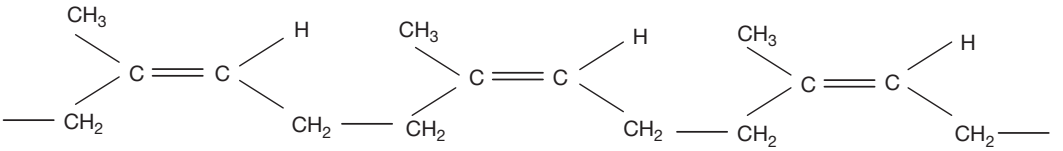

C is 1,4-Polyisoprene

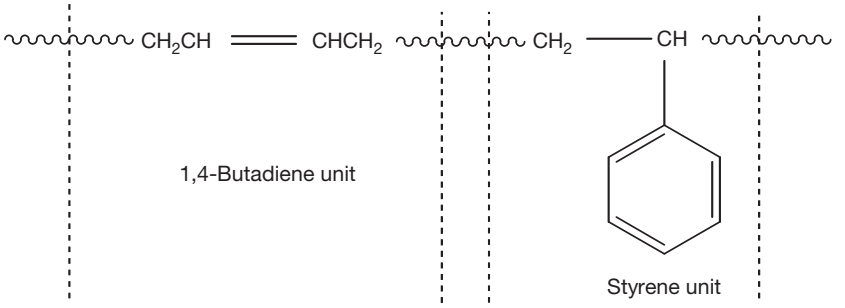

Styrene butadiene rubber (SBR)

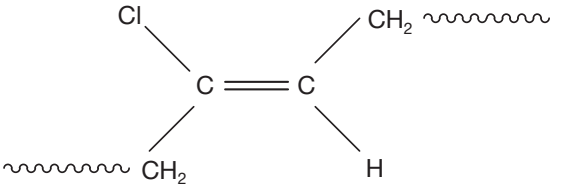

Trans 1,4 polychloroprene

Figure 4 Chemical structure of general-purpose elastomers.

Besides NR, polychloroprene rubber (CR) can also crystallize. Indeed CR crystallizes more readily than NR does because trans 1,4 configuration allows better molecular packing than cis 1,4 configuration.

3.33.3.1.2 Oxidation and ozone resistance

All unsaturated elastomers are susceptible to attack by oxygen and ozone which ultimately leads to chain scission followed by progressive loss in the physical properties. This aspect of oxidation will be discussed further in a later section. Almost all specialty elastomers have saturated bonds on the main backbone as well as high bond dissociation energy. Thus, specialty elastomers are highly resistance to heat, oxidation and ozone cracking.

3.33.3.1.3 Swelling resistance

The swelling resistance of rubber towards hydrocarbon oil depends on the extent of the polarity of the elastomer. The more the polar groups attached to the rubber molecules the higher is the polarity, and the better is the swelling resistance towards hydrocarbon oil. The solubility parameter of elastomers and liquids determines the extent of compatibility and swelling resistance. The closer the solubility parameters between the elastomer and the liquid, the better is their compatibility. Indeed, the greater the thermodynamic compatibility between liquid and elastomer, the greater the absorption of liquid occurring when both have similar solubility parameters. The solubility parameter δ is related to a parameter to measure the specific interaction between molecules known as cohesive energy density (CED) by the following mathematical relationship.

$$\delta = (\mathrm{CED})^{1/2} \quad [1]$$

$$\mathrm{CED} = (\Delta H - RT)/(M/\rho) \quad [2]$$

where ΔH is the latent heat of vaporization, T is the absolute temperature, M is the molecular weight of the polymer, ρ is the density of the polymer, and R is the molar gas constant. For example, natural rubber has a solubility parameter value of 16.7 and NBR has

a solubility parameter between 21.0 and 22.0 $MPa^{1/2}$. Most of the petroleum oils have a solubility parameter of 16.3 $MPa^{1/2}$. Thus NR will swell markedly in petroleum oil because their solubility parameters are similar. In contrast, NBR has a solubility parameter very much higher than that of petroleum oil, so the two are not compatible. For this reason, polar NBR shows higher swelling resistance than nonpolar NR towards petroleum oil. Elastomers with higher polarity such as polyurethane rubber (AU) show even higher swelling resistance to nonpolar solvents than nonpolar elastomers. Based on the solubility parameter, polar rubbers swell more in polar solvents. Nonpolar rubbers are resistant to swelling in polar solvents.

3.33.3.1.4 Glass-transition temperature T_g

The glass-transition temperature (T_g) is the temperature at which molecular mobility begins to take place, below which molecular mobility is frozen and the elastomer becomes rigid and glassy. The T_g of the elastomer depends on the chemical structure of the elastomer. The presence of a polar atom, side groups, length of side chains, and crosslink reduces molecular mobility which would increase T_g of the elastomer. The glass-transition temperature affects a number of important technological properties such as strength, damping, low temperature flexibility, rolling resistance, wet grip, etc. High T_g elastomers are preferred to low T_g elastomers for applications where high mechanical strength, high damping, and excellent wet traction are required. For applications where excellent low temperature flexibility, low heat generation, high resilience and low rolling resistance are required, low T_g elastomers are preferred to high T_g elastomers.

Table 6 summarizes the respective T_g, ozone cracking resistance, chemical resistance and heat aging resistance of some of the important commercial elastomers.

3.33.4 Rubber Technology and Compounding

3.33.4.1 Mastication and Mixing

Rubbers find very limited applications in their raw form. In their raw form, rubbers may be suitably used as binders and adhesives because of their inherent tack. To become useful products, they have to undergo various processes from mastication, mixing, shaping or fabrication prior to molding, as shown by the schematic flow chart in Figure 5.

3.33.4.2 Rubber Compounding

Rubber compounding is the term used to denote the art and science of selecting and combining elastomers and additives to obtain an intimate mixture that will develop the necessary physical and chemical properties for a finished product. In compounding, one must cope with literally hundreds of variables in materials and equipment. There are three main areas of concern in rubber compounding, namely, (i) to secure certain properties in the finished product to

Table 6 Some important technological properties of some important commercial elastomers

Elastomer	*T_g (°C)*	*O_3 resistance*	*Swelling resistance (%)[a]*	*Heat resistant up to (°C)[b]*
NR	−72	L	200 (120 °C)	100
SBR	−63	L	130 (120 °C)	100
BR	−112	L	>140 (70 °C)	100
EPDM	−55	H	>140 (70 °C)	150
IIR	−66	M	120 (120 °C)	150
CIIR	−66	M	>140 (150 °C)	150
ACM	−22 to −40	H	25 (150 °C)	175
CO	−26	H	5 (150 °C)	150
CR	−45	M	65 (120 °C)	125
NBR (med ACN)	−34	L	10 (100 °C)	125
MVQ	−120	VH	50 (150 °C)	225
CSM	−25	H	50 (150 °C)	150
H-NBR	−30	H	15 (150 °C)	150
FKM	−18 to −50	VH	2 (150 °C)	250
EU	−55	H	40 (100 °C)	100

[a]Swelling after 70 h in ASTM oil 3.[5,9]
[b]Classification after ISO/TR 8461, aerobic condition, Method ISO 4632/1 3 days, (Retention properties).[9]
L = low resistance M = medium resistance H = high resistance.[5,9]

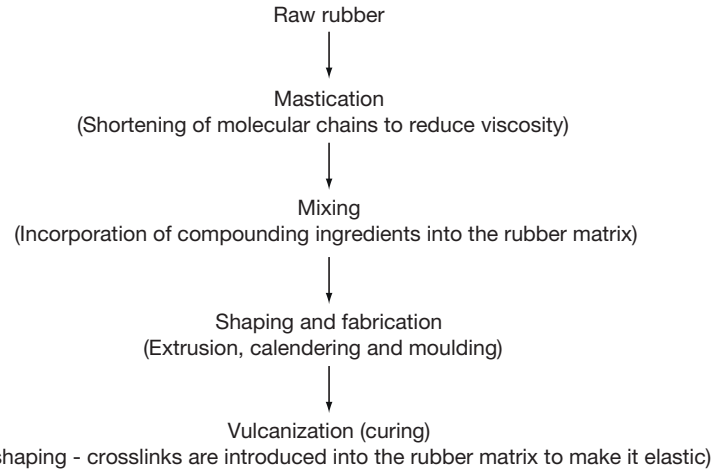

Figure 5 Schematic flow process chart.

satisfy service performance; (ii) to be able to meet processing characteristics for efficient utilization of available equipment, and (iii) to meet conditions (i) and (ii) at the lowest possible cost. In other words, the most important criteria in compounding are to secure an acceptable balance among demands arising from the three concerned areas.

Theoretically, a rubber compound may consist of an elastomer and a cross linking agent. However, in practice, a rubber compound may contain 5 ingredients or even more than 10 ingredients, depending on the intended products, types of application and their service conditions. Each ingredient has a specific role and function(s). Each has an impact on properties, processability, and price. The real challenge is to develop a high quality rubber product at the lowest cost possible. The materials utilized by the rubber compounder can be classified into nine major categories, which are defined as follows:

- *Elastomers*: The basic component of all rubber compounds may be in the form of rubber alone, or master batches of rubber–oil, rubber–carbon black, or rubber–oil–carbon black.
- *Vulcanization agents*: These materials are necessary for vulcanization processes where chemical crosslinks are introduced into the rubber matrix to form a three-dimensional network. Crosslinks inhibit permanent flow under deformation or heat and prevent dissolution in solvents. Strength, stiffness and resilience increase upon cross linking, and set, stress-relaxation and creep decrease.
- *Accelerators*: In combination with vulcanizing agents, these materials reduce the vulcanization time (cure time) by increasing the rate of vulcanization. In most cases, the physical properties of the products are also improved.
- *Activators*: These ingredients form chemical complexes with accelerators, and thus aid in obtaining the maximum benefit from an acceleration system by increasing vulcanization rates and improving the final properties of the products.
- *Age-resistors*: Antioxidants, antiozonants, and other materials are used to slow down ageing processes in the vulcanizates.
- *Fillers*: These materials are used to reinforce or modify physical properties, impart certain processing properties, and reduce cost.
- *Processing additives*: Formerly known as processing aids, the new term currently used is processing additives. These are materials used to modify rubber during the mixing or processing steps, or to aid in a specific manner during extrusion, calendering, or molding operations.
- *Softeners*: They are materials that can be added to rubber either to aid mixing, produce tack, or extend a portion of the rubber hydrocarbon (e.g., oil extended).
- *Miscellaneous ingredients*: These materials can be used for specific purposes but are not normally required in the majority of rubber compounds. They include retarders, colors, blowing agents, abrasives, dusting agents, odorants, etc.

3.33.4.3 Vulcanization

Vulcanization is a process of cross-linking rubber molecules chemically with organic/inorganic substance through the action of heat and pressure. The

rubber which is cross linked chemically is known as vulcanizate. The introduction of crosslinks into the rubber matrix may be comparatively few in number but are sufficient to prevent unrestricted flow of the whole molecules past neighboring ones. The low concentration of crosslinks implies that the vast majority of the segments making up the long chain molecules are free to move by virtue of kinetic energy. An unvulcanized rubber dissolves completely in its solvent. In contrast, a vulcanized rubber only swells. The chemical crosslinks prevent complete dissolution. A vulcanized rubber in this sense is a solid and will retain its shape and dimensions.

Vulcanization is a very important process in the rubber industry and conducted at relatively high temperatures (140–200 °C). For latex dipped goods, vulcanization is conducted at relatively low temperatures (60–120 °C) and requires no pressure as the latex is in fluid form and flows to take the final shape of the former and mold.

One of the most important chemicals in vulcanization is the cross linking agent. Elemental sulfur is the most widely used cross linking agent in the rubber industry because it is very cheap, abundant and easily available. Besides, sulfur is very easy to mix and readily soluble in the rubber. By varying the amount of sulfur to the accelerator ratio one can get different types of crosslink in the rubber matrix. **Table 7** summarizes the types of sulfur vulcanization system,[10] nature of crosslinks produced and their influence on technological properties. Thus sulfur vulcanization provides flexibility as one can control the type of crosslink intended for specific use or applications. The most basic requirement for sulfur vulcanization is the availability of double bonds on the rubber hydrocarbon. The nonsulfur cross-linking agents include organic peroxides, quinines and their oximes and imines, metallic oxides and high energy radiation. The detailed mechanisms of vulcanization with these vulcanizing agents are discussed by Elliot and Tidd.[10]

There is another type of sulfur vulcanization system known as soluble efficient vulcanization (EV)[10] intended for engineering products that require consistent stiffness, low creep, low stress-relaxation and low set. This vulcanization system employs certain soluble accelerators, activators, and sulfur that completely dissolve in rubber giving a truly homogeneous compound.[10] In practice, this is achieved by selecting accelerators and activators that have a fairly high solubility in rubber at room temperature. Suitable accelerators for soluble EV include diphenyl guanidine, tetrabutylthiuram disulphide and *N*-oxydiethylenebenzothiazole-2-sulphenamide. Zinc oxide is insoluble in rubber, but it has to be included in the system as it plays a major role in sulfur vulcanization. However, 2-ethyl hexanoic replaces the common coactivator stearic acid as the latter reacts with zinc to form an insoluble zinc stearate which induces creep and the former forms a rubber-soluble zinc salt. The sulfur dosage employed in soluble EV must not exceed 0.8 pphr (parts per hundred of rubber) to ensure that it remains dissolved in the rubber and with no tendency to bloom to the rubber surface.

Nonsulfur vulcanization such as the peroxide vulcanization system produces carbon–carbon type of crosslink that gives excellent heat aging resistance and very low compression set. However, the mechanical strengths are lower than polysulfidic and monosulfidic crosslinks. The choice of vulcanization system depends on the service environment as well as the mode of deformation for the intended rubber product.

3.33.5 Rubber-to-Metal Bonding – Engineering and Automotive Applications

Most of the rubber springs involve bonding of rubber to metal. In many cases the metal parts are required for fixing purposes, particularly those of automotive components such as rubber bushes, engine mounts

Table 7 Sulfur vulcanization systems, types of crosslink produced and their effect on technological properties

Vulcanization system	*Sulfur*	*Accelerator*	*Type of crosslink*	*Technological properties*
Conventional	2.0–3.5	1.0–0.4	Polysulfidic	Increase tensile and tear strengths, high compression set, and poor heat aging
Efficient (EV)	0.3–0.8	6.0–2.5	Monosulfidic	Excellent heat aging, low compression set, low tensile, and tear strengths
Semi-EV	1.0–1.7	2.5–1.0	Mixtures of poly, di- and mono	Compromise or balance in terms of strength and heat aging

and couplings. **Figure 6** shows some typical rubber-to-metal bonded products. In tank lining, the main function of rubber is to protect the metal against attack by corrosive chemicals as well as to protect the metal parts from oxidation by air and moisture, which leads to rusting.

The laminated rubber bearing consists of alternate layers of metal plates. The metal plates serve to restrain the lateral expansion of the rubber on compression. Because of restriction at the rubber metal interface, due to friction or when the rubber is bonded to metal, the rubber bulges at the end plates to maintain a constant volume. As a result, the effective compression modulus is dependent on the shape factor, S, defined as the ratio of loaded area to force free area.[2]

$$S = \text{Loaded area}/\text{Force free area} \quad [3]$$

For a rectangular rubber block of length L, width W, and thickness h, shape factor S is given by eqn [4]:

$$S = LW/[2h(L + W)] \quad [4]$$

The dependence of the compression modulus on the shape factor has a significant advantage where the vertical stiffness increases substantially, by inserting horizontal metal spacer plates into the rubber. For a rectangular rubber block having length L, width W, and height h, the shear stiffness and compression stiffness are given by eqns [5] and [6] respectively.

$$k_s = GA/h \quad [5]$$

$$k_c = 3G(1 + 2S^2)A/h \quad [6]$$

Here, G is the shear modulus of the vulcanizate and A is the cross-sectional area of the rubber surface subjected to shear or compression. Equation [6] shows

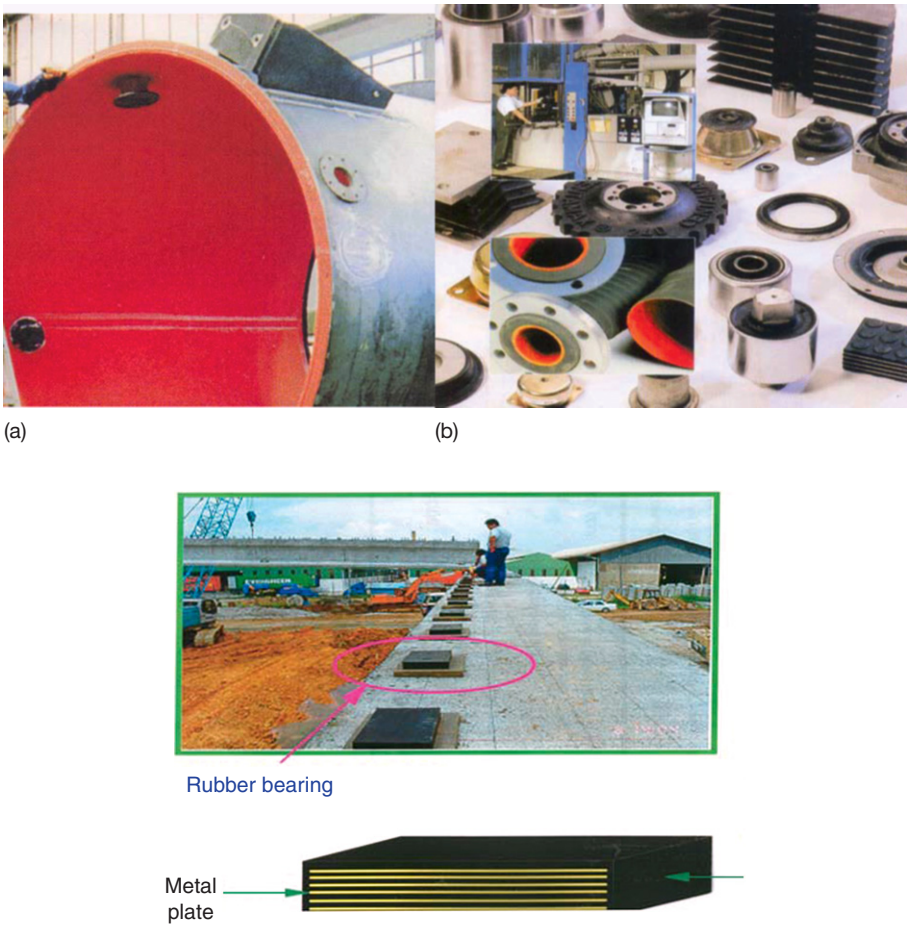

Figure 6 Rubber-to-metal bonding products – (a) tank lining (LHS), (b) various automotive rubber products (RHS) and (c) below rubber bridge bearing.

that the compression stiffness can be increased substantially by increasing the shape factor. The shape factor does not affect shear stiffness. For these reasons, laminated steel rubber bearings are used in bridges, where high compression stiffness is necessary to support all dead and live loads of the deck, and very low shear stiffness to accommodate movements associated with thermal expansion and contraction due to temperature changes.

To achieve efficient bonding at the rubber–metal interface, it is necessary that the rubber is chemically bonded to the metal surface. This is achieved in practice by following proper procedures laid down in the following section.

3.33.5.1 Bonding of Rubber to Metal

3.33.5.1.1 Preparation of metal plates

The metal plates must be clean and free from any contamination such as oil, grease, protective coating, and rust. Exposing the contaminated metal surface to the vapor of a suitable organic solvent (e.g., chlorinated solvent) removes oil and grease. The next step is to remove metal oxides and rust on the metal surface, usually by the sandblasting technique or wire brushing. Apart from cleaning, sandblasting increases the surface area, which is very beneficial for strengthening the bonded area. Acid etching provides an alternative means of removing metal oxides from the metal surface.

It is very vital that the metal surface is completely free from oil, grease and rust to ensure efficient wetting of the bonding agent on the metal surface so that during vulcanization the bond formed between rubber and metal via the bonding agent is very strong. However, a few precautions need to be observed when sandblasting on the metal surface. The grit size, gun pressure and shooting distance must be correct to get the right surface topology, thus avoiding excessive wear or too little wear.

3.33.5.1.2 Types of bonding agent and methods of applications of bonding agent to metal plates

The common bonding agents for bonding rubbers to metals include ebonite solution or sheet, brass and proprietary adhesives. In the past, the bonding agent as well as the lining material for making tank lining was ebonite solution and calendered ebonite sheet. The ebonite compound contains a high amount of sulfur, about 25–35 pphr. This high sulfur content makes ebonite a hard and brittle material. Indeed ebonite is a thermoset as it is highly cross linked. The high sulfur content of ebonite introduces high polarity that makes it a very suitable bonding agent. Despite the superior chemical resistance of ebonite, there are a few limitations such as its brittleness after cure, long cure time and potential of fire hazard due to exothermic reaction during curing, especially when a thicker lining is involved. For this reason, soft rubber linings are preferred to ebonite linings.

Brass is a very good bonding agent, and is widely used in the tire industry. Brass is coated on steel wire cords by the electroplating process. Brass-coated steel wire cords are used as breakers or belts placed underneath the tread and on top of the carcass of the green tire. During vulcanization, the sulfur forms covalent bonds with both the rubber and the component metals of the brass, leading to a very strong bond.[11]

In most rubber-to-metal bonded products, a proprietary bonding agent is preferred to the other two bonding agents. A proprietary bonding agent usually requires two coatings, *viz.* a primer and an adhesive cement. There are reasons why a two-coat system offers more insurance for the rubber to metal bond. The first coating known as a primer helps to eliminate corrosion in corrosion-prone metals when they are in contact with the rubber.[12] By using a primer, secondary cement (second coating–adhesive) that has a greater degree of bondability to the stock being used can be selected, rather than a one-coat system.[12] It is claimed that the two-coat system allows more metal adhesion into the primer, and more stock adhesion into the cement coat.[12] This results in a higher intrinsic bond with the two-coat system than a single coat system.

Bonding agents are applied by painting, spraying or dipping on treated metal parts in the form of a solution or aqueous suspension.

3.33.5.1.3 Molding of rubber-to-metal bonded parts

Finally, the dried, coated metal parts are loaded into the mold and the rubber is vulcanized in contact with these substrates by the conventional rubber molding techniques such as compression, transfer and injection molding. It is during this vulcanization process that the rubber is chemically bonded to the metal surface when the cross linking agents react with the adhesive.

However, in the case of tank lining, the method is different from the conventional rubber-to-metal bonded products. The method of applying calendered rubber sheeting onto the prepared metal surfaces is

analogous to that of applying rolls of wallpaper to the walls of a room. However, care must be taken to avoid entrapment of air between rubber and metal. The rubber sheet is laid down at the correct angle, and is rolled down into close contact with the adhesive. Applying the rubber sheet at the corner or edges of the tank is quite tricky. In practice, this is achieved by making joints at corners by inserting and rolling down an extruded rubber fillet of triangular cross-section and forming the sheet joints on top of the fillet. This technique gives to the lining a well finished appearance and reduces the danger of weak joints occurring in corners.

Upon completion of laying the rubber sheet onto the metal surface, the covered lining tank is usually allowed to rest for at least 24 h before being vulcanized. This resting period allows any air trapped between rubber and metal to diffuse, apart from enabling the adhered rubber sheet to recover and settle down before it is heated.

3.33.5.2 Vulcanization

It is usually done in an open steam autoclave for tanks or vessels that are small enough to go into the autoclave. When the lined vessel is too large to be accommodated in an autoclave it may be vulcanized in one of the following methods:

3.33.5.2.1 Low or high pressure steam

This method is applicable to a vessel that has sufficient strength to withstand internally applied pressure. This procedure can be adopted if the vessel such as road or rail tank cars can be lined and then sealed and bolted to give a strong and steam proof pressure container. The steam pressure is passed through the lined vessel to the desired vulcanization temperature until the rubber is fully vulcanized. There are some elements of danger when dealing with high pressure steam. So it is very important that all the safety regulations are met in terms of design and material of the vessel. The work should be done under skilled engineering supervision.

3.33.5.2.2 Water curing technique

This method is suitable for tanks or vessels that are too weak structurally to be put under steam pressure. Here, the lined tank is filled with water or brine. The water is heated by passing live steam into the water until it approaches boiling point. This temperature is maintained for a few hours until the rubber is fully vulcanized. Care must be taken to ensure that live steam does not impinge on the rubber lining to avoid the occurrence of a large blister between the rubber and metal at the point of impingement. It is necessary to conserve heat by shielding the unit against draughts and cold to minimize temperature variations which would affect the uniformity of the cure.

3.33.5.2.3 Hot air or ambient temperature vulcanization

This method is suitable for tanks or vessels which do not work with the methods discussed above. The choice of accelerator is very important. Ultrafast or very fast accelerator is usually used in the rubber compound. Care has to be taken to ensure that the rubber does not vulcanize prematurely (scorched) before it is applied onto the treated metal surface. One of the means to overcome the problem is to avoid mixing the accelerator and sulfur together, but to prepare sulfur masterbatch and accelerator masterbatch separately. The two masterbatches are blended together just prior to calendering, and the calendered sheet applied as soon as possible to the metal to avoid the risk of being scorched.

3.33.5.3 Types of Bond Failure and Possible Remedies

A rubber shear mount may be expected to deform up to 300% shear strain, and the mean shear stress acting on the rubber-to-metal bond can be as high as 10 MPa or 2/3 tons per square inch.[11] Steel laminated rubber bearings for bridges must have a minimum bond strength of about 9 N mm^{-1} (MS 671, 1991).

It is important to observe the failure mode that occurs in rubber-to-metal bonded products because it throws some light and clues to the root cause of the problem. It is usual to conduct peel test to determine the interfacial bond strength between the rubber and metal. There are two basic types of bond failure either adhesive or cohesive. Adhesive failure may occur at the interfacial between the rubber and substrate, or between cement and substrate. Cohesive failure occurs within the rubber itself. There are three modes of adhesive failure.[13] First is called CM failure that takes place between primer and metal interface. Second is CP failure that occurs at the primer to cover cement interfacial. Third is RC failure where the bond fails at the rubber–cover cement interface. RC failures are the most common and the most difficult to solve.[13] There are a number of causes, which bring about these bond failures. They include the following: metal surface not cleaned efficiently due to poor cleaning procedure,

contamination of metal surface during handling, incomplete wetting of adhesive on the metal surface, variations of temperature of metal surface, precured adhesive, sweeping of adhesive during molding etc.[13] There are remedies to overcome these problems. First, ensure that the metal surface is free from all forms of contamination. Second, avoid contamination of metal surface during handling. Third, apply the primer and adhesive cement onto the metal surface evenly by taking care of the correct viscosity of the adhesive, and correct spraying distance and thickness of the adhesive film. Fourth, use the correct type of adhesive and follow strictly the instruction and procedure recommended by the chemical supplier.

If during the peel test, cohesive failure occurs within the bulk of the rubber, then this indicates that the interfacial bond strength between the rubber and metal plate via the bonding agent is stronger than the cohesive strength of the rubber itself.

3.33.6 Oxidation of Rubber

Metals oxidize in the presence of air and water and consequently they corrode, become rusty and weak. **Figure 7** shows the old version of using steel rollers to accommodate movements of the bridge deck brought about by expansion and contraction due to temperature changes.[14] The steel rollers corroded and suffered high wear and tear. In contrast, laminated steel rubber bearing did not show any sign of wear out after nearly twenty years of installation.[14] However, this does not mean that elastomeric bearing will last forever. Like metals, rubbers are also prone to corrosion. Corrosion of rubbers is associated with the aging process known as degradation. All unsaturated rubbers are subject to degradation due to the attack of heat, ultraviolet (UV) light, oxygen, ozone etc. The more is the amount of unsaturation the more it is susceptible to degradation. The term aging as applied to rubber, covers a variety of phenomenon arising out of the factors described above. Aging properties of raw rubber differ from vulcanized rubber because of the latter's specific network structure and extra network material. When natural rubber is heat-aged in the presence of oxygen or air, it invariably loses strength, in particular its tensile strength decreases. The pattern of modulus change during aging is not so straight forward because there are two opposing reactions which can occur simultaneously. One is degradation of the molecular chains and crosslinks which causes softening; the other is additional cross linking which causes stiffening. Under any given set of aging conditions (time and temperature) either softening or stiffening reactions may predominate depending on the type of vulcanization system, type of filler and antidegradants employed in the rubber compound.

Oxygen reacts with rubber only after the rubber has been acted upon by energy. This is usually from UV light, heat or mechanical energy (flexing). This energy dislodges a hydrogen atom from the rubber molecule, resulting in the formation of a radical. The oxidation of polymer with elemental oxygen is called autoxidation because it is an autocatalytic. The rate of autoxidation is affected by temperature, the presence of catalyst and also the presence of antioxidant. When the oxygen attacks the rubber it produces hydroperoxide. The hydroperoxides break to form free radicals. This is an autocatalytic, self generated free radical process. The autoxidation process involves three main stages, namely, initiation, propagation and termination. In view of the complexity of autoxidation reaction with rubber, Bolland and Gee[15,16] used model olefins to study the kinetics of autoxidation. **Figure 8** shows the mechanism of autoxidation as proposed by Bolland.[15,16]

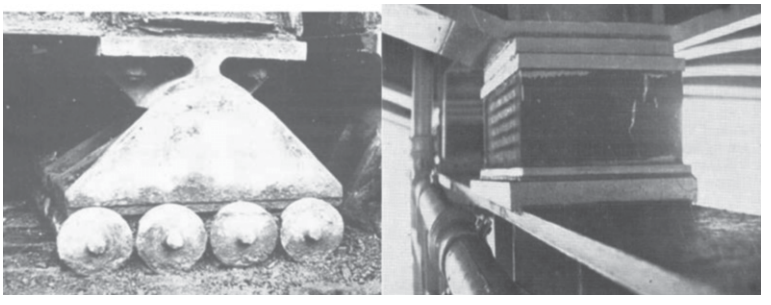

(a) (b)

Figure 7 (a) Steel roller bridge bearing and (b) steel laminated rubber bearing installed in 1955. Adapted from Mullins, L. *Proc. Rubb. in Eng. Conf*. Kuala Lumpur, 1974, pp. 1–20, with permission from the Malaysian Rubber Board.

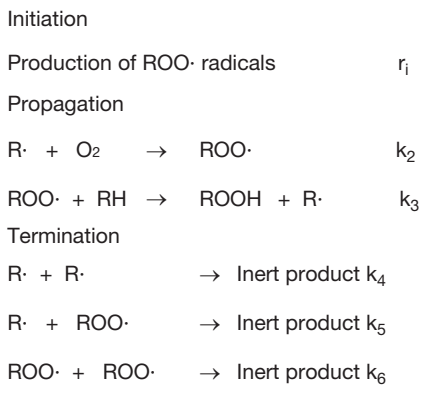

Figure 8 Mechanism of autoxidation of natural rubber as outlined by Bolland. Adapted from Barnard, D.; Lewis, P. M. In *Natural Rubber Science and Technology*; Robert, A. D., Ed. Oxford University Press, 1988; Chapter 13, pp 621–673, with permission from · · ·.

The autoxidation is initiated with the generation of free radicals due to the relatively facile homolysis of traces of peroxide present in the elastomer.[17] The rate of oxidation is related to the concentration of the hydroperoxide [ROOH] as shown by eqn [I] below[16].

$$r_i = k_i[\mathrm{ROOH}]^2 \qquad [\mathrm{I}]$$

The resultant free radicals react with oxygen to form the deleterious peroxides and propagate the autoxidation reaction. The rate of propagation is controlled by the hydroperoxide yields and those of decomposing. The hydroperoxide yields for a large number of olefins range from almost 100% downwards to values controlled by side reactions of the peroxy radicals, such as addition to olefinic double bonds, when hydrogen abstraction becomes relatively difficult.[16] Such side reactions would continue the propagation chain. However, when the value of the rate constant k_2 becomes large, the reaction of alkenyl radicals with oxygen become independent of oxygen pressure. Under these conditions, rate-determining step is no longer controlled by the rate constant k_3, of the hydrogen abstraction step. Termination would occur primarily by the interaction of alkenyl radicals. Then the propagation rate is given by eqn [II] below[16].

$$r = r_i^{1/2} k_2 k_4^{-1/2}[\mathrm{O_2}] \qquad [\mathrm{II}]$$

Termination occurs solely by the mutual destruction of peroxy radicals and represented by the following rate equation[16]:

$$r = r_i^{1/2} k_3 k_6^{-1/2}[\mathrm{RH}] \qquad [\mathrm{III}]$$

The outcome of this autoxidation is either chain-scission or cross-linking. If chain-scission occurs, the degraded rubber will be soft and tacky. On the other hand, if cross linking occurs the degraded rubber will be hard and brittle. In both cases, the mechanical strength of the rubber decreases markedly. Model olefins were used to study the mechanism of oxidation of NR due to complexity of the oxidation reaction in particular when the rubber is vulcanized.[16] The oxidation of rubber vulcanizate is technologically important since the absorption of only a small amount of oxygen (1%) by rubber vulcanizate results in a considerable change in the physical properties.

It is believed that the oxidation of natural rubber follows the same route and analogous to that of the model olefins where the polyisoprene chain undergoes scission.[16] An essential concept of this process is the number of molecules of oxygen absorbed per scission event. According to Bolland,[15] the oxidation reaction would finally lead to an alkoxy radical disproportionate to butan-2-one-4-al rather levulinaldehyde, and the vinylic radical would have to be oxidized further to the methyl ketone end group. Minute amount of certain heavy metals such as copper, iron and manganese catalyze autoxidation reactions. However, this catalytic action can be prevented by applying protective or chelating agent such as metal deactivator like *p*-phenylenediamines.

In the case of vulcanized rubber, the oxidation reaction is more complex than that of raw rubber since the various different types of crosslink (e.g., ploysulfidic, disulfidic, monosulfidic, cyclic sulfides, conjugated dienes and treines, etc.) present in the network structure may affect oxidation in some way or another.[16] Most types of sulfur vulcanizates initially hardens on aging before degradation occurs. This hardening is due to cross linking associated with oxidative reactions of sulfur species in the network that takes place before chain scissions take place.[16]

Barnard and Lewis[16] listed out some useful and important points concerning chain scission mechanism for unprotected NR at modest temperature as follows:

- Scission occurs once approximately for every 20 molecules of oxygen absorbed.
- The scission is of the rubber chain even in peroxide or sulfur vulcanizates although concomitant crosslink can occur in the latter.
- Kinetically, scission appears to take place in the propagation step.

- Each scission event results in a stable terminal ketone group being formed on one of the new chains and a transient terminal aldehyde group on the other.

Since autoxidation results in chain scission, means and ways were introduced to determine accurately chain scissions caused by a known quantity of oxygen absorbed. A parameter known as scission efficiency ε defined as the number of molecules of oxygen absorbed which bring about one scission event[16] was introduced to monitor chain scission quantitatively. There are two methods either physical or chemical to monitor chain scission. The common physical methods involved measuring molecular weight reduction, stress-relaxation, sol–gel analysis, and stress–strain characteristics.[16] For example, in stress-relaxation method, a rubber sample of a uniform cross-section is held at a constant extension and maintained at a constant temperature. When a network is oxidized due to the cleavage of stress-supporting chains, then the stress would decay and this event would lead to occurrence of stress-relaxation. The change in moles of stress-supporting chains per gram can be calculated from eqn [7][16]:

$$f_t/f_0 = N_t/N_0 \qquad [7]$$

where the subscripts t and 0 refer to the samples after time t and time zero respectively, and f derived from the statistical theory of rubber elasticity[18] is given by eqn [8]:

$$f = \rho NRTA_0(\lambda - \lambda^{-2}) \qquad [8]$$

where ρ is the density of rubber, N is the number of moles of stress-supporting chains per gram, R is the gas constant, T is the absolute temperature, A_o is the unstrained cross-sectional area, and λ is the extension ratio. Stress-relaxation method has the advantage of being able to monitor scission event continuously, and if the amount of oxygen absorbed is also known then the scission efficiency ε can be calculated.[16] However, on a short time scale, the decay in stress level as function of time at constant deformation and temperature is associated with the rearrangement of molecular chains and it is predominantly attributed to viscoelastic behavior of the rubber.

Almost all technical specifications of elastomeric products require passing an aging test. The use of aging tests is extremely important in assessing the service life of elastomeric products because properties of vulcanizate could change during service. The basic principle of the test is to expose rubber test-pieces to air at an elevated temperature (70 or 100 °C) for a specified period (7 or 14 days or longer). This so-called accelerated aging test causes deterioration of rubber in air due to combined effects of oxidative and thermal aging. The tensile properties, set and hardness are measured on these samples before and after ageing. If minor changes in these properties result, long service life may be expected; if appreciable changes occur, service life may be short. However, it must be stressed here that accelerated ageing test is a useful quality control and specification tests. There are significant difficulties in predicting service life from accelerated aging test. Use of test temperatures much above the anticipated service temperature is not advisable because the correlation between the results of such tests and service performance becomes increasingly tenuous.

3.33.7 Ozone Cracking of Rubber

Apart from oxygen, all unsaturated elastomers are also susceptible to ozone attack although ozone concentration in the outdoor atmosphere at ground level is about 1 pphm (part per hundred million of air by volume).[19,20,21] However, this can be significant because the reaction of ozone with the double bond is extremely fast and causes cracking on strained rubber. The cracks appear slowly at right angle to the direction of the strain applied, that grow slowly and consequently lead to a break of the vulcanizate. Ozone being very reactive attacks the double bonds of the rubber and produces ozonide that cleaves to produce zwitterions.[17] The zwitterions are unstable and will breakdown to form other zwitterions. These zwitterions may react with other zwitterions to produce diperoxide compound, or react with carbonyl compound to produce ozonide. In both cases, the ultimate result is chain scission. The mechanism of ozone attack on olefin is as shown in **Figure 9**.[17]

However, there is a subtle difference between ozone cracking and auto-oxidation where the former requires a certain critical strain level (~5% for unprotected NR) for its occurrence.[19,20,21] The severity of ozone cracking increases rapidly with strain level. Braden and Gent,[19] and subsequently Lake *et al.*[20,21] investigated various factors affecting ozone cracking. For example, Lake and Thomas[20] came out with a boundary layer theory for ozone attack on rubber surface to explain the rate of ozone crack growth. According to their theory, the variation in

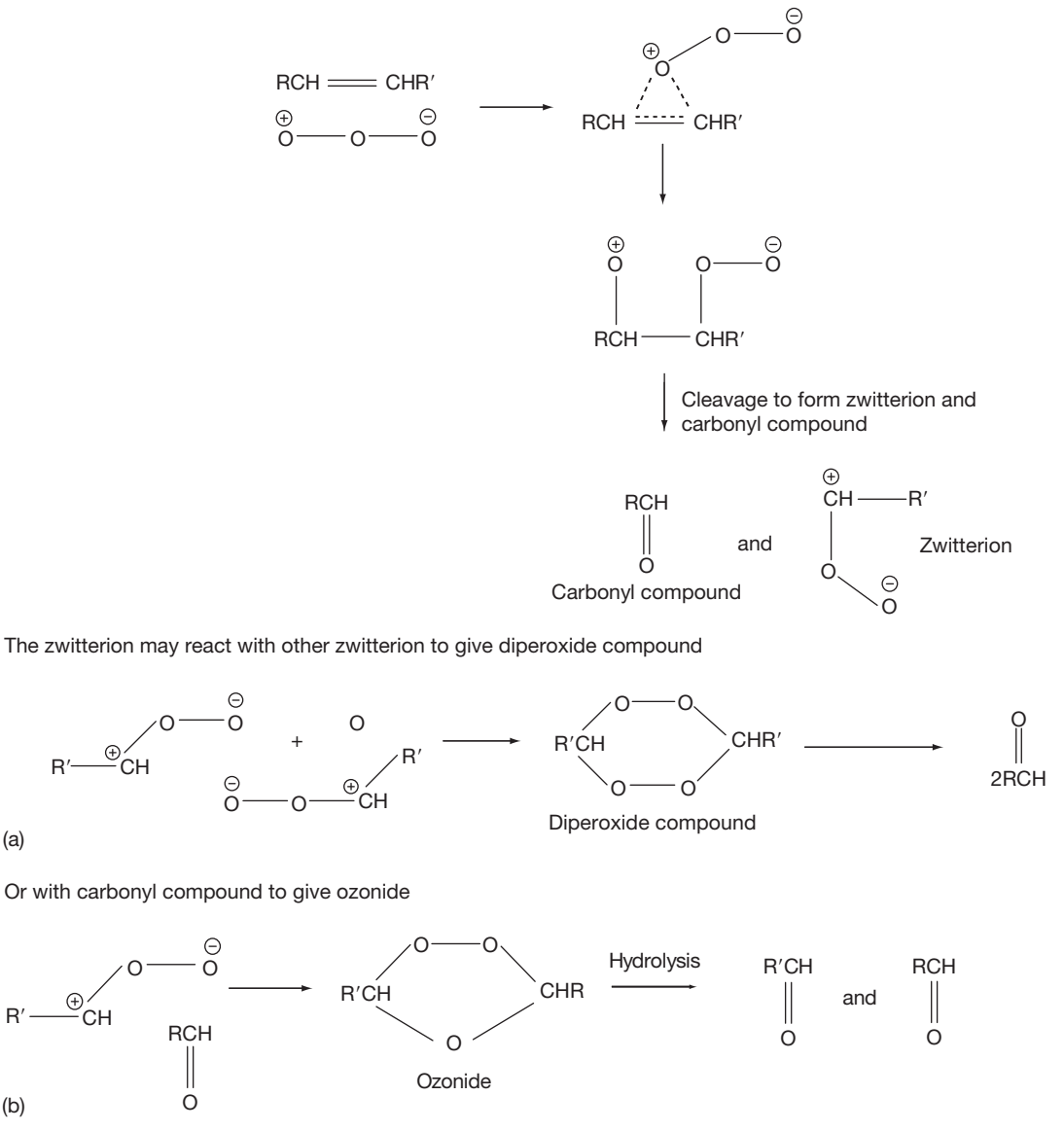

Figure 9 Mechanism of ozone attack on olefins.

the rate of ozone attack on stretched rubber surfaces produced by changes in the air velocity and magnitude of the strain is controlled by the diffusion of ozone across the relatively stationary boundary layer adjacent to rubber surface. The boundary layer effect is important because of the readiness with which ozone is destroyed by stretched rubber.[20] As mentioned earlier, ozone cracking occurs only in elastomers subject to tensile stresses. Elastomeric components used in compression will crack only in the regions of the surface where tensile stresses are induced. These cracks are unable to penetrate very far because they soon encounter compressive rather than tensile stresses. Thus ozone cracking is not a serious problem for large elastomeric components such as rubber bearings which are used in compression. Nevertheless, ozone cracks are unsightly and may initiate fatigue crack growth, which ultimately leads to mechanical failure. In view of this deleterious effect, it is necessary to carry out test on ozone resistance. The test involves exposing the stretched test-pieces (20% strain) in an ozone-rich atmosphere at a fixed temperature (23 or 40 °C) and inspecting the surfaces for cracks with the aid of a magnifying

glass at intervals of time. If cracks are not observed after completion of test, the vulcanizate is said to have good resistance to ozone cracking.

3.33.8 Heat Aging Resistance

Elastomers can survive over long periods in service at ambient temperatures without any measurable deterioration if the products are sufficiently thick. For a thick section of rubber, the availability of oxygen will be limited by diffusion, and components with bulky rubber layers can be considerably more resistant to elevated temperatures than thin rubber sections. For example, bearing pads of NR installed in 1890 had been examined, and although the outer 1–2 mm of rubber had degraded after 96 years of exposure to the atmosphere, the inner core of the rubber was still in good condition as shown by the photograph in Figure 10.[2] Rubber samples taken from the interior portion were found to retain good physical properties as that of freshly prepared compounds.[2] At sufficiently elevated temperatures, all types of elastomer will undergo degradation. However, conventional NR vulcanizates can be used safely at 60 °C, the maximum ambient temperature likely to be encountered practice.[2] At temperatures of 300 °C and above, NR vulcanizates first softens as molecular breakdown occurs, then resinify, becoming hard and brittle.[2] Flammable vapor are emitted and ignition occurs. However, the rate of burning is extremely slowly for the case of large block rubber.[2]

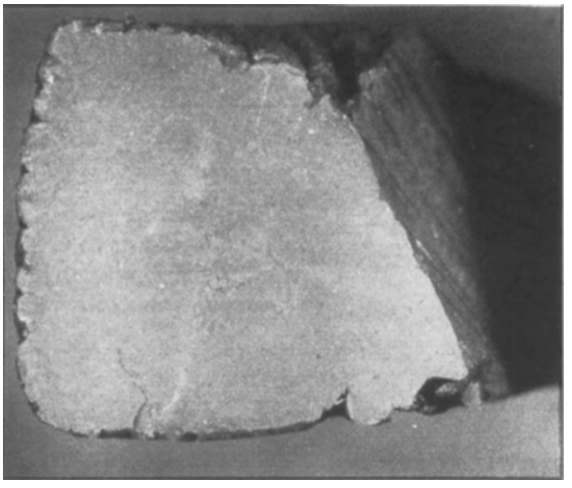

Figure 10 Cross-sectioned view of a 100-year old bridge bearing pad showing the very small depth of penetration of atmospheric degradation. Adapted from Fuller, K. N. G.; Muhr, A. H. *Engineering design with natural rubber, NR Technical Bulletin*, 5th ed.; The Malaysian Rubber Producers' Research Association, London, 1992; pp 1–33, with permission from Tun Abdul Razak Research Centre, Brickendonbury Hertford, England.

In recent years, new performance demands for automotive elastomers have been proposed[22] to perform at high operating temperatures. This move was made to accommodate increasing concern for improved fuel economy, which resulted in a significant downsizing and redesign of the automobile. Concomitantly the engine compartment became smaller and more difficult to cool thus raising the temperature of the under hood. Current automotive elastomers are expected to perform well under a 120 °C in-service temperature at least until the life of the car.[22]

There is a growing expectation those future automotive elastomers to perform well in a 150 °C environment for over 100 000 miles.[22] This is a clear signal that specialty elastomers would find very strong markets over general-purpose elastomers for high temperature performance.

3.33.9 Flex Cracking

Flexing and cyclic stresses can lead to premature failure during service. There are two basic mechanisms of crack growth, (i) ozone crack growth, due to primarily chain scission, and (ii) mechanico-oxidative crack growth, due to mechanical rupture at the tip of a flaw, which is considerably facilitated by the presence of oxygen.[23] Both types of growth can occur under static or dynamic conditions or together. The amount of crack growth in a given time is directly proportional to the ozone concentration. The crack growth rate dc/dt of a single ozone crack under static conditions is given by eqn [9]:

$$dc/dt = \alpha q \qquad [9]$$

where q is the ozone concentration and α a constant (the rate at unit ozone concentration) which is a property of the rubber.[23] The cyclic crack growth rate is given by eqn [10]:

$$r = (dc/dn)\text{ozone} = (F/f_f)\alpha q \qquad [10]$$

where F is the time fraction of cycle for which the test-piece is strained, and f_f is the frequency.[23] Based on fracture mechanics approach, and assuming that the growth of naturally occurring flaws of a fatigue test has the same characteristics as that of a crack growth test, Lake and Lindley[23] worked out

the fatigue life of vulcanized elastomer as given by eqn [11]:

$$N_f = 1/(16BW_s^2 c_0) \qquad [11]$$

where N_f is the number of cycles to failure from a naturally occurring flaw of size c_0. B is the crack growth constant, and W_s is the strain energy density. Thus the fatigue life N can be predicted from known parameters of eqn [11].

3.33.10 Oil Absorption

An unvulcanized elastomer becomes solution when immersed in its solvent; in contrast, a vulcanized elastomer will only swell. The extent of swell depends on the amount of solvent absorbed, which in turn depends on the crosslink concentration and types of solvent. Swelling is undesirable because apart from dimensional instability, the modulus and mechanical strengths are all decreased making the swollen vulcanizate unsuitable for most engineering applications.[2] In the case of rubber-to-metal bonded, bond failure occurs if the liquid is able to reach the metal plate. **Figures 11 and 12** show some of the typical automotive elastomeric components such as fuel and oil hoses, gaskets, O-rings and seals which are in contact with automotive fuels. These rubber components are thin and susceptible to damages when swollen excessively by the oil. Additives such as ethanol, methanol, and methyl *t*-butyl ether are being placed in gasoline with a view to improve its octane number.[22] Increasing the alcohol content of the gasoline increases the amount of swell, which is very undesirable not only because of dimensional instability, but also reduces tensile strength and elongation at break of the swollen elastomer.

It is well established that swelling is diffusion-controlled and the volume of liquid absorbed is initially proportional to the square root of the time of immersion.[2] For most organic liquids, the rate of penetration depends on their viscosity rather than

(a) (b)

Figure 11 Automotive rubber products in contact with oil and heat: (a) hoses – hydraulic, fuel, gasoline pump, and steam hose and (b) gaskets, O-rings, seals, and exhaust hanger, etc.

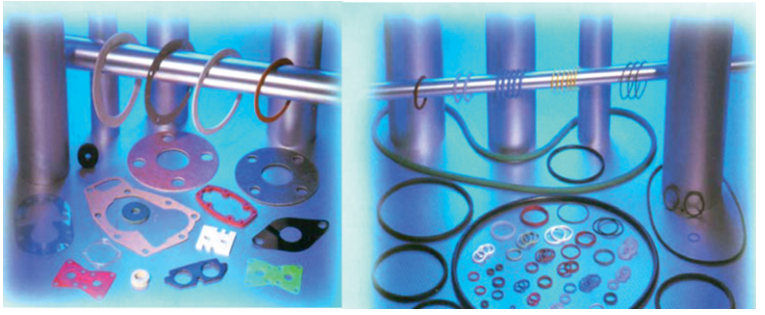

(a) (b)

Figure 12 Automotive rubber components: (a) gaskets and (b) O-rings and seals.

their chemical nature[2]. **Figure 13** shows the time–viscosity relationship for the liquid to penetrate 5 mm into the rubber interior.[2]

For NR, it takes about 4 days for a volatile liquid such as toluene to penetrate 5 mm depth, 1–2 years for engine lubricating oil, and about 30 years for a petroleum jelly, even with continuous immersion.[2] It is possible to estimate the distance of liquid in a given time provide that the penetration rate is known.[2] Alternatively, the viscosity of the liquid may be used if penetration rate is not known since the penetration rate is related to viscosity as shown earlier in **Figure 13**.

Southern[24] has introduced a nomogram as illustrated in **Figure 14** to facilitate the calculation in estimating the penetration depth of liquid into the elastomer. Although the data were obtained for NR, but would be expected to work with other elastomers of similar T_g.[24] As an illustration to use the nomogram, Southern[24] has calculated, a liquid with penetration rate of 7×10^{-5} cm $s^{-1/2}$ would take 4 weeks to penetrate 1 mm, but 100 years to penetrate 40 mm of the rubber block. The penetration rate–viscosity relationship does not hold for water because of the presence of hydrophilic impurities which complicate transport of water in elastomers.[24]

3.33.10.1 Effect of Crosslink Concentration and Polarity on Swelling Resistance

Natural rubber (NR) latex has found very wide applications in the glove industry since the 1920s. This is attributed to the excellent tear and puncture resistance of NR latex films. Besides, NR latex film exhibits very high extensibility (600–1000%) before its breaking point. These properties make NR latex film an excellent barrier protection against infectious liquids and gases. Most of the examination and surgical NR latex gloves are used in hospitals and clinics. However, recently NR latex gloves have entered the fast food industry where good swelling resistance is an essential requirement. Being a nonpolar rubber, NR latex gloves have a poor swelling resistance which limits its application in the fast-food industry. The fast-food industry is growing very fast all over the world. There is a growing concern over the cleanliness and hygiene of the food. It is essential that the workers wear rubber gloves to avoid contact with the food they serve. Rahim and Samsuri[25] investigated the effect of crosslink concentration and effect of blending carboxylated nitrile rubber (XNBR) with NR latex on the swelling resistance of NR latex film towards cooking oil. The amount of sulfur was varied to produce different crosslink concentrations. The crosslink concentration was determined by immersing the latex film sample in a solvent until equilibrium swelling was attained. The crosslink concentration was calculated by using the Flory–Rehner equilibrium swelling equation as proposed by Mullins[18] given by eqn [12]:

$$-\ln(1-v_r) - v_r - \chi v_r^2 = 2\rho V_1 [X]_{phy} v_r^{1/3} \qquad [12]$$

where v_r is the volume fraction of rubber in the swollen gel, ρ is the density of rubber, V_0 is the molar volume of solvent, χ the rubber–solvent interaction parameter, and $[X]_{phys}$ is the physically manifested crosslink concentration. The diffusion coefficient D was calculated from eqn [13][24]:

$$M_t/M_\infty = (2/l)(Dt/\pi)^{1/2} \qquad [13]$$

where M_t is the total amount of liquid absorbed per unit area of the sheet after immersion for time t, M_∞ is the amount of liquid absorbed after infinite time (in this case time to reach equilibrium swelling), and l is the half thickness of the film sheet. It is necessary to plot M_t against square root time as shown in **Figure 15** to calculate D in eqn [13].

The effect of crosslink concentration on the diffusion coefficient of cooking oil in the latex film is shown in **Table 8**.[25] The results show that increasing the crosslink concentration decreases the diffusion coefficient significantly. Increasing the sulfur content from 0.6 to 3 pphr increases the crosslink concentration by about 90%, which merely decreases the

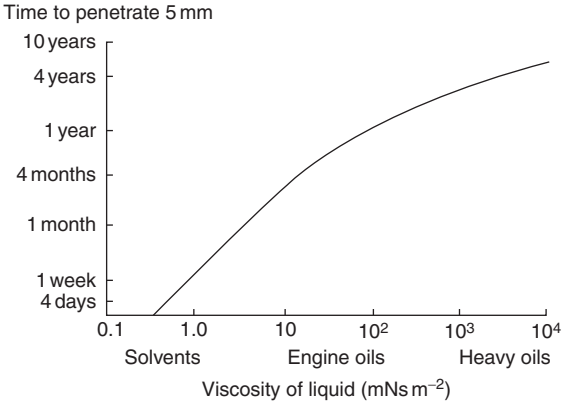

Figure 13 Effect of viscosity of liquid on penetration time. Adapted from Fuller, K. N. G.; Muhr, A. H. *Engineering design with natural rubber, NR Technical Bulletin*, 5th ed.; The Malaysian Rubber Producers' Research Association, London, 1992; pp 1–33, with permission from Tun Abdul Razak Research Centre, Brickendonbury Hertford, England.

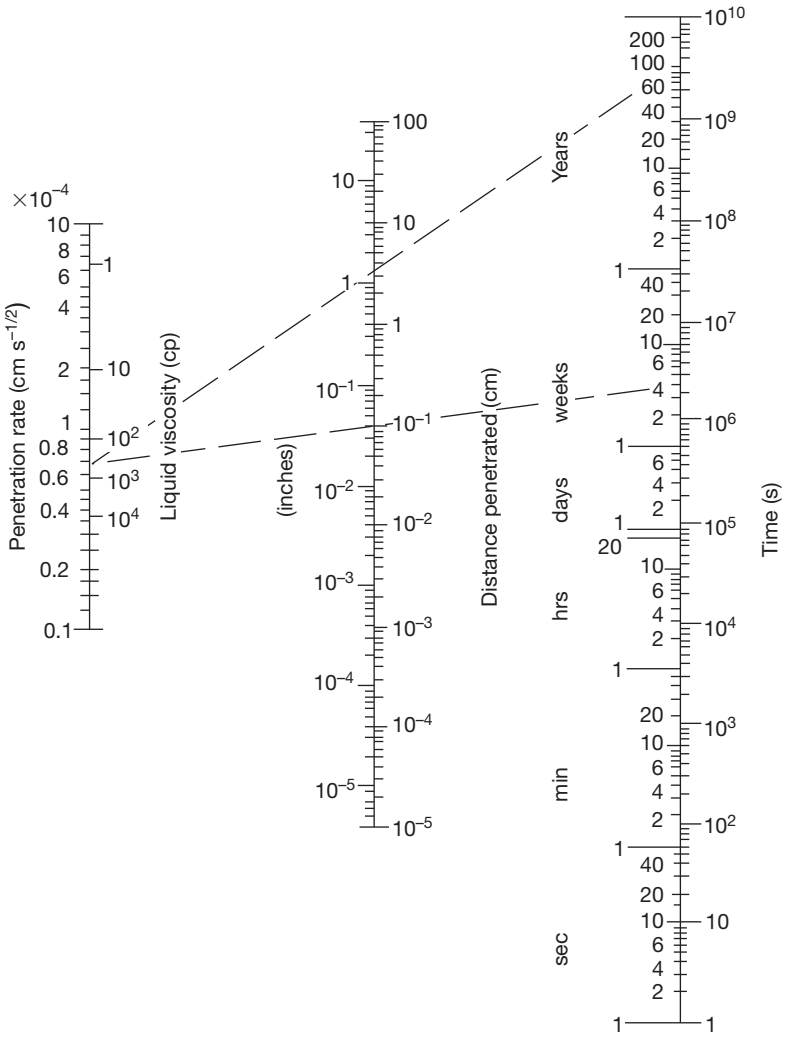

Figure 14 Nomogram to facilitate rapid calculation of distance penetrated by liquid into rubber. Adapted from Muniandy, K.; Southern, E.; Thomas, A. G. In *Natural Rubber Science and Technology*; Robert, A. D., Ed.; Oxford University Press, Oxford, UK, 1988; Chapter 13, pp 820–851, with permission from Oxford University Press.

diffusion coefficient by about 23%. However, the most efficient method to increase swelling resistance is through physical blending of NR latex with XNBR latex, where the diffusion coefficient D of the oil into the film decreases by a factor of 2.7 compared with NR latex having the highest crosslink concentration. Thus, this work shows strong evidence that blending of nonpolar elastomer with polar elastomer enhances the swelling resistance of the former.

3.33.11 Water Absorption

Elastomers find wide uses in marine and offshore engineering applications. The application of elastomers in water management is attributed to its high impermeability to water. A rubber sheet is used to line the water reservoir and pond, while inflatable rubber is used as a dam. Rubber dock fenders rely on the energy absorption capacity of the rubber. Inevitably, the rubber will absorb some quantity of water as these rubber products spend a considerable time under water. It is of great concern whether the absorption of water would impair the strength of the rubber.

The true solubility of water in rubber is very low.[24] Nonetheless, relatively large amounts of water can be absorbed during prolonged immersion as shown in **Figure 16**.[2] The diffusion of water in elastomers is not straightforward, but complicated by the presence of hydrophilic materials. In the case of NR it is mainly

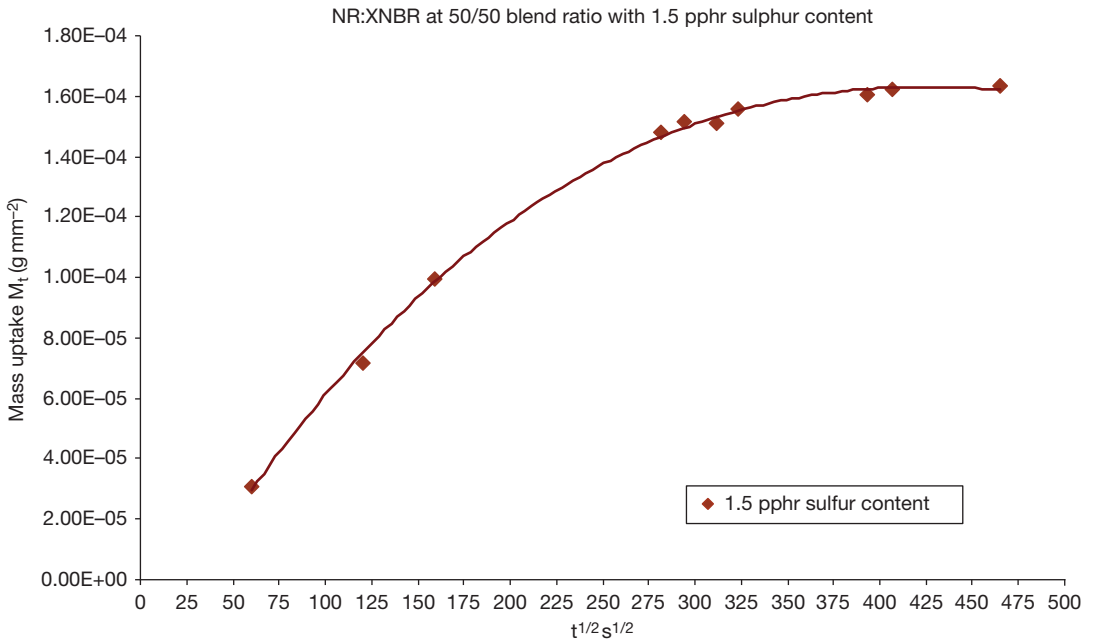

Figure 15 Typical mass uptake curve for NR/XNBR blend latex film.[25]

Table 8 Effect of crosslink concentration on diffusion coefficient *D* of cooking oil into NR latex film

Sulfur level (pphr)	*$[X]_{phy}$ (mol per kg RH)*	*D ($m^2s^{-1} \times 10^{-13}$)*
0.6	4.46×10^{-2}	4.70
1.0	4.60×10^{-2}	4.00
2.0	4.89×10^{-2}	3.70
3.0	5.82×10^{-2}	3.57
NR:XNBR (50:50) 1.5	–	1.30

proteinaceous.[24] When water diffuses into the rubber, the water-soluble hydrophilic materials dissolve forming droplets of solution within the rubber. Osmotic pressure gradient would exist between watery domains in the rubber and that of the external solution immersing the rubber.[24] This results in more water diffusing into the internal solution droplet. Water absorption reaches its equilibrium when the elastic stresses acting on the droplets balance the osmotic pressure difference. Muniandy and Thomas[24] proposed a mathematical model for water absorption to derive equations for the equilibrium water uptake and to evaluate the kinetics of water absorption and desorption. From the model, they calculated the equilibrium water uptake and the apparent diffusion coefficient. They found very good agreement between theory and experimental results.

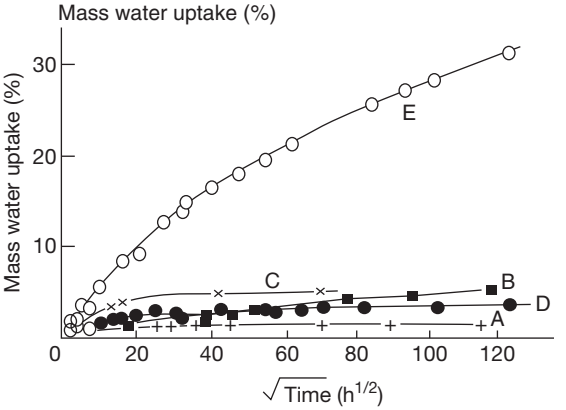

Figure 16 Corrected mass uptake measurements for engineering rubbers in seawater at 23 °C: (a) deproteinized NR, (b) lead oxide cured polychloprene, (c) nitrile rubber, (d) conventional NR, and (e) conventional polychloroprene Adapted from Fuller, K. N. G.; Muhr, A. H. *Engineering design with natural rubber, NR Technical Bulletin*, 5th ed.; The Malaysian Rubber Producers' Research Association, London, 1992; pp 1–33, with permission from Tun Abdul Razak Research Centre, Brickendonbury Hertford, England.

Later, Lake[26] investigated the kinetics of water (tap water) absorption in elastomers and their effects on properties. He reported that when the absorption was large (50% or more), the rubber test-piece degraded. Severe degradation leads to porosity of the surface layer, and when pressed, water exudes.[26] However, at a low level of absorption, Lake observed

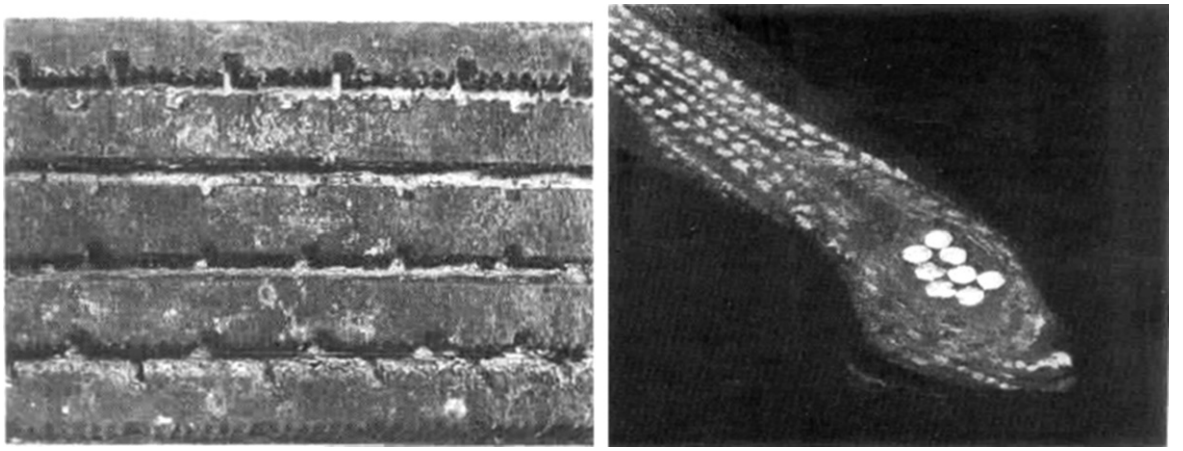

Figure 17 A natural rubber tire after 40 years' exposure to seawater. Adapted from Mullins, L. *Proc. Int. Rubb. Conf*. Kuala Lumpur, 1985, with permission from Malaysian Rubber Board.

the formation of droplets similar to the blisters that occur in plastics or under protective coatings, consistent with an osmotic diffusion mechanism.[24] In saltwater, water absorption reached steady state at much lower levels than in freshwater, again consistent with an osmotic pressure mechanism. Thus seawater is less damaging than freshwater and may not have any serious consequences for many elastomers. This latter point is consistent with findings of Ab. Malek and Stevenson[27] who evaluated the physical properties of a rubber tire as shown in **Figure 17**, recovered from seawater at a depth of 80 ft. They found that the rubber tire had absorbed about 5% of seawater after 42 years of immersion. They found no evidence of microbiological attack. What is more interesting, the physical properties of the rubber tire were within normal specifications for new rubber of the same type. They even suggested storing elastomers in deep seawater in view of its inert nature. Indeed, elastomer is a very suitable material to coat metal surfaces against corrosion in deep seawater. The photograph in **Figure 17** shows clear evidence that the steel cords making up the bead of the tire are corrosion-free after a 42-year immersion in seawater.[27]

3.33.12 Protective Measures

3.33.12.1 Selection of Elastomer

All elastomers experience aging. Some age faster than others. The rate of aging depends on a number of factors such as the chemical structure of the polymer, service environment, which includes length of exposure to heat and light, oxygen and ozone concentration, size and shape of elastomers, and mechanical stresses. One cannot stop the aging process, but one can slow it down. The most effective means of combating aging is to select the correct elastomers to meet the maximum service temperature and environment. Fully saturated elastomers having high bond dissociation energy making up their backbone chains are the best choice to meet high service temperature applications. Fully saturated rubbers such as ethylene propylene copolymer and very low unsaturation butyl rubber are excellent resistance to heat aging, oxidation and ozone cracking. Not only the maximum service temperature, but also other environmental factor such as oil or solvent determines the aging resistance. In cases like these, the elastomers having high bond dissociation energy and solvent resistance are desired. These include specialty elastomers such as acrylic (ACM), chloro-sulfonyl-polyethylene (CSM), ethylene propylene copolymer (EPM), fluoroelastomers (FKM), silicones (MQ, VMQ), polyester urethanes (AU), etc. Alternatively, for unsaturated elastomers are to use antioxidants and antiozonants, with correct vulcanization system can slow down the aging process quite efficiently.

3.33.12.2 Blends of Elastomers

It is a common practice to blend two elastomers of different properties with a view to combining the best features in terms of technical and economic values. Natural rubber is blended with EPM for applications requiring very high resistance to attack by ozone as the latter is fully saturated. A blend of NR and EPDM is used for applications that require a combination of good resistance to attack by ozone and high

strength properties. Nitrile rubber (NBR) is blended with EPM to meet the requirements for very good oil resistance as well as conferring high resistance to oxidation and ozone cracking. The former is polar rubber and provides very good oil resistance, while the latter provides excellent weather resistance. However, blending two or more elastomers is not as easy as one would imagine. The work on blending various elastomers conducted by Tinker[28] and coworkers has thrown some light on the importance of compatibility, distribution of crosslinks in each rubber phase, distribution of filler and plasticizer and interfacial tension of each phase which have very strong influence on the service performance of the blend. When the elastomers are not compatible with each other, the associated problems that may arise include maldistribution of crosslinks, partition of chemicals (sulfur, accelerators, etc.) due to mechanism associated with preferential solubility and others. Lewan[29] worked on crosslink density distribution in NR/NBR blend and reported the effects of large difference in polarity and solubility parameters between these two rubbers. The large difference in polarity has the following effects:

(i) causes high interfacial tension that is detrimental to mixing since it interferes with efficient mixing at the interface, hence minimizing the opportunity for crosslinking between the rubbers;
(ii) causes poor phase morphology, which is characterized by large phase sizes;
(iii) causes uneven distribution of crosslinks arises through preferential solubility of the curatives and vulcanization intermediates. Sulfur will be preferentially soluble (partition in favor of) the more polar NBR. One phase is over-crosslinked and the other is lowly crosslinked.

However, Lewan[29] overcame these problems by selecting the correct type of curing system such as semi-EV based on sulfur – TBBS, to obtain an even distribution of crosslinks in each phase and maximizing crosslinking between rubbers at the interface. The use of compatibilizer is highly recommended to enhance the compatibility between rubber phases. Polychloroprene rubber serves as a very good compatibilizer for the NR/NBR blend with just a small quantity (5 pphr) added to the blend. The addition of this compatibilizer reduced phase sizes, gave an even distribution of crosslinks and increased tensile strength.[30] Blends of elastomers provide alternative means of improving both aging resistance and oil resistance.

3.33.12.3 Antidegradants

Chemical antioxidants and antiozonants combat aging by scavenging harmful radicals, absorbing UV light, deactivating catalytic metals like copper, manganese, iron, etc., and decomposing initiating peroxides.[16,17] Two main types of chemical antioxidants and antiozonants are widely used in rubber compounds; they are amines and phenolics. Amine types are more effective and powerful antioxidants than phenolic types. However, the former is staining and the latter is not. Thus, this limits applications of amine types to black and dark colored elastomeric products. Phenolic types are exclusively used for white and bright colored products, especially in electrical wire insulation where colors are useful for identification purposes. Both amines and phenolics provide protection against aging by scavenging the harmful free radicals during the oxidative chain reaction.[16,17] The proposed mechanism[17] by which these two types of antioxidants work is shown in **Figure 18**. During the initiation stage, the free radicals produced by the peroxides abstract a labile hydrogen atom from the antioxidant and produce an antioxidant radical. This antioxidant radical is more stable than the peroxy radical, which terminates by reaction with other radicals in the system.[16,17]

The transfer step (c) and termination step (f) remove the free radical functionality from the elastomer, which consequently halts the oxidative degradation reaction.[17] Metal deactivators such as 2-mercaptobenzimidazole and its salt when added into the rubber compound containing amine or phenolic antioxidant give a synergistic effect to enhance the protection against aging.[31] These chemicals form

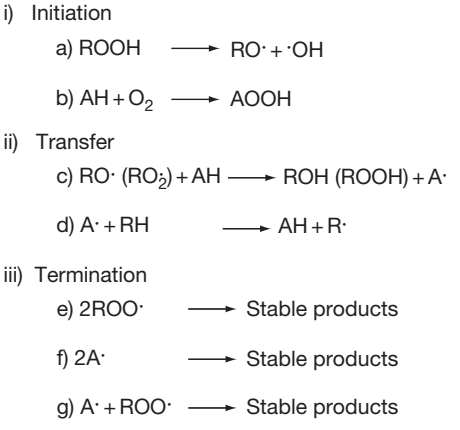

Figure 18 Mechanism of amine and phenolic antioxidant activity, where AH is the antioxidant.[17]

coordination complexes with catalytic metals and inhibit metal-activated oxidation. Carbon black is a natural UV light absorber, and for nonblack compounds, it is useful to incorporate a UV light absorber such as benztriazole derivative.

3.33.12.3.1 Mechanism of antiozonant action

The mechanism by which an antiozonant protects unsaturated rubber against ozone cracking has received attention from many rubber chemists and physicists. A number of suggestions have been proposed as to how antiozonants confer protection, ranging from competitive reaction with ozone (scavenging) to various types of protective layer formation.[17,19–21] There are three theories to describe the mechanism of antiozonant action[17]:

(i) The antiozonant blooms to the surface of the rubber compound and reacts preferentially with the incident ozone.
(ii) The antiozonant blooms to the surface of the rubber and forms a protective layer of film on the surface.
(iii) The antiozonant reacts with intermediates formed in the ozonation of rubber, preventing chain scission or recombining severed rubber chains.

Lake[32] has conducted some work to elucidate the mechanism of antiozonant action to protect natural rubber against ozone cracking. He used dioctyl-*p*-phenylenediamines (DOPPD) antiozonant for his rubber compound. Exposing the rubber test-piece to ozone-rich atmosphere has reportedly resulted in a layer of film 10^{-3} cm thick and visible to the naked eye forming on the rubber surface.[32] The protective layer can be removed by physical means either by scraping or using adhesive tape, or by swabbing with cotton wool dipped in acetone. The mass of the film can be determined by weighing the test-piece before and after its removal. In this way, the kinetics of layer formation can be determined by monitoring changes in weight after various periods of exposure to ozone.

Lake[32] has derived a mathematical expression to relate the mass of layer per unit area of surface M_L formed after time t to the concentration C_0 of antiozonant in the rubber and diffusion coefficient D_L as shown by eqn [14]:

$$M_L = [2\rho_L D_L S_L C_0 t]^{1/2} \qquad [14]$$

where ρ_L is the density of the layer material and S_L is the solubility, relative to that in the rubber, of the antiozonant in the layer. In deriving this equation, Lake[32] assumed that the layer to be formed entirely of reacted antiozonant and the concentration of unreacted material within it to be small. The product $D_L S_L$ was determined experimentally by measuring the rate of transfer of antiozonant through the layer formed on a test-piece to a controlled rubber test-piece containing no antiozonant initially. This was done experimentally by pressing two cylindrical discs (test-piece A contains antiozonant, test-piece B has no antiozonant) together so their surfaces are in intimate contact with each other. The antiozonant from test-piece A would migrate into test-piece B as a function of time. The mass of the layer formed per unit area of surface was plotted against the square root of time to produce a straight line whose slope gave the value of $M_L/t^{1/2}$, that is mass of film deposited per square root time. Lake[32] obtained very good agreement between theory and experimental data.

Lake[32] proposed the mechanism of antiozonant action as follows: The protective layer formed on the rubber surface is composed predominantly of the antiozonant which has reacted with ozone. The film formed remained essentially in the unstrained state, independent of the type of deformation applied. For this to happen, it is necessary that the antiozonant is soluble in the rubber, and that its reaction product should be insoluble. However, once the protective layer becomes coherent and compact, it will reduce substantially the flux of ozone reaching the rubber surface. Thus it appears that the ability of the antiozonant to prevent cracking is likely to be determined by what occurs during the initial stages of exposure when the layer is starting to form, rather than by the long-term behavior. Indeed, Lake[32] suggested that a coherent monomolecular layer of film that formed on the rubber surface is sufficient to confer protection against ozone cracking. However, the time for this monolayer to form must be faster than the time for the crack to grow to the same depth, so that the monolayer is able to bridge any cracks that have begun to grow.

3.33.12.3.2 Theories of layer formation

The thin layer of protective film covering the rubber surface is a direct consequence of the chemical reaction between chemical antiozonant and ozone. Lake and Mente[21] proposed two diffusion models to work out a theory for layer formation. The two models are shown in **Figure 19**. The first model describes the rate of layer formation that is controlled by the diffusion of the antiozonant across the already-formed layer to react with ozone at its outer surface. Under

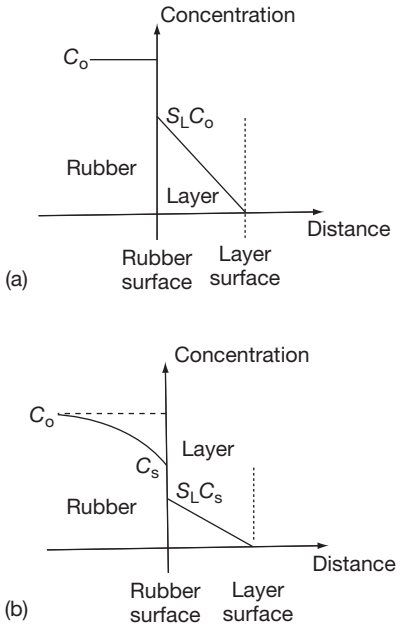

Figure 19 Diffusion models for antiozonant layer formation: (a) rate governed by diffusion of antiozonant within the layer only, and (b) rate governed by both diffusion in the layer and in the rubber. Adapted from Lake, G. J.; Mente, P. G. *J. Nat. Rubb. Res.* **1992**, *7*(1), 1–13, with permission from Malaysian Rubber Board.

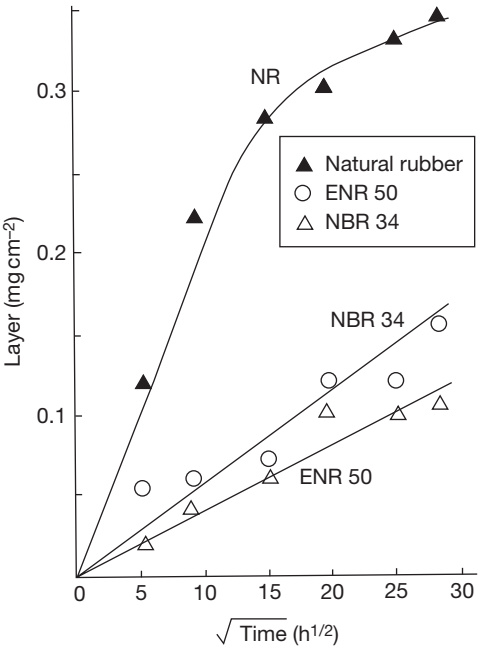

Figure 20 Dependence of the mass of antiozonant layer formed on the square root of the time of exposure to an ozone concentration of 200 pphm at 40 °C for vulcanizates of NR, ENR 50, and NBR 34. Adapted from Lake, G. J.; Mente, P. G. *J. Nat. Rubb. Res.* **1992**, *7*(1), 1–13, with permission from Malaysian Rubber Board.

these circumstances, the mass per unit area M_L, of layer formed after time t is given by eqn [14].[21,32] The concentration gradient in the layer will be essentially linear as shown in **Figure 19(a)**. The second diffusion model takes into account diffusion within the rubber in addition to diffusion across the layer. In this case, an equation similar to eqn [14] applies, when C_0 is replaced by C_s, the concentration at the rubber surface is lower than C_0 as shown schematically in **Figure 19(b)**. C_s is a function of C_0 and the relative permeabilities of the rubber and the layer to the antiozonant, and with the assumptions made, are given by eqn [15]:

$$C_s/C_0 = 1 + \xi - [(1+\xi)^2 - 1]^{1/2} \qquad [15]$$

where

$$\xi = (\pi/4)(\rho_L D_L S_L / DC_0) \qquad [16]$$

and D is the diffusion coefficient of the antiozonant in the rubber. The mass of layer per unit area of surface plotted against square root of time as shown in **Figure 20** enabled Lake and Mente[21] to determine the rates of layer formation of the antiozonants formed on NR, ENR 50, and NBR 34, respectively. These three rubbers differ greatly in terms of polarity and glass-transition temperature, which may affect the rate of film formation on the rubber surface. Their experimental results as shown in **Figure 20** indicate that the rate of layer formation for NR is about four times faster than that of NBR 34 and ENR 50, which is in accordance with the dependence of the diffusion coefficient on the glass-transition temperature of the rubber. The diffusion coefficient decreased in the increasing order of the T_g of the rubber.[21] Thus the diffusion coefficient of NR is fastest and that of ENR 50 is the slowest as T_g of NR is about −69 °C and that of ENR 50 is about −24 °C.[21] NBR34 has a slightly faster diffusion coefficient than ENR 50 as its T_g (−28 °C)[19] is slightly lower than that of ENR 50. Lake and Mente[21] also conducted experiments to investigate the effect of temperature on layer formation on the NR surface at −17 and 23 °C respectively as shown in **Figure 21**. They found that the rates of layer formation at these two temperatures were the same for NR. However, the diffusion coefficient of this particular antiozonant (DOPPD) in NR at −17 °C was very similar to that in ENR 50 and NBR 34 at 23 °C. They attributed this finding to the partitioning of the antiozonant

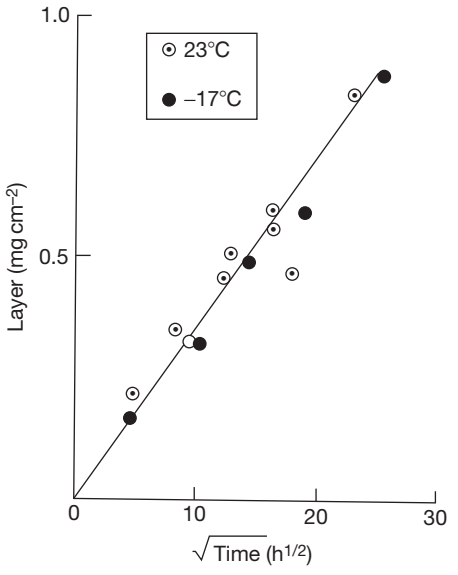

Figure 21 Mass of antiozonant layer formed versus square root of the time of exposure to 10^5 pphm ozone for an NR vulcanizate containing 10 pphr DOPPD at 23 and −17 °C. Adapted from Lake, G. J.; Mente, P. G. *J. Nat. Rubb. Res.* **1992**, *7*(1), 1–13, with permission from Malaysian Rubber Board.

between the elastomer and the layer material, as the polarity of the elastomer affects the solubility of the antiozonant in the rubber. The solubility of the antiozonant varies in the ascending order of polarity of elastomer, that is NR < NBR 34 < ENR 50.[21] Lake and Mente concluded that for elastomers with high T_g, the antiozonant offers better protection at temperatures above room temperature than at low temperature, as the protective agents are more mobile at high temperatures rather than at low temperatures.

3.33.12.4 Blooming of Wax

Besides chemical antiozonants, paraffin wax is also a useful ingredient to confer protection against ozone cracking. Wax provides a protective layer surrounding the surface of the elastomer through the diffusion process commonly known as blooming, which prevents direct contact between ozone and the elastomer. Blooming occurs when the supersaturated solution of the ingredient in the rubber crystallizes more readily on the surface than in the rubber itself.[24,33] This basic mechanism of blooming is not only applicable to wax but other ingredients as well. When other ingredients such as sulfur, accelerators and strearic acid bloom to the rubber surface, they reduce the tackiness of the rubber, which can bring detrimental effects to products relying on adhesion and bond strength involving different components plied together. These include rubber-to-metal bonded components, tires, belts, and hoses. However, blooming of waxes and antioxidants brings advantages.

Nah and Thomas[33] investigated the mechanism and kinetics of diffusion of wax to the rubber surface. They envisaged that the driving force for the blooming process arises from the elastic forces acting around the wax precipitates in the rubber when the wax concentration is in excess of its equilibrium solubility. They then proposed a model and theory for wax blooming base on thermodynamic concept of diffusion, where the driving force of the diffusion process is predominantly associated with free energy gradient rather than the concentration gradient of the wax that is dissolved in the rubber. The initial rate of wax bloom per unit area $(M_t/t^{1/2})$ is given by eqn [17][33]:

$$(M_t/t^{1/2})_{x=0} = [(24 v_f D_t s_x \rho_x V_x G)/RT]^{1/2} (d\lambda/dy)_0 \quad [17]$$

where D_t is diffusion coefficient, v_f is volume fraction of seeding particles or flaws present in the rubber. s_x is solubility of wax in the rubber, ρ_x is density of wax, and V_x is molar volume of solid wax. G is shear modulus of the rubber, R is molar gas constant, T is absolute temperature. $(d\lambda/dy)_0$ is equivalent to the concentration gradient of the wax at the surface of the rubber, and is determined by numerical methods for the appropriate boundary conditions and a suitable value of v_f. The symbol λ stands for the extension ratio of the rubber around the precipitated wax particle, assumed spherical. Nah and Thomas[33] verified eqn [17] experimentally, and obtained satisfactory agreement between their experimental and theoretical values for the migration of paraffin waxes in peroxide cured natural rubber. The theory was applicable to predict the blooming of wax mixtures with success, indicating that the mechanism of wax blooming has been identified correctly. Although Nah and Thomas developed the theory for blooming of wax, with minor adjustments, it is also applicable to predict migration and blooming of sulfur, fatty acids and antidegradants in vulcanized elastomers.

3.33.12.5 Choice of Vulcanization System

Anaerobic aging usually decreases the stiffness, resilience, and tensile, tear and fatigue properties; the extent is mainly determined by the type of vulcanization system, which affects aging of elastomers. There are three types of sulfur vulcanization systems known as conventional, efficient (EV) and

semi-efficient (semi-EV) respectively[8,10] as discussed briefly in Section 3.33.4.3. The conventional system has a higher sulfur dosage than the accelerator that produces predominantly polysulfidic crosslinks, where the rubber molecular chains are linked by three or more sulfur atoms. Polysulfidic crosslinks have poor resistance to heat aging because the –S–S– bond has low thermal stability. In contrast, EV makes use of the low sulfur level and high accelerator dosage. This EV system produces predominantly monosulfidic crosslinks which are thermally very stable. The rubber network consists of other structural features as described briefly in subsequent sections.

3.33.12.5.1 Sulfur vulcanization system and types of crosslinks on aging resistance

Polysulfidic crosslink

A chain of three or more sulfur atoms (maximum of six atoms) in this crosslink bridges two polymer chains. The bond energy of this crosslink is less than 268 kJ mol^{-1}, which is relatively low.[10] A polysulfidic crosslink can be produced by using the conventional vulcanization system where the quantity of sulfur is more than the quantity of the accelerator in the ratio 5:1 (sulfur: accelerator). Therefore the conventional sulfur cure system is not suitable for high temperature applications.

Disulfidic crosslink

In a disulfidic crosslink, there are two sulfur atoms bridging the two polymer chains. Its bond energy is about 268 kJ mol^{-1}. Little is known of the properties of this crosslink, mainly because it is very difficult to prepare a network in which disulfides are predominant. In both conventional and efficient sulfur vulcanizates the proportion of disulfidic crosslink is seldom more than 20–30% of the total.

Monosulfidic crosslink

In the case of a monosulfidic crosslink, the two polymer chains are bridged by one sulfur atom. Its bond energy[10] is relatively high, about 285 kJ mol^{-1}. A monosulfidic crosslink can be produced from an EV system where the amount of the accelerator is higher than the amount of sulfur, about 5:1 (accelerator:sulfur). Thus the EV system is suitable for medium high temperature applications.

Cyclic sulfides

These are intra-crosslinks which are useless as the crosslinks are formed on the same polymer chain. This phenomenon is also known as main chain modification. The main source of these main chain modifications is the thermal decomposition of polysulfide crosslinks. The conventional vulcanization system creates more cyclic sulfides than the EV system as the former produces more polysufide crosslinks than the latter.

Conjugated diene and triene groups

These main chain modifications are also formed by the thermal decomposition of polysulfide crosslinks. The concentration of these conjugated groups increases on overcure. The presence of these groups tends to catalyze oxidative aging as they are much more susceptible to oxidation than the polyisoprene main chain.[8,10,16]

Pendent accelerator group

It is generally accepted that in accelerated sulfur vulcanization, crosslinks are formed from initial rubber-bound pendent groups in which disulfide or polysulfide chains are terminated by accelerator fragments. Like the crosslink, some of these intermediates undergo progressive desulfuration and are converted into stable monosulfidic links between the polymer chain and accelerator fragments. The extent of main chain modification will depend on the amount of accelerator available and on the ease with which the initial pendent group can be desulfurated.

Extra-network material

The extra-network material formed by a sulfur vulcanizing system can be put into two categories. The first consists of unreacted zinc oxide and fatty acid activators, their zinc soap reaction products and zinc sulfide. The second consists of accelerator reaction products.

3.33.12.5.2 Peroxide vulcanization system

Unlike sulfur vulcanization, peroxide vulcanization does not require the presence of double bonds. In fact, peroxide vulcanization is possible for rubbers having either saturated or/and unsaturated carbon–carbon backbone chains. However, peroxide vulcanization is quite impossible with the following elastomers because of their tendency to decompose:

- IIR – butyl rubber
- CIIR – chlorinated butyl rubber
- CO – polyepichlorohydrin rubber
- ECO – copolymer of epichlorohydrin and ethylene oxide
- PP – polypropylene
- ACM – polyacrylic rubber

The most common peroxide is dicumyl peroxide (DCP or dicup). Others include ditert butyl peroxide, dibenzoyl peroxide and bis(2,4-dichlorobenzoyl) peroxide. Peroxide vulcanization[10] produces a vulcanizate which will impart good aging resistance and excellent resistance to compression at high temperatures (70–100 °C). To obtain the best compression set performance, freedom from certain other compounding ingredients, especially zinc oxide and stearic acid, is essential. Peroxide vulcanization is essentially nonreverting. However, there are certain deficiencies such as poor hot tear strength and incompatibility with chemical antiozonants. Other technical limitations include slow cure rate with no delayed action, and degradation of the rubber giving a sticky surface if it comes into contact with air during the cure. Thus peroxides are not suitable for hot-air or steam-pan curing. The reaction of peroxide must be carried through to completion to obtain the best heat resistance; therefore long cure times are inevitable. In addition, nearly all antidegradants and aromatic oils affect the efficiency of the peroxide cure.

Co agents, which are highly reactive materials, are usually added in peroxide vulcanization to increase the efficiency of the organic peroxide, but do not affect the rate of cure.[10,31] They are used either to enhance the modulus and hardness or to reduce the level of peroxide required. They can be absolutely essential for the efficient cure of chlorinated polyethylene. Typical solid coagents are zinc diacrylate, zinc dimethacrylate, and *m*-phenylene dimaleimide. Liquid coagents are materials such as triallyl cyanurate (TAC), triallylisosyanurate (TAIC), etc. High vinyl polybutadiene is a polymer which can act as a coagent.

3.33.12.5.3 Vulcanization with urethane

This (urethane) crosslinking system for natural rubber was developed in the early 1980s by the scientists at the Malaysian Rubber Producers Research Association (MRPRA).[10,31] It was marketed under the trademark Novor. The basic reagent is a reaction product of a nitroso compound and a diisocyanate which dissociates at vulcanizing temperatures into its component species. The free nitroso compound then reacts by addition to rubber molecules giving attached pendent groups which subsequently react with the diisocyanate to form urea type crosslinks. The main features of the vulcanizates are excellent reversion resistance and, when protected with a TMQ/ZMBI antioxidant combination, excellent heat aging resistance.

3.33.12.5.4 Metallic oxide vulcanization

Elastomers containing halogens can be cured with metallic oxides such as oxides of zinc, magnesium, and lead. The oxides form an ether type of crosslink (R–O–R′) which gives good heat aging resistance. Elastomers which can be vulcanized metallic oxides are polychloroprene, halogenated butyls, and polychlorosulphunated rubber.

3.33.12.5.5 Resin vulcanization

Resin vulcanization has established itself to some degree in butyl (IIR) crosslinking, giving excellent heat and steam stability.[10] Example of a typical resin cross linker is polymethylolphenolic resin. The amount used is at the level of 5–12 pphr.

3.33.12.5.6 Quinonedioximes vulcanization

p-Benzoquinonedioxime (CDO) as well as its dibenzoyl derivative are cross linkers for many rubbers because of their free radical reactions.[10] Best known and of greatest interest is their use in IIR because of the excellent heat and steam stability that can be obtained. They are used mainly for rubbers having low unsaturation where sulfur vulcanization is slow. They have been unimportant for the classic diene rubbers.

3.33.13 Future Developments in Materials or Applications

Natural rubber and synthetic elastomers are likely to maintain their roles and contributions in domestic and industrial applications, buildings and structures, automotives, and marine and engineering products. With the emergence of nanomaterials for rubber compounding, it is envisaged that future elastomeric products will provide better service and longer life performance than they are capable of providing now. High heat resistant elastomers and highly oil resistant elastomers are the main players of the future to meet the high demands of the automotive industry and aeronautical engineering. More developmental work in these areas is expected.

Acknowledgements

I am very grateful to Dr. Stuart Lyon, Reader in Corrosion Control Engineering, School of Materials (Corrosion and Protection Centre), University of Manchester, England, who gave me the opportunity to write as part the prestigious Shier's Corrosion

book. I feel much honored to be among the experts who contributed to this fourth edition of Shier's Corrosion.

It gives me great pleasure to thank the Publication Divisions of the Malaysian Rubber Board (MRB) (formerly Rubber Research Institute of Malaysia), and its sister concern the Tun Abdul Razak Research Centre (TARRC) (formerly Malaysian Rubber Producers Research Association) at Brickendonbury Hertford, England. In particular, Dato' Dr. Kamarul Baharin Basir, Director General, MRB and Mdm Rabeatun Awaliah Awalludin, MRB, and Dr. A.J. Tinker (Director Research) TARRC and Ms. K. Lawson TARRC who helped me to obtain the permission to reproduce data and figures from their respective Publication Divisions.

I would like to express my sincere appreciation and thanks to Oxford University Press and the American Chemical Society (Rubber Division) for giving permission to reproduce figures and data from their respective publications.

Last but not least, Associate Prof. Dr. Mohamad Kamal Harun, Dean of Faculty of Applied Sciences, MARA University of Technology, Malaysia (UiTM) for his encouragement.

References

1. International Standard, Rubber – *Vocabulary, ISO1382*, 3rd Ed, 1996-08-01.
2. Fuller, K. N. G.; Muhr, A. H. *Engineering design with natural rubber, NR Technical Bulletin*, 5th ed.; The Malaysian Rubber Producers' Research Association: London, 1992; pp 1–33.
3. Chadwick, J. C. *Shell Polym.* **1981**, *5*, 44–50.
4. ISO 4632/1-1982 (E), ISO Classification system.
5. Hashimoto, K.; Maeda, A.; Hosoya, K.; Todani, Y. *Rubb. Chem. Technol.* **1998**, *70*(3), 449–519.
6. Fogg, G.; Swift, P. M. *NRPRA Tech. Bull.* **1962**, *4*, 1–26.
7. Brydson, J. A. *Plastics Materials*, 4th ed.; Butterworths: Newton, MA, 1989; Chapter 29, pp 730.
8. Brown, P. S.; Porter, M.; Thomas, A. G. In *Proceedings of the International Rubber Conference*; Kuala Lumpur, October 21–25, 1985, RRIM, 1986; pp 20–46.
9. Hofmann, W. *Rubber Technology Handbook*; Hanser, 1989; Chapter 3, Synthetic Rubber, pp 1–171.
10. Elliott, D. J.; Tidd, B. K. *Prog. Rubb. Technol.* **1974**, *34*, 83–126.
11. Gregory, M. J. In *Rubber to metal bonding, Adhesives, Sealants, and Encapsulants Conference*, London, November 5–7, 1985.
12. Gage, F. *J. IRI* **1968**, 47–49.
13. Gibbs, E. H., Jr.; Seber, J. N. ACS Rubber Division Mtg., Indianapolis, IN, May 1984, pp 1–9.
14. Mullins, L. In *Proc. Rubb. in Eng*. Conf. Kuala Lumpur, 1974, pp 1–20.
15. Bolland, J. L.; Hughes, H. *J. Chem. Soc.* **1949**, 492.
16. Barnard, D.; Lewis, P. M. In *Natural Rubber Science and Technology*; Robert, A. D., Ed.; Oxford University Press: Oxford, UK, 1988; Chapter 13, pp 621–673.
17. Keller, R. W. *Rubb. Chem. Technol.* **1985**, *58*, 637–651.
18. Mullins, L. *J. Polym. Sci.* **1956**, *19*, 225–236.
19. Braden, M.; Gent, A. N. *J. Appl. Polym. Sci.* **1960**, *3*, 90–106.
20. Lake, G. J.; Thomas, A. G. In *Proceedings of the Int. Rubb. Conf*. 1967, Maclarens: London.
21. Lake, G. J.; Mente, P. G. *J. Nat. Rubb. Res.* **1992**, *7*(1), 1–13.
22. Kinro, H.; Akio, M.; Kiyoshi, H.; Yoshihiro, T. Speciality Elastomers for Automotive Applications, *Rubber Chemistry Technology*; **1998**, *71*(3).
23. Lake, G. J.; Lindley, P. B. *Rubber J.* **1964**, *10*, 24–30, 79, 11, 30–36, 39.
24. Muniandy, K.; Southern, E.; Thomas, A. G. In *Natural Rubber Science and Technology*; Robert, A. D., Ed.; Oxford University Press: Oxford, UK, 1988; Chapter 13, pp 820–851.
25. Rahim, R.; Samsuri, A., Effect of crosslink concentration and XNBR:NR ratio on swelling resistance of NR latex film towards cooking oil, in press.
26. Lake, G.J. In *Conf. Polymers in a Marine Environment*, London, 31 Oct.–2 Nov., 1984, pp 157–160.
27. Ab-Malek, K.; Stevenson, A. *J. Mater. Sci.* **1986**, *21*, 147–154.
28. Tinker, A. J. In *Blends of Natural Rubber*; Tinker, A. J., Jones, K. P., Eds.; Chapman & Hall: London, 1998; Chapter 1, pp 1–7.
29. Lewan, M. V. In *Blends of Natural Rubber*; Tinker, A. J., Jones, K. P., Eds.; Chapman & Hall: London, 1998; Chapter 5, pp 53–67.
30. Kongsin, K.; Lewan, M. V. In *Blends of Natural Rubber*; Tinker, A. J., Jones, K. P., Eds.; Chapman & Hall: London, 1998; Chapter 7, pp 80–93.
31. The Natural Rubber Formulary and Property Index, Malaysian Rubber Producers' Research Association, 1984, pp 1–24.
32. Lake, J. G. *Rubb. Chem. Chem.* **1970**, *43*, 1230–1238.
33. Nah, S. H.; Thomas, A. G. *J. Polym. Sci., Polym. Phys. Ed.* **1980**, *18*, 511–521.

3.33 Degradation of Natural Rubber and Synthetic Elastomers

A. bin Samsuri
Department of Polymer Technology, MARA University of Technology (UiTM), 40450 Shah Alam, Selangor, Malaysia

Glossary

Damping Basic property of an elastomer to dampen, absorb or reduce vibrations. High damping elastomers are those having high glass-transition temperature (T_g), which are widely used to isolate vibrations.

Glass-transition temperature (T_g) It denotes the temperature below which the elastomer becomes glassy and brittle, above which it is soft and rubbery. T_g reflects molecular mobility and hence the internal viscosity of the elastomer. High T_g indicates low molecular mobility or high internal viscosity and vice versa.

Heat build-up The amount of heat accumulated in the elastomer when subject to cyclic deformation. It is closely related to hysteresis.

Hysteresis It is a term to denote energy dissipated as heat when the elastomer is subject to cyclic stresses or in a single stress–strain cycle. The area bounded by the extension and retraction curve gives a quantitative measure of hysteresis.

Raw rubber Fresh rubber or an elastomer as received from the supplier.

Scorch It is a rubber technology term to denote the occurrence of a premature crosslink, which is an undesirable feature during the shaping process.

Vulcanizate or vulcanized elastomer Indicates rubber or elastomer that has been vulcanized or cured, and thus, contains network structure or chemical crosslinks.

Abbreviations

ACM Polyacrylic rubber
ASTM American Society for Testing Materials
CED Cohesive energy density
CIIR Chlorinated butyl rubber
CM Cement metal failure
CP Cement primer failure
CR Polychloroprene rubber
CSM Chlorosulfonated polyethylene rubber
DCP Dicumyl peroxide
DOPPD Dioctyl-*p*-phenylenediamines
ECO Copolymer of epichlorohydrin rubber
ENR50 Epoxidized natural rubber (50 mol% epoxidation)
EPM Ethylene propylene rubber
EV Efficient vulcanization
GRG General rubber goods
IHRD International Rubber Hardness Degrees
IIR Isobutylene isoprene (butyl) rubber
IR Synthetic polyisoprene rubber
IRG Industrial rubber goods
ISO International Organization for Standardization
MRB Malaysian Rubber Board
MRPRA Malaysian Rubber Producers Research Association
MS Malaysian standard
NBR Nitrile rubber
NR Natural rubber
PP Polypropylene
PTR Polysulphide rubber
SBR Styrene butadiene rubber
TAC Triallyl cyanurate
TAIC Triallylisosyanurate
TARRC Tun Abdul Razak Research Centre
UiTM Mara University of Technology
UV Ultraviolet light
XNBR Carboxylated nitrile rubber

Symbols

A Cross-sectional area (m^2)
***A*$_o$** Unstrained (original) cross-sectional area (m^2)
B Crack growth constant
c Crack length (mm, m)
***c*$_o$** Natural flaw size (mm, m)
***C*$_o$** Concentration of antiozonant ($mg\,cm^{-2}$)

C_s Concentration of antiozonant at the rubber surface (mg cm^{-2})
D Diffusion coefficient ($m^2\,s^{-1}$)
dc/dt Crack growth rate ($m\,s^{-1}$)
f Force (N)
f_f Frequency (Hz)
h Height (m)
k_c Compression stiffness ($N\,m^{-1}$)
k_s Shear stiffness ($N\,m^{-1}$)
l Half thickness of film sheet (mm, m)
L Length (m)
M Molecular weight ($g\,mol^{-1}$)
M_∞ Total mass of liquid absorbed after an infinite time (g, kg)
M_L Mass of layer per unit area of surface ($g\,mm^{-2}$, $kg\,m^{-2}$)
M_t Total amount of liquid absorbed per unit area after immersion time, t ($g\,mm^{-2}\,s^{1/2}$)
N Number of molecules per unit volume of rubber ($mol\,cm^{-3}$)
N_f Fatigue life (number of cycles of failure) (cycles, kilocycles)
R Molar gas constant (8314 $J\,mol^{-1}\,K^{-1}$)
S Shape factor
T Absolute temperature (K)
t Time (s)
T_g Glass-transition temperature (°C, K)
V_1 Molar volume of solvent (m^3)
v_f Volume fraction of seeding particles present in the rubber
v_r Volume fraction of rubber in the swollen gel
W Width (m)
W_s Strain energy density ($J\,m^{-3}$)
$[X]_{phy.}$ Physically manifested crosslink concentration ($mol\,kg^{-1}$)
δ Solubility parameter $(MPa)^{1/2}$
ΔH Latent heat of vaporization (J)
λ Extension ratio
ρ Density ($kg\,m^{-3}$)
χ Rubber–solvent interaction parameter

3.33.1 Introduction

Natural rubber and elastomers belong to the same group of materials known as high molecular weight polymers. According to the International Organization for Standardization (ISO) rubber vocabulary,[1] an elastomer is a macromolecular material which returns rapidly to approximately its initial dimensions and shape after substantial deformation by a weak stress and release of the stress. However, an elastomer has always been recognized as a synthetic elastic polymer.[1] A polymer is a high molecular weight material having many units of small molecules chemically joined or linked by normal covalent bonds to form long chain molecules. These flexible and soft materials find wide uses in many engineering applications, such as natural rubber (NR) bridge bearings, and earthquake and seismic bearings. Indeed NR has had a sound track record in many engineering applications for over 150 years.[2] Elastomers have some unique properties that metals do not have. These include

- high bulk modulus (2000–3000 MPa) relative to their Young's modulus (0.5–3.0 MPa),
- some inherent damping, and
- large strain deformation.

Rubbers having high bulk modulus hardly change their volume when deformed. In simple words, rubber is incompressible. Like incompressible liquids, it has a Poisson's ratio close to 0.5. If rubber is constrained, to prevent changes in shape, it becomes much stiffer, a feature that is used to full advantage in the design of compression springs. Elastomeric bridge bearings and seismic bearings are examples of products that rely on these properties.

The damping inherent in the elastomer is a very important property as it helps to prevent the amplitude of the vibration of the spring from becoming excessive if resonant frequencies are encountered. Elastomeric products such as vibration isolators and engine mounts rely on the inherent damping properties of the elastomer.

The elastomer undergoes large strain deformation (a few hundred percent) without failure by an applied stress below its breaking stress. This means that it can store much more energy per unit volume than steel. Elastomeric dock fender systems make use of its large stored energy capacity to absorb shocks, blows and the impact exerted by ships.

Some of the merits of elastomeric springs over metal springs are as follows[2]:

- no maintenance is required,
- the energy storage capacity is high,
- with correct design, the rubber spring can provide different stiffness in different directions, or nonlinear load–deflection characteristics,
- a certain amount of misalignment is tolerable as the rubber spring can accommodate this tolerance,
- easier to install,
- hysteresis inherited by the elastomer is able to dampen dangerous resonant vibrations.

Another important property of an elastomer is its strong resistance to inorganic acids, salts, and alkalis. In contrast, acids attack metals. For these reasons, the linings of chemical tanks and pipes, especially those containing caustic solutions, are made from elastomers. The function of the elastomer here is to protect the metal against attack by corrosive chemicals.

Every product has its own life span. The designed lifetime of a product depends on the environmental conditions and the nature of the application. It is very important to choose the materials correctly to meet the intended service conditions and the surrounding environment. The aging process is the determining factor that limits the life span of the product. The term aging is always associated with the degradation or corrosion process as applied to metals, which may take many forms. In metals, corrosion takes place in the form of rusting, which involves oxygen and moisture. In elastomers, the term degradation is preferred to corrosion and covers a wider scope than that of metals. Degradation takes place in the form of oxidation, ozone cracking, flex cracking, liquid absorption and heat aging. Degradation in elastomers is very complex as it involves oxygen, ozone, mechanical strain, heat, trace metals, etc. There are other agencies such as solvents, oils, fuels, hot air (steam) and water, which may degrade elastomers and affect the service life of elastomeric products. A specific section on the degradation of elastomers discusses all these issues again later.

3.33.2 Classifications of Rubber and Elastomers

3.33.2.1 Classification in Terms of Origins

Natural rubber comes from trees known as *Hevea brasiliensis*, and shrubs called guayule. The pictures in **Figure 1** show typical rubber trees grown in the hot tropical climate of Malaysia, and the fresh latex that exudes from the bark of the rubber tree, after tapping with a sharp tapping knife. The fresh latex that exudes from the tree known as field latex contains about 70% water. After removing this large amount of unwanted water, the latex is known as concentrated latex and has about 60% of rubber content. Centrifuging is the preferred method of concentrating field latex because of its efficiency and rapidness compared to creaming and evaporation methods. Apart from latex, natural rubbers are available commercially in standard bale form, weighing about 33.33 kg. These bales of NR are produced specifically to meet certain technical requirements such as minimum dirt content, viscosity consistency, ash content, etc.

Figure 1 Pictures of (a) natural rubber trees (top), (b) NR latex exudes from natural rubber tree (middle), and (c) closer view of NR latex collected in a cup (bottom).

All synthetic elastomers are produced by the polymerization process. The early production of synthetic elastomers such as styrene butadiene rubber (SBR), polychloroprene rubber (CR), and nitrile rubber (NBR) relied on emulsion polymerization. One of the main drawbacks of emulsion polymerization is the lack of uniformity of polymer molecules with respect to stereo regularity. This is due to the

different ways in which diene monomer molecules can react, and it applies to all free radical polymerization processes of diene monomers. However, there was a real breakthrough with the discovery of the Ziegler–Natta catalyst in 1954, which enabled the control of the microstructure of polyisoprene.[3] Synthetic polyisoprene is produced by the solution polymerization process using catalysts of the alkyl lithium types such as trialkyl aluminum/titanium tetrachloride mixtures.[3] The Al/Ti mole ratio is critical for achieving high cis content. Currently, there are about 27 types of rubbers or more commercially available in the market. The choice depends on the nature of application, service conditions and environment.

3.33.2.2 Classification in Terms of Purposes

Elastomers can be classified further either as general-purpose rubbers or as specialty rubbers. General-purpose rubbers are those elastomers that are widely used in the manufacture of tires, industrial rubber goods (IRG), and general rubber goods (GRG). Most of the general-purpose elastomers cannot meet high service temperature and high oil resistance specifications or the combinations of these two requirements. The most common general-purpose rubbers include NR, SBR, CR, NBR, ethylene–propylene–diene rubber (EPDM), and BR. In contrast, specialty rubbers are those elastomers that are tailor made to meet certain specific requirements, such as low temperature flexibility, high swelling resistance towards oil (hydrocarbon, fuel, gasoline, etc.) and very high service temperature or combinations of these requirements. Specialty rubbers include silicone rubber, fluoroleastomers, epicholorohydrin, cholorosulfonated rubber, etc. **Table 1** shows some of the rubbers which belong to these grades and their typical applications.

3.33.2.3 Classification in Accordance with International Organization for Standardization

Elastomers can also be classified according to the ISO 4632/1-1982(E)[4] which provides information about rubber as a material with specifications. They are classified and designated in terms of their performance to heat aging, swelling resistance towards oil and low temperature flexibility. This method of classification is very helpful as it facilitates the purchasers and suppliers to make the correct selection of suitable materials, and avoid wasting time and energy.

These designations are determined by a type based on resistance to heat aging, by a class based on resistance to swelling in oil, and by a group based on low temperature resistance.[4] These classification criteria are used to establish a characteristic material designation consisting of three capital letters, where

- the first letter signifies Type (heat resistance)
- the second letter signifies Class (oil resistance)
- the third letter signifies Group (low temperature resistance).

Tables 2–4 show the heat aging temperature, limits of volume swell and brittleness temperature for establishing Type, Class and Group respectively.[4] Type is determined by the maximum temperature at which heat (air oven) aging for 70 h, in accordance with ISO 188, causes a change in tensile strength of not more than ±30%, a change in elongation at break of not more than −50%, and a change in hardness of not more than ±15 International Rubber Hardness Degrees (IHRD). Class is based on the resistance of the material to swelling in American Society for Testing Materials (ASTM) Oil No. 3, when tested in accordance with ISO 1817. In the test, the immersion time shall be 70 h at a temperature determined in **Table 2**. Group is based on the brittleness temperature of the material when measured in accordance with ISO/R 812.

Thus if an elastomer is designated as BCD, it means that it is classified as Type B, Class C and Group D. This implies that the elastomer resists temperatures up to 100 °C, with volume swelling not exceeding 120% in oil No. 3 and is not brittle at −40 °C.

Most of the general purpose elastomers shown in **Table 1** have poor heat resistance except for ethylene propylene rubber (EPM) as shown in **Figure 2**. EPM can withstand service temperature of about 150 °C as it is categorized as Type D. General purpose elastomers also have poor swelling resistance towards hydrocarbon oil except nitrile rubber (NBR) which is classified as Class H with maximum volume swell of 30%. A majority of the specialty elastomers shown in **Table 1** have both excellent heat resistance and swelling resistance. From the chart shown in **Figure 2**, silicone rubber having both methyl and vinyl substituent groups on the polymer chain (VMQ) has equivalent heat resistant (Type G) with silicone rubber having methyl, vinyl, and fluorine substituent groups on the polymer chain (FVMQ). However, they have different Class with respect to swelling resistance. VMQ belongs to Class E while FVMQ belongs to Class J. Clearly

Table 1 General purpose rubbers and specialty rubbers

General purpose rubbers	*Typical applications*	*Specialty rubbers*	*Typical applications*
Natural rubber (NR)	Mainly for tires, industrial and general rubber goods, bridge and earthquake bearings, bridge expansion joints, etc.	Carboxylated nitrile rubber (XNBR)	Oil resistant hoses, boots, seals and gaskets and other automotive components with very good oxidation resistance
Synthetic polyisoprene (IR)	Tires, sports goods, earthquake rubber bearings, IRG.	Polysulphide rubber (PTR)	Used mainly where good resistance to solvents is required
Styrene butadiene rubber (SBR)	Passenger car tires, IRG, GRG	Polyurethane rubber (AU, EU)	Gaskets, seals, solid tires, and foams
Butyl rubber (IIR)	Tire tubes, tube liners, enclosures, air bags, and curing bladders	Silicone rubber (Si)	Able to withstand a very wide range of service temperatures from −45 to 200 °C. Various grades are available covering a very wide range of applications such as baby teats, catheters, medical applications, wire and cables, electronic components, etc.
Butadiene rubber (BR)	Tires, sports goods	Chlorosulfonated polyethylene rubber (CSM)	Electrical insulator in cable and wire industry, tank lining, colored-stable weather-resistance products, oil resistant hoses and gaskets
Ethylene–propylene–diene rubber (EPDM)	Gaskets, seals, automotive components, IRG, and GRG	Polyacrylic rubber (ACM)	Seals and gaskets for high temperature applications, 180–200 °C
Polychloroprene rubber (CR)	Hoses, rubber bearings, expansion joints, belts, and conveyors	Fluorocarbon rubber (FPM)	Products which are resistant to chemicals, oils and solvents. Able to withstand high service temperatures exceeding 250 °C. Outstanding oxidation and ozone resistance. Flame resistant. Hoses, gaskets and seals for aircraft, jets, and rockets
Nitrile rubber (NBR)	Oil-resistant hoses, seals, O-rings, gaskets	Epichlorohydrin rubber (ECO)	Automotive industry – gasket, seals, hoses to withstand service temperatures above 130 °C

Table 2 Heat aging temperature for establishing Type[4]

	Type									
	A	B	C	D	E	F	G	H	J	K
Test temperature (°C)	70	100	125	150	175	200	225	250	275	300

Table 3 Limits of volume swelling for establishing Class[4]

	Class										
	A	B	C	D	E	F	G	H	J	K	L
Vol. swell max. (%)	No rqmt.	140	120	100	80	60	40	30	20	10	5

Table 4 Limiting brittleness temperatures for establishing Group[4]

	Group						
	A	B	C	D	E	F	G
Limiting brittleness temperature (°C)	0	−10	−25	−40	−55	−75	−85

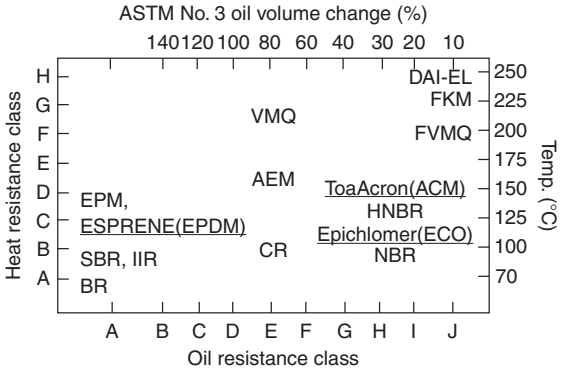

Figure 2 A chart showing type and class of elastomers. Adapted from Hashimoto, K.; Maeda, A.; Hosoya, K.; Todani, Y. *Rubb. Chem. Technol.* **1998,** *70*(3), 449–519, with permission from American Chemical Society.

FVMQ is more resistant to swelling towards the solvent than VMQ grade, as the fluorine atom is highly polar. Figure 3 shows the general chemical structure of silicone rubber with different substituent groups.

The main backbone chain is made of repeating −Si−O− groups while the methyl groups are attached at the side. Both Si–O and Si–CH_3 bonds are thermally stable. This explains why VMQ and FVMQ grades have the same Type of heat resistance, as the main chain backbone is the same for both. The Si–O bond is partially ionic and it is relatively easy to be broken by concentrated acids and alkalis even at room temperature. Another important feature of the chemical structure of silicone rubber is the relatively large bond angle of Si–O (about 140–160°).[7] The intermolecular forces between silicone chains are very low probably because of the large distance between the adjacent chains, as silicone atoms are relatively large. Thus this facilitates ease of chain rotation which accounts for the lowest glass-transition temperature T_g (∼−120 °C) among the commercially available elastomers. The dimethyl rubbers swell more in aliphatic and aromatic hydrocarbons than in acetone and diesters. However, the swelling resistance towards hydrocarbon oil can be enhanced by the replacement of one methyl group on each silicon atom by a more polar group such as trifluropropyl group ($-CH_2CH_2CF_3$), that is, the FVMQ grade.

3.33.3 General Properties of Elastomers

All elastomers have some common properties such as being flexible, tough, relatively impermeable to both water and air, and elastic when vulcanized. One of the unique features of a vulcanized elastomer is its ability to exhibit high elasticity: the elastomer can be stretched to a few hundred percent and recover its original shape and dimensions almost instantaneously when the deforming force is released. For a material to exhibit high elasticity, it must fulfill the following conditions:

- flexible long chain molecules with relatively low molecular interaction forces,
- the long chain molecules must be cross linked (at least 2% cross linked network),
- rubbery above T_g.

The elasticity of an ordinary solid such as metal is associated with its internal energy. In contrast, the elasticity of rubber is entropy driven.

Elastomers are also well known for their good resistance to acids, alkali and chemical solutions. Elastomers have a proven record of accomplishment as the material used for tank lining or related chemical vessels. Beyond these common characteristics, each rubber has its own unique properties depending on the chemical structure as discussed briefly below.

3.33.3.1 Structure–Property Relationship

The effects of chemical structure on some important physical and technological properties are summarized in Table 5.

3.33.3.1.1 Mechanical strength

Tensile strength, tear strength, crack-growth resistance and fatigue life of the vulcanized elastomer depend on the chemical structure and its geometrical configurations. Elastomers having regular microstructure are able to crystallize, and those that have irregular microstructure are amorphous. Figure 4 shows the chemical structure of general-purpose elastomers such

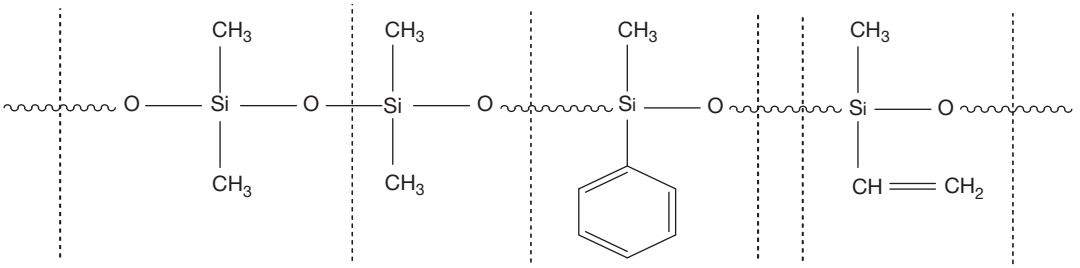

Figure 3 Chemical structure of silicone rubber: MQ grade consists of methyl, PMQ grade consists of benzene rings and VMQ grade consists of vinyl.

Table 5 Influence of chemical structure on physical and technological properties of elastomers

Basic structure	*Technological significance*
1. Nature of carbon–carbon backbone chain (i) Double bonds (ii) Single bonds	Unsaturated elastomers (having double bonds) are capable of being vulcanized with sulfur. Saturated elastomers (having single bonds) cannot be vulcanized with sulfur, but with peroxide. Unsaturated elastomers have poorer ozone cracking resistance and poorer oxidative resistance than saturated elastomers
2. Geometrical configurations	Regular microstructure would favor crystallization. Irregular microstructure leads to amorphous elastomers. The degree of crystallization affects mechanical strength
3. Polarity	Affects the degree of swelling resistance, rubber to metal bond strength, T_g and electrical resistivity
4. Chain flexibility and glass transition temperature, T_g	Affects hysteresis and damping, and other related properties such as resilience, heat build-up, mechanical strengths, etc.
5. Molecular weight distribution	Broad molecular weight distribution provides easier processing than narrow molecular weight distribution

as natural rubber (NR), styrene butadiene rubber (SBR) and polychloroprene rubber (CR).

Natural rubber is 100% *cis*-1,4-polyisoprene indicating that it has regular microstructure, thus enabling it to crystallize. NR will crystallize at low temperatures. Crystallization has its own kinetic; in the case of NR the maximum rate of crystallization occurs at −26 °C.[2,6] When the rubber crystallizes, it hardens progressively and eventually loses its flexibility and rubber-like elasticity. The maximum amount of crystalline region is about 33% in the case of NR. However, if a tensile strain (more than 200%) is applied to NR it crystallizes almost instantaneously even at high temperatures. This phenomenon is known as strain-induced crystallization. Since crystallization is a reversible process, the crystals are completely melted once the applied strain is removed.

Low temperature crystallization brings few disadvantages to NR, particularly when it involves mixing. When NR crystallizes, it becomes very stiff and may cause damage to the mills. To overcome this problem, the common practice is to place the crystallized NR in a hot room (oven) to melt the crystals so that the rubber regains its flexibility. Any unmelted crystals present during the mixing process would interfere with the incorporation and dispersion of the compounding ingredients. In contrast, strain-induced crystallization offers a big advantage in that it helps to enhance the mechanical strength of the rubber. For example, an unfilled or gum NR vulcanizate gives higher tensile strength (23–27 MPa) than unfilled SBR gum vulcanizate (2–3 MPa). Unfilled (gum) vulcanizate refers to a vulcanized rubber containing no filler apart from the compounding ingredients necessary for vulcanization. The crystals that are formed during straining act like a reinforcing filler to enhance the tensile strength. Thus for a noncrystallizing elastomer, it is necessary to incorporate a reinforcing filler into the rubber to enhance its strength.

In addition to the reinforcing filler, the types of chemical crosslink such as polysulfidic(C–S_x–C), monosulfidic (C–S–C), or carbon–carbon (C–C) also affect the strength of the vulcanized elastomer.[8] Polysulfidic crosslinks are weak and labile with lower bond energy than monosulfidic and carbon–carbon links. Polysulfidic crosslinks enhance mechanical strengths such as tensile and tear strengths because these weak and labile crosslinks relieve stresses by 'yielding.'[8]

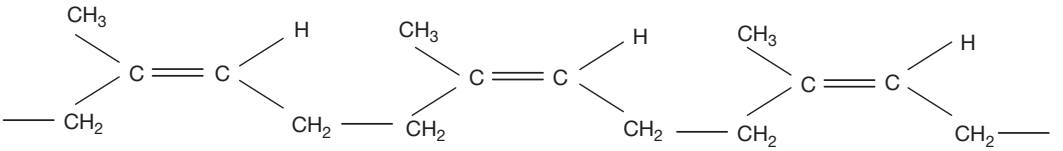

C is 1,4-Polyisoprene

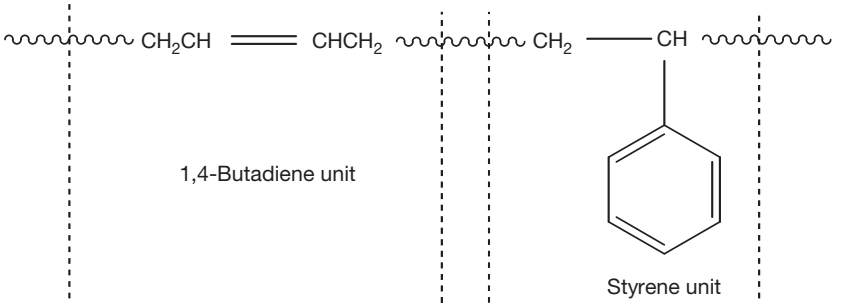

Styrene butadiene rubber (SBR)

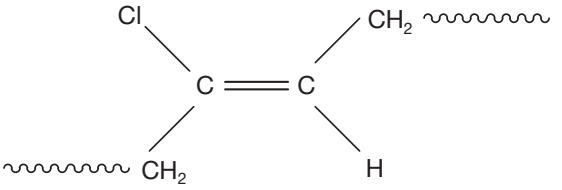

Trans 1,4 polychloroprene

Figure 4 Chemical structure of general-purpose elastomers.

Besides NR, polychloroprene rubber (CR) can also crystallize. Indeed CR crystallizes more readily than NR does because trans 1,4 configuration allows better molecular packing than cis 1,4 configuration.

3.33.3.1.2 Oxidation and ozone resistance

All unsaturated elastomers are susceptible to attack by oxygen and ozone which ultimately leads to chain scission followed by progressive loss in the physical properties. This aspect of oxidation will be discussed further in a later section. Almost all specialty elastomers have saturated bonds on the main backbone as well as high bond dissociation energy. Thus, specialty elastomers are highly resistance to heat, oxidation and ozone cracking.

3.33.3.1.3 Swelling resistance

The swelling resistance of rubber towards hydrocarbon oil depends on the extent of the polarity of the elastomer. The more the polar groups attached to the rubber molecules the higher is the polarity, and the better is the swelling resistance towards hydrocarbon oil. The solubility parameter of elastomers and liquids determines the extent of compatibility and swelling resistance. The closer the solubility parameters between the elastomer and the liquid, the better is their compatibility. Indeed, the greater the thermodynamic compatibility between liquid and elastomer, the greater the absorption of liquid occurring when both have similar solubility parameters. The solubility parameter δ is related to a parameter to measure the specific interaction between molecules known as cohesive energy density (CED) by the following mathematical relationship.

$$\delta = (\mathrm{CED})^{1/2} \quad [1]$$

$$\mathrm{CED} = (\Delta H - RT)/(M/\rho) \quad [2]$$

where ΔH is the latent heat of vaporization, T is the absolute temperature, M is the molecular weight of the polymer, ρ is the density of the polymer, and R is the molar gas constant. For example, natural rubber has a solubility parameter value of 16.7 and NBR has

a solubility parameter between 21.0 and 22.0 $MPa^{1/2}$. Most of the petroleum oils have a solubility parameter of 16.3 $MPa^{1/2}$. Thus NR will swell markedly in petroleum oil because their solubility parameters are similar. In contrast, NBR has a solubility parameter very much higher than that of petroleum oil, so the two are not compatible. For this reason, polar NBR shows higher swelling resistance than nonpolar NR towards petroleum oil. Elastomers with higher polarity such as polyurethane rubber (AU) show even higher swelling resistance to nonpolar solvents than nonpolar elastomers. Based on the solubility parameter, polar rubbers swell more in polar solvents. Nonpolar rubbers are resistant to swelling in polar solvents.

3.33.3.1.4 Glass-transition temperature T_g

The glass-transition temperature (T_g) is the temperature at which molecular mobility begins to take place, below which molecular mobility is frozen and the elastomer becomes rigid and glassy. The T_g of the elastomer depends on the chemical structure of the elastomer. The presence of a polar atom, side groups, length of side chains, and crosslink reduces molecular mobility which would increase T_g of the elastomer. The glass-transition temperature affects a number of important technological properties such as strength, damping, low temperature flexibility, rolling resistance, wet grip, etc. High T_g elastomers are preferred to low T_g elastomers for applications where high mechanical strength, high damping, and excellent wet traction are required. For applications where excellent low temperature flexibility, low heat generation, high resilience and low rolling resistance are required, low T_g elastomers are preferred to high T_g elastomers.

Table 6 summarizes the respective T_g, ozone cracking resistance, chemical resistance and heat aging resistance of some of the important commercial elastomers.

3.33.4 Rubber Technology and Compounding

3.33.4.1 Mastication and Mixing

Rubbers find very limited applications in their raw form. In their raw form, rubbers may be suitably used as binders and adhesives because of their inherent tack. To become useful products, they have to undergo various processes from mastication, mixing, shaping or fabrication prior to molding, as shown by the schematic flow chart in Figure 5.

3.33.4.2 Rubber Compounding

Rubber compounding is the term used to denote the art and science of selecting and combining elastomers and additives to obtain an intimate mixture that will develop the necessary physical and chemical properties for a finished product. In compounding, one must cope with literally hundreds of variables in materials and equipment. There are three main areas of concern in rubber compounding, namely, (i) to secure certain properties in the finished product to

Table 6 Some important technological properties of some important commercial elastomers

Elastomer	*T_g (°C)*	*O_3 resistance*	*Swelling resistance (%)[a]*	*Heat resistant up to (°C)[b]*
NR	−72	L	200 (120 °C)	100
SBR	−63	L	130 (120 °C)	100
BR	−112	L	>140 (70 °C)	100
EPDM	−55	H	>140 (70 °C)	150
IIR	−66	M	120 (120 °C)	150
CIIR	−66	M	>140 (150 °C)	150
ACM	−22 to −40	H	25 (150 °C)	175
CO	−26	H	5 (150 °C)	150
CR	−45	M	65 (120 °C)	125
NBR (med ACN)	−34	L	10 (100 °C)	125
MVQ	−120	VH	50 (150 °C)	225
CSM	−25	H	50 (150 °C)	150
H-NBR	−30	H	15 (150 °C)	150
FKM	−18 to −50	VH	2 (150 °C)	250
EU	−55	H	40 (100 °C)	100

[a]Swelling after 70 h in ASTM oil 3.[5,9]
[b]Classification after ISO/TR 8461, aerobic condition, Method ISO 4632/1 3 days, (Retention properties).[9]
L = low resistance M = medium resistance H = high resistance.[5,9]

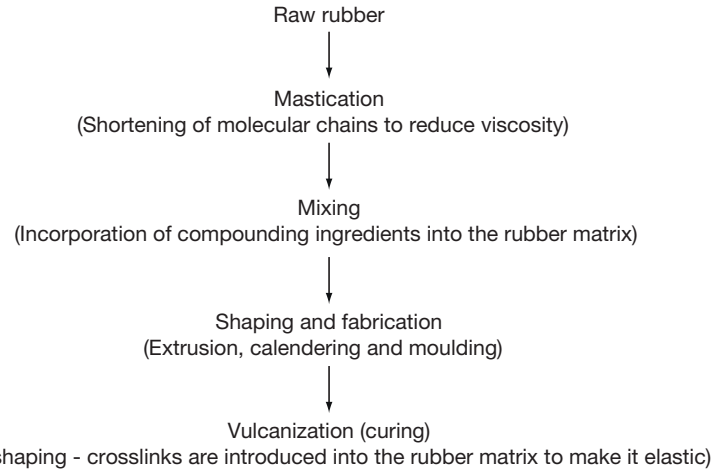

Figure 5 Schematic flow process chart.

satisfy service performance; (ii) to be able to meet processing characteristics for efficient utilization of available equipment, and (iii) to meet conditions (i) and (ii) at the lowest possible cost. In other words, the most important criteria in compounding are to secure an acceptable balance among demands arising from the three concerned areas.

Theoretically, a rubber compound may consist of an elastomer and a cross linking agent. However, in practice, a rubber compound may contain 5 ingredients or even more than 10 ingredients, depending on the intended products, types of application and their service conditions. Each ingredient has a specific role and function(s). Each has an impact on properties, processability, and price. The real challenge is to develop a high quality rubber product at the lowest cost possible. The materials utilized by the rubber compounder can be classified into nine major categories, which are defined as follows:

- *Elastomers*: The basic component of all rubber compounds may be in the form of rubber alone, or master batches of rubber–oil, rubber–carbon black, or rubber–oil–carbon black.
- *Vulcanization agents*: These materials are necessary for vulcanization processes where chemical crosslinks are introduced into the rubber matrix to form a three-dimensional network. Crosslinks inhibit permanent flow under deformation or heat and prevent dissolution in solvents. Strength, stiffness and resilience increase upon cross linking, and set, stress-relaxation and creep decrease.
- *Accelerators*: In combination with vulcanizing agents, these materials reduce the vulcanization time (cure time) by increasing the rate of vulcanization. In most cases, the physical properties of the products are also improved.
- *Activators*: These ingredients form chemical complexes with accelerators, and thus aid in obtaining the maximum benefit from an acceleration system by increasing vulcanization rates and improving the final properties of the products.
- *Age-resistors*: Antioxidants, antiozonants, and other materials are used to slow down ageing processes in the vulcanizates.
- *Fillers*: These materials are used to reinforce or modify physical properties, impart certain processing properties, and reduce cost.
- *Processing additives*: Formerly known as processing aids, the new term currently used is processing additives. These are materials used to modify rubber during the mixing or processing steps, or to aid in a specific manner during extrusion, calendering, or molding operations.
- *Softeners*: They are materials that can be added to rubber either to aid mixing, produce tack, or extend a portion of the rubber hydrocarbon (e.g., oil extended).
- *Miscellaneous ingredients*: These materials can be used for specific purposes but are not normally required in the majority of rubber compounds. They include retarders, colors, blowing agents, abrasives, dusting agents, odorants, etc.

3.33.4.3 Vulcanization

Vulcanization is a process of cross-linking rubber molecules chemically with organic/inorganic substance through the action of heat and pressure. The

rubber which is cross linked chemically is known as vulcanizate. The introduction of crosslinks into the rubber matrix may be comparatively few in number but are sufficient to prevent unrestricted flow of the whole molecules past neighboring ones. The low concentration of crosslinks implies that the vast majority of the segments making up the long chain molecules are free to move by virtue of kinetic energy. An unvulcanized rubber dissolves completely in its solvent. In contrast, a vulcanized rubber only swells. The chemical crosslinks prevent complete dissolution. A vulcanized rubber in this sense is a solid and will retain its shape and dimensions.

Vulcanization is a very important process in the rubber industry and conducted at relatively high temperatures (140–200 °C). For latex dipped goods, vulcanization is conducted at relatively low temperatures (60–120 °C) and requires no pressure as the latex is in fluid form and flows to take the final shape of the former and mold.

One of the most important chemicals in vulcanization is the cross linking agent. Elemental sulfur is the most widely used cross linking agent in the rubber industry because it is very cheap, abundant and easily available. Besides, sulfur is very easy to mix and readily soluble in the rubber. By varying the amount of sulfur to the accelerator ratio one can get different types of crosslink in the rubber matrix. **Table 7** summarizes the types of sulfur vulcanization system,[10] nature of crosslinks produced and their influence on technological properties. Thus sulfur vulcanization provides flexibility as one can control the type of crosslink intended for specific use or applications. The most basic requirement for sulfur vulcanization is the availability of double bonds on the rubber hydrocarbon. The nonsulfur cross-linking agents include organic peroxides, quinines and their oximes and imines, metallic oxides and high energy radiation. The detailed mechanisms of vulcanization with these vulcanizing agents are discussed by Elliot and Tidd.[10]

There is another type of sulfur vulcanization system known as soluble efficient vulcanization (EV)[10] intended for engineering products that require consistent stiffness, low creep, low stress-relaxation and low set. This vulcanization system employs certain soluble accelerators, activators, and sulfur that completely dissolve in rubber giving a truly homogeneous compound.[10] In practice, this is achieved by selecting accelerators and activators that have a fairly high solubility in rubber at room temperature. Suitable accelerators for soluble EV include diphenyl guanidine, tetrabutylthiuram disulphide and *N*-oxydiethylenebenzothiazole-2-sulphenamide. Zinc oxide is insoluble in rubber, but it has to be included in the system as it plays a major role in sulfur vulcanization. However, 2-ethyl hexanoic replaces the common coactivator stearic acid as the latter reacts with zinc to form an insoluble zinc stearate which induces creep and the former forms a rubber-soluble zinc salt. The sulfur dosage employed in soluble EV must not exceed 0.8 pphr (parts per hundred of rubber) to ensure that it remains dissolved in the rubber and with no tendency to bloom to the rubber surface.

Nonsulfur vulcanization such as the peroxide vulcanization system produces carbon–carbon type of crosslink that gives excellent heat aging resistance and very low compression set. However, the mechanical strengths are lower than polysulfidic and monosulfidic crosslinks. The choice of vulcanization system depends on the service environment as well as the mode of deformation for the intended rubber product.

3.33.5 Rubber-to-Metal Bonding – Engineering and Automotive Applications

Most of the rubber springs involve bonding of rubber to metal. In many cases the metal parts are required for fixing purposes, particularly those of automotive components such as rubber bushes, engine mounts

Table 7 Sulfur vulcanization systems, types of crosslink produced and their effect on technological properties

Vulcanization system	*Sulfur*	*Accelerator*	*Type of crosslink*	*Technological properties*
Conventional	2.0–3.5	1.0–0.4	Polysulfidic	Increase tensile and tear strengths, high compression set, and poor heat aging
Efficient (EV)	0.3–0.8	6.0–2.5	Monosulfidic	Excellent heat aging, low compression set, low tensile, and tear strengths
Semi-EV	1.0–1.7	2.5–1.0	Mixtures of poly, di- and mono	Compromise or balance in terms of strength and heat aging

and couplings. **Figure 6** shows some typical rubber-to-metal bonded products. In tank lining, the main function of rubber is to protect the metal against attack by corrosive chemicals as well as to protect the metal parts from oxidation by air and moisture, which leads to rusting.

The laminated rubber bearing consists of alternate layers of metal plates. The metal plates serve to restrain the lateral expansion of the rubber on compression. Because of restriction at the rubber metal interface, due to friction or when the rubber is bonded to metal, the rubber bulges at the end plates to maintain a constant volume. As a result, the effective compression modulus is dependent on the shape factor, S, defined as the ratio of loaded area to force free area.[2]

$$S = \text{Loaded area}/\text{Force free area} \quad [3]$$

For a rectangular rubber block of length L, width W, and thickness h, shape factor S is given by eqn [4]:

$$S = LW/[2h(L + W)] \quad [4]$$

The dependence of the compression modulus on the shape factor has a significant advantage where the vertical stiffness increases substantially, by inserting horizontal metal spacer plates into the rubber. For a rectangular rubber block having length L, width W, and height h, the shear stiffness and compression stiffness are given by eqns [5] and [6] respectively.

$$k_s = GA/h \quad [5]$$

$$k_c = 3G(1 + 2S^2)A/h \quad [6]$$

Here, G is the shear modulus of the vulcanizate and A is the cross-sectional area of the rubber surface subjected to shear or compression. Equation [6] shows

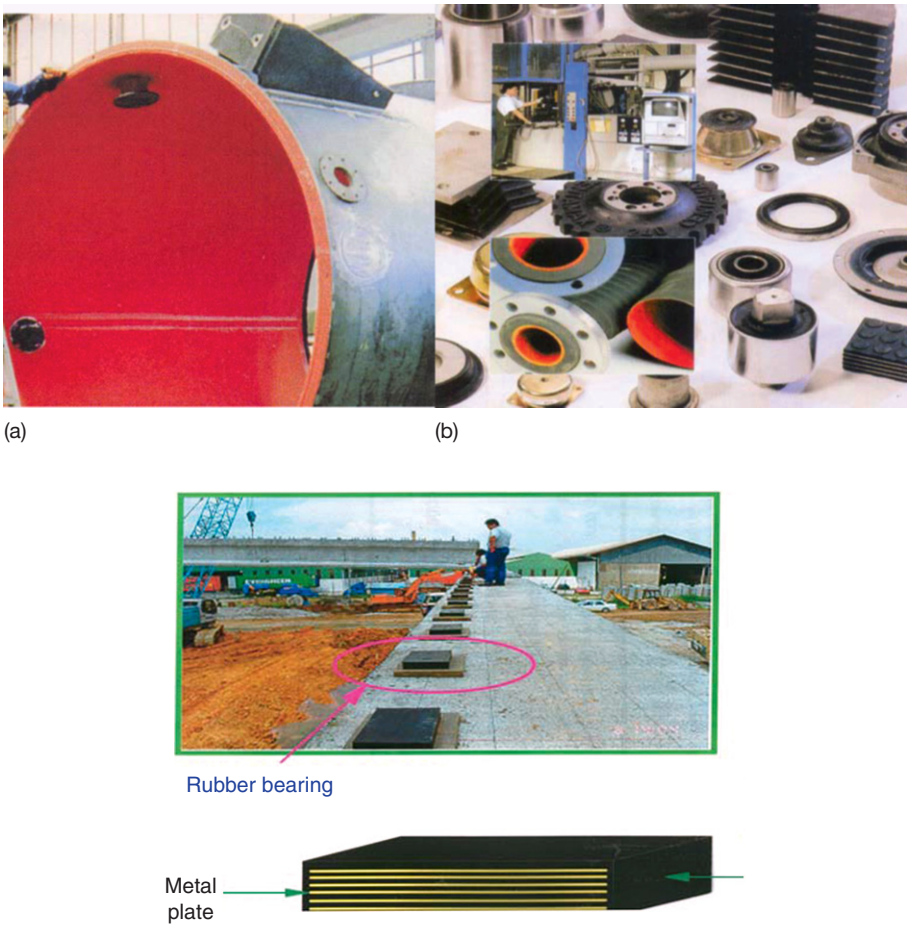

Figure 6 Rubber-to-metal bonding products – (a) tank lining (LHS), (b) various automotive rubber products (RHS) and (c) below rubber bridge bearing.

that the compression stiffness can be increased substantially by increasing the shape factor. The shape factor does not affect shear stiffness. For these reasons, laminated steel rubber bearings are used in bridges, where high compression stiffness is necessary to support all dead and live loads of the deck, and very low shear stiffness to accommodate movements associated with thermal expansion and contraction due to temperature changes.

To achieve efficient bonding at the rubber–metal interface, it is necessary that the rubber is chemically bonded to the metal surface. This is achieved in practice by following proper procedures laid down in the following section.

3.33.5.1 Bonding of Rubber to Metal

3.33.5.1.1 Preparation of metal plates

The metal plates must be clean and free from any contamination such as oil, grease, protective coating, and rust. Exposing the contaminated metal surface to the vapor of a suitable organic solvent (e.g., chlorinated solvent) removes oil and grease. The next step is to remove metal oxides and rust on the metal surface, usually by the sandblasting technique or wire brushing. Apart from cleaning, sandblasting increases the surface area, which is very beneficial for strengthening the bonded area. Acid etching provides an alternative means of removing metal oxides from the metal surface.

It is very vital that the metal surface is completely free from oil, grease and rust to ensure efficient wetting of the bonding agent on the metal surface so that during vulcanization the bond formed between rubber and metal via the bonding agent is very strong. However, a few precautions need to be observed when sandblasting on the metal surface. The grit size, gun pressure and shooting distance must be correct to get the right surface topology, thus avoiding excessive wear or too little wear.

3.33.5.1.2 Types of bonding agent and methods of applications of bonding agent to metal plates

The common bonding agents for bonding rubbers to metals include ebonite solution or sheet, brass and proprietary adhesives. In the past, the bonding agent as well as the lining material for making tank lining was ebonite solution and calendered ebonite sheet. The ebonite compound contains a high amount of sulfur, about 25–35 pphr. This high sulfur content makes ebonite a hard and brittle material. Indeed ebonite is a thermoset as it is highly cross linked. The high sulfur content of ebonite introduces high polarity that makes it a very suitable bonding agent. Despite the superior chemical resistance of ebonite, there are a few limitations such as its brittleness after cure, long cure time and potential of fire hazard due to exothermic reaction during curing, especially when a thicker lining is involved. For this reason, soft rubber linings are preferred to ebonite linings.

Brass is a very good bonding agent, and is widely used in the tire industry. Brass is coated on steel wire cords by the electroplating process. Brass-coated steel wire cords are used as breakers or belts placed underneath the tread and on top of the carcass of the green tire. During vulcanization, the sulfur forms covalent bonds with both the rubber and the component metals of the brass, leading to a very strong bond.[11]

In most rubber-to-metal bonded products, a proprietary bonding agent is preferred to the other two bonding agents. A proprietary bonding agent usually requires two coatings, *viz.* a primer and an adhesive cement. There are reasons why a two-coat system offers more insurance for the rubber to metal bond. The first coating known as a primer helps to eliminate corrosion in corrosion-prone metals when they are in contact with the rubber.[12] By using a primer, secondary cement (second coating–adhesive) that has a greater degree of bondability to the stock being used can be selected, rather than a one-coat system.[12] It is claimed that the two-coat system allows more metal adhesion into the primer, and more stock adhesion into the cement coat.[12] This results in a higher intrinsic bond with the two-coat system than a single coat system.

Bonding agents are applied by painting, spraying or dipping on treated metal parts in the form of a solution or aqueous suspension.

3.33.5.1.3 Molding of rubber-to-metal bonded parts

Finally, the dried, coated metal parts are loaded into the mold and the rubber is vulcanized in contact with these substrates by the conventional rubber molding techniques such as compression, transfer and injection molding. It is during this vulcanization process that the rubber is chemically bonded to the metal surface when the cross linking agents react with the adhesive.

However, in the case of tank lining, the method is different from the conventional rubber-to-metal bonded products. The method of applying calendered rubber sheeting onto the prepared metal surfaces is

analogous to that of applying rolls of wallpaper to the walls of a room. However, care must be taken to avoid entrapment of air between rubber and metal. The rubber sheet is laid down at the correct angle, and is rolled down into close contact with the adhesive. Applying the rubber sheet at the corner or edges of the tank is quite tricky. In practice, this is achieved by making joints at corners by inserting and rolling down an extruded rubber fillet of triangular cross-section and forming the sheet joints on top of the fillet. This technique gives to the lining a well finished appearance and reduces the danger of weak joints occurring in corners.

Upon completion of laying the rubber sheet onto the metal surface, the covered lining tank is usually allowed to rest for at least 24 h before being vulcanized. This resting period allows any air trapped between rubber and metal to diffuse, apart from enabling the adhered rubber sheet to recover and settle down before it is heated.

3.33.5.2 Vulcanization

It is usually done in an open steam autoclave for tanks or vessels that are small enough to go into the autoclave. When the lined vessel is too large to be accommodated in an autoclave it may be vulcanized in one of the following methods:

3.33.5.2.1 Low or high pressure steam

This method is applicable to a vessel that has sufficient strength to withstand internally applied pressure. This procedure can be adopted if the vessel such as road or rail tank cars can be lined and then sealed and bolted to give a strong and steam proof pressure container. The steam pressure is passed through the lined vessel to the desired vulcanization temperature until the rubber is fully vulcanized. There are some elements of danger when dealing with high pressure steam. So it is very important that all the safety regulations are met in terms of design and material of the vessel. The work should be done under skilled engineering supervision.

3.33.5.2.2 Water curing technique

This method is suitable for tanks or vessels that are too weak structurally to be put under steam pressure. Here, the lined tank is filled with water or brine. The water is heated by passing live steam into the water until it approaches boiling point. This temperature is maintained for a few hours until the rubber is fully vulcanized. Care must be taken to ensure that live steam does not impinge on the rubber lining to avoid the occurrence of a large blister between the rubber and metal at the point of impingement. It is necessary to conserve heat by shielding the unit against draughts and cold to minimize temperature variations which would affect the uniformity of the cure.

3.33.5.2.3 Hot air or ambient temperature vulcanization

This method is suitable for tanks or vessels which do not work with the methods discussed above. The choice of accelerator is very important. Ultrafast or very fast accelerator is usually used in the rubber compound. Care has to be taken to ensure that the rubber does not vulcanize prematurely (scorched) before it is applied onto the treated metal surface. One of the means to overcome the problem is to avoid mixing the accelerator and sulfur together, but to prepare sulfur masterbatch and accelerator masterbatch separately. The two masterbatches are blended together just prior to calendering, and the calendered sheet applied as soon as possible to the metal to avoid the risk of being scorched.

3.33.5.3 Types of Bond Failure and Possible Remedies

A rubber shear mount may be expected to deform up to 300% shear strain, and the mean shear stress acting on the rubber-to-metal bond can be as high as 10 MPa or 2/3 tons per square inch.[11] Steel laminated rubber bearings for bridges must have a minimum bond strength of about 9 N mm^{-1} (MS 671, 1991).

It is important to observe the failure mode that occurs in rubber-to-metal bonded products because it throws some light and clues to the root cause of the problem. It is usual to conduct peel test to determine the interfacial bond strength between the rubber and metal. There are two basic types of bond failure either adhesive or cohesive. Adhesive failure may occur at the interfacial between the rubber and substrate, or between cement and substrate. Cohesive failure occurs within the rubber itself. There are three modes of adhesive failure.[13] First is called CM failure that takes place between primer and metal interface. Second is CP failure that occurs at the primer to cover cement interfacial. Third is RC failure where the bond fails at the rubber–cover cement interface. RC failures are the most common and the most difficult to solve.[13] There are a number of causes, which bring about these bond failures. They include the following: metal surface not cleaned efficiently due to poor cleaning procedure,

contamination of metal surface during handling, incomplete wetting of adhesive on the metal surface, variations of temperature of metal surface, precured adhesive, sweeping of adhesive during molding etc.[13] There are remedies to overcome these problems. First, ensure that the metal surface is free from all forms of contamination. Second, avoid contamination of metal surface during handling. Third, apply the primer and adhesive cement onto the metal surface evenly by taking care of the correct viscosity of the adhesive, and correct spraying distance and thickness of the adhesive film. Fourth, use the correct type of adhesive and follow strictly the instruction and procedure recommended by the chemical supplier.

If during the peel test, cohesive failure occurs within the bulk of the rubber, then this indicates that the interfacial bond strength between the rubber and metal plate via the bonding agent is stronger than the cohesive strength of the rubber itself.

3.33.6 Oxidation of Rubber

Metals oxidize in the presence of air and water and consequently they corrode, become rusty and weak. **Figure 7** shows the old version of using steel rollers to accommodate movements of the bridge deck brought about by expansion and contraction due to temperature changes.[14] The steel rollers corroded and suffered high wear and tear. In contrast, laminated steel rubber bearing did not show any sign of wear out after nearly twenty years of installation.[14] However, this does not mean that elastomeric bearing will last forever. Like metals, rubbers are also prone to corrosion. Corrosion of rubbers is associated with the aging process known as degradation. All unsaturated rubbers are subject to degradation due to the attack of heat, ultraviolet (UV) light, oxygen, ozone etc. The more is the amount of unsaturation the more it is susceptible to degradation. The term aging as applied to rubber, covers a variety of phenomenon arising out of the factors described above. Aging properties of raw rubber differ from vulcanized rubber because of the latter's specific network structure and extra network material. When natural rubber is heat-aged in the presence of oxygen or air, it invariably loses strength, in particular its tensile strength decreases. The pattern of modulus change during aging is not so straight forward because there are two opposing reactions which can occur simultaneously. One is degradation of the molecular chains and crosslinks which causes softening; the other is additional cross linking which causes stiffening. Under any given set of aging conditions (time and temperature) either softening or stiffening reactions may predominate depending on the type of vulcanization system, type of filler and antidegradants employed in the rubber compound.

Oxygen reacts with rubber only after the rubber has been acted upon by energy. This is usually from UV light, heat or mechanical energy (flexing). This energy dislodges a hydrogen atom from the rubber molecule, resulting in the formation of a radical. The oxidation of polymer with elemental oxygen is called autoxidation because it is an autocatalytic. The rate of autoxidation is affected by temperature, the presence of catalyst and also the presence of antioxidant. When the oxygen attacks the rubber it produces hydroperoxide. The hydroperoxides break to form free radicals. This is an autocatalytic, self generated free radical process. The autoxidation process involves three main stages, namely, initiation, propagation and termination. In view of the complexity of autoxidation reaction with rubber, Bolland and Gee[15,16] used model olefins to study the kinetics of autoxidation. **Figure 8** shows the mechanism of autoxidation as proposed by Bolland.[15,16]

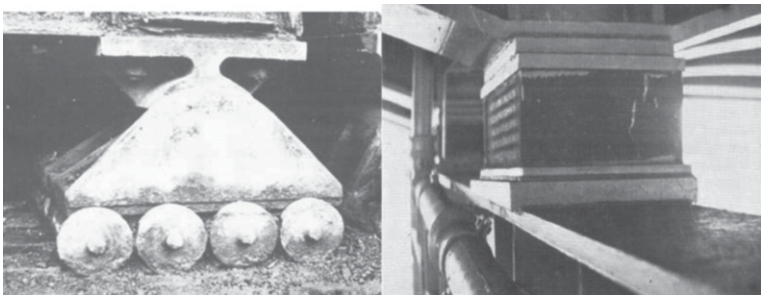

(a) (b)

Figure 7 (a) Steel roller bridge bearing and (b) steel laminated rubber bearing installed in 1955. Adapted from Mullins, L. *Proc. Rubb. in Eng. Conf*. Kuala Lumpur, 1974, pp. 1–20, with permission from the Malaysian Rubber Board.

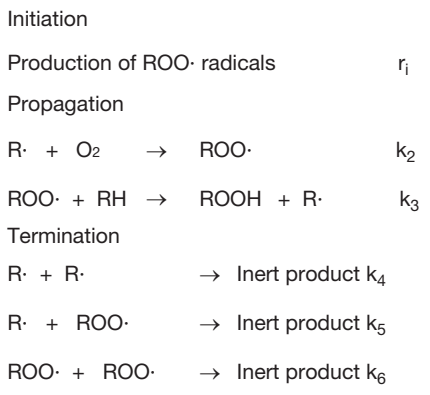

Figure 8 Mechanism of autoxidation of natural rubber as outlined by Bolland. Adapted from Barnard, D.; Lewis, P. M. In *Natural Rubber Science and Technology*; Robert, A. D., Ed. Oxford University Press, 1988; Chapter 13, pp 621–673, with permission from · · ·.

The autoxidation is initiated with the generation of free radicals due to the relatively facile homolysis of traces of peroxide present in the elastomer.[17] The rate of oxidation is related to the concentration of the hydroperoxide [ROOH] as shown by eqn [I] below[16].

$$r_i = k_i[\mathrm{ROOH}]^2 \qquad [\mathrm{I}]$$

The resultant free radicals react with oxygen to form the deleterious peroxides and propagate the autoxidation reaction. The rate of propagation is controlled by the hydroperoxide yields and those of decomposing. The hydroperoxide yields for a large number of olefins range from almost 100% downwards to values controlled by side reactions of the peroxy radicals, such as addition to olefinic double bonds, when hydrogen abstraction becomes relatively difficult.[16] Such side reactions would continue the propagation chain. However, when the value of the rate constant k_2 becomes large, the reaction of alkenyl radicals with oxygen become independent of oxygen pressure. Under these conditions, rate-determining step is no longer controlled by the rate constant k_3, of the hydrogen abstraction step. Termination would occur primarily by the interaction of alkenyl radicals. Then the propagation rate is given by eqn [II] below[16].

$$r = r_i^{1/2} k_2 k_4^{-1/2}[\mathrm{O_2}] \qquad [\mathrm{II}]$$

Termination occurs solely by the mutual destruction of peroxy radicals and represented by the following rate equation[16]:

$$r = r_i^{1/2} k_3 k_6^{-1/2}[\mathrm{RH}] \qquad [\mathrm{III}]$$

The outcome of this autoxidation is either chain-scission or cross-linking. If chain-scission occurs, the degraded rubber will be soft and tacky. On the other hand, if cross linking occurs the degraded rubber will be hard and brittle. In both cases, the mechanical strength of the rubber decreases markedly. Model olefins were used to study the mechanism of oxidation of NR due to complexity of the oxidation reaction in particular when the rubber is vulcanized.[16] The oxidation of rubber vulcanizate is technologically important since the absorption of only a small amount of oxygen (1%) by rubber vulcanizate results in a considerable change in the physical properties.

It is believed that the oxidation of natural rubber follows the same route and analogous to that of the model olefins where the polyisoprene chain undergoes scission.[16] An essential concept of this process is the number of molecules of oxygen absorbed per scission event. According to Bolland,[15] the oxidation reaction would finally lead to an alkoxy radical disproportionate to butan-2-one-4-al rather levulinaldehyde, and the vinylic radical would have to be oxidized further to the methyl ketone end group. Minute amount of certain heavy metals such as copper, iron and manganese catalyze autoxidation reactions. However, this catalytic action can be prevented by applying protective or chelating agent such as metal deactivator like *p*-phenylenediamines.

In the case of vulcanized rubber, the oxidation reaction is more complex than that of raw rubber since the various different types of crosslink (e.g., ploysulfidic, disulfidic, monosulfidic, cyclic sulfides, conjugated dienes and treines, etc.) present in the network structure may affect oxidation in some way or another.[16] Most types of sulfur vulcanizates initially hardens on aging before degradation occurs. This hardening is due to cross linking associated with oxidative reactions of sulfur species in the network that takes place before chain scissions take place.[16]

Barnard and Lewis[16] listed out some useful and important points concerning chain scission mechanism for unprotected NR at modest temperature as follows:

- Scission occurs once approximately for every 20 molecules of oxygen absorbed.
- The scission is of the rubber chain even in peroxide or sulfur vulcanizates although concomitant crosslink can occur in the latter.
- Kinetically, scission appears to take place in the propagation step.

- Each scission event results in a stable terminal ketone group being formed on one of the new chains and a transient terminal aldehyde group on the other.

Since autoxidation results in chain scission, means and ways were introduced to determine accurately chain scissions caused by a known quantity of oxygen absorbed. A parameter known as scission efficiency ε defined as the number of molecules of oxygen absorbed which bring about one scission event[16] was introduced to monitor chain scission quantitatively. There are two methods either physical or chemical to monitor chain scission. The common physical methods involved measuring molecular weight reduction, stress-relaxation, sol–gel analysis, and stress–strain characteristics.[16] For example, in stress-relaxation method, a rubber sample of a uniform cross-section is held at a constant extension and maintained at a constant temperature. When a network is oxidized due to the cleavage of stress-supporting chains, then the stress would decay and this event would lead to occurrence of stress-relaxation. The change in moles of stress-supporting chains per gram can be calculated from eqn [7][16]:

$$f_t/f_0 = N_t/N_0 \qquad [7]$$

where the subscripts t and 0 refer to the samples after time t and time zero respectively, and f derived from the statistical theory of rubber elasticity[18] is given by eqn [8]:

$$f = \rho NRTA_0(\lambda - \lambda^{-2}) \qquad [8]$$

where ρ is the density of rubber, N is the number of moles of stress-supporting chains per gram, R is the gas constant, T is the absolute temperature, A_o is the unstrained cross-sectional area, and λ is the extension ratio. Stress-relaxation method has the advantage of being able to monitor scission event continuously, and if the amount of oxygen absorbed is also known then the scission efficiency ε can be calculated.[16] However, on a short time scale, the decay in stress level as function of time at constant deformation and temperature is associated with the rearrangement of molecular chains and it is predominantly attributed to viscoelastic behavior of the rubber.

Almost all technical specifications of elastomeric products require passing an aging test. The use of aging tests is extremely important in assessing the service life of elastomeric products because properties of vulcanizate could change during service. The basic principle of the test is to expose rubber test-pieces to air at an elevated temperature (70 or 100 °C) for a specified period (7 or 14 days or longer). This so-called accelerated aging test causes deterioration of rubber in air due to combined effects of oxidative and thermal aging. The tensile properties, set and hardness are measured on these samples before and after ageing. If minor changes in these properties result, long service life may be expected; if appreciable changes occur, service life may be short. However, it must be stressed here that accelerated ageing test is a useful quality control and specification tests. There are significant difficulties in predicting service life from accelerated aging test. Use of test temperatures much above the anticipated service temperature is not advisable because the correlation between the results of such tests and service performance becomes increasingly tenuous.

3.33.7 Ozone Cracking of Rubber

Apart from oxygen, all unsaturated elastomers are also susceptible to ozone attack although ozone concentration in the outdoor atmosphere at ground level is about 1 pphm (part per hundred million of air by volume).[19,20,21] However, this can be significant because the reaction of ozone with the double bond is extremely fast and causes cracking on strained rubber. The cracks appear slowly at right angle to the direction of the strain applied, that grow slowly and consequently lead to a break of the vulcanizate. Ozone being very reactive attacks the double bonds of the rubber and produces ozonide that cleaves to produce zwitterions.[17] The zwitterions are unstable and will breakdown to form other zwitterions. These zwitterions may react with other zwitterions to produce diperoxide compound, or react with carbonyl compound to produce ozonide. In both cases, the ultimate result is chain scission. The mechanism of ozone attack on olefin is as shown in **Figure 9**.[17]

However, there is a subtle difference between ozone cracking and auto-oxidation where the former requires a certain critical strain level (~5% for unprotected NR) for its occurrence.[19,20,21] The severity of ozone cracking increases rapidly with strain level. Braden and Gent,[19] and subsequently Lake *et al.*[20,21] investigated various factors affecting ozone cracking. For example, Lake and Thomas[20] came out with a boundary layer theory for ozone attack on rubber surface to explain the rate of ozone crack growth. According to their theory, the variation in

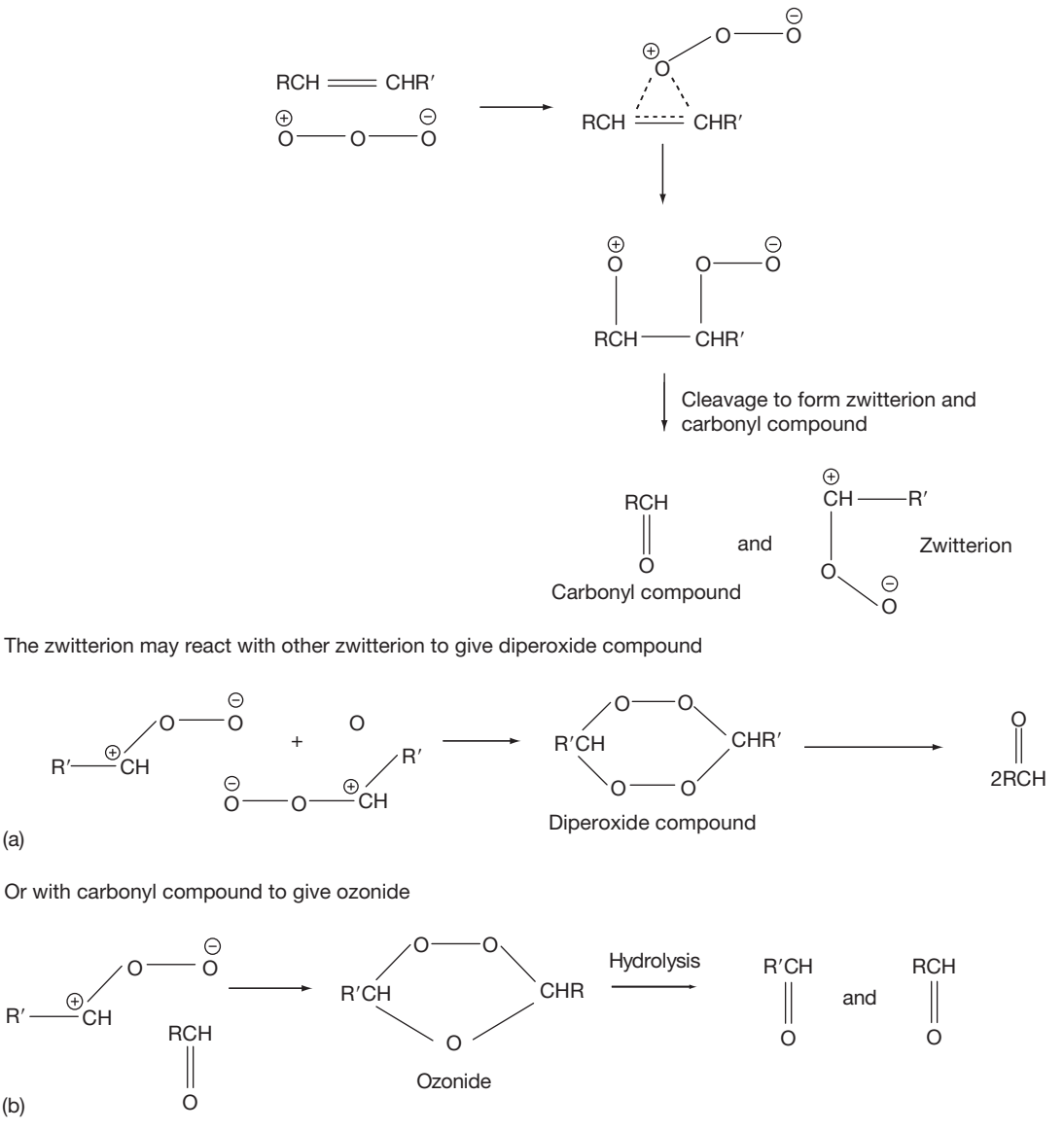

Figure 9 Mechanism of ozone attack on olefins.

the rate of ozone attack on stretched rubber surfaces produced by changes in the air velocity and magnitude of the strain is controlled by the diffusion of ozone across the relatively stationary boundary layer adjacent to rubber surface. The boundary layer effect is important because of the readiness with which ozone is destroyed by stretched rubber.[20] As mentioned earlier, ozone cracking occurs only in elastomers subject to tensile stresses. Elastomeric components used in compression will crack only in the regions of the surface where tensile stresses are induced. These cracks are unable to penetrate very far because they soon encounter compressive rather than tensile stresses. Thus ozone cracking is not a serious problem for large elastomeric components such as rubber bearings which are used in compression. Nevertheless, ozone cracks are unsightly and may initiate fatigue crack growth, which ultimately leads to mechanical failure. In view of this deleterious effect, it is necessary to carry out test on ozone resistance. The test involves exposing the stretched test-pieces (20% strain) in an ozone-rich atmosphere at a fixed temperature (23 or 40 °C) and inspecting the surfaces for cracks with the aid of a magnifying

glass at intervals of time. If cracks are not observed after completion of test, the vulcanizate is said to have good resistance to ozone cracking.

3.33.8 Heat Aging Resistance

Elastomers can survive over long periods in service at ambient temperatures without any measurable deterioration if the products are sufficiently thick. For a thick section of rubber, the availability of oxygen will be limited by diffusion, and components with bulky rubber layers can be considerably more resistant to elevated temperatures than thin rubber sections. For example, bearing pads of NR installed in 1890 had been examined, and although the outer 1–2 mm of rubber had degraded after 96 years of exposure to the atmosphere, the inner core of the rubber was still in good condition as shown by the photograph in Figure 10.[2] Rubber samples taken from the interior portion were found to retain good physical properties as that of freshly prepared compounds.[2] At sufficiently elevated temperatures, all types of elastomer will undergo degradation. However, conventional NR vulcanizates can be used safely at 60 °C, the maximum ambient temperature likely to be encountered practice.[2] At temperatures of 300 °C and above, NR vulcanizates first softens as molecular breakdown occurs, then resinify, becoming hard and brittle.[2] Flammable vapor are emitted and ignition occurs. However, the rate of burning is extremely slowly for the case of large block rubber.[2]

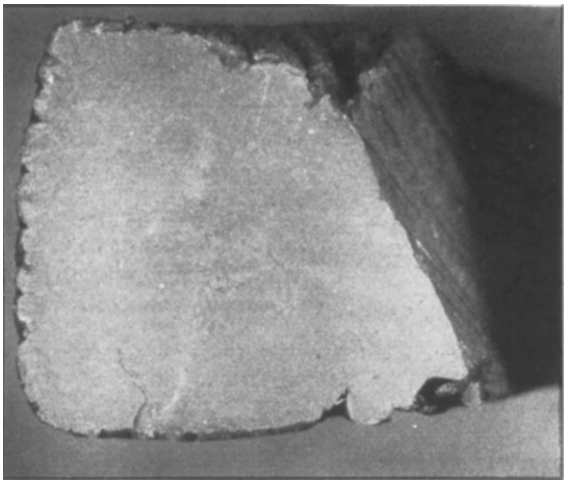

Figure 10 Cross-sectioned view of a 100-year old bridge bearing pad showing the very small depth of penetration of atmospheric degradation. Adapted from Fuller, K. N. G.; Muhr, A. H. *Engineering design with natural rubber, NR Technical Bulletin*, 5th ed.; The Malaysian Rubber Producers' Research Association, London, 1992; pp 1–33, with permission from Tun Abdul Razak Research Centre, Brickendonbury Hertford, England.

In recent years, new performance demands for automotive elastomers have been proposed[22] to perform at high operating temperatures. This move was made to accommodate increasing concern for improved fuel economy, which resulted in a significant downsizing and redesign of the automobile. Concomitantly the engine compartment became smaller and more difficult to cool thus raising the temperature of the under hood. Current automotive elastomers are expected to perform well under a 120 °C in-service temperature at least until the life of the car.[22]

There is a growing expectation those future automotive elastomers to perform well in a 150 °C environment for over 100 000 miles.[22] This is a clear signal that specialty elastomers would find very strong markets over general-purpose elastomers for high temperature performance.

3.33.9 Flex Cracking

Flexing and cyclic stresses can lead to premature failure during service. There are two basic mechanisms of crack growth, (i) ozone crack growth, due to primarily chain scission, and (ii) mechanico-oxidative crack growth, due to mechanical rupture at the tip of a flaw, which is considerably facilitated by the presence of oxygen.[23] Both types of growth can occur under static or dynamic conditions or together. The amount of crack growth in a given time is directly proportional to the ozone concentration. The crack growth rate dc/dt of a single ozone crack under static conditions is given by eqn [9]:

$$dc/dt = \alpha q \qquad [9]$$

where q is the ozone concentration and α a constant (the rate at unit ozone concentration) which is a property of the rubber.[23] The cyclic crack growth rate is given by eqn [10]:

$$r = (dc/dn)\text{ozone} = (F/f_f)\alpha q \qquad [10]$$

where F is the time fraction of cycle for which the test-piece is strained, and f_f is the frequency.[23] Based on fracture mechanics approach, and assuming that the growth of naturally occurring flaws of a fatigue test has the same characteristics as that of a crack growth test, Lake and Lindley[23] worked out

the fatigue life of vulcanized elastomer as given by eqn [11]:

$$N_f = 1/(16BW_s^2 c_0) \qquad [11]$$

where N_f is the number of cycles to failure from a naturally occurring flaw of size c_0. B is the crack growth constant, and W_s is the strain energy density. Thus the fatigue life N can be predicted from known parameters of eqn [11].

3.33.10 Oil Absorption

An unvulcanized elastomer becomes solution when immersed in its solvent; in contrast, a vulcanized elastomer will only swell. The extent of swell depends on the amount of solvent absorbed, which in turn depends on the crosslink concentration and types of solvent. Swelling is undesirable because apart from dimensional instability, the modulus and mechanical strengths are all decreased making the swollen vulcanizate unsuitable for most engineering applications.[2] In the case of rubber-to-metal bonded, bond failure occurs if the liquid is able to reach the metal plate. **Figures 11 and 12** show some of the typical automotive elastomeric components such as fuel and oil hoses, gaskets, O-rings and seals which are in contact with automotive fuels. These rubber components are thin and susceptible to damages when swollen excessively by the oil. Additives such as ethanol, methanol, and methyl *t*-butyl ether are being placed in gasoline with a view to improve its octane number.[22] Increasing the alcohol content of the gasoline increases the amount of swell, which is very undesirable not only because of dimensional instability, but also reduces tensile strength and elongation at break of the swollen elastomer.

It is well established that swelling is diffusion-controlled and the volume of liquid absorbed is initially proportional to the square root of the time of immersion.[2] For most organic liquids, the rate of penetration depends on their viscosity rather than

(a) (b)

Figure 11 Automotive rubber products in contact with oil and heat: (a) hoses – hydraulic, fuel, gasoline pump, and steam hose and (b) gaskets, O-rings, seals, and exhaust hanger, etc.

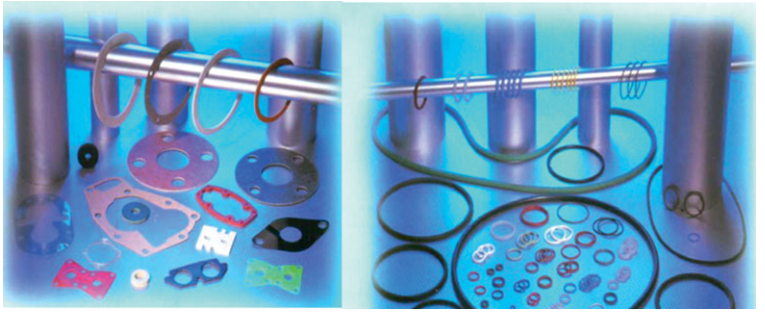

(a) (b)

Figure 12 Automotive rubber components: (a) gaskets and (b) O-rings and seals.

their chemical nature[2]. **Figure 13** shows the time–viscosity relationship for the liquid to penetrate 5 mm into the rubber interior.[2]

For NR, it takes about 4 days for a volatile liquid such as toluene to penetrate 5 mm depth, 1–2 years for engine lubricating oil, and about 30 years for a petroleum jelly, even with continuous immersion.[2] It is possible to estimate the distance of liquid in a given time provide that the penetration rate is known.[2] Alternatively, the viscosity of the liquid may be used if penetration rate is not known since the penetration rate is related to viscosity as shown earlier in **Figure 13**.

Southern[24] has introduced a nomogram as illustrated in **Figure 14** to facilitate the calculation in estimating the penetration depth of liquid into the elastomer. Although the data were obtained for NR, but would be expected to work with other elastomers of similar T_g.[24] As an illustration to use the nomogram, Southern[24] has calculated, a liquid with penetration rate of 7×10^{-5} cm $s^{-1/2}$ would take 4 weeks to penetrate 1 mm, but 100 years to penetrate 40 mm of the rubber block. The penetration rate–viscosity relationship does not hold for water because of the presence of hydrophilic impurities which complicate transport of water in elastomers.[24]

3.33.10.1 Effect of Crosslink Concentration and Polarity on Swelling Resistance

Natural rubber (NR) latex has found very wide applications in the glove industry since the 1920s. This is attributed to the excellent tear and puncture resistance of NR latex films. Besides, NR latex film exhibits very high extensibility (600–1000%) before its breaking point. These properties make NR latex film an excellent barrier protection against infectious liquids and gases. Most of the examination and surgical NR latex gloves are used in hospitals and clinics. However, recently NR latex gloves have entered the fast food industry where good swelling resistance is an essential requirement. Being a nonpolar rubber, NR latex gloves have a poor swelling resistance which limits its application in the fast-food industry. The fast-food industry is growing very fast all over the world. There is a growing concern over the cleanliness and hygiene of the food. It is essential that the workers wear rubber gloves to avoid contact with the food they serve. Rahim and Samsuri[25] investigated the effect of crosslink concentration and effect of blending carboxylated nitrile rubber (XNBR) with NR latex on the swelling resistance of NR latex film towards cooking oil. The amount of sulfur was varied to produce different crosslink concentrations. The crosslink concentration was determined by immersing the latex film sample in a solvent until equilibrium swelling was attained. The crosslink concentration was calculated by using the Flory–Rehner equilibrium swelling equation as proposed by Mullins[18] given by eqn [12]:

$$-\ln(1-v_r) - v_r - \chi v_r^2 = 2\rho V_1 [X]_{phy} v_r^{1/3} \qquad [12]$$

where v_r is the volume fraction of rubber in the swollen gel, ρ is the density of rubber, V_0 is the molar volume of solvent, χ the rubber–solvent interaction parameter, and $[X]_{phys}$ is the physically manifested crosslink concentration. The diffusion coefficient D was calculated from eqn [13][24]:

$$M_t/M_\infty = (2/l)(Dt/\pi)^{1/2} \qquad [13]$$

where M_t is the total amount of liquid absorbed per unit area of the sheet after immersion for time t, M_∞ is the amount of liquid absorbed after infinite time (in this case time to reach equilibrium swelling), and l is the half thickness of the film sheet. It is necessary to plot M_t against square root time as shown in **Figure 15** to calculate D in eqn [13].

The effect of crosslink concentration on the diffusion coefficient of cooking oil in the latex film is shown in **Table 8**.[25] The results show that increasing the crosslink concentration decreases the diffusion coefficient significantly. Increasing the sulfur content from 0.6 to 3 pphr increases the crosslink concentration by about 90%, which merely decreases the

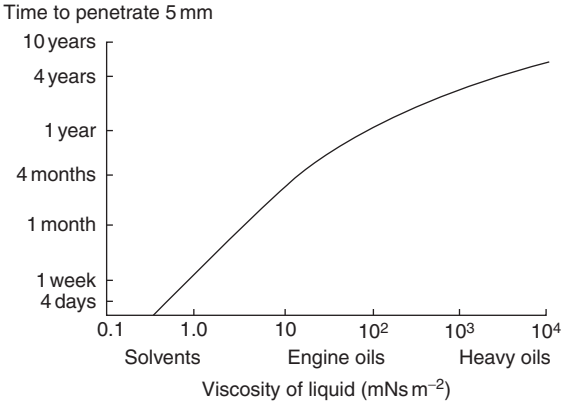

Figure 13 Effect of viscosity of liquid on penetration time. Adapted from Fuller, K. N. G.; Muhr, A. H. *Engineering design with natural rubber, NR Technical Bulletin*, 5th ed.; The Malaysian Rubber Producers' Research Association, London, 1992; pp 1–33, with permission from Tun Abdul Razak Research Centre, Brickendonbury Hertford, England.

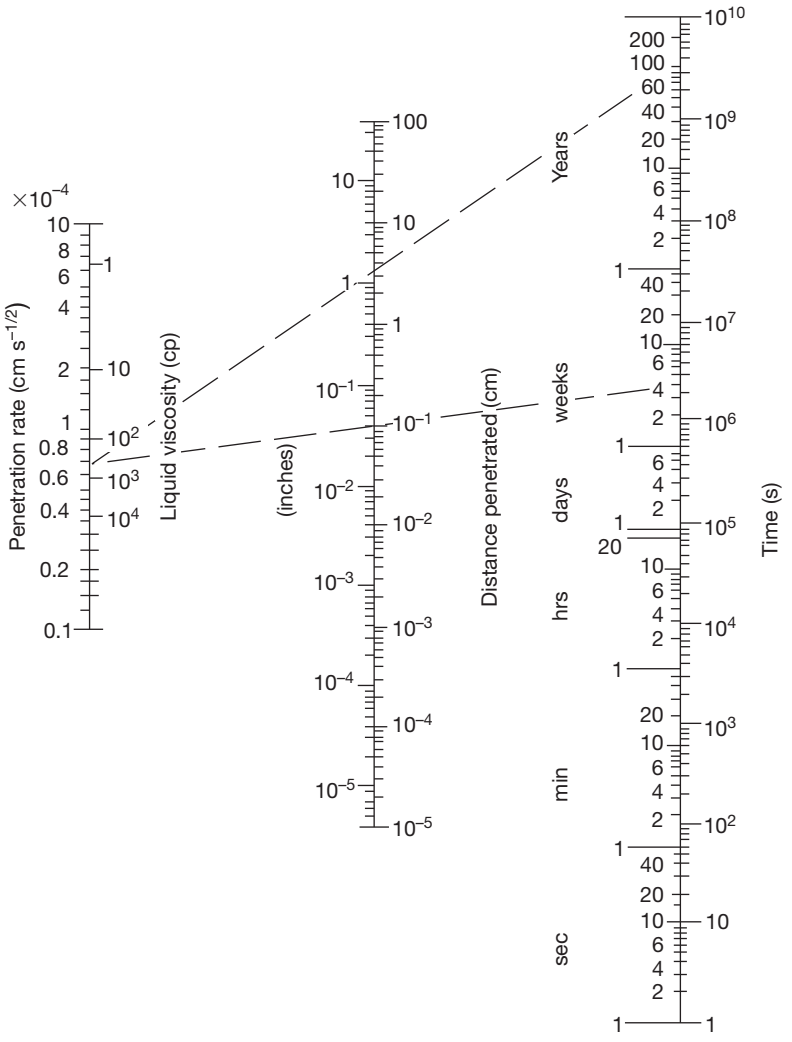

Figure 14 Nomogram to facilitate rapid calculation of distance penetrated by liquid into rubber. Adapted from Muniandy, K.; Southern, E.; Thomas, A. G. In *Natural Rubber Science and Technology*; Robert, A. D., Ed.; Oxford University Press, Oxford, UK, 1988; Chapter 13, pp 820–851, with permission from Oxford University Press.

diffusion coefficient by about 23%. However, the most efficient method to increase swelling resistance is through physical blending of NR latex with XNBR latex, where the diffusion coefficient D of the oil into the film decreases by a factor of 2.7 compared with NR latex having the highest crosslink concentration. Thus, this work shows strong evidence that blending of nonpolar elastomer with polar elastomer enhances the swelling resistance of the former.

3.33.11 Water Absorption

Elastomers find wide uses in marine and offshore engineering applications. The application of elastomers in water management is attributed to its high impermeability to water. A rubber sheet is used to line the water reservoir and pond, while inflatable rubber is used as a dam. Rubber dock fenders rely on the energy absorption capacity of the rubber. Inevitably, the rubber will absorb some quantity of water as these rubber products spend a considerable time under water. It is of great concern whether the absorption of water would impair the strength of the rubber.

The true solubility of water in rubber is very low.[24] Nonetheless, relatively large amounts of water can be absorbed during prolonged immersion as shown in **Figure 16**.[2] The diffusion of water in elastomers is not straightforward, but complicated by the presence of hydrophilic materials. In the case of NR it is mainly

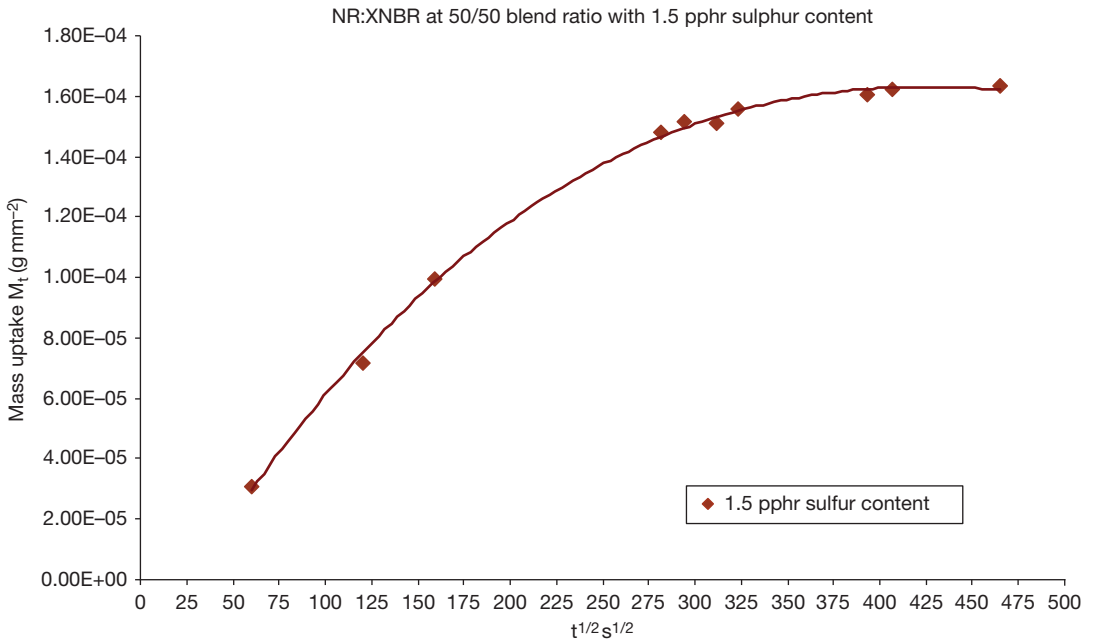

Figure 15 Typical mass uptake curve for NR/XNBR blend latex film.[25]

Table 8 Effect of crosslink concentration on diffusion coefficient *D* of cooking oil into NR latex film

Sulfur level (pphr)	*$[X]_{phy}$ (mol per kg RH)*	*D ($m^2s^{-1} \times 10^{-13}$)*
0.6	4.46×10^{-2}	4.70
1.0	4.60×10^{-2}	4.00
2.0	4.89×10^{-2}	3.70
3.0	5.82×10^{-2}	3.57
NR:XNBR (50:50) 1.5	–	1.30

proteinaceous.[24] When water diffuses into the rubber, the water-soluble hydrophilic materials dissolve forming droplets of solution within the rubber. Osmotic pressure gradient would exist between watery domains in the rubber and that of the external solution immersing the rubber.[24] This results in more water diffusing into the internal solution droplet. Water absorption reaches its equilibrium when the elastic stresses acting on the droplets balance the osmotic pressure difference. Muniandy and Thomas[24] proposed a mathematical model for water absorption to derive equations for the equilibrium water uptake and to evaluate the kinetics of water absorption and desorption. From the model, they calculated the equilibrium water uptake and the apparent diffusion coefficient. They found very good agreement between theory and experimental results.

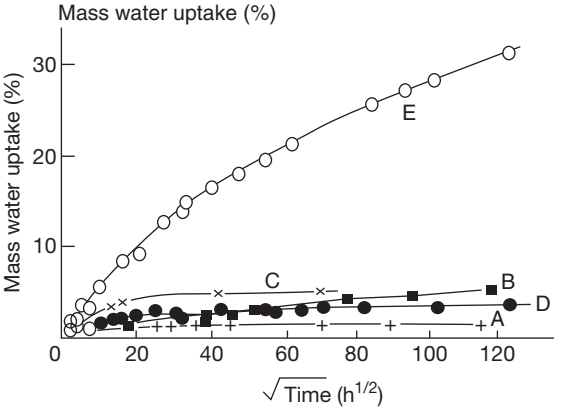

Figure 16 Corrected mass uptake measurements for engineering rubbers in seawater at 23 °C: (a) deproteinized NR, (b) lead oxide cured polychloprene, (c) nitrile rubber, (d) conventional NR, and (e) conventional polychloroprene Adapted from Fuller, K. N. G.; Muhr, A. H. *Engineering design with natural rubber, NR Technical Bulletin*, 5th ed.; The Malaysian Rubber Producers' Research Association, London, 1992; pp 1–33, with permission from Tun Abdul Razak Research Centre, Brickendonbury Hertford, England.

Later, Lake[26] investigated the kinetics of water (tap water) absorption in elastomers and their effects on properties. He reported that when the absorption was large (50% or more), the rubber test-piece degraded. Severe degradation leads to porosity of the surface layer, and when pressed, water exudes.[26] However, at a low level of absorption, Lake observed

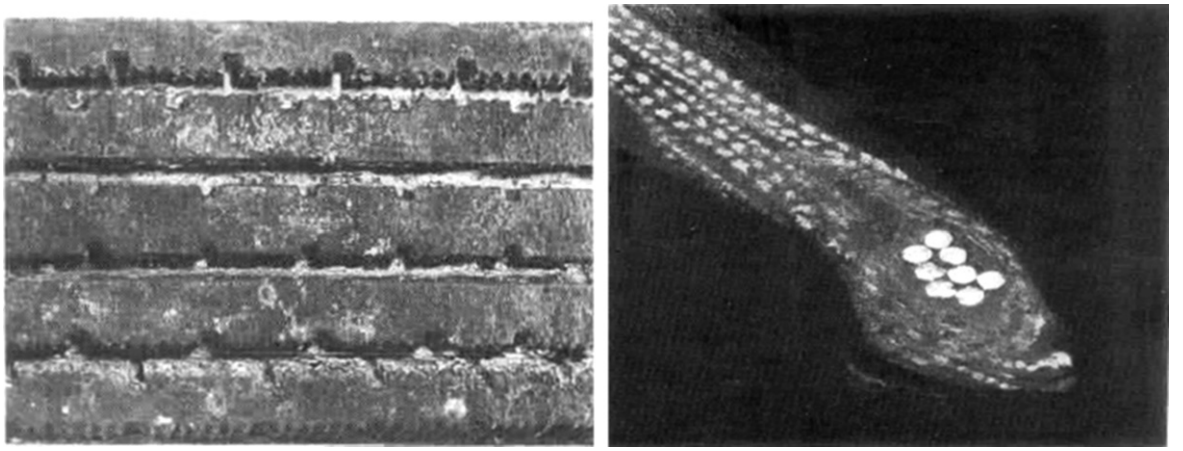

Figure 17 A natural rubber tire after 40 years' exposure to seawater. Adapted from Mullins, L. *Proc. Int. Rubb. Conf*. Kuala Lumpur, 1985, with permission from Malaysian Rubber Board.

the formation of droplets similar to the blisters that occur in plastics or under protective coatings, consistent with an osmotic diffusion mechanism.[24] In saltwater, water absorption reached steady state at much lower levels than in freshwater, again consistent with an osmotic pressure mechanism. Thus seawater is less damaging than freshwater and may not have any serious consequences for many elastomers. This latter point is consistent with findings of Ab. Malek and Stevenson[27] who evaluated the physical properties of a rubber tire as shown in **Figure 17**, recovered from seawater at a depth of 80 ft. They found that the rubber tire had absorbed about 5% of seawater after 42 years of immersion. They found no evidence of microbiological attack. What is more interesting, the physical properties of the rubber tire were within normal specifications for new rubber of the same type. They even suggested storing elastomers in deep seawater in view of its inert nature. Indeed, elastomer is a very suitable material to coat metal surfaces against corrosion in deep seawater. The photograph in **Figure 17** shows clear evidence that the steel cords making up the bead of the tire are corrosion-free after a 42-year immersion in seawater.[27]

3.33.12 Protective Measures

3.33.12.1 Selection of Elastomer

All elastomers experience aging. Some age faster than others. The rate of aging depends on a number of factors such as the chemical structure of the polymer, service environment, which includes length of exposure to heat and light, oxygen and ozone concentration, size and shape of elastomers, and mechanical stresses. One cannot stop the aging process, but one can slow it down. The most effective means of combating aging is to select the correct elastomers to meet the maximum service temperature and environment. Fully saturated elastomers having high bond dissociation energy making up their backbone chains are the best choice to meet high service temperature applications. Fully saturated rubbers such as ethylene propylene copolymer and very low unsaturation butyl rubber are excellent resistance to heat aging, oxidation and ozone cracking. Not only the maximum service temperature, but also other environmental factor such as oil or solvent determines the aging resistance. In cases like these, the elastomers having high bond dissociation energy and solvent resistance are desired. These include specialty elastomers such as acrylic (ACM), chloro-sulfonyl-polyethylene (CSM), ethylene propylene copolymer (EPM), fluoroelastomers (FKM), silicones (MQ, VMQ), polyester urethanes (AU), etc. Alternatively, for unsaturated elastomers are to use antioxidants and antiozonants, with correct vulcanization system can slow down the aging process quite efficiently.

3.33.12.2 Blends of Elastomers

It is a common practice to blend two elastomers of different properties with a view to combining the best features in terms of technical and economic values. Natural rubber is blended with EPM for applications requiring very high resistance to attack by ozone as the latter is fully saturated. A blend of NR and EPDM is used for applications that require a combination of good resistance to attack by ozone and high

strength properties. Nitrile rubber (NBR) is blended with EPM to meet the requirements for very good oil resistance as well as conferring high resistance to oxidation and ozone cracking. The former is polar rubber and provides very good oil resistance, while the latter provides excellent weather resistance. However, blending two or more elastomers is not as easy as one would imagine. The work on blending various elastomers conducted by Tinker[28] and coworkers has thrown some light on the importance of compatibility, distribution of crosslinks in each rubber phase, distribution of filler and plasticizer and interfacial tension of each phase which have very strong influence on the service performance of the blend. When the elastomers are not compatible with each other, the associated problems that may arise include maldistribution of crosslinks, partition of chemicals (sulfur, accelerators, etc.) due to mechanism associated with preferential solubility and others. Lewan[29] worked on crosslink density distribution in NR/NBR blend and reported the effects of large difference in polarity and solubility parameters between these two rubbers. The large difference in polarity has the following effects:

(i) causes high interfacial tension that is detrimental to mixing since it interferes with efficient mixing at the interface, hence minimizing the opportunity for crosslinking between the rubbers;
(ii) causes poor phase morphology, which is characterized by large phase sizes;
(iii) causes uneven distribution of crosslinks arises through preferential solubility of the curatives and vulcanization intermediates. Sulfur will be preferentially soluble (partition in favor of) the more polar NBR. One phase is over-crosslinked and the other is lowly crosslinked.

However, Lewan[29] overcame these problems by selecting the correct type of curing system such as semi-EV based on sulfur – TBBS, to obtain an even distribution of crosslinks in each phase and maximizing crosslinking between rubbers at the interface. The use of compatibilizer is highly recommended to enhance the compatibility between rubber phases. Polychloroprene rubber serves as a very good compatibilizer for the NR/NBR blend with just a small quantity (5 pphr) added to the blend. The addition of this compatibilizer reduced phase sizes, gave an even distribution of crosslinks and increased tensile strength.[30] Blends of elastomers provide alternative means of improving both aging resistance and oil resistance.

3.33.12.3 Antidegradants

Chemical antioxidants and antiozonants combat aging by scavenging harmful radicals, absorbing UV light, deactivating catalytic metals like copper, manganese, iron, etc., and decomposing initiating peroxides.[16,17] Two main types of chemical antioxidants and antiozonants are widely used in rubber compounds; they are amines and phenolics. Amine types are more effective and powerful antioxidants than phenolic types. However, the former is staining and the latter is not. Thus, this limits applications of amine types to black and dark colored elastomeric products. Phenolic types are exclusively used for white and bright colored products, especially in electrical wire insulation where colors are useful for identification purposes. Both amines and phenolics provide protection against aging by scavenging the harmful free radicals during the oxidative chain reaction.[16,17] The proposed mechanism[17] by which these two types of antioxidants work is shown in **Figure 18**. During the initiation stage, the free radicals produced by the peroxides abstract a labile hydrogen atom from the antioxidant and produce an antioxidant radical. This antioxidant radical is more stable than the peroxy radical, which terminates by reaction with other radicals in the system.[16,17]

The transfer step (c) and termination step (f) remove the free radical functionality from the elastomer, which consequently halts the oxidative degradation reaction.[17] Metal deactivators such as 2-mercaptobenzimidazole and its salt when added into the rubber compound containing amine or phenolic antioxidant give a synergistic effect to enhance the protection against aging.[31] These chemicals form

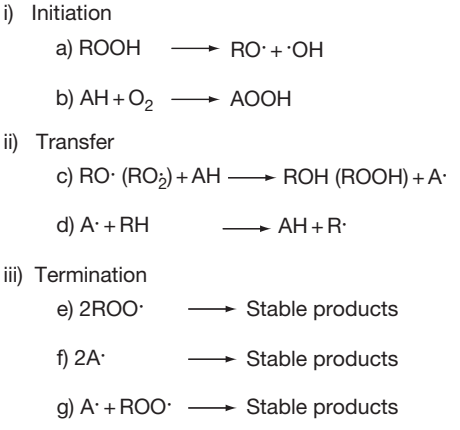

Figure 18 Mechanism of amine and phenolic antioxidant activity, where AH is the antioxidant.[17]

coordination complexes with catalytic metals and inhibit metal-activated oxidation. Carbon black is a natural UV light absorber, and for nonblack compounds, it is useful to incorporate a UV light absorber such as benztriazole derivative.

3.33.12.3.1 Mechanism of antiozonant action

The mechanism by which an antiozonant protects unsaturated rubber against ozone cracking has received attention from many rubber chemists and physicists. A number of suggestions have been proposed as to how antiozonants confer protection, ranging from competitive reaction with ozone (scavenging) to various types of protective layer formation.[17,19–21] There are three theories to describe the mechanism of antiozonant action[17]:

(i) The antiozonant blooms to the surface of the rubber compound and reacts preferentially with the incident ozone.
(ii) The antiozonant blooms to the surface of the rubber and forms a protective layer of film on the surface.
(iii) The antiozonant reacts with intermediates formed in the ozonation of rubber, preventing chain scission or recombining severed rubber chains.

Lake[32] has conducted some work to elucidate the mechanism of antiozonant action to protect natural rubber against ozone cracking. He used dioctyl-*p*-phenylenediamines (DOPPD) antiozonant for his rubber compound. Exposing the rubber test-piece to ozone-rich atmosphere has reportedly resulted in a layer of film 10^{-3} cm thick and visible to the naked eye forming on the rubber surface.[32] The protective layer can be removed by physical means either by scraping or using adhesive tape, or by swabbing with cotton wool dipped in acetone. The mass of the film can be determined by weighing the test-piece before and after its removal. In this way, the kinetics of layer formation can be determined by monitoring changes in weight after various periods of exposure to ozone.

Lake[32] has derived a mathematical expression to relate the mass of layer per unit area of surface M_L formed after time t to the concentration C_0 of antiozonant in the rubber and diffusion coefficient D_L as shown by eqn [14]:

$$M_L = [2\rho_L D_L S_L C_0 t]^{1/2} \qquad [14]$$

where ρ_L is the density of the layer material and S_L is the solubility, relative to that in the rubber, of the antiozonant in the layer. In deriving this equation, Lake[32] assumed that the layer to be formed entirely of reacted antiozonant and the concentration of unreacted material within it to be small. The product $D_L S_L$ was determined experimentally by measuring the rate of transfer of antiozonant through the layer formed on a test-piece to a controlled rubber test-piece containing no antiozonant initially. This was done experimentally by pressing two cylindrical discs (test-piece A contains antiozonant, test-piece B has no antiozonant) together so their surfaces are in intimate contact with each other. The antiozonant from test-piece A would migrate into test-piece B as a function of time. The mass of the layer formed per unit area of surface was plotted against the square root of time to produce a straight line whose slope gave the value of $M_L/t^{1/2}$, that is mass of film deposited per square root time. Lake[32] obtained very good agreement between theory and experimental data.

Lake[32] proposed the mechanism of antiozonant action as follows: The protective layer formed on the rubber surface is composed predominantly of the antiozonant which has reacted with ozone. The film formed remained essentially in the unstrained state, independent of the type of deformation applied. For this to happen, it is necessary that the antiozonant is soluble in the rubber, and that its reaction product should be insoluble. However, once the protective layer becomes coherent and compact, it will reduce substantially the flux of ozone reaching the rubber surface. Thus it appears that the ability of the antiozonant to prevent cracking is likely to be determined by what occurs during the initial stages of exposure when the layer is starting to form, rather than by the long-term behavior. Indeed, Lake[32] suggested that a coherent monomolecular layer of film that formed on the rubber surface is sufficient to confer protection against ozone cracking. However, the time for this monolayer to form must be faster than the time for the crack to grow to the same depth, so that the monolayer is able to bridge any cracks that have begun to grow.

3.33.12.3.2 Theories of layer formation

The thin layer of protective film covering the rubber surface is a direct consequence of the chemical reaction between chemical antiozonant and ozone. Lake and Mente[21] proposed two diffusion models to work out a theory for layer formation. The two models are shown in **Figure 19**. The first model describes the rate of layer formation that is controlled by the diffusion of the antiozonant across the already-formed layer to react with ozone at its outer surface. Under

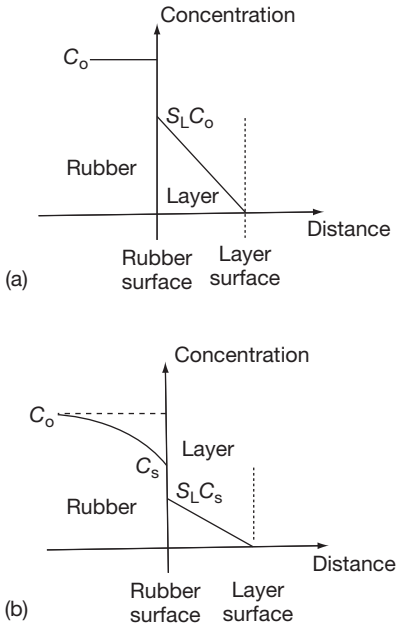

Figure 19 Diffusion models for antiozonant layer formation: (a) rate governed by diffusion of antiozonant within the layer only, and (b) rate governed by both diffusion in the layer and in the rubber. Adapted from Lake, G. J.; Mente, P. G. *J. Nat. Rubb. Res.* **1992**, *7*(1), 1–13, with permission from Malaysian Rubber Board.

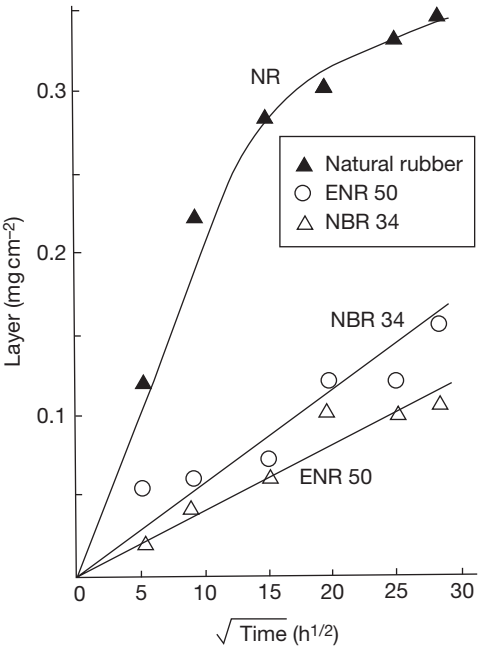

Figure 20 Dependence of the mass of antiozonant layer formed on the square root of the time of exposure to an ozone concentration of 200 pphm at 40 °C for vulcanizates of NR, ENR 50, and NBR 34. Adapted from Lake, G. J.; Mente, P. G. *J. Nat. Rubb. Res.* **1992**, *7*(1), 1–13, with permission from Malaysian Rubber Board.

these circumstances, the mass per unit area M_L, of layer formed after time t is given by eqn [14].[21,32] The concentration gradient in the layer will be essentially linear as shown in **Figure 19(a)**. The second diffusion model takes into account diffusion within the rubber in addition to diffusion across the layer. In this case, an equation similar to eqn [14] applies, when C_0 is replaced by C_s, the concentration at the rubber surface is lower than C_0 as shown schematically in **Figure 19(b)**. C_s is a function of C_0 and the relative permeabilities of the rubber and the layer to the antiozonant, and with the assumptions made, are given by eqn [15]:

$$C_s/C_0 = 1 + \xi - [(1+\xi)^2 - 1]^{1/2} \qquad [15]$$

where

$$\xi = (\pi/4)(\rho_L D_L S_L / DC_0) \qquad [16]$$

and D is the diffusion coefficient of the antiozonant in the rubber. The mass of layer per unit area of surface plotted against square root of time as shown in **Figure 20** enabled Lake and Mente[21] to determine the rates of layer formation of the antiozonants formed on NR, ENR 50, and NBR 34, respectively. These three rubbers differ greatly in terms of polarity and glass-transition temperature, which may affect the rate of film formation on the rubber surface. Their experimental results as shown in **Figure 20** indicate that the rate of layer formation for NR is about four times faster than that of NBR 34 and ENR 50, which is in accordance with the dependence of the diffusion coefficient on the glass-transition temperature of the rubber. The diffusion coefficient decreased in the increasing order of the T_g of the rubber.[21] Thus the diffusion coefficient of NR is fastest and that of ENR 50 is the slowest as T_g of NR is about −69 °C and that of ENR 50 is about −24 °C.[21] NBR34 has a slightly faster diffusion coefficient than ENR 50 as its T_g (−28 °C)[19] is slightly lower than that of ENR 50. Lake and Mente[21] also conducted experiments to investigate the effect of temperature on layer formation on the NR surface at −17 and 23 °C respectively as shown in **Figure 21**. They found that the rates of layer formation at these two temperatures were the same for NR. However, the diffusion coefficient of this particular antiozonant (DOPPD) in NR at −17 °C was very similar to that in ENR 50 and NBR 34 at 23 °C. They attributed this finding to the partitioning of the antiozonant

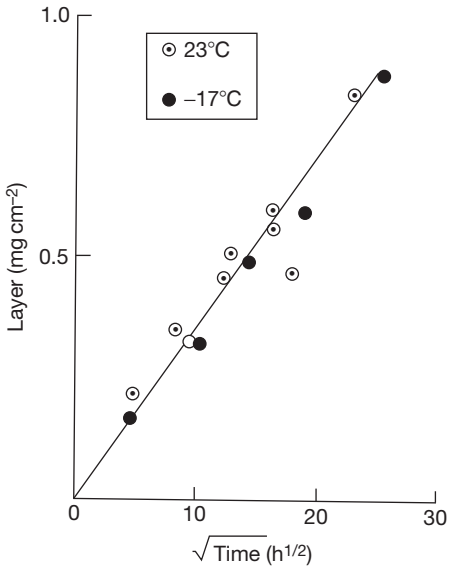

Figure 21 Mass of antiozonant layer formed versus square root of the time of exposure to 10^5 pphm ozone for an NR vulcanizate containing 10 pphr DOPPD at 23 and −17 °C. Adapted from Lake, G. J.; Mente, P. G. *J. Nat. Rubb. Res.* **1992**, *7*(1), 1–13, with permission from Malaysian Rubber Board.

between the elastomer and the layer material, as the polarity of the elastomer affects the solubility of the antiozonant in the rubber. The solubility of the antiozonant varies in the ascending order of polarity of elastomer, that is NR < NBR 34 < ENR 50.[21] Lake and Mente concluded that for elastomers with high T_g, the antiozonant offers better protection at temperatures above room temperature than at low temperature, as the protective agents are more mobile at high temperatures rather than at low temperatures.

3.33.12.4 Blooming of Wax

Besides chemical antiozonants, paraffin wax is also a useful ingredient to confer protection against ozone cracking. Wax provides a protective layer surrounding the surface of the elastomer through the diffusion process commonly known as blooming, which prevents direct contact between ozone and the elastomer. Blooming occurs when the supersaturated solution of the ingredient in the rubber crystallizes more readily on the surface than in the rubber itself.[24,33] This basic mechanism of blooming is not only applicable to wax but other ingredients as well. When other ingredients such as sulfur, accelerators and strearic acid bloom to the rubber surface, they reduce the tackiness of the rubber, which can bring detrimental effects to products relying on adhesion and bond strength involving different components plied together. These include rubber-to-metal bonded components, tires, belts, and hoses. However, blooming of waxes and antioxidants brings advantages.

Nah and Thomas[33] investigated the mechanism and kinetics of diffusion of wax to the rubber surface. They envisaged that the driving force for the blooming process arises from the elastic forces acting around the wax precipitates in the rubber when the wax concentration is in excess of its equilibrium solubility. They then proposed a model and theory for wax blooming base on thermodynamic concept of diffusion, where the driving force of the diffusion process is predominantly associated with free energy gradient rather than the concentration gradient of the wax that is dissolved in the rubber. The initial rate of wax bloom per unit area $(M_t/t^{1/2})$ is given by eqn [17][33]:

$$(M_t/t^{1/2})_{x=0} = [(24 v_f D_t s_x \rho_x V_x G)/RT]^{1/2} (d\lambda/dy)_0 \quad [17]$$

where D_t is diffusion coefficient, v_f is volume fraction of seeding particles or flaws present in the rubber. s_x is solubility of wax in the rubber, ρ_x is density of wax, and V_x is molar volume of solid wax. G is shear modulus of the rubber, R is molar gas constant, T is absolute temperature. $(d\lambda/dy)_0$ is equivalent to the concentration gradient of the wax at the surface of the rubber, and is determined by numerical methods for the appropriate boundary conditions and a suitable value of v_f. The symbol λ stands for the extension ratio of the rubber around the precipitated wax particle, assumed spherical. Nah and Thomas[33] verified eqn [17] experimentally, and obtained satisfactory agreement between their experimental and theoretical values for the migration of paraffin waxes in peroxide cured natural rubber. The theory was applicable to predict the blooming of wax mixtures with success, indicating that the mechanism of wax blooming has been identified correctly. Although Nah and Thomas developed the theory for blooming of wax, with minor adjustments, it is also applicable to predict migration and blooming of sulfur, fatty acids and antidegradants in vulcanized elastomers.

3.33.12.5 Choice of Vulcanization System

Anaerobic aging usually decreases the stiffness, resilience, and tensile, tear and fatigue properties; the extent is mainly determined by the type of vulcanization system, which affects aging of elastomers. There are three types of sulfur vulcanization systems known as conventional, efficient (EV) and

semi-efficient (semi-EV) respectively[8,10] as discussed briefly in Section 3.33.4.3. The conventional system has a higher sulfur dosage than the accelerator that produces predominantly polysulfidic crosslinks, where the rubber molecular chains are linked by three or more sulfur atoms. Polysulfidic crosslinks have poor resistance to heat aging because the –S–S– bond has low thermal stability. In contrast, EV makes use of the low sulfur level and high accelerator dosage. This EV system produces predominantly monosulfidic crosslinks which are thermally very stable. The rubber network consists of other structural features as described briefly in subsequent sections.

3.33.12.5.1 Sulfur vulcanization system and types of crosslinks on aging resistance

Polysulfidic crosslink

A chain of three or more sulfur atoms (maximum of six atoms) in this crosslink bridges two polymer chains. The bond energy of this crosslink is less than 268 kJ mol^{-1}, which is relatively low.[10] A polysulfidic crosslink can be produced by using the conventional vulcanization system where the quantity of sulfur is more than the quantity of the accelerator in the ratio 5:1 (sulfur: accelerator). Therefore the conventional sulfur cure system is not suitable for high temperature applications.

Disulfidic crosslink

In a disulfidic crosslink, there are two sulfur atoms bridging the two polymer chains. Its bond energy is about 268 kJ mol^{-1}. Little is known of the properties of this crosslink, mainly because it is very difficult to prepare a network in which disulfides are predominant. In both conventional and efficient sulfur vulcanizates the proportion of disulfidic crosslink is seldom more than 20–30% of the total.

Monosulfidic crosslink

In the case of a monosulfidic crosslink, the two polymer chains are bridged by one sulfur atom. Its bond energy[10] is relatively high, about 285 kJ mol^{-1}. A monosulfidic crosslink can be produced from an EV system where the amount of the accelerator is higher than the amount of sulfur, about 5:1 (accelerator:sulfur). Thus the EV system is suitable for medium high temperature applications.

Cyclic sulfides

These are intra-crosslinks which are useless as the crosslinks are formed on the same polymer chain. This phenomenon is also known as main chain modification. The main source of these main chain modifications is the thermal decomposition of polysulfide crosslinks. The conventional vulcanization system creates more cyclic sulfides than the EV system as the former produces more polysufide crosslinks than the latter.

Conjugated diene and triene groups

These main chain modifications are also formed by the thermal decomposition of polysulfide crosslinks. The concentration of these conjugated groups increases on overcure. The presence of these groups tends to catalyze oxidative aging as they are much more susceptible to oxidation than the polyisoprene main chain.[8,10,16]

Pendent accelerator group

It is generally accepted that in accelerated sulfur vulcanization, crosslinks are formed from initial rubber-bound pendent groups in which disulfide or polysulfide chains are terminated by accelerator fragments. Like the crosslink, some of these intermediates undergo progressive desulfuration and are converted into stable monosulfidic links between the polymer chain and accelerator fragments. The extent of main chain modification will depend on the amount of accelerator available and on the ease with which the initial pendent group can be desulfurated.

Extra-network material

The extra-network material formed by a sulfur vulcanizing system can be put into two categories. The first consists of unreacted zinc oxide and fatty acid activators, their zinc soap reaction products and zinc sulfide. The second consists of accelerator reaction products.

3.33.12.5.2 Peroxide vulcanization system

Unlike sulfur vulcanization, peroxide vulcanization does not require the presence of double bonds. In fact, peroxide vulcanization is possible for rubbers having either saturated or/and unsaturated carbon–carbon backbone chains. However, peroxide vulcanization is quite impossible with the following elastomers because of their tendency to decompose:

- IIR – butyl rubber
- CIIR – chlorinated butyl rubber
- CO – polyepichlorohydrin rubber
- ECO – copolymer of epichlorohydrin and ethylene oxide
- PP – polypropylene
- ACM – polyacrylic rubber

The most common peroxide is dicumyl peroxide (DCP or dicup). Others include ditert butyl peroxide, dibenzoyl peroxide and bis(2,4-dichlorobenzoyl) peroxide. Peroxide vulcanization[10] produces a vulcanizate which will impart good aging resistance and excellent resistance to compression at high temperatures (70–100 °C). To obtain the best compression set performance, freedom from certain other compounding ingredients, especially zinc oxide and stearic acid, is essential. Peroxide vulcanization is essentially nonreverting. However, there are certain deficiencies such as poor hot tear strength and incompatibility with chemical antiozonants. Other technical limitations include slow cure rate with no delayed action, and degradation of the rubber giving a sticky surface if it comes into contact with air during the cure. Thus peroxides are not suitable for hot-air or steam-pan curing. The reaction of peroxide must be carried through to completion to obtain the best heat resistance; therefore long cure times are inevitable. In addition, nearly all antidegradants and aromatic oils affect the efficiency of the peroxide cure.

Co agents, which are highly reactive materials, are usually added in peroxide vulcanization to increase the efficiency of the organic peroxide, but do not affect the rate of cure.[10,31] They are used either to enhance the modulus and hardness or to reduce the level of peroxide required. They can be absolutely essential for the efficient cure of chlorinated polyethylene. Typical solid coagents are zinc diacrylate, zinc dimethacrylate, and *m*-phenylene dimaleimide. Liquid coagents are materials such as triallyl cyanurate (TAC), triallylisosyanurate (TAIC), etc. High vinyl polybutadiene is a polymer which can act as a coagent.

3.33.12.5.3 Vulcanization with urethane

This (urethane) crosslinking system for natural rubber was developed in the early 1980s by the scientists at the Malaysian Rubber Producers Research Association (MRPRA).[10,31] It was marketed under the trademark Novor. The basic reagent is a reaction product of a nitroso compound and a diisocyanate which dissociates at vulcanizing temperatures into its component species. The free nitroso compound then reacts by addition to rubber molecules giving attached pendent groups which subsequently react with the diisocyanate to form urea type crosslinks. The main features of the vulcanizates are excellent reversion resistance and, when protected with a TMQ/ZMBI antioxidant combination, excellent heat aging resistance.

3.33.12.5.4 Metallic oxide vulcanization

Elastomers containing halogens can be cured with metallic oxides such as oxides of zinc, magnesium, and lead. The oxides form an ether type of crosslink (R–O–R′) which gives good heat aging resistance. Elastomers which can be vulcanized metallic oxides are polychloroprene, halogenated butyls, and polychlorosulphunated rubber.

3.33.12.5.5 Resin vulcanization

Resin vulcanization has established itself to some degree in butyl (IIR) crosslinking, giving excellent heat and steam stability.[10] Example of a typical resin cross linker is polymethylolphenolic resin. The amount used is at the level of 5–12 pphr.

3.33.12.5.6 Quinonedioximes vulcanization

p-Benzoquinonedioxime (CDO) as well as its dibenzoyl derivative are cross linkers for many rubbers because of their free radical reactions.[10] Best known and of greatest interest is their use in IIR because of the excellent heat and steam stability that can be obtained. They are used mainly for rubbers having low unsaturation where sulfur vulcanization is slow. They have been unimportant for the classic diene rubbers.

3.33.13 Future Developments in Materials or Applications

Natural rubber and synthetic elastomers are likely to maintain their roles and contributions in domestic and industrial applications, buildings and structures, automotives, and marine and engineering products. With the emergence of nanomaterials for rubber compounding, it is envisaged that future elastomeric products will provide better service and longer life performance than they are capable of providing now. High heat resistant elastomers and highly oil resistant elastomers are the main players of the future to meet the high demands of the automotive industry and aeronautical engineering. More developmental work in these areas is expected.

Acknowledgements

I am very grateful to Dr. Stuart Lyon, Reader in Corrosion Control Engineering, School of Materials (Corrosion and Protection Centre), University of Manchester, England, who gave me the opportunity to write as part the prestigious Shier's Corrosion

book. I feel much honored to be among the experts who contributed to this fourth edition of Shier's Corrosion.

It gives me great pleasure to thank the Publication Divisions of the Malaysian Rubber Board (MRB) (formerly Rubber Research Institute of Malaysia), and its sister concern the Tun Abdul Razak Research Centre (TARRC) (formerly Malaysian Rubber Producers Research Association) at Brickendonbury Hertford, England. In particular, Dato' Dr. Kamarul Baharin Basir, Director General, MRB and Mdm Rabeatun Awaliah Awalludin, MRB, and Dr. A.J. Tinker (Director Research) TARRC and Ms. K. Lawson TARRC who helped me to obtain the permission to reproduce data and figures from their respective Publication Divisions.

I would like to express my sincere appreciation and thanks to Oxford University Press and the American Chemical Society (Rubber Division) for giving permission to reproduce figures and data from their respective publications.

Last but not least, Associate Prof. Dr. Mohamad Kamal Harun, Dean of Faculty of Applied Sciences, MARA University of Technology, Malaysia (UiTM) for his encouragement.

References

1. International Standard, Rubber – *Vocabulary, ISO1382*, 3rd Ed, 1996-08-01.
2. Fuller, K. N. G.; Muhr, A. H. *Engineering design with natural rubber, NR Technical Bulletin*, 5th ed.; The Malaysian Rubber Producers' Research Association: London, 1992; pp 1–33.
3. Chadwick, J. C. *Shell Polym.* **1981**, *5*, 44–50.
4. ISO 4632/1-1982 (E), ISO Classification system.
5. Hashimoto, K.; Maeda, A.; Hosoya, K.; Todani, Y. *Rubb. Chem. Technol.* **1998**, *70*(3), 449–519.
6. Fogg, G.; Swift, P. M. *NRPRA Tech. Bull.* **1962**, *4*, 1–26.
7. Brydson, J. A. *Plastics Materials*, 4th ed.; Butterworths: Newton, MA, 1989; Chapter 29, pp 730.
8. Brown, P. S.; Porter, M.; Thomas, A. G. In *Proceedings of the International Rubber Conference*; Kuala Lumpur, October 21–25, 1985, RRIM, 1986; pp 20–46.
9. Hofmann, W. *Rubber Technology Handbook*; Hanser, 1989; Chapter 3, Synthetic Rubber, pp 1–171.
10. Elliott, D. J.; Tidd, B. K. *Prog. Rubb. Technol.* **1974**, *34*, 83–126.
11. Gregory, M. J. In *Rubber to metal bonding, Adhesives, Sealants, and Encapsulants Conference*, London, November 5–7, 1985.
12. Gage, F. *J. IRI* **1968**, 47–49.
13. Gibbs, E. H., Jr.; Seber, J. N. ACS Rubber Division Mtg., Indianapolis, IN, May 1984, pp 1–9.
14. Mullins, L. In *Proc. Rubb. in Eng*. Conf. Kuala Lumpur, 1974, pp 1–20.
15. Bolland, J. L.; Hughes, H. *J. Chem. Soc.* **1949**, 492.
16. Barnard, D.; Lewis, P. M. In *Natural Rubber Science and Technology*; Robert, A. D., Ed.; Oxford University Press: Oxford, UK, 1988; Chapter 13, pp 621–673.
17. Keller, R. W. *Rubb. Chem. Technol.* **1985**, *58*, 637–651.
18. Mullins, L. *J. Polym. Sci.* **1956**, *19*, 225–236.
19. Braden, M.; Gent, A. N. *J. Appl. Polym. Sci.* **1960**, *3*, 90–106.
20. Lake, G. J.; Thomas, A. G. In *Proceedings of the Int. Rubb. Conf*. 1967, Maclarens: London.
21. Lake, G. J.; Mente, P. G. *J. Nat. Rubb. Res.* **1992**, *7*(1), 1–13.
22. Kinro, H.; Akio, M.; Kiyoshi, H.; Yoshihiro, T. Speciality Elastomers for Automotive Applications, *Rubber Chemistry Technology*; **1998**, *71*(3).
23. Lake, G. J.; Lindley, P. B. *Rubber J.* **1964**, *10*, 24–30, 79, 11, 30–36, 39.
24. Muniandy, K.; Southern, E.; Thomas, A. G. In *Natural Rubber Science and Technology*; Robert, A. D., Ed.; Oxford University Press: Oxford, UK, 1988; Chapter 13, pp 820–851.
25. Rahim, R.; Samsuri, A., Effect of crosslink concentration and XNBR:NR ratio on swelling resistance of NR latex film towards cooking oil, in press.
26. Lake, G.J. In *Conf. Polymers in a Marine Environment*, London, 31 Oct.–2 Nov., 1984, pp 157–160.
27. Ab-Malek, K.; Stevenson, A. *J. Mater. Sci.* **1986**, *21*, 147–154.
28. Tinker, A. J. In *Blends of Natural Rubber*; Tinker, A. J., Jones, K. P., Eds.; Chapman & Hall: London, 1998; Chapter 1, pp 1–7.
29. Lewan, M. V. In *Blends of Natural Rubber*; Tinker, A. J., Jones, K. P., Eds.; Chapman & Hall: London, 1998; Chapter 5, pp 53–67.
30. Kongsin, K.; Lewan, M. V. In *Blends of Natural Rubber*; Tinker, A. J., Jones, K. P., Eds.; Chapman & Hall: London, 1998; Chapter 7, pp 80–93.
31. The Natural Rubber Formulary and Property Index, Malaysian Rubber Producers' Research Association, 1984, pp 1–24.
32. Lake, J. G. *Rubb. Chem. Chem.* **1970**, *43*, 1230–1238.
33. Nah, S. H.; Thomas, A. G. *J. Polym. Sci., Polym. Phys. Ed.* **1980**, *18*, 511–521.

3.35 Corrosion of Metal Joints

G. Pimenta
Materials Laboratory, Instituto de Soldadura e Qualidade, Av. Prof. Cavaco Silva 33 – Talaide, 2780-994 Porto Salvo, Portugal
R. A. Jarman
Formerly School of Engineering, University of Greenwich, Old Royal Naval College, Park Row, Greenwich, London SE10 9LS, UK

Glossary

Bead A single run of weld metal on a surface.

Brazing A metal joining process that is identical to soldering except that the joining takes place at temperatures generally above 500 °C. The molten non-ferrous filler metal is distributed between properly fitted surfaces of the joint by capillary attraction.

Butt joint A connection between the ends or edges of two parts making an angle to one another of 135°–180° inclusive in the region of the joint.

Edge preparation The preparation of an edge, by squaring, grooving, chamfering, or bevelling, prior to welding.

Electroslag welding A fusion welding process that utilizes the combined effects of current and electrical resistance in a consumable electrode and conducting bath of molten slag, through which the electrode passes into a molten pool, both the pool and the slag being retained in the joint by cooled shoes which move progressively upwards.

Electron-beam welding A welding process in which the joint is made by fusing the parent metal by the impact of a focused beam of electrons.
Filler metal The metal that is added during welding, braze welding, brazing, or surfacing.
Flux A material that is used during welding, brazing, or braze welding to clean the surfaces of the joint, prevent atmospheric oxidation, and to reduce impurities.
Friction welding A welding process by which the joint metals are fused together by the conjoint action of frictional heating and pressure.
Fusion penetration The depth to which the parent metal has been fused.
Fusion zone That part of the parent metal which is melted into the weld metal.
Heat affected zone That part of the parent metal that is metallurgically affected by the heat of the joining process, but not melted.
Laser welding A welding process employing a laser as the source of heat.
Metal arc welding An arc welding process that uses a consumable metal electrode.
MIG welding Metal-inert gas arc welding using a consumable electrode.
Gas welding A welding process in which the heat source is a flammable gas (commonly acetylene) that is burnt in an oxygen atmosphere.
Parent metal The metal that is to be joined.
Pressure welding A welding process in which a weld is made by a sufficient pressure to cause plastic flow of the surfaces, which may or may not be heated.
Resistance welding A welding process in which force is applied to surfaces in contact and in which the heat for welding is produced by the passage of electric current through the electrical resistance at, and adjacent to, these surfaces.
Run The metal melted or deposited during one passage of an electrode, torch, or blow-pipe.
Soldering A metal joining process that is identical to brazing except that the joining takes place at temperatures generally below 500 °C. The molten nonferrous filler metal is distributed between closely fitted surfaces of the joint by capillary attraction.
Submerged arc welding Metal-arc welding in which a bare wire electrode is used; the arc is enveloped in flux, some of which fuses to form a removable covering of slag on the weld.
TIG welding Tungsten inert-gas arc welding using a nonconsumable electrode of pure or activated tungsten.
Thermal cutting The parting or shaping of materials by the application of heat with or without a stream of cutting oxygen.
Weld A union between pieces of metal at faces rendered plastic or liquid by heat or by pressure, or by both. A filler metal whose melting temperature is of the same order as that of the parent material may or may not be used.
Welding The making of a weld.
Weld metal All metal melted during the making of a weld and that is retained in the weld.
Weld zone The zone containing the weld metal and the heat-affected zone.

Abbreviations

CP Cathodic protection
HAZ Heat affected zone
IGA Intergranular attack
MIG Metal inert gas
MMA Manual metal arc
PWHT Postweld heat treatment
SCC Stress corrosion cracking
SSCC Sulfide stress corrosion cracking
TIG Tungsten inert gas

Symbols

ΔK Stress intensity range (MPa $m^{1/2}$)

3.35.1 Introduction

A jointed fabrication is the one in which two or more components are held in position by one of:

1. A mechanical fastener (screw, rivet, bolt, etc.).
2. A fusion joining process (e.g., welding, brazing, soldering, etc.).
3. An adhesive bond.

The components of the joint may be metals of similar or dissimilar composition and structure, metals and nonmetals, or they may be wholly nonmetallic. Since the majority of fabrications are joined at some stage of their manufacture, the corrosion behavior of joints is of utmost importance, and the nature of the materials involved in the joint, and in the geometry of the joint, may lead to a situation in which one of the materials is subjected to accelerated and/or localized attack. Although galvanic corrosion is dealt with elsewhere in this book, it is necessary to emphasize the following in relation to corrosion at joints in which the metals involved may be either identical or similar:

1. A difference in electrochemical potential may result from differences in structure or stress brought about during or subsequent to the joining process.
2. Large differences in area may exist in certain jointed structures, for example, between weld metal and parent metal.
3. Many joining processes lead to a crevice, with the consequent possibility of crevice corrosion.

The corrosion of adhesive joints is described in a separate chapter in this book.

3.35.2 Mechanical Fasteners

These require little further description and take the form of bolts, screws, rivets, etc. Mechanical failure may occur as a result of the applied stress in shear or tension exceeding the ultimate strength of the fastener, and can normally be ascribed to poor design. However, other failure modes are possible, including the failure of steel fittings below their ductile-to-brittle transition temperature, or by hydrogen embrittlement. Also, failure mechanisms that combine mechanical and corrosion aspects are of particular risk, that is, corrosion fatigue, stress corrosion cracking (SCC), etc. Thus, the corrosion problems associated with mechanical fixtures are often one of three types, that is, crevice corrosion, galvanic corrosion, or stress related.[1–3] Individually, these topics are dealt with in some detail in the relevant chapters elsewhere in this book.

As an example, the mechanical joining of aluminum alloys to steel using rivets and bolts, a combination which is difficult to avoid in the shipbuilding industry, represents a typical example of a situation where subsequent galvanic corrosion could occur. Similarly, other examples of an ill-conceived choice of materials, which should normally be avoided, can be found in, for example, brass screws used to attach aluminum plates or steel pins used in the hinges of aluminum windows.

The relative areas of the metals being joined is of primary importance in galvanic corrosion. For example, stainless steel rivets can be used to join aluminum sheet (small cathode, large anode), whereas the reverse situation would lead to rapid deterioration of aluminum rivets (large cathode, small anode). However, in the former case a more dangerous situation could arise if a crevice was present, for example, a loose rivet, since under these circumstances the effective anodic area of the aluminum sheet would be reduced, with consequent localized attack. In general, under severe environmental conditions, it is always necessary to insulate the components from each other by use of insulating washers, sleeves, gaskets, etc. as shown in **Figure 1**. The greater the danger of galvanic corrosion, the greater the necessity to ensure complete insulation; washers may suffice under mild conditions but a sleeve must be used additionally when the conditions are severe.[4]

The fasteners themselves may be protected from corrosion and made compatible with the metal to be fastened by the use of a suitable protective coating, for example, a metallic or organic coating, etc. The choice of fastener and protective coating, or the materials from which it is manufactured, must be made in relation to the components of the joint and environmental conditions prevailing. A point that cannot be overemphasized is that, in the long term, stainless steel fasteners should always be used for securing joints of stainless steel parent metal.

In the case of protection with organic coatings, it is dangerous to confine the paint to the more anodic component of the joint because if the paint is scratched, intense localized attack is likely to occur on the exposed metal. In general, organic coatings should be applied to both the anodic and cathodic metal, but if this is not possible, the more cathodic metal rather than the more anodic metal should be painted. The use of high-strength steels for bolts for fastening mild steel does not normally present problems, but a serious situation could arise if the structure is to be cathodically protected, particularly if an impressed current system is to be used, since failure could then occur by hydrogen embrittlement; in general, the higher the strength of the steel and the higher the stress, the greater the susceptibility to cracking.

In summary, mechanical joints are important joining methods. However, attention must be given to materials compatibility in order to avoid dissimilar metal

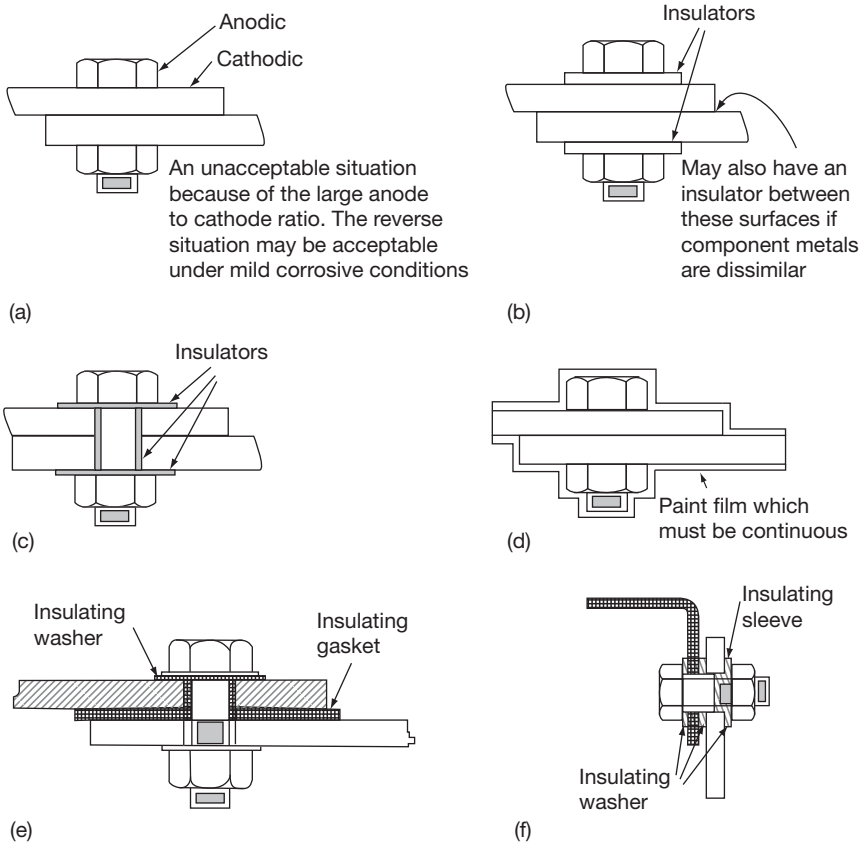

Figure 1 Design of insulated joints. Reproduced from Layton, D. N.; White, P. E. *Br. Corros. J.* **1966**, *1*(6), 213.

corrosion problems, crevice corrosion, for example, for aluminum,[5,6] stress corrosion, and corrosion fatigue.

3.35.3 Soldering and Brazing

These metal joining processes are essentially identical apart from the temperature of joining, which is lower for soldering (generally below ~500 °C) than for brazing (generally above ~500 °C). A characteristic of both processes is the formation of an interdiffusion layer between the parent and filler metal that, if properly formed, constitutes the main metallurgical bond, which results in the strength of the joint. Since a filler material is used for joining which is necessarily different from the parent metal, galvanic corrosion is one of the characteristic failure mechanisms.

3.35.3.1 Soldered Joints

Soldering and brazing are methods of joining components together with a lower-melting-point alloy such that the parent metal (the metal or metals to be joined) is not melted. Traditional alloys for this purpose are summarized in **Table 1**, although it should be noted that many of the lead-containing alloys are no longer in use. In the case of soft soldering, the maximum temperature employed is usually of the order of 250 °C, and the filler alloys used for joining are generally based on a tin alloy composition. The components must present a clean surface to the solder to allow efficient wetting and flow of the molten filler and to provide a joint of adequate mechanical strength. To obtain the necessary cleanliness, degreasing and mechanical abrasion may be required followed by the use of a flux to remove any remaining oxide film and to ensure that no tarnish film develops on subsequent heating.

Soldered joints present their own characteristic corrosion problems usually in the form of dissimilar metal attack often aided by inadequate flux removal after soldering. Such joints have always been a source of concern to the electrical industry.[7,8] However, in view of the toxicity of lead and its alloys, the use of lead solders, particularly in contact with potable waters and foodstuffs, is effectively no longer permitted.

Table 1 Traditional soldering and brazing alloys

Process	*Temperature range(°C)*	*Typical fillers*	*Fluxes*
Soldering			
Hot iron, oven, induction, ultrasonic, dip, resistance, wave and cascade	60–300	70Pb–30Sn 40Pb–60Sn 70Pb–27Sn–3Sb 40Pb–58Sn–2Sb Sn–Zn–Pb	Chloride based Fluoride based Resin based
Brazing			
Torch, dip, salt bath, furnace, induction, resistance	500–1200	90Al–10Si 50Ag–15Cu–17Zn–18Cd Ag–Cu–Ni–In 60Ag–30Cu–10Zn 50Cu–50Zn 97Cu–3P 70Ni–17Cr–3B–10Fe 82Ni–7Cr–5Si–3Fe 60Pd–40Ni	Borax based Fluoride based Hydrogen gas Town's gas Vacuum

In the case of carbon and stainless steels, and many of the nonferrous alloys, the fluxes are based on acidic inorganic salts, for example, chlorides, which are highly corrosive to the metal unless they are removed subsequently by washing in hot water. For soldering tinplate, copper, and brass, it is possible to formulate resin-based fluxes having noncorrosive residues, and these are essential for all electrical and electronic work. Activators are added to the resin to increase the reaction rate, but these must be such that they are thermally decomposed at the soldering temperature if subsequent corrosion is to be avoided.[9] Corrosion is always a particular risk with soldered joints in passive materials such as aluminum owing to the relatively large difference in electrochemical potential between the filler alloy and the parent metal and the highly corrosive nature of the flux that is generally used for soldering. With aluminum soldering, it is imperative that the joints be well cleaned both prior and subsequent to the soldering operation, and the design should avoid subsequent trapping of moisture.

3.35.3.2 Brazed Joints

When stronger joints or higher temperature service are required, brazing may be used.[10] The filler alloys employed generally melt at much higher temperatures (600–1200 °C), but the effectiveness of the joining process still depends upon surface cleanliness of the components to ensure adequate wetting and spreading. Metallurgical and mechanical hazards may be encountered in that the filler may show poor spreading or joint filling capacity in a certain situation or may suffer from hot tearing, whilst during furnace brazing in hydrogen-containing atmospheres there is always the possibility that the parent metal may be susceptible to hydrogen embrittlement or steam cracking. Furthermore, brittle diffusion products may be produced at the filler base-metal interface as a result of the reaction of a component of the filler alloy with a base-metal component, for example, phosphorus-bearing fillers used for steel in which the phosphorus diffuses into the steel.

Damage during the brazing procedure can be caused by excessive diffusion into the parent metal of the molten brazing alloy, especially where the parent contains residual or applied stresses, which can lead to liquid metal embrittlement. Nickel and nickel-rich alloys are particularly prone to liquid-braze-filler attack especially when using silver-based braze fillers at temperatures well-below the annealing temperature of the base metal, since under these conditions there is no adequate stress relief of the parent metal at the brazing temperature. The problem may be avoided by annealing prior to brazing and ensuring the maintenance of stress-free conditions throughout the brazing cycle. A range of silver-, nickel-, and palladium-based braze fillers of high oxidation and corrosion resistance have been developed for joining the nickel-rich alloys; however, the presence of sulfur, lead, or phosphorus in the base-metal surface or in the filler can be harmful, since quite small amounts can lead to interface embrittlement. In the case of nickel–copper alloys, the corrosion resistance of the joint is generally less than that of the parent metal and the design must be such that as little as possible of the joint is exposed to the corrosive media.

With carbon and low-alloy steels, the braze fillers are invariably noble to the steel so that there is less likelihood of corrosion (small cathode/large anode system). However, for stainless steels a high-silver braze filler alloy is often used to retain the corrosion resistance of the joint. However, embrittlement of the filler is always a possibility if any zinc, cadmium, or tin are present. An interesting example of the judicious choice of braze filler is to be found in the selection of silver alloys for the brazing of stainless steels to be subsequently used in a tap-water environment.[11] Although the brazed joint may appear to be quite satisfactory, after a relatively short exposure period, failure of the joint occurs by a mechanism which appears to be due to the breakdown of the bond between the filler and the base metal. Dezincification is a prominent feature of the phenomenon[12,13] and zinc-free braze alloys based on the Ag–Cu system with the addition of nickel and tin have been found to inhibit this form of attack. A similar result is obtained by electroplating of nickel over the joint area prior to brazing with a more conventional Ag–Cu–Zn–Cd alloy. Interface corrosion of brazed stainless steel joints has been reviewed by Kuhn and Trimmer,[14] whilst Lewis[15] has used X-ray photo-electron spectroscopy to confirm the dezincification theory. On the other hand, the corrosion resistance of a high temperature brazed joint in a Mo-containing low-C stainless steel exposed to drinking water gave no problems.[16]

When, in an engineering structure, an aluminum–bronze alloy is selected for corrosion resistance, the choice of braze filler becomes important. Thus, although copper–zinc brazing alloys are widely used, the corrosion resistance of the resultant joint (effectively of brass) will be significantly worse than that of the bronze. Crevice corrosion has also been found when joining copper tubes using Cu–Ag–P fillers, the presence of scale adjacent to the joint being deemed responsible.[17] Brazing with copper alloys is unsuitable for equipment exposed to ammonia and various ammoniacal solutions because of the likelihood of increased corrosion, especially SCC with copper- and nickel-base alloys; however, an alloy based on Fe–3.25B–4.40Si–50.25Ni has been shown to be suitable for such applications.[18]

3.35.4 Welded Joints

3.35.4.1 Welding Processes

A weld differs from all other forms of joint in that the intention is to ideally obtain a homogeneous material (i.e., continuous and of similar microstructure and composition) throughout the volume of the welded joint. There are a large variety of processes by which this may be achieved, most of which depend upon the application of thermal energy to bring about a plastic or molten state of the metal surfaces to be joined. The more common processes used are classified in **Table 2**.

Examination of a welded joint shows several distinct zones, namely the fusion zone with its immediate surroundings, the heat affected zone (HAZ) adjacent, and the parent metal that remains unaffected, **Figure 2**. It is apparent that welding necessarily produce differences in microstructure between the (effectively) cast deposit, the HAZ which has undergone a variety of thermal cycles, and the parent plate. Furthermore, differences in chemical composition are often present between parent and weld metal. Other characteristics of welding include:

1. The production of a residual stress system which remains after welding is completed, and which, in the vicinity of the weld, is tensile and can exceed yield.
2. In the case of fusion welding, the surface of the deposited metal has a generally rough surface profile that is both a stress raiser and a site for the condensation of moisture.
3. The joint area is covered with an oxide scale and possibly a slag deposit which may be chemically reactive, particularly if hygroscopic.
4. Protective coatings on the metals to be joined are inevitably removed during welding so that the weld and the parent metal in its vicinity become unprotected compared with the bulk of the plate.

Table 2 Typical joining processes

Joining process	*Types*
Mechanical fasteners	Nuts, bolts, rivets, screws
Soldering and brazing	Hot iron, torch, furnace, vacuum
Fusion welding	Oxyacetylene, manual metal arc, tungsten inert gas, metal inert gas, carbon dioxide, pulsed arc, fused arc, submerged arc, electro slag, and electron beam
Resistance welding	Spot, seam, stitch, projection, butt, and flash butt
Solid-phase welding	Pressure, friction, ultrasonic and explosive

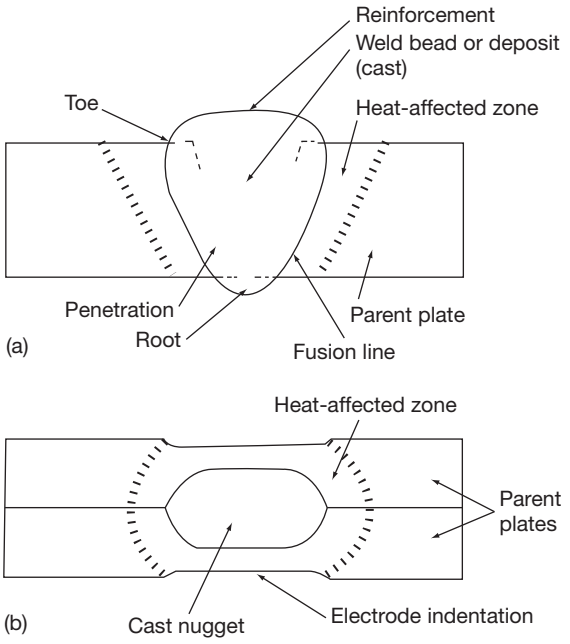

Figure 2 Weld definitions. (a) fusion weld and (b) resistance spot weld.

Therefore, the use of welding as a method of fabrication may modify the corrosion behavior of an engineering structure, and this may be further aggravated by removal of protective systems applied before welding, whilst at the same time the use of such anticorrosion coatings may lead to difficulties in obtaining satisfactorily welded joints.[19–21]

3.35.4.2 Weld Defects

There is no guarantee that defect-free joints will automatically be obtained when fabricating 'weldable' metals. This is a result of the fact that weldability is not a specific material property but a combination of the properties of the parent metals, filler metal (if used), and various other factors that are summarized in **Table 3**.[22] The consequence of the average structural material is to produce a situation where defects may arise in the weld deposit or HAZ, as summarized in **Table 3** and **Figure 3**.

It is obvious that these physical defects are dangerous in their own right but it is also possible for them to lead to subsequent corrosion problems, for example, pitting corrosion at superficial nonmetallic inclusions and crevice corrosion at pores or cracks. Other weld irregularities which may give rise to crevices include the joint angle, the presence of backing strips and spatter, as summarized in **Figure 4** and **Table 4**.

Table 3 Factors affecting weldability after Lundin

Parent metal	*Filler metal*	*Other factors*
Composition	Composition	Degree of fusion
Thickness	Impact strength	(Joint formation)
State of heat treatment	Toughness	Degree of restraint
Toughness	Hydrogen content	Form factor
Temperature	Purity	(Transitions)
Purity	Homogenicity	Deposition technique
Homogenicity	Electrode diameter (heat input during welding)	Skill and reliability of the welder

Source: Lundin, S. *ESAB, Göteborg* **1963**, 2.

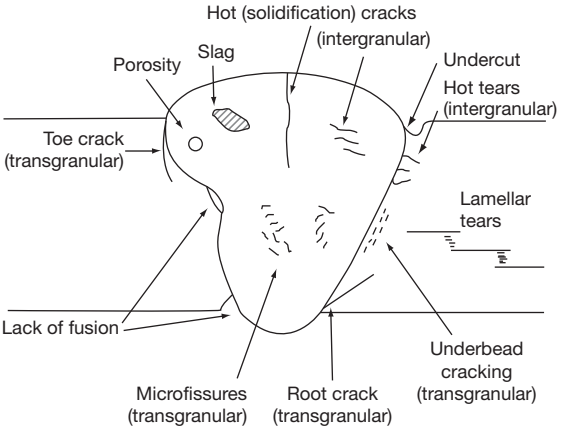

Figure 3 Possible weld defects.

3.35.4.3 Factors Affecting Weldment Corrosion

Corrosion of welds may result from one or more of a number of factors, including:

1. Deficient weld design
2. Residual stresses
3. Inadequate consumables
4. Deficient welding procedure or welding technique
5. Incomplete penetration
6. Weld features such as the geometry of the weld bead
7. Surface finish, due, for example, to oxide film or scales on the weld surface, weld slag or spatter.

3.35.4.3.1 Weldment design

Weld joint design is a relevant factor to be considered in the overall corrosion performance assessment of equipment, and the design stage provides the best

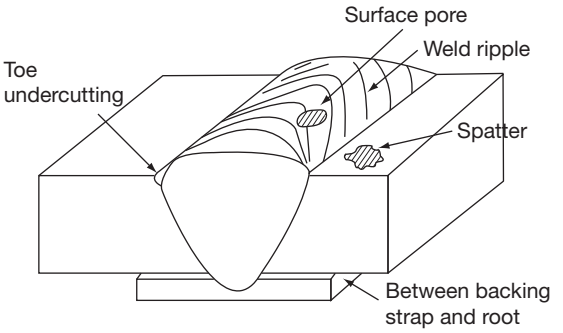

Figure 4 Possible crevice sites.

opportunity to avoid future corrosion problems relating to both the weld material and the weld geometry. The specification of the ideal geometry in regard to corrosion resistance has sometimes to be sacrificed in favor of the necessity to attend to other relevant construction aspects, for example, component flexibility. When possible, the weld should be located in an easily accessible area that allows for easy inspection, for example by nondestructive testing or even by visual inspection, and avoids stress concentration.

Some of the more significant features of weldment geometry are those that might cause crevice corrosion problems. These can be eliminated at the equipment design stage by a proper weld design, for example, by the use of butt rather than overlap welds. Weld joint geometry may affect the corrosion performance of a welded structure by creating conditions leading to dead volumes that may lead to accumulation of debris or corrosion products. These causes exacerbate corrosion by:

1. Allowing the area to remain wet longer than the rest of the equipment.
2. Contributing to the accumulation of aggressive species beneath them.
3. Allowing differentiated access of oxygen to the surface.
4. Preventing adequate drainage of equipment during downtime periods, rendering the fluid stagnant, and increasing the localized corrosion rate.

Some weld joint geometries may also cause crevice corrosion. For example, an overlap or T weld is an inevitable crevice former. Also, the use of skip welding instead of continuous welding introduces crevices, as illustrated in Figure 5. In principle, these problems can be avoided by the application of a sealing weld. However, sometimes the solution is not so straightforward because this might introduce unacceptable constraints into the equipment that can cause cracking or even promote other corrosion phenomena, such as SCC.

Table 4 Weld defects

Defect	*Causes*	*Remedies*
Hot cracks	Large solidification range Segregation Stress	More crack-proof filler Less fusion
Under bead cracks	Hardenable parent plate Hydrogen Stress	Low hydrogen process Planned bead sequence Preheating
Microfissures	Hardenable deposit Hydrogen Stress	Low hydrogen process Pre- and post-heating
Toe cracks	High stress Notches Hardenable parent plate	Planned bead sequence Pre-heating Avoidance of notches
Hot tears	Segregation Stress	Less fusion Cleaner parent plate
Porosity	Gas absorption	Remove surface scale Remove surface moisture Cleaner gas shield

3.35.4.3.2 *Weldment backing*

A common deficiency of weld joint geometry is faulty weld penetration through the complete thickness of the section to be joined. Incomplete or excess penetrations are the two most serious defects in root passes, both of which have an impact on corrosion performance. In some geometries and welding positions, the root pass liquid weld metal pool tends to fall toward the interior of the structure resulting in excessive penetration. This can cause flow disturbance, particularly in small diameter pipes. Furthermore, splatter can also form on the internal surface. Both defects can compromise the corrosion performance of the equipment, and welders often tend to produce incompletely penetrated welds, which produce crevices in which corrosion can occur by the accumulation of aggressive species. To avoid this, backing rings can be used. These accessories help control the weld pool on the root pass, which is essential to produce a

satisfactory weld, allowing an easier inner surface alignment and an acceptable internal root profile. Furthermore, backing rings can have a chilling effect on the weld metal and the HAZ, reducing the total heat input which often has a positive impact on the HAZ width and weldment microstructures resulting from the welding operation. A common backing material is copper, which has a high thermal conductivity. However, other backing materials are also used such as anodized aluminum, stainless steel, mild steel, or even nonmetallic materials like ceramics.

Although the use of backing materials is positive from the welding standpoint, a permanent backing material may reduce the corrosion resistance of the weld joint. It creates an internal obstruction that will disturb flows and may induce erosion–corrosion, a crevice that may lead to crevice corrosion and possible galvanic incompatibility that may promote galvanic corrosion if the material is not chosen correctly. To overcome the disadvantages associated with permanent backings, inserts have been developed, that are consumed in the root pass, assuring complete penetration and a smooth root pass.

3.35.4.3.3 Welding procedure or technique

Apart from incomplete or excessive penetration, other incorrect or inadequate aspects of welding operations can have an impact on the weldment corrosion performance. A weld is always a metallurgically inhomogeneous area compared to the parent material. Often, depending on welding parameters or cooling rates, this may lead to the formation of second phases, precipitates, grain boundary segregation, or even grain growth, which has consequences for the mechanical and corrosion properties of the weldment. Thus, an inappropriate thermal cycle can lead to a severe reduction in fracture toughness due to martensite formation in the case of carbon or low alloy steels, sensitization in the case of stainless steels, an inappropriate proportion of phases as in the case of duplex stainless steels, or secondary phase formation/distribution in the case of aluminum alloys.

Weld metal surface roughness or finish, or even the geometrical transition of the weld cap to the parent material, can provide stress raisers and therefore crack initiators in conditions with the potential for SCC or corrosion fatigue. Also, weld slag or spatter can create the conditions for crevice corrosion. Insufficient shielding gas protection can produce excessive oxidation of the welded area resulting in the formation of films or even scales that reduce the localized corrosion resistance, particularly in the case of stainless steels. Note that welding is much more readily controlled in the fabrication shop than in the field, and field repair welding presents particular challenges in relation to the control of procedures and techniques.

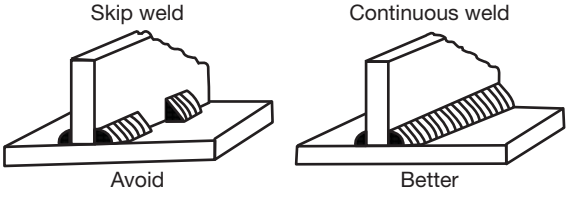

Figure 5 Skip welding and crevice corrosion versus continuous welding. Reproduced from Landrum, R. J. *Fundamentals of Designing for Corrosion Cont*rol; NACE, 1989.

3.35.4.3.4 Residual stresses and stress concentration

A weld is a geometric discontinuity that may concentrate residual, service, or applied stresses. Thermal contraction in the cooling stage and phase transition resulting from the welding process may introduce residual stresses in or at the vicinity of the weld joint, as shown schematically in Figure 6. Furthermore, surface irregularities associated with the roughness of the weld bead or other defects may act as stress raisers. The resulting applied stress, that is, the sum of all stresses in a component, may introduce a vulnerability to phenomena such as corrosion fatigue, SCC, hydrogen induced cracking, or hydrogen embrittlement. The crack orientations will vary with the relevant stress fields:

1. Longitudinal cracks oriented parallel to the weld cord arise as consequence of transverse contraction.
2. Longitudinal cracks located on the middle of the weld cord arise as a consequence of an abnormal

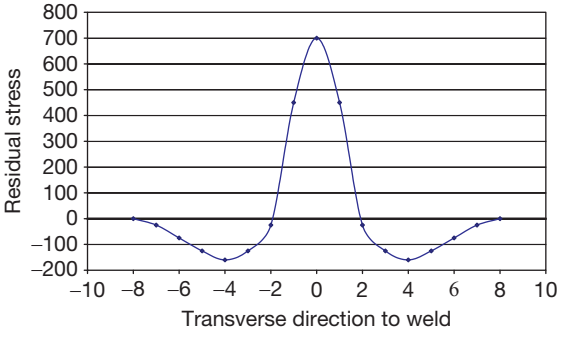

Figure 6 Schematic diagram of typical stress distribution across a butt weld.

stress level on the weld cord resulting from an improper welding technique.
3. Cracks on the weld edges result from the contraction stresses amplified by an edge effect.
4. Cracks on the HAZ parallel to the weld arise as a consequence of transverse contraction.

3.35.4.3.5 Postweld heat treatment

Sometimes, welding procedures require a postweld heat treatment (PWHT). This may be required by the construction code and may have an impact on the corrosion behavior of the weld area. PWHT is undertaken for a number of reasons depending on the requirements of the joint:

1. Annealing to produce recrystallization and eventually grain growth.
2. Softening to reducing the weld hardness in the HAZ.
3. Precipitation hardening to increase the strength
4. Stress relieving to reduce residual fabrication stresses.

These heat treatments may have an impact on the corrosion performance of the weld area to the extent that they might change the microstructure of the weld metal and HAZs, as well as the material surface condition, namely in regard to oxide formation. If a heat treatment is required and it is not adequately performed, it can induce detrimental changes, such as the sensitization of stainless steels or secondary phase precipitation that will strongly affect the corrosion performance of the weld. One of the most common examples of softening relates to materials intended for sour service in the oil and gas industry where materials are submitted to environments in which sulfide stress corrosion cracking (SSCC) may occur.

3.35.4.3.6 Filler metal composition

The weld metal composition is important from the corrosion standpoint. If the weld metal has a lower potential than the materials to be joined, it will corrode preferentially. Furthermore, due to its lower surface area, the corrosion current density for the corrosion process will be very high. In the case of autogenous welds, in which there is no separate filler material, the composition of the weld, *albeit* not necessarily the microstructure, is determined by the adjacent parent material. However, if a filler material is used, it should ideally be more noble than the material, or materials to be joined. Furthermore, when possible, the weld root should face the most aggressive fluid, because it will expose a smaller area.

3.35.5 Welding of Specific Materials

3.35.5.1 Introduction

A review of the extensive work that has been undertaken since the previous edition on the corrosion performances of weldments in specific materials is beyond the scope of this chapter and the reader is referred to other sources such as The Corrosion of Weldments, edited by J. R. Davis, published by ASM International and the publications of relevant alloy suppliers. The pointers to weldment performance that are provided in the following sections are based mostly upon the material published in the previous edition with only minor updating.

3.35.5.2 Carbon and Low-Alloy Steels

Carbon steels undergo metallurgical transformations across the weld and HAZ, and a wide range of microstructures can be developed depending on cooling rates that in turn depend on factors, such as energy input, preheat, metal thickness, weld bead size, etc. Some typical microstructures for a carbon steel weld are shown in **Figure 7**. Clearly, weld metal microstructures will be very different from those of the HAZ and parent material. Preferential corrosion of the HAZ is a common feature in a wide range of aqueous environments. Hardness levels will tend to be lower for high heat input processes such as submerged-arc welding than lower energy processes such as shielded metal arc.

The subject of weldment corrosion in offshore engineering was reviewed by Turnbull.[23] Galvanic effects are possible if the steel weld metal is anodic to the surrounding parent plate and is enhanced by the high anode to cathode surface area ratio that exists. Lundin[24] showed, for carbon steel, that weld metal deposited using a basic flux was less noble; acid fluxes resulted in a more noble weld metal, while rutile-based fluxes were intermediate. The nature of the surface and its prior treatment (e.g., peening) seemed to have no effect. It was also noted that the HAZ was no less corrosion resistant than the unaffected plate. Millscale and other heat oxides should always be removed by grit blasting as its presence can cause serious corrosion problems around welded joints. On the other hand, Saarinen and Onnela[25] considered that weld metal corrosion can be eliminated by using a suitably balanced electrode type, the remaining problem then being in the HAZ whose tendency to corrode (i.e., become more active) increased with increasing Mn content. Thus, the heat input during welding must be

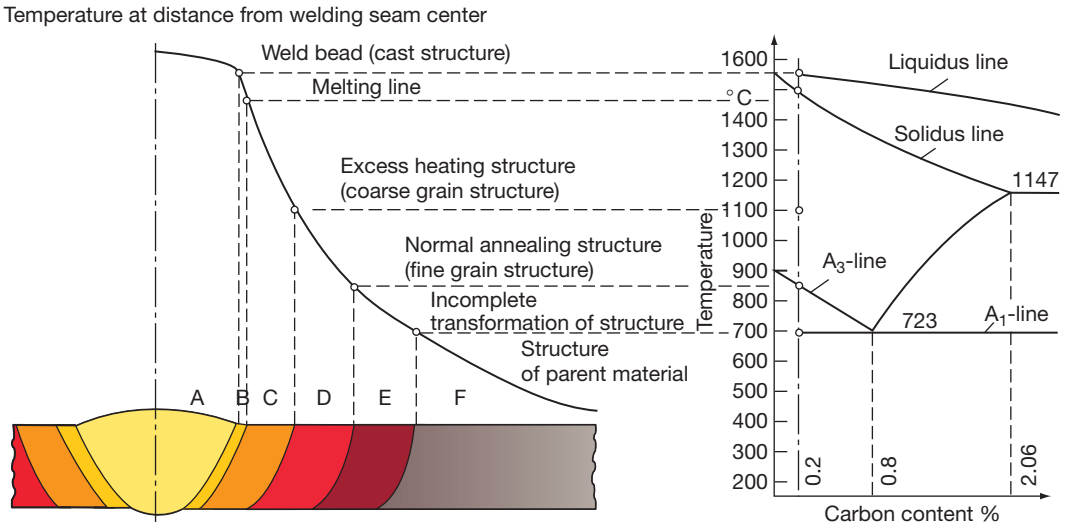

Figure 7 Variation of weld structure with distance from the welding seam center. Reproduced from ISQ training material.

important since a significant factor will be the cooling rate of the HAZ after welding. These findings have been substantiated by Ousyannikov *et al.*[26] using a scanning reference electrode probe. Increasing the heat input changed the weld metal from anodic to cathodic relative to the parent plate, although the presence of Ni reduced the magnitude of the effect.

The problem of grooving corrosion in line-pipe steel welded by high frequency induction or electric resistance welding has been studied. In sea water, it seems to be related to high sulfur content in the weld zone, the type of environment, its temperature, and velocity.[27] The importance of sulfur is significant since Drodten and Herbsleb have reported that localized corrosion at welded joints is more a function of S, Si, microstructure, and nonmetallic inclusion type and shape than of the local oxygen concentration.[28]

One of the major concerns in offshore construction is that of the corrosion fatigue. Turnbull[24] discusses this at length. Cracks usually originate at weld toes, the point of initiation being associated with crack-like defects (slag, nonmetallics, cold laps, undercuts, hot tears). These can constitute sharp notches situated at a point of maximum stress concentration due to the weld geometry. It is to be noted that although cracks initiate in the HAZ at the weld toe, the majority of crack propagation occurs in what is essentially unaffected parent plate. In air, it is possible to have cracks that grow at a decelerating rate until no further growth occurs, this is the 'short crack' problem widely discussed by Miller,[29] and the cracks are referred to as nonpropagating cracks. On the other hand, similar cracks may continue to grow at an accelerating rate in a corrosive environment even though the stress may be below the fatigue limit. Burns and Vosikovsky[30] have given considerable attention to corrosion fatigue of tubular joints in structural and line-pipe steels. Crack initiation at the toe occurs after a small fraction of life, and long surface cracks can exist for over 50% of the life. On the other hand, laboratory tests on plate-to-plate welded specimens of the cruciform type show cracks which are much smaller for a larger percentage of the life, but their growth rate accelerates as the depth increases.

In sea water, the effects of cyclic frequency, stress ratio, electrochemical potential, oxygen content, and intermittent immersion at 5–12 °C have all been evaluated.[31] There is some evidence that at lower temperatures, seawater is less detrimental to fatigue life, but at all temperatures studied, the crack growth rate was always faster than in air. At intermediate ranges of stress intensity range (ΔK), there was a significant reduction in crack growth rate as the seawater temperature was reduced from 25 °C to 0 °C. Whilst the cracks are small and ΔK low, calcareous blocking is very effective, and under these conditions and correctly applied cathodic protection (CP) consequently reduces the crack growth rate. As the crack length increases, blocking becomes less effective and the increased hydrogen embrittlement can accelerate the growth rate to values greater than experienced for the unprotected joints. Similarly,

Nibbering *et al.*[31] obtained data showing that CP raises the initial fatigue crack resistance but has little effect at a later stage of crack propagation. Even so, they considered that CP is still the most effective method for prolonging structural life under corrosion fatigue conditions. This is not unreasonable since crack initiation and early growth can represent a large proportion of the total life.

Marine fouling leading to the local production of H_2S increases crack growth rate, but what the effect is when combined with CP is uncertain. Some of the factors mentioned earlier in connection with other steel corrosion problems are important to sulfide stress-corrosion cracking (SSCC). For example, the use of high strength low alloy steels in which carbon is reduced to below 0.05% combined with reduced sulfide segregation are beneficial to preventing SSCC of weldments.[32,33] SSCC of weld repairs in well-head alloys was investigated by Watkins and Rosenberg[34] who found that the repairs were susceptible to this problem because of the hard HAZs developed by welding. Postweld heat treatment was an essential but not complete cure compared with unrepaired castings. In the case of hydrogen-assisted cracking of welded structural steels, composition is more important than mechanical properties and the carbon equivalent should be $<0.5\%$.[35,36] McMinn has presented much useful data concerning the fatigue crack growth rate in simulated HAZs of A533-B steels,[37] whilst Ray *et al.* have demonstrated the role of pitting corrosion of mild steel on crack initiation.[38]

3.35.5.3 Stainless Steels

There are four groups of stainless steels, each possessing their own characteristic welding problems:

1. Ferritic: Welding tends to result in a large grain size throughout the weld zone causing significant reduction in ductility. Also, the ferritic microstructure is susceptible to hydrogen embrittlement.
2. Martensitic: HAZ cracking is likely and may be remedied by employing the normal measures required for the control of hydrogen-induced cracking.
3. Austenitic: These steels may be readily welded but are susceptible to hot cracking, which may be controlled by permitting a small amount of residual delta ferrite in the weld.
4. Duplex: Welding of duplex alloys requires correct choice of weld material and procedures, in particular weld heat input, in order to ensure the retention of a satisfactory weld microstructure.

The corrosion of stainless steel welds was reviewed in the 1970s by Pinnow and Moskowitz[39] and, although this article is clearly dated in detail, the main general issues are still of relevance. Thus, main problems that might be encountered are weld decay, knife-line attack, and SCC, as illustrated in **Figure 8**.

3.35.5.3.1 Ferritic and martensitic stainless steels

The more traditional compositions with a relatively high (C + N): Cr ratio carry a risk of martensite formation in the HAZ during cooling.

Furthermore, there is a risk for carbide precipitation and therefore, for intergranular corrosion. More modern grades of ferritic stainless steel have a low (C + N): Cr ratio and possess stabilizing elements added to the material to reduce the likelihood of intergranular corrosion. Ferritic stainless steels are also liable to grain growth in the HAZ, as illustrated in **Figure 9**. Therefore, heat input should be kept to a minimum, **Figure 9**. Also, insufficient gas protection during welding may lead to chromium nitride formation due to N_2 uptake from the atmosphere, and consequently, to embrittlement and decreased corrosion resistance. Finally, the gas used for shielding as well as the metal surface should be free of H_2 sources (e.g., moisture, oil, and grease) in order to avoid hydrogen embrittlement.

3.35.5.3.2 Austenitic stainless steels

Although readily welded, these are susceptible to hot cracking which may be overcome by balancing the weld metal composition to allow the formation of a small amount of δ-Fe (ferrite) in the deposit, optimum crack resistance being achieved with a δ-ferrite content of 5–10%, as illustrated in **Figure 10**. More than this

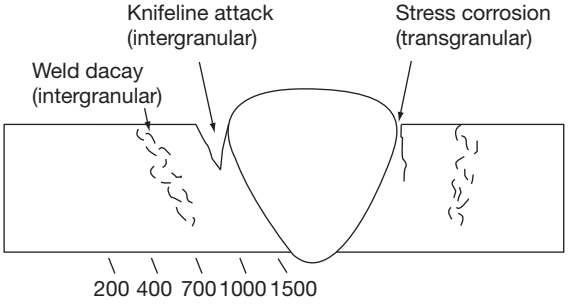

Figure 8 Common sites of corrosion in stainless steel welds; typical peak temperatures attained during welding (°C) are given at the foot of the diagram. Note that knife-line attack has the appearance of a sharply defined line adjacent to the fusion zone.

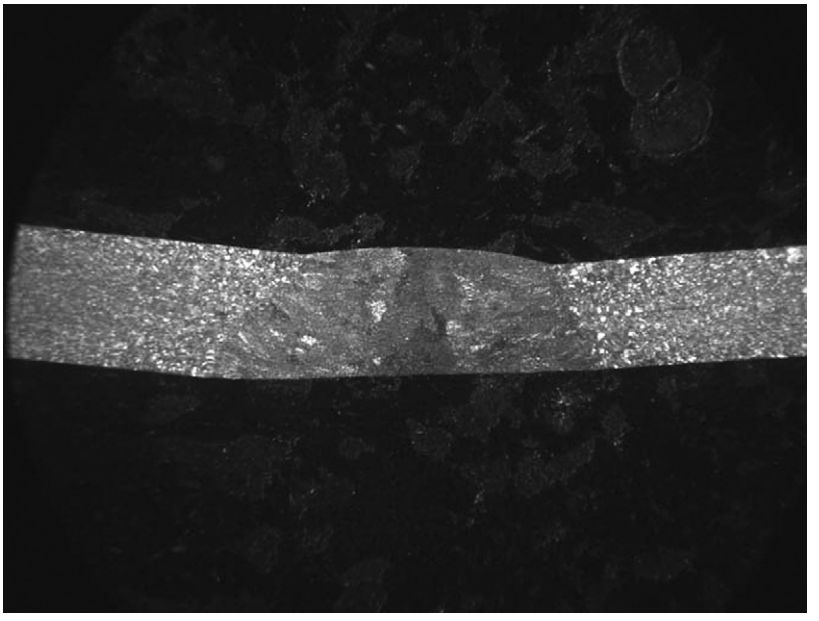

Figure 9 Ferritic stainless steel weld showing large grain size in the weld and heat affected zone.

Figure 10 Dendritic ferrite in an austenite weld (left); heat affected zone (center); equiaxed austenitic grains in the parent metal (right).

concentration increases the possibility of σ-phase formation if the weldment is used at elevated temperature consequently reducing both mechanical and corrosion properties. Any adverse effects of the δ-ferrite on corrosion resistance are usually overcome by slight enrichment of the filler metal composition relative to the parent material. However, in certain critical applications such as the manufacture of urea, δ-ferrite can reduce corrosion resistance to an unacceptable extent in which case fully austenitic welds are required.

Prasad Rao and Prasanna Kumar[40] undertook electrochemical studies of austenitic stainless steel claddings to find that heat input and delta ferrite content significantly affected the anodic polarization behavior under active corrosion conditions, whilst Herbsleb and Stoffelo found that two-phased weld claddings of the 24Cr–13Ni type were susceptible to intergranular attack (IGA) as a result of sensitization after heat treatment at 600 °C.[41]

3.35.5.3.3 Duplex stainless steels

These steels have a better weldability than ferritic steels. They are purely ferritic at high temperatures, and if quenched rapidly they may remain predominantly ferritic and the ferrite phase is sensitive to chromium nitride and brittle phase formation. Modern duplex stainless steels have a high content of nitrogen, which is an austenite stabilizer. This facilitates austenite formation at high temperatures and consumes the nitrogen, preventing the formation of nitrides in the ferritic phase. Duplex filler metal is also formulated with more nickel than the parent

material to promote austenite formation. As a result, the as-welded structure has a balance of ferrite and austenite that is close to the equilibrium structure of the parent material. Nitrogen additions to the weld shielding gases also assist in maintaining the correct composition of the weld and heat affected zones. Duplex stainless steels are also susceptible to intermetallic phase formation approximately in proportion to their chromium and molybdenum contents. This decreases the corrosion resistance and mechanical properties such as toughness. Precipitation of intermetallic phases is favored by high heat inputs that need to be controlled, particularly in thick sections, to avoid adverse effects.

3.35.5.3.4 Sensitization

Carbide precipitation and growth causes the formation of a chromium depleted area around the grain boundaries and chromium carbide formation at the grain boundaries. When sensitized material is subjected to an aggressive medium, preferential attack occurs.

Sensitization results from exposure of the material to high temperatures, either during production, or as a result of welding operations. Sensitization temperatures are in the range 425–815 °C. Although sensitization is primarily caused by chromium and carbon, other elements present in the stainless steel may play a secondary role in sensitization. Thus, Ni increases carbon activity in the solid matrix; favoring carbide precipitation and Mo has behavior similar to chromium, although it is usually present in lower amounts.

Nowadays, most commercial grades of stainless steel are of an 'L' grade and low in carbon. Hence, sensitization rarely occurs; as can be seen in **Figure 11**, reduction in carbon concentration greatly increases the time required for sensitization to occur. However, surface sensitization, most commonly from surface hydrocarbon contamination (i.e., from oil and grease) remains an issue. Sensitization can only be reversed by heat-treatment to affect a re-solution of the chromium carbide (preferably at ~1050 °C), which is generally impractical in most structures.

Under certain conditions, it is possible for a weldment to suffer corrosive attack which has the form of a fusion line crack emanating from the toe of the weld; this is termed knife-line attack. It is occasionally experienced in welded stainless steels that have been stabilized against sensitization by addition of titanium, niobium, or tantalum. The niobium-stabilized steels are more resistant than the titanium-stabilized types by virtue of the higher solution temperature of NbC, but the risk may be minimized by limiting the carbon content of the steel. Knife-line attack is described in detail in **Chapter 2.24, Corrosion in Nitric Acid**.

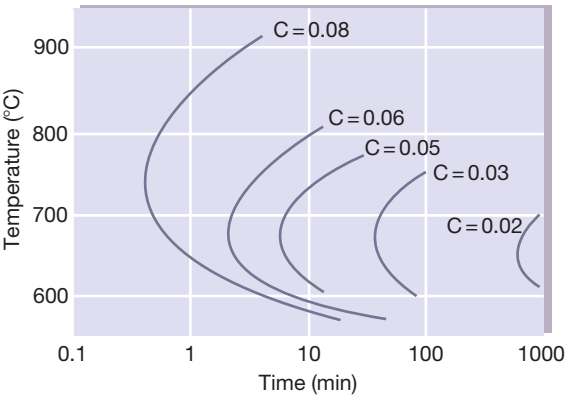

Figure 11 Time–temperature diagram for IGA of 18Cr 9Ni stainless steels with different carbon contents in sulfuric acid–copper sulfate tests showing that lower carbon contents increase the time required for sensitization. Reproduced from Corrosion Handbook, Stainless Steels; AB Sandvik Steel, 1994.

3.35.5.3.5 Localized corrosion at weldments

The various forms of SCC are described in separate chapters in this book. SCC is particularly dangerous because of the insidious nature of the phenomenon. The residual stresses arising from welding are often sufficiently high to provide the necessary stress condition, whilst a chloride-containing environment in contact with the austenitic stainless steels induces the typically transgranular and branched cracking. Increased nickel content marginally improves the resistance of the steel to this type of attack. Also, the ferritic steels and duplex steels with at least 50% ferrite have high resistance to chloride-induced transgranular SCC.

IGA, pitting, and crevice corrosion are problems commonly associated with the stainless steels and their welds. For example in the duplex stainless steels, the corrosion resistance, particularly in terms of pitting and crevice corrosion, depends on microstructure, that is, the relative proportions of ferrite and austenite, the lattice concentration of dissolved nitrogen, and the segregation of alloying elements between the ferrite and austenite phases.[42–44] These may be affected by heat input and welding procedures.[45] Grekula *et al.*,[46] studying pitting corrosion of gas tungsten arc welds in austenitic steels, found that the final interdendritic regions to solidify in primary austenite welds and the austenite interfaces in primary δ-ferrite welds are the most susceptible sites for pit initiation. Sulfur also affects pitting

potential and increases the pit density but has no effect on the pit growth rate.[47] Also, pitting in or adjacent to tungsten inert gas (TIG) weld beads in tap-water may be caused by the surface oxides formed during welding and is generally due to inadequate root gas shielding.[48] It is essential, for optimum resistance to localized corrosion initiation, to remove any weld tint using appropriate pickling fluids/pastes such as nitric acid or light blasting with, for example, rounded glass beads.

Controlled additions of nitrogen have been made to 439 steel weld metal to prevent IGA,[49] whilst additions of Y or Ce to an 18Cr–12Ni steel have also been found to be beneficial.[50] In the case of TIG-welded Mo-containing stainless steels, σ-phase formation can be responsible for IGA in hot oxidizing (e.g., nitric) acids.[51]

3.35.5.4 Nickel Alloys

In the main, welding does not seriously affect the corrosion resistance of the high nickel alloys, and the resistance to stress corrosion is particularly high. Earlier versions of the N–Cr–Mo and Ni–Mo families of alloys had limited thermal stability and were vulnerable to the precipitation of deleterious intermetallic phases during welding. Thus, in the case of the Ni–Cr–Mo–Fe–W type alloys, Samans[52] suggested that the material should be given a two-stage heat treatment prior to single-pass welding in order to produce a dependable microstructure with a thermally stabilized precipitate. In the case of the Ni–28Mo alloy, it was suggested that a special case of selective corrosion analogous to the weld-decay type of attack could be removed by solution treatment or using an alloy containing 2% V.[53] The more recent grades of these alloys have been alloyed to provide much greater thermal stability and are much less vulnerable to loss of corrosion resistance during welding. The chromium-containing alloys can be susceptible to weld decay and should be thermally stabilized with titanium or niobium, and where conditions demand exposure to corrosive media at high temperatures a further post-weld heat treatment may be desirable.

Of the weldability problems, nickel and nickel-based alloys are particularly prone to solidification porosity, especially if nitrogen is present in the arc atmosphere, but this may be controlled by ensuring the presence of titanium as a denitrider in the filler and maintaining, a short arc length. The other problem that may be encountered is hot cracking, particularly in alloys containing Cr, Si, Ti, Al, B, Zr, S, Pb, and P. For optimum corrosion resistance, it is recommended that similar composition fillers be used wherever possible, although overmatching with, for example, molybdenum can compensate for any elemental segregation inherent in the weld metal. Obviously any flux residues that may be present must be removed.

3.35.5.5 Aluminum Alloys

These alloys are susceptible to hot solidification cracking and in order to overcome this problem some aluminum alloys have to be welded with a compensating filler of different composition from that of the parent alloy; this difference in composition may lead to galvanic corrosion. A further problem in the welding of these materials is the high solubility of the molten weld metal for gaseous hydrogen which causes extensive porosity in the seam on solidification; the only effective remedy is to minimize hydrogen pick-up by using a hydrogen-free gas shield with dry, clean consumables (e.g., welding rods, wire), and parent plate.

In general, however, the corrosion resistance of many aluminum alloys is not significantly reduced by welding. Any adverse effects that may be encountered with the higher strength alloys can be largely corrected by postweld heat treatment; this is particularly true of the copper-bearing alloys. Pure aluminum fillers impart the best corrosion resistance, although the stronger Al–Mg and Al–Mg–Si fillers are normally suitable; the copper-bearing fillers are not particularly suitable for use in a corrosive environment.

The HAZ may become susceptible to SCC, particularly in the high-strength precipitation hardened alloys. In this context for Al–Zn–Mg type alloys, it has been shown that maximum sensitivity appears to occur when there is a well-developed precipitation at the HAZ grain boundaries adjacent to the fusion line, a fine precipitate within the grain and a precipitate-free zone immediately adjacent to the grain boundaries.[54]

3.35.6 Protection of Welded Joints

Structural steels are frequently protected from corrosion by means of a paint primer, but these materials can have an adverse effect on the subsequent welding behavior, and this is mainly observed as porosity.[20] Hot-dip galvanizing for long-term protection can also lead to porosity and intergranular cracking after welding, in which case it may be necessary to remove the zinc coating from the edges of the parent material prior to welding. The presence of zinc can also lead to operator problems due to the toxicity of the fume

evolved unless adequate fume extraction is employed. After welding and prior to painting, all welding residues must be removed and the surface prepared by grinding, grit blasting, wire brushing, or chemical treatment. This preparation is of fundamental importance, the method of applying the paint and the smoothness of the bead apparently having little effect on the final result.[55]

In the electric-resistance welding of hot-dipped galvanized steel, welding had little effect on the seawater corrosion of the coated steel when compared with the uncoated steel, the latter showing considerable corrosion after 12 months exposure.[56] The subject of galvanizing and the welding of structural steels has been given special attention by Porter,[57] but by far the most common method of protection is by painting which McKelvie[58] discusses in terms of fundamentals of paint as a corrosion barrier and the cleaning and coating procedures necessary to achieve protection of welded structures. In these articles, he covers the type of contaminants arising from welding as well as cleaning methods, blast primers, galvanizing, coating removal for repair welding, wire brushing, and chemical treatments. Lloyds Register of Shipping lists the proprietary products that have no significant deleterious effects on subsequent welding work.[59]

References

1. Booth, F. F. *Br. Corros. J.* **1967**, *2*(2), 55.
2. Everett, L. H.; Tarleton, R. D. J. *Br. Corros. J.* **1967**, *2*(2), 61.
3. Layton, D. N.; White, P. E. *Br. Corros. J.* **1967**, *2*(2), 65.
4. Layton, D. N.; White, P. E. *Br. Corros. J.* **1966**, *1*(6), 213.
5. Hahn, F. P. *Ind. Corros.* **1984**, *2*(6), 16.
6. Bauer, I. C. O. *Aluminium* **1982**, *58*(5), E146.
7. Costos, L. P. *Weld. J.* **1982**, *61*(10), 320s.
8. Yamaguchi, S. *Werkstoffe Korros.* **1982**, *33*(11), 617.
9. Allen, B. M. *Soldering Handbook;* Iliffe: London, 1969.
10. Collard Churchill, S. *Brazing;* The Machinery: London, 1963.
11. Sloboda, M. H. *Czech. Conf. Brazing* **1969**, 18.
12. Jarman, R. A.; Myles, J. W.; Booker, C. J. L. *Br. Corros. J.* **1973**, *8*(1), 33.
13. Linekar, G. A. B.; Jarman, R. A.; Booker, C. J. L. *Br. Corros. J.* **1975**, 10.
14. Kuhn, A. T.; Trimmer, R. M. *Br. Corros, J.* **1982**, *17*(1), 4.
15. Lewis, G. *Corros. Sci.* **1980**, *20*(12), 1259.
16. Lugscheider, E.; Minarski, P. *Schweissen Schneiden* **1989**, *41*(11), 590.
17. Stevernazel, G. *Werkstoffe Technik.* **1981**, *12*(12), 439.
18. Stenerson, R. N. *Welding J.* **1969**, *48*(6), 480.
19. Gooch, T. G.; Gregory, E. N. *Br. Corros. J.* **1968**, 348.
20. Baker, R. G.; Whitman, J. G. *Br. Corros. J.* **1967**, *2*(2), 34.
21. Hoar, T. P. *Br. Corros. J.* **1967**, *2*(2), 46.
22. Lundin, S. *ESAB, Göteborg* **1963**, 2.
23. Turnbull, A. *Rev. Coat. Corros.* **1982**, *5*(1–4), 43.
24. Lundin, S. *Svetsaren (ESAB)* **1967**, *2*(2).
25. Saarinen, A.; Onnela, K. *Corros. Sci.* **1970**, *10*(11), 809.
26. Ousyannikov, V. Yu.; Chernov, B. B.; Semenchenko, V. S.; Tyul 'Kin Yu, K. *Svar. Proizvod.* **1986**, *4*, 38.
27. Düren, C.; Treiss, E.; Herbsleb, G. *Mater. Perform.* **1986**, *25*(9), 41.
28. Drodten, P.; Herbsleb, G.; Schwenk, W. *Steel Res.* **1989**, *60*(10), 471.
29. Miller, K. J. *Fatigue Eng. Mater. Struct.* **1982**, *5*(3), 223.
30. Burns, D. J.; Vosikowsky, O. *Time-Dependent Fracture*; Krauz, A. S., Ed.; Martinus Nijhoff: Dordrecht, 1985; pp 53.
31. Nibbering, J. J. W.; Buisman, B. C.; Wildschut, H.; Rietbergen, E. *Laser Tech.* **1986**, *9*, 187.
32. Choi, J. K.; Kim, H. P.; Pyun, S. I. *Korean Inst. Met.* **1986**, *24*(1), 14.
33. Terasaki, F.; Ohtani, H.; Ikeda, A.; Nakanishi, M. *Proc. Inst. Mech. Eng. A. Power Process Eng.* **1986**, *200*(A3), 141.
34. Watkins, M.; Rosenberg, E. L. *Mater. Perform.* **1985**, *22*(12), 30.
35. Pircher, H.; Sussek, G. *Stahl und Eisen* **1982**, *102*(10), 503.
36. Drodten, P. *Stahl und Eisen* **1982**, *102*(7), 359.
37. McMinn, A. *FCGR in HAZ-Simulated A533-B steel*; H.M.S.O.: London, 1982.
38. Ray, G. P.; Jarman, R. A.; Thomas, J. G. N. *Corros. Sci.* **1985**, *25*(3), 171.
39. Pinnow, K. E.; Moskowitz, A. *Weld. J.* **1970**, *49*(6), 278.
40. Prasad Rao, K.; Prasanna Kumar, S. *Corrosion* **1985**, *41*(4), 234.
41. Herbsleb, G.; Stoffelo, H. *Werkstovfe Korros.* **1978**, *29*(9), 576.
42. Tamaki, K.; Yasuda, K.; Kimura, H. *Corrosion* **1989**, *45*(9), 764.
43. Fujiwara, K.; Tomasi, H. *Corros. Eng.* **1988**, *37*(11), 657.
44. Angelini, E.; Zucchi, F. *Br. Corros. J.* **1986**, *21*(4), 257.
45. Grekula, A. I.; Kujanpaa, V. P.; Karjalainen, V. P. *Corrosion* **1984**, *40*(11), 569.
46. Chen, J. S.; Levine, T. M. *Corrosion* **1989**, *45*(1), 62.
47. Edling, G. *Svetsen* **1979**, *38*(3), 61.
48. Engelhard, G.; Mattern, U.; Pellkofer, D.; Seibold, A. *Weld. Cutting (Düsseldorf)* **1988**, *40*, 19.
49. Deverell, H. E. *Mater. Perform.* **1985**, *24*(2), 47.
50. Watanabe, T.; El, K.; Nakamura, H. *J. High Temp. Soc. Japan* **1988**, *14*(4), 185.
51. Zingales, A.; Quartarone, G.; Moretti, G. *Corrosion* **1985**, *41(3)*m, 136.
52. Samans, C. H.; Meyer, A. R.; Tisinai, G. F. *Corrosion* **1966**, *22*(12), 336.
53. Lancaster, J. F. *Metallurgy of Joining*; Chapman and Hall: London, 1986.
54. Kent, K. G. *Met. Revs.* **1970**, *15*(147), 135.
55. Keane, J. D.; Bigos, J. *Corrosion* **1960**, *16*(12), 601.
56. Roswell, S. C. *Met. Constr.* **1978**, *104*(4), 163.
57. Porter, F. C. *Met. Constr.* **1983**, *15*(10), 606.
58. McKelvie, A. N. *Met. Constr.* **1981**, *13*(11/12), 693–744.
59. *Approved Prefabrication Primers and Corrosion Control Coatings*; Lloyds Register of Shipping: London, 1983.

Further Reading

Davis, J. R. Ed. *Corrosion of Weldments*; ASM International: Materials Part, OH, 2006.

3.36 Role of Corrosion in the Failure of Adhesive Joints

J. F. Watts
Surrey Materials Institute and Faculty of Engineering & Physical Sciences, University of Surrey, Guildford, Surrey, GUZ 7XH, UK

3.36.1 Introduction

It may seem rather at odds with the general scope of Shreir's Corrosion to include a section on adhesives as these materials are not normally employed as a mechanism of combating corrosion, or recognized as being susceptible to it, although they will, and do undergo environmental degradation. The justification is, however, very straightforward; adhesives are now widely used to bond metal components; metal components corrode, and such corrosion processes may compromise the performance of an adhesive joint, either at the bonded interface or adjacent to it. This chapter seeks to bring together the current state of knowledge regarding failure mechanisms in adhesive joints (much of it obtained from studies of the behavior of organic coatings applied to effect corrosion protection of a metallic substrate) and provide guidelines as to how various failure types may be identified.

Adhesive bonding has reached a level in manufacturing industry where the process can truly be said to be ubiquitous. Applications range from the rapid robotic assembly of small components to the structural adhesive bonding of massive parts in the aerospace and civil engineering industries. Against this background, there is a need to understand failure mechanisms that may occur in adhesively bonded structures during their lifetime and design out such weaknesses. In terms of the initial load-bearing capacity, and subsequent lifetime under well defined conditions, of an adhesive joint, this can be readily determined from standard monotonic or fatigue tests. Arguably, however, the most important attribute of an adhesive joint is the durability that it possesses, that is the level of the original joint strength that will be retained over the lifetime of the structure. The life expectation of an adhesive joint can vary from a few days or weeks for foodstuffs packaging to more than 25 years for an aircraft! Thus, the focus of much adhesive bonding research over the last three decades has sought to catalogue and understand the issues associated with the durability of adhesive joints. The term durability in its strictest sense refers to the exposure of an adhesive joint or adhesively bonded structure to any aggressive liquid (or vapor) phase and as such includes reagents as diverse as fuel, deicing liquid and brake fluid! The generally accepted definition, however, of joint durability refers to the environmental exposure to water. The reason for this is that although durability is the performance of an adhesive bond in any chosen environment, the most aggressive environment as far as the metallic substrate–adhesive interface is concerned is water, and the term durability,

when applied to adhesives, has become synonymous with bond performance when exposed to water in its vapor or liquid form.

In seeking to understand the role of water on the degradation of joint durability, one must be aware that there are several distinct processes that can take place, leading to failure, resulting from different diffusion paths for water molecules in the adhesive and the presence, or otherwise, of electrochemical activity at the coated metallic surface. This gives rise to three distinct failure processes; interfacial failure as a result of hydrodynamic displacement of the adhesive from the substrate, the degradation of the adhesive itself in the environs of the substrate–adhesive (known in the adhesives community as plasticization), and the interfacial failure as a result of cathodic or anodic activity at the substrate, referred to as either cathodic delamination or anodic undermining. The mechanistic aspects of these three processes are well understood and can be related to exposure parameters.

The kinetics of failure is a function of both the environment and design parameters. In some situations, there may be more than one mechanism in operation, and the one that proceeds fastest will invariably become the rate-controlling step, but although it may prove possible to stifle such a mechanism, failure may still occur, albeit at a slower pace, as a result of the kinetics associated with the minor process. A number of authors have attempted to relate experimental observables to a unified mechanism that may serve as a design guide. Test geometries employed have varied from very simple tension or peel geometries to more sophisticated fatigue test pieces. Similarly, some authors have set out to investigate a particular failure process, such as cathodic delamination, while others have set out to study joint performance and have related durability to corrosion processes in an effort to gain a complete understanding of how failure has occurred. This chapter reviews mechanisms of failure, considers the various rate models that have been derived on the basis of empirical results, and finally, suggest ways in which adhesive joint design and specification can be used to reduce the detrimental effects of corrosion on joint durability.

3.36.2 Mechanisms of Failure

3.36.2.1 Hydrodynamic Displacement

The interfacial thermodynamics associated with an adhesive joint are readily addressed using the concepts of interfacial free energy of the substrate, adhesive, and water. Following is the well known Young–Dupré, which defines the thermodynamic work of adhesion (W_A) as

$$W_A = \gamma_S + \gamma_A - \gamma_{AS} \quad [1]$$

where γ_S is the surface free energy of the (oxidized) metal substrate, γ_A is the surface free energy of the adhesive (normally a figure for a generic type of adhesive, such as epoxies, will be used), and γ_{AS} is the interface free energy associated with the substrate–adhesive junction. In a dry environment, the W_A parameter will assume a positive value indicating that the joint is thermodynamically stable. Something that is self evident by visual inspection and mechanical testing will invariably yield a failure within the adhesive layer, often at about the midpoint of the glue line thickness. The important feature here is that from both a thermodynamic standpoint and by experiment, when tested in a dry environment, the interface between substrate and adhesive is strong and stable. The exception to this observation is if a contaminant layer is present on the substrate, such an occurrence will compromise joint strength and lead to an interfacial failure. For this reason, such contamination, known as a weak boundary layer, is to be avoided at all costs in adhesive bond fabrication.

Although stable in a dry atmosphere, the exposure of such a joint to a humid or wet environment can lead to the diffusion of water along the interface, from the exposed joint edge, as indicated in **Figure 1**. Following the approach of Gledhill and Kinloch,[1] eqn [2] can be written to predict the work of adhesion W_A^* in the presence of a third liquid phase, considering the three interfaces that are now involved:

$$W_A^* = \gamma_{SL} + \gamma_{AL} - \gamma_{AS} \quad [2]$$

where the addition of subscript L indicates the interface free energy of substrate or adhesive in contact with the liquid, as indicated in **Figure 1**. Gledhill and Kinloch were able to show that when the values of

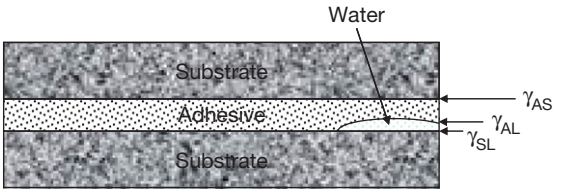

Figure 1 The spontaneous displacement of an adhesive layer on an oxidized metal substrate (e.g., aluminum); the quantity W_A^* will be negative as predicted by eqn [2].

W_A^* were negative (indicating that the process is thermodynamically favorable), there was a good correlation with empirical results in which a variety of joints were exposed to various liquids. Calculated values of W_A^* from these systems were either positive or negative, and those with a negative value showed spontaneous (but not instantaneous) separation when exposed to the liquid. (The term spontaneous is used in the thermodynamic sense, meaning energetically favorable, and has no implications regarding the kinetics of the process. This usage should not be confused with the same word taken in a sense to mean instantaneous, as in the term spontaneous combustion much favored by the popular press!)

Although outside the scope of this article, it must be appreciated that such an approach is only valid when the forces of adhesion are a result of van der Waals forces, more usually subdivided into dispersion and polar forces. These forces are generally rather weak and readily compromised by the presence of water. Specific interaction at interfaces, such as covalent bonds or donor–acceptor interactions (also known as acid–base bonds, of which hydrogen bonds are an important subcategory), are not so susceptible to degradation by water, and for this reason, the energetics approach described above is not applicable, and the presence of such bonds at the substrate–adhesive interface has, in itself, the propensity to improve bond durability.

Thermodynamic considerations indicate a true interfacial failure, as described above, and this can be established by the use of surface analysis methods such as X-ray photoelectron spectroscopy (XPS) and time-of-flight secondary ion mass spectrometry (ToF-SIMS). As some failure mechanisms may leave vanishingly thin adhesive residues on the substrate (<5 nm), the use of optical or scanning microscopy, analysis by EDX or FT-IRS is really not good enough, and methods than can explicitly provide a chemical analysis of such very thin layers are required.

Although the study of organic coatings provides valuable mechanistic information regarding failure modes that can be transferred directly to studies of the failure of adhesive joints, there is one major difference that must be considered when making this analogy. In the case of coatings, downward diffusion of water molecules, perhaps mitigated by the concomitant diffusion of solvated ions, is always likely to occur, whereas in the case of adhesively bonded substrates, this is only an important consideration if one or other substrate is permeable to water. This is clearly not the case in the adhesive bonding of metallic substrates, although it may become so if one or other of the substrates is a polymeric material, or if so-called 'open-face' model joints are being considered. Thus, the usual pathway for the diffusion of water and other aggressive or deleterious species is laterally from the joint edge, either along the interface, as considered in **Figure 1**, or within the adhesive layer itself. This route gives rise to a characteristic failure that moves inwards from the edge of the joint, giving rise to the characteristic picture-frame morphology as illustrated in **Figure 2**. This failure appearance may be a result of thermodynamic displacement or any of the other failure mechanisms discussed in the following section.

In summary, the presence of water at the interface of an adhesive joint generally leads to instability at the interface, resulting in interfacial failure, readily identified by XPS and ToF-SIMS. Simple thermodynamic calculations enable joint stability to be predicted from the knowledge of surface and interface free energies. It must be noted, however, that it provides no indication of the kinetics of failure, which must be established by empirical studies.

3.36.2.2 Adhesive Plasticization

All polymeric adhesives are permeable to water, and although water molecules can only enter through the edge of the joint, there is then the possibility that they can diffuse throughout the glue-line thickness. This can give rise to a degradation of the mechanical properties of the adhesive that is usually known by the catch-all term of plasticization. Water molecules can aggregate close to the interface with the substrate, which leads to swelling of the polymer and the subsequent reduction in durability. This process is analogous to the wet adhesion phenomenon observed in paints and shows the same behavior, in that, it is reversible to a large extent. Heating, or simply leaving joints that have been exposed to

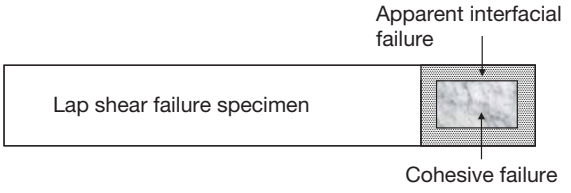

Figure 2 Picture frame failure, the typical appearance of a joint, which has been exposed to water, leading to an apparent interfacial failure from the edge inwards (the picture frame) and a central cohesive region (the picture), which has not been affected by water and provides the joint with residual strength.

water in relatively dry air is able to remove the water, and values approaching the original dry strength can easily be achieved.[2,3] The diagnostic of this type of failure is once again made by a careful examination of the substrate failure surface. Unless there is ready route to the interface from the bulk of the adhesive for the water molecules, they will not aggregate at the interface but only very close to it. Once again, surface analysis has an important role to play in the forensic analysis of failures in order to define the locus of failure at the molecular level. **Figure 3** indicates, schematically, the concepts of interfacial and cohesive failure, and the thinner the layer of adhesive remaining on the substrate in the cohesive example, the more challenging the analysis. The role of surface analysis in adhesion studies has recently been reviewed,[4] and examples of different failure types, as deduced from the application of such methods, will be presented at the end of this section.

3.36.2.3 Corrosion Induced Failure

3.36.2.3.1 Cathodic failure

The occurrence of corrosion at the exposed substrate of an adhesive joint leads to a localized corrosion phenomenon, in that the anodic and cathodic sites are separated with the exposed metal undergoing anodic oxidation, and the electrons produced are consumed at a cathodic site at the adhesive–substrate interface, where hydroxide ions are produced by the reduction of water and oxygen molecules. The reactions involved are the standard ones and are given below for an iron substrate.

At the exposed metal, the anodic reaction occurs

$$Fe^0 \rightarrow Fe^{2+} + 2e^- \qquad [3]$$

While at the cathode, two reactions are possible depending on the electrode potential, the more usual one being

$$O_2 + 2H_2O + 4e^- \rightarrow 4OH^- \qquad [4]$$

Although at potentials more noble than 1020 mV (versus the saturated calomel electrode), water reduction, leading to the evolution of hydrogen, is dominant:

$$2H_2O + 2e^- \rightarrow 2OH^- + H_2 \uparrow \qquad [5]$$

Reaction [5] occurs at a potential below that, which develops at the free corrosion potential of iron, and is generally considered to be important only when metal substrates are deliberately polarized cathodically, such as in impressed current cathodic protection schemes or laboratory based simulations of the same. Both cathodic reactions lead to the generation of hydroxide ions, which creates an alkaline environment in and around the adhesive–substrate interface.

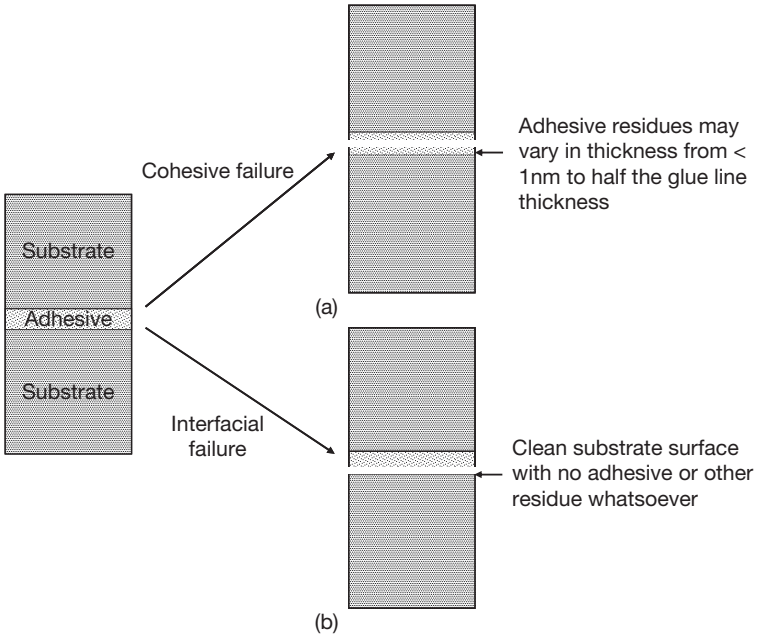

Figure 3 Schematic representation of (a) cohesive and (b) interfacial loci of failure.

The deleterious effect of such an alkaline environment on polymer to metal adhesion was first reported by Evans in 1929[5] in a paper entitled 'The Electrochemical Corrosion of Painted Steel with Special Reference to the *Alkaline Peeling* of the Coat.' This phenomenon received scant attention until the 1970s when the term cathodic disbondment (or variously disbonding or delamination) was coined to describe the separation of a polymer from the cathodic region of a coated metal. At the time, the examples of cathodic delamination that were cited included the adhesion loss of a paint film adjacent to a stone chip on an automobile or the failure of powder coatings on cathodically protected gas and oil transmission line pipe. Interestingly, both these examples had important technological consequences and led to an upsurge in research activity in the process of the mechanisms of cathodic delamination, most notably by groups led by Leidhesier, using electrochemical methods[6,7] and Dickie (at Ford USA)[8,9] and Castle (at the University of Surrey UK),[10,11] using XPS. The various mechanisms implicated in the cathodic delamination process were reviewed in the following decade by Leidhesier[12] and Watts.[13] Castle attempted to shed fresh light on the process in 1996, with a critical assessment of the role of water within the polymer in the failure process.[14]

The basic premise of cathodic delamination is very straightforward in that oxygen and water arrives at the cathodically polarized metal surface and, following eqn [4], hydroxide ions are produced, leading to an increase in the pH in the environs of the polymer–metal interface. This underfilm alkalinity attacks the interfacial bonding directly, in the manner proposed by Evans,[5] leading to adhesion loss. In practice, such a failure is observed visually on low carbon steel as the rather unusual and counter intuitive observation in that the organic coating readily peels from the steel, but the steel has a very clean, unrusted, appearance. The classic situation of a localized defect in an organic coating on steel is indicated in **Figure 4**. In this situation, the exposed metal undergoes anodic dissolution, the electrons produced are consumed in the annular cathodic zone surrounding the initial defect, water may arrive at the tip of the disbondment crevice by lateral diffusion from the defect or by downwards diffusion through the thickness of the coating, and the process which supplies the water molecules most quickly will be the one that is rate controlling. As the process continues, the anodic area will grow, consuming the delaminated cathodic area that will also extend, leading to increased coatings failure. This type of failure is

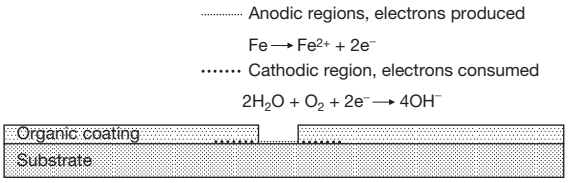

Figure 4 The electrochemical reactions that occur at a defect in an organic coating exposed to an aqueous solution. The anodic reaction occurs at the defect and cathodic reduction of water is localized within an extending crevice beneath the coating.

readily observed on painted steel structures where macroscopic or microscopic defects in the coating have developed. The cathodic and anodic areas are visually quite easy to separate, but in some cases, there is a need to be absolutely certain about the mechanism of failure, and in such cases, a useful analytical solution is to make use of the observation that electrode surfaces will retain their electrochemical signature once removed from the electrolyte and analyzed by a surface analysis method such as XPS.[15] In essence, the surface alakalinity needs metal cations (often Na^+) to balance the cathodically generated hydroxide ions, and as most electrolytes will have sufficient ionic species, the cathodic region can be identified by retained cations of this type. In a similar vein, anodic regions will retain marker anions such as Cl^-. Although the concentration of such ions is at monolayer coverage or less, it is a routine matter to determine their presence and concentration by XPS. Thus, in XPS, there is a useful methodology in which mechanism of failure can be confirmed, as will be shown in the next section.

The scenario of **Figure 4** is clearly the situation that exists when a polymer–metal system, be it adhesive or coating, is at the rest potential (free corrosion potential) of the metallic substrate. Although this situation occurs quite often, there is another regime that can render the cathodic delamination process even more destructive, that is, when the metal substrate bearing the adhesive or coating is polarized cathodically. This can occur as a result of a deliberately applied potential (as is the situation with impressed current cathodic protection), but more often, it occurs when the metal is coupled to a more active metal. Much of the early work relating to cathodic delamination was carried out in this manner using either an ASTM Specification[16] in which coated steel was coupled to a zinc anode or a UK approach[17] in which the coated panel was polarized

cathodically to a potential of 1.5 V versus the saturated calomel electrode, as shown in **Figure 5**. This latter test was much favored by the coatings end-users who found that it was able to discriminate coating performance very rapidly at a fairly rudimentary level. Many in the business found that it was a very severe test, with oxide reduction occurring as a precursor to coatings failure, something which the Pourbaix diagram for iron predicts will only happen at the extremes of cathodic potential and pH! Notwithstanding these possible shortcomings, this test is widely used, and performance of high performance fusion bonded coatings is frequently quoted against such a test by coatings manufacturers.

The mechanisms for destruction of the polymer–metal interface and failure of coating or adhesive appear to be fairly similar, irrespective of the source and magnitude of the cathodic potential; however, the kinetics of failure vary quite considerably, and this in turn is a direct consequence of the flux of hydroxide ion produced during the cathodic reduction process. It is informative to consider the quantities involved using data published many years ago.[11] In the examination of the delamination of a powder sprayed epoxy coating from a cathodically polarized (−1.5 V versus SCE) mild steel substrate, a delamination rate of 0.4 mm day^{-1} was established for a range of surface profiles once a correction for interfacial path length had been made. By converting the delamination rate to a more convenient unit, one arrives at a crack growth rate of 5 nm s^{-1}. From the knowledge of the rate at which a typical interface separates, the rate at which such an interface is exposed can be calculated, and then, by the application of Fick's law of diffusion, the flux of hydroxide ions required to sustain these kinetics can be inferred. The results of such a modeling approach lead to a flux of 10^{-15} mole of hydroxide ions per second, and the application of Fick's Law indicates a concentration gradient within a disbondment crevice of 10^{-3} mole dm^{-3} cm^{-1}, that is, a pH of at least 11. Using a similar approach, the current density required to sustain a rate of 5 nm s^{-1} is estimated at 6×10^{-11} A cm^{-2}. This is extremely low, and it is unlikely that this is the rate-controlling step in the disbondment process, and this leads one to the inescapable conclusion that diffusion of hydroxide ions along the metal–polymer interface is, indeed, the rate-controlling step, and when the required concentration gradient is maintained, the process will continue unabated.

3.36.2.3.2 *Anodic failure*

The two failures described above, hydrodynamic displacement of the organic phase, and the cathodic delamination of the coating or adhesive as a result of a local increase in pH, are routinely observed, whereas the failure of the polymer–metal interface as a result of localized anodic activity is unusual. In the coatings filed, there are well documented examples of the anodic undermining of a lacquer on tin plate for foodstuffs[18] and the failure of an acrylic repair coat on an aluminum brass substrate,[19] but otherwise, examples are rare. In the examination of the failure mode of adhesively bonded hot dipped galvanized steel, Fitzpatrick and Watts[20] showed that failure was a result of localized microelectrodes occurring at the metal–adhesive interface, but it was in the regions of cathodic activity that interfacial failure occurred; the other failure regions, presumably in the region of the microanodes, were essentially cohesive in nature,

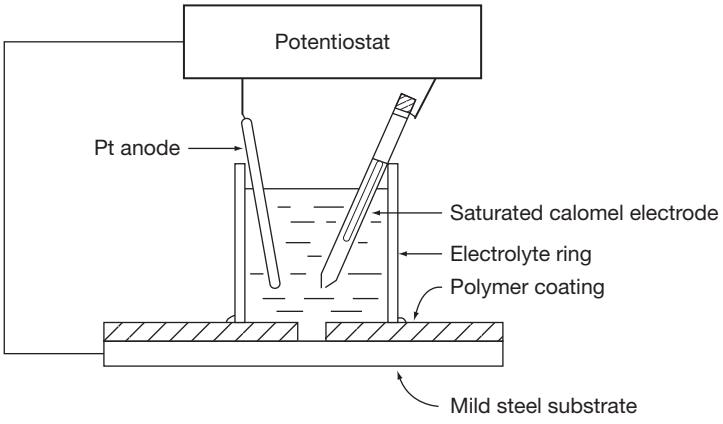

Figure 5 Schematic representation of the cathodic disbondment test.

indicating that the electrochemical activity in the environs of the anodic sites was not as deleterious as the increase in pH experienced at the microcathodes.

3.36.3 Identification of Locus of Failure and Failure Classification

As described above, there are four possible failure mechanisms that may be encountered as a result of the exposure of an adhesive joint to water. If we also consider the cohesive failure that may occur in a dry joint or a joint exposed to water for a relatively short time, there are five potential modes of failure. Of these five, four may look remarkably similar, and upon cursory examination, all will be described as an interfacial failure. This can be a gross oversimplification, and it is now informative to consider the characteristics of the failure modes that will be generated by each process in turn. The types of failure can be divided into cohesive failure within the adhesive (**Figure 3(a)**) or interfacial failure, when separation occurs exactly at the junction between substrate and adhesive (**Figure 3(b)**). Although conceptually easy, this definition is extremely difficult to confirm in practice as the layer of adhesive remaining on the substrate can range from many hundreds of micrometers (which can be established with the naked eye) to vanishingly thin layers of a few nanometers or less, which require surface analysis methods to detect and identify them. Thus, one of the greatest problems faced by those attempting to classify a failure mode can be the experimental techniques at their disposal; at some point, if only microscopy is used, a cohesive failure will appear, and be classified, as an interfacial failure!

If a joint is tested in a dry condition or if only exposed to water for a short time, the expectation is that the locus of failure will run through the glue-line thickness, a phenomenon that is readily observed by optical or electron microscopy and even, in some instances, by the naked eye. The diagnosis of such a failure is simple, but the edges of the joint should be examined for evidence of an interfacial failure generated by water diffusion along the interface. Even in instances of dry failure, it is possible that under some loading geometries, the locus of failure will pass so close to the metal–adhesive interface that the failure will appear interfacial to all forms of microscopy. This is the nub of any investigation into an adhesive joint failure – the identification of the failure path (or locus of failure to use the adhesion scientists term) at the molecular level. Thus, unless a failure is demonstrably within the glue-line thickness, the emphasis is on the investigator to use techniques that are appropriate to characterize the exact locus of failure and also the thermodynamic or electrochemical cause of the failure under consideration. The most useful method for failure analysis in this type of investigation has been shown to be XPS, which is a surface chemical analysis technique with a characteristic sampling depth of ~5 nm. In addition, XPS is able to provide chemical specificity, a quantitative analysis, overlayer thickness values and the identification of any characteristic ions from solution that are associated with the failure, and for this reason, it has been widely used in adhesion investigations over the last three decades.[21–23] The XPS characteristics of a cohesive failure close to the metal polymer interface are shown in **Figure 6**. This sample is a tin free steel substrate coated with an epoxy lacquer that has been hot molded to nylon, and then tested on a lap shear configuration. A macroscopic image (**Figure 6(a)**), shows that the failure appears to occur between metal substrate and epoxy or epoxy and nylon, depending on the position on the failure surface. Small spot XPS analyses (at 400 μm) were taken from the region that appeared to be a metal interfacial failure surface and a mirror image position on the adhesive side. These spectra (**Figures 6(b)** and **6(c)**) are extremely similar, and the characteristic of the epoxy coating itself is showing that the locus of failure is within this phase and not at the epoxy–steel interface, as one would assume from a visual inspection of the failure surfaces. Moving on to the situation wherein water is responsible for the (hydrodynamic) displacement of the adhesive from the metal substrate, an example can be seen in the work of Kinloch *et al.*[24] on the structural adhesive bonding of aluminum. After fatigue tests of a tapered double cantilever beam test piece, the joint is cracked open, and XPS analysis of the metal failure surface (**Figure 7(b)**), when compared with the unbonded surface (**Figure 7(a)**), indicates that an interfacial failure has occurred. However, the absence, in the spectrum, of any specific marker ion indicating electrochemical activity leads to the conclusion that this failure has been the result of the thermodynamic displacement, by water, of the adhesive from the metal substrate. This conclusion is entirely logical as the aluminum substrate will be covered with a passive oxide film and will only be susceptible to localized corrosion at points of metallurgical heterogeneity such as intermetallic precipitates (which will be cathodic to the surrounding matrix).

The observation that the electrochemical history of an electrode could be deduced from the spectrum

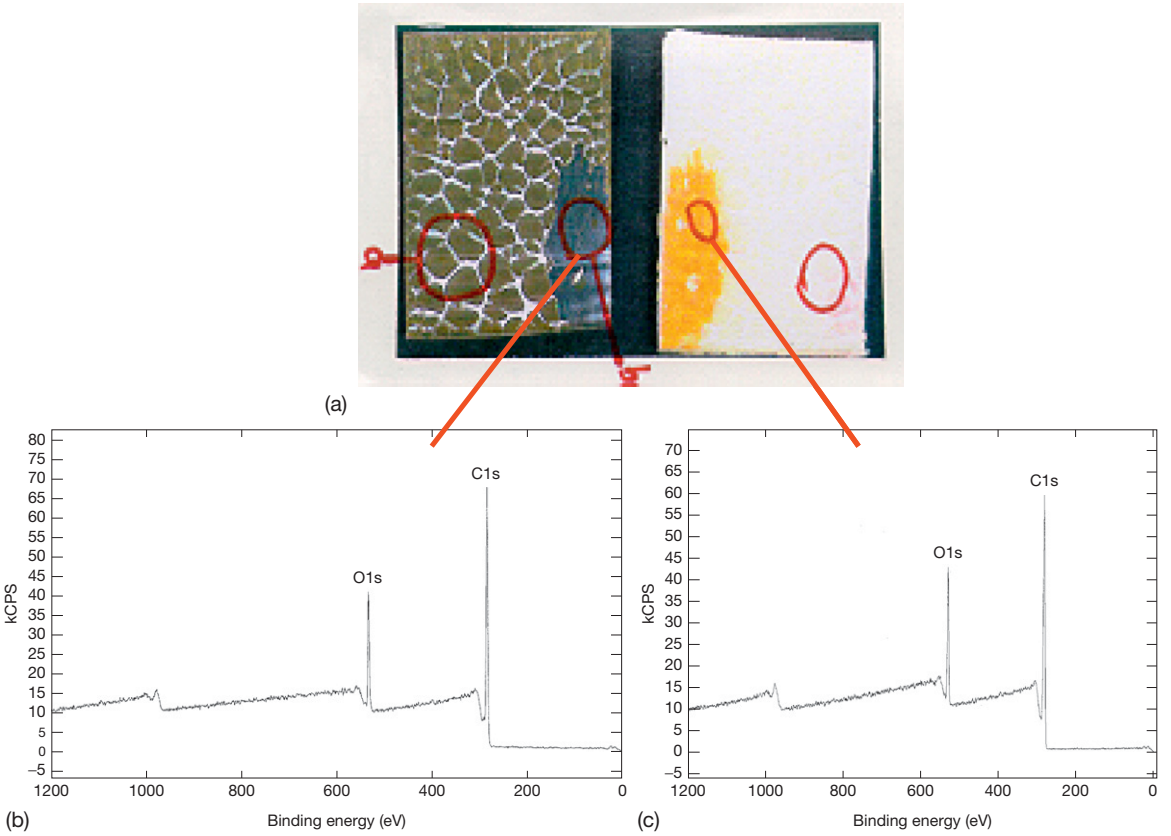

Figure 6 Optical microscopy image of a failure between epoxy coated tin-free steel and a nylon coating (a). XPS survey spectra taken from the apparent interfacial failure between the steel substrate (b) and epoxy coating (c). The similarity of the spectra establish unambiguously that the failure is a cohesive failure within the epoxy lacquer.

of ions adsorbed on the surface was first made by Castle and Epler,[15] using XPS, and more recently, work from the authors laboratory has extended this approach to analysis using ToF-SIMS. The important observation, initially made more than 30 years ago, was that if a metal electrode is exposed to a cathodic potential in an aqueous electrolyte, it will, not unreasonably, adsorb cations from the electrolyte. On removal from the electrolyte and subsequent washing, these adsorbed ions are retained (often at submonolayer concentrations) on the electrode surface and can be detected and quantified by a surface chemical analysis technique such as XPS. Initial work envisaged that such an approach would be useful in identifying whether a corrosion feature, such a pit, was active or benign, but the widest application of this approach is probably in guiding the definition of failure mode of organic coating and adhesives. This can be illustrated from very early work on the delamination of an organic coating from cathodically polarized (−1.5 V versus saturated calomel electrode in 0.5 M NaCl) steel.[10] The test was set up as shown in **Figure 5** with a central defect in the coating so that the cathodic reduction reaction could readily occur at the exposed metal surface and lateral diffusion of hydroxide ions could occur unimpeded. In addition, water could diffuse through the thickness of the coating in regions well removed from the coating defect. The metal interfacial failure surfaces that are generated in these two regions are very different, as shown in **Figures 8(a)** and **8(b)**. The failure close to the defect is once again characterized by an interfacial failure, but the very intense sodium concentration (~7 at.%) shows that there has been cathodic activity, the Na^+ acting as a counter ion for the cathodically generated OH^-. Farther from this defect, the carbon peak in the spectrum is very intense and the Fe 2p peak (at a binding energy of ~710 eV) is barely visible, being identified by an abrupt change in the background region of the spectrum. This change in background is

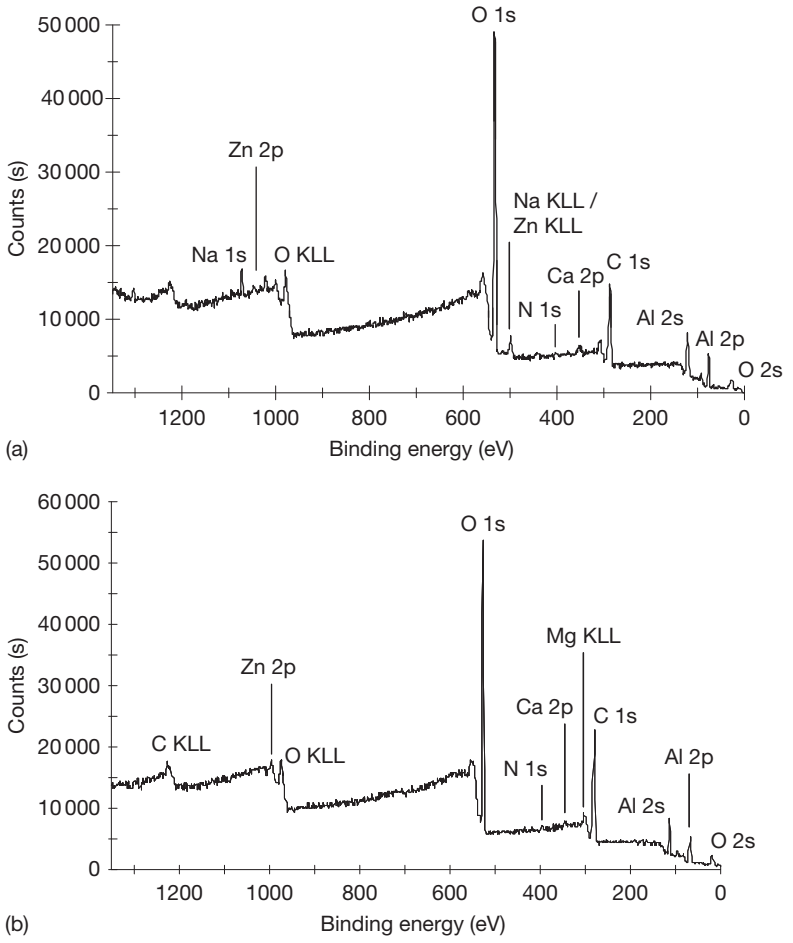

Figure 7 XPS survey spectra from grit blasted/degreased aluminum surfaces (a) prior to bonding and (b) following failure after exposure to liquid water. Reproduced from Kinloch, A. J.; Korenberg, C. F.; Tan, K. T.; Watts, J. F. *J. Mater. Sci.* **2007**, *42*, 6353–6370.

itself very informative, in that it indicates to the electron spectroscopist that most of the iron signal is being attenuated by a thin overlayer of, in this case, carbon (polymeric coating). Thus, this spectrum indicates that the failure is cohesive within the polymer but with a very thin (<10 nm) overlayer, indicating the locus of failure is ~10 nm from the metal oxide–polymer interface.

Although failure of adhesion as a result of cathodically generated alkali is one of the most usual failure mechanisms when corrosion is involved, there are very few documented examples of the advancing disbondment front acting as an anodic crevice. The most cited system and example of great importance to the food packaging industry is the anodic undercutting of the tin coating on tinplate[18] in times gone by but less so nowadays. An example of the manner in which the polymer–metal interface may develop as anodic crevice is afforded by the work of Castle *et al.*[19] who investigated the failure of an acrylic coating on aluminum brass on exposure to hot saline solution. The XPS survey spectra of **Figure 9** are from the interfacial failure metal surfaces of the acrylic–aluminum brass systems when subjected to a mechanical test before exposure (**Figure 9(a)**) and the failure following saline exposure (**Figure 9(b)**). Both failures are cohesive, as indicated by the intense C1s peak at a binding energy of ~285 eV, and the intense Cl2p peak for the exposure surface (**Figure 9(b)**) is in marked contrast to the failure surfaces of **Figure 8(a)** and indicates that the system is behaving as an anodic crevice. The localization of anodic activity within the crevice was reported to be enhanced by the application of increased thickness of organic coating, which represents a situation similar to that in adhesive bonds.

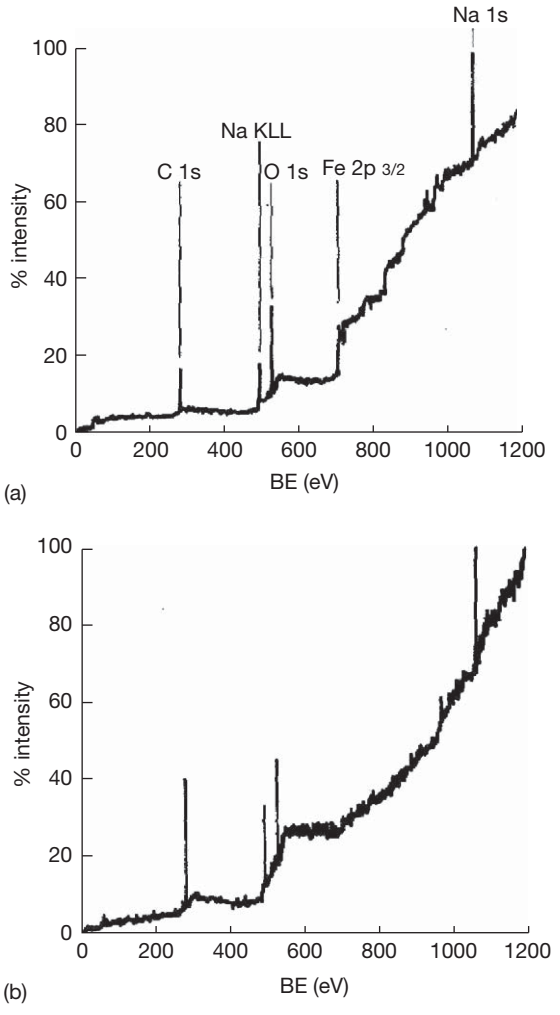

Figure 8 Failure of a polybutadiene coating on steel exposed to the cathodic disbondment test of Figure 5. XPS survey spectra from (a) immediately adjacent to the defect, resulting from the cathodic generation and lateral diffusion of hydroxide ions and (b) the wet adhesion failure region well removed from the defect arising from the downward diffusion of water molecules through the thickness of the coating. Reproduced from Watts, J. F.; Castle, J. E. *J. Mater. Sci.* **1983**, *18*, 2987–3003.

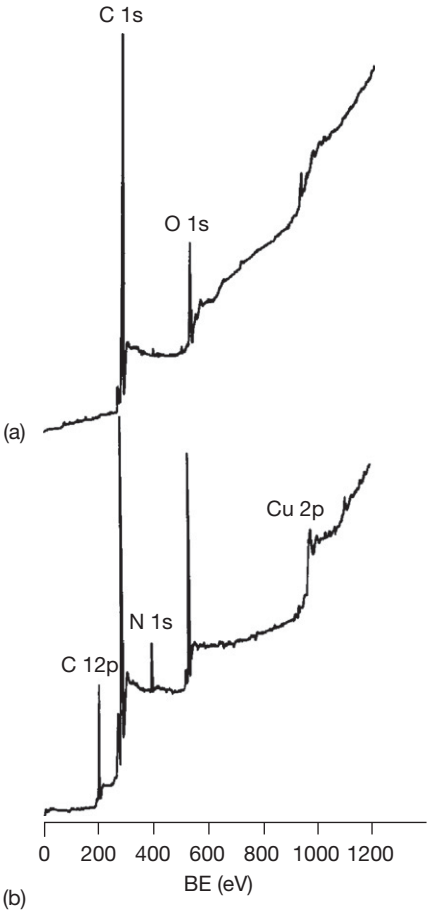

Figure 9 The failure of an acrylic coating on brass. XPS survey spectra of the interfacial metal surface following (a) dry test and (b) test in hot saline solution. Reproduced from Castle, J. E.; Luklinska, Z. B.; Parvizi, M. S. *J. Mater. Sci.* **1984**, *19*, 3217–3223.

In this section, the various mechanisms that may be observed in adhesive joints exposed to aqueous environments have been reviewed. When inspecting a failure surface, the first step in establishing the process responsible for failure is the assessment of the exact locus of failure. If failure is clearly within the glue-line thickness, as established by visual inspection or optical or electron microscopy, then it is reasonable to assume that failure is a result of exceeding the load-bearing capacity of the adhesive, and corrosion does not play a significant role in the failure process. If the failure path is very close to the substrate–adhesive interface, it is very likely that degradation based on exposure to water or corrosion reactions is responsible for failure, and without resorting to surface analysis techniques, such as XPS, it is probable that the locus of failure will be described as interfacial, even if examined at high resolution in an SEM. The reason for this is that failure is often extremely close (within 10 nm) to the interface, and thus, to fully understand failure, a surface chemical analysis is needed. A true interfacial failure can be easily recognized (although there will be a small amount of adventitious carbon – 20–35 at.% in a quantitative surface analysis), and this may be a result of hydrodynamic separation on exposure to water or cathodic delamination, which is recognized by the adsorption of cations, such as sodium, from the

test solution. If there is a small residual layer of adhesive on the substrate, it may be a result of water- or alkali-induced degradation of the polymer phase; once again, the presence of cations will indicate a significant involvement of the cathodic reduction process. The presence of anions, such as chloride, to excess, is unusual and is indicative of failure being the result of a developing anodic crevice, and seems to be associated with a cohesive failure.

Having reviewed the corrosion processes that may be responsible for failure of an adhesive joint and the manner in which the forensic analysis of failed surfaces can help identify the failure mechanism, and the role of corrosion in the failure process, it is helpful to consider the failure characteristics of various adhesively bonded substrate materials.

3.36.4 Adhesively Bonded Substrate Materials

In this section, the role of corrosion in adhesive bond failure will be considered with a series of case histories involving common metallic substrates for adhesive bonding. It is interesting to note that some authors set out to establish performance data, which can be used for adhesive bond design purposes, and the unraveling of the failure mechanism, takes on a secondary role, while others set out with the main purpose of establishing failure mechanism and use durability data on a merely comparative basis. It is important to note that there are two clear philosophies that are in use regarding the durability testing of adhesive joints; the first, easiest, and probably least realistic is to expose the joint to the aggressive environment with no load applied: at the point of test, the joint is removed from the test solution, dried, and tested, to obtain performance data. The alternative approach is to load (either monotonically or in cyclic mode) within the test environment, and once failure has occurred, remove specimens for microscopy and/or analysis. Both methods have their own particular merits; the first practice avoids the possibility of post-failure contamination (or back deposition) from the test solution, while the second is clearly much more realistic and generates data that can be included in the appropriate design codes. Examples of both types of testing will be considered in this section.

3.36.4.1 Low Carbon Steel Substrates

As one might imagine, the rapid corrosion that is experienced by adhesively bonded low carbon steel, if the joint is not protected by additional measures, leads to the domination of cathodic delamination as a failure process, and significant problems in the post failure analysis of failed joints as all surfaces that have been exposed during failure will inevitably become anodic sites. There are two potential measures for alleviating these difficulties; the cathodic polarization of the entire joint and the exposure of a joint in water with a low concentration of dissolved oxygen. Both approaches have been successfully employed, and examples are described below.

The bonding of neoprene to mild steel is of particular importance in the maritime industry, and there is a fairly extensive body of literature dealing with the failure modes of this system when the steel substrate is protected by either impressed current or sacrificial anode cathodic protection. The mechanistic aspects of the failure of this system was investigated by Boerio *et al.*[25,26] who employed a strip blister specimen, illustrated in Figure 10, polarized at a

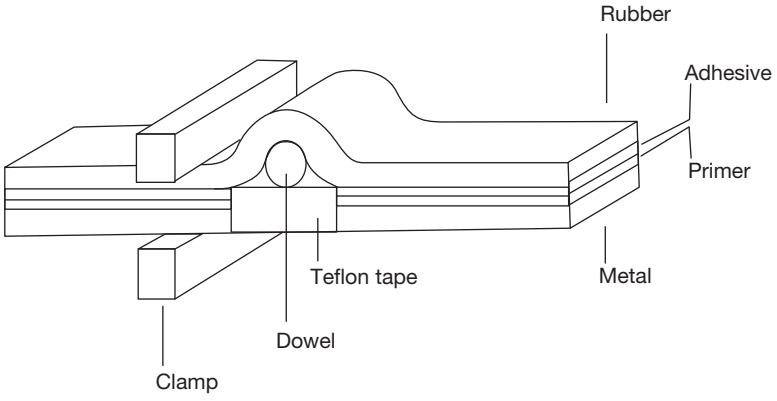

Figure 10 Schematic diagram of the strip specimen used for the study of the cathodic delamination of neoprene rubber from steel. Reproduced from Boerio, F. J.; Hudak, S. J.; Miller, M. A.; Hong, S. G. *J. Adhes.* **1987**, 99–114.

potential of −1.5 V versus the saturated calomel electrode. They were able to show, by XPS and FT-IRS analysis of the failure surfaces, that degradation occurred as a result of the degradation of the phenolic primer and dehydrohalogenation of the rubber in both the primer and the adhesive.[25] Such dehydrochlorination resulted in the formation of inorganic solutes soluble in the alkaline solution used as a test medium. These authors also showed a critical dependence on surface roughness, indicating the importance of mechanical effects in the performance of adhesive joints, presumably as a result of the increased extent of interfacial contact achieved with the rougher substrate. In subsequent work, Boerio and Hong[26] used FTIR to refine the chemistry of the failure mechanism, and showed that methylene groups linking phenyl species in the primer were rapidly oxidized in alkaline solution to form benzophenone linkages, which could oxidize further to carboxylic acids and quinines. $ZnCl_2$ was observed to form a soluble reaction product at the bondline, as a result of the reaction between chlorine from the chlorinated rubber and ZnO filler in the primer. It is concluded, on the basis of these studies, that both the oxidation of phenolic resins in the primer and osmotic effects related to $ZnCl_2$ have important roles to play in the failure mechanism of rubber to steel adhesive joints. Complemented by the studies of Hamade and Dillard, in a series of papers spanning almost 20 years, have concentrated on relating the experimental observables (strength and extent of disbondment) to experimental parameters, such as time, temperature, and cathodic potential. The study of these authors is informative as it shows how a simple, diffusion-based model can be developed to provide a semiempirical model that is able to accurately predict the disbondment rates upon exposure to cathodic environments. These authors also differentiate between a separated zone (the picture-frame failure appearance) and a weakened zone ahead of the true delamination zone. Although mechanistic aspects of this are not fully explored, one assumes that the separated zone is the region of cathodic delamination resulting from alkaline attack of the interfacial bonding, while the weakened zone results from aqueous plasticization of the adhesive. The latter zone may show recovery of strength on removal from the aqueous environment as described by Watts *et al.* in their work on epoxy and other systems.[27] Hamade *et al.* in their extensive studies have produced data on the rate of disbondment in both the failed and weakened zone, and also strain energy release rate, G, as a function of time. This led to the development of a semiempirical model for the cathodic weakening of adhesive joints,[28,29] in which failure kinetics were related to the harshness of the environment (as exemplified by extent of cathodic activity and temperature of test) and the strain energy release rate. This can be represented very conveniently in the diagram of **Figure 11**, which illustrates the generic behavior of delamination rate ($\log \mathrm{d}Z_2/\mathrm{d}t$) versus strain energy release rate for weakening (region I), delamination (region II) as well as region III, where environmental and corrosion process play no discernible role in the failure process. These authors also provide guidance on the extent of delamination that will occur for a given set of exposure conditions in the form of nomographic scales or nomograms. In this manner, the extent, for a particular bond, in a particular aqueous environment, can be estimated as a function of cathodic potential and temperature. Two such nomograms are reproduced in **Figure 12** for a mild steel adhesively bonded system of a chlorinated rubber adhesive and a phenolic resin/chlorinated rubber primer. **Figure 12(a)** represents the calculated delamination values (Z_2) for the above system in artificial seawater, while **Figure 12(b)** represents complementary data in a 1 M NaOH environment. The arrows on the nonograms indicate example applications for the time for 12 mm of delamination to occur in the strip blister test of **Figure 10** at a potential of −1100 mV and at a temperature of 298 K. In the case of artificial seawater, a time of 180 days is predicted, while in 1 M NaOH, a much reduced time of ∼30 days is indicated. Although very specifically related to a certain system, such nomographs are clearly of much practical use, allowing changes in environment and pretreatment to be predicted.

An alternative way in which gross corrosion of a mild steel substrate can be alleviated in order to examine the interfacial chemistry associated with failure is to expose the joints in water containing a low concentration of dissolved water. In studies of this type, Davis and Watts[30] assembled adhesively bonded mild steel coupons in a lap shear configuration and then immersed them in pure water in sealed glass jars, removing specimens periodically for mechanical testing and surface analysis of the interfacial failure surfaces. After 1200 h of testing, a characteristic picture-frame failure surface was observed, while after 7500 h, the picture was greatly reduced in size, and visual and spectroscopic differences were observed at the surrounding metal surface. In the early stages of exposure, adhesive–substrate separation is driven by cathodic delamination, but on longer exposure times,

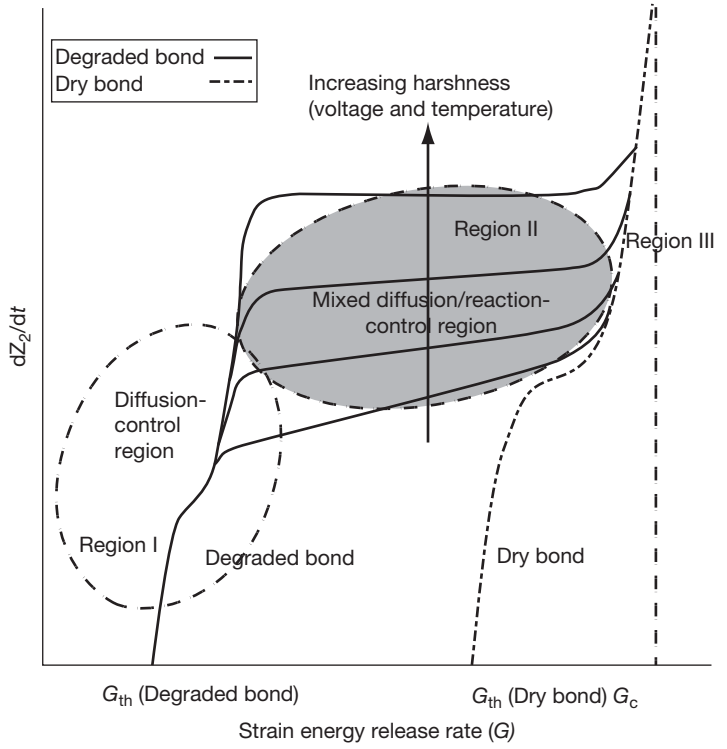

Figure 11 A plot illustrating the generic behavior of log delamination rate (log dZ_2/dt) versus log G. The diagram shows the regimes of diffusion control, leading to weakening (region I), the mixed diffusion/reaction control region (region II) and the environment independent region (region III). Reproduced from Hamade, R. F.; Seif, C. Y.; Merhij, F.; Dillard, D. A. *J. Adhes. Sci. Technol* **2008**, *22*, 775.

the crevice opens at the mouth as a result of oxide thickening, which appears as a dull rather than bright outer region. XPS analysis confirmed oxide dissolution at the crack tip with oxide growth subsequently occurring, as indicated in **Figure 13**. As the experiments were undertaken in pure water, the deposition of marker cations was at a very low concentration (below the detection limit of XPS); however, ToF-SIMS, with its better detection limit, allowed such marker ions to be profiled across the failure crevice. This example illustrates the concept of a so-called zero volume debond (sometimes referred to as a kissing bond in the aerospace industry) in which the adhesive and failure surfaces are in contact but have no load carry ability as a result of the adhesion between the two, having been compromised.

3.36.4.2 Aluminum Substrates

As a result of its importance in the aerospace industry, the adhesive bonding of aluminum has been studied very widely over the last three decades, and there is a large body of literature relating to the mechanical performance and durability of these systems. Generalized corrosion of aluminum is unusual, and it has very rarely been identified as a primary cause of failure in adhesively bonded systems, although localized corrosion in the form of pitting may sometimes be seen on test pieces immersed in water. The more usual forms of failure are associated with adhesive degradation at short exposure times, and interfacial separation of adhesive and oxidized aluminum substrate is as a result of thermodynamic displacement of adhesive by water. Using simple T-peel joints, exposed to water prior to testing, Watts *et al.*[27] were able to show failure associated with adhesive degradation at the edge of the joint. **Figure 14** shows the physical appearance of the failure surface of adhesively bonded chromic acid anodized aluminum following 10 weeks exposure at 50 °C in deionized water. The characteristic picture-frame type of failure morphology is seen running along the length of the joint, and visual assessment would identify the edge effect as being an interfacial failure. Small area XPS analyses were recorded from the interfacial failure surfaces at the edge of the joint and the centre of the

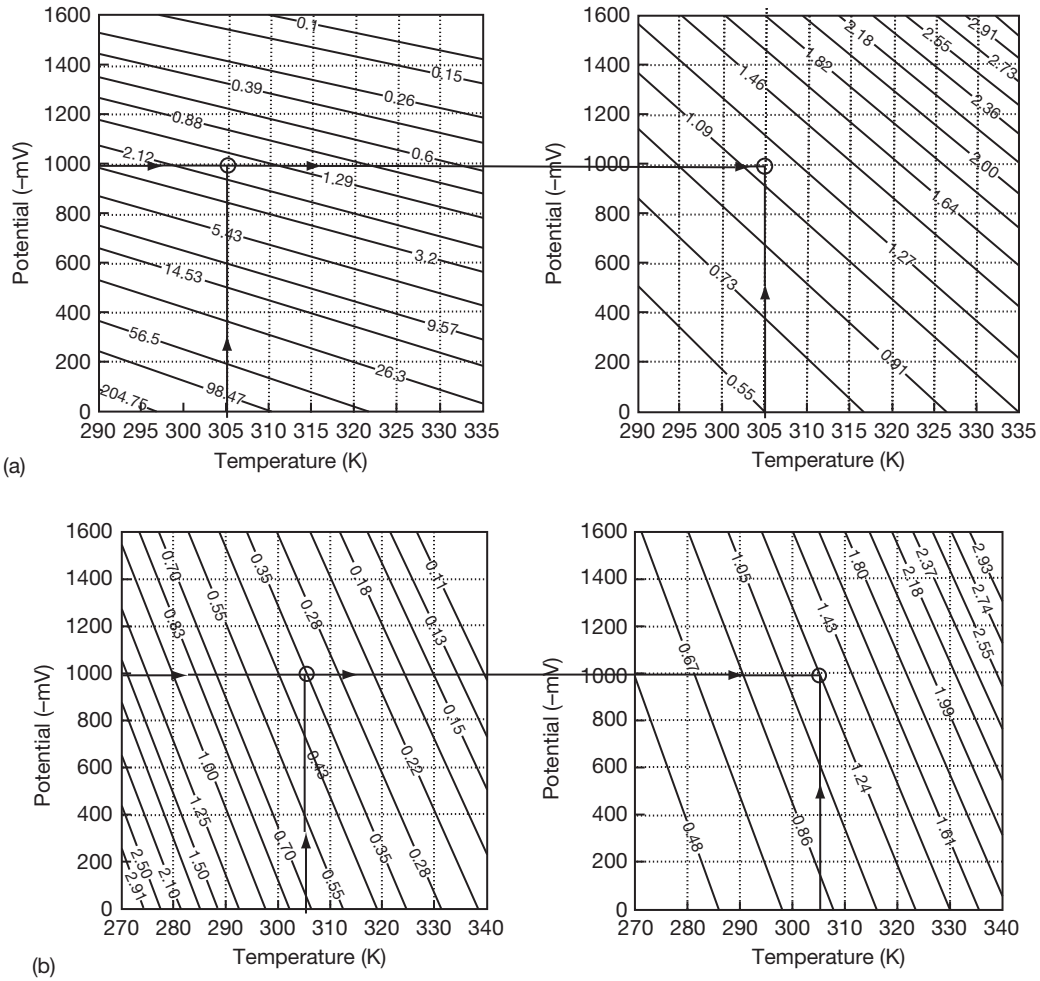

Figure 12 Nomographs for estimating bond weakening distances in (a) artificial seawater and (b) 1 M NaOH. The left plot of each pair represents the contours of the square root of delay time, t_d, while the right plots represent contours of the bond weakening rate WR_e. Examples of the use of such nomographic scale are provided in the original reference. Reproduced from Hamade, R. F.; Dillard, D. A. J. *Adhes. Sci. Tech.* **2003**, 1235–1264.

joint width. As expected, the general cohesive failure zone yields a spectrum characteristic of the bulk adhesive with no unexpected elements present, but the spectrum from the edge region, **Figure 15(a)**, is of an oxidized aluminum substrate attenuated with ~5 nm of adhesive. This clearly indicates that failure is associated not with environmental attack of the adhesive–substrate interface but with the aqueous degradation of the adhesive itself. Work in this paper also shows that such degradation is physical rather than chemical in nature and that a drying schedule at elevated temperature is able to reverse the damage, the locus of failure moving into the bulk of the adhesive, as observed in the central part of the joint of **Figure 15(b)**.

As part of a wide-ranging fracture mechanics study, Kinloch *et al.*[24] have studied the durability of adhesively bonded aluminum joints, steel joints, and aluminum–steel couples bonded in a similar manner. In the case of the aluminum and steel joints, the failure mechanisms were as expected; in the case of bonded 7075 aluminum, there is little corrosion observed, and failure is attributed to the thermodynamic displacement of the adhesive from the substrate as predicted by eqn [2]; when the substrates are both medium carbon (0.6%), steel failure follows the predicted path of cathodic delamination, both failure mechanisms being confirmed by an extensive XPS and ToF-SIMS study. In the case of dissimilar substrates (aluminum and steel beams), the situation is rather complex, and it is worthwhile considering this situation in some detail as an exemplar of how corrosion processes may have an unexpected role to

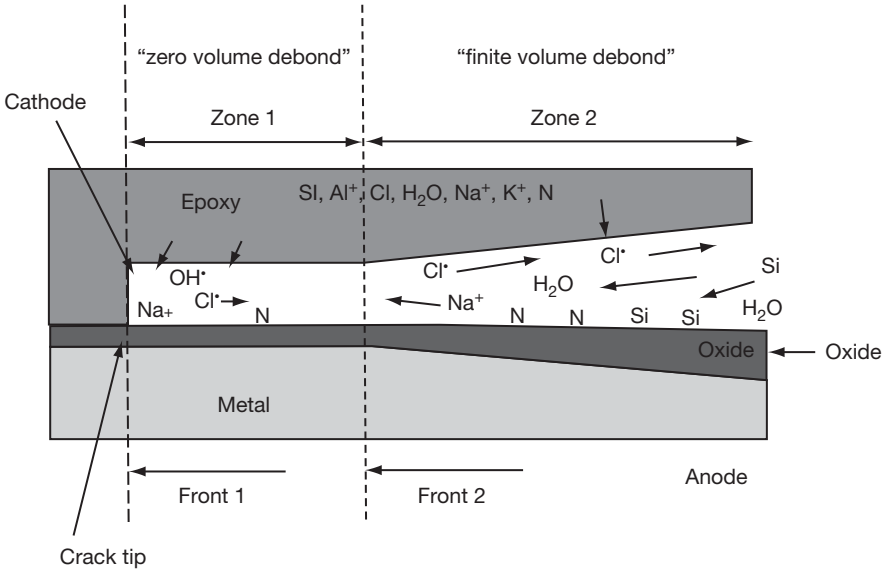

Figure 13 Schematic illustration of the failure processes that occur within the extending crevice at the edge of an adhesive joint exposed to an aqueous solution with a low partial pressure of oxygen. The crevice mouth acts as the anode and subsequently opens as a result of oxide growth and other processes, while the crevice tip forms the cathodes and leads to a zero-volume debond within which mass transport of the reactive and other species is restricted. Reproduced from Davis, S. J.; Watts, J. F. *J. Mater. Chem.* **1996**, *6*, 479–494.

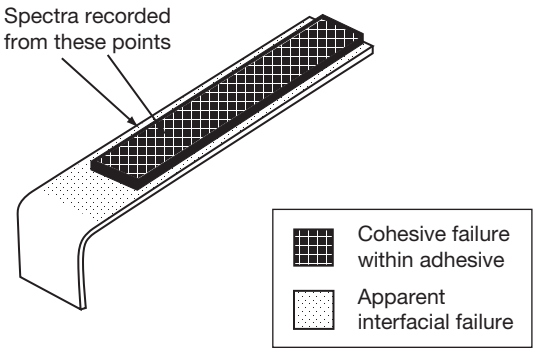

Figure 14 The schematic appearance of the failure surface of a T-peel assembly of adhesively bonded aluminum exposed for water at 50°C prior to testing. Reproduced from Watts, J. F.; Blunden, R. A.; Hall, T. J. *Surf. Interf. Anal.* **1990**, *16*, 227–235.

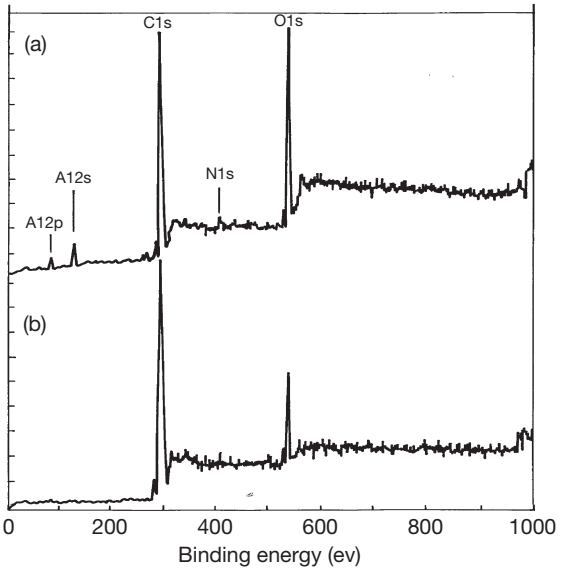

Figure 15 Small area XPS (250 μm) taken from the edge (a) and the central (b) regions of the failure illustrated in Figure 14.

play in the failure of an adhesively bonded structure, and the manner in which it is necessary to consider the environment surrounding the joint as well as the specific environs of the bondline itself. In the case described by Kinloch *et al.*, the joints were assembled in a tapered cantilever beam geometry (to ensure constant compliance as crack propagation occurs) and tested under fatigue loading in pure water. Failure always occurred adjacent to the adhesive–steel interface, and not at the aluminum–adhesive interface. At first sight, the occurrence of the failure at the steel–adhesive interface would seem to be the simple case of galvanic corrosion, as an aluminum alloy will be at the more active end of the galvanic series than steel. For such galvanic coupling to occur, there needs to be electrical contact between the aluminum-alloy

and steel substrates. This was not the case, and experiments were performed to ensure that there was no electrical coupling of the two substrates. There was also extensive corrosion on the steel beam, which would not be present had the beam been the cathodic part, in its entirety, of a galvanic cell. Now, the reason for the inferior durability of the dissimilar joints lies in the diffusion of oxygen molecules into a developing crevice and the concomitant outward diffusion of the cathodic reaction product (OH^-). It is helpful at this point to consider the situation in terms of the oxygen supply that exists for the steel–steel joint. Along the sides of both beams, the anodic reaction will take place, and soluble Fe(II) ions will pass into the solution, leading to a local increase in density. Thus, this solution of water and Fe(II) ions will sink to the bottom of the testing tank, and the solution in the environs of the adhesive layer will be refreshed with aerated water. This situation ensures that there is a ready supply of reactants for the cathodic reaction, which develops a crevice normal to the direction of crack propagation (i.e., the length of the test piece). As the diffusion of hydroxyl ions is known to be rapid in aqueous solution, it is more likely that the aggregation of these species at the crack tip is modest; in other words, the diffusion coefficient of water molecules into the crevice is much the same as that of hydroxide ions diffusing outwards. Thus, the rate-controlling step may be taken to be the rate of arrival of the water molecules, which must feed the two developing cathodic crevices. This situation is illustrated schematically in Figure 16. In the case of an aluminum-alloy–steel joint, the two metal interfaces will not behave in the same manner; the steel adhesive interface will develop a cathodic crevice as described above, but as the aluminum-alloy has a passivated film present, the extent of cathodic reactions at this surface will be confined to regions surrounding localized corrosion, such as pitting on the failure surface of the beam. Thus, any corrosion on the aluminum-alloy beam will be a post-failure event. This means that the majority of the oxygen molecules dissolved in the aqueous bath adjacent to the adhesive layer are available for consumption by the cathodic half reaction at the steel–adhesive interface. Assuming the outward diffusion of hydroxide ions remain the same, the situation that now exits is that the inward diffusion of oxygen molecules exceeds the outward diffusion of hydroxide ions. This will lead to an aggregation of hydroxide ions at the crevice tip and an increase in pH in this region. This will have an increased damaging effect on the level of adhesion between adhesive and steel substrate and the associated reduction in performance. To summarize, the increased concentration of oxygen molecules available in solution to feed the crevice developing normal to the beam side at the steel–adhesive interface weakens the joint and leads to more rapid advancement of the crack tip. As the crevice develops, the crevice mouth becomes anodic and the corrosion product is back deposited, reducing the inward diffusion of water and oxygen molecules, but by this time, the damage is already done and the mechanical perturbation of the reduced area at the advancing crack tip has brought about failure. The development of the cathodic crevice

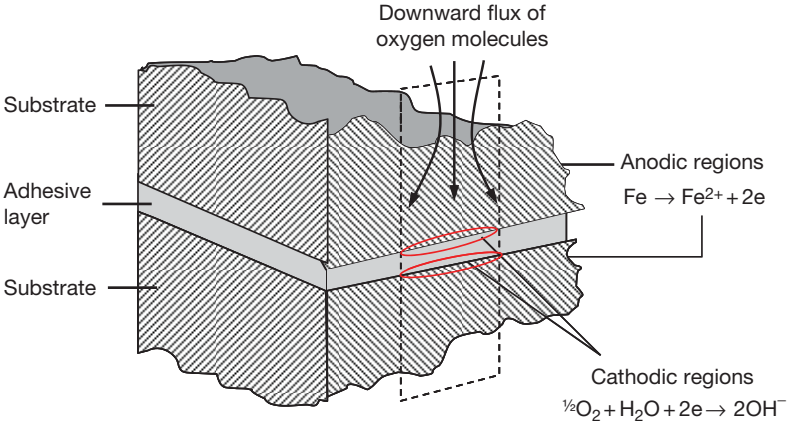

Figure 16 Schematic illustration of the supply of oxygen to the crevices developing at the adhesive–substrate interface of an adhesive joint. As freshly aerated water arrives, it must supply oxygen to both crevices in the case of a steel–steel joint, but only the steel–adhesive interface in the case of an aluminum–steel joint. Reproduced from Kinloch, A. J.; Korenberg, C. F.; Tan, K. T.; Watts, J. F. *J. Mater. Sci.* **2007**, *42*, 6353–6370.

happens along the beam simultaneously; thus the effect is most serious in the mid-regions where the crevice has developed significantly but not been blocked by corrosion product. The situation is summarized schematically in **Figure 17**.

3.36.4.3 Zinc Substrates

The need to bond zinc structures is, of course, very specialized and outside the scope of the review; however, the bonding of zinc coated steel (whether hot dipped or electrogalvanized (HDGS or EGS)) is becoming increasingly important as a production process, particularly in the automobile industry. In essence, the failure is brought about by the gross corrosion of the substrate, a situation that is improved by the chemical pretreatment of the substrate, for example, by the application of a zinc phosphate process. Dickie *et al.* showed quite convincingly that the failure of adhesively bonded EGS in an aqueous environment is a result of an electrochemically driven process,[31] with the XPS survey spectra of both the metal and adhesive interfacial failure surfaces being dominated by zinc oxide. These observations indicate that failure is associated with gross corrosion of the zinc when the surface is not stabilized by the application of an appropriate treatment, such as a conversion coating. Work by Fitzpatrick *et al.*[20,32] points the way to a better understanding of the manner in which such a conversion coating improves bond durability. Studies by small area XPS indicate that failure initiation is associated, at least in part, by the dissolution of the phosphate crystal by cathodically-generated alkali in regions of some 50–100 µm in size within 1 mm of the edge of the adhesive bond. ToF-SIMS successfully identifies electrochemical activity, although not gross phosphate dissolution, within the central region of the joint, and it is clear that this precedes the

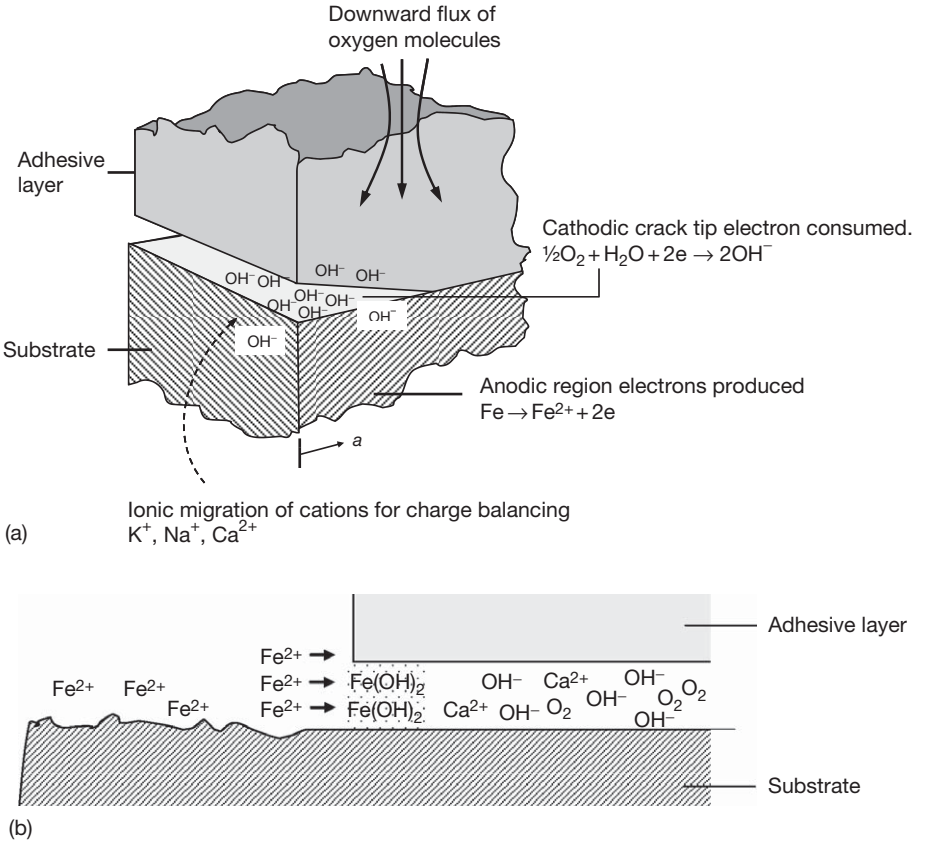

Figure 17 Schematic representation of the factors influencing supply of oxygen in the developing crevices. (a) In the early stages of failure, oxygen is supplied at the advancing crevice tip as the crack proceeds along the length of the beam and also normal to the direction of crack growth to establish a small but significant developing crevice at the edge of the specimen. (b) The edge crevice may become blocked with corrosion products in this manner in the later stages of joint failure and thus have a disproportionate effect on the failure kinetics. Reproduced from Kinloch, A. J.; Korenberg, C. F.; Tan, K. T.; Watts, J. F. *J. Mater. Sci.* **2007**, *42*, 6353–6370.

phosphate degradation process identified at the bond edge. This points the way to a more purposeful design and selection of conversion coatings for the pretreatment of zinc-coated steel for adhesive bonding, the use of those that have a better resistance to alkaline dissolution than the traditional zinc phosphate product.

3.36.5 The Improvement of Bond Durability

The solution to the need to improve the resistance of adhesive joints to the ravages of corrosion-related phenomena, leading to premature failure, is well-catalogued and can be readily appreciated by consideration of the examples above. There are two potential routes by which durability can be improved; one is the exclusion or immobilization of water by the adhesive so that the kinetics of diffusion toward the reaction zone are reduced to a manageable or acceptable level. The other is to modify the interface in some manner so that the forces responsible for adhesion become less susceptible to cathodically generated alkali or the interfacial path length between substrate and adhesive, which is increased to such an extent that the delamination process at the interface translates to a lateral or planar value that will no longer compromise the joint performance.

Exclusion of water is most commonly achieved by the simple expedient of the application of a bead of silicone, polysulfide or similar sealant along the external surface of the adhesive. Similar in use to a typical domestic product for bathroom use, such a sealant not only seals the joint against the ingress of water, but being hydrophobic, it also physically repels water from the vicinity of the joint. A similar approach is to use a hydrophobic binder for the adhesive, which will repel water from the adhesive, although not necessarily from the interface region. An alternative possibility, not widely explored, is to add extenders to the pigment that will either absorb and immobilize water or increase the path length for water to reach the interface.

The modification of the interface to improve performance would seem to be a much more elegant approach to take, and clear improvements in performance can be achieved by the use of organo-functional silanes as either primers[24,28] or components of the adhesives formulation, and most commercial structural adhesives have these additives included by the manufacturer. The benefit derives from the formation of a bond more resistant to both hydrodynamic displacement and cathodic delamination; that is a covalent bond as opposed to van der Waals bonding.[33] The increase of the interfacial path length is achieved by simple expedients, such as grit blasting, but in the case of aluminum, this is never adequate, and the complex microtopography achieved by acid anodizing processes is always required.[34] The porous deposit produced by these processes is filled by the adhesive on joint manufacture forming an interlocking region sometimes referred to as a microcomposite interphase zone.

The empirical test approach for a particular set of variables (substrates, adhesive type, loading conditions and environment) is an important way of extending our understanding of failure mechanisms and at the same time providing an indication of the manner in which improved performance can be obtained. This does not necessarily help the design engineer and certainly provides no predictive capability outside the narrow spectrum of conditions that have been examined. The solution to this, as outlined by many authors in recent years, is to develop predictive models that take into account the important variables that are experienced by adhesive joints. There are two basic approaches here that can be described, by analogy with nanotechnology production methods, as top-down or bottom-up. Models based on empirical results, of the required level of sophistication, can be extended to accommodate different adhesive bonding situations, and elegant examples of this approach is provided by the work of Kinloch[24] and Hamade.[35] The alternative approach is to consider a particular joint geometry, load and environment, and the development of closed form adhesive joint stress analyses as described by Crocombe.[36] The particular challenge with this method has been the incorporation of environmental degradation into such closed form solutions, and recent work shows that this can be achieved in a relatively straightforward manner.[37]

3.36.6 Conclusions

There is a very large body of literature that documents the deleterious effect of water on adhesively bonded metal structures, and the prime causes of joint failure are well understood. Corrosion of the substrate, leading to cathodic delamination of the adhesive from the metal is particularly important in the failure of steel joints, while for aluminum, with its passive native oxide layer, thermodynamic displacement of the adhesive from the substrate by the water is the most

commonly encountered failure mode. If the interface is modified chemically (e.g., using an organosilane) or physically to increase surface topography and then the interfacial path length, environmental degradation of the adhesive itself may occur. In order to improve a joint performance, it is necessary to first define the failure mode, and the surface analysis methods of XPS and ToF-SIMS have important roles to play here, not only in the exact definition of the locus of failure, measurement of the thickness of vanishingly thin residual adhesive layers, and relating their composition to the adhesive formulation, but also in the identification of tracer anions and cations, which can indicate whether the region of the substrate that the adhesive has separated from has experienced anodic or cathodic condition as an electrochemical cell has been set up.

There is still much active research to establish new pretreatments that will improve the durability of joints and provide improved corrosion resistance of the substrate. The driving force over the last decade has been to remove hexavalent chromium from pretreatment processes, and the stage is almost upon us where this reagent can be removed totally from the pretreatment stage of the bonding process, even in the aerospace industry, with no adverse effect on performance.

References

1. Gledhill, R. A.; Kinloch, A. J. *J. Adhes.* **1974**, *6*, 315–330.
2. Watts, J. F.; Castle, J. E.; Hall, T. J. *J. Mat. Sci. Lett.* **1988**, *7*, 176–178.
3. Leidheiser, H., Jr; Funke, W. *J. Oil Colour Chem. Assoc.* **1987**, *70*, 121–132.
4. Watts, J. F. In *Handbook of Surface and Interface Analysis: Methods for Problem Solving*; Riviere, J. C., Myhra, S., Eds.; Marcel Dekker, 1998; pp 781–833. Second Edition in press, publication 2009.
5. Evans, U. R. *Trans. Electrochem. Soc.* **1929**, *5*, 243–248.
6. Leidheiser, Jr. H.; Kendig, M. W. *Corrosion* **1976**, *32*, 69–76.
7. Standish, J.; Leidheiser, H., Jr. In *Corrosion Control by Organic Coatings*; Leidheiser, H., Jr., Ed.; NACE: Houston, TX, 1981; pp 38–44.
8. Hammond, J. S.; Holubka, J. W.; de Vries, J. E.; Dickie, R. A. *Corr. Sci.* **1981**, *21*, 239–253.
9. Dickie, R. A.; Hammond, J. S.; Holubka, J. W. *Ind. Eng. Chem. Prod. Res. Dev.* **1981**, *20*, 339–343.
10. Watts, J. F.; Castle, J. E. *J. Mater. Sci.* **1983**, *18*, 2987–3003.
11. Watts, J. F.; Castle, J. E. *J. Mater. Sci.* **1984**, *19*, 2259–2272.
12. Ledheiser, H., Jr. *J. Adhes. Sci. Technol.* **1986**, *1*, 79–98.
13. Watts, J. F. *J. Adhes.* **1989**, *31*, 73–85.
14. Castle, J. E. In *Organic Coatings*; AIP Conference Proceedings 354; Lacaze, P.-C., Ed.; AIP Press: Woodbury, NY, 1996; pp 432–449.
15. Castle, J. E.; Epler, D. C. *Surf. Sci.* **1975**, *53*, 286–296.
16. ASTM G8–72.
17. British Gas Specification PS/CW6.
18. Koehler, E. L. *J. Electrochem. Soc.* **1985**, *132*, 1005–1009.
19. Castle, J. E.; Luklinska, Z. B.; Parvizi, M. S. *J. Mater. Sci.* **1984**, *19*, 3217–3223.
20. Fitzpatrick, M. F.; Watts, J. F. *Surf. Interf. Anal.* **1999**, *27*, 705–715.
21. Watts, J. F.; Castle, J. E.; Ludlam, S. J. *J. Mater. Sci.* **1986**, *21*, 2965–2971.
22. Watts, J. F.; Dempster, B. R. *Surf. Interf. Anal.* **1992**, *19*, 115–120.
23. Sautrot, M.; Abel, M.-L.; Watts, J. F.; Powell, J. *J. Adhes.* **2005**, *81*, 163–187.
24. Kinloch, A. J.; Korenberg, C. F.; Tan, K. T.; Watts, J. F. *J. Mater. Sci.* **2007**, *42*, 6353–6370.
25. Boerio, F. J.; Hudak, S. J.; Miller, M. A.; Hong, S. G. *J. Adhes.* **1987**, 99–114.
26. Boerio, F. J.; Hong, S. G. *J. Adhes.* **1989**, *30*, 119–134.
27. Watts, J. F.; Blunden, R. A.; Hall, T. J. *Surf. Interf. Anal.* **1990**, *16*, 227–235.
28. Hamade, R. F.; Dillard, D. A. *J. Adhes. Sci. Technol.* **2003**, 1235–1264.
29. Hamade, R. F.; Dillard, D. A. *Int. J. Adhes. Sci. Technol.* **2005**, 147–163.
30. Davis, S. J.; Watts, J. F. *J. Mater. Chem.* **1996**, *6*, 479–494.
31. Dickie, R. A.; Haack, L. P.; Jethwa, J. K.; Kinloch, A. J.; Watts, J. F. *J. Adhes.* **1998**, 1–37.
32. Fitzpatrick, M. F.; Ling, J. S. G.; Watts, J. F. *Surf. Interf. Anal.* **2000**, *29*, 131–138.
33. Abel, M.-L.; Fletcher, I. W.; Digby, R. P.; Watts, J. F. *Surf. Interf. Anal.* **2000**, *29*, 115–125.
34. Clearfield, H. M.; McNamara, D. K.; Davis, G. D. In *Adhesive Bonding*; Lee, L.-H., Ed.; Plenum Press: New York, NY, 1991; pp 203–238.
35. Hamade, R. F.; Seif, C. Y.; Merhij, F.; Dillard, D. A. *J. Adhes. Sci. Technol.* **2008**, 775–793.
36. Crocombe, A. D. In *Adhesive Bonding: Science, Technology and Applications*; Adams, R. D., Ed.; Woodhead Publishing Ltd.: Cambridge, UK, 2005; pp 91–122.
37. Crocombe, A. D. *J. Adhes.* **2008**, *84*, 212–230.